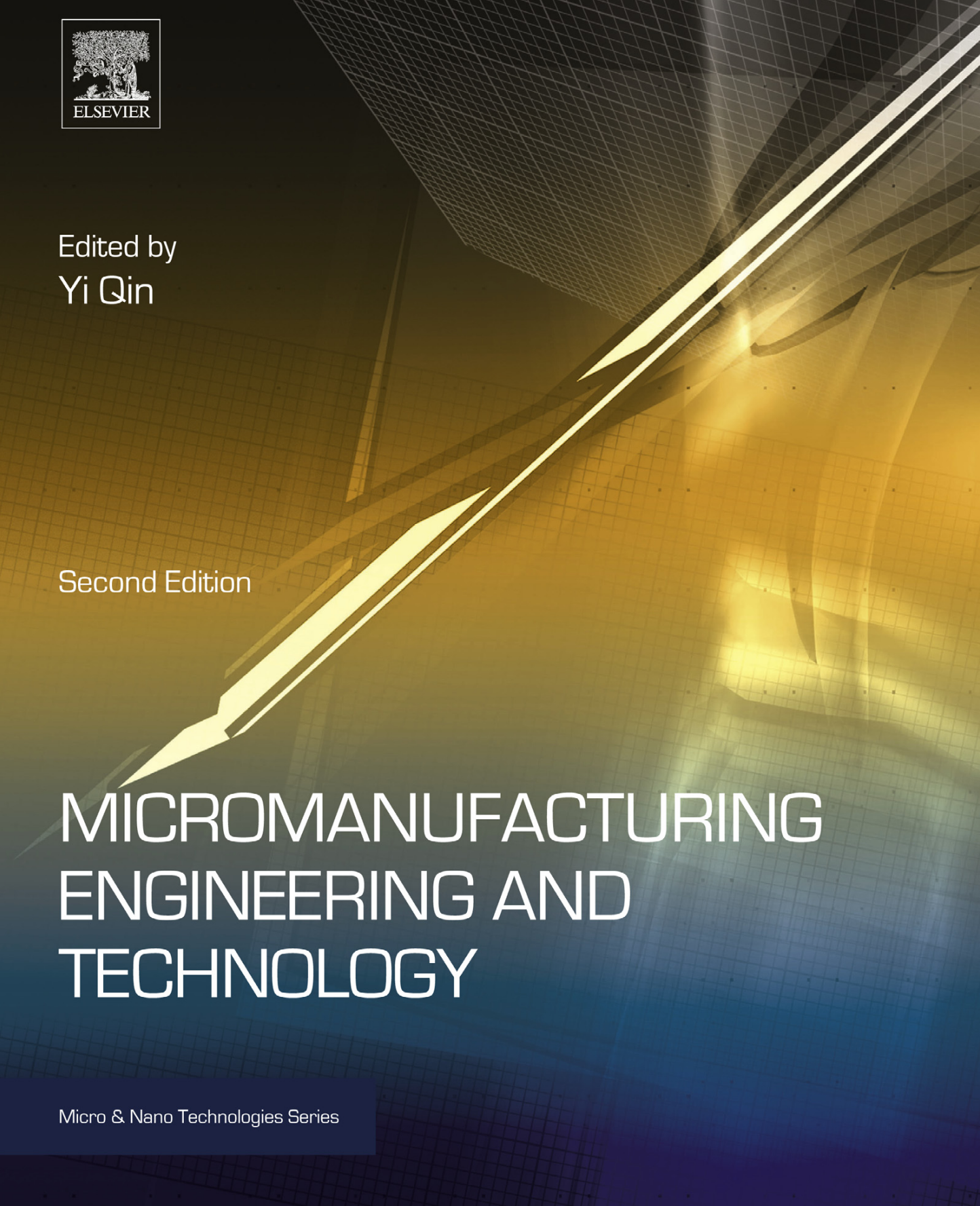
ELSEVIER
Edited by
Yi Qin
Second Edition
MICROMANUFACTURING ENGINEERING AND TECHNOLOGY
Micro & Nano Technologies Series

Micromanufacturing Engineering and Technology

This page intentionally left blank

Micromanufacturing Engineering and Technology

Second Edition

Yi Qin

ELSEVIER

AMSTERDAM • BOSTON • HEIDELBERG • LONDON
NEW YORK • OXFORD • PARIS • SAN DIEGO
SAN FRANCISCO • SINGAPORE • SYDNEY • TOKYO

William Andrew is an imprint of Elsevier

William Andrew is an imprint of Elsevier
The Boulevard, Langford Lane, Kidlington, Oxford, OX5 1GB, UK
225 Wyman Street, Waltham, MA 02451, USA

Notices
Knowledge and best practice in this field are constantly changing. As new research and experience broaden our understanding, changes in research methods, professional practices, or medical treatment may become necessary.

Practitioners and researchers must always rely on their own experience and knowledge in evaluating and using any information, methods, compounds, or experiments described herein. In using such information or methods they should be mindful of their own safety and the safety of others, including parties for whom they have a professional responsibility.

To the fullest extent of the law, neither the Publisher nor the authors, contributors, or editors, assume any liability for any injury and/or damage to persons or property as a matter of products liability, negligence or otherwise, or from any use or operation of any methods, products, instructions, or ideas contained in the material herein.

British Library Cataloguing-in-Publication Data
A catalogue record for this book is available from the British Library

Library of Congress Cataloging-in-Publication Data
A catalog record for this book is available from the Library of Congress

ISBN: 978-0-323-31149-6

Publisher: Matthew Deans
Acquisition Editor: Simon Holt
Editorial Project Manager: Peter Gane
Production Project Manager: Susan Li
Designer: Greg Harris

Typeset by TNQ Books and Journals
www.tnq.co.in

Printed and bound in the United Kingdom

Contents

This page intentionally left blank

Contributors

Gerald Anyasodor
University of Strathclyde, UK

Mogens Arentoft
IPU Technology Development, Kgs. Lyngby, Denmark

Giuliano Bissacco
Department of Mechanical Engineering, Technical University of Denmark, Kgs. Lyngby, Denmark

Matthias Burgard
Fraunhofer Institute for Manufacturing Engineering and Automation IPA, Stuttgart, Germany

Ivan Calderon
Sysmelec, Switzerland

Jian Cao
Department of Mechanical Engineering, Imperial College London, London, UK

Kai Cheng
Advanced Manufacturing & Enterprise Engineering, Brunel University, Uxbridge, UK

Ioannis S. Chronakis
Technical University of Denmark, DTU-Food, Søltofts Plads, Lyngby, Denmark

Mauro Comoglio
Diad Group, Italy

Sergio Durante
Diad Group ES, Spain

Rasmus Solmer Eriksen
IPU Technology Development, Kgs. Lyngby, Denmark

Bertrand Fillon
CEA/LITEN, Rue des Martyrs, Grenoble Cedex 9, France

Gonzalo G. Fuentes
Asociación de la Industria Navarra, Carretera Pamplona, Cordovilla, Spain

Arnold Gillner
Fraunhofer Institute for Laser Technology ILT, Aachen, Germany

Patrick Gretzki
Fraunhofer Institute for Laser Technology ILT, Aachen, Germany

Bin Guo
School of Materials Science and Engineering, Harbin Institute of Technology, Harbin, China

Hans Nørgaard Hansen
Department of Mechanical Engineering, Technical University of Denmark, Kgs. Lyngby, Denmark

Klaus S. Hansen
IPU Technology Development, Kgs. Lyngby, Denmark

Christoph Hartl
Faculty of Automotive Systems Engineering and Production Engineering, Cologne University of Applied Sciences, Cologne, Germany

Hany Hassanin
School of Mechanical Engineering, The University of Birmingham, Birmingham, West Midlands, UK

Riku Heikkilä
Department of Mechanical Engineering and Industrial Systems, Tampere University of Technology, Tampere, Finland.

Dr Jens Holtkamp
Fraunhofer Institute for Laser Technology ILT, Aachen, Germany

Kunlan Huang
School of Manufacturing Science and Engineering, Sichuan University, Chengdu, Sichuan, P.R. China; Centre for Precision Manufacturing, Department of DMEM, University of Strathclyde, Glasgow, UK

Atanas Ivanov
Brunel University London, Uxbridge, Middlesex, UK

Eeva Järvenpää
Department of Mechanical Engineering and Industrial Systems, Tampere University of Technology, Tampere, Finland.

Kyle Jiang
School of Mechanical Engineering, The University of Birmingham, Birmingham, West Midlands, UK

Seung Hwan Ko
Applied Nano and Thermal Science (ANTS) Lab, Department of Mechanical Engineering, Seoul National University, Gwanak-gu, Seoul, Korea (R.O.K)

Konstantin Konrad
Fraunhofer Institute for Manufacturing Engineering and Automation, Germany

Malte Langmack
TU Berlin

Pietro Larizza
MASMEC SpA, Bari-ITALY

Rebecca Leese
Brunel University London, Uxbridge, Middlesex, UK

Jianguo Lin
Department of Mechanical Engineering, Imperial College London, London, UK

Xichun Luo
Department of Design, Manufacture and Engineering Management, University of Strathclyde, Glasgow, UK

Matthias Meier
Robert Bosch GmbH, Stuttgart, Germany

P. Meyer
Institute of Microstructure Technology, Karlsruhe Institute of Technology, Eggenstein-Leopoldshafen, Germany

Johann Michler
Laboratory for Mechanics of Materials and Nanostructures, EMPA, Swiss Federal Laboratories for Materials Testing and Research, Thun, Switzerland

Alexander Olowinsky
Fraunhofer Institute for Laser Technology ILT, Aachen, Germany

Fredrik Östlund
Laboratory for Mechanics of Materials and Nanostructures, EMPA, Swiss Federal Laboratories for Materials Testing and Research, Thun, Switzerland

Laetitia Philippe
Laboratory for Mechanics of Materials and Nanostructures, EMPA, Swiss Federal Laboratories for Materials Testing and Research, Thun, Switzerland

Timo Prusi
Department of Mechanical Engineering and Industrial Systems, Tampere University of Technology, Tampere, Finland.

Yi Qin
Centre for Precision Manufacturing, Department of DMEM, University of Strathclyde, Glasgow, UK

Nitul S. Rajput
Department of Design, Manufacture and Engineering Management, University of Strathclyde, Glasgow, UK

Ursula Rauschecker
Fraunhofer Institute for Manufacturing Engineering and Automation IPA, Stuttgart, Germany

Nicola Ridgway
Teks, France

Markus Röhner
Fraunhofer IPK

Karolina Rzepiejewska-Malyska
Laboratory for Mechanics of Materials and Nanostructures, EMPA, Swiss Federal Laboratories for Materials Testing and Research, Thun, Switzerland

Antonio J. Sánchez
Universitat Politècnica de València, Valencia, Spain

Tassilo-M. Schimmelpfennig
Fraunhofer IPK

Felix Schmitt
Fraunhofer Institute for Laser Technology ILT, Aachen, Germany

J. Schulz
Institute of Microstructure Technology, Karlsruhe Institute of Technology, Eggenstein-Leopoldshafen, Germany

Patrick Schwaller
Laboratory for Mechanics of Materials and Nanostructures, EMPA, Swiss Federal Laboratories for Materials Testing and Research, Thun, Switzerland

Debin Shan
School of Materials Science and Engineering, Harbin Institute of Technology, Harbin, China

Niko Siltala
Department of Mechanical Engineering and Industrial Systems, Tampere University of Technology, Tampere, Finland.

Alexandre Spieser
Brunel University London, Uxbridge, Middlesex, UK

David Stifter
Center for Surface and Nanoanalytics (ZONA), Johannes Kepler University Linz, Linz, Austria

Xizhi Sun
Advanced Manufacturing & Enterprise Engineering, Brunel University, Uxbridge, UK

Peter T. Tang
IPU Technology Development, Kgs. Lyngby, Denmark

Rafa López Tarazón
Robotnik Automation SLL

Guido Tosello
Department of Mechanical Engineering, Technical University of Denmark, Kgs. Lyngby, Denmark

Reijo Tuokko
Department of Mechanical Engineering and Industrial Systems, Tampere University of Technology, Tampere, Finland.

Eckart Uhlmann
TU Berlin; Fraunhofer IPK

Wan-Nawang W.A.
Centre for Precision Manufacturing, The University of Strathclyde, Glasgow, UK

Chunju Wang
School of Materials Science and Engineering, Harbin Institute of Technology, Harbin, China

Shiwen Wang
Department of Mechanical Engineering, Imperial College London, London, UK

Matthias Worgull
Karlsruhe Institute of Technology, Institute of Microstructure Technology, Eggenstein-Leopoldshafen, Germany

Yi Yang
School of Manufacturing Science and Engineering, Sichuan University, Chengdu, Sichuan, P.R. China

Gang Yang
School of Manufacturing Science and Engineering, Sichuan University, Chengdu, Sichuan, P.R. China

Deqiang Yin
School of Manufacturing Science and Engineering, Sichuan University, Chengdu, Sichuan, P.R. China

Jie Zhao
Centre for Precision Manufacturing, The University of Strathclyde, Glasgow, UK

Yu Zhou
School of Manufacturing Science and Engineering, Sichuan University, Chengdu, Sichuan, P.R. China

Weimin Zhuang
College of Automotive Engineering, Jilin University, Changchun, Jilin, PR China

This page intentionally left blank

Author Biographies

Professor Yi Qin (FIMechE, FIoN, FHeA, CEng, PhD) is chair/professor in Manufacturing Technology and Systems and director of the Center for Precision Engineering and Micro-Manufacturing (CePMM) at the University of Strathclyde, UK. His research interests include micro/nano-manufacturing, precision forging/forming, manufacturing system technology, and numerical simulation. He has managed a series of funded RTD projects, including overall management of EU FP6 IP MASMICRO ("Integration of manufacturing systems for mass-manufacture of miniature/micro-products") as the project coordinator, project technical coordinator of EU FP7 POLYTUBES and Micro-FAST project. He is editor-in-chief of the Journal of Manufacturing Review, a member of the editorial board of IJMTM and advisor to the International Commercial Magazine on Micro-Manufacturing. Prof. Qin has published over 180 technical papers and given keynote speeches and invited presentations at more than 30 conferences and workshops worldwide.

E-mail: qin.yi@strath.ac.uk.

Professor Kai Cheng holds the chair professorship in manufacturing systems at Brunel University. Professor Cheng's current research interests focus on micro-/nano-manufacturing, design of high precision machines, smart machining, and sustainable manufacturing and systems. His research team is currently working on a number of research projects funded by the EU 7th Framework Programs, Technology Strategy Board (TSB), EPSRC, KTP Programs and the industry. Professor Cheng and his team have enjoyed working closely with manufacturing companies in the UK, Europe, the USA, and Far East. Over the last eight years, Professor Cheng and his team has built up one of the international centers of excellence in high precision and micro-/nano-manufacturing at Brunel, as evidenced by the team's research outcomes and academic track records. He is a fellow of the IET and IMechE and also the European editor of the International Journal of Advanced manufacturing Technology and a member of the editorial board of International Journal of Machine Tools and Manufacture.

E-mail: Kai.Cheng@brunel.ac.uk.

Dr Xizhi Sun received her BSc and MSc degrees in mechanical engineering from Harbin Institute of Technology, China, in 2001 and 2003, respectively. She obtained her PhD in Precision and Micro-Machining in 2009 at Brunel University. Her current research interests include modeling and simulation of micro-manufacturing processes and design of precision machine tools. She has published more than 15 technical papers in these fields.

E-mail: xizhi.sun@brunel.ac.uk.

Dr Nitul Rajput received his PhD degree in 2013 from the Department of Physics, Indian Institute of Technology, Kanpur, India. Subsequently, he has joined the

DMEM department, University of Strathclyde to carry out post-doctoral research in micro-/nano-engineering using FIB tool. His primary research interest is on investigation of ion−matter interaction processes at the nanoscale and their applications in the design of next generation micro-/nano-devices.

E-mail: nitul.rajput@strath.ac.uk.

Dr Xichun Luo is a professor in ultra precision manufacturing at the University of Strathclyde (Glasgow). He obtained his PhD in ultra precision manufacturing at Harbin Institute of Technology (China) in 2002 and second PhD in precision engineering at Leeds Metropolitan University (UK) in 2004. Before Strathclyde, he worked as a research officer, lecturer, and reader at Cranfield University, Heriot-Watt University and University of Huddersfield, respectively. His primary research interests include ultra precision machining process and facility development, micro-machining, and nano-fabrication.

E-mail: xichun.luo@strath.ac.uk.

Professor Eckart Uhlmann worked as a scientific engineer and chief engineer in IWF (1986−1994), and assumed various management responsibilities at Hermes Schleifmittel GmbH & Co., Hamburg (1994−1997), including responsibility as the vice president of the company (1995). Professor Uhlmann became the director of the Fraunhofer Institute IPK and director of the Chair of Machine Tools and Manufacturing Technology at the IWF of the Technical University Berlin in the Production Technology Center, Berlin (1997).

E-mail: Eckart.Uhlmann@ipk.fraunhofer.de.

Mr Markus Röhner studied mechanical engineering at the Technical University Dresden and then worked as a scientific engineer and deputy leader of the group Micro-Production Technology, Institute for Machine Tools and Factory Management (IWF), Technical University Berlin (2005−2008). Since October 2008 Markus has been working as a research engineer at the Fraunhofer Institute IPK where he is responsible for technology and strategic consultancy with various industrial partners.

E-mail: Markus.Roehner@ipk.fraunhofer.de.

Mr Malte Langmack studied Mechanical Engineering with focus on micro and precision engineering at the Technical University Berlin, Germany. Since 2007 he has been working as a research engineer in the field of micro-electrical discharge machining at the Centre of Micro Production Technology of the Fraunhofer IPK.

E-mail: Malte.Langmack-projekt@ipk.fraunhofer.de.

Dr Arnold Gillner studied physics at the University of Darmstadt and obtained his PhD in mechanical engineering at the RWTH AACHEN in 1994. Since 1985 he has worked as a scientist at the Fraunhofer-Institute for Laser Technology (ILT). Starting

in 1992, he developed the Department for Micro-Technology at the ILT, which has since become a leading department. Together with more than 20 scientists he is developing industrial laser processes for micro-joining and packaging, micro- and nano-structuring, polymer applications, and life science applications.

E-mail: arnold.gillner@ilt.fraunhofer.de.

Mr Patrick Gretzki studied Physics at RWTH Aachen University. After finishing his diploma thesis in the department for process sensoring at Fraunhofer ILT he moved to another group the department for micro- and nano-structuring, where he now works on development of new laser processes for the industry. He started to integrate and develop new technique regarding diffractive beam shaping using spatial light modulator to increase the throughput in ultra-short pulse material ablation and to improve the process quality.

E-mail: patrick.gretzki@ilt.fraunhofer.de.

Dr Atanas Ivanov is senior lecturer and course director of Advanced Engineering Design at Brunel University. Main interest of Atanas is development of nontraditional manufacturing technologies, and he has special inters in development micro-manufacturing technologies and techniques. He developed within FP6 the first hybrid micro-EDM micro-ECM machine. Within FP7 he developed first micro-ECM machine for German automotive sector. Atanas has many years experience in developing manufacturing technologies and providing consultancy to many companies. He teaches sustainable design and manufacturing, design experience, process capability, tolerancing, and process planning.

E-mail: Atanas.Ivanov@brunel.ac.uk.

Alexandre SPIESER graduated with a MEng in electronics and electrical engineering in France (ESIEE-Amiens) and also has an MSc in advanced manufacturing systems. He is currently a researcher at Brunel University, where he also teaches electromechanical interfaces and industrial systems to MSc students. His work experience mainly involves the development of control systems and power electronics design. His research interests are power electronics, embedded systems, automation and nonconventional machining processes such as electrochemical micromachining. He took part in the development of the first micro-ECM machine for the German automotive industry.

Rebecca Leese completed a Masters of Chemistry (MChem) and at present is researcher at Brunel University. Rebecca worked on a project for measurement of pH with National Physical Laboratory (NPL) in Teddington. The research conducted at NPL won the “best paper” award from CITAC. Rebecca joined Brunel after graduating from the University of Southampton to begin her PhD focusing on the chemical details of micro-electrochemical machining. Her research interests are in the electrochemistry and its applicability for the manufacturing processes.

Dr Matthias Worgull currently works at the Institute for Microstructure Technology at Forschungszentrum Karlsruhe (Karlsruhe Institute of Technology), Germany. His degree from the University of Karlsruhe was in Mechanical Engineering. He has been the leader of the Nanoreplication Group at the Institute since 2005 and the leader of the replication division since 2008.

E-mail: matthias.worgull@imt.fzk.de.

Ms Jie Zhao obtained her first degree in electronic and information engineering in China and an MSc in mechatronics and automation engineering at the University of Strathclyde, in 2006. In 2007, she started research in micro-manufacturing as a full time researcher. Her work has been a mix of mechatronics, machine/tool development, experimentation for micro-manufacturing, as well as project management. Currently, she is working toward a PhD in micro-manufacturing.

E-mail: j.zhao@strath.ac.uk.

Dr Gerald Anyasodor obtained his PhD and is working as a post-doctoral research fellow at the University of Strathclyde. His expertise is in tool/machine design and control development for metal and polymer forming as well as in micro-manufacturing, FE-analysis, laser technology, and project management. He is currently working on the heating, cooling, and handling system in the development project for the hot stamping of AL-Alloys at the University of Strathclyde. Before joining the University of Strathclyde, he had worked as a project engineer and research assistant in Africa and Germany, respectively for over 10 years.

E-mail: gerald.anyasodor@strath.ac.uk.

Prof. and Dr Christoph Hartl has been professor at the Cologne University of Applied Sciences since 2002. He worked as a general manager responsible for the Hydroforming R&D Center of a German press manufacturer. He is also the managing director of the Institute of Production Technology and Production Organisation, GmbH and President of the Society for Technical and Scientific Education e.V. in Cologne. His current research is focused on micro-hydroforming technology, laser processing, and process simulation.

E-mail: christoph.hartl@fh-koeln.de.

Klaus Schütt Hansen graduated in 2008 as mechanical engineer from the Technical University of Denmark. Since then, he has been working at IPU Technology Development providing expertise on thermal processes with focus on laser processes. In addition, he has worked on the development of equipment for laser processes. In 2011, he began working on an industrial PhD entitled: "Multi-fiber laser beam welding" in cooperation with the Department of Mechanical and Manufacturing Engineering at Aalborg University. The purpose of this is to establish methods for the optimization of beam patterns during laser welding. He has worked as work-package coordinator contributing on behalf of IPU to the FP7 project "Polytubes," where he developed the concept and a machine for the cross-rolling of micro-plastic tubes.

In addition to expertise in thermal processes and laser processes, he has a broad interest in mechanics and electronics.

E-mail: ksh@ipu.dk.

Mogens Arentoft, Head of IPU Technology Development, has wide contacts over most of IPU's technical areas. For more than 20 years he has worked with innovation, focusing on process technology. It is also in this area that he obtained his MSc. and PhD degrees and he frequently publishes scientific articles. As chairman of the Danish Cold Forging Group (DKFG), the Danish Metallurgical Association, ESAFORM and Danish Sheet Metal Forming Group; board member of ATV-Semapp; member of "International Cold Forging Group" and "CIRP"; he has established a large network within material and process technology, which he maintains by participating in international research projects and conferences. Mogens is in close contact with researchers at the Technical University of Denmark and holds a position as external lecturer to ensure that he is always updated on the latest research to the benefit for the customers of IPU.

E-mail: ma@ipu.dk.

Ivan Calderon obtained a master's degree in micro-engineering in 1997 followed by a biomedical engineering post grade. He continuously broadens his engineering and management expertise in the automation field: industrial machinery, semiconductor industry, instrumentation, automotive, high precision applications, laser materials processing, biomedical products, and life science applications. More precisely, he fosters competences on risk deconstruction and assessment, complex processes/projects analysis and management, development of industrial validation methods and tools. He held engineering positions at Torit Donaldson, Babcok & Wilcox, Valeo, Etel SA and Sysmelec SA and senior technology project manager at Unitechnologies AG.

Konstantin Konrad received a master's degree in cybernetics engineering 2007 and was awarded a doctorate (magna cum laude) for the research of semantically supported ramp-up of assembly systems in 2013. He is a project manager and senior scientist at the Fraunhofer Institute for Manufacturing Engineering and Automation IPA in Stuttgart, Germany and has been working in the field of manufacturing IT, factory logistics, and systems integration for many years. He has sound expertise in the design, analysis, and optimization of flexible production and IT system. Since 2009 he is also actively involved in the definition of Roadmaps and Strategic Research Agendas for the European Community.

Dr Ioannis S. Chronakis, associate professor at Denmark Technology University, and previously an associate professor and research project manager with Swerea IVF, Sweden, takes a lead in the research for the development and applications of micro-/nano-structured materials and their processing technologies. He received his PhD in physical chemistry in Cranfield University, worked respectively in

Lund University (Sweden) and INRA (France), published over 60 research papers and book chapters and holds three patents in micro-nanotechnology.

E-mail: ioach@food.dtu.dk.

Dr Guido Tosello is associate professor on polymer micro-/nano-processing at the Department of Mechanical Engineering of the Technical University of Denmark. He received his PhD titled "Precision Moulding of Polymer Micro Components" in 2008 and has 10 years of experience of research on precision engineering, micro-technology, polymer micro-processing, micro-/nano-manufacturing metrology. He is member of the NanoMicro Moulding Special Interest Group of SPE (Society of Plastic Engineers), member of Euspen (European Society for Precision Engineering and Nanotechnology), and associate member of CIRP (The International Academy for Production Engineering). He is author and coauthor of more than 90 peer-reviewed international publications including journal articles, conference papers, and book chapters in the field of micro-/nano-precision manufacturing. He is currently leading research in European and national projects in the fields of micro-product design, injection molding at micro-/nano-scale, process optimization, simulation, and quality control.

E-mail: guto@mek.dtu.dk.

Dr Hany Hassanin has been a research fellow within the Advanced Materials and Processing Laboratory (AMPLab) in the School of Metallurgy and Materials, University of Birmingham, since 2012. Hany received his PhD at the University of Birmingham in 2010. Before joining the AMPLab, he worked on an industrial project entitled "Net Shape Manufacturing of Ceramic Micro Gas Turbine" in the School of Mechanical Engineering's Micro-engineering and Nano-technology Research Centre since 2010. His current research project is "Rapid Manufacturing as a Key Enabler for Enhanced Monopropellant Ceramic Catalyst Bed" funded by The European Space Agency (ESA). He also has successfully carried out several manufacturing techniques in other projects. Hany has more than 30 of the publications including journal and conference papers, one book, two book chapters, and three patent applications.

E-mail: h.s.s.hassanin@bham.ac.uk.

Kyle Jiang is professor of nanotechnology and director of Biomedical Engineering and Micro/Nanotechnology Research Centre. Kyle Jiang received his PhD in mechatronics at King's College London in 1994. He has been with the University of Birmingham as a member of academics since 1999. Prior to his current appointment, he was a research assistant at King's College London. In 1998, he joined the University of Liverpool as a lecturer. His current research interest is in nanotechnology for energy and bio-medical applications. He has authored about 200 publications in books, scientific journals, and refereed international conferences. He is the inventor of five patents. His research in micro-engine has received wide public media reports.

Kyle is regularly involved in organizing international conferences and gives keynote speeches. He reviews papers for a wide range of journals.

E-mail: k.jiang@bham.ac.uk.

Prof Yi Yang received the BS degree in casting technology from the Department of Mechanical Engineering, Wuhan Institute of Technology, Hubei, China, in 1982, the MS degree in casting technology from the Department of Metal Materials, Shenyang Polytechnic University, Liaoning, China, in 1986, and the PhD degree in material forming engineering from Sichuan University, Chengdu, China, in 2004. He is currently a professor and the vice dean of the School of Manufacturing Science and Engineering, Sichuan University. He has published more than 160 journal papers and is in charge of more than 20 projects funded by the Chinese Central Government, Sichuan Provincial Government, and some industrial companies. His research interests include casting technology, powder metallurgy, and micro-fabrication technology.

E-mail: yangyi@scu.edu.cn.

Ms Kunlan Huang received her BSc degree in material forming and control engineering from Sichuan University, China, in 2010. From 2013, she is working toward a PhD in micro-forming under the joint-program of Sichuan University and University of Strathclyde (Glasgow, Scotland, UK). Her current research works include experimentation for Micro-FAST, modeling, and simulation of sintering process of Micro-FAST.

E-mail: huangkunlan0311@163.com.

Prof Gang Yang received the BSc degree in foundry technology from the Department of Metal Materials, Chengdu University of Science and Technology, Chengdu, China, in 1988, the MS degree in metal materials and heat treatment from the Department of Metal Materials, Sichuan Union University, Chengdu, in 1995, and the PhD degree in metal materials from Sichuan University, Chengdu, in 2006. He is currently an associate professor of the School of Manufacturing Science and Engineering, Sichuan University. He has been undertaking research work in the field of material forming, powder metallurgy, and micro-fabrication technology since 1990. He has published more than 50 journal papers and has participated in more than 20 research projects.

E-mail: yanggang@scu.edu.cn.

Dr Deqiang Yin received his BSc degree in mechanical engineering from Chongqing University, China, in 2006. He obtained his PhD in solid mechanics in 2012 under the joint program of Chongqing University and University of Strathclyde (Glasgow, Scotland, UK). His current research interests include modeling and simulation of nano-multilayered coatings and micro-field-activated sintered technology, including investigating the hardening and densification mechanism from

the atomic scale and macro/micro/nano-multi scale. In addition, he is a lecture at Sichuan University, China.

E-mail: deqiang.yin@scu.edu.cn.

Mr Yu Zhou obtained his first degree in material forming and control engineering at JiangHan University, China, in 2011. In 2011 he started research in material forming, powder metallurgy, and micro-fabrication as a postgraduate at Sichuan University. Currently, he is working toward a PhD in machine design manufacturing and automation.

E-mail: logr@foxmail.com.

Mr Rasmus Eriksen, a trained technician, has worked with industrial production machines for several years. He received MSc in 2005 in electrical engineering at Technical University of Denmark, Denmark, then worked for 1 year at IPU as engineer consultant in the division of technology development. In 2006 Rasmus joined the group of micro/nano-manufacturing at Technical University of Denmark. His research is focused on tool design for bulk-forming of micro-components and was a part of the research team designing a fully functional prototype machine for micro-bulk-forming with the EU MASMICRO project.

E-mail: rser@mek.dtu.dk.

Mr W.A. Wan Nawang is currently doing his PhD research in sheet metal micro-forming at the University of Strathclyde, UK. His work focused on stochastic characteristics in micro-sheet metal and developing methods to improve the quality of micro-forming process. He is also a lecturer at University of Kuala Lumpur, Malaysia teaching manufacturing subjects as well as having industrial experiences in various manufacturing industries. He holds his first degree in manufacturing systems engineering, MEng in aeronautics and Astronautics and a holder of FAA Airframe and Powerplant Certificate before pursuing his PhD.

E-mail: wan.wan-nawang@strath.ac.uk.

Ms Jie Zhao obtained her first degree in electronic and information engineering in China and an MSc in mechatronics and automation engineering at the University of Strathclyde, in 2006. In 2007, she started research in micro-manufacturing as a full-time researcher. Her work has been a mix of mechatronics, machine/tool development, experimentation for micro-manufacturing, as well as project management. Currently, she is working toward a PhD in micro-manufacturing.

E-mail: j.zhao@strath.ac.uk.

Dr Jens Holtkamp studied mechanical engineering at the Aachen University of Technology (RWTH). Since 2004 he has been a research engineer at the Fraunhofer Institute for Laser Technology (ILT), Aachen, with the Department of

Micro-Technology. He is currently the group leader of the 'Micro Structuring' group at ILT and his main field of the research is laser-assisted forming processes.

Email: jens.holtkamp@ilt.fraunhofer.de.

Dr Bertrand Fillon is the CTO of CEA/LITEN for new energy technologies, organic electronic and nanomaterials, France, and the scientific president of the French Polymer Cluster "Plastipolis." He has been the initiator of the polymer platform involving the different CEA research teams and Swiss laboratories CSEM. Between 1990 and 2003, he worked with Pechiney Packaging as a coordinator of their Global Packaging R&D activities and the leader of the Pechiney polymer expert group.

E-mail: bertrand.fillon@cea.fr.

Dr Seung Hwan Ko received the BS (2000) from Yonsei University, MS (2002) from Seoul National University, and PhD (2006) in mechanical engineering from UC Berkeley. Currently he is an associate professor, Department of Mechanical Engineering, Seoul National University. His Current interests include digital low temperature direct printing process development, flexible and stretchable electronics fabrication process development, laser micro-/nano-fabrication, hierarchical nano-structuring for high efficiency energy devices.

E-mail: maxko@snu.ac.kr.

Dr Hans Nørgaard Hansen, professor of micro manufacturing, Technical University of Denmark, is heading the research group on Micro/Nano Manufacturing as well as the Manufacturing Engineering Section of the department. His research is focused on industrial production of products and components in metals, polymers, and ceramics with critical dimensions in the micrometer range (product and material development, development of processes, process chains and production systems for micro-mechanical systems).

E-mail: hnha@mek.dtu.dk.

Dr Peter T. Tang holds an MSc in chemical engineering and a PhD in electrochemical engineering and micro-technology. He has worked for more than 15 years on electroplating and electrochemistry, and is a project leader of several national and EU research projects as well as contracted industrial projects. Peter has worked on pulse plating of nickel, copper, silver, zinc and various alloys, lately, mainly within the field of micro-technology. He is the author of more than 65 scientific papers and holds seven patents in the field of electrochemistry, electroforming, pulse plating, and selective metallization.

E-mail: tt@ipu.dk.

Dr Giuliano Bissacco, assistant professor of manufacturing engineering at the University of Padova, was research assistant (2001−2004) and assistant professor

(2005−2007) at Technical University of Denmark, Denmark. Giuliano's research activities include design and manufacture of micro-mechanical components in metals, polymers and ceramics; development and optimization of micro-manufacturing processes for production of micro-components characterized with complex 3D geometry; development of innovative process-chains for manufacture of micro-components, tooling processes and machine tools.

E-mail: giuliano.bissacco@unipd.it.

Dr Gonzalo G Fuentes, got his PhD in material science and thin films from the Autonomous University of Madrid, and researched in hetero-nanotubes and macro-molecular systems in Germany. Since 2003 he is responsible for the international projects at the Center of Advanced Surface Engineering (with AIN), Spain. He participated in seven EU funded research projects and coordinated several national and regional projects. He has published over 50 scientific articles in the peer-reviewed journals.

E-mail: gfuentes@ain.es.

Dr Chunju Wang, MSc in Material Processing Engineering, PhD in Mechatronics Engineering, works as an associate professor at the School of Materials Science and Engineering of Harbin Institute of Technology. His research interests are micro-forming processes with metallic materials including micro-bulk forming and micro-sheet forming, and development of micro-forming apparatus. These days, his investigations are mainly focused on micro deep drawing with DLC-coated tools and ultrasonically-assisted micro-blanking.

E-mail: cjwang1978@hit.edu.cn.

Prof. Debin Shan, vice-head of the National Key Laboratory for Precision Hot Processing of Metals at Harbin Institute of Technology, managed a series of the funded projects and published over 120 technical papers. His current research interests include micro-forming, spinning, and isothermal forging technologies.

E-mail: shandb@hit.edu.cn.

Prof. Bin Guo, vice president of Harbin Institute of Technology, has published over 100 peer reviewed papers and three books. He is the director of China Society of Micro-Nano Technology, and has an excellent track record in attracting research funding from NSFC, etc. Currently, he also heads a research group of 10 researchers working on various metal forming processes.

E-mail: bguo@hit.edu.cn.

Dr Eeva Järvenpää obtained her MSc degree in mechanical engineering in 2007 and PhD degree in production engineering in 2012 from Tampere University of Technology (TUT). Currently she is a post-doctoral researcher at the Department of Mechanical Engineering and Industrial Systems at TUT. Since 2006 she has

been working in several international and national research projects relating to manufacturing process and system design, micro and desktop factories, information modeling, and digital manufacturing. Her current research interest lies around production planning and scheduling systems, production system adaptation, co-evolution of products, processes and systems and information modeling relating to these domains. She has published more than 20 scientific articles in refereed conference proceedings, journals, and compilations.

E-mail: eeva.jarvenpaa@tut.fi.

Mr Niko Siltala (MSc) is a researcher at Tampere University of Technology, Department of Mechanical Engineering and Industrial Systems. Siltala has 16 years experience in discrete manufacturing, robotics and manufacturing automation, and more than 6 years in micro and desktop manufacturing. He possesses expertise on control and communication systems, which culminates in this field to control the parallel kinematic structures. He has involved on making two international standards applicable on the field, and several open specifications like standards. He is the author of over 30 technical and scientific publications.

Mr Timo Prusi (MSc) is a researcher and university teacher at Tampere University of Technology, Department of Mechanical Engineering and Industrial Systems. He has been working in the micro-factory research group since 2002. He has been responsible for developing the machine vision solutions used in TUT-Microfactory concept demonstrations and he is also involved in teaching machine vision, production automation, and desktop manufacturing for undergraduate students. He is an author of 19 technical or scientific publications and he has organized several training sessions dealing with machine vision also in industry.

Reijo Tuokko, Professor Emeritus, Tampere University of Technology, has 40 years experience in discrete manufacturing, robotics and manufacturing automation, and more than 10 years in micro and desktop manufacturing, including 12 years in responsible positions in manufacturing industry in machine tool and factory automation business, 4 years as an associate professor and 24 years as a full professor. He is the author of over 300 technical and scientific publications, and a worldwide recognized expert and scientist in micro and desktop manufacturing and frequently invited keynote speaker in different international manufacturing-related events around the world. He has coordinated two large national programs in manufacturing, and has strong experience in European and other international research collaboration.

E-mail: reijo.tuokko@tut.fi.

Matthias Burgard received his Dipl.-Ing. degree in micro-system technology from the University of Freiburg, Germany, in 1996. He is a project manager in the field of precision assembly and fluidic handling technologies for the micro-manufacturing at the Fraunhofer Institute for Manufacturing Engineering and Automation. He is managing national and European funded projects as well as industrial projects

with application-oriented focus. His research interests include manipulation and assembly of micro-components, e.g., micro-electromechanical systems (MEMS, and the handling and dispensing of fluid for micro-manufacturing in the field of e.g., life science, measurement devices and aerospace. A focus of his research is the use of fluids and their surface tensions for the manipulation of micro-components and the further development into application.

Mr Felix Schmitt studied mechanical engineering at the Aachen University of Technology (RWTH) and finished his study with a major in micro-production technology there. Since 2005, he has been working as a research engineer at the Fraunhofer Institute for Laser Technology (ILT) and in Aachen, with the Department of Micro-Technology. He is part of the group "Micro-Joining Technology." His main field of the research is laser-beam micro-welding and soldering.

E-mail: felix.schmitt@ilt.fraunhofer.de.

Dr Alexander Olowinsky studied mechanical engineering at the Aachen University of Technology (RWTH), and joined the Fraunhofer Institute for Laser Technology in 1996 as a project engineer in the Department of Microtechnology. He received his doctoral degree in 2002 in the field of laser beam micro-forming. Since 2001 he has headed the group "Micro-Joining Technology" with the activities in laser-based micro-joining processes such as welding, soldering, bonding, and polymer welding.

E-mail: alexander.olowinsky@ilt.fraunhofer.de.

Antonio-Jose Sanchez-Salmeron received the BEng and MSc degrees in computer science in 1992 and 1994, respectively, and the PhD degree in control engineering in 2001, all from the Universitat Politècnica de València (UPV), Valencia, Spain. He has been professor of automatic control with the UPV since 1995, where he is currently an associate professor with the Department of Systems Engineering and Control. He has been involved in more than 48 research and mobility projects funded by local industries, government, and the European community. His current research interests include robotics and computer vision, especially 3D computer vision and intelligent robot systems.

E-mail: asanchez@isa.upv.es.

Dr Rafael Lopez Tarazón owns a degree in Telecommunications Engineering (Communications Branch). He worked in the R&D department of Althea Productos Industriales, Spain, in 2000. In 2001 he was contracted by IBM as a system engineer for wide-area networks in Madrid and Barcelona. He was a founding member of Robotnik Automation SLL in 2002. Since then he holds the position of the R&D manager of the company.

E-mail: rlopez@robotnik.es.

Dr Pietro Larizza, in charge of the R&D Division of the Masmec Srl, Italy, is carrying industrial research devoted to the robotics, automation, measurement and

advanced production technologies. He is named as an Expert of the MIUR for the disciplines of electronics, electronics measurement and automatic controls. He has published various technical papers and holds several industrial patents on identification techniques and processing of medical images.

E-mail: piero.larizza@masmec.com.

Dr David Stifter studied solid state and semiconductor physics at the Johannes Kepler University (JKU) Linz, Austria, and worked at Profactor GmbH and then at UAR GmbH where he focused his research on optical coherence tomography (OCT) for metrology and nondestructive material charxacterization. He is now again with JKU as associate professor at the Center for Surface and Nanoanalytics (ZONA) and head of the Christian Doppler Laboratory for Microscopic and Spectroscopic Material Characterization (CDL-MS-MACH). Beside his activities in electron spectroscopy for surface analysis, he is currently working on full-field coherent imaging methods and advanced nonlinear optical techniques for the characterization of surfaces and thin films. He is reviewer for several international scientific journals and author/coauthor of more than 90 peer-reviewed articles.

E-mail: david.stifter@jku.at.

Mr Fredrik Östlund, has an MSc in engineering physics from Uppsala University, Sweden, and has been working in the field of compression tests of semiconductor micro-pillars at the Laboratory for Mechanics and Materials at the Swiss Federal Laboratories for Materials Testing and Research (EMPA) during last several years.

E-mail: Fredrik.Oestlund@empa.ch.

Dr Karolina Rzepiejewska-Malyska, got her MSc in Engineering at the Warsaw University of Technology in the field of Micromechanics, and she studied for her PhD focusing on the mechanical and tribological behaviors in the micro- and nano-scale of thin multilayered ceramic films for MEMS applications, in EMPA, Switzerland.

E-mail: Karolina.Rzepiejewska@empa.ch.

Dr Laetitia Philippe got her PhD and completed her postdoctoral research in the field of local electrochemical processes and influences of mechanical deformations on electroformed nanomaterial properties. She is currently the group leader in Nanostructuration by Electrochemical Methods, in EMPA, Switzerland. Her research deals with the fabrication of metallic, semiconductor and composite nanostructures (wires and dots), their nano-manipulation and mechanical characterizations.

E-mail: Laetitia.Philippe@empa.ch.

Dr Patrick Schwaller got his PhD at the University of Zurich in the field of angle-resolved photoelectron spectroscopy. Since 2001 he has been working at EMPA

(Switzerland) in the field of micro- and nano-mechanics with a focus on instrumented indentation techniques. In addition, he is also a lecturer at the Bern University of Applied Science.

E-mail: Patrick.Schwaller@empa.ch.

Dr Johann Michler got his PhD at the Swiss Federal Institute of Technology Lausanne (EPFL) in the field of thin film mechanics. He has been working at EMPA since 2000 and is currently heading the Laboratory for Mechanics of Materials and Nanostructures of EMPA. He has published over 100 scientific publications and is cofounder of two companies on scientific instrumentation.

E-mail: Johann.Michler@empa.ch.

Dr Shiwen Wang, AMIMechE, worked as a research fellow with Prof. Jianguo Lin at Birmingham University and Imperial College London. He is an expert on solid mechanics with strong expertise on the nonlinear constitutive modeling of polycrystalline materials using crystal plasticity finite element (CPFE) theory. Dr Wang is currently working as a senior consultant engineer for nuclear and energy industry. He has extensive experiences on creep, fracture, and fatigue analysis for components at elevated temperatures using several industrial codes, including British Energy R5 V2/3, ASME VIII, DNV, API and ISO-13,628.

E-mail: shiwen_wang@yahoo.co.uk.

Prof. Weimin Zhuang, PhD, is deputy head of Vehicle Body Engineering Department of Jilin University, PR China. Her expertise is on the area of vehicle body weight optimum through the mixture of materials and radical manufacture/assembly technology development. She is an expert on multiscale finite element modeling and structure optimization. She had taken part two EU Framework projects: MASMICRO and M3-2S. She is the principal investigator of several major projects, including the use of hot forming and cold quenching technique to optimum design the aluminum body parts weight based on multiscaled FE analysis. Her publications had been widely cited at EI and SCI publications.

E-mail: zhuangwm@jlu.edu.cn.

Dr Jian Cao, worked with Prof. Jianguo Lin for determination of materials modeling since 2002. He then worked as a research fellow at the University of Birmingham on EU FP6 Project (MASMACRO), cooperated with EMPA, Switzerland. Dr Cao has multidisciplinary background knowledge with degrees of BSc in accounting and Finances, MSc in computer science, and PhD in mechanical engineering at the University of Birmingham. Dr Cao founded RTC Innovation Ltd in 2009 and plays leading roles in technology transfer, technology-based spin-out. He currently sits on the board as directors of two companies: Oxford Multi Spectral Ltd and Oxford Vacmedix HK ltd.

E-mail: j.cao@rtcinnovation.com.

Prof. Jianguo Lin, PhD, MASME, FIMechE, FREng, is a professor in the mechanics of materials and head of mechanics of materials division in the Department of Mechanical Engineering at Imperial College London. He is a leading expert on the modeling of materials for use in the manufacturing industry and he has developed a method for predicting different types of metal failure mechanisms. Professor Lin's work has widespread applications such as the forming of lightweight complex panel shapes for automotive, aerospace and other transportation industries.

E-mail: Jianguo.Lin@imperial.ac.uk.

Dr Matthias Meier is project manager at Bosch Corporate Sector Research and Advance Engineering. Formerly, he worked as project manager and researcher at the Ultraclean Technology and Micromanufacturing department of the Fraunhofer Institute for Manufacturing Engineering and Automation (Fraunhofer IPA) in Stuttgart, Germany. His main area of research at Fraunhofer IPA targeted issues in the Production-IT environment. Mr Meier holds a Dr.-Ing. from the University of Stuttgart, Germany.

E-mail: meiermat@online.de.

Ms Ursula Rauschecker is a senior scientist and project manager at the Fraunhofer Institute for Manufacturing Engineering and Automation (Fraunhofer IPA). She holds a diploma in mechatronics and a master in logistics management and is active in the field of manufacturing IT for several years now. Among other activities, she has successfully contributed to numerous public and contract research projects in production IT with special regard to IT-based manufacturing systems and related requirements analysis, implementation and roll out.

E-mail: ursula.rauschecker@ipa.fraunhofer.de.

Dr Sergio Durante is currently the executive vice president of the DIAD Group. He was the project manager of Business Lines with FIAT Sector and responsible of public relation with Fiat Group companies. He was the President of the Advanced Manufacturing Club there. As the head of a Machining Team in FIAT, he gained valuable experience in advanced design of machine tools structure and the reengineering of the machining manufacturing processes. He was the Coordinator of six European projects, and a member of the Scientific Committees of the technical revue "Thermal Treatment and Coatings" and "Advanced Machine Tools."

Dr Mauro Comoglio is graduated in mechanical engineering at Politecnico of Torino and for several years has been responsible of advanced research projects on machining technologies in an automotive research center, where he was leader of the machining department and responsible of technology transfer to FIAT Group Companies. He has been involved in several European projects, where the most important European universities, industries, and research institutes are involved in. Today he is general manager of DIGRO, where he is also responsible for

innovation transfer in aeronautic and space sectors. Author of several publications, he is member of the scientific committees of several technical international conferences.

Dr Pascal Meyer, got his PhD in 1996 from the University of Franche-Comté (Neutron dosimetry with a solid state nuclear track detector: the CR-39). After two years as an assistant professor at the Franche-Comté University, he worked as a post-doctorial researcher at the Institute of Microstructure Technology of the Forschungszentrum Karlsruhe, since 1998. His interests include the commercialization of micro-products, particularly those made with the LIGA process and their production (repeatability, quality, reliability, customer satisfaction, etc.).

E-mail: Pascal.Meyer@imt.fzk.de.

Dr Joachim Sechulz, received his PhD in solid state physics, started the research as a post-doctorial researcher at the Institute of Microstructure Technology of the Forschungszentrum Karlsruhe in 1991, where he led a group in LIGA-Sensor-Technology and the technology department for several years. After concentrating on implementing an automated production line for LIGA-products (FELIG) he founded the company Microworks in 2007, which focuses on the production of high-precision parts using X-ray-LIGA technology.

E-mail: Joachim.Schulz@imt.fzk.de.

CHAPTER

Overview of Micro-manufacturing

1

Yi Qin
Centre for Precision Manufacturing, Department of DMEM, University of Strathclyde, Glasgow, UK

CHAPTER OUTLINE

INTRODUCTION

Manufacturing, in a general term referring to industry, is to make products that have been designed for certain application purposes. The meaning of "manufacture" has ever changed, especially during the last 20 years, in terms of what are being made, how they are made, how the manufacturing is organized, etc. Desire for better quality of life, good health, and high working efficiency has been one of the major drivers recently to the development of micro- and nano-technology products. As a consequence, issues concerning the length scales in manufacturing have been often mentioned and researched.

When manufacture is examined with reference to different length scales, such as nano-, micro-/meso-, or macro-scale, it is almost inevitable that people will realize that the methods, approaches, and techniques that could be used are quite different: from bottom-up approaches to top-down approaches, different manufacturing strategies can be clearly seen. When the first edition of this book was prepared in 2009, "micro-manufacturing" referred to the "manufacturing of micro-products with

Micromanufacturing Engineering and Technology. http://dx.doi.org/10.1016/B978-0-323-31149-6.00001-3

scaled-down manufacturing-processes, effected with miniature-manufacturing machines/systems, and with optimised process chains," which obviously gave an emphasis on "applying conventional manufacturing processes to the manufacture of miniature, micro or nano-products." Over recent years, what has been done and what is being carried out, however, has indicated that there may be the need to redefine the scope of micro-manufacturing as follows:

- Micro-precision manufacturing of macro-sized components
- Micro-/nano-feature manufacturing over large and small areas
- Manufacturing of micro-sized components
- Manufacturing with micro-/nano-structured materials
- Manufacturing with controlled micro-structures of materials

These may concern manufacturing methods, technologies, equipment, organizational strategies, and systems. Micro-manufacturing engineering is a general term, which concerns a series of relevant activities within the chain of manufacturing micro-products/features, including design, analysis, materials, processes, tools, machinery, operational management methods and systems, etc.

There is a huge diversity in micro-products, the main types of these including micro-electronics products, micro-optical electronics systems, micro-electronics mechanical systems (MEMS), and micro-optical electronics mechanical systems (MOEMS), depending on the combinations of product functionalities and/or working principles. Correspondingly, there are different methods and strategies, which could be used to manufacture these products. Micro-manufacturing, in a wider context, should cover all these of the aspects relating to the manufacturing of these products/features. The definition given to it, or its gravity/focus, often varies between different sources.

There has been an enormous amount of literature produced on the manufacture of MEMS and micro-systems in the past and also becoming available currently. The technologies relating to design and fabrication with these methods are sometimes referred to as either Micro-system technology or MEMS techniques. In order to differentiate the techniques from other manufacturing techniques, micro-manufacturing techniques are often categorized respectively as MEMS manufacturing and non-MEMS manufacturing, where MEMS manufacturing involves, largely, techniques such as photolithography, chemical etching, plating, lithography, electroplating, and moulding (LIGA), laser ablation, etc., while non-MEMS manufacturing often involves techniques such as electrical-discharge-machining (EDM), micro-mechanical cutting, laser cutting/patterning/drilling, micro-embossing, micro-injection molding, micro-extrusion, micro-stamping, etc. Regarding the materials to be dealt with, micro-manufacturing is also sometimes categorized as silicon-based manufacturing and nonsilicon material manufacturing. The purpose of differentiating these is sometimes to emphasize the importance of the latter as being in urgent need of development, whereas silicon-based manufacturing is often seen as a "mature" business, i.e., well developed and established.

This book is focused on the description of nonsilicon-based manufacturing, especially non-MEMS manufacturing techniques and systems, although there are

several chapters dealing with the techniques for both MEMS and non-MEMS manufacturing. This chapter intends to give an overview of micro-manufacturing, which may serve as an introduction to the readers of the book.

What has been happening over the last 10 years reflects three major trends associated with micro-manufacturing: (1). manufacturing is often a multilength scale problem, and hence, micro-manufacturing cannot be an isolated activity; (2). nano-sciences and technology look very likely to have significant impact on future products and technological equipment, while realizing this potential will largely rely on micro-manufacturing technology to bridge "nano-manufacturing" and "macro-manufacturing" and to produce low-cost products; and (3). research on micro-manufacturing is being shifted from "process and technology focus" to "market/product"-driven activities. These trends will be reflected in the following sections of this overview as well as in the other chapters of this new edition of the book.

PRODUCTS AND MARKET

There are ever-increased demands on miniaturized/micro-products/systems and components, e.g., MEMS and micro-systems, micro-reactors, fuel cells, micro-mechanical devices, micro-medical components, etc., which are now popularly used in vehicles, aircraft, telecommunication and IT facilities, home appliances, medical devices, and implants. The manufacturing of these products has received great attention over the last 15 years. At the same time, as nano-technology has become increasingly more mature and influential, more nano-technology-based products have emerged, such as nano-devices for sensors, communication and medical treatment, nano-materials and coating/functionalized surfaces for enhanced performance, etc. According to Yole's forecast [1], in terms of MEMS, a significant volume growth is foreseen (around 20% expected between 2013 and 2019). Globally, the predicted values of the increases of micro- and nano-technology products vary between different sources. According to ISuppli 2011 report [2], the micro-products' CAGR (compound annual growth rate) between 2011 and 2016 will be over 20%.

Typical micro-products for automotive and aerospace uses include pressure sensors, thermal sensors, temperature sensors, gas sensors, rate sensors, sound sensors, injection nozzles, etc., and the components include those for electrostatic, magnetic, pneumatic, and thermal actuators, motors, valves, and gears. There are more than 200 micro-actuators and sensors now integrated into modern automobiles.

The products also include sensors for mass flow, micro-heat exchangers, micro-chemical reactors, tools/molds for forming/replication, etc., and the components include those for miniaturized electronics products such as mobile phones, iPads, laptops, etc. Especially, smart phones are the main targeted market for emerging MEMS devices and micro-sensors, such as those for better communication performance, sound quality, visual experience, navigation and environmental sensing, etc.

In the medical sector, micro-fabricated parts span over a wide range for implantable applications in various clinical areas. Typical examples are sensors for cardiovascular, micro-machined ceramic packages, implantable devices, coatings on

micro-polymers or metal parts, etc. It is fair to say that micro-products and components are almost everywhere in life.

Another significant application market for micro- and nano-technology is the equipment market. Micro- and nano-technology products will play a significant role in evolving future factory equipment and production environment, such as enabling miniaturization of the equipment, lightweight structures, longer life span, manufacturing intelligence, low energy consumption, and excellent human—machine interfaces.

The micro- and nano-product market is influenced, currently, by three significant trends:

1. Disruptive development of manufacturing technologies, which helped/is helping the development of new products: the development of accelerometers has been helped greatly by the development of precision engineering, piezo-technology, bulk micro-machining and surface micro-machining technology. It is expected that new development of micro- and nano-manufacturing technologies (continuous and disruptive) will furthermore enable and accelerate technical and commercial breakthroughs in other application areas such as organic photovoltaics, micro-engines, E-cars, battery technology, etc.
2. Shortened development time, compared to what happened 20 years ago. Currently, from concept, through research and development (R&D), to the diffusion of the product into the market, the time has been shortened considerably: 35 years for pressure sensors to develop from R&D to commercial ramp-up, while it is about 16 years for oscillators to reach commercial ramp-up.
3. Emerging markets driven by needs of specific sectors such as energy, transport, health care, and consuming electronics, which are closely linked to important social and environmental issues. There have been targeted developments of micro- and nano-manufacturing technology for particular sectors and markets, e.g., that for energy sourcing, conversion, storage, transport, and utilization which involve largely thin-film technologies, ceramic technologies, nano-materials, and integration into surfaces and bulk parts, etc.

The future markets for micro- and nano-technology products are promising. The manufacturing cost will, however, be a key competitive factor, which raises a significant challenge to the development of micro- and nano-manufacturing technologies to meet the requirement for low-cost and high-quality products.

MEETING MANUFACTURING REQUIREMENTS AND ADDING VALUES

The requirements for micro-manufacturing may be classified into two levels: the component level and the product level (assembly/packaging). The following table presents some examples of the products/parts which can be made with micro-fabrication techniques, particularly with mechanical and/or thermal micro-manufacturing processes:

Components/ Parts	Sample Geometry/ Features	Possible Enabling Techniques	Typical Part Materials	Processing Accuracy	Typical Products/ Applications
Surface 2.5D functionalized structures	Local features in 100 nm to 10s microns	Hot embossing/coining/ imprinting, ink-jetting, plating, direct writing, laser ablation, etc.	Polymers, glass, aluminum, copper, brass, steel, etc.	Several microns to tens nanometers	Micro-optical, fluidic devices, force transmit. Surfaces, dies/molds, etc.
Lead frames	Various geometry, local features as small as tens microns, thicknesses vary, such as between 0.3 and 0.01 mm.	Micro-stamping, with/ without laser assistance, laser cutting, photochemical etching, etc.	Copper and alloys, nickel steel, etc.	Several microns or to 10% of the sheet thickness	Electronics products
Micro-pins	Diameters in 0.2–1 mm ranges, can wall thickness in 50–200 μm possible, and tolerances <5 μm	Forward, and/or combined with backward extrusion, micro-shape rolling, micro-machining/electrical-discharge-machining (EDM).	Various types of metals.	Several microns to submicrons	Various applications as IC carriers, micro-device assemblies, electric contacts, etc.
Electrothermal mechanical actuator	2.5D/3D structural parts, various sectional geometries.	Chemical etching and micro-stamping, laser cutting, Efab.	Shape memory alloy (SMA) and other metal materials	Several microns	Microactuating devices.
Micro-cups	Micro-cups, less than 1 mm in diameter, various thicknesses.	Micro-deep drawing, micro-stamping, micro-spinning, micro-machining.	Molybdenum, copper, aluminum, steel.	Several microns	Electron guns, pressure sensors, UV sensors, etc.
Micro-gears	Diameters of 1 mm or less, local features in 10s microns.	Micro-forging, micro-extrusion, micro-stamping, LIGA, micro-casting, photo-chemical-etching (PCE), micro-EDM, Efab, etc.	Metals, polymers	Several microns to submicrons	Micro-mechanical devices, watches.

Continued

Continued

Components/ Parts	Sample Geometry/ Features	Possible Enabling Techniques	Typical Part Materials	Processing Accuracy	Typical Products/ Applications
Shafts for micro-mechanical drivers	Less than 1 mm in diameter.	Micro-extrusion, micro-machining/EDM.	Steels and alloys	Several microns to submicrons	Micro-driving devices, e.g., micro-spindles.
Micro-screws, micro-cans	Diameters in 0.1–0.5 mm ranges.	Micro-forging, extrusion, shape rolling, micro-machining.	Various metals	Several microns to submicrons	Micro-devices, housing and assembly, etc.
Micro-gear shafts	Local features in 30–50 μm.	Extruded with local heating, micro-radial extrusion, micro-machining, EDM.	Metals	Several microns to submicrons	Micro-mechanical driving devices, Watches
Casing/ housing of micro-devices	Thin sheets, from 0.1 to 0.01 mm	Micro-stamping, dipping, drawing, hydroforming.	Stainless steel, aluminum, copper, etc.	Several microns	Micro-mechanical, electronics, medical, optical, chemical devices, etc.
Micro-tubular components	Outer diameter less than 1 mm, wall thickness larger than 20 μm.	Micro-hydro-tube forming, micro-rolling, micro-bending, laser machining, etc.	Metals	Several microns	Micro-shafts, micro-heat exchangers, micro-medical devices/implants.
Micro-molds, dies, and punches	Die bore or inner pockets in less than 1 mm; punch diameter from 0.05 to 1 mm.	Micro-EDM, laser cutting, micro-machining, electroforming, sintering, etc.	Tool steels, glass, powder, etc.	Several microns to submicrons	Forming/replicating processes e.g., injection molding, embossing, extrusion, etc.

Micro-manufacturing technology is being developed not only to meet these manufacturing requirements but also for creating new values. For example, to be able to make metallic and ceramic micro-components for micro-robots and micro-engines, produce high-quality 3D electrical interconnections for 3D micro-assemblies, create micro-/nano-structural surface/parts for batteries and micro-fuel cells, develop standard mechanical and mechatronics parts/elements for micro-machines or miniaturized equipment, etc., would itself add value to the associated products.

Considering where the value could be added to a product through micro-/nano-manufacturing, the following are some suggestions:

- Improving surface quality through precision manufacturing (e.g., nano-machining and focused ion beam (FIB) machining);
- Adding surface functionalities of the component/system surfaces through surface texturing (e.g., micro-machining, laser ablation, micro-EDM, micro-electrochemical machining (ECM)) and/coating (e.g., multilayered nano-coating);
- Creating new functional structures of the components/systems through micro-/nano-forming/casting/sintering (e.g., hollow-sectioned, channeled, functionally graded structures);
- Converting low-value materials into high-value products such as nano-materials/nano-composite products (e.g., micro-/nano-forming, casting, and sintering of high-quality components);
- Creating value by high-quality assembly from low-value components/materials (e.g., micro-injection molding assembly, high-precision mechanical, micro-joining, and self-assembly).

The main challenges to micro-manufacturing technology and equipment to meet manufacturing requirements and customers' needs continue to be cost, accuracy/precision, and standardization.

MICRO-MANUFACTURING METHODS AND PROCESSES

Compared to the manufacture of macro-products, manufacturing methods and strategies in micro-manufacturing may be different. Manufacturing macro-products may be effected with manufacturing individual components/parts by removing and/or deforming and/or adding materials, and then assembling them. These operations can be carried out either in a single industrial site or in different sites. The manufacturing of micro-products may be effected with patterning, deposition, and layering methods within a single machine/manufacturing platform, e.g., integrating components/parts fabrication with assembly/packaging that is often used in MEMS and micro-systems manufacturing. Micro-manufacturing largely uses nontraditional manufacturing methods or scaling down or modifying the traditional methods, as appropriate, to fully address issues related to manufacturing in the micro-world. Further, manufacturing chains may also be different, compared to traditional manufacturing, which may be due to:

- *Material properties*: conventional manufacturing methods may not be able to cope with special material properties, e.g., either too hard or too weak for a process, sticking onto micro-tools, not to the mask materials, or the original material properties cannot be altered during the manufacturing, e.g., affected by mechanical work induced heat or direct heating processes, etc.
- *Structural strength and stiffness*: components/parts may be too fragile to sustain any mechanical forces that are needed for processing the materials, or too difficult to handle during processing and/or assembly/packaging.
- *Shape and size—length scale factors*: all factors associated with small dimensional scale manufacturing apply, e.g., inability of tool fabrication for mechanical cutting and plastic forming may force the consideration of nonmechanical approaches. Normal geometric shapes such as holes, slots, pockets, threads, etc., may not be a problem in macro-scale manufacturing, but these may be extremely difficult to be achieved if the dimensions go down to submillimeters. Alternative manufacturing methods to conventional methods such as patterning, deposition, and layer manufacturing methods, may have to be considered.
- *Difficulties for clamping/releasing*: Due to the sizes and structuring strength/stiffness issues, it may be difficult to clamp/release the components/parts to be made by mechanical manufacturing methods such as mechanical cutting and forming. Alternative methods such as laser ablation, electroforming, and chemical etching may be considered.
- *Residual stress and surface integrity*: The existence of the residual stresses and weakened surface integrity, induced by plastic deformations, cyclic loadings, thermal gradients, etc., may not be acceptable for some critical components/parts for micro-products, e.g., those for medical implants and high-grade sensors. Selection of processes may have to consider such issues and process chains may have to be optimized to address these issues.

The fundamentals of the roles that the reduced length scales could play in various processing mechanisms need to be understood, e.g., roles of the surface at different length scales and in different manufacturing processes with respect to surface fabrication and micro-/nano-manipulation, surface metrology, etc. [3]. These play a significant role in selecting manufacturing methods and in optimizing the manufacturing chains.

Both conventional and nonconventional methods have been used to manufacture micro-products. There have also been emerging methods such as hybrid manufacturing methods. According to the type of the energy to be deployed, manufacturing may be classified as processes such as mechanical, chemical, electrochemical, electrical, and laser processes. The working principles include mechanical forces, thermal, ablation, dissolution, solidification, recomposition, polymerization/lamination, and sintering [4]. According to the way in which the components/products are to be made, general manufacturing processes can also be classified into subtractive, additive, forming, joining, and hybrid processes. The classification is equally

applicable to micro-manufacturing. Typical manufacturing methods for producing components/products are as follows:

Typical methods/processes of micro-manufacturing (edited based on a table presented in [4])

Subtractive processes	Micro-mechanical cutting (milling, turning, grinding, polishing, etc.); Micro-EDM; Micro-ECM; Laser beam machining; Electrobeam machining; Photochemical machining; etc.
Additive processes	Surface coating (chemical vapor deposition, physical vapor deposition); Direct writing (inkjet, laser-guided); Micro-casting; Micro-injection molding; Sintering; Photoelectroforming; Chemical deposition; Polymer deposition; Stereolithography; etc.
Deforming processes	Micro-forming (stamping, extrusion, forging, bending, deep drawing, incremental forming, superplastic forming, hydroforming, etc.); Hot embossing; Micro-/Nano-imprinting; etc.
Joining processes	Micro-mechanical assembly; Laser welding; Resistance, Laser, and Vacuum soldering; Bonding; Gluing; etc.
Hybrid processes	Micro-laser-ECM; LIGA and LIGA combined with laser machining; Micro-EDM and laser assembly; Shape deposition and laser machining; Efab; Laser-assisted micro-forming; Micro-assembly injection molding; Combined micro-machining and casting; etc.

Some typical micro-manufacturing methods/processes are included in this book. They are described in detail in corresponding chapters respectively. The following texts give an overview of some key methods and processes as well as the current state of the development.

Micro-Mechanical Cutting: Micro-machining may be seen as an ultraprecision material removal process, which is able to achieve micro-form accuracy and a several nanometers finish [5]. From precision machining to micro-machining, some challenging issues are being met such as predictability, producibility, and productivity in micro-scale manufacturing [6]. Effort is being made to achieve complex 3D, intricate micro-features/components with mechanical micro-machining, e.g., the systems for micro-instrumentation, inertial sensing, biomedical devices, wireless communication, high-density data storage, etc., as well as producing dies and molds for other manufacturing processes such as micro-forming and injection molding. Current efforts also include machining of difficult-to-cut materials such as metal matrix composites, silicon carbide, ceramics, etc., as well as nano-surface patterning [7–11].

Due to the working principle of removing chips by mechanical forces, significant efforts have been devoted to the improvement of the precision of machine tools and development of error compensation methods to ensure the required machine tool—workpiece system precision. The main issues addressed include

understanding of chip formation mechanisms and micro-machining mechanics, machine tool design with "optimal" dynamics stiffness, optimal cutter geometry/materials and motion control, in-process inspection with high-resolution metrology, etc. Benchtop machine tool designs have now become a trend showing the design being shifted from large scale, ultrahigh precision designs to miniature structures and low-cost system designs. Ultrahigh precision and high-speed spindle design is another topic attracting many researchers and industries. Diamond cutting tools, tools with nano-crystalline diamond coating, etc., are also important in micro-machining.

Micro-EDM: Electrophysical and chemical micro-machining processes play important roles in micro-manufacturing due to their special material removal mechanisms [12]. EDM is especially suitable for manufacturing micro-components/tools due to its thermal material removal mechanism, which allows an almost process force-free machining independently of the mechanical properties of the processed material. High-precision EDM can process functional materials such as hardened steel, cemented carbide, and electrically conductive ceramics with submicron precision [13]. Its applications have extended far beyond dies/molds fabrication to such as micro-gears, micro-fluidic devices, medical implants, etc. The processes include micro-wire EDM, micro-die sinking, micro-electrical discharge drilling, micro-electrical discharge contouring, and micro-electrical discharge dressing [14,15].

Compared to conventional EDM, micro-EDM places more emphasis on the following:

- Precision of the machine, e.g., high-precision control on the motion of the electrodes;
- Qualification of the wear of the electrodes, damage on the wire, and compensation for the wear/damage;
- Careful control on the frequency of discharge, level of the energy input, e.g., current and voltage;
- Better understanding of material properties, thermal conduction of the workpiece, melting and recasting processes, and their effect on the surface finish/integrity;
- Careful considerations of the setup of gaps, component forms to be produced, flash of the debris, etc.

Micro-ECM (MECM): ECM is another popular choice for making micro-parts, due to less effort being needed for handling during the ECM, easy control of the process, being relatively simple for the machine design/setup (computer numerical control (CNC) possible), and the capability of processing various materials, including high-strength materials. Other attractive characteristics include a burr-free surface produced, no thermal damage, no distortion of (part) parts and no tool wear. The issues needing to be addressed in micro-manufacturing applications include controlling material removal, machining accuracy, power supply, design and development of micro-tools, roles of interelectrode gap and electrolyte, etc. [16–19]. High surface roughness, relatively poor fatigue properties, difficulty to make sharp corners,

etc., are some negative aspects to be taken into account when the process is to be considered for manufacturing. For micro-machining, masks may be used (one side or two sides possible) for making finer geometry.

Micro-forming: Micro-products may be produced with forming configurations, i.e., micro-forming. Metal-forming offers some attractive characteristics that are superior to those of other processes, for example, machining and chemical-etching, considering such features as higher production rates, better material integrity, less waste, lower manufacturing costs, etc. Various forming/forging configurations are possible such as forging, extrusion, stamping, bending, hydroexpansion, superplastic forming, etc. Micro-forming may be achievable by effective scaling down of the process configurations, tools, and even machines [20–23]. Some challenges do arise when the sizes/features reduce to such as tens or hundreds of microns, or the precision requirements for macro-/miniature parts reduce to such as less than a few microns. Major issues being addressed include understanding of material deformation mechanisms and material/tool interfacial conditions, materials property characterization, process modeling and analysis, qualification of forming limits, process design optimization, etc., with emphasis on the related size effects. Current effort also includes the development of micro-tooling techniques such as diamond-like carbon coating and FIB modification, etc. [24–28]. To date, various micro-forming configurations have been investigated [20–29], including:

- Laser shock/pulsed/bulging/peening forming and laser-heating-assisted forming
- Micro-forging/micro-cold and warm and hot and isothermal forging
- Micro-extrusion and backward can extrusion/ultrasonic vibration micro-extrusion
- Micro-rolling/roll-to-roll stamping/micro-dimple forming and incremental forming
- Micro-stamping (hard and soft tools)/micro-deep drawing/micro-bending (laser)
- Micro-superplastic forming
- Micro-cold and hot embossing (on metals)/micro-/nano-imprinting/micro-coining
- Micro-hydroforming (tubes)
- Liquid impact micro-forming
- Semisolid micro-forming

Laser Machining: Laser technology is qualified as an efficient micro-technology because of its high lateral resolution by minimized focusability down to a few microns, low heat input, and high flexibility. One major advantage is its capability of processing various, nonsilicon materials that are increasingly needed for manufacturing micro-products. Some examples for laser applications are micro-cutting, micro-drilling, micro-welding, soldering, selective bonding, micro-structuring, and laser-assisted forming [30]. Femtosecond laser micro-machining is a new approach emerging in MEMS area in recent years, and some promising results have been shown in micro-machining and micro-system applications, including industrial material processing, biomedicine, photonics, and semiconductors [31].

The ultrafast, or ultrashort laser means that the laser pulse has a duration that is somewhat less than about 10 ps—usually some fraction of a picosecond (femtosecond) (a picosecond $= 1 \times 10^{-12}$ s) [32]. It utilizes the ultrashort laser pulse properties to achieve an unprecedented degree of control in sculpting the desired micro-structures internal to the materials without collateral damage to the surroundings. It has been proven that micro-structuring with femtosecond laser pulses is an excellent tool for the free design micro-fabrication of almost all kinds of materials [33,34]. With the filament, spatially scanning and other methods, many types of optical micro-structures (including 3D) such as optical memory, waveguides, gratings, couplers, and photonic crystals, have been produced successfully inside a wide variety of transparent materials in the sold state and also in the liquid state (laser-induced plasma micro-machining) [35] and laser dimpling strategies on TiN coatings for tribological applications with a highly energetic Q-switched fiber laser have been developed [36].

Replication Techniques: The LIGA technique is seen as a solution for the precision manufacturing of high-aspect ratio micro-components and systems [37], while other replication techniques such as micro-hot embossing, micro-injection molding, micro-casting/soft molding, micro-sintering, etc., are seen as better solutions to low cost, mass production of micro-components/features [38–48], reel-to-reel UV embossing being a good example for mass production. Materials that can be processed with replicating techniques include metals, glass, polymers, etc. Especially, embossing, molding, and casting are very effective for fabricating micro-structures for optical elements/devices, which can produce high resolutions possibly in the nanometer ranges with some processes, and allow the fabrication of large areas and complex micro-structures. Processes for gratings, holograms, and diffractive foils are well established. Efforts are continually being made to extend the process capability such as increasing the aspect ratios of the micro-structures, producing these in larger areas (such as replicating micro-structures with optical functions with dimensions between 200 nm and 50 μm on areas of up to half a square meter), combining embossing with other processes such as lithography, dry etching, and thin-film coating, etc. Micro-powder injection molding is a low-cost mass fabrication process for manufacturing micro-structures and micro-components. It can be used for processing many different materials (e.g., ceramics and metals) for very complex geometries. For making small geometries, silicon mold inserts may be used, taking advantages of deep reactive ion etching. The processing parameters need to be carefully set in order to produce the required quality and small features. LIGA, an alternative micro-fabrication process combining deep X-ray lithography, plating-through-mask, and molding, enables the highly precise manufacture of high-aspect ratio micro-structures with large structural height ranging from hundreds to thousands of micrometers thickness which are difficult to be achieved with other manufacturing techniques. Significant progress in MEMS manufacturing is largely due to introduction of the LIGA process. The polymer LIGA process is especially suitable for mass production. There is a chapter in this book especially describing this process.

Deposition methods: The methods are seen as effective for fabricating multimaterial devices with no need to increase the process chain. Possible methods for micro-manufacturing include laser-assisted chemical vapor deposition, laser-guided direct write and flow-guided direct write, shape deposition manufacturing (SDM), localized electrochemical deposition and forming, etc. [49–59]. For example, a similarity between the silicon-based MEMS methods and SDM is that "both integrate additive and subtractive processes and use part and sacrificial materials to obtain functional structures" [50], while the latter is able to deal with more types of the materials. Electro-forming has been used widely already to produce micro-components and micro-/nano-structures, and is, to date, still a powerful technique for securing fine geometry and low-cost production [59].

A micro-rapid prototyping system based on a deposition technique may include micro-deposition, ultrasonic-based micro-powder feeding, dry powders cladding/sintering, and laser micro-machining (a laser beam with a wavelength of 355 nm, for example) [50]. Fabrication of meso- and micro-structured devices by direct-write deposition and laser processing of dry fine powders is also possible [51], which is also seen to be an effective way to fabricate 3D structures with heterogeneous material compositions. The direct-write deposition system is able to produce a "100 μm minimum attainable feature size for device footprints ranging from submillimeter to a few centimeters" on a movable substrate. The prototype devices produced included micro-batteries, interdigitated capacitor, fractal antennae, Swiss-roll micro-combustors, and functionally graded polymeric bioimplants. By combining an electric-chemical method and an etching method, a new manufacturing technique, so-called Efab manufacturing (a system developed by MEMGen, USA) has been developed [52]. The method adds layers from 2 to 20 μm thickness and is able to create 3D metallic features with support of the sacrificial material, which is later etched away.

SDM combining micro-casting with other intermediate processing operations (CNC machining and shot peening) was also attempted to create metallic parts [53]. A better product quality could be achieved with proper control of interlayer metallurgical bonding (through substrate remelting) and the cooling rates of both the substrate and the deposited material. Another good example of fabricating complex metallic micro-structures is to use lithography and etching techniques to make sacrificial silicon molds. Multiple silicon layers are stacked and metallic glass is then forced into the cavities under heat and pressure in an open-air environment. Such an approach could be a solution for low-cost manufacturing [54].

Inkjet technology offers a prospect for the reliable and low-cost manufacture of flat panel displays (FPD). Compared to other conventional processes, an inkjet printing method for color filters (C/F) in LCD or RGB patterning in organic light-emitting diode offers potential for the mass production of the enlarged display panels with low costs [55] while the possibility of depositing nano-particles offers more potential applications and higher quality of products [56–58].

Assembly/Packaging: Basic processes for micro-assembly and packaging include mechanical placement/insertion/pressing, micro-welding; resistance/laser/vacuum

soldering, micro-casting/molding, bonding; gluing, etc. [60–65]. Interconnection and packaging solutions (e.g., 3D-molding of interconnect devices) are the key technologies for connecting micro-systems to the macro-world. Molded interconnect devices technologies include insert molding, one-shot molding, and two-shot molding. Assembly/packaging gains more importance with the growth of complexity and miniaturization of the products and systems. Although significant progress has been made in the manufacture of individual micro-components/parts, as well as MEMS, there is still a significant amount of manual work involved in the assembly/packaging of the micro-products and systems. Assembly of individual technical components to hybrid micro-systems is often a bottleneck to large-scale production, which is evident especially in the areas of heterogeneous assembly, online inspection, and quality control. Integration of micro- and nano-devices through assembly is still a new area of challenges. A method for achieving electrical and mechanical interconnects for use in heterogeneous integration has been to combine metal reflow and a self-aligned, 3D micro-assembly, which allows for the batch processing of a large number of heterogeneous devices into one system without sacrificing performance. Micro-assembly injection molding gives another option for joining plastics and some inlay parts such as fiber reinforced needles and other elements. The use of lasers for welding has exhibited tremendous growth over the last decade for improving efficiency and reducing costs in a broad range of industries for the manufacture of both macro- and micro-components. Efforts are continually being made for better understanding of the processes and for controlling the key parameters for better quality and efficiency. Online inspection of joint quality is an important issue for industry. For some micro-devices assembly, there has been almost no efficient online inspection system available for industry to use, and therefore, quality control was extremely difficult. Another key issue for both MEMS- and non-MEMS-based manufacturing is the need of effective and efficient gripping techniques/systems and corresponding manipulation strategies/means for micro-assembly.

Process Chains and Hybrid Processes: Manufacture of a component/product often cannot be completed with a single process only: it may involve a process chain. Better quality and efficiency of the manufacture could be achieved with a properly defined process chain. This also applies to micro-manufacturing which often needs several processes to complete a component manufacturing. A typical example is the combination of plating/coating, chemical etching, and stamping to make 3D micro-sheet components. If including micro-tooling, the process chain is extended even longer. Various process chains are possible in order to meet various design and manufacturing specifications. For example, combining lithographic tooling and injection molding techniques can enable the mass production of micro-components with various materials such as polymers, metals, and ceramics [66]; and an LIGA process could be improved by fabricating micro-molds with direct femtosecond laser micro-machining [67]—an approach may lead to practical, cost-effective 3D MEMS with various materials. Ultraprecision manufacturing of self-assembled micro-systems is another example of this kind of development,

which combines ultraprecision micro-machining such as milling, turning, drilling, and grinding with sacrificial/structural multilayer manufacturing processes to produce self-assembled, 3D micro-systems and associated meso-scale interfaces from a variety of materials for MEMS applications [68]. With this process, a new class of micro-systems could be developed that is highly three dimensional, precisely machined, and automatically assembled. Rapid fabrication of micro-components may also be effected with the combination of UV-laser assisted prototyping, laser micro-machining of the mold inserts, and replication via photo molding [69] which was found to be able to deal with materials such as polymers and composites. Another example is equipment development and applications of the pulsed laser for the micro-machining of large-area polymer substrates with micro-structures which involve rapid prototyping, bow tie scanning, synchronized image scanning (mask projection technique), etc. The applications include FPD, solar panels, superlong inkjet printer nozzles, micro-lenses, diffusing structures fabrication, etc. [70].

Ideally, a process chain for micro-manufacturing should be short in order to achieve high efficiency, reduce manufacturing errors, and eliminate unnecessary handling/transport/packaging of micro-components among different processes. Hybrid manufacturing processes may take advantage of the merits of individual micro-manufacturing methods/processes while some of the inherited disadvantages may be reduced or eliminated, e.g., shortening the process chains [71]. For example, micro-EDM and laser assembly may be combined to fabricate 3D metal micro-structures [72]. The system may use a micro-EDM process to fabricate micro-parts and laser welding to assemble these micro-parts. By such a combination, increased numbers of the patterns, higher aspect ratios, and higher joint strength of the micro-structures can be achieved. Another merit is reduction or elimination of the number of postassembly operations which may involve various efforts in handling and high-precision positioning. A new technology based on laser transmission welding, combined with a photolithographic mask technique, enables the assembly of plastic micro-fluidic devices, MOEMS, and micro-arrays which require high positioning and welding accuracy in the micrometer range [73]. The system created consists of a diode laser with a mask and an automated alignment function to generate micro-welding seams with freely definable geometries. A fully automated mask alignment system with a resolution of less than or equal to 2 μm and a precise, noncontact energy input allows a fast welding of micro-structured plastic parts with high reproducibility and excellent welding quality, as reported. Combining the ECM and EDM, i.e., so-called hybrid ECM−EDM, is another example of improving the material processing efficiency. In EDM, sparks are needed (dielectrics), while these are unwanted for ECM (electrolyte, short circuit). The sparks would be encouraged for combined ECM−EDM with appropriate control. The applications include the drilling of small holes in hard alloys, wire-machining removal of metallurgical samples, manufacture of dies and molds, etc. Other hybrid processes include laser-ECM and electrolytic in-process dressing (ELID) processes.

MANUFACTURING SYSTEMS/EQUIPMENT FOR MICRO-MANUFACTURING

Traditionally, some micro-manufacturing processes (non-MEMS manufacturing) were often effected with large-scale equipment, such as that for micro-mechanical machining, micro-EDM, and micro-metal forming. To perform micro-manufacturing tasks with such equipment, significant efforts have been made to improve the precision of the machine structures, to compensate for mechanical and thermal errors, as well as to increase the functionality, resolution, and reliability of the monitoring systems. The cost paid to achieve these objectives has been very high, while the resulting equipment is too expensive, which actually limits their applications.

MINIATURE MANUFACTURING SYSTEMS AND BENCHTOP MACHINES

During the last 20 years benchtop/desktop machines or miniature manufacturing systems have been gradually developed and introduced to industry. The development of such machines/systems has attracted a lot of interest from research organizations and industries. A main consideration is that conventional facilities for manufacturing miniature/micro-products are not compatible, in sizes, to the products to be made in miniature/micro-manufacturing. Therefore, it is necessary to reduce the scale of the equipment which could, in turn, reduce the energy consumption and material requirements, reduce pollution, create a more user-friendly production environment, reduce equipment cost, etc. At the same time, as the scales of the machinery and auxiliary equipment are reduced, the mass of the mechanical parts is reduced dramatically and, as a result, the speed of the manufacturing tools could be increased, which could result in increase of the production rates. Another advantageous feature often mentioned is that the force/energy loop and the control loops are significantly short for small machinery, therefore, the precision of the machinery could be increased comprehensively. Micro-factories are typical examples of such facilities.

During the last 20 years several demonstration micro-factories (also called miniature manufacturing systems) have been developed [22,74–76], notably in Japan, but now a worldwide effort. These systems and machines indicate a trend in the development of the equipment for micro- and nano-manufacturing. The development of a micro-factory itself renders significant challenges to the development of manufacturing facilities, e.g., stringent requirements on machine elements and assembly, as well as monitoring and inspection. In turn, the development of miniature machines or micro-machines also promoted the development of a micro-factory, which has resulted in various new micro-factory concepts [3,22,77]. To date, many miniature machines/desktop machines have been put on the market, such as desktop milling machines, EDM machines, injection molding machines, laser-processing equipment, miniature-forming presses, multiprocess equipment, etc. Compared to the traditional micro-machine concepts, currently commercially

available desktop machines are relatively larger but closer to industrial application requirements [3]. These may be seen as bridging the gap between micro-machines and conventional, large-scale machines.

Led by the Institute of Product Development (IPU) of Denmark, a miniature press and flexible tool system was developed for the forming of micro-bulk products [78,79]. The press is driven by a linear servo motor and is capable of fast and accurate motion. The tool system enables eight different bulk-forming processes to be carried out by changing only small portions of the tool elements. The precision of the tool system is crucial due to narrow tolerances on the dimensions of the micro-components to be formed, which requires the manufacture of die cavities to within the submillimeters range in diameter and within a few microns in geometrical accuracy. To match the mass production characteristics of micro-metal forming, a high-precision and fast handling system is an important part of the system.

A linear motor-driven micro-sheet forming machine system (benchtop machine) was developed at the University of Strathclyde, UK [80,81], in collaboration with Pascoe Engineering of Scotland, Tekniker of Spain, and other EU partners. The machine is capable of a series of micro-sheet forming processes for forming thin-sheet metal parts with thickness below 100 μm. The machine has capability of up to 800−1000 strokes per minute, a force capacity of 5 KN, and a machine precision of 2−5 μm, with a modular and flexible setup. The machine is equipped with a newly designed, linear stage-driven, high-speed feeder which enables a feeding accuracy (thin strips) of less than 5 μm [82]. With properly designed pilot pins deployed in micro-sheet forming, higher positioning accuracy could be achieved. Another novel development was to transport the parts directly out of the tooling system with a novel part-carrying system [83]. The machine is also equipped with a force-displacement monitoring system which reads the data directly from the tooling.

The Institute of Production (IFP) of the University of Applied Science Cologne, Germany, leads the development of the first generation hydroforming machine for the forming of miniature/micro-tubular components [84,85]. Hydorforming processes have been employed successfully in industry to produce mass products predominantly relating to lightweight automotive components. The mass production of such components is, however, limited largely to parts with cross sections of above about 20 mm width. There was a lack of understanding in the hydroforming of tubular, miniature/micro-parts [86]. A machine system was developed for the forming of miniature tubes down to 0.8 mm diameter with thickness down to 20 μm. The applications of the system significantly extends micro-manufacturing capabilities, especially in the manufacture of hollow-sectioned parts, such as those used in micro-housings, fluidic devices, lightweight structures in micro-mechanical devices, etc., which has not been achieved before.

A benchtop, multiple axis machine tool capable of machining intricate 3D geometries in components with nano-scale tolerances has been developed [87,88], led by Brunel University and Ultra-Precision Motion Ltd of the United Kingdom. The associated new series developments include an air bearing slideway and a rotary table

with improved damping capacity (Patented) and an ultrahigh speed air bearing spindle (Loadpoint Ltd/Ultra-Precision Motion Ltd of the United Kingdom), a piezo-driven fast tool servo system and a piezoelectric actuation unit for vibration-assisted machining (CEDRAT Technologies S.A. of France), new micro-diamond tools (Contour Fine Tooling Ltd of the United Kingdom), a robotic arm unit for micro-components/tools handling and management (Carinthian Tech Research AG of Austria), and a tool and spindle condition monitoring system (University of Patras of Greece).

MULTIPLE-PROCESS EQUIPMENT

Multiple-process equipment is an ideal solution to implement various process chains within an integrated platform, which could significantly reduce the number of component handlings. Another resulting benefit is reduction of the possible accumulation of manufacturing errors. The majority of the equipment/devices developed in micro-factory or miniature manufacturing systems cannot be classified as multiprocess equipment/devices, since each of these is a stand-alone machine which deals with a particular process.

The idea of multiple process equipment received very positive response in Asia, typical developments in this region including the multifunctional micro-machining equipment developed in one of Chinese universities which was able to perform several micro-machining operations on the same machine tool [89]—micro electrical discharge machining (EDM), MECM, micro-ultrasonic machining (USM) as well as their combination. Using micro-EDM, micro-rods with a diameter of less than 5 μm were ground on a block electrode, and micro-holes and 3D microstructures were obtained. Shaped holes were machined with a combination of micro-EDM and micro-USM. Another similar multifunctional micro-machining system was developed in Ibaraki University of Japan, which is capable of micro-milling, turning, grinding, buffing, polishing, EDM, ECM, laser machining, and their combinations [90]. The applications included the fabrication of micro-lens molds. Another development undertaken in National Taiwan University was a multifunction high-precision tabletop CNC machine [91]. With this machine, machining processes such as micro-high-speed milling and micro-EDM (die sinking and wire EDM) could be performed on the same machine without need of unloading, reloading, and readjusting the workpiece for the subsequent operations. The system was also equipped with an in-process workpiece/features geometrical measurement system. Micro-electrodes as small as 8 μm in diameter and diameter/slenderness ratios as high as 100 could be achieved. Similar development was also seen in Singapore [92]—a multiprocess miniature machine tool which included processes such as micro-EDM, MECM, micro-turning, drilling, and milling, as well as ELID grinding and single-point diamond tool cutting. A micro-factory as a whole may be seen as a platform that integrates several processes through several micro-machines on the same platform and hence, is seen as an item of the multiprocess equipment.

The EU POLYTUBES consortium developed a common platform integrating several processes (micro-rolling, micro-hot embossing, micro-blow forming, laser drilling/trimming) in a form of integrating individual modular machines [77]. The small machines were linked through a global handle system (robotic manipulator), aiming at producing polymeric, tubular micro-components, while each of the modular machines has its own interhandling device that is able to feed the tubes and to pick up the shaped components. In such a way, each modular machine can be a stand-alone machine for different applications but can also be integrated onto a common platform for an integrated process chain. Other advantages are: high manufacturing flexibility—the process combinations can be programmable, there is high modularity (a highly modular system) and the system is easily reconfigured, etc.

SUPPORTING TECHNOLOGIES/DEVICES/SYSTEMS FOR MICRO-MANUFACTURING

Handling and inspection/measurement are still two major features to be taken into account in micro-manufacturing. Considering handling at the micro-scale, factors such as gravity cannot be considered as a main force applied to the parts to be handled. Unwanted surface forces such as van der Waals, electrostatic, and surface tension forces are dominant at such a scale [93]. The pick-and-place issue has to be addressed fully, due to adhesive forces existing. In micro-handling, the possible joint backlash and structural vibration due to link flexibility may have to be controlled at the level of several microns during automated positioning. Higher care on manipulation and cleanliness are also required. The problems associated with micro-handling may be well understood, but a key challenge is still handling to match the high production rates to be deployed with some miniature/micro-manufacturing machines such as micro-forming machines [94]. This is far more difficult to achieve, compared to that in a slow assembly/packaging process.

Sensor systems play an important role in many fields of manufacturing. Their applications in micro-manufacturing such as that in equipment and that for online inspection require high levels of accuracy/resolution of the sensors. Data processing close to the sensors, extracting more information from the directly sensed information by signal analysis, system miniaturization, multisensors uses, etc., are the demands to be met [95]. Single-function transducers may now not be sufficient to meet the needs, and system-based sensors as system components are being introduced: systems containing both sensors, actuators and electronics, are being developed.

Micro-manufacturing technologies are still being developed, and quality assurance plays an even more important role in order to efficiently support the transition of micro-production processes from nonrobust to stable processes [96–100]. Quality assurance faces particular challenges at the production level—some common quality methods for macro-length scale manufacturing may be difficult or even impossible to be applied/implemented. The need for the development of the

technologies and systems for dimensional metrology at different length scales and integrating them is evident. As critical dimensions are scaled down for both components and manufacturing machines/tools, and the geometrical complexity of the objects increases, the available technologies and systems may not be able to meet current and development needs [101−103]. New measuring principles and instrumentation, tolerancing rules and procedures as well as traceability and calibration, etc., are being developed for micro- and nano-manufacturing. 3D measurement technologies that enable fast, accurate measurement of solid shapes in the submicron and even nanometer region are also being developed [104,105]. Providing all possible measuring means available and integrating them into a flexible system to allow users to deal with different inspection requirements in micro- and nano-manufacturing could be a solution to meet various manufacturing needs. Current, significant interest and effort in developing micro- and nano-metrology will significantly help further the development of micro- and nano-manufacturing technologies and production systems.

DESIGN CONSIDERATIONS AND MATERIAL FACTORS

DESIGN CONSIDERATIONS

Design of products for micro-manufacturing needs to address production issues fully, compared to the prototype products based on micro-technologies. High volume production of micro-components should be a target for the design for micro-manufacturing. When these products are designed, not only will functional requirements need to be considered but also micro-manufacturing related factors will have to be taken into account. This is because, as briefly described above, manufacturing these products renders more significant challenges, compared to the manufacture of macro-products. The following are some typical issues to be addressed at the design stage:

- *Overall dimensions of the parts/products*: overall dimensions of a part/product, such as diameters, widths, lengths, and thicknesses, are very much constrained by the overall capabilities of the processes and manufacturing facilities (machines, handling devices, tools, etc.). Both the maximum and the minimum dimensions are the parameters to be checked with reference to the manufacturing system's capabilities. Complexity around dimensional scale issues is a dominant factor in micro-/nano-manufacturing. The question often asked may be how small a part can be dealt with rather than how large a part can be handled.
- *Part/component local features*: design of local features, such as hole/pocket radii and aspect ratios, widths/depths of channels or aspect ratios, wall thickness, area reductions, density of the local features, will be largely constrained by the processing capability in micro-/nano-manufacturing, especially those features relying on the uses of tools such as replicating processes. There is also the factor

of the relevant grain sizes of the material to be used. The local features will not only determine the tool geometry, but will also affect the stiffness/rigidity of the part/product structures, and hence, affect the manipulation of the part/product. The manufacture of local features spread over a large area also renders challenges to many micro-manufacturing processes and equipment, even not mentioning nano-manufacturing.

- *Shape capability*: shape capability considers the capability/limitation of a manufacturing process in dealing with the shapes to be produced. For example, a lot of processes are only able to deal with 2D/2.5D shapes, while making 3D shapes may need much more significant effort in respect of such as new processes and expensive equipment. Rotational symmetry is probably favorite for micro-extrusion, for example, considering the effects of grains and grain sizes on the process. Any asymmetry may bring in difficulty in controlling the quality in micro-shaping. Excessive material accumulation, large reductions in area, and sudden changes of the sections should also be avoided in forming/shaping. Others include the design of the draft for the workpiece for micro-forging, permitted drawing ratios and profiles of the drawn products in micro-sheet forming, etc. Conventional rules on shape capability of manufacturing may not be applicable to micro-manufacturing largely due to size effects needing to be considered and limitations to the tool shapes that can be produced.
- *Tolerance and surface quality capability*: the design of a macro-product would (expect) require the designer to consult handbooks/standards before specifying a grade of tolerance and surface quality requirements. Design for micro-manufacturing may not be as straightforward as the design of a macro-product. Standards on manufacturing tolerances for design for micro-manufacturing, especially for non-MEMS-based manufacturing, have not been established fully, while most of the data are "in-house" determined/used. The designer may have to consult with the manufacturing engineers who are responsible for manufacturing using their own manufacturing capability.
- *Material capability*: selection of a material for micro-manufacturing will be constrained largely by the availability of the material for volume production, due to the limited number of suppliers operating in this field currently, although the trend is improving, such as that happening with nano-material suppliers, the number of which have increased significantly, recently. New study/qualification of material properties may be needed if the material suppliers are not able to provide the material data relevant to micro-manufacturing, such as size effects and material property descriptions. The properties will have to be qualified for design uses, with consideration of size effects, and these have to be available with inclusion of mechanical, thermal, electrical, and magnetic properties, as appropriate, others including bio- and chemical compatibility, hydrophilic and hydrophobic properties, etc. Grain sizes of the material to be selected must also be known for most of the micro-manufacturing processes. Ultimately, the designer has to know which processes are most suitable for the materials selected, or which materials are most suitable for the available processes, etc.

- *Part/component material properties after processing*: the involvement of large plastic deformations, damage, and possibly, significant temperature rise locally and thermal stresses during mechanical and thermal processes, which, very likely, will result in alteration of the material properties after processing, need to be considered. The micro-part/component material properties will play significant roles in determining part/component performance under working conditions than that for macro-components, such as those used in micro-sensors and medical implants. Part/component design is, therefore, constrained by the applicability of certain micro-manufacturing processes, e.g., chemical and high-temperature processes, due to considerations of possibly adverse effects on the material properties.
- *Characteristics of volume production*: the design should also address significant characteristics of volume production in micro-manufacturing. Prototyping in a lab-scale is significantly different from manufacturing the products in a production-scale. Achievable/targeted production yield, which is prescribed largely by the capability of the processes, machinery, tools, and auxiliary equipment, will have an influence on the selection of the materials for the manufacturing and design of the part/component and their features. Among those factors, handling the parts/components and interactions with tools are particular concerns that should be taken into account at the design stage.
- *Manufacturing cost*: Manufacturing cost is a major issue to be addressed. This is largely because micro-manufacturing often involves high investment in facilities and human resources and low product quantity requirements from each customer. Many factors prescribe the manufacturing cost, and a balance, however, will have to be maintained between the feasible reduction of the cost for core processes and the cost involving the use of auxiliary processes. Some sophisticated geometry and tight tolerances may not be achievable solely with a single process, and using a process chain which may involve various processes is often inevitable. The designer has to be aware of how the design specifications will impact on the planning for the manufacturing chains. He/she has to realize that the cost for tooling for some micro-manufacturing processes may be very high. A comparison among available manufacturing processes/chains and even involving supply chains may be needed, even at the design stage.
- *Synthesis factors*: Design synthesis may be conducted by considering all of the factors discussed above. The results can be a basis for design optimization. Strong dependences of the component/part design on the manufacturing processes in micro-manufacturing suggest that design iterations and interactions with manufacturing personnel are often inevitable and necessary.

The design of micro-products is still a challenging task due to lack of sufficient standards, design/manufacturing rules, and understanding of the manufacturing processes theirselves. There is also lack of effective software to support the design activities. Incorporating size effects into conventional design and analysis software and/or developing domain-specific design and analysis tools (software) will help to

improve the situation. Modeling for different length scales such as micro-mechanics modeling and molecular dynamics modeling, and multiscale modeling, and integration of these into commercial software, are urgent needs for design for micro-manufacturing. Some of these will be mentioned in several chapters of this book.

MATERIAL FACTORS

Material properties have much more significant impact on the design/planning for micro-manufacturing, compared to that in macro-manufacturing, which, for example, is reflected in the following aspects:

- Size effects on mechanical, thermal, electrical, magnetic properties, bio- and chemical compatibility, hydrophilic and properties, etc., need to be understood, and some of these may be significantly different, compared to the material behavior in the macro-scale.
- As a consequence of the above, the mechanisms of material conversion processes (separation, deformation, joining/deposition chemically and physically) will be different or affected, as well as interactions between the materials and processing tools (for tool-based processes).
- As a consequence of the above, selection of the means for enabling material convention processes will be affected, the considerations involved including effectiveness and efficiency and the effects on the material properties of the processing methods (mechanical, chemical, thermal, electric-chemical method, etc.).
- Grain and grain boundaries, which may have less impact on the material conversion processes in macro-manufacturing, will have more significant impact on the material conversion mechanisms as the dimensional scale goes down and the sizes of the grains become more relevant, such as their influence on interfacial friction and the dislocation of grains and damage. This is particularly relevant in mechanical material conversion processes.
- Emphasis on the importance of the material-related issues in micro-manufacturing is also due to, currently, lack of sufficient, effective means for qualifying some material properties in the micro-scale, and hence, insufficiently understanding these.

In design and planning for micro-manufacturing, special attention should be given to the micro-structures of the materials, such as grain sizes, grain boundaries, precipitations, and intermetallics as second-phase particles and their size and distribution in multicrystalline structures, in relation to the sizes of the micro-products/features (less than 1 mm in dimension). Developing new materials and increasing the volume of the materials available for particular micro-manufacturing processes are needed: otherwise, micro-manufacturing will be constrained significantly by the limited number of materials that can be processed in the micro-scale with the required quality and efficiency. A typical example is that the type of the materials usable in micro-replication/forming processes is quite limited by the material flow ability, strength, hardening, and surface adhesion behavior. For volume production,

fine grains and high plastic flow ability of the material, either at room temperature or at elevated temperature, are preferred.

The following are some examples of the materials used in micro-manufacturing: materials with finer grain sizes; materials alloyed with elements of high purity grades; modification of surface roughness, e.g., laser defined micro-structured surfaces; materials with defined strain-hardening characteristics; materials originating from galvanic processes; single-crystal materials with a mono-crystalline structure; materials produced by thin-wire processing, e.g., bond wires for micro-electronics; materials produced by thin foil precision cold rolling; materials with special coatings; materials with total or selective plating of strips; materials for thin films coating; materials for the roll cladding of strips; etc.

DEVELOPMENT AND UTILIZATION STRATEGIES OF MICRO-MANUFACTURING TECHNOLOGIES

A series of methods and technologies have been developed in the micro-manufacturing field and the trend will continue. These methods and technologies are, mostly, materials and products oriented. This is particularly the case for manufacturing, since many particular considerations need to be taken into account in the manufacture of micro-products, as discussed in previous sections. As far as a method and technology developer is concerned, it is particularly important to understand how the end-users assess the methods and technologies developed, and how a decision is made on the selection and utilization of the manufacturing methods and technologies, even when the product manufacturing requirements are known. Since significant knowledge gaps still exist, especially for those emerging micro-manufacturing technologies, plus significant lack of standards and manufacturing/production guidelines, selecting an appropriate technology/process for the manufacture of a particular micro-product may not be a straightforward task.

In some cases, to have a clear view on issues such as the competitiveness of the technologies and the unpredictability of the technological development is not easy to achieve, while the issues relating to possible manufacturing difficulties and institutional change needs are particularly important to an industry. Similarly, life cycle assessment methods may be introduced to the assessment of emerging technologies such as micro-/nano-manufacturing technologies, e.g., assessment of the impact on the environment (eco-efficiency improvement) which may consider materials, production, uses, and disposal, possibly taking future changes into account. Other methods for assessing micro-manufacturing methods and technologies are also possible, each of which may be focused on particular issue such as scientific and technological issues, collaborative issues, etc.

Assessment of the emerging technologies to be utilized with a view to fully understanding the implication and impact on the business is very important. Experience should be learnt from previous cases in the MEMS field which saw that some enterprises were struggling to survive or disappeared from the business. A business

built on immature prototype designs and products with low volumes always takes a risk. Micro-/nano-manufacturing, at the moment, may still be an expensive business which is characterized by high investment in resources (facilities, knowledge, and skills) and often by low volume production and lack of a complete business chain locally. Decision-making on the development or utilization of the technologies should take these factors into account, together with other technological issues, such as dealing with multimaterials, small geometries, increased and complex functionalities of products, etc.

The following aspects should be particularly looked at strategically, in relation to the strategies of the development and utilization of micro-manufacturing methods and technologies:

Manufacturing and supply chains: The development of micro-manufacturing technologies largely depends on the demands and enthusiasm from industry. The industry's decision is influenced significantly by the perspectives of new business to be brought or improvement which could be made to the existing business. Besides the efforts in developing individual manufacturing technologies, completing manufacturing chains and providing industry with flexibility to optimize the manufacturing chains are also very important. This is not just because significant numbers of micro-parts/components often cannot be produced/completed with a single technology alone but also because an optimized manufacturing chain may result in better quality and efficiency. Since no single technology could claim to be dominant, a possible solution to the industrial applications of micro-manufacturing is to provide various technologies and means for the industry to be able to effectively and efficiently form the required process chain(s), with lower cost. Completing supply chains for micro-manufacturing-based business is another important issue to be addressed. Forming effective micro-manufacturing business chains is often affected by the lack of the required material and high-quality tool supply, as well as auxiliary facilities such as that for inspection and testing, although demands on micro-parts/components is highly evident. Without complete and efficient and manageable supply chains, a sustainable micro-manufacturing industry cannot be established. Strategic efforts should be made to complete manageable micro-manufacturing supply chains regionally and/or globally.

Advanced methods and systems for supply chain management for the semiconductor industry, and the micro-electronics manufacturing industry in general, are mature and have been applied to the industry widely. These have not been developed exclusively for addressing the emerging micro-manufacturing industry. One of the main challenges also results from the fact that significant numbers of enterprises in micro-manufacturing are small and only of a short time in business, etc. Development in material and production planning with good knowledge of cost implications is insufficient for emerging micro-manufacturing, including lack of advanced material resource planning (MRP) systems exclusively for micro-manufacturing. The lack of standards exclusively for micro-products, materials, manufacturing methods and technologies also makes management of the supply chains more difficult. Good strategies are needed for marketing and financing, considering the nature

of micro-manufacturing for a new business. Attention should also be paid to the recycling and reusing of micro-manufactured products and materials.

Integration with other manufacturing activities/sectors: a good solution for fostering a micro-manufacturing industry may be to have some other business to be associated with or to give support to the micro-manufacturing, at an early stage of the development. There are two considerations. First, micro-manufacturing cannot be an isolated activity and it should be an efficient means for linking macro- and nano-manufacturing. There will only be limited impact from nano-manufacturing if it is not effectively integrated with micro-manufacturing. It is the same for micro-manufacturing—effectively building micro-systems or integrating results from micro-technologies and science, into macro-systems, will be a key measure to the success of micro-manufacturing. Second, development of new micro-manufacturing business needs strong backing from successful business in macro-manufacturing, technologically and financially. Currently, significant numbers of business and research activities in micro-manufacturing are actually transformed from macro-manufacturing, which has helped the development of micro-manufacturing tremendously. More attention should, however, be paid to the issues associated with the micro-world for which some methods and technologies cannot be simply "scaled down" from the macro-world.

The micro-/nano-manufacturing industry may still be small, compared to other industries, such as automotive, aerospace, health care, etc. However, it will be playing significant roles in driving other industries to a new level. These may be reflected in the following aspects:

- Traditional industry needs breakthrough/transformation/improvement, considering significant competition and demands on the new products and higher quality. Achieving these cannot rely on organizational measures only, but also requires, significantly, technological measures. Research and technological development in micro-/nano-manufacturing is one of most promising areas that could deliver the required solutions.
- Research in developing new micro-/nano-materials will meet many material challenging issues faced in the traditional materials and manufacturing industry—an area in which currently, significant competition exists.
- Manufacturing process concepts evolved in micro-/nano-manufacturing research will significantly change/update traditional manufacturing concepts in terms of effectiveness and efficiency, these being due to the need of better understanding and control of the manufacturing processes as well as due to the new way in which the products are manufactured in micro-/nano-manufacturing. No matter which length scale is to be dealt with, the process development in micro-/nano-manufacturing is of general significance to all length scale manufacturing.
- To be able to meet much more stringent requirements in tool fabrication for micro-/nano-manufacturing will deliver new knowledge and enabling techniques for the whole tool industry, which will better equip the traditional tool

industry for meeting new challenges and competition. Typical examples include tool dimensional precision and surface quality, tool material performance, etc.
- New manufacturing machine and system concepts, such as benchtop, miniature, micro-machines and systems, will have significant impact on all manufacturing sectors in design, fabrication, and use of the machines, in relation to the performance, impact on users and environment, energy saving, etc.
- Micro-/nano-technology products designed and/or prototyped in other sectors may have to be brought to the market in order to have real impact/economical gains—Micro-/nano-manufacturing is a sector to make it happen.

Technological performance/maturity level: Compared to macro-manufacturing, one of the difficulties in assessing the technological performance/competitiveness of a micro-manufacturing process and the equipment lies in the significant number of uncertainties existing. Capabilities on material, geometry, tolerance, production rate, ease to link with other processes and equipment, etc., are often difficult to be defined in general terms, as these are often affected by many factors, as described in several sections of this chapter. The strong material, dimensional, and environmental dependence in micro-manufacturing, including the skills of the workers, makes comparison of different processes and equipment very difficult to achieve. Nevertheless, the following aspects should be examined in terms of assessing the technological performance and maturity level of a micro-manufacturing process and equipment:

- Geometry associated performance: achievable overall dimensions, feature geometry, tolerances, surface finish, possibility for length scale integration manufacturing, etc.;
- Material-associated performance: type of the materials processable, material property requirements/constraints (e.g., micro-structures and surface integrity), postprocessing requirements, etc.;
- Production-associated performance: yield, reliability, scalability, online/in-process monitoring/inspection ability, ease for integration into process chains, dependence on the skills/environment, impact on the environment, etc.;
- Cost factors: all costing items including those for auxiliary processes and equipment (e.g., that for handling, assembly/packaging, cleaning, etc.).

Other issues: besides a series of activities such as economic analysis, decision analysis, technological forecasting, information monitoring, risk assessment, market analysis, and externalities/impact analysis, etc., education and training is important for a micro-manufacturing industry. This is needed largely due to micro-manufacturing being generally a knowledge-intensive business.

REFERENCES

[1] http://www.i-micronews.com/reports/Status-MEMS-Industry-2014/1/454/, (accessed in August 2014).
[2] MINAM Roadmap 2012, Version 1.4, October 2012.

[3] Qin Y, Brockett A, Ma Y, Razali A, Zhao J, Harrison C, et al. Micro-manufacturing: research, technology outcomes and development issues. Int J Adv Manuf Tech 2010;47:821−37.
[4] Alting L, Kimura F, Hansen HN, Bissacco G. Micro engineering. CIRP Ann Manuf Tech 2003;52(2):635−57.
[5] Liang SY. Mechanical machining and metrology at micro/nano scale. In: Proc. of SPIE − int. soc. for optical eng., v. 6280 I, third int. symp. on prec. mech. measurements; 2006. p. 628002.
[6] Luo X, Cheng K, Webb D, Wardle F. Design of ultraprecision machine tools with applications to manufacture of miniature and micro components. J Mats Proc Tech August 30, 2005;167(2−3):515−28.
[7] Sun X, Chen K. Multiscale simulation of the nano-metric cutting process. Int J Adv Manuf Tech 2010;47:891−901.
[8] Biermann D, Kahleyss F, Krebs E, Upmeier T. A study on micro-machining technology for the machining of NiTi: five-axis micro-milling and micro deep-hole drilling. J Mats Engng Perform 2011;20(4−5):745−51.
[9] Huo D, Lin C, Dalgarno K. An experimental investigation on micro machining of fine-grained graphite. Int J Adv Manuf Tech 2014;72(5−8):943−53.
[10] Liu J, Xu C. Interaction of the cutting tools and the ceramic-reinforced metal matrix composites during micro-machining: a review. CIRP J Manuf Sci Tech 2014;7(2): 55−70.
[11] Choi S, Lee S-M, Hong L, Park J-K, Lee DW. Nano/micro machining using multi-arrayed tool for nano/micro surface patterning. Proc ASPE 2011 Spring Top Meet Struct Free Surfaces 2011;51:59−62.
[12] Rajurkar KP, Levy G, Malshe A, Sundaram MM, McGeough J, Hu X, et al. Micro and nano machining by electro-physical and chemical processes. CIRP Ann Manuf Tech 2006;55(2):643−66.
[13] Uhlmann E, Sascha P, Schauer K. Micro milling of sintered tungsten−copper composite materials. J Mats Proc Tech 2005;167(2−3); 402−07.
[14] Maradia U, Boccadoro M, Stirnimann J, Beltrami I, Kuster F, Wegener K. Die-sink EDM in meso-micro machining. Proc 5th CIRP Conf High Perform Cut 2012;1(1):166−71.
[15] Richard J, Demellayer R. Micro-EDM-milling development of new machining technology for micro-machining. Procedia CIRP 2013;6:292−6.
[16] Bhattacharyya B, Munda J, Malapati M. Advancement in electrochemical micro-machining. Int J Mach Tools Manuf December 2004;44(15):1577−89.
[17] Mithu MAH, Fantoni G, Ciampi J, Santochi M. On how tool geometry, applied frequency and machining parameters influence electrochemical microdrilling. CIRP J Manuf Sci Technol 2012;5:202−13.
[18] Choi SH, Kim BH, Shin HS, Chung DK, Chu CN. Analysis of the electrochemical behaviors of WC−Co alloy for micro ECM. J Mats Proc Tech 621−30.
[19] Bassu M, Surdo S, Strambini LN, Barillaro G. Electrochemical micromachining as an enabling technology for advanced silicon microstructuring. Adv Funct Mats 2012; 22(6):1222−8.
[20] Geiger M, Kleiner M, Eckstein R, Tiesler N, Engel U. Micro-forming. Ann CIRP 2001;50(2):445−62.
[21] Engel U, Geibdorfer S. Microforming technology − on the way to industrial application?. In: Proc. 1st int. conf. micro-manufacturing, Urbana-Champaign, USA; September 2006. p. 21−30.

[22] Qin Y. Micro-forming and miniature manufacturing systems − development needs and perspectives. In: Keynote paper (plenary address) of the 11th int. conf. of metal forming, September 2006. J Mats Proc Tech 2006;177(1−3):8−18.
[23] Qin Y. Development of an integrated manufacturing facility for mass-manufacture of miniature/micro-products. In: Keynote paper, proc. of the 1st int. conf. on micro-manufacturing, Urbana-Champaign, USA; September 2006. p. 35−40.
[24] Vollertsen F. Size effects in micro forming. Key Engng Mats 2011;473:3−12. Sheet Metal 2011.
[25] Wang C, Shan DB, Guo B, Xu J, Zhang H. Effect of nano-crystals at surfaces induced by ion beam irradiation on the tribological behaviour in microforming. Vacuum 2013; 89:267−70.
[26] Castagne S, Taureza M, Song X. Surface textures and friction control in microforming. Adv Mats Res 2014;966−967:111−9.
[27] Hu Z, Wielage H, Vollertsen F. Economic micro forming using DLC- and TiN-coated tools. J Techn Plast 2011;36(2):51−8.
[28] Hung JC, Shieh CS. Development of an ultrasonic-vibration microforming apparatus. Adv Mats Res 2011;189−193:4092−6.
[29] Fu MW, Chan WL. A review on the state-of-the-art microforming technologies. Int J Adv Manuf Tech 2013;67(9−12):2411−37.
[30] Gillner A, Holtkamp J, et al. Laser applications in microtechnology. J Mats Proc Tech 2005;167(2−3):494−8.
[31] Xia M, Tu Y. An investigation of femtosecond laser micromachining. Proc 2005 Int Conf MEMS NANO Smart Syst: 2005:296−300.
[32] Bado P, Clark W, Said A. Micromachining Handbook. 2001. Clark-MXR, Inc. Ultrafast Laser Machining Division, 7300 West Huron River Dr. Ann Arbor, MI 48130.
[33] Li Y, Tian J, Sun Q. Micro-fabrication by femtosecond laser pulses. Proc SPIE Int Soc Opt Engng 2006;6149:61490X.
[34] Lehr J, Kietzig A-M. Production of homogenous micro-structures by femtosecond laser micro-machining. Opt Lasers Engng 2014;57:121−9.
[35] Malhotra R, Saxena I, Ehmann K, Cao, Jian J. Laser-induced plasma micro-machining (LIPMM) for enhanced productivity and flexibility in laser-based micro-machining processes. CIRP Ann Manuf Tech 2013;62(1):211−4.
[36] Demir AG, Previtali B, Lecis N. Development of laser dimpling strategies on TiN coatings for tribological applications with a highly energetic Q-switched fibre laser. Opt Laser Tech 2013;54:53−61.
[37] Malek CK, Saile V. Applications of LIGA technology to precision manufacturing of high-aspect-ratio micro-components and -systems: a review. Microelectron J February 2004;35(2):131−43.
[38] Hansen HN, Hocken RJ, Tosello G. Replication of micro and nano surface geometries. CIRP Ann 2011;60/2:695−714.
[39] Worgull M, Kolew A, Heilig M, Schneider M, Dinglreiter H, Rapp B. Hot embossing of high performance polymers. Microsyst Technol 2011;17(4):585−92.
[40] Kuo CC, Hsu HJ. Micro-hot embossing of fresnel lens using precision micro-featured mold. Mater Manuf Process 2013;28(11):1228−33.
[41] Schelb M, Vannahme C, Kolew A, Mappes T. Hot embossing of photonic crystal polymer structures with a high aspect ratio. J Micromech Microeng 2011;21:025017 (5 pp).

[42] Loh NH, Tor SB, Tay BY, Murakoshi Y, Maeda R. Micro powder injection molding of metal microstructures. Mater Sci Forum 2003;426−432(5):4289−94.
[43] Tosello G, Griffiths CA, Dimov SS, Scholz SG, Rees A, Whiteside B, et al. Analysis of demoulding in micro injection moulding of cyclic-olefin-copolymer microfluidic systems. 4M 2013, San Sebastian October 2013;8−10:65−8.
[44] Tosello G, Costa FS, Hansen HN. Micro injection moulding high accuracy three-dimensional simulations and process control. In: Proc. of polymer process enging. 11 − enhanced polymer processing, vols. 6−7; December 2011. p. 413−35. Bradford (UK).
[45] Hassanin H, Jiang K. Fabrication and characterization of stabilised zirconia micro parts via slip casting and soft moulding. Scr Mater 2013;69:433−6.
[46] Hassanin H, Jiang K. Net shape manufacturing of ceramic micro parts with tailored graded layers. J Micromech Microeng 2014;24:015018 (8 pp).
[47] Lu D, Yang Y, Qin Y, Yang G. Forming microgears by Micro-FAST technology. J Microelectromech 2013;22:708−15.
[48] Huang K, Yang Y, Qin Y, Yang G. 316L stainless steel powder densification during the coupled multi-Fields activated micro-forming. Mater Manuf Process 2013;28:183−8.
[49] Kadekar V, Fang W, Liou F. Deposition technologies for micromanufacturing: a review. ASME Trans J Manuf Sci Engng Nov. 2004;126:787−95.
[50] Li XC, Choi H, Yang Y. Micro rapid prototyping system for micro components. Thin Solid Films December 2, 2002;420−421:515−23.
[51] Kumar P, Das S. Fabrication of meso- and micro-structured devices by direct-write deposition and laser processing of dry fine powders. ASME Int Mech Engng Congr Expo 2004:519−24.
[52] Dvorak P. Manufacturing macro and micro designs. Mach Des October 10, 2003:76−8.
[53] Amon CH, Beuth JL, Merz R, Prinz FB. Shape deposition manufacturing with microcasting: processing, thermal and mechanical issues. J Manuf Sci Engng Tran ASME August 1998;120(3):656−65.
[54] Bardt JA, Ziegert JC, Schmitz T, Sawyer WG, Bourne G. Precision molding of complex metallic micro-structures. In: Proc. of the 1st int. conf. on micro-manufacturing, Champaign, IL, USA; September 2007. p. 274−9.
[55] Ryu BH, Choi YM. Application of inkjet technology in flat panel display. Proc Int Meet Information Disp 2006;2:913−8.
[56] Ko SH, Pan H, Lee D, Grigoropoulos CP, Park HK. Nanoparticle selective laser processing for a flexible display fabrication. J Appl Phys 2010;49:05EC03.
[57] Ko SH, Chung J, Hotz N, Nam KH, Grigoropoulos CP. Metal nanoparticle direct inkjet printing for low temperature 3D micro metal structure fabrication. J Micromech Microeng 2010;20:125010.
[58] Kullmann C, Hotz N, Schirmer NC, Lee M-T, Ko SH, Grigoropoulos CP, et al. 3D micro-structures by piezoelectric inkjet printing of gold nanofluids. J Micromech Microeng 2012;22:055022.
[59] Tang PT. Electroforming: from rocket engines to nanotweezers. J Micro Nanosyst 2011;3(3):180−7.
[60] Najafi K. Micropackaging technologies for integrated microsystems: applications to MEMS and MOEMS. Proc SPIE Int Soci Opt Engng 2003;4982:ix−xxvii.
[61] Huang T, Nilsen E, Ellis M, Kim K, Tsui K, Skidmore G, et al. 3-D, self-aligned, micro-assembled, electrical interconnects for heterogeneous integration. Proc SPIE Int Soci Opt Engng 2003;4981:189−201.

[62] Michaeli W, Opfermann D. Micro assembly injection moulding. Microsyst Technol June 2006;12(7):616−9.
[63] Martukanitz RP. A critical review of laser beam welding. In: Proceedings of SPIE − int. soci. for optical engng., v. 5706, critical review: industrial lasers and applications; 2005. p. 11−24.
[64] Cecil J, Vasquez D, Powell D. A review of gripping and manipulation techniques for micro-assembly applications. Int J Prod Res February 15, 2005;43(4):819−28.
[65] Fantoni G, Santochi M, Dini G, Tracht K, Scholz-Reiter B, Fleischer J, et al. Grasping devices and methods in automated production processes. CIRP Ann 2014;63/2:679−701.
[66] Heaney DF. Mass production of micro-components utilising lithographic tooling and injection molding technologies. In: Proc. of the 1st int. conf. on micro-manufacturing, Champaign, IL, USA; September 2007. p. 280−3.
[67] Palmer JA, Williams JD, Lemp T, Lehecka TM, Medina F, Wicker RB. Advancing three-dimensional MEMS by complimentary laser micro manufacturing. Proc SPIE Int Soci Opt Engng 2006;6109:61090A.
[68] Sharon A, Bilsing A, Lewis G, Zhang X. Manufacturing of 3D microstructures using novel UPSAMS process (ultra precision manufacturing of self-assembled micro systems). Proc IEEE Micro Electro Mech Syst (MEMS) 2003:542−5.
[69] Pfleging W. Rapid fabrication of microcomponents − UV-laser assisted prototyping, laser micro-machining of mold inserts and replication via photomolding. Microsyst Technol 2003;9(1−2):67−74.
[70] Booth HJ. Recent applications of pulsed lasers in advanced materials processing. Thin Solid Films 2003;453−454:450−7.
[71] Lauwers B, Klocke F, Klink A, Tekkaya E, Neugebauer R, Mcintosh D. Hybrid processes in manufacturing. Ann CIRP 2014;63/2:561−83.
[72] Kuo CL, Huang JD, Liang HY. Fabrication of 3D metal microstructures using a hybrid process of micro-EDM and laser assembly. Int J Adv Manuf Tech 2003;21(10−11): 796−800.
[73] Chen JW, Zybko J, Clements J. Diode laser bonding of planar MEMS, MOEMS, and microfluidic devices. In: Mater. res. soci. sympo. proc., v. 872, micro- and nanosystems − materials and devices; 2005. p. 309−14.
[74] Okazaki Y, Mishima N, Ashida K. Microfactory − concept, history and development. ASME Trans J Manuf Sci Engng November 2004;126:837−44.
[75] Ashida K, Nakano S, Park J, Akedo J. On-demand MEMS device production system by module-based microfactory. Int J Automation Technol 2010;4(2):110−6.
[76] Tuokko R, Järvenpää E, Heikkilä R, Nurmi A. Micro and desktop factories for micro/meso-scale manufacturing applications and future visions. Appl Mech Mater 2013; 289:1−12.
[77] Qin Y, Perzon E, Chronakis I, Calderon I, Konrad K, Hartl C, et al. Process chain and POLYTUBES micro-factory concept. In: The 8th int. conf. on micro-manufacturing, Victoria, Canada; March 2013. p. 211−8.
[78] Arentoft M, Eriksen RS, Hansen HN, Paldan NA. Towards the first generation micro bulk forming system. CIRP Ann Manuf Tech 2011;60(1):335−8.
[79] Mahshid R, Hansen HN, Arentoft M. Characterization of precision of a handling system in high performance transfer press for micro forming. CIRP Ann 2014;64(1):497−500.
[80] Qin Y, Ma YL, Harrison C, Brockett A, Zhou M, Zhao J, et al. Development of a new machine system for the forming of micro-sheet-products. Int J Material Form April 2008:1−4. http://dx.doi.org/10.1007/s12289-008-0098-9.

[81] Qin Y, Razali AR, Zhou M, Zhao J, Harrison C, Nawang W. Dynamic characteristics of a micro-sheet-forming machine system. Key Engng Mater 2012;504−506:599−604.
[82] Razali A, Qin Y, Zhao J, Harrison C, Smith R, Eguia J, et al. A newly developed high-precision feeder for micro-sheet-forming. J Manuf Sci Engng Trans ASME December 2012;133(6). p. 061025−1 to 7.
[83] Zhao J, Brockett A, Razali A, Qin Y, Harrison C, Ma Y. Micro-sheet-forming and case studies. Steel Res Int September 2010;81(9). In: 13th int. conf. on metal forming, Toyohashi, Japan; 1185−88.
[84] Hartl C, Lungershausen J, Eguia J, Uriarte G, Lopez Garcia F. Micro hydroforming process and machine system for miniature/micro products. In: Proc of int conf 7th euspen, Bremen, vol. 2; 2007. p. 69−72.
[85] Hartl C, Anyasodor G. Experimental and numerical investigations into micro-hydroforming processes and machine design. In: Proc. of the 13th int. conf. on metal forming, Toyohashi, Japan; 2010. p. 1193−6.
[86] Hartl C, Anyasodor G, Lungershausen J. Formability of micro-tubes in hydroforming. In: Proc. of int. EASEFORM conf., Belfast; 2011. p. 529−34.
[87] Huo D, Cheng K. Design of a 5-Axis ultraprecision micro milling machine − ultramill: part 1: holistic design approach, design considerations, and specifications. Int J Adv Manuf Tech April 2010;47(9−12):867−77.
[88] Huo D, Cheng K. Design of a 5-Axis ultraprecision micro milling machine − ultramill: part 2: integrated dynamic modelling, design optimization and analysis. Int J Adv Manuf Tech April 2010;47(9−12):879−90.
[89] Jia BX, Wang ZL, Hu FQ, Li XH, Zhao WS. Research on multifunctional micro machining equipment. In: Materials science forum. Adv. in mater. manuf. sci. and tech, vols. 471−472; 2004. p. 37−42.
[90] Zhou LB, Yaguchi Y, Fujii T, Shimizu J, Eda H. Development of a multifunctional micro-machining system and its applications. Key Engng Mater 2003;238−239:3−8.
[91] Liao YS, Chen ST, Lin CS. A multi-function high precision tabletop CNC machine for making micro-parts developed in National Taiwan University. In: Proc. of the 1st ICOMM; September 2006. p. 48−52.
[92] Rahman M, Lima HS, Neo KS, Senthil Kumara A, Wong YS, Li XP. Tool-based nano-finishing and micromachining. J Mats Proc Tech 2007;185(1−3):2−16.
[93] Sanchez-Salmeron AJ, Lopez-Tarazon R, Guzman-Diana R, Ricolfe-Viala C. Recent development in micro-handling systems for micro-manufacturing. J Mats Proc Tech August 30, 2005;167(2−3):499−507.
[94] Sanchez AJ, Ricolfe C. A flexible packaging station for micro-bulk-forming applications based on a standard carrier. Int J Adv Manuf Tech 2012;61(5−8):529−36.
[95] Hauptmann PR. Selected examples of intelligent (micro) sensor systems: state-of-the-art and tendencies. Meas Sci Tech March 1, 2006;17(3):459−66.
[96] Fleischer J, Lanza G, Schlipf M, Behrens I. Quality assurance in micro production. Microsyst Technol June 2006;12(7):707−12.
[97] Hansen HN, Carneiro K, Haitjema H, De Chiffre L. Dimensional micro and nano metrology. CIRP Ann Manuf Tech 2006;55(2):721−43.
[98] Tosello G, Hansen HN, Gasparin S. Applications of dimensional micro metrology to the product and process quality control in manufacturing of precision polymer micro components. CIRP Ann Manuf Tech 2009;58(1):467−72.
[99] Qian J, Wang J, Ferraris E, Reynaerts D. A holistic approach for zero-defect micro-EDM milling. Proc IEEE Int Sympo Assembly Manuf 2013:226−9.

[100] Gasparin S, Tosello G, Hansen HN, Islam A. Quality control and process capability assessment for injection-moulded micro mechanical parts. Int J Adv Manuf Tech 2013;66(9−12):1295−303.
[101] Fleischle D, Lyda W, Mauch F, Osten W. Optical metrology for process control: modeling and simulation of sensors for a comparison of different measurement principles. Proc SPIE Int Soci Opt Engng 2010;7718. Article number: 77181D.
[102] Li Y, Su R, Hedlind M, Ekberg P, Kjellberg T, Mattsson L. Model based in-process monitoring with optical coherence tomography. In: 1st CIRP global Web conf.: interdisciplinary research in production engineering, CIRPE 2012 Procedia CIRP 2012; 2(1):70−3.
[103] Moylan SP, Damazo B, Donmez MA. Implementation of a metrology frame to improve positioning of MICRO/MESO-scale machine tools. Trans NAMRI SME 2009;37:573−80.
[104] Manske E, Jäger G, Hausotte T, Fül R. Recent developments and challenges of nanopositioning and nanomeasuring technology. Measur Sci Tech 2012;23(7). Article number: 074001.
[105] Schitter G, Steininger J, Heuck F, Staufer U. Towards fast AFM-based nanometrology and nanomanufacturing. Int J Nanomanuf 2012;8(5−6):392−418.

This page intentionally left blank

CHAPTER

Micro-/Nano-machining through Mechanical Cutting

2

Xizhi Sun, Kai Cheng

Advanced Manufacturing & Enterprise Engineering, Brunel University, Uxbridge, UK

CHAPTER OUTLINE

INTRODUCTION

The emergence of miniature and micro-products and components is increasingly demanding the production of parts with dimensions in the range of a few tens of nanometers to a few millimeters. Micro-/nano-cutting is one of the key technologies

Micromanufacturing Engineering and Technology. http://dx.doi.org/10.1016/B978-0-323-31149-6.00002-5

to enable the realization of micro-products, while a great many micro-manufacturing processes have been developed.

In this chapter, micro-/nano-cutting is defined as the fabrication of miniature and micro-components using geometrically defined cutter edges. Typical micro-/nano-cutting operations include micro-milling, micro-turning, micro-drilling, and micro-grinding.

Similarly to the conventional cutting operation, in micro-/nano-cutting, the surface of the workpiece is mechanically removed using tools, but the depth of cut is normally at the level of a micrometer or less. As the unit removal size decreases, issues of tool cutting edge geometry, grain size, orientation, etc., considered to have little or no influence at larger scales, become dominant factors with strong influences on the resulting machining accuracy, surface integrity, and quality of the machined component [1]. In this chapter, therefore, emphasis is placed on the issues that prevail in micro-/nano-cutting, which is essentially different from the conventional cutting process. Furthermore, the chapter focuses on the precision machines for micro-/nano-cutting and the application of the process in various fields.

FUNDAMENTALS OF THE MICRO-/NANO-CUTTING PROCESS

While the mechanisms of conventional cutting are well established, micro-/nano-cutting mechanics and the associated intricate issues are less well understood. The depths of cut involved are several orders of magnitude smaller than those of conventional cutting, so that it is necessary to examine closely the micro-/nano-cutting process. Unlike conventional machining, where shear and friction dominate, micro-/nano-cutting may involve significant sliding along the flank face of the tool due to the elastic recovery of the workpiece material. The effects of plowing may also become important due to the large effective negative rake angle resulting from the tool edge radius. In addition, the subsurface plastic deformation and the partition of thermal energies may also be quite different from those of traditional cutting [2]. This section discusses the fundamentals of the micro-/nano-cutting process.

SPECIFIC ENERGY AND CUTTING FORCE

Specific energy and cutting force are important physical parameters for understanding cutting phenomena, as they clearly reflect the chip removal process. As shown in Figure 1 [3], the specific energy generally increases with the decreasing depth of cut, within the range from 10 nm to 20 μm. This is because the effective rake angle will increase as the depth of cut decreases, and the larger the rake angle the greater the specific energy. This phenomenon is often called the "size effect."

Micro-/nano-cutting is also characterized by the high ratio of the normal to the tangential components of the cutting force, as shown in Figure 2 [3], that is, the resultant cutting force becomes closer to the thrust direction when the depth of cut becomes smaller. Since the depth of cut is very small in micro-/nano-cutting, the workpiece is mainly processed by the cutting edge and compression will thus

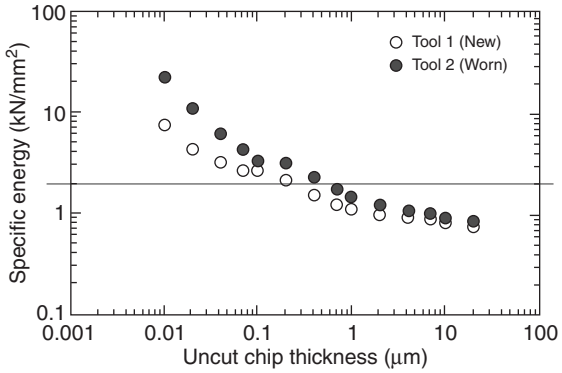

FIGURE 1

Specific energy versus uncut chip thickness for new and worn diamond tools.

become dominant in the deformation of the workpiece material, which will result in larger friction force at the tool/chip interface and consequently in a greater cutting ratio. This indicates a transition from the shearing-dominated process in conventional cutting to a plowing-dominated process in micro-/nano-cutting.

MINIMUM CHIP THICKNESS AND CHIP FORMATION

The definition of minimum chip thickness is the minimum undeformed chip thickness below which no chip can be formed stably.

Figure 3 shows the chip formation with respect to the chip thickness [4]. In Figure 3(a), where the uncut chip thickness, h, is smaller than the minimum chip thickness, h_c, only elastic deformation results and no workpiece material will be removed by the cutter. When the uncut chip thickness approaches the minimum

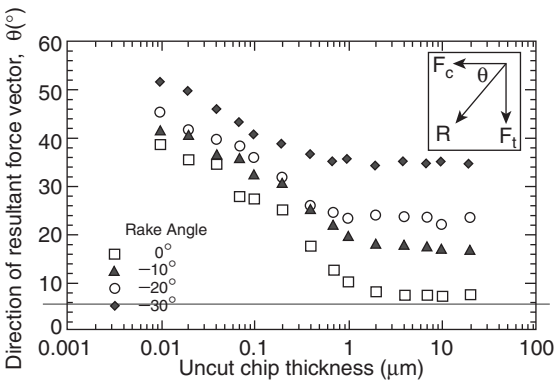

FIGURE 2

Resultant force vector versus uncut chip thickness at various rake angles.

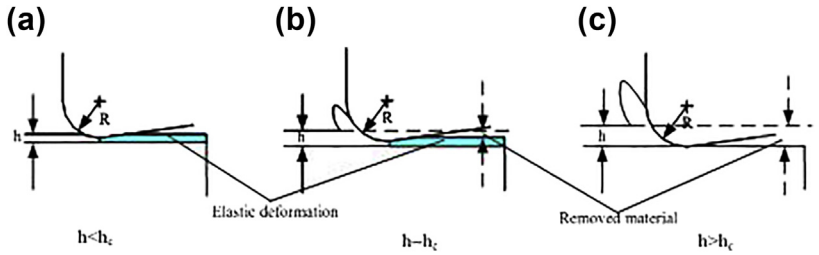

FIGURE 3

Schematic diagram of the effect of the minimum chip thickness.

chip thickness, as shown in Figure 3(b), chips will be formed due to the shearing of the workpiece. However, since elastic deformation still exists, the removed depth is generally smaller than the desired depth. If the uncut chip thickness is larger than the minimum chip thickness, as shown in Figure 3(c), elastic deformation is significantly reduced and results in the removal of the entire depth of cut as a chip.

Due to this minimum chip thickness effect, the micro-/nano-cutting process is affected by two mechanisms: chip removal ($h > h_c$) and plowing/rubbing ($h < h_c$). From a practical point of view, the minimum chip thickness is a measure of the extreme machining accuracy attainable because the generated surface roughness is mainly attributed to the plowing/rubbing process when the uncut chip thickness is less than the minimum chip thickness. The extent of plowing/rubbing and the nature of the micro-deformation during plowing/rubbing contribute significantly to increased cutting forces, burr formation, and increased surface roughness. Therefore, knowledge of the minimum chip thickness is essential in the selection of appropriate machining conditions [5]. Ikawa et al. [6] obtained an undeformed thickness on the order of a nanometer, as shown in Figure 4, by a well-defined diamond tool with an edge radius of around 10 nm.

The minimum chip thickness depends on the cutting edge radius, workpiece material, and the micro-cutting of steel. For example, Vogler et al. [7] conducted finite element (FE) simulation of the micro-cutting of steel, finding that the minimum chip thickness is 20% and 30% of the cutting edge radius for the pearlite and ferrite, respectively. However, Shimada et al. [8] observed that the minimum chip thickness can be around 5% of the cutting edge radius for the cutting of copper and aluminum, through molecular dynamics (MD) simulation.

DUCTILE MODE CUTTING

The machining of brittle materials such as germanium, silicon, and optical glasses at a large depth of cut in conventional cutting has a tendency to generate a rough surface and subsurface cracking. As a result, the machining of brittle materials is normally achieved using conventional processing techniques such as polishing. However, intricate features, the surface finish quality of the workpiece produced,

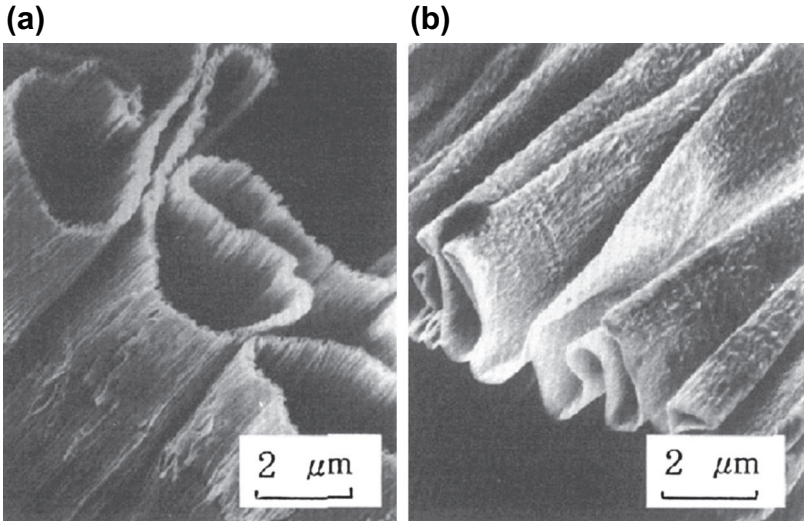

FIGURE 4

Scanning electron micrographs of chips generated from nanometric cutting; (a) thickness of chip 1 nm; (b) thickness of chip 30 nm.

and a greater material removal rate of processing demand an effective means for the fabrication of brittle materials.

There is a transition in the material removal mechanism of brittle materials, from brittle to ductile, when the depth of cut decreases [9]. Based on this feature, cutting in a ductile mode below the critical depth of cut has been attempted with the aim of obtaining a good surface finish and an uncracked surface. Since the chip thickness in micro-cutting can be of the order of the critical depth of cut, micro-cutting can serve as a novel means of fabricating unique features with brittle materials that are not achievable by polishing or other techniques [1].

The results of many research studies indicate that the tool geometry and the cutting conditions are two major factors affecting the value of the critical depth of cut. It was found that the critical depth of cut increases with the increase of the cutting velocity and the negative rake angle [10,11]. However, it is difficult to achieve ductile mode cutting with a greater feed rate, as shown in Figure 5 [12].

EFFECT OF WORKPIECE MATERIAL MICRO-STRUCTURE

The crystalline grain size of most workpiece materials is of the same order as the depth of cut in micro-cutting, so that chip formation normally takes place by the breaking up of the individual grains of a polycrystalline material. Most polycrystalline materials are thus treated as a collection of grains with random orientation and anisotropic properties [1]. The crystalline graphic orientation affects the chip formation, the surface generation, and the variation of the cutting forces [13]. There is a

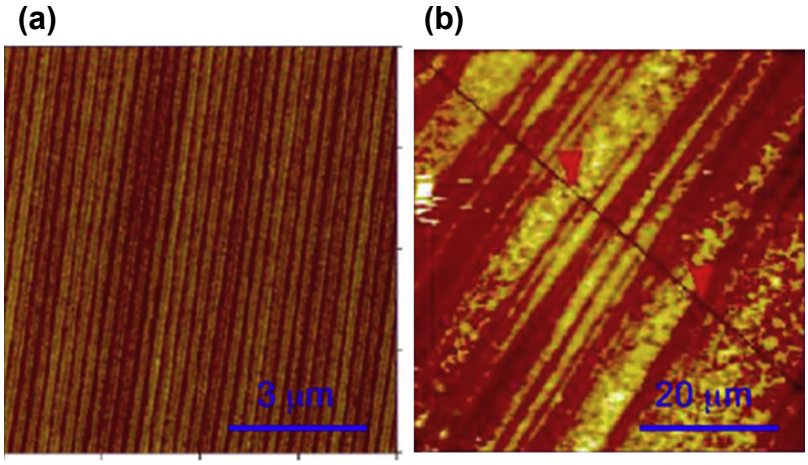

FIGURE 5

Silicon surfaces machined at a cutting speed of 90 m/min and a depth of cut of 1 μm: (a) feed rate of 0.4 mm/min (ductile mode cutting) and (b) feed rate of 1 mm/min (brittle mode cutting).

distinct difference between micro-cutting and conventional cutting, where the material can be treated as isotropic and homogeneous. To et al. [14] obtained the effects of the crystallographic orientation and the depth of cut on the surface roughness by conducting the diamond turning of single-crystal aluminum rods, as illustrated in Figure 6.

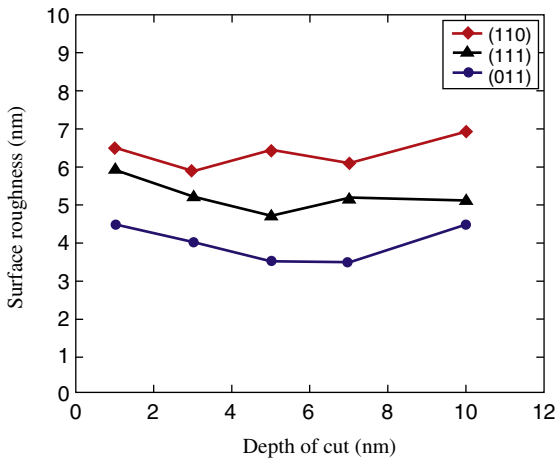

FIGURE 6

The effects of the crystallographic orientation and the depth of cut on the surface roughness.

MODELING THE MICRO-/NANO-CUTTING PROCESS

In the past, extensive cutting tests were performed to understand cutting mechanics and optimize various cutting process variables. However, it is difficult to investigate the micro-/nano-cutting process solely by the experimental approach due to the substantial cost of micro-tooling, the required careful preparation of samples, and the considerable amount of testing involved on machine tools, which is both time consuming and expensive. Furthermore, the in-process observation and accurate measurement of results are also very challenging.

The micro-/nano-cutting process is very complex because of the size effect, elastic/plastic deformation and fracture with high strain rates, and varying material properties during the process. Analytical modeling is thus considered extremely difficult at the current level of understanding of material behavior. Most analytical modeling efforts are based on kinematics from empirical observation combined with classical cutting models at the macro-level. The applicability and accuracy of these models are subject to many limitations [1].

Although analytical models involve many assumptions, the numerical modeling of micro-/nano-cutting provides a powerful tool to assist scientific understanding of the process. Using numerical models, the effects of various cutting conditions can be obtained easily and effectively while undertaking less expensive experiments. FE modeling (FEM) and MD modeling are two popular numerical modeling and simulation techniques for micro-/nano-cutting. More recently, multiscale modeling methods based on combining FEM and MD have emerged to overcome the disadvantages of each method and to enable the simulation of the cutting process more realistically.

In the following subsections, details of these key modeling methods of micro-/nano-cutting are discussed, with examples presented from published research work.

FE MODELING

The FE method is based on the principle of continuum mechanics, in which materials are defined as continuous structures and the effects of micro-constituents such as crystal structure, grain size, and interatomic distances are ignored. In an FE model, only the value of the variables of nodes can be obtained exactly between the nodes, the values of the variables are determined by interpolation [15]. Hence, the number of nodes and the distances between the nodes are selected based on the required calculation accuracy.

The application of FE simulation to the cutting process provides an effective means to understand the mechanics and characteristics of the cutting process. A typical FE cutting model is shown in Figure 7 [15], where the workpiece is fixed and the tool is in motion. During cutting simulation, the interaction of nodes between the interface of the workpiece and the tool is transferred to other nodes of the workpiece. The interactions between nodes can be described by three kinds of FE formulation: Lagrangian formulation, which requires a remeshing algorithm

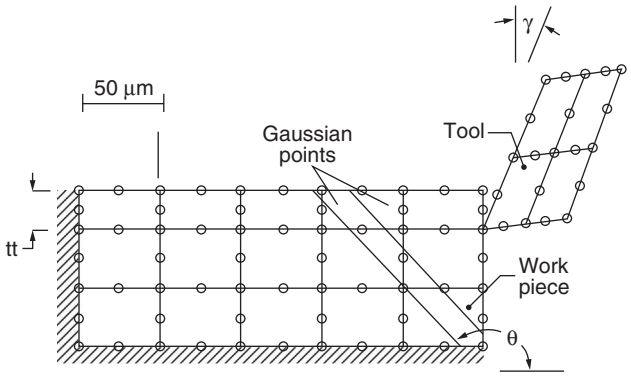

FIGURE 7

An illustration of a finite element modeling cutting model.

or a chip separation criterion to form the chip; Eulerian formulation, which needs a prior assumption of a chip shape; and arbitrary Lagrangian Eulerian formulation. For the description of large plastic deformation and large strain rate of a material during the cutting process, the well-known Johnson–Cock formulation is often used.

The application of the FE method in cutting has been attracting a lot of research interest since the 1970s. Although micro-cutting could be significantly different from conventional cutting, the governing principles, e.g., plasticity and tool/chip tribology, should remain but be heavily subject to the size effect [16]. According to these principles, various aspects in the micro-cutting process have been investigated using the FE method, which include the following:

- Material removal and chip formation;
- Effects of tooling geometry and process parameters;
- Effects of material micro-structure;
- Residual stress in micro-cutting.

Moreover, some research areas that usually are conducted by MD have been recently investigated with FE method, such as:

- Influence of workpiece crystallographic orientation on the cutting and thrust-specific energies of the process.
- Size effect and minimum cutting thickness.
- Temperature of tool tip and workpiece.

MD MODELING

MD simulation is a well-established methodology for detailed microscopic modeling at the molecular scale. It is based upon a model of the molecules of the matter or system concerned, according to their atomic structure. Potential

functions are used to describe the molecular interactions, and the interatomic forces can be derived from the differentiation of the potential function. The motions of individual atoms are usually assumed to be governed by Newton's second law. The numerical solutions to the motion equations give the trajectories of the atoms, which can be used to determine the macroscopic static and dynamic characteristics of the system.

In the late 1980s, a research group in Lawrence Livermore National Laboratory (LLNL) started the MD simulation of the diamond turning of single-crystal copper [17]. Since then, MD has been successfully applied to a variety of phenomena in micro-/nano-cutting.

A typical nanometric cutting MD model is shown in Figure 8 [8], which was used to study the feasibility of ultimate accuracy of micro-cutting by Shimada [8]. The model consists of a workpiece and a rigid diamond tool. In the model, the two layers of atoms in the left side of the workpiece and the bottom of the work material are kept fixed, and a thermostat zone is applied to conduct away the heat generated in cutting region. The temperature of the thermostat atoms is maintained same by scaling the velocities of the atoms. Parameters used in the simulation are summarized in the Table 1 [8].

The topics investigated by MD simulation are as follows:

1. The effect of crystal orientation on surface roughness;
2. Chip formation and the machined surface generation;
3. Minimum undeformed chip thickness in nanometric cutting;
4. Cutting forces and cutting temperature;
5. Side flow and pileup phenomena in the cutting process;
6. Surface integrity.

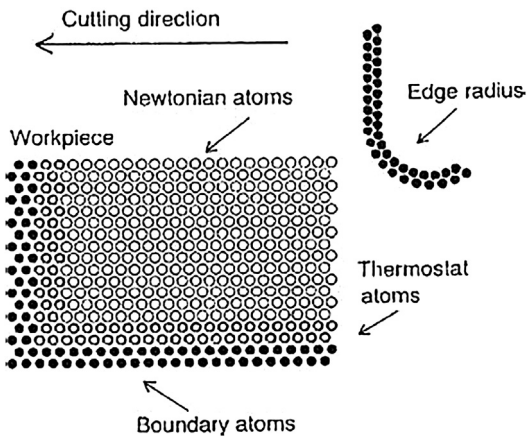

FIGURE 8

An illustration of an molecular dynamics simulation model.

Table 1 Parameters of the Molecular Dynamics Simulation

Material	2-D Morse potential (Cu, Al)
Configuration	2-D orthogonal cutting
Cutting speed	20,200 m/s
Uncut chip thickness	0.1–1.2 nm
Tool edge radius	2,5,10 nm
Rage angle	0
Clearance angle	7
Width of cut	1 atomic layer
Bulk temperature	293 K
Number of work atoms	54,008,000
Number of tool atoms	676,172
Computation time step	1,10 fs

Although MD simulation has become a useful tool in analyzing the nanometric machining process, further research and development are expected in the following areas:

1. Improvement of the model dimensions and computational speed;
2. Establishing more accurate potential functions for workpieces and cutting tools;
3. Developing a material model including defects, such as vacancies, dislocations, grain boundaries;
4. Tool wear simulation.

MULTISCALE MODELING

MD simulation and the FE method have been successfully applied in the simulation of the machining process. However, the two methods have their own respective limitations. For example, MD simulation can only cover the phenomena occurring at nanometric scale because of the physical dimension, computational cost, and scale, while the FE method is suited to model meso- and macro-scale machining and to simulate macro-parameters such as the temperature in the cutting zone, the stress/strain distribution, and cutting forces, etc. A natural approach to the simulation of multiscale processes is to combine an MD simulation for the critical regions within the system with an FE method for continuum coverage of the remainder of the system. The hybrid approach provides an atomistic description near the interface and a continuum description deep into the substrate, increasing the accessible dimensional scales and greatly reducing the computational cost while increasing the modeling accuracy and capacity.

Several multiscale simulation methods have been developed such as the FE atomistic method, the quasi-continuum (QC) method, the macro-atomistic ab-initio dynamics method, and the coarse-grained molecular dynamics method. A remarkably successful approach is the QC method proposed by Tadmor et al. in 1996 [18].

QC is a way of simulating the macro-scale nonlinear deformation of crystalline solids using MD.

Application of multiscale methods to micro-/nano-machining is still in their earlier stage, and only a few studies have been conducted on the multiscale simulation of micro-/nano-cutting. Shiari et al. performed multiscale simulation on nanometric cutting of single-crystal aluminum, in which the atomistic details of material removal, chip formation, surface evolution, generation and propagation of dislocations for a wide range of tool speeds are investigated [19]. Before that, authors developed a multiscale model for nanometric cutting of single-crystal copper showing capabilities of the QC approach. Later, the chip formation and propagation of atomistic dislocations were examined for nanometric cutting of single-crystal aluminum by the authors using the QC method [20,21].

Figure 9 is a schematic diagram of the model developed by the authors for the multiscale simulation of nanometric cutting of single-crystal copper [20]. It can be seen that the mesh density becomes greater when proceeding upward. At the top the interface meshes disappear, and there are atoms instead of mesh, entirely. The size of the work material is 0.2×0.1 μm, taking into account the transition from nanometer to micrometer. The number of atoms to be computed at the 50th step time is no more than 20,000, which is much less compared to 1.25×10^7 atoms included in the model for MD simulation. This model is an embodiment of the concept of multiscale simulation for micro-machining.

Figure 10 shows the simulation plots at the first time step, the 50th time step, and the corresponding atoms' velocity contour line.

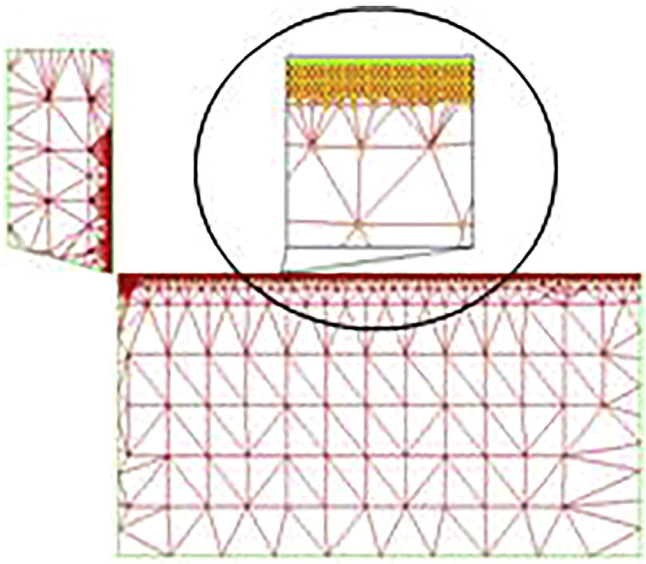

FIGURE 9

Multiscale model for nanometric cutting of single-crystal copper.

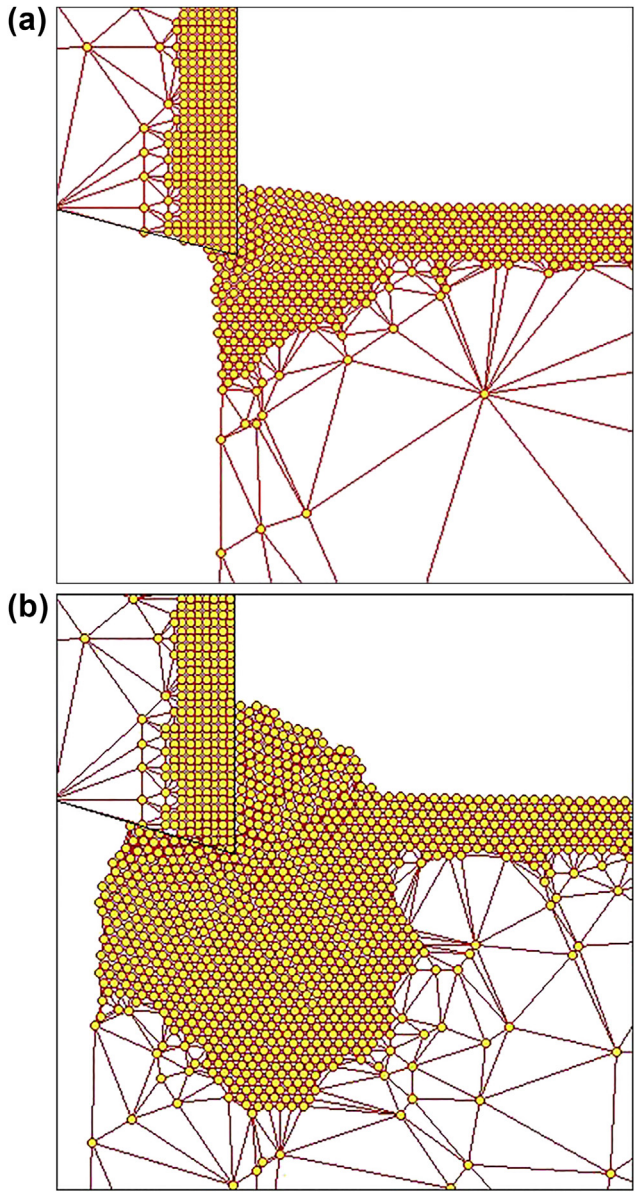

FIGURE 10

Instantaneous diagram of copper's cutting simulation by the multiscale method: (a) at the first time step; (b) at the 50th time step.

In addition, Aly et al. proposed a hybrid MD-FEM approach via hierarchical modeling for the simulation of micro-machining of silicon. In this method, the material properties applied in the FE model were achieved from the MD simulation of a uniaxial tension performed on silicon [22].

The future research studies on the multiscale simulation of micro-/nano-cutting should focus on the following areas:

- Improving the model dimensions and speed.
- Developing more material models at multiscale.
- Investigating phenomenon occurred during micro-/nano-cutting processes such as size effect, effect of crystal orientation on the surface roughness, etc., using multiscale method.

PRECISION MACHINES FOR MICRO-/NANO-CUTTING

ULTRAPRECISION MACHINE TOOLS

Ultraprecision machine tools play an important role in the implementation of micro-/nano-cutting, while they directly determine machining accuracy, productivity, producibility, and repeatability. There have been great market demands for ultraprecision machine tools, which are capable of machining increasingly more complex-structured components and products (e.g., axially asymmetric surfaces and free-form surfaces) with greater accuracy and finer surface finish, and coping with any newly emerging materials for high-throughput and cost-effective manufacturing. These demands and requirements have led to the significant development of a new generation of machine tools.

Figure 11 illustrates a five-axis ultraprecision micro-milling machine, developed at Brunel University. A typical ultraprecision machine tool has five major subsystems, including a mechanical structure, a spindle and drive system, a control system, a position measurement and feedback system, and an in-process condition monitoring and inspection system. These subsystems critically determine the performance of the overall machine tool system.

MECHANICAL STRUCTURE

The mechanical structure provides a framework and mechanical support for all the machine components. It encompasses important components such as the machine base, column, worktable, slide, spindle cases, and carriages. The major factors for machine design and selection include [24] the following:

1. Structural configuration;
2. Stiffness and damping;
3. Structural connectivity and interface;
4. Structure dynamics and associated performance.

FIGURE 11

Schematic figure of a five-axis micro-milling machine [23].

A robust design of mechanical structure should aim to achieve high structural loop stiffness, good damping properties, a symmetrical and closed-loop structural configuration, minimization of heat deformation, long-term stability, and isolation of environmental effects.

Material is also a key factor in determining the final machine performance. While cast iron and granite have been widely used for fabricating machine bases and slideways, polymer concrete has become popular for ultraprecision machine tools where light weight with high damping capacity and rigidity is required. Structural materials with a low thermal expansion coefficient and high dimensional stability have also found application, including super invar, synthetic granite, ceramics, and Zerodur.

SPINDLE AND DRIVE SYSTEM

The spindle is a key component of a precision machine and it has significant impact on machined components in terms of form/dimensional accuracy and surface quality. Two types of spindles are most commonly used in precision machine tools, i.e., aerostatic bearing spindles and oil hydrostatic bearing spindles. They are capable of high rotational speed with high motion accuracy. Aerostatic bearing spindles usually have lower stiffness than oil hydrostatic bearing spindles, but they have lower thermal deformation than the latter. Aerostatic bearing spindles are widely used in machine tools with medium and small loading capacity, whereas oil hydrostatic bearing spindles are more suitable for large and heavily loaded machine tools.

More recently, the groove technique has been used in the design of bearings. A grooved hybrid air bearing combines aerostatic and aerodynamic design principles to optimize ultrahigh speed performance.

Several drive mechanisms can be used for ultraprecision machine tools, including piezoelectric actuators, linear motor direct drives, and friction drives. Piezoelectric actuators usually have a short stroke with high motion accuracy and wide response bandwidth. They have been employed in fine tool positioning so as to achieve high precision control of the cutting tool (e.g., a diamond-cutting tool).

Linear motor direct drives (AC or DC) usually have a long stroke and they do not need conversion mechanisms such as lead screws, and racks and pinions. They offer better stiffness, acceleration, speed, motion smoothness, repeatability, accuracy, etc. [24], although their applications in the machine tools industry are still relatively new.

Friction drives also have a long stroke and usually consist of a driving wheel, a flat or round bar, and a supporting backup roller. They offer low friction force, smooth motion, and good repeatability and reproducibility due to elastic deformation induced by the preload.

CONTROL SYSTEM

Following the invention of Computer Numerical Control (CNC) in the early 1970s, many companies started to develop their control systems for machine tools. The control system typically includes motors, amplifiers, switches, and the controller. High-speed multiaxis CNC controllers play an essential role in efficient and precision control of servo drives, error compensation (thermal and geometrical errors), optimized tool setting, and direct entry of the equation of shapes [25]. Advanced PC-based control systems have achieved nanometer or even subnanometer levels of control resolution for ultraprecision and micro-manufacturing purposes, such systems also being used commonly in the majority of commercially available ultraprecision machines.

POSITION MEASUREMENT AND FEEDBACK SYSTEM

Ultraprecision machine tools necessarily require an ultraprecision position measurement and feedback system. Laser encoders (laser-interferometer based) are particularly suitable because interferometers have an intrinsically high resolution. Interferometers also have the ability to eliminate Abbe errors. They have a typical resolution of 20 nm (digital), and subnanometer resolution can also be achieved with an analog system via external interpolation. The installation may be made simpler by means of fiber-optics laser launch and integrated interferometer optics. Some laser holographic-linear scales have a resolution of better than 10 nm.

Another alternative technique is to use ultrahigh resolution optical encoders. They can provide resolution close to that of laser encoders, but in a more industrially feasible and simple manner. There is a trend of more optical encoders being adopted on industrially used precision and ultraprecision machines.

IN-PROCESS CONDITION-MONITORING AND INSPECTION SYSTEM

Intelligent and smart machine tools are an important development for ultraprecision applications. To meet these requirements, some sensors are generally required to monitor the operation of the machine tool and to combine multifunctionality, reliability, sensitivity, and compactness. Monitoring the machining status during ultraprecision machining is usually difficult because of the associated very small energy emissions and cutting forces compared with the conventional machining processes. Thermal effects have been known to be the largest source of dimensional errors. It is therefore important to implement online temperature monitoring. Condition monitoring may be also applied to other parameters or variables, e.g., cutting force, chatter, and vibration. It is desirable to use multiple sensors to realize the smart and intelligent machine tool. Furthermore, tool wear, tool breakage, and its engaging process demand a great deal of attention in micro-/nano-machining because of the high precision and fragile micro-tools involved.

MICRO- AND MESO-MACHINES

Traditional ultraprecision machines are currently the major means for undertaking micro-/nano-cutting because of their feasible performance and availability. However, these machines are generally very expensive, working in a tight temperature control environment, and they are energy and resources inefficient. To match the micro-manufacturing of miniature and micro-components, the concept of micro- and meso-machine tools has been proposed by some researchers, as shown in Figure 12 [4].

Micro- and meso-machines and their integration for the micro-manufacturing system/micro-factory are suitable for the fabrication of micro-products at low cost, requiring the occupation of less space, and being of low energy consumption and greater mobility, etc. Compared to a conventional ultraprecision machine, a micro- or meso-machine has the five essential characteristics of decreased heat deformation, less material consumption, smaller vibration amplitudes, smaller footprint and thus smaller space occupation, and less energy consumption [26].

At Brunel University, three meso-machines have been developed for machining micro-components and micro-products. Figure 13(a) shows a desktop micro-milling/turning test rig, which has a two-dimensional piezo-driven stage for vibration-assisted cutting. Figure 13(b) shows a three-axis bench-top diamond-turning machine, a mirror surface, as illustrated in Figure 14, being achievable on this machine. Figure 13(c) is a five-axis bench-top micro-milling machine, which is still under development with the specifications as follows:

1. Overall size: 1140 × 910 × 1865 mm.
2. Working XYZ: 150 × 150 × 100 mm.
3. Slides and rotary table: direct drive and air bearings with squeeze film dampers to achieve a nanometric level of positioning and machining accuracy.
4. Spindle speed: 250,000 rpm to cope with small diameter of tools and micro-features.

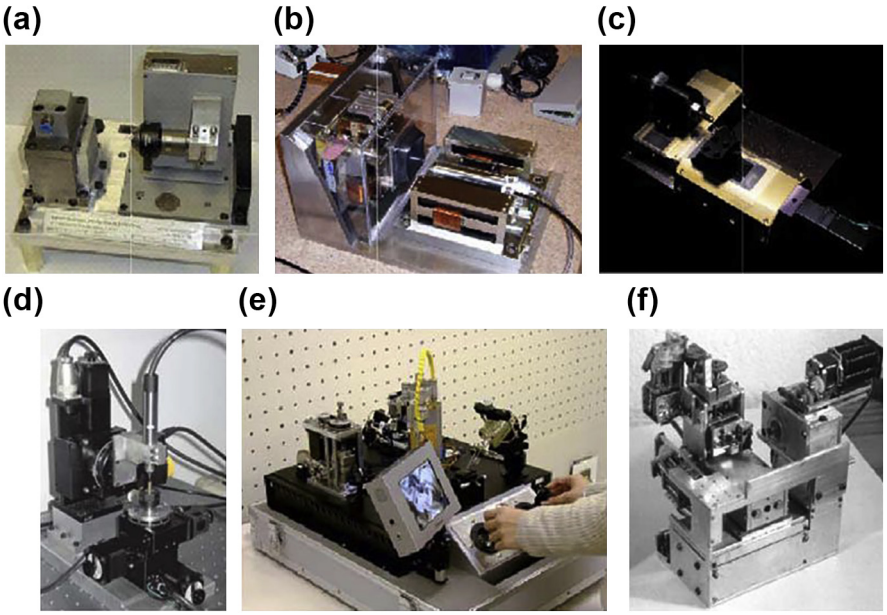

FIGURE 12

Typical micro- and meso-machines [4]. (a) Micro-factory; (b) second generation miniature machine; (c) commercial miniature machine; (d) miniature machine; (e) micro-factory; (f) micro-machine tool.

5. Mechanical handling and visual inspection integrated into the machine design.
6. Machining accuracy: <100 nm.
7. Surface roughness: <10 nm.
8. Control system: UAMC five-axis.

MICRO-TOOLING

Micro-tooling is the essential enabler for micro-/nano-cutting processes. It also determines the feature sizes and surface quality of the miniature and micro-components machined. Smaller tools have decreased thermal expansion relative to their size, increased static stiffness from their compact structure, increased dynamic stability from their higher natural frequency, and the potential for decreased cost due to smaller quantities of material utilized [4].

Single-crystal diamond is the preferred tool material for micro-/nano-cutting due to its outstanding hardness, high thermal conductivity, and elastic and shear moduli. The crystalline structure of the diamond makes it easy to generate a very sharp cutting edge, e.g., a cutting edge in tens of nanometers can be achieved. More recently, chemical vapor deposition diamond-cutting tools have become available, as shown

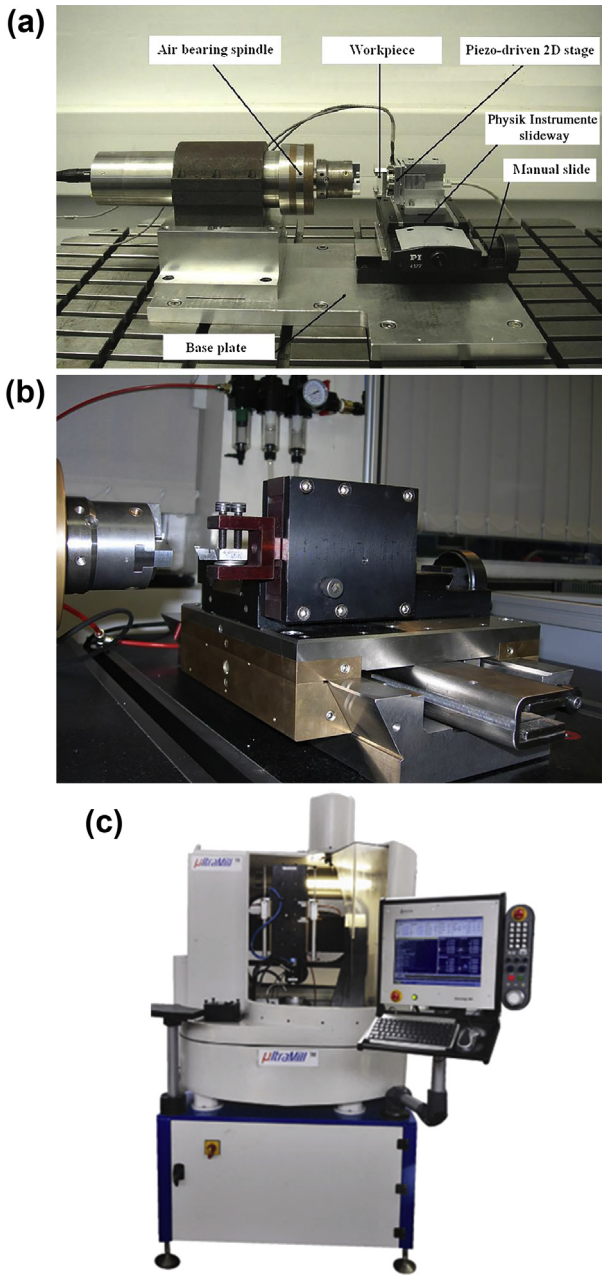

FIGURE 13

Micro- and meso-machines developed at Brunel University: (a) a desktop micro-milling/turning test rig; (b) a three-axis bench-top diamond-turning machine; and (c) a five-axis bench-top micro-milling machine.

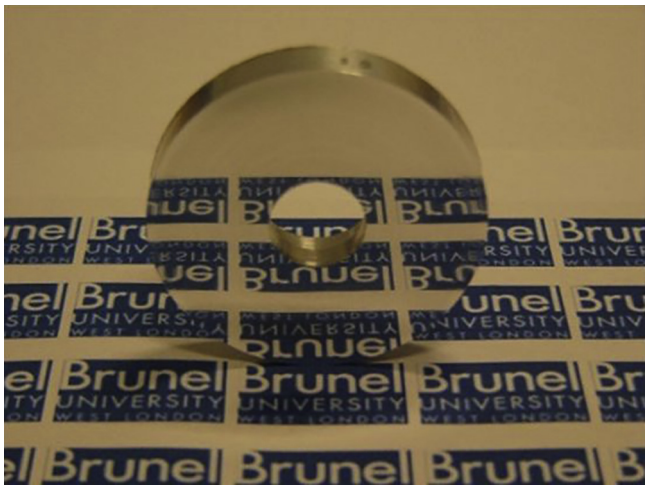

FIGURE 14

Mirror surface achieved on the three-axis diamond-turning machine.

in Figure 15 [27]. They are extremely hard and can be used to cut tungsten carbide with a cobalt of 6% or greater.

However, diamond is limited to the cutting of nonferrous materials because of the high chemical affinity between diamond and iron. Micro-tools that are used to machine ferrous materials are normally made from tungsten carbide. As shown in Figure 16 [28], these micro-milling tools are made from tungsten carbide with a diameter from ∅0.2 to ∅1.5 mm.

Commercially available micro-drills are typically on the order of 50 μm diameter [1]. However, methods for minimizing micro-tools continue to be developed, such as focused ion beam, electrical discharge machining, wire electrical discharge grinding, and grinding, etc. Figure 17 [29] shows micro-end mills developed by the focused ion beam process, their diameter being less than ∅25 μm.

Other trends in the development of micro-tools include: the optimization of the geometric and coating properties of micro-tools for longer tool life and accuracy enhancement, and characterization and condition monitoring of micro-tools.

APPLICATIONS

Micro-/nano-cutting has many applications, which are directly related to the overall application markets of micro-products. For instance, micro-electromechanical system (MEMS), as shown in Figure 18, is and will remain one of major driving forces for micro-cutting. It is expected that the MEMS/micro-system technology market volume will reach $24 billion in 2009 from $12 billion in 2004. Moreover, completely new products such as micro-fuel cells, MEMS memories, chip coolers, liquid lenses for cell phone zoom and autofocus will be included in this category.

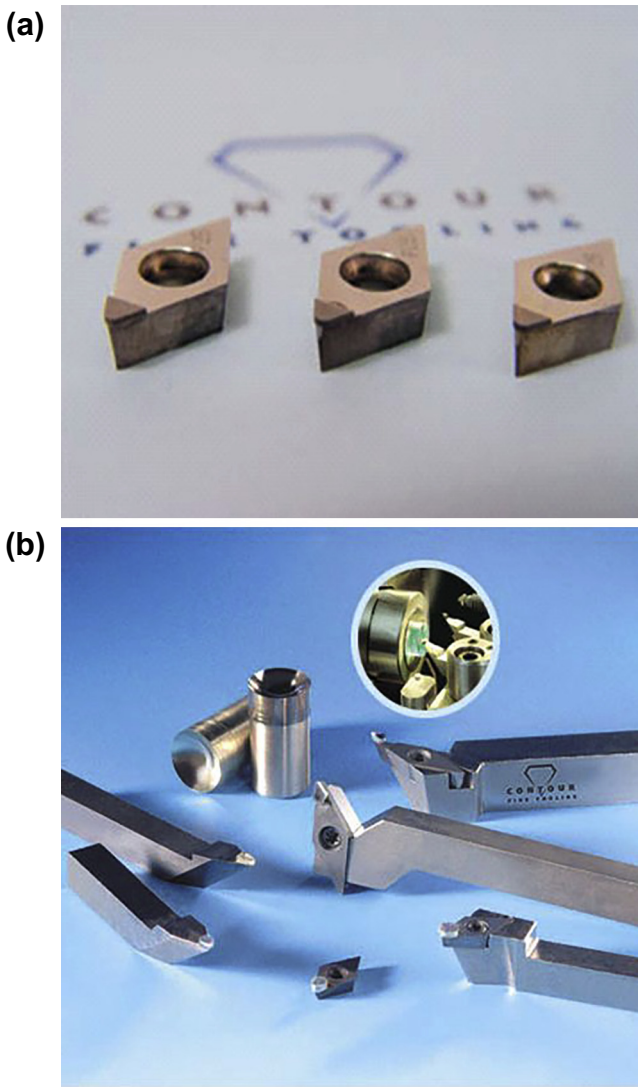

FIGURE 15

Micro-turning tools manufactured by: (a) Diamond-turning tools; (b) Chemical vapor deposition diamond-turning tools.

Courtesy: Contour Fine Tooling Ltd.

The EU FP6 4M Network has organized the major applications into the following three divisions [31], i.e.,

1. **Micro-optics:** telecommunication, biotechnological, instrumentation, and medical applications.

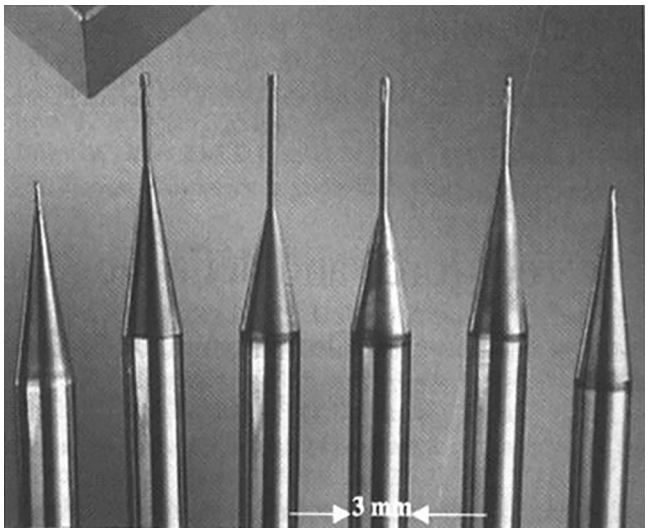

FIGURE 16

Micro-milling tools.

2. **Micro-sensors and actuators:** medicine, biomedical field, health and safety, environment, and process control.
3. **Micro-fluidics:** biological, medical, pharmaceutical, and chemical engineering applications.

Micro-/nano-cutting is very promising in the production of micro-products used in the above three divisions, such as sensors, accelerometers, actuators, micro-mirrors, fiber-optics connectors, micro-display, etc. Some typical application samples resulting from micro-/nano-cutting are shown in Figure 19 [32].

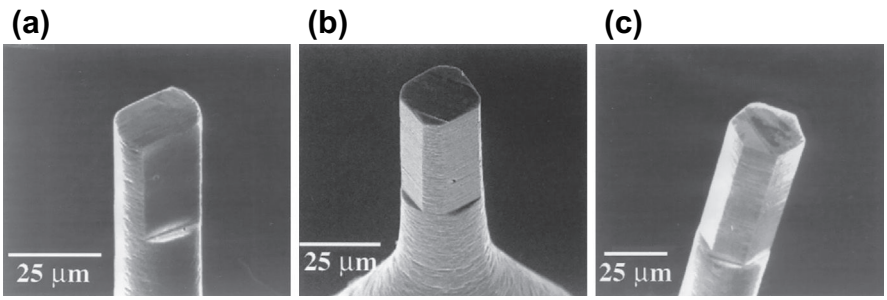

FIGURE 17

Micro-end mills made by focused ion beam sputtering having: (a) two cutting edges; (b) four cutting edges; and (c) five cutting edges (scanning electron micrographs).

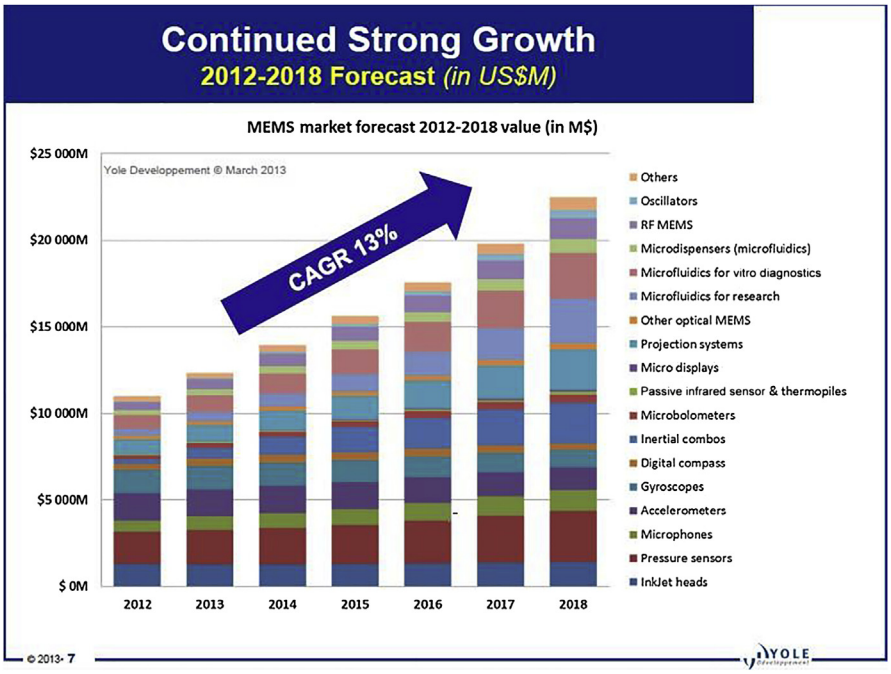

FIGURE 18

Market for micro-system technology/MEMS products in the future [30].

Figure 19(a) is a joining element (steel) for optical fiber connections. There are 18 drill holes with a diameter of 0.23 mm ± 5 μm and a drilling depth of 1.5 mm. The positional tolerance of the drill holes is 10 μm. The complete machining time was 25 min.

The part shown in Figure 19(b) is a mixing disc of a rocket motor, produced by five-axis machining. Six tools were used and precision adjustment on spot faces was required.

Figure 19(c) shows three turbine wheels for micro-fluid pumps, produced by five-axis machining. The wheels are made of vespel and ceramic with diameters of 2−7 mm and a circumferential tolerance of 2 μm.

Figure 19(d) shows watch base-plates made by fully automatic production using 30 tools including milling, drilling, and tapping. The positional tolerances between the drill holes and drill depths are ±3 μm.

The cataract lens shown in Figure 19(e) has a surface finish of $R_a < 0.2$ μm. Its outside contour is machined with a milling tool (0.4 mm), and the positioning holes are produced by drilling.

The indispensable advantage of micro-/nano-cutting is applicable to the manufacture of 3D complex-shape/form micro-molds. It is anticipated that micro-/nano-cutting will be intensively used in the fabrication of compression molds and

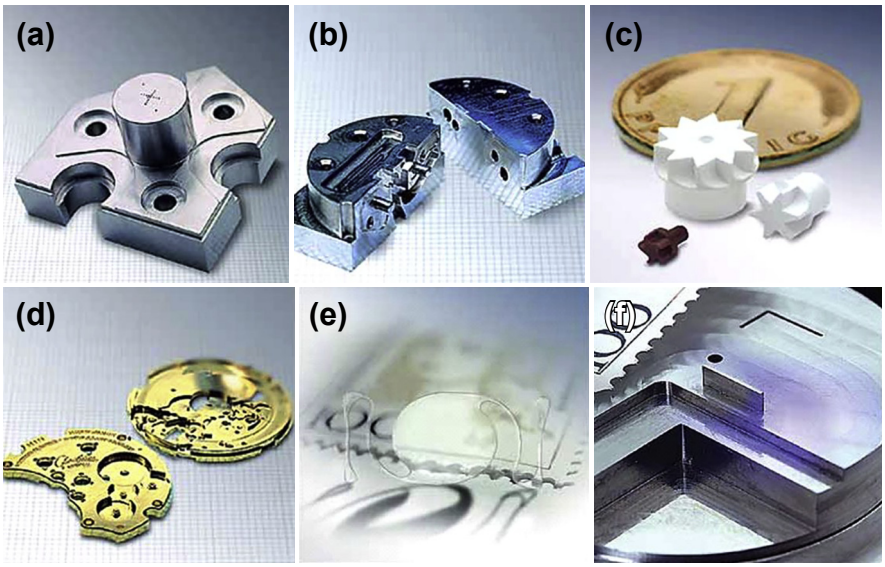

FIGURE 19

Micro-product samples.

Courtesy: KERN Micro- & Feinwerktechnik GmbH.

injection molds. Figure 19(f) shows an injection-molding tool for watch making, machined by micro-milling. The material of the mold is hardened steel 54 HRC, its position and form tolerance is ± 5 μm, and its surface quality is $R_a > 0.25$ μm.

COMPETITIVE TECHNOLOGIES AND ECONOMIC CONSIDERATIONS

Micro-/nano-cutting brings many potentialities to the fabrication of miniature and micro-products/components with arbitrary geometry. The micro-/nano-cutting process is particularly suitable for the manufacture of individual personalized components rather than large batch sizes, which is largely indispensable for the current vibrant markets. With the high level of machine accuracy of ultraprecision machine tools, good surface finish and form accuracy can be achieved. Micro-/nano-cutting is also capable of fabricating 3D free-form surfaces. The high machining speed of micro-/nano-cutting is another advantage over other micro-manufacturing technologies. Moreover, it can fabricate a huge range of materials, such as steel, aluminum, brass, plastics, ceramic, polymers, etc. Unlike micro-laser beam machining and lithographic techniques, it does not require a very expensive setup, which enables the fabrication of miniatures at an economically reasonable cost.

ACKNOWLEDGMENTS

The authors would like to thank all research colleagues in the Advanced Manufacturing and Enterprise Engineering (AMEE) research group at Brunel University for stimulating discussions, and relevant research publications and projects to access and refer to. Thanks are also extended to the EU MASMICRO project consortium, practically to its RTD five-subgroup for frequent meetings and discussions, which are always very helpful.

REFERENCES

[1] Dornfeld D, Min S, Takeuchi Y. Recent advances in mechanical micromachining. CIRP Ann 2006;55(2):745−68.
[2] Lucca DA, Rhorer RL, Komanduri R. Energy dissipation in the ultraprecision machining of coppers. CIRP Ann 1991;40(1):69−72.
[3] Lucca DA, Seo YW. Effect of tool edge geometry on energy dissipation in ultraprecision machining. CIRP Ann 1993;42(1):83−6.
[4] Chae J, Park SS, Freiheit T. Investigation of micro-cutting operations. Int J Mach Tool Manuf 2006;46(3−4):313−32.
[5] Liu X, Devor RE, Kapoor SG. An analytical model for the prediction of minimum chip thickness in micromachining. J Manuf Sci Technol Trans ASME 2006;128(2):474−81.
[6] Ikawa N, Shimada S, Tanaka H. Minimum thickness of cut. Nanotechnology 1992;3(1):6−9.
[7] Vogler MP, Kapoor SG, Devor RE. On the modeling and analysis of machining performance in micro-end milling. J Manuf Sci Technol Trans ASME 2004;126(4):685−705.
[8] Shimada S, Ikawa N, Tanaka H, Ohmori G, Uchikoshi J, Yoshinaga H. Feasibility study on ultimate accuracy in microcutting using molecular dynamics simulation. CIRP Ann 1993;42(1):91−4.
[9] Shimada S, Ikawa N, Inamura T, Takezawa N, Ohmori H, Sata T. Brittle-ductile transition phenomena in microindentation and micromachining. CIRP Ann 1995;44(1):523−6.
[10] Li D, Dong S, Zhao Y, Zhou M. The influence of rake of diamond tool on the machined surface of brittle materials with finite element analysis. In: Proceedings of the 1st international conference and general meeting of the European society for precision engineering and nanotechnology Bremen, Germany; 1999. p. 338−41.
[11] Ichida Y. Ductile mode machining of single crystal silicon using a single point diamond tool. In: Proceedings of the 1st international conference and general meeting of the European society for precision engineering and nanotechnology Bremen, Germany; 1999. p. 330−3.
[12] Fang FZ, Wu H, Zhou W, Hu XT. A study on mechanism of nano-cutting single crystal silicon. J Mater Process Technol 2007;184(1−3):407−10.
[13] Liu X, Devor RE, Kapoor SG. The mechanics of machining at the microscale: assessment of the current state of the science. J Manuf Sci Technol Trans ASME 2004;126(4):666−78.
[14] To S, Lee WB, Chan CY. Ultraprecision diamond turning of aluminium single crystals. J Mater Process Technol 1997;63(1−3):157−62.
[15] Luo X. High precision surfaces generation: modelling, simulation and machining verification [Ph.D. thesis]. Leeds Metropolitan University; 2004.

[16] Woon KS, Rahman M, Fang FZ. Investigations of tool edge radius effect in micromachining: a FEM simulation approach. J Mater Process Technol 2008;195(1−3):204−11.
[17] Hoover WG. Molecular dynamics. In: Lect. notes phys., vol. 258. Berlin: Springer-Verlag; 1986. p. 13.
[18] Tadmor EB, Ortiz M, Phillips R. Quasicontinuum analysis of defects in crystals. Philos Mag A 1996;73:1529−63.
[19] Shiari B, Miller RE, Klug DD. Multiscale simulation of material removal processes at the nanoscale. J Mech Phys Solids 2007;55:2384−405.
[20] Sun X, Chen S, Cheng K, Huo D, Chu W. Multiscale simulation on nanometric cutting of single crystal copper. Proc Inst Mech Eng B J Eng Manuf 2006;220(7):1217−22.
[21] Sun X, Cheng K. Multiscale simulation of the nano-metric cutting process. Int J Adv Manuf Technol 2010;47:891−901.
[22] Aly MF, Ng E, Veldhuis SC, Elbestawi MA. Prediction of cutting forces in the micromachining of silicon using a "hybrid molecular dynamic-finite element analysis" force model. Int J Mach Tool Manuf 2006;46:1727−39.
[23] Huo D, Cheng K. A dynamics-driven approach to the design of precision machine tools for micro-manufacturing and its implementation perspectives. Proc Inst Mech Eng B J Eng Manuf 2008;222(1):1−13.
[24] Luo X, Cheng K, Webb D, Wardle F. Design of ultraprecision machine tools with application to manufacture of miniature and micro components. J Mater Process Technol 2005;167:515−28.
[25] Ikawa N, Donaldson R, Komanduri R, König W. Ultraprecision metal cutting − the past, the present and the future. CIRP Ann 1991;40(2):587−94.
[26] Alting L, Kimura F, Hansen HN. Micro engineering. CIRP Ann 2003;52(2):635−57.
[27] http://contour-diamonds.com/GB/turningtools.html [accessed 03.03.14].
[28] Dow T, Miller E, Garrard K. Tool force and deflection compensation for small milling tools. Precis Eng 2004;28(1):31−45.
[29] Adams DP, Vasile MJ, Benavides G, Campbell AN. Micromilling of metal alloys with focused ion beam-fabricated tools. Precis Eng 2001;25:107−13.
[30] Katano Y, Leroy S. NEXUS market briefing organized by Yole development. http://www.suframa.gov.br/minapim/news/visArtigo.cfm?Ident=147&Lang=EN [accessed 03.03.14].
[31] Dimov SS, Bramley AN, Eberhardt W, Engel U, Fillon B, Johander P, et al. 4M network of excellence, process report 2004−2006. In: 4M2007 conference on multi-material micro manufacture, Borovets, Bulgaria; October 3−5, 2007.
[32] http://www.kern-microtechnic.com/2-Sub-Samples.html accessed 19.11.07.

This page intentionally left blank

CHAPTER

FIB Micro-/Nano-fabrication 3

Nitul S. Rajput, Xichun Luo
Department of Design, Manufacture and Engineering Management, University of Strathclyde, Glasgow, UK

CHAPTER OUTLINE

Micromanufacturing Engineering and Technology. http://dx.doi.org/10.1016/B978-0-323-31149-6.00003-7

INTRODUCTION

The focused ion beam (FIB) is one of the state-of-the-art micro-/nano-fabrication tools. It adopts both bottom-up and top-down approaches to generate micro-/nano-structures and the biggest advantage of FIB lies in its maskless fabrication capability. The efficacy of the machine is now well proven among the scientific community. Modern FIB systems offer a highly focused and precise beam of ions, which are effectively used for fabricating precise, high-aspect ratio, micro-/nano-structures.

FIB was first developed in the early 1970s as a result of research on liquid metal ion source (LMIS) [1,2]. Subsequently, the potential of the technology as a maskless fabrication technique was realized [3]. Initially, FIB was used mostly for mask repairing purposes. Gradually, with the help of the development of the ion source and the charge particle lens system the technology has become a reliable and precise fabrication tool for researchers and engineers. The research and development of the technology has been carried out mostly by industrial companies such as, FEI, JEOL, ZEISS, HITACHI, which also provide state-of-the-art FIB machines for customers.

The number of FIB users is growing rapidly with a wide variation in area where FIB is being used: this is shown in Figure 1. The plot shows the number of published papers, where FIB has been directly or indirectly used, as a function of year and clearly indicates the rapid growth of FIB users and the importance of the tool in modern research.

FIB has been used in all branches of science and engineering. In material science, FIB has been mostly used for material modification and characterization

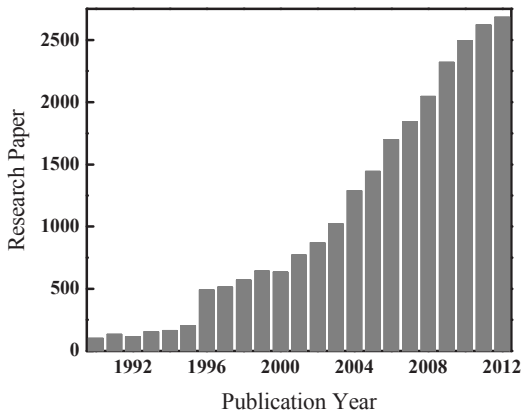

FIGURE 1

Published focused ion beam papers versus publication year.

source: www.scopus.com.

[4–6]; in physics and chemistry, FIB structures are used to study phenomena at the nano-scale [7–10]. FIB is also used in the development of prototype nano-electromechanical systems/micro-electromechanical systems, actuators, sensors, bio–nano-tools, etc. [11–17].

FIB micro-/nano-fabrication is based on the principle of the ion beam milling and deposition technique. FIB systems can provide a high milling and deposition rate of the order of 1 $\mu m^3\ nC^{-1}$. Using the flexibility that a modern FIB system offers, such as eucentric position, auto-FIB, and advanced user interface software, complicated 3-D micro-/nano-structures, or a large number of patterned structures can be fabricated rapidly and smoothly.

ARCHITECTURE OF FIB

In an FIB system, an ion beam column is the backbone of the tool. The function of the ion column is to provide a highly energetic, focused, and monochromatic beam of ions. These are done with the help of a stable ion source, extractor, suppressor, lens system, scan generator, etc. Nowadays, in most of the FIB systems, an electron beam column is integrated. These kinds of system are generally referred as dual-beam or cross-beam systems. The electron column is used for imaging the sample during or after the FIB processing. The electron beam can also be used for depositing extra material, the process then being called electron beam-induced deposition (EBID). The electron and the ion column are normally aligned at 52°. A schematic view of a dual-beam system is presented in Figure 2. Modern FIB equipment is

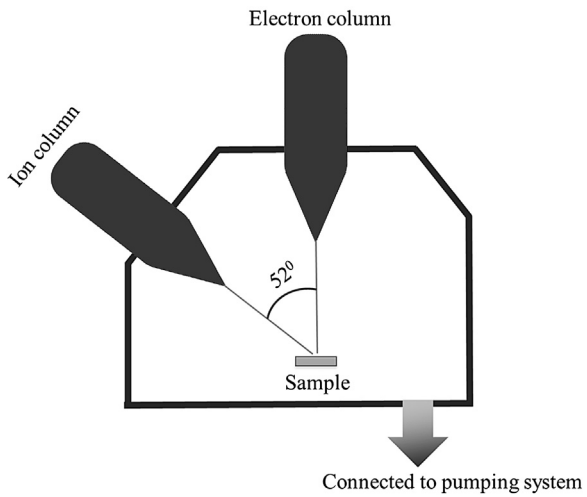

FIGURE 2

Schematic diagram showing the geometry of a dual-beam focused ion beam system.

mostly integrated with various characterization facilities, such as energy dispersive spectroscopy (EDS), residual gas analyser (RGA), electron backscattered diffraction (EBSD), along with other accessories such as a manipulator, gas injection system (GIS). These are discussed briefly below.

ION COLUMN

In order to produce a high quality beam of ions, a stable ion source is required. The beam should have high brightness and resolution. There are two types of ion sources available which can produce high quality ion beams: LMIS and gas-filled ion source. However, LMIS sources have better angular intensity, which is related to the focusing capability, and so LMIS sources are preferable for FIB systems.

In the LMIS type, heated metallic liquid flows from the reservoir to a tungsten needle, and wets the latter. A high voltage is applied at the wet tip and eventually the liquid assumes a conical shape. This conical shape is known as a "Taylor cone." Ions are subsequently extracted from the metallic cone to form a jet [18].

In LMIS, Ga is the first choice to use as an ion source for various reasons. It has a melting point of 29.8 °C and hence it is very convenient to make an LMIS gun with limited heating. Also, the low M_p minimizes the possibility of interdiffusion of the Ga ions with the W needle through which the Ga ions are extracted. Ga sits in the middle of the periodic table and thus the momentum transfer capability (which is an important parameter for FIB milling, discussed in details in the FIB processing section) to the target atoms is optimal for a wide variety of target samples. Low volatility at the melting point of Ga conserves the supply of the Ga source. The low vapor pressure of Ga helps the ion source to retain a longer life. In addition, Ga has excellent mechanical, electrical, and vacuum properties.

The ions are extracted from the source and to suppress the strayed ions, a suppressor electrode is used. Subsequently, the beam is passed through the lens system, a variable aperture system, and scan plates before it reaches the sample. Nowadays, with the advance of the ions lens system and the ion beam source, a resolution of several nanometers can be easily achieved.

ELECTRON COLUMN

The structure of the electron beam column is similar to that of the ion column. The source of the electron beam is kept at the top of the column. Mostly three types of electron sources are used: tungsten, lanthanum hexaboride (often called "lab six"), and the field emission gun (FEG). Tungsten and lab six can provide a high current density of the electron beam, however, for better resolution, an FEG type source is generally used. Once the beam of electrons is emitted from the source gun, they are passed through the electric and magnetic lenses to focus it. Since the

mass of an electron is much smaller than that of an ion, magnetic force acts more efficiently on an electron. Thus, in contrast to the ion column, where electric lenses are used to focus and align the beam, here, electromagnetic lenses are used to do the same. Also magnetic lenses produce lower aberration than the electric lenses. Finally, in order to scan the focused electron beam onto the sample, scan plates are used. More information about the SEM system can be found in electron microscopy books [19,20].

A modern SEM system based on an FEG source can provide a focused electron beam of less than 1 nm diameter. Focused electron beam can be used for high-resolution SEM imaging and nano-structure deposition (EBID).

STAGE

In most FIB systems, the sample stage has the ability to move in the x, y, and z directions along with rotation and tilting capability. The stage movement can be controlled smoothly with the help of graphical user interface (GUI) software. In a few FIB systems, users can also handle the stage manually. Instead of a general stage, users can also have a piezostage, which works on the piezoelectric principle to generate precision motion and, by means of feedback control, with a feedback signal provided by optical encoders. This kind of stage provides precise movement of the stage, in steps of as small as 10 nm, in the x, y, and z directions.

IMAGING DETECTORS

FIB systems are integrated with various detector types. For the available range of secondary electrons (SE) and backscattered electrons (BSEs) devices, an Everhart—Thornley detector and in-lens detectors are often selected, and mounted inside the sample chamber. In order to collect the BSEs efficiently, a dedicated BSEs detector can be mounted near the mouth of the electron column.

For a live view inside the chamber, a CCD camera is often used, which helps the user to realize the movement of the stage and identify the workpiece.

GAS INJECTION SYSTEM

GISs are the sources of gases, used with fine needles to supply precursor gas molecules during the FIB deposition and etching processes. During the processing, the gas reservoirs are heated for a few minutes and then gas is sprayed over the sample surface with the help of the needles. The needle tip should be kept at a close proximity of a few hundreds of microns so that the sufficient local gas flux at the

processing site is adsorbed by the sample surface. The local gas flux at the sample site also depends on the needle diameter and the reservoir temperature. These conditions are generally kept constant. Normally, one injector system contains one type of reservoir, i.e., one GIS needle is dedicated for only one type of deposition or etching. However, multiple GISs are available nowadays, where there are several reservoirs for different precursor gases with a single GIS port. This helps to reduce congestion inside the chamber.

PUMPING SYSTEM

In an FIB system, different portions of the system require different levels of vacuum. The ion and the electron column require a higher level vacuum of the order of 10^{-8}–10^{-11} mbar. These vacuum levels are achieved with the help of ion gutter pumps. The sample chamber requires a low level vacuum of the order of 10^{-6} mbar. This is achieved with the help of a turbo molecular pump that is backed by an oil-free fore pump. Contamination may affect the FIB processing and degrade the quality of the fabricated structure. In order to avoid such issues, the sample chamber should be pumped for a sufficient time before a job is started.

ENERGY DISPERSIVE SPECTROSCOPY

EDS is an auxiliary facility, which can be integrated with an SEM system or a cross-beam FIB system. EDS detects the elements present in the sample. EDS can be used to collect the elemental information along a line or a box or a dot drawn over the sample.

RESIDUAL GAS ANALYZER

RGA is a technique to analyze the elements present inside the chamber. The environmental molecules or the elemental composition inside the chamber may vary as a result of FIB processing. These can be monitored with the help of an RGA [21].

ELECTRON BACKSCATTER DIFFRACTION

EBSD is a structural analysis technique [22]. Thus, in a cross-beam system, EBSD can be integrated as a sample analysis technique. FIB can be used to section a sample layer by layer and the EBSD can be harmoniously used to collect crystalline information of a sample layer by layer. Using this approach, crystalline information of the

whole structure can be extracted efficiently and rapidly, and a 3-D map of the sample showing the grains, grain boundaries as well as the crystalline orientations of the grains can be constructed.

MANIPULATOR

It is often required to handle micro-/nano-structures inside the FIB chamber, mainly for transmission electron microscopy (TEM) sample preparation, circuit editing, failure analysis, etc. To allow the users to perform these tasks efficiently, a manipulator in the form of needles or a gripper is mounted inside the chamber. These needles or grippers can be moved inside the chamber smoothly and efficiently in x, y, z, T (tilt), and R (rotation) with the help of micro-motors. The micro-/nano-manipulator, which acts as a hand to the microscopy can also be used for the measurement of other physical properties of the sample. The manipulator can be integrated with a conventional FIB system as a third-party tool.

FIB PROCESSES

The basic processes related to FIB technology are given below.

1. FIB milling,
2. FIB deposition,
3. FIB imaging, and
4. FIB etching.

These processes are discussed in details in the following sections.

FIB MILLING

FIB milling is the process of material removal from the target sample. The ejection of the target material depends highly on the ion beam energy, ion beam type, and the target material. The physical mechanism of the milling process will be discussed in the subsequent subsections.

MODE OF ENERGY LOSS

When an ion particle enters into the solid, it transfers its energy and momentum to the target atoms and electrons. This energy loss can occur through two modes:

1. Nuclear energy (NE) loss and
2. Electronic energy (EE) loss

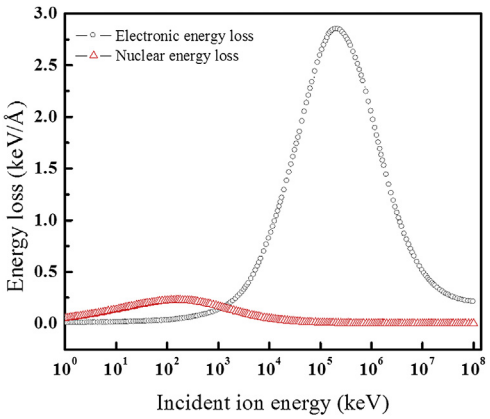

FIGURE 3

Energy loss profile of Ga ions in Au sample as simulated using Stopping and Range of Ions in Matter [23].

NE loss happens when the energy and the momentum of the injected particle are transferred to the target atoms which will result in atomic displacements. NE loss is an elastic process. It dominates at relatively lower beam energy (∼keV).

On the other hand, if the energy of the incoming ion beam is transferred to the electronic part of the target atoms, it is referred as the EE loss. This process is an inelastic process as the energy loss occurs through excitation and ionization of the target atoms, which in turn produces additional particles such as X-rays, secondary electrons (SEs). EE dominates when the energy of the incoming ion is relatively high (∼MeV).

To have a comparative idea about the energy loss profile, an SRIM (Stopping and Range of Ions in Matter) plot is shown in Figure 3, where the energy loss profile of Ga ions in an Au sample is shown. SRIM is a Monte Carlo-based program, which has been developed by Ziegler and can be used efficiently to determine the implantation depth and the energy loss profile of the ions [23].

SPUTTERING PROCESS

During the NE loss process, the target atoms are displaced and voids are created. Further, if the energy of a displaced atom is sufficient, it can knock on further atoms and produce further defects in the sample. The process continues until the energy of the displaced atom is no longer sufficient to create any further voids. This collision process is known as a collision cascade. During the collision cascade process, some of the displaced atoms may reach the surface of the sample and if the kinetic energies of these atoms are higher than the surface binding energy, then the atoms can come out from the surface. The physical term to define this process is sputtering

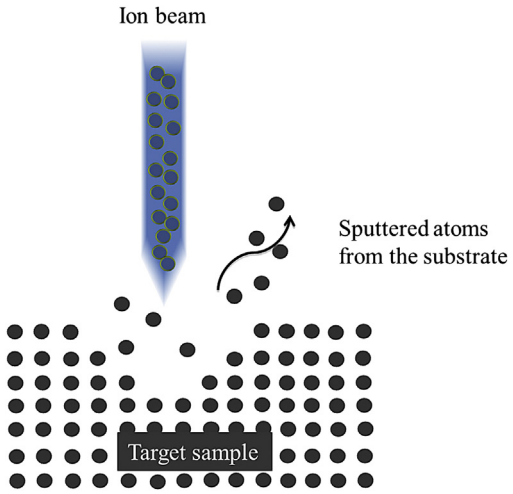

FIGURE 4

Focused ion beam sputtering/milling process.

(Figure 4). This material removal process is popularly known as FIB milling. The efficiency of the FIB milling process is evaluated by the term "sputtering yield" (Υ), which is defined as:

Υ = Mean number of atoms sputtered or emitted/incoming ions.

The sputtering yield is a function of various parameters, such as the sample type and the beam type, beam energy, which can be expressed as follows [24–27]:

$$\Upsilon = \Lambda F_D(E_0) \tag{1}$$

where Λ contains the material properties of the sample such as surface binding energy, the range of displaced target atoms, and $F_D(E_0)$ is the density of the transferred energy within the surface. $F_D(E_0)$ depends on the type (atomic number, mass number, etc.), energy, and the direction of the incident particle as well as on the type of the target atoms (atomic number, mass number, etc.).

The typical value of Υ varies from 10^{-1} to 10^2 for a keV beam [25].

Υ increases with E_0, however, it remains nearly constant after 30–40 keV beam energy. Υ is an important characteristic in FIB processing (milling) and as Υ does not change much after $E_0 \sim 30$ keV, in most of the FIB systems, the beam voltage has been kept between a few keV and 30 keV.

The dependence of sputtering yield on θ, the incident angle (the angle made by the incident ion particle with the surface normal of the sample), is nonlinear. As the ion beam is tilted from the normal direction, the collision cascade produced by the ion beam becomes shallower to the surface and the probability of the displaced atoms coming out from the surface becomes higher. The sputtering yield is plotted as a function of θ in Figure 5. As can be seen, Υ increases with the incident angle, however, after $\sim 80^\circ$, Υ gradually decreases with θ. At a higher tilted angle, the

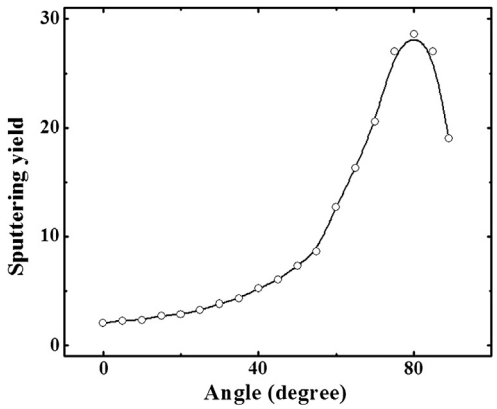

FIGURE 5

Sputtering yield versus angle of incidence of a 30 keV Ga ion beam irradiated on a Si sample [23].

incoming ion beam becomes much more inclined to the surface and at this grazing angle the probability of reflection of the incident ions increases and the initiated collision cascades could not fully develop: as a result the yield drops accordingly.

Sputtering is an outcome of energy and momentum transfer from the incident ions to the target atoms and thus Y depends highly on the density of the target sample. It is found that in the case of body-centered cubic samples, Y is higher along the [111] direction as compared to other directions and in case of face-centered cubic materials, Y is higher along the [110] direction as compared to other directions [24]. The atomic density along these specified directions is relatively higher than that in the other directions and as a result the yield is greater along these directions.

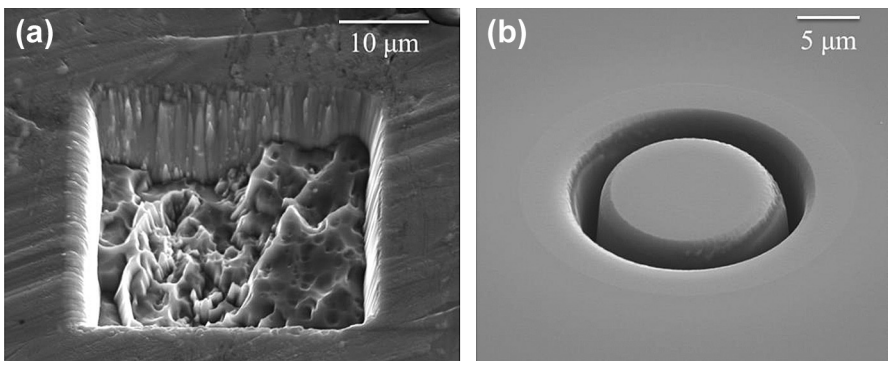

FIGURE 6

Examples of the focused ion beam milling process. SEM pictures of (a) a milled area on an Al sample; (b) a circular ring milled on a Si (111) sample.

In Figure 6, two examples of FIB milling are shown. In Figure 6(a), the SEM image shows an Al sample milled using the FIB milling technique. The nonuniformity occurs because of the polycrystalline nature of the Al sample. The milling rate is different at different portions of the sample and as a result the milled area is not smooth.

Figure 6(b) shows a circular hole fabricated on an Si (111) sample. The milling rate is uniform throughout the patterned area and this results in uniform and smooth milling.

FIB DEPOSITION

When gas molecules (often called a "precursor gas") are sprayed over a sample surface, gas molecules may become stuck to the surface, which can be either adsorptive or absorptive. If it is of adsorptive type, the gas molecules sit over the surface and if an ion beam is irradiated on the adsorbed sites, the ion beam can crack the adsorbed gas molecules into different smaller components, volatile and nonvolatile parts. The cracking process occurs through the SEs produced by the incident ions. The nonvolatile component remains on the surface while the volatile part is pumped out by the pumping system. This process is illustrated in Figure 7. Precursor gas molecules normally contain a ligand which can be metallic or nonmetallic and elements, such as C, H, O. After the cracking, the ligand part remains on the surface (the nonvolatile part) and the other dissociated components (C, O, H, CO, H_2O, CO_2, etc.) are pumped out. With continuous supply of precursor gas and ion irradiation, the chosen material can be deposited on a predefined area. The layer by layer growth of the material leads to a structure. This process is called FIB-induced chemical vapor deposition.

The FIB deposition process, particularly, the growth rate of the deposited material, depends on various parameters, which can be discussed with the help of the following equation [18]:

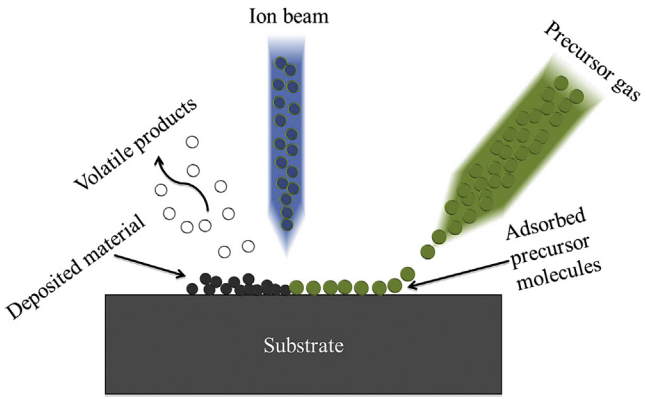

FIGURE 7

Focused ion beam deposition process.

$$\frac{dn}{dt} = gF(1-\theta) - k_d N_0 \theta - \frac{JN_0\theta\sigma}{e} - \frac{JY(1-\theta)}{e} \quad (2)$$

where:

$\frac{dn}{dt}$ is the rate of change in the density of the adsorbed molecules;
g is the sticking coefficient;
F is the gas flux;
θ is the precursor monolayer coverage;
k_d is the thermal desorption rate constant;
N_0 is the precursor monolayer density;
J is the primary ion current density;
σ is the decomposition cross section;
Y is the film sputter yield; and
e is the charge of electrons.

Here, the first term on the right side of the equation refers to the gas molecules that become stuck to the sample surface. The second term infers the desorptive part of the already adsorbed molecules. The third term represents the decomposition by the ion beam and the last term shows the sputtered portion of the deposited material.

Thus, the FIB deposition process depends highly on the sample surface and the precursor gas type, which determine the sticking probability. In addition, the sample site should be filled with the adsorbed gas molecules, i.e., the precursor gas flux at the site should be sufficient. Since the ion beam also removes material (the last term in Eqn (2)), FIB deposition is an outcome of the competition between the ion beam-induced cracking and continuous milling. If the ion beam flux is more than the required amount to crack all the available gas molecules on the sample site, the beam starts milling the sample. Thus, an optimized value of ion beam current should be used in order to carry out an FIB deposition.

Modern FIB systems are integrated with GIS needles, which are used to supply precursor gas molecules.

Most commonly used GIS or precursor gas molecules are listed in Table 1.

Figure 8 shows a pillar deposited using the FIB deposition process. Methyl cyclopentadienyl trimethyl platinum precursor gas is used for the deposition process.

Table 1 Various Popular Precursor Gas Types and Their Purpose of Deposition

Precursor Gas	Function
Naphthalene: $C_{10}H_8$	Carbon deposition
Methyl cyclopentadienyl trimethyl platinum: $(CH_3)_3Pt(CpCH_3)$	Platinum deposition
Tungsten hexacarbonyl: $W(CO)_6$	Tungsten deposition
Tungsten hexafluoride: WF_6	Tungsten deposition
Tetramethyl orthosilicate: $Si(OCH_3)_4$	SiO_2 deposition
Au(hexafluoro acetyl acetanoate)$(CH_3)_2$	Au deposition

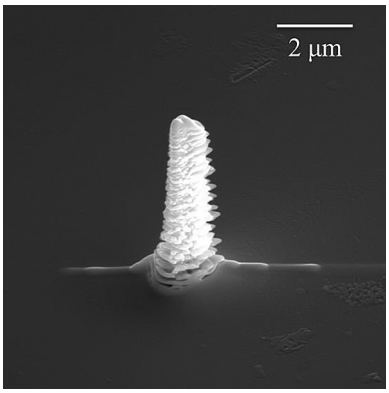

FIGURE 8

A Pt pillar deposited using the focused ion beam deposition process.

The deposited Pt pillar also contains other elements, such as, O, CO, H, CO_2, in addition to Pt [28]. The guest atoms appear because of the insufficient cracking of the precursor gas molecules. Ga ions are also implanted during the FIB processing. The amount of contamination also depends on the ion beam deposition parameters [28].

FIB IMAGING

As a result of the collision cascade process, a large number of SEs are produced. The SEs, which are coming out from the sample surface can be collected and used for image formation. This process is known as scanning ion microscopy (SIM). It is shown schematically in Figure 9. The major difference between SEM and SIM is

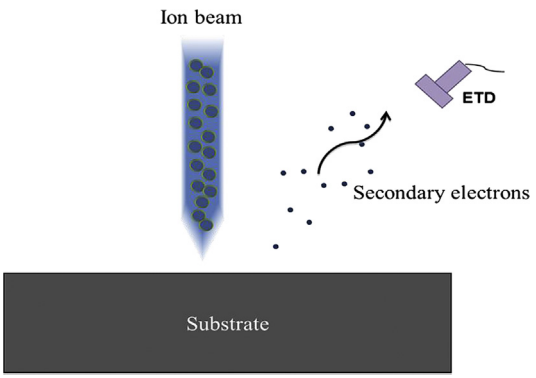

FIGURE 9

Illustration of the working principle of SIM imaging. ETD, Everharte–Thornley detector.

that the SEs in SEM are produced by the incident electrons, whereas in SIM, the SEs are produced by the incident ions.

The range of ions in matter is much lower than an electron beam having the same beam energy. The SEs produced in SIM carry information only from the surface and thus SIM has been very useful for extracting surface information of the sample.

FIB ETCHING PROCESS

The FIB etching process is similar to the FIB deposition process, in the sense that both processes use external gas molecules to interact with the ion beam [4]. In FIB etching, the selected chemical gas molecules are adsorbed on the sample site. As a result of the adsorption, the adsorbed gas molecules may react with the target atoms and molecules, and produce a different reaction product. This reaction product may have higher or lower sputtering yield than that of the native sample. If the reaction product has a higher sputtering yield, then the overall milling rate of the sample will be increased. This will enhance the FIB milling performance. If the sputtering yield of the reaction product is lower than that of the native sample, the FIB milling performance will decrease. Thus, depending on the requirement of the user, a different chemical agent can be used to change the milling rate.

Similarly to the FIB deposition process, where optimized parameters are used in order to enhance or retard the deposition performance, proper beam flux and beam energy should also be used during the FIB etching process to increase or decrease the milling rate.

Halogen or halogen-containing gases are generally preferred for the FIB etching process. I_2, Br_2, and XeF_2 are the most commonly used chemical agents during the FIB etching process. These etching agents are supplied to the sample site with the help of the GIS needles.

SCANNING STRATEGIES

During ion beam irradiation, the beam is moved in steps from one pixel to the next pixel. The beam remains in each pixel for a particular time before it jumps to the next pixel. This time is defined as the beam dwell time. The beam dwell time can be varied from a few tens of nanoseconds to microseconds order. The movement of the beam, i.e., the scanning of the beam over the sample, can be done through two ways. These are (1) serpentine and (2) raster. In serpentine scan, the beam moves from one end of the row to the other end of the row (say from left end to the right end) and then jumps to the next row to start from the right end pixel and moves toward the left end pixel as shown in Figure 10(a). It continues until the beam finishes the whole pattern window and then flies back to its initial pixel and continues

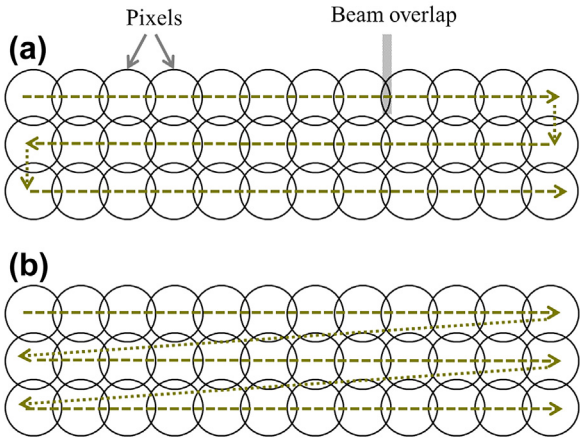

FIGURE 10

FIB scanning mode: (a) serpentine scanning; and (b) raster scanning.

the scanning in this fashion until the patterning is over. On the other hand, in raster scan, the beam scans the patterned site in one direction only. Thus, in raster scan, when the beam scans from left end pixel and finishes the right end pixel, it jumps to the next row and starts from the left end pixel and finishes the right end pixel (Figure 10(b)).

The beam scans the patterning site pixel to pixel and there can be overlapping between two successive pixels. This is defined as "beam overlapping" and is calculated in terms of percentage of area.

FIB processing depends highly on the beam dwell time, the scan direction, and beam overlapping [25]. These parameters can be changed using GUI software and optimized for a particular process.

PATTERNING STRATEGIES

In the case of multiple patterning, an FIB system can employ two approaches to finish the job. These are (1) serial patterning and (2) parallel patterning. In serial patterning, FIB does the patterning one by one. Thus, if there are five patterns of different shapes or sizes to fabricate, the patterning/fabrication will be done from pattern 1, then pattern 2, and continue up to pattern 5. On the other hand, in the case of parallel patterning, all the patterns are carried out simultaneously. Thus, the user has the flexibility to use serial patterning or parallel patterning during the sample fabrication stage. Depending upon the requirement of the user, these processes can be used to remove material from, as well as to deposit material onto, a particular site.

APPLICATIONS OF FIB

The processes discussed above help the user to fabricate complex 3-D structure, which might not be feasible when using any other technique. FIB can also be utilized in circuit editing or failure analysis, reverse engineering, sample modification, characterization, etc. Several specific examples are discussed in the following subsections.

3-D MICRO-/NANO-STRUCTURING

FIB is a maskless fabrication technique and the highly precise focused nano-beam of ions extends the capability of the technique to fabricate complex micro-/nano-structures. The GUI software provides a patterning page, where patterns of different shapes and sizes can be drawn and ion beam parameters, such as beam dwell time, beam overlapping, GIS needle operations, can be set. Figure 11(a) shows an example of an FIB-made structure which is fabricated using a circular pattern of outer diameter $\sim$9.5 μm and inner diameter $\sim$7 μm. The circular structure is deposited using a $C_{10}H_8$ needle which provides the required carbon material. The structure is deposited on top of a self-supporting thin Au film. The structure is further cut at the base region and made to fall onto the ground using an ion-induced bending technique [10]. The final tube-like structure can be seen in Figure 11(b).

Using both the milling and deposition process, complicated structures or devices can be designed. Figure 12 shows an example of such an attempt to fabricate a nano-Langmuir probe to detect local plasma. A thin metallic film is deposited on a glass substrate and subsequently three separate pads are made using the FIB milling process. Two vertical walls of tungsten were made using the FIB deposition process and further, the inner sides of the walls were polished with selective ion beam irradiation.

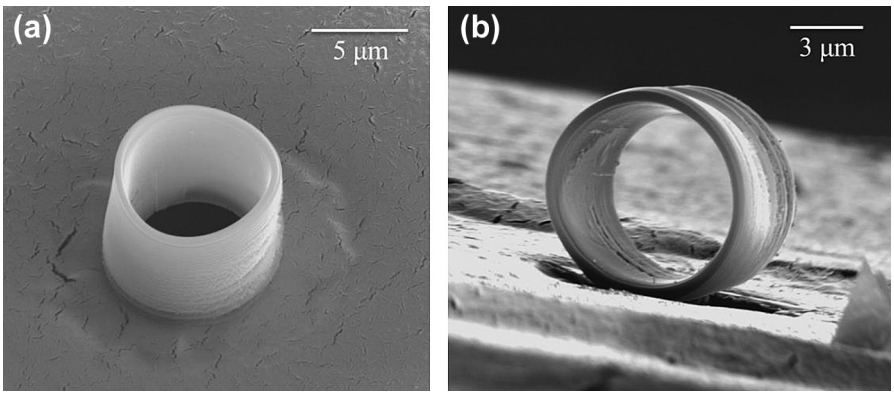

FIGURE 11

A cylindrical structure fabricated using the FIB deposition process.

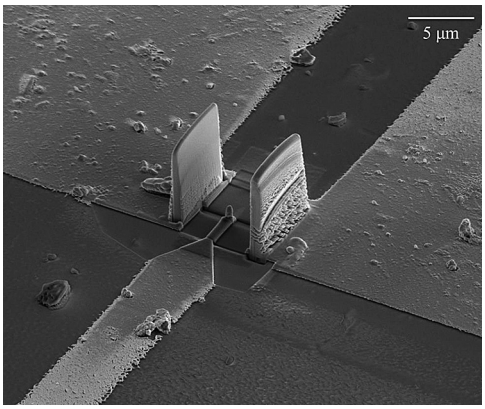

FIGURE 12

A nano-Langmuir probe along with two vertical side walls.

The purpose of the vertical walls was to create local plasmas within the micron region. To detect the plasmas, tungsten material was deposited on the third pad to make a nano-tip which acts as a nano-Langmuir probe.

Using the layer by layer deposition approach, complex structure can be smoothly and rapidly fabricated. In the patterning page of the GUI software, numbers of circular blocks are drawn which form a complete human-like structure (shown schematically in Figure 13(a)). In order to replicate this design into a product, the serial patterning approach is used. In this approach, the bottommost block is fabricated first. Subsequently, the next upper block is patterned. This is continued until

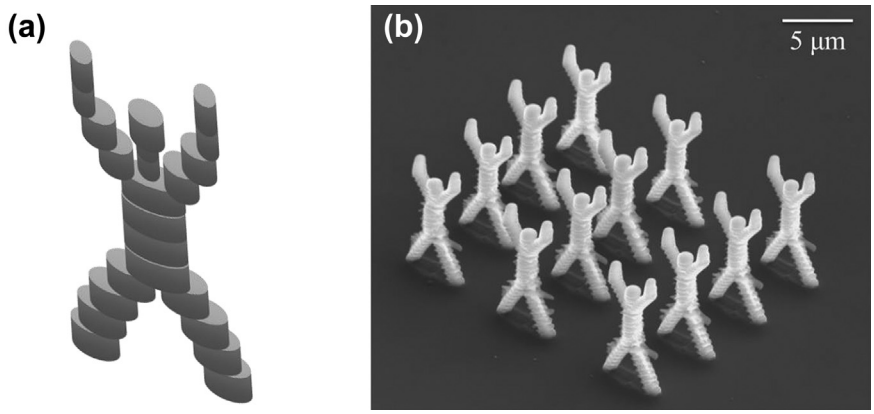

FIGURE 13

(a) Pattern of a human-like structure; (b) a fabricated branch of human-like structures using the pattern (a).

the topmost blocks are completed. The whole procedure can be used to fabricate a branch of such structures. In Figure 13(b), an army of such structures is shown.

CIRCUIT EDITING AND FAILURE ANALYSIS

Commercially, FIB has been used widely for circuit editing and design modifications. The precise cutting capability of the technique is used to remove/cut unwanted wiring and the deposition functionality of FIB helps in changing or adding new connections on the chip. Since different types of material (metallic or insulating) can be deposited on the site, accordingly circuit modifications or new design can be carried out efficiently. Thus, FIB can be used powerfully for debugging as well as for circuit modification. The process is simple and rapid, and highly used commercially.

TEM/STEM SAMPLE PREPARATION

The precised milling capability of the FIB cutting technique has been used successfully for TEM sample preparation. As a part of the preparation, a μ-sample (the dimension can be of the order of a few tens of microns) is prepared using the FIB cutting technique. Subsequently, it is attached to the manipulator needle with the help of the FIB deposition process. The sample is then mounted on the TEM grid with the following procedure: first the sample is attached with the help of the FIB deposition process; then the sample is detached from the manipulator by FIB cutting again. Further, with controlled and continuous FIB irradiation on the sample, a thin slice can be made, which can be used as a TEM or scanning TEM sample.

FIB AS AN ANALYTICAL TECHNIQUE

Apart from using the ion beam for milling, deposition, and imaging, FIB can also be used as an analytical technique. As a result of ion matter interaction, X-rays are also produced along with ions, cluster of atoms, SEs, photons, etc. In most of the samples, for keV ions, the collision cascade produced lies mostly within tens of nanometer from the sample surface. Also, the X-rays produced during the FIB processing can be utilized for elemental characterization. This process is known as particle-induced X-ray emission (PIXE). This has a special advantage over the EDS technique which uses an electron beam for the excitation. In EDS, the data collected carry information from a deeper part of the sample; on the other hand, X-rays produced during the FIB-PIXE process carries information from the surface only and for surface analysis purposes, this technique can provide more accurate information.

During the FIB milling, a huge amount of materials, particularly secondary ions, are produced. These ions can be collected and analyzed by magnetic lenses and filters.

In this way, the elemental composition of the sample can be determined easily. This secondary ion mass spectroscopy is a handy and useful analytical technique.

Auger electron spectroscopy (AES) is a surface analysis technique, which can be integrated with an FIB system. AES provides surface elemental information. Using the FIB milling technique, the sample can be cut slice by slice and simultaneously, surface elemental information can be collected efficiently.

SUMMARY: ISSUES AND FUTURE OF FIB

The efficacy of FIB technology is well accepted nowadays, even though FIB has several drawbacks. FIB is a destructive process. It damages the sample and modifies the inherent substrate properties. FIB uses ion particles (mostly Ga ions), and during the milling or deposition process, a large amount of Ga ion can remain on the site, which can modify the sample properties. The FIB deposition process is not a pure deposition process, in the sense that a large amount of impurity remains in the fabricated structure. This changes the electrical properties of the deposited structures. Moreover, the deposited materials are generally amorphous in nature.

During the FIB processing, the Ga ions can scatter. This is known as the "scattering effect" [29,30]. Because of the scattering, unwanted deposition often happens and additional ion beam irradiation has to be used to remove the unwanted deposition. To predict and compensate for the divergence through adjustment of the FIB processing parameters based on premachining simulation is another approach for the precise fabrication of 3-D micro-structures [31].

It is found that the postannealing of an FIB-made structure can help to reduce contamination [32]. Adding additional foreign molecules can also help in reducing a significant amount of impurity [33]. These techniques to improve FIB processing show a promising development in respect of securing a future flawless nanofabrication tool. Modern FIB systems based on He and Ne ion sources provide a low scattering effect because of the low masses of He and Ne. For precise nanomilling requirements such as in circuit designing on grapheme sheet or carbon nano-tube, nano-metric cutting on a chip, these modern FIB systems have a promising role.

REFERENCES

[1] Krohn VE. Progr Astronaut Rocketry 1961;5:73.
[2] Krohn VE, Ringo GR. Appl Phys Lett 1975;27:479.
[3] Seliger RL, Fleming WP. J Appl Phys 1974;45:1416.
[4] Yao N. Focused ion beam systems: basics and applications. Cambridge University Press; 2007.
[5] Archanjo BS, Barboza APM, Neves BRA, Malard LM, Ferreira EHM, Brant JC, et al. Nanotechnology 2012;23:6. 255305.

[6] Hirayama Y, Okamoto H. J Vac Sci Tech 1988;B 6:1018.
[7] Castillo-Garza R, Chang Chia-Cheng, Yan D, Mohideen U. J Phys Conf Ser 2009;161: 012005.
[8] Frabboni S, Gazzadi GC, Pozzi G. Appl Phys Lett 2008;93:073108.
[9] Banerjee A, Banerjee SS. Nanotechnology 2013;24:12. 105306.
[10] Rajput NS, Banerjee A, Verma HC. Nanotechnology 2011;22:7. 485302.
[11] Matsui S. Nucl Instrum Methods 2007;B 257:758.
[12] Kometani R, Morita T, Watanabe K, Hoshino T, Kondo K, Kanda K, et al. J Vac Sci Technol 2004;B 22:257.
[13] Stratton FP, Kubena RL, McNulty HH, Joyce RJ, Vajo J. J Vac Sci Technol 1998;B 16: 2449.
[14] Khizroev S, Hijazi Y, Chomko R, Mukherjee S, Chantrell R, Wu X, et al. Appl Phys Lett 2005;86:042502.
[15] Hoshino T, Ozasa A, Kometani R, Suzuki T, Matsui S, Mabuchi K. J Vac Sci Technol 2006;B 24:2538.
[16] Satriano C, Carnazza S, Licciardello A, Guglielmino S, Marletta G. J Vac Sci Technol 2003;A 21:1145.
[17] Wagner A, Levin JP, Mauer JL, Blauner PG, Kirch SJ, Longo P. J Vac Sci Technol 1990; B 8:1557.
[18] Orloff J, Utlaut M, Swanson L. High resolution focused ion beams: FIB and its applications. New York: Kluwer Academic/Plenum Publishers; 2003.
[19] Egerton RF. Physical principles of electron microscopy: an introduction to TEM, SEM, and AEM. New York: Springer; 2005.
[20] Zhou W, Wang ZL. Scanning microscopy for nanotechnology, techniques and applications. New York: Springer; 2006.
[21] Banerjee A, Mankad T, Dhamodaran S, Ramkumar J, Kulkarni VN. Nanotechnology 2009;20:7. 345501.
[22] Stojakovic D. Process Appl Ceram 2012;6(1):1−13.
[23] Ziegler JF. Nucl Instr Meth 2004;B 219−220:1027.
[24] Ohring M. The materials science of thin films. 2nd ed. Academic Press; 2002.
[25] Giannuzzi LA, Stevie FA. Introduction to focused ion beams: instrumentation, theory, techniques and practice. New York: Springer; 2005.
[26] Sigmund P. Phys Rev 1969;184:383.
[27] Feldman LC, Mayer JW. Fundamentals of surface and thin film analysis. New York: Elsevier Science Publishing Co; 1986.
[28] Tripathi SK, Shukla N, Kulkarni VN. Nucl Instrum Methods Phys Res 2008;B 266:1468.
[29] Tripathi SK, Shukla N, Rajput NS, Kulkarni VN. Nanotechnology 2009;20:6. 275301.
[30] Tripathi SK, Shukla N, Rajput NS, Singh AK, Kulkarni VN. Micro & Nano Lett 2010; 5(5):254−7.
[31] Sun J, Luo X, Ritchie J, Hrncir T. Proceedings for institution of mechanical engineers, part B. J Eng Manuf 2012;226(2):229−38.
[32] Langford RM, Wang T-X, Ozkaya D. Microelectron Eng 2007;84:784−8.
[33] Mehendale S, Mulders JJL, Trompenaars PHF. Nanotechnology 2013;24:7. 145303.

CHAPTER

Micro-electrical Discharge Machining

4

Eckart Uhlmann[1,2], Markus Röhner[2], Malte Langmack[1], Tassilo-M. Schimmelpfennig[2]

TU Berlin[1]; Fraunhofer IPK[2]

CHAPTER OUTLINE

Micromanufacturing Engineering and Technology. http://dx.doi.org/10.1016/B978-0-323-31149-6.00004-9

INTRODUCTION

Nowadays, micro-electrical discharge machining (μ-EDM) is applied in all kinds of fields concerning micro-machining. Especially in single part or small batch production μ-EDM can be used economically to produce micro-tools and micro-molds. By combining different process variants of μ-EDM with current machining processes such as micro-milling or laser ablation, a cost efficient mass production can be realized [30,31,36,39,40,42,43].

Based on a thermal material removal process, μ-EDM is working almost free of process forces. It is also independent of mechanical workpiece properties such as the Young's modulus or hardness. Bringing together huge geometrical freedom and precision, μ-EDM allows the machining of a wide range of electroconductive materials with a minimal conductivity of $\kappa = 0.01$ S/cm including high-temperature alloys, cemented carbide, and electroconductive ceramics.

WORKING PRINCIPLE

MACHINING PRINCIPLE OF ELECTRICAL DISCHARGE MACHINING

Electrical discharge machining (EDM) is a nonmechanical thermal shaping process with which material is removed by spatially and temporally separated electrical discharges between a workpiece electrode and a tool electrode. The high-frequency discharges cause melting and vaporization of material on the surface of both electrodes. To enhance the material removal, EDM operates in a nonconducting fluid, the dielectric fluid (Figure 1) [35,45].

During machining, the tool and workpiece electrode are positioned relatively to each other that a working gap s filled with dielectric fluid remains between them. Applying a voltage—depending on the working gap width and conductivity of the dielectric fluid—causes an expanding energetic plasma channel and a current flow after exceeding the dielectric strength of the fluid. Temperatures above $T = 10{,}000$ K [1] inside the plasma channel effect melting and vaporization processes of the material on the surfaces of both electrodes. By switching off the current, melted material is abruptly erupted due to an implosion of the plasma channel [2–5].

The result of a single discharge is a crater-shaped pit on the electrodes' surfaces named discharge crater (Figure 2(a)). Depending on the erosion

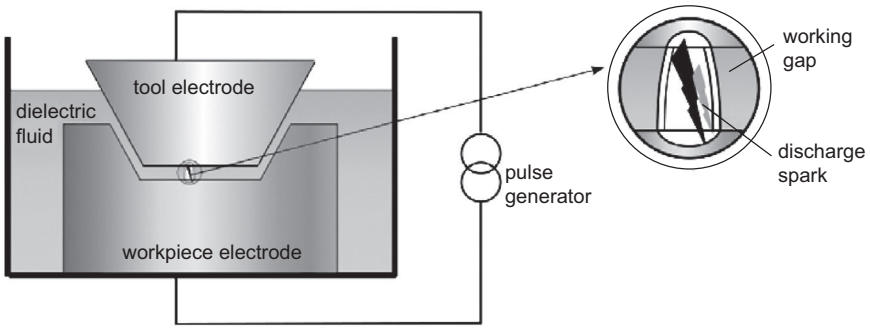

FIGURE 1

Principle illustration of the EDM process.

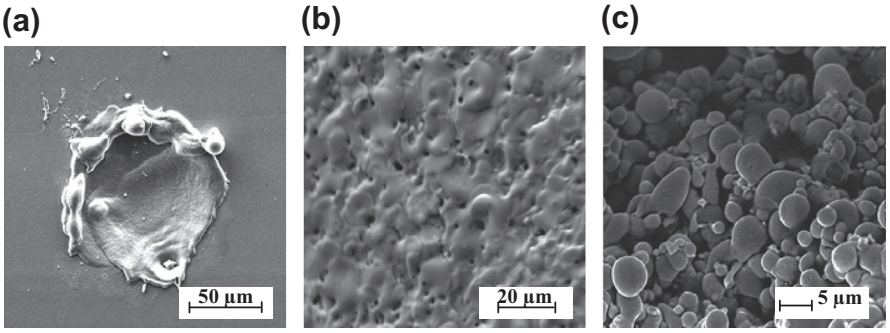

FIGURE 2

Single discharge crater (a), surface topography (b), and removed particles (c).

parameters such as the discharge time, discharge current or the type of dielectric fluid, typical crater diameters vary from around $d_c = 1$ µm [6] to around $d_c = 100$ µm. The EDM-specific surface topography is caused by a multitude of overlapping discharge craters (Figure 2(b)). The removed material mostly consists of ball-shaped particles (Figure 2(c)) [38].

PROCESS VARIANTS

With different variants µ-EDM is a very flexible machining process. Three variants of big industrial relevance are micro-die sinking (µ-die sinking) (Figure 3(a)), micro-wire electrical discharge machining (µ-WEDM) (Figure 3(b)), and micro-electrical discharge drilling (µ-ED drilling) (Figure 3(c)). In µ-die sinking, a shaped tool electrode is used for manufacturing three-dimensional shapes and free-forms. µ-WEDM comes into operation for cutting defined contours by using a fine wire electrode. µ-ED drilling, a special option of µ-die sinking, operates with a rotating pin electrode to produce micro-holes, e.g., as needed in fuel injection systems.

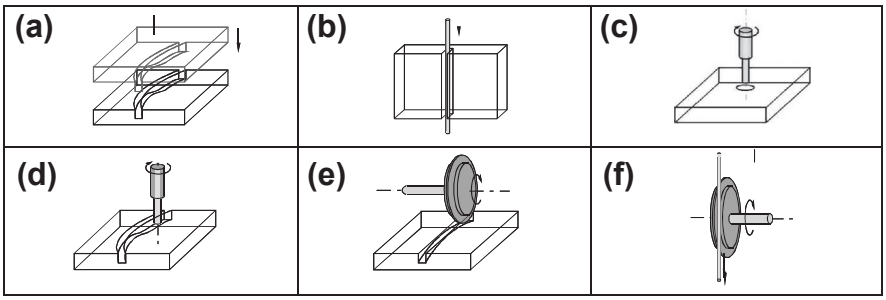

FIGURE 3

Process variants of micro-electrical discharge machining: micro-die sinking (a), micro-wire electrical discharge machining (b), micro-electrical discharge drilling (c), micro-electrical discharge milling (d), micro-electrical discharge grinding (e), and micro-wire electrical discharge grinding (f).

Processes with less industrial relevance are micro-electrical discharge milling (μ-ED milling) (Figure 3(d)), micro-electrical discharge grinding (μ-EDG) (Figure 3(e)), and micro-wire electrical discharge grinding (μ-WEDG) (Figure 3(f)). μ-ED milling is a further development of μ-ED drilling. In combination with a path-controlled motion in three dimensions, free-forms and cavities can be produced. The importance of this process is increasing because it delivers an option to relinquish laborious 3D-shaped tool electrodes. In analogy toward the kinematics of conventional grinding processes, μ-EDG is used for producing, e.g., micro-fluidic channels. For manufacturing, e.g., ejector pins, μ-WEDG is applied.

DIELECTRIC FLUID

The dielectric fluid has several main functions in the EDM process.

It isolates the tool electrode [7] from the workpiece electrode to achieve a high current density in the plasma channel. It cools down the heated surfaces of the electrodes and exerts a counter pressure to the expanding plasma channel [8]. Flushing with dielectric fluid removes the particles after the discharge process and prevents developing particle linkages causing process interruptions by short circuit, or damage of the electrodes' surfaces [9,32,34,37,44,46].

There exist two main types of dielectric fluids: deionized water and dielectric fluids based on hydrocarbon compounds also known as dielectric oil [35].

Deionized water, mostly tap water which was filtered by deionization resin to decrease electrical conductivity to $\kappa_w \sim 1$ μS/cm, has a higher conductivity and therewith a lower dielectric strength than hydrocarbon-based dielectric fluids with $\kappa_{hdf} < 0.1$ μS/cm. Due to the lower dielectric strength of deionized water, discharge sparks ignite more easy at bigger working gaps compared to dielectric oil. The higher vaporization heat of water-based dielectric fluids also removes more thermal energy from the process than hydrocarbon dielectric fluids. This especially becomes very important at short discharge durations and high effective pulse frequencies.

Table 1 Differences of Hydrocarbon Dielectric Fluids and Deionized Water

Type of Dielectric Fluid	Hydrocarbon Dielectric Fluids	Deionized Water
Electrical conductivity	<0.1 μS/cm	~1 μS/cm
Technological behavior	High material removal rate, small tool wear, big influence on peripheral zone	High material removal rate, high surface quality, high wear
Properties	No corrosion of workpiece, no deionization necessary, special disposal, low flash point, hazardous vapors	Not flammable, no hazardous vapors, no special disposal, corrosion
Application	Micro-die sinking	Micro-wire electrical discharge machining

In comparison to dielectric oil, deionized water effects a higher surface quality [10] and a higher material removal rate [9]. Furthermore, the influence on the subsurface formation also known as white layer is much lower using deionized water. Disadvantages of water-based fluids are high tool wear, workpiece corrosion, and deionization. Due to the high dielectric strength, dielectric oil can be used for high discharge energies with small working gaps applied for micro-die sinking operations. Special disposal of used oil and contaminated filters, low flash point, and hazardous vapors during the machining process cause problems while machining with hydrocarbon dielectric fluids [9]. Table 1 shows an overview of properties and technological behavior of hydrocarbon-based dielectric fluids and deionized water.

GENERAL FLUSHING STRATEGIES

To force a circulation in dielectric fluid and to clean the working gap from removed material particles, different flushing strategies are used. There are direct and indirect flushing strategies (Figure 4). Direct flushing, such as lateral flushing (Figure 4(a)),

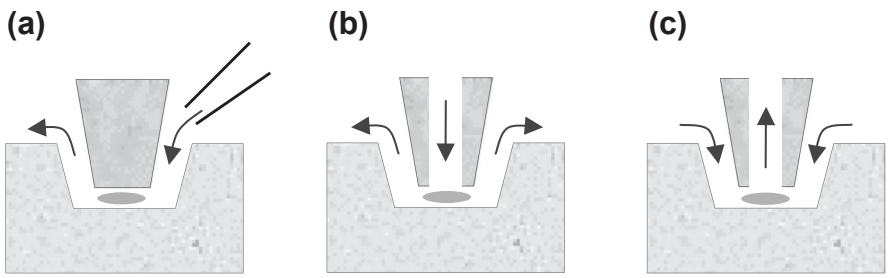

FIGURE 4

Illustration of direct flushing strategies: lateral flushing (a), pressure flushing (b) and suction flushing (c).

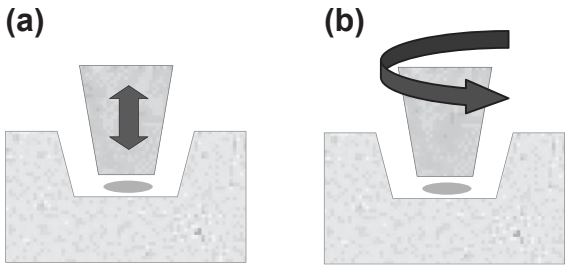

FIGURE 5

Illustration of indirect flushing strategies: lifting (a) and rotation (b).

pressure flushing (Figure 4(b)), or suction flushing (Figure 4(c)), is produced by a fluid pump. Flushing can also be pulsatory or intermittent.

In μ-EDM, flushing through the electrode is often impossible because of small electrode dimensions. Thus, a circulation in the dielectric fluid is realized by indirect flushing strategies (Figure 5). Indirect flushing is a result of a relative motion between the tool electrode and the workpiece that is superimposed onto the tool feed. The relative motion can be generated by a periodic high-frequency vibration (Figure 5(a)) or a rotary motion of the tool electrode (Figure 5(b)) created by a high speed spindle.

PROCESS

PROCEDURE OF A SINGLE DISCHARGE

A single discharge can be differentiated into four phases: the buildup phase, the ignition phase, the discharge phase, and the breakdown phase, as shown in Figure 6.

During the **buildup phase**, a voltage, which is called open circuit voltage u_0, is applied between the tool electrode and the workpiece. The voltage, with a level from $u_0 = 60$ V to $u_0 = 400$ V depending on the machining process [9], causes a strong electrical field at the working gap between the electrodes. An acceleration of existing free charge carriers inside the dielectric fluid takes place along the streamlines of the field [11]. Additionally, the electrical field effects an emission of electrons out of the cathode (field emission). With electrons moving toward the anode and ions that are attracted by the cathode, a current starts to flow. As a consequence, the dielectric fluid is heated above its boiling temperature, then vaporizes, and as a result a plasma channel is formed.

In the **ignition phase**, the accelerated electrons prompt an ionization, the so-called impact ionization, of neutral particles or molecules which rapidly increases the number of existing charge carriers. Passing a defined threshold causes the working fluid's dielectric strength to exceed. The ignition phase is directly

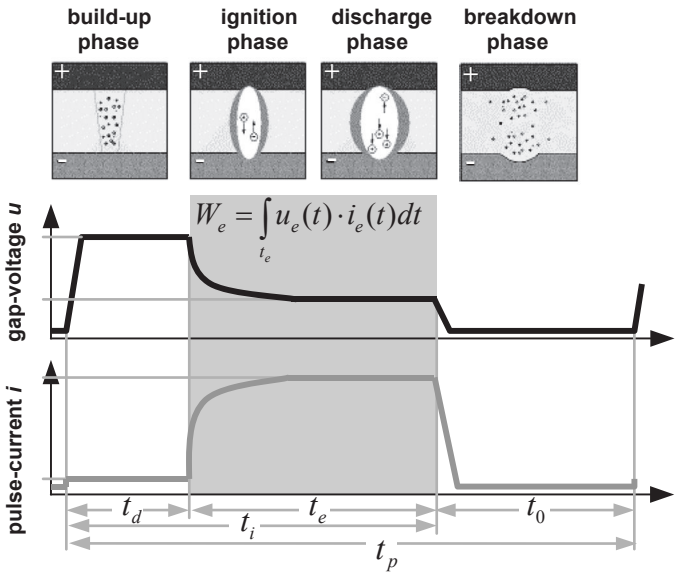

FIGURE 6

Illustration of a single discharge.

connected to a change in current and voltage. With building up a discharge channel, the open-circuit voltage u_0 drops to discharge voltage u_e which depends on the ohmic resistance in the working gap, and a discharge current i_e begins to flow on the superficial surface of the plasma channel [8]. Common discharge currents of μ-EDM range from $i_e = 1$ mA to a maximum of $i_e = 1$ A [9]. The time from applying the open circuit voltage u_0 to exceeding the dielectric strength is called the ignition delay time t_d.

During the third phase, named the **discharge phase**, the electrical energy is changed into heat energy because of the kinetic impact of charge carriers on the electrodes' surface. Due to different particle masses, the amount of melted material created by impacting electrons on the anode is less compared to that created by ions on the cathode. Furthermore, the material from the anode is mainly removed at the beginning of the discharge phase. For long discharge durations, t_e, the anodic material removal decreases toward zero, while the cathodic material removal increases and converges toward a specific value. This phenomenon, known as the polarity effect, can also be explained by the different mobility of the charge carriers [11]. Since μ-EDM operates at very short discharge durations from $t_e = 10$ ns to $t_e = 1$ μs, the tool electrode is usually charged as the cathode to reduce tool electrode wear [9].

The primary material removal takes place during the **breakdown phase**. Switching off the discharge current causes a collapse of the plasma channel. An induced low pressure reduces the boiling temperature of the melted material on the electrodes' surfaces and the material is vaporized or explosively erupted by

hydromechanical forces [2–5]. The amount of removed material mainly depends on the discharge energy W_e which is defined by:

$$W_e = \int_0^{t_e} u_e(t) i_e(t) dt \approx u_e \cdot i_e \cdot t_e \quad (1)$$

After discharge, the working gap is deionized and cleaned from particles by flushing with dielectric fluid during the pulse interval time t_0. The pulse interval time is generally set to be as long as the pulse duration t_i.

MICRO-WIRE EDM

Wire electrical discharge machining (WEDM), a process variant introduced industrially in 1969 [1], is characterized by a path programmed cut of the workpiece contour by a traveling wire electrode. The kinematics of WEDM is comparable to that of a band saw. The wire electrode is fed from a spool and "cuts" the workpiece along the programmed contour. Either the workpiece or the wire is moved relatively to each other in the *x*- and *y*-directions. For this reason, only two-dimensional and no free-form shapes can be machined. Conical shapes can be manufactured by a sloping position of the wire. Hereby the upper guide of the unwinding wire tool electrode is relatively adjustable in the *u*- and *v*-directions (Figure 7) to the lower guide. Due to wear and an associated decrease of the wire diameter, the wire electrode can only be used once. A reuse causes an increasing risk of tearing the wire electrode and of deviations in contour.

Multiple cutting strategies

To reach high surface quality and geometrical accuracies at efficient cutting speeds, multiple cutting strategies are used. The main cut is applied at the highest available

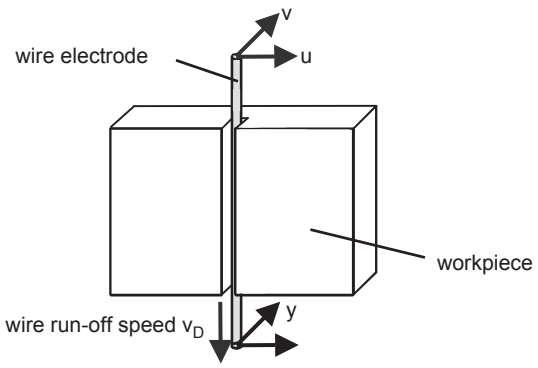

FIGURE 7

Illustration of wire electrical discharge machining.

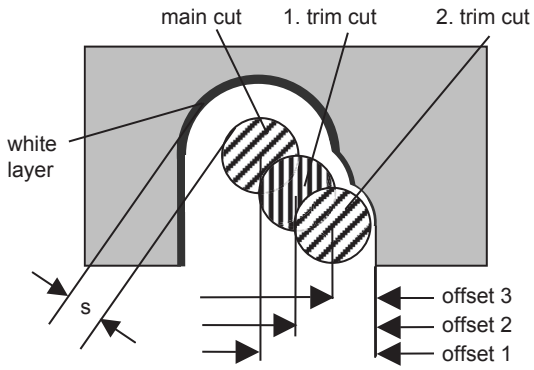

FIGURE 8

Multiple cutting strategy.

discharge energy. It is related to a maximum material removal rate, low surface quality, and a high thermal influence of the workpiece's peripheral zones, the white layer. Applying several trim cuts, where the discharge energy, working gap, and tool offset are successively decreased (Figure 8), causes a lower material removal, a thinner white layer (<1 μm), and a surface roughness down to $R_a = 0.07$ μm.

Micro-wire electrodes

In contrast to conventional wire electrodes that are generally made of copper or brass, premium electrodes for μ-WEDM have a more complex buildup, which is also very cost-intensive. Based on a steel or tungsten core which is coated with several layers (e.g., copper, zinc, silver) (Figure 9), it is possible to achieve a combination of high thermal and mechanical stability and high electrical conductivity. Additionally, the soft upper layers decrease abrasive wear of the machine's wire

FIGURE 9

Buildup of a micro-multilayer wire electrode.

guiding system. Micro-wires ranging from $d_w = 10$ µm to $d_w = 100$ µm have a tensile strength of $\sigma_z = 2000$ N/mm^2 to $\sigma_z = 3600$ N/mm^2.

Dielectric fluid and flushing

As in conventional WEDM, deionized water is also used as a dielectric fluid for µ-WEDM. To minimize the working gap and to increase shape contouring accuracy, the electrical conductivity of the water is reduced to $\kappa_w = 1$ µS/cm. Due to limited mechanical properties of the micro-wire, vibrations easily lead to inaccuracies in shape and a decrease in surface quality. To reduce occurring vibrations and the risk of a damaged micro-product, a very low flushing pressure $p_f < 1$ bar or no flushing is used during machining.

Dimensions and applications

µ-WEDM allows the production of very complex and fine 2 1/2D structures (Figure 10(a)). In combination with high-precision machines and special relaxation generators, shape accuracies of around ±1 µm at high aspect ratios of more than 100 can be machined by using several trim cuts [6]. An aspect ratio is the relation between a characteristic lateral dimension of a micro-structure and its height.

µ-WEDM is mainly used in the field of high-precision tool making for micro-mechanical and optical devices (Figure 10(b)). Other applications are micro-gears for the clock and watch industry (Figure 10(c)) and punching dies for electronic components. Micro-tools such as micro-grabbers or components for micro-reactor systems can also be machined by µ-WEDM [7].

Micro-wire electrical discharge grinding

A special variant of µ-WEDM is µ-WEDG (Figure 11). In µ-WEDG, the wire is moved along two axes of motion through a rotating cylindrical workpiece.

The rotation of the workpiece causes a uniform material removal that allows fabricating pin electrodes with minimal diameters of 5 µm or machining disc electrodes with thicknesses down to 7 µm used in electrical discharge contouring. Industrial applications of the µ-WEDG process are contact pins for micro-assembly [12],

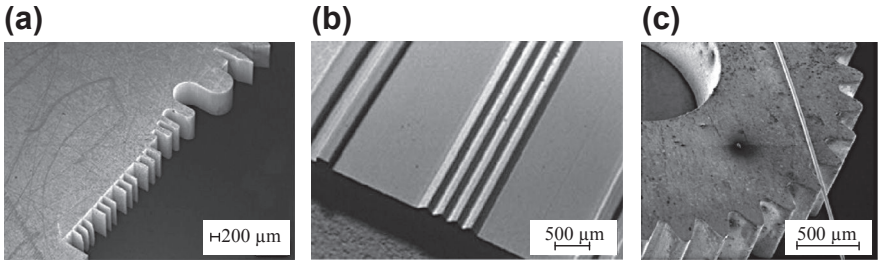

FIGURE 10

Micro-structured referential workpiece (a), mold insert for hot embossing micro-optoelectronic connecting plugs (b), and micro-gear of a micro-planetary drive (c).

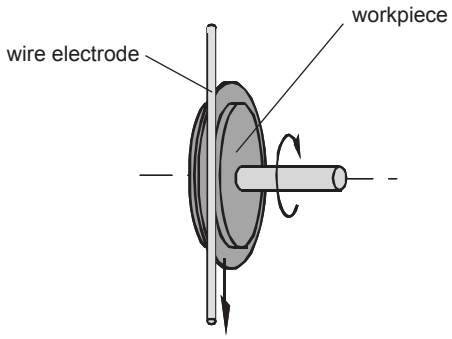

FIGURE 11

Illustration of the micro-wire electrical discharge grinding process.

ejector pins for injection molds, or micro-single blade milling tools [13,14]. Other examples are gear shafts that are free of join patches [14,15] or components for micro-turbines [16].

MICRO-DIE SINKING EDM

μ-Die sinking EDM is characterized by the replication of the tool electrode's shape into the workpiece. The tool's path motion is basically single axial and the machining is realized in several steps to achieve high surface and geometrical quality. For the finishing of lateral surfaces, planetary machining steps come into operation.

To receive smallest discharge energies for μ-die sinking EDM and high surface quality, generators based on capacities, so-called relaxation generators, are used. Discharge capacitors of $C_e = 10$ pF are able to generate impulses with discharge durations of $t_e = 40$ ns at discharge currents of $i_e = 100$ mA to obtain discharge energies of $W_e = 0.1$ μJ [9]. To allow an adequate material removal rate, maximum pulse frequencies of up to $f_p = 10$ MHz are generated [17]. Due to the very short discharge duration, the tool electrode (Figure 12) is charged cathodic and the workpiece is anodic.

Micro-die sinking electrodes

The shape accuracy is mainly influenced by electrode wear. For this reason, suitable materials must offer high electrical conductivity as well as high thermal conductivity and a high melting temperature. Since the main rate of all shaped electrodes is formed by milling processes, these materials should be easy to machine. Further shaping processes for micro-tool electrodes are μ-WEDM and lithography, electroplating, and moulding (LIGA) technology (Figure 13). Even though thermally and mechanically resilient materials such as graphite, cemented carbides, or tungsten-copper are used for tool electrodes, the relative wear can rise above 30% and is extremely noticeable at structure edges and corners due to increased electric field strength.

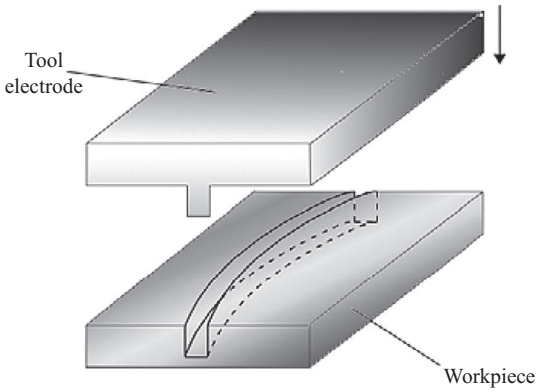

FIGURE 12

Illustration of the micro-die sinking process.

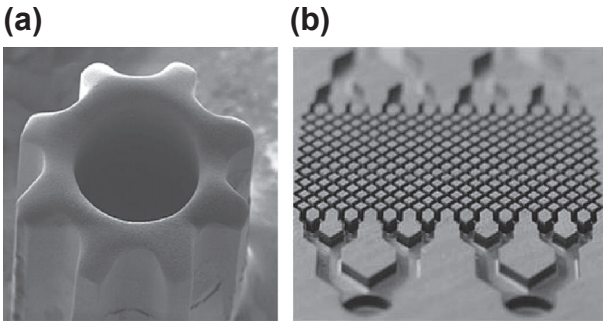

FIGURE 13

Micro-tool electrodes: gearwheel (a) and fluid mixer (b).

Dielectric fluid and flushing

Often small dimensions or low mechanical stabilities of the structures on the tool electrode or the workpiece prevent direct flushing strategies. In this case, either no or indirect flushing is used. Due to its high dielectric strength, dielectric oil with low viscosity around $\nu_o \leq 1.8\,mm^2/s$ is applied as dielectric fluid in the micro-die sinking process. Compared to deionized water, the oil's higher dielectric strength causes smaller working gaps and therewith higher shape accuracies of the workpiece.

Dimensions and applications

Nowadays, μ-die sinking is mostly used in single or small batch production. The main application field is the fabrication of tools for micro-embossing (Figure 14(a)) or micro-injection molding (Figure 14(b) and (c)). Minimal structure

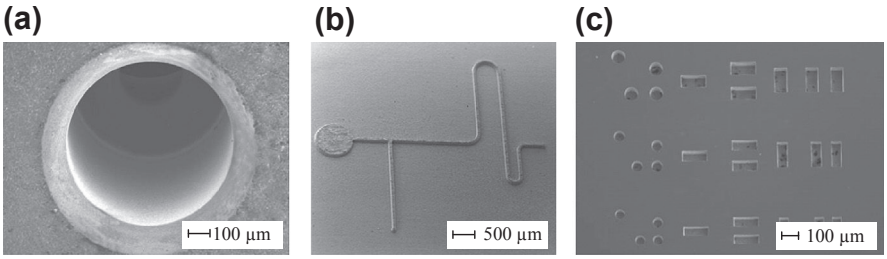

FIGURE 14

Micro-fabricated die for shaping small silver pins (a), mold insert for hot embossing fluidic micro-components ("lab-on-a-chip") (b), and mold insert with different referential structures (c).

widths that can be achieved by µ-die sinking vary from 20 µm to 40 µm [1,6]. Also, channels of around 20 µm and corner radii of 10 µm at aspect ratios of up to 25 can be produced. Deviations of contouring accuracies are ±1 µm [1].

MICRO-ELECTRICAL DISCHARGE DRILLING

A special application of µ-die sinking is µ-ED drilling, which uses small pin electrodes for the manufacturing of boreholes. The rotating or stationary pin electrode is moved single axially into the workpiece (Figure 15).

Micro-drilling electrodes

Conventional electrodes for µ-ED drilling made from cemented carbide are available with diameters down to $d_p = 45$ µm. Production, handling, and positioning

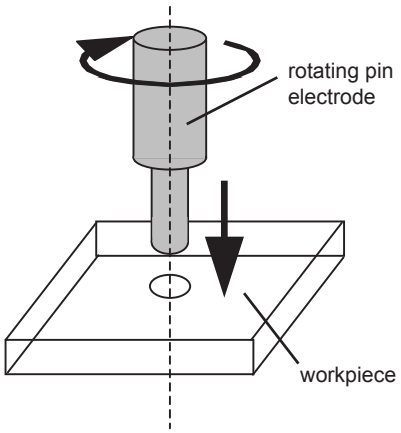

FIGURE 15

Illustration of the micro-electrical discharge drilling process.

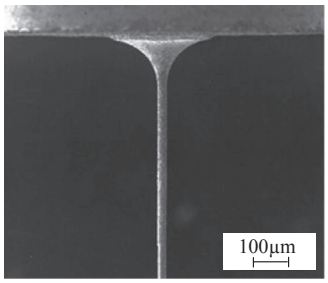

FIGURE 16

Electrode for micro-electrical discharge drilling made of cemented carbide.

(Figure 16) of these electrodes are challenging [6]. Special guiding systems also made from cemented carbide or ceramics are needed for the exact guiding and positioning. Tungsten, tungsten-copper, copper, and brass is used as electrode material. Pin electrodes with diameters smaller than $d_p = 45$ µm can be produced using µ-WEDG.

Dielectric fluid and flushing

As in µ-die sinking, either deionized water or oil with a low viscosity is used as dielectric fluid. To improve flushing conditions inside the gap and to obtain higher accuracies in roundness, higher aspect ratios and higher material removal rates, the electrodes are rotated at speeds of up to $n_r = 2000$ l/min [6,18–22]. Additionally, the effectiveness of the flushing is increased by a translatory vibration with an amplitude between 4 µm and 20 µm and a frequency of 50 Hz to 300 Hz which can be superimposed onto the feed of the electrode.

Dimensions and applications

Boreholes with aspect ratios of 10 to above 50 for tool electrodes with diameters ranging from $d_e = 25$ µm to $d_e = 100$ µm can be machined by µ-ED drilling [6]. Reproducible hole diameters of $d_h = 30$ µm can be produced with a shape accuracy of ± 2 µm. Minimal diameters of $d_h = 6$ µm [28] and $d_h = 2.9$ µm have been achieved. µ-ED drilling is mainly used for the fabrication of common rail injection nozzles, cooling boreholes of turbine blades, or starting holes for µ-WEDM [6]. Figure 17 shows examples for applications like boreholes for ejector pins in embossing tools (Figure 17(a)) or spinning nozzles in a ceramic plate with a depth of 1 mm and a diameter $d_h = 80$ µm (Figure 17(b)).

MICRO-ELECTRICAL DISCHARGE CONTOURING

Using process variants such as µ-die sinking or µ-WEDM, the fabrication of large molds with widely spread micro-structures of different heights is sometimes very cost-intensive or not possible at all. Reasons for this are the limited workpiece heights caused by the micro-wire's mechanical and thermal stability, or maximal

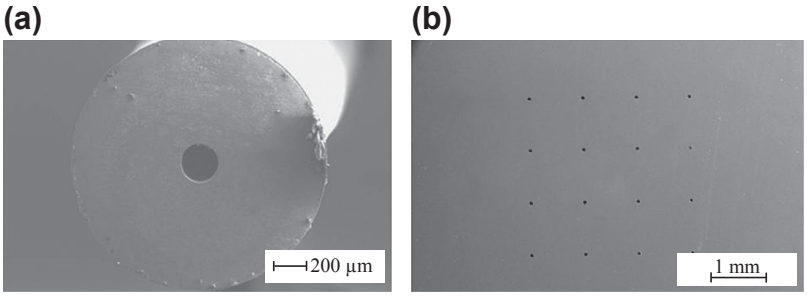

FIGURE 17

High-precision borehole in an ejector pin (a), spinning nozzles in a ceramic plate (b).

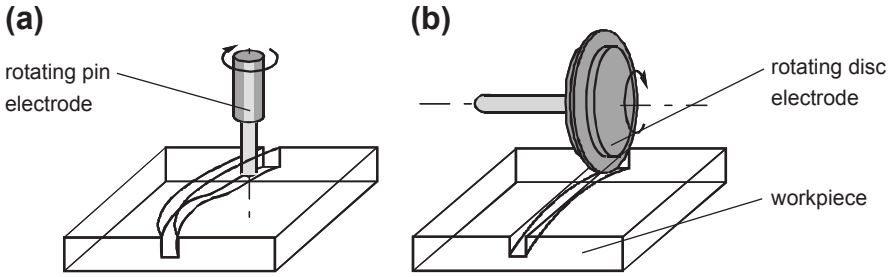

FIGURE 18

Illustration of micro-electrical discharge milling (a), and micro-electrical discharge grinding process (b).

overall dimensions of the die considering adequate flushing conditions inside the working gap. As an alternative, micro-electrical discharge contouring process variants such as µ-ED milling or µ-EDG can be used.

In contrast to µ-ED drilling which only works in one direction, µ-ED milling uses a rotating pin electrode that is moved through the workpiece on a defined three-dimensional path (Figure 18(a)). Typical infeed rates of the pin vary from 0.5 µm/s to a maximum of 10 µm/s [23]. Thus, in electrical discharge milling, it is possible to produce free-forms and cavities without fabricating a special tool electrode.

µ-EDG (Figure 18(b)) uses a rotating disc electrode instead of a pin electrode. The profile of the disc is reproduced in the workpiece as a channel. Similar to µ-ED milling, the electrode can also be moved in three dimensions which enables the fabrication of long, curved channels of different depths.

Micro-electrical discharge contouring electrodes

Even though high strength materials such as cemented carbide, tungsten, or tungsten-copper are applied, the tool wear of the pin electrode with a minimal

diameter of $d_m = 45$ µm is very high. In electrical discharge contouring, it is possible to regulate the wear by using special wear compensation algorithms that converted into computer numerical-controlled (CNC) language. Disc electrodes can be used for the manufacturing of extensive channel structures which cannot be produced by µ-WEDM. A main advantage of disc electrodes is the allocation of the wear on the circumferential length. Disc electrodes made of tungsten copper can either be produced by cutting removal processes or µ-WEDG. Electrodes with minimal widths of 7 µm have been successfully manufactured by µ-WEDG and have been applied [24–26].

Dielectric fluid and flushing

Due to the open shape of the workpiece and the rotating electrode in micro-electrical discharge contouring, the flushing conditions inside the working gap are comparable to micro-die sinking EDM. With regard to the variant of µ-ED milling, flushing through the electrode can be applied to increase material removal and decrease machining time.

Dimensions and applications

Today, µ-ED milling is used for the fabrication of cavities (Figure 19(a)) or channels in injection molds, reliefs in embossing dies, or prismatic micro-molds [23]. Due to its novelty, long machining time and disadvantages regarding finishing strategies, µ-ED milling has only a small relevance in industrial application so far. µ-EDG realizes the fabrication of very long structures which predetermine this process variant for the production of micro-fluidic channels (Figure 19(b)). Other industrial applications are the postproduction of cutting inserts made of polycrystalline diamond or cemented carbides and micro-structuring of grinding wheels [27].

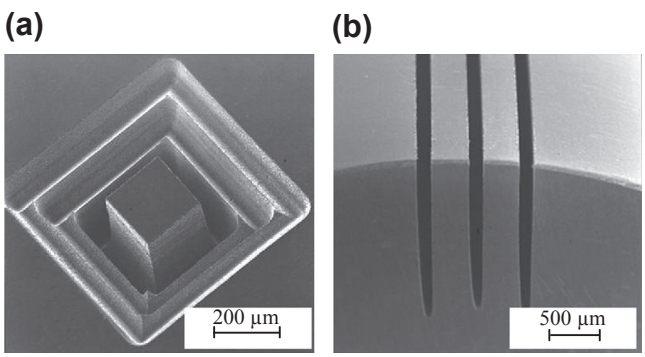

FIGURE 19

Cavity fabricated by micro-electrical discharge milling (a), micro-electrical discharge grinding produced micro-fluidic channels (b).

MATERIAL

Every material with an electrical conductivity above $\kappa = 0.01$ S/cm can be machined by EDM (Figure 25). Mechanical properties such as Young's modulus, hardness, or strength do not have an influence on the process behavior. Consequently, EDM is especially used for the machining of hard and difficult-to-cut materials such as cemented carbides for punching tools, polycrystalline diamond for cutting inserts, or high alloy steels for injection molding tools.

The amount of material being removed is influenced by its thermal and electrical properties. Contrary to a high electrical conductivity (Figure 26(a)) that promotes material removal, high thermal conductivity, and high melting temperature reduce the material removal (Figure 26(b) and (c)). This is of special importance when selecting wear resistant electrode materials.

TOOL ELECTRODES

Up-to-date tool electrode materials for μ-EDM are electrolyte copper, tungsten, and tungsten composites such as tungsten copper or tungsten carbide.

The attractive attributes of **electrolyte copper** are its high electrical and thermal conductivity. Electrolyte copper is easy to obtain, very consistent in quality, and low in cost. A disadvantage of the material is its limited grind ability [8]. Due to mechanical instability, the material's ductility and softness can cause problems when milling small structures. Another problem is the high wear of electrodes made from electrolyte copper.

Tungsten is a metal of very high strength, density, and hardness. With a melting point near 3400 °C, it resists thermal damaging effects of the EDM process very well. Disadvantages of tungsten are a very high material price. It is also difficult to machine because of its high hardness. To make tungsten more attractive for certain applications, it is combined with ductile materials such as copper.

The resulting material, **tungsten-copper**, is easier to machine, more conductive than normal copper, and extremely wear resistant. Especially in the field of microstructuring and surface finishing, tungsten copper is used as the tool electrode material [41].

MACHINERY

MACHINE DESIGN

Basic EDM equipment consists of the machine unit with actuation components, the generator, the dielectric unit including pumps, filters, and cooling (Figure 20), and in the case of WEDM, a deionization unit (Figure 21). To ensure the high precision of μ-EDM, many components of the system are produced with materials of a long-term thermal and mechanical stability such as ceramics. Also, servo drives with positional accuracies of around 1 μm and high-precision clamping systems are used.

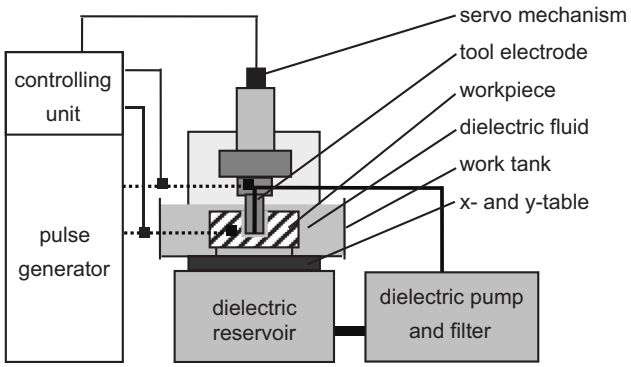

FIGURE 20

Die-sinking electrical discharge machine tool.

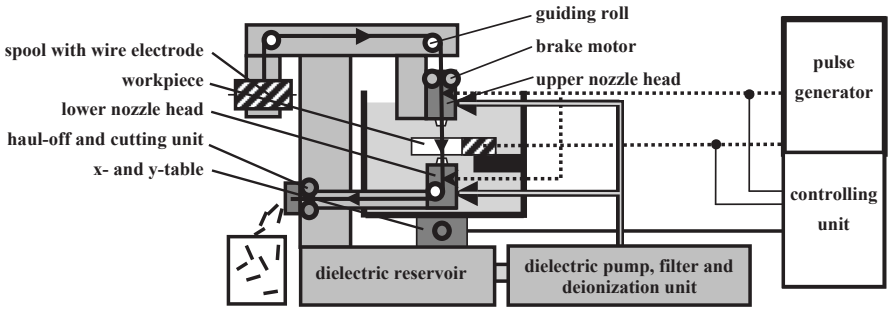

FIGURE 21

Wire electrical discharge machining system.

Die-sinking EDM machine

Die-sinking EDM machines are mainly built as a C-frame construction (Figure 20). The tool electrode is moved along the z-axis by a servo drive which is controlled by the machine control. The controlling unit is connected to a power supply that provides a pulsed DC output, the so-called pulse generator. The power supply is also controlled. The workpiece, which is immersed in a tank of dielectric fluid, is connected to one lead of the pulse generator. The tool electrode is linked to the other lead of the power supply. The tank is placed on an x- and y-axis table and is moved during the machining process. It is combined with a dielectric pump, a fluid reservoir, and a filter system. The pump provides pressure for flushing the working gap. The filter system refines removed material particles from the dielectric fluid. The dielectric reservoir stores and cools additional dielectric fluid and provides a container for draining the dielectric fluid between the operations.

Wire EDM machine

In wire EDM machines (Figure 21), which are built as a C-frame or gantry portal construction, the wire electrode is constantly fed from a spool. It is guided by rolls through an upper and lower nozzle head. The lower nozzle head is fixed. The upper nozzle head can be moved horizontally (u, v) and vertically (z). Thus, in combination with an x- and y-motion of the workpiece, it is possible to machine conical shapes of different heights with angles ranging from 0° to 15°, depending on the machine design. To reduce oscillations caused by electromagnetic, electrostatic, or hydromechanical forces, the wire is strained with a defined force that is generated by a brake motor and a haul-off unit. After use, the wire is cut, chopped, and recycled.

GENERATOR TYPES

Modern EDM machines provide two different types of generators in order to fit a wide range of different applications: static pulse generators for roughing operations and relaxation generators for micro-structuring and finishing operations.

Static pulse generators

Static pulse generators are characterized by a controlled current or voltage source which generates rectangular single pulse discharges [8]. The source is directly connected to the discharge path via electronic switching elements (Figure 22). Pulse shape, pulse duration t_i, and discharge duration t_e can be adjusted and controlled for the realization of a relatively low wear of the working electrode.

In contrast to relaxation generators, static pulse generators allow the setting of the discharge duration t_e independently of the discharge current i_e and are normally used for intensive material removal processes with long discharge durations t_e and high discharge currents i_e [34,38,46].

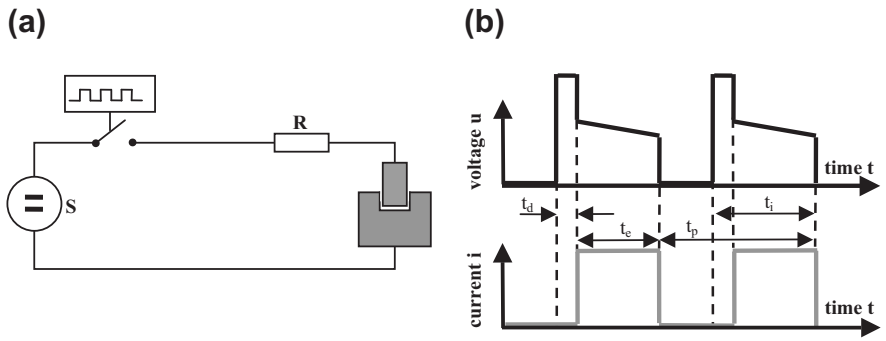

FIGURE 22

Static pulse generator: schematic illustration (a), voltage and current diagram including ignition delay time (t_d), discharge duration (t_e), pulse duration (t_i), and pulse cycle time (t_p) (b).

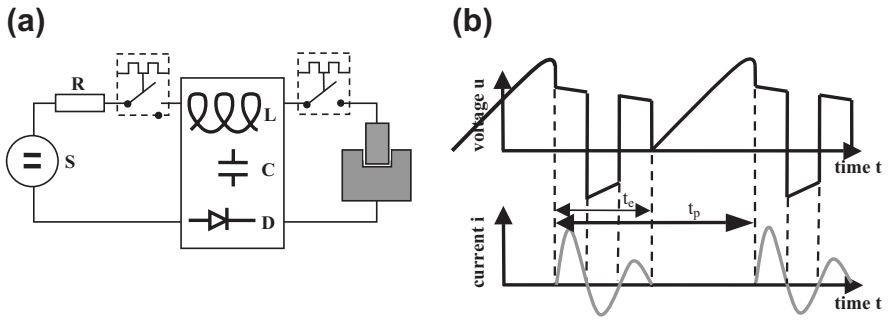

FIGURE 23

Relaxation generator: schematic illustration (a), voltage and current characteristic including discharge duration (t_e), and pulse cycle time (t_p) (b).

Relaxation generators

The principle setup of a relaxation generator is a direct current source in combination with different storage elements (RC, RLC, or LC circuits) [8] (Figure 23). In case of charged storage elements, the gap between the tool electrode and the workpiece serves as a switch. After exceeding the dielectric strength of the dielectric fluid, an oscillating discharge is released. Discharge duration t_e and discharge current i_e depend on the value of the capacity and cannot be controlled independently as this is the case with a static pulse generator. Additionally, the pulse frequency depends on the charging voltage of the capacity. Due to very small discharge energies of down to $W_e = 0.1\ \mu J$ at high pulse frequencies of up to $f_p = 10\ MHz$, relaxation generators are used for micro-machining and precise surface finishing [29,33,38,41].

Adaptive feed control

In contrast to cutting technologies, the feed rate in EDM is adaptively controlled by the control of the EDM machine. A constant feed rate can lead to short circuits, resulting in a destruction of the micro-structures. The adaptive feed control analyzes the measured parameters of the electrical impulse characteristics and classifies them using a pulse detection unit. According to that detection, the feed rate is regulated by a control circuit.

The electrical impulses are classified in four different types (Figure 24) which result from the conditions inside the gap: no-load discharge, normal discharge, arc discharge, and short circuit.

No-load discharges occur when the working gap is oversized. As a consequence the buildup of a plasma channel is prevented and the discharge current does not flow. The adaptive feed control reacts with an increase of the feed rate. At a **normal discharge**, the width of the working gap has an optimal size. For the following discharges, the adaptive feed control tries to keep a constant feed rate. An **arc discharge** is characterized by a premature ignition of the spark. The real ignition delay time t_{dr} is far below the set value of the ignition delay time t_d. This type of

Discharge type	No-load discharge	Normal discharge	Arc discharge	Short circuit
Cause	Working gap is too big	Working gap is optimal	Working gap is too small	Working gap $s = 0$
Illustration	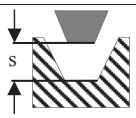	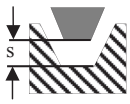		
Effect	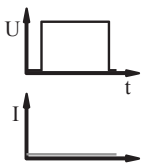	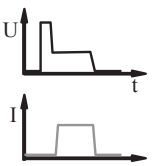	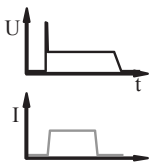	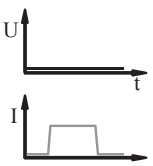
Reaction	Increase of feed rate	Constant feed rate	Decrease of feed rate	Pullback of tool electrode

FIGURE 24

Illustration of the principle controlling strategies.

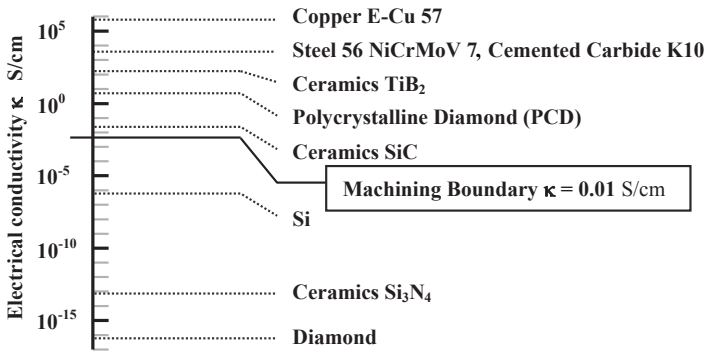

FIGURE 25

Machinable and nonmachinable materials.

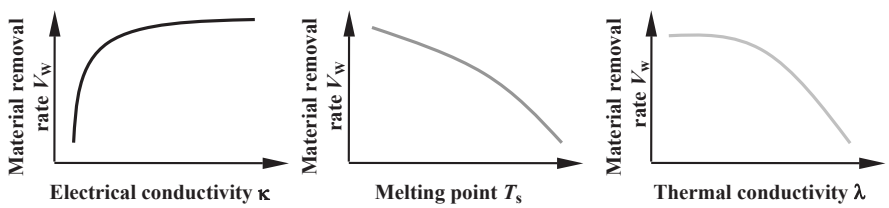

FIGURE 26

Influence of thermal and electrical properties on material removal rate.

Table 2 Table of μ-EDM Process Variants According to Performance and Applications

Process Variant	Geometry Complexity	Structure Dimension	Surface Quality	Application Examples
Micro-wire EDM (μ-EDM)	• 2½D • Tapered surfaces with maximal angles of 15°	• Minimum inner radii, cutting width, and maximum workpiece height depends on wire diameter, e.g., at $d_{wmin} = 0.03$ mm, $s_{min} = 0.005$ mm, $h_{max} = 5$ mm	$R_a \sim 0.07$ $R_z \sim 0.35$ (with multiple cutting strategy)	• Forming tools for optoelectronic components • Lead frame stamping tools • Spinning nozzles • Micro-gears
Micro-die sinking (μ-die sinking)	• 3D • Freeform surfaces • Undercuts possible by planetary erosion • Limited by electrode manufacturing	• Minimum structure width ~0.02 mm • Aspect ratio ~20	$R_a \sim 0.1$ μm $R_z \sim 0.5$ μm (in all directions)	• Micro-injection molds • Embossing molds for micro-optics
Micro-electrical discharge drilling (μ-ED drilling)	• 2D • Boreholes	• Borehole diameters down to $d_{min} = 0.04$ mm • Aspect ratio from 25 to 50	$R_a \sim 0.3$ μm $R_z \sim 1.5$ μm (lateral)	• Injection nozzles • Micro-fluid systems • Starting holes for μ-WEDM
Micro-electrical discharge grinding (μ-EDG)	• 2½D • Straight partly vertically curved channel structures • Profile of structure depends on cross-section of disc	• Minimum structure widths of 0.07 mm • Aspect ratio ~15 • Possible length depends on electrode wear (>50 mm)	$R_a \sim 0.2$ μm $R_z \sim 0.8$ μm (in all directions)	• Embossing and coining tools • Micro-fluid channels
Micro-electrical milling (μ-ED milling)	• 3D • Free-form surfaces	• Minimum inner radii depend on pin diameter • Applicable electrode diameter $d_{min} = 0.1$ mm	$R_a \sim 0.2$ μm $R_z \sim 0.8$ μm (in all directions)	• Cavities for micro-injection molding • Embossing or coining tools
Micro-wire electrical discharge grinding (μ-wire EDG)	Rotational symmetric structures (discs, pins)	• Minimum pin electrode diameter $D_{min} \sim 0.02$ mm • Aspect ratio ~30	$R_a \sim 0.15$ μm $R_z \sim 0.75$ μm	• Pin electrodes • Rolling tools

Table 3 Cost Listing AGIE Evolution/Classic 2/3 S

Wearing parts	€0.30
Filter	€0.61
Deionization resin	€0.51
Water	€0.06
Electricity	€0.58
Wire costs	€2.52
Total	**€4.58**

discharge is caused by a high concentration of electroconductive particles inside the gap. This status is normally followed by a series of normal discharges. The adaptive feed control reacts with a decrease in feed. **Short circuits** can either occur due to contact between the tool electrode and the workpiece or because of remaining particles that form an electrical linkage [9]. To leave that state, the tool electrode is pulled back along the machining path.

Depending on the application, different control technologies and strategies based on fuzzy logic are used in modern μ-EDM machines such as adaptive control optimization or adaptive control constraint.

APPLICATIONS

A final summary of the chapter and the wide application field of μ-EDM are shown in Tables 2 and 3.

REFERENCES

[1] Menz W, Mohr J, Paul O. Mikrosystemtechnik für Ingenieure. KGaA, Weinheim: Wiley-VCH Verlag GmbH Co; 2005.
[2] Lazarenko BR, Lazarenko NI. Elektrische Erosion von Metallen. Moskau: Cosenergoidat; 1944.
[3] Lazarenko BR. Die Elektrofunkenbearbeitung von Metallen. Vestuik Maschinostroia; 1974.
[4] Zolotych BN. Physikalische Grundlagen der Elektrofunkenbearbeitung von Metallen. Berlin: SVT 175 VEB-Verlag Technik; 1955.
[5] Zolotych BN. Über die physikalischen Grundlagen der elektroerosiven Metallbearbeitung, Bd. 1: Elektroerosive Bearbeitung von Metallen. Moskau: Akademie der Wissenschaften der UdSSR; 1957.
[6] Uhlmann E, Piltz S, Doll U. Machining of micro/miniature die and moulds by electrical discharge machining – recent development. J Mater Process Technol Elsevier 30 August 2005;167(2–3):488–93.
[7] Brück R, Rizvi N, Schmidt A. Angewandte Mikrotechnik – LIGA – laser- Feinwerktechnik. Carl Hanser Verlag München Wien; 2001.

[8] König W. Fertigungsverfahren band 3. Düsseldorf: VDI-Verlag GmbH; 1990.
[9] Piltz S. Grundlagen und Prozessstrategien der Mikrofunkenerosion für die Bearbeitung von Rotationsbauteilen. Stuttgart: Fraunhofer IRB Verlag; 2007.
[10] Siebers F-J. Funkenerosives Senken mit wässrigen Arbeitsmedien, Grundlagen, Technologie und Wirtschaftlichkeit [dissertation]. RWTH Aachen; 1994.
[11] Schönbeck J. Analyse des Drahterosionsprozesses. Carl Hanser Verlag München Wien; 1993.
[12] Langen HH, Masuzawa T, Fujino M. Modular method for microparts machining and assembly with self-alignment. Ann CIRP 1995;44(1).
[13] Fleischer J, Masuzawa T, Schmidt J, Knoll M. New applications for micro EDM. In: Proc. of the 14th international symposium for electromachining (ISEM XIV), March 30−April 1, 2004, Edinburgh, Scotland, UK, published in J. of materials processing technology, 149(1−3); 2004.
[14] Fleischer J, Schmidt J, Knoll M, Haupt S, Müller C, Förster R, et al. Mikrobearbeitung durch Abtragen, 94. Jahrgang: wt Werkstattstechnik Online; 2004. C H. 11/12.
[15] Förster R. Untersuchung des Potenzials elektrochemischer Senkbearbeitung mit oszillierender Werkzeugelektrode für Strukturierungsaufgaben der Mikrosystemtechnik [dissertation]. Albert-Ludwig-Universität Freiburg; 2004.
[16] Masaki T, Kawata K, Masuzawa T. Micro electro-discharge machining and its applications. Proc IEEE MEMS 1990, INSPEC Accession Number: 3764171.
[17] Masaki T. Micro electro-discharge machining. In: Proceedings of the 9th international symposium for electromachining-ISEM IX. Nagoya (Japan); 1989.
[18] Allen D, Almond H, Logan P. A technical comparison of micro-electro-discharge machining, microdrilling and copper vapour laser machining for the fabrication of ink jet nozzles. In: Proc. of SPIE conference on design, test, integration and packaging of MEMS/MOEMS, 4019, Paris, France, May 9−May 11, 2000.
[19] Ghoreishi M, Atkinson J. Vibro-rotary electrode, a new technique in EDM drilling − performance evaluation by statistical modelling and optimisation. In: Proc. of the 13th international symposium for electromachining (ISEM XIII), vol. II, Bilbao, Spain, May 9−May 11, 2001.
[20] Ghoreishi M, Atkinson J. A comparative experimental study of machining characteristics in vibratory, rotary and vibro-rotary electro-discharge machining. J Mater Process Technol 2002;120.
[21] Muttamara A, Fukuzawa Y, Mohri N, Tani T. Probability of precision machining of insulating Si_3N_4 ceramics by EDM. J Mater Process Technol 2003;140.
[22] Uhlmann E. Funkenerosives Feinbohren keramischer Werkstoffe. Abschlussbericht zum DFG-Forschungsprojekt UH 100/22−2. Berlin: Technische Universität; 2002.
[23] Meeusen W, Reynaerts D, Peirs J, Van Brussel H, Dierickx V, Driesen W. The machining of freeform micro moulds by micro EDM − work in progress. In: Proc. of micromechanics Europe workshop, Cork, Ireland (MME 2001).
[24] Wolf A, Ehrfeld W, Lehr H, Michel F, Richter T, Gruber H, et al. Mikroreaktorfertigung mittels Funkenerosion, 105. F&M Fernwerk- und Mikrotechnik; 1997. C 6.
[25] Chow H-M, Yan B-H, Huang F-Y. Micro slit machining using electro-discharge machining with a modified rotary disk electrode (RDE). J Mater Process Technol 1999;91.
[26] Kuo C-L, Huang J-D. Fabrication of series-pattern micro-disk electrode and its application in machining micro-slit of less than 10 μm. Int J Mach Tools Manuf 2004;44.

[27] Appel S. Funkenerosive Bearbeitung von ploykristallinem Diamant [dissertation]. Technische Universität Berlin; 1998.
[28] Allen DM. Micro electro discharge machining for MEMS applications. In: IEE seminar on demonstrated micromachining technologies for industry; 2000. Ref. No. 2000/032.
[29] Ekmekci B, Sayar A, Öpöz TT, Erden A. Geometry and surface damage in micro electrical discharge machining of micro-holes. J Micromech Microeng 2009;19:1−16.
[30] Ho KH, Newman ST. State of the art electrical discharge machining (EDM). Int J Mach Tools Manuf 2003;43:1287−300.
[31] Jahan MP, Wong YS, Rahman M. A comparative experimental investigation of deep-hole micro-EDM drilling capability for cemented carbide (WC-Co) against austenitic stainless steel (SUS 304). Int J Adv Manuf Technol 2010;46:1145−60.
[32] Karden A. Funkenerosive Senkbearbeitung mit leistungssteigernden Elektrodenwerkstoffen und Arbeitsmedien [dissertation]. RWTH Aachen; 2001.
[33] Klitzing A. Mikrosenkerosion auf konventionellen Erodiermaschinen [dissertation]. RWTH Aachen; 2008.
[34] Klocke F, König W. Fertigungsverfahren 3-Abtragen, Generieren, Lasermaterialbearbeitung. Berlin: Springer; 2007.
[35] Kunieda M, Lauwers B, Rajurkar KP, Schumacher BM. Advancing EDM through fundamental insight into the process. CIRP Ann Manuf Technol 2005;54(2):64−87.
[36] Lim HS, Wong YS, Rahman M, Edwin Lee MK. A study on the machining of high-aspect ratio micro-structures using micro-EDM. J Mater Process Technol 2003;140: 318−25.
[37] Oelheld GmbH. Wissenswertes zur Senkerosion. Stuttgart: Firmenschrift; 2004.
[38] Piltz S. Grundlagen und Prozessstrategien der Mikrofunkenerosion für die Bearbeitung von Rotationsbauteilen [dissertation]. TU Berl; 2007.
[39] Tsai YY, Masuzawa T. An index to evaluate the wear resistance of the electrode in micro-EDM. J Mater Process Technol 2004;149:304−9.
[40] Uhlmann E, Piltz S, Doll U. Funkenerosion in der Mikrotechnik − Einsatzgebiete und Verfahrensgrenzen. wt Werkstattstech Online 2001;91(12):733−7.
[41] Uhlmann E, Klocke F, Neyer A, Doll U, Lung D, Neumann F, et al. Potentiale der Funkenerosion für Anwendungen in der Mikrotechnik. In: Tagungsband zum Abschlusskolloquium des DFG-Schwerpunktprogramms 1012 "Mikromechanische Produktionstechnik", Shaker, Aachen; 2003. p. 488−93.
[42] Uhlmann E, Piltz S, Doll U. Machining of micro/miniature dies and moulds by electrical discharge machining − recent development. J Mater Process Technol 2005;167: 488−93.
[43] Vallance RR, Morgan CJ, Shreve SM, Marsh ER. Characterizing form, waviness, and roughness of micro EDM electrodes. In: Proceedings of ASPE 19th annual meeting, Orlando, USA; 2004.
[44] Wong YS, Lim LC, Lee LC. Effects of flushing on electro-discharge machined surfaces. J Mater Process Technol 1995;48:299−305.
[45] Fertigungsverfahren Abtragen − Einordnung, Unterteilung, Begriffe. Berlin: Beuth; 2003.
[46] Elektroerosive Bearbeitung − Begriffe, Verfahren, Anwendung. Düsseldorf: VDI-Verlag GmbH; 1975.

This page intentionally left blank

CHAPTER

Laser Micro-structuring

5

Arnold Gillner, Patrick Gretzki
Fraunhofer Institute for Laser Technology ILT, Aachen, Germany

CHAPTER OUTLINE

INTRODUCTION

In the production of micro-scaled products and micro-replication tools, laser ablation becomes a more and more important tool which is able to generate structure sizes in the range of 10–100 μm, not only in metals but also in hard and ultra-hard materials such as tungsten carbide and ceramics [1–14]. Especially for micro-machining, laser processes have been qualified for a wide range of materials starting from semiconductors in the field of micro-electronics, hard materials for tool technology to very weak and soft materials such as polymers for medical products. Even ceramics, glass, and diamond can be processed with laser technologies with accuracies of better than 10 μm. In comparison to the classical technologies, laser processes are generally used for small and medium lot sizes but with strongly increased material and geometry variability.

The development and industrialization of ultra-short pulsed lasers with pulse durations in the range of some 100 fs up to 10 ps made it possible to further increase the palette of workable materials and the achievable process quality. Using ultra-short pulsed lasers in pulse bursts of several pulses with a time spacing of 20 ns each and adapted pulse energies, the surface quality of metal micro-ablation has

Micromanufacturing Engineering and Technology. http://dx.doi.org/10.1016/B978-0-323-31149-6.00005-0

been increased significantly and allows the production of tools and parts with R_a values less than 0.5 μm. Compared to conventional EDM (electrical discharge machining/spark eroding) processing, laser manufacturing of parts and tools can be performed without additional working tools in reasonable times directly from the CAD-CAM system without any tool wear.

Micro-ablation by means of laser-based vaporization of materials has been used in a large variety of applications to produce micro-molds, functional components in electronics and micro-drilling applications. Most of these processes were focused on small parts, where the laser has its unique position in selectivity and low thermal damaging without changing the properties of the entire part. Recent developments in solar cell manufacturing, display manufacturing, and the manufacturing of products based on electrically conducting polymers such as organic light-emitting diodes have opened a new field of laser micro-manufacturing with laser radiation, where the specific advantages and outstanding properties of laser radiation are highly required.

Properties of laser micro-ablation and surface functionalization:

- Ablation depth accuracy: Submicron scale
- Depth of heat input: Nanometer scale
- Lateral accuracy: Micron scale lateral

(Submicron scale with special process techniques)

When the production of components cannot be met by conventional processes, laser ablation allows new manufacturing processes on almost all types of materials. In this way, laser ablation and surface functionalization has been already proven as a nonconvertible tool in solar cell and display manufacturing.

BASIC PROPERTIES OF LASER ABLATION

The precision of laser ablation is given by a combination of different effects, which are related to the following:

- working tool (geometry of the laser beam);
- laser process (laser—material interaction);
- positioning system for the part; and
- laser steering system.

Laser radiation is used as a working tool to structure matter by thermal vaporization with well-defined volumes and high lateral precision. For this, depending on the type of laser and processing technology, laser radiation is focused or projected by objectives onto the surface, thereby being formed to a specific spatial intensity distribution. Depending on the intensity, the absorption conditions of the materials and the interaction time, several aspects have to be considered, which define the ablation geometry and the precision of the ablation process.

The precision of the resulting structures depend not only on the focus diameter and the positioning stage, but also on the precision of the process resulting from the reactions of the matter during and after irradiation. Thus, the processing diameter

depends not only on the beam radius w_0, but also on the physical properties of the material, such as the reflectivity, absorption, melting, and evaporation enthalpy. Depending on the optical properties of the material and on the applied radiation, the precision of the process diameter depends on the absorption of the radiation, which can be linear or nonlinear. Additionally, the ablation depends strongly on the pulse duration and on the wavelength (Figure 9).

ABSORPTION EFFECTS ON ABLATION GEOMETRY

Generally, the interaction of photons and matter is based on the absorption of the electromagnetic energy at the free and bound electrons of a material. The electrons are heated and transfer their energy after a characteristic time to the lattice of the material. After transfer of the optical energy to the lattice, the material heats up and starts to melt and subsequently vaporizes with further energy deposition. The laser-induced ablation itself can be distinguished between photo-induced and thermal ablation. The precision is greater for photo-induced ablation being comparable to the precision of the working tool, here resulting in the processing diameter. In the case of the thermal ablation, additional processes such as heat diffusion decrease the precision and give rise to a larger processing diameter than the focus diameter.

For most of the materials in laser material processing, surface absorption is the dominating process. Materials absorb laser radiation linearly, when an absorption band at the laser wavelength (Figure 1) or due free or quasi-free electrons being present (such as metals or graphite) is given. This can be described by Lambert–Beer's law

$$I(x) = (1 - R)I_0 e^{-\alpha x} \tag{1}$$

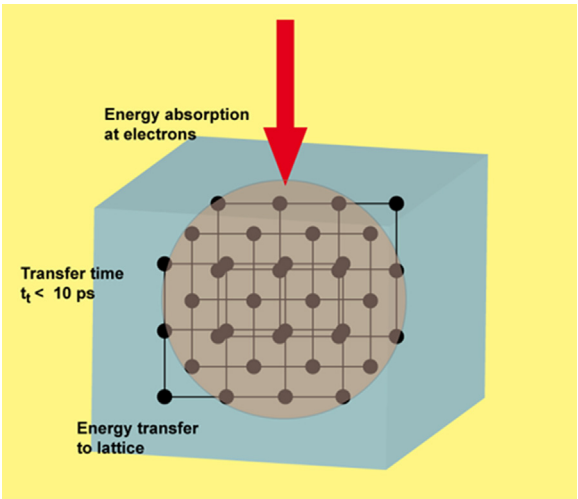

FIGURE 1

Principle of laser beam interaction with materials.

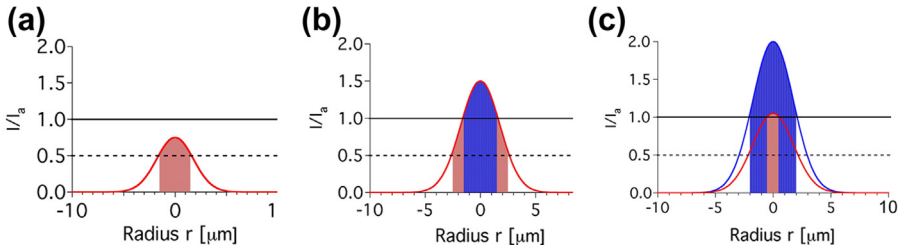

FIGURE 2

Extension of the melted (faint) and ablated (dark) region for intensities smaller (a), larger (b), then I_a. For $I \approx I_a$ and $I > I_a$ demonstrates differences in the extension of the ablated region (c).

with R the reflectivity, α the absorption coefficient (cm^{-1}), and I_0 the threshold intensity for ablation [W/cm^2]. Based on this, a logarithmic dependence of the ablation depth h [cm] on the intensity can be found:

$$h = \frac{1}{\alpha} \ln\left(\frac{I}{I_0}\right). \tag{2}$$

The ablation depth defines the precision of the structures in depth.

Applying Gaussian radiation with a focus diameter $2w_0$, the processing diameter can be controlled by the intensity of the radiation, depending on the ratio of the applied intensity to the threshold intensity for ablation. Threshold intensities are given for homogenous material by the threshold intensity for melting, I_m and for evaporation, I_v (Figure 2). Solid materials feature a melt enthalpy that is always smaller than the evaporation enthalpy, resulting in larger processing diameters for melting than for evaporation (Figure 2(b) for $I_m = I_v/2$).

The processing diameter of focused Gaussian radiation can be reduced steadily by decreasing the intensity close to the threshold intensity for ablation, I_a. Processing diameters much smaller than the focal diameter $2w_0$ are achievable (Figure 2(c)).

Thermal and/or photo-physical processes govern ablation. Thermal processes are represented by heating of matter without change in the chemical constitution, whereas photo-physical processes imply changes in the chemical constitution or irradiated matter.

THERMAL EFFECTS ON ABLATION PRECISION AND ABLATION GEOMETRY

Today, for precise laser ablation, single nanosecond pulses with time spacing between the pulses in the range of 10 μs are used. Ablation rates of between 0.1

and 1 mm^3/min are achieved with depth accuracies of 1−2 μm. In the nanosecond range, the thermal influence of the laser irradiation results in typical melting depths of several micrometers and a surface quality which is controlled and defined by the melt resolidification and the surface tension of the melt. With this technology, ablation accuracies of typically 1 μm can be achieved and a surface roughness of 0.6 μm can be obtained. Recent investigations using ps-lasers showed even higher accuracy, which is due to a totally different laser interaction regime with significant differing thermal influence and resulting quality. In nanosecond beam interaction, the energy deposition and heat transfer in the material is taking place within the pulse duration. In ultra-short pulse processing, the energy transfer to the lattice occurs after the entire pulse duration. The temperature increase and thermal behavior is then described by a two-temperature model which takes into account that laser−material interaction takes place generally between photons and electrons with an overheated electron gas; and an energy transfer to the lattice by a material-specific coupling coefficient [2].

The effect of the absorbed optical energy on thermal ablation of matter is driven by the pulse duration and is subdivided into four regimes for linearly absorbing matter:

- absorption of the optical energy by quasi-free electrons ($t_{\gamma e} < 10$ fs);
- thermalization of the electrons, called the electron system ($t_{ee} < 100$ fs);
- interaction between the electron and the phonon system ($t_{ep} < 10$ ps); and
- thermalization of the phonon system ($t_{pp} < 100$ ps).

The durations of the single processes within the brackets are exemplary if given for copper. Two limiting cases can be distinguished:

Pulse duration larger than the thermalization of phonons $\tau > t_{pp}$

For $\tau > t_{pp}$, the times for absorption of the photons and the thermalization of the electron and phonon system are much smaller than the pulse duration, resulting in the description of heating by one temperature for the electron and the phonon system. Ablation affects the subsystems as an instantaneous process. The threshold fluence for ablation (fluence = energy per area) scales with the square root of the pulse duration and a thermal penetration depth can be defined as:

$$\delta_{therm} = 2\sqrt{\frac{\kappa t_p}{c_p \rho}} \tag{3}$$

depending on the thermal property of matter, with κ the thermal conductivity, c_p the heat capacity, ρ the density, and t_p the pulse duration of the applied radiation. The thermal penetration depth δ defines the region beyond the focus diameter (tool diameter), which can be thermally modified, such as by the amorphization of crystalline substrate. This regime is called the heat-affected zone. The processing diameter is given by $2(w_0 + \delta)$.

Pulse duration smaller the electron–phonon relaxation time $\tau < t_{ep}$

For $\tau < t_{ep}$ the processes within the electron and the phonon system are decoupled. The temperature development for these systems are described by a two-temperature model representing two coupled differential equations:

$$C_e \frac{dT_e}{dt} = \frac{\partial}{\partial z}\left(\kappa_e \frac{\partial T_e}{\partial z}\right) + S - \mu\left(T_e - T_p\right) \tag{4}$$

$$C_p \frac{dT_p}{dt} = \mu\left(T_e - T_p\right)$$

C_e and C_p represent the heat capacities of the electron and the phonon system, κ the heat conductivity of the electron system, S the applied optical energy, μ the electron–phonon coupling constant, and T_e and T_p the temperatures of the two systems. Ablation of materials is characterized by negligible melt and small mechanical load of the irradiated region. The processing diameter is comparable to the focus diameter.

In nanosecond laser processing, this energy transfer occurs during the duration of the laser pulse, whereas in picosecond laser processing, the energy transfer occurs after a certain interaction time. For metals, this transfer time is generally in the range of some picoseconds. In this case, the material is heated up after the end of the laser pulse, so that there is no interaction of the photons with melted and evaporated material. The result is a much more accurate ablation because the ablation is mainly due to vaporization of the material and not by melt expulsion. The second reason for the use of picosecond pulse durations in laser ablation is the very high intensity of the pulses. With peak intensities of more than 10^{10} W/cm^2, all materials are vaporized rather than merely melted. As a consequence of these high intensities, the ablation rate per pulse is quite low, because for vaporization an excessive amount of energy is needed. In Figure 3, a direct comparison of laser-ablated steel with nanosecond pulses and picosecond pulses is shown. It can be seen clearly, that in nanosecond ablation, the residual melt after ablation is much stronger and the geometry is affected by melt resolidification. In picosecond ablation, almost no melt can be found in the ablation area and clean surfaces with a surface roughness of <0.5 μm can be produced by laser ablation.

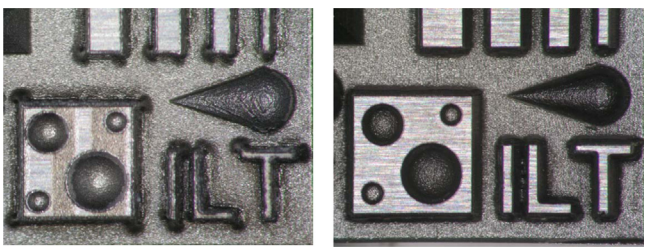

FIGURE 3

Comparison of nanosecond laser ablation (left) and picosecond laser ablation (right) of steel.

PROCESS PRINCIPLES FOR LASER ABLATION

Micro-structuring with laser radiation adopts one of the following techniques:

- mask technique, and
- scribing technique.

The mask technique is appropriate for 2.5-dimensional structuring, for example, application in lithography and the generation of micro-fluidic systems and nano-scaled optical devices such as gratings. The scribing technique is adopted for full-3D structuring and is comparable to mechanical milling.

MASK TECHNIQUE

For mask-based laser ablation, the laser radiation is formed and homogenized by a telescope and projected onto a mask representing the desired intensity distribution. The mask is imaged by an objective to the final intensity distribution. The transversal miniaturization m is given by:

$$|m| = \frac{f}{g - f}, \tag{5}$$

This relation is known from the optical geometry, with the focal length of the lens f and the distance of the mask to the lens g (Figure 4).

The precision of the working tool is described by Abbe's law, which gives the theoretical resolution limit Δx of an objective for noncoherent radiation:

$$\Delta x = 1.22 \frac{\lambda f}{D_L} = 0.61 \frac{\lambda}{NA} \tag{6}$$

and depends on the objective diameter D_L and on the numerical aperture of the objective NA.

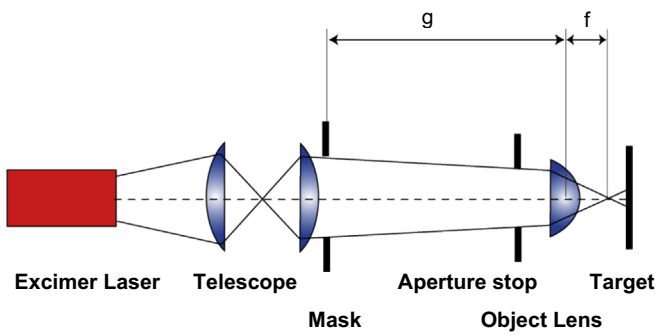

FIGURE 4

Principle of mask projection imaging. Laser radiation is collimated and homogenized by a telescope and a homogenizer to illuminate the mask. The mask itself is imaged on the target.

SCRIBING TECHNIQUE

Scribing is a common technique for structuring with laser radiation. Similar to milling, the working tool "laser radiation" is moved relatively to the substrate and removes matter in the focal regime by melting, vaporization, or photo-ablation.

The spatial intensity distribution of the laser radiation depends, among others, on the applied laser resonator. Of special importance for micro-structuring concerning focusability is the radiation, which should exhibit a spatial Gaussian intensity distribution. Micro-structuring applying this radiation benefits of the property of Gaussian radiation to be focused to the smallest possible value, called the diffraction-limited focus, resulting in a beam radius of:

$$w_0 \approx \frac{2\lambda f}{D} \approx \frac{\lambda}{NA}, \tag{7}$$

with λ the wavelength of the applied radiation, f the focal length of the objective, and D the beam diameter of the radiation close to the objective. The working tool diameter is given by $2w_0$ and defines the working tool precision. The numerical aperture is given by $NA = D/f$ for objectives with large focal length ($f >> 15$ mm) and by $NA = n \sin\theta$ for microscope objectives ($f < 15$ mm), with the refractive index of the medium between objective and the substrate and θ the aperture angle of the objective.

Micro-structures, like a cavity, are generated by ablation with laser radiation displacing the laser radiation relative to the work piece and carrying out a meander trajectory, removing the material in layers (Figure 5). In general, the laser displacement of the laser beam is realized by high-speed galvanometer mirrors. Focusing

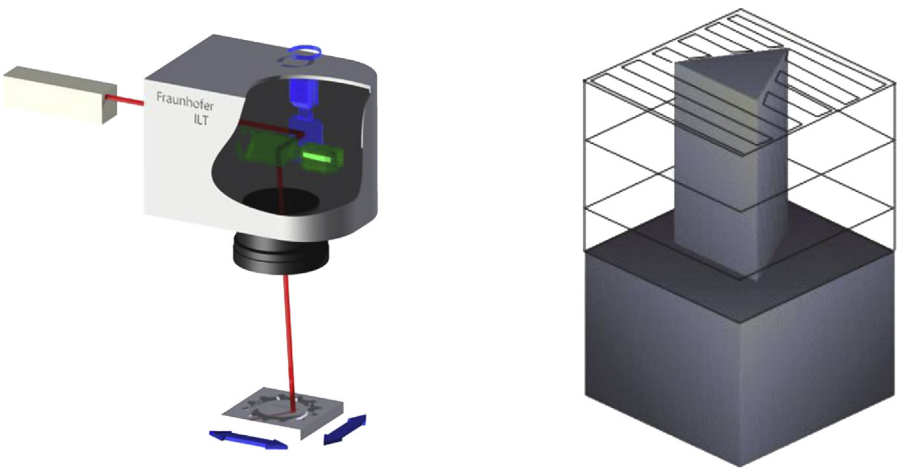

FIGURE 5

Principle of 3D-laser machining by laser scribing technology.

of the laser beam is either made by either adjustable lenses set before the scanning mirrors or by telecentric lenses.

The ablation rate per length depends on the ratio between the applied intensity to the threshold intensity for ablation and on the overlap, o:

$$o = 1 - \frac{\mathrm{v}}{2 f_p w_p}. \tag{8}$$

where w_p represents the processing diameter, v the relative velocity, and f_p the pulse repetition rate. The processing diameter for mechanical ablation (e.g., milling) is given by the tool diameter, whereas the processing diameter for laser ablation is given by the focal diameter (tool diameter) and the process precision, described below. Applying laser radiation for micro- and nano-structuring, the appropriate tool diameter is obtained by reducing the wavelength and increasing the numerical aperture. The last one is obtained by decreasing the focal length of the objective or by increasing the beam diameter close to the objective (Example: $\lambda = 355$ nm; $NA = 0.5 \Rightarrow w_0 \approx 0.7$ μm).

Microscope objectives are often used for focusing laser radiation to small focal diameters <10 μm. The focal diameter is varied during processing by changing the objective, or changing the beam diameter in front of the objective, or positioning the laser radiation extra focally. Different to mechanical milling, laser radiation is contact-free and massless, resulting in reduced delay times for positioning of the working tool. Mechanical micro-milling with tool diameter <100 μm exhibits positioning times in the range of minutes, whereas laser radiation is positioned within fractions of seconds.

EXAMPLES

In the production of micro-scaled products and products with micro- and nano-scaled surface functionalities, laser ablation becomes a more and more important tool which is able to generate structure sizes in the range of 10−100 μm and with new machining strategies, even within a range smaller than 1 μm. Using ultra-short pulsed lasers with pulse durations of 10 ps in pulse bursts of several pulses with a time spacing of 20 ns each and adapted pulse energies, the surface quality of metal micro-ablation has been increased significantly. With a combination of ultra-short pulses and high-resolution interference methods, structures with dimensions of less than 300 nm can be generated, either in polymer parts directly, or in steel replication tools. For mass replication of those structures to achieve improvements in wetting capabilities or optical properties of surfaces, a new laser-supported embossing technology has been developed.

The availability of these new process variants and improved beam sources qualifies the laser as a universal tool, especially in the area of micro-mold processing. The wide range of materials processed by lasers spread out from hard materials such as tungsten carbide for tool technology to even ceramics, glass, and diamond, with

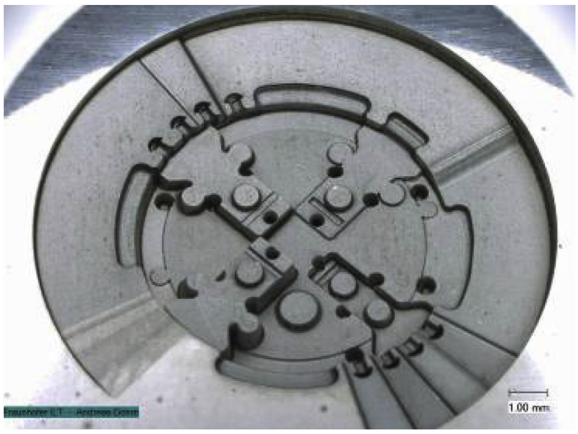

FIGURE 6

Laser-manufactured micro-injection molding tool insert.

accuracies of better than 10 μm, which make the technology useful for the processing of innovative tools, and also for high-temperature mass replication processes.

With the newly developed laser ablation technology using ultra-short pulsed lasers in the picosecond range, accuracies of better than 5 μm and surface roughness of less than 0.5 μm can be provided for the manufacturing of micro-molding tools (Figure 6).

Using this new laser ablation technology opens a new field of the micro-processing of tools, which allows the manufacturing of micro- and even nano-scaled functional structures on polymer, metal, and glass components. With laser ablation using picosecond lasers, a machining technology with accuracies <1 μm is available which can be applied to all kind of materials. In Figure 7, the surface of a replication tool

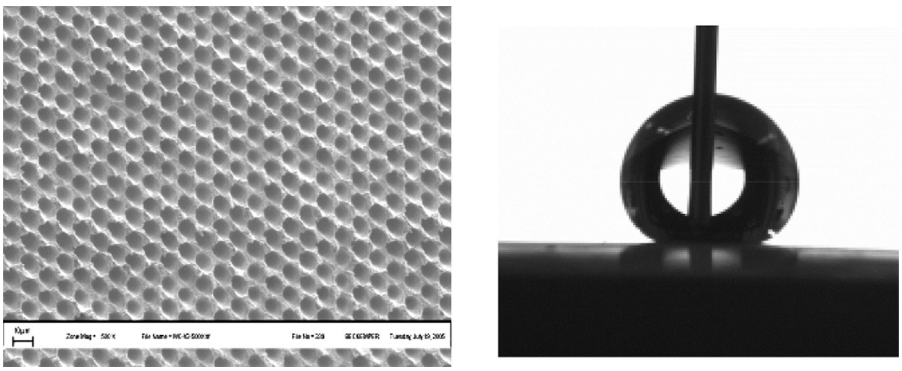

FIGURE 7

Micro-structured replication tool for self-cleaning surfaces (left), super lotus effect on micro-structured polymer surface (right).

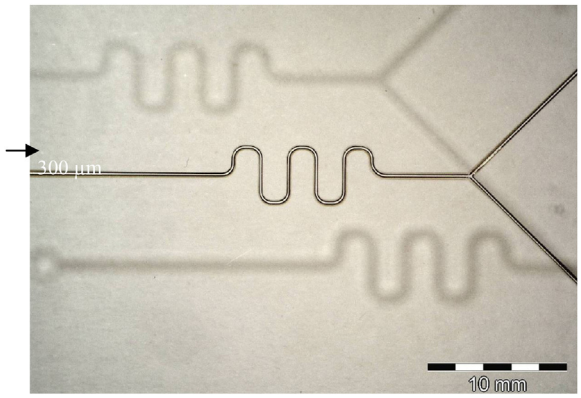

FIGURE 8

Micro-fluidic channels ablated with excimer laser radiation.

is shown, whereby laser ablation in tungsten carbide micro-pits with sizes between 1 and 5 µm have been produced. Due to the process characteristics of laser ablation, submicrometer-scaled substructures are produced, which further increase the surface area. Tools like this have been successfully tested for the replication of polymers to achieve functional surfaces. In Figure 7, the result of a wetting test shows that by micro-structuring, a super hydrophobic effect can be produced.

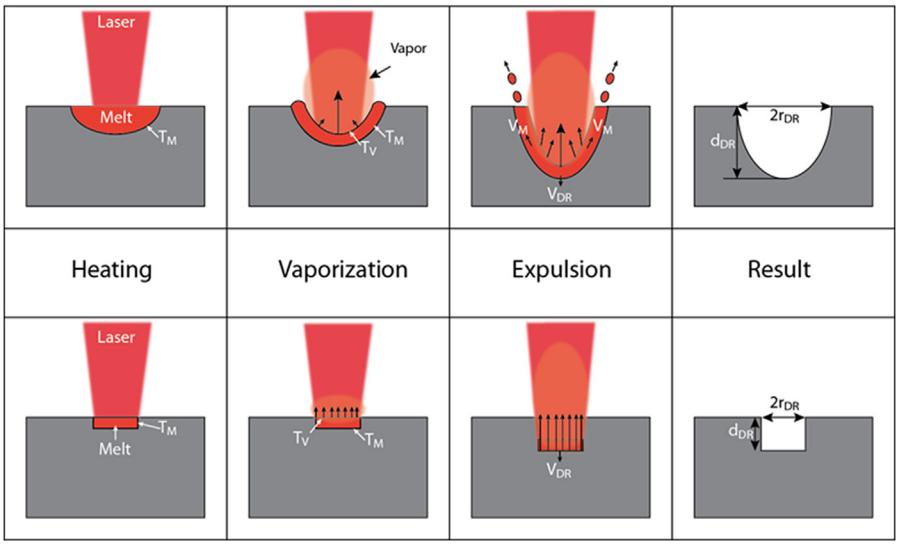

FIGURE 9

Comparison of characteristic states during laser processing with short pulsed (upper) and ultra-fast pulsed lasers (lower).

By mask technique, ablation with UV-excimer lasers, especially polymer parts can be produced in a very flexible way. Among others, micro-fluidic systems require very small channels and reservoirs in the geometry range of several 10 μm. With mask-based excimer ablation, a tool for rapid prototyping is available for the manufacturing of single parts in small lot sizes [6] (Figure 8).

CONCLUSIONS

Laser micro-ablation has been shown to be a versatile tool in the machining and production of micro-parts and micro-replication tools. Using ultra-short pulsed lasers with material-adapted wavelengths, the quality of the ablation process can be increased significantly compared to long pulses (Figure 9). With an optimized energy deposition, a significant reduction of the surface roughness down to $Ra < 0.7$ μm could be achieved over a wide parameter range, the best achieved roughness being $Ra = 0.5$ μm. Using this optimized parameter, laser ablation can be used for the generation of micro-replication tools as well as for the direct manufacturing of small parts in different materials such as ceramics, steel, and sintered metals showing the potential for high-precision tool manufacturing for high-accuracy parts.

REFERENCES

[1] Ashkenasi D, Müller G, Rosenfeld A, Stoian R, Hertel IV, Bulgakova NM, et al. Fundamentals and advantages of ultrafast micro-structuring of transparent materials. Appl Phys A 2003;77(2):223−8.

[2] Neuenschwander B, Jaeggi B, Schmid M, Rouffiange V, Martin PE. Optimization of the volume ablation rate for metals at different laser pulse-duration from fs to ps. Laser Appl Microelectron Optoelectron Manuf (LAMOM) 2012;8243.

[3] Jandeleit J, Horn A, Weichenhain R, Kreutz EW, Poprawe R. Fundamental investigations of micromachining by nano-and picosecond laser radiation. Appl Surf Sci 1998;127:885−91.

[4] Korte F, Adams S, Egbert A, Fallnich C, Ostendorf A, Nolte S, et al. Sub-diffraction limited structuring of solid targets with femtosecond laser pulses. Opt Express 2000; 7(2):41−9.

[5] Schoonderbeek A, Biesheuvel CA, Hofstra RM, Boller KJ, Meijer J. Shadowgraphic imaging of material removal during laser drilling with a long pulse excimer laser. Appl Phys A 2005;80(4):769−75.

[6] Wehner M. Excimer laser technology. In: Basting D, editor. Göttingen: Lambda Physik AG; 2001.

[7] Poprawe R, Gillner A, Hoffmann D, Gottmann J, Wawers W, Schulz W. High speed high precision ablation from ms to fs. Proc SPIE 2000;7005:12 S.

[8] Gillner A, Holtkamp J, Hartmann C, Olowinsky A, Gedicke J, Klages K, et al. Laser applications in microtechnology. J Mater Process Technol 2005;167:494−8.

[9] Schmitz GJ, Brücker C, Jacobs P. Manufacture of high aspect-ratio micro-hair sensor arrays. J Micromech Microeng 2005;15:1904−10.
[10] Wehner M, Beckemper S, Jacobs P, Schillinger S, Schibur D, Gillner A. Processing of polycarbonate by high-repetition rate ArF excimer laser radiation. Proc Lasers Manuf 2005;3:557−61.
[11] Bremus-Köbberling E, Meier-Mahlo U, Henkenjohann O, Beckemper S, Gillner A. Laser structuring and modification of polymer surfaces for chemical and medical micro components. In: Proceedings of SPIE 5662; 2004. p. 274−9.
[12] Bremus-Köbberling E, Gillner A. Laser structuring and modification of surfaces for chemical and medical micro components. In: Proceedings of the 4th international symposium on laser microfabrication LMP 4; 2003. p. 1−5.
[13] Hartmann C, Fehr T, Brajdic M, Gillner A. Investigation on laser micro ablation of steel using short and ultrashort IR-multipulses. Kyoto, Japan: LAMP; 2006.
[14] Hartmann C, Gillner A, Aydin U, Noll R, Fehr T, Gehlen C, et al. Investigation on laser micro ablation of metals using ns-multi-pulses. J Phys 2007;59:440−4.

This page intentionally left blank

CHAPTER

Micro-electrochemical Machining

6

Atanas Ivanov, Rebecca Leese, Alexandre Spieser
Brunel University London, Uxbridge, Middlesex, UK

CHAPTER OUTLINE

INTRODUCTION

Products are becoming smaller, lighter, and more compact, and standards and quality requirements are rising. Micro-machining is finding more applications in many products in the aerospace, automotive, medical device, jewelry, and consumables industries. There are many forms of micro-machining processes such as micro-milling, laser machining, electrodischarge machining (EDM).

All micro-manufacturing technologies are constantly evolving and new technologies are also joining the initial set of micro-technologies due to the new research developments and the growing demand for more accurate, defects-free, machined micro-surfaces as well as special requirements for the machined surface integrity like requirements for roughness suitable for optical applications and no defective layer after the machining process.

Electrochemical machining (ECM) and especially electrochemical micro-machining (μECM) became an attractive area of research due to the fact that this process does not create any defective layer after machining and that there is a growing demand for better surface integrity on different micro-applications such

Micromanufacturing Engineering and Technology. http://dx.doi.org/10.1016/B978-0-323-31149-6.00006-2

as micro-fluidics systems, optical systems, and stress-free drilled holes in the automotive and aerospace sectors.

ECM is considered as a nonconventional machining process and there is no direct contact between the tool electrode and the workpiece. The process requires maintaining a small gap—the interelectrode gap (IEG)—between the anode (workpiece) and the cathode (tool electrode) in order to achieve acceptable machining results (i.e., accuracy, high aspect ratio with appropriate material removal rate, and energy efficiency). Other major advantage of this process is that there is no wear on the tool electrode unlike the micro-EDM process and the final roughness of the machined surface depends severely on the type of the electrolyte and the grain structure of the workpiece material and easily can be achieved surfaces with optical quality.

This chapter presents the μECM process and its suitability for micro-applications and research challenges. Technological characteristics of the process together with basic calculations are explained. It is also presented here the latest developments in the area of μECM and future steps of this rapidly growing research area in order the process to become more predictable and easy to use.

WORKING PRINCIPLES

ECM is an electrolytic process which works on the basis of anodic dissolution of the workpiece. Electrolysis is the passing of current between two electrodes in an electrically conductive solution called an electrolyte which completes the circuit [1]. A simple example of an electrolysis process is between an impure copper anode and a pure copper cathode in a temperature-controlled, quiescent solution of copper sulfate with a constant current source connecting the two electrodes [2]. Copper atoms from the anode are dissolved and travel through the electrolyte to the cathode where it is subsequently deposited. The process discussed above can be used to purify copper as any impurities within the copper anode are not deposited at the cathode due to either being insoluble or having a different deposition potential to copper [3]. The copper ions move through the solution via several mechanisms. The first being diffusion; diffusion is the movement of ions within a solution influenced by concentration gradients with ions moving from high concentrations to lower concentrations in an attempt to equalize the concentration throughout the solution [1]. In this case the concentration of copper ions at the anode surface is much higher than the concentration of copper ions in the bulk of the solution; hence the copper ions diffuse away from the anode toward the bulk solution and the copper cathode. The concentration of copper ions at the cathode surface is lower than the bulk concentration because copper ions are consumed at the cathode surface. The copper ions also travel through the solution via migration; migration is the movement of ions due to a potential field [1]. In the example, the positive copper ions are electrostatically attracted to the negatively charged cathode. Usually in electrochemical experiments examining electrode reactions, a background electrolyte with a high concentration is used to mitigate the effects of migration in the solution [1]. The majority of the current is carried by the background electrolyte so the effect of

migration on the species being studied is negligible. The third mechanism in which the ions could move through the solution is convection. Convection is movement due to external mechanical forces such as stirring or bubbling gas through the solution [1]. In the case of copper electrolysis the solution is unstirred and kept at a constant temperature so the ions are not subjected to any large convection effects, be that natural or forced convection, e.g., stirring the solution. This allows the effects of convection to be ignored in the analysis.

The reactions happening at the electrodes are as follows:

$$\text{At the anode}: \quad \mathrm{Cu} \rightarrow \mathrm{Cu}^{2+} + 2\mathrm{e}^{-}$$

$$\text{At the cathode}: \quad \mathrm{Cu}^{2+} + 2\mathrm{e}^{-} \rightarrow \mathrm{Cu}$$

These two reactions happen simultaneously. This prevents charge accumulation anywhere within the circuit [1]. There are also counter ions in the solution so the solution remains neutrally charged.

Figure 1 shows a schematic of the reactions occurring within the electrolyte during the purification of copper.

The impure copper anode is dissolved and hence reduces in mass. The insoluble impurities collect underneath the anode. No other reactions take place at either electrode as copper is less reactive than hydrogen, determined in the electrochemical series. If a metal more reactive than hydrogen had been used, hydrogen gas would have been produced at the cathode, i.e., if the standard potential of the half-reaction relating to the working electrode material is negative with respect to hydrogen, hydrogen will be formed at the electrode [4].

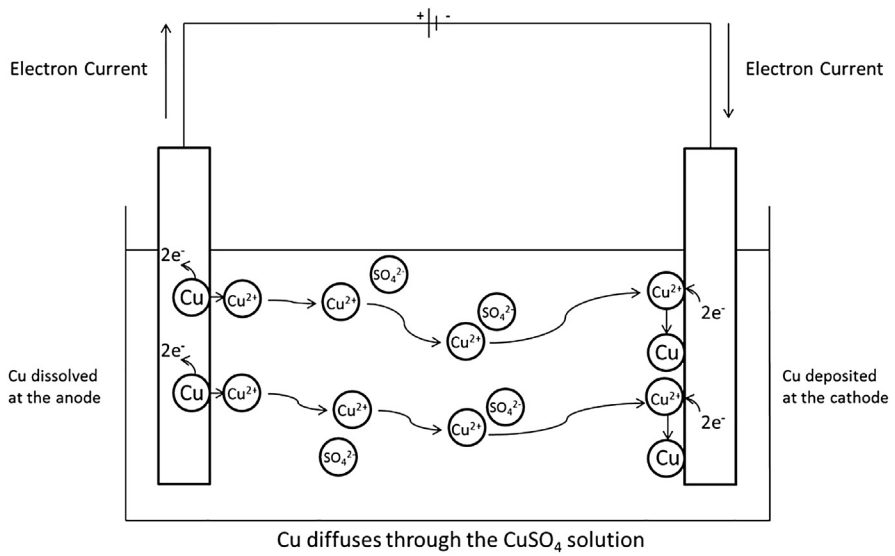

FIGURE 1

Schematic of copper purification process.

ECM works on a similar basis as described above for the purification of copper. ECM utilizes the anodic dissolution process used in copper electrolysis but confines the current to allow more precise and accurate machining. This enables different shapes and contours to be machined using this method.

Here the controlled anodic dissolution of iron in sodium nitrate electrolyte will be used as an example to show the differences in the process compared to the electrolysis of copper. In order to control the areas on the workpiece which are affected by the anodic dissolution the gap between the tool and the electrode is reduced to the micrometer range [5]. This helps to confine the current to the desired areas. The iron ions are dissolved in the same way as the copper ions, however the two processes differ once the ions have been dissolved. In the electrolysis of copper, the ions remain in the solution until they are deposited onto the cathode. This is undesirable in the ECM process as it will alter the shape of the cathode tool over time [6]. To avoid this, the electrolyte is selected to react with the iron ions once they have been dissolved. The iron ions react with hydroxide ions which have been formed from the electrolytic breakdown of water to form insoluble metal hydroxides. These precipitate out of the solution [7], removing the ions from the solution and preventing them from being deposited onto the cathode. This process, however, is electroless, meaning it is a spontaneous reaction that will happen regardless of a current being passed or not and it does not occur at the electrode surface. The total current passed is not affected by this reaction. Figure 2 below schematically shows the processes occurring during ECM of an iron workpiece in sodium nitrate.

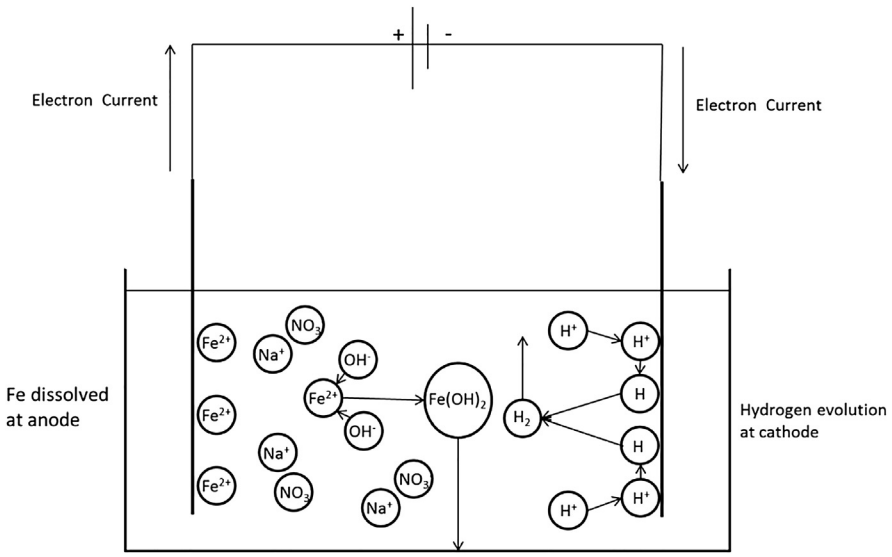

FIGURE 2

Schematic for the anodic dissolution of iron in $NaNO_3$.

The reactions occurring at the electrodes are as follows:

$$\text{Anode}: \quad \text{Fe} \rightarrow \text{Fe}^{2+} + 2\text{e}^-$$

$$\text{Cathode}: \quad 2\text{H}_2\text{O} + 2\text{e}^- \rightarrow \text{H}_2 + 2\text{OH}^-$$

The formation of the iron hydroxide happens away from the electrode surface in the electrolyte and happens via the following electroless reaction:

$$\text{Fe}^{2+} + 2\text{OH}^- \rightarrow \text{Fe(OH)}_2$$

MECHANISM OF THE ANODIC DISSOLUTION

The molecules of substances in aqueous solutions dissociate into cations and anions carrying an electric charge depending on the valence, n. As the amount of the cations is equal to the anions, the whole solution stays electrically neutral. When a metal electrode is submerged into the solution, and the metal electrode is negatively charged, it attracts the positively charged cations. If the metal is positively charged, it attracts the negatively charged anions. In this way the so-called electrical double layer (EDL) is formed, which is similar to the effect observed in a thin capacitor where one layer represents the surface charges on the solid electrode and the other the charges of the ions in the electrolyte (see Figure 3). Therefore on the anode appears potential V_{anode} and on the cathode appears potential $V_{cathode}$. The EDL plays very important role in the micro-ECM process.

The value and the sign of the open circuit potential for different metal electrodes can be determined according to the standard hydrogen electrode. When there is no applied external potential, the transition of metal cations from one phase into another is inhibited. In order to have a process of anodic dissolution, it is necessary to apply an external potential U_0, which should be higher than U (see Figure 4)

$$U_0 > U = [V_{anode} + (-V_{cathode})].$$

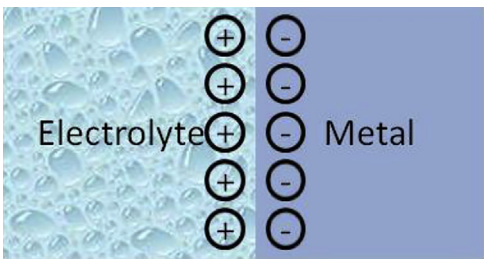

FIGURE 3

Appearing of a potential on the boundary between the metal electrode and the electrolyte.

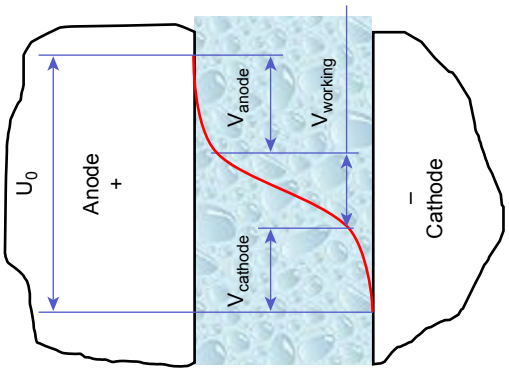

FIGURE 4

Potentials appearing on the two electrodes forming the electrical double layer in the electrolytic cell and applied external U_0 potential.

After applying U_0, there is no more electrostatic forces holding the cations to the surface and dissolving the anode becomes the dominant process. Now there are conditions for anodic dissolution of the anode material. The ions in the IEG start to move under the influence of the applied electric field. Current, I, starts flowing in the IEG. The current value is determined by the $V_{working}$ and the resistance of the IEG R.

$$U_0 = V_{anode} + (-V_{cathode}) + V_{working}$$

ECM process is very popular for material volume removal (ECM sinking) and shaping the anode using DC current by using complex-shaped cathode electrodes. Recent developments in this area aim at the use of much smaller electrodes with a smaller IEG size for machining complex features with simple shape electrode. This requires improving severely the resolution of the anodic dissolution and respectively the achieved accuracy. These developments led to the appearance of a new area of ECM technology defined as "pulsed electrochemical machining."

Pulse electrochemical micro-machining (also referred to as μECM, μPECM, EMM, PECMM, PEMM) exploits the capacitive properties of the EDL at the electrode/electrolyte interfaces: it has been demonstrated that the electrical model of the electrochemical cell behaves as an RC circuit [8–12]. The charging constant ($\tau = RC_{DL}$, where C_{DL} is the overall capacitance of the cell and R is the electrolyte resistance) of the EDL depends on the distance between the tool and the workpiece (which actually corresponds to the charging current path): the farther the tool is from the workpiece surface, the longer the charging time of the EDL will be [13]. By using this property, the localization of the material removal can be controlled very accurately by setting the pulse duration according to the charging time of the EDL. This became the stepping stone for the development of the micro-ECM technology. The frequency and the pulse duration vary respectively depending on the application [14–17].

More detailed behavior of the process can be obtained by the so-called polarization curves which will depend on a number of conditions like material of the electrodes, electrolytes, working temperatures, and many others.

POLARIZATION CURVES AND POURBAIX DIAGRAMS

In ECM, polarization curves are used to determine whether the electrolyte selected is a suitable choice for the metal workpiece material. The polarization curve can also reveal at what potential the machining should be conducted at [17]. Pourbaix diagrams disclose information about how the potential and pH affect which phases of the metal are stable [17].

Polarization curves show the current–potential relationship of a metal–electrolyte system. The experiment is set up with a working electrode made from the material of interest, a counter electrode, e.g., a platinum flag and a reference electrode, e.g., an Ag/AgCl electrode [18]; see Figure 5.

Within the potentiostat there is a voltmeter to measure the potential difference between the working electrode and the reference electrode. There is also an ammeter to measure the current being passed through the counter electrode. The potentiostat controls the potential of the working electrode with respect to the reference electrode throughout the experiment while recording the current being passed between the working electrode and the counter electrode. The shape of the curve is unique for each metal–electrolyte combination.

Figure 6 shows a typical polarization curve observed for a surface that undergoes passivation and then the breakdown on the passivation layer, plotted as the potential versus the logarithm of the current. On Figure 6, section AB shows the current

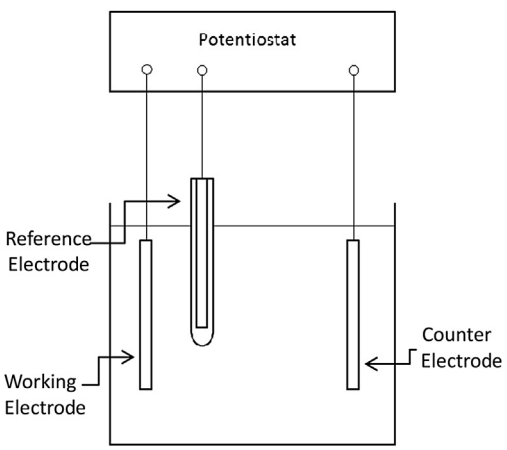

FIGURE 5

Experimental setup for polarization experiment.

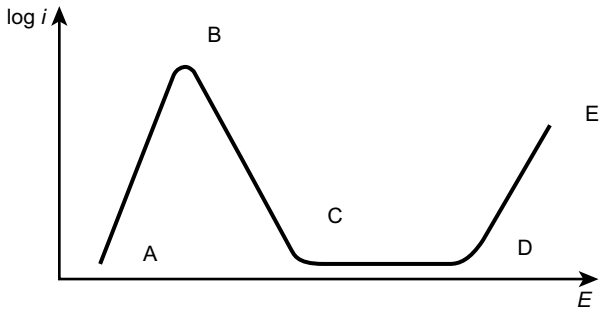

FIGURE 6

Polarization curve showing passivation.

increasing due to the anodic dissolution of the workpiece; section BC shows the current decreasing due to the passivation of the surface layer; CD is the transpassive region where there is no electrical connection due to the insulating passive film; section DE shows the current rising again as the passive layer is broken down regaining electrical contact and continuing anodic dissolution.

Pourbaix diagrams, also known as a potential/pH diagram, map possible stable phases in an aqueous electrochemical system at room temperature only [19]. These can be used as a guide to determine the pH and potential at which the ECM could be carried out at by considering whether the stable phases are solid or aqueous. If the stable phase is aqueous it is highly likely that anodic dissolution will be successful [17]. This is because the workpiece should react to form a soluble compound and therefore the workpiece would dissolve. However, if the stable phase is a solid, it is more likely that a passive film will form on the surface of the workpiece rendering the dissolution process unsuccessful [17]. They do not reveal any kinetic information so the information gained should not be used in isolation but can be used as a preliminary guide to help decide initial machining parameters. Pourbaix diagrams are read much like a standard phase diagram but with different axes (see Figure 7).

BASIC CALCULATIONS IN ECM AND/OR MICRO-ECM PROCESS

In the calculations shown below is assumed that material removal is purely due to electrochemical processes, i.e., there is no mechanical material removal or crumbling of grains of material or hydrodynamic erosion, electric erosion, or micro-cutting by abrasive. The material removal rate in ECM can be expressed by Faraday's first law.

According to the first law of Faraday, the mass of metal ions removed Δm is proportional to the current ΔI during time Δt:

$$\Delta m = k\Delta I\Delta \mathrm{t}$$

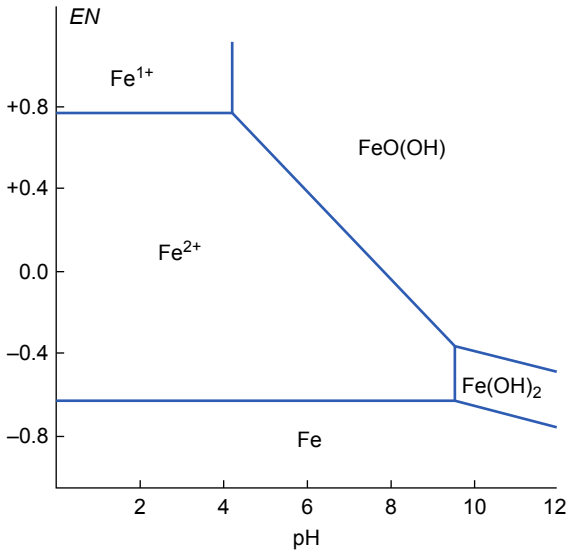

FIGURE 7

Pourbaix diagram for an iron–water system at room temperature [19].

where, k is the so-called electrochemical equivalent of the workpiece material, which equals the mass of ions carrying 1 unit of electric charge, 1C (i.e., 1 As).

This equation also can be written using the volume of the removed material ΔV and the density of the material ρ:

$$\Delta V\rho = k\Delta I\Delta t \rightarrow \Delta V = \frac{k\Delta I\Delta t}{\rho}$$

Using Faraday's second law, the electrochemical equivalent for the reaction: $\mathrm{Me} \rightarrow \mathrm{Me}^{n+} + \mathrm{ne}^{-}$ can be expressed in the following way:

$$k = \frac{A}{nF}$$

A is atomic weight of the metal Me
F is Faraday's constant (96,500C)
n is valency of the workpiece material

For example, iron has an atomic weight of $A = 55.85$. In its divalent form ($n = 2$) this metal has an electrochemical equivalent $k = 29 \times 10^{-5}$ g/As;

The trivalent iron ($n = 3$) has $k = 19 \times 10^{-5}$ g/As.

If an alloy consists of i elements such that each element accounts for a fraction z_i of the total and it is assumed that each element dissolves independently and simultaneously with the others, the electrochemical equivalent of alloy may be found by the following equation:

$$k = \frac{1}{F \sum \frac{z_i n_i}{A_i}}$$

The current efficiency of anodic dissolution, η, is calculated using the ratio between the current responsible for metal dissolution, ΔI_{dis}, and the total current, ΔI_{total}. It can also be calculated using the ratio between the mass removed from the electrode, Δm_{real}, versus the calculated mass loss, Δm_{calc}. Alternatively volumes can also be used in the same way.

$$\eta = \frac{\Delta I_{dis}}{\Delta I_{total}} = \frac{\Delta m_{real}}{\Delta m_{calc}} = \frac{\Delta V_{real}}{\Delta V_{calc}}$$

Efficiency of 100% means that the total current is carried by ions of dissolved metal. For zero efficiency, the current passes without metal dissolution. It is often convenient to express the current efficiency in terms of a percentage ratio. Current efficiency η depends greatly on the material of the workpiece, type of electrolyte as well as the machining conditions, mainly on the current density, the temperature, and the flow rate of electrolyte as well as the type of power supply. The current efficiency in micro-ECM, where short pulsed DC current is used, is much lower than in the volume (sinking) ECM process using normal uninterrupted DC power supply.

The coefficient of electrochemical machinability, K_V is equal to the volume of material dissolved from the anode per unit electrical charge and can be given by the following equation:

$$K_V = \frac{\eta \kappa}{\rho}$$

The coefficient K_V can only be determined experimentally and its value for some commonly used metals is given in Table 1 below.

Table 1 Coefficient for Electrochemical Machinability K_V for Most Commonly Used Metals

Metal (Unit)	Atomic weight (g)	Valence	Density (g/cm^3)	K_V at current efficiency 100% ($\eta = 1$) (mm^3/Amin)
Aluminum (Al)	26.98	3	2.71	2.06
Cadmium (Cd)	112.40	2	8.67	4.1
Chromium (Cr)	51.896	2 3 6	7.2	2.25 1.51 0.75
Cobalt (Co)	58.93	2 3	8.92	2.05 1.38
Copper (Cu)	63.546	1 2	8.97	4.39 2.20
Gold (Au)	196.967	1 3	19.33	6.40 2.13

Table 1 Coefficient for Electrochemical Machinability K_V for Most Commonly Used Metals—cont'd

Metal (Unit)	Atomic weight (g)	Valence	Density (g/cm^3)	K_V at current efficiency 100% ($\eta = 1$) (mm^3/Amin)
Iron (Fe)	55.847	2 3	7.86	2.21 1.47
Lead (Pb)	207.19	2 4	11.36	5.74 2.79
Magnesium (Mg)	24.312	2	1.75	4.43
Manganese (Mn)	54.938	2 3 4 6 7	7.48	2.26 1.48 1.15 0.77 0.65
Molybdenum (Mo)	95.94	3 4 6	10.22	1.95 1.47 0.98
Nickel (Ni)	58.71	2 3	8.92	2.11 1.36
Platinum (Pt)	195.09	2 4	21.47	2.79 1.47
Silver (Ag)	107.9	1	10.5	6.39
Tantalum (Ta)	181	5	16.62	1.31
Tin (Sn)	118.69	2 4	7.31	5.05 2.52
Titanium (Ti)	47.90	3 4	4.52	2.19 1.65
Tungsten (W)	183.85	6 8	19.31	0.98 0.74
Vanadium (V)	50.95	3 5	6.09	1.74 1.05
Zinc (Zn)	65.37	2	7.15	2.85

Material removal rate (MRR) can be defined either as the volume removed per time:

$$MRR = \frac{dv}{dt},$$

or the mass removed per time.

$MRR = \frac{dm}{dt}$ which also leads to equation

$$MRR = K_v I$$

From this equation can be concluded that MRR in ECM is dependent on electrochemical properties of the workpiece material (K_V) and proportional to the total current.

Specific energy consumption of an ECM process is defined as energy needed for removal of unit volume of machining material, i.e., $e = \frac{dE}{dV}$.

During time dt, energy consumed in ECM is equal to $dE = UIdt$, where U is the applied voltage and the volume of dissolved material is $dV = K_v Idt$.

Therefore, $e = \frac{U}{K_v}$, which means that the specific energy consumption is ratio between the applied voltage and coefficient of electrochemical machinability.

ELECTROLYTES

The electrolyte has three main roles in the ECM process: it carries the current between tool and the workpiece, it removes the product of the reaction from the IEG, and it removes the heat produced from the passage of current [20].

The most common electrolyte used for ECM is a concentrated salt electrolyte, namely sodium chloride or sodium nitrate. These are used as they are relatively inexpensive and they do not cause damage to the machinery [21].

The choice of electrolyte determines the reactions that happen at both the workpiece and the tool electrode but also within solution. Firstly there are two main types of electrolyte: passivating and nonpassivating electrolytes [22]. Passivating electrolytes will encourage the development of a passive layer on the workpiece. A passive layer is usually formed of metal oxides and hydroxides which can spontaneously form upon contact with the electrolyte or only once a current is flowing through the system [23]. This will depend on both the electrolyte and the metal involved. Many passive films are electrically insulating and form a barrier on the workpiece surface. This is usually detrimental to the machining process and in some cases can completely prevent any dissolution from occurring. This is not to say that the formation of all passive layers is unwanted. Sometimes the formation of a passive layer, which is more easily broken down, can improve the resolution of the machining, obtaining a more precise shape with sharper edges and corners [17]. The energy consumption for this method is higher due to the increased potential required to break through the passive layer [12]. A surface is said to be passive if the corrosion resistance is increased under conditions where bare metal would significantly react [23]. Nonpassivating electrolytes do not, as the name suggests, form a passive layer. They usually contain aggressive ions, such as chloride, which destabilize the formation of a film [17]. This results in a higher machining rate but the surface finish is compromised along with the machining resolution [24].

The concentration of the electrolyte can also affect the machining quality and rate [25]. An electrolyte with a higher concentration can carry more current as there are more ions available within the solution [26]. This means that the machining rate will be higher as the amount of material removed is proportional to the amount of current passed over time. The current lines extend further into the solution when

the concentration is higher as the resistance of the electrolyte is reduced. This means the reaction at the workpiece can occur further away from the tool electrode which decreases the resolution of the machining process [13]. This issue has been overcome by the use of pulsed potential waveforms allowing the use of high-concentration electrolytes to maintain high machining rates [13].

When an alloy is used as the workpiece, choosing an appropriate electrolyte can be difficult. One electrolyte may be a good choice to machine one component of the alloy but may hinder the dissolution of the other components leading to an evenly machined surface. A way to combat this is to use a mixed electrolyte. This has been successfully demonstrated by S H Choi et al. [27] in the machining of a WC-Co alloy. It was demonstrated that while sodium nitrate was a good electrolyte for the tungsten element of the alloy it encouraged the formation of an oxide film on the cobalt element. Sulfuric acid was added to the electrolyte at a concentration of 0.2 M which helped dissolve the cobalt binder in the alloy allowing for even machining of the surface.

The electrolyte also serves the purpose of removing the reaction products from the machining gap [28]. The gap between the tool and the workpiece is very small, just a matter of micrometers, to enhance the precision of the machining. This gap can very quickly become blocked with the solid metal hydroxides which are formed when the dissolved metal ions react with the hydroxide ions in solution. It is imperative to remove this precipitate from the IEG to prevent a short circuit occurring or causing damage to either the workpiece or the tool electrode. This is done by pumping the electrolyte through the gap at high rates to flush any precipitate from the gap [28]. This is carried out in different ways; the most popular way is to expand the IEG, pump electrolyte through in a pulse before closing the gap to its previous position [13]. There is no electrolyte flowing while the electrodes are at their closest positions. Another method is to constantly pump the electrolyte through the system but this requires a much sturdier tool electrode to prevent the tool from being misplaced or bent by the electrolyte flow. Flushing the electrolyte through the gap also reduces the thickness of the static diffusion layer at the electrode surfaces. This is beneficial as it increases the machining rate by reducing the time it takes ions to diffuse to the electrode surface from the bulk solution and vice versa [26].

The third role of the electrolyte is to remove excess heat from the reaction zone [17]. Joule heating is the heat released when current is passed through a conductor. The heat produced is proportional to the square of the current and the electrical resistance. The heat is generated due to the resistance encountered when passing current through the electrolyte.

There are several reasons as to why it is important to remove the heat from the IEG. One being to prevent the electrolyte from boiling in the gap [29]; this creates bubbles in the gap, increasing the resistance across the gap and can cause sparks to occur between the two electrodes. This damages both the tool and the workpiece and can prevent any further machining taking place.

Another reason the temperature of the electrolyte needs to be controlled is to ensure the surface finish is of an acceptable standard. It was reported that when

the electrodes were heated above 40 °C, the surface quality of the machined part was reduced [17]. Hence it is clear to see that the temperature needs to be controlled to enable good quality machining to take place.

IEG CONTROL AND MODELING

IEG CONTROL METHODS

During the machining process, the tool electrode is moved in order to maintain constant IEG. The dimension of this gap can vary from a few μm to 100 μm depending on the application and has a dramatic influence on the machining accuracy. When drilling micro-holes, the feedrate of the tool electrode should match the material removal rate of the process to maintain the gap size and at the same time to reduce the chances for short circuits to occur [30]. The IEG is very difficult to control because it cannot be measured directly.

The different issues influencing the IEG size that can be met during an ECM process have been summarized as follows [31,32]: (1) local variation of the electrical conductivity in the IEG caused by the appearance of bubbles in the electrolyte; (2) difficulty in determining anodic overpotential changes; variation in local anodic current efficiency; (3) nonuniformity in the distribution of the electric field in the gap region; (4) presence of stray current lines.

In 1996, Wei et al. proved that the machining current could be used as a sensing parameter to evaluate the IEG [33]. It was concluded that it is therefore possible to conceive an online gap measurement system that can be used to control this parameter in real time—which confirmed the statements from Rajurkar et al. [34]. This technique was used by Schuster et al. who monitored the distance between the tool and workpiece by measuring the current flowing through the cell [8]. Since then, most of the published gap control strategies use the machining current to assess the IEG conditions and control the motion of the tool electrode.

Different control methods have been experimented and they can be summarized according to the logic used.

- Binary logic control methods: constant tool feedrate associated with tool retraction when the overcurrent protection is triggered

  This method is based on setting a maximum machining current value.

  Authors such as Yong et al. (Figure 8) and Ozkeskin developed a control system based on the measurement of the current passing through the system [35]. To be able to control the gap during the machining process, they moved the tool toward the workpiece until a “current jump-up” and then retracted the tool by a few micrometers. Mithu et al. used the same logic [30]. A similar approach has been adopted by Bhattacharyya et al. who controlled the IEG using an “electrical conduction method”: 1 V was applied to the IEG and the resulting current was measured to check if there was electrical contact (short circuit) between the tool electrode and the workpiece. This event then triggered the retraction of the tool (moved upward)

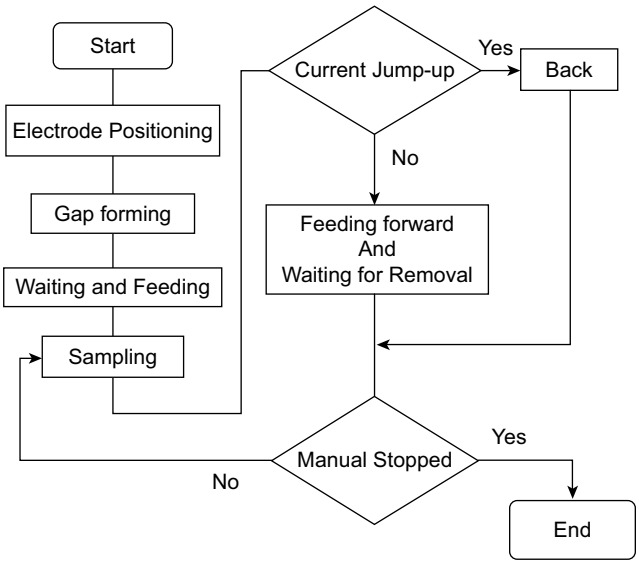

FIGURE 8

Flowchart for a control of the interelectrode gap [7].

to break this contact [36]. Recently, Mithu et al. were able to determine the short situation by analyzing the shape of the current during machining [37] which is an encouraging step to develop a process monitoring system.

Cagnon et al. and Choi et al. controlled the motion of the tool by using a short-circuit detector: if a short circuit occurred during machining the tool was retracted until there was no more contact between the tool electrode and the workpiece to the initial value of the IEG [38,39].

- Analog control method

In 2004, Schuster et al. proposed a patented "method for electrochemically processing material" [35]. They also presented a way to control the IEG within a 10 μm range. The current peaks were measured via a current peak detector and their values were compared with the desired value. The output of the comparator was passed through a low-pass filter (integrator) and a downstream amplifier. This amplifier controlled an electromagnetic mechanism that had a 10 μm travel distance. The position of the workpiece was then adjusted with respect to the measured current peaks. The authors claimed that the gap was "sufficiently small to obtain the desired local resolution" and "sufficiently high to avoid short circuits." However, no specific distances were mentioned.

- Fuzzy logic control (FLC)

Labib et al. [35] pointed out the necessity for the controller to have decision-making capabilities. They observed that the occurrence of sparking was efficiently

prevented when FLC was applied to the ECM process and encouraged further research to develop FLCs for the EMM process. Moreover, it is worth mentioning that fuzzy logic was also used to control the process in EDM, wire EDM [40,41], and electrochemical discharge machining [42,43].

The combination of an active control loop with adaptive neuro-fuzzy inference system or optimization algorithms seems very promising as some authors have already used neural networks to tune the machining parameters in ECM [44–47]. Recently, micro-herringbone grooves were machined in hydrodynamics bearings using a simulation-assisted μECM process [42]. Fuzzy logic was also applied to control the gap during an ECM process using a 6D force sensor while measuring the machining current [43].

- Computer numerical control (CNC) system with tool retraction and constant feed rate

Finally, in 2010 a CNC system was developed for μECM process using a soft-CNC architecture based on RT-Linux. This system used a real-time module to handle the motion, short-circuit detection (the detection signal was coming from the pulse generator), and gap adjustment aspects [44]. The authors managed to mill a hexagonal star and micro-stepped cavities at a feedrate of 6 μm/min using G code generated from standard CAD/CAM software.

As mentioned previously, the majority of the authors consider that the most reliable sensing parameter to control the IEG is the current [34,35,38,48,49], so a good relationship between the current and the gap size must be defined. The only way to answer this demand is to create electrical model(s) of the IEG.

INTERELECTRODE GAP MODELING

In 2000, Schuster et al. experimented μECM with ultrashort pulses by taking into account the effect of the EDL [50,51]. Studies showed that a capacitor was a suitable representation of the EDL in this process [50,52]. The electrical model of the gap that they used is presented on Figure 9.

Kozak [47] and Marla et al. [53] improved this model by adding nonlinear resistors (r_a and r_k) in parallel with the EDLs (Figure 10).

They claimed that the current going through the double layer was actually the sum of two different currents (Figure 11):

- *The charging current:* It is the current density that flows through the double layer when the latter is getting charged.
- *The faradaic current:* It is the current that causes the dissolution of the material when the EDL is fully charged.

It can be said that the current representing the gap size is the faradaic current because it only starts flowing through the cell when the EDL is fully charged, and is therefore strongly related to the IEG resistance. The use of this model has been reported by other authors as well [52,54,55].

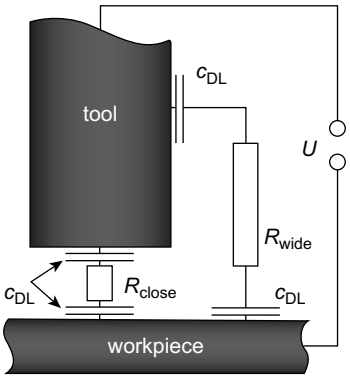

FIGURE 9

Schematic of an electrochemical cell, the double layer capacity (C_{DL}) is charged via the electrolyte resistance [8].

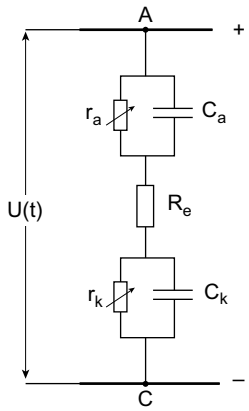

FIGURE 10

Electrical model of the interelectrode gap proposed by Kozak J et al. [47] for the electrochemical micro-machining process.

To increase the amount of faradaic current contained in each pulse, Kozak et al. made μECM trials by combining a DC voltage source and a pulsed voltage. The role of the DC voltage was to keep the EDL partially polarized, then the voltage pulses would remove material more efficiently and at the same time, the tool would be protected from corrosion. The DC voltage was therefore relatively low and below the activating potential of the electrochemical reaction [14]. However, some other authors claimed that applying an appropriate value of negative voltage during the pulse off-time would improve the unloading/reloading times of the EDL without the dissolution of the tool [56].

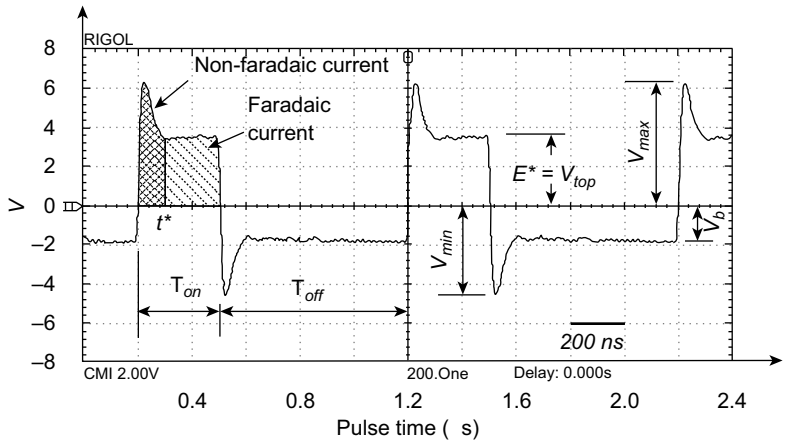

FIGURE 11

Charging and discharging waveforms during electrochemical micro-machining [56].

The amount of faradaic current per pulse decreases when the pulse width becomes shorter since the charging time takes a greater portion of the pulse. Furthermore, if the pulses are too short, then the EDL cannot fully charge and therefore no faradaic current is created.

The current is mainly influenced by the conductivity of the electrolyte and the gap size. However, the conductivity of the electrolyte is influenced by several parameters including the ionic concentration (i.e., pH, Cl^-, NO_3^-) and the temperature.

Therefore, if the current is used as a sensing parameter, the properties of the electrolyte have to be carefully maintained constant within the IEG, otherwise the relationship between the measured current and the gap size changes.

In order to have a more accurate representation of the gap, the side walls of the cathode (tool electrode) should be insulated to prevent the current from flowing through them: only the current flowing through the front face of the cathode can be used to indirectly measure the IEG size unless a very complicated algorithm is created to compensate for the change of the active zone on the cathode electrode.

EQUIPMENT FOR MICRO-ECM

Micro-ECM is a relatively new process and it is still trying to secure its place on the market among the other micro-manufacturing technologies. The main problem is that the process is very complex and requires a set of interdisciplinary skills and knowledge. Existing equipment is predominantly in the laboratories and in the last few years there is noticeable increase of the research activities in this area. Still there are many obstacles linked with the needed equipment for micro-ECM process to be securely placed on the market of micro-manufacturing technologies.

- Power supplies for micro-ECM process should be special as they should be able to provide pulses with amplitude 1−15 V, current up to 5 A (depending on the cathode working area), and frequency range from 1 KHz to 5 MHz with minimum pulse width (on time) of 50 ns. This kind of device is hard to design mainly because it requires the metal-oxide semiconductor field effect transistors (MOSFETs) to be switched at a very high frequency. Indeed, most of the silicon-based power transistors commercially available are designed to work at a maximum switching frequency of 1 MHz and are limited by their turn-on and turnoff times. To make a MOSFET turn on in a few nanoseconds, a high current pulse (of several amperes) has to be applied to quickly charge the capacitor at its gate. Therefore in most cases a special gate driver needs to be developed [51].
- Short-circuit protection: Machining at a very small IEG dramatically increases the chances for short circuits to occur. Short circuits are very undesirable as they might damage the tool, alter the quality of the workpiece surface, and even damage the pulse generator. Therefore, an ultrafast short-circuit protection is necessary to be built into the power supply unit. Most of the solutions implemented for that purpose measure the current flowing through the system via a sensing resistor in series with the gap. Moreover, the measured current is used as a machining parameter to control the IEG [31].
- Electrical connections: One of the critical parameters of the μECM process circuitry is the inductance of the cables connecting the power supply unit (PSU) to the electrodes [52]. The parasitic cable inductance increases the rise time of the voltage pulses especially for pulse durations below 1μs. At high frequency, the impedance of the cable becomes so big that only a portion of the output power is delivered to the IEG and the pulses are distorted. The cabling therefore limits the frequency at which machining can occur and problems have been reported above 1 MHz [54]. To solve this issue, or at least diminish the effect, special low-inductance cables should be used and still though their length must be minimized. The electrical connection of the anode electrode is also complicated and important as few rules have to be followed:
  - Only the machined material has to be exposed to the electrolyte and the electrical connection.
  - The cables should be with low inductance and with minimum length.
  - In the best case the working zone should be in a structure acting like a Faraday cage to shield/prevent RF emissions and reduce parasitic inductance.

In the case of on-the-machine electrode preparation (similar to the micro-EDM process) the power supply should be able to reverse the polarity of the pulses and the wiring should support this as well.

- Spindle: The spindle also can be designed so that it can accommodate the PCB from the power supply with the high frequency and severely reduce the length of the connection cables. In the case of high frequency power supply and high current (up to 5A) it is not suitable to use the traditional carbon or silver brushes

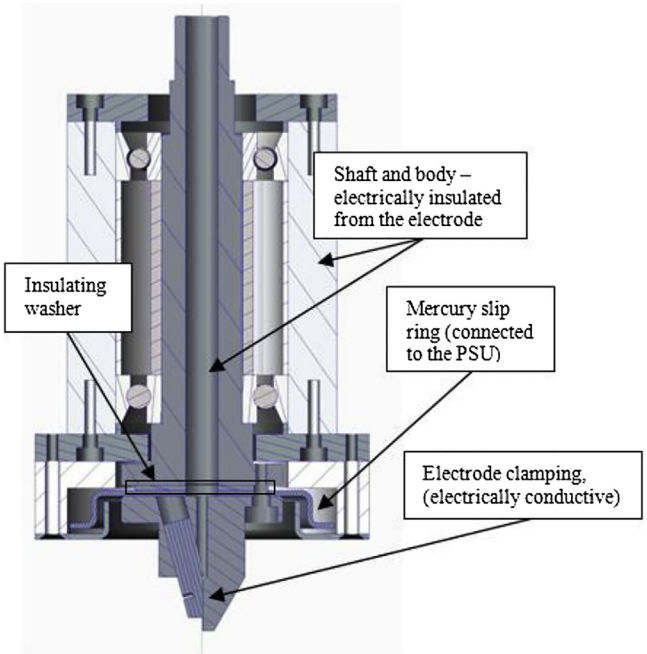

FIGURE 12

Proposed electrochemical micro-machining spindle design with built-in mercury slip ring for minimizing the current path and minimizing the inductance.

because the transmission of high current has a detrimental effect on them and they do not work well at high frequency (parasitic inductance). At the moment the authors propose a solution to reliably transmit high frequency pulses through a liquid metal bath (e.g., mercury or galinstan) by designing a slip ring (see Figure 12).

APPLICATIONS AND EXAMPLES

Micro-ECM is a diverse process that can, theoretically, anodically dissolve any electrically conductive material provided the right machining conditions are applied, including the correct choice of electrolyte. This machining process has many applications including die sinking, profiling and contouring, grinding, drilling, and polishing.

Die sinking is used to form items such as watch cases or other 3D microstructures. In these cases 3D micro-features are machined on the cathode electrode which is then used to create the features onto the anode workpiece (Figure 13) [54]. This allows a complex shape to be fashioned quickly, easily, and repeatedly once a tool electrode has been designed.

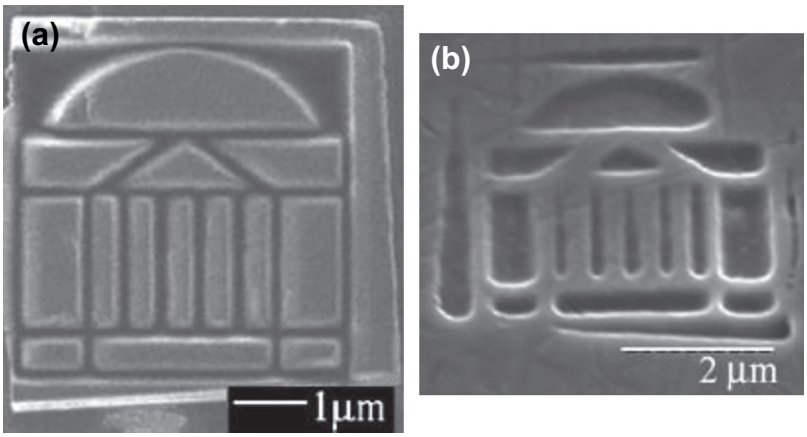

FIGURE 13

Scanning electron micrographs (a) the tool and (b) structure in Ni substrate [54].

ECM can also be used to polish a surface, a technique also known as electrochemical polishing. This is used to remove burrs from a product created using a conventional machining method [54].

Drilling is conducted using a thin tool electrode that is approached to the workpiece as machining commences. Usually the outer edge of the tool is insulated to prevent an overcut from forming. In some cases, the pulse duration was increased when the tool reached a desired location during drilling, in order to create cavities (undercuts) into the workpiece and machine complex features (Figure 14) [55].

To enable micro-contouring machining the ECM process has to be adapted. Generally a tool electrode is moved along a designated, computer-controlled pathway to create the desired shape in the workpiece. In this way complex shapes and contours can be created without the long process of designing a tool electrode and the tool electrode shape is simple. The tool position is important here, but using

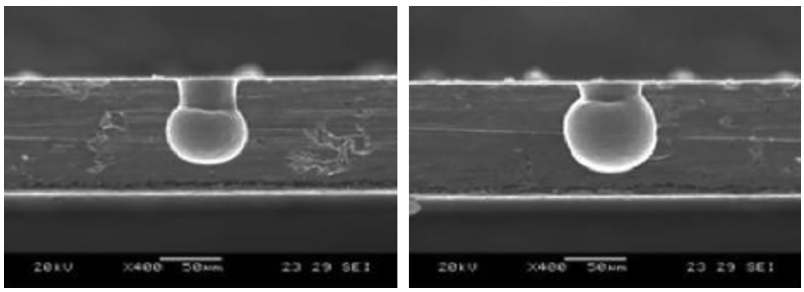

FIGURE 14

Micro-cavities machined by controlling dissolution time and pulse duration [55].

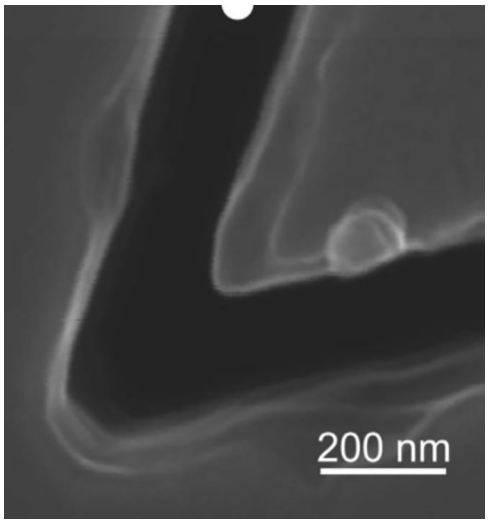

FIGURE 15

Triangular trough created using electrochemical machining [13].

a very small tool, on the micrometer scale, it can be difficult to place the tool accurately. To solve this issue, the tool is created in situ creating a fine electrode from a thicker piece of wire similar to the electrode grinding in micro-EDM process. To achieve the high precision required for micro-features the potential is applied in short pulses. The accuracy is dependent on the pulse duration; the shorter the pulse the higher the accuracy. A triangular-shaped trough measuring just 1 μm deep and approximately 200 nm wide was successfully machined with a 500 ps pulse [13]. Figure 15 shows the feature using a scanning electron microscope.

For micro-ECM, each machining is possible to find the optimal range for the IEG; a gap too small may cause sparking or short circuits which could cause damage to either the workpiece or tool electrode and a gap too large would not facilitate machining as the potential pulse would not be of a duration long enough to charge the workpiece surface sufficiently to enable anodic dissolution. This is because the dissolution is exponentially dependent on the potential drop, which is linked to the IEG. Still a methodology how to determine the optimal IEG has not been suggested.

REFERENCES

[1] Pletcher D. A first course in electrode processes. 2nd ed. Southampton: The Royal Society of Chemistry; 2009.

[2] McGeough J. Electrochemical machining (ECM). Electrochemistry encyclopedia [Online]. 2005. electrochemm.cwru.edu/encycl/art-m03-machining.htm.

[3] Pletcher D. Metal finishing. Industrial electrochemistry. Chapman and Hall Ltd; 1982.
[4] Lewis E, Berry M. As and a level chemistry. Longman; 2000.
[5] Hotoiu L, Deconinck J. In: Time-efficient simulations of Nano-pulsed electrochemical micro-machining, vol. 6. CIRP; 2013. p. 469−74.
[6] Cook NH, Loutrel SP, Meslink MC. Increasing electrochemical machining rates. Cambridge Massachusetts: US Army Materials Research Agency; 1967.
[7] INDEC. Precision electrochemical machines and technologies. INDEC; 2011.
[8] Schuster R, Kirchner V, Allongue P, Ertl G. Electrochemical micromachining. Science 2000;289:98−101. http://dx.doi.org/10.1126/science.289.5476.98.
[9] Schuster R. Electrochemical microstructuring with short voltage pulses. Chemphyschem A Eur J Chem Phys Phys Chem 2007;8:34−9. http://dx.doi.org/10.1002/cphc.200600401.
[10] Schuster R, Kirchner V. Method for electrochemically processing material [US 6689269 B1]; 2004.
[11] Trimmer AL, Hudson JL, Kock M, Schuster R. Single-step electrochemical machining of complex nanostructures with ultrashort voltage pulses. Appl Phys Lett 2003;82:3327. http://dx.doi.org/10.1063/1.1576499.
[12] Cagnon L, Kirchner V, Kock M, et al. Electrochemical micromachining of stainless steel by ultrashort voltage pulses. Z für Phys Chem 2003;217:299−314. http://dx.doi.org/10.1524/zpch.217.4.299.20383.
[13] Berlin: s.n Kock M, Kirchner V, Schuster R. Electrochemical micromachining with ultrashort voltage pulses − a versatile method with lithographical precision. Electrochim Acta 2003;48:3213−9.
[14] Kozak J, Rajurkar KP, Makkar Y. Study of pulse electrochemical micromachining. J Manuf Process 2004;6:7−14. http://dx.doi.org/10.1016/S1526-6125(04)70055-9.
[15] Kamaraj AB, Sundaram MM. Mathematical modeling and verification of pulse electrochemical micromachining of microtools. Int J Adv Manuf Technol 2013;68:1055−61. http://dx.doi.org/10.1007/s00170-013-4896-y.
[16] Kozak J, Rajurkar KP, Makkar Y. Selected problems of micro-electrochemical machining. J Mater Process Technol 2004;149:426−31. http://dx.doi.org/10.1016/j.jmatprotec.2004.02.031.
[17] Bannard J. Electrochemical machining. J Appl Electrochem 1977;7:1−29.
[18] Thomas JGN, Hind G. The electrochemistry of corrosion. www.npl.co.uk. [Online] [Cited: October 16, 2013.] http://www.npl.co.uk/upload/pdf/the_electrochemistry_of_corrosion_with_figures.pdf.
[19] Rayner-Canham G, Flynn C. Iron ocean Seeding. Royal Society of Chemistry. [Online] 2010. [Cited: October 16, 2013.] http://www.rsc.org/Education/EiC/issues/2010September/IronOceanSeeding.asp.
[20] Hanamant Surekar Suresh, Gajanan Kharche Wasudwv. Electrolytes in electrochemical machining process. In: Proceeding of 9th international symposium on advances in electrochemical science and technology; 2010.
[21] Lesch Andreas, et al. External control of anodic dissolution mechanisms of 100Cr6 in nitrate/chloride mixed electrolytes. J Electrochem Sci Eng 2011;1:39−54.
[22] Wolters H-H. Electrochemical machining − a non-conventional metal machining technology. ECM Technologies; 2010 [SIG Materials Analysis].
[23] Schultze JW, Lohvengel MM. Stability, reactivity and breakdown of passive films. Problems of recent and future work. Electrochim Acta 2000;45:2499−513.
[24] Datta M. Anodic dissolution of metals at high rates. IBM J Res Dev 1993;37.

[25] Bhattacharyya B, Munda J, Malapati M. Advancement in electrochemical micromachining. Int J Mach Tools Manuf 2004;44:1577−89.
[26] Pletcher D. A first course in electrode processes. 2nd ed. Romsey: Electrochemical Consultancy; 2009. 136.
[27] Choi S Hwan, et al. Analysis of electrochemical behaviours of WC-Co alloy for micro-ECM. J Mater Process Technol 2013;213:621−30.
[28] Kozak J, Rajurkar KP, Makkar Y. Study of pulse electrochemical micromachining. J Manuf Process 2004;6(1).
[29] Loutrel SP. Electrochemical machining: prediction of operating parameters including extreme operating conditions. Massachusetts Institute of Technology; 1971.
[30] Mithu MAH, Fantoni G, Ciampi J, Santochi M. On how tool geometry, applied frequency and machining parameters influence electrochemical microdrilling. CIRP J Manuf Sci Technol 2012;5:202−13. http://dx.doi.org/10.1016/j.cirpj.2012.07.006.
[31] Yong L, Yunfei Z, Guang Y, Liangqiang P. Localized electrochemical micromachining with gap control. Sens Actuators A 2003;108:144−8. http://dx.doi.org/10.1016/S0924-4247(03)00371-6.
[32] Ozkeskin FM. Feedback controlled high frequency electrochemical micromachining. Texas A&M University; 2008.
[33] Wei B, Rajurkar KP, Talpallikar S. On-line identification of interelectrode gap sizes in pulse electrochemical machining (PECM). In: Proc. Symp. High Rate Met. Dissolution Process; 1996. p. 248.
[34] Rajurkar KP, Wei B, Kozak J, McGeough JA. Modelling and monitoring interelectrode gap in pulse electrochemical machining. CIRP Ann - Manuf Technol 1995;44:177−80. http://dx.doi.org/10.1016/S0007-8506(07)62301-4.
[35] Labib AW, Keasberry VJ, Atkinson J, Frost HW. Expert systems with applications towards next generation electrochemical machining controllers: a fuzzy logic control approach to ECM. Expert Syst Appl 2011;38:7486−93. http://dx.doi.org/10.1016/j.eswa.2010.12.074.
[36] Bhattacharyya B, Munda J. Experimental investigation on the influence of electrochemical machining parameters on machining rate and accuracy in micromachining domain. Int J Mach Tools Manuf 2003;43:1301−10. http://dx.doi.org/10.1016/S0890-6955(03)00161-5.
[37] Mithu MAH, Fantoni G, Ciampi J. A step towards the in-process monitoring for electrochemical microdrilling. Int J Adv Manuf Technol 2011;57:969−82. http://dx.doi.org/10.1007/s00170-011-3355-x.
[38] Mediliyegedara TKKR, De Silva AKM, Harrison DK, McGeough JA. New developments in the process control of the hybrid electro chemical discharge machining (ECDM) process. J Mater Process Technol 2005;167:338−43. http://dx.doi.org/10.1016/j.jmatprotec.2005.05.043.
[39] Skrabalak G, Zybura-Skrabalak M, Ruszaj A. Building of rules base for fuzzy-logic control of the ECDM process. J Mater Process Technol 2004;149:530−5. http://dx.doi.org/10.1016/j.jmatprotec.2003.11.058.
[40] Asokan P, Ravi Kumar R, Jeyapaul R, Santhi M. Development of multi-objective optimization models for electrochemical machining process. Int J Adv Manuf Technol 2008;39:55−63. http://dx.doi.org/10.1007/s00170-007-1204-8.
[41] Zare Chavoshi S. Analysis and predictive modeling of performance parameters in electrochemical drilling process. Int J Adv Manuf Technol 2011;53:1081−101. http://dx.doi.org/10.1007/s00170-010-2897-7.

[42] Chang D-Y, Shen P-C, Hung J-C, et al. Process simulation-assisted fabricating micro-herringbone grooves for a hydrodynamic bearing in electrochemical micromachining. Mater Manuf Process 2011;26:1451−8. http://dx.doi.org/10.1080/10426914.2011.551905.
[43] Yonghua L, Kai L. Fuzzy controlling interelectrode gap of ECM based on 6 dimensional forces and machining current. In: 2010 Int. Conf. Intell. Syst. Des. Eng. Appl. Ieee; 2010. p. 775−9.
[44] Wang Y, Chen H, Wang Z, et al. Development of a Soft-Computer Numerical Control System for Micro − Electrochemical Machining. Am J Nanotechnol 2010;1:51−55.
[45] Kirchner V, Cagnon L, Schuster R, Ertl G. Electrochemical machining of stainless steel microelements with ultrashort voltage pulses. Appl Phys Lett 2001;79:1721. http://dx.doi.org/10.1063/1.1401783.
[46] Ahn SH, Ryu SH, Choi DK, Chu CN. Electro-chemical micro drilling using ultra short pulses. Precis Eng 2004;28:129−34. http://dx.doi.org/10.1016/j.precisioneng.2003.07.004.
[47] Kozak J, Gulbinowicz D, Gulbinowicz Z. The mathematical modeling and computer simulation of pulse electrochemical micromachining. In: IAENG Trans. Eng. Technol. Spec. Ed. World Congr. Eng. Comput. Sci. AIP Conf. Proc., San Francisco (CA), vol. 2; 2008. p. 174−85.
[48] Çaydas U, Hasçalk A, Ekici S. An adaptive neuro-fuzzy inference system (ANFIS) model for wire-EDM. Expert Syst Appl 2009;36:6135−9. http://dx.doi.org/10.1016/j.eswa.2008.07.019.
[49] Abuzied HH, Awad MA, Senbel HA. Prediction of electrochemical machining process parameters using artificial neural networks. Int J Comput Sci Eng 2012;4:125−132.
[50] Choi SH, Kim BH, Shin HS, et al. Analysis of the electrochemical behaviors of WC−Co alloy for micro ECM. J Mater Process Technol 2013;213:621−30. http://dx.doi.org/10.1016/j.jmatprotec.2012.10.018.
[51] Tang T, Burkhart C. Hybrid MOSFET/driver for ultra-fast switching. IEEE Trans Dielectr Electr Insul 2009;16:967−70. http://dx.doi.org/10.1109/TDEI.2009.5211841.
[52] Burkert S, Schulze H, Gmelin T, Leone M. The pulse electrochemical micromachining (PECMM) − specifications of the pulse units. Int J Mater Form 2009;2:645−8. http://dx.doi.org/10.1007/s12289-009-0464-2.
[53] Marla D, Joshi SS, Mitra SK. Modeling of electrochemical micromachining: comparison to experiments. J Micro/Nanolith, MEMS MOEMS 2008;7:033015. http://dx.doi.org/10.1117/1.2964215.
[54] Landolt D, Chauvy P-F, Zinger O. Electrochemical micromachining, polishing and surface structuring of metals: fundamental aspects and new developments. Electrochim Acta 2003;48:3185−201.
[55] Jo CH, Kim BH, Shin HS, et al. Micro electrochemical machining for complex internal micro features. In: Internal conference on smart manufacturing application; 2008. p. 247−50. http://dx.doi.org/10.1109/ICSMA.2008.4505651.
[56] Mithu Ma H, Fantoni G, Ciampi J. The effect of high frequency and duty cycle in electrochemical microdrilling. Int J Adv Manuf Technol 2011;55:921−33. http://dx.doi.org/10.1007/s00170-010-3123-3.

This page intentionally left blank

CHAPTER

Hot Embossing

7

Matthias Worgull
Karlsruhe Institute of Technology, Institute of Microstructure Technology, Eggenstein-Leopoldshafen, Germany

CHAPTER OUTLINE

Micromanufacturing Engineering and Technology. http://dx.doi.org/10.1016/B978-0-323-31149-6.00007-4

INTRODUCTION

A further distribution of applications with integrated micro-features or micro-systems requires technologies to replicate the corresponding micro-structures. In addition to the structuring of silicon, glass, or metals by different structuring processes, the replication of micro-structures is based typically on polymers. Polymers, especially thermoplastic polymers, are commercially available and are characterized by a large bandwidth of properties. Here for most applications a suitable polymer which fulfills the requirements of the application can be found.

Hot embossing is one of the established replication technologies for the replication of a micro-structured master, a so-called mold insert. The available replication processes are listed below [1−4,30]:

- Micro-reaction injection molding,
- Micro-injection molding,
- Micro-injection compression molding,
- Micro-hot embossing,
- Micro-thermoforming,
- Nano-imprint lithography (NIL) processes.

All these processes are not in competition to each other, since they have their own specific characteristics and merits. Therefore, depending on the requirements like stress in molded parts, flow length, number of replications, or cost-effectiveness, the replication process can be determined. Nevertheless, the design and the arrangement of the structures will define the suitable replication technology. Hot embossing is a technology which is suitable for the replication of a large bandwidth of structures especially structures with high aspect ratios. In this chapter, such a process is presented. The technology of hot embossing machines, hot embossing tools, and examples of typical applications will underline the merits and flexibility of hot embossing.

The replication technique of hot embossing of micro-structures can be traced back to the second half of the twentieth century. Already in 1970, hot embossing had been implemented by a group of researchers from RCA Laboratories at Princeton, NJ, USA [5]. The objective of their work was to develop a low-cost reproduction technique of surface hologram motion pictures for television playback. A master tape was made by electroplating nickel into photoresist patterns. The master was run through heated rollers together with a vinyl tape and, thus, the micro-structure was transferred into the vinyl. The molded structures were characterized by a depth of 0.1 μm and a lateral resolution of 1 μm. In 1978, Gale et al. [6] used a hot embossing technique for the replication of surface relief structures for color and black-and-white reproductions. These relief phase grating structures refer to a recording of light in zero-order diffraction. These structures, with a height of 1−2 μm and a spacing of around 1.4 μm, were replicated from a nickel mold insert into transparent PVC by hot embossing at a molding temperature of 150 °C and a pressure of 0.3 MPa. The structures were also replicated in polycarbonate and acetate.

The structures replicated by hot embossing today are characterized by high aspect ratios, smaller feature sizes down to the nanometer range, and vertical sidewalls with a surface roughness below 40 nm (Figure 1).

Before the hot embossing process was established in micro-structure technology experiments were done by reaction injection molding. This process enables injection of mixed liquid monomers and a starter into a micro-structured mold and the molding occurs by polymerization in the mold [7]. Micro-structures of polymethylmethacrylate (PMMA) and polyamide were molded successfully, but at the beginning of these experiments the filling and the demolding of filigree micro-structures with high aspect ratio was a challenging aspect. Nevertheless, because of the difficulties in controlling the polymerization and the high shrinkage of the molded part, the hot embossing technique based on polymer foils was investigated. Beside fundamental tests with micro-injection molding, basic experiments in 1989 with an embossing technique of PMMA material marked the start of the use of micro-hot embossing for the production of LIGA structures [8] (LIGA is a German acronym for lithography, electroplating, and molding—Lithographie, Galvanik, Abformung). With further development of the LIGA technique, the development of the hot embossing technique also proceeded. At the beginning the technique was based on laboratory machines with a low grade in automation which required the control of every molding step by the user. The precision of the molding machine regarding the press force, the molding velocity, and the temperature distribution was also improved. A milestone in the development was the use of computer-controlled tensile testing machines for hot embossing applications. Such machines, already available in many material testing laboratories, can fulfill the requirements for micro-hot embossing, including high stiffness of the machine, precise motion, the control system for force and velocity combined with a measurement system, and an interface to the user. An integration of a molding tool with a heating and cooling system completed the required components for hot embossing. Subsequently, this concept was further developed into commercially available machines. Together

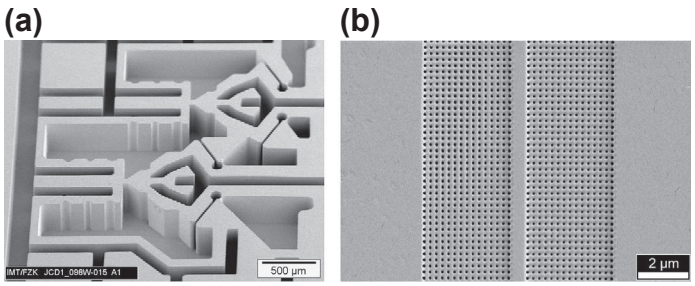

High aspect ratio structures nano structures [32]

FIGURE 1

Polymethylmethacrylate replicated structures. (a) High aspect ratio structures and (b) nanostructures [32].

with further development of the hot embossing technique, these kinds of machines are now part of state-of-the-art hot embossing technology [9]. Independently from the developments based on the use of tensile testing machines, new concepts based on the use of the hydraulic drives were also established [10]. There are also other types of machines existing in various research laboratories and industries, as a result of independent development and/or customized applications.

On the basis of the hot embossing technology available at the present time, hot embossing is a well-established process in industry and science with a large bandwidth of process variations. The replication of Fresnel lenses for overhead projectors or concentrating solar systems [11] is also established, like the replication of CDs by the related process of injection compression molding. The development of NIL with thermal and UV curable materials opens a way for hot embossing technology to be extended to the nano-structuring methods. A new level of different applications, such as surface modifications in the nano-range or the replication of structures in the wavelength dimensions of light, will pave a way to a new class of applications. The development of the hot embossing technique is closely linked to the development of structuring techniques for the fabrication of mold inserts. Today, structures of mold inserts in a range below 10 nm can be fabricated. The hot embossing process in combination with polymers is well suited for the replication of these structures and it can make contributions to the volume production of new applications based on nano-structuring. One of the key merits is its flexibility in setup, which allows for convenient changing of the mold and molding material. Therefore, hot embossing is also a popular process in laboratories for micro-structuring. The process is characterized by a large bandwidth of possible process variations, such as double-sided aligned molding, molding of through holes, molding of polymer stacks, thermoforming by polymer melts or structuring by hot punching. These variants offer attractive characteristics for micro- and nano-replications and for the development of micro- and nano-systems.

HOT EMBOSSING PROCESS

To illustrate the fundamental of the process, the case of single-sided hot embossing is described below. The principle of a one-sided hot embossing cycle is represented schematically in Figure 2. Between the micro-structured mold insert and a metal plate with a rough surface, the so-called substrate plate, a semifinished product, i.e., a polymer foil, is positioned. The thickness of the foil exceeds the structural height of the tool. The surface area of the foil covers the structured part of the tool. The tool and substrate are heated under vacuum to the polymer molding temperature. When a constant molding temperature is reached, the two steps of the molding cycle are initiated. In the first step, the mold insert and substrate are moved toward each other (in the range of 1 mm/min) until the preset maximum embossing force is achieved. In the second step, the embossing force achieved is held at a constant value for a defined holding time. To generate a constant force, the relative

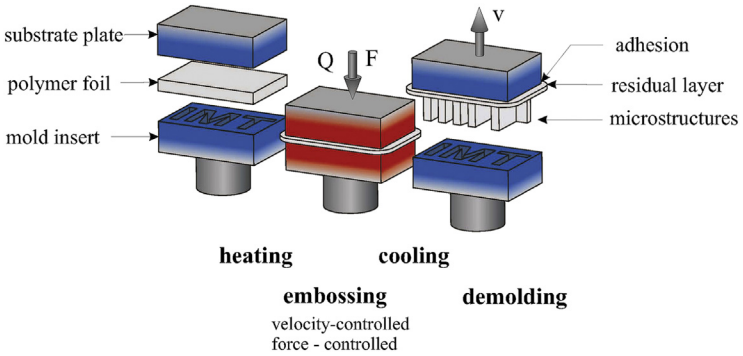

FIGURE 2

Schematic view of the hot embossing process.

movement between the tool and substrate has to be controlled. The force is now kept constant over an additional time period (packing time, holding time). During this period, the plastic material flows in the radial direction and the residual layer will be reduced under the acting constant force (packing pressure). At the same time, the tool and substrate move further toward each other, while the thickness of the residual layer decreases with packing time. During this molding process, the temperature remains constant. This isothermal embossing under vacuum is required to fill the cavities of the tool completely. Air inclusions or cooling during mold filling may result in an incomplete molding of the micro-structures, in particular at high aspect ratios. Upon the expiry of the packing time, cooling of the tool and substrate starts, while the embossing force is maintained. Cooling is continued until the temperature of the molded part drops below the glass transition temperature or melting point of the plastics. When the demolding temperature of the polymer is reached, the molded part is demolded from the tool by relative movement between the tool and the substrate. Demolding only works in connection with an increased adhesion of the molded part to the substrate plate. Due to this adhesion, the demolding movement is transferred homogeneously and vertically to the molded part. Demolding is the most critical process step of hot embossing. Depending on the selected process parameters and the quality of the tool, demolding forces may vary by several factors. In extreme cases, demolding is no longer possible, the structures are destroyed during demolding.

Apart from the one-sided molding described, the process is also used for double-sided positioned embossing. The principle of the process remains the same. Instead of the substrate, however, another tool is applied. To demold the molded part from one of the two tool halves, special demolding mechanisms, such as ejector pins or pressurized-air demolding, are used. For a better understanding, the schematic representation of embossing in Figure 2 is limited to the major process steps. Depending on the tool and the polymer used, the process and process parameters have to be adapted to any changes.

The characteristics and merits of hot embossing may be summarized as follows:

- The molding process is characterized by short flow paths, only from the molten polymer film into the micro-cavities;
- Because of the moderate molding velocities in the range of 1 mm/min only moderate shear stress in the polymer will be generated. This results in comparative low residual stress in the molded parts;
- If the molding temperature is set to the range where the relaxation times of a polymer corresponds to the cycle times of molding, the stress induced by molding can be decreased by relaxation processes. This option requires the knowledge of the temperature-dependent relaxation behavior of the polymer;
- The use of standardized mold inserts allows for the quick change of a micro-structured mold, which underlines the flexibility of the technology;
- Beside the quick change of the mold insert, the polymer can also be changed quickly. Only a new polymer foil has to be placed between the mold insert and the substrate plate (Figure 1). This allows for replicating a mold insert into several polymers in a short time.
- The technology allows for a variety of process variations, for example, double-sided molding, molding of through holes, multilayer molding, and also thermoforming of a high-temperature polymer foil by a low-temperature polymer melt;
- Compared to injection molding, the process may be characterized by longer cycle time. Although the development shows that with an effective technology the cycle times could be reduced, the process is economically well suited for small and medium series production. Nevertheless, because of the high flexibility this process can be adapted to several requirements and it, therefore, is of high potential for the development of prototypes within laboratories.

PROCESS VARIATIONS

As mentioned above hot embossing is not limited to the case of a single-sided molding cycle. The concept of hot embossing allows for modifying the process according to the requirements of further applications of the molded parts. Representative of a large number of modifications, the concepts of double-sided molding, multilayer molding, the molding of through holes, and roller embossing, are described in this section.

DOUBLE-SIDED MOLDING

Double-sided molding paves the way to a further large family of molded parts. For example, double-sided structured parts are part of micro-fluidic systems where through holes are essential features. Although fraction lines with thin residual layers can be designed to separate molded parts, in general, with double-sided molding,

the possibility of three dimensional structuring could be enabled. A precondition for such designs is the correlation of two mold inserts which are positioned opposite to each other and adjustable laterally relative to each other. Use of markers or the orientation on characteristic structures of the design is recommended. After a coarse adjustment of both mold inserts, a first part should be molded. In a second step the differences in the lateral dimension between the markers on the top side and the bottom side of the molded part have to be measured. The transparency of the most polymer is helpful, because it enables the determination of the misalignment of the markers with an optical measurement system, focusing on the top and on the bottom of a thin molded part. The misalignment can be split into a transversal (x,y) direction and a rotational (in the perpendicular axis of the part) misalignment. With this measured data the alignment of both mold inserts can be corrected by an alignment system integrated in a hot embossing tool. The alignment can be done separately in the transversal and rotational directions (Figure 3). These alignment systems are optional components of commercial hot embossing machines (for example, Jenoptik Hex03) and are a precondition for double-sided molding.

MULTILAYER MOLDING

Another illustrated approach [12], e.g., for the fabrication of through holes is the use of a polymer composite, a stack of two different polymer films (polymer 1 and polymer 2). The structured part with through holes will be molded onto a layer of a second polymer (polymer 2) (Figure 4). After demolding of the molded composite the first polymer can be separated from the second polymer, in this case the carrier layer, by peeling. The advantage of this method is the maintenance of the adhesion on the substrate plate. This allows for demolding the molded composite in the vertical direction by the precise movement of the hot embossing machine. The adhesion between the first polymer and the second polymer has to be high enough

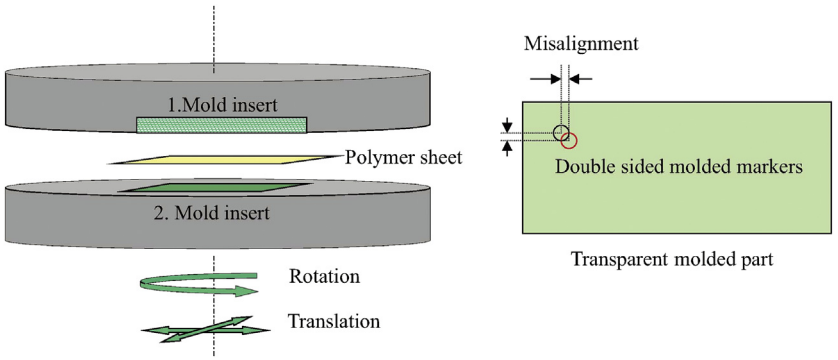

FIGURE 3

Principle of alignment for double-sided molding.

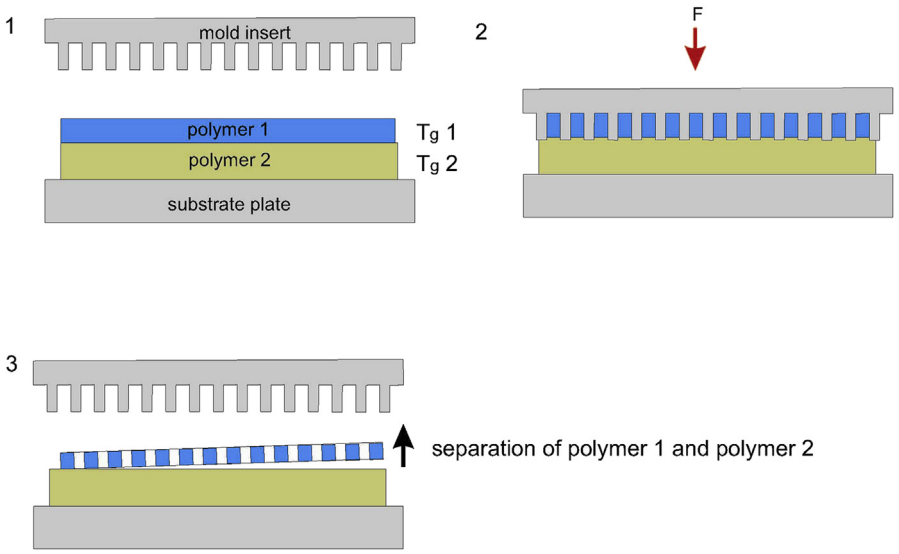

FIGURE 4

Principle of two layer molding for molding through holes.

to withstand the tensile forces during demolding. Additionally, a form closed connection, effected by the penetration of the mold insert into the second polymer, will support the connection of both polymers. This approach is only suitable for selected material combinations, because of the required adhesion and further separation.

THROUGH HOLES

In micro-system technology the need of molded parts with through holes is increasing, especially micro-fluidic components like micro-pumps, micro-valves, or fluidic components for lab-on-a-chip systems, are common examples. The fabrication of through holes is, therefore, an actual aspect in fabrication of micro-system components. To reduce the postprocessing steps, through holes should be fabricated already during molding. Because of the molding principle, this requirement is difficult to achieve. As mentioned above, hot embossing is characterized by a squeeze flow of a polymer melt. Typical molded parts are therefore characterized by a residual layer. On the one side this residual layer is necessary to obtain the pressure for filling micro-cavities, on the other side for the fabrication of parts with through holes, these residual layer should be completely displaced. The methods for fabricating these holes can be split into the postprocessing methods to remove thin residual layers and in methods that are characterized by the selected substrate plates allowing for fabricating through holes already during molding. Finally, a new development is discussed—a

principle that allows for fabricating through holes with a two-step process, a molding cycle and a cutting cycle which gives the name of this process—hot punching.

To avoid any postprocessing of molded parts, through holes should be fabricated already during the embossing cycle. This can be achieved by the use of a combination of modified mold inserts and selected substrates [13]. The principle refers to a complete displacement of the residual layer in selected areas, achieved by embossing free standing structures of the mold inserts into modified substrates. This enhanced molding principle requires a sensitive setup of the process parameters and a proper selection of the substrate materials, because of the relatively high load on the structures during molding. The risk of damaging filigree structures of the mold insert increases, especially when the diameter of the through holes decreases.

Representative of the process variation of molding through holes, the approach of molding onto a stack of foils is described here. In this approach, additional to the conventional metal substrate plate, a flexible layer is put on top. This layer consists typically of a polymer layer and a metal film. By the selection of the materials and film thickness, the flexibility of this combination can be influenced. Figure 5 illustrates the principle. Because of the flexibility of the layer, in selected areas the polymer melt can be displaced completely from the top-side of the mold insert. By using this technique it is possible to retain the residual layer in large contact surfaces, e.g., at the margin regions of the mold insert, and to completely displace the residual layer in small contact areas. During the cooling state the desired dwell pressure will be generated by the flexible layer and not by the residual layer.

HOT PUNCHING

The principle of hot punching is a two-step method for molding through holes (Figure 6). In the first step a selected mold insert will be replicated in an amorphous polymer with high glass transition or a semicrystalline polymer with high melting temperature. The replication refers to a single molding on a rough substrate plate. Instead of peeling off the molded part from the substrate plate, the replicated part remains on the residual layer after demolding. The molded part will be used as a second, to the first mold aligned mold insert, here the so-called matrix. In the second process step a thin film of another polymer with a lower glass transition temperature

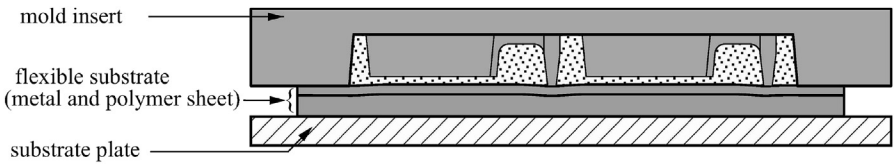

FIGURE 5

Schematic view of a configuration for the molding of through holes with the use of a stack of foils.

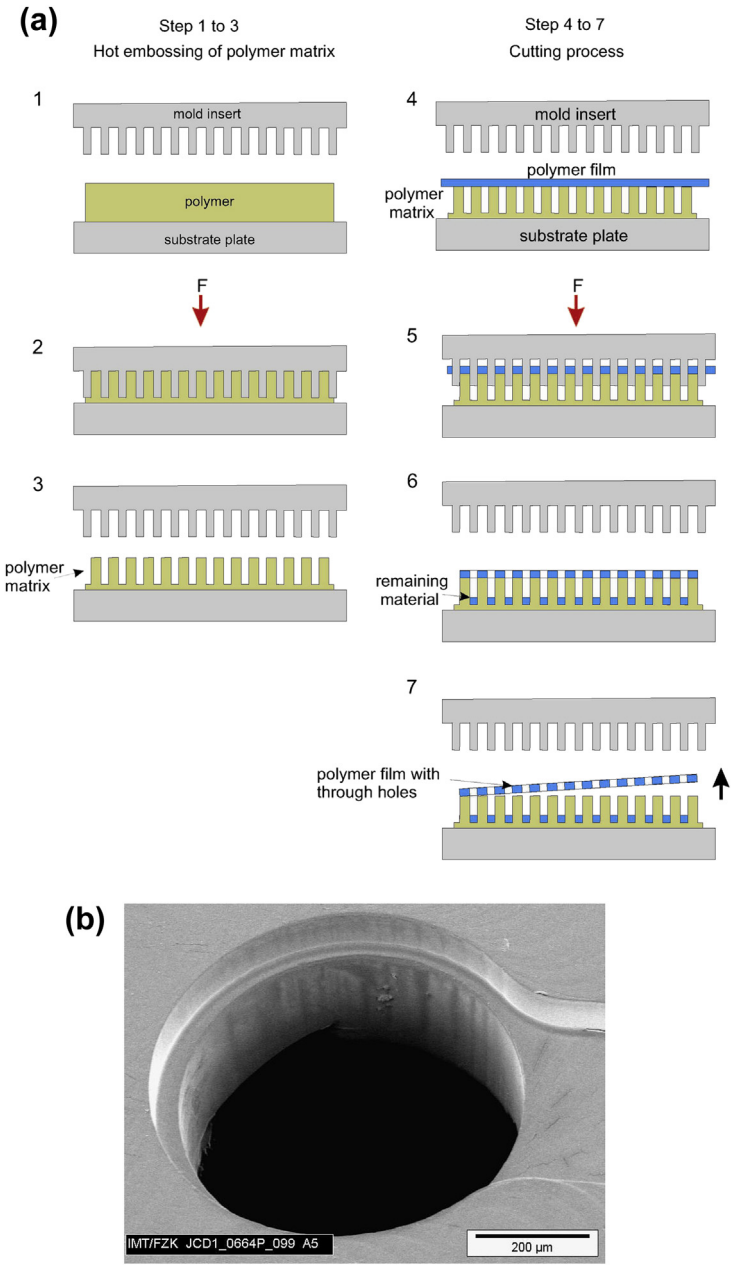

FIGURE 6

(a) Principle of hot punching for molding through holes and (b) holes fabricated by hot punching [14].

than the matrix is positioned between the mold insert and the molded part. The mold insert and substrate are heated to a temperature in the range of the glass transition temperature of the thin polymer film which should be significantly below the glass transition temperature of the matrix. The third step of this method is simply another embossing cycle structuring the thin film of polymer between the mold insert and the remaining matrix. Because of the high accuracy of the alignment of the previously molded matrix compared to the mold insert, the structures of the mold insert will match the inverse structures of the matrix properly. Differences of thermal expansions will be compensated for by the relative flexibility of the polymer matrix, compared to that of the mold insert of metal. During the second molding step the mold insert now cuts holes inside the thin polymer film. This principle can be seen as a shearing process. The punched areas will remain in the matrix, where the matrix has to renewed after several punching steps. Depending on the design and the thickness of the polymer film, the demolding of the punched polymer film from the matrix can be difficult to achieve and should be accomplished carefully, otherwise damage of the polymer film will occur. To help the process a release agent may be used [14].

The advantage of this method is the use of a wide range of mold inserts without any modifications. The material combinations are manifold. Besides the differences in softening temperatures, no adhesion between the used polymers is a precondition. Because of the two-step molding, this method is more time-consuming. For series production the method has to be improved.

THERMOFORMING OF HIGH-TEMPERATURE POLYMERS BY HOT EMBOSSING

In accordance with the molding of through holes the concept of two-layer molding can also be used for the thermoforming of thin films of semicrystalline high-temperature materials like LCP or polyether ether ketone (PEEK). Thermoforming refers to the straining of a polymer, typically by air pressure. The gas pressure is substituted for by a polymer melt. The starting point refers to a combination of two polymer films, a thin film of a high-temperature polymer and a second film of a material with lower softening temperature. A suitable combination is, for example, PMMA as molding material and PEEK as thermoforming material on top. Similar to multilayer molding, the combination of materials has to be selected carefully. The molding temperature has to be set such that the low-temperature polymer is in the melting range and the semicrystalline high-temperature polymer foil is in a temperature range above the transition temperature but below the melting temperature. In this temperature range the amorphous part is softened which reduces the elastic modulus of the high-temperature semicrystalline polymer which supports the straining of the polymer film. A characteristic of this method is the combination of a molding step (PMMA) and a simultaneous thermoforming step of the high-temperature polymer foil (PEEK).

The achievable thickness of the foils depends on the process parameters and the necessary molding force. Experiments show that good results for this kind of thermoforming can be achieved up to a film thickness of 100 µm. The thickness of the polymer film has to be selected in relation to the size of the cavities. To obtain a three-dimensional shape the thickness of the polymer foils has to be much lower than the lateral dimensions of the mold cavity, otherwise the polymer foil will not fill the cavity completely. Further, the material combination has to be selected in such way that only a moderate adhesion is effective between both foils after molding, because the thin foil has to be separated from the molded low-temperature polymer manually by peeling. With this method a three-dimensional structuring is possible, the rear side of the thin polymer foil showing the inverse structure of the front side that is similar to the mold insert (Figure 7).

ROLLER EMBOSSING

Roller embossing or roll-to-roll embossing is a well-established modification of the hot embossing process. Using rolls instead of plates, a continuous molding can be achieved with advantages regarding the molding times and disadvantages regarding the height and the aspect ratio of the molded structures (Figure 8). Tan et al. [15] used this approach, the so-called roller nano-imprint lithography, to fabricate sub-100-nm patterns. Two methods were investigated. The cylinder mold method refers to a thin-structured metal film bent around a smooth roller. In particular, a compact disk master with a thickness of 100 µm was used. The second method, the so-called flat mold method, refers to a structured silicon wafer mold placed on a polymer substrate. A smooth roller mold is rotated over the mold and the deformation of the mold under the pressure of the roll imprints the structures into the polymer. In both methods the roller temperature is set significantly above the glass transition temperature. For PMMA, the roller temperature is set in a range between 170 and

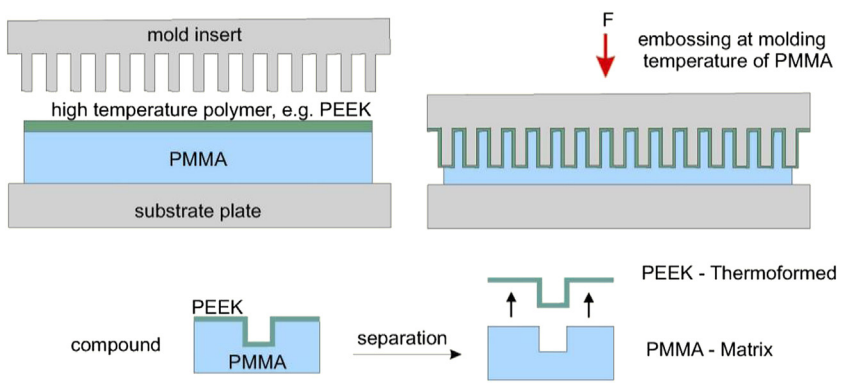

FIGURE 7

Principle of thermoforming of a thin polymer film by hot embossing.

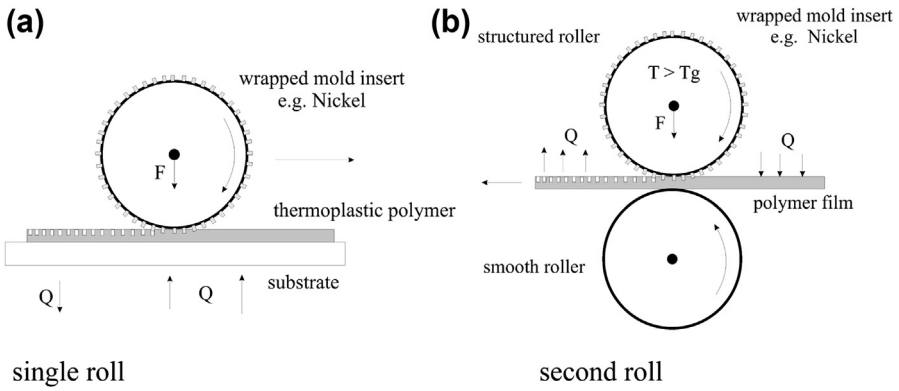

FIGURE 8

Thermal roller hot embossing. (a) single roll and (b) second roll.

200 °C and the platform temperature in a range of 50−70 °C. Roller speeds from 0.5 up to 1.5 cm/s were investigated, the pressure being set in the range between 300 and 4800 psi.

MATERIALS FOR HOT EMBOSSING

Most applicable materials for hot embossing are thermoplastic polymers [28]. During a molding cycle a thermoplastic polymer undergoes several temperature-dependent aggregate states. Switching to another aggregate state changes the material properties significantly. Based on the molecular structure of amorphous and semicrystalline polymers, different aggregate states and different transition ranges can be determined. The thermal behavior of thermoplastic polymers may be described with the time-dependent shear modulus over temperature.

Based on the shear modulus−temperature diagram, typical molding windows for embossing amorphous and semicrystalline polymers can be specified. Amorphous polymers show, theoretically, a wide temperature range for hot embossing, beginning at the glass transition temperature and ending before the decomposition range. In practice the molding window depends on several other parameters and has to be set in dependency of the design, the molding area, and the technique used in the embossing machine. Due to these factors, the actual molding window is smaller than the theoretical window and can be set approximately in the range of 20 up to 100 K above the transition temperature. In contrast to the amorphous polymers, semicrystalline polymers show only a small gap of temperature suitable for hot embossing. As described above, the decrease of the shear modulus occurs in a small temperature gap in the melting range. At the beginning of this range the stiffness of the polymer is too high for molding. The risk of damage to a micro-structured mold is high. At the end of the range, marked by a low shear modulus, semicrystalline polymers show typically a behavior like a fluid with low

viscosity, which is not suitable for hot embossing because the pressure needed for embossing with free flow fronts cannot be achieved. Therefore, the molding window can be found approximately in the middle of the small gap of the melting range. In practice, an exact temperature has to be set during molding. The temperature range of amorphous polymers is considerably larger than that for semicrystalline polymers, which in practice makes it easier to mold amorphous polymers in hot embossing (Figure 9).

Beside thermoplastic polymers alternative materials become more important. Glass, metallic glass, metals with low softening temperature can also be structured by this technology. In this case, the technique has to be modified to achieve temperatures in the range of 600 °C or higher. Especially if metallic glass is replicated the heating and cooling rates have to be taken into account which makes it necessary to develop special molding tools.

HOT EMBOSSING TECHNIQUES

COMPONENTS

The technology components for micro-hot embossing mainly include four groups (Figure 10):

- The embossing machine—this is responsible for delivering the press force and the accurate molding velocity. The challenge of the technology is to obtain a high stiffness at high force and also a precise relative motion between the mold and the substrate plate. This requirements result in a stiff frame design consisting of two crossbars and mostly four massive guiding pillars. To obtain a press force one of the crossbars is fixed. Another crossbar is moved by a precise motion system, like a spindle drive or a hydraulic drive.
- The tool—this is mounted between the two crossbars and is responsible for the heating and cooling of the mold, substrate plate, and polymer sheet. A typical tool consists of two halves, the top half fixed onto the top crossbar and the bottom half fixed at the lower crossbar, each with a single heating and cooling system. With an approximation of both halves, an integrated vacuum chamber will be closed and isolates the micro-structured mold insert and the substrate plate against the ambient pressure. Optionally, an alignment system is integrated that allows to adjust, for example, two mold inserts against each other or to mold on prestructured substrates.
- The micro-structured mold insert—this is reversibly fixed onto the tool. Opposite the mold insert another mold insert or a substrate plate will be positioned. A wide range of micro-structured mold inserts can be used, for example, inserts produced by mechanical machining or mold inserts fabricated by lithographic techniques.
- A precise controlling system—the precise control of the press force, the motion of crossbars and the temperature is one of the technological challenges. Besides

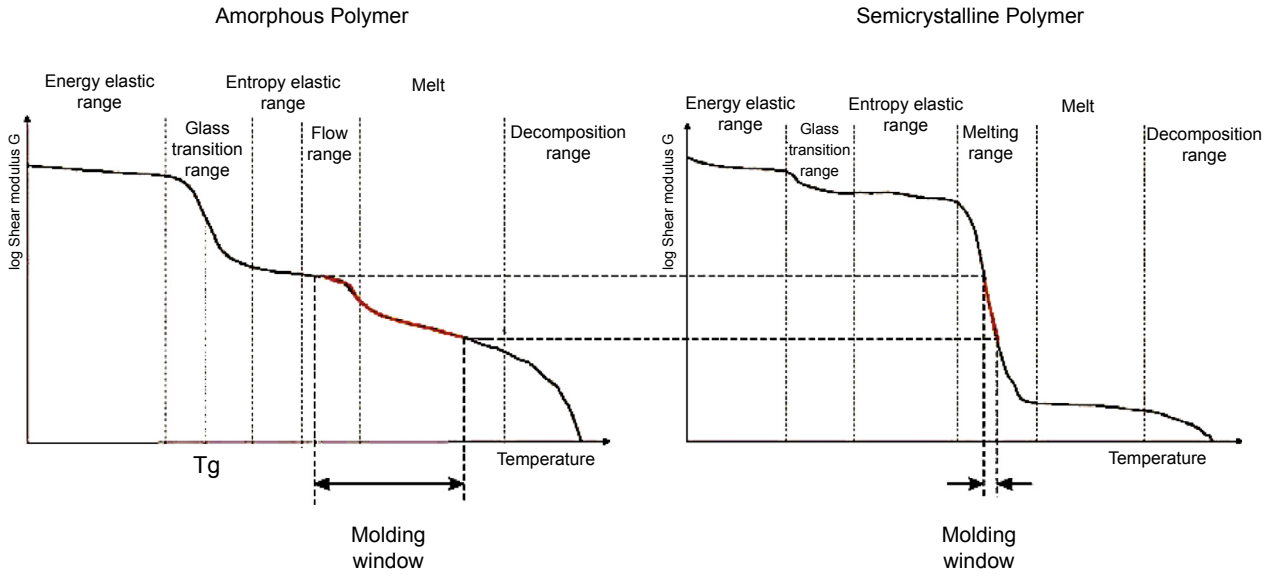

FIGURE 9

Thermal molding windows for hot embossing.

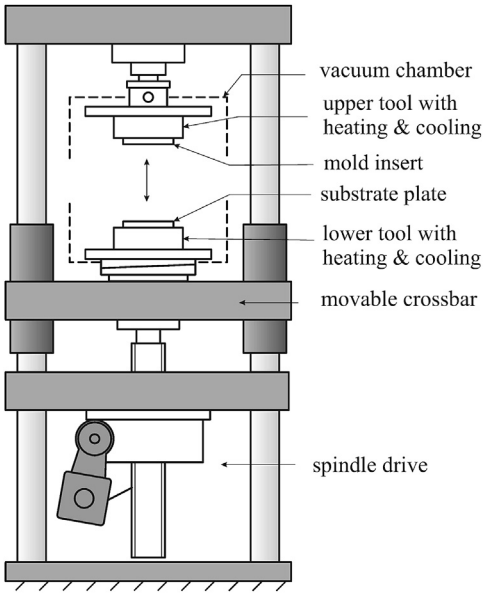

FIGURE 10

Schematic view of the components of a hot embossing machine.

the control of the process parameters, the measurement of the press force, temperatures inside mold inserts, and the distances between the mold insert and the substrate plate is the task of the control unit. As an interface to the user, it is also a task to prepare and visualize all data, allowing the user to set up and control the process in an effective way.

Hot embossing machines have been developed to different levels, beginning with simple manually controlled hot embossing machines, for example, for general laboratory use, up to high level machines with a high grade in automation, used in industry and in scientific research.

COMMERCIALLY AVAILABLE MACHINES

The market of commercially available hot embossing machines is comprehensive. The first hot embossing machine suitable for hot embossing of high aspect ratio was developed in Karlsruhe at FZK in cooperation with Jenoptik Mikrotechnik.

Jenoptik Mikrotechnik

Jenoptik Mikrotechnik [9] was one of the first companies providing a complete family of hot embossing machines. Each member of the hot embossing machine family is suited for different kinds of embossing tasks. The machine HEX01 is the smallest machine, compact and with a maximum force of 100 kN already

suitable for the most molding tasks, especially up to a molding area of 4 inches. If larger areas should be molded the machine HEX02 fulfill the requirements regarding molding forces up to 200 kN and molding temperatures up to 300 °C. If, further, double-sided molding is required, the machine HEX03 additionally is equipped with a precise alignment system and an integrated microscope that allows the alignment of the tool to be accomplished very easily. The latest machine, HEX04, is especially designed for large area replication under high molding force of up to 600 kN. All these machines are characterized by an electrical heating unit, a convective cooling system, a spindle drive, and flexible controlling by a macro-language. The family of hot embossing machines is shown in Figure 11. Jenoptik stops the fabrication of their embossing machines in 2011.

Wickert press

Another company that manufactures hot embossing machines is Wickert Maschinenbau [10]. Already in the past this company build the first machine

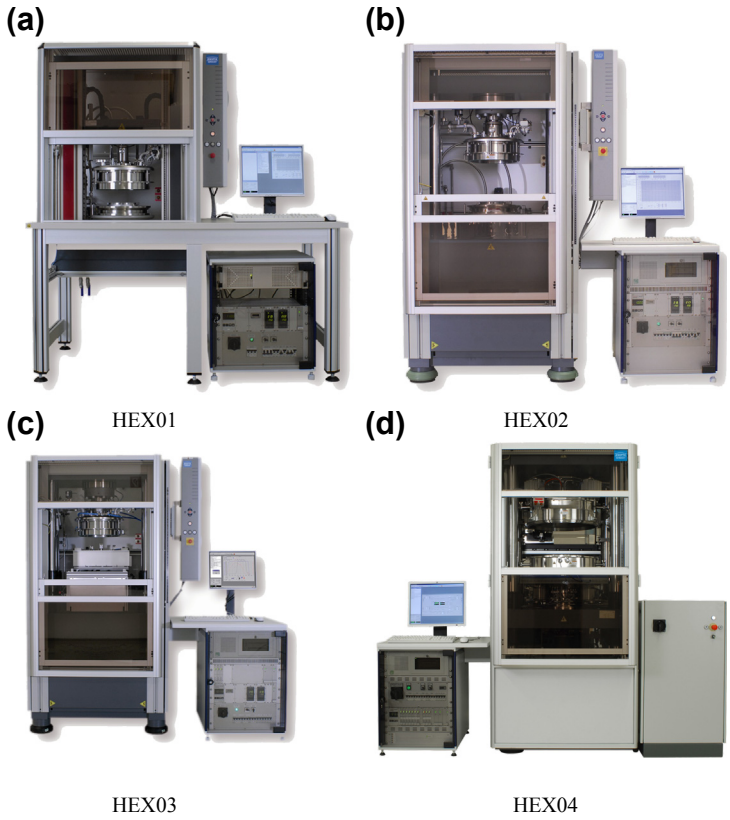

FIGURE 11

The hot embossing family of Jenoptik. (a) HEX01, (b) HEX02, (c) HEX03, and (d) HEX04.

"MS1" used in industry for hot embossing of micro-spectrometers. In 2003, a new generation of hot embossing machine was developed. The machine WMP1000 (Figure 12) is characterized by a hydraulic drive, a molding area larger than 8 inch and a maximum force of 1000 kN. The machine was developed in particular for industrial use, therefore an automatic handling system was integrated with the machine. In parallel an optimized molding tool was developed to reduce the heating and cooling times, which finally resulted in a significant reduction of cycle times. Further, a user-friendly control panel was integrated, allowing the control of the machine in an effective way. Nevertheless, the realized concept requires more infrastructure for the operation of the machine. For example, a separate room for the hydraulic pumps and a solid foundation for the heavy machine which also has with a large overall height will be required.

EVGroup

The company EVGroup [16] offers three hot embossing machines with different levels of automation [17]. The hot embossing machine EVG510HE is a basic machine for lab applications, focused on high accuracy and flexibility. The machine EVG520HE is characterized by a semiautomatic molding process, while the hot embossing machine EVG750 is, in contrast, fully automated (Figure 13). This high level of automation is suited for large serial production. The machines are compatible with standard semiconductor manufacturing technologies and allow the molding on substrates up to 200 mm. The hot embossing system EVG520HE includes a vacuum chamber, a drive unit with a high press force up to 600 kN, and a heating system which allows the molding of a wide range of polymers. Both machines are equipped with an alignment system.

FIGURE 12

Hot embossing machine Wickert WMP1000.

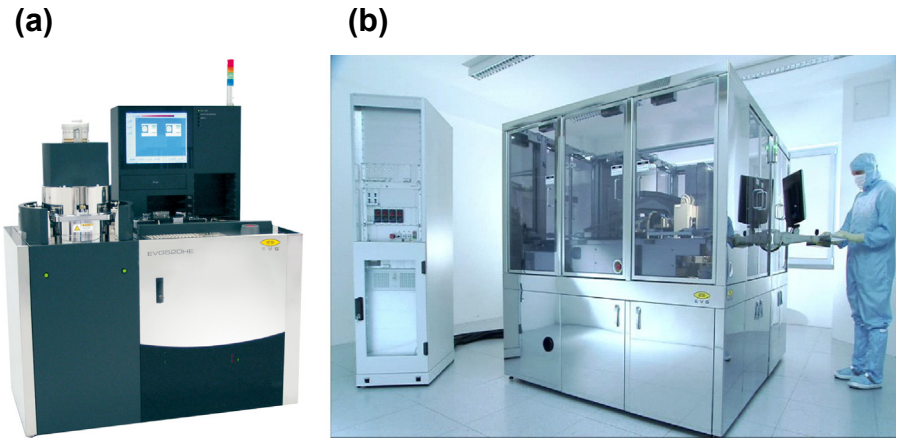

FIGURE 13

Nano-imprint machines. (a) EVG520HE and (b) EVG750.

HOT EMBOSSING TOOLS

Apart from the molding press and the micro-structured mold insert, hot embossing tools are essential components for any hot embossing system. The hot embossing tool may be defined as an interface between the molding press that is responsible for applying the molding force and molding velocity and the micro-structured mold insert to be replicated in polymers. Compared to macroscopic molding tools, such as tools for injection molding, where the structures are part of the tool, tools for micro-replication are characterized by a reversible integration of a micro-structured mold insert. This concept results from the different and incompatible fabrication processes of the macroscopic tool and microscopic structures. The tasks of a hot embossing tool are similar to tasks known from macroscopic molding tools, on the one hand. On the other hand, the embossing tool has to fulfill tasks that are specific to the molding of micro-structures, such as the generation of a vacuum. In detail, a hot embossing tool has to fulfill the following tasks.

- Heating and cooling of the polymer film by heat conduction of the mold insert and substrate plate;
- Fixation of different kinds and sizes of mold inserts;
- Hermetic sealing of the mold insert, polymer, and substrate plate against ambient pressure;
- Generation of a vacuum to fill the micro-cavities completely;
- A demolding unit which allows the demolding of the embossed parts in the vertical direction at a controlled demolding velocity;
- Optional alignment of both mold halves, if double-sided molding or positioned molding is desired.

From these tasks, the requirements to be met by a molding tool can be deduced, including minimum requirements for molding and optional requirements for specific tasks.

BASIC TOOLS FOR HOT EMBOSSING

The requirements and concepts underlying the design of tools for hot embossing were described above. An example of a hot embossing tool with an optimized heating and cooling concept was developed at the Institute of Microstructure Technology at the research center of Karlsruhe. In this case, thermal mass is reduced, while the stability and evenness of the surfaces needed for molding micro-structures on large areas of a thin residual layer are maintained (Figure 14).

The functioning of this tool is illustrated in Figure 15. To reduce the heated masses by the largest possible extent, the hot and cold areas of the tool are separated thermally. Hence, such a tool is divided into a heating plate and a so-called cooling block (Figure 15). In the basic state of the tool, both functional units are insulated thermally by an air gap produced with the help of springs (Figure 15(a)). This air gap is retained when melting the polymer. The contact force is generated by the springs only (Figure 15(b)). Due to thermal insulation, the relatively thin heating plate and the mold insert can be heated rapidly. In the displacement- and force-controlled embossing process, the molding force presses the heating plate onto the massive cooling block, which results in a mechanically stable setup, by means

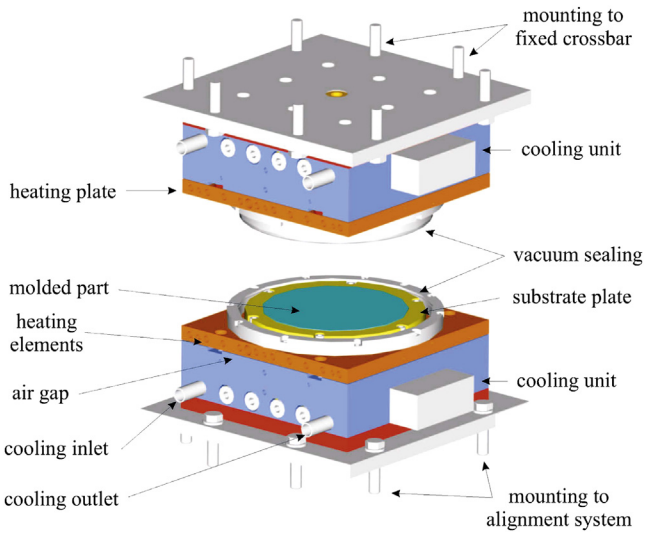

FIGURE 14

Schematic view of a basic molding tool with reduced thermal mass.

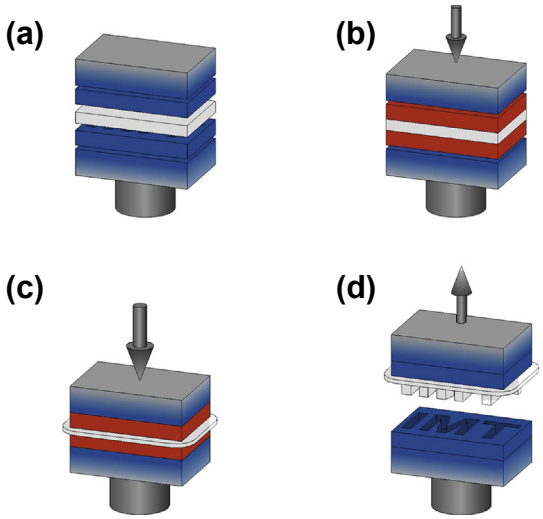

FIGURE 15

Schematic view of the process steps of hot embossing with the basic molding tool. (a) Insertion of the semi-finished product, (b) heating of heating plates, (c) build up of molding force and pressing of the heating plates onto the cooling block, and (d) cooling and demolding.

of which homogeneously thin residual layers may be produced even on large areas (Figure 15(c)). As soon as the heating plate is in contact with the cooling block, heat is removed from the heating plate to the comparably large and permanently cooled cooling block. As the cooling block acts like a heat sink, the heating plate and the mold insert can be cooled down rapidly. Subsequently, the components can be demolded (Figure 15(d)). Except for the vacuum chamber, the tool halves are designed symmetrically and consist of a water-cooled cooling block and a heating plate each. The heating plate is lifted off the cooling block by prestressed disk spring packages. Mold inserts of 250 mm in diameter can be fixed onto the heating plate, and the maximum molding temperature is 300 °C. In this tool, the heating plate can be clamped to the cooling block using a magnetic clamping system. A tolerance-free opening movement of the hot embossing machine thus allows for offset-free demolding. As in conventional hot embossing tools, substrate plates roughened by lapping or sand blasting may be used for demolding. The demonstration tool is presented in Figure 16.

For precise temperature control, the heating plates of the basic tool are divided into four zones each, which are controlled separately and may be set to various temperatures. In this way, a highly homogeneous temperature distribution can be achieved in the mold insert. In the hot embossing process, three different temperatures can be input for each tool half: the molding temperature is the temperature to which

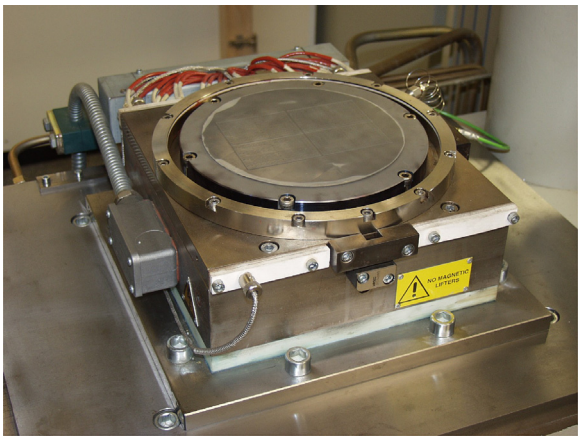

FIGURE 16

Lower half of a basic molding tool with a moldable surface area of up to 250 mm diameter.

the heating plates are heated, while the embossing temperature is the temperature at which the embossing force starts to build up. At the demolding temperature, demolding of the embossed component starts. The molding temperature is measured directly in the individual zones of the heating plates, and the embossing and demolding temperatures are measured in the mold insert and substrate plate, respectively. As the mold insert cools quickly when the embossing force is generated, it may be reasonable to select a molding temperature far above the embossing temperature. As a result of the thermal inertia of the heating plate and the cooling block, cooling of the polymer melt is then slowed slightly: this allows the fabrication of very thin components of low stress.

The heating concept based on a spring was also implemented by Schift et al. [18] for the molding of wafer-type substrates. A clamped stack of the stamp and substrate was preassembled in an alignment system, and it was not in contact with the heating plate, under action of the spring system. The gap was closed by the acting of force, pressing the stack onto the heating plate. After embossing, the force was set to a low value which results in the separation of the stack from the heating plate under action of the springs. The molded part is cooled and can be demolded manually.

MICRO-STRUCTURED MOLD INSERTS

For every replication process a mold or the so-called master is necessary to copy the structures of the mold into a molding material. The mold is split into the tool and the mold insert with the micro-structured surface. In theory every micro-structured surface can be used as a mold insert. A precondition is that the mold material and the micro-structures will withstand the temperature and mechanical load during

molding. Nevertheless, for successful molding, and especially demolding, the mold inserts has to fulfill the following requirements:

- The yield stress of the mold material at the maximum molding temperature has to be significantly higher than the stress effected by the molding force;
- To avoid any bending and to ensure the greatest possible evenness of the mold, the residual stress inside the mold, caused by the fabrication process, should be reduced to a minimum;
- The mold material should show chemical resistance against the polymer;
- A high heat conductivity of the mold material to reduce the heating and cooling times;
- For cost effectiveness the lifetime of the mold should be extended over many cycles;
- To support successful demolding, the surface roughness, especially of vertical sidewalls, should be reduced to an unavoidable minimum;
- Demolding angles are advantageous because they facilitate demolding. In contrast, undercuts prevent the successful demolding of micro-structures. Even small undercuts in the submicron range can increase demolding forces significantly.

Regarding the requirements, especially the requirement of high yield stress, it is obvious that mold inserts, fabricated in metals, are well suited. The technique of micro-structuring of metals is therefore essential for mold fabrication, but also glass or polymers like UV-transparent polydimethylsiloxane (PDMS) or high-temperature-resistant PEEK can be used for selected replication tasks [29]. Nevertheless, regarding the lifetime of a mold insert, high stiffness molds fabricated of metals are widely used for replication. An overview over the different mold fabrication processes is shown in Figure 17.

The structuring processes can be split into two groups: direct structuring methods like mechanical machining, electric discharge machining, or laser structuring [19]; and lithographic methods like E-Beam lithography, UV lithography. For structures with high aspect ratios, X-ray lithography is also used to structure the mold inserts. All lithographic processes require the step of electroforming to obtain a metal mold insert. Each structuring method has different characteristics and is therefore suitable for different kinds of applications.

Representative for the large number of suitable mold inserts two electroplated mold inserts are shown in Figure 18: a typical LIGA mold insert with high aspect ratio structures with dimensions of $28 \times 66\ mm^2$ and a thickness of 5 mm and as an alternative for larger structured areas a 4-inch nickel shim mold insert with a typical thickness of approximately 300 up to 500 μm.

APPLICATIONS

This section presents some applications where hot embossing plays an important role for their fabrication.

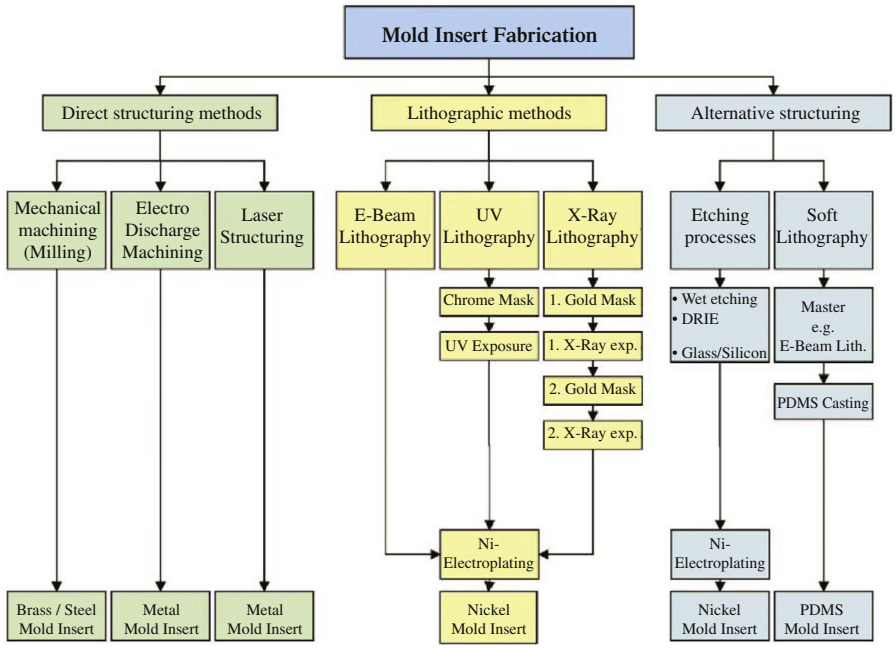

FIGURE 17

Overview of the mold fabrication processes [30]. PDMS, polydimethylsiloxane.

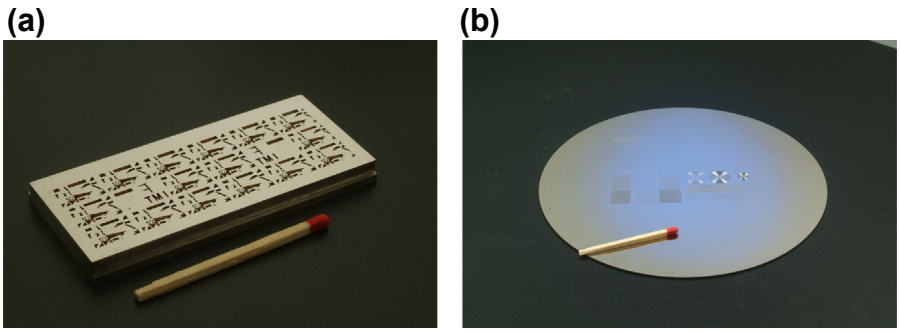

FIGURE 18

Electroplated LIGA mold insert, structured by X-ray lithography. The height of the structures is 750 μm. Nickel shims are characterized by a thickness in the range of several hundred micrometers and are well suited for the replication of structures with low aspect ratios on large areas, typically 4 or 6 inch. (a) LIGA mold insert and (b) Nickel shim mold insert.

MICRO-OPTICAL DEVICES

Micro-optical devices are one of the main applications in micro-system technology. The devices that can be replicated by hot embossing are manifold, beginning at micro-optical components like lenses, mirrors, optical benches, or waveguides, up to micro-systems like micro-spectrometer, distributed feedback laser systems, optical switches, fiber connectors, photonic crystals, or antireflection films [20–21]. Because of the requirements regarding structure sizes, surface quality, and accuracy of lateral distances, the mold inserts for hot embossing are typically fabricated by lithographic processes.

Optical wave guides

For optical interconnection the replication of polymeric waveguides opens a new field of applications. Depending on the application, monomode or multimode waveguides with different sizes are required, beginning with lateral dimensions of approximately 6 μm [22] up to 500 μm [23]. Sufficient for the most applications is an aspect ratio in the vicinity of unity, but typically a guiding path over several millimeters or centimeters is desired. The design refers typically to freestanding rectangular shapes without any additional supporting structures, which makes it necessary to reduce internal stress inside the structures to avoid any deformation of the shape of the waveguides. Several techniques allow the modification of the refractive index of the material, for example, the UV radiation of PMMA, which makes this material suitable for the replication of waveguides. Representative for a variety of polymer waveguides, replicated rectangular waveguides and further optical splitters are presented in Figure 19.

MICRO-FLUIDIC DEVICES

Micro-fluidic systems are part of life science technology and diagnostic and therapeutic biomedical engineering. Passive micro-components like capillary micro-channel structures and the so-called wells, reservoir areas, or miniaturized sample chambers, can be part of micro-total analysis systems or lab-on-a-chip systems [24]. Representative for passive micro-fluidic systems are, for example, capillary electrophoresis chips. Active micro-fluidic components like pumping systems or valve systems are mostly part of complex total analysis systems.

Capillary analysis systems

The functioning of a capillary electrophoresis system can be explained principally by Figure 20. The systems consist of two intersecting micro-channels with wells at the beginning (buffer) and at the end (waste). The first shorter channels will contain the sample material which should be analyzed, the longer channels contains a buffer solution. To achieve a flow an injection of the sample fluid into the buffer fluid at the intersection point, a difference in potential has to be obtained by electrodes integrated in the wells. By an electric switching the sample volume located in the intersection area can be injected into the longer separation channel.

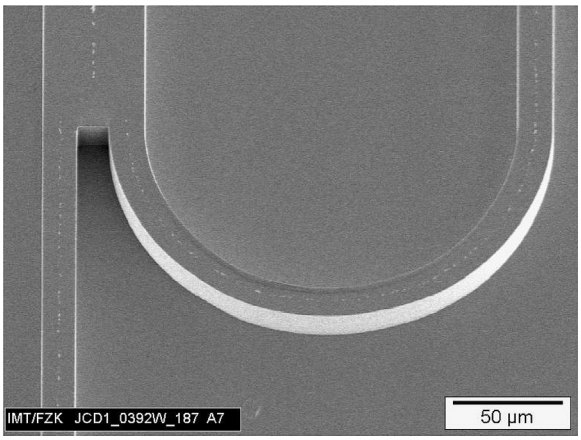

FIGURE 19

Molded optical waveguides with a cross-section and height of approximately 6 µm [22,31]. The electroplated nickel shim mold was fabricated by UV lithography and replicated into polymethylmethacrylate. The refractive index of the molded waveguides was modified after replication by UV radiation. The basic optical waveguide elements allow further the development of interactions between waveguides for subsequent applications.

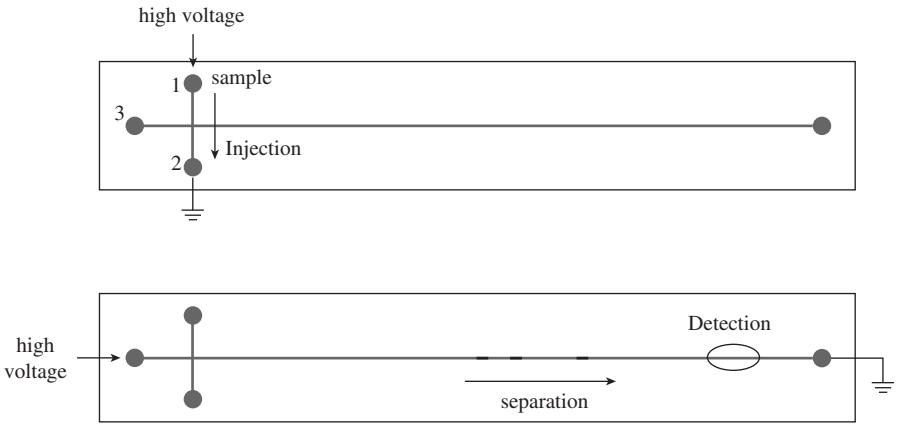

FIGURE 20

Principle of a capillary electrophoresis system. The principle refers to an intersection of two micro-channels where a small volume of the sample fluid is injected into the long fluid channel with a buffer fluid inside. During the flow the sample volume will be separated into its components, which can be detected at the end of the flow path. The injection and the flow are supported by a high voltage difference between the buffer and the waste.

In this channel the plug is separated into its components, depending on molecule size and electric charge [25]. Characteristic for micro-fluidic structures are grooves typically with an aspect ratio in the vicinity of unity and a flow path of up to several centimeters which can be arranged in a shape of a meander to achieve compact systems. For easy handling of these structures it is recommended to arrange such capillary electrophoresis (CE) systems onto standardized platforms, for example, micro-titerplates with an area of 125 mm × 85 mm. On this area, for example, 96 CE systems could be integrated (Figure 21).

MICRO-NEEDLES

Another application for the hot embossing technique is an example of a medical technique, in particular in drug delivery. Micro-needles are one of the minimal invasive drug delivery systems entering the body through the skin. Therefore the outer layer of the skin (stratum corneum) with a typical thickness in a range between 10 and 20 µm has to be disrupted. The thickness of this layer determines the minimum height of the needles. The biocompatibility of selected polymers and the fabrication of an array of micro-needles for the drug delivery make this application well suited for polymer replication processes. One of the requirements is a hollow needle which makes it necessary to integrate a fluid channel inside the polymer needles.

A suitable fabrication method is the replication of micro-needles by double-sided, positioned hot embossing. In this case a cone-shaped needle on the one side hits a cone-shaped hole in the other side of a two-sided molding mold insert (Figure 22). The achievable accuracy regarding the homogeneous thickness of the sidewalls depends here on the overlay accuracy of both mold halves. The advantage of this method is that only a thin residual layer on the tip of the cone has to be

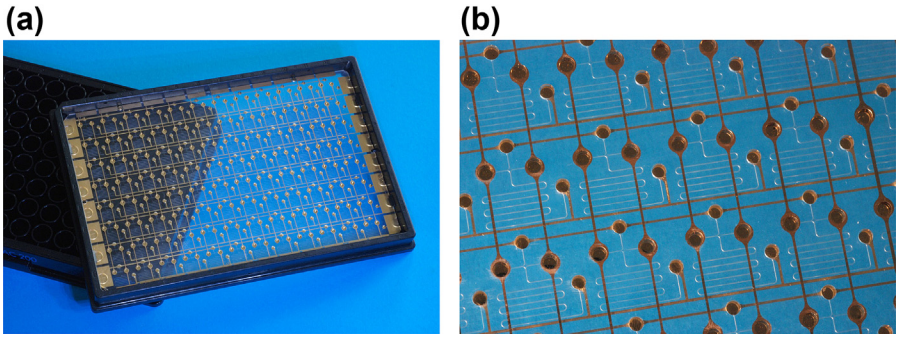

FIGURE 21

Micro-titerplate with 96 capillary electrophoresis (CE) systems [24,25]. (a) Microtiteplate with 96 CE-systems and (b) micro-fluidic channels with electrical connections.

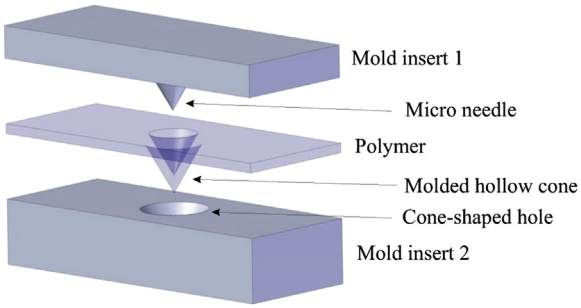

FIGURE 22

Double-sided molding of micro-needles. To achieve hollow cone-shaped needles, double-sided positioned molding of a cone-shaped needle into a cone-shaped hole is required.

disrupted. This can be done, for example, easily by laser structuring. The fabrication of the mold inserts, the positive cone- and the negative cone-shaped hole can be done by mechanical machining.

Finally, the residual layer of the needle has to be eliminated. In this case the residual layer is beside the carrier layer of the needle, also located in the tip of cone. To achieve a fluid channel through the needle, the residual layer has to be removed. A molded micro-needle with a fine hole in the tip is shown in Figure 23.

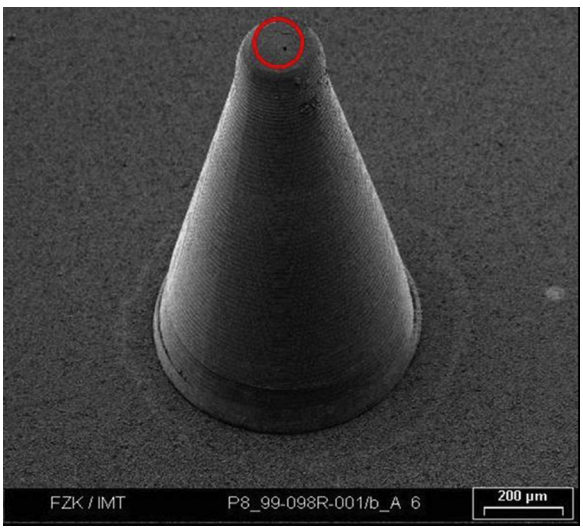

FIGURE 23

Molded micro-needles with a through hole on top of the cone-shaped needle.

CHANGE OF SURFACE PROPERTIES

As already mentioned the process of hot embossing is well suited to structure the surface of thin films, even in the nano-range. Using a surface structuring the surface properties can be changed, for example, from hydrophilic to superhydrophobic surfaces [26,27]. By this replication process the surface properties can be controlled on large scale, for example, by roll-to-roll process (Figure 24).

THE OUTLOOK

The examples presented above are only part of a pool of applications, but they underline the relevance of the hot embossing or thermal nano-imprint process as established replication technology. Further developments in hot embossing and nano-imprinting will be supported by new applications, especially if large series are required. Here the kind of automation and standardization of, e.g., molding

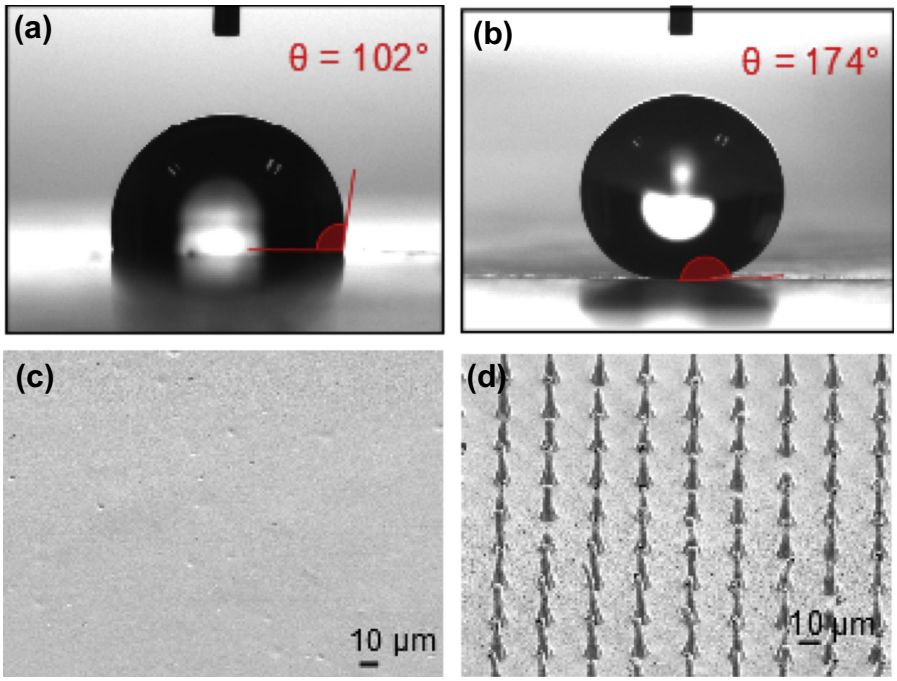

FIGURE 24

Change of wetting behavior by surface structuring. The unstructured surface (c) shows a contact angle of around 100° (a). With surface structuring by hot embossing (d) the contact angle of the same material increases to around 170° (b). In this example a cellulose-based biodegradable material was used [26].

formats will also help to establish this technology in the industry as replication technology. Especially, the cycle times have to be minimized in future, which corresponds to an efficient heating and cooling system. Optimized molding tools are therefore a key issue for cost-effective molding. In combination with already well-established handling systems in macroscopic processing the process times can be minimized and hot embossing can be established as an industrial replication technology. A cost-effective replication also requires large molding areas. These molding areas correspond to the fabrication methods of the mold inserts which are limited individually. To overcome these limits, molding tools with multiple mold inserts can be used. These aspects are mainly in the foreground of interest for a cost-effective use of hot embossing. Independently of the potential to optimize the cost-effectiveness, hot embossing will still be a well-suited process for the first replications of prototypes. In this case the future may shift the replication to structures with smaller structure sizes in the nano-range in combination with high aspect ratios, e.g., larger than 5. Further, those structures will be replicated over large areas such as 8 inches or more. Nevertheless, all replication processes are inspired by the requirements of the further applications and these applications will finally determine the structure sizes, the molding areas and the kind of automation. A further development will focus on the roll-to-roll embossing to upscale the small areas of the conventional embossing to cost-effective large area fabrication. In this case also the mold fabrication technology has also to be upscaled. Here beside laser structuring and etching technologies the structuring area of lithography processes should be increased to provide large format molds with structures in the nano-range for roll-to-roll applications. Here the development on hot embossing also corresponds to the development in molding tool fabrication and master structuring.

REFERENCES

[1] Becker H, Gärtner C. Polymer microfabrication technologies for microfluidic systems. Anal Bioanal Chem 2008;390:89−111.
[2] Becker H, Heim U. Hot embossing as a method for the fabrication of polymer high aspect ratio structures. Sens Actuators 2000;83:130−5.
[3] Heckele M, Bacher W, Mueller KD. Hot embossing − the moulding technique for plastic microstructures. Microsyst Technol 1998;4:122−4.
[4] Heckele M, Schomburg WK. Review on micro moulding of thermoplastic polymers. J Micromech Microeng 2004;14:R1−14.
[5] Bartolini R, Hannan W, Karlsons D, Lurie M. Embossed hologram motion pictures for television playback. Appl Opt 1970;9(10):2283−90.
[6] Gale MT, Kane J, Knop K. Zod images: Embossable surface-relief structures for color and black-and-white reproduction. J Appl Photogr Eng 1978;4(2):41−7.
[7] Becker EW, Ehrfeld W, Hagmann P, Maner A, Münchmeyer D. Fabrication of microstructures with high aspect ratios and great structural heights by synchrotron radiation lithography, galvanoforming and plastic moulding (ligaprocess). Microelectron Eng 1986;4:3556.

[8] Harmening M, Bacher W, Bley P, El-Kholi A, Kalb H, Kowanz B, et al. Moulding of three dimensional microstructures by the liga process. In: Proc. MEMS '92, Travemünde, Germany. IEEE; 1992. p. 202.
[9] Jenoptik Mikrotechnik. http//www.jenoptik.com; 2014.
[10] Wickert Press. http//www.wickert-presstech.de; 2014.
[11] ORAFOL Fresnel Optics. http://www.orafol.com/energy/europe/de/home; 2014.
[12] Mueller K-D. Herstellung von beweglichen metallischen Mikrostrukturen auf Siliziumwafern. In: Scientific report FZKA 6254. Forschungszentrum Karlsruhe; 1999.
[13] Mehne Ch. Grossformatige Abformung mikrostrukturierter Formeinstze durch Heissprägen. [Ph.D. thesis], University of Karlsruhe, Institute for Microstructure Technology; 2007.
[14] Rapp BE, Schneider M, Worgull M. Hot punching on an 8 inch substrate as an alternative technology to produce holes on a large scale. Microsyst Technol 2010;16(7): 1201−6. http://dx.doi.org/10.1007/s00542-009-0943-x.
[15] Tan H, Gilbertson A, Chou SY. Roller nanoimprint lithography. J Vac Sci Technol B 1998;16(6):3926−8.
[16] EVG. http//www.EVGroup.com; 2014.
[17] Schaefer Ch, Farrens S, Glinser T, Lindner P, Roos N. State of the art automated nanoimprinting of polymers and its challenges. In: Seventh international conference on the commercialization of micro and nano systems (COMS); September 8−12, 2002.
[18] Schift H, Bellini S, Gobrecht J, Reuther F, Kubenz M, Mikkelsen MB, et al. Fast heating and cooling in nanoimprint using a spring-loaded adapter in a preheated press. Microelectron Eng 2007;84:932−6.
[19] Fleischer J, Kotschenreuther J. The manufacturing of micro moulds by conventional and energy-assisted processes. I J Adv Manuf Technol 2007;33:75−85.
[20] Ting C-J, Huang M-C, Tsai H-Y, Chou C-P, Fu C-C. Low cost fabrication of large-area anti-reflection films from polymer by nanoimprint/hot-embossing technology. Nanotechnology 2008;19:1−5.
[21] Seekamp J, Zankovych S, Helfer AH, Maury P, Sotomayor Torres CM, Böttger G, et al. Nanoimprinted passive optical devices. Nanotechnology 2002;13:581−6.
[22] Bruendel M. Herstellung photonischer Komponenten durch Heissprägen und UV-induzierte Brechzahlmodifikation von PMMA. [Ph.D. thesis], University of Karlsruhe (TH), Institute for Microstructure Technology; 2008.
[23] Mizuno H, Sugihara O, Kaino T, Okamoto N, Hosino M. Low-loss polymeric optical waveguides with large cores fabricated by hot embossing. Opt Lett 2003;28(23): 2378−80.
[24] Guber AE, Heckele M, Herrmann D, Muslija A, Saile V, Eichhorn L, et al. Microfluidic lab-on-a-chip systems based on polymers-fabrication and application. Chem Eng J 2004;101:447−53.
[25] Gerlach A, Knebel G, Guber AE, Heckele M, Herrmann D, Muslija A, et al. Microfabrication of single-use plastic microfluidic devices for high-throughput screening and DNA analysis. Microsyst Technol 2002;7:265−8.
[26] Worgull M, Schneider M, Röhrig M, Meier T, Heilig M, Kolew A, et al. Hot embossing and thermoforming of biodegradable three-dimensional wood structures. RSC Adv 2013;3:20060−4.
[27] Worgull M, Heckele M, Mappes T, Matthis B, Tosello G, Metz T, et al. Sub-µm structured lotus surfaces manufacturing. Microsyst Technol 2009;15(8):1327−33. http://dx.doi.org/10.1007/s00542-008-0744-7.

[28] Worgull M, Kolew A, Heilig M, Schneider M, Dinglreiter H, Rapp B. Hot embossing of high performance polymers. Microsyst Technol 2011;17(4):585–92.
[29] Kolew A, Münch D, Sikora K, Worgull M. Hot embossing of micro and sub-micro structured inserts for polymer replication. Microsyst Technol 2011;17(4):609–18.
[30] Worgull M. Hot embossing – theory and technology of micro replication. Elsevier; 2009, ISBN 978-0-8155-1579-1.
[31] Bruendel M, Henzi P, Rabus DG, Worgull M. Hot embossing of optical waveguides. In: Conference proceedings of 50. Internationales Wissenschaftliches Kolloquium 2005. Ilmenau, Germany: Mechanical Engineering from Macro to Nano; September 19–23, 2005, ISBN 3-932633-98-9. p. 351–2.
[32] Schelb M, Vannahme C, Kolew A, Mappes T. Hot embossing of photonic crystal polymer structures with a high aspect ratio. J Micromech Microeng 2011;21. 025017 (5pp).

CHAPTER

Forming of Polymeric Tubular Micro-components

8

Yi Qin[1], Jie Zhao[1], Gerald Anyasodor[1], Klaus S. Hansen[2], Ivan Calderon[3], Konstantin Konrad[4], Christoph Hartl[5], Mogens Arentoft[2], Ioannis S. Chronakis[6]

University of Strathclyde, UK[1]; IPU Technology Development, Kgs. Lyngby, Denmark[2]; Sysmelec, Switzerland[3]; Fraunhofer Institute for Manufacturing Engineering and Automation, Germany[4]; Faculty of Automotive Systems Engineering and Production Engineering, Cologne University of Applied Sciences, Cologne, Germany[5]; Technical University of Denmark, DTU-Food, Søltofts Plads, Lyngby, Denmark[6]

CHAPTER OUTLINE

INTRODUCTION

As the trend of miniaturization of various products, devices, and equipment continues, demands for complex micro-components increase significantly. The emerging needs include tubular micro-components (e.g., diameters <1000 μm), such as those used in micro-fluidic devices, medical instruments, thermal management systems, and laboratory analysis equipment, and within a variety of other areas, for which micro-tubes need to be shaped into components with functionalized features [1].

Shaping polymeric tubes was, traditionally, enabled with processes such as tipping, necking, expanding, and flaring. These are used largely for the shaping of

Micromanufacturing Engineering and Technology. http://dx.doi.org/10.1016/B978-0-323-31149-6.00008-6

polymeric tubes to be used for the connections in fluidic devices, containers, or for medical use, such as catheter tubes [2,3]. The corresponding items of equipment, which are mainly manually operated for the shaping of medium-sized tubes, e.g., those often used in hospitals, usually involve a very slow process, and the quality of the part is hard to measure and control. Therefore, such equipment cannot be used for volume production purposes, nor for the shaping of micro-tubes, as had been proposed earlier. Research activities dealing with the application to high-volume production of tubular components with cross-sectional dimensions below 1000 μm have shown that traditional forming techniques cannot be directly transferred to the manufacture of polymeric micro-components [4]. Alternative processes and equipment, which are of shaping capabilities and volume production characteristics for the manufacture of polymeric tubular micro-components were required.

Furthermore, in most cases, a single process may not be able to complete the task of manufacturing a component with all of the designed features, due to the different requirements on raw materials and specific forming requirements. Hence, a proper process chain or the combining of several processes can be a solution, to enable the achieving of desired processing efficiency and product quality. Some process chains developed/used in micro-manufacturing have been commented upon in the literature [5–8], such as combining lithographic tooling and injection molding techniques, combining a LIGA (a German acronym for lithography, electroplating, and molding–Lithographie, Galvanoformung, Abformung) process with direct laser micro-machining, ultra precision manufacturing of self-assembled micro-systems, etc. Ideally, a process chain for micro-manufacturing should be short in order to achieve high efficiency, reduce manufacturing errors, and eliminate unnecessary handling/transport/packaging of micro-components between different processes. Hybrid manufacturing processes may take advantage of the merits of individual micro-manufacturing methods/processes while some uentialherited disadvantages may be overcome, e.g., combining electrical discharge machining (EDM) with laser machining, combining EDM with electrochemical machining, etc. Around the concepts of either integrating process chains or realizing the hybrid processes, some manufacturing platforms and systems have been evolved worldwide [9–13]. The multiple processes manufacturing platform discussed here is one of these hybrid process machines mentioned above, which will focus on the mass production of polymeric micro-tubes into functional micro-tubular components.

PRINCIPLE

HOT EMBOSSING

Hot embossing may be categorized mainly as a polymer molding process and has long been established as a capable technology for the precise and qualitative manufacture of plastics parts with fine micro-structures and nano-structures [14,15]. As a fabrication technique for creating micro-structures at the surfaces, hot embossing often uses mold inserts for the forming/shaping of polymeric parts, which is similar to other replication techniques such as micro-injection molding and

micro-closed-die-forging. Compared with other micro-replication processes, the material flow distances are normally much shorter and the velocity is much lower, which results in a significantly lower shear stress of the polymer. This will give the hot embossing technology a good advantage for a reduced system complexity, shorter production cycle time, cost efficiency, etc. Over the last 20 years, the process variants of hot embossing have been developed, including double-sided molding, multilayer molding of polymer composites, molding of through holes, hot-punching, roller embossing, and found to be within the range required for micro-system applications [15]. These process variants highlight the flexibility of hot embossing to satisfy different requirements according to existing and emerging applications of the molded components. Among the various hot embossing processes, there are some that are often used for the molding of the structures on plane surfaces such as polymeric sheets and thin films or foils, to produce mostly 2.5D features, but were not designed specifically for the forming of micro-tubes. Hot embossing of polymeric micro-tubes is to form 3D features (both outer and inner features), which would require more dedicated tool design and process control, including consideration of the stiffness of tubular structures and relevant material flow.

The hot embossing process for the shaping of polymeric micro-tube is designed to achieve reduced features at the tips or intermediate sections of the micro-tube. With some variations from the conversional hot embossing process, the processing sequence of sharing micro-tubes is as shown in Figure 1 (a) the tool-set would be heated to the required temperature either by an external heating device, e.g., a cartridge heater or by hot air; (b) the tube would be fed into the lower shaping die (a short tube or a continuous tube coil is possible, depending on the application); (c) the tube would be heated rapidly by contact with the die due to the small volume of the material involved; (d) the lower die would secure the tube properly while it is embossed by the upper tool. A proper pressure would be maintained for a specific time to allow shape-setting and even fusion-bonding at the inner folded interfaces,

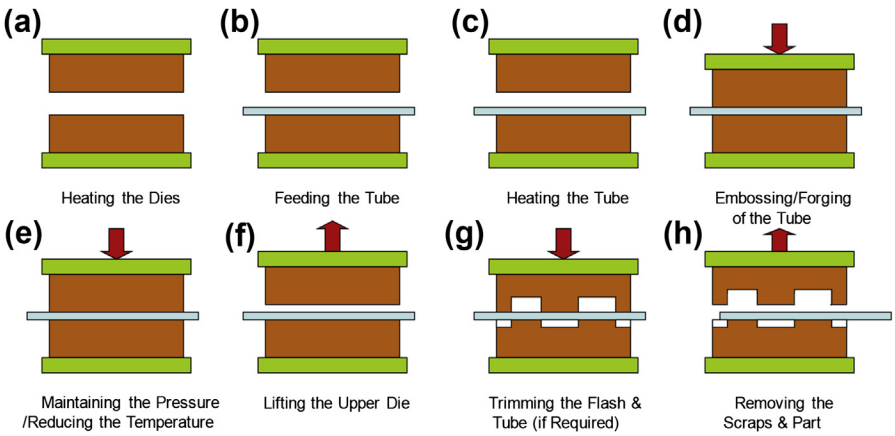

FIGURE 1

Processing sequence of a hot embossing polymeric micro-tube.

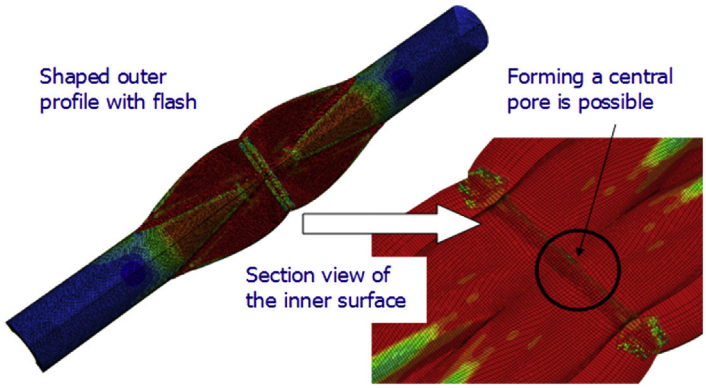

FIGURE 2

Three dimensional finite element simulation of embossing of a micro-tube.

and hence, an inner pore/feature would be formed. At this stage, to maintain shape stability, a cooling mechanism may be necessary (e.g., compressed air cooling or water cooling), depending on the polymeric material to be used. (e) The upper-tool would then be lifted while a mechanical gripper would hold the shaped tube; (f) the flash formed may also be trimmed off by a following sharing process (optional) after the shaped tube is moved into another station (similar to progressive stamping); and (g) finally, the scrap and shaped part are removed from the lower die.

Finite element (FE) simulation of the embossing of micro-tubes is aiming to examine the shaping capability of the proposed process and in-depth understanding of the influential parameters. Shown in Figure 2, is a 3D model illustrating the forming a necked-profile at the intermediate section of a polytetrafluoroethylene micro-tube (outer diameter 0.37 mm and inner diameter 0.27 mm) which leads to the formation of a large amount of flash and a small central pore ($<$10 μm is possible).

A plane strain model simulation of the central section of the tube (smallest necked part) is shown in Figure 3, in order to demonstrate the sequence of the material flow during the embossing. Subjected to the compression by the upper and lower dies, four clear shearing sections at the tube wall are formed, accompanied by material flow in both the vertical and horizontal direction. After both of the die cavities are filled, the transversal flow of the material prevails, which leads to the formation of flash as well as to a reducing size of the pore, until the pore disappears due to the continuing compression from the upper die.

In order to confirm the shaping capability of the micro-tubes, a comparison of a series of simulations with different die cavity shapes and dimensions can be seen in Figure 4. Employing the same micro-tube, by controlling the ratio of the material flow in the vertical direction (the direction of the tool movement) and the transversal direction it is possible to control the ratio of the height to the width of the formed central pore as well as its transitional shape of the pore edges. In general, an oval pore is inevitably formed due to the tube being compressed in one direction only. However, the FE simulation also showed that controlling the shape of the central

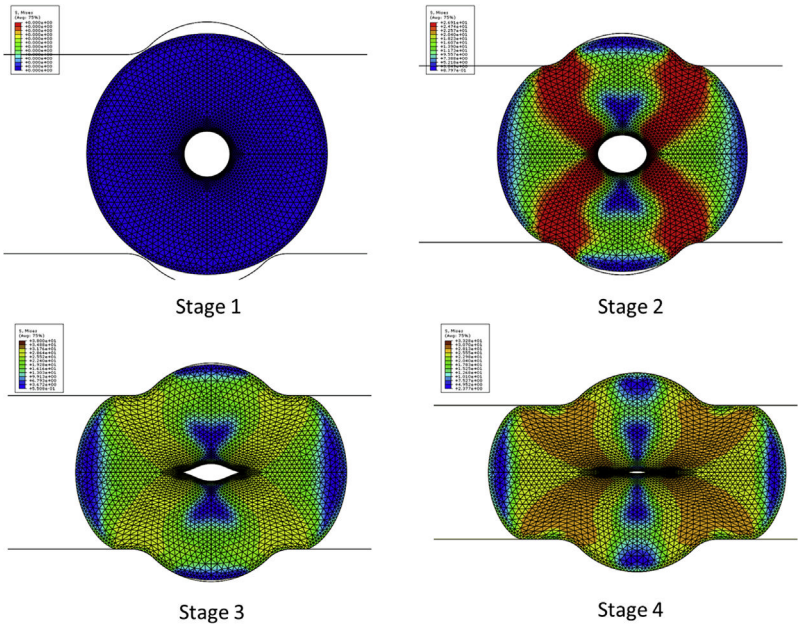

FIGURE 3

Material flow sequences during the embossing of a polytetrafluoroethylene micro-tube.

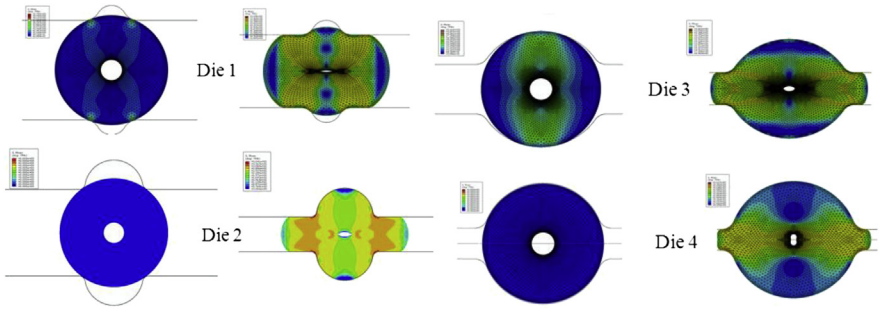

FIGURE 4

Illustration of influences on the pore formation from the die cavity geometry.

pore is possible by controlling the die cavity shapes and dimensions properly. It was further confirmed that the die geometry and die/tube material interface conditions are major factors in determining the material flow and, hence, the formation of the central pore: among these factors, the depth of the die cavity, the transition of the die entry, as well as the friction between the die and workpiece are the most influential and need to be thoroughly studied. For a particular tube material and initial geometry, an optimal setting of these parameters/conditions is necessary.

To demonstrate the technical and commercial viability for volume production at a full industrial scale by manufacturing prototype products which meet all of the

functional requirements for applications, a series of experiments were conducted, with a hot embossing machine developed by researchers in University of Strathclyde [16]. These experiments were also useful for the study of the material characteristics such as thermal behavior, flow behavior, shaping ability, and quality of end products. Several typical thermoplastic polymeric tubes with different materials, wall thicknesses, and glass transition temperatures were tested with their corresponding settings of the forming parameters. The experimental results showed that various outer profiles can be formed at the tips and/or at the intermediate sections of the tubes, and inner features (pores) below 5 μm in length along the long and short axis of the oval shapes formed can be achieved with properly controlled processes (a sample result is shown in Figure 5). The forming results obtained from the experiments are very similar to those observed from the process simulations.

There are a number of factors that are considered to be the main influences in the hot embossing process and its application as well as the quality of formed micro-tubular parts, these being discussed as follows.

The hot embossing process for shaping polymeric micro-tubes can be regarded as a good solution for mass production. The cycle time is relatively short. Compared with the conventional methods for the shaping of polymeric materials such as injection molding and injection compression molding, the required forming temperature is much lower. The good repeatability of the component quality achievable with the hot embossing machine is also an advantage for the shaping of micro-tubular components.

The processing temperature is important for hot embossing as it influences significantly the material flow under the embossing force. Compared to the hot embossing on a plane area for creating surface micro-structures, shaping a micro-tube involves longer material-flow paths, e.g., the formation of flash when shaping necked sections. Therefore, the heating of the polymer should be maintained at a higher level that

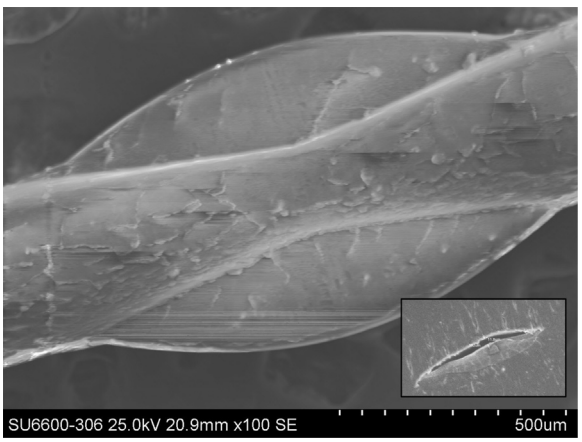

FIGURE 5

Scanning electron microscope image of a polytetrafluoroethylene tube after hot embossing; and its cross section (insert).

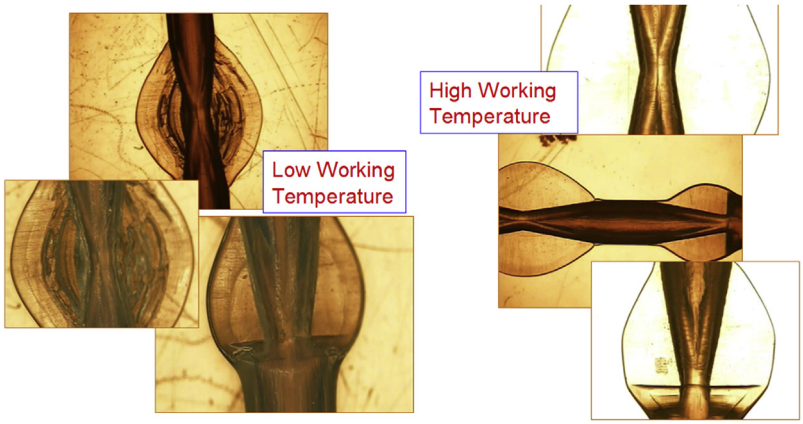

FIGURE 6

Comparison of the specimens produced at two different temperatures.

allows for the viscous flow of the material. This reduces the shrinkage of the shaped micro-structures as well as the friction which occurs at the workpiece/die interfaces. Figure 6 shows a comparison of the shaped tubes with two different temperatures for polyethylene terephthalate (PET) tubes. With a higher temperature, the shaped sections were seen clearly to have even material flows. The high temperature also results in better performance in respect of bore-reduced necking (external and internal), noted upon examination of the tube cross sections.

Similar to the hot embossing of polymers on plane surfaces, a constant pressing force and a relatively slow shaping process are preferable for the hot embossing of polymeric micro-tubes in order to achieve a fully shaped geometry, to reduce the shear stress on the heated polymeric tube and to reduce residual stresses within the shaped part. This helps to reduce the level of defects such as distortion in the formed component and separation of the bonded surfaces.

Holding time is crucial to the formation of fully sealed interfaces due to bonding of the polymer under an elevated temperature. Longer holding-time will allow for the fusion-bonded interfaces to settle down without separation after cooling. It is obvious that it is a parameter which will affect the production rate. However, to ensure good quality of the part to be produced, a longer holding-time is preferred. On the other hand, a longer hold-time may affect the tool life due to the sustained hot condition of the die/tool.

MICRO-BLOW MOLDING

Micro-blow molding applied to serial production is a new manufacturing method for tubular polymeric micro-components. The process principle is based on the forming of polymeric tubes by internal pressurization with a superimposed axial tensile stress under optimized temperature. As an important advantage, this forming technology

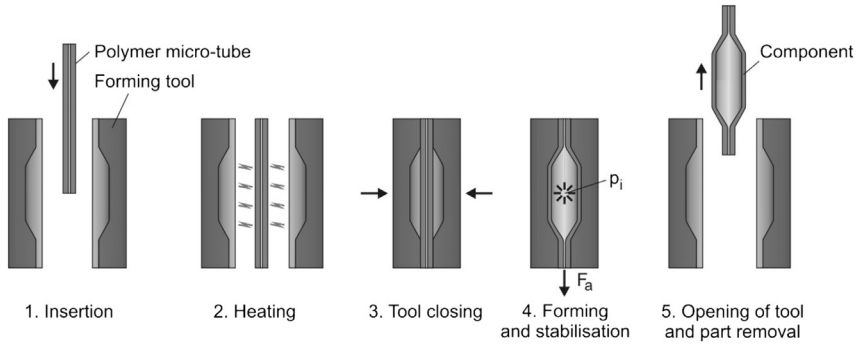

FIGURE 7

Principle of the micro-blow molding process.

enables the manufacture of hollow complex-shaped components in a one-piece design on an economic basis for volume production. Additionally, a vast variety of available polymeric materials allows the starting material to be tailored to the desired properties for processing and application. For this reason, a wide range of conventional products is manufactured today by the blow molding processes at macro-scale, such as containers for the food industry and the pharmaceutical industry, and for components for the automotive applications [17].

Blow molding comprises a category of forming processes for polymeric materials, based on the expansion of tubular or hollow shaped initial products by internal pressurization within a die cavity which corresponds to the final component geometry. Figure 7 shows the principle of a micro-blow molding process, developed with the intention to transfer blow molding technology to the high-volume production of polymeric micro-components. The initial polymeric tube is positioned between two die halves which contain forming die cavities having the final shape of the component to be produced. While in this position, the tube is sealed and connected at one end to an air pressure supply. The tool elements which are sealing and the workpiece ends are designed in such a way that an axial tensile force F_a can be superimposed on the force resulting from the application of the internal pressure p_i.

The forming process is started after the closing of the forming die halves, with a controlled application of the forming loads p_i and F_a to the now expanded workpiece, until the latter achieves complete contact with the surrounding die cavity. While raising the internal pressure to form the workpiece, the temperature of the forming dies, which was kept constant until this stage, is decreased rapidly by means of an integrated tool-cooling system, to stabilize the formed component shape, and to reduce its excessive shrinkage. After opening the die halves, the formed component can be ejected. Figure 8 shows, as an example, micro-blow molded components, manufactured with the process described above. For the forming of these components, polymeric micro-tubes made from PET with an outer diameter of 1340 µm and a wall thickness of 170 µm were expanded at a forming temperature of 90 °C, and calibrated with an internal pressure of 18 bar.

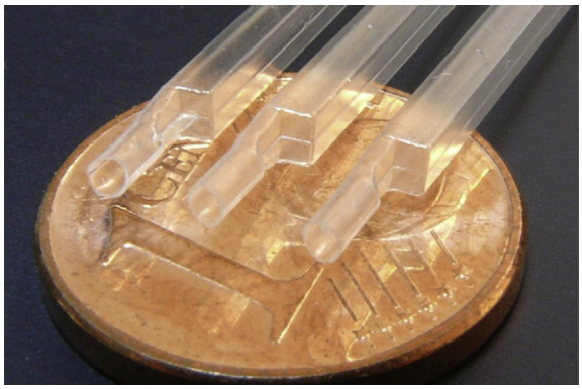

FIGURE 8

Micro-blow molded components.

Particularities which have to take into consideration when scaling down blow molding processes for serial production concern not only the reliable handling of the micro-workpieces and the suitable thermal management, but also the component removal from the forming die cavities, forming tool design, and sealing strategies to pressurize the formed workpiece.

The necessary modifications in thermal management as well as the factors that have to be taken into account concerning the component removal are caused by the so-called size effects. These result here from the increased ratio of the workpiece surface to its volume A/V. The ratio A/V is relevant for all effects which are dominated by surface effects, in particular, concerning heating or cooling, friction, and adhesion [18]. Regarding a thin-walled initial tube as an example, its outer surface can be determined roughly by $A \approx d\,\pi\,l$, where d is the mean tube diameter and l the tube length, and the volume by $V = d\,\pi\,t\,l$, where t is the tube wall thickness. Hence, for a tube with $t << d$, the surface to volume ratio can be written as:

$$A/V \approx t^{-1} \tag{1}$$

This means that the importance of size effects will increase with the factor $1/t$, when decreasing the component size.

Shaping of polymer micro-components by blow molding requires, as well as for the conventional forming of polymer macro-parts, the application of a specific and elevated workpiece temperature. In conventional processes, this heat energy is either already provided by the extrusion process which delivers the extruded and heated tube directly between the forming dies, or by a preheating in case where, for example, injection molded components are used for the initial parts. A comparable strategy, where the micro-tube is provided to the process as a preheated part, was considered not to be feasible. Due to the above-mentioned higher ratio of outer surface to volume A/V of micro-tubes compared to conventionally sized tubes, upon a heat energy being applied, it dissipates faster by emission, which results in an insufficient forming temperature at the start of the process.

For this reason, in the micro-blow molding process as described above, the necessary heat energy is provided by the heated forming die halves. This ensures also a constant distribution of the heat energy applied by the surrounding tool, and avoids the local stiffening of the formed micro-component by a local temperature decrease. However, this heating strategy requires that the formed component has to be cooled down at the end of the process to improve its dimensional quality. Further, in the case that the expanded tube wall stays for a comparatively long time within the heated die cavity without being cooled down, local overheating of the component may occur. In conventional blow molding processes this cooling effect is provided by the unheated cavity of the forming die.

Adhesion of the heated and formed micro-component to the shaping die cavity has a significant impact on process reliability and product quality. Exceeding a critical amount of adhesive force can result in distortion of the formed component when it is removed from the forming die cavity. Due to the increased ratio A/V, this impact of adhesion forces is higher for micro-tube forming compared with conventional blow molding. Although the adhesion forces are of similar dimension for micro- and macro-forming, the resulting stresses within the wall of the micro-component, when it is removed from the die cavity, are higher due to the lesser wall thickness of these parts. In principle, common mold-release agents can be applied to reduce adhesion. However, this application means additional effort and process time as well as the eventuality of the deposition of release agent residue in the die cavity.

CROSS ROLLING

Cross rolling is a cold forging process to reduce the micro-tube diameter uniformly on a desired section by means of a pair of rotating rollers. Applying a pressure higher than the yield stress to the material, results in a permanent deformation. The principle in cross rolling (Figure 9) is to use two symmetrical rollers to apply such a pressure to a micro-tube on only two sides while it rotates. In this way the diameter of the tubes is reduced gradually until the desired shape is achieved. It is possible to control

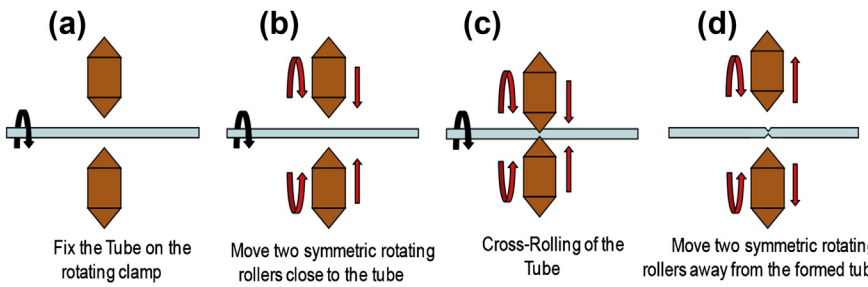

FIGURE 9

Processing sequence of the cross rolling polymeric micro-tube.

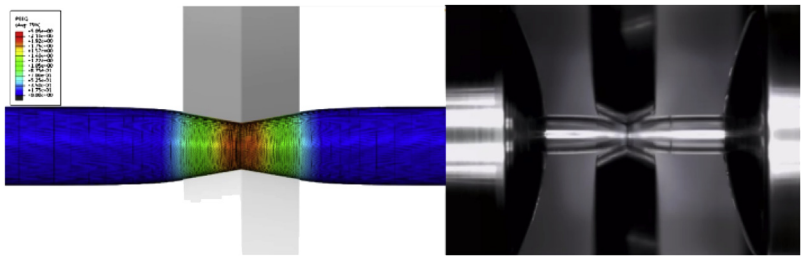

FIGURE 10

Comparison of the results of cross rolling process simulation and experiment.

the diameter by adjusting the motion of the rollers. When the rollers are removed, and the procession stops, the tube expands slightly due to elastic recovery. This action gives rise to a demand for the material to have a low yield strain.

As shown in Figure 10, the process simulations are in good agreement with the experiment results. In general, there is no limit on the outer diameter of a tube to be cross rolled. One small drawback of the process is that it works mainly for relatively thick-walled tubes, e.g., for polycarbonate the wall thickness should be around 1/3 of the outer radius.

Figure 11 shows some sample parts of polycarbonate tubes, produced with the cross rolling process.

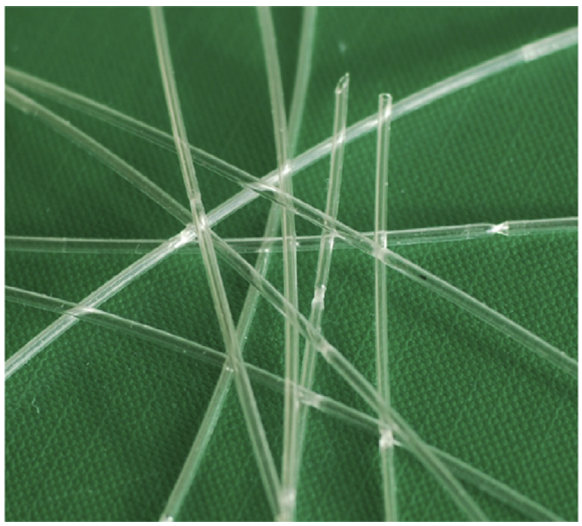

FIGURE 11

Micro-blow molded micro-tubular parts.

THE WHOLE SYSTEM

As an innovative micro-manufacturing solution for the manufacture of functionalized, tubular micro-components for a variety of applications from a range of polymeric materials and geometries, the system targets for applications are that the shaping would normally be required at either of the two ends of a micro-tube or/and at intermediate sections of the tube where basic shapes such as a reduced section, e.g., a tip, or an expanded section, V-shaped or U-shaped opens; or/and reduced diameters, e.g., necks and other profiles; or/and expanded hollow sections with certain outer profiles, etc. The identification of the requirements on the shaping led to a definition of the processes needed to convert micro-tubes into functionalized components. The processes included in the platform are tip-forming is to be effected with the hot embossing process, and reduced sections effected with cross rolling and/or hot embossing, while expanded sections are to be enabled with a blow molding/thermal expansion process. Moreover, sectioning tubes, creating micro-sized holes in the tube-walls as well as the removal of flash would rely on the use of a dedicated layer system. At the same time, the platform also took the requirement for volume production into account, such as effectiveness of the handling, efficiency of the shaping, ease for quality control, etc. These processes together form a high-yield, high-flexibility process chain for the shaping/fabrication of polymeric, tubular micro-components.

The manufacturing platform is to integrate individual processes in the form of integrating individual modular machines which are linked through a global handle system: a robotic manipulator (Figure 12) capable of feeding the tubes; while each of the modular machines has its own inter-handling device and can pick up the shaped components. In such a way, each modular machine can be a

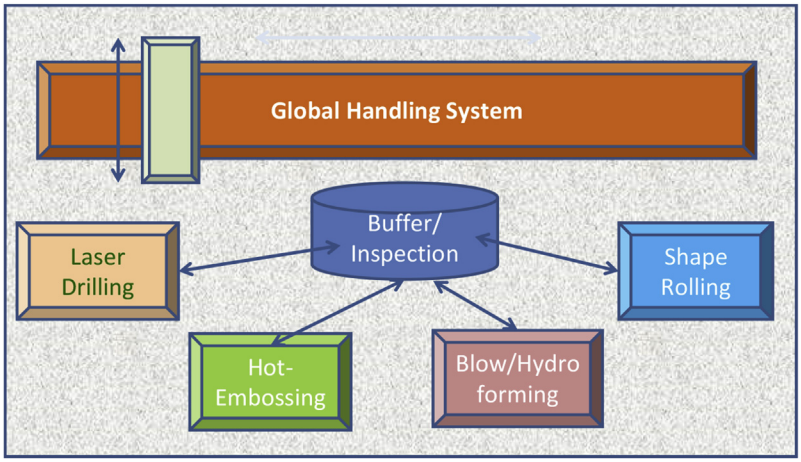

FIGURE 12

Schematic diagram of the "Polytubes micro-factory."

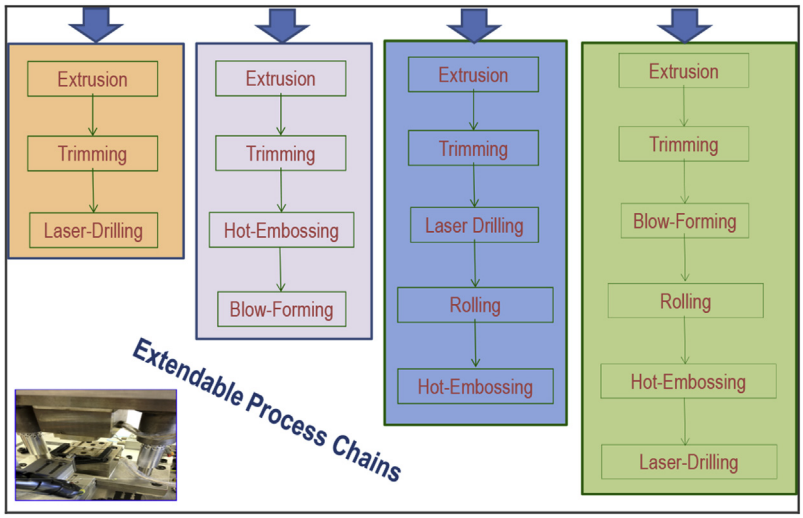

FIGURE 13

Polytubes process chain variations.

stand-alone machine for different applications, but can also be integrated onto a common platform for an integrated process chain (Figure 13). Other advantages are high manufacturing flexibility (the process combinations can be easily reprogrammed); high modularity (a highly modular system); and the system is easily configured, etc.

MATERIALS

All three micro-tube forming technologies were tested, with series polymer materials, including PI, PEEK, PP, PA, PC, PET, COC materials, etc., ranging from outer diameters of 1.5−0.037 mm with various thicknesses. All processes must not exceed the maximum strain of the material, which may lead to breaks, cracks, or other types of failure of the tubes. It was found that a certain process is particularly suitable for certain materials, and challenges arose when there was the need to link these processes into a process chain to process the same material for a component. For instance, processes such as hot embossing and cross rolling are mostly suitable for the shaping of thicker tubes, while blow molding is ideal for the shaping of thin tubes: this situation is similar to that encountered in laser-drilling and trimming. In general, amorphous polymeric materials are ideal for shaping and quality control, while more effort is required when dealing with semicrystalline polymeric materials. Nevertheless, the manufacturing platform mentioned above does provide a flexibility to form different process chains to deal with different materials/geometry combinations.

FORMING TOOLS AND MACHINES

HOT EMBOSSING

To enable the high-quality hot embossing of polymeric micro-tubes, tools (Figure 14) were designed and constructed to enable modular insertion of core dies; precision guiding of the micro-tube within the dies; heating and cooling units with a temperature-control system; heat insulation for improved heating efficiency; precise alignment of the upper and lower die sets, etc. The tool design also took the requirement for automated handling into account.

To demonstrate the technical and commercial viability for volume production at a full industrial scale by manufacturing prototype products which meet all functional requirements for applications, a series of tests with the hot embossing machine that had been developed was conducted. The hot embossing machine is a miniature desktop machine (Figure 15) which integrates a linear press, forming dies and tool components with heating and cooling units, precision guides and machine frames, and an automated micro-tube handling system. To ensure fully automated operation, a multiaxis micro-tube handling system was developed as an automatic raw material feeding and component pickup device to serve the hot embossing machine. The machine and process parameters such as press force, travel speed and distance, temperature as well as holding time can be easily set with a software interface developed within the project. In summary, the system has the following features: integrated force, position, and signal control; maximum force 3 kN; smallest force measuring 0.83 N; maximum stroke 100 mm; distance resolution 0.049 μm; working temperature up to 500 °C; four axis micro-tube handling unit; and a selection of the integration interface.

A programmable logic controller was used to control and automate the various electromechanical operations of the machine. With the implementation of the control system, the following key parameters can be controlled during the hot embossing process.

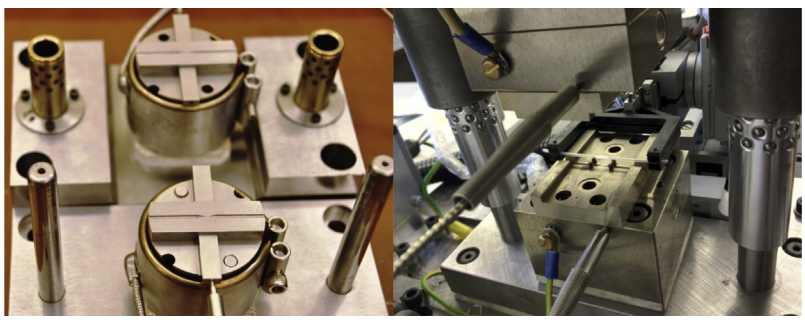

FIGURE 14

A close-up view of the hot embossing tooling (cylindrical and cuboid tooling).

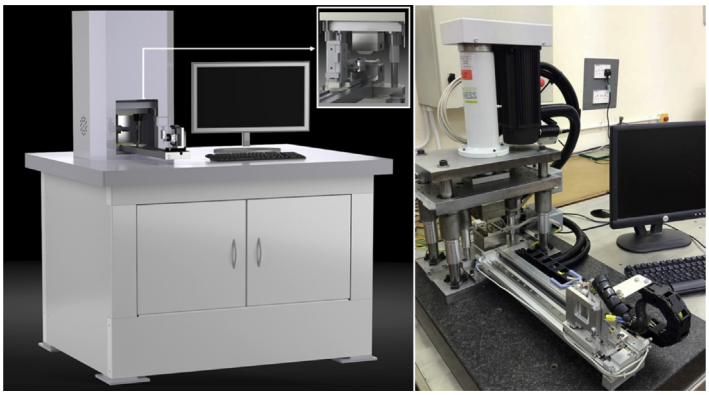

FIGURE 15

The micro-tube hot embossing machine system (computer model and prototype machine).

Press force: The hot embossing force and holding force generated by the linear actuator during hot embossing can be preset accordingly for each polymeric material and geometry to be dealt with. Control of how long the holding force should be maintained (holding time) is a key factor in determining the quality of the shaped micro-component. Another associated factor is the production rate. A higher production rate to be achieved suggests that a shorter holding time may have to be used, which may mean a sacrifice of part quality.
Press stroke: This parameter can be controlled independently of the press force, which gives flexibility for micro-shaping which needs separate control on both parameters. It is especially useful for the shaping of polymeric materials where maintaining a certain level of the pressure is necessary when the deformation needs time to be settled/completed, e.g., when accompanied by a cooling process.
Machine RAM speed: The machine RAM speed should be adjusted to suit the shaping of a particular material where it is desirable to meet the cycle time requirement as well as to address the strain rate sensitivity of the deforming thermoplastic material. The latter has an effect on the shaping ability of the material as well as on the failure forms of the part.
Heating temperature: This is an important parameter in the hot embossing of thermoplastic materials. Depending on the tubular material and final shapes to be achieved, the temperature at the tool surface may be expected to be raised above the glass transition temperature, T_g, or melting point, Tm, for easier shaping. To form a bonding at the folded surfaces of the inner surface of a tube and, hence, a sound central pore, a temperature above the Tm (for crystalline thermoplastics) is expected, in order to achieve viscous fluid and sufficient fusion at the interfaces.
Holding time: This parameter can be preset. While maintaining a constant force on the upper tool, the tool will be held for a period of time after the machine

RAM stroke is completed. Compared with the hot embossing of a polymeric material on a large plane area, the micro-tube cools down rapidly to below the glass transition temperature due to small material-volume being involved.

MICRO-BLOW MOLDING

To obtain short cycle times for high-volume production, an appropriate design for the forming tools and the thermal management is required to ensure that the heat energy to heat the next tube to be formed, is provided within a comparatively short time. In comparison to conventional blow molding process design, the tool elements are heated by embedded heat cartridges. This enables the continuous application of heat energy to the formed component, in order to retain it at a stable forming temperature. In accordance with investigations into the thermoforming of micro-polymeric bulk components presented in Ref. [19], a suitable forming temperature is about 20 up to 30 °C above the glass transition temperature T_g of the formed polymeric material.

Important aspects concerning the design and manufacture of the forming tools are the determination of a suitable mold parting line and the taking of measures for die cavity venting. Parting lines with a symmetrical material distribution within the two forming die halves are recommended. For the case of parting lines that lead to unsymmetrical material distribution, a locally adapted thermal energy supply is often necessary, in order to obtain the required forming results. Suitable knowledge concerning the tool manufacture in the presently required micro-dimension is of importance to ensure the intended accuracy of the formed components is obtained. This concerns, in particular, the design of measures for die cavity venting to avoid air becoming trapped between the formed component and the die cavity wall. Figure 16 shows an example of forming tool inserts for micro-blow molding which were used for the fabrication of the formed components presented in Figure 8.

New strategies are necessary for the robust sealing and pressurization of the blow molded micro-tubes. Conventional blow forming processes, which are working with just extruded polymeric tubes, use mandrels to supply pressurized air into the workpiece. The mandrel, which has to be inserted with precision into the tube end, is clamped by closing the forming die halves to achieve sealing. A sealing system for micro-tube molding has to be designed in such a way that it avoids loss of process reliability, which latter may be caused by imprecision when inserting the mandrel into the initial workpiece.

Figure 17 presents an automated micro-blow molding machine system capable of the volume manufacture of polymer components made from micro-tubes, designed on the basis of the findings developed in Ref. [4]. The machine system contains various actuators for the controlled application of the process loads, sealing, and thermal management, as well as for component handling, and enables the pressurization and forming of micro-tubes below a diameter of about 1300 μm with pressures of up to 50 bar.

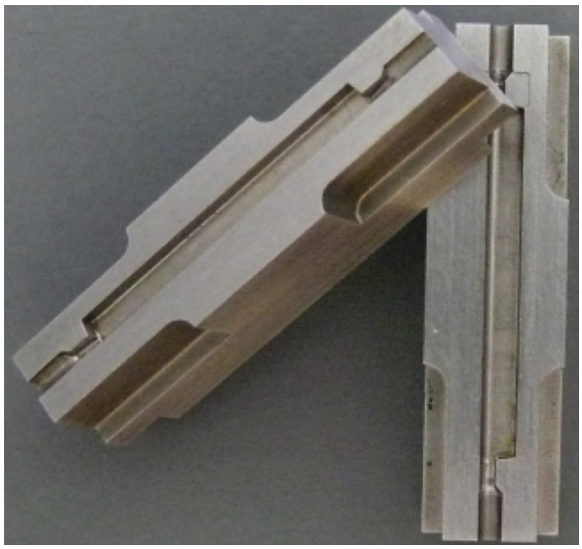

FIGURE 16

Example of forming tool inserts for micro-blow forming.

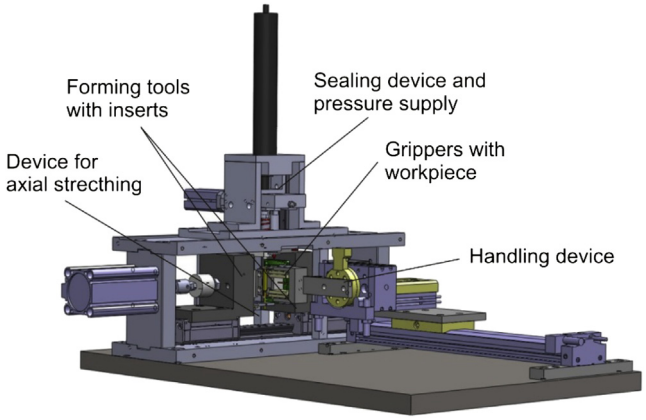

FIGURE 17

Micro-blow molding machine system.

CROSS ROLLING

Cross rolling has been used successfully with large-size metal bars but not with micro-tubes. The development work reported here was undertaken at Institute of Product Development (IPU) of Denmark, which developed a machine that is flexible and can produce any cross rolled shapes, with minimum changes in the size of the clamps and in the shape of the shaping tools (Figure 18).

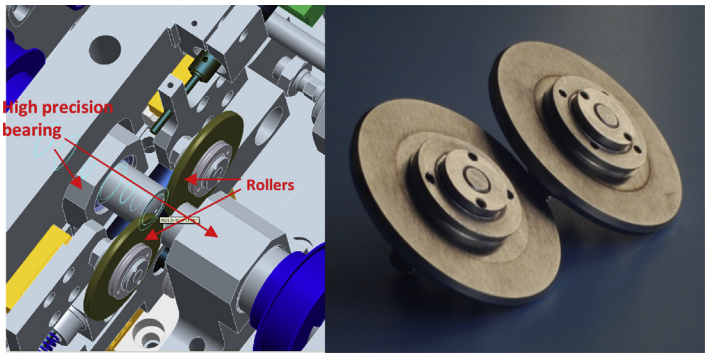

FIGURE 18

Roller for cross rolling forming.

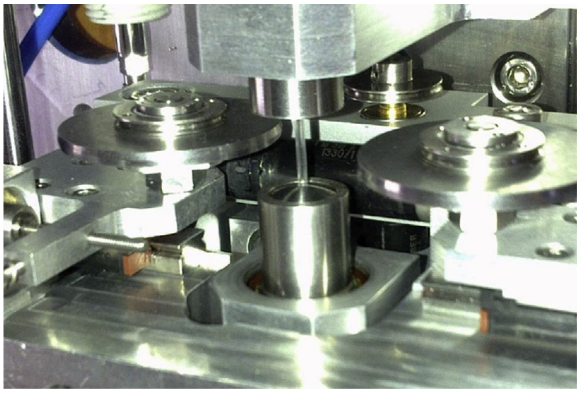

FIGURE 19

Modular cross rolling machine.

This machine reveals the full potential of the process and also enables volume production in an automated way. The whole cross rolling machine (Figure 19) is $525 \times 150 \times 150$ mm in size. The rollers are interchangeable so that it is possible to deal with the forming of different geometries. The tube is clamped firmly by a set of two pneumatically controlled rotational clamps so that it cannot be bent during the process. The whole setup is mounted on a guide rail to allow for the small tension generated when the tube is necked during which the surface length of the tube may be increased to enable it to form to the curvature of the rolls, but its overall length measured along the axis of the machine may be decreased. The rotation of the tube and the rollers is controlled by two servomotors and the rotational speed of the tube can be adapted to the rotational speed of the rollers giving a minimum of sliding

between the rollers and the tube. The speed of the tube can, in this way, also be increased during processing, when the diameter changes, to keep the sliding to a minimum. The pitch of the rollers is controlled by a small servomotor. The mean considerations for this system development are repeatability and precision; flexible regarding tube diameter; and flexible regarding length and a possibility to apply tension during processing.

POLYTUBES "MICRO-FACTORY"

The micro-factory (manufacturing platform) has been demonstrated to provide flexibility to form/configure different process chains to deal with different materials/geometry combinations or applications. Each modular machine is stand-alone equipment that could be used for on-site production separately or in a combination, and they are also extendable for processing other materials in addition to polymers. With proper programming, different process chains could be enabled to suit different applications—several possible process chains, developed by Sysmelec, Switzerland, are illustrated in Figure 20. Other relevant modules, as part of whole system, such as laser drilling, part handling are detailed and can be found in the relevant chapters.

Three levels of integration were considered: (1) process control and handling integration on individual modular machines; (2) manufacturing platform control which links individual machines/modules; and (3) platform management system integration for production management (Figure 21). The dialogue interfaces for communicating with the platform from the individual modular machines and the requirements on the mechanical integration (mechanical and safety interfaces and others) were defined prior to the software development which was tested later on its integration functionalities and effectiveness.

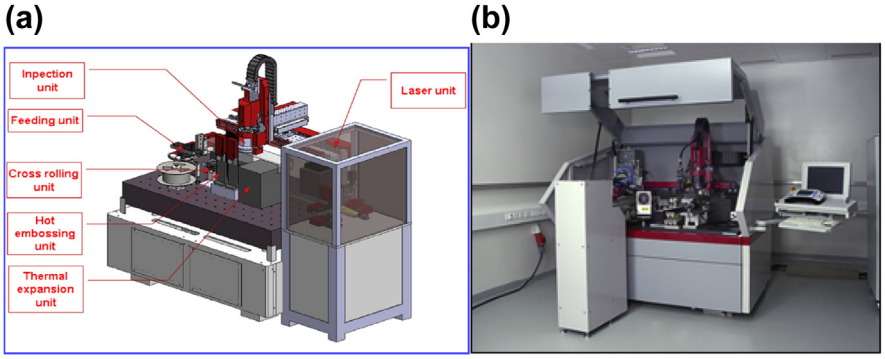

FIGURE 20

(a) Graphical illustration of the micro-factory concept; (b) The manufacturing platform used for testing the concept (Sysmelec, Switzerland).

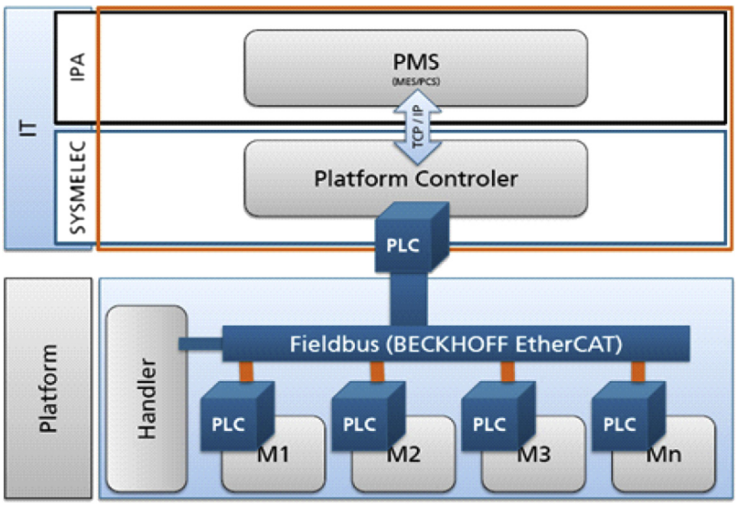

FIGURE 21

Scheme of the manufacturing platform integration. PMS, production management system.

APPLICATIONS

Major advantages of the three micro-tube forming technologies consist in the possibility to generate hollow shaped complex geometries in a single forming step from economically priced extruded polymer tubes. Creating new micro-manufacturing facilities with new manufacturing capabilities was also aimed to support product innovations, e.g., expanding applications of polymeric-tubes at much smaller length scales—potential applications including medical engineering (e.g., catheters (cardiovascular, intravenous), endotracheal tubes (for intubation or anesthesia), medical balloon tubing (angioplasty and stent delivery), intravascular drug delivery tubing, urological retrieval devices, etc.); biotechnological medical engineering (e.g., shaped inlet and outlet channels for biochemical analysis of liquids in biochips for easy connection to "macro-world"); chemical industry and medical engineering (e.g., micro-pipettes for chemical and pharmacy dosage systems, micro-tubes and micro-needles for drug delivery, micro-capillary reactors for development of chemical, cosmetic, or pharmacy products, etc.); and general sensor and actuator applications such as those used in chemical, medical, and biotechnological products as well as consumer goods.

Several typical tubular instruments were developed as the demonstrators for testing different forming processes combinations: instruments for electrophysiological study of ion channel patch clamp; micro-heat exchangers; and a system for capillary electrophoresis study. One of the medical instruments developed is shown in Figure 22. The processes and equipment developed were used for producing parts for the product demonstrators which were then subjected to laboratory validations

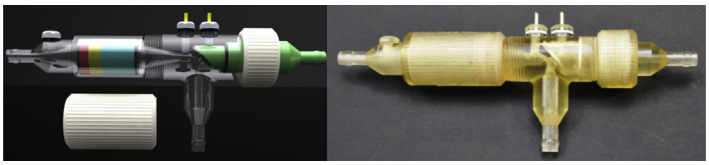

FIGURE 22

A medical instrument as a typical application of a micro-tubular component.

and testing. The results from these evaluations were further used to update the design and manufacturing knowledge which was further used to optimize the process and machine development.

REFERENCES

[1] Qin Y, Brockett A, Ma Y, Razali A, Zhao J, Harrison C, et al. Micro-manufacturing: research, technology outcomes and development issues. Int J Adv Manuf Tech 2010; 47(9−12):821−37.

[2] Saab MA. Heat transfer catheters and methods of making and using same. US; 1997.

[3] Choudhury N, Debergue P, Diraddo R, Truckenmueller R, Giselbrecht S. Micro-blow moulding and micro-thermoforming: simulation and validation. In: Polymer processing society 24th annual meeting. Salemo; 2008.

[4] Anyasodor G, Hartl C. Investigations into fundamentals and forming system design for micro-tube expansion with pressurized media. In: XXI international symposium, research-education-technology. Gdansk; 2013.

[5] Qin Y. Micro-manufacturing engineering and technology. 1st ed. Elsevier; 2010.

[6] Heaney DF. Mass production of micro-components utilising lithographic tooling and injection molding technologies. In: 1st international conference on micro-manufacturing; 2006. p. 280−3.

[7] Palmer JA, Williams JD, Lemp T, Lehecka TM, Medina F, Wicker RB. Advancing three-dimensional MEMS by complimentary laser micro manufacturing. In: The international society for optical engineering; 2006.

[8] Sharon A, Bilsing A, Lewis G, Zhang X. Manufacturing of 3D microstructures using novel UPSAMS process (ultra precision manufacturing of self-assembled micro systems). In: IEEE the sixteenth annual international conference; 2003.

[9] Okazaki Y, Mishima N, Ashida K. Microfactory—concept, history, and developments. J Manuf Sci Eng 2005;126(4):837−44.

[10] Jia BX, Wang ZL, Hu FQ, Li XH, Zhao WS. Research on multifunctional micro machining equipment. Materials Science Forum Adv Mater Manuf Sci Tech 2004; 471−472:37−42.

[11] Zhou LB, Yaguchi Y, Fujii T, Shimizu J, Eda H. Development of a multifunctional micro-machining system and its applications. Key Eng Mater 2003;238−239:3−8.

[12] Liao YS, Chen ST, Lin CS. A multi-function high precision tabletop CNC machine for making micro-parts developed in National Taiwan University. In: 1st ICOMM; 2006. p. 48−52.

[13] Rahman M, Lim HS, Neo KS, Senthil Kumar A, Wong YS, Li XP. Tool-based nanofinishing and micromachining. Mater Process Technol 2007;185(1−3):2−16.
[14] Heckele M, Bacher W, Müller KD. Hot embossing - the molding technique for plastic microstructures. Microsyst Technol 1998;4(3):122−4.
[15] Worgull M. Hot embossing: theory and technology of microreplication. Elsevier; 2009.
[16] Zhao J, Qin Y, Razali A, Yip ALK, Fei Z. Hot-embossing of polymeric micro-tubes. In: International conference on micromanufacturing; 2012.
[17] Lee NC. Practical guide to blow moulding. Rapra Technology Limited; 2006.
[18] Vollertsen F. Size effects in manufacturing. In: 1st colloquium process scaling. Bremen; 2003. p. 1−9.
[19] Heilig M, Schneider M, Ide T, Worgull M. Technology of microthermoforming of complex three-dimensional parts with multiscale features. Microsyst Technol 2011;17(4): 593−600.

CHAPTER

Micro-injection Molding

9

Guido Tosello

Department of Mechanical Engineering, Technical University of Denmark, Kgs. Lybgby, Denmark

CHAPTER OUTLINE

INTRODUCTION

The essential condition for the market success of micro-systems is the cost-effective production of micro-structures on a large scale. In recent years, plastic molding techniques such as injection molding, which is a suitable process for medium- and large-scale fabrication, have been adapted for the necessities of micro-components fabrication. Injection molding is a process technology that has been well established in the production of polymer parts in the macro-dimensional range for decades. Therefore, vast know-how and machine technology is available to be made use of in micro-injection molding (μIM) as well.

Moreover, the fabrication costs of molded micro-parts are only slightly affected by the complexity of the design. Once a mold insert has been made, several thousand parts can be molded with little effort. The cost of raw material in most cases is negligibly low, because only small material quantities are required for micro-components.

Micromanufacturing Engineering and Technology. http://dx.doi.org/10.1016/B978-0-323-31149-6.00009-8

Therefore, parts fabricated by μIM, even from high-end materials, are suitable for applications requiring low-cost and disposable components [1]. The result is that plastic products manufactured by μIM have made successful entry into the market. In fact, peculiar characteristics such as production capability, disposability, biocompatibility, optical properties, just to mention a few, pose plastics as the best choice for numerous micro-products. Fields of application of micro-molded products are micro-optics (waveguides, micro-lenses, fiber connectors, micro/sub-micrometer gratings), micro-mechanics (micro-gears, micro-actuators, micro-pumps, micro-switches), information storage and data carrier devices (CDs, DVDs, Blu-ray Discs, sensor discs), micro-fluidic systems (blood analysis, DNA analysis), medical technology (hearing aid, components for minimal invasive surgery, micro-dispensers, micro-needle arrays), micro-reactors (micro-mixers, micro-heat exchangers), biomedical applications (bioreactors, artificial skin, cell culturing).

When downscaling systems, products, and their components, the limits of conventional manufacturing techniques are reached. This initiated the improvement of conventional techniques and the further development of new ones, as in the case of the μIM process. Lateral dimensions in the micrometer range, structural details in the sub-micrometer dimensional level and high aspect ratio (aspect ratio = depth/width) of 10 and above are achieved. There are a variety of applications already known for the micro-molding of thermoplastic polymers and many more are expected to arise in the future.

μIM SCENARIO

Injection molding is one of the most versatile and important operations for the mass production of complex plastic parts. Injection-molded parts typically have good dimensional tolerance and require almost no finishing and assembly operations. In addition to thermoplastics and thermosets, the process is also being extended to such materials as fibers, ceramics, and metal powder materials, with polymer as binders. Among all the polymer-processing methods, injection molding accounts for 32% by weight of all the polymeric materials processed [2]. Innovations of the conventional injection molding process have been continuously developed to further extend the applicability, capability, flexibility, productivity, and profitability of this versatile mass production process.

In particular, μIM is an innovative technology for replication on the medium-to-large scale of micro-components. μIM introduces additional design freedom, new application areas, unique geometrical features, and sustainable economical benefits, as well as material properties and part quality that cannot be accomplished by the conventional injection molding process.

μIM (also called micro-molding) refers to the production of parts that have

- weight in the range of milligrams, overall dimensions, functional features, and tolerance requirements that are expressed in terms of micrometers, as well as miniaturized gate and runner system (see Figure 1, top);

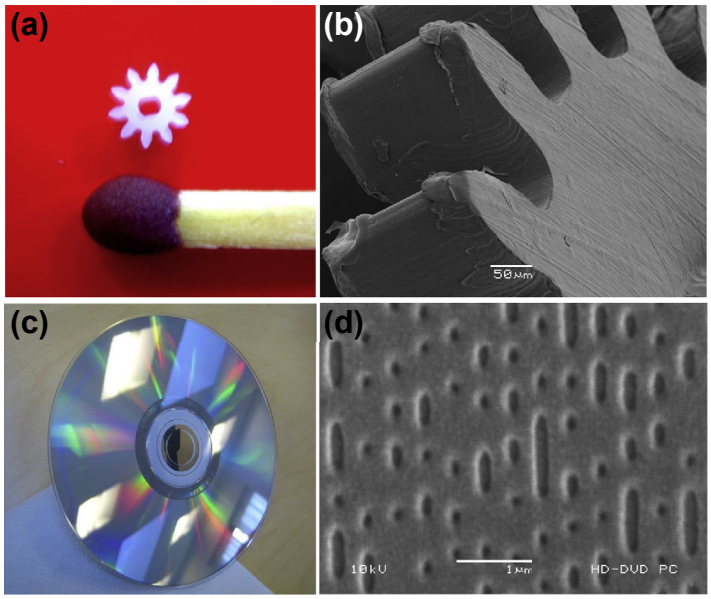

FIGURE 1

Example of a micro-molded part: (a) micro-gear and (b) detail view of micro-teeth, material: polyoxymethylene; macro-part with a sub-micro-structured region; (c) high-density DVD disc; and (d) detail view of sub-micro-features, material: polycarbonate.

- overall dimensions in the macro-range, weight of the order of grams, and areas with micro-features. Such micro-structures have dimensions, functional features, and tolerance requirements that are expressed in terms of micrometers down to nanometers (see Figure 1, bottom).

On the basis of these definitions, micro-molding can be also regarded as one type of molding technology recently defined as "precision injection molding" [3].

Among the various micro-manufacturing processes, μIM possesses the advantage of having a wealth of experience available in conventional plastics technology, standardized process sequences, and a high level of automation and short cycle times.

Due to the miniature characteristics of the molded parts, however, a special molding machine and auxiliary equipment are required to perform tasks such as shot volume control, process parameters control, injection, ejection, plastification, inspection, handling, packaging of molded parts, etc. Furthermore, micro-machining technologies are needed to produce the micro-cavity.

μIM TECHNOLOGY

The development of micro-injection technology entered a first phase between 1985 and 1995 [4]. During that period, injection molding technology for macro-parts with

micro-structured details started and no appropriate machines were available. Only modified commercial units, hydraulically driven and with a clamping force of usually 25 up to 50 tons, could be applied for the subtle way of replicating micro-structured mold inserts with high aspect ratios by injection molding. After, a second stage occurred from 1995 to 2000 when, with the collaboration between mechanical engineering companies and research institutes, special micro-injection units or even completely new machines for the manufacturing of real micro-parts were developed. The task was to reduce the minimal amount of injected resin, which is necessary to guarantee a stable process (i.e., improve the process repeatability) and increase replication capabilities of very small features (down to 20 μm).

Following this intense developing stage, a number of machines equipped with special features for micro-injection have been produced by leading manufacturers. Minimum shot weights down to 25 mg are now feasible, micro-features can be replicated in a short cycle time, and three-dimensional micro-products are produced, which can now successfully enter the market.

MICRO-MOLDING WITH CONVENTIONAL INJECTION MOLDING MACHINE

The fabrication of micro-molded parts becomes a challenge when conventional injection molding machines (see Figure 2) are used for the replication of very small parts. If such machines are adapted to the direct production of a micro-product, i.e., parts with a part weight down to a milligram, they produce precise but large sprues to achieve the minimum necessary shot weight to perform the process properly. Very often, over 90% of the polymer is wasted and this waste can be an important cost factor (considering, e.g., plastic material for medical applications, it is not unusual for 1 kg of special material, e.g., polyaryletheretherketone, to cost €100). Moreover, the large sprue increases the cooling time and, simultaneously, the cycle time [6].

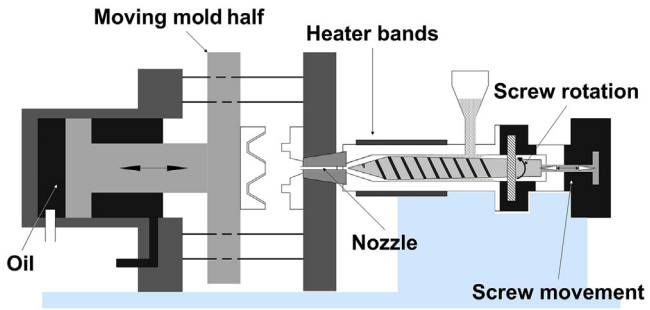

FIGURE 2

Schematic view of a hydraulic injection molding machine with its main components [5].

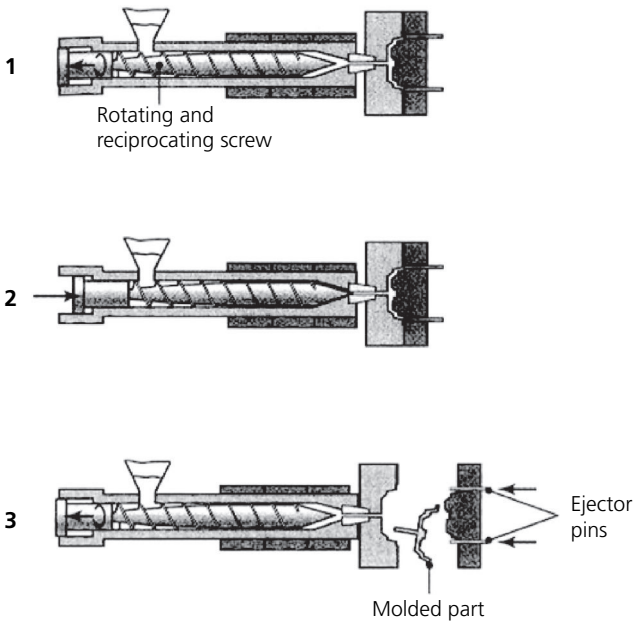

FIGURE 3

Phases of the injection molding process.

In conventional injection molding, an injection cycle is composed of the main phases described in the following (see Figure 3).

1. **Plastification**—during the plastification phase, the screw is rotating to build up the melt polymer necessary for the injection phase. The pressure pushes the screw backward. When sufficient polymer has built up (i.e., shot volume is plastificated), rotation stops.
2. **Injection, filling, and packing phase**—when the mold is closed, the screw is advanced (injection). The melt polymer fills the sprue, the runners, and the mold cavity (filling). The screw begins rotating again to build up more polymer (packing).
3. **Cooling and ejection**—after the polymer is solidified (cooling), the mold opens and ejector pins remove the molded part (ejection).

A problem which occurs with the small shot weight typical of micro-parts is related to the size of pellets used in standard injection molding. Conventional injection molding machines utilize screws with diameters down to 14 mm. Thus the depth of the screw channels should have at least the dimensions of a single grain. Hence, when the screw moves just 1 mm, about 185 mg of plastic are injected. For example, even one single pellet of poly(methylmethacrylate) (PMMA) weighs 24 mg. This exceeds the part weight of, e.g., gears for the watch industry of 0.8 mg. Again, to

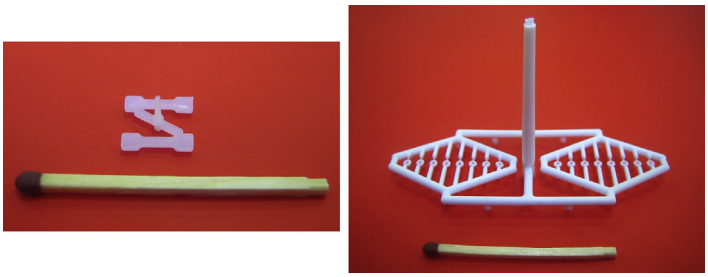

FIGURE 4

Comparison of runner systems to mold micro-part with conventional injection molding machines (right) and with micro-injection molding machine (left) [7].

produce such gears, relatively huge runner systems are used to compensate for this issue (Figure 4).

It is clear that these data represent a limit for correct processing of an injection-molded micro-part: the minimum shot weight for a stable production lies in the range of tenths of a gram. When producing parts at the lower limit of the machine capacity, problems such as dwelling time of the material will appear, with risk of polymer degradation [5].

A screw for melting and injecting polymers combines four functions in one single unit:

- Plastification and homogenization
- Metering
- Locking
- Injection

A conventional reciprocating screw used in macro-machines presents the following problems when it is employed on molding micro-parts:

- It is difficult to control the melt metering accuracy as a result of the screw structure and the limitation to reduce screw size.
- Because of the channel configuration, there is a melt backflow when high injection pressure is applied to fill small and micro-cavities.

For further downscaling of the injection molding process, these issues have to be solved by dividing the four functions of the screw at least in two different units:

- A screw for plasticizing and homogenizing
- A piston for metering and injection

μIM MACHINE

In order to control the metering accuracy and the homogeneity of the very small quantities of melt in the μIM process, a new micro-molding machine that uses an

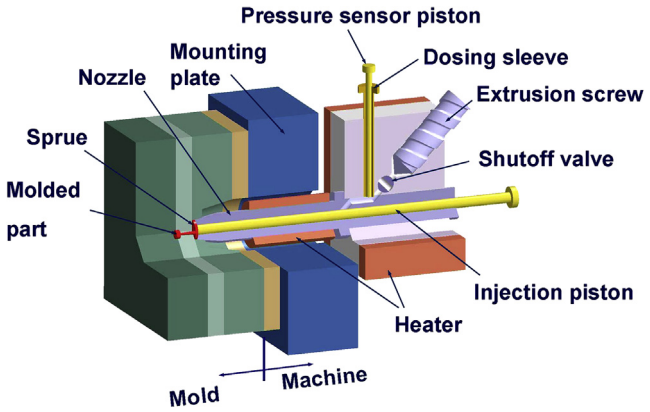

FIGURE 5

Injection unit of a micro-injection molding machine [7].

injection system comprising a screw extruder and a plunger injection unit has been developed over the last 10 years.

The main difference between the new micro-molding machine design and the conventional macro-machines with the conventional reciprocating screw injection system is that by separating melt plastification and melt injection, a small injection plunger of a few millimeters in diameter can be used for melt injection to control metering accuracy. At the same time, a screw having sufficient channel depth to properly handle standard plastic pellets and yet provide the required screw strength can be employed in micro-molding machines.

The typical solution provided by a μIM machine consists of the splitting of the four functions of the reciprocating screw (plastification, metering, locking, injecting) into different components (see Figure 5).

The plastification takes place in a dedicated functional part of the machine, which is separated from the injection unit.

- The very small amount of plastics needed is plasticized either by a plasticizing small screw (diameter of 14 mm, see Figure 6) or in an electrically heated cylinder, and then fed into the injection cylinder by a plunger (diameter of 5 mm) (Figure 7).
- A second plunger with a diameter of just 5 mm down to 2 mm, depending on the machine configuration, injects the molten material into the cavity. It is driven by an electric motor and a precise linear drive. Typically, the shot weight can be varied between 5 and 300 mg.

The μIM process steps are the following (see Figure 9):

1. Plastic pellets are plasticized by the fixed extruder screw and fed into the metering chamber.
2. The shutoff valve closes in order to avoid backflow from the metering chamber.

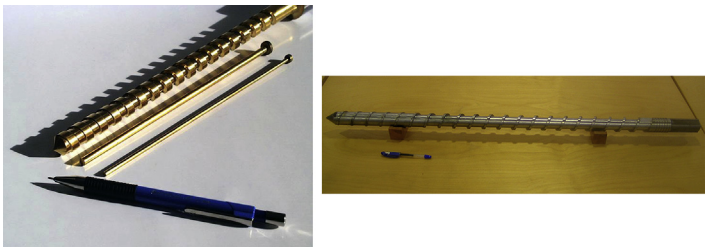

FIGURE 6

Comparison of dimensions between screw and injection plungers for micro-injection molding (left) and a screw for conventional injection molding (right).

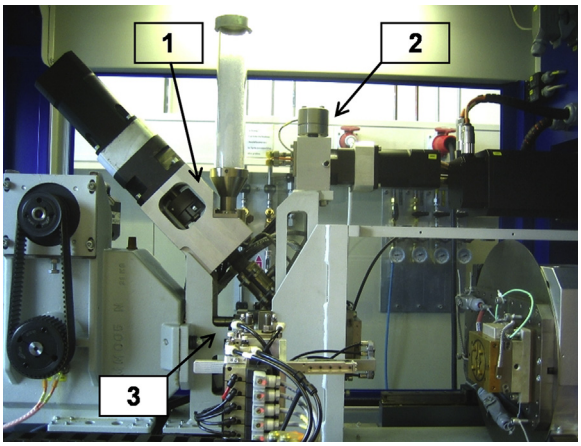

FIGURE 7

Micro-molding machine and the three-stage unit: (1) plastication, (2) metering, and (3) injection [8].

3. After the set volume has been achieved, the plunger in the dosage barrel delivers the shot volume to the injection barrel.
4. The injection plunger then pushes the melt into the mold.
5. Once the plunger injection movement is completed, a holding pressure may be applied to the melt. This is achieved by a slight forward movement (maximum 1 mm) of the injection plunger.

The injection piston is usually capable of a maximum injection speed of 400–900 mm/s and it is able to inject up to the parting line of the micro-cavity (i.e., the pinpoint gate); in this way no sprue is attached to the molded part (see Figure 8). This design feature is particularly suitable for the mass production of micro-injection-molded components for the following reasons: it allows shorter filling time due to the lower volume to be filled, it avoids short shots due to

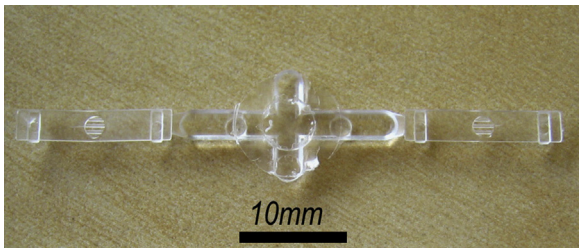

FIGURE 8

Micro-molded components and runner systems [9]: thin tensile bar test part ($15 \times 3 \times 0.3\ mm^3$) including three micro-features (width = 300 μm, length = from 1500 μm up to 2000 μm), material = polystyrene, weight of the complete molded part = 119 mg (17% for each of the two parts and 64% for the miniaturized runner system) [8].

premature melt freezing allowing better micro-features replication, and it decreases the cycle time due to shorter cooling time (Figure 9).

More recently, variations of this dedicated machine design developed for micro-injection molding have been developed. The main drivers for further developments appeared to be a simplification of the micro-injection unit architecture, an extension of the maximum injection volume, increased modularity to provide flexibility in terms of injection piston dimensions, improved melt homogeneity and high accuracy. Examples of recently developed micro-molding machine architectures that use injection units suitable for micro-injection in alternative of the small screw (diameter 14 mm) and two plungers (diameter of 5 mm) design include the following components:

- A small screw for plastication (diameter 14–18 mm) and one injection plunger (diameter 4–8 mm) [10–12];
- Two pistons, one for plastication (e.g., diameter 6 mm) and one for metering/injection (diameter 2–5 mm) [13];
- Two screws, one for plastication and one for injection (diameter 15–18 and 8 mm, respectively) [14].

PROCESS CONTROL AND ANALYSIS

μIM is a process which enables the mass production of polymer micro-products. In order to produce high-quality injection-molded micro-parts, a crucial aspect to be fully understood and optimized is the filling of the cavity by the molten polymer. As a result, the relationships between filling performance and the different process parameter settings have to be established.

Characterization of the filling phase during μIM is a challenging task, mainly due to the dimensions of the cavity (typically in the sub-millimeter range, and even down

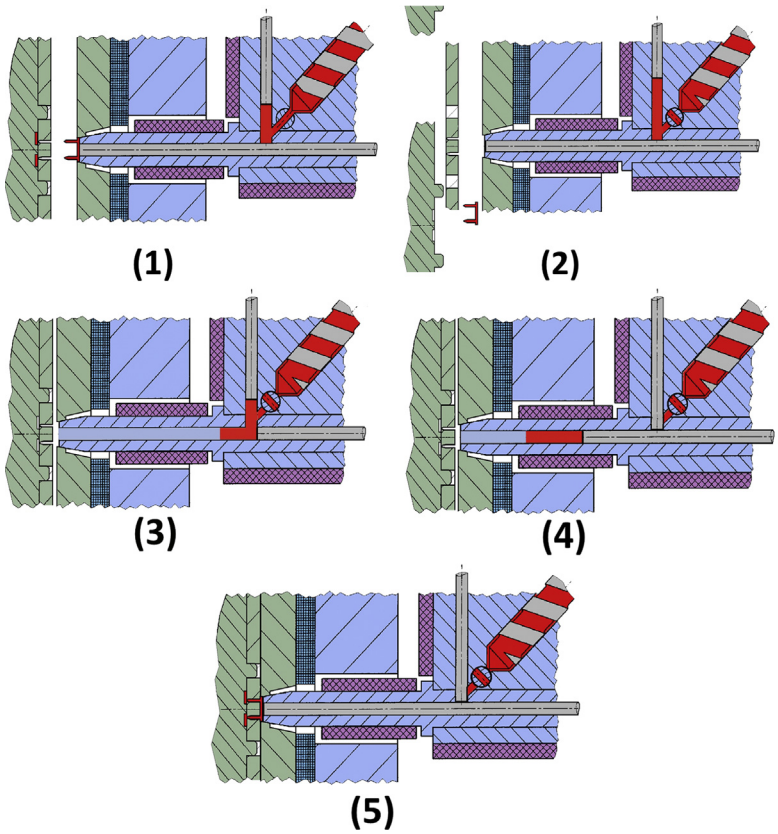

FIGURE 9

Micro-injection molding steps [7].

to a few micrometers) and the filling time of the cavity (in the order of a few tens of milliseconds).

Different approaches have been recently applied in order to accurately describe the filling of the micro-cavity depending on the process parameter settings. For example, methods for the analysis of filling performance are the short shots method, the flow-melt visualization method, and the flow length test.

MICRO-CAVITY FILLING ANALYSIS

Different approaches can be employed for the analysis of the filling stage of the μIM process. In particular, three methodologies can be applied in order to characterize filling performances.

- Short shots, where partial filling is obtained by means of part-filled moldings of increasing volume.

- Flow visualization, used to show the progress of the melt front in the cavity during the injection phase.
- The length flow test, used to evaluate the filling capability of the molding system in terms of achievable flow length and aspect ratio.

SHORT SHOTS METHOD

In conventional injection molding (i.e., in the macro-dimensional range), a common approach to study the development of the melt flow inside the cavity is the short shot analysis. This consists of the injection of a fraction of the molten polymer volume necessary to completely fill the cavity (see Figure 10).

The application of the short shots method to micro-injection-molded parts has been shown to be possible when using a μIM machine provided with an injection plunger [3,8]. One of the main conditions for the applicability of such a method is that the resolution of the machine (i.e., the smallest shot volume that can be injected in a controlled manner) has to be smaller than a fraction of the part which is significant to give information about intermediate stages of the filling. This condition can be fulfilled by injection molding machines having an injection unit with a plunger. On the other hand, small injection molding machines with the conventional plastification unit with a reciprocating screw cannot provide controlled short shots in the order of a fraction of 1 mm^3 (typical volume of polymer micro-parts and/or micro-features). Furthermore, in conventional machines, the acceleration of the screw may not be high enough to provide the required injection speed in the very short time needed to produce micro-short shots. As a result, despite the fact that it is actually possible to inject mold micro-parts with conventional injection molding

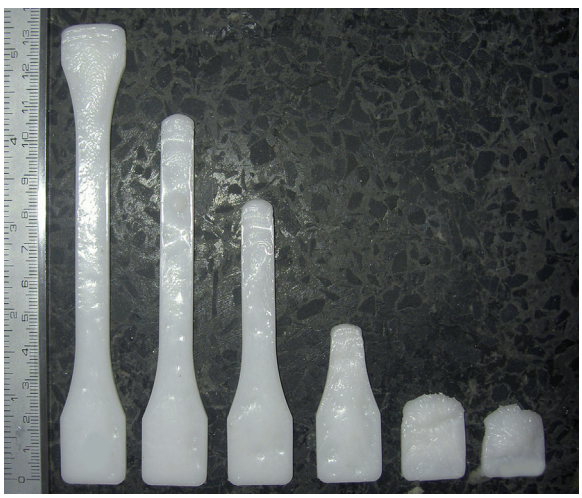

FIGURE 10

Short shots of an injection-molded dog bone (material: polyoxymethylene (POM)).

Experimental short shots	Parameters	Experimental short shots	Parameters
	Inj. Vol. = 55 mm^3 Inj. Time = 21 ms Weight = (52.1 ± 0.4) mg		Inj. Vol. = 105 mm^3 Inj. Time = 38 ms Weight = (96.9 ± 0.2) mg
	Inj. Vol. = 65 mm^3 Inj. Time = 25 ms Weight = (61.0 ± 0.5) mg	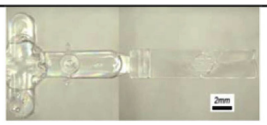	Inj. Vol. = 110 mm^3 Inj. Time = 41 ms Weight = (101.2 ± 0.2) mg
	Inj. Vol. = 75 mm^3 Inj. Time = 26 ms Weight = (70.0 ± 0.4) mg	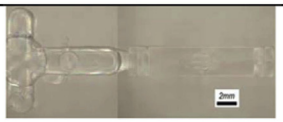	Inj. Vol. = 125 mm^3 Inj. Time = 51 ms Weight = (114.4 ± 0.2) mg
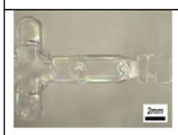	Inj. Vol. = 90 mm^3 Inj. Time = 29 ms Weight = (84.0 ± 0.3) mg	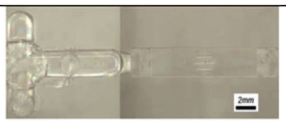	Inj. Vol. = 130 mm^3 Inj. Time = 83 ms Weight = (118.8 ± 0.2) mg
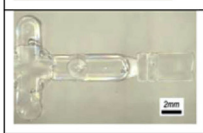	Inj. Vol. = 95 mm^3 Inj. Time = 31 ms Weight = (88.0 ± 0.2) mg		

FIGURE 11

Series of short shots of a thin wall micro-molded part with micro-features [8].

machines (especially if electrically driven and capable of high injection speed), with such machines it is not possible to produce reliable micro-short shots. Process condition repeatability in terms of actual speed and injection pressure at the beginning of the screw movement is lower than when it has reached a steady state injection movement. Moreover, the produced incomplete micro-parts present free surfaces with a deformation due to stress relaxation and thermal contraction. This causes an approximation on the dimensional accuracy of the determination of the actual flow front during the filling, especially if the target is accurate in the micrometer range. On the other hand, the short shots method has been proven to be a feasible method to represent the evolution of the filling stage when performing μIM (see Figure 11).

FLOW VISUALIZATION TESTS

Flow visualization can also be used to describe the advancement of the flow front into the cavity during the filling stage. It consists of the use of a high-speed camera capable of actually recording at high frame rates (in the order of 10^3—10^4 frames per second) of the flow advancement inside the micro-cavity. In order to achieve such results, the mold has to be provided with a lateral opening (camera access to the

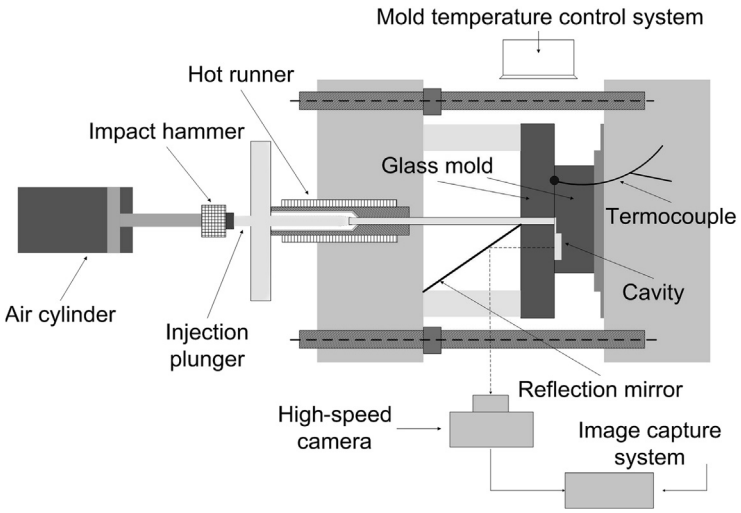

FIGURE 12

Schematic diagram of a machine equipped with a glass mold cavity and a flow visualization setup.

mold) and one side of the cavity made of glass [9,15] (see Figure 12). By subsequent image processing of the recorded film of the cavity filling, it is possible to perform a time-dependent analysis on the displacement of the melt-flow front depending of different setting of process parameter such as melt temperature, mold temperature, and injection speed. Further, by using a high-speed infrared thermal camera, it is possible to combine a flow visualization test with a measurement of the melt temperature development inside the cavity, for example, to verify injection rate settings in the machine and evaluate shear heating effects [16, 17].

The flow visualization method offers a better resolution than the short shots method. Furthermore, it can be applied not only to μIM machines but also to conventional reciprocating screw machines (mainly because the high resolution is provided by the high-speed camera). On the other hand, the construction of the mold itself is quite complicated due to the presence of a perfectly aligned optical glass and an optical mirror conveying the image from the cavity, through the glass and on to the external camera. As a consequence, the method appears to be of difficult implementation in an industrial environment.

LENGTH FLOW TESTS

Length flow tests are used to evaluate the filling capacity of the molding system in terms of flow length in the cavity and aspect ratio. Usually, a test cavity having constant cross section and a dominant dimension parallel to the flow front advancing direction is used for the purpose; typically, aspect ratios above 10 are desired. Downscaling of such an approach, commonly employed on conventional injection

molding, has been proposed for the investigation of filling behavior and processability during μIM of semicrystalline polymers (i.e., polypropylene and polyoxymethylene) as well as amorphous polymers (i.e., acrylonitrile-butadiene-styrene) [18]. Investigations are usually carried out by performing injection molding under different process factors affecting the replication capabilities and the filling performance of the process. Then, the achieved flow lengths in miniaturized channels, defined as the actual length reached by the melt during the molding, are determined and compared in order to establish the relation between flow lengths and process parameter settings (see Figures 13 and 14).

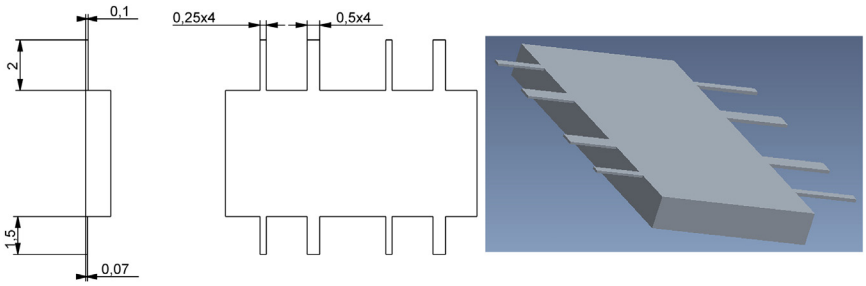

FIGURE 13

Part design for process analysis based on flow length test [18].

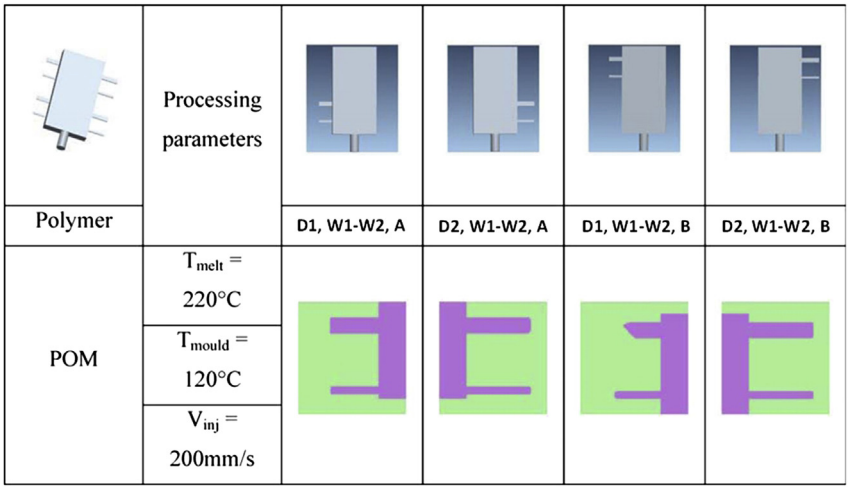

FIGURE 14

Flow length evaluation of micro-injection-molded features for different thicknesses (D1 = 70 μm, D2 = 100 μm), widths (W1 = 250 μm, W2 = 500 μm), and feature distance from the injection location (A = near the gate, B = far from the gate).

To identify which process parameters are the most influential on the achievable aspect ratios during the filling stage of the μIM process, the effects of process factors (e.g., barrel temperature, mold temperature, injection speed, holding pressure) and geometrical/dimensional factors (e.g., width, thickness) are investigated. The main processing conditions increasing the achievable flow length are determined by high settings of melt and mold temperatures and of the injection speed. A decrease of width and thickness of micro-channels limit the melt flow length because it leads to an increase of the surface-to-volume ratio in micro-cavities.

The venting of cavity is another aspect that has an effect on the achievable aspect ratio in μIM. Air entrapment in the cavity can counteract the effect of suitable processing conditions and limit the cavity filling capability of the micro-molding process. Process monitoring applied to different processing and venting conditions can be used to study the effects of air evacuation conditions in micro-cavities when replicating polymer micro-parts. The effects of melt and mold temperatures, type of air evacuation, and injection speed on micro-features flow length and airflow rates indicate that the considered process factors have a significant influence on airflow rate and mass of evacuated air. A mold design including an additional venting capability increases significantly the flow length and the uniformity of the flow front pattern. This is due to the combined effect of high process settings required in μIM and the limited venting through the primary split line of the mold, because of the high accuracy and surface quality of tools used in μIM, which have a significant impact on the filling performance. Micro-molding experiments using ABS (acrylonitrile butadiene styrene) on a micro-structured component have shown that the presence of additional cavity venting can extend the flow length by 30% under the same μIM processing conditions [19].

FILLING ANALYSIS IN μIM USING WELD LINES AS FLOW MARKERS

In injection molding, during the filling of cavities, when two or more flow fronts meet, an imperfection observable as a line is created. This defect of injection-molded parts is referred to as a weld line. Weld lines are influenced by material composition, mold design, and process conditions [20]. Particularly related to mold design, the basic situations that are conducive to weld line formation are the presence of [21] inserts in the cavity (i.e., insert molding, see Figure 15), two or more gates for the part filling, the presence of regions of varying depths, features in the mold (e.g., pins all through the thickness of the cavity). Weld lines are visible on the surface of the part (their depth was measured with the atomic force microscope and found to be in the range between 500 and 1500 nm [22]) and they are a clear trace of the development of the flow melt during the filling of the cavity (see Figures 16 and 17).

Therefore, weld lines can be used as flow markers and, in particular, represent the position of the flow front at the end of filling. The analysis of the positions of weld

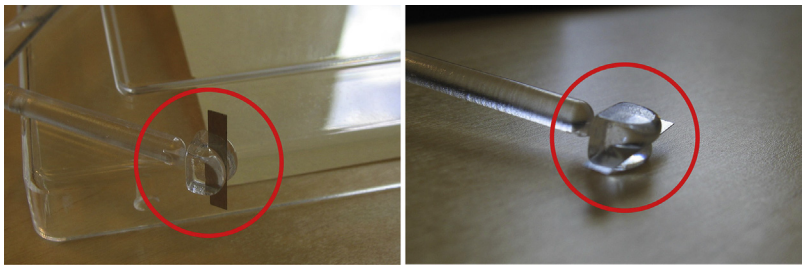

FIGURE 15

Weld line formation due to the presence of an insert in the cavity during insert molding [8].

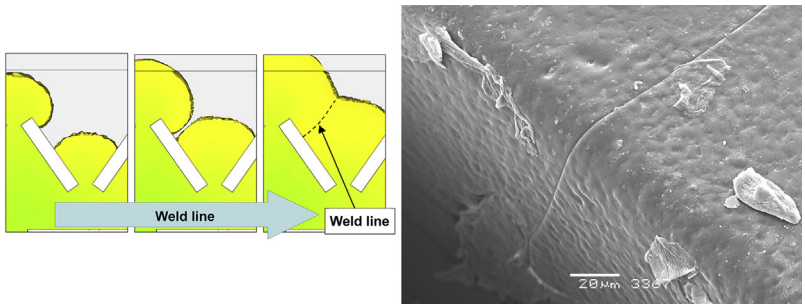

FIGURE 16

Simulation of the formation of a weld line due to the presence of a micro-feature (width = 200 µm) in the cavity (left). Scanning electron microscope images of the actual weld line shown in the simulation (polymer = polystyrene) (right) [8].

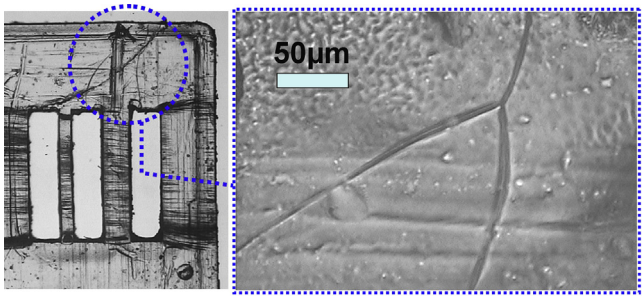

FIGURE 17

Optical image of weld lines due to melt flow front separation.

lines permits study of the influence of different processing conditions on the filling capability of the micro-molding process.

In fact, the different paths of weld lines obtained with the different settings of process parameters can be employed to study the effect of different process parameters and determine the conditions for better cavity filling conditions [23]. In particular, a variation of mold temperature and of injection speed produces modification of the path of the weld lines, pushing toward the end of micro-features as the polymer melt flows. For example, in the case of polystyrene, the effect of melt temperature and packing pressure was extremely limited.

The flow front depth of filling (i.e., the ease of the melt flow to fill micro-structures) increases with the width of the structures to be filled. The meeting points of weld lines out of channels 200- and 300-μm wide, as well as the horizontal weld line in the channel 150 μm, show such behavior (see Table 1).

Table 1 Experimental Depth of Filling Depending on the Channel Width

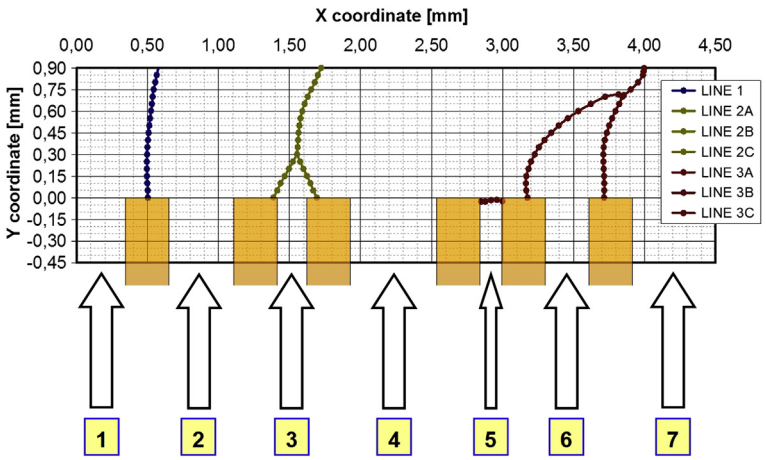

Channel No.	Width (μm)	Depth of Filling (μm)	End of Cavity
1	400	900	Yes
2	450	900	Yes
3	200	301	–
4	600	900	Yes
5	150	−22	–
6	300	710	–
7	600	900	Yes

Complete filling of micro-injection-molded features (i.e., a good filling performance) can be therefore obtained by using a high temperature of the mold (which decreases the viscosity of the melt and prevents premature solidification) and high injection speed (which also decreases the viscosity of the melt due to viscous thinning and viscous heating, as well as decreasing the injection time, thus avoiding premature short shots and incomplete filling). On the other hand, it is not convenient to increase the temperature of the melt, first due to the limited benefit on the filling performance, and second to avoid material degradation due to material overheating. An elevated packing pressure is also not advantageous because it can produce high internal tension on the polymer matrix as well as induce high stress on the mold itself.

μIM PROCESS CONTROL AND ANALYSIS

The reliable manufacturing of polymer-based micro-components on a mass production perspective is directly connected to the capability of controlling the μIM process. The influence of process parameters on μIM can be investigated with a mold with a sensor applied at injection location. It can be used to monitor actual injection pressure and to determine the cavity filling time (Figures 18–20).

At the injection location where the melt is pushed into the cavity (see Figure 21, detail A) by the injection piston, a piezoelectric pressure sensor is usually placed (see Figure 21, detail B). The recording of the in-cavity pressure at injection location over time is one of the methods to monitor conventional and μIM processes. It allows comparative studies to be performed on different process conditions and evaluation of the process repeatability when molding under the same process conditions. Moreover, especially in the case of micro-molding, it is a powerful method to calculate the cavity filling time which would not be possible by other means, since filling of micro-cavities takes place in times in the order of tens of milliseconds.

The cavity pressure profile, in μIM as well as in precision injection molding, is a factor directly correlated to the quality of the part [24]. The cavity pressure control, expressed in terms of both absolute value and repeatability (i.e., standard deviation), is fundamental for an optimized part and process realization and it is the critical process parameter for the precision molding of high accuracy thermoplastic parts [25] as micro-molded components. For example, an excessive value of the cavity pressure will lead to defects such as flashes (see Figure 22); whereas a large value of the standard deviation of the pressure indicates a poor cycle-to-cycle process repeatability (i.e., different filling conditions) and therefore different properties of the molded part.

Analysis of the cavity injection pressure shows that an increase of the temperature of the melt causes an increase of the cavity injection pressure. This is due to the fact that higher temperature reduces the melt viscosity, which has as a consequence the reduction of the pressure drop through the nozzle and runners, resulting in higher cavity injection pressure. To attain higher injection speed, a higher injection pressure

must be applied, which in turn increases the cavity injection pressure. The influence of the temperature is also of importance. At higher mold temperature, close to the glass transition temperature of the polymer, the melt viscosity is decreased, which in turn reduces the pressure drop, resulting in a higher cavity injection pressure.

The cavity injection pressure cycle-to-cycle repeatability can provide a valuable parameter to determine the process stability (see Figure 23). In micro-molding, a standard deviation in the order of 10−50 bar, which corresponds to a coefficient of variation between 1% and 5%, can be obtained [26,27]. As result of the high process repeatability, the mass of micro-molded parts in the 100-mg range can be reproduced with a standard deviation within 0.1−0.7 mg [26,28]. Dimensional accuracy of micro-moldings over repeated cycles is in the order of 0.1−1% of the measured characteristic feature (e.g., diameter, height, etc.), form error such as flatness and position error as concentricity lower than 5−10 μm can be obtained [29,30].

The injection pressure rises at the injection location and the subsequent reaching of the maximum cavity pressure can be employed to determine the cavity injection time (see Figures 23 and 24) under different process conditions. Due to the very short filling time in micro-molding (of the order of a few tens of milliseconds), sampling rates of the order of 5−25 kHz are recommended to be employed. Experimental results show that an increase of both the temperature of the mold and of the injection speed lead to a shorter cavity injection time, with injection speed having the greatest influence. The cavity injection time can be used also to estimate the cycle-to-cycle repeatability of the micro-molding process. Standard deviation values in the range between 1 and 3 ms are usually encountered during micro-molding (which correspond to a coefficient of variation lower than 1%).

Once the micro-injection molding process has been realized and its performance optimized, the key stage of demolding needs to be considered. High micro-molding process settings in terms of temperatures, injection speed, and packing pressure can contribute to increase the demolding force needed to eject the part. High temperature settings increase the surface replication at the polymer/mold interface creating a mechanical interlocking at the surface micro-topography level, which can have a detrimental effect on the integrity of the part due to higher ejection forces. High injection speed and packing pressure increase the demolding force as consequence of higher stresses induced in the parts. An increase of 20−25% of the demolding force at high mold temperature and packing pressure settings, respectively was observed during the injection molding of micro-fluidic systems using a cyclic-olefin-copolymer [31].

DEFECTS OF MICRO-INJECTION-MOLDED PARTS: WELD LINES

Weld lines are a reality of the injection molding of complex parts. Multiple gating, splitting of the melt flow due to inserts in the cavity or through-holes, as well as changes of thickness give rise to points within the structure where the flowing fronts

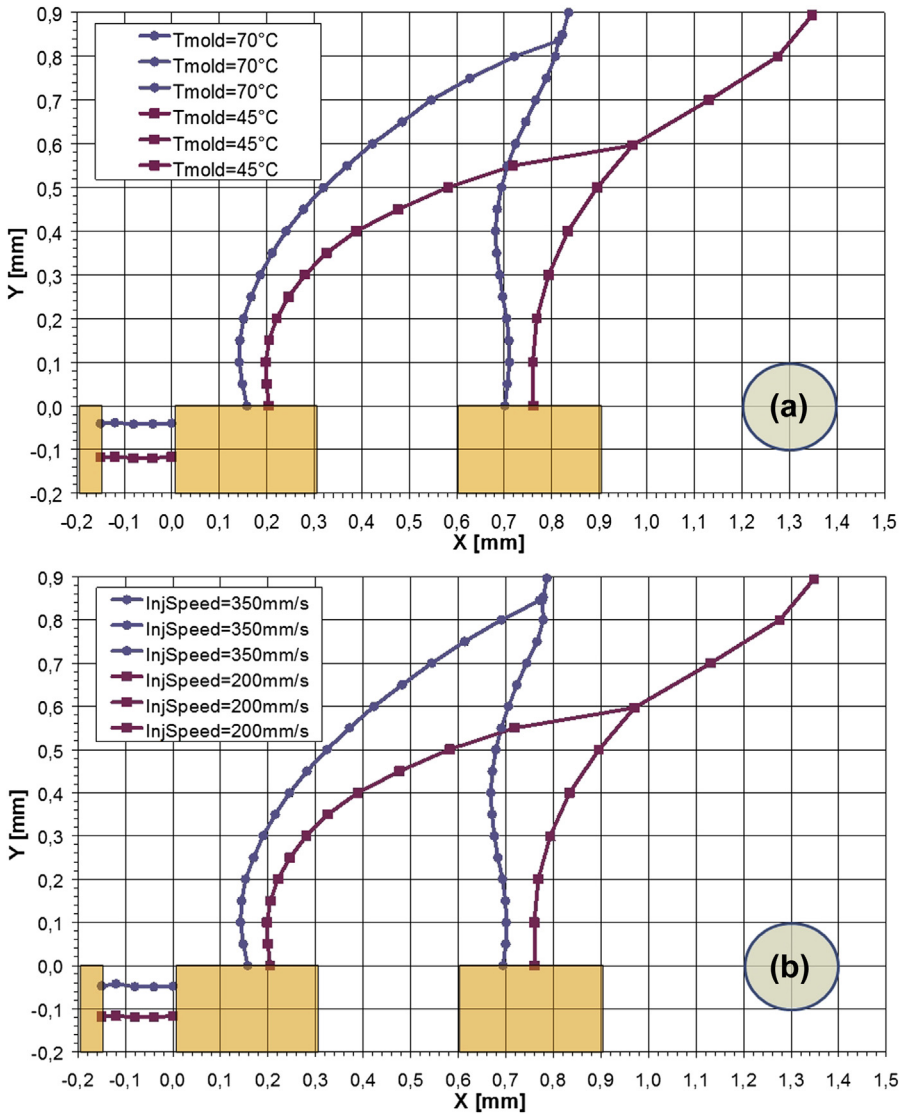

FIGURE 18

Effect of (a) mold temperature, (b) injection speed, (c) packing pressure, and (d) melt temperature on the positions of weld lines shown in Figure 17 [8].

will recombine and weld. An imperfection is observed as a line on the surface of the molded part (see Figure 25). In the molding of very complex components, a multiplicity of weld lines is generated. The weld lines are formed as the mold is being filled. Weld lines reduce the mechanical strength of components in the macro [21]

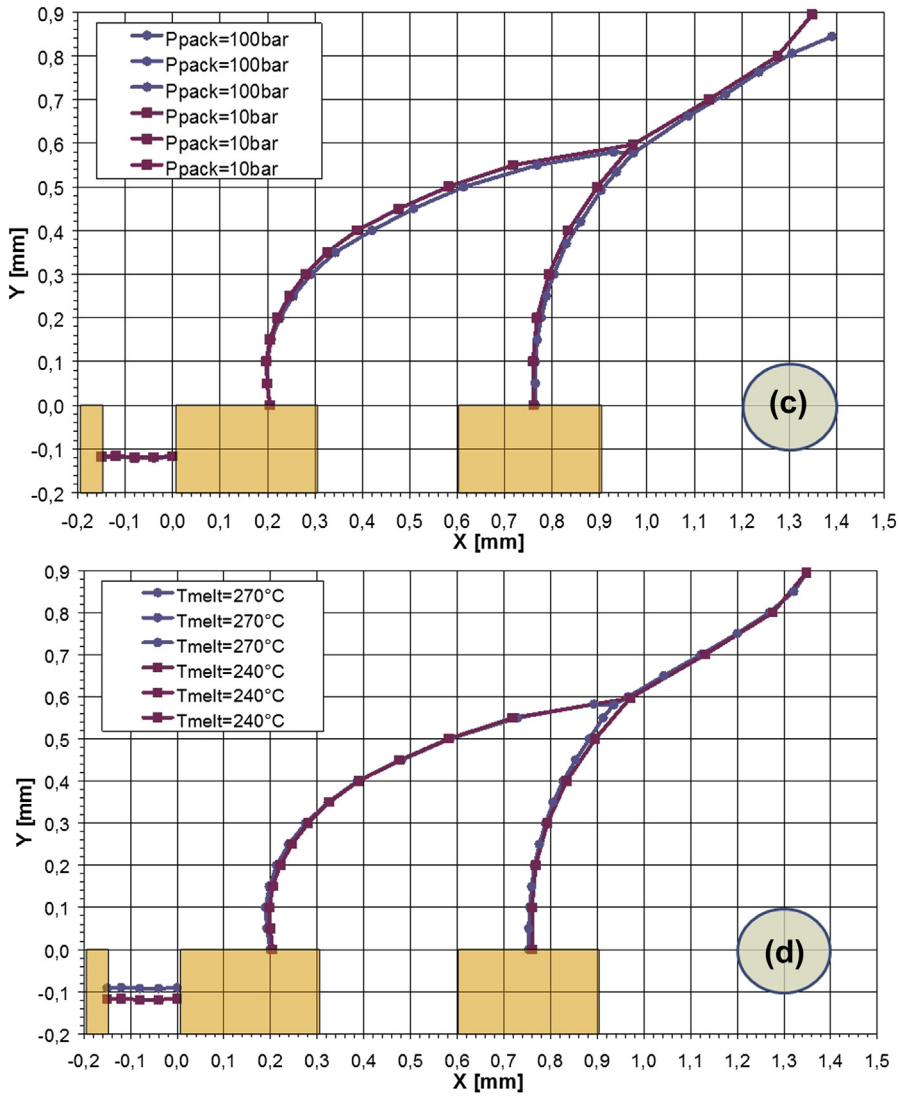

FIGURE 18 cont'd.

as well as in the micro-dimensional range [20,33]. In particular, an area where the properties are different from the bulk is created. Weld-line factors (defined as the ratio between the strength of workpieces containing a weld line and workpieces with the same geometry but without weld lines) as low as 20% were found on micro-injection-molded tensile strength specimens. The main causes are incomplete molecular entanglement or diffusion, the formation of V-notches at the weld surface,

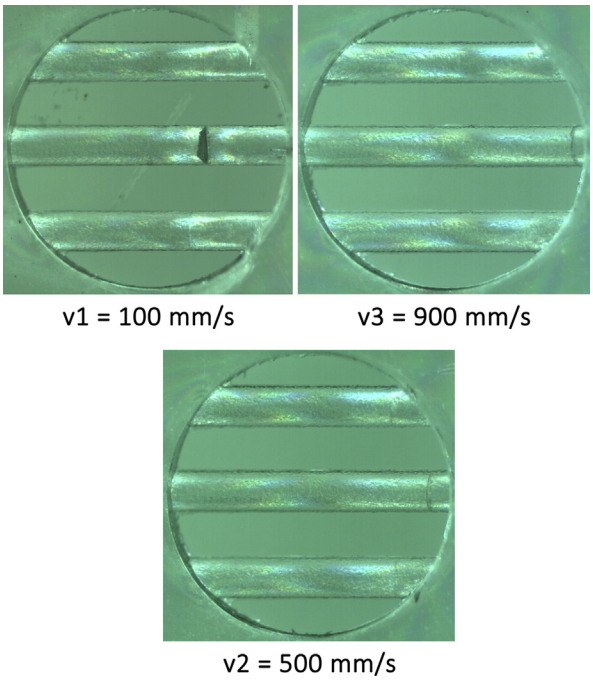

FIGURE 19

Injection molding of 300-μm wide micro-features: optical microscope images of the flow front position shift due to an increase of injection velocity (injection direction from left to right, $T_{melt} = 220\,°C$, $T_{mold} = 55\,°C$) [8].

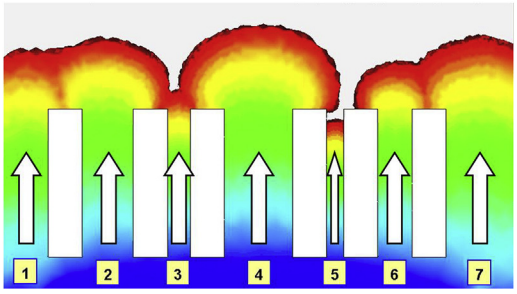

FIGURE 20

Simulated flow front pattern to be compared with weld lines used as flow markers [8].

the presence of contamination of micro-voids at the weld-line interface, and unfavorable molecular or fiber orientation at the weld [20] (Figures 26–28).

It is therefore of great importance to optimize the injection molding process, and especially the filling phase, in order to decrease such defects. In particular, injection

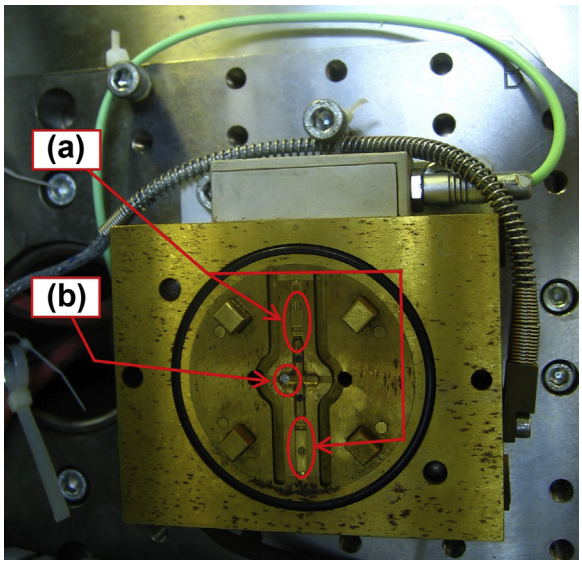

FIGURE 21

Two micro-cavity mold (a) equipped with in-cavity pressure sensor at injection location (b) [8].

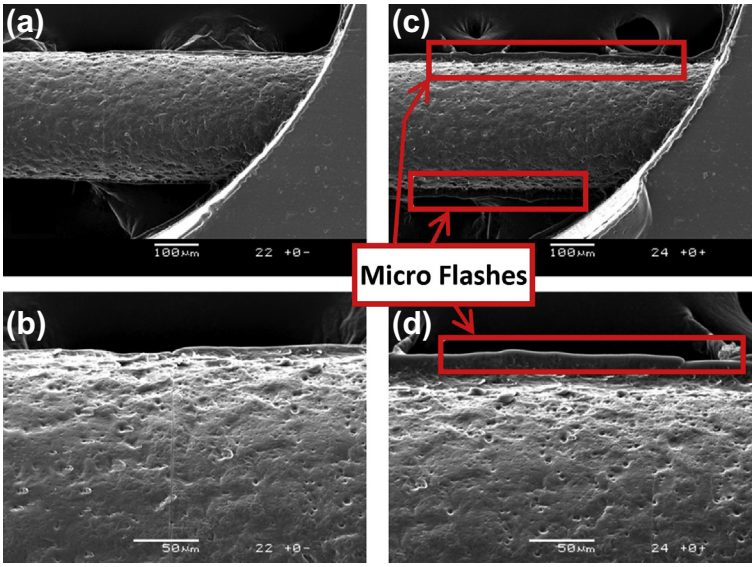

FIGURE 22

Effect of cavity injection pressure: micro-flashes do not occur at lower pressure (553 bar (a,b)) and appear at higher pressure (778 bar (c,d)). Melt temperature, mold temperature, and injection speed were: (a,b) 260°C, 70 °C, 100 mm/s and (c,d) 260°C, 70 °C, 900 mm/s [8].

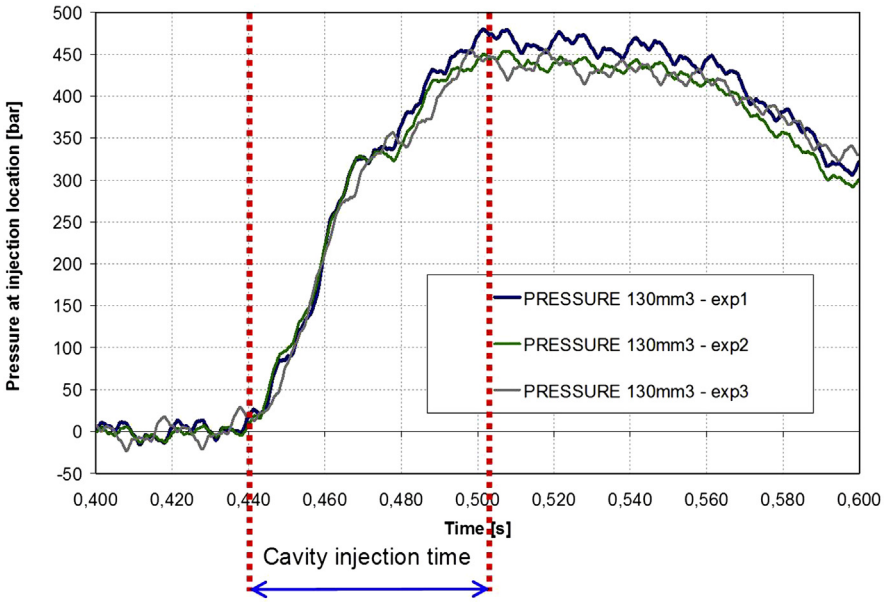

FIGURE 23

Cavity injection time determination from the cavity pressure versus time plot [8].

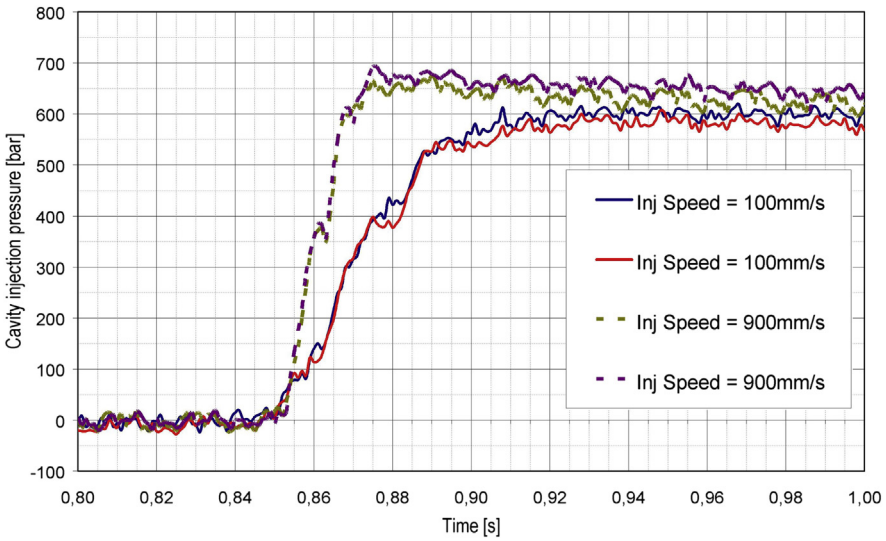

FIGURE 24

Pressure versus time curves from the in-cavity sensor. Moldings at two different injection speeds (100 and 900 mm/s) are shown. Temperatures of the melt and of the mold were 220 °C and 55 °C, respectively. In the chart, two curves sampled from the same molding, carried out under the same processing conditions, are shown. The increase of the injection speed produced a decrease of the average cavity injection time from 67 to 30 ms and an increase of the average maximum cavity injection pressure from 612 to 672 bar [8].

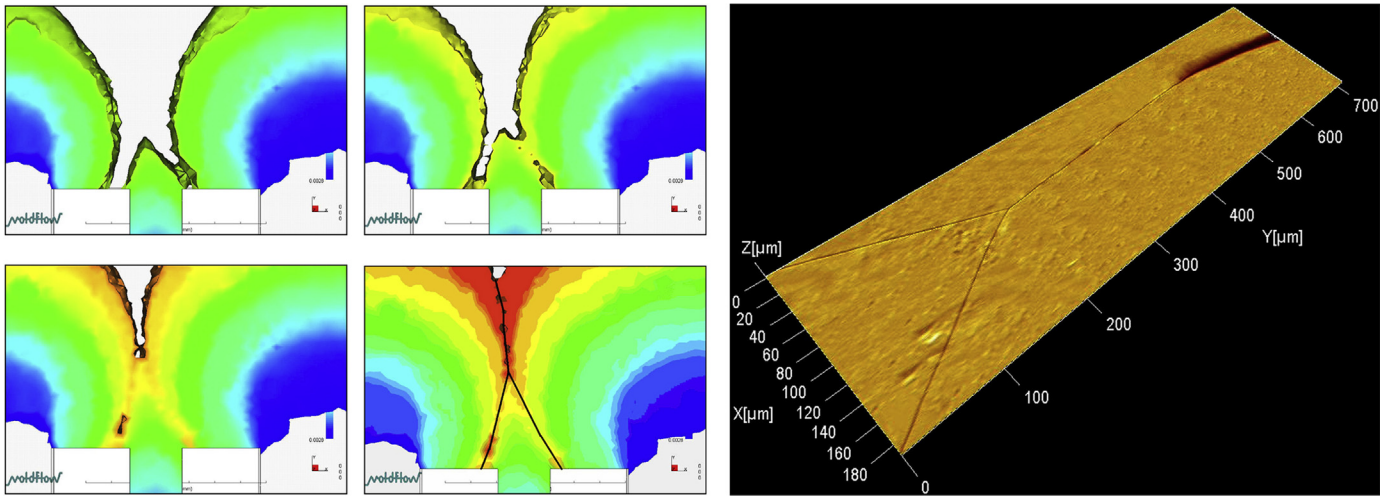

FIGURE 25

Simulation of the formation of a weld line due to the presence of two micro-features and the meeting of three melt flow fronts (left) and large-range AFM scanning of the actual meeting area on a polystyrene micro-molded part (right). The large-range scanning of 700 × 200 μm was obtained using a software tool for stitching three-dimensional surface topography data sets [32]: 18 different scannings (50 × 100 μm) were employed for the reconstruction [8].

speed and mold temperature set at a convenient level can be beneficial in order to decrease the depth and width of weld lines (see Figures 29–31). A higher temperature of the mold allows a higher molecular mobility (i.e., lower viscosity) which permits obtaining of smaller weld lines. Higher injection speed causes a decrease of the injection time, which has the consequence of avoiding premature freezing of the polymer melt, allowing higher mobility of the polymer at the interface melt front/mold surface. As a conclusion, higher temperature of the mold and higher injection speed are preferable when molding micro-components with polystyrene polymer grade in order to decrease the importance of weld lines.

Furthermore, the position of the gate with respect to a considered area of the part with weld lines is also important. In particular, the longer the flow length, the larger the weld lines that will form. Increase of width and depth of 30% were observed when measuring weld lines far from the gate compared with weld lines near to the gate. To this respect, multigating solutions can be employed to shorten the flow length along the part of the polymer melt during the filling of the cavity (see Figure 32).

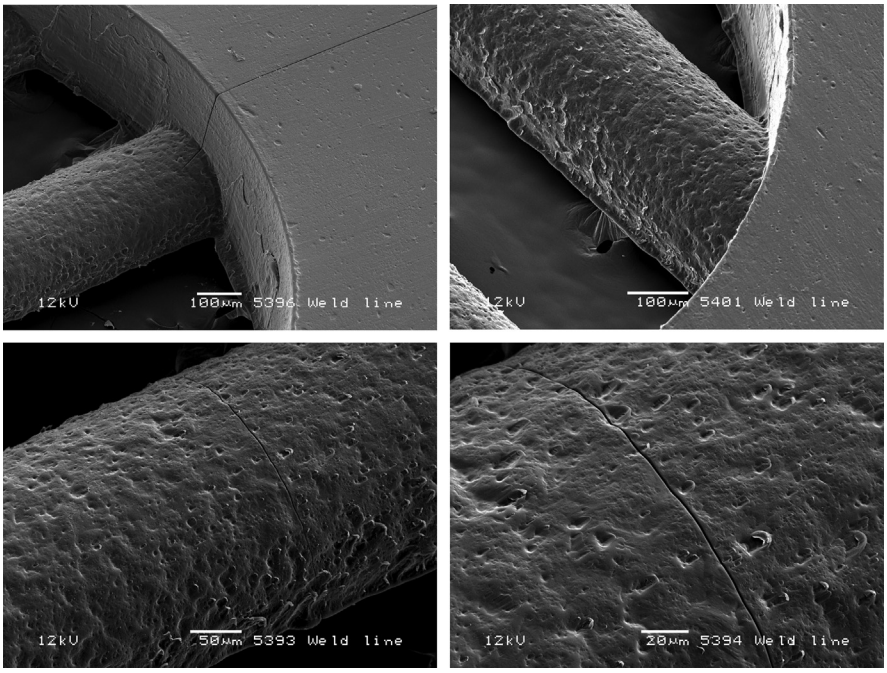

FIGURE 26

Scanning electron microscope images of weld lines on the surface of the 300-μm wide microfeatures [8].

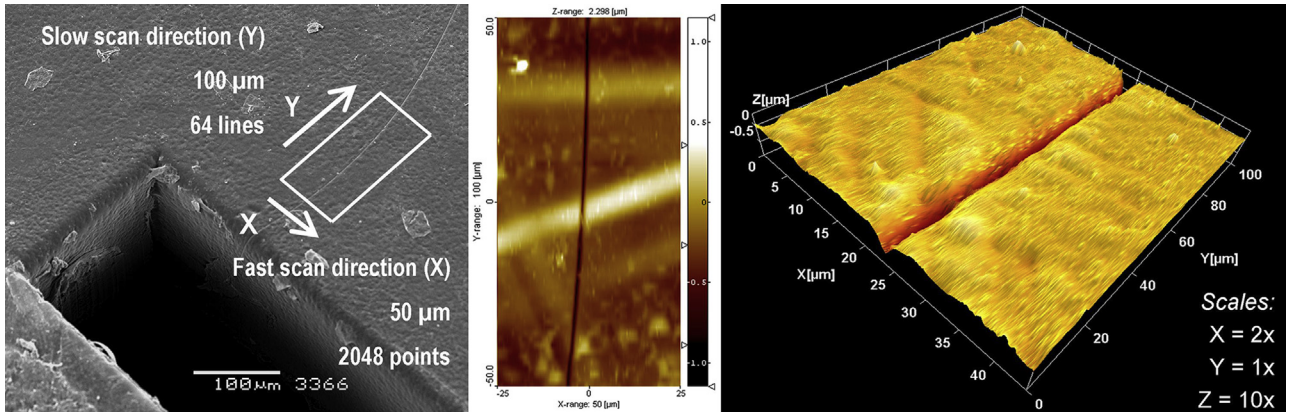

FIGURE 27

Atomic force microscope measurement of weld lines produced at the meeting area of two flow fronts [8].

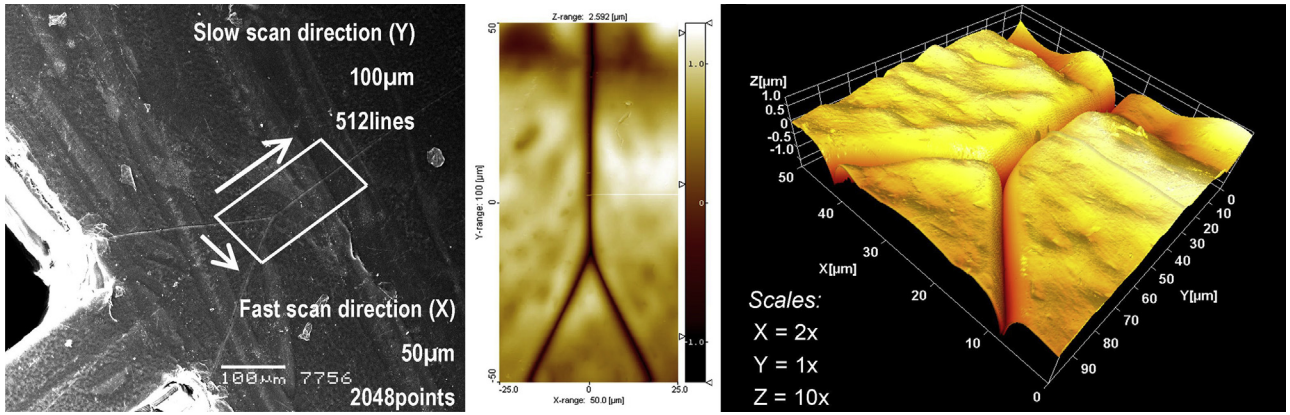

FIGURE 28

Atomic force microscope measurement of weld lines produced at the meeting area of three flow fronts [8].

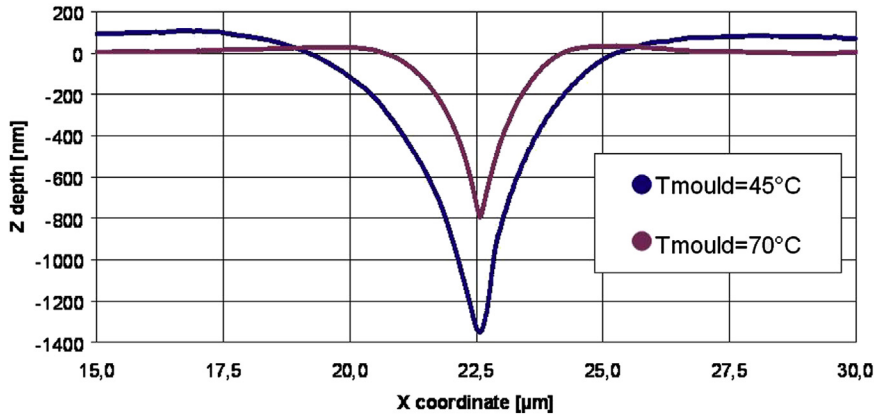

FIGURE 29

Effect of the temperature of the mold on the weld line profile [8].

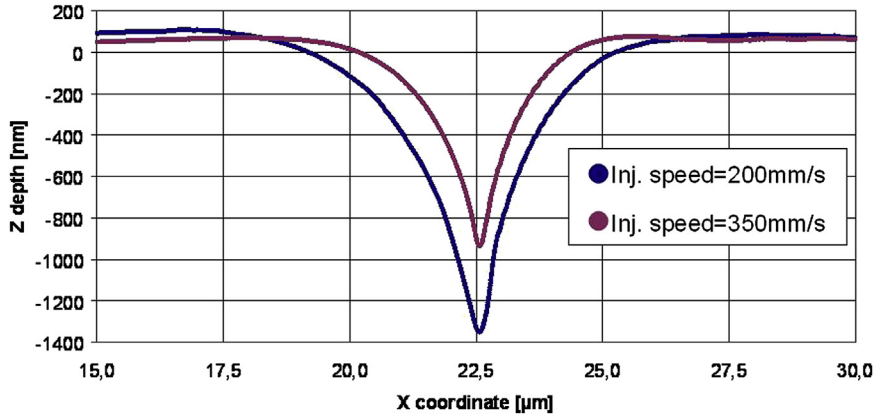

FIGURE 30

Effect of the injection speed on the weld line profile [8].

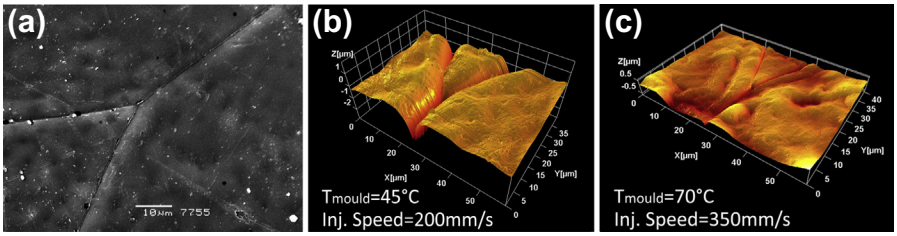

FIGURE 31

Three-dimensional visualization of the effect of temperature of the mold and of injection speed on weld line topography: (a) scanning electron microscope image of the weld lines meeting point; atomic force microscope of weld line obtained at (b) mold temperature = 45°C, injection speed = 200 mm/s, (c) mold temperature = 70°C, injection speed = 350 mm/s [8].

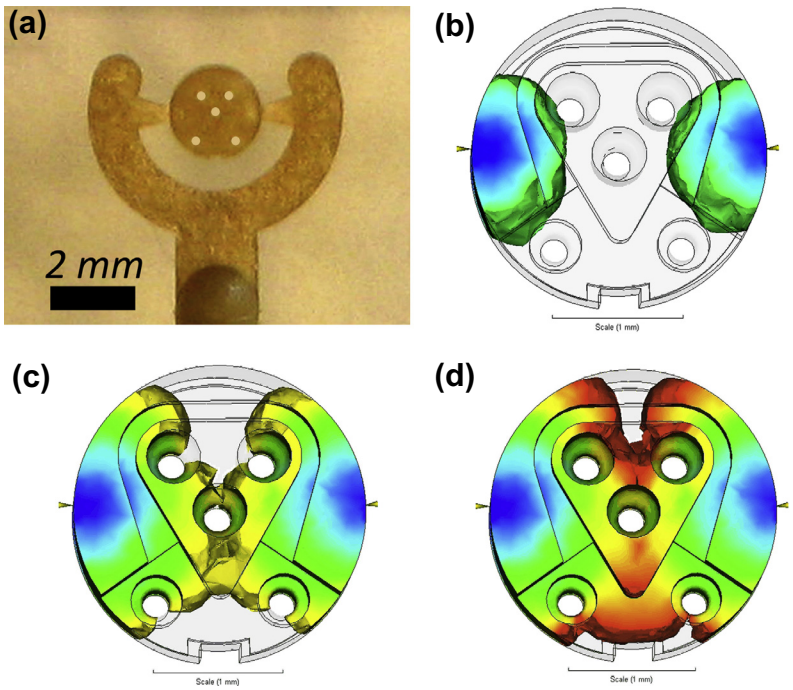

FIGURE 32

Multigating design of a polymer micro-product produced by injection molding (hole diameter is 300 μm): (a) micro molded part; simulated flow fronts position at (b) 40%, (c) 75% and (d) 95% cavity fill volume. [8].

PROCESS SIMULATION

Simulation programs in polymer replication micro-technology are applied with the same purposes as in conventional injection molding. To avoid the risks of costly reengineering, the functions of the final products as well as the manufacturing steps are simulated extensively before starting the actual manufacturing process: important economic factors are the optimization of the molding process and of the tool, using different simulation techniques.

In polymer micro-manufacturing technology, software simulation tools adapted from conventional injection molding can provide useful assistance for the optimization of molding tools, mold inserts, micro-component designs, and process parameters.

At present, commercially available simulation tools can work adequately from a qualitative point of view but numerical values cannot be calculated as precisely as necessary [34] and therefore simulation is not integrated in the product development process as extensively as for macro-products. A dedicated software module

developed for μIM is still not available and therefore experimental validation of simulation results is needed. To assess and optimize the performance of commercial simulation software for modeling of micro-scale polymer flows, results from μIM process monitoring (e.g., sensor measurements), part quality control (e.g., in-process flow visualization, short shots method), material characterization (e.g., rheology measurements) have been employed. The calibration data for quantitative validation of simulative results are a critical factor for all comparisons. In addition, most programs have difficulties in simulating exactly the filling of micro-structures with high aspect ratio. The reason is that commercial software tools developed for macroscopic applications do not consider microscopic aspects properly.

The main limitations encountered are related to the fact that the rheological data used in current packages are obtained from macroscopic experiments and that a no-slip boundary condition is employed, with the consequence that wall slip cannot be predicted [35]. Moreover, surface tension is not taken into account, but plays a role on the filling of micro-structures [36]. Usually a constant heat transfer coefficient is assumed, but it cannot describe the flow through micro-channels [35,37] and its standard value suitable for the simulation of macro-parts differs substantially from values indicated for μIM [37–39]. Moreover, rheology data provided by the software's database are obtained at shear rates and pressures typical of capillary rheometers (i.e., over significantly lower ranges if compared with those of micro-molding), and therefore are not directly applicable and not suitable for micro-scale polymer flow applications.

However, a proper implementation strategy employed during the set up of the simulation can improve the quality (i.e., the accuracy) of the simulated results. There are a number of aspects to be considered in order to improve existing software packages' results [40]:

- **At the machine–software interface boundary:** the implementation of the actual injection speed profile during the filling stage of the cavity and the verification of the actual cavity injection time [41]. The injection speed is the most affecting parameter in terms of prediction accuracy of flow length, shear stress, and melt temperature and it needs to be implemented in the simulation filling setting according to the strategy adopted in the μIM machine injection unit control (e.g., the injection profile could be controlled either in a speed vs time, or in speed vs position configurations).

  Further, the nozzle geometry has a large effect on the cavity pressure compared with the injection pressure; it has to be considered during both pre-processing (i.e., the geometry model preparation) and postprocessing (i.e., the evaluation of simulated pressure results) and should be included in the simulation model [42,43].
- **Part modeling guidelines:** three-dimensional modeling of the whole molding system including sprue, runner, gate, mold block, part, and micro-features, to consider the meshing tolerance compared to the actual dimensions of the micro-features: a tolerance between the meshed model and the solid

geometry of 10 μm or lower should be maintained to ensure volume conservation and correct geometrical representation of the micro-part and its micro-features. The full molded geometry, including sprue, runners, gates, and cavities need to be simulated in order to calculate actual filling times, injection pressure, shear stress, melt temperature in the cavity [44,45] (see Figures 34).

- **Concerning mesh element size:** typical mesh size (i.e., element edge length) settings to achieve the validation of micro-molding simulation results are in the sub-millimeter to 100-μm range for miniaturized sprue and runners; in the sub-100 to 100-μm range for the micro-molded part, depending on cross-section thickness; micro-features and gating areas could have even higher density mesh with element size down to 10 μm. Best accuracy of simulation results can be obtained with a number of at least 10 elements across the section [46,47] (see Figures 34d and 35).
- **Regarding the material characterization:** the use of experimental micro-rheological data of the polymer material instead of the default rheology available in the software database, to use experimental data obtained with micro-sized cavities (see Figure 33) and high-speed rheometry experiments (at higher shear rates of 10^6 1/s and higher) [8,48–50].

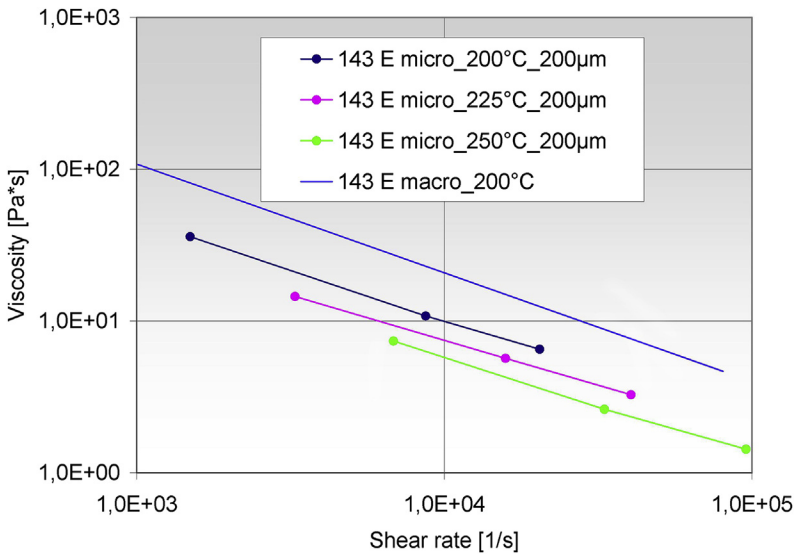

FIGURE 33

Polystyrene 143 E micro-rheology curves for a channel 200-μm wide at melt temperatures of 200, 225, and 250 °C and 143 E macro-rheology at 200 °C (i.e., obtained with conventional capillary rheometer). Viscosity of polymer melt flowing in micro-channels is lower than in the macro-dimensional range due to the wall-slip effect [8].

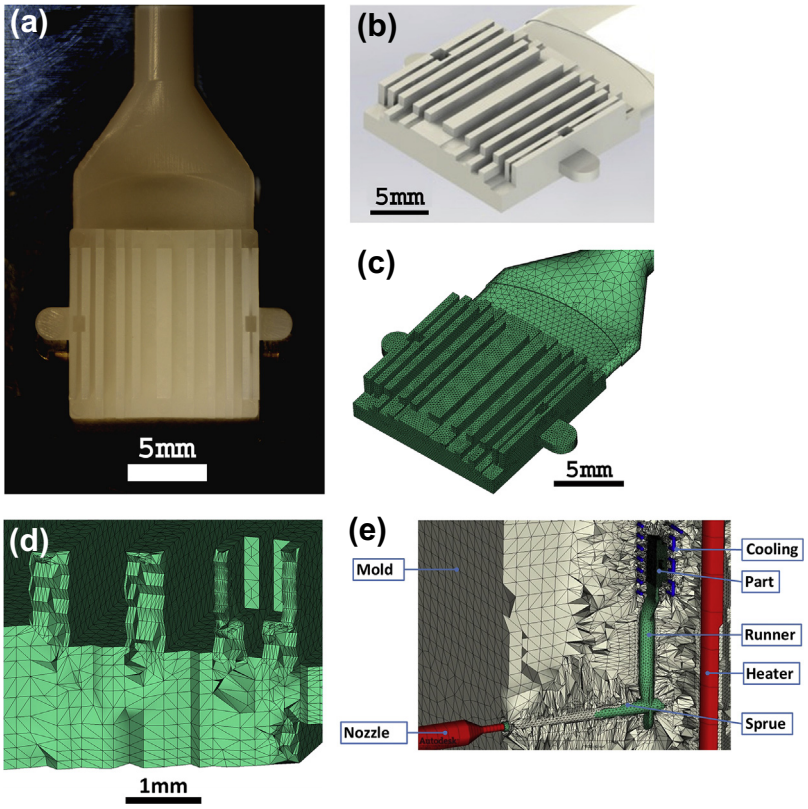

FIGURE 34

(a) Micro-injection-molded part (material = polyoxymethylene); (b) three-dimensional meshing of the part including the gate; (c) three-dimensional modeling of part and micro-features; (d) three-dimensional mesh of the part and its micro-features with 10 layers of element in the thickness direction; (e) three-dimensional mesh of the complete molding system including mold block, nozzle, sprue, runner, part, heating elements, cooling channels.

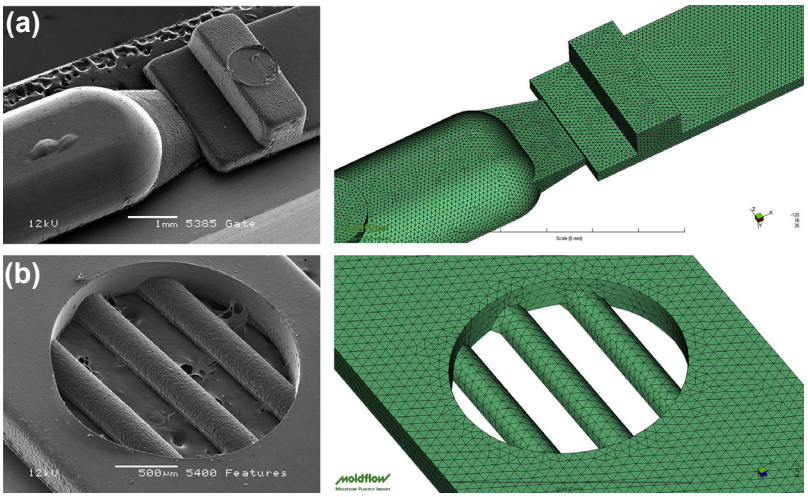

FIGURE 35

Accurate 3D meshing (right) of gate (a) and micro-features (b) (width = 300 μm) of micro-injection-molded part (left) [8].

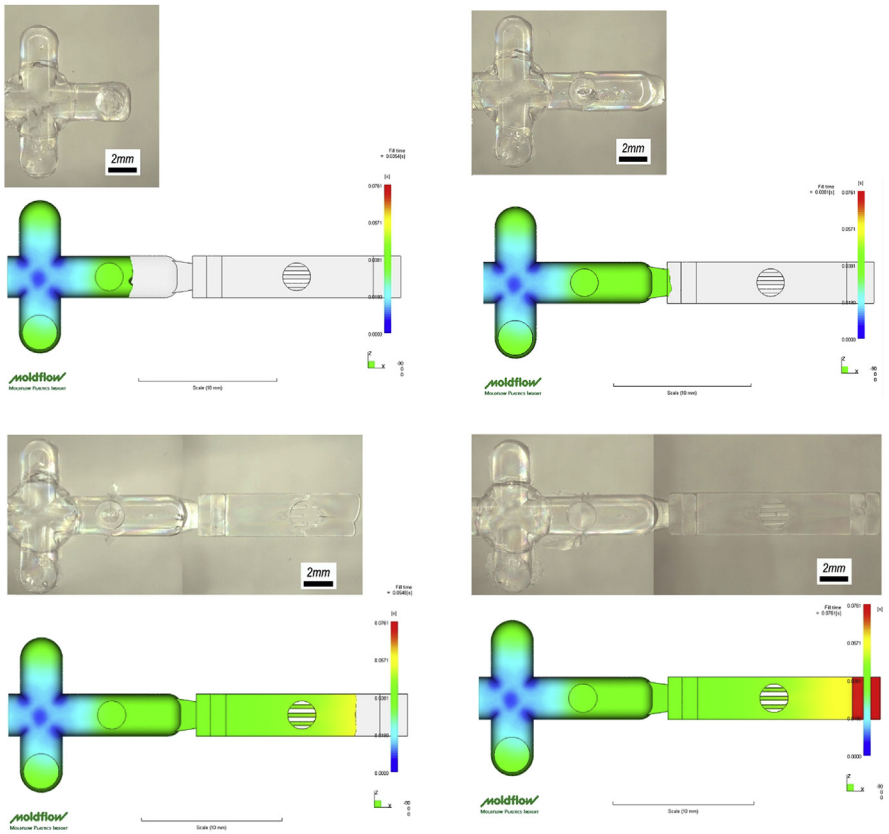

FIGURE 36

Experimental and simulated short shots method: flow front positions at (a) 42%, (b) 58%, (c) 81% and (d) 100% of the total fill volume [8].

Optimized simulations can provide results with improved accuracy and they can effectively be employed to validate μIM experimental results in terms of cavity injection pressure, cavity injection time, mass/length/flow pattern of short shots and full part (see Figure 36), weld lines position [41,46], optimized micro-molding design features such as runner system configuration and dimensions [45], as well as increase in the μIM process understanding by verifying critical conditions of the melt flow such as shear stress, melt flow front temperatures [51], flow micro-jetting [46], and surface micro-features replication [52–55].

CONCLUSIONS

μIM is recognized as a manufacturing process enabling the mass fabrication of polymer micro-components. Fundamental process parameters for the control of both the

micro-product and the process are the temperature of the melt, the temperature of the mold, the injection speed, and the cavity injection pressure. Process simulation can be used for polymer micro-product and process design, and can provide at the present time mostly qualitative input to the designer and the process engineer. Further, process analysis methods and optimization tools are being used in order to provide reliable validation of both process and simulations.

REFERENCES

[1] Heckele M, Schomburg WK. Review on micro molding of thermoplastic polymers. J Micromech Microeng 2004;14(3):R1−14.

[2] Turng L-S. Special and emerging injection molding processes. J Injection Molding Technol 2001;5(3):160−79.

[3] Whiteside BR, Martyn MT, Coates PD. Introduction to micromolding. In: Greener J, Wimberger-Friedl R, editors. Precision injection moulding. Munich (Germany): Hanser; 2006. p. 239−64.

[4] Piotter V, Bauer W, Benzler T, Emde A. Injection molding of components for microsystems. Microsyst Technol 2001;7(3):99−102.

[5] Michaeli W, Spennemann A. Micro injection moulding − improving the efficiency of a classical processing technology. In: Proceedings of international conference on microtechnologies: MICRO.tec 2000, vol. 2; 2000. p. 593−6.

[6] Michaeli W, Spennemann A, Gärtner R. New plastification concepts for micro injection moulding. Proc Conf Micro Syst Technol 2002;8:55−7.

[7] Ganz M. Micro injection moulding and compression moulding, Workshop at the 1st international conference on multi-material micro manufacture (4M): polymer technology toward nano, future technology for Europe, Karslruhe (Germany) (June 29−July 1, 2005).

[8] Tosello G. Precision moulding of polymer micro components [Ph.D. thesis]. Department of Mechanical Engineering, Technical University of Denmark, ISBN 978-87-89502-77-9; 2008.

[9] Han X, Yokoi H. Visualization analysis of the filling behaviour of melt into microscale V-groove during the filling stage of injection molding. Polym Eng Sci 2006;46(11): 1590−7.

[10] Sodick Plustech. V-LINE two-stage plunger system − precision injection molding machines, http://www.plustech-inc.com/technology.htm; [last access February 2014].

[11] Männer. Micro moulding systems, http://www.maenner-group.com/text2/233/en/jump,233/hot-runner/micro-molding-systems/micro-maen-50.html; [last access February 2014].

[12] Wittmenn-Battenfeld. MicroPower series − for small, high-precision and micro injection molding, http://www.wittmann-group.com/injection-molding/electric/micropower-5-15.html; [last access February 2014].

[13] DesmaTec. Micro injection moulding machine for small shot weights, http://www.desmatec.com/en/machines/micro_injection/micro_injection.php; [last access February 2014].

[14] Arburg. Micro moulding on ALLROUNDERs, http://www.arburg-injection-moulding-machines.com/micro-moulding.htm; [last access February 2014].

[15] Whiteside BR, Spares R, Coates PD. Rheo-optical measurements in micromoulding. In: Society of plastics engineers − 67th annual technical conference (ANTEC2009), Chicago (Illinois, USA) (22−26 June 2009); 2009. p. 1803−10.
[16] Yang SY, Nian SC, Sun IC. Flow visualization of filling process during micro-injection molding. Int Polym Process 2002;17(4):354−60.
[17] Spares R, Whiteside BR, Coates PD. High speed thermal imaging of micromoulding. In: Society of plastics engineers − 67th annual technical conference (ANTEC2009), Chicago (Illinois, USA) (22−26 June 2009); 2009. p. 2570−3.
[18] Sha B, Dimov S, Griffiths C, Packianather MS. Micro-injection moulding: factors affecting the achievable aspect ratios. Int J Adv Manuf Technol 2007;33:147−56.
[19] Griffiths CA, Dimov SS, Scholz S, Tosello G. Cavity air flow behavior during filling in microinjection molding. J Manuf Sci Eng Trans ASME Am Soc Mech Eng February 2011;133(1):011006. http://dx.doi.org/10.1115/1.4003339 (10 pages).
[20] Wu CH, Liang WJ. Effect of geometry and injection-molding parameters on weld line strength. Polym Eng Sci 2005;45(7):1021−30.
[21] Fellahi S, Meddad A, Fisa B, Favis BD. Weld lines in injection molded parts: a review. Adv Polym Technol 1995;14(3):169−95.
[22] Tosello G, Gava A, Hansen HN, Lucchetta G, Marinello F. Characterization and analysis of weld lines on micro injection moulded parts using atomic force microscopy (AFM). Wear 2009;266(5−6):534−8 (Metrology and Properties of Engineering Surfaces).
[23] Tosello G, Gava A, Hansen HN, Lucchetta G. Study of process parameters effect on the filling phase of micro injection moulding using weld lines as flow markers. J Adv Manuf Technol 2010:81−97. http://dx.doi.org/10.1007/s00170-009-2100-1.
[24] Varela AE. Self-tuning pressure control in an injection moulding cavity during filling. Chem Eng Res Des Trans IChemE 2000;8:A:79−86.
[25] Kazmer D, Barkan P. The process capability of multi-cavity pressure control for the injection molding process. Polym Eng Sci 1997;37(11):1880−95.
[26] Tosello G, Hansen HN, Guerrier P. Process condition monitoring of micro moulding using a two-plunger micro injection moulding machine. In: 7th international conference on multi-material micro manufacture (4M/ICOMM 2010), Bourg en Bresse and Oyonnax (France), 17−19 November 2010, vol. 138; 2010, ISBN 978-981-08-6555-9. p. 283−6. http://dx.doi.org/10.3850/978-981-08-6555-9. Research Publishing.
[27] Tosello G, Hansen HN, Schoth A. Process and part filling control in micro injection molding. In: Society of plastics engineers − 66th annual technical conference (ANTEC2008), Milwakee (Wisconsin, USA), 4−8 May 2008; 2008. p. 2529−33.
[28] Attia UM, Alcock JR. Optimising process conditions for multiple quality criteria in micro-injection moulding. Int J Adv Manuf Technol 2010;50:533−42.
[29] Tosello G, Hansen HN, Gasparin S. Applications of dimensional micro metrology to the product and process quality control in manufacturing of precision polymer micro components. Ann CIRP Int Acad Prod Eng 2009;58(1):467−72.
[30] Marson S, Attia UM, Lucchetta G, Wilson A, Alcock JR, Allen DM. Flatness optimization of micro-injection moulded parts: the case of a PMMA microfluidic component. J Micromech Microeng 2011;21:115024 (9pp). http://dx.doi.org/10.1088/0960-1317/21/11/115024.
[31] Tosello G, Griffiths CA, Dimov SS, Scholz SG, Rees A, Whiteside B, et al. Analysis of demoulding in micro injection moulding of cyclic-olefin-copolymer microfluidic

systems. In: International conference on multi-material micro manufacture (4M 2013), san Sebastian (Spain), 8−10 October 2013; 2013. p. 65−8.
[32] Marinello F, Bariani P, De Chiffre L, Hansen HN. Development and analysis of a software tool for stitching three dimensional surface topography data sets. Meas Sci Technol 2007;18:1404−12.
[33] Xie L, Ziegmann G, Hlavac M, Wittmer W. Effect of micro tensile sample's cross section shape on the strength of weld line in micro injection molding process. Microsyst Technol 2009;15:1031−7.
[34] Piotter V, Mueller K, Plewa K, Ruprecht R, Hausselt J. Performance and simulation of thermoplastic micro injection molding. Microsyst Technol 2002;8:387−90.
[35] Kemann O, Weber L, Jeggy C, Magotte O, Dupret F. Simulation of the micro injection moulding process. In: Society of Plastics Engineering (SPE) - 58th Annual Technical Conference (ANTEC2000), vol. 1. 2000. p. 576−580.
[36] Cao W, Hassager O, Wang Y. Surface tension effect on micro injection molding. In: Polymer processing society (PPS) 24th annual meeting proceedings S08; 2008. p. 141.
[37] Yu L. Experimental and numerical analysis of injection moulding with microfeatures [Ph.D. thesis]. Ohio University; 2004.
[38] Gava A, Tosello G, Lucchetta G, Hansen HN, Salvador M. A new approach for the validation of filling simulations in micro injection moulding. In: Proceedings of 9th international conference on numerical methods in industrial forming processes (NUMIFORM); 2007. p. 307−12.
[39] Nguyen-Chung T, Jüttner G, Löser C, Pham T, Gehde M. Determination of the heat transfer coefficient from short-shots studies and precise simulation of microinjection molding. Polym Eng Sci 2010;50(1):165−73.
[40] Tosello G, Griffiths CA, Hansen HN, Dimov SS. The COTECH knowledge database: assessment of critical factors in micro moulding. In: Proceedings of international conference on multi-material micro manufacture (4M 2012), Vienna (Austria), 9−11 October 2012, ISBN 978-981-07-3353-7. p. 229−36. Research Publishing.
[41] Tosello G, Gava A, Hansen HN, Reinecke H, Lucchetta G, Schoth A. Influence of different process settings conditions on the accuracy of micro injection molding simulations: an experimental validation. In: Society of plastics engineers − 67th annual technical conference (ANTEC2009), Chicago (Illinois, USA) (June 22−26, 2009); 2009. p. 1787−93.
[42] Costa F, Tosello G, Whiteside BR. Best practice strategies for validation of micro moulding process simulation. In: Polymer process engineering '09 conference (PPE'09). Bradford (United Kingdom); 27−28 October 2009. ISBN 13 978 1 85143. 262 2. p. 331−64.
[43] Vietri U, Sorrentino A, Speranza V, Pantani R. Improving the predictions of injection molding simulation software. Polym Eng Sci 2011;51(12):2542−51.
[44] Tosello G, Schoth A, Hansen HN. Implementation strategies for the optimization of micro injection moulding simulations. In: 4th international conference on multi-material micro manufacture (4M2008) Cardiff (United Kingdom) September 9−11, 2008; 2008. p. 271−4.
[45] Griffiths CA, Dimov SS, Brousseau EB. Microinjection moulding: the influence of runner systems on flow behaviour and melt fill of multiple microcavities. Proc Inst Mech Eng Part B J Eng Manuf 2008;222(9):1119−30.
[46] Tosello G, Costa H, Hansen HN. Micro injection moulding high accuracy three-dimensional simulations and process control. In: Proceedings of polymer process

engineering 11 − enhanced polymer processing. Bradford (UK); 6−7 December 2011. ISBN 13 978 1 85143 268 4. p. 413−35.

[47] Marhöfer DM, Tosello G, Hansen HN, Islam A. Advancements on the simulation of the micro injection molding process. In: International conference on multi-material micro manufacture (4M 2013), San Sebastian (Spain), 8−10 October 2013; 2013. p. 77−81.

[48] Chien RD, Jong WR, Chen SC. Study on the rheological behaviour of polymer melt flowing through micro-channels considering the wall-slip effect. J Micromech Microeng 2005;15(8):1389−96.

[49] Chen C-S, Chen S-C, Liaw W-L, Chien R-D. Rheological behavior of POM polymer melt flowing through micro-channels. Eur Polym J 2008;44:1891−8.

[50] Kelly AL, Gough T, Whiteside BR, Coates PD. High shear strain rate rheometry of polymer melts. J Appl Polym Sci 2009;114(2):864−73.

[51] Griffiths CA, Dimov SS, Brousseau EB, Packianather MS. The finite element analysis of melt flow behaviour in micro-injection moulding. Proc Inst Mech Eng Part B J Eng Manuf 2008;222(9):1107−18.

[52] Tosello G, Hansen HN, Islam A. Two-component injection moulding simulation of ABS-POM micro structured surfaces. In: Proceedings of the 13th international conference of euspen (European society of precision engineering and nanotechnology), 27−30 May 2013, Berlin, Germany, vol. 2; 2013, ISBN 978-0-9566790-2-4. p. 47−50.

[53] Lee JG, Bong-Kee L, Kang TG, Kwon TH. Experimental and numerical investigation of injection molding with microrib patterns. Polym Eng Sci 2010;50(6):1186−98.

[54] Tada K, Fukuzawa D, Watanabe A, Ito H. Numerical simulation for flow behaviour on micro- and nanomoulding. Plast Rubber Compos Macromol Eng 2010;39(7):321−6.

[55] Yang C, Li L, Huang H, Castro JM, Yi AY. Replication characterization of microribs fabricated by combining ultraprecision machining and microinjection molding. Polym Eng Sci 2010;50(10):2021−30.

CHAPTER

10 Net Shape Manufacture of Freestanding Ceramic Micro-components through Soft Lithography

Hany Hassanin, Kyle Jiang
School of Mechanical Engineering, The University of Birmingham, Birmingham, West Midlands, UK

CHAPTER OUTLINE

INTRODUCTION

The advent in micro-electromechanical systems (MEMS) through the past decade has been the driving force for the development of manufacturing techniques for high-temperature resistant micro-components. Most MEMS technology-based micro-components are constructed using silicon-based materials fabricated using conventional technologies such as UV lithography, etching, or micro-machining. However, silicon does not withstand the high temperature, which poses one of the biggest technical challenges in several high-temperature applications. Ceramics have outstanding properties such as high temperature resistance, high wear resistance, and high compression strength [1–3].

Conventional ceramic-forming techniques are well established for shaping fine features in the millimeter scale. However, it is a challenging to get net shape ceramic parts when they have micrometer size features. Additive manufacturing (AM) is a group of fabrication processes where three-dimensional parts are constructed by adding layers of materials on point, line, or planar surfaces. The structure formation of this technique is computer controlled. AM is a direct writing technique, which does not require molds. A moving device such as laser, light, or ink-jet performs the shaping of the designed pattern. Objects in this technique are created

Micromanufacturing Engineering and Technology. http://dx.doi.org/10.1016/B978-0-323-31149-6.00010-4

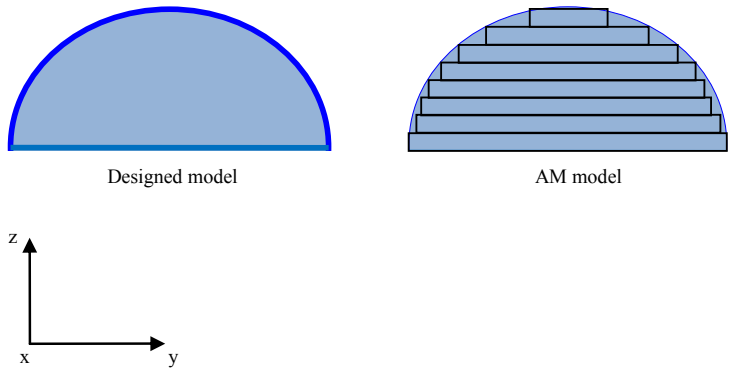

FIGURE 1

Schematic diagram represents stair stepping properties of additive manufacturing (AM) built.

incrementally [4]. AM processes include stereolithography, laser micro-sintering, three-dimensional printing, fused deposition modeling, laminated object manufacturing, and ink-jet printing [5–8]. There are two main drawbacks of these techniques. First, the resultant parts normally exhibit unfavorable surface roughness on all inclined surfaces, which is a typical consequence of the stair-stepping effect due to the formation of the buildup layers. Second, the final components from the AM usually suffer from relatively low density and large shrinkage. This is because the employed ceramic suspension has a low solid loading, which affects the dimensional tolerance and the utility of the designed micro-components (Figure 1).

Micro-injection molding is a productive forming technique for ceramic microfabrication. It can be used to fabricate a wide variety of sizes, complexity, and materials. This technique is much similar to plastic injection molding. Polymer or wax is melted and put together with ceramic powder to form a composite slurry. A micro-injection molding machine injects the molds with the mixture under heat and pressure (Figure 2). Afterward, the molds are left to cool and solidify to form the green parts, which can be later demolded. For micro-components with high aspect ratio, demolding becomes a problem. A photoresist fabricated by UV or X-ray lithography is typically utilized as a lost mold to overcome the demolding problems. After forming a component, the mold is removed by plasma etching to avoid the micro-components damage caused by the conventional melting or dissolving methods [5–7].

Electrophoretic deposition has been successfully used to shape ceramic micro-components. In this process, electric current is applied to a well-dispersed colloidal suspension, which results in migration of the suspended particles and forming a consistent deposition on the electrode surface (Figure 3). The mold is then being demolded and sintered in order to densify the powder compact. To produce parts with high mechanical properties and low surface roughness, well-dispersed suspensions should be employed. One of the disadvantages of this technique is the resultant low sintered density and the necessity to burnout the mold, which can easily damage the micro-components due to high organic content of the mold [8–12].

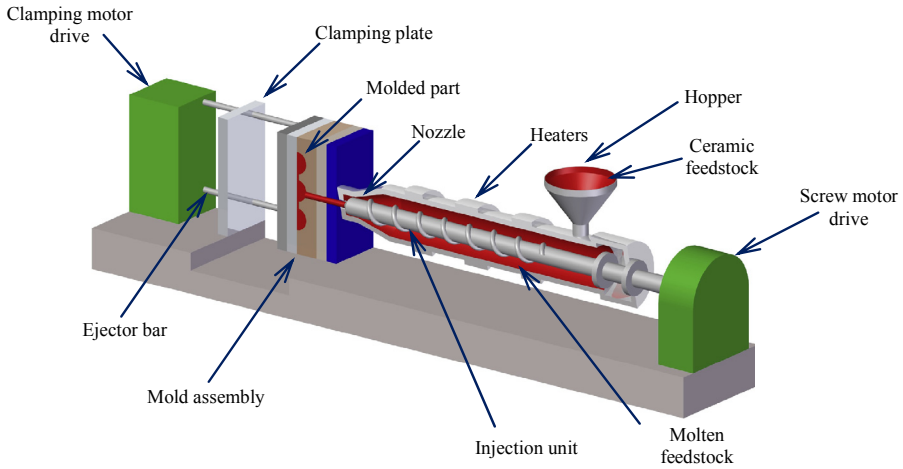

FIGURE 2

Schematic diagram of injection molding setup.

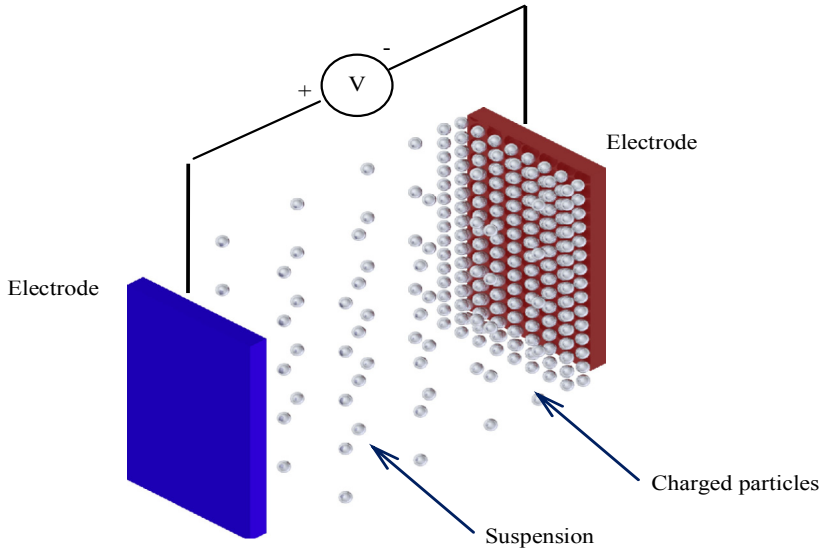

FIGURE 3

Schematic diagram of electrophoretic deposition principle.

Soft lithography is a nonphotolithographic fabrication technique, which established on replica molding (REM) for fabrication of micro- and nano-structures from nonphotosensitive materials. Soft lithography is an increasingly popular technique for its low-cost template replication feature for a wide variety of applications. In soft lithography, a soft mold is used as a stamp with patterned relief micro-structures on

its surface to generate components with micro- and nano-features. The elastomeric stamp or mold is the key element in this process. There are several materials that have been used for the elastomeric stamps, for example, poly(dimethylsiloxane) (PDMS) elastomers (or silicone rubbers) are used in most applications; some groups have used polyurethanes, cross-linked Novolac resins, and polyimides. On the other hand, five subtechniques have been developed, and they are micro-contact printing, REM, micro-transfer molding, micro-molding in capillaries, and solvent-assisted micro-molding [13–16].

Based on the analysis of the reviewed ceramic micro-fabrication techniques, one can say that soft lithography is regarded the most suitable technique to develop freestanding ceramic micro-parts. When compared to the reported techniques, micro-parts fabricated using soft lithography does not suffer from low resolution, poor surface finish, and low density, which are the main limitations reported by other methods. In addition, soft lithography is considered productive and low-cost fabrication method where the mold can include many micro-molds.

PROCESS

Soft molding is considered an efficient technique for replication of pattern in the surface of a mold. Various kinds of ceramic materials can be patterned using this technique. The whole fabrication procedure starting is illustrated in Figure 4.

The process starts with the conventional UV lithography process. A clean wafer is coated by a photoresist followed by a soft baking process. Afterward the exposure is performed by applying UV radiation onto the silicon substrate through a chrome mask. In negative photoresists such as SU-8, parts exposed to UV radiation become insoluble while the unexposed parts remain soluble in the resist developer. After development, the design is formed from the remaining solid resist on the wafer. Finally, a hard baking step is performed to ensure that mold properties do not change during the use of the mold, especially at higher temperature, and to anneal any surface cracks. A soft mold is an elastomeric mold that produces the inverse of the master mold. It is often used to manipulate suspensions or slurries that are dried or cured as part of the soft lithography process. The replication process starts by casting a prepolymer mixture into the fabricated master mold. The mold is then cured and transformed to an elastomeric material, which is then peeled off from the master. Afterward, the soft molds are filled with a ceramic material. Finally, the green patterns are demolded and sintered to produce the micro-parts.

FABRICATION AND CHARACTERIZATION OF THE MOLDS

Master and soft molds are crucial parts in the soft lithography process, which affect the quality of each subsequent step. The master carries a micro-pattern design on the surface that serves as a template for the production of soft mold replicas. There are

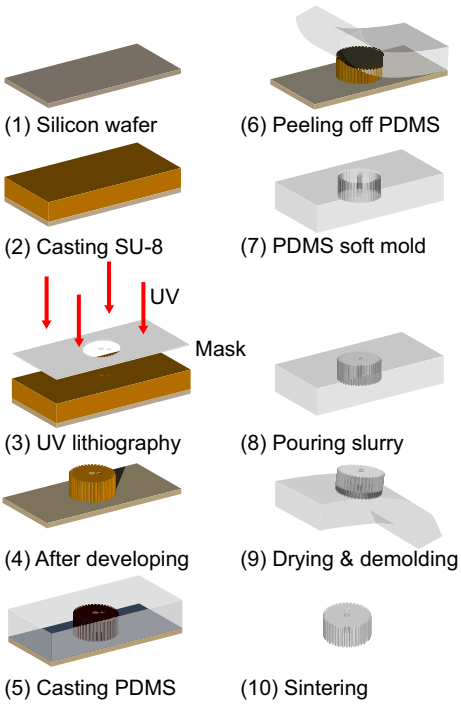

FIGURE 4

Schematic diagram of the fabrication process. PDMS, poly(dimethylsiloxane).

various materials and methodologies used for the production of master and soft molds. Hassanin and Jiang have compared several of them [17]. In particular, they used SU-8, BPR100, and silicon to pattern master molds by using either UV lithography or deep reactive ion etching (DRIE). In addition, they used PDMS and Dragon Skin in the replication process. SU-8 is a high-contrast epoxy-based negative tone photoresist. The main advantages of SU-8 are its simple processing, high chemical stability, good planarization capability, and ability to form thick layers. High aspect ratio structures with smooth sidewalls are achieved by UV lithography [18,19]. In addition, BPR100 (Rohm and Haas) photoresist has a wide variety of applications including electroforming, etching, and wafer-level packing processes [20]. BPR100 is a liquid negative tone type with a solid content of 58−62% and is typically used to form layers with a thickness ranging from 40 to 130 μm. DRIE using the Bosch process is one of the most important silicon micro-fabrication techniques. The main advantage of the Bosch process is that it provides means for deep etching of high aspect ratio patterns with almost vertical sidewalls and high etching rates. The process consists of many repetitions of alternating etch and passivation cycles. The first cycle is to etch. Repeating the etch and

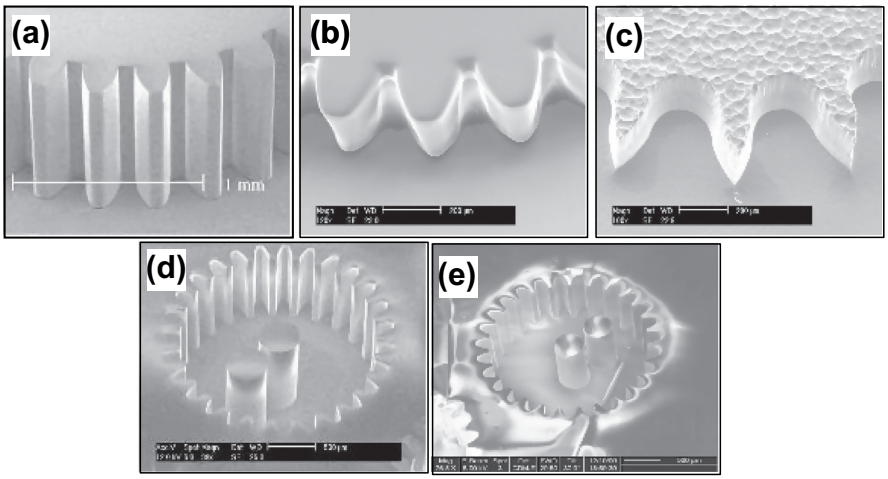

FIGURE 5

SEM images of (a) SU-8, (b) BPR100, (c) Deep reactive ion etching silicon, (d) Poly(dimethylsiloxane), and (e) Dragon Skin molds.

passivation loop results in a high rate and selective etching. Photoresist with a low etching rate is necessary for optimal results [21]. Soft molds made from PDMS and Dragon Skin were prepared by mixing their prepolymer and cross-linking agents in a glass beaker, and degassing the mixture under vacuum to remove bubbles formed during the mixing. The mixtures were then poured onto the master molds and the wafer was then placed in a vacuum again to fill the micro-molds and to remove all residual bubbles. It was then cured by heating. After cooling down, the cured soft molds were gently peeled off from the SU-8 master mold. SEM images of various master and soft molds are shown in Figure 5, [17]. The authors concluded that BPR100 and DRIE silicon molds are not suitable for thick molds. In addition, their surface roughness values were higher than those found for the SU-8 mold. On the other hand, Dragon Skin soft molds were shown to have demolding problems due to strong adhesion with the SU-8 master mold. Therefore, it was not suitable for use as a soft mold despite having a smoother surface than PDMS.

CERAMIC SLURRY PREPARATION AND CONTROL

Properties of ceramic powders play an important role in the fabrication of ceramic micro-components. Powder sizes can be varied from nanometers to several micrometers, see Figure 6.

Ceramic slurry is obtained by mixing ceramic powder, carrying vehicle, binder, and dispersant to produce uniformly dispersed ceramic slurry. It is important to optimize the slurry composition in order to obtain high green density, low green

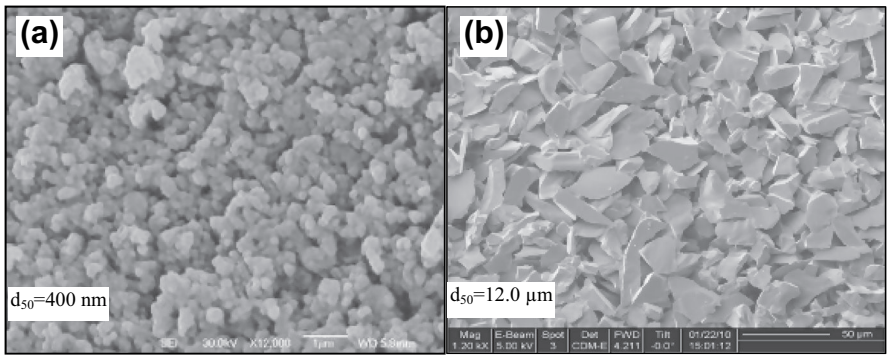

FIGURE 6

SEM images of alumina powders of different powder sizes (a) 400 nm, (b) 12.0 μm.

shrinkage, and sufficient green strength to produce defect-free demolding. Dispersant is used to separate the agglomerated particles in a slurry by controlling the interparticle forces affecting the colloidal stability of the system. Dispersion of ceramic powder processing is very important to obtain a high reliability sintered structure. Any inhomogeneity is a potential flaw in the sintered parts. Hence, the agglomerates, which exist in most commercially supplied powders, either have to be broken down or removed [22]. The dispersion condition of slurry has a direct impact to the green density. Well-dispersed slurry is required to produce green bodies with high packing densities and uniform micro-structures. Therefore, density and shrinkage measurements of the green parts are typically carried out for the optimization of dispersant concentration. Green density indicates how tightly the ceramic particles are packed in the green part. In addition, it is the key for achieving low sintered shrinkage, high dimensional resolution, and less distortion on resultant sintered part. Therefore, it is considered as a dominant parameter in forming ceramic micro-components.

Ceramic binder is a substance that is used to bind ceramic particles into the desired shape in the mold. In addition, it enhances green strength and improves flexibility of the ceramic parts. Polymers and waxes are the two major ingredients that are mainly present equally in a typical ceramic binder [23–25]. In most of slurry systems, binders play a crucial part in preparing optimum ceramic slurry. The more binder added, the stronger the green body is expected. Additionally, binders must be taken off from green parts before sintering. The more added binder, the more difficult the debinding process will be. Because of large amount of binder, more gas will be formed during the binder burnout step, which causes internal stresses, possible part damage, and geometry distortion.

Water-, preceramic polymer-, and wax-based slurries are employed and their process parameters are optimized for the fabrication of ceramic micro-components using soft lithography [24]. Water-based slurry process has been employed extensively in many forming techniques, such as tape casting and slip casting. The use of water as a dispersing liquid is attractive because of cost, environmental, and

health benefits. Aqueous binders such as Duramax B-1000 (Rohm and Haas, USA) and Duramax B-1007 (Rohm and Haas, USA) were used together in the experiments. They are commercially available low-foaming binders. In addition, their high dispersion in water enables an effective adsorption on the powder in water, reducing possible cracks on the green body during drying. The high solid loading of the binders increases the particle binding in the green body, which improves its flexibility. During the drying of the slurry, the polymer particles bind the particles together and increase the green strength. On the other hand, Duramax D-3005 (Rohm and Haas, USA) was used as a dispersant. D-3005 is an ammonium salt of a polyelectrolyte, commercially available for dispersing different ceramic powders in aqueous suspensions. D-3005 has a low molecular weight, which makes it effective at low use levels. The dispersant is supplied as a 35% solution in water. It was found that the minimum binder concentration used in the slurry without damaging the resultant green parts during both drying and demolding processes was about 20:25 mg/g powder for different powder sizes. Less binder concentration increases the possibility to damage the green parts. Using the optimum binder concentration resulted in complete and crack-free green parts as shown in Figure 7.

Polymer-derived ceramics are fabricated through pyrolysis of preceramic polymers. They offer a great variety of chemical and micro-structure modifications, allowing molecular tailoring of ceramic materials with improved properties compared to conventional ceramic materials. They gain in importance with the increase of advanced precursor materials, such as polycarbosilane, polysilazane, polysiloxane, and polyborosilazane. They have been used to fabricate net shape monolithic ceramic MEMS by either micro-casting a ceramic precursor liquid into a mold that has been prepared by conventional lithographic methods or by micro-forged molds [26]. Recently, polymer ceramics have been successfully used to fabricate alumina composites by hot pressing of poly(allyl)carbosilane-coated alumina

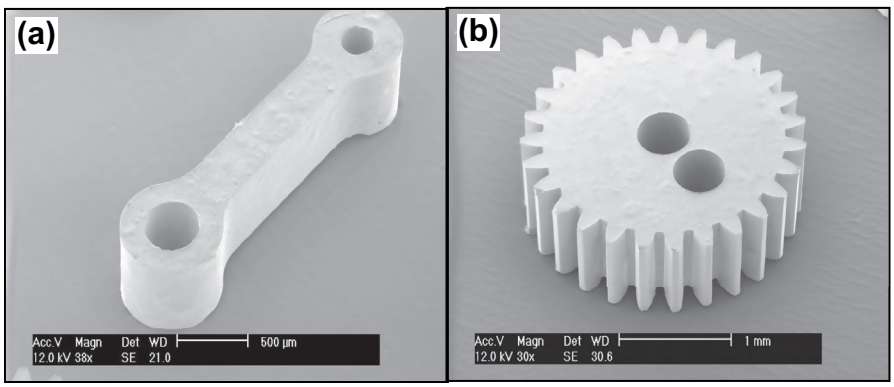

FIGURE 7

SEM images of green ceramic micro-components fabricated using water-based slurry (a) Micro-connecting rod, (b) Micro-gear.

powder into green pattern shapes, with subsequent pyrolysis and pressureless sintering. Polysiloxazane preceramic coatings resin (PCR) was used as a binder [27]. The commercial product of PCR used in the experiments was HTA 1500 Slow Cure (KiON Speciality Polymers, Germany). It is a clear and low-viscosity coating resin designed to cure at room temperature curable with 100% solids within 1 h. The polymer pyrolysis after curing results in conversion of the cured polymer to amorphous and crystalline ceramic phases. Therefore, using PCR over organic binders is expected to be better than conventional polymeric binders as it works both as the binder and as the additive of ceramic inclusion within the sintered ceramic matrix [27]. However, many of the green micro-components suffer from several defects (Figure 8). By adjusting the slurry composition and curing time, a few undamaged near-net shape green micro-pistons were produced (Figure 9).

Paraffin wax is a mixture of alkane hydrocarbons having C_nH_{n+2} formula where $20 \leq n \leq 40$. They are solid in room temperature and start to melt in temperature starting from 37 °C. Paraffin wax is a very popular binder in low-pressure injection molding for its low cost and versatile working temperatures. In addition, the resultant high-strength green parts make it effective binder for complex shape ceramics [28]. Paraffin wax (Sigma−Aldrich, UK) has the melting point of 53−57 °C. Ceramic slurry based on paraffin wax could be improved with the addition of dispersants, which improves ceramic particle dispersion and enhances wetting of the binder on the ceramic particles [28]. Stearic acid ($C_{18}H_{36}O_2$) supplied by Sigma−Aldrich, UK with a melting point of 69−71 °C was used as a dispersant in the paraffin wax-based slurry. Paraffin wax played the role of both the binder and the carrying medium. In the mixing step, the minimum amount of binder, which provides the necessary convenient molding process, was decided as the optimization criterion. For binder concentration less than 50 mg/g powder, it was found that it is difficult to mix the ceramic slurry using mechanical stirrer. By increasing the binder concentration to about 200 mg/g and 100 mg/g, it was easier to get homogeneous slurry using mechanical stirring. However, the slurry freezes faster before completing the filling, especially in thin micro-features, due to its high viscosity. As a result, incomplete micro-parts were obtained. Further increasing the binder content to about 260 mg/g, the filling process was improved and a complete filling was achieved, as shown in Figure 10.

Based on the assessments of the given slurries, water-based slurry proved to offer the greatest potential to realize suitable ceramic micro-components fabrication approach.

Sedimentation behavior of aqueous ceramic suspensions with different particle sizes and dispersant concentrations was studied to find the conditions for the maximum dispersion [29,30]. Suspensions stability is closely related to particle size and the amount of dispersant concentration as shown in Figure 11. All particles have a natural tendency to settle, generating higher sedimentation heights when no dispersant is added. The sedimentation height of the suspension with the smallest particle size is the highest when compared to the other suspensions. On the other hand, the stability is improved with the addition of the dispersant. It is notable

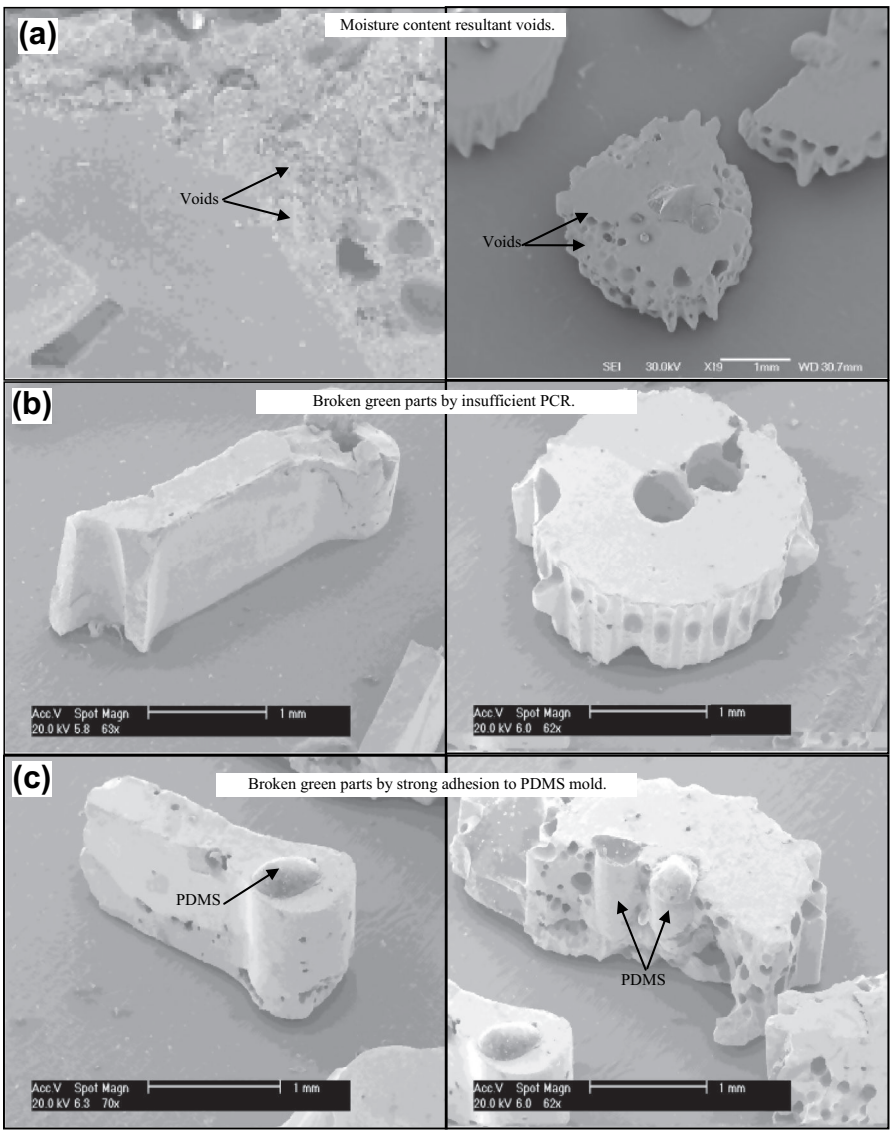

FIGURE 8

SEM images of defected green parts fabricated using solvent-based slurry (a) Moisture content resultant voids, (b) Broken green parts by insufficient preceramic coatings resin (PCR), (c) Broken green parts by strong adhesion to poly(dimethylsiloxane) (PDMS) mold.

that as the powder particle size is increased, the required amount of the dispersant to affect suspension stability is reduced. This is because a higher specific surface area requires more dispersant. With further increase of the dispersant, the settled height of all suspensions remained almost constant.

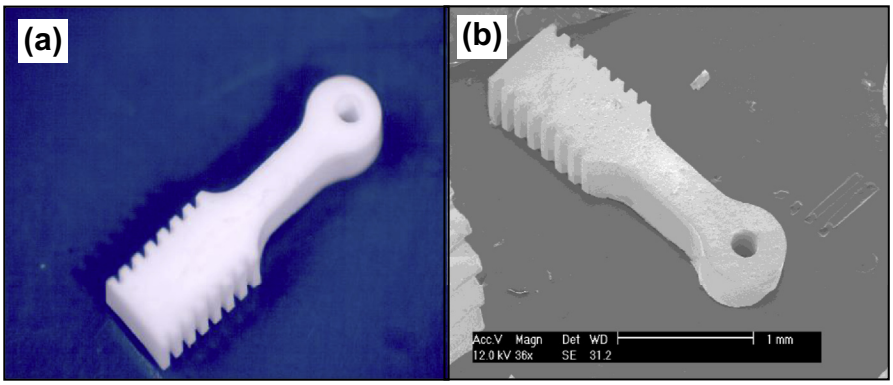

FIGURE 9

(a) Optical and (b) SEM images of ceramic green micro-pistons fabricated using solvent-based slurry.

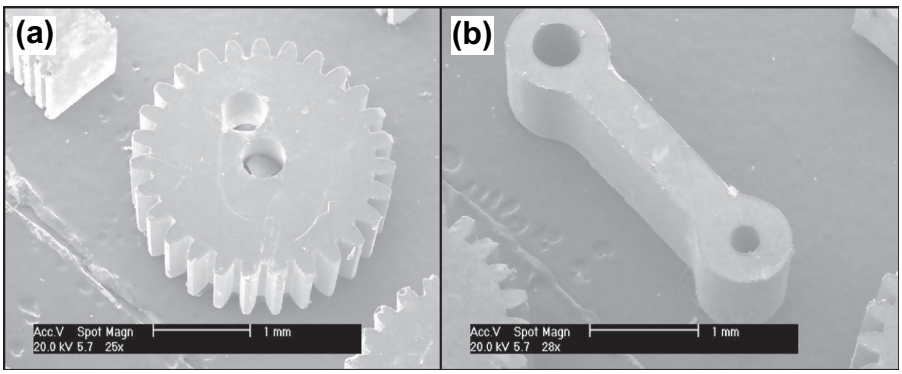

FIGURE 10

SEM image of complete green micro-components fabricated using paraffin wax-based slurry (a) Micro-gear, (b) Micro-connecting rod.

Viscosity of aqueous ceramic suspensions with different particle sizes and dispersant concentrations was studied to find the conditions for the maximum flowability and the results are shown in Figure 12. Viscosities of all suspensions are initially improved when the dispersant is added. The addition of the dispersant can gradually break down ceramic suspension structure by overcoming the attractive forces according to the Derjaguin, Landau, Vervey, and Overbeek (DLVO) theory, and thus the viscosity of the suspension decreases. After showing a minimum viscosity, further increasing of dispersant concentration resulted into an increased viscosity, which may be due to the saturation of the particle surfaces with the adsorbed dispersant. It can be noted that the amount of the dispersant required for ceramic suspensions to have a minimum viscosity increased with decreasing of the particle size. This is

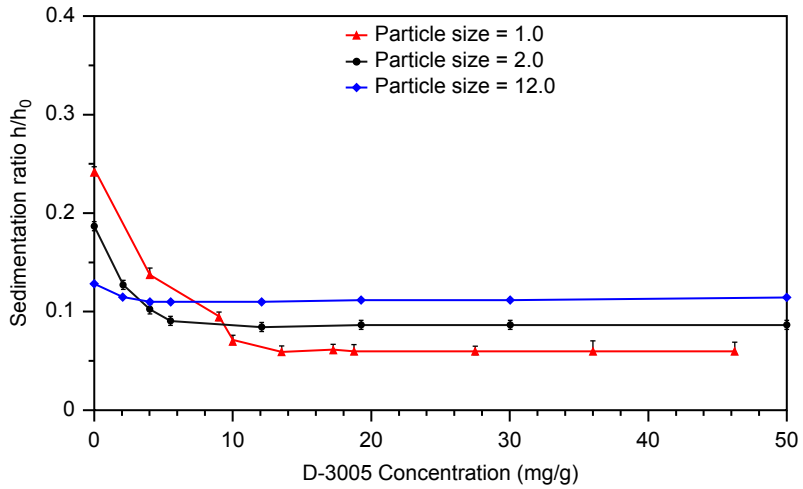

FIGURE 11

Sedimentation behavior of aqueous ceramic suspensions of various particle sizes as a function of dispersant concentration.

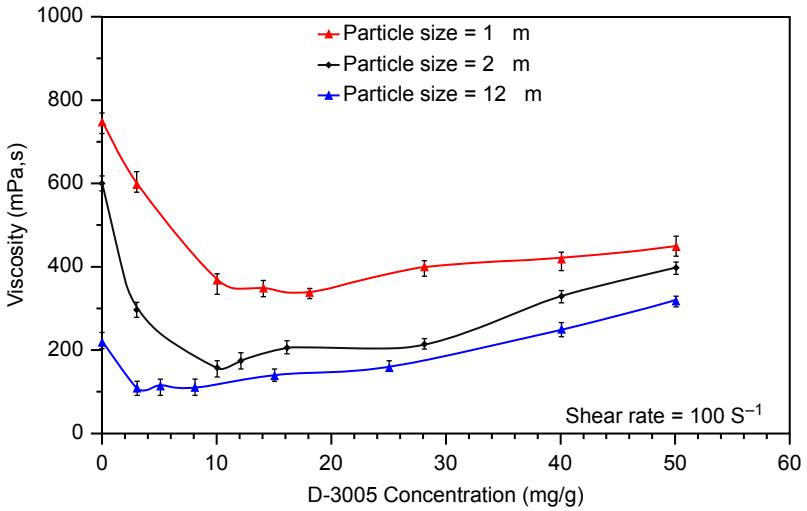

FIGURE 12

Relationship between the suspensions viscosity and concentration of dispersant for suspensions with particle size of 1, 2, and 12 μm.

because a higher specific surface area absorbs more dispersant. Furthermore, it can be clearly noted that viscosities of alumina suspensions are higher when powder particle sizes become finer. The high viscosity of alumina suspension with a small particle size can be attributed to its highest specific surface area and as a result the highest attractive forces, which restrict particles movements [29].

SINTERED MICRO-COMPONENTS

Sintered properties are important to study in order to assess the performance of the net shape micro-components. High sintered density, low and uniform sintered shrinkage, high hardness and fracture strength are essential for mechanical applications. Green ceramic micro-components are typically sintered using a specified heating cycle. Sintered density and linear shrinkage of alumina samples with different particles sizes can be measured. For example, Figure 13 shows this relation with respect to the dispersant concentration in the ceramic mixture. It can be clearly seen that by increasing the concentration of the dispersant to an optimum amount, the densification behavior of the micro-components was enhanced. Further addition of the dispersant caused sintering density to gradually decrease. It is clearly noted that the smaller the powder size, the higher the sintered density, and hence the higher the linear shrinkage. Smaller powders have a higher surface energy, and hence a greater sintering rate and higher density are expected.

The effect of sintering temperature on sintered density and linear shrinkage of alumina micro-components fabricated using different powder sizes is shown in Figure 14. The relative density and linear shrinkage of alumina samples increased

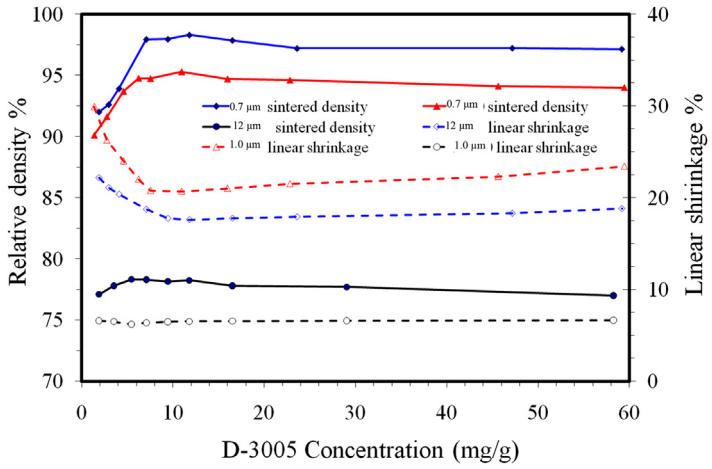

FIGURE 13

Sintered density and linear shrinkage as a function of dispersant concentration.

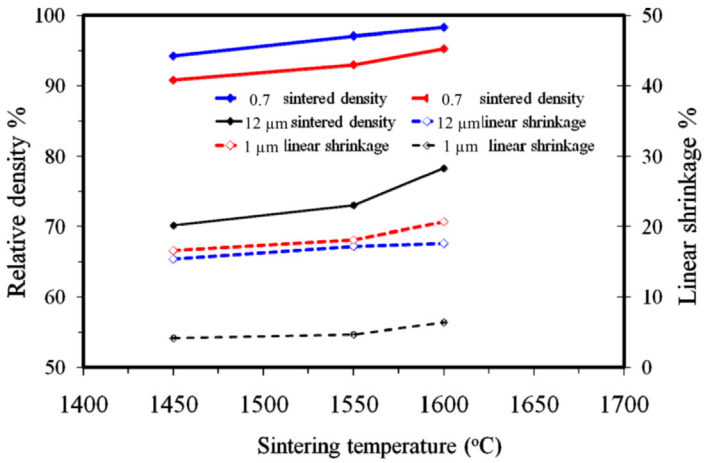

FIGURE 14

Sintered density and linear shrinkage of alumina micro-parts as a function of sintering temperature.

gradually as the sintering temperature rose. The relative density of the sample reached a maximum of 98.3%, 95.3%, and 78.3% with linear shrinkage of 17.6%, 20.7%, and 6.4% for micro-parts fabricated using powder size of 0.7, 1.0, and 12.0 μm respectively and sintered at 1600 °C. The smaller the powder size, the higher the sintered density and linear shrinkage was obtained when sintering temperature was increased.

Vickers micro-hardness of alumina micro-components sintered at different sintering temperatures is shown in Figure 15. Vickers micro-hardness increased with the increase of the sintering temperature. This is mainly because of the increase of sintered density when sintering temperature increased. High density means fewer pores and hence strengthens the material. In addition, it can be concluded that the smaller the powder size, the higher hardness the sintered micro-components will have. The highest Vickers values were 23.05 and 22.1 GPa for 0.7 and 1.0 μm-based samples after sintering at 1600 °C.

Figure 16 shows flexural strength of alumina samples as a function of sintered temperature. Flexural strength of alumina increased with the increasing sintering temperature. The samples reached to the highest flexural strength of 366 MPa for alumina samples made from 0.7 μm and sintered at 1600 °C. In addition, these samples have higher flexural strength than alumina samples made from 1 μm throughout the sintering temperatures. It is generally accepted that denser material has higher strength.

The fabricated alumina micro-components were inspected using SEM to investigate the effect of the powder size on the shape retention and edge resolution. Figure 17 shows SEM images of complete sintered micro-gears fabricated using

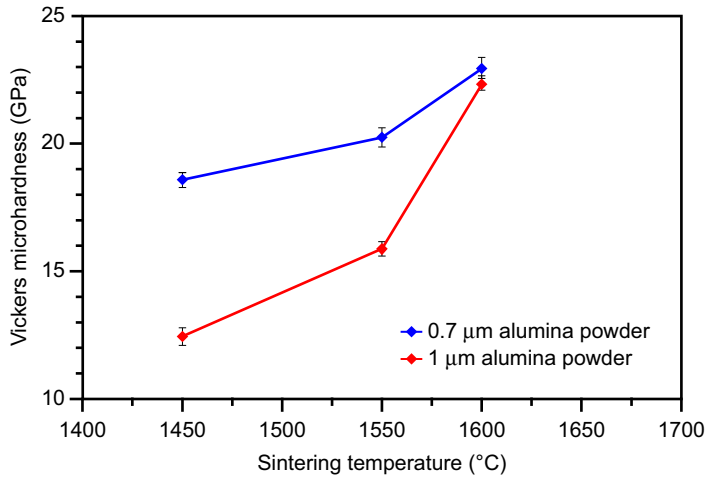

FIGURE 15

Vickers hardness of alumina micro-parts as a function of sintering temperature.

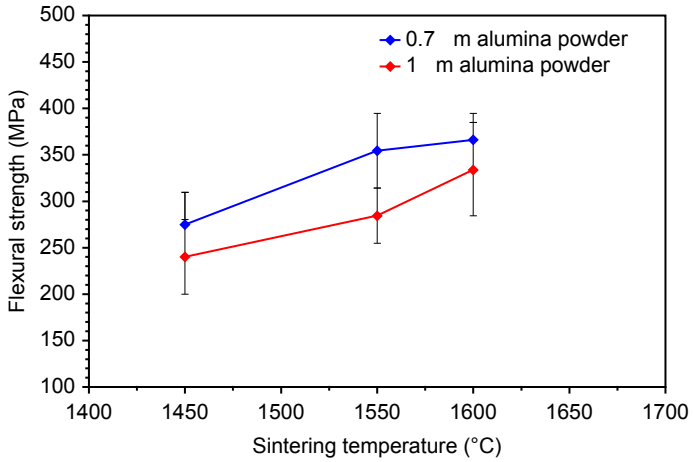

FIGURE 16

Flexural strength of alumina samples as a function of sintering temperature.

Al_2O_3 powders with average particle size of 0.7, 1.0, and 12.0 μm. It can be clearly seen that the Al_2O_3 micro-gears preserve their shapes completely after sintering. A close look to the magnified teeth from the top of the gears was performed for selected gears. The images demonstrate good edge profiles of the 0.7 and 1.0 μm-based micro-gears. On the other hand, the 12.0 μm-based micro-gear demonstrates irregular edge profile and poor resolution.

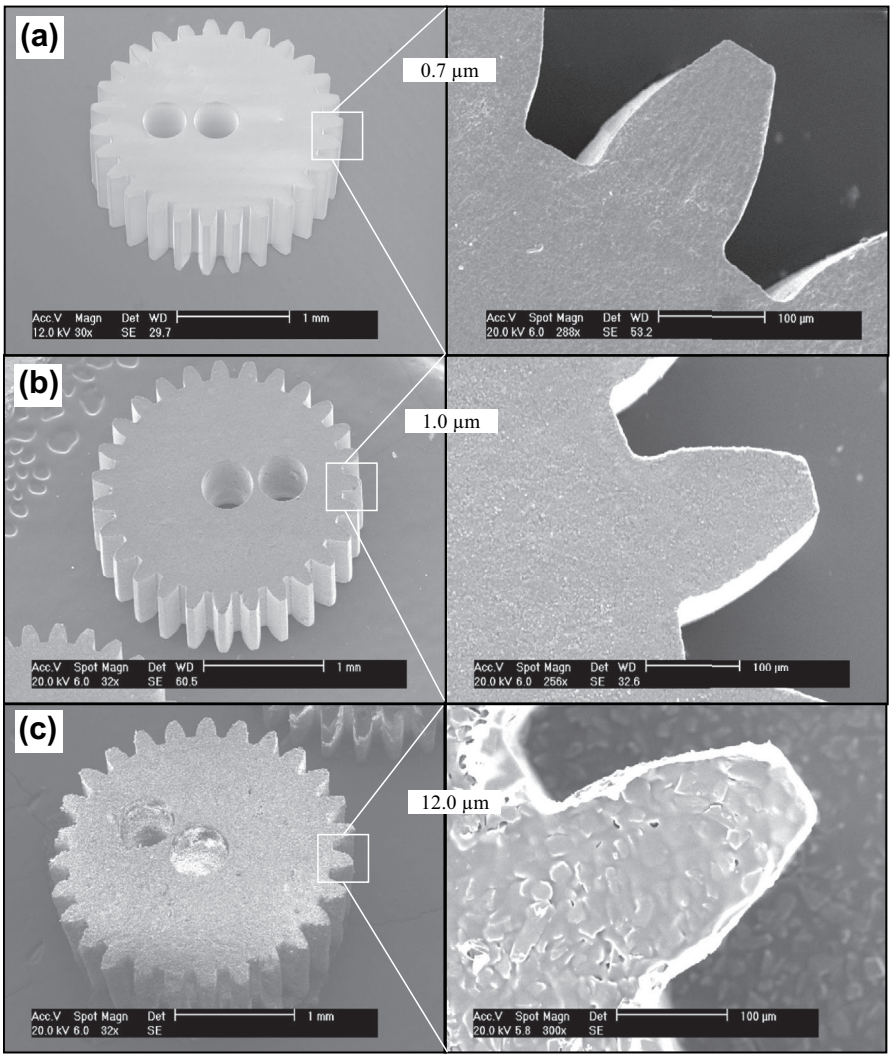

FIGURE 17

SEM images of alumina micro-gears fabricated using powder size of (a) 0.7 μm, (b) 1.0 μm, and (c) 12.0 μm.

CONCLUSIONS

This chapter reviewed the state of art of ceramic micro-fabrication using soft lithography as one of the most robust techniques to fabricate ceramic micro-components. In this technique, soft molds have been realized from the traditional solid molds to make a convenient demolding and to reduce the damage of green patterns. The

complete soft lithography involves the following steps: (1) fabricating rigid master molds using UV light lithography; (2) producing soft molds from the masters; (3) making ceramic suspension; (4) filling patterned molds with the ceramic suspension; (5) demolding and sintering. The entire process chain can be monitored and optimized through different characterization techniques, which lead to develop net shape ceramic micro-parts with optimum properties.

REFERENCES

[1] Hassanin H, Jiang K. Fabrication and characterization of stabilised zirconia micro parts via slip casting and soft moulding. Scr Mater 2013;69:433−6.

[2] Hassanin H, Jiang K. Fabrication of near net shape alumina nickel composite micro parts using aqueous suspension. In: Micro electro mechanical systems, 2009. MEMS 2009. IEEE 22nd international conference on, Piscataway, NJ, USA; 2009. p. 721−4.

[3] Hassanin H, Jiang K. Fabrication of alumina composite microengine parts using soft lithography. SAE Tech Pap 2009;0118.

[4] Edirisinghe MJ. Solid freeform fabrication of ceramics. In: TMS fall meeting, Rosemont, IL, USA; 1998. p. 139−49.

[5] Hill S. Micromoulding − a small injection of technology. Mater World 2001;9:24−5.

[6] Griffiths CA, Dimov SS, Brousseau EB, Hoyle RT. The effects of tool surface quality in micro-injection moulding. J Mater Process Technol 2007;189:418−27.

[7] Stone VN, Baldock SJ, Croasdell LA, Dillon LA, Fielden PR, Goddard NJ, et al. Free flow isotachophoresis in an injection moulded miniaturised separation chamber with integrated electrodes. J Chromatogr A 2007;1155:199−205.

[8] Ju Hyun Y, Wei G. Near-net ceramic micro-tubes fabricated by electrophoretic deposition process. Int J Mod Phys B 2003;17:1147−51.

[9] Sarkar P, Prakash O, Wang G, Nicholson PS. Micro-laminate ceramic/ceramic composites (YSZ/Al2O3) by electrophoretic deposition. Ceram Eng Sci Proc 1994;15: 1019−27.

[10] Von Both H, Dauscher M, Hauelt J. Fabrication of microstructured ceramics by electrophoretic deposition of optimized suspensions. Cocoa Beach (FL, USA). 2004. p. 135−40.

[11] Bonnas S, Ritzhaupt-Kleissl H-J, Hauelt J. Electrophoretic deposition for fabrication of ceramic microparts. J Eur Ceram Soc 2010;30:1159−62.

[12] Laubersheimer J, Ritzhaupt-Kleissl HJ, Hausselt J, Emig G. Electrophoretic deposition of sol-gel ceramic microcomponents using UV-curable alkoxide precursors. J Eur Ceram Soc 1998;18:255−60.

[13] Brittain S, Paul K, Xiao-Mei Z, Whitesides G. Soft lithography and microfabrication. Phys World 1998;11:31−6.

[14] Xia Y, Whitesides GM. Soft lithography, vol. 28. Palo Alto (CA, USA): Annual Reviews Inc.; 1998. p. 153−84.

[15] Rogers JA, Nuzzo RG. Recent progress in soft lithography. Mater Today 2005;8:50−6.

[16] Brehmer M, Conrad L, Funk L. New developments in soft lithography. J Dispersion Sci Technol 2003;24:291−304.

[17] Hassanin H, Ostadi H, Jiang K. Surface roughness and geometrical characterization of ultra-thick micro moulds for ceramic micro fabrication using soft lithography. Int J Adv Manuf Tech August 2013;67:2293−300.

[18] Peng J, Jiang K, Nianjun S. Microfabrication of ultra-thick SU-8 photoresist for micro-engines. In: Micromachining and microfabrication process technology VII, 27−29 January 2003, USA; 2003. p. 105−10.
[19] Jiang K, Jin P. Lithographic process. LOS ANGELES, CA US Patent, 2004.
[20] Xue Yong W, Chen Han L, Kyle J. Nickel electroforming of 3D microstructure by using BPR100 photoresist mould. Int J Nanomanufacturing 2007;1:499−505.
[21] Urban A, Laermer F. Bosch-process − DRIE success story, new applications and products. Boston (MA, USA). 2009. p. 133−44.
[22] Solomon MJ, Saeki T, Wan M, Scales PJ, Boger DV, Usui H. Effect of adsorbed surfactants on the rheology of colloidal zirconia suspensions. Langmuir 1999;15:20−6.
[23] Dang-Hyok Y, Lee BI. Processing of barium titanate tapes with different binders for MLCC applications-part I: optimization using design of experiments. J Eur Ceram Soc 2004;24:739−52.
[24] LeBeau JM, Boonyongmaneerat Y. Comparison study of aqueous binder systems for slurry-based processing. Mater Sci Eng A 2007;458:17−24.
[25] Baklouti S, Chartier T, Gault C, Baumard JF. The effect of binders on the strength and Young's modulus of dry pressed alumina. J Eur Ceram Soc 1998;18:323−8.
[26] Stearns LC, Junhong Z, Harmer MP. Processing and microstructure development in Al2O3-SiC 'nanocomposites'. J Eur Ceram Soc 1992;10:473−7.
[27] Hassanin H, Jiang K. Alumina composite suspension preparation for softlithography microfabrication. Microelectron Eng 2009;86:929−32.
[28] Moballegh L, Morshedian J, Esfandeh M. Copper injection molding using a thermoplastic binder based on paraffin wax. Mater Lett 2005;59:2832−7.
[29] Hassanin H, Jiang K. Effects of particle size on soft lithography process, the green and sintered micro alumina parts. Int J Appl Ceram Technol 2013;10:1014−22.
[30] Hassanin H, Jiang K. Net shape manufacturing of ceramic micro parts with tailored graded layers. J Micromech Microeng January 2014;24:015018 (8 pp.).

CHAPTER

Micro-sintering through a FAST Process

11

Yi Yang[1], Kunlan Huang[1,2], Gang Yang[1], Deqiang Yin[1], Yu Zhou[1], Yi Qin[2]

School of Manufacturing Science and Engineering, Sichuan University, Chengdu, Sichuan, P.R. China[1]; Centre for Precision Manufacturing, Department of DMEM, University of Strathclyde, Glasgow, UK[2]

CHAPTER OUTLINE

INTRODUCTION

On the technology front, during the last decade, the manufacture of micro-components and the miniaturization of manufacturing equipment/devices, which deals with the manufacturing at miniature (e.g., <10 mm), micro- (<1.0 mm), and sub-micro-scale (0.1−1.0 μm), has obtained notable development globally. Various manufacturing methods have emerged, which deal with a wide range of materials and applications. Micro-system technology is one of the leading technologies for producing micro-components ranging from nanometers to millimeters [1−3].

Micromanufacturing Engineering and Technology. http://dx.doi.org/10.1016/B978-0-323-31149-6.00011-6

For the manufacture of large-sized components from the materials, e.g., ceramics, cermets, super conductors, magnets, metal composites, and glass, traditionally, the processes called powder metallurgy would be used. However, these were not developed for the manufacture of small-sized components due to the manufacturing routines not being suitable for micro-scale manufacture. Injection molding [4] and compressive molding [5] are alternative processes often used to make these components from powders, but such processes, however, involve the use of the so-called green compacts (mixing the powders with binders, and then shaping them into the required shapes, followed by high-temperature sintering which often takes place in furnaces or chambers with a transfer belt). The drawbacks involved include a long-process chain, difficulty in controlling component accuracy, the binders, hence affecting the environment, etc.

A process aimed at resolving these problems is called micro-fields-activated sintering technology (Micro-FAST)—a manufacturing process to make micro-components usage directly from powders. The powders are pressed when an external electric field is applied to them while the powders are joined together through fusion bonding under high temperatures created either by resistance heating at the powder interfaces and/or by the mold due to the high current flowing through it. High density of the structure can be achieved by the coupled actions from the electrical field and mechanical pressure, i.e., coupled multiphysics fields-activated forming and sintering. One of the exciting prospects on this method is its efficiency in shaping the component, e.g., with a high current applied (e.g., 10,000 A) and a fast heating rate (e.g., a rate of increase of current of 1000 A per second); due to only a micro-volume of the material to be heated, a component can be formed in a few seconds, while with a conventional sintering method, usually tens of minutes and even 2 h are required.

The impact of the technology being researched will be high, not only due to its high efficiency but also because of several other advantages:

1. No binders are used and hence there is less impact on the environment;
2. It is possible to use all types of materials, even in combinations (e.g., feeding different kinds of powders into a mold);
3. The materials are fully recyclable;
4. The nano-structures of the materials in the formed parts can be maintained, due to the ultrafast processing time, hence excellent mechanical properties can be obtained.

MICRO-FAST SINTERING PROCESS

The Micro-FAST [6–10] sintering process can be seen in Figure 1. It is a method which has been successfully applied in the forming of micro-components with a variety of material systems, for instance, metals (Cu, Steel) and alloys (MnZn, WC-Co). Compared to conventional sintering methods, Micro-FAST is a promising and energy-efficient technique that uses electricity to quickly raise the compact's

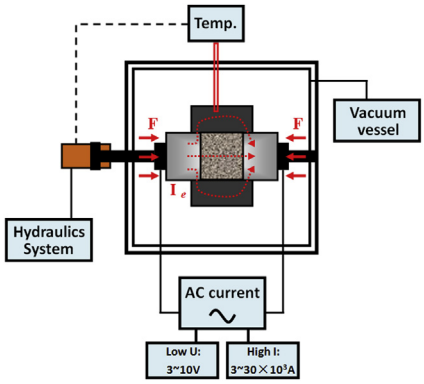

FIGURE 1

Illustration of the Micro-FAST sintering and forming process.

temperature and exert pressure simultaneously, which can be turned off immediately after the preset sintering time. In Micro-FAST, the powder is formed/sintered under simultaneous actions from the current, high temperature, and forming pressure. Moreover, loose powder is loaded directly into the die, and the heating is achieved by passing an AC current through the die to generate the necessary temperature in the powders, while pressure is applied onto the powders simultaneously. The entire forming process can be accomplished within 50 s. The direct manufacture from powder and no additional binders being added to the powder indicate that it is an energy-conserving and environment-friendly forming process.

Figure 2 is a schematic illustration of the tool-set used in the experiments with a Gleeble-1500D thermal simulation machine from Dynamic System Inc., USA. The electric field produced by the machine has low voltage and high current (3−10 V and 3000−30,000 A). The as-received powder consists of agglomerates which were

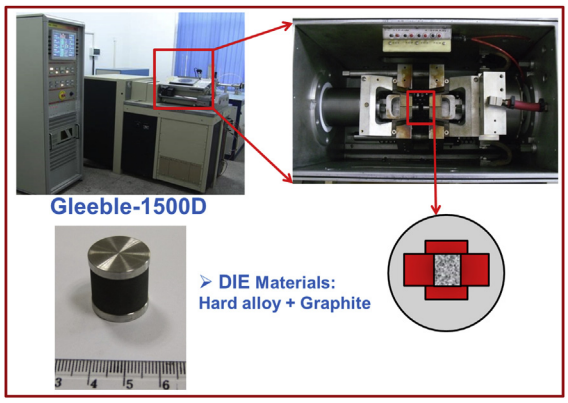

FIGURE 2

Tool-set used and experimental setup with the Gleeble-1500D.

sufficient for making up a micro-product. The weighted powder was loaded into the die, a model of the die being shown in the lower right-hand corner of Figure 2. Next, the die, filled with copper powder, was placed into the Gleeble-1500D machine, then heated rapidly to a certain sintering temperature at a preset heating rate in a vacuum ($<10^{-4}$ Pa) (a high electric current passes through the die-set), and at the same time, a preset pressure was applied to the punch and die-bottom.

ANALYSIS OF PROCESS

ANALYSIS OF SINTERING PROCESS

So far, there are two kinds of sintering process that have been developed for Micro-FAST, these being constant temperature sintering and electro-heating loops sintering, as shown in Figure 3. From these two processes, the sintering may be generally described as a four-stage process: (1) a preheating period, during which the compacts were heated to a low temperature (e.g., 200 °C) and then held for a certain time, during which dwell time at the low temperature the gas trapped inside the sintered powder system is driven out; (2) a calefactive period, during which the compacts are heated to the preset sintering temperature from the dwell temperature; (3) a sintering period, when the compacts were held for a certain time at the preset sintering temperature, or the sintering temperature is fluctuating and cycles for a fixed number of times; and (4) a cooling period, when the electrical current was reduced and the compacts were cooled to room temperature. According to the results of the present experiments, different material powders should be sintered by different sintering processes.

It should be noted that the division of the process into four stages is purely to enable a simple explanation of the process: there is no clear boundary between two neighboring stages for the whole work-piece since individual powders in the die cavity at the same time may be in different states. However, such a treatment will lead to a meaningful analysis and may yield instructive insight into the forming and sintering mechanism of the powders.

EFFECTS OF COUPLED MULTIFIELDS ACTIVATION

As described above, the process used for the forming of micro-compacts is actually one coupled with multifields activation, i.e., a coupled multifields-activated forming process: forming of the component is enabled under a simultaneous pressure field, temperature field, and electrical field.

Under the condition of an external pressure-field, the equation of densification rate may be expressed as follows [9]:

$$\left(\frac{d\rho}{dt}\right)_{p>0} = \frac{3}{2}\cdot\frac{\gamma}{\eta r_1}\cdot\left(1+p\frac{r_1}{2\gamma}\right)(1-\rho)\left[1-\frac{\sqrt{2}\tau_c r_1}{2\gamma\left(1+p\frac{r_1}{2\gamma}\right)}\cdot\ln\frac{1}{(1-\rho)}\right] \quad (1)$$

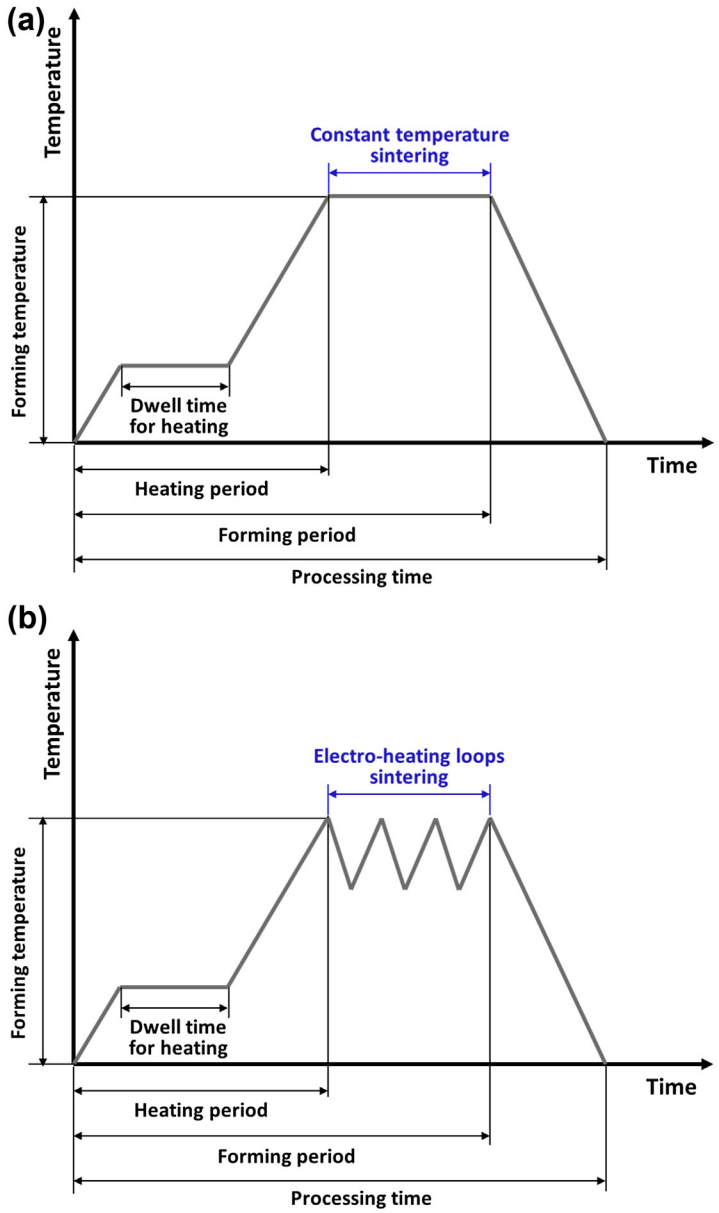

FIGURE 3

Temperature—time curve of the compact during the sintering process: (a) constant temperature sintering; (b) electro-heating loops sintering.

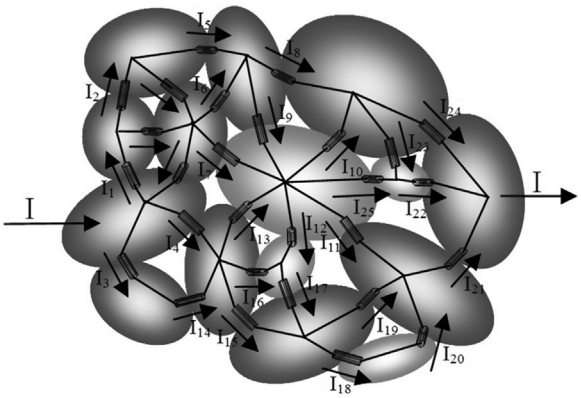

FIGURE 4

Illustration of the distribution of the current in a compact.

where $\frac{d\rho}{dt}$ is the densification rate; γ is the surface tension of the materials; η is the viscosity of the materials; r_1 is the radius of the closed gap; ρ is the relative density of the sintering sample; τ_c is the yield stress of the material; and p is the external pressure. It can be seen that external pressure can contribute to the densification rate during sintering. When the grain boundary is a perfect sink for vacancies, two particles approach each other, driven by a force that is obtained by integrating the stress over the boundary area and by adding the surface tension along the circumference. A porous material shrinks when the total energy decreases with decrease of the pore volume. Sintering stress is a concept that gives the relationship between the total energy change and the pore volume change [11].

When an AC current passes through the compacts, Joule heat will be generated at an interface due to the contact resistance. Figure 4 illustrates the distribution of the current in the compacts. According to the Joule−Lenz's law, the heat generated by the current passing through the compact is:

$$Q = I^2Rt \tag{2}$$

in which Q is the generated heat when current passes through the compact; R is the resistance of the compact; and t is the electrify time. In the process of sintering, the change of Joule heat is affected by the interfacial contact resistance and the current of the particles.

As observed, the greater the temperature and electric current density, the greater is the Joule heat and emission current intensity. Collision of emission current with the adjacent particles resulted in the transfer of the emission current's kinetic energy to internal energy, which accelerated atomic diffusion at a lower temperature under the action of an electric field. The powders used in the experiments were discontinuous, trapping a lot of gas between the particles. During the heating process, the gas trapped inside the sintered powder system was driven out and a

liquid phase was formed. At the same time, the liquid phase flow was accelerated at large pressure due to the extra pressure applied to the powders, and parts of the liquid phase filled into the vicinal pores by plastic flow.

It should be emphasized that the pressure field greatly influences the formation of the temperature field and electrical field, and correspondingly, the increased temperature and Joule heat also further change the distribution of the pressure field. These are particularly important at the micro-scale, where the extremely small contact-areas (and hence, high contact pressure) and localized high-temperature (due to the high heating-rate) play significant roles during the densification of the powders. As a result of which, the coupled multifields activation causes intensive densification of the powders.

APPLICATIONS OF MICRO-FAST

Micro-FAST is able to form net-shaped products with the advantage of high material utilization and fabricate micro-components under low temperature with loose powder materials. Examples of suitable micro-components are micro-gears and blades in a variety of materials. In the following sections, micro-components sintered with different materials will be introduced.

FABRICATION OF MnZn FERRITE

MnZn ferrites are already widely used in mini DC−DC converters and inductors. Further, recently MnZn ferrite components have found new applications and form essential parts of the electrical circuit of renewable energy production units [12,13]. For the manufacture of large-sized components from MnZn ferrite, traditionally, the processes called solid-state reaction or continuous solid-state crystallization would be used. However, these processes were not developed for the manufacture of small-sized components due to the manufacturing routines not being suitable for micro-scale manufacture. Furthermore, during the sintering, the temperature was higher than 1050 °C, such a high sintering temperatures leading to a series of problems, including high losses of magnetic properties at high frequency; low densities of components; and more power consumption during the sintering process. Microwave sintering [14] and injection molding [15] are alternative processes often used to make MnZn ferrite components from powders. These, however, involve use of green compacts, drawbacks including a long-process chain, difficulty in controlling component accuracy, using binders, hence affecting both the environment and the components. In Micro-FAST, however, MnZn ferrite micro-components can be sintered with good magnetic performance at a lower temperature and in a shorter time.

During the sintering process, MnZn ferrite powders are rapidly heated to 800 °C, the rate of temperature increase being 50 °C/s. A pressure of 75 MPa is applied to the powders through the punches at the start of the heating process. After

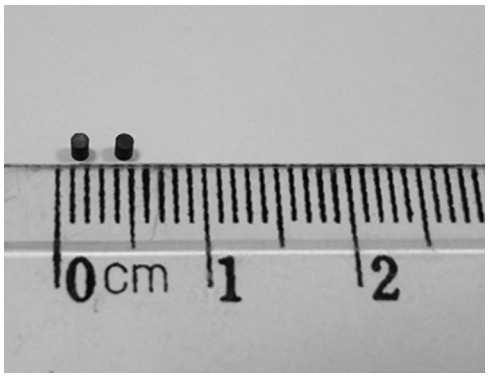

FIGURE 5

The fabricated MnZn ferrite cylindrical bulks.

an 8 min thermal holding time, the Gleeble-1500D thermal simulation instrument is turned off and the sample is allowed to cool to room temperature in a vacuum atmosphere.

As shown in Figure 5, cylindrical bulk MnZn ferrite with diameters of 1.0 mm, and heights of 1.0 mm were sintered by Micro-FAST. The density of the samples reached 4.69 g/cm^3 when they were sintered at a relatively low sintering temperature (800 °C) for 8 min, at a higher heating rate (50 °C/s) and pressure 75 MPa.

Microstructure of the formed samples

In order to compare the methods of Micro-FAST and conventional sintering, MnZn ferrite samples of identical composition were sintered for 4 h at 1280 °C by conventional protective atmosphere sintering carried out in a furnace, the resulting microstructure being shown in Figure 6. Compared to Figure 7, it can be seen that for the sample sintered at much lower temperature (800 °C) and much shorter sintering time (8 min) in Micro-FAST, the microstructure of the sintered MnZn ferrite is almost as dense as that of the conventionally sintered MnZn ferrite. In addition, it can be seen that solid phase reaction of MnZn ferrite materials was not completely finished in the sample, the dark areas shown by the arrows in Figures 6 and 7 in the samples are raw materials.

During the sintering process, when the energy obtained by the system was sufficiently large to surmount the activation energy for reactions at a certain temperature, the reaction of $MnO + Fe_2O_4 \rightarrow MnFe_2O_4$ and $ZnO + Fe_2O_4 \rightarrow ZnFe_2O_4$ may occur in the powder system, and then the $MnFe_2O_4$ and $ZnFe_2O_4$ will form a solid solution after sintering, which results in MnZn ferrite synthetic [16]. The X-ray Diffraction (XRD) patterns of the sample before and after sintering are presented in Figure 8. It can be seen that the sample both before and after sintering (both in Micro-FAST and in the solid-state reaction method) has a typical spinel structure. However, the composition and structure of spinel have changed after sintering.

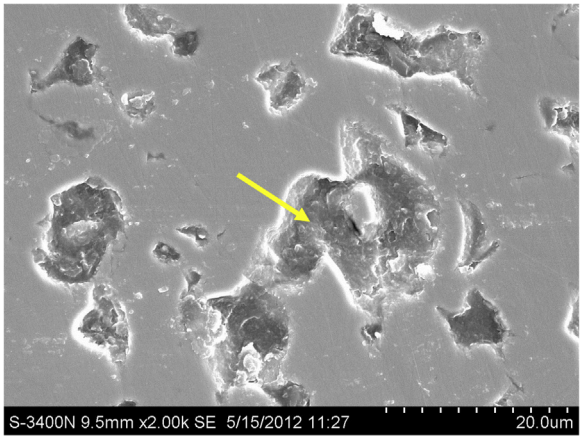

FIGURE 6

Microstructure of MnZn ferrite sintered for 4 h at 1280 °C by the solid-state reaction method.

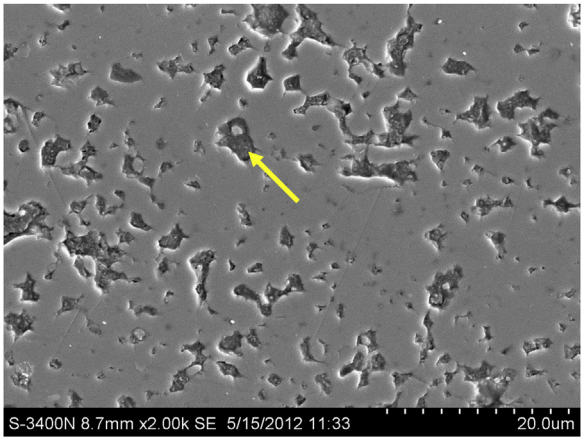

FIGURE 7

Microstructure of MnZn ferrite sintered for 8 min at 800 °C by Micro-FAST.

Magnetic properties of the formed samples

A comparison of the magnetic properties of MnZn ferrite sintered with the two different methods is shown in Table 1, from which it can be seen that the density of the sample sintered by Micro-FAST is 4.69 g/cm^3, which is almost the same as the density of the sample sintered by the solid-state reaction method. As shown in Table 1, the maximum energy product of MnZn ferrite sintered by Micro-FAST is 50.362E+3 GOe, while the maximum energy product of the same composition MnZn ferrite sintered by the solid-state reaction process is 116.61E+3 GOe. At

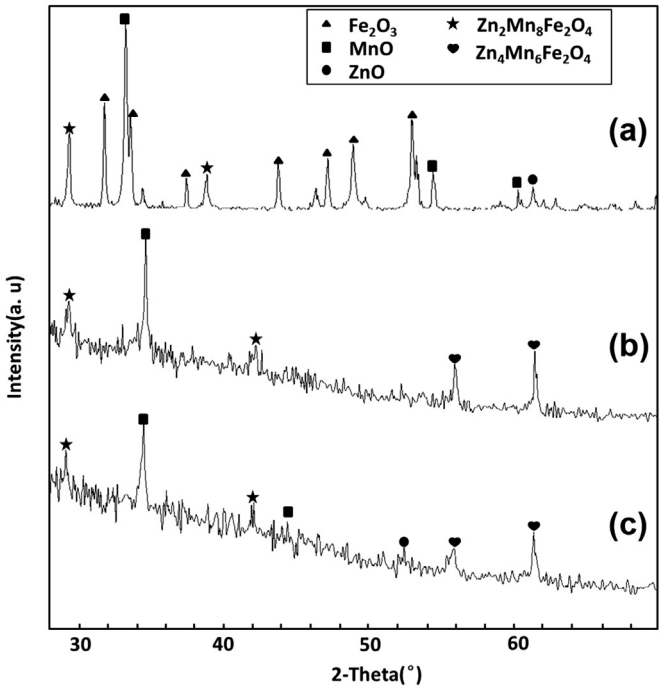

FIGURE 8

XRD patterns of the sample: (a) before sintering; (b) after sintering in solid-state reaction; and (c) after sintering in Micro-FAST.

Table 1 Effects of Different Sintering Methods on Magnetic Properties of MnZn Ferrites

Sintering Method	Sample Size/(mm)	ρ/(g/cm^3)	BH_{max}/(GOe)	B_r/(G)	H_{ci}/(G)	Ms/(emu)
Solid-state reaction for 4 h at 1280 °C	Φ 8 × 8	4.74	116.61E+3	6.5790	0.262	7.5522
Micro-FAST for 8 min at 800 °C	Φ 1 × 1	4.69	50.362E+3	52.143	30.152	2.0340

the same time, the saturation magnetization of the sample sintered by Micro-FAST is 2.0340 emu, while the saturation magnetization of the sample sintered by the solid-state reaction method is 7.5522 emu. It could be concluded that the effect of coupled multiphysical fields activation treatment process (in Micro-FAST) resulted in a high-density sintered product with a relative low magnetic performance. This could be attributed to very small material volumes involved. However, the remanence of

MnZn ferrite is 52.143 G, and the remanence of the sample sintered by the solid-state reaction method is 6.5790 G, this demonstrating that remanence of MnZn ferrite sintered by Micro-FAST is greater than that of the solid-state reaction sintered sample. Moreover, considering the merits of Micro-FAST, e.g., being a simple sintering process, with an ultrafast processing time, and no binder being used in the powder system, the conclusion can be reached that Micro-FAST is a good alternative technology to fabricate magnetic materials.

FABRICATION OF HARD ALLOY

WC-Co composites are widely used as cutting tools and dies due to their high wear resistance and toughness [17]. WC-Co composites are normally prepared by a powder metallurgy route, which is a procedure consisting of a series of long-time processes, such as the synthesis of WC powder, mixing with metal, granulation, pressing, and sintering. Moreover, the carbonization temperature of WC is as high as 1400−1600 °C. In order to improve its properties and simplify the preparation procedure, the consolidation of WC-Co powder has been studied using a variety of techniques including hot isostatic pressing [18], as well as unconventional processes such as microwave sintering and spark plasma sintering (SPS), rapid omni compaction, and ultrahigh pressure rapid hot consolidation [19]. However, the hardness and toughness are in contradiction with each other for the conventional coarse-grained WC-Co alloys [20]. To date, numerous processes have been dedicated to the study of densification and grain growth control during sintering of the WC-Co powders in order to achieve the goal of obtaining fully dense WC-Co materials.

One of the keys for controlling the grain growth of WC-Co composites is a suitable selection of additives as grain growth inhibitors, such as vanadium carbide (VC) and chromium carbide (Cr_3C_2). At the same time the grain growth can be inhibited by using special sintering technologies allowing very high heating rates, increasing the densification rate, even at lower sintering temperature and shorter holding times, such as microwave sintering and SPS. Moreover, Bonache et al. [21] have investigated the effect of grain growth inhibitors on the WC grain growth and its mechanical properties when they are combined with the use of the pulsed electric current sintering technique. The results have demonstrated that the addition of inhibitors, especially VC, is an efficient method for controlling the grain growth in the solid state, even in rapid sintering processes.

In Micro-FAST, WC-6Co cemented carbide can be directly fabricated from powders and no additional binders need to be added to the powders. The advantages of this technique over the conventional techniques include lower sintering temperature, shorter forming time, and remarkable inhibition of grains coarsening.

Also in the present work, cylinders of Φ 4.0 × 4.0 mm have been formed with ultrafine WC-6Co powders. The detailed technological parameters of the experiments are shown in Table 2. The "Electro-heating loop" means the fluctuation of the temperature and cycles for a fixed time. The relative properties of sintered

Table 2 Process Conditions and Relative Density of the Formed Samples

Specimen Designation	Heating Rate (°C/s)	Sintering Temperature (°C)	Pressure (MPa)	Times of Electro-Heating Loop (T ~ 400 °C)	Relative Density (%)
1#	50	850	75	1	92.90
2#	50	850	75	3	93.30
3#	50	850	75	4	93.80
4#	50	850	75	6	97.80

WC-6Co cemented carbides, such as the hardness and the microstructures, have been obtained, as presented in Table 2.

Properties of the sintered WC-6Co cemented carbide

Results selected from the experiments can be found in Table 2. The micro-formed samples show high relative density (92.90−97.80%). It can be seen that the dependence of the relative density on the electro-heating loop is strong and a tendency toward an increase in relative density with increase in these two parameters was noted. The morphology of a formed sample can be seen in Figure 9.

Table 3 shows properties of WC-6Co cemented carbide material that was prepared by different shaping technologies. It can be concluded that the effect of the coupled multiphysical fields activation treatment process was to produce a

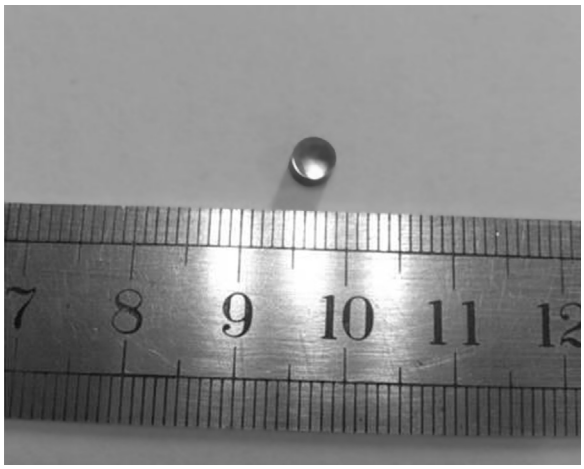

FIGURE 9

The formed samples (solid cylinders) with a size of Φ 4.0 × 4.0 mm.

Table 3 Properties of WC-6Co Cemented Carbide Material

Shaping Technology	Relative Density (%)	Rockwell A Hardness (HRA)
Die pressing (Shi, 2006)	97.40	93.1
PEM (Shi, 2006)	97.00	92.8
Die pressing plus CIP (Shi, 2006)	99.50	93.6
Coupled multiphysical fields activation	97.80	87.2

harder sintered product with a relatively low strength. This should be attributed to the residual holes in the samples (Figure 11) and the very small material volumes involved.

XRD inspection of the WC-Co system

During the sintering process, the reactions of WC and Co can be expressed as follows [21]:

$$WC + Co \rightarrow Co_3W_3C \tag{3}$$

$$WC + Co \rightarrow Co_6W_6C \tag{4}$$

$$Co_6W_6C \rightarrow Co_3W_3C \tag{5}$$

$$Co_6W_6C \rightarrow Co_3W_3C + WC + Co \tag{6}$$

$$Co_3W_3C \rightarrow WC + Co \tag{7}$$

The XRD pattern of the composition of WC-6Co samples sintered by coupled multiphysical fields activation technology can be seen in Figure 10. The XRD results show that there is no evidence of η phase (Co_3W_3C or Co_6W_6C) formation in the composition. The absence of secondary phases confirms that the WC-Co powder system had been sintered in solid phase. This clearly indicates that the incomplete densification in the solid state can be ascribed to the effect of coupled multiphysical fields activation, especially the high-density current field, is associated with the limitation of the diffusion phenomena and migration of Co [22]. On the other hand, it is difficult for the WC-Co system to react because of the short length of heating period (a few seconds).

Microstructure of the formed samples

Comparing the micrographs of the formed samples shown in Figure 11, the following conclusions can be drawn: (1) WC-6Co powders can be well sintered to dense compacts under the coupled actions from multiphysical fields within relatively short sintering time (e.g., <4 min), while conventional sintering could take a couple of hours. It is worthy of mention that the pores in a composite decrease as the times of the electro-heating loops increase, which is accompanied by the densification of the compact. At the same time, when the times of the electro-heating loop increased,

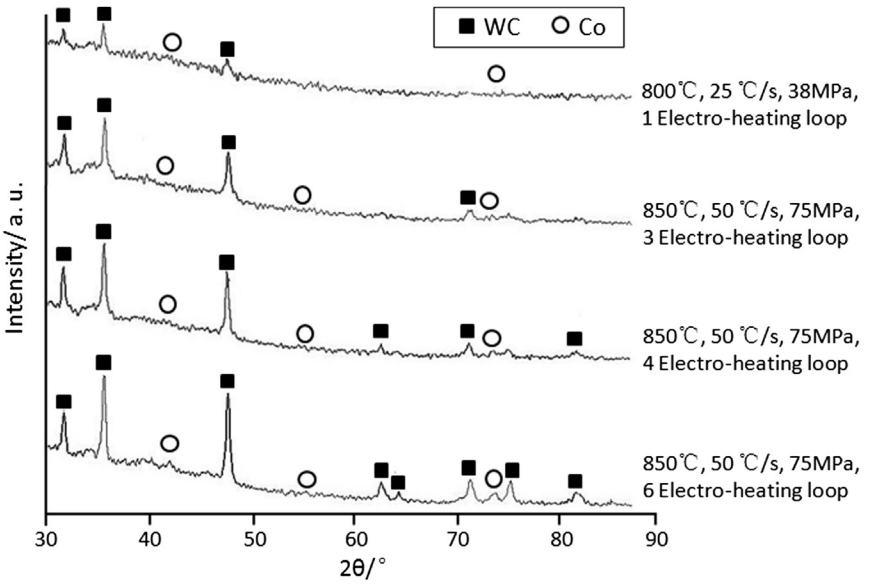

FIGURE 10

The XRD pattern of the composition of WC-6Co samples sintered by Micro-FAST.

the round WC grains combined together with the Co binder phase in WC-6Co cemented carbides, for the liquid Co binder phase was formed during the sintering process. (2) It was found that no coarsening of grains accompanied the process of the densification of the dense compact, this conclusion being obtained from the comparison between the grain size of samples in Figure 11(b—e) and that of raw materials in Figure 11(a). Therefore, the coupled multiphysical fields activation technology is a suitable selection for controlling the grain growth of WC-6Co composites and enabling the retention of the good properties of density and hardness.

FABRICATION OF PURE COPPER

In Micro-FAST, a variety of material micro-parts can be sintered with good densification at a lower temperature and shorter time. In order to improve the process understanding and component quality, this section reports a study on the evolution of the micro-structure and characteristics of a micro-gear fabricated using this novel powder micro-forming/sintering method. The densification of copper powder in the micro-gear can be accomplished, if not entirely, then mostly, during the temperature-rise period. Therefore, the influences of the heating rate and sintering temperature on the densification are investigated in detail.

Pure copper powder (99.5% purity) with an average particle size of 35 μm was used for the experiments. The detailed technological parameters of the experiment are given in Table 4. The morphology of a formed sample can be seen from

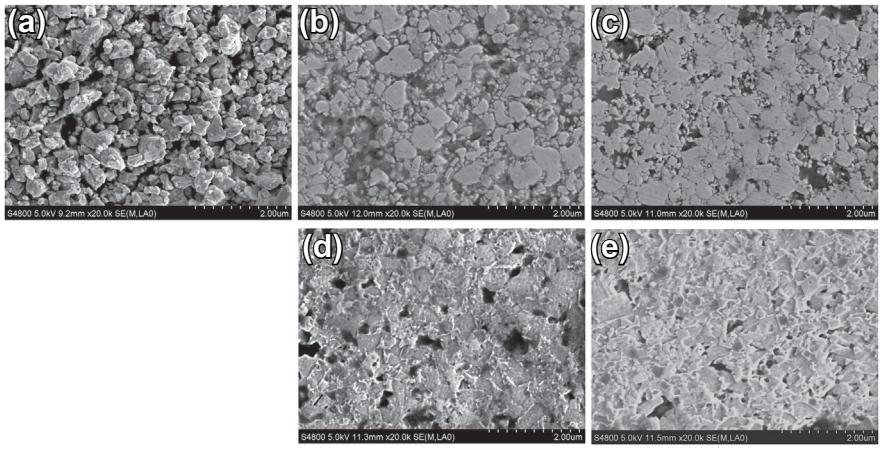

FIGURE 11

SEM micrographs of formed samples: (a) WC-6Co mixed raw powders; (b) WC-6Co sintered at 850 °C, in heating rate 50 °C/s and under 75 MPa for 1 time electro-heating loop; (c) WC-6Co sintered at 850 °C, in heating rate 50 °C/s and under 75 MPa for 3 times electro-heating loop; (d) WC-6Co sintered at 850 °C, in heating rate 50 °C/s and under 75 MPa for 4 times electro-heating loop; (e) WC-6Co sintered at 850 °C, in heating rate 50 °C/s and under 75 MPa for 6 times electro-heating loop.

Figure 12. Micro-gears with 8 teeth were fabricated with a module of 0.2 and a pitch diameter of 1.6 mm.

The heating process of a micro-gear

Figure 13(a) shows the temperature and axial reduction (in height) profiles of the sample during the heating process. According to the characteristics of this temperature profile, the process can be described as consisting of three periods:

1. Preheating period (from room temperature to the end of holding at 200 °C). The onset temperature at the point where the reduction in simple height increases quickly represents the loose powder becoming rearranged and compressed tightly due to the pressure exerted on the punch.

Table 4 The Processing Parameters Corresponding to the Samples Formed

Specimen Designation	Heating Rate (°C/s)	Sintering Temperature (°C)	Pressure on the Punch (MPa)	Number of the Heating Cycle[a] (T ~ 400 °C)
1#	50	500	100	3
2#	50	600	100	3
3#	100	600	100	3
4#	50	700	100	3

[a] *A heating cycle is defined as a cycle during which the temperature rises to the maximum value and then drops to about 400 °C.*

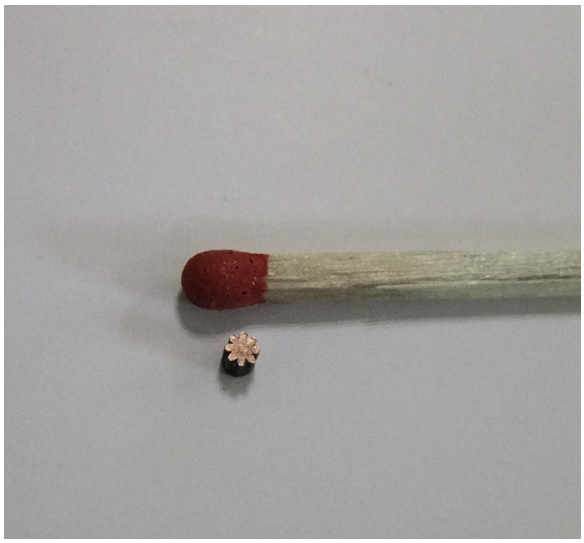

FIGURE 12

Fabricated copper micro-gear compared with a match.

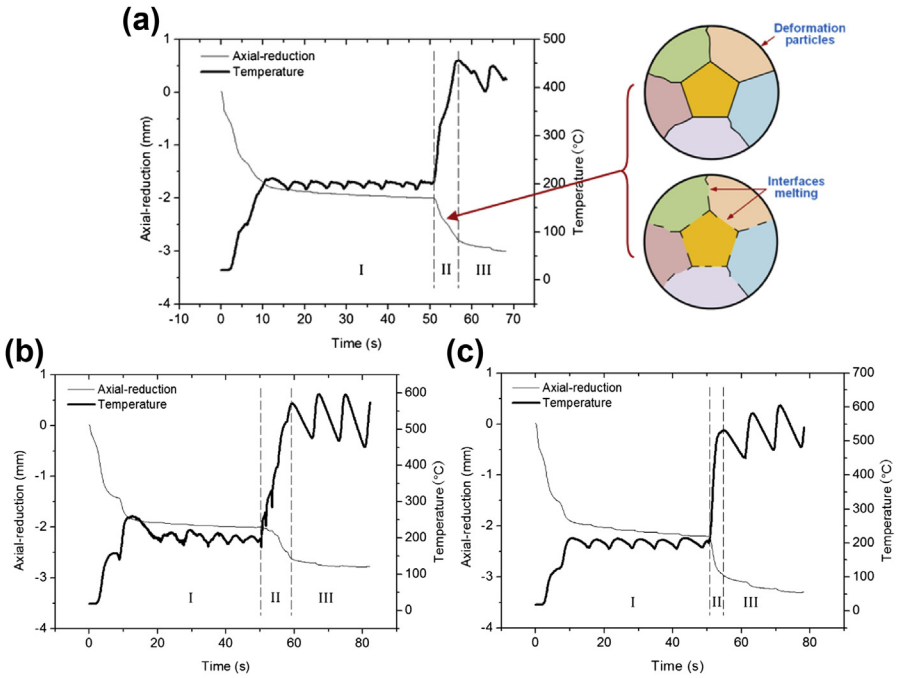

FIGURE 13

The temperature and axial reduction of the workpiece as a function of time: (a) sample 1#; (b) sample 2#; (c) sample 3#.

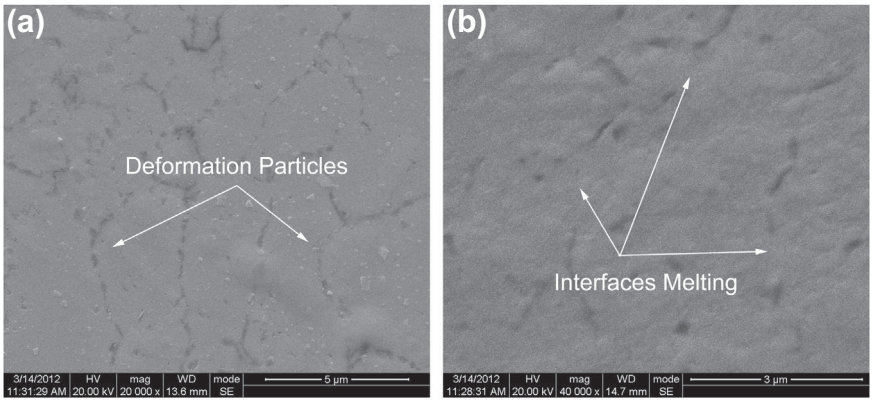

FIGURE 14

Particle deformation and interface formation: (a) 2#, deformed particles; (b) 3#, melting of interfaces between particles.

2. Temperature-rise period (from the end of holding at 200 °C to the ignition temperature). A comparison on the temperature and axial-reduction profile for the samples 1#, 2#, and 3# is given in Figure 13(a–c), and this period is defined as the main densification period where the axial reduction of the sample increases rapidly with the rising temperature. It is worth noting that there was a significant reduction in height in the sample, which can be attributed to the deformation and interface melting of particles, as shown in Figure 14(a) and (b).
3. Final-heating period. According to the trend of the height reduction of the samples, cyclic heating only made a small contribution to the densification of the samples.

Effect of the coupled multiphysics fields activation during the temperature-rise period

As described above, the process used for the forming of the micro-compacts is actually one that was coupled with multiphysics fields activation, i.e., a coupled multifields-activated forming process: forming of the component is enabled simultaneously under the pressure field, temperature field, and electrical field.

Under the effect of an external pressure-field, initially, only elastic deformation develops in the material's particles. For a low density body, the contact areas between particles, where stress is transmitted, are small, and hence, stresses are, locally, much higher than the macroscopic applied stress. Thus, particles or their edges are deformed under the effect of the forming pressure. This greatly increases the interface area among particles and hence minimizes the porosity of the sample and increases the contact resistance of the particles.

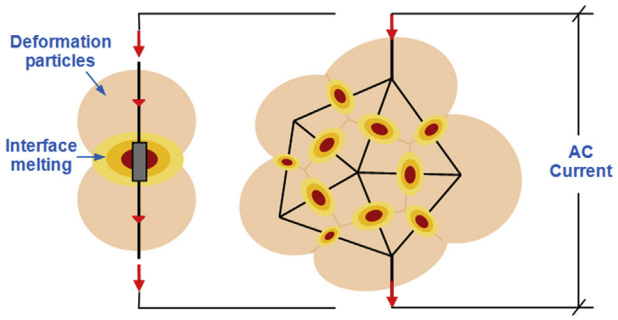

FIGURE 15

Illustration of the principle of the heating process.

Joule heating is the main heat source during the heating process which occurs without generating sparks, compared to SPS [23]. When an AC current passes through a compact, Joule heat will be generated at an interface due to the contact resistance. Figure 15 illustrates the distribution of the current in the compacts. According to the Joule–Lenz's law, the heat generated by the current passing through the compact is:

$$Q = I^2Rt \tag{8}$$

where Q is the generated heat when current passes through the compact; R is the resistance of the particles; and t is the electrify time. In the process of sintering, the change of Joule heat is affected by the interface contact resistance and current of the particles. As observed, the greater the temperature and electrical current density, the greater the Joule heat.

As the surface area of the particles increases, the resistance of the particles' interface decreases, namely, the contact surface between particles can gain local high temperature in the temperature-rise period. A certain amount of liquid phase is formed when the local temperature is greater than the Cu liquidus temperature, which leads to the melting of the contact surface between particles [24,25].

Although the Joule heating is still the main heat source during the sintering process, it has a different densification mechanism compared to that of a conventional SPS process. For example, this study has identified that the mechanical plastic deformation and interface melting of particles make a great contribution to the densification of powder during the coupled multiphysics fields-activated micro-forming process.

The results of the present study have shown that the axial reduction of the samples increased rapidly with the increase of temperature during the sintering while the external pressure was maintained. Based on the experimental observations, it can be concluded that the deformation of the particles resulted in an increase in, and then subsequent disappearance of, the interface areas between the particles, the feature which plays a key role in the densification of the copper powder.

CONCLUSIONS

A new process concept—Micro-FAST, was proposed and developed. Based on the present experiment results, it can be concluded that Micro-FAST is ideal for the manufacture of micro-components with all kinds of material powders at a relatively low sintering temperature and within a very short sintering time. Besides further efforts in fundamental studies being needed, more effort should be made to develop industrial equipment that matches the needs of production of small-size products, these include the following:

1. A new size-effect theory system should be established in order to create a guideline for the design of the Micro-FAST process;
2. Precision of the components formed needs to be improved further;
3. Development of the process and equipment should consider mass-production characteristics.

REFERENCES

[1] Alting L, Kimura F, Hansen HN, Bissacco G. Micro engineering. CIRP Ann Manuf Technol 2003;52:635−57.
[2] Brinksmeier E, Riemer O, Twardy S. Tribological behavior of micro structured surfaces for micro forming tools. Int J Mach Tool Manuf 2010;50:425−30.
[3] Qin Y, Brockett A, Ma Y, Razali A, Zhao J, Harrison C, et al. Micro-manufacturing: research, technology outcomes and development issues. Int J Adv Manuf Tech 2010; 47:821−37.
[4] Tay BY, Loh NH, Tor SB, Ng FL, Fu G, Lu XH. Characterisation of micro gears produced by micro powder injection moulding. Powder Tech 2009;188:179−82.
[5] Cheng J, Wan L, Cai Y, Zhu J, Song P, Dong J. Fabrication of W-20wt.%Cu alloys by powder injection molding. J Mater Process Tech 2010;210:137−42.
[6] Lu D, Yang Y, Qin Y, Yang G. Forming microgears by micro-fast technology. J Microelectromech S 2013;22:708−15.
[7] Huang K, Yang Y, Qin Y, Yang G. Densification behavior of copper powder during the coupled multi-physics fields-activated microforming. Int J Adv Manuf Tech 2013;69: 2651−7.
[8] Lu D, Yang Y, Qin Y, Yang G. Effect of particle size and sintering temperature on densification during coupled multifield-activated microforming. J Mater Res 2012;27: 2579−86.
[9] Huang K, Yang Y, Qin Y, Yang G. 316 L stainless steel powder densification during the coupled multi-fields activated micro-forming. Mater Manuf Process 2013;28:183−8.
[10] Du A, Yang Y, Qin Y, Yang G. Effects of heating rate and sintering temperature on 316 L stainless steel powders sintered under multiphysical field coupling. Mater Manuf Process 2012;28:66−71.
[11] Wakai F, Shinoda Y. Anisotropic sintering stress for sintering of particles arranged in orthotropic symmetry. Acta Mater 2009;57:3955−64.

[12] Kogias G, Tsakaloudi V, Van der Valk P, Zaspalis V. Improvement of the properties of MnZn ferrite power cores through improvements on the microstructure of the compacts. J Magn Magn Mater 2012;324:235−41.
[13] Sun K, Lan Z, Yu Z, Jiang X, Huang J. Phase formation, grain growth and magnetic properties of NiCuZn ferrites. J Magn Magn Mater 2011;323:927−32.
[14] Reddy MP, Madhuri W, Reddy NR, Kumar KVS, Murthy VRK, Reddy RR. Influence of copper substitution on magnetic and electrical properties of MgCuZn ferrite prepared by microwave sintering method. Mat Sci Eng C 2010;30:1094−9.
[15] Zlatkov BS, Mitrović NS, Nikolić MV, Maričić AM, Danninger H, Aleksić OS, et al. Properties of MnZn ferrites prepared by powder injection molding technology. Mat Sci Eng B 2010;175:217−22.
[16] Zaspalis VT, Sklari S, Kolenbrander M. The effect of heating rate on the microstructure and properties of high magnetic permeability MnZn-ferrites. J Magn Magn Mater 2007; 310:28−36.
[17] Pan Y, Li DY, Zhang H. Enhancing the wear resistance of sintered WC−Co composite by adding pseudo-elastic TiNi constituent. Wear 2011;271:1916−21.
[18] Trung TB, Zuhailawati H, Ahmad ZA, Ishihara KN. Grain growth, phase evolution and properties of NbC carbide-doped WC-10AISI304 hardmetals produced by pseudo hot isostatic pressing. J Alloy Compd 2013:20−5.
[19] Machado IF, Girardini L, Lonardelli I, Molinari A. The study of ternary carbides formation during SPS consolidation process in the WC-Co-steel system. Int J Refract Met H 2009;27:883−91.
[20] Zhao S, Song X, Zhang J, Liu X. Effects of scale combination and contact condition of raw powders on SPS sintered near-nanocrystalline WC-Co alloy. Mat Sci Eng A 2008; 473:323−9.
[21] Bonache V, Salvador MD, Fernández A, Borrell A. Fabrication of full density near-nanostructured cemented carbides by combination of VC/Cr3C2 addition and consolidation by SPS and HIP technologies. Int J Refract Met H 2011;29:202−8.
[22] Carroll DF. Sintering and microstructural development in WC/Co-based alloys made with superfine WC powder. Int J Refract Met H 1999;17:123−32.
[23] Zhou Y, Hirao K, Yamauchi Y, Kanzaki S. Effects of heating rate and particle size on pulse electric current sintering of alumina. Scr Mater 2003;48:1631−6.
[24] Beri N, Maheshwari S, Sharma C, Kumar A. Technological advancement in electrical discharge machining with powder metallurgy processed electrodes: a review. Mater Manuf Process 2010;25:1186−97.
[25] Olmos L, Martin CL, Bouvard D. Sintering of mixtures of powders: experiments and modelling. Powder Tech 2009;190:134−40.

CHAPTER

Micro-bulk Forming 12

Mogens Arentoft[1], **Rasmus Solmer Eriksen**[1], **Hans Nørgaard Hansen**[2]
IPU Technology Development, Kgs. Lyngby, Denmark[1]*; Department of Mechanical Engineering, Technical University of Denmark, Kgs. Lyngby, Denmark*[2]

CHAPTER OUTLINE

INTRODUCTION

Forming of metals is a well-established process, dating back more than a thousand years. During the early colonization in Europe, the village blacksmith formed fittings and weapons using hammer, anvil, and forge.

The idea of plastically deforming metals into a desired shape makes good use of the material and can even enhance the performance of the material [1,2]. In the ancient Asian cultures the forging of the Samurai sword was considered to be a black art. By forging steel alloys with different carbon content into a sword blade, it was possible to combine the ductility of low carbon steel with the hardness of high carbon steel into a blade which was both flexible and sharp. The subsequent heat

Micromanufacturing Engineering and Technology. http://dx.doi.org/10.1016/B978-0-323-31149-6.00012-8

treatment of the sword blade included the addition of a mixture of water and clay to the cutting edge of the blade in order to reduce the cooling gradient in this area. Only by mastering the craftsmanship of forming, and using his knowledge of materials and empirical skills for the hardening procedure, was the Samurai sword maker able to make the ultimate weapon [3].

BASIC COLD FORMING PROCESSES

Today bulk forming is used extensively in a wide range of industrial applications. Within the production of transmission elements for the automotive industry, the bulk forming process is the standard. Huge tonnages of rack, axles, and other components are manufactured by the bulk forming process, either into near-net components that subsequently undergo light machining or net shape components which are finished after the forming process.

A typical forming process requires multiple forming steps and comes in a wide range of variants. Each of the variants can, however, be categorized into the eight basic bulk forming operations depicted in Figure 1.

The industrial popularity of the bulk forming process still relies on the underlying theory of material flow and behavior, something that has not changed since the early days of forging. Even with the employment of numerical simulation and modern computer aided design systems, a well-functioning bulk forming system requires extensive knowledge of the strain hardening of the material and its flow behavior as well as of friction and lubrication conditions (tribology). These parameters generally dictate the forming limits of the bulk forming process and thereby also the achievable geometry of the components.

A medium advanced bulk forming process often consists of three to five consecutive forming steps, either mounted in the same press system or as individual

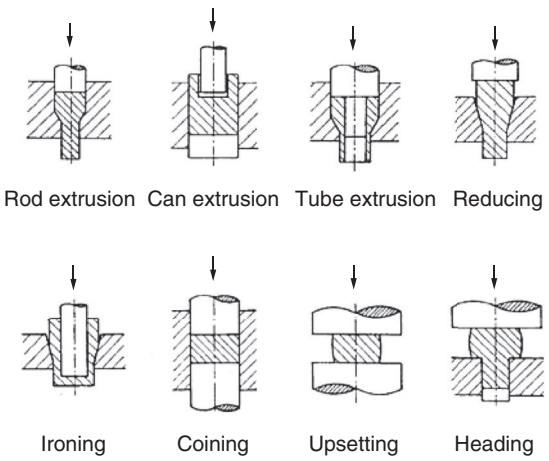

FIGURE 1

Basic cold forging processes [4].

operations. This means that a typical bulk forming process actually is a process chain of several forming operations, each carefully designed and analyzed to arrive at the best possible end result for the finished component.

Micro-bulk forming is the utilization of the bulk forming process to form micro-components. Compared to more traditional micro-manufacturing processes, such as turning and milling, this process holds the potential of producing high quality components, faster and with no or only little material waste.

THE SIZE EFFECT

By definition, a micro-component is a component with one or more geometrical dimensions or functional features of less than 1 mm in size [5]. By decreasing the size of the components in small mechanical systems, the weight and volume of the device can be reduced without sacrificing functionality, and often the micro-component technology is the enabler of a new miniaturized product. Micro-components are often a central part of the mechanical systems in consumer products such as hearing aids, computer drives, or mobile phones. The medical sector is another important application for micro-components. Here the components are used as parts of dental implants, in spine fracture repair kits, or as elements in drug delivery systems. These applications often require low failure rate in combination with high functionality; giving rise to strict quality and tolerance requirements on the components making up the system. It is not uncommon to see 100% inspection rate requirements for these types of components, something that is incompatible with mass production at low cost.

Size effect is a term for the deviation from the linear continuum theory, when the scale is reduced to micro-size. That is, when the scale is reduced to the micro-level, some of the rules change and a new set of theories have to be applied. Or putting it in another way, when the size on the component is within orders of magnitude of the physical elements of the process, e.g., material grain size, the linear theory of the macro-domain breaks down [6].

The contributors to size-effects can be put into three groups: density, shape, and structural effects.

Density effects relate to the inhomogeneity of materials at small scale. If the average grain size of a material is considered to be of the order of 40 μm, a macro-size component would contain millions of grains, meaning that the material could be modeled as homogeneous. Going to the micro-domain, a 500 μm feature would only contain about 12 grains over the cross section, resulting in the properties of the individual grains influencing the forming process.

Shape effects are closely related to the surface-to-volume ratio of the component. Consider a dice with a scalable side length of α. The volume then scales with the third power α^3, whereas the surface area scales to the second power α^2, meaning that a small component will have a higher surface-to-volume ratio, by α, when compared to its larger equivalent. The surface-to-volume ratio is an important parameter when considering an ejection or handling situation, where the friction is a factor of the component surface area and the component strength is related to the material

volume. Designing an ejector system to remove a micro-component from the forming die is challenging, due to the risk of collapse or reverse forming during ejection. Further, small components are prone to the sticking effect, where adhesive forces between the gripper and the component outweigh gravitational forces. These adhesive forces primarily consist of surface tensions, van der Waals, and electrostatic forces, and can be the limiting factor of a handling system for micro-components.

The third effect contributing to the size effect is the group of micro-structural effects. This group of effects is made of physical elements which either experience a physical length limitation, where it is not practical to scale the micro-geometry or where secondary scaling effects come into play. Surface roughness is an example of a quantity that, in practice, is not fully scalable. The roughness topography of a tool is often an inherit property of the manufacturing process and is only scalable within a certain window, resulting in higher relative roughness at smaller size.

Manufacturing tolerance is another important property prone to the size effect. High precision tooling machines are costly with an approximately exponential correlation between achievable precision and machine cost. However, the machine precision is independent of workpiece size and is strictly bound to the precision of the tooling machine itself. However, when the overall size of the component is reduced to the millimeter scale, it is seldom acceptable to inherit the tolerance band of the macro-scale, which is normally within a few orders of magnitude of a millimeter.

Figure 2 depicts prominent scaling effects affecting the micro-forming process; the boundary roughness characteristics, the fixed tolerances inherited from the tool manufacturing process, the grain size determined by the physics of metallurgy, and the geometrical nonlinearity of the surface/volume ratio.

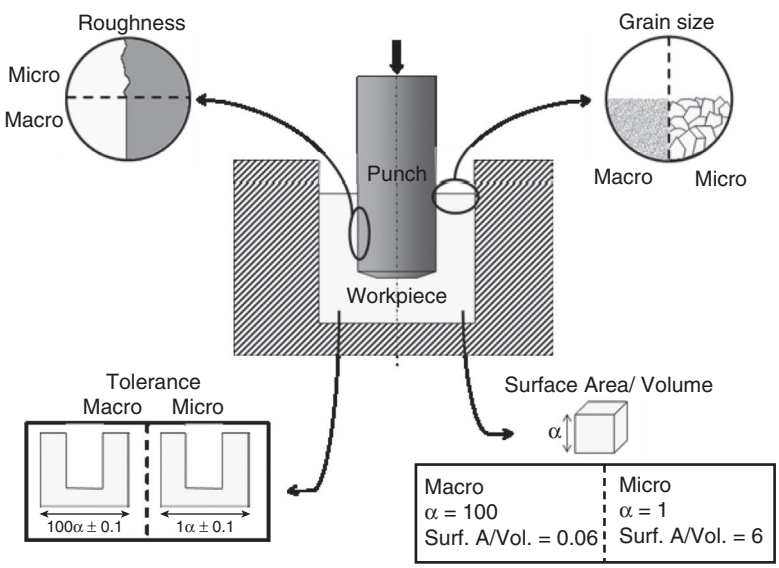

FIGURE 2

Overview of dominant size-effects in micro-bulk forming, the influence of roughness scaling, grain size scaling, tolerance scaling the nonlinear scaling for surface-to-volume ratio.

WORKPIECE MATERIALS

Material knowledge is central for the bulk forming process, which fundamentally relies on differences in flow stress between two materials. These two materials are often termed "workpiece material" and "tooling material," relating to their respective functional purpose in the bulk forming process. Properties such as price, flow stress, ductility, and strain hardening are important for the forming material, whereas the yield strength, machinability, and ductility are performance parameters for the tool material.

In order to accurately analyze and simulate the forming process, workpiece material data are needed. These data can be acquired by performing an upsetting test, where the mechanical strain/stress curve of the material can be acquired using length and force transducers connected to a data acquisition device. The resulting data can be fed into a numerical simulation program and the forming process can be simulated.

The selection of workpiece material is normally a trade-off between requirements set by the component application and formability performance. Materials with a high strength are generally desirable, leading to lower mass and a more compact design; however, these materials are often difficult to form in a bulk forming process. On the other hand, a soft material is easier to extrude or form but the strength of the finished component is often not adequate for high-performance applications. The choice of workpiece material further influences tool life expectancy, forming temperature, the choice of lubricant, coating, and the number of forming operations required.

AMORPHOUS METALS

Amorphous metals are a new range of noncrystalline materials with interesting properties for manufacturing of micro-metallic components. The amorphous structure of the materials is generally realized by combining alloying metallic elements of considerably different atom sizes with rapid cooling when transitioning from the liquid to the solid phase. By rapid cooling the alloy is frozen in the amorphous state, thereby not allowing the metallic atoms to combine into the well-known lattice structure characterizing conventional metals. The required critical cooling rate generally sets limits on the achievable forms in which amorphous metals can be realized, typically thin ribbons, foils, and wires. However, recent development has enabled the casting of amorphous metals with dimensions exceeding 1 mm: these are known as bulk metallic glasses (BMGs).

BMGs are interesting for the forming of micro-components because the material is not subject to the grain size forming limitations, dislocations, and sliding planes of normal crystalline materials and can be formed at the micrometer scale with good results. The forming of BMGs takes place between the glass transition temperature T_g and the crystallization temperature T_x. At T_g the BMG becomes a supercooled viscous liquid exhibiting decreasing flow stress with increasing temperature. A second dependent parameter of the forming temperature is the crystallization time t_{cryst}, at which the amorphous structure is lost and the material turns crystalline. There is a time/flow stress trade-off when selecting the forming temperature; a higher temperature equals

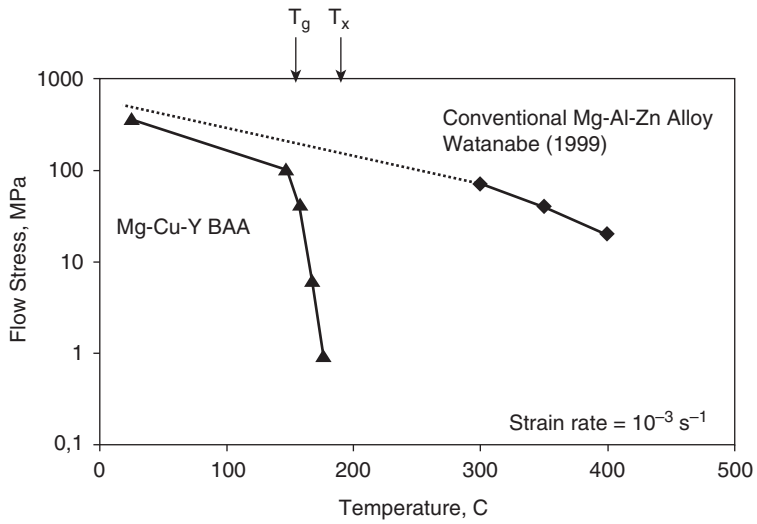

FIGURE 3

Flow stress for Mg60Cu30Y10 bulk amorphous alloy.

low flow stress and low viscosity but limited forming time due to the decreasing crystallization time. On the other hand, a lower forming temperature results in increased flow stress and viscosity of the BMG, resulting in longer process time and increased tool loads, whereas the window of amorphous processing time increases.

Further, BMG materials are generally very strain-rate-dependent and fast processing results in high flow stresses. It has been claimed that BMG above the glass transition temperature behaves like asphalt on a summer's day, since the viscosity of both BMG and asphalt is strongly dependent on temperature and strain rate. Figure 3 depicts the flow stress dependency of Mg60Cu30Y10 bulk amorphous alloy in comparison to a conventional crystalline magnesium—aluminum alloy.

Figure 4 depicts a micro-component formed by bulk forming in BMG and a soft aluminum alloy. By comparison, it is observed that there is better form filling in the case of the BMG material (Figure 4(a)) even though the forming process is not fully completed. As marked by the arrows, the outer rim of the component is subject to rounding in the case of the aluminum material whereas the BMG case exhibits sharp edges.

The forming of BMG material is not trivial and remains a topic of research [7,8]. Some of the issues yet to be solved relate to fracture strength and high-temperature tool development. Low-temperature BMG, with a glass transition temperature below 200 °C, is brittle with fracture strength as low as 500 MPa and may easily fracture during ejection or use. Zirconium and iron-based BMGs are formed between 360 and 600 °C and have a higher yield and fracture strength, but here the design of the tooling setup becomes challenging due to the high temperature that gives rise to thermal deflection, oxidation, and lubrication breakdown.

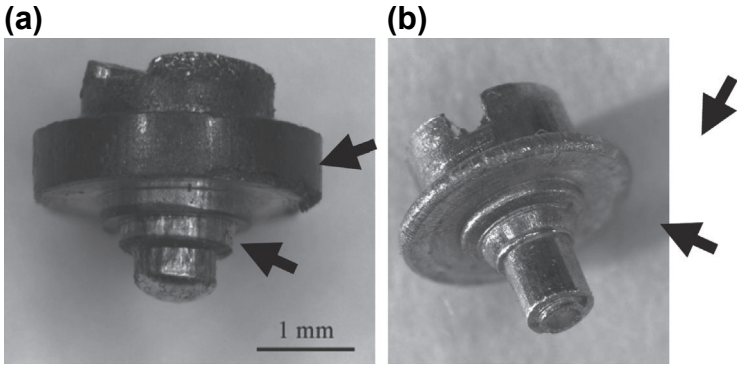

FIGURE 4

Side-by-side comparison of a potentiometer axle for a hearing aid bulk formed in: BMG Mg60Cu30Y10 (a); and in an annealed aluminum EN AW-6060 (b).

TOOL MATERIALS

The most dominant tool steels for bulk forming tools are state-of-the-art powder metallurgical steels with high toughness, hardness, and metallurgical homogeneity. Due to the high surface pressures involved in bulk forming, a tool material hardness of greater than 50 HRC is normally required. The tool steels used to be cut in their soft state and subsequently heat-treated to their maximum hardness and ultimately polished or surface-treated. However, modern tooling machines can directly cut hardened steel, allowing for better tolerances of the finished tool by avoiding the inevitable geometrical deflections arising during heat treatment.

In micro-bulk forming the geometrical tolerances of the tool are very narrow and deflections of the tool during heat treatment often exceed the total allowable tolerance deviation of the tool. Thus tooling materials for micro-bulk forming need to be hardened already from bulk and will be machined in their hard state using grinding, hard micro-milling, or electro discharge machining (EDM). Owing to the small size of the tools it can be time and cost-effective to use known prefab elements such as standard industrial punch needles or bushings as a starting point for a bulk forming tool, as these ISO-standardized machine elements are cost-effective, easy to source, and have the mechanical properties required.

Hard metal, ceramics, or solid tungsten carbide materials are other options for tooling materials. The cost of these materials is often much higher than traditional tool steel but since the amount of material used for a micro-bulk forming die is small, the solid tungsten carbide can be an economically viable tool material. The benefits of using tungsten carbide as tool material are the increased hardness of 62−70 HRC and a very low elasticity. The drawbacks of using tungsten carbide are the limited available machining processes, normally only electrical discharge machining, and the low tensile fracture strength of the material (as low as

400 MPa). Especially, the presence of tensile hub stress is unwanted for hard metal dies because of the crack initiation risk. With a correctly dimensioned prestress system, in the form of conical stress rings, it is possible to superimpose compressive stresses onto the hard metal forming die. As a result, the stress rings counteract the tensile stresses arising from the forming process, thereby eliminating any effective tensile stresses on the hard metal die. This is also touched upon in the next section dealing with machine and tool design.

MACHINE AND TOOL DESIGN

The design and manufacturing of machine and tooling elements play an important role in the overall performance of a micro-bulk forming process. Ideally the machine should scale accordingly, meaning that the micro-bulk forming could take place on small mobile tabletop machines. This vision has been proposed by several researchers as the factory lines of the future. In order to realize this vision, several technologies have to work together to form a fully working micro-bulk forming plant, from raw material to the final component.

BILLET PREPARATION

Workpiece material is delivered in bulk, typically as rods. These have to be split into billets with the right volume for the subsequent bulk forming operation. A straightforward way to split the bulk material is by machining. This is, however, not very appealing for the reasons of cost and time. Rightfully, a claim could be made that if the billets have to be machined, the whole component should be finished when the part is in the cutting machine.

By cropping billets from rods the machining operation is avoided. Cropping is a process where the bulk material rod is divided into smaller pieces by a static and a moving cutting edge. Cropping is not a high precision process and some volume deviation is to be expected between the final billets. An investigation of the cropping quality of an Ø1.9-mm aluminum rod has been made and the results are depicted in Figure 5 [9]. It is clear that the cut in Figure 5(b) exhibits only little scatter in volume among the cut billets due to the high quality cut. It was further found that the billet was geometrically deformed in the high-speed cutting scenario, where the faces of the cutting dies move with speeds exceeding 10 m/s, Figure 5(c).

It was further found that cropping is a fast and inexpensive way of manufacturing billets for micro-bulk forming. The best results are achieved using a cropping process where the bulk material is kept under axial stress, close to the yield strength of the material, while the billet is sheared from the bulk.

PRESS SYSTEM

Conventional macro-size hydraulic or excenter presses are not suitable for micro-bulk forming processes due to their size, and their low load control capability.

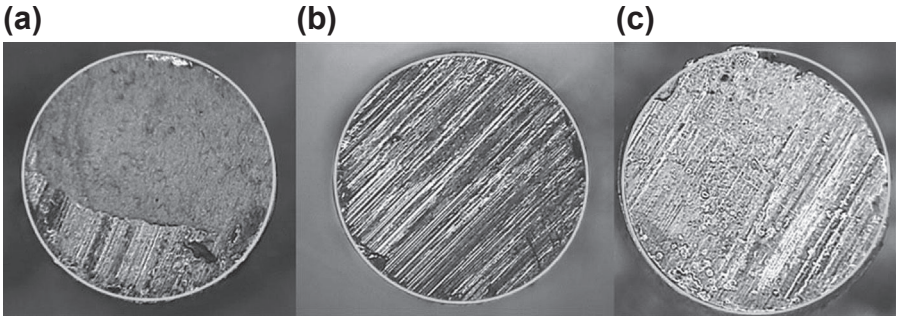

FIGURE 5

Cropping quality comparison of an Ø1.9-mm aluminum rod with three different cropping scenarios. (a) conventional cropping, (b) cropping under hydrostatic pressure, and (c) high-speed cropping.

Bulk forming of high-quality components requires high stiffness of the press frame, high speed and good load and position control of the press. The load requirements often range between 5 and 30 kN, depending on the component and the material. With these requirements in mind a number of micro-bulk forming press systems have been built [9–11]. By using a servomotor as the actuator for the press movement, the required speed and force can be delivered while maintaining good control over the position of the press axis. The actuator itself can be a direct drive linear motor, where a linear rod is moved by the magnetic field of surrounding coils. This solution offers very high speeds and accelerations of up to 40*G* while having a peak force output at about 0.5 kN. Another commonly used setup is a configuration with a nut and roller screw driven by a servomotor, through a gearbox. The roller screw solution is capable of positioning to within a few micrometers while delivering high loads at moderate speed. The press frame should be designed for high stiffness in order to minimize elastic deflections of the frame and the consequent positional inaccuracy and lateral defections. The press frame system is normally not prestressed, as deflections can be kept within tolerable limits.

THE TOOL DIE SYSTEM

Due to the required precision on tooling elements and the machine in general, manufacturing process chain design decisions will have to be made in order to keep tolerances within acceptable limits. Examples of such process chain design decisions include machining several tooling elements in the same run, thereby eliminating inaccuracies arising from fixation and long-term deflections of the tooling machine.

PRECISION AND ALIGNMENT OF TOOLING ELEMENTS

In general the precision requirements of a tooling system for micro-bulk forming can be divided into precision issues relating to the precision of the individual tooling

element, such as the die and the punch, and the precision of the relative alignment of the individual parts, relating to the framework of the tooling system.

Achieving the required tolerances on the individual tooling parts is relatively easily done by an appropriate choice of tooling machine and process chain. Here high speed milling and turning, and EDM, are processes of choice. These processes can work directly in hardened material and can achieve good precision down to about 5 μm. With subsequent surface treatment such as polishing or micro-spraying, high-quality tooling components can be achieved with a short lead time and at low cost.

When considering the alignment of the individual tooling elements, there are a number of approaches to achieving the alignment of the tooling parts. The straightforward way of ensuring the alignment of tooling elements is by a framework supporting the tooling elements. This could be the utilization of a standard die set where ball-cage bearings ensure the alignment of the upper and lower part of the die set. The use of a reference plane, as depicted in Figure 6(a), such as a ground flat back plate, is another way of ensuring good alignment. By placing the high accuracy reference element in the middle of the tolerance chain, it is possible to reference all other tooling elements to this element. This approach requires strict control of the tool tolerance chain to ensure that alignment errors are within an acceptable level. It is often challenging to ensure that the macro-size framework tooling elements, such as the stand and the base-plate, are within the precision required for the alignment of the micro-size forming tools. In Figure 6(b), the punch is loosely fitted into a

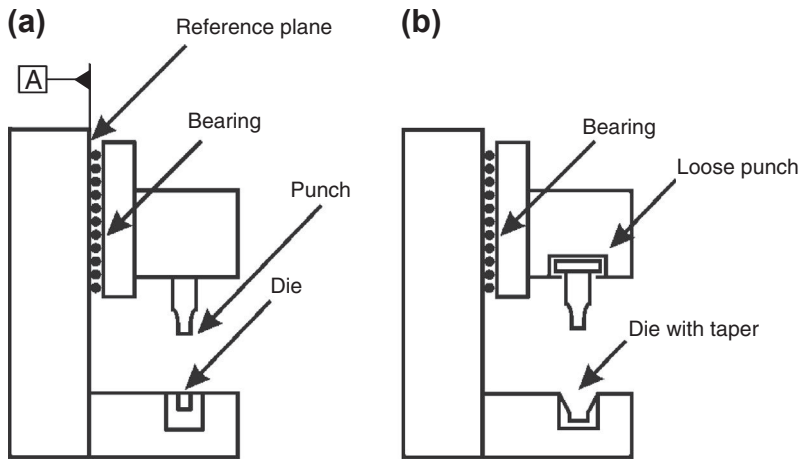

FIGURE 6

(a) Example of a bulk forming setup where the back-plate is used as a reference for the tooling elements. (b) A die with a tapered inlet and a flexible punch fixture is used to form a self-aligning bulk forming tool.

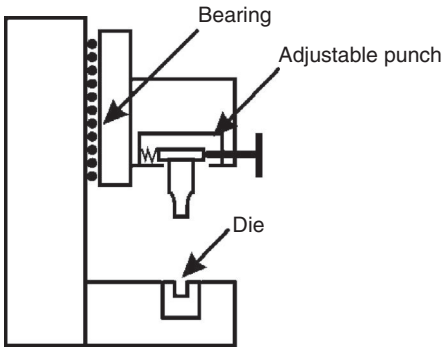

FIGURE 7

An adjustable punch fixture allows for the alignment of the punch and die through an adjustment screw.

slot of the moving fixture allowing the punch to center on the die during closure. It is important that the alignment occurs before any load is applied to the punch, meaning that this property should be included into the design of the forming tools. This alignment approach is simple and self-contained, but is generally only suitable for simple forming operations of rotationally symmetrical components.

A hybrid solution for the alignment of tooling elements is depicted in Figure 7. Here the punch holder fixture is spring loaded with a micrometer screw, allowing for adjustment of the punch position. With this flexible solution it is easy to achieve good alignment and long-term stability, and re-establishing the alignment is tolerable.

FLEXIBILITY OF TOOL SYSTEM

With the vision of small desktop style factories of the future in mind, flexibility and low changeover times are important factors of focus. With the trend toward smaller production series and more customized products, several components should be produced on the same setup with a quick change of only the central forming dies and handling fixtures. This idea of modularization is easy to grasp and has been widely adopted in the manufacturing industry. When considering micro-bulk forming, it is suggested to realize a flexible bulk forming system through the utilization of modified normal machine elements.

Figure 8(a) depicts an example of a two-step flexible micro-forming setup. The forming dies, punches, and ejectors are manufactured from standard punch needles. By standardizing the diameter and tooling material and allowing for easy setup, the central tooling elements can easily be changed and the machine can manufacture different components with low change times. With an outer diameter of 8 mm and a ground surface finish, the forming dies in Figure 8(b) can be easily interchanged.

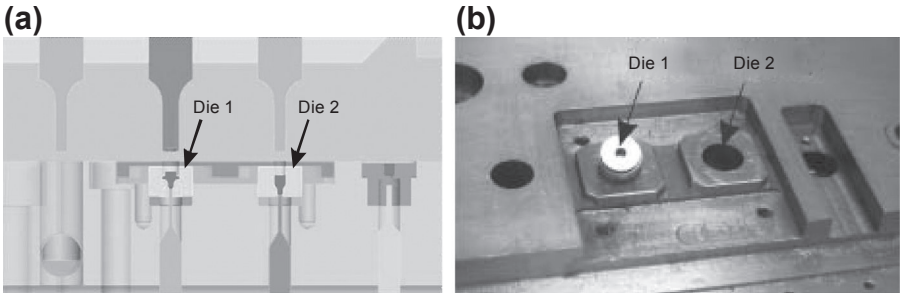

FIGURE 8

Sectional view of a two stage micro-bulk forming machine.

WARM FORGING OF MICRO-COMPONENTS

Micro-components are often manufactured using precious metals such as alloys of palladium, titanium, or magnesium. The choice of material is often given by the end applications, where the environment of use can be humid, corrosive or have special demands for strength or biocompatibility. Also new age materials, such as BMGs, are expected to find wide use within micro-bulk forming. With some of these advanced materials it can be beneficial to utilize warm forging, where the central forming tool elements are operating at elevated temperature. The main benefits of warm forging are a decreased tooling load, increased ductility of the workpiece material, and elimination of the heat treatment process prior and post to forging. For some materials, such as BMGs or high-grade titanium, it is required to warm the forming tools in order to have an acceptable lifetime of the tooling elements. Warm forging is defined as forging at elevated temperatures above the ambient temperature and below the material recrystallization temperature, typically in the range 100−400 °C. The use of warm forming tools requires an advanced tooling setup with good thermal isolation, heat shields, and possible external cooling. It is essential to control the temperature gradient between the warm forging tool elements and the cold framework elements to minimize thermal defections and the following misalignment and possible tool damage. Figure 9(a) depicts a prototype tool system for warm forging of a dental implant in titanium.

The system consists of a central heated core including die, punch, ejector supporting elements, and heaters. The framework die set is thermally isolated from the warm core by a calcium silicate-based ceramic material with a thermal conductivity of 0.4 W/mK. Heat shields, with an optical reflective finish, are placed around the upper and lower heated tooling elements. These heat shields prevent heat transfer to the frame by radiation and have a secondary function as a simple safety measure for avoidance of touching of the warm tool parts. Figure 9(b) illustrates the steady state temperature distribution of the tool system when heated to 200 °C. It can be observed that the tool frame is kept cold with only an insignificant temperature gradient over the supporting tool frame, thereby keeping thermal defections to an

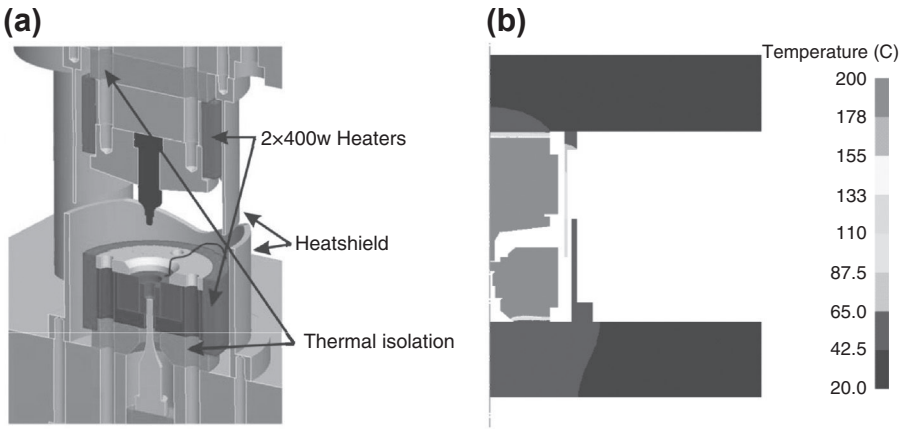

FIGURE 9

(a) A prototype tool system for warm micro-bulk forming of a dental implant in titanium. (b) Steady state thermal analysis of tool system including external die set for alignment.

acceptable level. In an industrial setup it is usually necessary to apply external temperature control as known from tools for thermoplastic injection molding.

The elevated temperature in warm forging imposes some additional design challenges on the tooling parts located in the heated zone of the tool. For an open-die forging scenario the primary adjacent factors to handle are more challenging tribological conditions. The tribological conditions can be controlled by applying suitable coatings to the punch and die, and matching the workpiece material and the lubricant: the section on tribology later in the chapter touches more on these issues. Further, periodical cleaning of the punch and die might be needed to remove residues of lubricant and workpiece material pickup. For closed-die forming the tribological challenges remain and are followed by oxidation and lubricant entrapment issues. When tempering the punch and die at temperatures near to the recrystallization point, oxides will form on the surface of these parts. The oxide layer, having a high friction coefficient, will give rise to a narrowing of tool clearances and increased friction between the tool pieces and between the tool and workpiece. This can lead to tool breakdown and should be avoided. Further, pickup due to lubricant breakdown and lubricant entrapment is more dominant at elevated temperatures. Most lubricants are unfit for warm forging because the base liquid components become volatile, leaving solid lubricant residues in the forming die and on the workpiece surface. However, by application of the right coatings in combination with the right type and amount of lubricant, it is possible to realize a micro-bulk forming process at elevated temperature.

HANDLING AND EJECTION SYSTEM

Today, most industrial machines handling micro-components are based on conventional circular vibrating screeners. These screeners are cross-vibrating vessels that

are able to align a specific component geometry by means of a custom-built mechanical gate system allowing only components that are rightly aligned to pass through. Depending on the component geometry, material, and the crafted design of the gate system, the mean failure rate of a vibrating screen system is usually around $\lambda = 1E\text{-}2$ to $\lambda = 1E\text{-}6$ pieces, meaning that one in every hundred to every million components will jam the system so that an operator will have to inspect the system. Further, the vibrating screeners are bulky, noisy, and inflexible, making them unsuitable as a handling system for a multistage micro-manufacturing machine. The sticking of matter is another issue that influences the handling of micro-components. With the increased surface-to-volume ratio for these small components, the van der Waals forces will cause sticking of the components. Primarily, the components will tend to stick to each other, requiring a strategy capable of both handling and separation. For this reason handling concepts of micro-components have been studied intensively in recent years [12,13]. The use of robot cells, advanced gripper systems, and self-assembly systems have been proposed, but none have been widely employed within micro-manufacturing because of the unfavorable combination of cost, complexity, and speed of these systems.

Figure 10 depicts a handling system for the micro-bulk forming process. A cut-out of the transfer system is illustrated in Figure 10(b), where the components can be ejected into the container fixture, moved laterally to the next station, and inserted into the succeeding forming die. This system is capable of transferring components at high speed and is simple to monitor for failure. The container is a precision

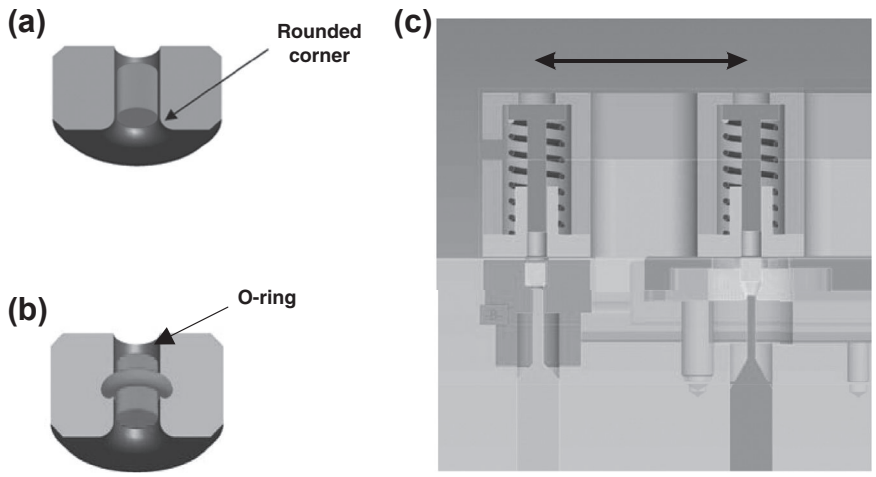

FIGURE 10

(a) Gripper for cylindrical micro-component functioning by a combination of friction and sticking forces. (b) Gripper with integrated rubber O-ring. The billet is centered in the carrier and is held in place by the friction of the O-ring. (c) Sectional drawing of a micro-bulk forming tool with an integrated ejector and transfer system.

element used to hold and transport the components from one forming station to the next. For the container depicted in Figure 10(a), the component is held in place by a combination of friction forces and surface tension forces. In order for the surface tension forces to overcome the gravitational forces and keep the component in the container, a specific clearance in the order of micrometers between the component and the container wall must be realized. Furthermore, wear of the container, production tolerances, and lubrication quantity must be under control.

Another concept for the component to be held in place in the transfer container is shown in Figure 10(b). In this design an O-ring is placed inside the container die and primarily functions as a friction gate. Secondarily the O-ring also has a centering function because the rubber O-ring will absorb minor misalignment and center the component in the container. The proposed transfer system is only capable of handling rotationally symmetrical components, but could be made to function for free-form workpiece geometries also.

PROCESS SUPERVISION

Intelligent process supervision is an area of increasing interest within manufacturing technology. By online monitoring of different process parameters and real-time comparison with a priori values or values acquired through earlier processing, it is possible to make sure that the process is performing correctly. Some common parameters that are monitored in a bulk forming process are the load/stroke curve for each forming cell, the tool temperature, the workpiece weight, and the position of the transfer rig.

The micro-bulk forming tool shown in Figure 11 employs online measurement of load on the individual forming cells by piezo force sensors. The tool setup is equipped with two piezo-type force transducers which measure the forming and ejection

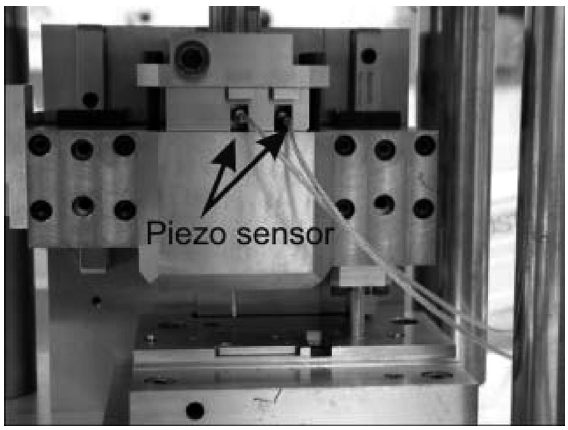

FIGURE 11

Online measurement of load on the individual forming cells by piezo force sensors.

forces on each of the two forming cells. By correlating the forming force with the stroke length, given by the actuator position encoder, the load/stroke curve can be determined and the curve can be compared with some preestablished curve envelopes. With this type of setup it is possible to detect machine errors such as tool breakdown, stuck workpieces, and misplaced aligned workpieces due to transfer errors. Secondary faults such as inconsistency in workpiece material, lubricant breakdown, and tool wear can also be monitored.

Data logging of the monitored values can serve as a quality assurance parameter of the manufactured components. As it is not uncommon to encounter inspection requirement rates of 100% within micro-manufacturing, the addition of traceability and online quality inspection can be valuable. Furthermore, the ability to stop the bulk forming machine in case of misalignment of workpiece or general tool malfunction can avoid machine breakdown, save tooling costs, and help to minimize production downtime.

MICRO-TRIBOLOGY

Tribology is the science and technology of interacting surfaces in relative motion. This includes the study of the phenomena of friction, lubrication, and wear phenomena. Micro-tribology is the subcategory of tribology dealing with the interaction of micro-size surfaces. As mentioned in the earlier section on the size effect, the laws of friction and lubrication are prone to the size effect. The main reason for this can be found in the underlying surface roughness (or surface asperities, as it is usually termed when referring to tribology), which only scales to a certain extent. This means that the relative surface roughness of a micro-component will be greater in the case of a micro-component compared with macro-size. However, the main parameter of interest in bulk forming is friction, which is dependent on surface load, lubrication, and surface characteristics, including surface roughness. Amontons' law of friction dictates a linear dependence between load and friction force: $F_f = \overline{\mu} \cdot L$, where F_f denotes the friction force, $\overline{\mu}$ is the friction coefficient, and L is the load. It can be noted that the friction force is independent of contact area, something that was later challenged by the Bowden and Tabor law of friction. Here the friction force F_f is expressed at the product of the effective shear stress, denoted by $\overline{\tau}$, and the sum of the areas of the asperities in contact: $F_f = \overline{\tau} \sum A_{asp}$. In bulk forming, the friction coefficient $\overline{\mu}$ is often established on the basis of experiment and there is seldom an explicit formulation for this quantity. The double-cup extrusion test (DCE test) is a recognized way of establishing the friction coefficient experimentally. The experimental setup, depicted in Figure 12, is based on a double-cup pressed between two punches with equal geometry. In the case of zero friction, the height ratio between the upper and lower cup will be unity, while no lower cup will be formed in the case of infinite friction.

A number of micro-scaled DCE tests were carried out by Engel and it was found that the measured friction coefficient depends on the scale of the experiment [14].

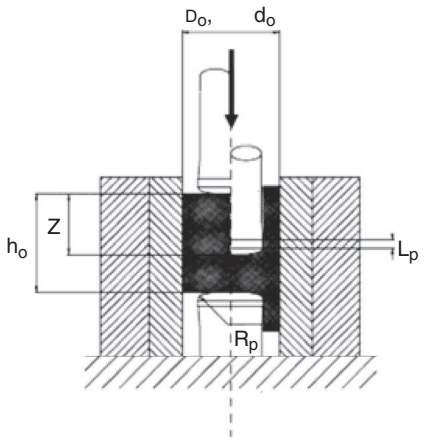

FIGURE 12

Sectional illustration of the double-cup extrusion test.

It was further found that the friction coefficient would increase by a factor of 20 when the experiment was scaled by a factor of 8. According to Engel, this is due to the fact that for micro-scale surfaces, more surface asperities reside close to the boundaries of the workpiece where they are less likely to form lubricant pockets under hydrostatic pressure. This influences the surface contact area, leading to an increase in friction force, as observed from the Bowden and Tabor law of friction. More studies of friction behavior can be found in references [15,16].

The influence of increase in friction coefficient when working in the micro-size domain brings about challenges for the handling and ejection of the bulk formed micro-components. Considering the increase of the surface-to-volume ratio, by the scaling factor α, while keeping in mind that surface area promotes friction and volume of material brings strength, this is an important frictional challenge encountered within micro-bulk forming. Further, with the increase in friction due to open lubricant pockets for the micro-size domain, it is evident that friction is a key challenge to be overcome in micro-bulk forming.

Figure 13(a) illustrates a simulation of a preform for a component to be manufactured by micro-bulk forming. In this case the lower pin extrusion, with a diameter of about 0.5 mm, must be able to withstand the total friction force during ejection. If the friction force is greater than the yield strength of the component the pin will collapse and reverse forming will occur. The photograph in Figure 13(b) presents an example of reverse forming of the component: this component is the realization of the simulation illustrated in Figure 13(a) where the forward rod extrusion has collapsed during ejection. The problem was resolved by a reduction of the press load, change of lubricant, and polishing of the forming die. The use and application of lubricants for micro-bulk forming is at the present time not very well researched. In conventional bulk forming, soaped-phosphate lubricant has been the lubricant of

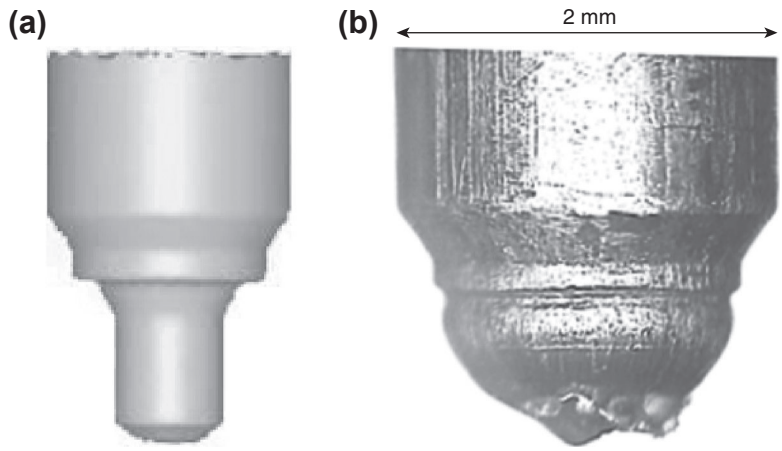

FIGURE 13

(a) Three-dimensional simulation of preform for a micro-axle. (b) Photograph of the formed component where unwanted reverse forming has occurred during ejection from the forming die.

choice for several decades. Unfortunately this lubricant is unsuitable for micro-bulk forming due to the chemical properties of the lubricant layer, allowing scaling down only to a certain thickness. In the example discussed above and other micro-bulk forming experiments at ambient temperature, the use of a commercial silicon paste showed good results. However, the application and removal of the lubricant as well as unintended confinement of lubricant in the forming die have been identified as challenges.

For warm forging and the forming of BMGs, a commercial sprayable lubricant based on $MoSO^2$ has been utilized. This lubrication approach worked fairly well and is suitable for forming at elevated temperatures. A drawback of utilizing a $MoSO^2$-based lubricant is the undesirable interaction with the workpiece surface. This will leave a dark-colored, rough surface which is difficult to remove and is generally unsuitable for use in any advanced or medical applications.

PROCESS ANALYSIS

The analysis of the bulk forming process normally takes place in a dedicated finite element method (FEM) computer simulation environment. In practice, the software is solving the underlying partial differential equations by doing incremental integration of an approximate set of equations. Due to the severe deformation of the workpiece in bulk forming, the software must be capable of doing accurate remeshing while retaining volume constancy. The process analysis is initiated by establishing the material parameters. The workpiece material flow curve is typically acquired by doing a tensile test or performing an upsetting test in a universal testing machine.

Once the material data are known, these can be fed into the material model of the FEM software together with the tool geometry. If the material is strain-rate-dependent or the process needs to run at high strain rates, this influence will have to be included in the model also. This forms the physical basis of the simulation and the simulation process proceeds by selection of simulation parameters.

The choice and analysis of simulation parameters depend on the type of forging process, tolerances, simulation accuracy, and several other influencing factors. The most important factor, however, is the number of elements in the simulation, *N*. The *N*-factor determines the number of nodes in the mesh and is thus responsible for the simulation accuracy. The number of calculations to be done by the computer increases linearly with *N*, and thus the number of elements becomes a trade-off between calculation workload and simulation accuracy. It is possible to use a zoned mesh where the user can define zones of the workpiece to have a more refined mesh, typically in areas of severe deformation.

Another important simulation parameter is the simulation step size. This is the time (or punch travel distance) between successive simulation steps. As in the case of number of elements, a large number of steps indicate a large calculation workload, while a low number of simulations steps will affect simulation accuracy. However, by taking notice of the rate of convergence of the simulation it is possible to choose the right step size within a few iterations.

For rotationally symmetrical workpieces, such as bolt, axle, or cup geometries, it is possible to cut down on the calculations by doing a two-dimensional simulation while retaining the full validity of the simulation. Even in the case of three-dimensional geometries it is often possible to impose symmetry constraints and cut down on the amount of calculations or increase the accuracy of the simulation. Figure 14(a)

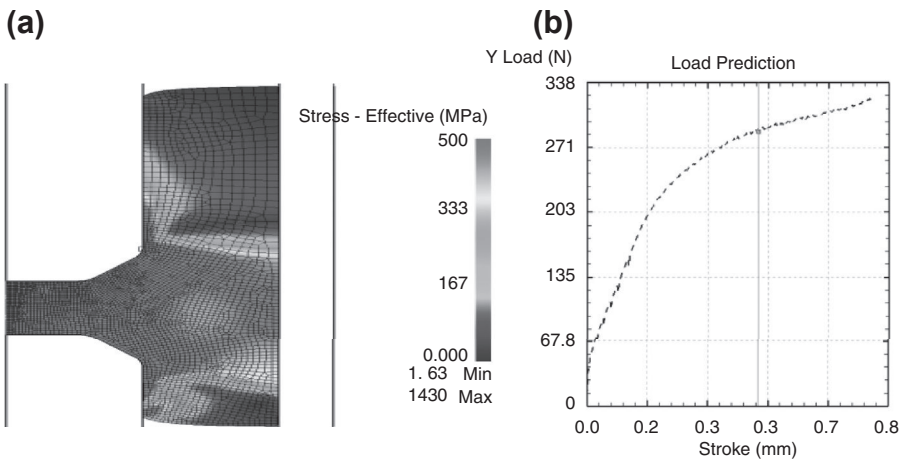

FIGURE 14

Finite element simulation of a double-cup extrusion: (a) stress distribution, and (b) load/stroke curve.

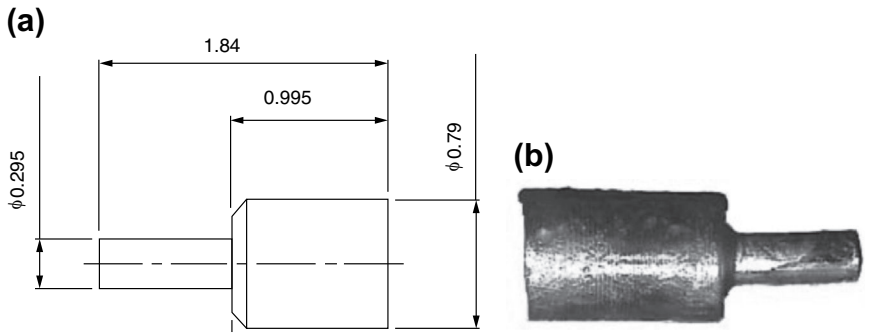

FIGURE 15

A sample of the extruded micro-pin (dimensions: mm).

illustrates the achieved geometry and stress distribution of a two-dimensional simulation of a double-cup extrusion. The simulation was done with a billet diameter of 1 mm of CuZn15 material and a friction coefficient $\mu = 0.15$ between the billet and container wall. Figure 14(b) is a plot of the corresponding load/stroke curve where the exponential progress of the envelope can be attributed to the work hardening of the workpiece material.

The benefits of simulations are manifold and simulations of traditional bulk forming processes often have exhibited a geometrical accuracy of better than 0.5%. If the simulation parameters are chosen carefully it is possible to predict the press load, unwanted forming folds, and tool stress without having to prepare costly prototype tools.

The micro-bulk forming process can be simulated in the same way as conventional macro-size bulk forming process with a few important exceptions. Most simulation models hold an underlying assumption of a continuous and isotropic material model. This means that the grain structure of the material is not taken into account, meaning that the model is only valid down to a certain size. Within normal limits, a material can be modeled as continuous and isotropic if it is indeed isotropic and the number of grain structures across all features is greater than 8−10 grains [15].

Figure 15 illustrates a forming experiment where a small copper pin was extruded. The original specification is reproduced in Figure 15(a). With an average grain size of about 80 μm, there are less than four grains across the pin, thereby invalidating the assumption of isotropy of the material. A photograph of the bulk-formed pin is shown in Figure 15(b) where a clear side tracing of the extruded pin can be noted. This behavior has been the topic of several research projects, and a range of new material models trying to incorporate the intergrain behavior have been proposed. By choosing a material with a fine grain structure or by changing the grain size by heat treatment or mechanical remodeling, it is possible to form micro-size components while keeping the assumption of homogeneity and isotropy in the material intact.

REFERENCES

[1] Cruise RB, Gardner L. Strength enhancements induced during cold forming of stainless steel sections. J Constr Steel Res 2008;64(11):1310–6.

[2] Ashraf M, Gardner L, Nethercot DA. Strength enhancement of the corner regions of stainless steel cross-sections. J. Constr Steel Res 2005;61(1):37–52.

[3] Inoue T. The Japanese sword: the material, manufacturing and computer simulation of quenching process. Mater Sci Res Int 1997;3:193–203.

[4] Nielsen LS, Lassen S, Andersen CB, Grønbæk J, Bay N. Development of a flexible tool system for small quantity production in cold forging. J Mater Process Technol 1997; 71(11/1):36–42.

[5] Engel U, Eckstein R. Microforming – from basic research to its realization. J Mater Process Technol 2002;125–126:35–44.

[6] Geiger M, Kleiner M, Eckstein R, Tiesler N, Engel U. Microforming. CIRP Ann Manuf Technol 2001;50:445–62.

[7] Wert JA, Thornsen C, Jensen RD, Arentoft M. Forming of bulk metallic glass microcomponents. J Mater Process Technol 2009;209:1570–9.

[8] Schroers J, Nguyen T, O'Keeffe S, Desai A. Thermoplastic forming of bulk metallic glass – applications for MEMS and microstructure fabrication. Mater Sci Eng A 2007;449–451(3/25):898–902.

[9] Arentoft M, Eriksen RS, Hansen HN, Paldan NA. Towards the first generation micro bulk forming system. CIRP Ann 2011;60/1:335–8. Elsevier.

[10] Okazaki Y, Mishima N, Ashida K. Microfactory – concept, history, and developments. J Manuf Sci Eng November 2004;126:837–44.

[11] Cao J, Krishnan N, Wang Z, Lu H, Liu WK, Swanson A. Microforming: experimental investigation of the extrusion process for micropins and its numerical simulation using RKEM. J Manuf Sci Eng November 2004;126:642–52.

[12] Van Brussel H, Peirs J, Reynaerts D, Delchambre A, Reinhart G, Roth N, et al. Assembly of microsystems. CIRP Ann Manuf Technol 2000;49:451–72.

[13] Eriksson T, Hansen H, Gegeckaite A. On the use of industrial robots in microfactories. Int J Adv Manuf Technol 2008;38(08/01):479–86.

[14] Engel U. Tribology in microforming. Wear 2006;260:265–73.

[15] Krishnan N, Cao J, Dohda K. Study of the size effects on friction conditions in microextrusion – Part I: microextrusion experiments and analysis. J Manuf Sci Eng August 2007;129:669–76.

[16] Mo Y, Turner KT, Szlufarska I. Friction laws at the nanoscale. Nature 2009;457: 1116–9.

This page intentionally left blank

CHAPTER

Forming of Micro-sheet Metal Components

13

Yi Qin, Wan-Nawang W.A., Jie Zhao

Centre for Precision Manufacturing, The University of Strathclyde, Glasgow, UK

CHAPTER OUTLINE

INTRODUCTION

Sheet metal components are used extensively in various applications such as vehicles, aircraft, electronics products, medical implants and packaging for consuming goods, typical parts/components including car panels, aircraft skins, cans for food and drinks, frames for TV/computer screens/monitors/displays, etc. Concerning miniature/micro-products, sheet metal parts include electrical connectors and lead frames, micro-meshes for masks and optical devices, micro-springs for micro-switches, micro-cups for electron guns and micro-packaging, micro-laminates for micro-motor and fluidic devices, micro-gears for micro-mechanical devices, casings/housings for micro-device assembly/packaging, micro-knives for surgery, etc. Therefore, miniature/micro-sheet metal parts are closely associated with everyday life.

Basic process configurations for the forming of macro-products include shearing, blanking, bending, stamping, deep drawing (including mechanical and hydromechanical), hydroforming, stretch forming, superplastic forming, age forming, spinning, explosive forming, incremental forming, etc. Some of these processes may be equally

Micromanufacturing Engineering and Technology. http://dx.doi.org/10.1016/B978-0-323-31149-6.00013-X

applied to the forming of miniature and even micro-products, if the issues related to "size effect" can be handled successfully [1–8]. General challenges associated with the manufacture of micro-products have been described in Chapter 1 of this book.

The forming of small/thin metal parts has been undertaken by industry for many years. New challenges arise when the overall sizes reduce to submillimeters, local features to such as tens of microns, or the precision requirements for macro-/miniature parts to such as less than a few microns. Studying the research reported previously and recent research conducted in-house resulted in the following observations:

1. Conventional metal-forming process configurations may be equally used for the forming of miniature/micro-parts, although the process capabilities are likely to be constrained more, due to additional material, interfacial and tooling considerations in micro-forming.
2. The types of materials which could be formable at micro-levels are prescribed more significantly than for forming at macro-levels by the micro-structures and grain-boundary properties of the materials. The forming limits for these materials are, therefore, somewhat different, compared to those for the forming of macro-parts.
3. Size effects may exist in material property and tool–material interfacial property characterization, depending largely on the micro-structures of the materials, which lead to the requirement of the definition of these parameters with reference to the actual materials and interfaces to be used.
4. Characteristics of the machines tools and feeding system are important to determine the quality of parts produced [9–15].

Regarding micro-sheet forming production, the following are the particularities which need to be paid attention, especially for the forming of sheets of less than 100 μm in thickness and feature sizes less than sub-millimeters, the reasons for which will be explained in the following sections of this chapter, wherever appropriate:

1. The need to use proper materials which are micro-formable, either under cold, warm, or localized heating conditions;
2. Special care in the handling of the raw materials (e.g., guiding thin strip, holding the strip during forming, etc.) and in collecting scrap, parts, or components effectively;
3. Constraints on the tool layouts due to the limited space and closeness of miniature/micro-tools, and hence, constraints on tool design;
4. The process capabilities, which are prescribed largely by the tool-fabrication capabilities, including tool coatings and the assembly of miniature/micro-tools;
5. Miniaturization of the forming machinery and improving the precision of the machinery at the corresponding scales;
6. Tool-cost issues, including process chains for micro-tooling, effective tool life affected by susceptibility to wear, fragile structures, damage to the tools caused by manufacturing, etc.;
7. Micro-products are subjects to probable uncertainties in their dimensional and material parameters that lead to variable product performance and reliability. Properties such as grain size and thickness play a major role in determining the

quality of micro-product which makes controlling and reducing defects become a crucial factor in micro-manufacturing environments [16].

MANUFACTURING PROCESSES AND FUNDAMENTALS

Traditionally, sheet metal may be defined as a metal having a thickness of between 0.4 and 6 mm, while micro-sheet forming usually deals with sheet metals of thickness is usually below 0.3 mm. Therefore, thin strips or coils may be proper words for defining these materials. As with conventional sheet metal forming, major material conversion mechanisms in micro-sheet forming include shearing/cutting, bending, unbending, stretching, compressing, stress-relaxation, etc., and their combinations.

Being the same as for conventional sheet metal forming, the mechanical properties of the materials such as elasticity, plasticity, stress−strain relations, strain rate, work-hardening, temperature effect, anisotropy, grain size, residual stress, etc., are very important for understanding of material deformation/separation mechanisms. The effects of grain sizes and orientations, and grain-boundary properties, are especially significant in micro-sheet forming, considering their effects on the definition of the overall stress−strain relationships, sheared section qualities, bending curvatures, springback phenomena, stress relaxation, etc.

For given micro-structures, the effects are more significant, in terms of the relative ratios between the grain sizes and the strip thickness/feature sizes/part dimensions. Moreover, the random/stochastic distribution of the grain will also lead to inhomogeneous material behavior which causes a variation in product quality [17].

The following sheet forming processes may be used in micro-sheet forming.

MANUFACTURE OF SHEET METAL PARTS BY BLANKING/PUNCHING

Cutting may be used to separate large sheets into smaller pieces, to cut out a part perimeter, or to make holes in a part, and can be accomplished by shearing action between two shared-cutting edges through the following stages of the material: (1) plastic deformation, (2) fracture initiation, and (3) separation (Figure 1). The parameters that influence the shearing/cutting quality significantly include: punch-die clearance, punch velocity, sheet metal materials, cutting tools, lubrication, alignment of the tools, strain rate, etc.

The clearance between the punch/cutting tool and the die is a very important parameter (Figure 2). For the clearance in conventional sheet metal forming, 4−8% of the sheet thickness is recommended. With too small clearance a greater cutting force is required and the fracture lines tend not to intersect, while with too large clearance excessive burr sizes develop. The best clearance value depends on the sheet metal type and thickness. The recommended clearance may be calculated from $C = at$, where t is the sheet thickness and a is a factor (provided from different sources).

The value of a for micro-blanking/punching needs to be determined by addressing actual cases because of the large influence of the micro-structure (size, orientation, and grain-boundary properties) relative to the overall scale of the part dimensions and/or cut geometries. For example, due to the size effect, the formation

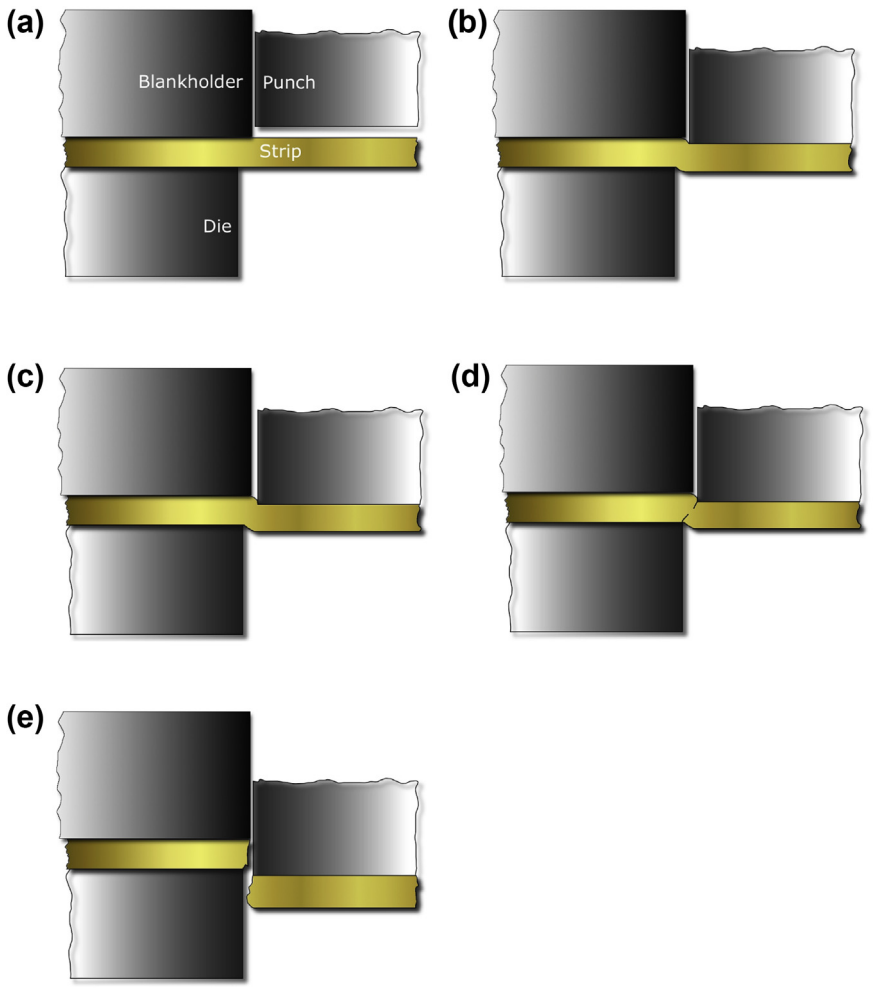

FIGURE 1

Stages of a shearing/cutting process. (a) Punch and die layout; (b) Contact with strip; (c) Plastic deformation; (d) Shearing as fracture meet; (e) Separation from sheet.

of edge draw-in, shear/plastic deformation, and fracture/burr (Figure 3) will be affected more significantly than that in a macro-blanking/punching process, by the micro-structure of the material. The level of the effect depends largely on the number of grains, the grain orientation, the possible number of sliding planes, etc., at the cutting areas. It was observed that the shearing resistance actually increases as the process/part dimensions are scaled down, but not in a linear manner [1]: this may be due to the limited number of sliding planes and the constrained position in which the shearing is taking place. A small number of grains may not be able to allow shear deformation to the same extent as would a polycrystal which

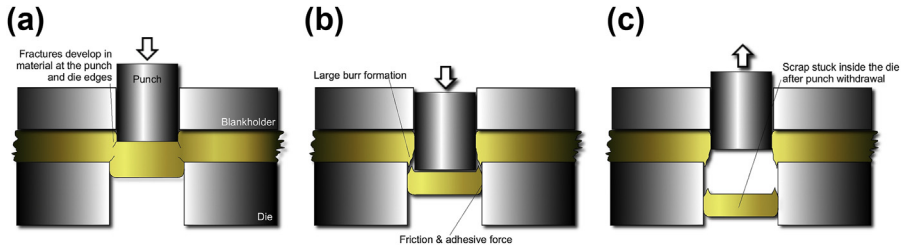

FIGURE 2

Illustration of the influence of the punch/die clearance. (a) Fracture develops due to small clearance; (b) Burr formation due to large clearance; and (c) Scrap stuck inside the die.

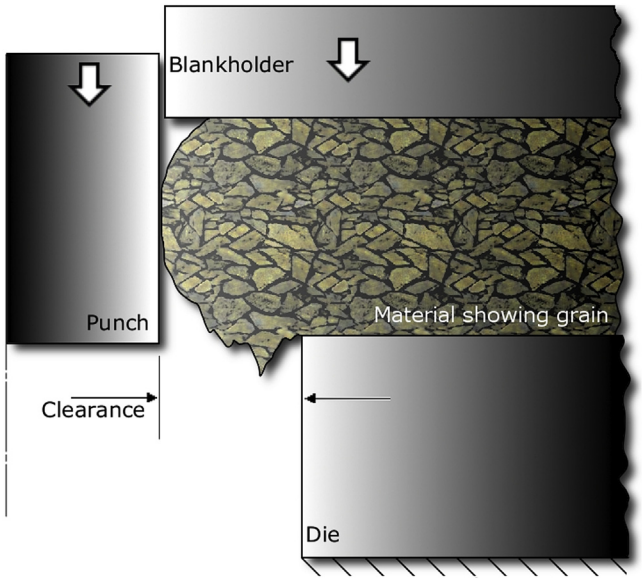

FIGURE 3

Illustration of the influence of grains on the sheared section.

has a large number of grains and grain boundaries [18]. The strain rate in shearing/cutting plays an important role, especially on the cutting quality, e.g., burr formation. It has been established that high velocities in blanking can lead to decrease of the blanking force and improved quality of cutting sections [19]: a dynamic fracturing mechanism and increase of the temperature locally for a short period of time may contribute to this. The same principle can be seen in high-speed chopping of metal billets for forging/forming. Considering that, the sheet metal is relatively thin in micro-forming, how the temperature factor could contribute to this is not clear. However, as a general principle, using a higher speed in cutting should normally help to improve the cutting quality.

A practical problem associated with micro-blanking/punching is that the punch/die clearance required may not always be able to be met. For example, for the stamping of a 20-μm thick sheet metal strip, the ideal clearance would be 1−2 μm. This would be a challenge to toolmaking and to the guiding of the tools (machine setup and tooling). Even though it is possible to achieve this in fabrication and assembly, the dynamic characteristics of the machine and tooling, including the resulting deflections, are very likely to cause an offset of the punch or the die of more than 1−2 μm. As a consequence, damage to the tools is likely to occur constantly. When using larger clearance values than the ideal values, if conventional process configurations are employed, burr formation in micro-forming of thin sheets may not be avoidable.

For micro-sheet metal parts, especially those to be used in important electronics products and micro-electromechanical systems (MEMS), the presence of burrs may not be acceptable. Therefore, a postprocess for burr removal may be necessary, e.g., laser ablation or mechanical methods. Burr-free blanking/punching processes have been explored in the past for the forming of thick sheet metals, and recently there were also attempts to use these to the forming of thin metal strips [20]. The process of using half-distance piercing without separating the material, then using a counter punch to effect a counter-direction piercing (pushback) to complete the blanking/punching (Figure 4), is feasible for eliminating burr formation for strip as thin as 50 μm. The several stages, including two stages shown in Figure 4, can be accommodated using a progressive die design in micro-stamping, e.g., punching for producing pilot holes, half-blanking (which may also be supported with a soft counterpunch), pushback blanking to complete the blanking operation, and, finally, clearing the cutting or cutting off the parts, etc. For micro-forming, for example, where the sheet metal thickness is less than 50 μm, controlling the half-blanking depth precisely will be crucial, and involves the control of not only the machine ram and the punch motion with the tooling, but also guiding and holding the metal strip inside the tooling.

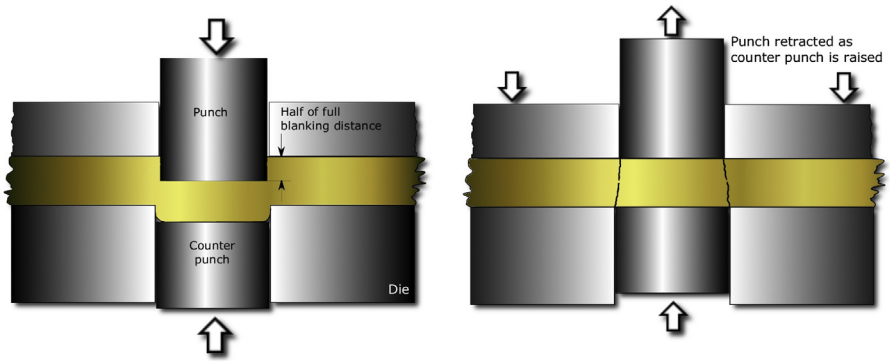

FIGURE 4

Illustration of a "burr-free" punching process.

Another useful process configuration called laser-assisted micro-stamping may be used for improving the quality of the cut section and extending the capabilities of the process to such as the stamping of greater aspect ratios (the ratio of the cutting thickness to the cutting area dimensions) and high-strength materials, including brittle/difficult stamping materials. The process is described in Chapter 10. The laser heating will provide a reduction of the strength of the local material and improve the flow ability of the material at the cutting section.

MANUFACTURE OF SHEET METAL PARTS BY BENDING

Bending is a major sheet forming process commonly used in fabrication of sheet metal parts. Bending may be defined as the straining of the metal around a straight axis. A neutral axis plane exists for the sheet metal around which the top section of the material may be stretched during bending while the bottom section is compressed (Figure 5). Bending operations may be performed using punches, rolls, wipe dies, the downward movement of the bending tools, depending on the bending processes, i.e., V-bending, U-bending, edge bending, etc., that are normally used in conventional sheet metal working. The manufacture of micro-sheet metal products, such as those used in electronics products and MEMS often needs bending to produce 3D profiles/sections. Typical applications include micro-electric-contacts/fingers/switches, 3D profiles for mechanical and thermo-mechanical sensors, and 3D sheet metal frames/housing for optical devices and micro-sensors. The manufacturing of these items may also require photochemical etching to produce fine geometry, while using bending to complete the 3D profiles/sections.

In employing bending for making micro-products, the bend angle, bend radius, bend allowance, length of bend, etc., are still key process parameters (Figure 5). The calculation of the strain value in bending, the minimum bend radius, the bend allowance, etc., may still be effected with the simplified equations that are normally used

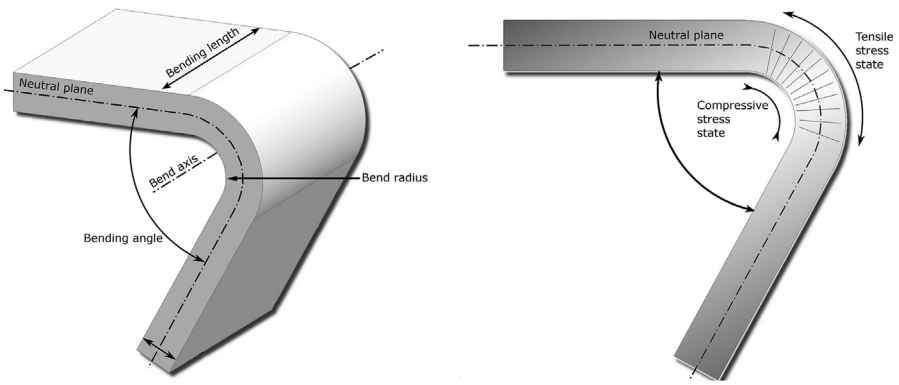

FIGURE 5

Illustration of a sheet metal bending process and parameters.

for macro/miniature-parts. These, however, need to include considerations concerning size effects. Similarly in the case of blanking/punching, the relative grain size to the sheet metal thickness, grain distribution, grain-boundary conditions, at the bend section, will have significant influences on the bending process and bending quality: a universal definition in terms of the level of these influences does not exist.

One of the main challenging issues in the bending of thin sheet metals is to prevent the distortion of the sheet and to overcome springback-related problems (Figure 6). Sheet metal may recover elastically after manufacturing, not only after bending, but also due to possible changes of the state of the stresses during/after secondary process, e.g., after trimming, i.e., the cutting of neighboring material which affects the stress balance in this or another section. This often occurs when microparts with condensed features or cutting/bending sections are produced with a progressive die-forming/stamping configuration. The springback may occur immediately after the release of the forming force, or occur due to the subsequent release of the residual stresses, and results in the distortion of the shape of the part or instability of the dimensions of the part under service conditions.

The component-form errors resulting from the springback may be compensated for by properly designing the die and the bending parameters, or introducing extra processes. Rebending, overbending, bottoming or stretch bending are the techniques often used to eliminate the errors caused by the springback in conventional sheet metal forming. It may be difficult to employ some of these techniques in microsheetforming, either due to the complexity of the geometry in small areas, or due to the difficulty in adding extra tools or forming stages in the limited tooling space, etc. Other limitations are those due to cost considerations. Feasible compensation measures include optimization of the bending stroke, bending angle, tool shape,

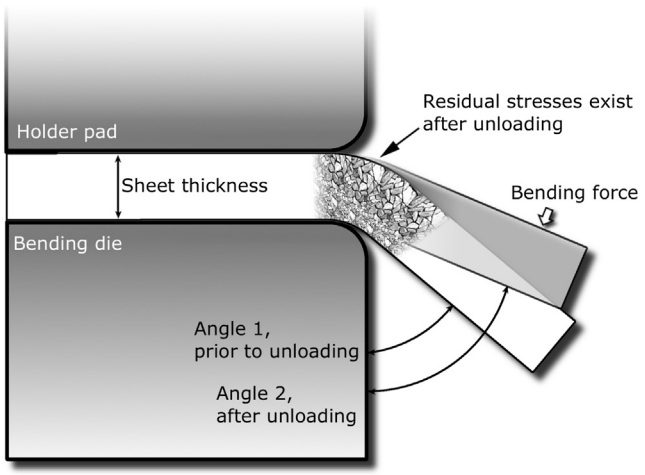

FIGURE 6

Illustration of the springback phenomena in sheet bending.

punch/die clearance, etc. In-process measurement of springback and adjusting the bending angle or bending speed is possible, if proper sensing (e.g., displacement and angular sensors, noncontact sensors such as laser-based sensors, etc.), an effective feedback loop and analysis, and control of the actuators, can be ensured. This is achievable mainly for simple bend geometry, not for a complex stamping process.

To avoid difficulties in handling micro-components/parts and in the fabrication of micro-tooling, noncontact processing approaches such as laser-assisted bending, may be introduced to achieve accurate bend geometries [21–23]. For example, short-pulse excimer laser radiation is able to result in a required level of thermally induced stress in very thin surface layers of a sheet metal, and the deformation of the thin sheet in the radiated area may be effected in the forms of bending by the released stresses. Laser heating can also assist in forming of 3D micro-sheet-structures effectively, e.g., combining bending and twisting [24].

DEEP DRAWING OF SHEET METAL PARTS

Deep drawing is a sheet metal forming process used industrially to produce cup-shaped, box-shaped, and other complex-curved hollow-shaped sheet parts. Micro-cups/micro-boxes may be produced with similar process configurations (Figure 7) for micro-housing applications, such as for the packaging of micro-sensors and micro-actuators. As for conventional deep drawing, the major parameters which influence the process and product quality include the dimensions of the blank, the punch and die dimensions, especially the punch corner radii, the clearance between the punch and the die, as well as the blank-holder geometry, the interfacial conditions, and the holding pressures. Deep drawing is a more complex process than shearing/cutting and bending because it usually combines processes such as bending, unbending, stretching, compression, and shearing, depending on the part geometry to be produced. These processes become more complex when the micro-structure of the sheet metal becomes a dominant factor as the scale decreases [2].

The drawing ratio (DR = diameter of the blank/diameter of the punch) achievable is usually about 2.0 (the limiting drawing ratio (LDR)), depending on the sheet material thickness and micro-structure. With fine-grain sheet metals, controlled friction at the contact surface of the blank-holder with the sheet, the sheet with the die, the punch to sheet metal interfaces, and possibly providing counterpressures under the sheet, the LDR value could be increased. A major challenge faced in micro-deep-drawing is to achieve these DR values within a limited space, which usually limits the tooling arrangement. Control of the interfacial conditions is even more difficult. Ideally, no other media should be used, and enhanced complexity of the tool/material interface conditions should be avoided. For example, a great potential use of various coating on micro-deep-drawing tools has made it possible to have a lubrication-free micro-deep-drawing. This technique is desirable because the friction between the surfaces can be precisely controlled compared to the use of lubrication. This will also avoid the complication during cleaning and handling of the micro-product because of its small size [25–27].

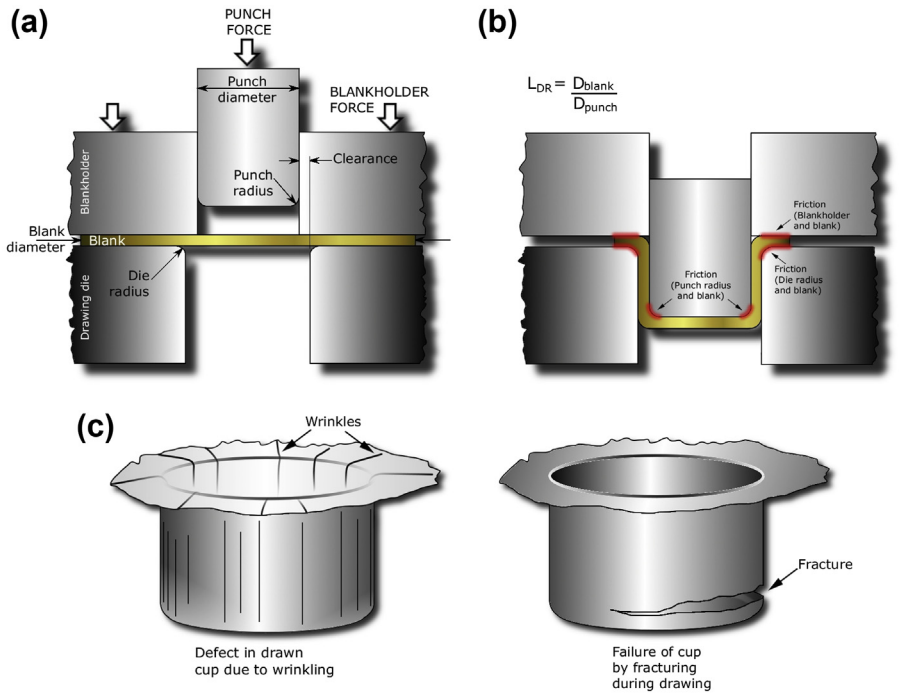

FIGURE 7

Illustration of the deep drawing process, influential parameters, and part failure forms. (a) Process configuration and basic parameters; (b) The areas where the friction has significant influences; and (c) Common defect in the drawn workpieces.

The actual *LDR* achievable in micro-deep-drawing production also depends on how the blanks and the formed cups will be toggled with the sheet metal strips in the forming/stamping layout design, since the blanks and the finally formed cups are unlikely to be detached from the strip during forming/stamping due to the difficulties associated with handling these small objects, while a reasonable production rate may have to be maintained. This is a special issue to be addressed, compared to the laboratory-based prototype process development.

Common defects in drawn thin sheet parts include the formation of wrinkles (due to buckling), material fracturing (especially at the punch and die corners), and surface scratching (Figure 7). Wrinkles often occur when very thin sheet metals are to be drawn (the material most likely buckles), such as 20-μm thick sheets. Blank holding will be crucial, but it may not be easily arranged due to the limited space for tool components in micro-deep-drawing. Fine-grain materials and materials with superplastic flow characteristics will be helpful in overcoming the fractures which often occur at the punch corner (small radius) and the flange/cup−wall interface. Smaller cups with thin sheet metals may not be achievable, due either to excessive springback for shallow geometries or to the initiation of fractures arising from the

use of small punches, similar to what can occur in a piercing process. Again, the avoidance of these features will also depend on how the blanks are to be toggled with the strip.

Redrawing is usually necessary, due to the limitation in the achievement of a feasible reduction value of a cup, in one stroke. Redrawing or reverse redrawing, even introducing an annealing process and ironing, is possible for miniature cups. These steps are unlikely to be introduced in the forming of a micro-cup, due to the difficulties occurring in the handling and alignment of the workpiece, etc. Ideal processes would be those without the need to reposition the workpiece while the tools are being changed.

OTHER MICRO-SHEET METAL FORMING PROCESSES

Other micro-sheet metal forming processes include (1) incremental (or die-less forming) forming: micro-sheet metal parts or micro-features on sheet metals can also be produced in incremental forming forms, such as by using CNC (computer numerical control)-controlled hammering, piezoelectric-actuated micro-probes for dimpling (high frequency vibration actuated), by which micro-features in small and large areas of thin sheet metals (down to 10 to 20 μm thickness) can be produced [28], (2) isostatic pressing: ultrathin metal foils may be pressed into a die with grooved surfaces to produce micro-channels. Foils as thin as several microns can be formed to produce such channels within the range of several to tens of microns [29], and (3) embossing/coining is also possible for use in producing surface micro-textures on the thin sheet metals, e.g., using silicon tools, on thin aluminum sheets, fine-grained alloy, amorphous alloy, in the cold and hot state, etc. [1,4].

GENERAL CONSIDERATIONS FOR MANUFACTURING

Similar to the planning for conventional sheet forming, the following aspects may have to be checked with a view to implementing micro-forming processes (some details concerning these issues being described in the next sections):

- Whether the maximum stamping-force requirements, machine static/dynamic characterization can be met with the available machines;
- Whether the machine strokes and manufacturing precision requirements can be met with available machines and tools;
- Whether the production rates achievable are acceptable, also considering the thickness of the sheet metals to be dealt with, the precision requirements and tool-life factors;
- Whether the raw materials obtainable meet the requirements, in terms of mechanical properties, grain sizes, and dimensional tolerances for production;
- What the stock/tool layout for progressive die design will be, including how the scrap and the parts will be dispatched;
- Whether the tool-design/manufacturing capabilities meet the requirements (especially micro-tooling capabilities, involving the whole process chains);

- Whether the punch/die clearance (recommended) is achievable by toolmaker(s);
- Whether a burr-removal process is required (for high quality/performance parts);
- What extra care for handling fragile thin strips and the structural parts stamped will be required, including that for careful strip/blank-holding designs;
- Whether a push−pull setup with two feeders is to be used or just a single feeder to be used for pulling/feeding the sheet metal;
- What extra measures for dealing with springback and distortions of the sheet parts with dense geometrical features will be required;
- How the scraps and parts will be collected from the tool system and the machine;
- How the process monitoring will be implemented (force, velocity, energy, etc.);
- How the tool condition, e.g., wear, breaking, damage to the coating, will be monitored;
- Whether a cleaning process is needed and a clean environment should be maintained;
- How the parts will be packed/transported;
- How the parts/products will be inspected (offline or online, or both), etc.;
- How to detect and monitor the errors that create defective product is important to maintain an acceptable product yield.

FORMING TOOLS

General considerations for tool design and manufacture for micro-sheet forming production include the scheme for progressive die forming/stamping or transfer die forming/stamping (need careful considerations on the part sizes, features and sizes, use of the strip material, etc.); the availability of the die-working-space provided by the machine as well as the connection to the feeder(s); the stock layouts considering micro-forming characteristics (especially the closeness of the features) as well as transport requirements; the blank-holding design considering limited spaces and precision; the feasible punch penetration distance (taking into account the punch diameter/free length ratio); the punch/die clearance achievable with micro-tooling capabilities; web-formation and limitation due to space arrangements and its potential effect on the distortion of the parts; the ejection/removal of the small/thin parts and scraps (if needed); burr generation and removal; punch stiffness/strength and assembly requirements (with limited spaces); the transport of the thin part/scrap ribbon at high speed; maintaining the flatness of the thin strip during transport; considerations for the implementation of a dry stamping process and its effects; the micro-tooling process chains and capabilities in dimension tolerances and surface finish; tool materials and cost; micro-tooling cost (considering the process chains); assembly and inspection techniques for micro-tools; the interfaces with the machine; special arrangements for the guiding of the punches/moving parts of the tooling; the proper selection of bearings and guides, prestressing parts, if possible; tool-surface polishing; tool-surface coating, etc.

Forming-tool design and manufacturing is a particularly challenging area for micro-sheet forming, and is mainly associated with the size effects induced as the scaling factor decreases:

1. Punch-die clearance in micro-stamping needs to be redefined (closely relating to the material properties qualified at micro-scales and to the micro-structures at the deformation/shearing sections). The recommended clearance (4−10% of the sheet thickness, Figure 2) for conventional stamping may not be correct. Increasing the punching velocity would affect the shearing section quality positively, which would, in turn, relax the clearance requirements.
2. For cutting thinner strips, tight clearances down to one to several microns may be needed, which may be achievable but at high cost. Constraints to this include whether the tool-fabrication capabilities are able to achieve one to several micron accuracy in manufacturing individual tool parts, to align these within a similar accuracy after assembly, and whether the dynamic characteristics of the tooling are able to maintain the tool bending, the tool offset due to loading eccentricity, and clearance between the bearings and guiding pillars to be within a similar precision range (a tool system is illustrated in Figure 8). Tool damage/breaking could be easily caused by these factors.
3. The reduced sizes of the cutting geometry restrict the punches to be of only a very short free length (to maintain sufficient stability). As a consequence, it may be difficult to punch the scrap out of the die exit (Figure 2(c)), if the punches are too short. It also requires extremely accurate control of the punch stroke to ensure that the stamping operation is completed.
4. Due to the limited space available, the number of tool parts/elements for constructing the tooling may have to be reduced to avoid difficulties in fabricating these parts/elements and assembling them in tiny spaces, as well as reducing the assembly errors accumulated. Using compound tool designs may be considered.

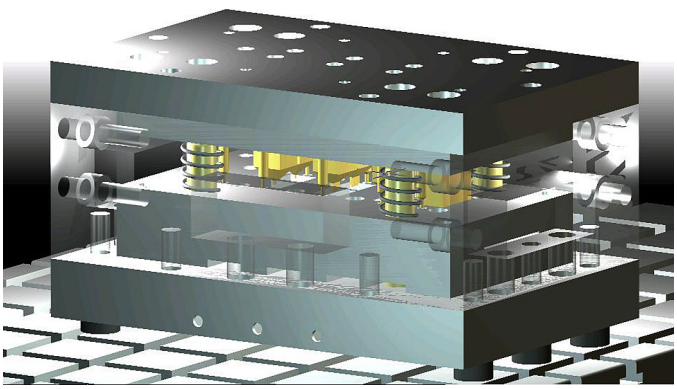

FIGURE 8

A tool system for micro-sheet forming.

5. The design of the pilot pins for positioning thin strip needs to be carefully done, by which the pins could correct the position of the strip (Figure 9) and help to reduce the positional errors significantly, thereby relaxing the stringent requirements on the strip feeder(s), in terms of feeding accuracy.
6. To prevent damage to the workpiece surfaces (e.g., coated strips for electronics applications) and to prevent sticking of the scrap and micro-parts to the tool

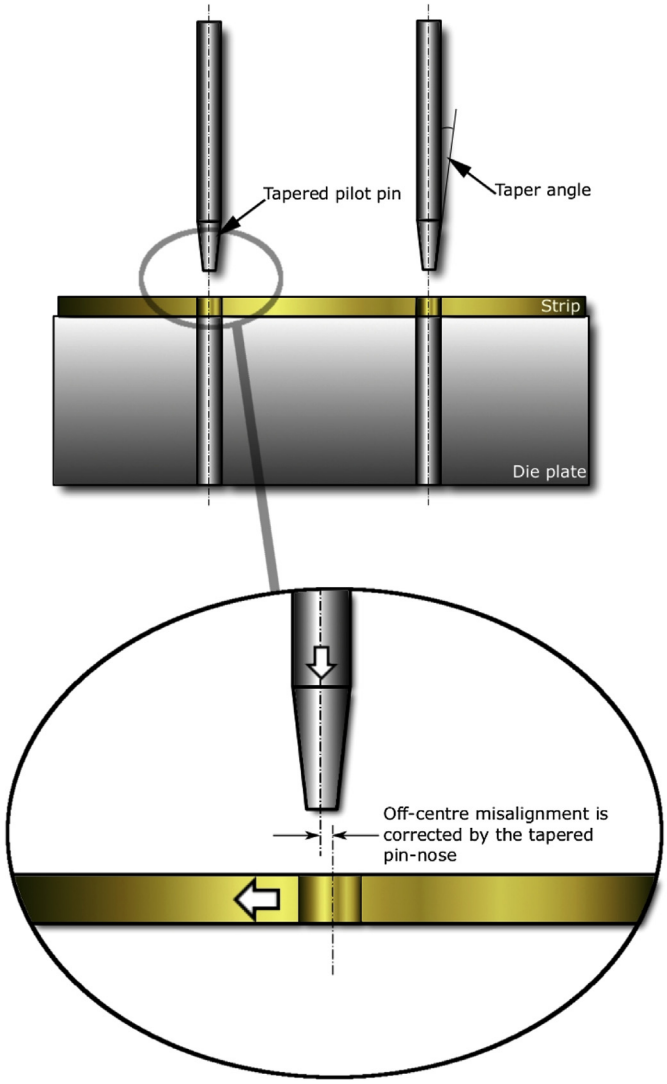

FIGURE 9

Illustration of the function of the pilot pins.

surfaces, dry stamping will be needed, for which special tool materials such as ceramic tools and self-lubricated tool coatings, etc., should be considered.

7. In micro-sheet forming, gravity cannot be considered as the main force being applied to the part. Unwanted surface forces such as van der Waals, electrostatic, and surface tension forces are dominant at such a scale. As a result, concepts for handling parts/scrap deployed in conventional forming (largely considering the gravity force of the parts) do not usually work. Parts may not drop out automatically and connecting these to the strip may be feasible in some cases. However, separation may still be needed, depending on the end users' and customers' requirements. A vacuum system directly connected to the dies or proper locations within a tool system will be helpful for collecting the scrap and even micro-parts.

Micro-tooling capabilities and process chains (e.g., mechanical cutting, electrical discharge machining (EDM), laser treatment, coating, electroforming, chemical etching, etc.) are especially important, which significantly prescribe the feasibility of realizing the processes and achievability of the required scales of the micro-parts, while maintaining proper production rates, product quality, and low manufacturing cost. These are addressed in several other chapters of this book.

MANUFACTURING PRESSES/MACHINES

Traditionally, sheet metal forming may be effected either with mechanical presses or hydraulic presses, in which latter are usually of large scale. These presses are usually not of sufficient precision for micro-forming applications, and they are not compatible, in terms of the scale, for the forming of the miniature/micro-sheet metal parts. Conventional, large-scale presses may be optimized/upgraded for the manufacture of miniature/micro-sheet metal parts with the required enhanced precision. Their manufacture may also be achievable through the use of delicately designed and fabricated forming tools. Conventional forming tools may be designed primarily for manufacturing metal parts with precisions in the millimeter range. However, with some specific engineering modifications implemented in these machines, they could be optimized for micro-forming applications. BSTA from Bruderer is a machine which can operate at up to 1400 strokes per minute (spm) and a press force of 300 kN [30]. Incorporated in the machine are specific modifications such as guides that are insensitive to thermal influences and additional features to secure high precision, a counterbalance system "acting irreversibly" to the movement of the ram with a view to keeping the machine free from vibration. The guides and levers that control the ram movement are arranged in such a way that the tilting of the ram due to the application of an eccentric load does not affect the position of the punch: This is achieved by placing the theoretical center of gravity of the ram at the tip of the punch.

Machines of smaller size such as bench-top machines may be built with newly enhanced elements/parts and/or designs particularly for micro-forming applications.

This category of machines are those of normal size but incorporating new concepts dedicated to micro-forming. A high-precision stamping press was developed jointly by Schuler, PtU Darmstadt, ILT, IPA and other partners [31]. The machine has a modular arrangement and a high-rigidity design. In this machine, linear motors are used for driving the ram. Linear driving has the advantages of high and reproducible accuracy. Lubrication is not needed and maintenance can be avoided, hence it is attractive option for clean room manufacturing. Other beneficial features include low noise emission and high reliability and endurance.

A new, low cost, bench-top machine dedicated for micro-sheet forming is being developed at the University of Strathclyde [8], with collaboration with its EU Masmicro consortium partners (Figure 10). A linear motor driving mechanism is used. The maximum frequency of the machine is 1000 spm, the maximum force is 5.3 kN, the vertical position resolution is 0.1 μm, and the load measurement resolution is 0.1 N. The machine enables the micro-stamping/forming of sheet metal parts (ideally for sheet metals of a thickness of less than 100 μm). The machine has a

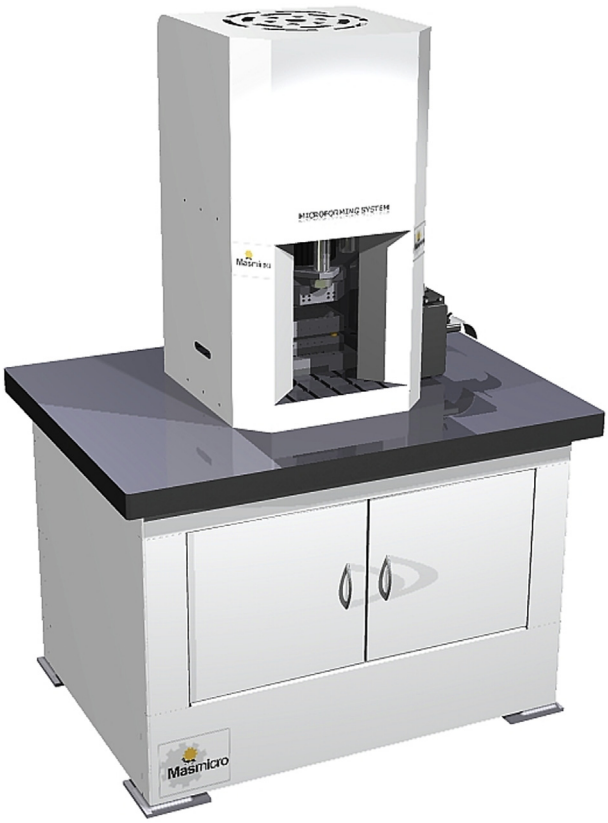

FIGURE 10

A bench-top micro-sheet-forming machine, designed by the University of Strathclyde.

maximum working space of 400 × 400 mm with a flexible setup, due to having a modular design (the ram-driven form/power is changeable, without need of changing other machine setups; four machine-frame columns and supports to the ram guiding bridge can be repositioned according to the requirements, as well as the sheet metal feeder, and the part carrier). The bridge for guiding the ram is separated from the main machine frame, and hence it is not affected significantly by the deflection of the main frame and by vibration. Other innovations include monitoring the displacement directly on the tooling (therefore being able to control the punch stroke more accurately), transporting the miniature/micro-parts directly out of the dies by a part carrier, a new vacuum/compression air chamber design, a new sheet metal holding design, etc. The machine design was supported by finite element dynamics analysis, which led to the development of a bench-top machine that has very good dynamic performance and machine stability (no connection to the bench is needed, and no significant vibration is felt at the shop floor).

Micro-forming may also be effected with micro-machines or similar setup, especially for research purposes. This category of machines are of much smaller size, compared to that of conventional, large-scale presses. The development of this type of machine has attracted much interest from researchers during the last 10 years [32–33]. Various new concepts are being experimented with to design and fabricate prototypes of new micro-machines. Force may be effected with linear motor actuation, piezoelectric actuation, piezoelectric/hydraulic actuation, electromagnetic launch and impact, etc. A micro-machine prototype using a working principle of incremental micro-forming has also been developed in Japan [28]. Small dents in a sheet metal can be generated by hitting the metal with a small punch installed at the end of a swinging arm. By repeating hammering, incremental deformation can be achieved across small areas of thin sheets. Other developments include the use of combinations of piezoactuating with hydraulic devices to amplify the punch stroke [34–35], e.g., the piezoelectric-driven press developed by Zentrum Fertigungstechnik Stuttgart (ZFS), Germany. A mechanical micro-press has been developed by the Mechanical Engineering Laboratory [36], Ministry of Trade and Industry, Japan. The machine has a size of 111 × 66 × 170 mm, and is powered by an AC servo motor of 100-W rated power which can generate a force of up to 3 kN. The transmission is effected by a ball screw/nut structure plus timing pulleys and belts. A micro-progressive die enables four blanking and two bending strokes. The stroke and speed of the machine can be controlled and 60 spm be achieved.

DESIGN CONSIDERATIONS FOR MICRO-SHEET METAL PARTS FOR FORMING

Various metals are possible for making micro-sheet parts, these including copper, brass, stainless steel, low carbon, mild- and high-strength steel, aluminum, nickel, etc. Fine grain sheet metals are preferable for micro-sheet forming, due to the reasons explained in Section Manufacturing processes and fundamentals of this

chapter. The description/characterization of material properties has to refer to the scaling factor for a particular part, material, process, and tooling, the values of which are normally expected to be obtained through a series of tests/measurements. The strength, the relationship of stress and strain, the anisotropy factor, the rate-dependent properties, the springback behavior, the thermal properties, etc., of the metal to be used are required to be corrected from the descriptions/definitions, which are based normally on a macro-scale.

General product design considerations include (1) thin sheet metal parts/structures should have sufficient strengths and stiffness, in relation to the functional and performance requirements; (2) thin sheet metal parts should have good dimensional accuracy, with reference to the applications; (3) thin sheet metal parts should have good surface finish, and precoating may be needed, depending on the application; (4) relatively low cost for manufacturing may be a key factor to be considered; (5) the design should consider the manufacturing constraints to the smallest features and tolerances, taking toolmaking and tooling construction capabilities into account; (6) the design should consider the manufacturing constraints to the closeness of neighboring smaller features (minimum web sizes) and the number of features; (7) the design should consider the specific aspect ratios achievable in stamping, considering size effects in micro-stamping; (8) the design should consider specific bending radius applicable for bending, considering size effects in micro-bending; (9) the design should consider the limiting specific drawing ratios for deep drawing, and the feasibilities of redrawing, considering size effects in micro-deep-drawing; (10) the design should consider the specific embossing/coining/denting ratios achievable in embossing/coining/incremental forming, considering size effects in these processes; and (11) the design should consider proper material selection and the availability of suitable materials, together with considering the "size effects" associated with their mechanical properties, surface/interface properties, and their influence on process design and tool design.

MICRO-SHEET FORMING—A CASE STUDY

In the following case study, the forming of a micro-sheet part—a sheet metal spring (Figure 11), is described. The part has overall dimensions of 2.4 × 3.0 mm, a sheet thickness of 50 μm, and it is used in a micro-device. Firstly, the part design was assessed and individual features identified for punching, blanking, and bending/forming. Subsequently, the stamping techniques were examined in detail before developing a suitable strip layout for progressive die stamping of the part. Five-stage stamping was employed, which included the following:

1. Punching to create carrier tabs and holes for pilot pins;
2. Blanking to create two side slots;
3. Forming of a center curve (bending);
4. Forming of edge features (bending/bottoming);
5. Blanking of the final part.

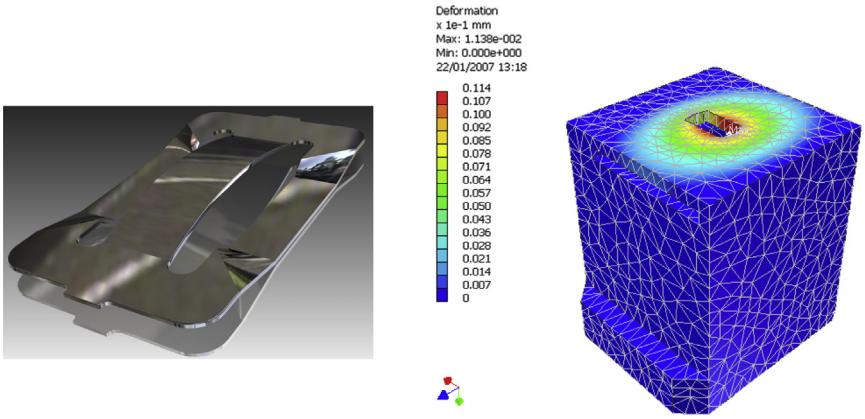

FIGURE 11

The sample part (left); and an finite element analysis study on one of the micro-dies (right).

The punch and die designs were supported with finite element analysis (Figure 11). A high-speed tool steel (hardened to a value of 62−64 HRC) was selected to fabricate the individual punches and dies, which were created using mechanical milling, followed by μ-EDM, and then precision grinding to allow the required tolerances to be achieved. A dedicated micro-forming tool system with a footprint of 250 × 160 mm was designed and fabricated (Figure 12), with the individual punches and dies designed as inserts. The tooling incorporates a specially

FIGURE 12

The micro-forming tool (left) and the micro-forming machine (right), developed at the University of Strathclyde.

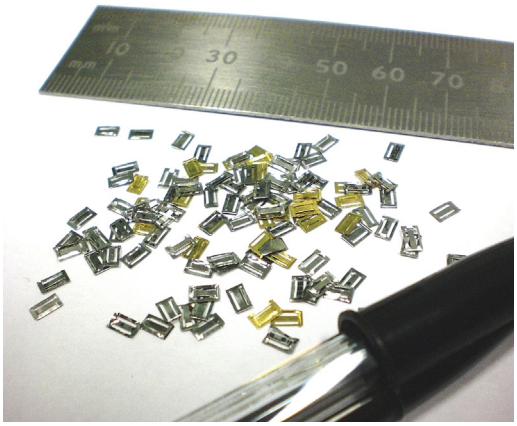

FIGURE 13

Samples of the formed micro-components in brass and stainless steel.

designed blank-holder to hold the strip during the stamping and four high-precision ball race guide units as the primary means of aligning the punches and dies. The formed features were generated using polyurethane pads and profiled punches. The pads under pressure adopt the negative feature of the solid punch and form the material of the strip.

The micro-forming tool was designed for use in a dedicated micro-forming machine (Figure 12), capable of providing high stamping rates (up to 1000 spm) while providing accurate control over the ram position. A load cell and positional encoder are integrated into the machine to allow for data collection from the stamping process and, additionally, for monitoring of the punch force to indicate breakages or problems in the system.

Copper and stainless steel were both used to produce the micro-spring (Figure 13). The scrap was collected through a vacuum system which is connected to the die blocks directly, while the parts were transported out of the final stage die via a tape—reel transport arrangement [8].

TECHNOLOGICAL COMPETITIVENESS AND OPERATIONAL ECONOMICS

Micro-fabrication in the past dealt with largely silicon-based materials due to economic considerations and the unique properties of these materials for micro-devices and systems. There are now increased demands on nonsilicon materials, e.g., polymers and metals, due to the need of multifunctional materials for the evolvement of multifunctional micro-systems and devices. There are various technologies available for the micro-fabrication of metals, among these micro-sheet forming renders unique advantages over other technologies. At the same time,

micro-sheet forming also competes with other technologies in the manufacture of micro-sheet metal parts, these including photonic etching and electroforming technology, electron beam lithography etching, laser micro-machining. It will be difficult for micro-sheet forming to compete with photochemical etching/electroforming, in the areas of fabricating 2D and 2.5D parts with smaller dimensions and finer features such as several to tens of microns in size, and thinner metal sheets, e.g., below 10—20 μm. Micro-sheet forming of these may be extremely expensive, or almost impossible to achieve. It is also difficult to compete with laser machining, in terms of the flexibility of the process setup, the type of materials that can be processed, and when finer geometries are involved. Micro-sheet forming, however, is able to produce metal parts with better integrity, and less deleterious effects on the properties of the material. It is also ideal for producing various 3D structured parts and connections. Most importantly, it can be implemented at a mass production scale (for suitable component forms) for which other processes/technologies cannot compete, if corresponding tooling technologies and machine capabilities are able to meet the manufacturing requirements. Good examples of applications include the high-speed stamping of leadframes for electronics products and the stamping of micro-laminates for micro-motors, etc.

The following table presents a comparison of the costs quoted for using photochemical etching and micro-stamping to produce a 2D flat sheet metal part:

Company	Technology	Quality	Quotation	Other Costs
A	Photochemical etching	10,000	£600	Tooling £125
B	Photochemical etching	10,000	£488	Tooling £395
C	Micro-stamping	10,000	349	Tooling £20,000 (first batch)

Without considering other merits of micro-sheet forming, just referring to the manufacture of this particular part, the data presented in this table suggest that the investment on tooling for the first batch production is extremely high for micro-sheet forming. However, for producing over one million pieces of this part, micro-sheet forming does have an advantage. Considering the feasibility of producing 1000 pieces of such a part (simple micro-blanking) per minute with micro-stamping, the advantage of micro-sheet forming in mass production is evident. Such an example does, however, not suggest a general calculating principle, in terms of comparison of costing. It should depend on the actual component form to be considered. Currently, there is a trend of combining photochemical etching, laser machining, and micro-sheet forming, in a process chain, to achieve the greatest efficiency of manufacturing.

The engineering applications of micro-sheet forming are not isolated issues. To enable realization of the potential of micro-sheet forming, in terms of its technological competitiveness and economic advantages, one should be able to manage the whole manufacturing and operation chain properly, including, in the chain, material supply and characterization of the material properties, stock preparation, forming

process selection/design, forming tool selection/design and fabrication, machine selection/setup, process/machine/tool control, material/parts/tool handling, postprocessing, linking to other processes/equipment, etc. The quality of the sheet metal and the quality of the tooling are extremely important, especially for the forming of thin sheet metals (thickness below 100 μm), smaller part sizes (several millimeters), and finer features (submillimeters). Fine grain sheet metals could be expensive and the tooling cost could be extremely high, while the tool life could be very short, due to the fragility of the small tools employed, such as slender punches, etc. Therefore, the development of overall consideration for the manufacture of a particular part is needed, which should take a balanced view of the manufacturing economics.

ACKNOWLEDGMENT

The authors would like to thank Andrew Brockett, Akhtar Razali, Yanling Ma, and Colin Harrison for their contributions to the development of the micro-sheet forming machine system at the University of Strathclyde and to the writing of this book chapter published in the first edition of this book.

REFERENCES

[1] Geiger M, Kleiner M, Eckstein R, Tiesler N, Engel U. Microforming. Ann CIRP 2001; 50(2):445−62.
[2] Vollerston F, Hu Z, Schulze Niehoff H, Theiler C. State of the art in microforming and investigations into micro-deep drawing. J Mater Process Tech 2004;151:70−9.
[3] Engel U, Geiβdšrfer S. Microforming technology − on the way to industrial application. In: Keynote paper proc. 1st int. conf. on micro-manufacturing, Urbana-Champaign, USA; September 2006. p. 21−30.
[4] EU Masmicro Consortium, Project Technical Reports (2004−2008), NMP2-CT-2004−500095.
[5] Qin Y. Micro-forming and miniature manufacturing systems − development needs and perspectives. In: Keynote paper 11th int. conf. of metal forming. J Mats Proc Tech September 2006;177:8−18.
[6] Qin Y. Development of an integrated manufacturing facility for mass-manufacture of miniature/micro-products. In: Keynote paper proc. 1st int. conf. on micro-manufacturing, Urbana-Champaign, USA; September 2006. p. 35−40.
[7] Qin Y. Advance in micro-manufacturing research and technological development, and challenges/opportunities for micro-mechanical machining. In: Keynote paper, the cutting tool congress 2007, Milan; November 2007. p. 1−8.
[8] Qin Y, Ma Y, Harrison C, Brockett A, Zhou M, Zhao J, et al. Development of a new machine system for the forming of micro-sheet-products. Proc ESAFORM Conf Int J Material Form 2008;1(Suppl. 1):475−8.
[9] Qin Y, Razali A, Zhou M, Zhao J, Harrison C, Nawang W. Dynamics characteristics of a micro-sheet-forming machine system. Key Eng Mater 2012;504−506:599−604.

[10] Razali A, Zhao J, Law F, Qin Y. A part-transport design and the system for micro-forming applications. J Plasticity Eng 2011;18(6):81−6.
[11] Razali A, Qin Y, Zhao J, Harrison C, Smith R, Eguia J, et al. A newly developed high-precision feeder for micro-sheet-forming. J Manuf Sci Eng Trans ASME December 2012;133(6). http://dx.doi.org/10.1115/1.4005046. p. 061025−1 to 7.
[12] Qin Y, Brockett A, Ma Y, Razali A, Zhao J, Harrison C, et al. Micro-manufacturing: research, technology outcomes and development issues. Int J Adv Manuf Technol 2010; 47:821−37.
[13] Zhao J, Brockett A, Razali A, Qin Y, Harrison C, Ma Y. Micro-sheet-forming and case studies. Steel Res Int September 2010;81(9):1185−8. 13th int. conf. on metal forming, Toyohashi, Japan.
[14] Zhou M, Qin Y, Harrison C, Brockett A, Ma Y. Finite element analysis and experimental measurement of dynamic behaviour of a micro-stamping tool. Int J Adv Manuf Technol 2010;47:839−44.
[15] Razali A, Qin Y, Harrison C, Brockett A. Design considerations for developing a new, ultra-high precision feeder for micro-sheet-forming applications. Int J Nanomanufacturing 2009;3(1/2):40−54.
[16] Raulea LV, Goijaerts AM, Govaert LE, Baaijens FPT. Size effects in the processing of thin metal sheets. J Mater Process Technol 2001;115:44−8.
[17] Eichenhueller B, Egerer E, Engel U. Microforming at elevated temperature − forming and material behaviour. Int J Adv Manuf Technol 2006;33:119−24.
[18] Geiger M, Vollertsen F, Kals R. Fundamentals on the manufacturing of sheet metal microparts. Ann CIRP 1996;45/1:277−82.
[19] Grünbaum M, Breitling J, Altan T. Influence of high cutting speeds on the quality of blanked parts. The Ohio State University; 1996. Report No. ERC/NSM − S-96-19.
[20] Kima SS, Hana CS, Lee Y-S. Development of a new burr-free hydro-mechanical punching. J Mater Process Technol 2005;162−163:524−9.
[21] Matsushita N. Laser micro-bending for precise micro-fabrication of magnetic disk-drive components. In: Int sympo on laser precision microfabrication, No 4, Munich, vol. 5063; 2003. p. 24−9.
[22] Ocaña JL. Laser shock microforming of thin metal sheets with ns lasers. Phys Procedia 2011;12(Pt 2):201−6.
[23] Ding H. Experimental analysis of sheet metal micro-bending using a nanosecond-pulsed laser. Int J Adv Manuf Technol 2013;69(1−4):319−27.
[24] Jeong H-W, Hata S, Shimokohbe A. Microforming of three-dimensional microstructures from thin-film metallic glass. J Microelectromech Syst 2003;12(1):42−52.
[25] Vollertsen F. Effects on the deep drawing diagram in micro forming. Prod Eng February 2012;6(1):11−8.
[26] Xu J, Guo B, Shan D, Wang C, Li J, Liu YW, et al. Development of a micro-forming system for micro-punching process of micro-hole arrays in brass foil. J Mater Process Technol November 2012;212(11):2238−46.
[27] Castagne S, Taureza M, Song X. Surface textures and friction control in microforming. Adv Mater Res 2014;966−967:111−9.
[28] Saotome Y, Okamoto T. An in-situ incremental microforming system for three-dimensional shell structures of foil materials. J Mater Process Technol 2001;113:636−40.
[29] Oh SI, Rhim SH, Joo BY, Yoon SM, Park HJ, Choi TH. Forming of micro channels with ultra-thin metal foil by cold isostatic pressing. In: 5th Japan-Korea joint symposium on micro-fabrication; 2005. p. 50−4.

[30] http://www.bruderer.com/bruderer-high-performance-presses/bsta-300, visited in May 2009.
[31] http://www.schulergroup.com/de/05_Extras/02_Publikationen/Broschueren_Anlagen_Herstellung_Elektrobleche/Download_Anlagen_Herstellung_Elektrobleche/extras_download_flyer_schnelllaeuferpressen_stanzrapid_linearantrieb_d.pdf.
[32] Mishima N, Ashida K, Tanikawa T, Maekawa H. Design of a microfactory. Proceedings of the ASME design engineering technical conference − 7th design for manufacturing conference, September 29−October 2, vol. 3. (Que., Canada): Montreal; 2002. 103−110.
[33] Okazaki Y, Mishima N, Ashida K. Microfactory and micro machine tools. In: Presented in the 1st Korea-Japan conference on positioning technology, October 15−17. Daejeon, Korea: KIMM; 2002. 1/6−6/6.
[34] Park JH, Yoshida K, Nakasu Y, Yokota S. A resonantly-driven piezoelectric micropump for microfactory. In: Proc. ICMT20002 Kitakyushu; 2002. p. 417−22.
[35] Hess A. Piezoelectric driven press for production of metallic microparts by forming. In: ACTUATOR 2000, 7th international conference on new actuators, 19th−21st June; 2000. p. 427−30. Bremen.
[36] http://www.mel.go.jp/.

CHAPTER

Micro-hydroforming 14

Christoph Hartl
Faculty of Automotive Systems Engineering and Production Engineering, Cologne University of Applied Sciences, Cologne, Germany

CHAPTER OUTLINE

INTRODUCTION

Hydroforming is a metal forming technology based on the application of pressurized liquid media to generate defined workpiece shapes from tubular materials or sheet metals. Numerous industries, for example, the manufacturers of automotive components and the piping industries, which are providing mass products, apply this technology productively today [1]. This successful adoption of hydroforming technology results from the advantages that hydroforming offers in comparison to conventional techniques such as the assembly of stampings by welding. Hydroforming provides the possibility to form hollow complex-shaped components with integrated structures from single initial workpieces, combined with improvements in stiffness and strength behavior due to the reduction of welding seams, and with reduced assembly costs [1].

Due to an increasing integration of micro-system technology into products of electronics, telecom, and medical devices for an ever-growing market, efficient and time-saving production technologies for micro-components become increasingly more important. Against this background, metal forming plays a decisive role for the mass production of respective components because it can offer the required productivity and accuracy for a comparatively large number of applications [2]. Concerning the mass production of hollow-shaped micro-components, this

Micromanufacturing Engineering and Technology. http://dx.doi.org/10.1016/B978-0-323-31149-6.00014-1

applies to hydroforming technology in cases where the manufacture of such parts currently still largely relies on time-consuming techniques based on the removal of material, either by chemical or mechanical means. Important existing technologies for the manufacture of complex-shaped hollow miniature and micro-components made from metals are, for example, techniques using electrodeposition of metal materials on subsequently removed mandrels (electroforming) [3] or rapid manufacturing techniques such as selective laser melting of metal powder [4]. Although these processes can offer the fabrication of high precision components, their application is limited to small and low volume production due to a comparatively high cycle time. Techniques working with the assembly of micro-surface structured component halves (for example, structured by laser or etching processes), which are used for the production of hollow-shaped metal parts, are predominantly restricted to planar workpieces. Also micro-injection molding techniques [5] enable the manufacture of complex-shaped components; however, these are limited to those with comparatively simple hollow inner shapes due to restricted possibilities in core design.

The design and optimization of micro-hydroforming processes require knowledge of the fundamentals to determine the necessary process loads, estimate feasibility, and obtain an improved comprehension of influences on the reliability and quality of component manufacturing. Additionally, size effects have to be taken into account when scaling down conventional hydroforming processes to micro-size. The objective of this chapter is to provide an overview of the respective hydroforming fundamentals and detailed information relevant for the practical application of micro-hydroforming.

PRINCIPLE OF HYDROFORMING AND PROCESS VARIANTS

Concerning existing hydroforming processes, a general distinction is to be drawn between the forming of tubular material, such as straight as well as bent tubes or profiles, and sheet material, such as single or multiple sheets. Currently, tubular material is predominantly applied for the manufacture of hydroformed components. The principle of these hydroforming processes is represented in Figure 1. At the beginning of the process, the initial part is placed into a die cavity that corresponds to the final shape of the component. The dies are closed with the closing force F_c while the tube is internally pressurized by a liquid medium with internal pressure p_i to effect the expansion of the component. Additionally, the tube ends are axially compressed by sealing punches with axial force F_a to force material into the die cavity. The component is formed under the simultaneously controlled action of internal pressure and axial force. Water/oil emulsions are typically used media to apply the internal pressure, which is usually increased from 1200 up to 4000 bar. The necessary amount of internal pressure is influenced significantly by the wall thickness of the component and the material strength and hardening, as well as by the component shape [1].

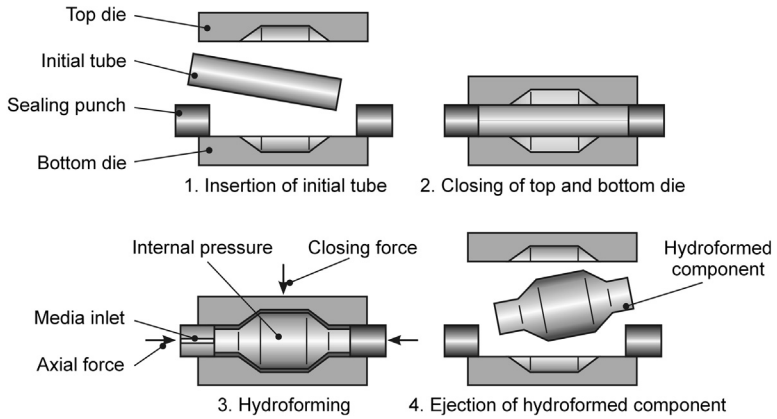

FIGURE 1

Hydroforming principle.

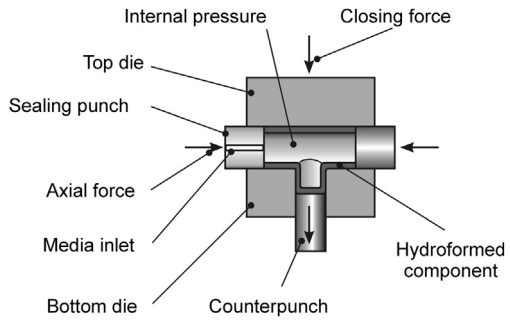

FIGURE 2

Principle of T-piece hydroforming.

Further mechanical loads can be applied to the workpiece, depending on the part and process type. An example is the hydroforming of T-shaped components, as shown in Figure 2. This process requires an additional counterpunch with a suitable control of the counterforce F_g during the forming process. The counterpunch acts on the end of the expanded protrusion and is displaced by the workpiece when the hereby exerted force achieves the current level of the counterforce.

Regarding the currently applied hydroforming process types, in Ref. [6], a first classification has been developed considering the acting stress state within the formed workpiece region and the specific characteristics of the expanded geometry. Based on this work, classifying engineering standards have been enhanced and updated regarding the description of hydroforming processes, for example, the engineering standard of manufacturing technologies DIN 8580, published by the German Institute for Standardization (DIN).

For conventional hydroforming processes, the integration of additional manufacturing operations in the hydroforming process itself is used to improve

productivity. Industrial hydroforming tools are often equipped with numerous piercing units to create holes for bolts, drain holes, reference points, collar formed holes, etc. [7]. Additionally, assembly operations within the hydroforming process have been shown to be feasible [8].

SEMIFINISHED PRODUCTS AND MATERIALS

Currently, predominantly, steel alloys and aluminum alloys are used as materials for the required semifinished products in hydroforming production. Copper and brass alloys are used for hydroformed products in the piping and sanitary industry. The applied alloys correspond, in the majority of cases, to materials which are used for common cold forming processes such as deep drawing or mass forming. In principle, all metal materials with sufficient formability are suitable for semifinished products in hydroforming processes. A fine-grained structure combined with large amounts of uniform elongation, elongation at fracture, and a large strain-hardening coefficient are advantageous in the feasible expansion of the initial workpiece, achievable without the occurrence of material instabilities. The strength of the final component is improved by a distinctive work-hardening of the formed material; however, work-hardening also causes an increase in the required forming loads.

Steel alloys used or tested for conventional hydroforming components are ductile low-carbon steels, case-hardened steels, heat-treatable steels, ferritic and austenitic stainless steels as well as high strength and ultrahigh strength steels, for example [9]. In general, tubular steel materials, which are used for hydroforming applications, are produced from flat sheet material by continuous roll forming and longitudinal high frequency welding to close the roll formed tubular cross section. Tubes with circular cross section as well as profiles which differ from a circular shape are able to be generated by the roll forming process using appropriate roll forming tools. However, predominantly semifinished products with circular cross sections are currently in use for the hydroforming production of steel components. Typical dimensions of conventionally hydroformed steel tubes are outer diameters, d_0, between about 20 mm and 140 mm with ratios of wall thickness to outer diameter, t_0/d_0, between about 0.012 and 0.16. Regarding micro-hydroforming, the market currently provides roll formed and welded metal micro-tubes with minimal outer diameters of about 0.2 mm and minimal wall thickness of about 0.03 mm.

When selecting appropriate tubes for hydroforming processes, a distinction is to be drawn between tubes without an annealing process after cold forming by roll forming or drawing, tubes drawn with a small resulting strain after a preceding annealing process, and tubes annealed after the final cold forming operation. Drawing processes, following the roll forming operation, serve for the adjustment of the final tube diameter and/or wall thickness as well as providing an increase in strength due to work-hardening effects.

Drawn and nonannealed tubes commonly provide reduced formability in hydroforming processes, depending on the characteristics of the steel alloy used and the

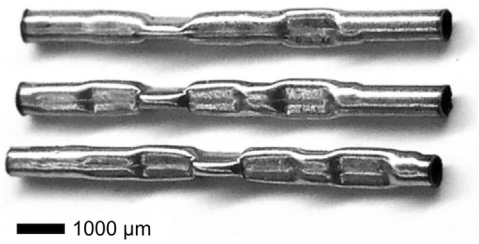

FIGURE 3

Micro-hydroformed components [10].

amount of strain induced by the drawing operation. Tubes which have been drawn with a small resulting strain after annealing show a cold formability within certain limits. The most extensive cold formability is obtained by the use of tubes which have been annealed after the final cold forming operation such as roll forming or drawing.

To avoid premature bursting of the workpiece within the hydroforming process, a highly satisfactory weld seam quality is required for roll formed and welded tubes. It is recommended to avoid locating the weld seam in the final hydroformed component within areas where excessive tensile stresses due to the expansion are acting on the component during the hydroforming process.

Figure 3 shows examples of hydroformed micro-prototype parts made from solution-annealed stainless steel tubes [10]. The initial tube material with an outer diameter of 0.8 mm and a wall thickness of 0.04 mm had been manufactured by continuous roll forming and subsequent drawing and annealing processes.

Concerning the use of aluminum alloys for conventional hydroforming applications, work-hardening aluminum 5000 alloys are currently used when priority is given to a high amount of formability and corrosion resistance, whereas precipitation-hardening aluminum 6000 alloys are applied for components requiring high strength, e.g., [11]. In general, tubes made from aluminum 5000 alloys are manufactured from flat sheet material by continuous roll forming with longitudinal welding, whereas aluminum 6000 alloys are produced as extruded profiles. Extruded profiles offer advantages in design flexibility for complex cross sections with sharp corners, multiple hollows, and flanges. However, the reduced formability of these semifinished products has to be considered when designing a respective hydroforming component. Additionally, the selection of extruded material for hydroformed micro-components is currently restricted by the minimal cross-sectional dimensions that can be produced by the relevant industries. The manufacturing of micro-extruded profiles as semifinished products was subject of several investigations, for example [12].

Due to their high strength-to-weight ratio, magnesium alloys offer a great potential for weight-reduced components. However, the use of these alloys in forming processes working at room temperature is limited due to their hexagonal atomic

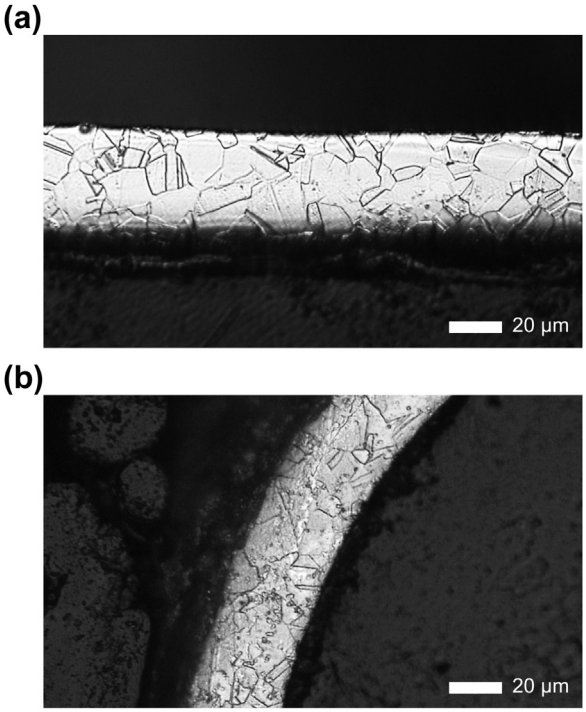

FIGURE 4

Microstructure of a micro-tube (material: AISI 304 solution annealed, outer diameter 800 µm, wall thickness 40 µm) [14], (a) section in longitudinal tube direction, (b) section perpendicular to longitudinal direction.

structure. An improvement in formability is achieved by the use of increased temperatures, above about 200 °C, when additional gliding planes become activated. Against this background, various investigations into the conventional hydroforming of semifinished products made from magnesium alloys by the use of an elevated temperature have been carried out during the last few years, e.g., [13].

In cases where hydroforming is applied to tubes with micro-dimensions, potential influences on the forming behavior, caused by the reduced ratio of tube wall thickness to average grain size diameter, t_0/d_k, of the tube microstructure, are to be taken into account [14]. This applies irrespective of the used tube material. As an example, Figure 4 shows the microstructure of the starting tubes, used for hydroforming of the stainless steel components presented in Figure 3. An average ratio, t_0/d_k, of tube wall thickness t_0 to grain size d_k between 1.54 and 2.56 was determined with a small number of single grains with $t_0/d_k \approx 1$ [14].

The design of hydroforming processes as well as the monitoring of semifinished product quality in hydroforming production requires suitable and reliable methods to obtain material parameters characterizing the forming behavior. Concerning

conventional tube hydroforming, predominantly traditional material testing methods are currently in use, such as tensile tests, mechanical expansion methods, and grid analysis. However, the suitability of these methods is often limited, as the typical biaxial stress state in hydroforming processes is not, or is only approximately, reproduced.

Most common method in use to characterize the forming behavior of the applied tubular material is the tensile test which is a standardized uniaxial material test method. A distinction is to be drawn between the application of this test to the initial sheet material before roll forming and the roll formed and welded workpieces. Testing the initial sheet material means that changes in material properties due to the manufacturing process of the tube remain unconsidered.

A method for strain analyses in hydroformed components consists in the application of circular or quadratic grids on the surface of the initial semifinished product. The measured distortion of the individual grid elements at the hydroformed workpiece enables the determination of local strains, which provides an assessment of the hydroforming process when comparing the analyzed strains with the forming limit curve of the respective tube material, e.g., [15]. There are restrictions in the use of this method in micro-hydroforming processes due to the minimal applicable grid size on micro-tubes.

An example of a standardized mechanical expansion testing method is the cone test, where the end of the investigated tube is expanded by a conical punch until fracture occurs. This test enables the principal determination of formability, for example, to compare different batches of tubular material. Also, failures at the tube surface or within the weld seam are able to be detected. When applying this test method, it has to be taken into consideration that variations in friction conditions or unequal prepared surface roughness at the tube end face influence the initiation of fracture of the expanded tube section. Figure 5 shows results of mechanically expanded micro-tubes made from stainless steel AISI 304 [16].

To improve methods for the characterization of tubes for hydroforming applications, several investigations have been carried out into tube expansion tests working with an inner pressurization of the tested tube, which is clamped at its ends according to Figure 6. This bulge test enables the determination of the bursting pressure p_b, the pressure-dependent expansion diameter $d(p_i)$, and the achievable expansion

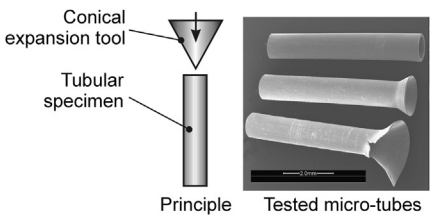

FIGURE 5

Expansion cone test and experimental results.

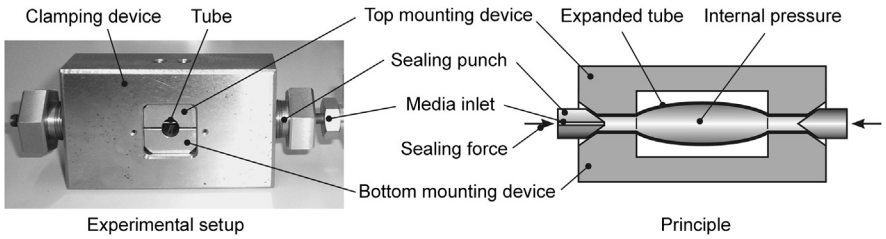

FIGURE 6

Bulge test device for micro-tubes.

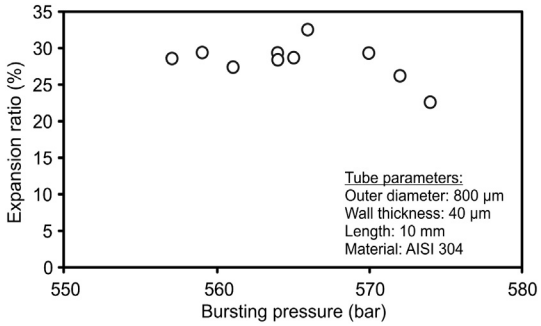

FIGURE 7

Expansion ratio versus bursting pressure of micro-tubes made of solution-annealed stainless steel.

diameter d_r under the biaxial tensile stress state. Strategies to determine the material properties of tubes as well as their yield curves based on the bulge test have been developed, for example in Refs. [17], [18]. When applying the bulge test, it has to be taken into consideration that the ratio of the expanded tube length l_d to the tube diameter d_0 influences the required pressure to expand a tubular specimen, if the ratio l_d/d_0 is below a certain limit [19,20]. The bulge test device shown in Figure 6 has been developed for the testing of micro-tubes with outer diameters below 1 mm and is suitable to apply up to 4000 bar of internal pressure [14,21]. Figure 7 shows as an example test results of micro-tubes conducted with this device which verified changing formability for downscaled hydroforming processes, as presented in [14].

PROCESS CHAIN FOR PART PRODUCTION

Depending on the component design, the industrial production of hydroforming parts requires several additional manufacturing steps in addition to the hydroforming process itself. Figure 8 shows schematically a typical process chain for the manufacture of hydroformed components.

FIGURE 8

Typical process chain for the production of hydroformed components.

The basic part of the process is the tube, which has to be cut to length in the first step. A comparatively high standard of quality for the cut tube ends is required to ensure reliable sealing during the hydroforming process. In general, tubes with conventional dimensions are cut and machined by sawing or mechanical cutting. However, the damage-free machining of thin-walled structures such as micro-tubes and micro-hydroformed components requires processes with a minimum of forces for clamping and processing. In general, lasers are predestined for the here-required operations because of their contact-free function. Also, cutting by wire electrical discharge machining provides reliable cut surfaces.

In the majority of cases, the complexity of the components requires that additional forming operations are to be applied preceding the hydroforming process. These operations can consist of bending and mechanical forming (preforming) of the initial component to enable its insertion into the hydroforming die or to obtain an optimized material distribution. Typical bending processes are, in general, rotary draw bending for complex bent components and press bending for less complex shapes with large bending radii [7]. However, it has to be taken into account that due to a preceding bending process of the initial tube, the wall thickness is decisively reduced within the outer bent areas and formability is exhausted to a large extent [22]. As a consequence, these workpiece areas tend to fail prematurely by necking and bursting. The increase of corner radii and/or the reduction of the overall expanded cross-sectional circumference are recommended to avoid the appearance of these instabilities.

In cases where the initial tube diameter d_0 is larger than the die cavity width w, a preforming operation is necessary to enable the reliable insertion of the initial workpiece into the hydroforming die. The preforming operation induces the reduction of the tube dimension within these areas in the direction of w. Typically used methods for preforming operations are shown schematically in Figure 9. For the preforming of straight as well as bent tube sections, methods working with beveled dies according to Figure 9(a) are suitable to be applied. In contrast to this, methods using cross-slides for local workpiece reduction are limited when bent tube sections are to be preformed (Figure 9(b)). In certain cases, preforming is also used to flatten tube sections, for example, when a flattening by closing of the hydroforming tool is not reliably feasible. Limits of preforming can consist in shape deviations which are caused by this operation and which remain after the hydroforming process; for example, wrinkles due to an inappropriate material distribution or excessive small radii

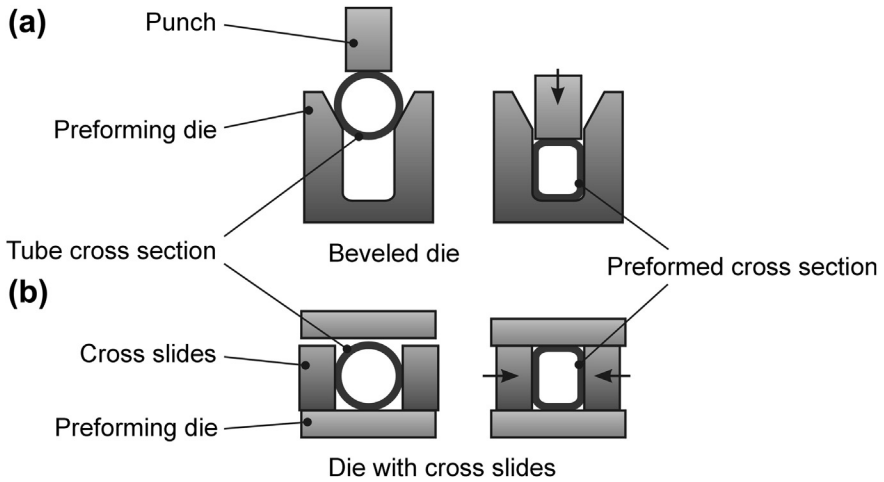

FIGURE 9

Principles of preforming, (a) with inclined tool surfaces, (b) with cross slides.

generated by local folding of the tube wall. Also excessive elastic springback of flat workpiece sections can occur due to an insufficient forming degree within the hydroforming process.

The following hydroforming of the preformed workpiece takes place by the controlled application of the forming loads p_i and F_a. Commonly, these process parameters are determined versus the time of the forming process. The suitable variation of internal pressure and axial force depends predominantly on the material properties and strain-hardening behavior, on the tube wall thickness, on the sizes of intricate sections of the component such as small corner radii, and on the potential occurrence of instabilities.

Further operations such as trimming, notching, or additional forming may need to be performed subsequent to the hydroforming process; for example, to enable the connection to other components by welding. For hydroformed parts with conventional dimensions, trimming operations consist in sawing, milling, mechanical cutting, or laser machining, depending on the required shape and quality of the component ends. Regarding micro-components, similarly to the cutting of the initial micro-tubes, lasers are suitable for final trimming and cutting operations due to their contact-free and flexible processing method.

HYDROFORMING PROCESS DESIGN

The design of process control for the forming loads during the hydroforming operation should be suitable to obtain the required forming result due to a continuously achieved yield stress of the material under the avoidance of failures such as

wrinkling, buckling, and bursting. The internal pressure p_i and the axial force F_a are the decisive parameters of the process control.

Currently, fundamentals to determine the correlation between applied loads and forming result have been developed predominantly for the conventional hydroforming of straight rotationally symmetrical workpiece shapes and of T-piece components, for example [19,23–26]. The methods used to derive applicable solutions have been the Membrane Theory, the Theory of Shells, and the Continuum Theory of Plasticity in the majority of cases. Due to the further development of commercial programs based on the finite element method within the last few years, the detailed and efficient analysis of forming processes is state of the art, where the component shape differs from parts with round cross sections and a straight axis [22].

From fundamental research work into miniaturization of forming processes, it is known that size effects have to be taken into account when scaling down forming processes [27,28]. Conducted experimental and theoretical investigations into micro-hydroforming already demonstrated the influence of these effects [14,29]. In Ref. [29], it was predicted theoretically by the use of a plain strain crystal plasticity finite element-based modeling technique that localized necking of a micro-tube wall is related to the angle between the crystal slip systems and the hoop stress direction. Hence, as a result of the small number of grains in tube wall direction, necking and following bursting progress faster in the expansion of micro-tubes than in macro-tubes, which can be regarded as a homogeneous continuum due to their larger number of grains.

To provide here a general basis to determine process parameters for micro-hydroforming, correlations are given in the following, which have been proven for conventional hydroforming. However, depending on the specific application, the aforementioned changes in material forming behavior (yield stress, forming limits), caused by the process miniaturization, have to be considered.

Based on the Membrane Theory, which considers a biaxial stress state, the condition for the initiation of yielding of a cylindrical straight tube under axial force F_a and internal pressure p_i and the resulting stress state can be derived [19]. The circumferential stress σ_θ and the axial stress σ_z within a thin-walled straight tube can be determined accordingly with:

$$\sigma_\theta = p_i \frac{d_0 - t_0}{2t_0} \tag{1}$$

$$\sigma_z = \frac{1}{\pi(d_0 - t_0)t_0}\left(p_i \frac{\pi}{4}(d_0 - 2t_0)^2 - F_a\right) \tag{2}$$

for an initial outer tube diameter d_0 and an initial tube wall thickness t_0. Plastic yielding of the tube starts when the effective stress σ_{eff}, which results from the combination of axial and circumferential stresses, corresponds to the local yield strength σ_Y of the tube material with:

$$\sigma_{eff} = \sqrt{\sigma_\theta^2 + \sigma_z^2 - \sigma_\theta \sigma_z} \tag{3}$$

according to the von Mises yield criterion. These equations enable the derivation of the correlation between the internal pressure p_i and the resulting axial force F_a, which is suitable to induce plastic deformation of the tube as follows [19]:

$$F_a = \pi(d_0 - t_0)t_0\left[\sqrt{\sigma_Y^2 - \frac{3}{16}p_i^2\left(\frac{d_0 - t_0}{t_0}\right)^2} - p_i\frac{d_0 - t_0}{4t_0}\right] + p_i\frac{\pi}{4}(d_0 - 2t_0)^2 \quad (4)$$

To ensure the sealing of the workpiece ends during the overall process, a minimum axial force is required which can be determined with:

$$F_p = p_i\frac{\pi}{4}(d_0 - 2t_0)^2 \quad (5)$$

If the axial force F_a is less than F_p, leakage between the hydroformed tube ends and the sealing punches occurs and with this a pressure loss.

In the final stage of the hydroforming process, the tube wall has to be formed into the corner radii of the die cavity, which was not formed during the main expansion of the tube. This is achieved by raising the internal pressure up to its maximum value p_k. Several theoretical and experimental investigations have provided correlations to determine this necessary calibration pressure, for example [30]. An empirically deduced equation suitable for a first estimation to determine the maximum necessary internal pressure is as follows [31]:

$$p_k = 1.2\sigma_{UTS}\frac{t_0}{r_c} \quad (6)$$

with the ultimate tensile strength σ_{UTS} of the formed tube material, the tube wall thickness t_0, and the minimal outer radius r_c which has to be formed.

The axial force F_a throughout the hydroforming process up to its end can be generally made up of three individual forces [32]:

$$F_a = F_z + F_p + F_f \quad (7)$$

The force F_z is the axial force component which is initiated in the tube wall and maintains, together with the action of the internal pressure, the plastic flow of the tube wall. F_p is the minimum sealing force according to Eqn (5). The force F_f is the frictional force that must be overcome throughout the forming process due to the contact between the tube ends with the hydroforming tool.

For practical use, the required force F_z can be estimated by:

$$F_z = \left(1.2\sigma_{UTS} + p_i\right)\pi t_0(d_0 - t_0) \quad (8)$$

with the initial tube dimensions d_0 and t_0 and the ultimate tensile strength σ_{UTS}.

When Coulomb's frictional behavior is taken as a basis, the following correlation to determine the friction force F_f in practical cases can be used:

$$F_f = \mu p_i d_0 \pi l_f \quad (9)$$

with the coefficient of friction μ, the tube diameter d_0 in the feeding zone, and the length l_f where frictional movement occurs.

The maximum values for the axial force and the internal pressure are commonly applied at the end of the forming process when the workpiece is calibrated with an increase in the internal pressure up to the magnitude of the calibration pressure p_k. Component-specific correlations to determine the axial force have been derived, for example in Ref. [19] for the hydroforming of rotationally symmetrical components and in Ref. [26] for the forming of T-shaped parts.

The occurrence of failures limits the applicable forming loads F_a and p_i and with this the feasible workpiece geometries produced by hydroforming processes. These instabilities are predominantly local necking and bursting of the workpiece wall, local or extensive wrinkling of the workpiece, and buckling of the initial tube [6].

Necking is caused by a locally exceeded formability of the workpiece material and introduces the bursting of the hydroformed workpiece. To predict the internal pressure p_b at the moment of the bursting of straight tubes within the state of free expansion, the correlation investigated in Ref. [19]:

$$p_b = \sigma_{UTS} \frac{2t_0}{d_0 - t_0} \tag{10}$$

has shown to be applicable for conventional tube hydroforming. Regarding the expansion of straight tubes, the bursting pressure p_b should not be exceeded within a hydroforming process as long as the tube is not in contact with the surrounding die cavity. Only if large areas of the expanded tube received alignment to the die cavity, can internal pressure be increased beyond p_b. Bursting and preceding necking predominantly occur within the area of largest expansion. In general, an increase in axial force F_a, within certain limits, raises the feasible expansion until necking and bursting are induced due to the resulting increase of axial compressive stress within the tube wall [6,19,24,25]. However, it has to be taken into consideration that long feeding sections and bent workpiece areas, where workpiece material has to be transported by the axial force into the area to be expanded, impede the material flow due to friction forces and additional bending forces [32]. In the case of complex-shaped components with varying cross-sections along the workpiece axis, bursting induced by necking predominantly occurs within the areas of cross-section corners. In addition to the influences from the process control and hydroformed component geometry, the occurrence of necking and bursting can also be induced by the properties of the applied semifinished product which result from their manufacturing process. Welding seams at longitudinally welded tubes or extruded profiles can be the starting points of these failures, for example.

Wrinkling of the component wall results predominantly from excessive axial load. Due to this possible failure case, the applicable axial stress to reduce the decrease in wall thickness during the hydroforming process is limited. An adapted control of axial force and internal pressure has to be applied to avoid this instability. Wrinkles in the longitudinal direction of the workpiece can be caused during closing of the hydroforming tool when improper dimensions for the semifinished product or for the preformed component geometry have been selected.

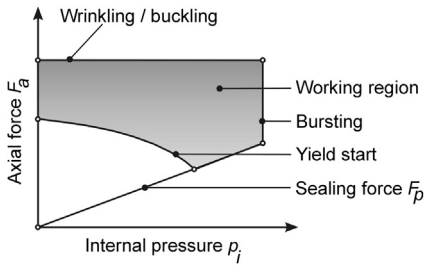

FIGURE 10

Range of feasible process controls (schematic).

In cases of comparatively long free-tube length, unsupported by surrounding tool surfaces, buckling of the workpiece can occur due to an excessive axial load. Also here, the application of an adequate control of axial load and internal pressure is required to avoid this failure case. In [33], an iterative method is presented to determine suitable load paths for the hydroforming of rotationally symmetrical workpieces with a maximum of compressive stress, derived on the basis of the determination of buckling with plastic material behavior.

The geometric parameters of the initial tube, the workpiece, and the tool as well as the tube material properties and friction conditions influence the range of failure-free process controls for the forming loads F_a and p_i. Figure 10 shows schematically the range for feasible process controls for a hydroforming process limited by the occurrence of instabilities, the initiation of yield of the workpiece, and the minimum required force to seal the tube, according to investigations reported in [19].

In [34] and [35], examples of achievable workpiece geometries within the here-discussed forming limits, considering comparatively satisfying formability of the component material and reliable and economic production, have been presented for conventional hydroforming.

DESIGN CONSIDERATIONS AND POTENTIAL APPLICATIONS OF MICRO-HYDROFORMING

Attributes which micro-components should have to be appropriate for a hydroforming production consist of the following:

1. a tubular shape with hollow cross sections;
2. changes in circumferences along the axis which are below the limits of possible expansion;
3. material properties which provide a reasonable formability;
4. a geometry which enables smooth die cavities with large corner radii to be formed by the hydroforming process to avoid uneconomic high internal pressures and high stresses within the tool elements;

5. an adequate ratio of wall thickness to tube diameter t_0/d_0 between 0.05 and 0.16 to ensure an economic amount of necessary internal pressure and to enable handling of the workpieces free of damage; and
6. comparatively rough tolerances demanded for inner dimensions [16].

For materials with a comparatively good formability, an expansion of 10% in circumference is feasible without an axial feeding of material and up to 30% is to be expected when axial forces are applicable to the component ends. However, corresponding to forming limits in conventional hydroforming [7], expansions within prebent tube sections should be avoided.

Micro-hydroforming offers the potential for the production of a wide range of products from the fields of *medical engineering* (e.g., needles and micro-tubes for drug delivery, micro-pipettes, tubular parts for endoscopes, elements for surgical tools or implants), *micro-fluidics* (e.g., components for micro-fluidic chips, elements for micro-dosage or pipe connections and housings), and *micro-mechatronics* (e.g., shafts and elements for micro-actuators, components for micro-sensors or connection pins). However, certain design changes of such products with an adaptation to the micro-hydroforming process will be required to enable a failure-free and reliable production by hydroforming.

TOOLS AND MACHINES

In addition to the applied process parameters and the quality of the tubular blanks used, the final quality of the hydroformed components is decisively influenced by the design of the hydroforming tool and the hydroforming machine. Also, production parameters such as cycle time, production reliability, equipment availability, and production costs depend on their design.

One important difference between hydroforming and other forming processes is the comparatively high level of loads acting on the tooling due to the closing force F_c and the internal pressure p_i. The minimum closing force which is required throughout the forming process to ensure that the hydroforming tool remains closed can be determined as follows:

$$F_c = p_i A_p \tag{11}$$

with the projected component surface A_p perpendicular to the closing direction, and the applied internal pressure p_i.

The acting loads generate elastic deformation of the tool elements which crucially influences part quality and tool lifetime. Figure 11 presents a schematic drawing and an example of hydroforming tooling for mass production with its essential components. The tool inserts, which contain the die cavity, are in general made of heat-treated tool steel to ensure a sufficient lifetime and wear resistance of these elements. The stresses within die inserts, resulting from the acting loads, are essentially influenced by the size of the corner radii of the die cavity, the positioning of the joint face between the top and bottom die, which determines the depth of the die

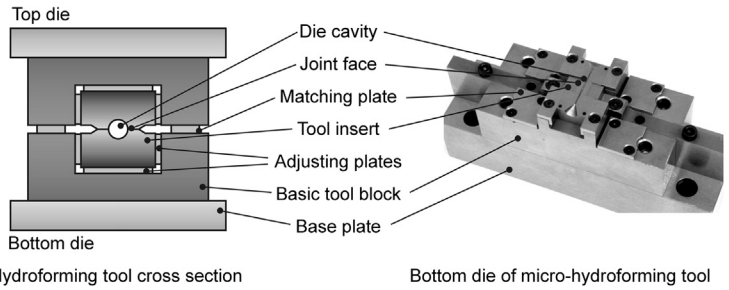

FIGURE 11

General design of micro-hydroforming tools.

cavity, and the surface quality of the die cavity [7]. On principle, the design of die inserts with deep cavities, small corner radii, and rough surfaces should be avoided. Due to these factors, the stresses within the inserts increase and, if a critical stress state is exceeded, fracture after a low number of cycles is the consequence. When positioning the joint face in the course of the tool design, it has to be taken into consideration that: (1) the initial component is able to be inserted into the bottom die without problems; (2) no undercuts exist within the die cavity; and (3) the hydroformed component is able to be removed failure free from the die cavity.

Die cavity deflections in micro-hydroforming processes can be reduced by superimposing bending stresses, as presented in Ref. [36]. Finite element simulations with systematic variation of closing force and tool parameters, which determine the amount of superimposed bending, were carried out to investigate their influence on die cavity deflection. The simulations were conducted on a cylindrical expanded shape. A tool cross section was selected representing a die cavity with diameter of $d = 1040$ µm, and an internal pressure of $p_i = 4000$ bar was applied. Without application of bending stresses ($a = 0$), the die cavity expands in horizontal direction (d_x) as well as in vertical direction (d_y) and cannot be kept constant to the nominal size of 1040 µm. The superimposition of bending deformation ($a = 20$ µm) enables to keep the die cavity closer to the nominal size in horizontal as well as in vertical direction as to be seen from Figure 12. However, the closing force F_c and the joint face width b have to be adapted to the selected amount of bending [36].

In general, part handling in automated conventional hydroforming production processes is done by robots equipped with grippers for the insertion of the initial tube into the tooling and to remove the hydroformed part from the tooling. Both actions, insertion and removal, are in most cases supported by so-called ejectors which are integrated into the top and bottom hydroforming tool halves [37]. These ejectors can be lifted and moved inward when the initial tube is inserted and they can be lifted to eject the part. Through lifting the part, a space is opened for the grippers to reach the workpiece. The disadvantages of ejectors are that they produce markings on the workpiece and that they reduce the stiffness of the tooling due to the necessary cutouts within the die in which to place the necessary drives. Additionally,

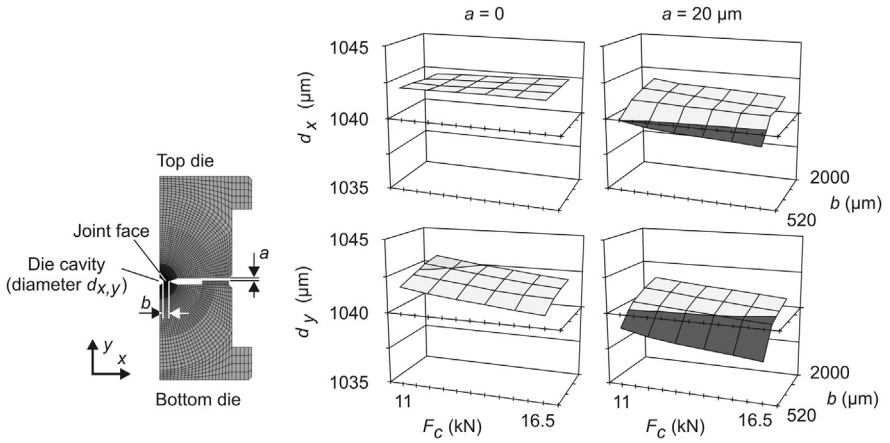

FIGURE 12

FE-simulation results of die cavity deformation analysis (according to [10,36]).

micro-hydroforming tools often allow a limited space for the integration of ejectors. Alternative concepts for efficient part removal for micro-hydroforming can consist in grippers, which take the component at its ends out the tooling while the tool is set in vibration to reduce the friction between the tool and the component and, with this, the forces for removal.

Adjusting plates, covering the contact areas between the basic tool blocks and the integrated tool inserts, serve to adjust the correct position of the die insert elements relative to each other and to the axis of the sealing punches. The basic tool blocks are commonly made of heat-treatable steel with a strength that is lesser in comparison to the strength of the tool insert.

Figure 13 shows examples of several design principles for the sealing of tubes during hydroforming from conventional practical applications and research works. In general, axial sealing punches are made from hardened tool steel. Punches working with rubber elements (Figures 13(c) and (d)) have shown an insufficient wear resistance in practical use for series production. Conical punches, as presented in Figure 13(b), show good behavior regarding sealing and wear resistance but do not enable the axial feeding of tube material into the die cavity. A suitable punch design proved in a practical series production is represented in Figure 13(a). Here, the sealing occurs mainly due to a sharp corner surrounding the contact area between the punch and the tube end. When the punch comes into contact with the tube end, this corner is pressed into the tube front and thereby creates the sealing. A general problem of axial sealing punches is their reduced durability due to the high level of stresses generated by the applied loads. The lifetime is mainly influenced by the level of loads, the tool material used, the surface roughness of the punch, the size of corner radii at the punch in critical areas, the size of the bore to feed the pressurizing media into the tube, and by additional bending moments

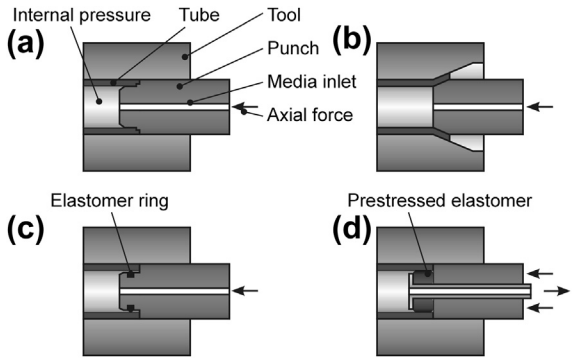

FIGURE 13

Sealing principles, (a) end-face contact, (b) conical punch, (c) elastomer ring, (d) prestressed elastomer.

acting on the punch which can result from elastic tool deflection caused by the closing force.

The hydroforming tool is mounted on the hydroforming machine, which performs the required actions and movements to conduct the forming process. The main tasks of this machine are

1. to open and close the tool for part insertion and removal;
2. to provide the required closing force F_c during the forming process;
3. to close the component ends using the axial sealing punches;
4. to fill the component with the pressurizing media;
5. to apply the internal pressure p_i according to a specified pressure−time curve;
6. to move the component ends for material transport by means of the axial sealing punches by applying the force F_a according to a specified stroke−time curve; and
7. to communicate with the handling system for component handling.

According to the tasks to be executed, hydroforming machines consist of corresponding subassemblies, as shown schematically in Figure 14. The predominant part of these subassemblies is mounted on the press frame, which has to provide sufficient stiffness against the loads to resist deformation and displacement of the structure and an adequate accessibility for part handling and die changing.

The opening and closing of the tool as well as the application of the closing force is, in general, conducted by one single drive. The requirements of this drive are a sufficiently high translational speed to enable short production times and enough force to close the hydroforming tool. It is recommended to synchronize the level of the required closing force with the currently applied internal pressure. This control strategy reduces tool deflection and improves with this the quality of the component produced. Hence, precision for force control of the drive is expected to be comparatively high, whereas precision of stroke control is secondary. When selecting a suitable drive, it has to be taken into consideration that the maximum force is

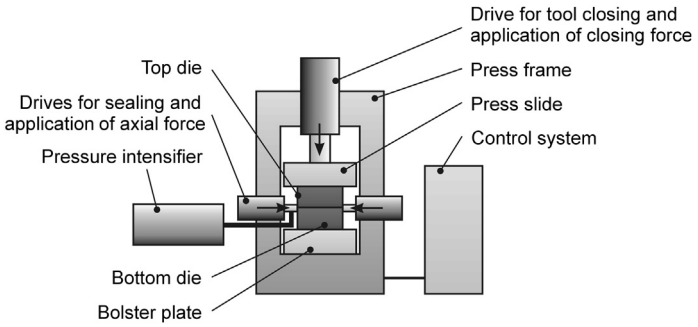

FIGURE 14

Elements and functions of the hydroforming machines.

applied without movement. Under these conditions, hydraulic cylinders are suitable for use as drives. Additionally, the overall stroke of the drive should be able to afford sufficient space for comfortable and fast tool changing and part handling. It should be mentioned here that for conventional hydroforming applications also, machine concepts exist which use one drive for a fast movement of the top die and a second drive with short stroke to apply the closing force [1].

The internal pressure p_i is applied by a pressure intensifier which is integrated into the high pressure system, consisting of valves, piping, equipment for media supply and maintenance such as filters and tanks, and the pressurizing medium. Due to the reduced volume of hydroformed micro-components, the required volume flow of the intensifier is comparatively small. However, depending on the component to be formed and its material, the required pressure is reasonably high. Pressure intensifiers can be driven mechanically, e.g., a spindle-driven plunger with an electric motor, by hydraulic power or by air pressure. The systems differ in minimum and maximum provided volume flow, achievable maximum pressure, and control accuracy.

Regarding the applied pressurizing media, predominantly water/oil emulsions, solutions based on water and in a few cases pure oil are in use as the pressurizing media. The applied water/oil emulsions and the solutions consist, in general, of about 95–98% water. The water-based systems have the advantage of a negligible compressive behavior whereas oil shows comparatively high compression under high pressure, which can influence the process control. Solutions show an improved resistance against micro-organisms in comparison to emulsions. Pure oil provides immunity against micro-organisms and good corrosion protection. Additionally, a crucial criterion for the decision of a suitable pressurizing medium is the pressure loss of the fluent liquid medium under increased pressure flowing through narrow bores, as is necessary for micro-hydroforming when providing the medium through the axial sealing punch into the workpiece [38]. In general, liquids with higher viscosity show an increased pressure loss.

The primary function of the axial driving system is the axial movement of the sealing punches toward the tube ends to ensure leakage-free sealing of the

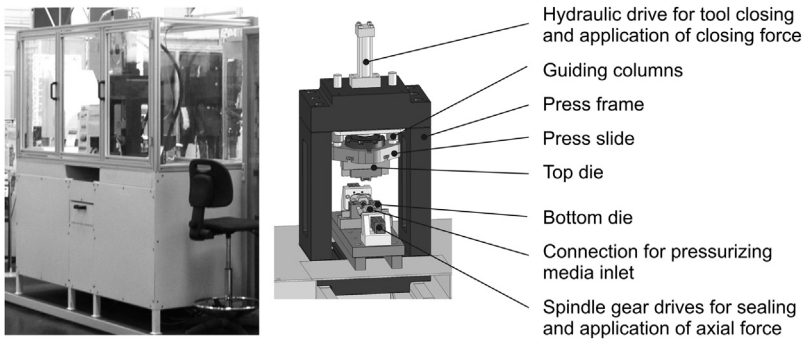

FIGURE 15

Micro-hydroforming prototype machine.

pressurized tube during the hydroforming process. The secondary function comprises the axial feeding of the tube material into the die cavity during the forming process to enable an extended formability of the tube. For example, linear actuators with a gear spindle can be used to drive the sealing punches. Hydraulic drives, as used in common hydroforming processes, generally deliver unnecessarily high levels of load for micro-hydroforming processes.

The control systems of industrial used hydroforming machines are based on conventional programmable logic controller systems, customary for press controls. Common sensors are used for measuring the strokes, speeds, and forces of all axes, and for measuring the pressures of the hydraulic system and the forming high pressure.

Figure 15 shows as an example a prototype micro-hydroforming press which was designed for investigations into the mass production of micro-components. This machine enables the micro-hydroforming of components with cross-sectional dimensions between 0.2 and 1 mm. It is equipped with a spindle-driven pressure intensifier which enables the application of up to 4000 bar internal pressure, the closing force being realized by a hydraulic drive, and the axial punches being moved by linear actuators with spindle gears. The investigation into this prototype machine served for the development of the first serial production micro-hydroforming machines [21].

CONCLUSIONS

Micro-hydroforming is a new manufacturing method for the mass production of tubular complex-shaped metal micro-components with integrated structures. It is based on the forming of initial tubes by internal pressurization with a liquid medium. Potential applications concern the production of corresponding components for

medical devices, micro-fluidic and micro-mechatronic technology. Important advantages of micro-hydroforming consist in the possibility to generate complex geometries with reduced effort in machining and joining operations as well as in process time, compared to methods used until now for the manufacture of such components. As micro-hydroforming is characterized by comparatively high forming loads and pressures, the application of this forming technology implies an enhanced knowledge of an adequate process design to obtain economic and reliable production.

REFERENCES

[1] Hartl Ch. Research and advances in fundamentals and industrial applications of hydroforming. J Mater Process Technol 2005;167:283−392.

[2] Qin Y, Brockett A, Ma Y, Zhao J, Harrison C, Pan W, et al. Micro-Manufacturing: research, technology, outcomes and development issues. Int J Adv Manuf Technol 2010;47:821−37.

[3] McGeough JA, Leu MC, Rajurkar KP, De Silva AKM, Liu Q. Electroforming process and application to micro/macro manufacturing. Annals CIRP 2001;50. 499−514.

[4] Yadroitsev I, Thivillon L, Bertrand Ph, Smurov I. Strategy of manufacturing components with designed internal structure by selective laser melting of metallic powder. Appl Surf Sci 2007;254:980−3.

[5] Piotter V, Gietzelt T, Merz L, Ruprecht R, Hausselt J. Powder injection molding in micro technology. In: Proceedings of PM2TEC, advances in powder metallurgy & particulate materials Orlando, US; 2002. p. 43−8.

[6] Dohmann F. In: Lange K, editor. Innenhochdruckumformen, vol. 4. Berlin: Umformtechnik Springer; 1993. p. 252−70.

[7] Hartl Ch. Case studies in hydroforming. In: Proceedings of int. conf. recent development on tube and sheet hydroforming Columbus, OH; 2003.

[8] Marré M, Gies S, Maevus F, Tekkaya AE. Joining of lightweight frame structures by die-less hydroforming. Int J Mater Form 2010;3:1031−4.

[9] Flehmig T, Schwarz S. Hydroforming complex hollow sections. Steel Grips 2003;1(6): 408−12.

[10] Hartl Ch, Anyasodor G. Experimental and numerical investigations into micro-hydroforming processes and machine design. In: Proceedings of 13th int. conf. on metal forming PC Toyohashi; 2010. p. 1193−6.

[11] Schuster C, Loretz C, Klaas F, Seifert M. Potentials and limits with hydroforming of aluminium alloys. In: Proceedings of int. conf. on hydroforming Stuttgart; 2005. p. 113−36.

[12] Rosochowski A, Wojciech P, Lech O, Richert M. Micro-extrusion of ultra-fine grained aluminium. Int J Adv Manuf Technol 2007;33(1−2):137−46.

[13] Geiger M, Merklein M, Celeghini M, Haldenwanger H-G, Prier M. Sheet and tube hydroforming at evaluated temperature. In: Proceedings of int. conf. on hydroforming Stuttgart; 2003. p. 259−78.

[14] Hartl Ch, Anyasodor G, Lungershausen J. Formability of micro-tubes in hydroforming. In: Proceedings of int. EASEFORM conf. on metal forming Belfast; 2011. p. 529−34.

[15] Green DE. Experimental determination of tube forming limits. In: Proceedings of int. conf. on hydroforming Stuttgart; 2003. p. 299−314.

[16] Hartl Ch, Lungershausen J, Biedermann H, Conzen J. Study of hydroforming processes for the production of micro-components. In: Proceedings of 1st jubilee scientific conf manufacturing engineering in time of information society Gdansk; 2006. p. 137−40.
[17] Groche P, Breitenbach G. Influence of tube manufacturing processes on hydroforming. In: Proceedings of int. conf. on hydroforming Stuttgart; 2005. p. 219−40.
[18] Altan T, Koc M, Aue-u-lan Y, Tibari K. Formability and design issues in tube hydroforming. In: Proceedings of int. conf. on hydroforming Stuttgart; 1999. p. 105−22.
[19] Klaas F. Aufweitstauchen von Rohren durch Innenhochdruckumformen. Duesseldorf: VDI; 1987.
[20] Hielscher C. Tube testing for the production of complex hydroforming parts. In: Proceedings of int. conf. on hydroforming Stuttgart; 2001. p. 63−84.
[21] Hartl Ch, Lungershausen J, Eguia J, Uriate L, Lopes Garcia P. Micro hydroforming process and machine system for miniature/micro products. In: Euspen 7th int. conf Brem 2; 2007. p. 69−72.
[22] Dohmann F, Hartl Ch. Hydroforming applications of coherent FE-simulations to the development of products and processes. J Mater Process Technol 2004;150:18−24.
[23] Fuchizawa S. Influence of strain hardening exponent on the deformation of thin-walled tube of finite length subjected to hydrostatic internal pressure. Adv Tech Plast I 1984: 297−302.
[24] Woo DM. Tube-bulging under internal pressure and axial force. J Eng Mater Technol 1973;10:219−23.
[25] Sauer WJ, Gotera A, Robb F, Huang P. Free bulge forming of tubes under internal pressure and axial compression. In: Proceedings of 6th North American metal working research conf. Gainsville; 1978. p. 228−35.
[26] Chalupzak J, Sadok L. The problem of forces and stresses in the hydromechanical process of bulge forming of tubes. Metalurgia I Odlewnictwo − Tqm 9 − Zeszyt 1984;1: 57−66.
[27] Vollertsen F. Size effects in manufacturing. In: Proceedings of 1st colloquium process-scaling Bremen; 2003. p. 1−9.
[28] Pawleski O. Beitrag zur Aehnlichkeitstheorie der Umformtechnik. Archiv für das Eisenhüttenwesen 1964;35:1−10.
[29] Zhuang W, Wang S, Cao J, Lin J, Hartl Ch. Modelling of localised thinning features in hydroforming of micro-tubes using crystal plasticity FE method. Int. J Adv Manuf Technol 2009;47:859−86. http://dx.doi.org/10.1007/s00170-009-2134-4.
[30] Koc M. Development of guidelines for tube hydroforming [Doctoral dissertation]. Columbus, OH; 1999.
[31] Braeutigam M, Rutsch H. Hydroformen − als Ausweg aus der Investitionsklemme. VDI Berichte N. R 1992;946. VDI, Duesseldorf.
[32] Hartl Ch. Theoretical fundamentals of hydroforming. In: Proceedings of int. conf. on hydroforming Stuttgart; 1999. p. 23−36.
[33] Dohmann F, Boehm A, Dudziak K-U. The shaping of hollow shaft-shaped workpieces by liquid bulge forming. Adv Tech Plast 1993:447−52.
[34] Klaas F. Innovations in high-pressure hydroforming. In: Proceedings of 2nd int. conf. on innovations in hydroforming technology Columbus, OH; 1997. p. 1−31.
[35] Dohmann F, Hartl Ch. Hydroforming components for automotive applications. Fabricator 1998;(2). 30−38.

[36] Hartl Ch, Anyasodor G, Ptaschlik T, Lungershausen J, Lippert S. Investigation into reduction of die-cavity deflection in micro-hydroforming processes using FEA. Int. J Adv Manuf Technol 2009;47:853−8. http://dx.doi.org/10.1007/s00170-009-2141-5.
[37] Hartl Ch, Abbey T. Product development of complex hydroformed parts and requirements regarding tool manufacture. In: Proceedings of int. conf. on technology of plasticity nuremberg; 1999. p. 1183−8.
[38] Cousin R. CFD-simulation of fast filling procedures in small fluid chambers for hydroforming processes. In: Proceedings of 1st jubilee scientific conf manufacturing engineering in time of information society Gdansk; 2006. p. 75−80.

This page intentionally left blank

CHAPTER

Laser-assisted Micro-forming

15

Dr Jens Holtkamp
Fraunhofer Institute for Laser Technology ILT, Aachen, Germany

CHAPTER OUTLINE

INTRODUCTION

Forming is one of the basic production technologies, and due to the potential and the low costs of the process, is widely spread in industrial applications. Nevertheless, there are specific limitations regarding the workpiece materials and the maximum strain within the forming operation. Brittle and high-strength materials cannot be accommodated without high process complexity or low product quality.

By heating the used materials prior to the forming process, with the corresponding change of their material properties, these drawbacks can be eliminated.

The use of laser radiation as the heat source enables short heating times, due to the associated high energy density. In addition, there are other advantages such as contactless heating, good focus ability, and good controllability. Lasers are, therefore, becoming a promising alternative to existing technologies such as induction or conductive heating.

In principle, every forming technique can be enhanced by laser technology. The basics for its integration and some exemplified processes are described in the following sections.

Micromanufacturing Engineering and Technology. http://dx.doi.org/10.1016/B978-0-323-31149-6.00015-3

SYSTEM TECHNOLOGY

Heating of the workpiece can be achieved by different methods: conductive through the contact of a heated tool, convective within a convection oven, or inductive by swirling currents generated in the material.

Preprocess heating of the workpiece outside of the tool leads to an increase of temperature within the whole part. Temperature gradients are not adjustable; therefore, local heating of selected areas of the part is not possible. Heating of micro-components is difficult due to their low mass. This low heat capacity leads to a cooling down after the transport into and the contact with the tool.

The disadvantage of methods based on heat convection is the bad controllability of the forming temperature and the resulting long cycle times. Similarly to the preheating method, the heating of local areas of the workpiece is not possible.

By using a laser as the heat source, the induced energy and the resulting temperatures can be easily controlled by laser power. Heating of selected areas is possible by forming the laser beam. The high energy density of the radiation and the direct absorption enable short cycle times. Therefore, a laser is a promising tool to achieve the potential of micro-forming at elevated temperatures.

The laser system causes the main additional cost in comparison to the cost of conventional machinery. Due to its low price in comparison with that of other laser systems, a diode laser is often favored, but there are also other effective systems such as fiber lasers. If absorption within transparent workpieces is intended, the wavelength of the laser has to be adapted.

The machinery used for laser-assisted processes is based on conventional forming machines. The system is then, beside the laser itself, enhanced with components for the integration and control of the laser. One basic additional element is an optical system which is placed inside the tool. Adapted to a fiber that connects the laser with this system, it guides the radiation through the forming tool onto the surface of the workpiece to be heated. If necessary, the shape of the radiation can be adapted to the geometry of the workpiece.

Figure 1 presents a schematic drawing of an exemplified configuration.

The laser radiation is first collimated and then reflected on a dichroic mirror through a focal lens toward the sheet metal surface.

By means of an additional camera, which is arranged coaxially with the optical path, the position of the laser radiation can be displayed on a monitor. This enables an easy adjustment of the tool to the optical system and the possibility of process monitoring.

Knowledge of, and the possibility to control, the process temperatures arising is important for reproducible and accurate process results. Additional sensors can be used such as thermocouples or pyrometers to detect these temperatures and, if necessary, to submit them to a controller. The value of a pyrometer depends on the emittance of the material and its surface properties. Therefore, it is necessary to "teach" the system before using new materials.

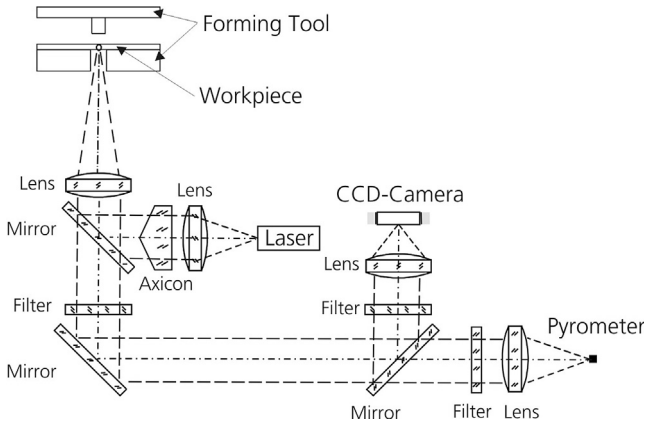

FIGURE 1

Example of an optical path.

Filtering is necessary to divide the radiation into the wavelengths that are important for the corresponding detectors: while the camera requires wavelengths in the visible range, the pyrometer detects a range just above 1 µm.

If a metal is used as the workpiece material, a circular shape of the laser focus leads to a nonuniform temperature distribution. Hot spots are generated in the middle of the area to be heated, whereas the border area remains cold due to the high thermal conductivity of metals. By using an axicon within the beam bath, this drawback can be substantially eliminated.

An axicon is a rotationally symmetric optical element, which consists of a cylindrical part and a cone, as shown in Figure 2. The axicon creates an annulus as the focus geometry. As a result, a more homogeneous temperature distribution can be achieved. Depending on the angle of the axicon and the focal lengths of the lenses used, the ring diameter can vary.

In addition to the optical system, the forming tool also has to be adapted, in such a way that the radiation can be guided onto the workpiece or the punch, depending on the workpiece material. For stamping operations, the radiation can be easily guided

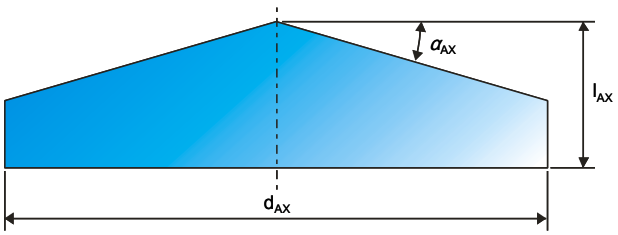

FIGURE 2

An axicon.

through the tool matrix. No additional elements are necessary, but it is important to remove the punched parts from the optical path at the end of the operation. Other forming processes require "tool windows." These can be made of sapphire or fused silica which are both, on the one hand, hard enough for the occurring process forces and, on the other hand, transparent for the laser radiation (as long as it is not in the infrared range). Through a breakout in the tool frame, the laser radiation is transmitted through the sapphire/glass onto the workpiece or the punch.

All devices—the laser and the press—are controlled by software, which controls the laser depending on the position of the punch relative to the tool and the required temperature, and switches it off after a defined distance or time has been reached.

In order to obtain short heating times and to maintain a constant temperature, a temperature controller can be used. The controller compares the signal of a thermal sensor with the demanded temperature and determines an according value for the laser system.

PROCESSES

STAMPING

Stamping is a well-established process, which enables the production of sheet metal or plastic parts in very short cycle times (up to 40 parts per second). In addition, the production of precise and complicated contours is possible. The process is characterized by a high material utilization [1].

The main components of a stamping tool usually consist of the punch and the female die (the matrix), sometimes with an additional pressure pad to build up compressive strength in the workpiece. The cutting forces are transferred from the surface of the punch and the female die to the sheet metal, which leads to an elastic deformation. With increasing force the deformation resistance is overcome and the elastic limit of the material is reached, whereupon the punch penetrates into the sheet metal [2]. This plastic deformation without separation leads to the rounded edges at the material surface [1]. Due to the plastic deformation in the cutting direction, the material yields in lesser loaded areas and leads to rollover. With increasing punch displacement, the rollover passes into a smooth shearing zone. Within zones of high material stressing, cracks appear. This leads to cleavage fracture and the creation of the fracture zone [2].

Figure 3 shows the three phases of the stamping process [3].

The process, the workpiece material, and the production accuracy of the tool are crucial for the quality of the stamped part. While a high shearing zone is intended, different defects occur on nearly every part. Figure 4 shows the different defects of the cut edge.

The height of the rollover depends on the cutting clearance and the yield-stress ratio. This ratio is defined as the quotient of the yield stress and the tensile strength.

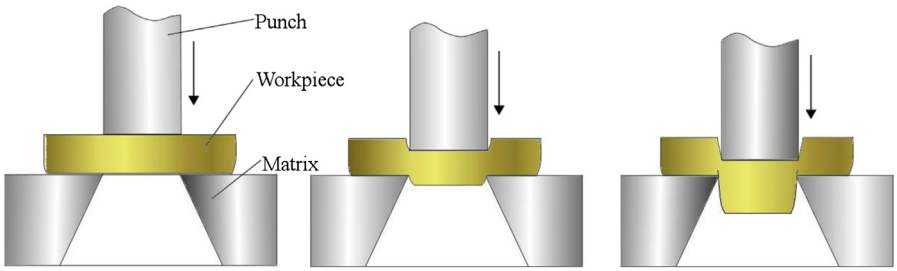

FIGURE 3

Process sequence.

The rollover increases with increasing cutting clearance and yield-stress ratio. Moreover, increase in cutting clearance also affects the fracture zone.

The height of the burr, an indication of the manufacturing quality, depends on the properties of the workpiece material. Whereas ductile materials, due to their formability, create a high burr and it is smaller on brittle materials [3]. Figure 5 shows the active tool parts for the stamping operation of gearwheels.

Depending on the temperature of the metal workpiece, the processes are divided into cold, warm, and hot forming. Cold forming takes place at ambient temperature. During the process, the mechanical properties of the workpiece materials change with the strength being most affected. The formability decreases, while the forming resistance increases, with a reduced cross section.

Within the hot-forming processes, the temperature of the workpiece is above the recrystallization temperature, which is estimated to be around 40–50% of the

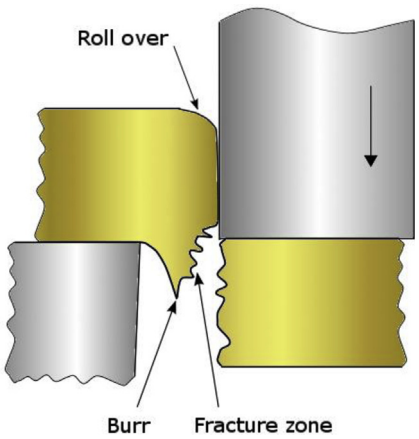

FIGURE 4

Defects of the cut edge.

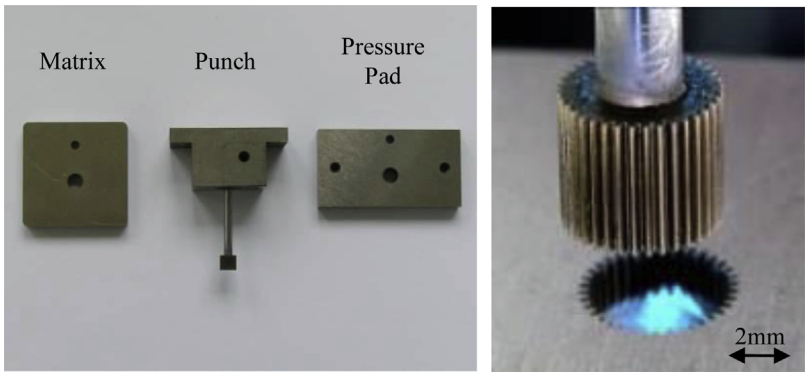

FIGURE 5

Active tool elements (manufactured by Fraunhofer IPK).

melting temperature [4] according to the Tamman rule. Hereby, the formability can be increased, whereas the required forming forces are lower.

The process of warm forming takes place at temperatures close to the recrystallization temperature but always below that point. In this region, even small increase in the temperature leads to a significant reduction of the yield strength within the material [5]. The mobility of defects in the crystal lattice and the amount of crystal regeneration will be increased at higher temperatures. This will cause a reduction of the defect density and thus a reduction of strain hardening. In comparison to recrystallization, the size and position of the crystallites will remain unchanged.

The influence of different forming temperatures on the material properties is shown in Figure 6. The yield stress and maximum strain are displayed for room and elevated temperatures. This points out that greater working temperatures ease plastic forming by reducing the yield stress. The reduction of the yield stress can be explained with the oscillation of atom crystals. The possibility to move is constricted at room temperature but increases at elevated temperatures until the melting point is reached [6].

Hot forming enables processes to be carried out that cannot be implemented at room temperature. Nevertheless, it is not an entirely satisfactory alternative to cold forming due to its disadvantages: e.g., bad surface quality, inaccuracy in size, and high tool loading because of the high temperatures. Since the whole tool is heated and not just the forming zone, the whole component is thermally loaded [7].

Warm forming uses the potentials of both the cold- and the hot-forming processes. These potentials are the constant strain hardening and good surface quality of cold forming and the low process forces and the high formability of hot forming [8]. High-alloyed steels are then plastically formable with constant quality and high accuracy in size.

As an example, the magnesium alloy AZ31 (MgAl3Zn; 3.5312) is chosen as the test material. The main alloying additions are aluminum and zinc. Due to their

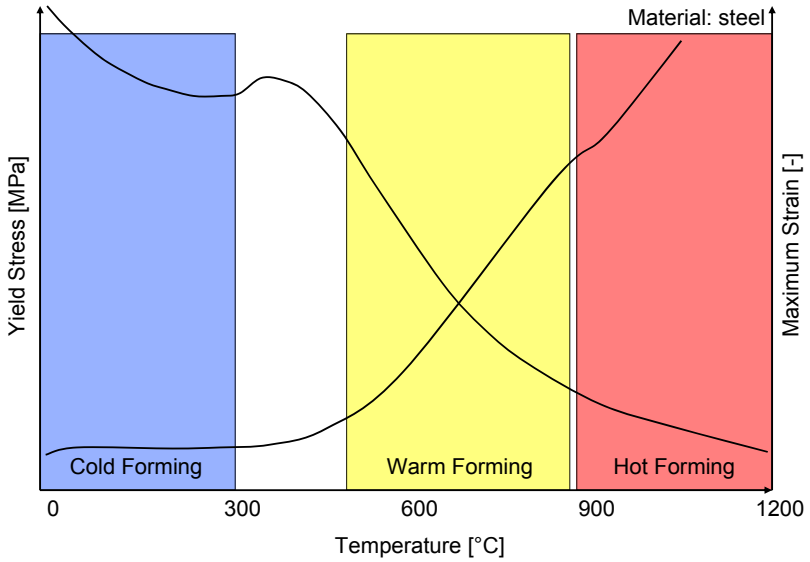

FIGURE 6

Forming temperature versus yield stress and maximum strain.

addition, the tensile strength and hardness are increased. However, the increased micro-porosity is disadvantageous [9] for forming operations.

Due to the hexagonal arrangement of the crystals of magnesium, the formability at room temperature is very low. Above 225 °C the formability increases through the activation of additional gliding planes [10,11]. Due to the hexagonal closed packed crystal structure, magnesium alloy sheets exhibit a low ductility and formability at room temperature, because only the basal plane can move [13].

The measured force–displacement curves confirm the influence of the elevated workpiece temperatures. The maximum punching force can be reduced by 30% (Figure 7).

Figure 8 shows two pictures made by a scanning electron microscope. The quality of both parts can be assessed concerning defects of form. The cold-formed part has significant defects. Many teeth are roughly removed, rather than smoothly sheared. The burr and the large fracture zones are indicators of bad quality. The warm-formed gearwheel has nearly no burr and fracture zones, but has a high shearing ratio.

EMBOSSING

Conventional technologies for the manufacturing of micro-structured components with geometries below 100 µm are injection molding and hot embossing. Both

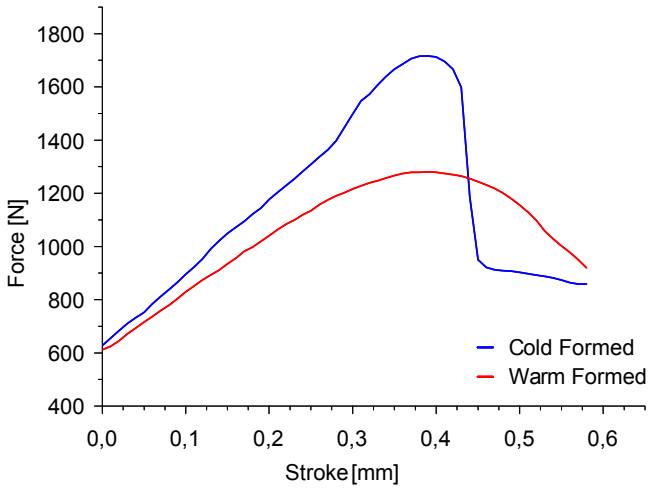

FIGURE 7

Force path.

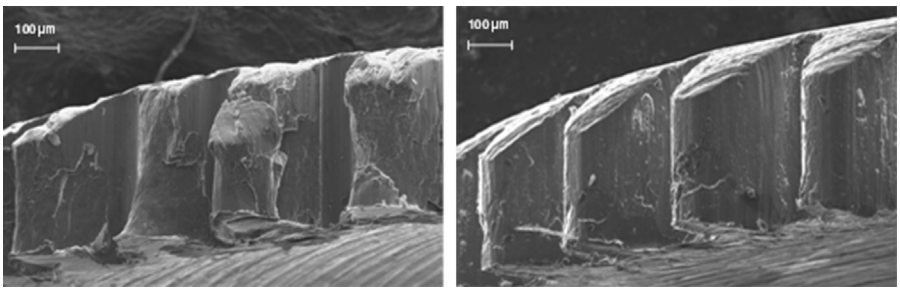

FIGURE 8

Gearwheels stamped without (left) and with (right) laser assistance.

technologies are mainly limited to polymer materials and require long cycle times due to different temperatures during forming and mold release. These drawbacks can be eliminated by laser-assisted hot embossing, where high-energy-density laser radiation is used for a selective and fast heating of the tool and the workpiece. Using controlled irradiation of the tool surface, a tool temperature of more than 500 °C can be achieved within seconds. At this temperature, even glass and metals can be structured with this technology. In comparison to other heating technologies such as induction heating, laser-assisted embossing enables the use of tool materials with low thermal and electrical conductivity such as ceramics.

In the use of transparent workpiece materials such as glass or polymers, the laser radiation heats the structured die, which, after achieving the required temperature, is

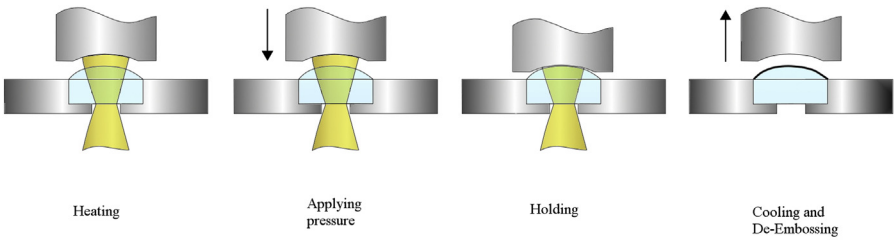

FIGURE 9

Process sequence in hot embossing.

then pressed onto the workpiece and heats it via heat conduction. In the case of non-transparent workpiece materials such as metals, the radiation is directly absorbed within the workpiece. The cold die then penetrates into the heated metal workpiece. With this technology, micro-structures from 200 nm to several tens of micrometers can be created at cycle times of below 1 min. The process sequence for transparent materials is shown in Figure 9.

The laser radiation is guided onto the structured surface of the punch. Transparent tool inserts, integrated into the lower tool part, enable the radiation to directly access through the tool onto the die.

The workpiece is heated to the forming temperature, which is between the glass transition temperature and the melting point. The tool then applies pressure on, and penetrates into, the workpiece. During the holding time, the material yields to the punch structure. The de-embossing phase is the most critical during the process: the structures are often destroyed in this phase due to tearing or overstretching. After the laser is switched off, the punch cools down again to below the heat transition temperature. Since only the structured face side is heated, the cooling phase is shorter in comparison to that for conventional technologies.

The advantages of laser-assisted hot embossing can be summarized as follows:

1. Tooling materials are independent of thermal or electrical conductivity;
2. Short heating times due to high energy density of laser radiation;
3. Short cooling times by heating the near-surface area only;
4. Accurate measurement of the embossing temperature;
5. Selective heating of single areas of the component.

Metals

As an example, the magnesium alloy AZ31 is used. A steplike structure with an edge length of 100 μm is pressed into the material both at room and elevated temperature. Figure 10 shows the top of the punch and the resulting metallographic cross sections of the embossed geometry.

Starting with a force of 5.9 kN, only the top of the geometry can be formed into the sheet metal. With increasing punch force, the penetration depth also increases. Even at 15.1 kN it is not possible to reproduce the hole structure in the sheet metal,

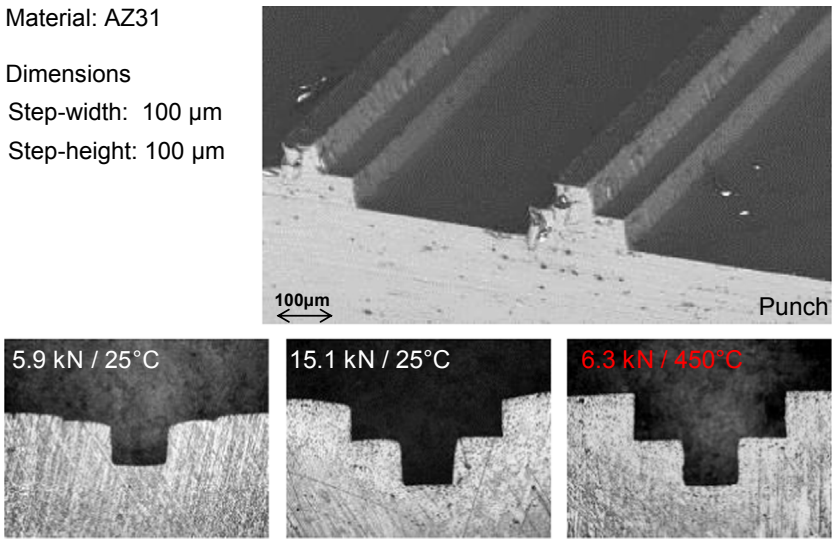

FIGURE 10

Hot embossing of magnesium (AZ31).

as shown in the middle picture. When the pressing force is increased further, the tool breaks. By heating the sheet metal with laser radiation, it is possible to reproduce the structure with just 6.3 kN of applied force. In addition, the rollover that occurred in the cold-formed part can be avoided. Thus, highly precise parts used for micro-fluidic applications, for example, can be produced.

Plastics

Amorphous thermoplastics are hard and brittle at room temperature. Above the softening or the glass transition temperature they transform into a plastic condition in which they can be formed.

The tooling requirements are low due to the low embossing temperatures of 150−250 °C. Different technologies can be used for tool manufacturing, such as lithography, whereby structure sizes in the nanometer range can be obtained with high flexibility regarding the geometry. Figure 11 shows two imprints into acrylic glass, both embossed with cycle times of below 1 min. The left-hand side picture has an overall size of 6 × 6 mm. It consists of pins with a structure size of around 15 µm. The picture on the right-hand side has a diameter of 7 mm. The structure size of 200 nm leads to the colored effects visible on the picture.

Glass

In comparison to plastics, the material glass has a higher optical quality, which is important for different applications such as camera lenses, sensors, or innovative lighting systems where aberration has to be avoided. The characteristic properties

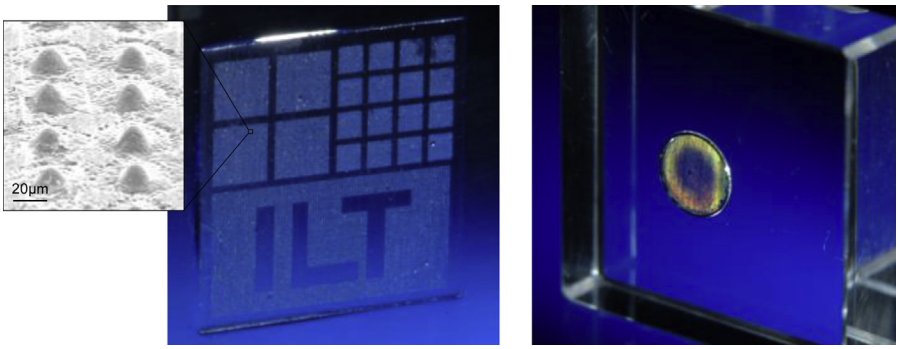

FIGURE 11

Hot embossing of acrylic glass.

of glass are, among others, high mechanical strength and environmental and temperature resistance, as well as joining ability. Due to its hardness and brittleness, this material is difficult to process. The mass manufacture of precise glass components is done by blank molding, but it is not possible to manufacture micro-optical functions such as diffractive optical elements on 3D-components with this technology.

Laser-assisted hot embossing is a suitable process for the cost-efficient processing of glass within short cycle times. Tool materials with high-temperature stability are necessary, which can be carbides, ceramics, or high-alloy high-speed steel—a subset of tool steels, which can withstand higher temperatures without losing its hardness.

The risk of glass breakage will be increased, if high temperature gradients occur on the glass surface. In order to reduce the thermal stress, therefore, a plane heat input is necessary to achieve an even heat distribution. As the glass material SK57 is used, which is characterized by a low melting point with a transition temperature of Tg = 493 °C. Starting at this temperature, imprints are possible with heating times of below 1 min.

Figure 12 shows embossed imprints made with this technology with structure sizes of between 30 and 80 µm.

BONDING OF PLASTIC WITH METAL AND CERAMIC—LIFTEC®

The ongoing trend regarding an increased level of integration in many technical products and the increased use of plastics as construction material is a challenge for many manufacturers regarding the connection of dissimilar materials, such as plastics with metals. The requirements for consumer products as well as for technical components are a flexible joining technique with short cycle times and a broad field of application.

Until now, the connection of these materials has been performed by gluing, screwed fastening, or the so-called mold-in technique. Hereby, the properties of

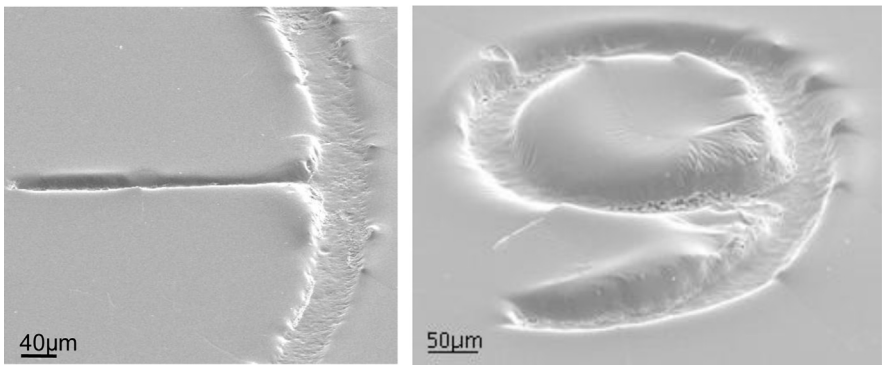

FIGURE 12

Hot embossing of glass (SK57).

the particular process define the area of application. Clamped or screwed joints enable a detachable connection while form-closed connections are able to transmit high power free of clearance. Gluing is applied for large areas. A complex preparation of the components is necessary for all mechanical connections. The most commonly used connection technique for plastics with metal is the mold-in technique during injection molding. The mechanical component is placed in an adapted tool prior to the injection molding process. An optimal process result requires tight tolerances of the tool and high precision components. The part handling is difficult. A subsequent joint of plastic with metal is not possible.

A process for a subsequent joint is the so-called postmolding technology, which is mainly used for thread inserts which are heated by induction and then pressed into the plastic component. However, the whole components may be heated, and ceramics cannot be processed. The positioning of the inductor is often difficult and the heat input not sufficient for small structure sizes.

Figure 13 displays a comparison of LIFTEC® with other joining techniques.

LIFTEC®—an acronym for "laser-induced fusion technology"—is a newly developed process. It is based on every thermoplastic being transparent or at least translucent in the unpigmented state. Based on this fact, a metal or ceramic component or a part of it is heated with laser radiation through the plastic part. The component is pressed onto the plastic part and heats this by heat conduction. After reaching sufficient plasticity the component penetrates into the plastic part. By choosing an appropriate geometry, a form-closed connection can be obtained. This can be, for example, a bump, a drilling, or a groove. The material displaced upward leads to unwanted bulging on the surface of the part. This can be eliminated or at least reduced by an additional cavity or by drilling within the part, where the plastic can yield.

An inevitable element of this technology is a component with a higher melting point in comparison to the plastic join partner. Possible materials are mainly metals and ceramics, but can also be a temperature-resistant plastic such as Teflon or even wood.

Process + good o average - bad	Properties					
	Strength	Backlash	Tolerance requirement	Additional joining part	Reversibility	Tightness
Screwed Joint	+	+	+	-	+	-
Press Fit	o	+	-	+	o	o
Gluing	o	o	o	+	-	+
Multi-Component-Injection-Moulding	+	+	-	+	-	o
Snap Connection	o	o	o	+	+	-
Riveting	o/+	+	+	-	o/-	-
In-Mould-Connection	+	+	-	+	-	o
LIFTEC®	+	+	+	+	-	o

FIGURE 13

Comparison of different joining techniques.

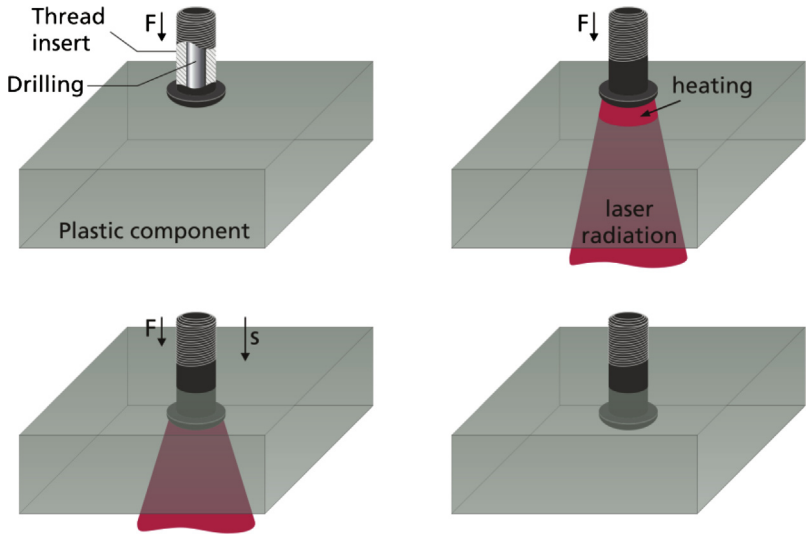

FIGURE 14

Process sequence.

Advantages of the technique are as follows:

1. Short cycle times
2. High mechanical strength
3. Nonloosening connection, free from backlash
4. Low requirements regarding tolerances and positioning accuracy
5. No pre- or postprocessing necessary
6. Postprocess assembly
7. Synergy effects by material combination

Figure 14 shows the sequence of this process:

1. Positioning and applying pressure;
2. Heating the metal part through the plastic component with laser radiation;
3. Penetration into the plastic component after exceeding the glass transition temperature;
4. Cooling down and the creation of positive locking.

When plastics are used that are not transparent for the laser radiation, the process can be adapted in the way that the radiation does not transmit through the plastic part, but is guided laterally to the component, as shown in Figure 15:

Heating with laser radiation is, in comparison to heating concepts already in use, quasi-independent of the heat conductivity and the electrical conductivity of the material used. This means that, in addition to metal, ceramic materials can also be joined with plastics. The combination of the properties of these hybrid components

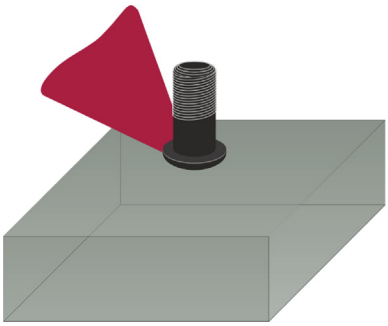

FIGURE 15

Alternative irradiation strategy for nontransparent plastics.

offers high mechanical strength, resistance to wear, high-temperature stability with, at the same time, reduced weight, and variable shape forming.

Due to the high energy density of laser radiation, quick heating is possible. If necessary, selected regions alone can be heated to limit the total amount of absorbed energy. The temperature of the part can be measured by a pyrometer to control the accurate joining temperature, dependent on the materials and geometries used. Thus, a stress-minimized insertion of the components is possible and damaging overheating does not occur.

The high laser intensities lead to a phase change in the irradiated region. In terms of heating and micro-structure formation, the process is almost the same for welding but with slight differences. Laser forming and embossing requires a shallow depth of phase change at the surface while laser welding requires deep penetration into the substrate material. The irradiated surface undergoes soled heating and melding followed by solidification in the forming process [12].

Transparent plates made of sapphire or fused quartz integrated into the tool enable the irradiation within the closed tool directly onto the surface of the metal even during the forming operation.

An essential process parameter is the joining temperature. When too high temperatures are applied, bubbling and discoloration occur. If the temperature is too low, cracks open due to high induced stress.

To reduce the cycle time, a peripheral software control for regulation of the power output is used, which allows reducing the heating time by a time-dependent power modulation.

A high power output is applied to reach the intended temperature, then the power is reduced to keep the temperature constant. An example of a temperature–time curve is shown in Figure 16.

In the present case, there is a heating period of 4 s at 25 Watts to achieve a temperature of 135 °C. Afterward, the laser power is reduced to 16.5 Watts.

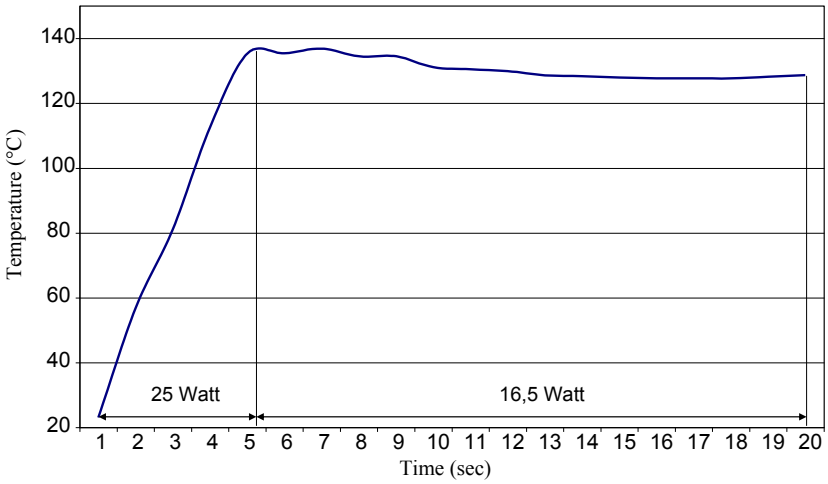

FIGURE 16

Reduction of heating time by modulation of laser power.

Plastic components can easily be formed, which thereby enables many design possibilities. Low density and chemical resistance are additional reasons for the increased application of this material. On the other hand, the high strength is a characteristic and important advantage of metals and ceramics. The combination of the materials results in the combination of their positive properties.

Principle fields of applications are anywhere, where this combination of properties is reasonable. For example, these are listed as follows:

1. Joining of rimless plastic eyeglasses with the arm. Beside higher strength of the bond and the security against loosening, new designs are possible. No pre- or postprocessing such as predrilling for screwed connections is necessary.
2. Joining of plastic windows with metal frames with high leak tightness.
3. Metallic pins at heavily and often loaded hinges in plastic components, e.g., cell phones. Beside having improved durability, the joint also ensures higher product quality.
4. Mounting of plastic components on metal components.
5. Plastic components with metallic inserts. The mechanical load can be absorbed by the mechanical part to reinforce the compound.

The main considerations of the process are as follows:

1. Accessibility of the laser radiation to the component to be heated
2. Different temperature stability of both components
3. Maximum size of the components
4. Geometry with positive locking

The following table shows some exemplified bonds:

Metallic thread insert
- Material: Steel, PMMA
- Thickness of plastic plate: 10 mm
- Screw diameter: M4
- Form closure by a bump

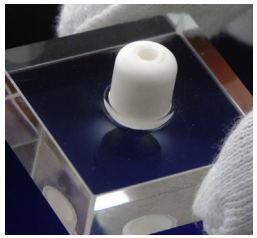

Plastic–ceramic bond
- Material: ZrO_2; PMMA
- Thickness of plastic plate: 10 mm
- Diameter of cylinder: 8 mm
- Form closure by surface roughness
- Additional drilling to avoid throw-offs

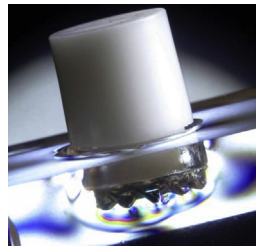

Plastic–plastic bond
- Material: Teflon, PMMA
- Thickness of plastic plate: 10 mm
- Diameter of cylinder: 10 mm
- Form closure by a groove

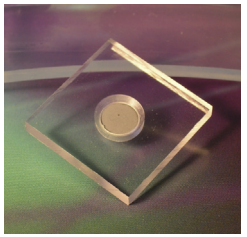

Plastic–Silicon bond
- material: Silicon; PMMA/PC
- Thickness of plastic plate: 3 mm
- Diameter of silicon plate: 7 mm
- Thickness of silicon plate: 0.3 mm

CONCLUSIONS

Warm forming with laser radiation is a promising technique to enable new processes or enlarge the processing limits of conventional processes. In comparison to other production technologies like lithography, no additional operations are necessary. Elevated temperatures of the workpiece material lead to a reduction of the yield stress and an increase of the forming ability. Laser radiation can be utilized as a selective heat source for fast and accurate heating of the workpiece. The demand toward reproducible and high-quality process results requires the accurate measurement of occurring temperatures during the forming operation, which can be achieved by the employment of a pyrometer. The system technology, the process basics as well as exemplified applications have been shown for the processes stamping, hot embossing, and LIFTEC.

REFERENCES

[1] Hellwig W. Spanlose Fertigung: Stanzen. Braunschweig (Wiesbaden): Friedl, Vieweg & Sohn Verlagsgesellschaft mbH; 2001.
[2] Pöllmann A. Prozessparameter beim Scherschneiden von Karosserieblechteilen. Berlin: Druckhaus Berlin-Mitte GmbH; 1997.
[3] König W, Klocke F. Blechbearbeitung, Fertigungsverfahren, Band 5. Düsseldorf: VDI Verlag; 1995.
[4] Schmann H, Oettel H. Metallographie. Weinheim: Wiley-VCH Verlag GmbH; 2005.
[5] Sieber K. Werkstoffe, Fertigungsverfahren und Maschinen der Massivumformung. Hamburg: VDI-Verlag GmbH; 1969.
[6] Lüpfert H. Metallische Werkstoffe. Leipzig: Akademische Verlagsgesellschaft Geest & Portig K.-G; 1958.
[7] Vollersten F, Schilf M, Seefeld T. Verbesserung der Umformbarkeit von Aluminiumlegierungen. In: UTF Sience 4; 2006. p. 1−5.
[8] Egerer E, Neudecker T, Engel U. Grundlagenuntersuchungen zum Halbwarmmikroumformen. Tagungsband zum DFG-Kolloqium SPP 2001;1074.
[9] Kleiner S. Magnesium und seine Legierungen. Feinstbearbeitung technischer Oberflächen − 6. Internationale IWF-Kolloqium; 2002.
[10] Doege E, Janssen St, Wieser J. Kennwerte für die Magnesiumumformung am Beispiel von AZ31. 2001.
[11] Yong MS, Hu BH, Enggalhardjo M, Choy CM. Development of warm forming technique to produce thin wall magnesium components, Initiatives of Precision Engineering at the Beginning of a Millennium. 2002. p. 334−8.
[12] Yilbas BS, Sohail A, Shuja SZ. Laser forming and welding processes. Mater Form Mach Tribol 2013:47−51.
[13] Park J, Jeounghan K, Nhokwang P, Youngsuk K. Study of forming limit for rotational incremental sheet forming of magnesium alloy sheet. Metall Mater Trans A 2010;41(1): 97−105.

CHAPTER

Deep X-ray Lithography 16

P. Meyer, J. Schulz
Institute of Microstructure Technology, Karlsruhe Institute of Technology, Eggenstein-Leopoldshafen, Germany

CHAPTER OUTLINE

INTRODUCTION

Several micro-fabrication technologies are available at the present time and are used to fabricate micro-components and systems. The most successful micro-machining technologies have been developed as extensions of standard IC and micro-electronics planar silicon-based processing. Others are based on advanced precision engineering and laser structuring. However, individual technologies including Si

Micromanufacturing Engineering and Technology. http://dx.doi.org/10.1016/B978-0-323-31149-6.00016-5

micro-machining or laser structuring are far from being sufficient to fulfill the needs of the variety of problems posed by:

- the great variety of functions of most of the devices to be made,
- the specificity of surroundings in which they will operate,
- the optimum cost/performance ratio for the targeted application.

Interest in a number of non-Si-based machining methods stems from major deficiencies of IC-based machining techniques:

- the need for using application-specific materials to optimize the functions and performance of various devices,
- the need to reduce cost by choosing low-cost materials,
- the difficulty in constructing truly 3D objects with planar-based processing, which continues to be a challenge.

Precision and ultraprecision mechanical, electro discharge, LIGA-based, and laser-based, micro-machining techniques, to mention the most current, are such alternative techniques, each with their specific application domains and relative merits. LIGA-based processing, a sequence of micro-fabrication steps combining a step of deep X-ray lithography (DXRL), also called by some authors deep etch X-ray lithography, and subsequent additive processing of plating-through-mask and molding, has moved from an emerging micro-fabrication technology to become a well-established nonsilicon alternative micro-fabrication technology for micro-electromechanical systems (MEMS). The LIGA technology provides unique advantages over other manufacturing methods in the fabrication of microstructures. LIGA-based technologies are used and are being further developed in a number of R & D institutes around the world. Spin-off companies and commercial companies have also evolved around large-scale synchrotron facilities.

The LIGA technology has been developed over the rather long time span of two decades [1–6]. During this time, other high aspect ratio technologies such as UV photolithography in thick resist such as SU-8, often referred to as UV–LIGA, and deep reactive ion etching of silicon have evolved also and challenge LIGA successfully in some specific application areas. For planning the role of LIGA in future manufacturing, a review of potential applications may serve as a useful basis. The basic LIGA process and some aspects of the process are recalled here to illustrate its strengths and discuss its challenges.

LIGA PROCESS AND STRENGTHS

BASIC PROCESS

The basic LIGA process is described in Figure 1. In the first step of the LIGA process, an X-ray sensitive polymer (resist) layer of up to several millimeters thickness is coated onto a conductive or nonconductive substrate. Typically, polymethylmethacrylate (PMMA) is used as positive resist and an epoxy-based resist like SU-8

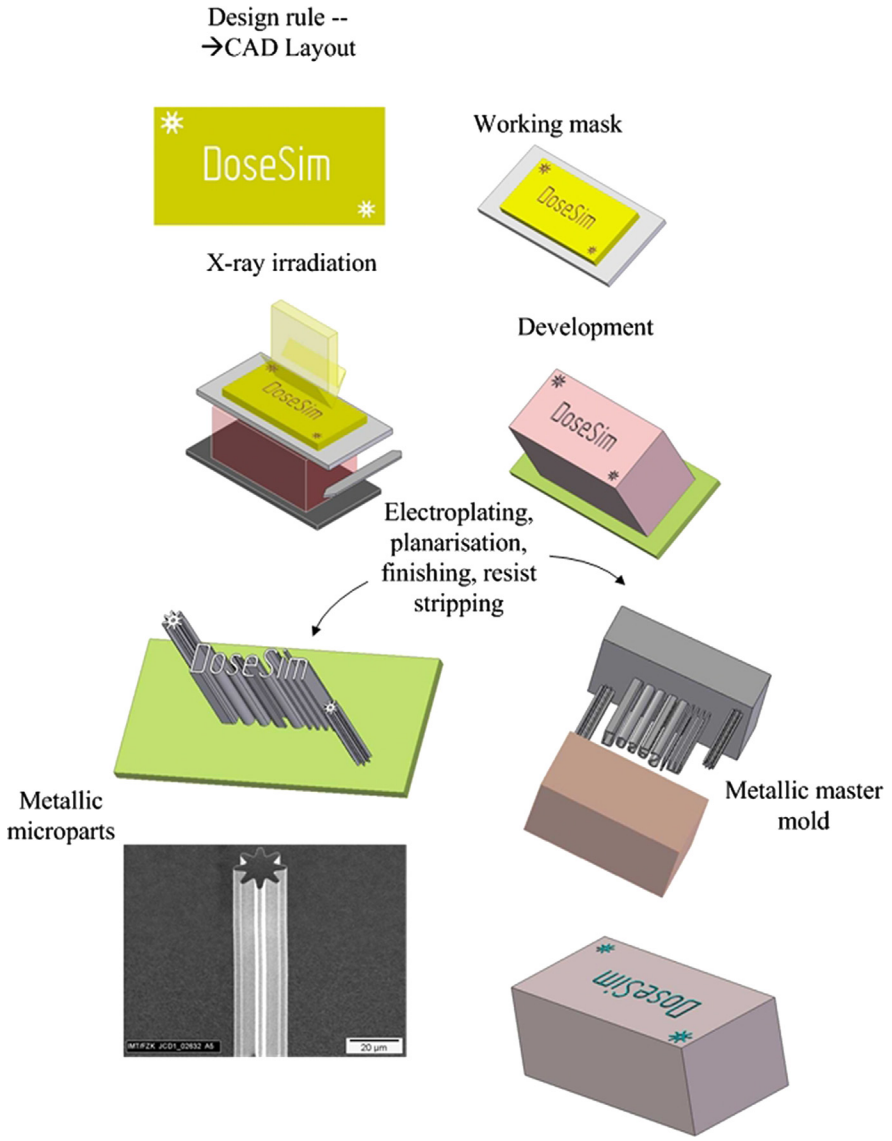

FIGURE 1

Illustration of the basic LIGA process steps.

[7–10] as negative resist. A pattern from a mask is therefore transferred into the thick resist layer via a 1:1 shadow proximity printing scheme using hard X-rays from a synchrotron radiation source. After exposure, selective dissolution of the chemically modified irradiated parts of the positive resist (or dissolution of the nonirradiated parts of the negative resist) in a chemical developer results in a polymeric relief replica of the mask pattern.

Then, depending on the material, number of parts selected for the final product, accuracy, quality, and price, different fabrication routes can be chosen, which may include further steps of micro-replication through electroforming and/or a variety of molding techniques (injection molding, embossing, casting, compression molding, etc.). The polymeric microstructure can be used as follows:

- simply as it is,
- as a lost mold for the formation of ceramic micro-parts,
- as an electroplating template to generate metallic micro-parts,
- as an electroplating template to produce a metallic master mold, which can then be used many times to mold cost-effective replicates in other materials, primarily polymers. When producing large numbers of electroplated components, the molded polymer parts are used as lost molds for a second plating process.

The unique processing feature that enables the manufacture of thick microstructures characterized by very steep walls and very tight tolerances is the creation of highly precise resist templates by DXRL using X-ray photons from a synchrotron radiation source.

LIGA MANUFACTURING STEPS

Resist technology

The resist technology consists of applying a resist onto a substrate. The substrates which can be used depend on the product to be made (for example, a mold insert), but they should meet the following criteria:

- a high planarity,
- the substrate and resist should have good adhesion,
- the substrate surface should be conductive if an electroplating step is needed,
- the resist developer should not etch the substrate.

Concerning the resist, a distinction should be made between positive and negative resist. In the first case, the radiation will damage the polymer by reducing its molecular weight; the most commonly used is PMMA; the exposed parts becoming soluble in a developer. In the case of a negative resist, the radiation typically generates an acid that acts as a catalyst for cross-linking usually activated by a post exposure bake; the irradiated volume being insoluble in a developer; the most commonly used are different epoxy-based negative resist formulations (one example is the resin SU-8). In the first case, it is necessary to know the dose to apply to the resist so that it becomes soluble in the developer; the developer must have negligible influence on the nonirradiated parts; while in the second case, it is necessary to know the dose to apply to the resist so that the exposed part becomes insoluble in the developer. Since a few years (2010), the epoxy-based negative resin has become the resist of choice for many applications. Its sensitivity compared to PMMA may be two orders of magnitude higher, and now its performance is reliable and reproducible except for very thick resists in excess of roughly 800 μm. Furthermore, the epoxy-based

negative resist removal is not a problem anymore. Basic idea is to use a very high density downstream of chemical radicals for etching attack to the resist but to separate the plasma from the place of the reaction with the cross-linked polymer [11,12]. This way, the etcher operates in a remote mode and bombardment with ions accelerated by electromagnetic fields is avoided at all.

Resist deposition

The epoxy-based negative resin is very often spin coated. Experimental results indicate that the coating qualities of SU-8 are affected by several factors, including the spinning speed, the photoresist viscosity, the initial acceleration, and the duration. After the resist has been applied to the substrate, it must be soft baked to eliminate the solvent. Since this is a diffusion process, the bake times increase at least quadratically with resist thickness. Lamination of dry epoxy-based films has been under investigation at Centre for Advanced Macromolecular Design (CAMD) [13].

Concerning PMMA, three possibilities depending on the thickness to be deposited exist:

- Gluing: gluing a commercially available PMMA sheet with a glue consisting of PMMA dissolved in methylmethacrylate (MMA). Prior to gluing, the PMMA sheet is cut and milled to the desired dimensions. The stress so induced is removed by annealing under controlled ramping conditions (the max temperature is slightly above the glass transition temperature of the PMMA used). The positioning of the sheet and the dispersing of the glue can be made using a robotic dispenser combined with a pick and place machine. This method is generally used for PMMA thicknesses greater than 100 μm.
- Casting. A resin consisting of PMMA dissolved in MMA is mixed with dibenzoylperoxide and dimethylaniline, and is applied to the substrate and hardened under a pressure of 4 bar at room temperature for 4 h; the dispensing can be effected using a robot dispenser. Subsequently, the resist-coated substrate is annealed under ramping conditions. This method is generally used for PMMA thicknesses of less than 100 μm.
- Spin coating: PMMA dissolved in a solvent (for example, anisole) could be spin coated onto a substrate, which will be baked after to evaporate the solvent and densify the film.

Irradiation technology

The LIGA technology needs a synchrotron beam line to perform the resist exposition, a scanner to move the sample, and a computer program to calculate the exposure dose, which defines the deposited dose in the resist.

Synchrotron source—scanner

At the heart of a synchrotron (see Figures 2 and 3) is a storage ring: a huge doughnut-shaped vacuum chamber. Electrons are accelerated and confined to travel around the storage ring at nearly the speed of light [14–16]. Because the electrons are constantly changing the direction they are accelerating, and the accelerating

FIGURE 2

Schematic view of a synchrotron.

Soleil.

FIGURE 3

View of the synchrotron ANKA.

electrons lose energy in the form of synchrotron light. Synchrotron produces X-rays, infrared, and ultraviolet light of exceptional quality and brightness: a million times more intense than that of a hospital X-ray machine! A charged particle constrained to move in a curved path experiences centripetal acceleration. Due to this acceleration, the particle radiates energy according to the Maxwell equations. A nonrelativistic particle emits radiation primarily at its frequency of revolution. However, as the speed of the particle approaches the speed of light, the radiation pattern is distorted by relativistic effects and changes to a narrow cone of radiation with angular spread. The total energy E for a particle of mass at rest m_0 moving at velocity v is:

$$E = \gamma \cdot m_0 \cdot c^2 \tag{1}$$

with

$$\gamma = 1 \Big/ \sqrt{\left(1 - \frac{v^2}{c^2}\right)} \tag{2}$$

The opening angle $\Delta\varphi$ of the radiation cone can be expressed, for high values of γ, as:

$$\Delta\varphi \cong \gamma^{-1} \tag{3}$$

Synchrotron radiation sources produce photons with a continuum of energies, from the infrared to the X-ray region. The spectral range of photons produced by electrons (energy $E_e(GeV)$) in a bending magnet (radius of curvature: R_b, magnet field: $B(T)$) can be characterized with the critical energy E_c, where

$$E_c = \frac{3 \cdot c \cdot \gamma^3}{2 \cdot R_b} \tag{4}$$

In practical units, the critical photon energy is also given by:

$$E_c = 0.6650 \cdot E_e(GeV) \cdot B(T) \tag{5}$$

E_c is defined in terms of the spectral power radiated by a relativistic particle: half of the power spectra is radiated at energies below E_c and the other half at energies above it. Wiggler (series of magnets designed to periodically horizontally deflect the charged particle) and undulator (series of magnets designed to periodically vertically deflect the charged particle) are also used to produce synchrotron radiation, the differences of which are indicated in Figure 4.

Presented in Table 1 is a nonexhaustive list of synchrotrons which possess a LIGA beam line.

For example, the synchrotron ANKA in Karlsruhe (Germany) is a second-generation medium-energy source, with an electron beam energy of 2.5 GeV. The X-rays are sent into the various beam lines (the straight lines branching out of the synchrotron). A typical LIGA beam line is presented in Figure 5. All of the beam lines are equipped with a scanner (see Figure 6) and optical elements, which modify the spectrum of the source. In fact, the synchrotron spectrum should be adapted to the needs of the user. The synchrotron ANKA has three LIGA beam lines (LIGA1, LIGA2, and LIGA3) sited on a bending magnet (1.5 T) with different optics. The characteristics of the beam lines are given in Table 2. The spectra of the lines after the front-end window and optics are given in Figure 7. The X-rays produced are highly parallel and to conserve this property for the lithography aspect, the diffraction (fresnel) effect should be as low as possible and also the absorption of the photons should take place only in the designed volume. In X-ray lithography, typically X-rays in the 0.5 to 5×10^{-10} m region are used, which interact with matter by the photoelectric effect, the Compton effect, and Rayleigh scattering. The total effect depends on the cross section of the different possibilities of interaction. The primary dose, which is about 95% of the deposited dose, is due

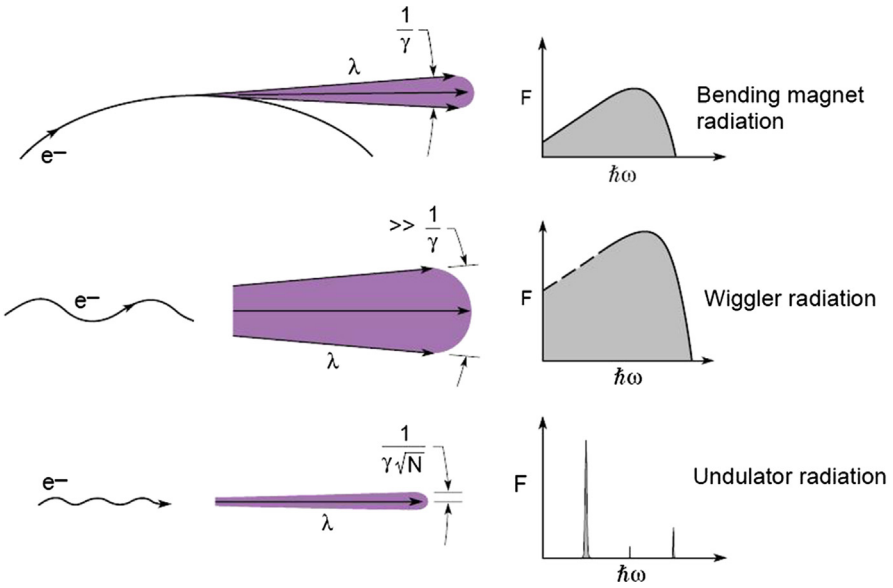

FIGURE 4

The different sources of synchrotron radiation with some of their characteristics.

Table 1 Synchrotron Location and Operating Energy (This is a Nonexhaustive List)

Name	CLS	ANKA	ELETTRA	CAMD	INDUS II
Country/ City	Canada Saskatoon	Germany/ Karlsruhe	Italy/Trieste	USA/Baton Rouge	India/ Indore, Madhya Pradesh
Operating energy (GeV)	2.9	2.5	2.0 or 2.4	1.3	2.5
Number of LIGA beam lines	2	3	1		1

CLS, http://www.lightsource.ca/beamlines/sylmand.php; ANKA, http://www.anka.kit.edu/1354.php; ELETTRA, http://www.elettra.eu/elettra-beamlines/dxrl.html; INDUS, http://www.rrcat.gov.in/technology/accel/srul/beamlines/lith.html; CAMD, http://www.camd.lsu.edu/beamlines.htm.

to the photoelectric effect in PMMA. Incident photon energy will be dissipated ultimately by secondary electrons generated by impact ionization; the distance over which the energy is spread should be as small as possible. The resolution limit of X-ray lithography is a function of diffraction in the mask-to-sample gap, and the effective range of the photo and auger electrons related when an X-ray is absorbed. In Figure 8, it is shown how the spectrum (source synchrotron ANKA; beam line

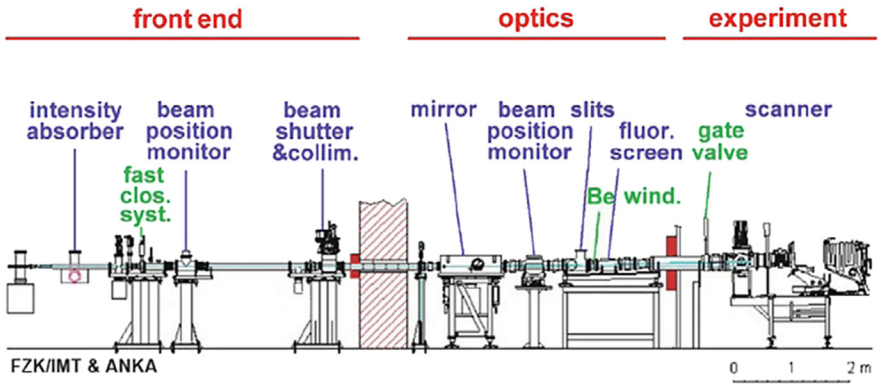

FIGURE 5

Schematic diagram of an X-ray lithography beam line (ANKA-LIGA2); side and top view.

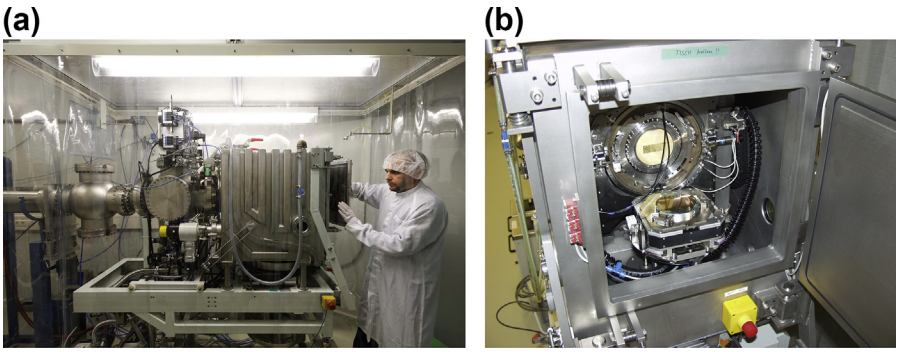

FIGURE 6

(a) Side view of the Jenoptik scanner—beam line: ANKA-LIGA3; (b) Front (scanner open) view of the Jenoptik scanner.

Table 2 Some Characteristics of the Three LIGA Beam Lines of the Synchrotron ANKA

Beam line	LIGA1	LIGA2	LIGA3
Window	175 μm beryllium	225 μm beryllium	225 μm beryllium
Optics	Single Cr mirror	Single Ni mirror	No optics
Dedicated to	X-ray lithography	Deep X-ray lithography	Ultra deep X-ray lithography
Structure height	Up to 100 μm	100–600 μm	600–2500 μm

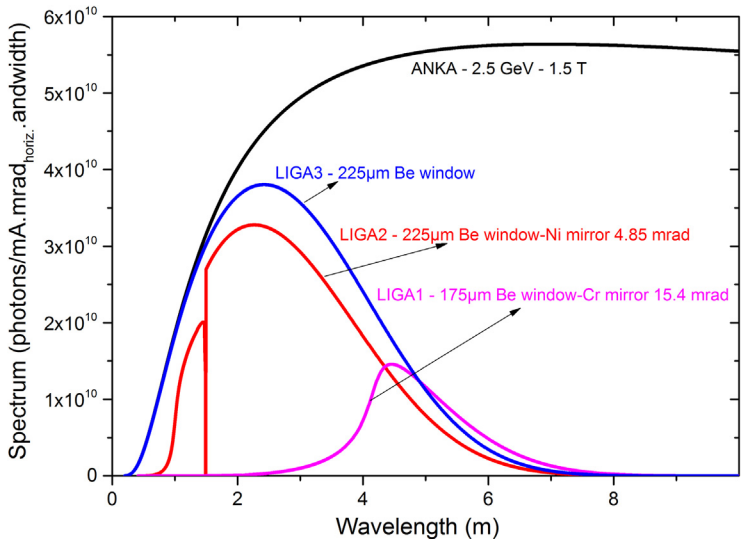

FIGURE 7

Spectrum of the three LIGA beam lines at ANKA Germany.

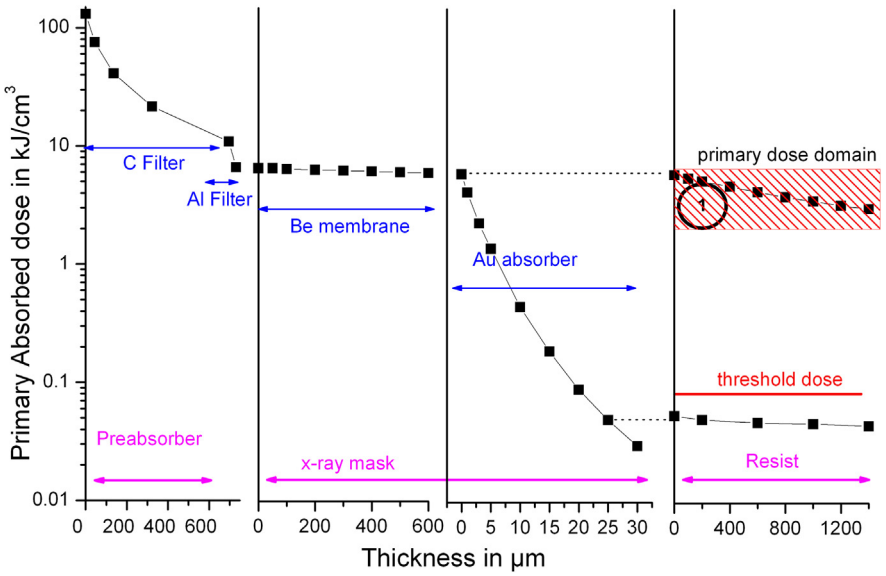

FIGURE 8

Primary absorbed dose along the X-ray trajectory, including a 1400-µm thick PMMA foil X-ray mask with a 550-µm beryllium membrane and carbon and aluminum filters.

ANKA; the beam line is LIGA3.

LIGA3) is attenuated during the exposure of a 1400-μm PMMA sample. The carbon and aluminum filters absorbed the low energy radiation to prevent overexposure of the top surface; the primary dose to be deposited in the resist should be situated in the region $D_{bottom}-D_{top}$. This region has been determined by many tests and is the best compromise between exposure and development time. The mask membrane (beryllium) is quasi-transparent, as is required. The absorber thickness should reach a minimum, which is defined by the threshold dose at which the resist starts to dissolve.

Epoxy-based resin

The resin is an epoxy made up of a bisphenol A novolac glycidyl ether [17]. As example, for the resist named SU-8, on average, there are eight epoxy groups in a typical molecule. This is a typical molecule because, in reality, molecules exist in a number of different sizes and shapes. The organic solvent used is gamma-butyrolacton, which varies in concentration depending on desired viscosity. Triarylsulfonium salt is the chemical that comprises the photoacid generator (PAG). The PAG releases acid after it absorbs a photon [18]. Thus, only regions that have been exposed with a light source have an acid present. A heating process is then required to give the reaction, the energy necessary for cross-linking to occur (post exposure bake). The combination of heating and the presence of acid allow the resist to cross-link. The noncross-linked resist will be dissolved in a solution of propylene glycol monomethyl ether acetate followed by a rinse in isopropyl alcohol.

The lithographic performance of the epoxy-based resin strongly depends on its response to irradiation, which can be examined by means of the so-called "contrast curve" [19,20]. The contrast curve describes the remaining resist fraction of a uniformly illuminated resist versus the logarithm of the applied exposure dose. The contrast γ is defined by the expression:

$$\gamma = \left(\log_{10}\left(\frac{D_2}{D_1}\right)\right)^{-1} \tag{6}$$

The value D_1 defines the dose for which the remaining resist fraction is 10% of the original value. The value D_2 defines the dose for which the remaining resist fraction is 90% of the original value. The sensitivity of the irradiated resist is defined as the point at which all of the film is retained. A higher contrast resist will usually yield more vertical sidewall profiles and is more tolerant to secondary radiation (fluorescence, photoelectrons) in the nonexposed areas.

PMMA degradation

During X-ray irradiation of PMMA, synchrotron light is absorbed in the exposed PMMA area, which results in a chemical modification; a scission of the polymer chain leads to a radiation-induced degradation of the molecular weight and becomes soluble in an organic developer. By increasing the dose of radiation, the average molecular weight decreases from an initial value $M_{W(Dose=0)}$ (about 1.5×10^6 g/mol) to a minimum limiting value of between 2500 and 3000 g/mol at very high dose

of radiation. The degradation mechanism of radiation-excited PMMA depends on the chemical structure of the resist and the exposure energy. The radiochemistry of PMMA is a complex mixture of consecutive reactions including excitations, fissions, cross-linking, recombinations, disproportions, rearrangements, and transfer reactions. The most important step of degradation is the scission of the methyl ester group, which is responsible for the major amount of the gases evolved. The remaining polymer chain stabilizes after hydrogen abstraction by formation of a double bond or chain scission. Radiochemical degradation of PMMA is categorized into two schemes:

- About 80% of the main-chain scissions have been observed after preceding side-chain degradation. The radiation-excited polymer molecule splits off an ester side chain. The remaining chain radical stabilizes after hydrogen abstraction by the formation of a double bond, or reacts by way of a main-chain scission. In the case of stabilization by hydrogen abstraction, the molecule has one ester side chain less than before irradiation.
- The remaining 20% of the main-chain scissions are due to a direct decomposition of the polymer into two macromolecules. Recombination of these fragments results in the primary polymer molecule.

PMMA development

The dissolution rate is a function of molecular weight, which is related to the initial PMMA molecular weight, the dose, and the main-chain scission yield [21–29]. This reduction of the average molecular weight causes the solubility of the resist in the developer to increase dramatically. A developer suitable for PMMA in X-ray lithography, commonly referred to as the GG developer, is composed of 15 vol% deionized water, 60 vol% 2-(2-butoxyethoxy)ethanol, 20 vol% tetrahydro-1-4-oxazine, and 5 vol% 2-aminoethanol. For X-ray lithography process simulation to calculate high aspect ratio microstructure and realistic MEMS devices of the size order of millimeter, a macroscopic resist dissolution and an easily measurable approach is required, rather than to describe the very complicated problem of microscopic resist dissolution. In chemistry, many models concerning polymer dissolution may be found. Due to the fact that a dose profile is deposited during X-ray lithography and the GG developer consists of four components, these models cannot be applied easily. The dissolution rate is described by the following equation (all other parameters being constant):

$$R(D) = R_0 + C \cdot \left(M_{W(Dose=D)} \right)^{-\beta} \tag{7}$$

R_0 corresponds to the development rate of an infinite molecular weight $M_{W(Dose=0)}$ (R_0 is negligible in the case of the PMMA-GG system), and C and β are characteristic constants of the polymer and solvent.

In reality, the relationship between the dissolution rate and the dose is influenced by a large number of parameters related to chemical reaction at the liquid (GG developer)—solid (PMMA) interface, e.g., the PMMA molecule weight, the developer temperature, and the development apparatus.

Special computer programs for X-ray lithography

Different computer programs have been developed, which meets the necessary requirements of a LIGA X-ray beam line [30–34]. The code currently permits the computation of synchrotron radiation from bending magnets, the effects of the optical properties of materials, and the necessary parameters for the resist exposure. The basic calculations needed for synchrotron beam line design are related to the spectral characteristics and to the modeling of the optical elements (mirrors, filters, beam stop). For example, the following calculations are performed: the dose rate, the dose profile from the top to the bottom of the resist, the exposure dose (the parameter that should be given to the scanner, which moves the sample), and the time needed to develop an irradiated resist sample. In Table 3 are listed computer programs especially dedicated to DXRL.

Micro-electroplating technology

Electroplating is the key step in the fabrication of metallic micro-components and tools such as masks and molding tools. Established routine processes are often referred to by simply giving the name of the plating solution. However, every user performs the base process with differences in electrolyte formulation and operation due to specific fabrication environments such as the plating apparatus or specific material properties. Nevertheless, some general aspects in micro-electroplating will be pointed out next. From the standpoint of a lithographic pattern, an ideal plating solution has the following properties:

- the resist structures are not changed (no swelling, no thermal-loading introduced),
- the mechanical stress remains very low (a few tens of MPa),

Table 3 Deep X-Ray Software Packages Available

Program	Platform	Status	Possibility
LEX-D[a]	Dos	Commercial	Source: bending magnet Optics: mirror, double mirror, beam stop Dose: primary and secondary Development: 4 dimensions
DoseSim[b]	Windows	Freeware	Source: bending magnet Optics: mirror, double mirror, beam stop Dose: primary and secondary—influence of the layer Development: 1 dimension
X3D[c]	LINUX	Freeware	Source: bending magnet Optics: none Dose: primary Development: 4 dimensions

[a] http://www.sandia.gov.
[b] http://www.kit.edu/imt.
[c] tabata@se.ritsumei.ac.jp.

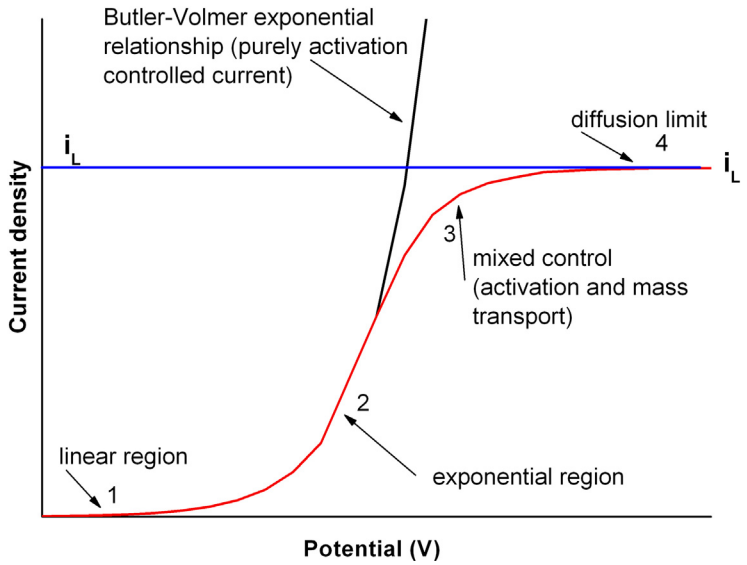

FIGURE 9

General current density–potential relationship [24].

- the grain structure does not change with height,
- small and large areas grow at the same rate.

Some limiting aspects arise from the desire to plate fairly thick layers in excess of 10 μm. This is usually referred to as electroforming and many commercial solutions can already be excluded. The complexity of LIGA-electroplating can best be described using a sketch of the current density versus voltage relationship (Figure 9) [35].

At the onset of the net current density (1 and 2), the rate is limited by the kinetics at the surface. The growth rate depends exponentially on the voltage, so this is not a robust working point. Furthermore, this corresponds to very low growth rates and unacceptably long plating times. In region 4, the current density is limited by diffusion of some species of which the concentration at the cathode becomes zero. To keep the diffusion zone small, both strong convection and high ion concentrations in the electrolyte are usually employed. Both aspects will raise the diffusion-limited current density.

From the electroplating point of view, the lithographic pattern is a nuisance. First, it distorts the flow across the surface (Figure 10(a)). On the one hand, eddy currents may form and on the other hand, convection into the structures, particularly for high aspect ratios, may be completely inhibited. In the latter case, the diffusion length corresponds to the total resist height while, for good convection, the diffusion length may be as small as a few micrometers. This means that locally, the current density–potential relationship will vary significantly. Secondly, the pattern distorts

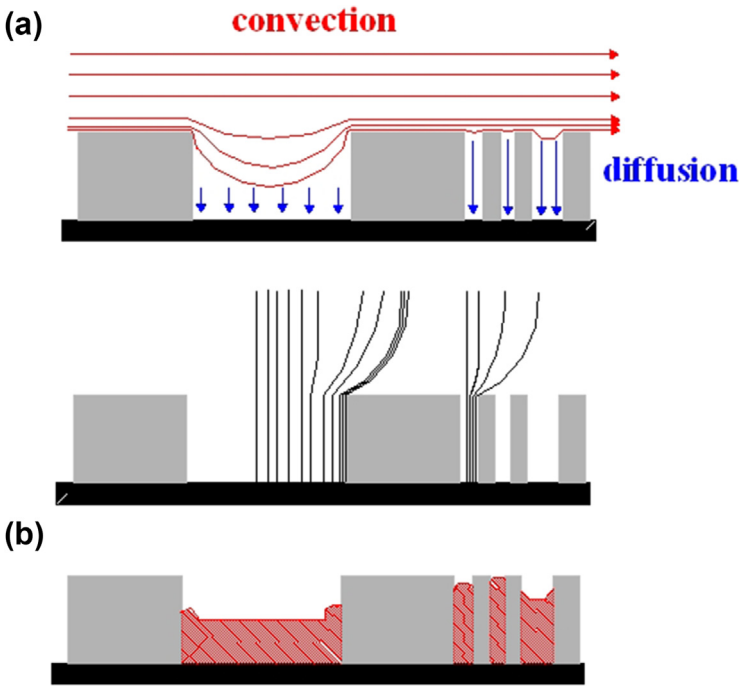

FIGURE 10

(a) Mass transport phenomena in micro-electroplating. The lithographic pattern may have a strong influence on the length of the diffusion zone which, in turn, will result in locally differing current densities. (b) Inhomogeneous field distribution due to the lithographic pattern. Isolated small features focus the field lines and grow faster than wider structures. The same effect leads to higher rates near resist edges.

the homogeneity of the electric field, with stronger fields corresponding to greater potentials on the current density–potential curve. This effect is sketched in Figure 10(b).

The art of electroplating therefore involves finding the right chemical composition that gives the desired properties of the deposited layers and making/keeping the solution stable against usage of the material to be deposited. The lithographic pattern introduces the requirement of low sensitivity to local variations in potential and mass transport. The use of additives alters the performance of the plating process drastically. Additives may be employed to change the current density–potential curve, where a leveler typically makes the curve near to the operating point flatter, an inhibitor reduces the current density at high voltages, and a brightener reduces the potential for the same current density by facilitating the nucleation of new grains. The finer grains usually are related to a greater hardness of the deposit. The electroplating procedures used in the LIGA process chain are gold plating for X-ray mask fabrication and nickel plating for molding tools and metallic micro-components.

Table 4 Plating Solution Characteristics

Property	Nickel	Nickel/Cobalt	Nickel/Iron
Composition	100	80/20	95/5
Bath temperature	40 °C	40 °C	52 °C
Plating rate	12 μm/h (1A/dm^2)	12 μm/h (1A/dm^2)	10 μm/h (1A/dm^2)
Hardness (Vickers)	280–330 (0.1)	450–500 (0.1)	580–630 (0.1)
Thickness accuracy	±50 μm	±50 μm	±100 μm

Further, alloys may be deposited in resist molds such as Ni—Co, Ni—P, or Ni—Fe. As an example, different plating solution properties (bath temperature, composition, thickness accuracy, aspect ratio) which produce a range of hardnesses of between 280 and 680 Vickers are listed in Table 4.

Finishing

When the thickness of the final parts must have a homogeneous thickness, the parts are typically "over plated" to ensure complete filling; an electroplating step is not available to deliver a homogeneous thickness all over the surface and a polished surface, which are sometimes needed. The top surface (electroplating front) is typically lapped and polished to the final part thickness and aspect. Other techniques are also available:

- Ultraprecision milling: This involves cutting with a milling tool while the workpiece is rotating. Using natural diamond cutting tools, a broad range of materials such as, for example, nonferrous metals (Ni—Co, Ni—P, Ni, Au, etc.) or plastics can be machined with a surface roughness of below 5 nm Ra. Only the diamond can be sharpened to the required level of accuracy. Cutting-edge sharpness and roundness are crucial to the manufacturing quality of the workpiece.
- Turning: This involves cutting with a rotating milling tool while the workpiece is fixed. Actually, only the hard Au can be turned using this technique.
- Grinding and polishing: The polishing can be supported electrolytically or chemically. All of the techniques should meet the following criteria:
  - to deliver a good thickness accuracy (±5 μm),
  - to avoid blur formation,
  - to deliver a specified surface quality (for example, optical quality).

Design rule—mask technology

A complete LIGA process database does not yet exist. Nevertheless, the LIGA centers (CAMD, IMT) have accumulated working design rules that enable them to advise customers on the feasibility of their needs. As an example, numerous parameters influence the quality of the final parts in terms of lateral

dimensions, and roughness of the sidewall. Some of the most important are listed here [36–39]:

- Secondary radiation: Divergence of the electrons and photons; fluorescence, Compton and Thomson diffusion emitted by the membrane, absorber, substrate; secondary electrons emitted by the membrane, absorber, substrate; Fresnel diffraction will deposit a certain dose in the unwanted parts of the resist.
- Thermal distortion: The mask, resist, and substrate develop heat during the irradiation. This leads to thermal distortion, which affects the accuracy of the copy. Cooling of the mask and the substrate is very important.
- Swelling and thermal expansion of resist.

X-ray masks are not available from commercial mask shops as is the case for Cr-masks. Therefore, the LIGA centers have developed their own technology to produce them. A variety of options exist (see Figure 11) requiring different tools using different mask membranes providing different performance for different costs. Nevertheless, a standard exists; it is limited to the characteristics of the support ring. X-ray masks consist of absorber patterns (generally Au) supported by highly X-ray-transparent membranes, the characteristics of which are given in Table 5.

In Figures 12 and 13 are shown the different mask format (layout area: 20×60–100 mm diameter; the use of the 100-mm diameter is actually under investigation) and as an example, a standard 4-inch X-ray mask (the membrane being a polished carbon membrane, the layout area having a diameter of 70 mm) respectively.

Metrology

This key production technology lacks extensive quality and process control; only a few consistent metrology studies concerning the X-ray LIGA process have been published to date [40,41]. Three dimensional (3D) micro-scale parts require accurate and traceable metrology. Very few metrology techniques fulfill these requirements. As an example, no metrology solution currently exists for the measurement of high aspect ratio X-ray LIGA gratings for phase contrast computer tomography [xx]. Even for larger structures in the millimeter range, there are very few instruments that can measure features to submicrometer accuracy. Currently, the best measurement techniques for high aspect ratio structures (for millimeter scale measurements) are those that use tactile probes, such as tactile coordinate measuring machines [42,43].

UNIQUE FEATURES OF THE LIGA PROCESS

Features characterizing this process are listed below:

- As a result of their high energy, these X-rays are capable of deeply penetrating thick (e.g., hundreds of micrometers or even millimeters) layers of polymeric

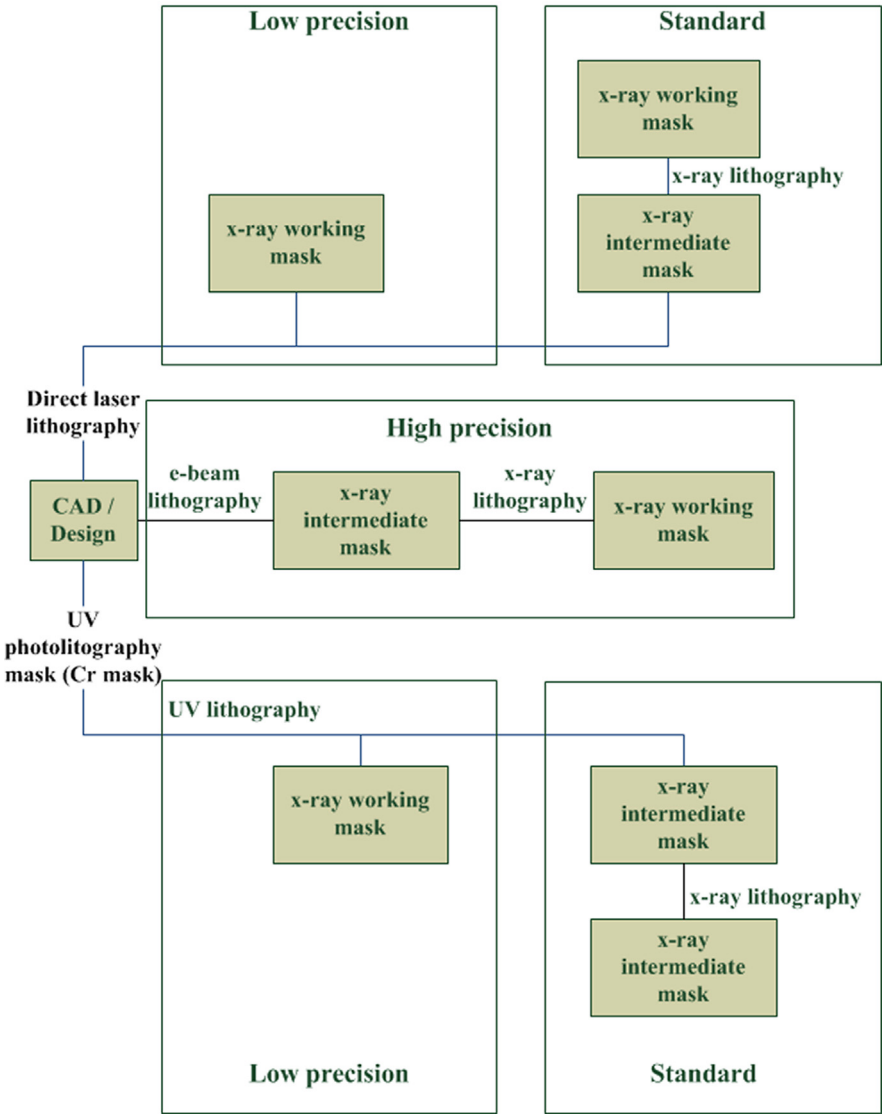

FIGURE 11

Different mask technology.

Table 5 Typical Mask Blank Characteristics

Material	Typical Thickness (μm)	Young's Modulus (GPa)	Thermal Expansion Coefficient (10^{-6}/K)	Thermal Conductivity (W/mK)	Density (g/cm^3)	Price
Titanium	2	116	9	22	4.5	High
Silicon	100	240	2.3	157	2.32	Low
Beryllium	500	318	12	230	1.85	High
Polished carbon	150	11	8.8	96	1.8	Low
Vitreous carbon	200	28	2.6	6.3	1.4	Low
Diamond	30	30	1.2	1000	3.51	High
Polyimide	10	2.5	20	0.12	1.42	Low

resist, allowing uniform deposition of energy in the depth of the resist and the formation of tall microstructures in one exposure step. Very precise shape definition of parts, both laterally in terms of dimensional control and straightness and planarity of sidewalls, are available.

- The short wavelengths of X-ray photons provide high resolution for patterning due to low diffraction effects. The smallest lateral dimension of a few micrometers with structural details in the submicrometer range can be manufactured.
- The very small vertical angular divergence of the X-ray beam achieves high accuracy in pattern transfer from the mask. Due to their excellent collimation, the X-rays penetrate thick resists with extremely low horizontal run-out (less than 0.1 μm/100 μm thickness), thereby producing the substantially vertical walls for which LIGA structures are well known.
- The almost parallel (well-collimated) light of X-ray beams produced by synchrotron radiation sources also allows printing with large depth of field. A large working gap between the mask and the substrate can then be used in nontraditional pattern transfer as for the manufacture of slanted structures or pattern formation on substrates presenting a large topography.
- The vertical sidewalls are optically smooth with a typical local roughness of the order of 10 nm and longer range waviness such as slope errors or steps determined solely by the accuracy of mask writing.

MARKET SITUATION OF DXRL

As mentioned earlier, the LIGA technique offers the possibility to manufacture microstructures with a number of unique features. With these properties, LIGA is on the leading edge of micro-fabrication. However, most of them consider LIGA to be very expensive, to employ much time from design up to realization and to

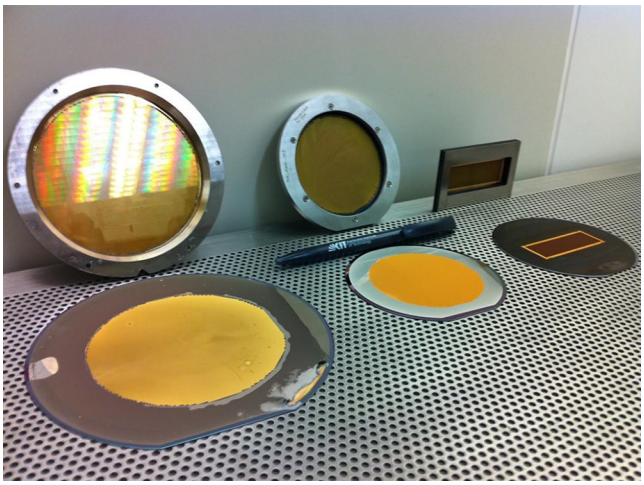

FIGURE 12

The different actually available mask format.

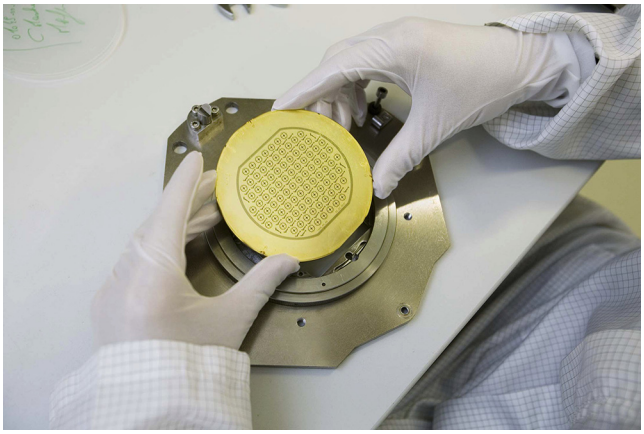

FIGURE 13

A standard X-ray mask (25 μm Au absorber supported by a 160 μm polished carbon membrane).

invoke a number of quality problems. They therefore try to avoid LIGA and only consider LIGA if the alternative fabrication methods fail to fulfill the requirements. These requirements, however, are often very challenging, even for LIGA, resulting in long development times, high-failure rates, and, of course, high cost. This reinforces the above described perception, resulting in a sort of vicious circle. De facto, DXRL is a small niche market, where the products are often unique or produced in small series.

COMMERCIAL APPLICATION

Examples are now given. For a more complete review of applications, see Ref. [6].

MICRO-SPECTROMETER [44—45]—MOLD

The spectrometer, as shown in Figure 14, consists of a molded base plate where the center hollow area, the gating profile, the location of the input fiber, and the 45′ mirror surface, are produced with a single pressing. The molded part is then placed in a vacuum chamber and a gold film deposited on both the grating surface and the mirror surface. This is then assembled into the complete spectrograph by fitting of the input fiber, the central hollow being filled with a polymer of different refractive index to that of the molding, and a lid of the same refractive index as that of the base glued into place. The assembly is then aligned with, and glued to, the diode array.

POLYMER COMPOUND REFRACTIVE X-RAY LENSES [46,47]

For hard X-rays, the refractive index r in matter is slightly smaller than 1. This implies a focal length F (given as $F = R/2Nr$ where R is the radius of the lens) of a single concave lens ($N = 1$) in the range of some 10 m. A compound refractive lens, consisting of a linear arrangement of N single lenses (see Figure 15), significantly reduces the focal length and thus can overcome this problem. For 14 keV photons, a focal spot of 0.32 μm (FWHM) was achieved using a focal distance of 242 mm. Crossed compound lenses are used for focusing the X-ray beam in two

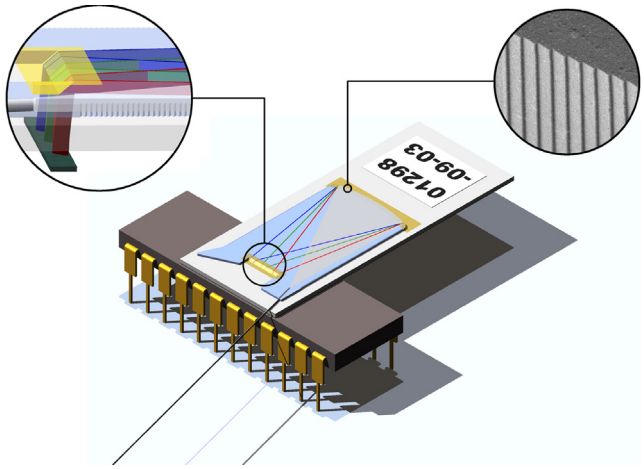

FIGURE 14

Micro-spectrometer.

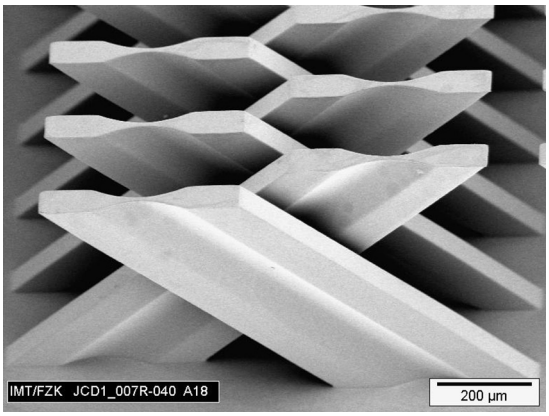

FIGURE 15

Rows of crossed parabolic lenses.

directions. For 28 keV photons, a focus spot of $0.5 \times 0.9\ \mu m^2$ (FWHM(x,y)) was achieved using a focal distance of 192 mm.

GRATINGS FOR DIFFERENTIAL PHASE CONTRAST IMAGING [48]

A novel approach in X-ray imaging yielding for reasonable imaging contrast of objects with little differences in absorption is differential phase contrast imaging (DPCI). The setup for DPCI consists of three gratings (see Figure 16): the source

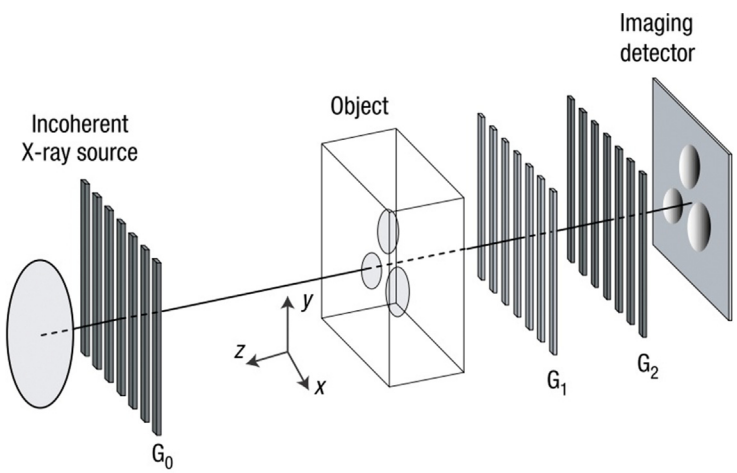

FIGURE 16

A Talbot–Lau grating interferometers setup for differential phase contrast imaging [48].

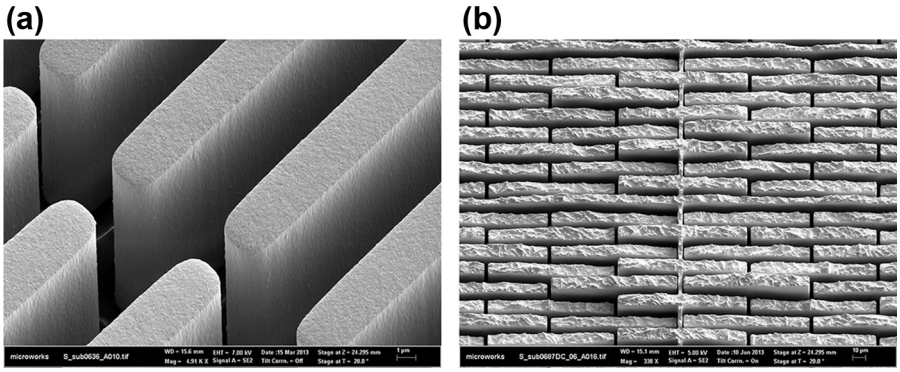

FIGURE 17

Scanning electron microscope pictures of a 4.8-μm (G0/G2) gratings. The Au thickness is 220 μm (AR: 91). (a) Top view and (b) 30° inclined view.

grating G0, used to generate small local coherent spots of the source; the phase grating G1, used to generate the Talbot carpet by shifting the phase of the X-rays periodically, typically either by π or $\pi/2$; and the analyzer grating G2, used to analyze the Talbot carpet in a phase stepping mode [46]. The periods and thickness of the gratings depend on the geometry of the whole setup; high aspect ratio feature concerning G0 and G2 are asked [49,50] because of the need to absorb the X-rays as much as possible, and the need of small periods (less than 5 μm) to get sufficiently short set ups and high detection efficiency. As example, Figure 17a and b present two G2 gratings; one with of period 7 μm and a gold thickness of 70 μm (AR: 20); the second one with a period of 14 μm and a gold thickness of 200 μm (AR: 29).

MICRO-GEARS—DIRECT METAL PARTS [51]

The search for the perfect product is one of the major preoccupations of the luxury watch-making industry. The combination of lithography with electroforming offers unparalleled-machining precision and extended design freedom for the manufacture of fine parts. The SU-8-based UV−LIGA technology undoubtedly attracts interest, in particular, when competing technologies fail to meet the precision and quality requirements. DXRL enables greater precision, better sidewall quality, and less restrictions, as almost any design can be realized. In Figure 18, are presented two parts (the cam in nickel−cobalt and the anchor in hart gold) of the newly developed IWC Schaffhausen constant force tourbillon, which combines a tourbillon with a constant force mechanism, guarantees a regular and precise rate for a period of at least 48 h.

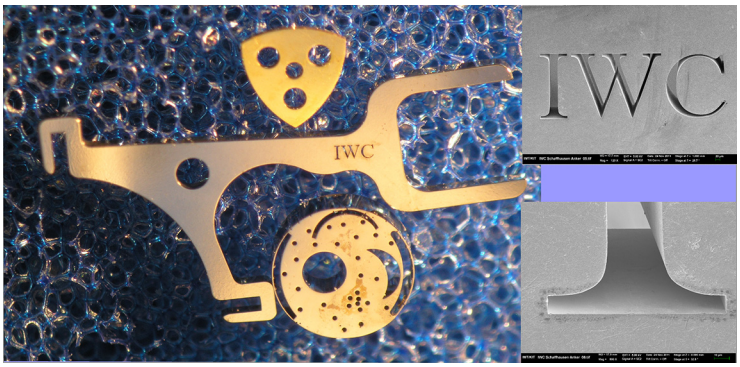

FIGURE 18

The two X-ray components (anker in nickel—cobalt with the IWC Schaffhausen's logo and the cam in hart gold) for the Portuguese Sidérale Scafusia next to a celestial disc of Nebra, celebrating the astrological complications of IWC Schaffhausen's new time piece.

CONCLUSIONS

Being invented in the 1980s, the potential of LIGA became evident in the 1990s when numerous examples for structures and devices were presented. The lead in MEMS technologies, however, was assumed by silicon micro-machining and not by LIGA, despite its technical superiority for many applications. The main reasons for this are the required technical infrastructure, process know-how, and cost issues. Silicon-based technologies could exploit the vast technology base developed for chip-making with billions of dollars invested. LIGA, on the other hand, was new and confined to research laboratories. Furthermore, as a key process step, LIGA required access to a synchrotron radiation facility, again a research laboratory provision, and often unacceptable for industries establishing manufacturing plants. Nevertheless, and this is a demonstration of the technical strength and superiority of LIGA, several industrial LIGA products have been launched by industries and synchrotron radiation facilities are currently widely used for micro-fabrication. In addition to the described efforts to make LIGA acceptable as a manufacturing technology for a large variety of industrial products, cutting-edge research in and with LIGA remains a hot topic. The goals include research in new materials, new replication techniques, and new lithography approaches exploiting the short-wavelength nature of X-rays. Questions such as "How small can we really get?" and "Can we overlap our top-down technologies with the typical bottom-up approach in nano-technology? At which dimensions?" are currently being addressed. Making devices much smaller than is possible today will open up entirely new fields in research and applications.

REFERENCES

[1] Becker EW, Ehrfeld W, Hagmann P, Maner A, Münchmeyer D. Fabrication of microstructures with high aspect ratios and structural heights by synchrotron radiation lithography, galvanoforming, and plastic moulding (LIGA process). Microelectron Eng 1986; 4:35−6.

[2] Kupka RK, Bouamrane F, Cremers C, Metgert S. Microfabrication: LIGA-X and applications. Appl Surf Sci 2000;164:97−110.

[3] Hruby J. LIGA technologies and applications. MRS Bull 2001;26(4):337−40.

[4] Hruby J. Overview of LIGA microfabrication. AIP Conf Proc 2002;625(1).

[5] Malek CK, Saile V. Applications of LIGA technology to precision manufacturing of high-aspect-ratio micro-components and -systems: a review. Microelectron J 2004; 35:131−43.

[6] Saile V, Wallrabe U, Tabata O, Korvink JG, editors. LIGA and its applications. Wiley; 2009, ISBN 978-3-527-31698-4.

[7] Cremers C, Bouamrane F, Singleton L, Schenk R. SU-8 as resist material for deep X-ray lithography. Microsyst Technol 2001;7:6−11.

[8] Nazmov V, Reznikova E, Mohr J, Snigirev A, Snigireva I, Achenbach S, et al. Fabrication and preliminary testing of X-ray lenses in thick SU-8 resist layers. Microsyst Technol 2004;10:716−21.

[9] Becnel C, Desta Y, Kelly K. Ultra-deep X-ray lithography of densely packed SU-8 features: I. An SU-8 casting procedure to obtain uniform solvent content with accompanying experimental results. J Micromech Microeng 2005;15:1242−8.

[10] Kouba J, Engelke R, Bednarzik M, Ahrens G, Scheunemann H-U, Gruetzner G, et al. SU8: promising resist for advanced direct LIGA applications for high aspect ratio mechanical microparts. Microsyst Technol 2007;13(3):311−7. http://dx.doi.org/10.1007/s00542-006-0178-z.

[11] Engelke R, Mathuni J, Ahrens G, Gruetzner G, Bednarzik M, Schondelmaier D, et al. Investigations of SU-8 removal from metallic high aspect ratio microstructures with a novel plasma technique. Microsyst Technol 2008;14(9):1607−12. http://dx.doi.org/10.1007/s00542-007-0537-4.

[12] http://www.muegge.de/products/plasma-systems/stp-2020/.

[13] Johnson DW, Goettert J, Singh V, Yemane D. SUEX process optimization for ultra-thick high-aspect ratio LIGA imaging. Proc. SPIE 7972, Adv Resist Mater Process Technol XXVIII April 15, 2011;79722U. http://dx.doi.org/10.1117/12.882872.

[14] Winick H. Synchrotron radiation research, Chapter 2: properties of synchrotron radiation. New York: Plenium Press; 1980.

[15] Margaritondo G. Introduction to synchrotron radiation, Chapter 2.2: bending magnet radiation. New York, Oxford: Oxford University Press; 1988.

[16] Attwood D. Intro synchrotron radiation, bending magnet radiation. EE290F. Berkeley: Univ. California; February 8, 2007.

[17] Nordt S, Pasch H, Radke W. Method development for epoxy resin analysis. Microsyst Technol 2010;16(8):1347−51. http://dx.doi.org/10.1007/s00542-010-1022-z.

[18] Stewart M, Tran H, Schmid G, Stachowiak T, Becker D, Willson G. Acid catalyst mobility in resist resin. J Vac Sci Technol B 2002;20:2946−52.

[19] Lemke S. Charakterisierung modifizierter Negativresiste für die Röntgentiefenlithographie [Ph.D. thesis]. Fakultät V -Verkehrs-und Maschinensysteme der Technischen Universität Berlin; 2011.
[20] Kunka D, Mohr J, Nazmov V, Meiser J, Meyer P, Amberger M, et al. Characterization method for new resist formulations for HAR patterns made by X-ray lithography. Microsyst Technol 2014;20(10):2023−9. http://dx.doi.org/10.1007/s00542-013-2055-x.
[21] El-Kholi A, Bley P, Göttert J, Mohr J. Examination of the solubility and the molecular weight distribution of PMMA in view of an optimised resist system in deep etch X-ray lithography. Microelectronic Eng 1983;21:271−4.
[22] Gad-el-Hak M. The MEMS handbook. New York, U.S.A.: CRC Press; 2001.
[23] Schmalz O, Hess M, Kosfeld R. Structural changes in poly(methyl methacrylate) during deep-etch X-ray synchrotron radiation lithography. Part II: radiation effects on PMMA. Die Angew Makromol Chem 1996;239:79−91.
[24] Glashauser W, Ghica GV. German patent, 3039110, 1982.
[25] Greeneich JS. Developer characteristics of poly-(methyl electron resist methacrylate). J Electrochem Soc 1975;122:970−6.
[26] Liu Z, Bouamrane F, Rouilliay M, Kupka R, Labeque A, Metgert S. Resist dissolution rate and inclined-wall structures in deep X-ray lithography. J Micromech Microeng 1998;8:293−300.
[27] Meyer P, El-Kholi A, Mohr J, Cremers C, Bouamrane F, Metgert S. Study of the development behavior of irradiated foils and microstructure. SPIE 1999;3874:312−20.
[28] Meyer P, El-Kholi A, Schulz J. Investigations of the development rate of irradiated PMMA microstructures in deep X-ray lithography. Microelectron Eng 2002;63:319−28.
[29] Pantenburg FJ, Achenbach S, Mohr J. Influence of developer temperature and resist material on the structure quality in deep X-ray lithography. J Vac Sci Technol 1998;16:3547−51.
[30] Meyer P, Schulz J, Hahn L. DoseSim: MS-Windows graphical user interface for using synchrotron X-ray exposure and subsequent development in the LIGA process. Rev Sci Instrum 2002;74(2):1113−9.
[31] Meyer P. Fast and accurate X-ray lithography simulation enabled by using Monte Carlo method. New version of DoseSim: a software dedicated to deep X-ray lithography (LIGA). Microsyst Technol 2012;18:1971−80. http://dx.doi.org/10.1007/s00542-012-1637-3.
[32] Griffiths SK, Ting A. LEX-D Version 7.54, Sandia LIGA exposure and development software. November 2002.
[33] Hafizovic S, et al. X3D: 3D X-Ray lithography and development simulation for MEMS. In: Transducers'03; 2003. p. 1570−3.
[34] Hirai Y, Hafizovic S, Matsuzuka N, Korvink JG, Tabata O. Validation of X-ray lithography and development simulation system for moving mask deep X-ray lithography. IEEE/ASME J Microelectromech Syst 2006;15(1):159−68. http://dx.doi.org/10.1109/JMEMS.2005.859191.
[35] Paunovic M, Schlesinger M. Fundamentals of electrochemical deposition. John Wiley and Sons; 1998.
[36] Griffiths SK, Hruby JM, Ting A. The influence of feature sidewall tolerance on minimum absorber thickness for LIGA X-ray masks. J Micromech Microeng 1999;9:353−61.

[37] Griffiths SK. Fundamental limitations of LIGA X-ray lithography: sidewall offset, slope and minimum feature size. J Micromech Microeng 2004;14:999−1011.
[38] Meyer P, Pantenburg FJ. A Monte Carlo study of the primary absorbed energy redistribution in X-ray lithography. Microsyst Technol 2014;20(10):1881−9. http://dx.doi.org/10.1007/s00542-013-1966-x.
[39] Chang W-J, Yang Y-C, Lin C-M. Estimating thermal transport in deep X-ray lithography with an inversion method. Appl Phys B-Lasers Opt 2005;81(4):543−8. http://dx.doi.org/10.1007/s00340-005-1909-z.
[40] Meyer P, Claverley JD, Leach RK. Quality control for deep X-ray lithography (LIGA): a preliminary study. Microsyst Technol 2012;18(4):415−21. http://dx.doi.org/10.1007/s00542-012-1448-6.
[41] Chinn D, Ostendorp P, Haugh M, Kershmann R, Kurgess T, Claudet A, et al. Three dimensional imaging of LIGA-made microcomponents. J. Manuf Sci Eng 2004;126:813−21.
[42] Cao S, Brand U, Kleine-Bestent T, Hoffmann W, Schwenke H, Bütefisch S, et al. Recent developments in dimensional metrology for microsystem components. J Microsyst Technol 2002;8:3−6.
[43] Brand U, Kirchhoff J. A micro-CMM with metrology frame for low uncertainty measurements, measurement science and technology. Meas Sci Technol 2005;16:2489−97.
[44] Müller C, Mohr J. Microspectrometer fabricated by the LIGA process. Interdiscip Sci Rev 1993;18(3):273−9.
[45] Last A. Fehllicht in LIGAMikrospektrometern [Ph.D. thesis]. Fakultät für Maschinenbau der Universität Karlsruhe; 2012.
[46] Nazmov V, Reznikova E, Somogyi A, Mohr J, Saile V. Planar sets of cross X-ray refractive lenses from SU-8 polymer. Proceedings of SPIE, Band 5539; 2004. S. 235−S. 243.
[47] Nazmov V, Mohr J, Simo R. Mosaic-like micropillar array for hard X-ray focusing one-dimensional version. J Micromech Microeng 2013;23. http://dx.doi.org/10.1088/0960-317/23/9/095015.
[48] Pfeiffer F, Weitkamp T, Bunk O, David C. Phase retrieval and differential phase-contrast imaging with low brilliance X-ray sources. Nat Phys 2006;2:258−61. http://dx.doi.org/10.1038/nphys265.
[49] Noda D, Tsujii H, Takahashi N, Hattori T. Fabrication of X-Ray gratings using X-Ray lithography technique for X-Ray talbot interferometer. J Electrochem Soc 2009;156(5):299−302. http://dx.doi.org/10.1149/1.3082377.
[50] Mohr J, Grund T, et al. High aspect ratio gratings for X-ray phase contrast imaging. AIP Conf Proc 2012;1466:41. http://dx.doi.org/10.1063/1.4742267.
[51] Meyer P, Schulz J, Hahn L, Saile V. Why you will use the deep X-ray LIG(A) technology to produce MEMS? Microsyst Technol 2008;14(9−11):1491−7.

This page intentionally left blank

CHAPTER

17 Polymer Thin Films—Processes, Parameters and Property Control

Bertrand Fillon
CEA/LITEN, Rue des Martyrs, Grenoble Cedex 9, France

CHAPTER OUTLINE

Micromanufacturing Engineering and Technology. http://dx.doi.org/10.1016/B978-0-323-31149-6.00017-7

INTRODUCTION

Over the last 10 years, the use of polymer thin films has increased significantly in various domains of application: in traditional industries (e.g., papers and metal strips), in the automotive industry, in packaging, etc. Moreover, emerging markets such as consumer electronics and photovoltaic energy use polymer thin films also. This growth has been driven mainly by important advances in the properties of polymer thin films (better barrier properties (water, oxygen, etc.), wear resistance, optical properties, etc.) and a much more extensive range of applications (solvent-based coatings, water-based coatings, plasma deposition, emulsions, etc.). It would indeed be very ambitious to attempt to cover all the properties of polymer thin films in the space of a few pages. Nevertheless, there are two major families of parameters which influence the properties of these thin films:

- Type of the polymer deposited;
- Implementation conditions.

Clearly, the properties of these thin films depend mainly on the type of polymer and its thickness. Certain polymers are better for improving barrier properties, while others offer very good sealing functions. As for the implementation conditions, three processes are used to produce most of these thin films: extrusion coating, deposition in solution with radiation cross-linking (thermal, UV, electron beam), and physical deposition involving plasma. The ranges of polymer thickness generally deposited by these three process types are respectively: >5 μm, $1 < t < 5$ μm, and <1 μm. Note that extrusion coating is at the upper limit of the range defined for the thin films.

Generally speaking, a key technological requirement is to provide all the desired functions of the coating (optical, barrier, adhesive, electrical, catalytic, etc.) while controlling the interfaces and micro-structures (film, charge dispersion, orientation, crystallinity, porosity, etc.).

This chapter is broken down into three major sections. Each section will focus on one of the three implementation processes mentioned above. The objective is to briefly describe these processes, indicating the most widely used polymers, and to show how thin film properties can be improved by the type of polymer deposited, but also through control of the interactions between process parameters and material parameters. Each of these sections will be illustrated by examples of applications requiring specific properties, e.g., water or oxygen barrier properties, optical properties, sealing properties, or surface properties.

THIN FILMS OBTAINED BY EXTRUSION COATING

The process of extrusion coating (Figure 1) enables covering a flexible substrate with a very thin polymer film. In industry, polyethylene is generally used to cover commercial substrates such as paper, cardboard, polyester, and other polymeric films, metal foils including aluminum foil, textiles, etc. The polymer deposited is often

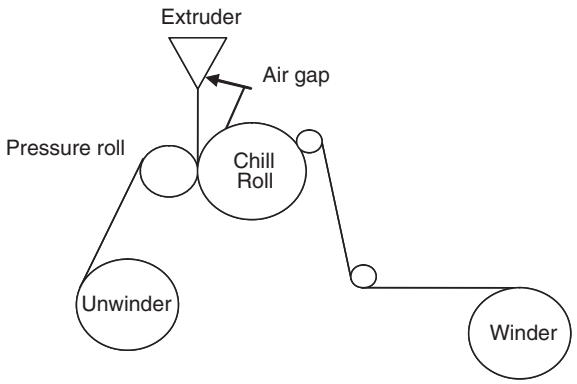

FIGURE 1

The process of extrusion coating.

a semicrystalline polymer such as polyolefin (polyethylene, copolymers such as ethylene methyl acrylate, ethylene butyl acrylate, etc.), polyesters, polyvinyl chloride (PVC), etc.

The objective is to coat a substrate with a polymer, combining the best properties of the two materials. The advantages of this process are a heat-sealable surface, improved resistance to tears and wrinkling, an excellent barrier against moisture, oxygen and odors, enhanced optical properties (dullness, gloss), and an imprintable surface.

PRINCIPLE OF EXTRUSION COATING

Polymer granules are extruded using a slot die to obtain a thin film of molten polymer. The role of this coating die is to present the molten polymer in a form similar to its final form (coating film), to keep it at a constant temperature, to obtain a stable flow of polymer and to coat the desired width of the substrate with it. The molten polymer travels over the distance between the slot die and the substrate: this distance is often called the air gap. The air gap value may vary depending on the desired extrusion conditions.

The film of molten polymer is pressed through two rollers positioned directly below the die. The first of these, coated with neoprene, is the pressure roll. It draws the substrate to be coated and presses it against the molten polymer film. This is the precise moment at which the extruded polymer adheres to the substrate. The pressure roll is cooled by internal water circulation with adjustable temperature. This prevents its temperature from rising too rapidly.

The second roller is chrome plated and called the chill roll. It is also cooled by internal water circulation with adjustable temperature. Its role is threefold:

- It must cool and solidify the polymer in a fraction of one rotation.
- Its rotational speed controls the quantity of polymer deposited on the substrate (coating thickness or grammage).

- Its surface (polished, matte, etc.) determines the surface appearance of the polymer coating.

The resulting complex is then directed toward the system's draw roll and winder.

PROCESS PARAMETERS AND INFLUENCES

Polymer suppliers and converters must deal with a growing market demand for low cost "deposited film/substrate" complexes which still offer high performance properties. Manufacturers, polymer and substrate suppliers, and converters must work together to reach these objectives. Various studies have enabled improving polymer performance while at the same time optimizing process parameters. For example, in the packaging industry, several complexes such as aluminum/polyethylene, paper/PE, etc., are used with low density polyethylene (LDPE) without a binder layer. These various structures are produced using extrusion coating. Good adhesion between the LDPE and the substrate is clearly vital. However, the adhesive strength is generally very weak between the substrate and the LDPE, due to the lack of polar or reactive functions in LDPEs. Likewise, following the extrusion coating process, the complexes alu/LDPE, paper/LDPE, etc., maintain the sealing properties of polyethylene.

Example: adhesive properties of an aluminum/LDPE structure

For adhesion to occur between LDPE and the aluminum foil, the LDPE has to oxidize during the extrusion process. This functionalization of the LDPE primarily occurs during the molten polymer's dwell time between the die's opening and the point of contact with the substrate, i.e., in the air gap. Adhesion between the LDPE and the substrate is affected by several factors, which can be categorized into three groups: extrusion parameters (melt temperature, air gap, etc.), polymer parameters (melt index (MI), density, etc.), and substrate parameters (type, surface roughness, etc.). Over the last 20 years, the practical problem of ensuring good adhesion between the LDPE and various substrates during extrusion coating has been the subject of much interest, both from a technical and a scientific point of view [1–7]. Whereas some parameters (corona treatment, ozone, posttreatment, etc.) generally increase adhesion, it is difficult to draw a single conclusion for process parameters overall, but most authors agree that interactions do exist between these parameters. The main process parameters with the greatest effect on adhesion between the polymer and the substrate are: temperature of the molten polymer, thickness of the film deposited, pressure of the rollers, extrusion speed, and air gap.

It is very difficult to separate the last two parameters: increasing the substrate speed effectively reduces the dwell time (d_t) in the air gap and LDPE oxidation becomes difficult, resulting in poor adhesion. If the air gap is increased, the dwell time d_t (or freeze time t_f) and LDPE oxidation will also increase, but the LDPE will cool and its viscosity will increase, reducing its wettability relative to the substrate's roughness. This in turn reduces mechanical adhesion. These two phenomena conflict

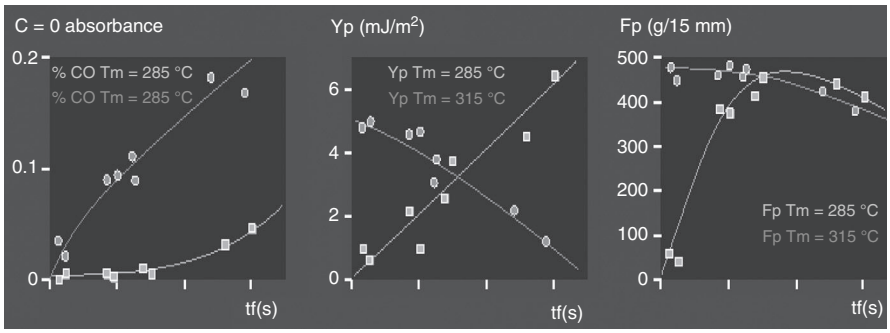

FIGURE 2

Freeze time (t_f) dependent changes in the oxidation rate, polar function (Y_p), and peel strength (F_p) of a low density polyethylene extruded on aluminum foil at two temperatures (285 °C and 315 °C). The thickness of the low density polyethylene film and the pressure between the rollers were constant ($e = 10$ μm; $P = 6$ bars).

with one another; hence the need for a compromise. According to most authors, line speed and air gap can be expressed as a single parameter, that of freeze time t_f:

$$t_f = \frac{H}{V_t - V_0} \times Ln \frac{V_t}{V_0}$$

where V_t = line speed, V_0 = material through P, and H = air gap.

Figure 2 illustrates the interactions between the process parameters and the polymer, which lead to changes in adhesive strength. At low temperatures ($T = 285$ °C), the adhesive strength (F_p) of the LDPE increases with dwell time, attaining a maximum value then falling. This increased adhesion is correlated with an increase in the LDPE's carboxylic functions and, as a result, in its surface energy (Y_p). The drop in adhesion at high t_f values is related to cooling of the LDPE, which becomes more viscous on contact with the substrate; as a result, the LDPE does not mold as well to the substrate's surface. At high temperatures ($T = 315$ °C), adhesion of the LDPE is very strong despite short dwell times. This adhesion decreases with high t_f values. Oxidation of the LDPE becomes excessive and initiates its degradation, resulting in a high number of ruptured chains and a drop in its surface energy (Y_p). This leads to a layer with poor cohesion at the surface of the LDPE film, in turn provoking the drop in adhesion.

Achieved through controlling process parameters, LDPE oxidation is necessary to attain good LDPE/aluminum adhesive strength.

Example: sealing properties of an aluminum/LDPE structure

Besides the adhesion between the aluminum foil and the polyethylene, the LDPE film should have good sealing properties. Figure 3 illustrates the changes in the seal strength of one alu/LDPE complex compared to another alu/LDPE complex, both obtained by extrusion coating. The sealing capacity of a polymer is most often

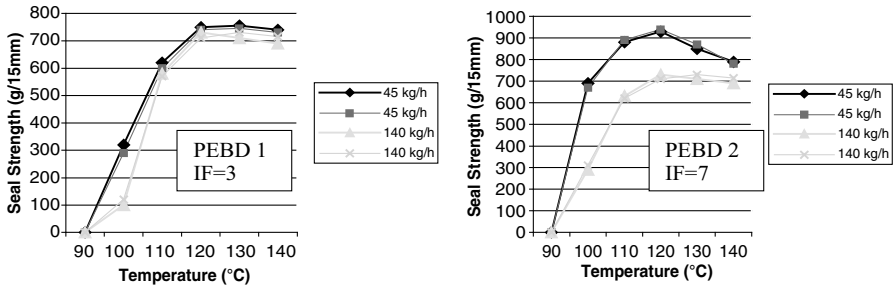

FIGURE 3

Changes in seal strength of two low density polyethylenes (LDPEs) (LDPE1: MI = 3; LDPE2: MI = 7) according to sealing temperature. The alu/LDPE complexes were obtained by extrusion coating at two different rates (45 and 140 kg/h) and at two different pressures (90 and 150 bar). The low pressure curves are represented by dotted lines.

linked to its MI. A high MI results in a high degree of fluidity and improves interfacial diffusion during sealing, allowing the polymer to attain a high seal strength at low temperatures. This is illustrated by Figure 3; the LDPE2 sealing curve (MI = 7) starts at a lower temperature than that of LDPE1 (MI = 3). Extruded at low pressure and a low rate (45 kg/h), LDPE1 attained a seal strength of 300 g/15 mm at a temperature of 100 °C. Under the same conditions, LDPE2 attained a seal strength of 700 g/15 mm.

Process parameters clearly have an influence on sealing properties as well as on adhesion. Figure 3 illustrates the effect of extrusion rate on seal strength. Within the operating range for the selected process parameters, when LDPE2 is deposited on aluminum foil at a lower rate (45 kg/h), seal strength goes from 300 g/15 mm to 700 g/15 mm. Likewise the air gap has an effect on seal strength, which is weaker when the air gap is reduced (Figure 4). Sometimes these process/material interactions do not exist; this is the case for pressure during the extrusion process [3].

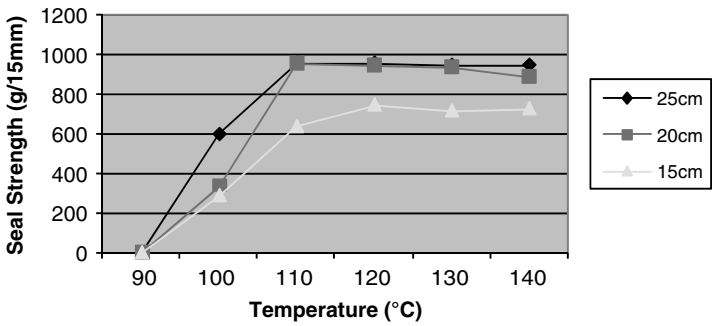

FIGURE 4

Changes in seal strength according to temperature for alu/LDPE complexes extruded with various air gaps.

SUMMARY ON EXTRUSION COATING

Variation in process parameters can have a significant impact on the final properties of film complexes such as alu/PE, paper/PE, alu/EVA, etc. Final products with excellent performance can be obtained at low cost through polymer selection and adjustment of the process parameters. In the section above, the examples presented for adhesive and sealing properties clearly illustrate the interactions between material and process parameters. Whatever be the target property—barrier, optical, etc.—these interactions between process and material parameters will always play an important role in determining the final properties of the product [8].

ORGANIC COATINGS DEPOSITED IN SOLUTION

Organic coatings deposited in solution (i.e., using wet methods) are found in very diverse areas. They are commonly produced by coating substrates with thin layers of a liquid or suspension, which are then transformed into solids by gelation, drying, or cross-linking. Such structures are vital elements for an extremely broad range of industrial products. They are developed for paper, steel, aluminum, polymer films, printed materials, selective membranes, photographic film, photosensitive coatings, adhesives, micro-electronics, integrated circuits, etc. However, deposition technologies may differ greatly depending on the final application. For example, the manufacture of microelectronic components uses spin coating, whereas varnish is generally deposited on steel foil using roll or spray coating.

This chapter focuses exclusively on organic coatings deposited with the roll coating technique; this covers a large majority of the polymer thin films produced industrially. Most of the deposition processes based on this technique involve a series of rollers-producing polymer thin films, which can have thicknesses below one micron. These varnishes offer an effective protective barrier for metal substrates (aluminum, steel), paper substrates, or polymer films. These coatings may also be used for decorative or aesthetic purposes (glossy or matte effects, colors, etc.), or act as sealants, etc. They must also offer specific characteristics of durability and resistance to temperature, solvents, or UV radiation depending on the final application of the coated product:

- Exterior applications (prefinished steel and aluminum for construction);
- Decorative interior elements, household appliances, etc.
- Packaging for food products, cosmetics, etc.

The composition of the varnishes or paints, the choice of substrate, and the conditions under which organic coatings are applied, dried, and cured are inextricably linked in determining the properties of the end product [8].

MAIN POLYMERS USED IN ROLL COATING

As in extrusion coating, the polymer used to coat the substrate will strongly influence the quality of deposition and the final properties. The most commonly used

Table 1 Performance of Main Coatings Used in Solution

Polymer Family	Polyester/ Amine	Polyester/ Polyurethane	Epoxy	PVDF	PVC
Flexibility	Good	Very good	Poor	Good	Very good
Hardness	Good	Average	Very good	Average	Poor
Adhesion to metal	Good	Good	Very good	Poor	Poor
Corrosion protection	Good	Good	Very good	Average	Very good
Weather resistance	Good	Very good	Poor	Very good	Average
Temperature resistance	Good	Good	Good	Good	Poor
Recyclability	Very good	Good	Good	Poor	Poor

coatings are indicated in Table 1. Note that the molecular weights of polymers deposited in solution are lower than those of polymers deposited by extrusion.

In general, six categories of basic polymers (Figure 5) are used in roll coating [9]. The different categories are based on:

- Solid state (amorphous or crystalline);
- Solubility in common solvents;
- Swellability of crystalline or cross-linked polymers.

Amorphous and soluble polymers (a), for example polyesters, epoxies, or acrylics, produce liquid varnishes and paints which are 30−70% nonvolatile. Amorphous and insoluble polymers (b), which are primarily polyesters, can be used in powder coating technology. Semicrystalline polymers (c), which form the basis of the extrusion coating films listed in the previous chapter, can also be used in roll coating after a process of precipitation or grinding to produce fine powders.

Dispersing these fine powders in other basic polymer solutions produces organosols (e), which are 40−60% nonvolatile. Examples of organosols include PVDF films and polyester polyurethane systems modified by polyamide fine powders.

Organosols can also be formulated with cross-linked polymers (d) in the form of micro-gels or ground into fine powders. Certain applications use these substances, specifically cross-linked amine polymers, acrylics, and unsaturated polyesters.

A plastisol (f) is obtained if a fine and crystalline powder polymer is dispersed in a plasticizer that homogeneously dissolves it at temperatures above the crystallite melting point, forming a gel after cooling. Plastisols are more than 90% nonvolatile. Little solvent is needed.

Note that in addition to the specific characteristics for roll application and "flash" forming or curing of the film, the varnishes or paints for the prefinishing of flat steel

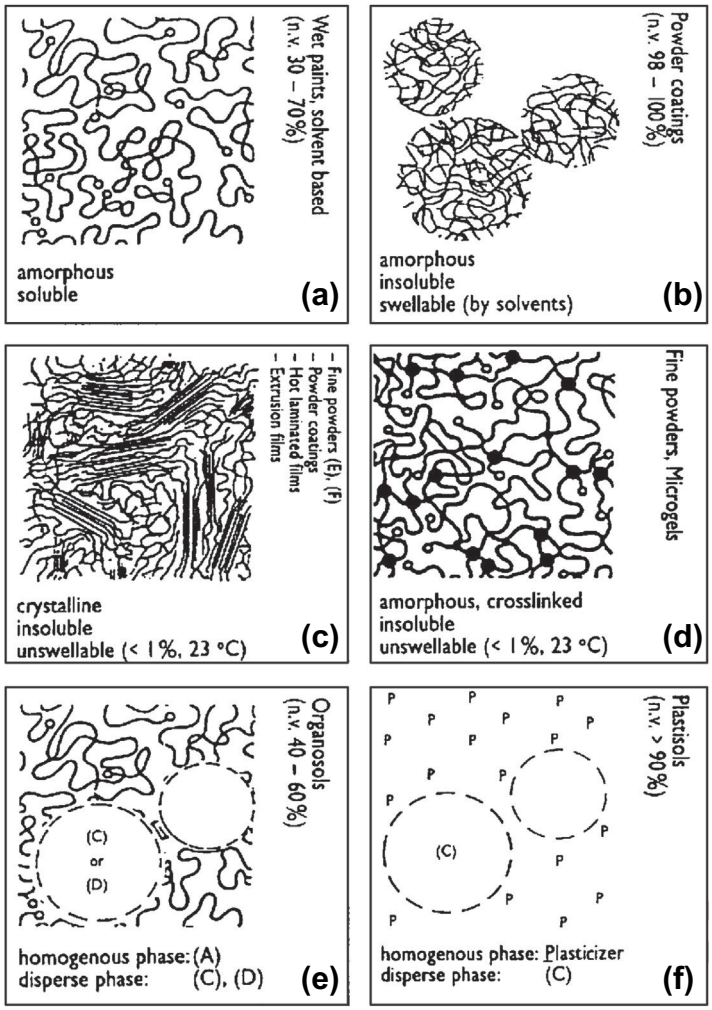

FIGURE 5

Morphology of basic resins [13].

or aluminum must offer excellent flexibility, e.g., meeting the postforming requirements for drawing food cans.

PRINCIPLE OF ORGANIC COATING DEPOSITION IN SOLUTION

Applying organic coatings to reels of flat substrate offers major technical and financial advantages due to the following:

- Increased productivity and yield of finishing systems (with linear speeds of up to 1000 m/min), reducing the cost of varnish and paint application.

- Flexibility of roll coating; rapid changes can be made without stopping the application process.
- Various curing temperature levels (80−250 °C), enabling a wide range of binder systems to be used via various film-formation processes (flash cross-linking, gelation, or fusion). Cross-linking increasingly involves the environment-friendly techniques of UV radiation or electron beams.
- Efficient effluent treatment systems (e.g., incineration of solvent vapors).

Generally, the process of roll coating includes three phases:

- **Surface preparation and treatment**: corona surface treatments are widely used on various substrates, e.g., chromate treatment of steel (no-rinse process) which helps to control film weight and eliminate releases.
- **Roll coating of the polymer**: can be performed on both sides of the reel simultaneously. Various approaches can be used for this step (Figure 6). More than 35 systems are available on the market to coat a variety of substrates [10]. The varnish properties, surface appearance, and thickness ranges differ according to the process used.
- **Solvent evaporation and flash curing**: necessary for forming the binding network.

The choice of technology is based on the application, but there are some country-specific trends emerging in the technologies chosen [11]. With the process of varnish deposition, it is possible to influence precision, coating weight, and also surface appearance (Table 2).

Most often, the coating is applied to the substrate using a series of application rollers. The reasons cited for using such a system are as follows: the ability to transmit shear to a liquid, to smooth the coating before its deposition, to attain an acceleration between the slow movement of the rollers and the speed at which the substrate passes through them (i.e., line speed), and to produce thin films by

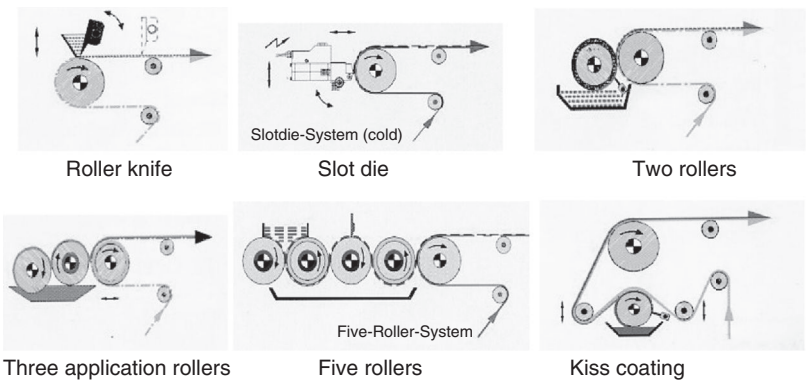

FIGURE 6

Various systems for varnish deposition [10]. Diagrams from Coatema sales documentation.

Table 2 Three Varnish Deposition Processes most Commonly Encountered

Type of Process	Characteristics	Main Comments on the Process
Knife coating	Thickness range: 5–500 μm Viscosity: 5000–50,000 mPas Maximum speed: 100 m/min	Very dependent on varnish and substrate. A very smooth film can be obtained with 4% precision over the full width of the substrate. For low viscosity varnishes, there may be problems with deposition uniformity. Solvent evaporation during the implementation process may lead to the appearance of agglomerates.
Slot die	Thickness range: <1–200 μm Viscosity: <1000 mPas Maximum speed: 1000 m/min	Possible to work with minimum contact. Substrate does not have a big influence. Precision is on the order of 1%. The low viscosity (<200 mPas) often Results in very good precision.
Roll coating	Thickness range: 2–100 μm Viscosity: <2000 mPas Maximum speed: 1000 m/min	Very dependent on the surface of the deposition roller (very smooth with very good precision or gravure roller). A very smooth film can be obtained. The precision of deposition depends on the parameters of the application roller and the roller opposite to it. For film thickness, precision is on the order of 2%.

multiplying the separation phases at each roller. The configurations are selected based on the deposition thickness and precision. In the two-roller configuration, there is only one gap for adjusting and controlling the thickness deposited. In a three-roller configuration, the additional gap allows this thickness to be optimized. Each roller has two functions. First, rollers act as a divider by reducing the thickness and uniformly spreading the varnish between all the rollers. Second, they create the necessary shear to provoke Newtonian behavior in the varnish. There are few publications [12–15] explaining how these deposits form, how a thin film is created, how good the sensitivity is, and how to perfectly control coating weight based on roller speed, gap, and varnish properties.

But obviously there will always be interactions between the varnish type, its viscosity, and the additives (size of charges, chemical nature, form, etc.). Note that for certain production processes, the central chemical treatment and coating section is isolated from the unwinding and winding sections by accumulators, allowing for uninterrupted operation during reel changing.

PROCESS PARAMETERS AND INFLUENCES

Example: optimizing optical properties

There is a great deal of demand for coatings with specific visual or optical properties (transparency, gloss, matte finish). By adjusting the parameters of the

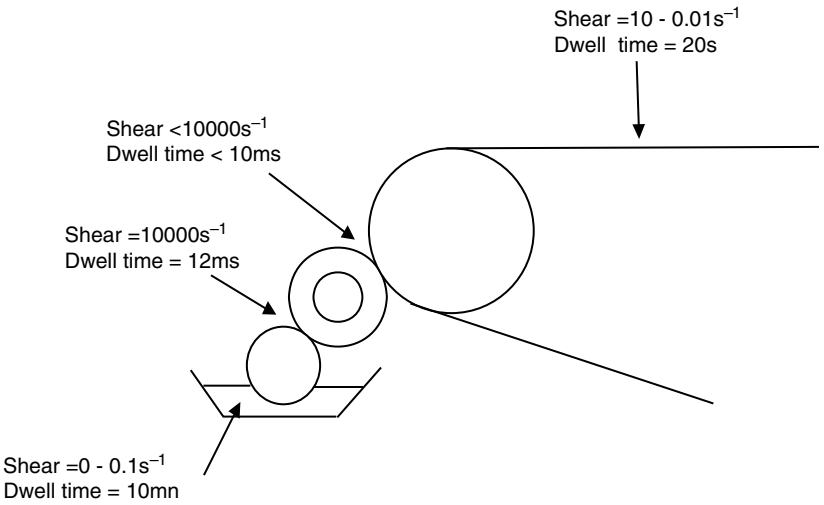

FIGURE 7

Timescale and typical values of process parameters for wet deposition.

implementation process, it is possible to influence a coating's surface appearance as well as its thickness and precision.

As the varnish is applied to the substrate, the shear rate changes abruptly, potentially attaining very high values (Figure 7), but this intense shear strain lasts only a short time (<0.01 s). Use of an elastomer roller can be estimated to increase the dwell time and reduce shear by a factor of around 10 compared to a rigid roller. The viscosity of the varnish will thus have a nonnegligible effect on its thickness and visual qualities, and it will interact with the system of application. Eleven types of flow between two rollers have been described. Experimental and theoretical studies have examined some of them [16] and have enabled correlating the quantity deposited with the flow characteristics. Likewise, a strong interaction between the implementation parameters and the optical properties has been demonstrated by the number of capillaries:

$$C_a = \frac{\eta_o V}{\sigma}$$

where η_o = viscosity, V = line speed, and σ = surface energy.

Whatever the mode of varnish transfer (corotating or reverse), the optical characteristics of the film vary strongly according to C_a. When C_a is high, an "orange peel" effect or bubbles appear (Figures 8 and 9). This is caused by a resonance phenomenon provoking a wave effect in the liquid solution when it is transferred by the application roller to the substrate. This defect can measure several microns [17] and increases in size when the film is thin and the line speed is high. It is generally agreed that competition exists between the viscosity of the varnish and the surface energy of the surface. This phenomenon is also observed for Newtonian liquids [18].

FIGURE 8

Typical optical defect with a "bulge" appearance.

Optical properties can be improved by increasing substrate surface energy or by decreasing the viscosity of the varnish as much as possible. However, one of the conditions essential to forming a continuous film of varnish at the surface of the substrate is that the latter has a surface energy higher than the surface tension of the liquid varnish, to ensure good wetting of the substrate. Figure 10 clearly illustrates that a critical surface energy is needed to eliminate these defects.

Coating quality also plays a very important role in determining its final properties, but several types of defects are possible, depending on the implementation conditions. They can include lines, pores, irregular thickness, etc. Extensive cracking of thin films may be linked to the internal strain in these fine organic coatings. This strain can also develop over time, either due to age or UV radiation. In addition to the loss of optical properties, aging often provokes delamination between the polymer thin film and the substrate [19,20]. There is also consensus that the film's glass transition temperature (T_g) plays a role in this mechanism, given that polymer chain mobility may facilitate the penetration of various species in the polymer matrix, leading to a loss of adhesion at the polymer/substrate interface. Figure 11 illustrates changes in glossiness for two families of varnish. Polyester varnish demonstrates poorer durability than PVDF under mercury lamp exposure [9].

FIGURE 9

Diagram of the two main appearance defects (bulges and bubbles).

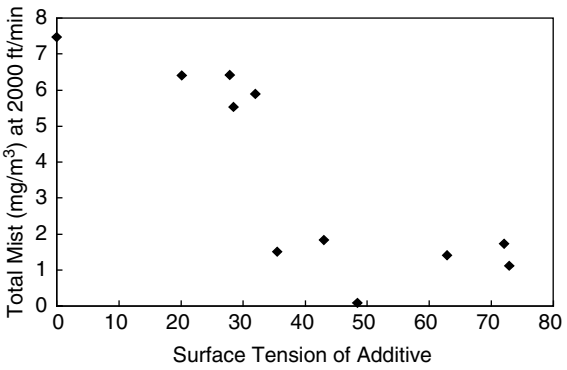

FIGURE 10

Changes in appearance defects according to substrate surface energy for an acrylic varnish on a polyethylene film.

Example: barrier properties

Another property in great demand for thin films deposited in liquid form is protection of the substrate by barrier properties or protection against corrosion. In the previous section, it was shown that the substrate's surface energy plays an important role in determining the optical properties of the thin film deposited. Figure 12 illustrates that surface energy is also important for water vapor barrier properties, obtained by depositing a film of polyvinyl alcohol (PVA) on a paper substrate [21,22]. Applying the corona treatment to the paper before PVA deposition increases the substrate's surface energy, while improving deposition quality and therefore, the water barrier properties [21]. This surface energy activation benefits calendered

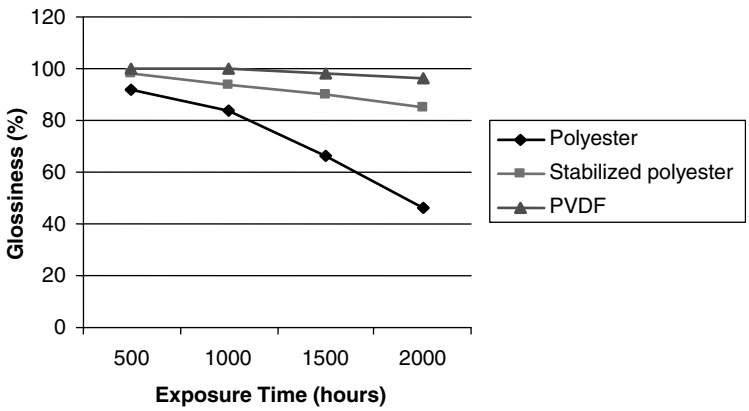

FIGURE 11

Variation in the glossiness of different polymer thin films according to exposure time under a mercury lamp.

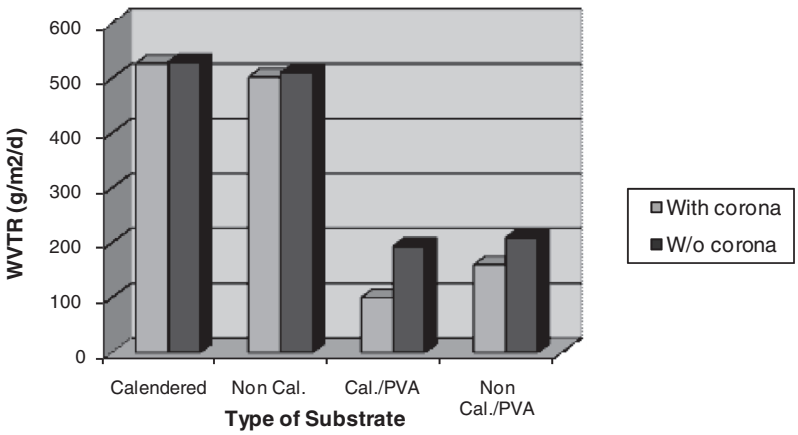

FIGURE 12

Changes in water barrier properties (WVTR) according to the type of paper and its surface treatment (with and without corona treatment). Calendered and noncalendered paper, with and without PVA.

papers as well as noncalendered papers. Note that the substrate's surface roughness also influences the uniform appearance of the film deposited [22].

A new generation of polymer thin films is currently being developed and involves integrating nano-fillers taken from sheet silicates (clays). Much work has been done on these nano-composites made from platelet nano-fillers, particularly in the packaging and automotive industries. These materials, with nanometric stiffeners that are strongly anisotropic (form factor of 200), offer very attractive properties, in terms of mechanical behavior under high temperatures as well as barrier properties, compared to materials with traditional stiffeners (talc, silica, etc.). Used on polymer, metal, and paper substrates, these thin film materials are opening up new possibilities for food-grade and cosmetic packaging, where additional requirements apply in terms of oxygen and odor barriers and resistance to heat and abrasion [23,24]. The industrial development of such impermeable structures, with their enhanced mechanical properties compared to standard thin films, depends on controlling nano-filler dispersion and exfoliation. Figures 13 and 14 illustrate the difference in nano-filler dispersion depending on the type of polymer matrix and the type of the nano-filler.

The filler in Figure 14 is not sufficiently polar and the filler/polymer interactions are not sufficiently strong to allow perfect exfoliation and dispersion of the platelets in the polymer matrix.

Example: sealing properties

Certain polymer thin films deposited in solution offer very attractive sealing properties, especially for substrates such as aluminum foil or paper. For example, Table 3

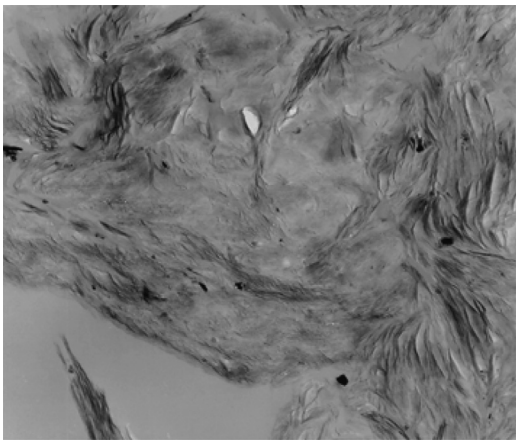

FIGURE 13

Homogeneous dispersion of the filler 2MHBT in a vinyl varnish.

indicates which family of sealing varnishes will be effective based on the substrate, for packaging applications such as seals, pouches, etc.

SUMMARY ON ORGANIC COATINGS

Depositing polymer thin films in solution is a widely used technique for diversifying the surface appearance and functionality of flat substrates. Selecting the binder system for the organic coating is decisive for substrate performance, whether in terms of

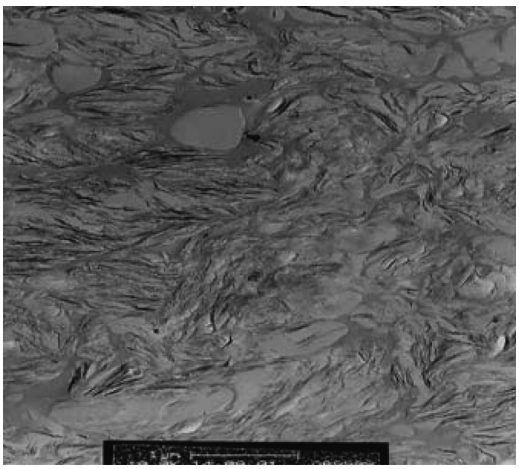

FIGURE 14

Inhomogeneous dispersion of 2M2HT in a vinyl varnish.

Table 3 Families of Sealing Varnish According to Type of Substrate

Varnish Family	Type of Substrate
Acrylic	Film or sheet of polystyrene or bi-oriented polypropylene (BOPP)
Vinyl	Aluminum foil, PVC
Polyester	Polyester, PVC
Modified acrylic on olefin	Film or sheet of polystyrene or bi-oriented polypropylene (BOPP)

appearance, moisture or gas barrier properties, corrosion protection, resistance to photochemical aging, or the capacity to undergo forming without cracking.

Prefinishing technologies offer diverse possibilities for new development, thanks primarily to the following:

- Coatings are constantly being improved;
- New developments in the area of organic coatings and their implementation.

For exterior applications, the use of new-generation flexible organic coatings with high or ultrahigh durability is enabling the development of wet thin films which are affordable and particularly effective. These new thin films meet the requirements of the final application domain and can ensure aesthetic qualities for over 15 years in some cases. In sectors such as household appliances, new, slightly thicker thin films offer better scratch resistance, for example.

It should be noted that other methods of applying organic coatings without a solvent are expanding rapidly, notably radiation cross-linking techniques (UV, electron beam).

VACUUM-DEPOSITED COATINGS

Over the past several years, vacuum deposition techniques have been developed for the industrial manufacture of high-quality products. Some of these techniques can be used in-process (ultrathin films for integrated circuits, magneto-optical films for magnetic discs or tapes, glass coatings for thermal insulation, electrical conductivity, or UV filtering for cars or construction, etc.). The main product objectives are as follows:

- Wide variety of deposition materials: pure metals, metal alloys, oligomers, ceramics.
- Deposits with composition gradients are possible, as well as multilayer deposition.
- Single or double-sided coatings are easy to obtain for various purposes.
- Reduced cost of finished products (productivity, energy, etc.).
- Environment-friendliness (low releases, little material used).

Since the end of the nineteenth century, it has been known that organic compounds in a discharge plasma form a solid deposit. These deposits were initially

considered undesirable by-products and little attention was paid to their properties. It was not until the 1960s that the material formed in plasma was recognized as a polymer and the process was named "plasma polymerization." During its early development, plasma polymerization was considered an exotic method of polymerization. It is now considered an important process for producing entirely new materials. The materials formed by plasma polymerization are very different from conventional polymers and inorganic materials, falling somewhere between the two. This technique is not limited to the production of organic materials, instead opening a broad field of possibilities including metals and inorganic components.

PRINCIPLE OF VACUUM POLYMER DEPOSITION

Generally speaking, there are three components to the technology of dry coating processes:

- A precursor, which can be the crucible in a vacuum evaporator, a bombardment target, or an effluent producer containing one or several precursor gases. The material to be deposited leaves this source in the form of ions, atoms, atom groupings, or molecules.
- A substrate, i.e., the part to be coated and the site of deposition, during which the source species develop progressively (growth), resulting in a more or less well-ordered film.
- An environment, which separates the source from the substrate and is the site of the vapor-phase transfer.

Various deposition methods are used:

1. Physical vapor deposition (PVD), for species produced by a purely physical phenomenon, such as thermal evaporation or ion bombardment.
2. Chemical vapor deposition (CVD), for species produced by a chemical reaction (e.g., reduction of a volatile halide by hydrogen) or by the decomposition of a molecule (hydrocarbon). In this case, the reactions are essentially surface reactions involving heat activation.

PVD, one of the most commonly used "dry" processes for inorganic coatings, includes two methods. The first is sputtering, involving bombardment of a solid to obtain a vapor phase, which is then condensed on a cold substrate to form another compound. The other method is vapor deposition, sometimes called thermal evaporation, which produces inorganic or organic thin films through evaporation of the source. In the case of polymer sources, the source is heated or irradiated. However, the deposition process (PVD) may decrease the molar mass of the resulting film.

CVD is a process in which a thin film is synthesized from a gas phase precursor that undergoes a chemical reaction (decomposition, grafting reaction) at the substrate's surface. These reactions distinguish CVD from physical deposition processes, such as evaporation, bombardment, or sublimation. CVD is a well-known process used to produce high purity inorganic and organic thin films.

This chapter examines chemical deposition, which is very relevant today. Thin film polymer coatings made from precursors using PECVD (plasma-enhanced chemical vapor deposition) are now common and can be found in a growing number of applications [25] (optics, mechanics, chemical protection, nano-systems, microelectronics, etc.). The success of these coatings in surface functionality is related to their high potential for innovation and their "clean" technology, which is environment-friendly with low material consumption.

In PECVD, "cold" plasmas are used because they are very thermodynamically unbalanced ($T_e >> T_i$ and T_n, where T_e, T_i, and T_n are electron, ion, and neutral temperatures, respectively). Plasma is an electrically neutral environment composed of ions, neutrals, radicals, electrons, and photons [26]. The gas precursors are dissociated in a controlled-pressure reactor (from a few millitorr to atmospheric pressure) in which an electrical discharge is applied. This partially ionizes the gas. In these plasmas, the electrons have high kinetic energy (1−10 eV or more); the ions, radicals, and neutrals have lower kinetic energies (around 0.5 and 0.1 eV, respectively). This is the advantage of plasma; the active species are produced in the plasma phase before contact with the surface, allowing the energy of the ions to be controlled when they reach the surface. The numerous collisions between neutrals and electrons generate active species at ambient temperature. This enables treatments on all types of substrate, with numerous reaction paths due to the large quantity of active species created. There are several ways to obtain these plasmas. However, thin film deposition techniques mainly use a capacitive discharge obtained by applying an alternating electrical field between two electrodes. There are three categories of excitation frequency: low frequency discharges (where 20 kHz $< f <$ 200 kHz) resulting in very low density plasma (low electron density), capacitive radio frequency (RF) discharges (where $f = 13.56$ MHz) resulting in electron density of around $10^{10}/cm^3$, inductive RF discharges (where $f = 13.56$ MHz) and microwave discharges (where $f = 2.45$ GHz) for which the electron density is much larger, i.e., greater than $10^{10}/cm^3$.

For polymerization to occur, the precursors must contain atoms capable of forming chains, such as carbon, silicon, or sulfur. Plasma polymerization is very different from conventional polymerization. Chemically speaking, polymerization is the reaction of activated monomers, producing a long repeating chain. During plasma polymerization, the notion of monomers does not really apply beyond the precursor stage. In fact, all the species created in the plasma participate in the reaction. In other words, activated radicals interact at the surface of the substrate and in the plasma, mainly through termination reactions. The terms "plasma polymerization" and "plasma-induced polymerization" are used because plasma produces free radicals and molecules with unsaturated bonds. The structure of the monomer (precursor) is not preserved and the product obtained is more or less disorganized, with variable cross-linking.

The very broad selection of precursors gives rise to a multitude of materials known as plasma polymers.

In summary, the growth of the films obtained by PECVD involves a series of elementary steps:

- Creation of reactive species (ions, excited neutral molecules, radicals).
- Migration of these species to the substrate.
- Absorption at the surface, followed by chemical reactions which produce new species that will form the thin film.

Figure 15 provides a general idea of how these processes work, and details of the various phenomena involved (plasma physics and chemistry, thermal hydraulics, and thermal kinetics of the gas- and solid-phase reactions, role of operational parameters) will not be given here. H. Yasuda [27], H. Biederman [28], and R. d'Agostino [29] provide an excellent overview of these topics. Because this technique introduces numerous interactions between process parameters and thin film properties, a few examples will be presented below.

The deposits obtained with these techniques offer interesting properties which depend on the substrate and the process conditions used. These properties include chemical and mechanical stability (adhesion, hardness, etc.) and optical, electrical, and gas barrier properties. Moreover, it is easy to obtain films with a gradient of chemical or physical properties by modifying the process parameters during the deposition cycle [30]. Numerous industrial machines are capable of processing reels of plastic film, often exceeding 2 m in width, on which they deposit thin SiO_x films,

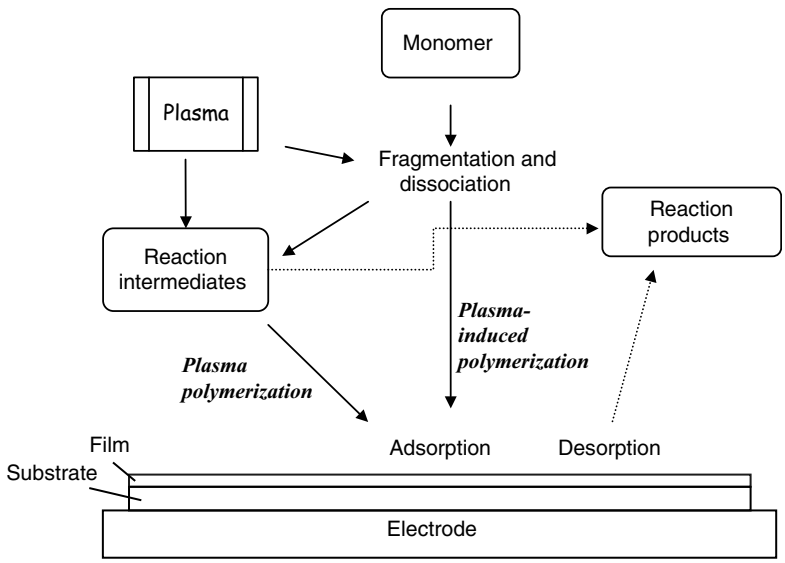

FIGURE 15

Schematic diagram of plasma polymerization.

with thicknesses of just a few dozen nanometers and substrate speeds of more than 100 m per minute.

MAJOR PRECURSOR FAMILIES

By analogy with traditional polymerization, the term "monomer" is also used for the precursor gas that reacts with the plasma. However, this term is inappropriate because there is no growth and no repetition of polymer chains in thin film deposition.

The various categories of common precursors are as follows:

1. **Hydrocarbons**: There is no need to have the traditional polymerizable groups. Thus, ethane, methane, and cyclohexane can be polymerized by plasma but with lower growth rates than acetylene, ethylene, and benzene [31].

Hydrocarbons contain polar groups, which can be used to produce far more polar films than hydrocarbons by themselves. Pyridine and amines are included in this group of precursors. Note that using nitrogen with a comonomer such as acetylene will produce very polar thin films with hydrophilic properties.

2. **Fluorocarbons**: These precursors are cited in the literature very frequently and are used in micro-electronics for plasma etching. However, depending on the precursor's C/F ratio, deposits with very antiadhesive properties may be obtained (e.g., C4F8 with F/C = 2).
3. **Siloxanes**: These are the most used precursors due to their ease of implementation. They include a broad range of siloxanes, silazanes, and linear or cyclical silanes. For example, hexamethyldisiloxane (HMDSO) with the chemical formula $OSi_2C_6H_{18}$ (162 g/mol) is liquid at ambient temperature ($\theta_f = -66\ ^\circ C$) and very volatile (vapor pressure of 56 mbar at 25 °C). With this precursor, polymer deposits containing polysiloxanes ($SiO_xC_yH_z$) or SiO_x can be easily obtained with PECVD by adding oxygen to the gas phase. Figure 16 is a schematic diagram of the molecule and Figure 17 shows its various bond energies.

Adding molecular oxygen to the discharge clearly modifies the composition of the film obtained. The atomic oxygen produced has an etching effect on the carbon compounds in the growing film. At high oxygen levels, this makes it possible to obtain SiO_2 films having practically no carbon.

Table 4 lists the main precursors used in PECVD, with the type of thin films produced and their properties.

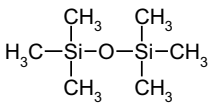

FIGURE 16

HMDSO molecule.

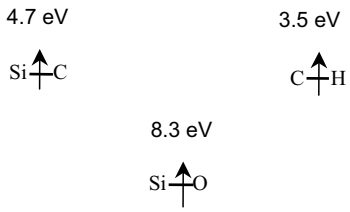

FIGURE 17

Bond energies of HMDSO.

PROCESS PARAMETERS AND INFLUENCES

In recent years and for diverse applications (packaging, electronics, etc.), the development of low temperature deposition of polymer thin films using the PECVD process has experienced very strong growth. Target properties currently include barrier properties [30–34] (oxygen, water, etc.), optical properties, hydrophobic or hydrophilic properties, antiadhesion, and abrasion resistance [35,36].

When the precursor is introduced into the plasma, the deposition rate and the physicochemical nature of the resulting polymer thin film will be affected by the main implementation parameters, such as:

- Excitation frequency of the plasma;
- Driving power;
- Flow rate of the precursor gas;
- Pressure in the chamber;
- Substrate temperature;
- Substrate polarization;
- Dwell time;
- Geometric factors (gas injection point, shape of gas nozzles, reactor dimensions, etc.).

In other words, the properties of a plasma polymer depend on the type of the precursor used, the implementation conditions in the plasma reactor, including its geometry, and the substrate on which the thin polymer film is deposited.

There is not yet complete understanding of the properties of PECVD films (prepared using given conditions and processes), including the range of possible interactions between all the parameters, but various publications describe the key roles of each parameter individually.

In this section, only the well-understood characteristics of polymer thin films will be presented.

Example: barrier properties

Improved barrier properties for plastic or paper substrates are certainly among the most sought-after characteristics. This can be achieved with PECVD thin films. Figure 18 illustrates changes in the moisture barrier of a polyethersulfone according

Table 4 A Few Precursors and the Polymer Deposits Obtained Using PECVD. The Main Properties of the Resulting Films are also Presented

	Surface Energy	**Barrier Properties**	**Porous Films**	**Optical Properties**
Precursors	Siloxanes: Fluorocarbons C3F8, C4F8	Siloxanes, silazanes, tetrafluoroethylene, perfluorobutene, ethylene, etc.	Fluorocarbons, perfluoro-1- methyldecaline, octamethylcyclo-tetrasiloxane, pentafluorostyrene, etc.	Hydrocarbons, fluorocarbons, vinyltrimethylsilane, perfluorobutene, tetrafluorobutene
Polymer thin films obtained	Polysiloxane (SiO_x), Teflon-like films (CF_x)	Polysiloxane (SiO_x), ($SiO_xC_yH_z$), polysilazane (SiN_x), amorphous carbon, Teflon-like films	Tetramethylsiloxane	Amorphous carbon, Teflon-like films, etc.
Target properties	Antiadhesive, wettability, hydrophobic, hydrophilic	Corrosion protection, water and oxygen barrier for plastic, paper and other substrates	Gas separation, permeable membrane	High refractive index, transparency, low extinction coefficient, etc.

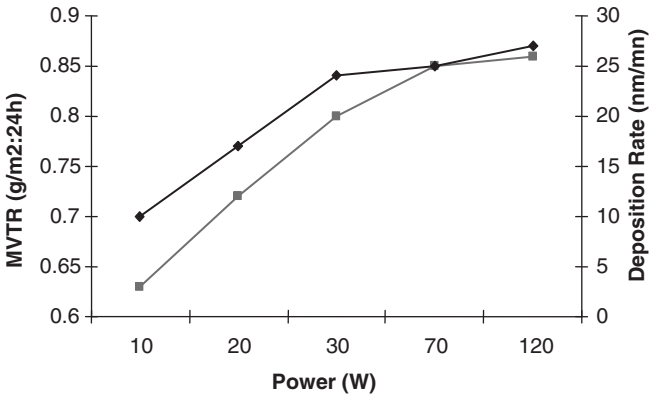

FIGURE 18

Changes in the moisture barrier (MVTR) and the rate of deposition according to the reactor's RF power, for a precursor composed of a mixture (N_2O/SiH_4) [32].

to the power used during deposition. First of all, increasing the reactor's power accentuates disassociation in the gas phase. A higher driving power can increase the deposition rate by creating a greater number of active species. Density saturation may also be observed at higher powers, which suggests that film production is limited by the supply of active species [32,37,38].

Figure 18 illustrates the increased deposition rate of an SiO_2 film obtained from a mixture of (N_2O/SiH_4) as the precursor.

The decrease in the MVTR (moisture vapor transmission rate) is due to the polymer thin film and its very high-internal stress level, resulting in the formation of defects such as pores, micro-holes, and cracks. When power increases, the energy of the plasma generates a significant number of oxygen radicals [39]. The faster deposition rate does not leave atoms enough time to reach low energy sites; this in turn increases the level of etching and, consequently, the surface roughness. In this manner, increased power causes a drop in the moisture barrier (MVTR).

For another commonly used precursor such as the mixture $HMDSO/O_2$, the driving power may have another effect on barrier properties. Figure 19 illustrates how increased power improves the oxygen barrier. This figure also shows that the concentration of silanol groups decreases at higher powers, resulting in better densification of the film. High energies lead to stronger ion bombardment and facilitate the formation of Si—O—Si bridges to the detriment of Si—OH [40].

This barrier property depends not only on the film's chemical nature and the power used during the process, but also on temperature and several other implementation parameters. For example, high substrate temperature generally leads to greater mobility of the species at the surface during deposition, and if there is also pyrolysis of the film, this leads to a decreased rate of growth. However, in both cases polymer cross-linking is increased, which modifies the thin film's barrier properties. For a

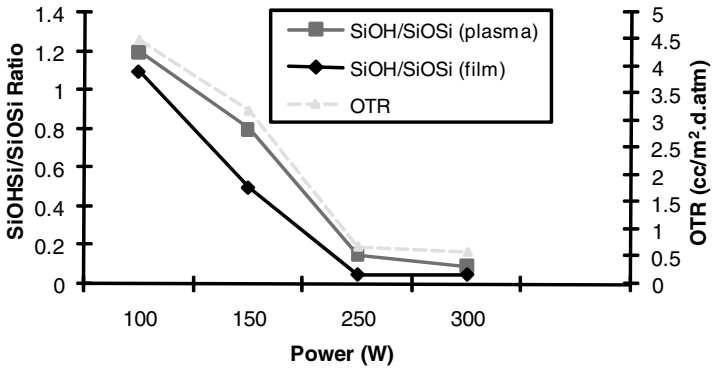

FIGURE 19

Changes in the oxygen barrier (OTR: oxygen transmission rate) and silanol groups, measured in the plasma and on the film according to the reactor's RF power [40].

deposit obtained with the precursor HMDSO, the chemistry of SiO_2 and $SiO_xC_yH_z$ formation at low temperatures differs significantly from that observed at high temperatures. Si—O—Si bonds are dominant at high temperatures, favoring the formation of SiO_2 thin films. In contrast, at low temperatures the formation of Si—OH (silanol) dominates under certain conditions and a great number of these groups can be incorporated in the thin layer obtained, producing a more flexible film with diminished barrier properties [41,42].

Thermal stability is an important parameter to control. Temperature plays a direct role in film thickness; generally, a drop in thickness is observed from a certain temperature, representing the film's stability limit.

Thus to obtain excellent barrier properties, the deposition thickness and the structure (chemical and physical) of the thin film must be perfectly controlled. The limitation of high barrier values, between 0.1 and 0.5 cc/m^2 d atm in the literature, can be explained by these various defects. The general permeation behavior of a polymer thin film system according to its thickness is schematically illustrated in Figure 20. It can be divided into three distinct phases.

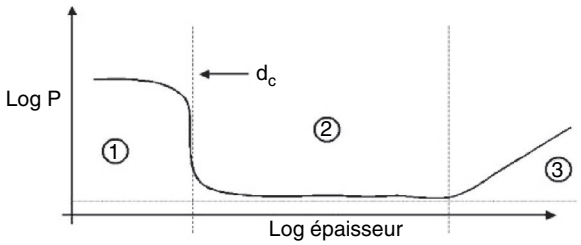

FIGURE 20

Variation in the permeability of the film—polymer system according to the thickness of the barrier film.

PHASE 1

Until the thickness of the barrier film reaches a critical value [43] commonly expressed as d_c, there is practically no barrier effect. This is particularly problematic in certain cases where d_c may reach several nanometers. The value of d_c varies strongly, depending on the type of film deposited and the type of polymer substrate. For example, in the case of PECVD SiO_x on polyethylene terephthalate (PET) using radio frequency this value is 12 nm, whereas for PECVD SiN it does not exceed 8 nm [39].

The following explanation has been proposed for this phenomenon: the substrate is initially coated with patches of material, which coalesce at d_c. In other words, a uniform layer would only be present at this precise time, explaining the drastic drop in P once d_c is reached.

PHASE 2

In this phase, permeability decreases slightly until reaching an asymptotic value that remains nonzero, even though the oxides used as barrier films are impermeable at high molecular weights. A.S. da Silva et al. [39] systematically and statistically demonstrated the presence of defects in PECVD SiO_x coatings on PET [44]. They arrived at the conclusion that a film's barrier performance is strongly correlated to the number of defects, n, it contains (Figure 21), thus proving that performance limits can be explained by the simple presence of holes in the film and the substrate. These defects can have various causes: e.g., coating defect due to an antiblocking agent in the substrate; coating defect due to the presence of a dust particle on the substrate surface during deposition.

PHASE 3

If the film's thickness becomes too great, the barrier effect disappears and permeability increases exponentially. This phenomenon is usually attributed to the

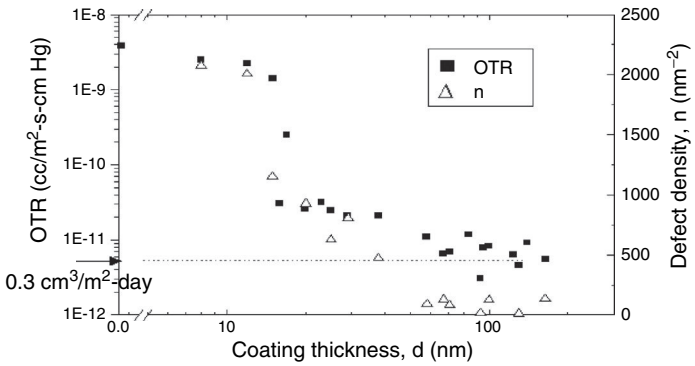

FIGURE 21

Correlation between OTR and the number of defects, n, in a PECVD SiO_x film on PET [45].

mechanical strain present within films. When film thickness is too great, the relaxation of this strain is not plastic; the film then becomes brittle and breaks. Permeant gases rapidly flow through the resulting holes. The thickness at which these breaks appear depends on the substrate, the type of barrier film, and the deposition method. For a system of PECVD SiO_x on PET, this thickness is around 200 nm.

Research in the area of thin barrier films is focusing more and more on developing super barriers whose oxygen permeation must not exceed 5×10^{-3} cc/m^2 d atm. Recently, J. Affino [45] proposed a very strong barrier ($<10^{-5}$ cc/m^2/d) based on the concept of a multilayer organic/inorganic structure obtained using PECVD. This concept of a series of nano-layers is receiving increasing attention and support [46]. A structure with three layers is often proposed [47]: the first polymer layer acts to reduce the surface roughness of the substrate, the second acts as a barrier, and the third serves to protect this barrier layer.

These various examples show that it is difficult to draw a single conclusion on how to control barrier properties. These characteristics are strongly dependent on the precursor type and the PECVD parameters used during the implementation process.

Example: surface properties

Even though the surface properties of the polymer thin film obtained using PECVD depend on process parameters, they are very strongly tied to the chemical nature of the precursor used. Low surface energy is obtained with fluorinated precursors, or with mixtures containing perfluorohydrocarbons or silanes. Surface energy for a hydrocarbon thin film is generally higher than that of a standard hydrocarbon polymer because carboxylic groups often appear at the surface during the deposition process. In contrast, it is more difficult to prepare a very high energy surface using the plasma process than a low energy surface. The reason is that organic precursors, which can be used to make very hydrophilic thin films, have very high evaporation temperatures due to their high polarity molecules and are thus difficult to use as precursors. Those with oxide groups lose a very significant portion of these functional groups during plasma polymerization.

In the literature, several strategies have been employed to obtain superhydrophobic surfaces. Washo describes contact angles close to 170° with PTFE deposited under process conditions (high temperature, high power) leading to the formation of powders. Another approach is to deposit PTFE and use plasma etching to structure the surface so as to obtain a contact angle very close to 170°. A great deal of research is currently under way on the PECVD process conditions necessary to obtain these very hydrophobic films all while structuring the surface [48].

Note that these PECVD deposits can be carried out in a localized manner using a masking technique. Figure 22 shows a surface that has undergone both hydrophobic and hydrophilic treatments [30].

These different localized treatments are very important for applications in biology and micro-fluidics.

The material in contact with physiological substances such as blood or cells has chemical properties that influence the organization of the protein layer, which is

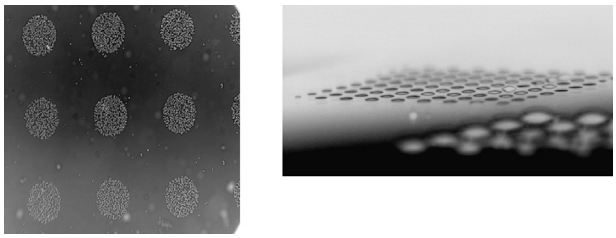

FIGURE 22

Localized hydrophobic and hydrophilic deposits obtained by PECVD with a masking technique.

adsorbed at the liquid/material interface within a few seconds of contact [48]. A good strategy for controlling the morphology and physiology of cells in contact with a biomaterial is to control the adsorption of proteins at its surface. Many applications such as diagnostic tools, implants, etc., call for substrates which are very or totally repulsive with regard to proteins or cells. Deposition techniques have been proposed to obtain polyoxymethylene thin films [49], which may offer antiadhesive properties in relation to cells.

Structured by multiple layers, texturing or by the addition of nano-fillers, these new-generation polymer thin films are currently being developed and will give plastic, paper, and steel substrates high-performance properties.

SUMMARY ON VACUUM-DEPOSITED COATINGS

Polymer thin films obtained by PECVD have a great deal of relevance for various industrial applications today, mainly due to their lower cost. Moreover, their structure is now very well controlled. This has given rise to systems with excellent new chemical and physical characteristics, such as barrier, friction, and hydrophobic properties.

The chemical nature of the precursors and their chemical reaction mechanisms are two significant factors in the vapor-phase deposition process which in turn affect reactor architecture.

Process parameters strongly influence the PECVD process. These parameters, including power, temperature, and pressure, allow modifications to film structure that can be controlled. The resulting properties can be very powerful. Numerous studies have been conducted on how to apply the final materials.

The application areas include packaging, with a focus on high barrier films, as well as steel, where the accent is on corrosion protection or adding properties such as high surface energy. A large number of emerging applications are also incorporating such films. Uses include biological, physical, and chemical sensors along with electronic, molecular, and nonlinear optical systems. Despite multiple studies in this area, these materials have only been successfully used for a small number of electronics and optical applications. This is primarily due to the low thermal

and chemical stability of thin films as well as their weak mechanical solidity. Hence the relevance of creating high-quality polymer thin films for a broad range of technological applications. The next generation of organic flat screens requires drastic encapsulation of their systems, which in turn necessitates jumping at least three to four orders of magnitude in barrier efficiency compared to the requirements of traditional industries such as packaging.

Today these thin films and the associated processes are used for the electronics market. Certain micro-electronics manufacturers, such as Applied Materials, are trying to push these processes to their limits, but when production of 65 nm transistors starts, they may no longer be satisfactory. A competing technology known as ALD (atomic layer deposition) seems very promising. For example, it should be possible to deposit 2 nm barrier films using ALD. Another emerging technology, electrografting, will be a competitor as well. Electrografting is an electrochemical technique. The chemical species present in a liquid bath migrate between an electrode and the part to be coated. Deposition is controlled through the electrical conditions.

CONCLUSIONS

There are various processes for producing polymer thin films, but whatever the deposition process (extrusion coating, wet or dry methods), the properties of the resulting film will depend strongly on the chemical nature of the polymer used. However, the numerous interactions between the process and material parameters significantly influence the final properties. Also it is very important to control the process parameters for maximum optimization of the target properties.

With control of these processes becoming more and more developed, films with an increasingly fine structure can be obtained (e.g., nanometric scale for PECVD). This in turn produces properties with very high performance.

The resulting thin films are used by traditional industries such as packaging and steel, but because there is enormous progress in the area of structure and properties, new emerging markets are focusing on the latest generation of polymer films. There are new products in optics, electronics, batteries, and micro-sources for which precision, multiple layers, and much localized deposition with micro-structures and texturing are required to attain the desired properties.

REFERENCES

[1] Briggs D, Brewis D, Koniecko MB. X-ray photoelectron spectroscopy studies of polyethylene-aluminium laminates. Eur Polym J 1978;14(1):1−4.
[2] Ulren L, Hjertberg TJ. J Adhesion 1990;31(2−4):117−36.
[3] Strälin A, Hjertberg TJ. Adhesion between LDPE and hydrated aluminium in extrusion-coated laminates. J Adhesion Sci Technol 1993;7(11):1211−29.

[4] Fillon B. Optimisation of aluminum/polyethylene adhesion with extrusion coating process. In: Polyethylene Maack business conference Zurich; 1995.
[5] Morris B. Prediction of polymer/metal adhesion. Polym Lamination Coat Conf, Tappi Proc 1996;191.
[6] Butruille JM, Fillon B, Frier JR. Analysis of polyethylene/aluminium adhesion mechanism. In: Proc. of the Eur Congr Appl Surf Interface Analysis, Montreux, 1997.
[7] Brentley B. Coating laminating PFFC, paper, film & foil converter. March 01, 2001.
[8] Morris B. In: Tappiconf., San Diego, Reducing curl in multilayer blown film, Part 1 experimental results, model development and strategies, Part 2 application of predictive modeling to barrier cereal line film, 2001 polymers laminations & coatings conference proceedings. 15 technology Parkway South, Norcross, GA: Technical Association of the Pulp and paper Industry; 2001. p. 112−3.
[9] Schmitthenner M. Eur Coat J 1998;9:618.
[10] Glawe A. Varnish deposition with various processes. In: Coatema Kuntsoffe conf; 2004.
[11] Urban D, Takamura K, editors. Polymer dispersions and their industrial applications. Wiley; 2002.
[12] Hull HH. The theoretical analysis and practical evaluation of roller ink distribution systems. TAGA − Tech Assoc Graph Arts 1968:228−315.
[13] MacPhee J. An engineer's analysis of the lithographic printing process. TAGA − Tech Assoc Graph Arts 1979:237−77.
[14] Benjamin D, Todd J, Scriven LE. Fluid mechanics and transport phenomena multiple roll systems: steady-state operation. AIChE J 1995;41(5):1045−60.
[15] Owens M, Scriven LE, Macosko CW. Technical session 5 − coating technology rheology and process control minimizes misting. In: 12th International coating science and technology symposium Rochester, New York; 2004.
[16] Benjamin D, Carvalho MS, Anderson TJ. Forward roll film-splitting: theory and experiment. In: TAPPI proceedings, 1994 TAPPI coating conference May 1−5, 1994, San Diego, 109, California; 1994.
[17] Bousfield DW, Salminen P, Urscheler R, Roper III JA. Wetting line in high-speed free jet coating. In: 1999 coating conference proceedings, proc. TAPPI coating conference. Atlanta, GA: TAPPI Press; 1999. p. 129−43.
[18] Coyle DJ. The fluid mechanics of roll coating: steady flows, stability and rheology [Ph.D. thesis]. Minneapolis, MN: University of Minnesota; 1984.
[19] Spadafora S, Leidheiser Jr H. Water disbondment characterization of polymer coating/metal substrate systems. JOCCA September 1988;71(9):276−85.
[20] Leidheiser H, Funke W. Water disbondment and wet adhesion of organic coatings on metals: a review and interpretation. JOCCA 1987;70(5):121−32.
[21] Schuman T, Wilström M, Rigdahl M. Coating of surface-modified papers with poly(vinyl alcohol). Surf Coatings Technol 2004;183(1):96−105.
[22] Schuman T, Wikström M, Rigdahl M. The effect of hot calendering of the substrate on the barrier properties of poly (vinyl alcohol)-coated papers. Nordic Pulp Pap Res J 2003;18(1):81−9.
[23] Burgentzle D, Duchet J, Fillon B, Jupin A, Gerard JF. Role of clay/solvent interactions for nanocomposite varnishes formulations, INSA Lyon. Cebal (France) 2003.
[24] Burgentzle D, Duchet J, Gérard JF, Fillon B, Jupin A. Study of clay/solvent interactions for varnish formulations. France: Laboratoire des Matériaux Macromoléculaires, Institut National Des, Sciences Appliquées de Lyon, Villeurbanne, University of Alicante; 2003.

[25] Biederman H, Slavinska D. Plasma polymer films and their future prospects. Surf Coatings Technol 2000;125(1−3):371−6.
[26] Held B. Physique des plasmas froids. Paris: Masson; 1994.
[27] Yasuda H. Plasma polymerisation. New York: Academic Press; 1985.
[28] Biedermann H. Plasma polymer films. London: Imperial College Press; 2004.
[29] D'Agostino R. Plasma deposition, treatment and etching of polymers. Academic Press; 1990.
[30] Fillon B. Polymer very thin film deposition. In: Hanst-007 conference Besançon; 2007.
[31] Morosoff N, D'Agostino R. Plasma deposition, treatment and etching of polymers. Academic Press; 1990.
[32] Wuu DS, Lo WC, Chang LS. Properties of SiO_2-like barrier layers on polyethersulfone substrates by low-temperature plasma-enhanced chemical vapor deposition. Thin Solid Films 2004;468(1−2):105−8.
[33] Creatore M, Palumbo F, D'Agostino R. IUPAC, Diagnostics and insights on PECVD for gas-barrier coatings. Pure Appl Chem 2002;74(3):407−11.
[34] Sahli S, Rebiai S, Raynaud P, Segui I, Segui Y, Wertheimer R. Deposition of SiO_2-like films by HMDSN/O_2 plasmas at low pressure in a MMP-DECR reactor. Plasmas Polym December 2002;7(4):327−40.
[35] Wu Y, Sugimura H, Ionue Y, Takai O. Preparation of hard and ultra water-repellent silicon oxide films by microwave plasma-enhanced CVD at low substrate temperatures. Thin Solid Films 2003;435(1−2):161−4.
[36] Sardella E, Gristina R, Senesi S, D'Agostino R, Favia P. Homogeneous and micropatterned plasma-deposited PEO-like coatings for biomedical surfaces. Plasma Process Polym 2004;1(1):63−72.
[37] Takahashi K, Itoh A, Nakamura T, Tachibara K. Radical kinetics for polymer film deposition in fluorocarbon (C4F8, C3F6 and C5F8) plasmas. Thin Solid Films 2000;374(2): 303−10.
[38] Shirafuji T, Kamisawa A, Shimasaki T, Hayashi Y. Plasma enhanced chemical vapor deposition of thermally stable and low-dielectric-constant fluorinated amorphous carbon films using low-global-warming-potential gas C5F8. Thin Solid Films 2000;374(2):256−61.
[39] da Silva Sobrinho AS, Latrèche M, Czeremuszkin G, Klemberg-Sapieha JE, Wertheimer MR. Transparent barrier coatings on polyethylene terephthalate by single- and dual-frequency plasma-enhanced chemical vapor deposition. J Vac Sci Technol A: Vac Surfaces, Films 1998;16(6):3190−8.
[40] Creatore M, Palumbo F, D'Agostino R. Deposition of SiO_x films from hexamethyldisiloxane/oxygen radiofrequency glow discharges: process optimization by plasma diagnostics. Plasmas Polym 2002;7(3):291−310.
[41] Lasorsa C, Morando PJ, Rodrigo A. Effects of the plasma oxygen concentration on the formation of SiO_xC_y films by low temperature PECVD. Surf Coatings Technol 2005; 194(1):42−7.
[42] Selamoglu N, Mucha J, Ibbotson D, Flamm D. Silicon oxide deposition from tetraethoxysilane in a radio frequency downstream reactor: mechanisms and step coverage. J Vac Sci Technol B: Microelectron Nanom Struct 1989;7(6):1345−51.
[43] Chatham H. Oxygen diffusion barrier properties of transparent oxide coatings on polymeric substrates. Surf Coatings Technol 1996;78:1−9.
[44] Da Silva Sobrinho A, Latrèche M, Czeremuszkin G, Dennler G, Wertheimer MR. A study of defects in ultra-thin transparent coatings on polymers. Surf Coatings Technol 1999;116−119:1204−10.

[45] da Silva Sobrinho AS, Czeremuszkin G, Latrèche M, Wertheimer MR. Defect-permeation correlation for ultrathin transparent barrier coatings on polymers. J Vac Sci Technol A: Vac Surfaces, Films 2000;18(1):149−57.
[46] Affinito JD, Graff GL, Gross ME, Hall MG, Mast ES, Shi MK. Environmental barrier material for organic light emitting device and method of making. US Patent 6,522,067; 2003.
[47] Affinito JD, Gross ME, Coronado CA, Graff GL, Greenwell EN, Martin PM. A new method for fabricating transparent barrier layers. Thin Solid Films 1996;2(290−291): 63−7.
[48] Cicala G, Milella A, Palumbo F, Rossini P, Favia P, D'Agostino R. Morphological and structural study of plasma deposited fluorocarbon films at different thicknesses. Diam Relat Mater 2003;12(10−11):2020−5.
[49] Griesser HJ, Chatelier CR, Gengenbach TR, Johson G, Steele JG. Growth of human cells on plasma polymers: Putative role of amine and amide groups. J Biomaterials Sci 1994;5(6):531−54 [Polymer Edition].

CHAPTER

18 Advanced Inkjet Technology for 3D Micro-metal Structure Fabrication

Seung Hwan Ko

Applied Nano and Thermal Science (ANTS) Lab, Department of Mechanical Engineering, Seoul National University, Gwanak-gu, Seoul, Korea (R.O.K)

CHAPTER OUTLINE

INTRODUCTION

Inkjet printing of functional materials with specific electrical, optical, chemical, biological, or structural functionalities has gained significant interest as an alternative to conventional vacuum deposition and photolithographic patterning methods, especially in the area of low cost, large-area electronics [1–4]. Conventional integrated circuit (IC) processes are multistep, environmentally hazardous, and involve expensive photomask, high-processing temperature, and toxic waste and therefore expensive. Since inkjet printing of functional materials is an additive and data-driven maskless process, material waste can be minimized. Furthermore, easier process modification can be integrated via computer-aided design system [5].

The noncontact and digital process nature of inkjet printing allows three-dimensional (3D) printing of functional materials. Since the material of interest needs to satisfy narrow low-viscosity (1–10 cP) conditions for successful inkjet printing, usually polymer resins [6] such as molten polymer resins, UV or thermally curable photopolymer resins are applied for 3D printing, especially in the area of rapid polymer prototyping [7]. Despite the ease in jetting, polymers have limited applications in the area of electronics due to their poor electric conductance. In this respect, metals are always preferred for high-quality electronics due to their high conductivity. Very few direct metal inkjet printing approaches have been demonstrated so far due to the

Micromanufacturing Engineering and Technology. http://dx.doi.org/10.1016/B978-0-323-31149-6.00018-9

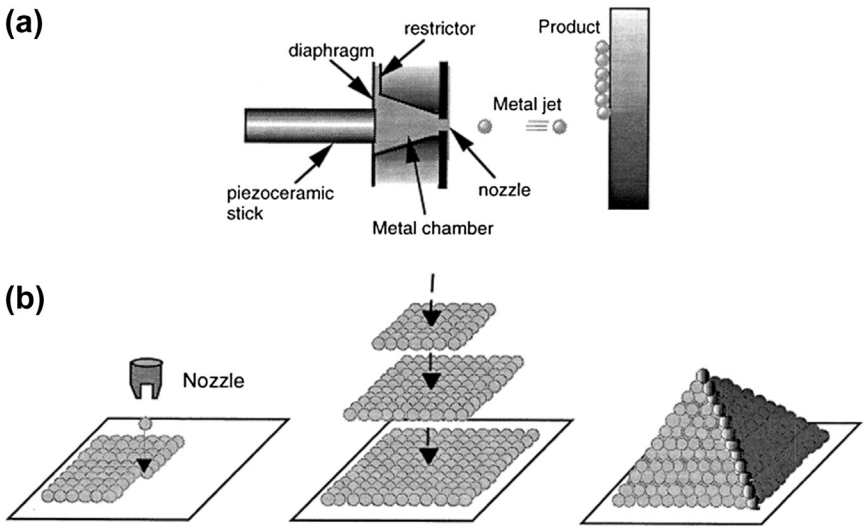

FIGURE 1

(a) Schematic illustration of metal jet nozzle and (b) the principle of modeling by Yamaguchi et al. [8].

high melting temperature of metals. As an approach toward 3D printing of metal components, Yamaguchi [8] first demonstrated 3D metal jetting of molten solder as shown in Figure 1. However, the molten metal jet process is limited in using low-melting temperature solder and needs high-temperature-resistant systems to keep the metal molten during the jetting process [9,10].

As an alternative to molten metal jet, metal nano-particles (NPs) have drawn tremendous interest in the area of low-temperature metal direct patterning by inkjet printing. Metal NPs exhibit low melting temperature due to thermodynamic size effect; for example, 3-nm Au NPs start to melt below 150 °C, i.e., considerably lower than bulk melting temperature (1064 °C) [11]. Metal NPs can easily form a nano-ink with optimum viscosity range for inkjetting and also can form metal structure without driving the processing temperature above the bulk metal melting temperature. These attributes enable metal inkjet printing on a polymer substrate. Fuller et al. [12], Chung et al. [13], and Ko et al. [14–17] demonstrated inkjet printing of 2D electrical circuits and 2D MEMS (micro-electromechanical system) structures by inkjet printing of gold NP ink. Later, by expanding 2D NP inkjet printing technologies were extended to 3D metal structure fabrication by metal NP inkjet printing demonstrated by Ko et al. [18] and Kullman et al. [19].

In this chapter, low-temperature 3D micro-metal structure fabrication by metal NP direct inkjet printing will be introduced. Parametric studies on the basic conditions for stable 3D inkjet printing of NP ink will be explained. Furthermore, diverse 3D metal micro-structures including micro-metal pillar arrays, helical, zigzag, and micro-bridges were demonstrated and electrical characterization will be given as examples. All processing and characterization steps can be carried out at plastic compatible low temperature and in air under ambient pressure.

INKJET PRINTING SYSTEM

Metal 3D micro-structures are fabricated on a glass or polymer substrate by the generation of picoliter sized NP ink micro-droplets using the piezoelectric drop-on-demand (DOD) printing system (Figure 2). DOD inkjet printing system makes picoliter size drops whenever the bipolar voltage is applied to the piezoelectric ceramic crystal surrounding glass capillary tube. This means each drop can be generated with precise time resolution. The complete DOD jetting system is composed of several system units; (1) a DOD inkjet printing unit, (2) an observation optics unit, (3) a mechanical translation unit, (4) a pneumatics and temperature control unit. About 10-mbar vacuum is maintained in the reservoir to prevent NP ink from leaking from the nozzle of the capillary tube due to the small viscosity and low surface tension of the toluene-based NP ink. A wide range of fluids can be dispensed with the requirement that the viscosity has to be lower than 40 cP. Drop volume is a function of the fluid, orifice diameter, and actuator driving parameters (voltage and timings) usually ranging from 50 pL to 200 pL. The operating frequency is limited by the total driving time of the actuator and on the dispensed fluid.

Piezoelectrically driven inkjet head (MicroFab, MJ-SF) with a 50 μm nozzle diameter is used to produce micro-droplets and a bipolar voltage waveform with amplitude of $\pm 13 - \pm 15$ V is applied (Figure 3). Briefly, the first rising voltage expands the glass capillary and a droplet is pushed outside the nozzle due to the falling voltage. The final rising voltage cancels some of the residual acoustic oscillations that remain after drop ejection and may cause satellite droplets. The optimum jetting parameters were found to be 2/40/4/80/2 μs ((A), (B), (C), (D), (E) in Figure 3(b)).

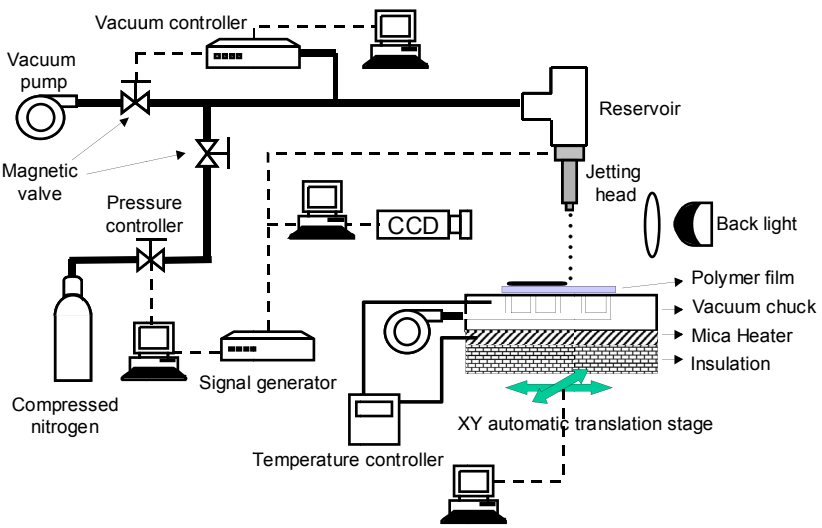

FIGURE 2

Complete Schematics of the Drop-on-Demand inkjet printing system [20].

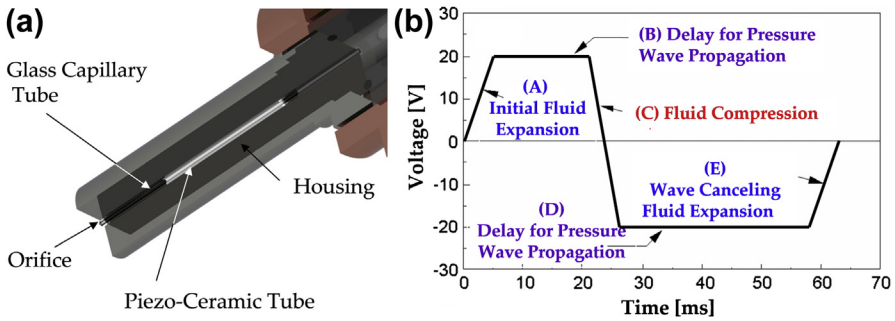

FIGURE 3

(a) Piezoelectric inkjet head and (b) bipolar voltage wave form applied to jet head.

The signal generator used to produce micro-droplets also triggers the CCD camera, so that the CCD captures images at the droplet generation frequency. The CCD camera provides in situ "frozen" transmission images of the droplet to check for satellite droplet generation as well as to measure the droplet velocity and size. After generating stable NP ink droplets of 50−60 μm diameter (i.e., 50−100 pL) at 30 Hz, various structures were made on the substrate by moving a precision translation stage. The gap between the jetting head tip and the glass substrate was maintained at 2 mm (Figure 4).

A vacuum controller and a magnetic valve were connected between the vacuum pump and the reservoir to minimize the loss of toluene due to continuous evaporation. To purge in the case of clogging, pressure-controlled nitrogen gas is used and the purging pressure was controlled at 0.4 psi.

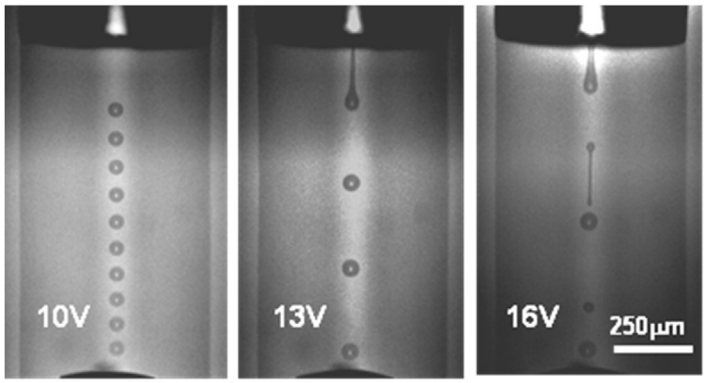

FIGURE 4

Multiple exposure CCD camera images of inkjetting process (2 μs exposures with a 98 μs delay) (50 μm diameter droplet) [20].

The temperature of the vacuum chuck is controlled by a thermocouple and Mica heater to facilitate evaporation of the solvent from the NP ink. Proper solvent evaporation is very important for growing 3D structures via inkjet printing of NPs. Vacuum (300 mbar) is applied through 0.5-mm diameter holes to assure the intimate contact between the heater and the substrate on the vacuum chuck.

Upon finishing inkjet printing, the inkjet printed micro-structure is composed of (self-assembled monolayer) SAM-protected metal NPs. The NP micro-structure has poor electrical conductivity. However, it can be easily converted into highly conductive continuous metal structure by low-temperature heating (around 150 °C). The electrical characteristics were measured in air using a semiconductor parameter analyzer (HP4155A) and a probe station with the micro-positioning manipulators in a dark Faraday cage.

MATERIALS (METAL NP INK)

To exploit the unique characteristics of metal NP ink, SAM-protected Au NPs were synthesized by a chemical two-phase method [21] to obtain 1−3 nm sized NPs and then dispersed in organic solvents (toluene or Alpha-terpineol) to form NP ink with desired low viscosity for inkjet printing. A piezoelectrically driven DOD inkjet head was used to generate stable picoliter NP ink droplets. First, parametric studies to find stable 3D NP inkjet printing conditions were carried out in terms of ink properties (viscosity, surface tension, NP concentration), jetting parameters (signal width, voltage magnitude, frequency), environment (pressure, temperature, humidity). Second, based on optimum 3D printing condition, various 3D metal micro-structures were demonstrated and characterized.

The SAM-protected gold NPs were prepared by a two-phase reduction method reported by Hostetler et al. [21]. Aqueous metal salts ($HAuCl_4$) were mixed in toluene solution containing long-chain alkylammonium surfactants to form a two-phase system. 1.5 g of tetraoctylammonium bromide ($C_{32}H_{68}BrN$) was mixed with 80 mL of toluene and added to 0.31 g of hydrogen tetrachloroaurate (III) hydrate ($HAuCl_4{:}xH_2O$) in 25 mL of deionized water. Vigorous stirring transferred the metal salt $(AuCl_4^-)$ into the organic phase (toluene) and the aqueous phase was removed. A measured quantity of capping agent, a long-chain thiol (hexanethiol), was added to the gold solution while stirring. Then, a reducing agent, sodium borohydride ($NaBH_4$), mixed in 25 mL of water was added into the organic phase over approximately 10 s to nucleate nano-crystals. The mixture reacted at room temperature for three and a half hours. The toluene was removed with a rotary evaporator and the leftover black particles were suspended in ethanol and sonicated briefly. The particles were washed with ethanol and acetone and air dried. Monolayer-protected gold NPs are suspended in toluene or alpha-terpineol at 10% in weight (Figure 5(a)). SAM is critical for NPs because it controls the size of the NPs in addition to enhancing long-term stability and achieving favorable optical properties through Au-thiol chemistry. The size of synthesized NPs is distributed 1−3 nm as measured by transmission electron microscopy

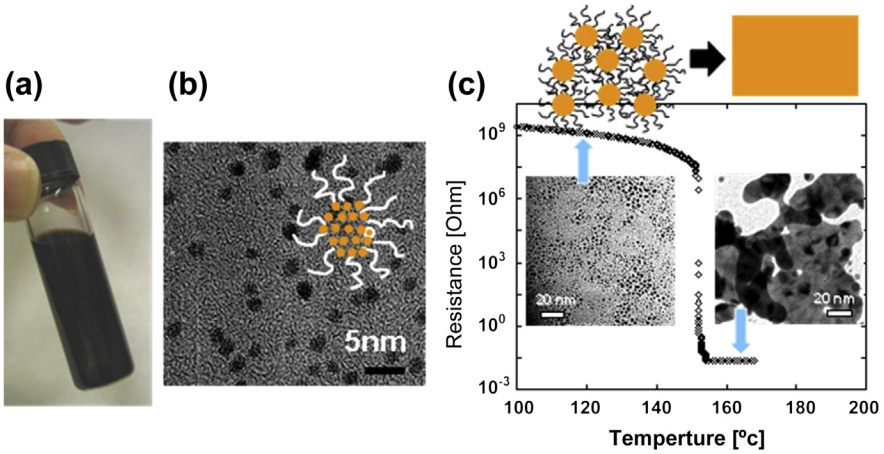

FIGURE 5

SAM-protected Au nano-particle. (a) Au nano-particle ink in toluene solvent. (b) TEM image of SAM-protected Au nano-particles. (c) Au nano-particle melting characterization. Transient resistance change on a hot plate; left top inset and left TEM picture before melting, right top inset and right TEM picture after melting.

(TEM) (Figure 5(b)). The NP melting characteristics were investigated at various temperatures. SAM-protected metal NPs do not exhibit good electrical conductivity despite having highly conductive cores. Electrical resistance (Figure 5(c)) dropped dramatically around 140−150 °C where the individual NPs (Figure 5(c) left top inset and left TEM picture) start to melt and SAM started to desorb and evaporate from the NPs (verified from thermo-gravimetry analysis) to form continuous metal (Figure 5(c) right top inset and right TEM picture).

INKJET PRINTED 3D METAL MICRO-STRUCTURE

Various 3D metal micro-structures could be demonstrated by the modified NP inkjet printing; (a, b) micro-pillar arrays, (c) micro-helix, and (d) micro-zigzag as shown in side view transmission images (Figure 6). The substrate was stationary for a micro-pillar array, rotating for a helix, and linearly translating back and forth for a zigzag while the metal NP ink was jetted at a fixed frequency (30 Hz) on the heated substrate (80 °C for toluene NP ink). The metal NP jetted droplet size was 50 μm with the speed of 1−2 m/s. The printed micro-structure of metal NP had a slightly bigger diameter (50−70 μm) than the original droplet size just after printing. The diameter shrank to 35−40 μm after thermal sintering (Figure 6(b)) due to melting and densification of printed metal NPs. The length of the NP pillar could be grown up to 1 mm at the rate of 10 μm/s depending on the jetting condition. The pillar maintained considerably constant diameter along the length direction.

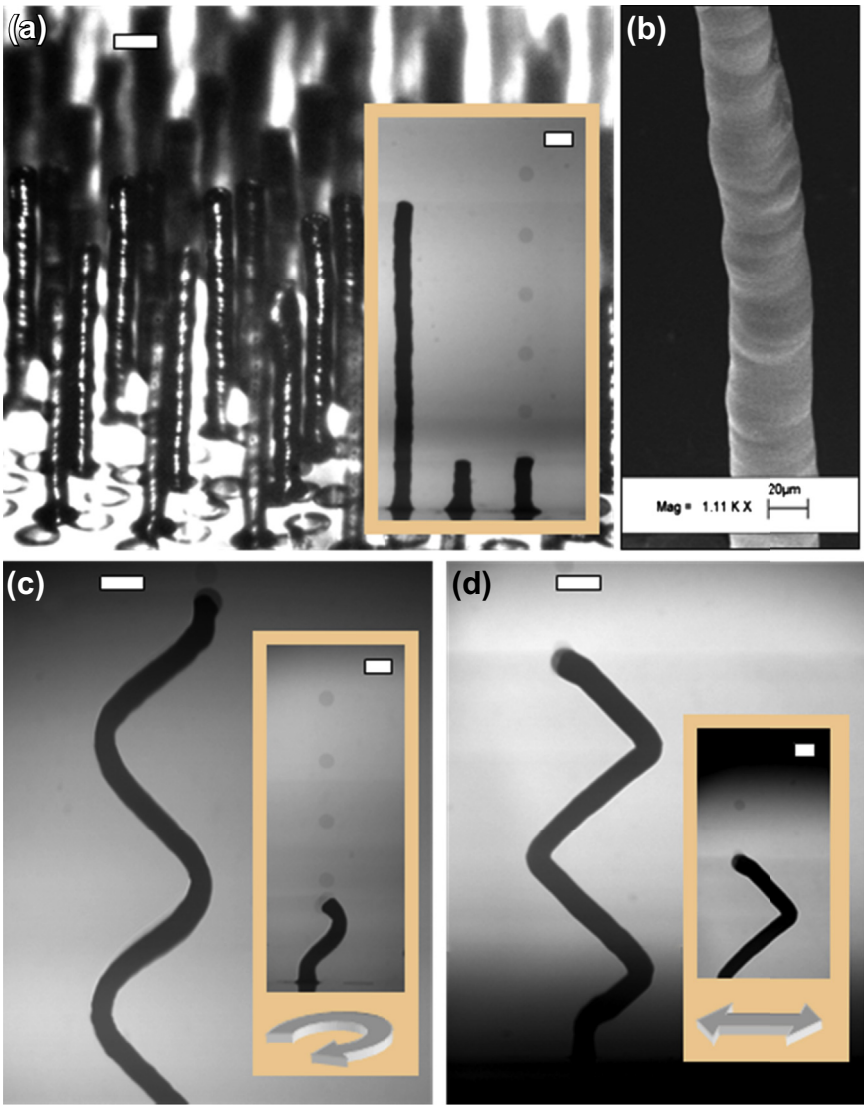

FIGURE 6

Various 3D micro-structures of metal NPs fabricated by the modified NP inkjet printing; (a, b) micro-pillar arrays, (c) micro-helix, (d) micro-zigzag, and (b) SEM picture of micro-pillar. Inset bars are 100 μm [18].

Successful inkjet printing of 3D micro-structures of metal NPs could be achieved within a certain jetting condition range. The basic requirement conditions for successful NP 3D printing are (1) stable jetting droplet generation, (2) sufficient droplet drying before the subsequent droplet arrives, and (3) a stable root initiating the 3D printing. The three requirements are strong functions of ink properties (viscosity, surface tension, NP concentration), jetting parameters (signal width, voltage magnitude, frequency), environment (pressure, temperature, humidity). Those parameters are strongly interconnected. However, the most fundamental inkjet printing parameters are: (1) jetting frequency and (2) substrate temperature. Figure 7(a) shows five regimes examined in searching for the optimum inkjet printing condition. Proper substrate temperature allowing sufficient drying of the NP is essential for successful 3D printing. When the substrate temperature is not high enough, the drying time will be longer. At high jetting frequency, the printed structure will not grow and the drop will just spread on the substrate because the root remains wet when the next drop arrives (Figure 7(a(v))). At low jetting frequency, the drying time may be long enough to grow a 3D structure, but the structure will be fat and short and will also take long time to build (Figure 7(a(iii))). When the substrate temperature is moderately high, the drying time will be short enough to sustain growth of longer 3D structures. At high jetting frequency, a stable pillar may grow on the substrate as a root. However, as the distance from the root increases, the drying time becomes longer. Consequently, the pillar stops growing and forms an accumulation of NP droplets (Figure 7(a(iv))). At the proper substrate temperature and jetting frequency to ensure sufficiently dry NP ink before the following NP ink arrives, a stable and straight 3D structure can be grown (Figure 7(a(ii))). Increasing substrate temperature is the basic requirement for printing 3D structures by shortening the drying time. However, too high substrate temperature also induces instability of the droplet trajectory and ultimately perturbs the jet printing process regardless of the jetting frequency (Figure 7(a(i))). Among the inkjet printing parameters, the magnitude of voltage signal to the piezoelectric material is critical to structure size and growth stability. As the voltage magnitude increases, the NP droplet size and droplet velocity increase, and thus the diameter of the structure increases (Figure 7(b)).

The required substrate heating temperature is dependent on the NP ink evaporation time as shown in Figure 8. Evaporation time varies, depending on the NP ink solvent material. Two organic solvents (Toluene and α-Terpineol) are commonly used to make SAM-coated NP ink due to good solubility. Toluene evaporation time was much shorter than α-Terpineol due to lower boiling temperature ($T_{b,\text{Toluene}} = 110\ ^\circ\text{C}$, $T_{b,\alpha\text{-Terpineol}} = 220\ ^\circ\text{C}$). Via in situ time-resolved droplet measurement technique [22], the evaporation time of 50-μm diameter toluene droplet was determined from 80 ms (at 25 °C) to 6 ms (at 110 °C) and that of α-Terpineol droplet ranging from 150 ms (at 100 °C) to 6 ms (at 200 °C). The jetting frequency should be determined according to the evaporation time for a certain substrate heating temperature. High substrate temperature clearly reduces the evaporation time and offers possibility for high frequency jetting. However, in addition to the jetting

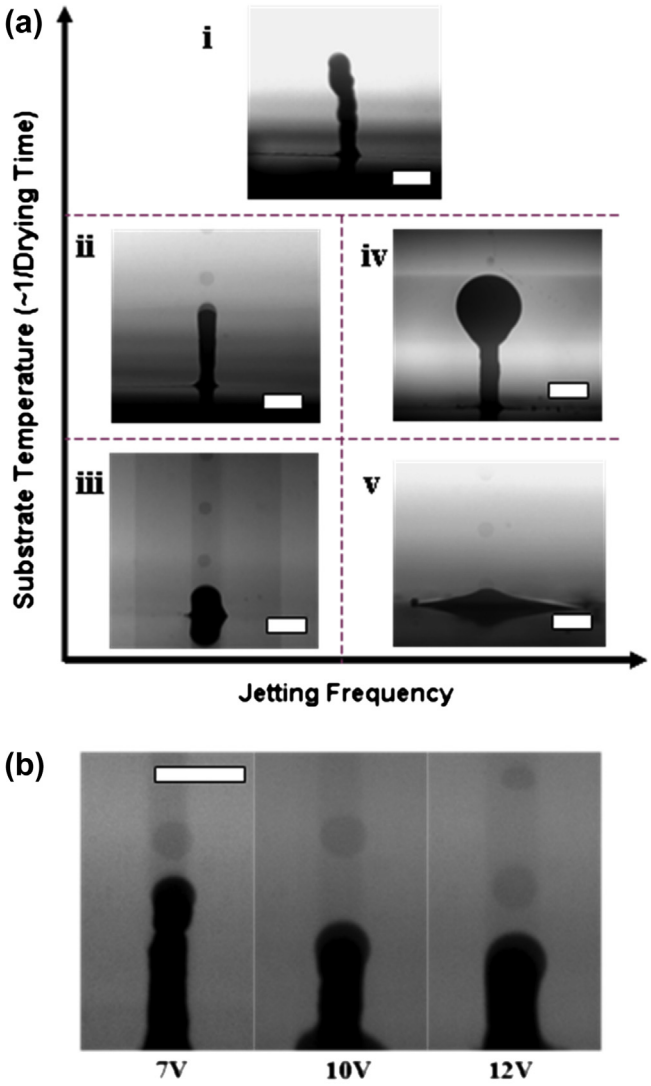

FIGURE 7

Important parameters for successful NP 3D inkjet printing (toluene NP ink). (a) Five regimes for the optimum inkjet printing condition. (b) Jetting voltage signal amplitude effects on 3D printing. Inset bars are 100 μm [18].

instability, a too high substrate temperature (indicated in blue box and red box in Figure 8) causes the so-called Leidenfrost effect and the NP droplet is not deposited on the substrate but instead bounces back away from the substrate and against the direction of incidence. Therefore, the heating temperature should be below the Leidenfrost temperature in order to successfully grow 3D structures. The 3D

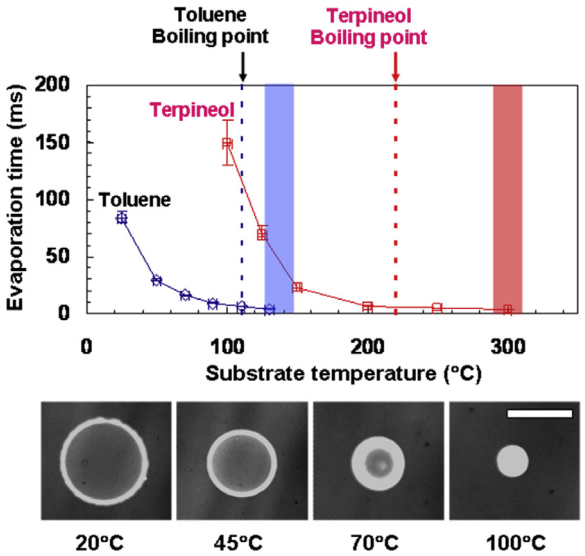

FIGURE 8

Effect of substrate heating temperature. Evaporation time at various substrate temperatures for NP in toluene (blue (light gray in print versions)) and α-Terpineol (red (gray in print versions)) solvent. Bottom pictures are printed toluene NP drops at various substrate temperatures. Inset bar is 100 μm [18].

structures shown in Figure 6 were printed on 80 °C substrate at the jetting frequency of 30 Hz using toluene NP ink to satisfy the drying time requirement. Besides ensuring the drying time requirement for 3D growth, substrate heating suppresses the droplet spreading and thereby reduces the lateral size of the printed structure. Figure 8 bottom inset pictures show the toluene NP ink droplet spreading on a substrate heated at 20, 45, 70, 100 °C. Substrate heating accelerates NP ink drying before the surface tension-driven spreading becomes dominant [22]. Both toluene NP ink and α-Terpineol NP ink could be used for 3D structure inkjet printing, confirming that metal NP direct 3D inkjet printing is possible regardless of the solvent type as long as the optimum jetting conditions are satisfied. However, higher processing temperature for α-Terpineol NP ink induced the instability more frequently than toluene NP ink.

Once the 3D structure starts growing, it will keep growing as long as stable jetting and drying time requirements are met. The drying time condition near the substrate can be easily satisfied by substrate temperature control. However, the temperature will drop as the structure grows due to conduction and natural convection. Figure 9 shows a numerical simulation of air temperature distribution during the jetting. When the jetting nozzle tip was 1.2 mm away from the heated substrate at 80 °C, the air temperature between nozzle tip and substrate was maintained between 60 °C and 80 °C. Within this temperature range, the NP ink evaporation time was

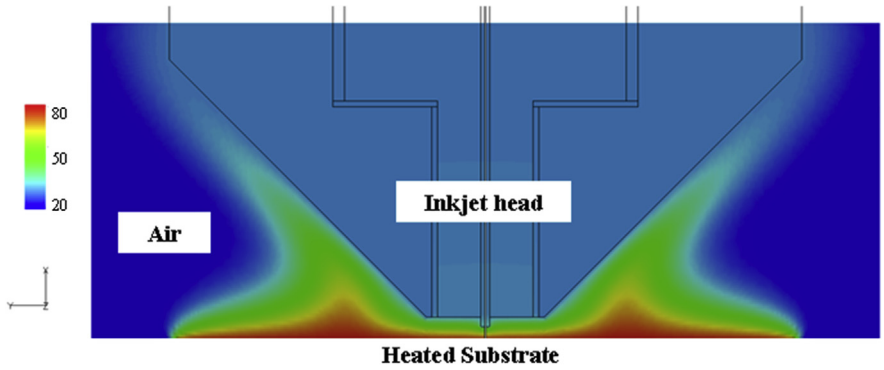

FIGURE 9

Numerical simulation of air temperature distribution due to conduction and natural convection [18].

found to be shorter than 25 ms for a toluene ink, as shown in Figure 8. The 30-Hz jetting frequency for 80 °C substrate heating was chosen to compensate the temperature drop as the structure grows even though 100-Hz jetting frequency is possible for 80 °C substrate temperature (Figure 8).

Based on the developed 3D inkjet printing of metal NP, more complex bridge structure (gable roof shape) was demonstrated. Figure 10(a) shows transmission side view images of the detailed 3D printing process at the jetting conditions stated above. First, a 300-μm vertical pillar grew by inkjetting at the same position, and then the translation stage moved to grow 45° tilted line on top of the printed vertical

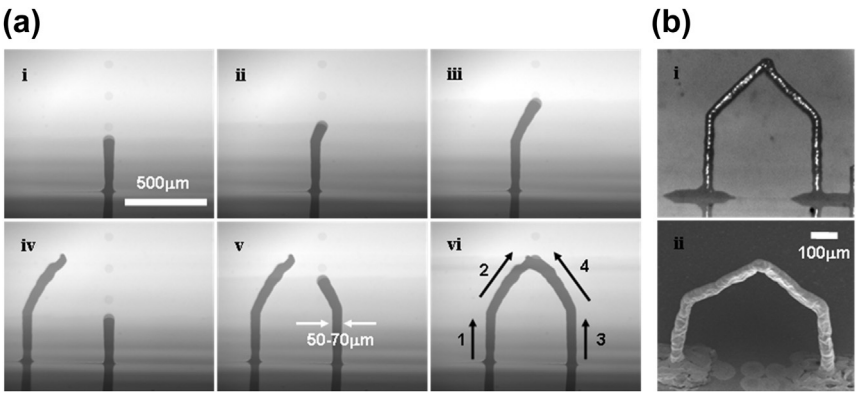

FIGURE 10

Metal micro-bridge interconnector fabrication process. (a) Transmission side view images of the detailed 3D printing process. (b) Optical and SEM images of fabricated metal bridge interconnector [18].

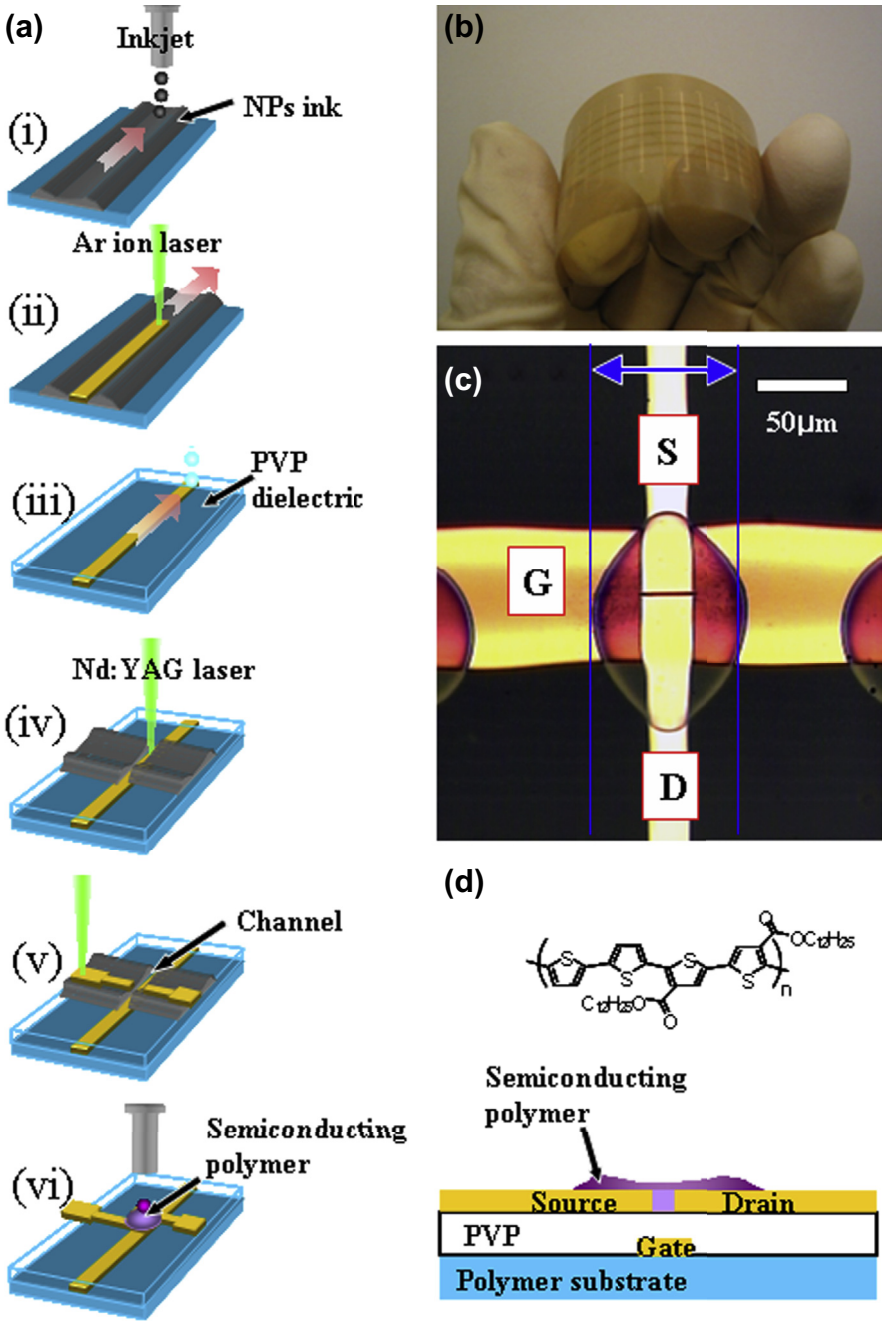

FIGURE 11

Hybrid metal nano-particle inkjet printing with selective laser sintering and ablation to realize flexible electronics [16]. (a) Process steps for the OFET fabrication. (b) Micrograph of arrays of OFETs fabricated on polyimide substrate. (c) Micrograph of an OFET fabricated on polyimide substrate by nanoparticle laser ablation and sintering combination. "S","D", and "G" indicate source, drain, and gate each. Purple circles are inkjet-printed semiconducting polymer. Two blue lines and arrow indicate the edges of an original inkjet printed line. Note how the selective laser sintering can reduce the feature size and laser ablation can obtain very short channel. (d) Schematics of an OFET. Inset shows the chemical structure of polythiophene derivative containing electron-withdrawing substituents.

pillar. Inkjet printing process video image can be found in the reference paper [18]. The other part (mirror image) of the bridge was grown in the same way to complete the gable roof-shaped micro-bridge. The bridge was mechanically stable and strong enough to sustain moderate bending force. The bridge can be easily converted to highly conducting electrical interconnector after low-temperature sintering at 150 °C. The electrical resistivity of the bridge-shaped interconnector was almost as low as the bulk gold resistivity (2.4 μΩ·cm) after the thermal sintering (Figure 10(b)). Good electrical conductivity and mechanical strength may allow implementation of the current process for metallic 3D micro-structuring on heat-sensitive polymer substrates. This is the first demonstration of direct 3D fabrication metallic micro-interconnector at plastic compatible low temperature compared with solder inkjetting above 300 °C [9,10] (Figure 11).

APPLICATIONS/CASES/COST ISSUES

Conventional lithographic processes are well developed for the 2D or 3D patterning of inorganic micro-electronics. However, there are many practical limitations existing in conventional IC fabrication processes that are multiprocess step, involve high-processing temperatures, toxic waste, and are therefore very expensive. Conventional 3D micro-fabrication could be optimized for the small item and mass production. In these days, customers' needs are highly diverse and change very fast. That is why customized small number item manufacturing is getting increasing attention, for example, recent social attention for the 3D printing even though the recent products were mainly limited to polymer parts which are relatively easier to be realized by 3D printer. This material choice can limit the application of 3D printing process. Therefore, metal 3D printing can extend the application to electrical parts with larger functionality such as MEMS devices. The low-temperature essence of the metal NP-based inkjet printing process can be further applied to flexible or stretchable electronics for wearable electronics fabrication.

Since the DOD inkjet printing is an additive process, many problems can be alleviated in a cost-effective manner. The fully data driven and maskless nature of DOD inkjet processing allows more versatility than other direct printing methods. The material is deposited in a carrier solution on the substrate by a piezoelectrically driven micro-capillary tube. This solution processing provides enhanced flexibility for choosing both the depositing material and the substrate. The inkjet process gains these advantages at the cost of the coarser resolution compared with IC process. The resolution of the inkjet process is mainly governed by the nozzle diameter (∼the droplet diameter) and the statistical variation of the droplet flight and spreading on the substrate. The currently achievable minimum feature size is of the order of 50−100 μm. To add more functionality to the metal NP inkjet printing, fast and low-temperature metal NP sintering steps are being developed by many groups such as *Ko* group at Seoul National University and *Grigoropoulos* group at UC Berkeley. Further recent research results and applications can be found their Web site [23,24].

The method can yield a fast, user-friendly and cost-effective manufacturing process appropriate for use in combination with a variety of delicate substrate materials. Besides proving the technological value of this approach, the research done has unveiled many important scientific issues that need to be addressed in order to improve the process. This will greatly facilitate progress extending to many other processes based on the utilization and manipulation of NPs.

REFERENCES

[1] Sirringhaus H, Shimoda T. Inkjet printing of functional materials. MRS Bull 2003;28:802−6.
[2] Burns SE, Cain P, Mills J, Wang J, Sirringhaus H. Inkjet printing of polymer thin-film transistor circuits. MRS Bull 2003;28:829−34.
[3] Zaugg FG, Wagner P. Drop-on-Demand printing of protein biochip arrays. MRS Bull 2003;28:837−42.
[4] Shimoda T, Morii K, Seki S, Kiguchi H. Inkjet printing of light-emitting polymer displays. MRS Bull 2003;28:821−7.
[5] Ko SH, Chung J, Pan H, Grigoropoulos CP, Poulikakos D. Fabrication of multilayer passive and active electric components on polymer using inkjet printing and low temperature laser processing. Sens Actuators A 2007;134:161−8.
[6] de Gans B-J, Duineveld PC, Schubert US. Inkjet printing of polymers: status of the art and future developments. Adv Mater 2004;16:203−13.
[7] Calvert P. Free forming of polymers. Curr Opin Solid State Mater Sci 1998;3(6):585−8.
[8] Yamaguchi K, Sakai K, Yamanaka T, Hirayama T. Generation of three-dimensional micro structure using metal jet. Precis Eng 2000;24:2−8.
[9] Kim HY, Karahalios T, Qiu T, Chun JH. Microsensor for impact of molten metal microdrops. Sens Actuators A 2004;116:417−23.
[10] Lee TM, Kang TG, Yang JS, Jo JD, Kim KY, Choi BO, et al. Theoretical analysis and experimental characterization of DoD metal-jet system. Proceeding KSME A 2007;31:11−7.
[11] Buffat P, Borel JP. Size effect on the melting temperature of gold particles. Phys Rev A 1976;13:2287−98.
[12] Fuller SB, Wilhelm EJ, Jacobson JM. Ink-jet printed nanoparticle microelectromechanical systems. J Microelectromech Syst 2002;11:54−60.
[13] Chung J, Ko S, Bieri NR, Grigoropoulos CP, Poulikakos D. Conductor microstructures by laser curing of printed gold nanoparticle ink. Appl Phys Lett 2004;84:801−3.
[14] Ko SH, Pan H, Grigoropoulos CP, Luscombe CK, Frechet JMJ, Poulikakos D. Air stable high resolution organic transistors by selective laser sintering of ink-jet printed metal nanoparticles. Appl Phys Lett 2007;90:141103.
[15] Ko SH, Pan H, Grigoropoulos CP, Frechet JMJ, Luscombe CK, Poulikakos D. Lithography-free high-resolution organic transistor arrays on polymer substrate by low energy selective laser ablation of inkjet-printed nanoparticle film. Appl Phys A 2008;92:579−87.
[16] Ko SH, Pan H, Grigoropoulos CP, Luscombe CK, Fréchet JMJ, Poulikakos D. All inkjet printed flexible electronics fabrication on a polymer substrate by low temperature high resolution selective laser sintering of metal nanoparticles. Nanotechnology 2007;18:345202.

[17] Ko SH, Pan H, Lee D, Grigoropoulos CP, Park HK. Nanoparticle selective laser processing for a flexible Display fabrication. Jpn J Appl Phys 2010;49:05EC03.
[18] Ko SH, Chung J, Hotz N, Nam KH, Grigoropoulos CP. Metal nanoparticle direct inkjet printing for low temperature 3D micro metal structure fabrication. J Micromech Microeng 2010;20:125010.
[19] Kullmann C, Hotz N, Schirmer NC, Lee M-T, Ko SH, Grigoropoulos CP, et al. 3D micro-structures by piezoelectric inkjet printing of gold nanofluids. J Micromech Microeng 2012;22:055022.
[20] Chung J, Ko SH, Grigoropoulos CP, Bieri NR, Dockendorf C, Poulikakos D. Damage-free low temperature pulsed laser printing of gold nanoinks on polymers. J Heat Transfer-Trans ASME 2005;127:724−32.
[21] Hostetler MJ, Wingate JE, Zhong CJ, Harris JE, Vachet RW, Clark MR, et al. Alkanethiolate gold cluster molecules with core diameters from 1.5 to 5.2 nm: core and monolayer properties as a function of core size. Langmuir 1998;14:17−30.
[22] Lim T, Han S, Chung J, Chung JT, Ko S, Grigoropoulos CP. Experimental study on spreading and evaporation of inkjet printed pico-liter droplet on a heated substrate. Int J Heat Mass Transfer 2009;52:431−41.
[23] Applied nano and thermal science lab. Korea: Seoul National University, http://ants.snu.ac.kr/.
[24] Laser thermal lab, USA: UC Berkeley, http://www.me.berkeley.edu/ltl/.

This page intentionally left blank

CHAPTER

Process Chains and Tooling Concepts

19

Hans Nørgaard Hansen[1], Mogens Arentoft[2], Peter T. Tang[2], Giuliano Bissacco[1], Guido Tosello[1]

Department of Mechanical Engineering, Technical University of Denmark, Kgs. Lyngby, Denmark[1]; IPU Technology Development, Kgs. Lyngby, Denmark[2]

CHAPTER OUTLINE

INTRODUCTION

Miniaturization has been one of the driving forces of technology during the last 20 years. As predicted by Taniguchi in 1983, by now the technology has moved into the nano-processing era and even for precision machining processes submicrometer precision is achievable [1]. This development has been made very clear in the semiconductor industry during the last 30 years, where the number of components on a chip has been approximately doubled each 18 months. This phenomenon is usually referred to as Moore's law. In recent years, the need for micro-mechanical systems has increased, for example, in connection with medical devices such as hearing aids, drug delivery systems, lab-on-chip systems, etc. The consequence is that traditional engineering materials such as metals and polymers are seen increasingly more often in micro-products. This requires the development of industrially viable manufacturing methods to support the demand for components and products.

Micromanufacturing Engineering and Technology. http://dx.doi.org/10.1016/B978-0-323-31149-6.00019-0

Replication methods such as injection molding and cold forging belong to the preferred choice of macro-scale manufacturing methods when the focus is on mass production and high productivity and yield. The same processes are found in micro-scale manufacturing, now typically referred to as micro-injection molding and micro-cold forging [2]. Special focus on size effects, process characteristics, optimization, etc., has been reported in, e.g., Refs [3–7]. However, a basic prerequisite for process realization is the availability of the tools to be used in the process. For example, the tolerances and dimensions of the tools cannot be scaled down directly, since no methods would then exist for fabrication, i.e., to meet the requirements. Consequently, the choice of processes and their integration into coherent process chains becomes one of the major decisive issues in micro-manufacturing.

DEFINITION OF TOOLING

A tool is a component that can be used (preferably more than once) to make other components. Normally the tool will be a durable component with a well-defined geometry, but tools that are only used once can be envisaged, for example, in casting. In most cases, the tool will be used to fabricate a large number of identical components before it is destroyed due to wear, corrosion, and mechanical failure. Tools are essential in replication processes such as hot embossing, injection molding, casting, hot and cold forging, cold forming (punching, stamping, etc.), and so on.

As product features are scaled down, the available technologies for tooling are changed, since traditional tooling technologies such as high-precision milling, die-sinking electrodischarge machining (EDM), wire EDM, etc., have lower limits as to the obtainable dimensions and geometries. New precision tooling technologies for potential micro-forming application have emerged as stand-alone technologies (e.g., micro-EDM milling, laser ablation, etc.) but equally interesting are the possibilities that emerge when processes are combined into new process chains. Figure 1

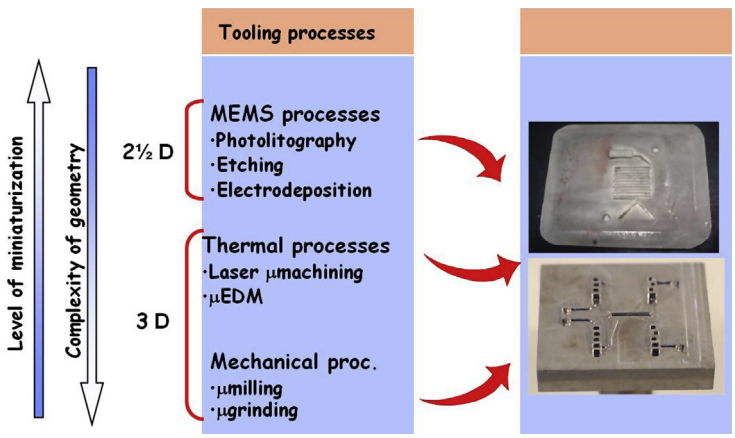

FIGURE 1

Example of mold-making technologies in micro-manufacturing.

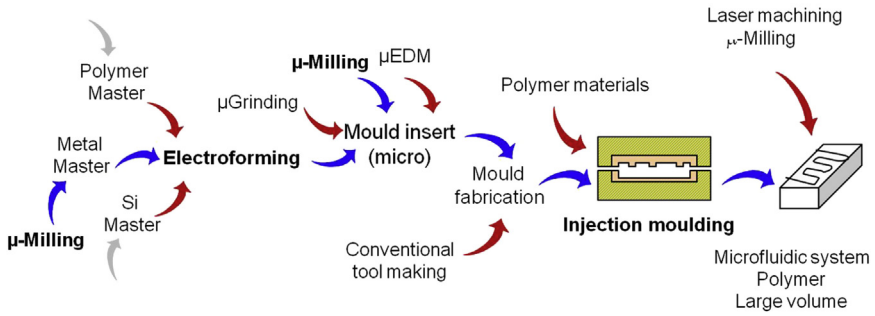

FIGURE 2

Possible process chains for the production of a polymer micro-component.

illustrates possible technology combinations in mold making for micro-manufacturing. Focus is usually given to the production of the part of the mold actually shaping the micro-part, and this is also the case for Figure 1. However, the integration of such inserts into larger tools actually placed into processing equipment (injection molding machines, presses, etc.) is also of great importance.

Hot embossing and injection molding are usually applied for polymeric materials, while casting, forging, and cold forming are applied to metallic materials. In special cases, it is possible to produce ceramic components by replication processes, e.g., the hot embossing of glass components is possible at temperatures of from around 550 °C and above.

DEFINITION OF "PROCESS CHAIN"

In the broadest definition, a process chain consists of all of the process steps necessary to produce the part or product in question. This means that a full process chain starts with design, selection of materials and processes, programing or other preparations of the production equipment, actual machining, quality assessment, cleaning, finishing, and packaging. If the product consists of more than one component, assembly processes are also included in the process chain (Figure 2).

TOOLING CONCEPTS

Utilizing a strictly systematic approach, the possible tooling concepts can be divided into four groups or schemes. The first division is made by identifying the most important shaping process, i.e., the process that creates the shape of the finished tool. This process can either place material on a substrate (additive process) or remove material from a substrate (subtractive process). The substrate is normally a homogeneous material, typically metallic or ceramic (silicon), but it could also be a hybrid material (multilayered, containing particles or fibers,

etc.). The shape of the substrate is typically that of a flat disc or plate, but other simple shapes (rods, spheres, etc.) are also possible.

The second division is made with regards to the way the final tool is obtained. If the tool is fabricated *directly* it is understood that the substrate—after additive or subtractive machining—will become the tool. In the case where the substrate is removed during one of the subsequent steps in the process chain, the tooling concept will be considered an *indirect* one.

Additive processes used in micro-fabrication include the following:

- electroforming
- laser sintering
- physical and chemical vapor deposition
- printing including 3D printing

Subtractive processes used in micro-fabrication are the following:

- milling, turning, or other machining processes
- electrodischarge machining (EDM)
- chemical etching
- electrochemical machining (ECM)
- laser machining/ablation (alternatively, other beam-processing technologies)
- combinations of the above in the so-called hybrid processes [8]

Some of the processes mentioned above require photolithography or other masking methods to define the areas that will be affected (and thus also the areas that will remain unchanged). To a certain extent, lithography can also be considered as belonging to the group of subtractive processes.

The various processes can be combined in almost infinite combinations, but in order to obtain the best and most accurate tooling concepts it is of the utmost importance to consider the various process properties such tolerances and material compatibility (see also Selection criteria for tooling process chains).

MATERIAL COMPATIBILITY

For almost every micro-machining process imaginable, perhaps with the exception of water jet erosion, the substrate or work piece material plays an immensely important role regarding the feature sizes, aspect ratios, surface roughness, and virtually any other property that can be obtained using the process. Table 1 lists some well-known material–process combinations, and some of the typical results that have been obtained in micro-machining.

Although the subtractive processes by far are the most widely used, the additive processes can in a similar manner also provide very different materials properties and results. For some of the additive processes, such as printing and laser sintering, the main geometrical limitations are inherently in the processes themselves. Other additive processes, mainly electroplating (or electroforming) and physical deposition (physical vapor deposition, chemical vapor deposition, magnetron sputtering,

Table 1 Typical Results Obtained Using Selected Subtractive Micro-machining Processes and Materials

Material	Process	Hole Diameter (μm)	Aspect Ratio	Roughness (Ra) (nm)
German silver	Diamond turning	–	–	5
Silicon	Reactive ion etching	10	10	500
Steel	EDM	60	20	500
Aluminum	Milling	50	10	1000
PMMA	CO_2 laser	100	20	2000
PEEK	Excimer laser	20	20	500

EDM, electrodischarge machining.

Table 2 Typical Results Obtained Using Selected Additive Micro-machining Processes and Materials

Process	Material	Hardness (HV)	Aspect Ratio	Deposition Rate (μm/h)
Magnetron sputtering	Copper	90	2	2
Electroforming	Nickel	440	2	70
PVD	TiN	1200	0.5	1
Pulse plating	NiCo alloy	580	3	20

PVD, physical vapor deposition.

etc.) rely on other (subtractive) processes for the definition of the minimum obtainable feature size and other machining properties (Table 2).

For laser-based additive processes the minimum feature size is strongly related to the spot size of the laser beam, which again is interacting with the thermal and optical properties of the material that is being formed (particles sintered together or polymerization of monomers).

Using the physical deposition processes, which are all based on the condensation of materials within a chamber with extreme control of gas flows and pressure, a number of pure metals, alloys, ceramics, and semiconductor materials can be deposited. Even with the best magnetron sputtering techniques, the deposition rate is relatively low. The processes are useful for building entire tools or tool inserts. However, the physical deposition processes are essential for the deposition of hard-wearing resistant coatings, for applying electrically conducting layers on top of insulators and for many other surface-treatment or enhancement steps.

Electrochemical deposition can be divided into two major subgroups, namely electroplating and electroless or chemical plating. The first group uses an external power supply to generate the electrons needed for the deposition of metal, while the second group utilizes a chemical reducing agent to supply the necessary electrons.

Typical deposition rates for electroplating are from 10 to 400 μm/h. The greatest deposition rates are obtained using highly concentrated sulfamate nickel baths for the deposition of nickel stampers for the manufacturing of optical storage discs (CD, DVD, HD-DVD, Blu-ray discs, etc.). Electroless deposition processes, which can be used for the metallization of nonconductors such as polymers or ceramics, are typically at least 10 times slower.

Since electrochemical deposition takes place at relatively low temperature (always below 90 °C, and sometimes even at room temperature), the mechanical properties of the deposited materials can be quite different as compared to the values found for forged or molded parts. This is mainly because the grain size of the deposited materials is smaller, due to the low deposition temperature. Materials with small grain sizes (electroless nickel is considered to be amorphous [9,10]) result in high hardness values and the possibility to reduce the surface roughness of parts machined by diamond turning or micro-milling (Figure 3).

DIRECT VERSUS INDIRECT TOOLING

Figure 4 is a simplified illustration of the four basic process chains for micro-tooling. The result of all four chains is a metallic tool insert, illustrating a simple tool for the replication of a micro-fluidic pattern.

For the indirect process chains, one particular process is common and has some special demands on the choice of materials. Indirect tooling, additive or subtractive, always requires—at some point—the separation of the substrate and the almost-finished tool. A complex tool, with micrometer-sized features and high accuracy, is not easy to separate from a substrate using mechanical methods or brute force. Consequently, the most gentle way to effect the separation is to chemically dissolve the substrate. In this case the substrate material should be one that can be dissolved easily and cleanly, without damaging the surface or structure of the tool. There are other ways to effect the separation, such as melting the substrate, providing a poor but well-controlled adhesion between the substrate and the tool, rapid cooling to enable the differences in thermal expansion to force the two materials apart, and many others.

One of the safest separation processes is to use a simple solution of sodium or potassium hydroxide to secure the dissolution of substrates such as aluminum, zinc, or silicon. This can be done cleanly and effectively without damaging tool surfaces of metals such as nickel or stainless steel, which form a passive layer that protects them from dissolution. In the case where aluminum or zinc alloys are used (typically on account of their easier machinability), the various alloying elements (Cu, Mn, Si, Fe, etc.) may create a layer on the tool surface, which can be difficult to remove [11] (Table 3).

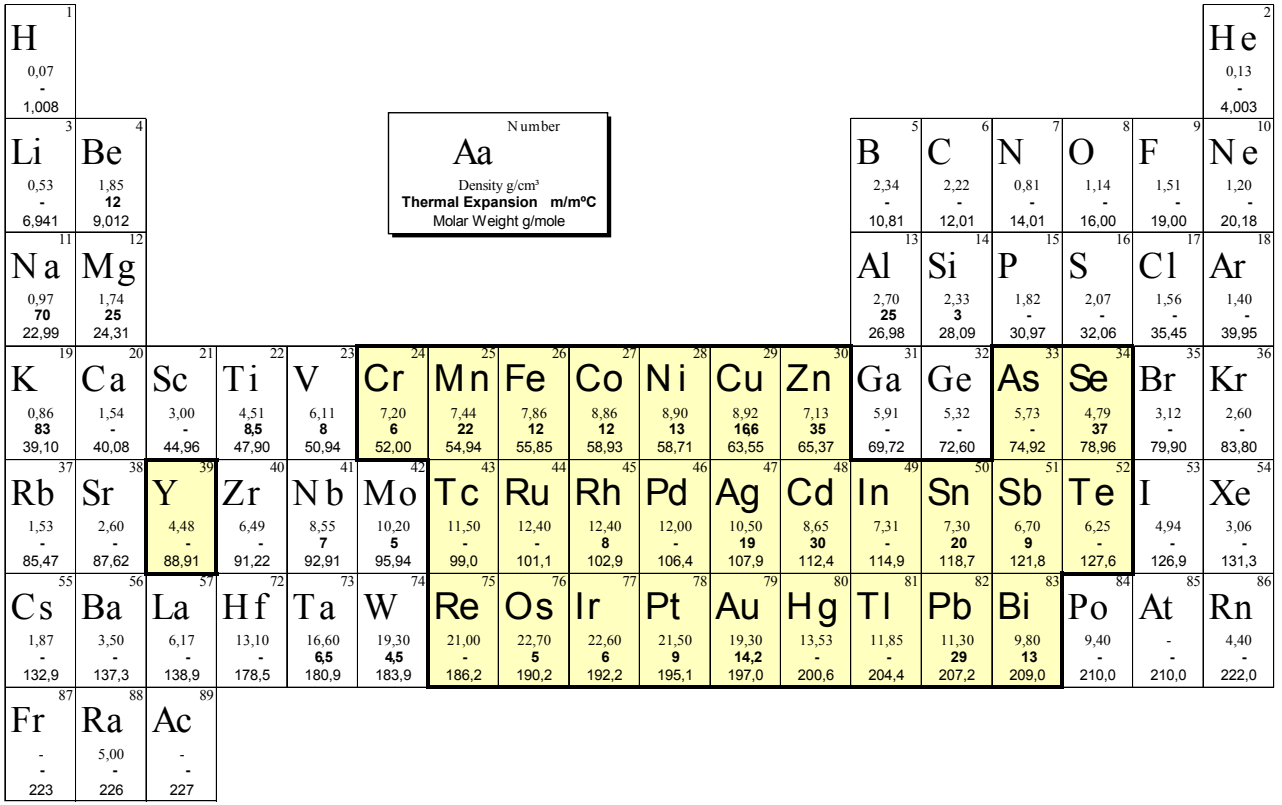

FIGURE 3

Portion of the periodic table of the element showing the elements that can be deposited electrochemically from an aqueous solution [6].

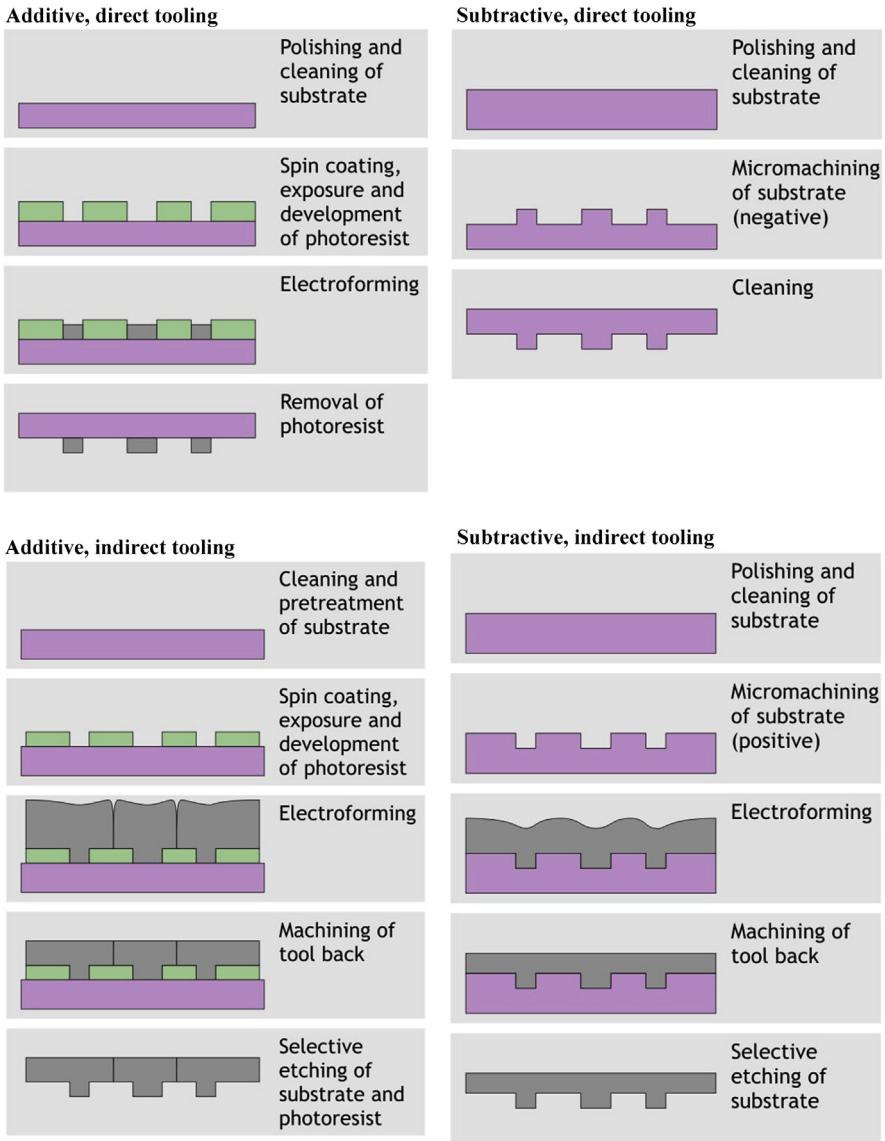

FIGURE 4

Schematic presentation of the four basic process chains for micro-tooling.

Table 3 Chemical Solutions Used in Indirect Process Chains for the Selective Etching of Substrates. Circle Means that the Material Is not Damaged by the Etching Solution, a Triangle Means that the Substrate Is Stained or Mildly Etched and a Cross Means that it Is Heavily Etched (and Eventually Completely Dissolved). In some Cases, the Etching Rate Is Listed in μm/h [6]

Name (Formula)	Concentration (g/l)	Temperature (°C)	pH	Etch Rate (μm/h)									
				Ni	Cu	Au	Zn	Pt	Al	Pd	Cr	Ti	Si
KOH	60	80	>14	O		O	X		X				X
$HCl + HNO_3$		38	<0	X	X	X	X	X	X		X		
$K_2S_2O_8$	25	25		Δ	20	O	X	O	X	O	O	O	O
	25	40		Δ	30	O							
$(NH_4)_2S_2O_8$	25	25		Δ	25	O	X		X	O	O	O	O
	25	40		Δ	35	O							
HNO_3	200	25	0.2	5	X	O		O	X	Δ	O	O	O
HCl	500	25	<0			O	X	O					
NaCN + NaOH	50 + 30	60	12.0	O	X	X	X						X

SELECTION CRITERIA FOR TOOLING PROCESS CHAINS

The focus of this section is on tooling for the mass replication of micro-components in polymers, metals, and ceramics. The tools considered are therefore essentially mold inserts, dies, punches, etc., carrying the negative geometry of the part to be produced. Normally micro-replication processes are used for the mass production of micro-components, with production volumes ranging from several thousands to millions of units. However, it is not uncommon in applications where replication processes are used for prototyping in the product development phase, particularly if the performance of the replication process has a critical influence on the design of the product. Thus the tool requirements will differ substantially, depending on the application.

The main issues influencing the tool requirements are as follows:

- the chosen replication process
- the production volume and thus the acceptable tooling cost
- the material of the replicated part
- the smallest feature size and the complexity (3D surfaces, through-holes, etc.)

For large series production, micro-mold inserts and dies must generally be characterized by high wear and corrosion resistance as well as by fatigue resistance. Except for these general requirements, the characteristics of the tool must match the demands set by the replication process. Hence, while mold inserts intended for polymer replication requires a surface hardness of 300−550 HV, dies for micro-forging will require a hardness of above 1000 HV as a consequence of the greater stresses necessary for the plastic flow of the material.

When a mold is produced for prototyping purposes, the surface hardness of the tool falls to a lower level of priority, while the functional performance of the tool and/or process is the main concern. In this case mold inserts can be made in soft metals or alloys, such as aluminum or brass, simplifying tremendously the manufacture of the tool. The complexity of the mold also influences the tool requirements. Tools with simple geometries and large tolerances are relatively inexpensive. In such cases, in the setup phase of a mass production process, it can be acceptable to change the tool design based on the initial evaluation of the performance of the tool and the process using prototype tools. If, on the other hand, the tool is very complex and the cost associated with producing the geometry is high, redesign iterations must be avoided and the tool will be produced to last for as long as possible, selecting harder materials and setting higher demands on the tool manufacturing processes. Recent investigations on the tool lifetime as a function of coatings have been performed in this area [12]. No significant difference in observed wear was found between uncoated and coated Ni tools. However, some delamination of the coating was observed after 25,000 injection molding cycles.

Once the tool requirements have been defined, a coherent process chain that enables the production of the tool can be selected/defined. It is very important to note that at this point the tool design must not be considered to be rigidly defined. Indeed,

based on the capabilities and limitations of the selected/available manufacturing processes, changes in the tool design are allowed in order to ease or improve manufacturing. The redesign (redesign for manufacturing) must of course ensure that the functionality of the tool and the final part is not compromised.

In many cases one single process will be able to generate the complete geometry of the part according to the requirements. However, in some cases more complex process chains might be chosen, either because they enable relevant improvements in terms of tool performance or simply because the tool cannot be produced otherwise. An important issue in drafting a process chain is the minimization of repositioning of the mold insert in proceeding from one process step to the next. Each time the insert is moved, alignment errors are introduced, reducing the tolerance window available for the individual manufacturing processes.

On the basis of the defined tool requirements a range of materials can be selected for the tool (mold insert, die, punch, etc.). The material must match the requirements in terms of surface hardness and at the same time allow the manufacture of all features within the prescribed tolerances by means of the available processes. In this respect, as seen earlier, it is important to consider that the tool may not need to be machined directly from material having all of the required properties. Indeed, indirect tooling is often a more suitable solution for all those applications where a high surface hardness is not mandatory. Mold inserts for polymer replication show, in general, lower demands in terms of wear resistance and can therefore take advantage of the indirect tooling approach.

Another important point when selecting a tooling process chain is the type of features to be realized and their relationship with the rest of the insert. As many microstructuring processes are based on material removal (e.g., subtractive processes such as micro-milling, micro-EDM, etc.), the lesser is the total amount of material to be removed, the faster will the tool production be completed. Thus when the tool is characterized by small cavities on a relatively large substrate, direct machining of the tool can be an advantage. By contrast, when the tool is characterized by small protrusions that are relatively isolated on a large substrate, indirect tooling is often the best approach, as in this case the machined master (having the opposite geometry to that of the tool) would consist of small isolated cavities on a large substrate (see Figure 5). The two cases considered here represent two extreme configurations, where the convenience of one approach or the other is apparent. There are many intermediate configurations between those two cases, such that the choice of the most convenient approach might not be so evident and other considerations might become determinant. In those cases when additive processes are used for the microstructuring of the mold or master, the convenience of either the direct or indirect approach with respect to features type is obviously reversed.

Tool requirements and thereby the final tool material, the type of geometry, and the type of processes (additive or subtractive) available for the generation of the basic 3D geometry, concur in determining the chosen tooling approach (direct or indirect). At this point the most critical choice regards the combination of the specific 3D structuring processes used to generate the insert geometry and their sequence.

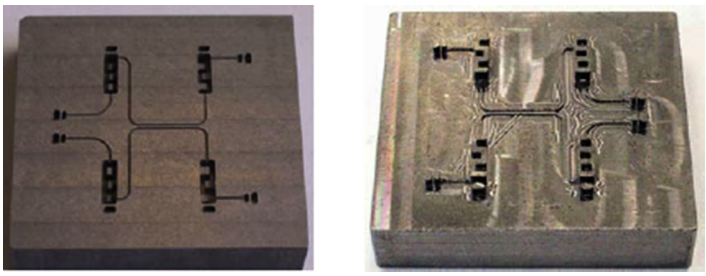

FIGURE 5

Micro-fluidic tooling. Aluminum master geometry for subsequent electroforming (left); hardened tool steel insert (right).

In selecting the tooling approach, an idea of the structuring processes available is of course necessary, as this could be a major limitation and enforce the employment of many of the choices discussed above. The process sequence selection must be compatible with the limitations of the individual processes with respect to machinable materials, machinable geometries, achievable accuracy, minimum feature size, surface and subsurface characteristics. The capabilities and limitations of a number of micro-structuring processes with respect to tooling applications will be discussed later. The sequential order of the micro-structuring processes concurring in the generation of the tool must be defined with focus on productivity, minimization of alignment errors, and compatibility of the succeeding process steps. In fact, subsequent process steps influence each other in complex ways, originating forward coupling (one process step influences the outcome of the following process steps) and backward coupling (one process step influences the features generated by the previous process steps).

APPLICATIONS

APPLICATION 1: POLYMER MICRO-FLUIDICS

Injection molding or hot embossing of polymer micro-fluidic components is a promising area, but also one of the relatively few areas that can already demonstrate real production capability and commercial applications.

Mainly depending on the required production capabilities, the first thing to decide upon is the replication process. Generally, injection molding is preferred for mass production applications, while hot embossing is adequate for smaller series and prototyping. In some cases, unusual requirement such as channels widths of below 100 μm, combinations of wide and narrow channels, through-holes, embedded optics, 3D channeling, etc., can change this general perception, since the two replication processes have their own unique features that might be exploitable for a special requirement (Figure 6).

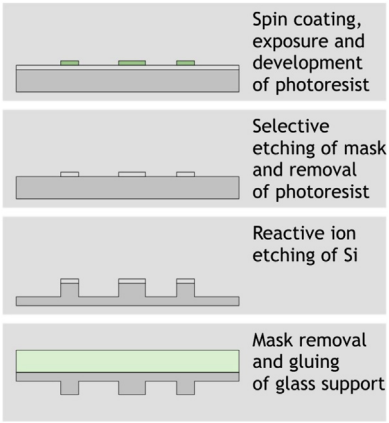

FIGURE 6

Process chain for the fabrication of a silicon embossing tool for the manufacturing of a small series of polymer micro-fluidic components.

A more durable tool, compared to the silicon/glass hybrid illustrated above, is necessary for injection molding. In order to be able to produce a metallic tool, and still be able to have channel widths and other features in the 20–40 μm range, an indirect tooling concept based on EDM and electroforming was reported [13]. Emphasis has also been put on realizing relatively large nano-structured areas in polymer materials. For that clean room-based technologies usually are combined with electroforming and subsequent molding. In this way surfaces with specific physical or optical behaviors can be achieved. Worgull et al. [14] report on such process chains. Furthermore, it has been reported to combine batch chemical processing with injection molding to establish submicrometer features [15]. This has resulted in tools for injection molding comprising nano-patterned micro-structures [16]. Figure 7 illustrates such an approach.

APPLICATION 2: DIE/MOLD FABRICATION FOR MICRO-BULK FORMING

Different tooling approaches were applied and compared on the basis of a cold-forged industrial micro-component as shown in Figure 8. The component consists of a series of different diameters and a non-symmetrical geometry at the top. The largest diameter is 3 mm, the smallest outer diameter is 0.6 mm, and the length is 3 mm. This component is currently fabricated using cutting. Micro-cold forging is highly attractive, since the productivity can be increased up to 100 times using cold forging compared to cutting. The component must be produced using a two-step cold forging procedure [17,18].

Two different approaches were followed in order to manufacture the die. The direct tooling approach includes micro-EDM milling. The chosen tool material is a slice of 8 mm ISO 8020 form B cutting punch made of Vanadis 23 hardened to

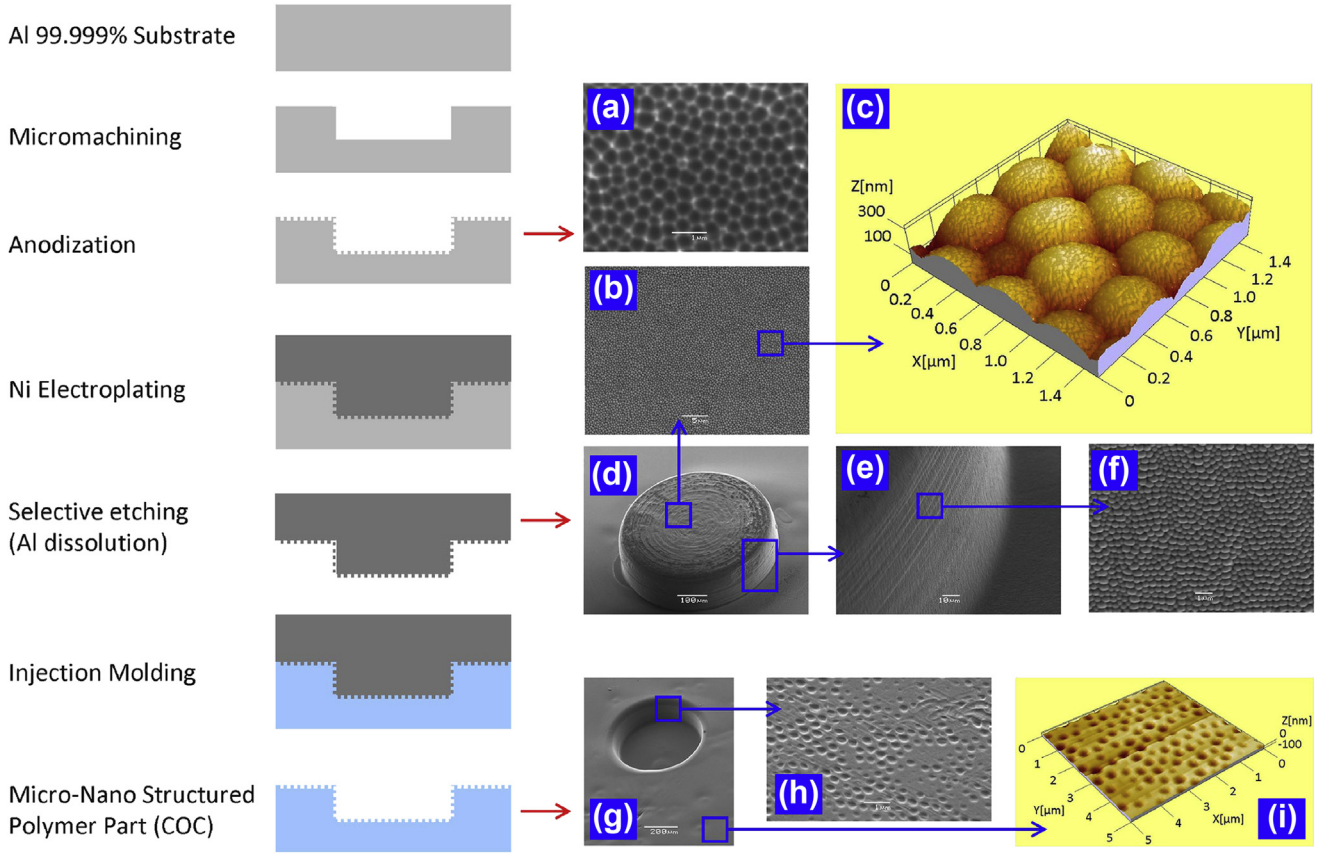

FIGURE 7

Process chain scheme for the manufacturing of metal and polymer large micro-structured areas with nano-surface texturing. (a) Scanning electron microscope (SEM) picture of anodized aluminum surface. (b–f) Details of nickel electroplated surface after dissolution of the aluminum master. (d) 3D micro geometry. (b, c) SEM and atomic force microscopy (AFM) of top surface. (e, f) SEM and AFM of side wall. (g–i) Details of injection molded plastic part. (h, i) SEM and AFM of vertical side wall of micro structure.

Inspired by Tosello et al. [16].

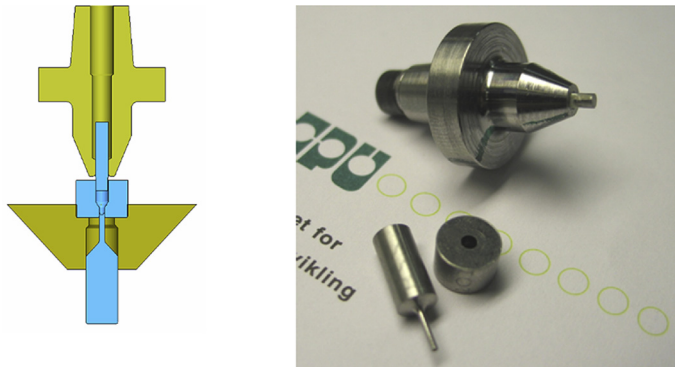

FIGURE 8

Direct Die manufacturing by micro-EDM milling.

HRC62-64. By using micro-EDM milling with a 0.3 mm electrode, the die was machined in less than 1 day. Figure 8 illustrates one of the dies.

In the indirect tooling approach, a cathode of aluminum was machined to an outer geometry similar to the inner geometry of the die. A hard nickel alloy is deposited on the aluminum. Subsequently, the aluminum can be etched away, leaving a die with the required inner geometry (Figure 9). The method has been tested with three different nickel alloys. At present, a die with a hardness of 440 HV25g has been tested in the forging of a lead billet. A die with a hardness of more than 800 HV25g is currently being produced. A qualitative and quantitative comparison of the two molds obtained using the two different methods was performed. A silicone replica of the inner geometry of both molds was taken and analyzed by optical methods (Figure 10). It is seen that the EDM approach yields nonsharp corners, whereas these can be obtained in the indirect approach. Furthermore, the dimensions are comparable and within specification for both methods.

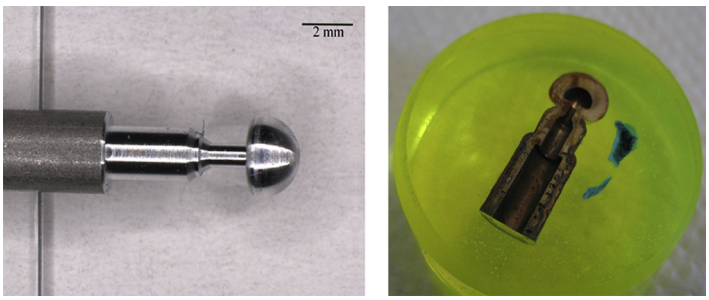

FIGURE 9

Indirect approach for dies for micro-metal forming. Turned geometry (left) and cross section of electroformed die (right).

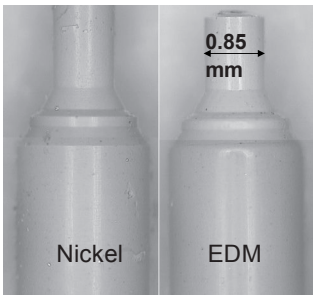

FIGURE 10

Replicas of dies for micro-metal forming.

CONCLUSIONS

This chapter has introduced the concept of tooling process chains for micro-manufacturing. Two main approaches have been described: indirect tooling and direct tooling. The building blocks of tooling process chains can be combined in numerous ways and obtainable dimensions and geometries are depending on specific choices of these building blocks. Selection criteria for tooling process chains were discussed and application examples presented.

REFERENCES

[1] Taniguchi N. Current status in, and future trends of, ultraprecision machining and ultrafine materials processing. Ann CIRP 2003;32(2):573−82.
[2] Alting L, Kimura F, Hansen HN, Bissacco G. Micro engineering. Ann CIRP 2003; 52(2):635−58.
[3] Geiger M, Kleiner M, Eckstein R, Tiesler N, Engel U. Microforming. Ann CIRP 2003; 50(2):445−62.
[4] Vollertsen F, Biermann D, Hansen HN, Jawahir IS, Kuzman K. Size effects in manufacturing of metallic components. Ann CIRP 2009;58(2):566−87.
[5] Theilade URA. Surface micro topography replication in injection moulding. Ph.D. thesis. Department of Manufacturing Engineering and Management, Technical University of Denmark; 2005.
[6] Theilade UA, Hansen HN. Surface microstructure replication in injection molding. Int J Adv Manuf Technol 2007;33:157−66.
[7] Hansen HN, Hocken RJ, Tosello G. Replication of micro and nano surface geometries. CIRP Ann 2011;60(2):695−714.
[8] Lauwers B, Klocke F, Klink A, Tekkaya E, Neugebauer R, Mcintosh D. Hybrid processes in manufacturing. Ann CIRP 2014;63(2):561−83.
[9] Tang PT. Fabrication of micro components by electrochemical deposition. Ph.D. thesis. Department of Manufacturing Engineering, The Technical University of Denmark; 1998.

[10] Tang PT. Electroforming: from rocket engines to nanotweezers. J. Micro & Nanosyst 2011;3(3):180−7.
[11] Tang PT. A method of manufacturing a mould part, WO (PCT) 2006/026989 A1.
[12] Tosello G, Hansen HN, Gasparin S, Albajez JA, Esmoris JI. Surface wear of TiN coated nickel tool during the injection moulding of polymer micro Fresnel lenses. CIRP Ann 2012;61(1):535−8.
[13] Tosello G, Bissacco G, Tang PT, Hansen HN, Nielsen PC. Micro tools manufacturing for polymer replication with high aspect ratio structures using μEDM of silicon, selective etching and electroforming. Microsyst Technol 2008;14:1757−64.
[14] Worgull M, Heckele M, Mappes T, Matthis B, Tosello G, Metz T, et al. Sub-μm structured lotus surfaces manufacturing. Microsystems Technol 2009;15:1327−33.
[15] Tosello G, Calaon M, Gavillet J, Tang PT, Ravn C, Hansen HN. Surface nano structures manufacture using batch chemical processing methods for tooling applications. In: Proc. of the 4th international conference in multi-material micro manufacture 4M, Stuttgart, Germany; 2011.
[16] Tosello G, Calaon M, Tang PT, Ravn C, Hansen HN. Process chain for nano surface texturing of metal and polymer micro structures. In: 10th international workshop on high aspect ratio micro and nano system technology (HARMNST2013) 21−24 April, Berlin (Germany); 2013.
[17] Hansen HN, Arentoft M. Precision tooling technologies for micro forming. In: Proc. of the 2nd international conference on new forming technology, Bremen; 2007. p. 157−65.
[18] Arentoft M, Eriksen RS, Hansen HN, Paldan NA. Towards the first generation micro bulk forming system. CIRP Ann 2011;60(1):335−8.

This page intentionally left blank

CHAPTER

Surface Engineering and Micro-manufacturing

20

Gonzalo G. Fuentes

Asociación de la Industria Navarra, Carretera Pamplona, Cordovilla, Spain

CHAPTER OUTLINE

INTRODUCTION

SURFACE ENGINEERING

Advanced surface technology or surface engineering is a key knowledge-based sector of great relevance for several manufacturing processes and consumer goods production. Surface engineering encompasses those technologies capable of modifying the surfaces of solids to provide them with superior performance or new functionalities.

During recent decades, part of the surface engineering sector has been devoted to the protection of the surfaces of manufacturing tools and industrial components working under severe conditions of friction, wear, oxidation, or corrosion. These phenomena are usually considered as catalysts of surface degradation, and yearly they cause huge production costs mainly related to tool reshaping or replacement, as well as

Micromanufacturing Engineering and Technology. http://dx.doi.org/10.1016/B978-0-323-31149-6.00020-7

component rejection. It is estimated that, in developed economies, surface degradation might cause losses of up to 4% of the gross domestic product (GDP). For the USA, these features represent approximately $280 billion/year. Moreover, other studies estimate that, in Germany alone, the consumption of oil-derived lubricants for wear prevention represents up to $1−2 billion/year [1] for manufacturing industries. In the US only, it is estimated that wear and friction costs exceed $100 billion per annum [2]. Additional costs related to surface protection are those caused by the generation of residues derived from galvanic techniques (e.g., hexavalent chromium).

Surface engineering is facing new and exciting challenges from the advent of micro- and nano-manufacturing technologies, and surface modification processes will have a major role in enabling the industrialization of several technologies in the near future, such as micro-forming, micro-machining, or micro-nano-texturing. Moreover, new and emerging technologies need to find novel functional surfaces which could introduce new products able to outperform those already existing from classical concepts. Some examples are (1) biomaterials, which require advanced techniques for surface biofunctionalization or (2) renewable energy, through the engineering of functional membranes and other functional coatings for H_2 fuel cells.

SURFACE CONTACT PHENOMENA AND TRIBOLOGY

The study of tribology (friction, wear, and lubrication) is a major, ongoing, priority for every manufacturing process. In fact, it is generally accepted in mechanical engineering that numerous failure cases in manufacturing are related to these surface degradation mechanisms. Tribology addresses the contact interactions between two surfaces in relative motion, and the physical−chemical response of such surfaces against the degrading action of the environment. A deep knowledge of the basic mechanisms of friction, wear, and lubrication is a major requirement to better understanding of the benefits of surface engineering and its role in improving the surface performance of tools and components. There exists an extensive amount of literature about tribology in general [3,4] and tribology in micro-manufacturing processes in particular [5,6]. A detailed revision over these studies and the reference therein will provide the reader with a better insight about surface-related failure mechanisms in manufacturing and the strategies for their prevention.

CHARACTERIZATION TECHNIQUES

Understanding the principles of surface functionalities and the strategies for their modification requires the utilization of purposely designed advanced characterization techniques. In fact, a good background on surface characterization enables mechanical engineers to better solve surface-related problems during prototype design, simulation, or process testing. In the specific case of manufacturing tools and component surface protection, the related characterization techniques focus on the chemical composition, the mechanical properties (hardness, fracture toughness, coefficient of friction, wear rate), the thermal−chemical stability (oxidation, corrosion), and the surface topography (roughness, texturing). It is noteworthy to

remark that several of the existing characterization techniques are today approved as validation standards under national and international standardization agencies, e.g., the American Society for Testing and Materials (ASTM) and the International Standards Organization (ISO) (www.astm.com and www.iso.org, respectively).

This chapter aims to provide the reader with a general and concise overview of the *surface engineering* field and its relevance for micro-manufacturing. In the first section, the fundamentals of the most extended advanced techniques for surface modification will be addressed, with special focus on those technologies which, due to their specific characteristics, might be more applicable in micro-manufacturing. The last section addresses different case studies, where surface engineering plays a decisive role.

FUNDAMENTALS OF ADVANCED SURFACE ENGINEERING PROCESSES FOR TOOLING PROTECTION

In this section, different advanced surface modification processes for tooling protection will be overviewed. Surface protection technologies have been developed during recent years in order to accomplish optimal material protection, depending on the environment, the working conditions, and the compatibility between the treatment itself and the substrate material. There exists a large variety of surface treatment techniques which have demonstrated their performance for surface protection or other functionalization purposes, and therefore they are already implemented at industrial scale. In general terms, all surface treatments can be classified within three main categories: *physical–chemical functionalization, mechanical–structural functionalization*, and *surface coating*, as illustrated in Figure 1.

In the case of micro-manufacturing, tools of submillimeter dimensions exhibit special features which limit the applicability of several of these techniques for surface protection. For instance, surface techniques must in this case prevent changes of the net shape of a tool which could reduce its performance or precision. Analogously, treatments carried out at excessive temperatures might degrade the bulk mechanical properties of the tool. In this context, this section presents a series of particular techniques which have proven their effectiveness in protecting small-size manufacturing tools. These techniques are framed within the groups of *physical–chemical functionalization*, including gas and plasma nitriding, ion implantation, and *coating techniques*, including electrodeposition, chemical vapor deposition (CVD), and physical vapor deposition (PVD).

PHYSICAL–CHEMICAL FUNCTIONALIZATION I: THERMAL AND PLASMA NITRIDING

Nitriding are surface techniques to harden the surfaces of several types of cold- and hot-work steels for forming operations. These are high-temperature surface treatments based on the incorporation of nitrogen species into metallic surfaces by

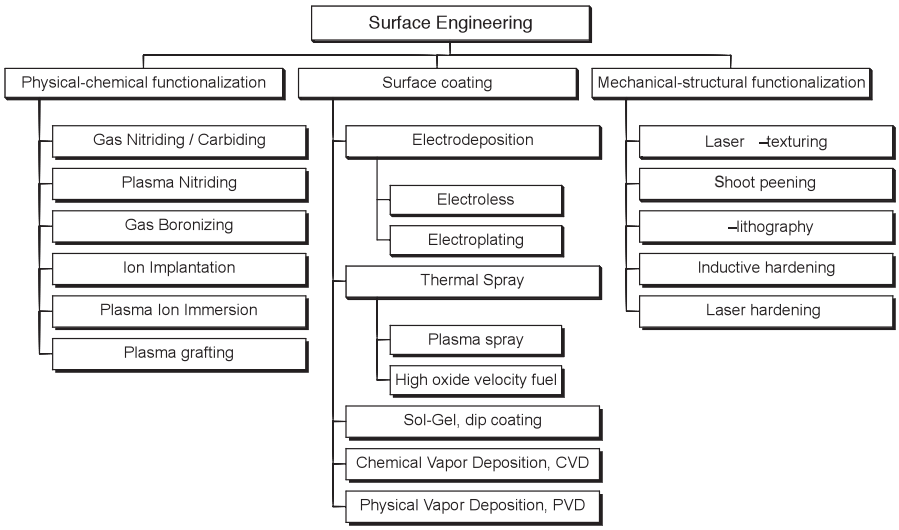

FIGURE 1

Classification of surface modification techniques in terms of physical–chemical functionalization, surface coating, and mechanical–structural functionalization.

different mechanisms of *thermal diffusion* or *plasma-activated thermal diffusion*. Carbon can also be incorporated into steel materials. These processes are denoted as carbiding. The nitrogen diffusion process in steels has two main effects. On the one hand, it induces the formation of a superficial layer (2–5 μm thick) containing hard metal nitrides, such as Al-N, V-N, or Cr-N. The formation of precipitates of these nitrides provides high-alloyed steels with high hardness and toughness. On the other hand, nitriding produces the so-called *diffusion layer* (10–100 μm thick) in which nitrogen atoms occupy interstitial sites in the crystalline lattice of the host metal, producing an induced lattice expansion effect. This expansion is well reported to cause compressive stresses, which leads to superior toughness and wear resistance properties. These effects have already been observed in different metallic alloys such as AISI H11-13 series steels [7], AISI-316L [8], Ti4Al6V [9], V5Ti [10], and others. The nitriding of steels often forms a shallow overlayer of iron nitrides (ε-$Fe_{2,3}N$, γ-Fe_4N, typically), denoted as *white layer*. It is usually recommended to remove such films by mechanical means (sand blasting, polishing) due to their brittleness, which can induce catastrophic crack propagation into the bulk component under normal or shear overloading. High vacuum-based plasma nitriding generally can avoid the formation of the white layer [11].

Thermal nitriding of tool steels requires temperatures above 500 °C and the use of reactive nitriding precursors such as pure N_2 or NH_3. Additionally, processing times could be of the order of 1–2 days to achieve a diffusion layer thickness of some hundreds of microns. Nitriding in molten salts at high temperatures (700–800 °C) is still widely utilized in various industrial sectors.

Nitriding/carburizing can also be carried out in the presence of activated glow discharges containing active species such as atomic nitrogen. The glow discharge activation permits the nitriding of tool steels at slightly lower processing temperatures (i.e., 400−500 °C) due to the larger reactivity of the ionized gases to penetrate the surface-to-bulk barrier of the material. Active screen plasma nitriding/carburizing [12], cathodic arc-activated nitriding [11], or triode plasma nitriding [13] are plasma-activated nitriding processes recently developed, which provide an extended range of solutions for a variety of metal alloys.

PHYSICAL−CHEMICAL FUNCTIONALIZATION II: ION IMPLANTATION

Ion implantation is a surface bombardment treatment widely implemented for tribological applications as well as for other technologies requiring special surface functionalities (e.g., micro-electronics, optics, biomaterials). The technique consists of the bombardment of ionized species and their implantation into the first atomic layers of a solid. Ion implantation essentially requires an ion generation source, an electrostatic acceleration system, and a vacuum chamber for the target housing. Ions are generated by physical means in a discharge chamber, using precursors appropriately converted to the vapor phase. There exist two main operative modes of ion implantation: *charge/mass selective mode* and *linear acceleration mode*. In *charge/mass selective mode*, the ionized species are preaccelerated until they reach a quadrupole magnet working as a charge/mass ion filter. The filtered beam is then postaccelerated and focused onto the target component. In the *linear acceleration mode*, all ionized species produced in the discharge chamber will be accelerated toward the target component. This latter implantation mode is less accurate, as the generated beam may contain some impurities from the different process stages.

The implantation process does not modify the net shape of sharp-edged tool features. On the other hand, ion implantation is a *line-of-sight* technique, meaning that all surfaces under treatment need to be directly exposed to the ion beam, which restricts the applicability of the technique to noncomplex surface geometries. To overcome this feature, new sources of plasma immersion ion implantation are being successfully developed. This technique allows the high energy bombardment of inhomogeneous surfaces with a variety of ionized atomic species.

For hardness-enhancement purposes on metallurgical components, nitrogen ion implantation has been found the most universal solution at industrial scale. Implanted nitrogen species (typically, N_2^+ and N^+) on transition metal surfaces form nitride phases that increase the hardness and toughness of the targeted surfaces. Some examples of hardness and coefficient of friction measurement of Aluminum Titanium, an AISI 316, after nitrogen ion implantations is depicted in Figure 2. In addition, implanted nitrogen induces crystalline lattice expansion at the surface of the bombarded metals. This effect is usually observable by the appearance of new diffraction peaks shifted to lower diffraction angles with respect to those of the original lattice structure. This lattice distortion provokes high compressive stress of the implanted surfaces and hence increases the hardness and toughness.

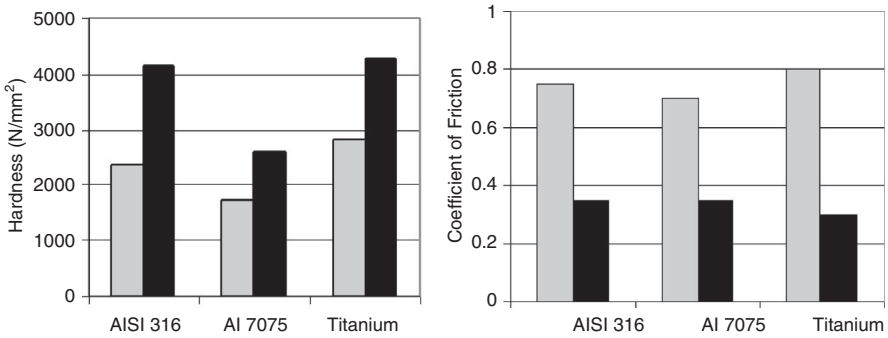

FIGURE 2

(left) Universal hardness. (right) coefficient of friction of three different metallic compounds AISI 316, Al 7075, and titanium before (gray) and after (black) nitrogen ion implantation treatment.

Nitrogen ion implantation increases the surface hardness of several alloyed steels, titanium or aluminum alloys [14], or even some thermoplastics such as polyethylene [15] (PE) and polycarbonate. Moreover, the hardness of Ni alloys can also be increased by the implantation of metal species, such as Cr, Ti, or Al. Finally, the corrosion protection of some alloys is improved upon gaseous and light atomic weight metals implantation.

COATING TECHNIQUES I: ELECTRODEPOSITION

Electrodeposition is a well-implemented technology in the surface treatment sector for its relatively easy installation and high performance. The technique is based on the chemical reduction of metallic precursors and the precipitation of a solid thin film onto the cathode (component) by either galvanic-induced (*electroplating*) or self-catalytic processes (*electroless*). The electroless process exhibits lower deposition rates than electroplating. Conversely, electroless coatings show larger homogeneity than electrodeposited films due to the absence of electric field lines during the process. The deposition parameters which drive the properties of electrodeposited coatings are the electrolyte composition and its chemical stability, the deposition speed, and the surface geometry of the substrates. Hard chromium, nickel, copper, and zinc are typical materials deposited by electrodeposition methods for tooling and component protection.

Hard chromium, produced by the galvanic reaction of CrO_3, H_2SO_4 in the presence of catalyst compounds which produce a metal Cr precipitation, leads to the formation of highly compact, porous-free films exhibiting high hardness and low coefficient of friction (COF). Hard chromium exhibits excellent wear resistance against abrasion and a very low adhesive COF. Nickel is also a widely utilized coating for tooling and component surface protection against wear and corrosion

Table 1 Vickers Hardness and coefficient of friction (COF) for Different Electroplated Engineered Coatings

Coating	Hardness HV	COF[a]
Hard chromium	1300–1500	0.15–0.25
Ni-electroplated	200–500	0.15–0.3
Electroless Ni	800–800	0.2–0.3
Ni-B	1300–1400	0.08–0.2
Ni-P	500–700	0.08–0.2
Ni-PTFE	400–500	0.05–0.1
Ni-W	900–1000	0.15–0.3

PTFE, polytetrafluroethylene.
[a] *COFs measured against chromium steels, using a ball-on-disc configuration.*

that can be precipitated by electroplating and electroless methods. Nickel is additionally used as a base material for electroformed tools, e.g., micro-embossing or micro-plastic injection molds. Ni-electroplated films show high hardness (see Table 1) and low COF, achieving efficient antiwear properties. Moreover, this material shows excellent protection against corrosion.

Electroless nickel-M (where M can be an atomic, molecular, or micro-particle additive) might show excellent antiwear properties and low COFs. Ni-phosphor and Ni-boron exhibit a hardness between 500 HV and 1300 HV. Ni-Teflon (Ni-PTFE) exhibits a very low COF in combination with hardness values of around 500 HV.

COATING TECHNIQUES II: CVD

CVD is a vacuum-plating technique by the precipitation reactions of gaseous precursors onto a given surface. Depending on the temperature and the presence or absence of plasma assisting processes, CVD can be classified into *thermal CVD* and *plasma-activated CVD* (PACVD).

In thermal CVD, the surfaces should be kept to temperatures of between 800 and 1000 °C, hence limiting the type of materials suitable to be coated by this technique due to thermal degradation effects. In fact, the high temperatures reached during CVD cycles often produce size distortions of the tools. A typical thickness of thermal CVD coatings for tooling protection could vary between 5 and 20 μm depending on the specific application and nature of the deposited material. Thermal CVD films exhibit very high adhesion strength, due to temperature-induced atomic diffusion at the coating/substrate interfaces. This fact converts thermal CVD into a recommended technique to be applied to tools subjected to strong normal and shear forces (cold/hot forging, metal forming). In addition, CVD coatings show low residual stresses and hence greater toughness and fatigue resistance.

The most commonly utilized coating materials for tooling protection are titanium nitride (TiN), titanium carbon nitride (TiCN), and chromium nitride (CrN). Other transition metal carbon nitrides such as hafnium or vanadium can be deposited by CVD, showing a good combination of hardness and low COF.

An alternative to thermal CVD is the plasma activation of the precursor gases, which can promote precipitation of dense thin films, even at deposition temperatures as low as 200−300 °C, which limits the size distortion effects on steel tools. These processes are named *plasma-activated CVD* (PACVD) [16] and represent a feasible alternative to deposit films onto a larger variety of substrate material. Other CVD activating processes can be found in the literature, such as hot-filament-assisted CVD, hollow cathode CVD, or microwave RF PACVD.

CVD is a well-implemented coating technique to deposit low friction carbon-based films containing different ratios of sp^3−sp^2 carbon−carbon bonds [17].

Highly containing sp^3 carbon films are usually known as polycrystalline diamond which is produced by high temperature CVD and it exhibits hardness close to this of natural diamond. Diamond-like carbon films (DLC), in its different forms ta-C; a-C; or H-terminated DLC, are low COF coatings (as low as 0.1 against bearing steels) used in automotive and machinery industry as an energy saving vector in power trains, bearings, cam shafts, and other elements. DLCs have high hardness (1500−3000 HV). DLC can be deposited even at relative low temperatures of around 300 °C with high adhesive strength using adequate bonding layers. Presently, silicon-based films produced by PACVD are predeposited to enhance the adhesion of DLCs on steel and hard metal substrates.

COATING TECHNIQUES III: PVD

PVD is a high vacuum coating technique used for tooling protection as well as for several technological applications (optics, photovoltaic conversion, decorative). PVD deposition is the result of producing a vapor stream in-vacuum from a solid material (usually named the *target*) by physical means (arc discharge, sputtering, heat transfer by laser or electron beams, etc.). *Cathodic arc evaporation* (CAE), *magnetron sputtering* (MS), and *electron beam* (EB) at the present time constitute the core group of PVD techniques for industrial tooling protection. In fact, there exists a great variety of PVD techniques, but those of the core group alone share more than 95% of the PVD market, in terms of both equipment sales and services.

CAE sources are probably the most widely utilized technique for industrial tooling protection. In CAE, a high electron current density is discharged onto a target material, producing a fast evaporation rate at its surface. The energy dissipated during the process sprays the evaporated atoms toward the substrate at energies of tens to some hundreds of eV (refer to Figure 3). This feature, and the high ionization produced during the electron discharge (up to 90% of the evaporated species), produces uniform and dense films, with compressive residual stresses. The deposition of metal compound films can be obtained by introducing reactive gases such as N_2, O_2, or C_2H_2 during the discharge process.

Part of the energy dissipated on the target surface during CAE is able to produce micro-sized particles (*micro-droplets*) that can also be sprayed toward the substrate. In general, these micro-droplets are barely detrimental for conventional machining tools provided the net shape of cutting edges remains unchanged upon deposition.

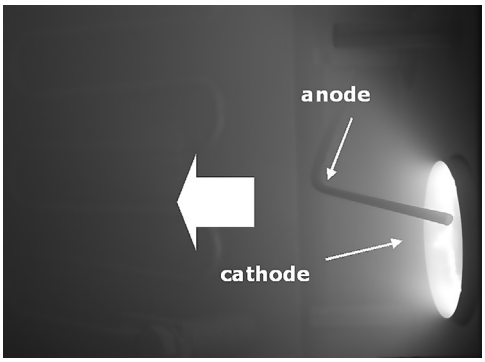

FIGURE 3

The reactive cathodic arc discharge physical vapor deposition working. The anode tip is a high temperature resistance metal alloy rod located near the surface of the target (glowing part of the photograph). The presence of ionized nitrogen provokes the red-like glow. The arrow indicates the vapor stream direction from the cathode.

The presence of these micro-particles, however, can be strongly detrimental for precision tools. In these cases, a surface repolishing process needs to be performed after a PVD CAE treatment. To avoid an excessive deposition of micro-particles, different arc sources design strategies are in use, such as the *lateral arc rotating cathode* configuration or the filtered arc.

MS sources are based on the confinement of a low pressure plasma around an evaporation target by an appropriate configuration of static or alternating electric/magnetic fields. The confined plasma bombards the target material, producing the sputtering of atoms from the target toward the substrate. The energy of the sputtered atoms is usually not greater than a few eV, and their ionization rate is generally poor (below 5% of the total sputtered atoms). Both factors, low ionization and energy, make necessary the postionization and acceleration of the sputtered species in order to achieve sufficient impact energy during the deposition process. This can be accomplished by polarizing the substrate with a negative potential (bias potential) of some tens of volts. Under these conditions, the deposition of sputtered atoms is produced simultaneously to the bombardment of ionized inert species (typically Ar ions) onto the growing film. This combined process, the so-called *ion beam-assisted deposition*, provides sufficient energy per arriving atom to form dense and well-adhered films. The ionization and energy of the sputtered atoms can also be increased using high power impulse magnetron sources (HIPIMS) [18]. HIPIMS utilizes high energetic electromagnetic megawatts/cm^2 millisecond pulses during the sputtering process to achieve ionization rates of almost 100% of the depositing species.

Sputtering techniques are able to deposit *low friction* coatings or *solid lubricant*. This family gathers the Me:C [19] coatings, where Me is a metal and C represents a variety of carbonaceous phases present in the film. In addition, MoS_2 or WS_2 low

COF films can also be deposited in the form of thin film by sputtering techniques (see Table 2).

Electron beam evaporation is based on the heat generated in a target material by the bombardment of an electron beam onto its surface. The technique retains the same principles as that of CAE and sputtering, in terms of vacuum process, coating thickness, reactive deposition, etc. Electron beam deposition is, in addition, currently used in industrial applications due to the surface finish properties achieved, along with good mechanical properties, such as those presented in Table 2. Plasma activation systems of the vapor stream are reported to contribute to the achievement of dense film growth, increasing hardness and toughness properties. A scheme of a *hollow cathode arc-activated deposition* is shown in Figure 4, the trajectory of the electron beam from the source to the target, and the plasma activation area, are indicated on the right of this figure.

The main application of PVD coating for mechanical engineering is in machining/cutting tooling protection against wear, overheating, and oxidation, this application representing almost 70% of all coating services worldwide. Forming tools, steel stamping dies, injection molds, cold-, and hot-forging dies constitute another important niche sector for PVD. Finally, a smaller ratio of the PVD market is devoted to solid lubricious films, especially for the protection of bearing parts in machines or engines.

The most common industrial PVD coatings for antiwear purposes are TiN, TiCN, AlTiN, and CrN, all deposited at processing temperatures of between 450 and 550 °C, in the presence of gaseous precursors, N_2, O_2, or hydrocarbons (see Table 2). The deposition temperatures are in general compatible with those in the tempering of tool steels (high speed steels (HSS), cold- and hot-work steels, etc.). Powder metallurgical tool steels additionally exhibit an excellent support to PVD hard coatings. Analogously, sintered hard metal cutting tools show excellent load support and adhesive strength for PVD hard coatings.

Titanium nitride (TiN) [20] is the most commonly used coating for cutting and forming tools due to its high hardness, low friction coefficient, and toughness. Additionally, its golden-like color makes TiN a suitable film for decoration/protection in household items and other consumer goods. Titanium carbon nitride (TiCN) shows a higher hardness and lower COF than TiN [21,22], but reduced thermal stability. In fact, this coating requires oil lubrication, especially during high-speed machining operations, to avoid its premature oxidation by overheating. Aluminum titanium nitride (AlTiN) coatings [23] were implemented for industrial products in the 1990s and are used widely at the present time for high-speed and dry-machining tools due to their high hardness (greater than that of TiN) and elevated thermal stability. Chromium nitride (CrN) [24] shows inferior hardness to that of TiN but very low adhesive COF, permitting its application in plastic injection molding and other forming operations, where galling needs to be attenuated. This is due to the low tendency of CrN to stick to the working material during processes requiring high contact stresses at the tool/material interface. At present, recently developed CrCN [25] coatings are found to exhibit even lower adhesive COF to those of

Table 2 Deposition Parameters and Properties of Common Physical Vapor Deposition Coating Materials for Mechanical Engineering Applications

Coating	[0,2–4]PVD Process[a]			Processing T°C	Hardness (GPa)	COF (ASTM G99-5)	Max Working T°C
	CA	EB	MS				
TiN	x	x	x	450–550	20–25	0.6–0.8	500
TiCN	x	x	x	450–550	25–30	0.3–0.5	300
TiAlN	x	x	x	450–550	25–30	0.6–0.8	500–700
AlTiN	x	x	x	450–550	30–35	0.6–0.8	600–800
nc-AlSiTiN[b]	x		x	450–550	35–40	0.6–0.8	800–1000
CrN	x	x	x	200–500	18–22	0.6–0.8	600–800
ZrN	x		x	450–550	25–28	0.5–0.7	400–500
WC/C			x	200–250	10–15	0.2–0.4	200–250
MoS_2			x		10–15	0.1–0.3	200–300
DLC[c]			x	200–300	10–40	0.1–0.2	200–300

PVD, physical vapor deposition; ASTM, American Society for Testing and Materials; DLC, diamond-like carbon films; COF, coefficient of friction.
[a] *CA = cathodic arc discharge; EB = electron beam evaporation; MS = magnetron sputtering.*
[b] *nc denotes a nano-composite phases, as produced by* Spinodal *decompositions of nonsoluble phases.*
[c] *In the case of DLCs, there is a large dispersion of results derived from the sp^3/sp^2 bonding relations.*

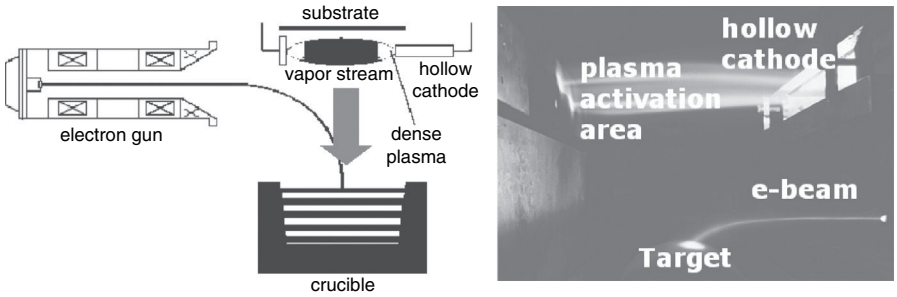

FIGURE 4

(right) Schematic representation of the hollow cathode arc-activated electron beam deposition. (left) Picture of the running process

Courtesy of Dr C. Metzner, Fraunhofer Institute for Electron Beam and Plasma Technologies.

CrN when sliding on stainless steels. Zirconium nitride (ZrN) exhibits a similar hardness to that of CrN and has a very low affinity for aluminum. These characteristics enable ZrN to be a recommended coating for Al-transformation dies (extrusion, injection), as well as for the machining of nonferrous alloys. Analogously to TiN, its brass-like color enables ZrN to be used as a decorative coating. Finally, the family of solid lubricious coatings WC-C [26,27] or MoS_2 [28] is utilized on bearing parts, as these are usually not subjected to excessively high temperatures.

PVD permits the design of a variety of film architectures with the aim to outperform the protective characteristics of single-layer configurations. Figure 5 shows different multilayer structures developed using the cathodic arc PVD technique. A common strategy to enhance the mechanical performance of PVD films is the design of load-adaptive layers [29]. Gradient composition films containing a hard layer at the interface and a low COF outer layer is a well-developed solution for several applications in the manufacturing sector [30]. A hard nitrided layer by nitriding processes can be an excellent load support surface for a PVD coating [31,32] (duplex processes).

Nanometer scale thin films are postulated [33]. Nano-multilayered coatings made of two different compounds (usually hard ceramic−ceramic or metal−ceramic) are found to exhibit the highest hardness/toughness when the nominal bilayer thickness ranges between 10 and 15 nm.

The deposition of immiscible phases in the form of thin film can lead to the formation of finely grained coatings (denoted as *nano-composites*). This variety of coatings shows superior values of hardness and toughness than the characteristics of their single counter-phases. It is commonly found that the incorporation of silicon in TiN [34,35], or AlTiN films [36], in quantities of around 8−10 at.%, increase their hardness values by a factor of 1.5−2. In addition, (Al,Si)TiN nano-composites retain their mechanical properties even after annealing temperatures of above 800−900 °C [37]. It has been shown how the tribological properties of TiAlSiN coatings deposited by CAE improve when the tests are done at temperatures between 200 and 400 °C with respect to wear tests carried out at room temperature. This intriguing

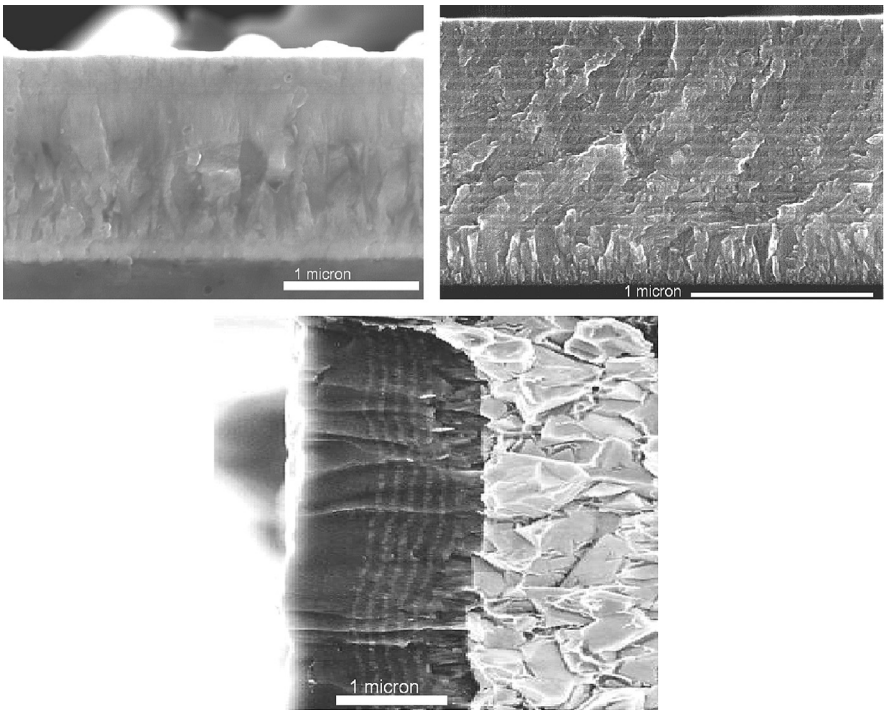

FIGURE 5

Different multilayer structures developed at AIN Surface Engineering Center using the cathodic arc physical vapor deposition technique. (left) Gradient CrCN, (center) damping coating AlTiN, (right) nano-multilayer TiN/CrN ($\lambda \sim 40$ nm).

phenomenon only observed for TiAlSiN is due to a combination of two factors: the elevated thermal stability and the formation of an oxide tribofilm at the sliding contact zone of the coated surface [38]. These outstanding properties have allowed these nano-composites to be utilized for the high speed and dry cutting of difficult-to-machine materials.

COATING FAILURE PREDICTION BY FINITE ELEMENT MODELING TECHNIQUES

In the recent years, the modelization of the mechanical performance of coating–substrate systems has gained a notable interest among the tooling protection industrial segment. In this context, it has been shown that multiscale models combining parameterized finite-element, cohesive-zone, and fatigue modeling [40] permit the prediction of the critical loads and failures due to fatigue effects. The model also permitted the prediction of the mechanical failures of multilayered systems consisting of hardened steels with plasma-nitrided cases and multistack coatings.

APPLICATIONS OF SURFACE ENGINEERING PROCESSES IN MICRO-MANUFACTURING

ADVANCED SURFACE TREATMENTS FOR MICRO-CUTTING TOOLS

As addressed in this chapter, micro-cutting technologies are one of the most important pillars of micro-manufacturing. With regards to tool design and development, strong efforts are being focused on the investigation of new materials and design concepts [39–43]. Nevertheless, few studies focus specifically on the problem of tool surface wear, which to some extent constitutes one of the main degradation mechanisms at this scale.

Some attempts to protect diamond tools have been made using DLC films deposited by CVD methods. DLC films were tested on diamond-based micro-cutting tools with different grain refinement, from coarse- to fine-grained structures [44]. Figure 6 compares the appearance of the drill point for two different cases: (a) DLC on coarse-grain diamond after 1800 holes had been processed; (b) DLC on fine crystal diamond after 15,500 holes had been processed. The results provide evidence that a DLC coating deposited on fine-grained diamond single crystal endmills enhances the cutting performance of the system.

Perucca et al. [45] investigated the machining performance of PVD-coated hard metal cutting tools for the precision turning of gray cast iron. They observed that

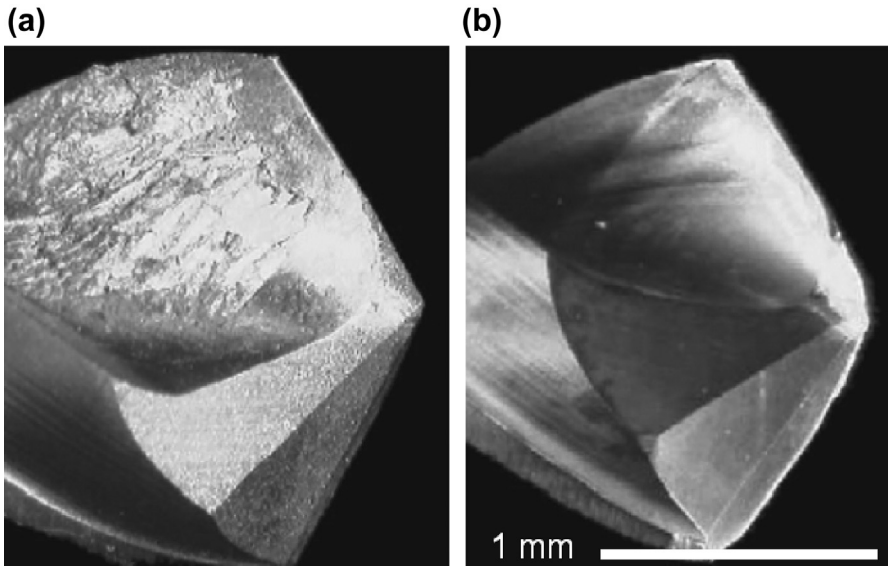

FIGURE 6

The appearance of drill points (width of chamfer 0.05 mm) ((a) diamond-like carbon films (DLC) coated on coarse-grain diamond after 1800 holes processed and (b) DLC coated on fine crystal diamond after 15,500 holes processed).

nano-crystalline TiN coatings outperformed other types of coatings such as multi-layered TiN/CrN or CrN films, as well as the naked tool. This is better observed in Figure 7, where the land wear width is depicted as a function of the total feed for gray cast iron turning tests. TiN coatings were also found to be optimal coatings for micro-milling of hardened tool steels [46], whereas TiAlN coatings became a preferred solution for micro-milling of austenitic stainless steel X5CrNi18-10 [47].

Yao et al. [48] investigated the wear properties and drilling precision of PVD-coated metal carbide micro-drilling tools. In particular, two different coating architectures were investigated: single hard TiN and nano-multilayered hard TiN/AlN coatings. The two architectures revealed different antiwear performances under the same working conditions. The TiN/AlN nano-multilayer exhibited greater protection against wear on both the tool flank and the rake faces than those shown by TiN films in the single-layer configuration, as depicted in Figure 8(a)–(d). Single TiN layers on the tool flank often tend to fail due to both the abrasion by hard particles and the accumulation of compressive stresses which originate from coating delamination.

Alternatively, nano-multilayered TiAlN/TiN-coated carbide endmills were found to outperform a single TiAlN coating, during the cutting of Cr-Mo-alloyed steels. In this study, different wear mechanisms were reported, depending on the cutting speed. At low cutting speed, built-up edge (BUE) formation was identified, caused by pressure-induced welding. High cutting speeds increased the temperatures at the contact zone, resulting in the diffusion of oxygen and enhancing the oxidation of the tool surface. It was observed that a metal-nitride PVD coating prevented both premature BUE and oxidation of the tool edge under low and high cutting speed,

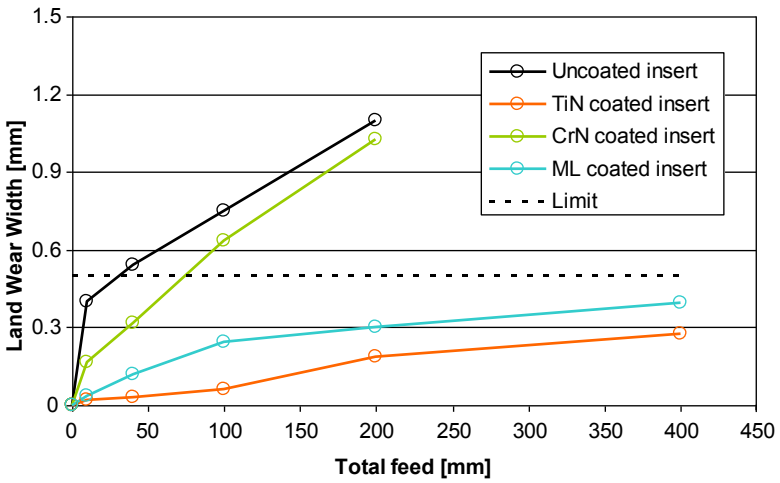

FIGURE 7

Land wear width for the cutting conditions: $f = 0.2$ mm, vc = 375 m/min; for uncoated, TiN coated, CrN coated, and TiN/CrN multilayered coated WC inserts.

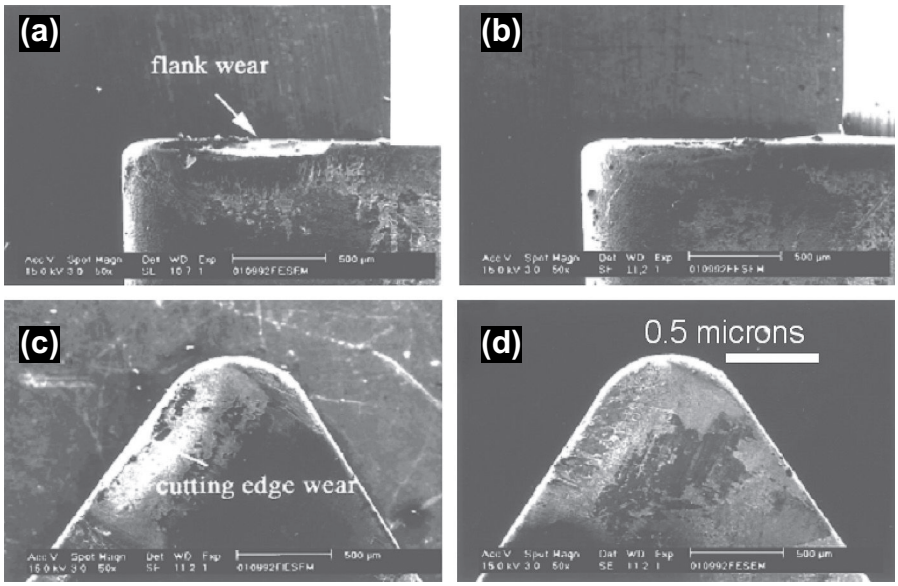

FIGURE 8

SEM wear morphology images of hard metal cutting tools with different coatings after running tests: flank wear for (a) single TiN layer and (b) nano-multilayer TiN/AlN film, and edge wear for (c) single-TiN layer, and (d) nano-multilayer TiN/AlN film.

respectively [49]. Additional studies were reported on the cutting performance of different MS-coated carbide precision tools in terms of the flank wear resistance.

Multilayered Cr/TiAlN and Mo-doped CrTiAlN coatings as deposited by MS exhibited the lowest flank wear rate during the micro-cutting of NiCrMoV-alloyed steels and CrCo alloys. The low wear rate obtained by these coated tools was attributed to the magnetic field configuration utilized for their deposition process, the so-called *close-field unbalanced* MS [50]. Analogously, the coating thickness distribution between the tool rake and the flank faces was considered to have a significant influence on the cutting performance of carbide micro-endmills [51]. More specifically, a lesser coating thickness on the tool rake with respect to the tool flank strongly diminishes the performance of the whole system due to uneven heat dissipation. In fact, when the coating on the rake is totally worn off during cutting, the tool base metal might come into contact with the working material, thereby increasing the COF and hence producing overheating at the tool/material interface. Thus thermal energy cannot be dissipated out of the tool due to the thermal barrier effect of the remaining unworn coating at the flank, causing rapid tool degradation. The optimal situation was identified when the coating thickness distribution was similar on the tool rake and the tool flank.

Alternative coating techniques such as atomic layer deposition (ALD) have been used in micro-milling of titanium. α-Al_2O_3 conformal coatings (200 nm thick) were

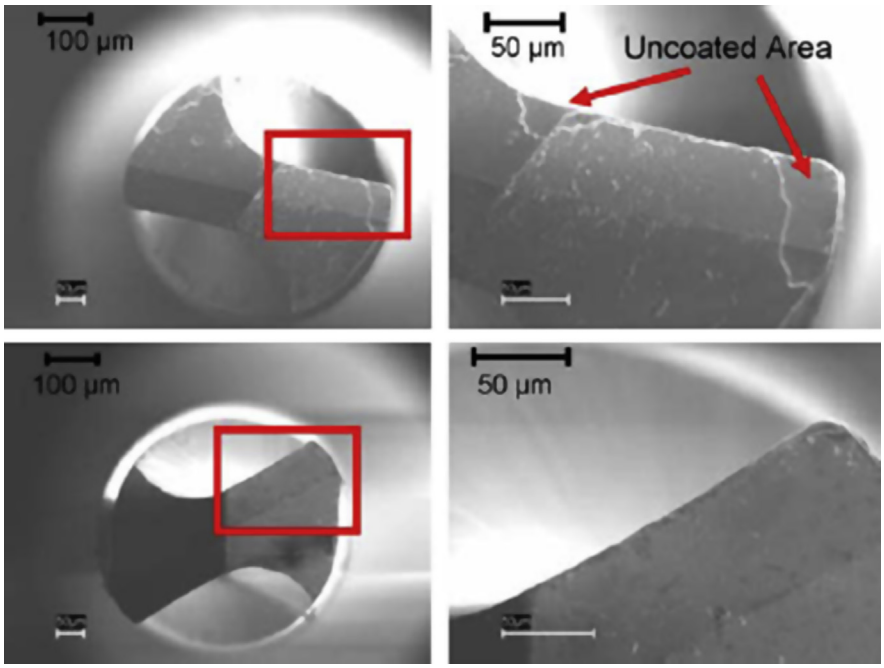

FIGURE 9

(top) 0.5 mm physical vapor deposition-coated tool; (bottom) 0.5 mm atomic layer deposition-coated tool.

deposited by ALD on HSS DIN 1899 drill tools (dia 0.5 mm) [52]. Figure 9 shows PVD-coated (top) and ALD-coated (bottom) micro-drill surfaces after a series of hole drills on grade 2-Ti. The results show clearly that the α-Al_2O_3 deposited by ALD retains the tool integrity.

ANTIADHESION AND WEAR RESISTANCE COATINGS ON MICRO-MOLDING TOOLS

The adhesion of the surface-forming materials (plastics, ductile metals, etc.) to the surface of the molding tool during demolding is a common feature in manufacturing which causes several problems of tool adhesive wear and workpiece quality. Additionally, waste production due to the use of oil lubricants or other wet demolding products is a common drawback associated with this surface–interface problem [53,54].

The reduction of the specific tool/material contact area in submillimeter microforming processes implies the loss of effective lubrication caused by a small lubricant retention capacity in the so-called closed valleys of the tool surface [5,55,56]. This fact leads submillimeter-scale contact interfaces to register COFs of up to one

order of magnitude greater with respect to the same interface systems scaled at macroscopic level. Micro-stamping, micro-embossing, and submillimeter metal bulk forming are a few examples where a high COF may provoke surface failures during component plastic deformation or workpiece demolding.

Different solutions are currently under development in this area. Polytetrafluoroethylene [57] (PTFE or Teflon) coatings are a standard solution for antiadhesive purposes in plastic injection molding. Silane and fluorinated silane were proposed as antiadhesive single films on electroplated Ni micro-featured molds for embossing or imprint operations. Different chemical formulations are able to produce self-assembled monolayers of silane derivatives which exhibit extremely low surface energy, therefore preventing the adhesion of plastic during demolding operations. The mechanical stability of silane-based films can be enhanced by depositing support SiO_2, NiO, or TiO_2 films [58,59] by vacuum plasma techniques such as plasma-enhanced CVD (PECVD).

Teflon- or silane-based films, however, have poor mechanical stability and high wear rates, making them unable to support mass production. In order to design mechanically stable surfaces on Ni-based micro-molds, other approaches are required. Ion beam-assisted DLC and SiO_x-doped coatings are proposed due to their self-lubricious properties, low surface energy, mechanical stability, and mimicking ability to replicate complex surfaces [60].

Chromium nitride-based PVD coatings with different stoichiometries and lattice structures have been investigated for their application in high precision plastic injection molding. It was found that the hexagonal Cr_2N phase deposited by MS exhibited the lowest surface energy among the most common transition metal nitrides [61], and therefore this film is proposed as an antiadhesive coating for Ni-based micro-embossing tools and other shape micro-replication processes.

Nano-multilayer coatings TiAlN/ZrN deposited by the MS technique have been applied on silicon micro-featured molds for the production of glass-based optical components. The tested coatings replicated well the original surface micro-pattern of the molds and exhibited an excellent thermal stability during the stamping of molten glass at 700 °C. Additionally, their good antioxidation behavior retarded the sticking of glass onto the coated Si molds [62].

Low friction coatings such as MoS_2, amorphous carbon (a-C:H), and WC-C deposited by MS were tested on Ni-electroplated tools providing different wear rates under sliding against steels [63]. In general, low friction coatings improve the wear rate of Ni molds for plastic micro-embossing, imprinting, or other surface-replication purposes.

DLC coatings deposited by PECVD techniques were reported to prevent the sticking of aluminum to the surfaces of hard metal molds during sliding in a ball-on-disc configuration at temperatures of between RT and 150 °C [64]. While the sticking of aluminum to the uncoated mold is found to occur at very early stages of the sliding contact, DLC inhibited the galling of aluminum on the surface of the hard metal tool even for temperatures greater than 120 °C.

Me-C:H PVD coatings have been used to enhance the tooling service of electro-discharge machining (EDM)-produced micro-compression molds for imprinting

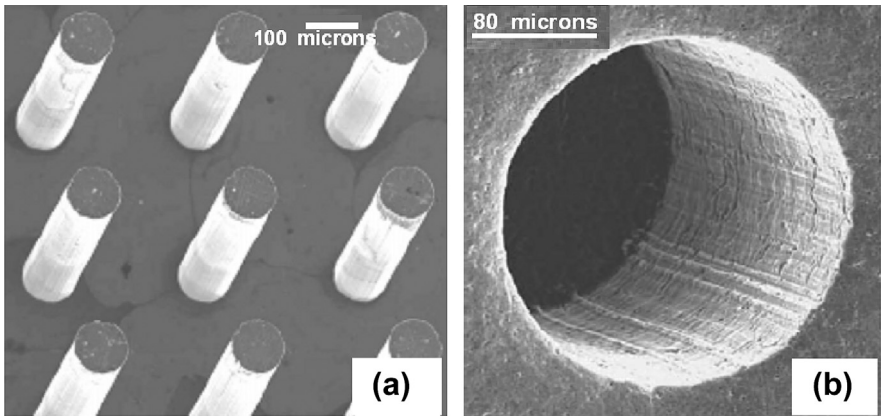

FIGURE 10

(a) SEM image of compression Ni micro-molds containing a series of parallel inserts in the form of cylinders and (b) imprinted hole produced by one-step stamping insert on aluminum plates at 450 °C. The inserts are coated with a hybrid chemical vapor deposition/physical vapor deposition Ti-C:H overlayer (2–3 μm thick).

applications on aluminum surfaces [65]. Figure 10(a) shows an SEM image of a coated compression Ni-based micro-mold containing a series of parallel inserts in the form of cylinders. The applied coating was a hybrid CVD/PVD Ti-C:H film (2.5 μm thick). Figure 10(b) shows the imprinted hole produced in a one-step stamping stroke.

The results of the Al-imprinting tests at different temperatures showed that the as-fabricated Ni inserts were not suitable for Al micro-molding due to strong abrasive surface wear. On the other hand, Ti-C:H deposition over Ni inserts enabled the Al micro-molding process to be carried out with near 100% shape replication.

Alternatively the hardness and wear resistance of electroformed Ni micro-embossing die surfaces can also be increased by the dual implantation of metal species such as Cr + N, or Ti + N atoms. It has been shown that the dual implantation of Cr and N reduced the COF of electroplated Ni surfaces from 0.5 down to 0.2 due to the hardening of the near surface [66].

Ti-MoS_2 cosputtered coatings onto Si-patterned dies increased the reproducibility of polymethylmethacrylate (PMMA) micro-channels produced by micro-embossing, as graphically depicted in Figure 11, where PMMA embossed micro-channels are shown for uncoated and Ti/MoS_2-coated Si dies [67]. The authors showed that the optimal coatings were those having Ti/Mo concentration ratio about 2/1, which exhibited the best trade-off between mechanical strength and COF.

Saha et al. ([68] and references therein) also investigated various coatings to improve the demolding operations of PMMA micro-channel embossing for micro-fluidic devices using patterned Si dies. N-DLC-based, Ti-Al-PTFE, or

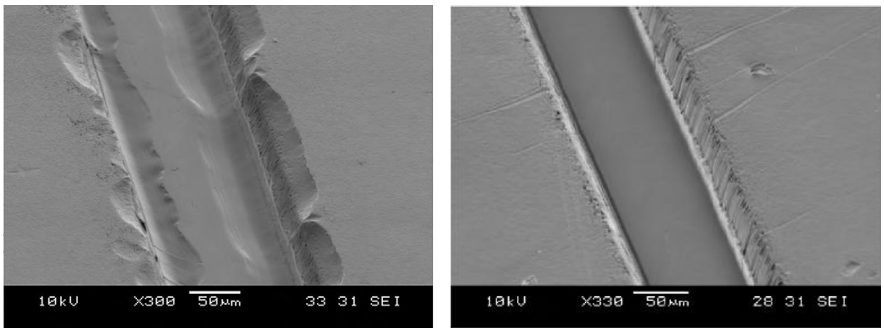

FIGURE 11

SEM micrographs of a channel of a polymethylmethacrylate micro-fluidic device fabricated using an uncoated (left) and a Ti-MoS_2-coated Si micro-mold (right).

N-Octadecyltrichlorosilane-based coatings facilitated the demolding steps and therefore the quality and reproducibility of the imprinted surfaces due to the reduction of the surface energy and COF of the Si micro-molds. Although, the delamination of the coatings during demolding represents a limiting factor the lifetime of such components.

MICRO-FORMING TOOL FABRICATION USING SURFACE ENGINEERING PROCESSES

Micro-manufacturing tool production at large scale represents a technological challenge due to the inherent difficulties found in the replication of submillimeter features in a reproducible manner. In this context, the increasing demand for smaller micro-components or micro-patterned surface textures has led researchers to explore new alternatives in the design and production of higher precision tool systems where such precision cannot be achieved by traditional manufacturing processes.

Downscaling traditional tool production methods is a well-known approach to achieve micro-tools, e.g., micro-cutting or micro-erosion by EDM techniques. However, mechanical removal processes by cutting often cause excessive burr formation, especially when the cutting process is made at submillimeter scale. On the other hand, the surface finishing of micro-forming molds as produced by micro-cutting or EDM is often too poor, and usually electropolishing posttreatments are required. Surface engineering has recently been emerging as a feasible method to fabricate custom-designed ultraprecision tools both for mass manufacturing as well as for flexible production systems.

Surface patterning by photolithography and electroforming are well-developed techniques within the family of surface engineering. Traditionally employed for the production of plates for integrated circuits, these technologies offer a great potential for the production of ultra-high precision micro-tools, e.g., molds for

micro-embossing, micro-stamping, and endmills for micro-cutting. Moreover, the combination of photolithography, in its different resolution ranges, visible light, UV, or X-ray, with electroforming is well suited for manufacturing with a high degree of repetitivity and rapidity, thus permitting its scalability to industrial production. As a drawback, photolithography technologies generate large amounts of residuals, which might compromise environmental regulations on waste production. Analogously, electroforming is limited to a small set of materials, often with low to medium hardness, having high wear rates in some applications. To overcome this problem, further engineered coatings might provide appropriate hardness values in combination with low coefficients of friction.

The production of Ni-based micro-embossing molds by using surface engineering methods [69] has been proposed, in which hard micro-textured DLC-deposited Ni plates are produced following a six-step chain according to Figure 12. In steps 1−3, a pattern of oxidized Si is produced by photolithography and chemical etching, leaving sharp cavities, of which each shape depends on the different etching speed of each family of crystalline planes. In step 4, the patterned Si surfaces are coated with a DLC hard film of 1−2 μm thickness, the DLC replicating accurately the original texture formed. In step 5, an electrodeposited Ni film of 1−2 mm thickness is deposited on top of the DLC. Interface-bonding films such as Ti could eventually enhance the adhesion strength between the DLC and the electroplated Ni film. Finally, the Si template is removed, and the Ni surfaces polished, leading to a master DLC-coated Ni-embossing tool.

These prototype embossing masters are successfully applied for texturing purposes on thermoplastics such as PMMA, PE-terephthalate, or polystyrene. Additionally, the hardness and toughness provided by the DLC film enables these masters to perform well on certain steels.

Figure 13 illustrates the result of stamping the DLC-Ni-embossing tool on steel plates. The grooves imprinted on the steel plates resemble those of a Vickers

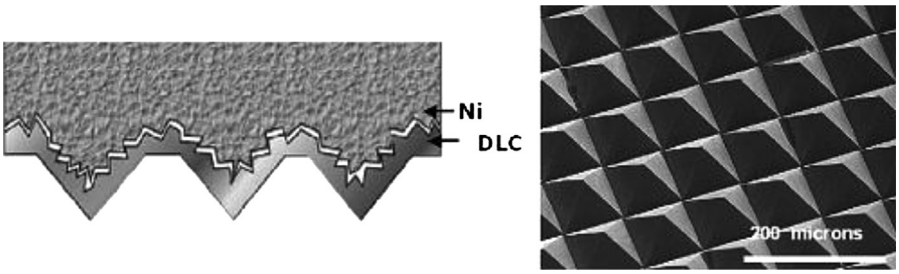

FIGURE 12

(a) Scheme of the design of a diamond-like carbon films-deposited Ni mold. (b) SEM image of micro-textured molds encompassing a well-defined pattern of indenter pyramids of 100 μm base side.

Courtesy of Petterson U. et al. Tribology International 2006;39:695.

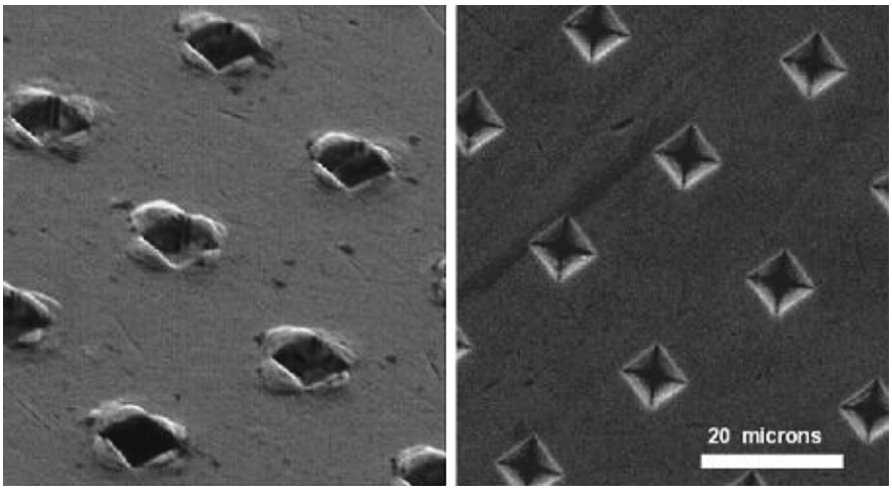

FIGURE 13

SEM images of flat steel plate grooves produced by diamond-like carbon films (DLC)-coated Ni-embossing tool molds—(left) ridges caused by the plastic flow of material during the indentation process and (right) ridges can be removed by a smooth polishing process.

indenter (Figure 13 left). The presence of prominent ridges is caused by the plastic flow of material during the indentation process. Such ridges are easily eliminated by a smooth polishing (Figure 13 right). On the other hand, industrially scalable molds should eventually work over nonplanar surfaces. In consequence, the mechanical performance of the molds depends strongly on the appropriate optimization of the Ni electrodeposition method and the adhesion and mechanical stability of the coating, in order to avoid premature crack failure under tool deflections.

Micro-textured DLC-based films where also produced by plasma-based ion implantation [70]. The procedure encompassed the imprinting of micro-patterns on a sacrificial aluminum foil, which is coated afterward by a thin DLC coating. The aluminum foil is then eliminated by chemical methods, leaving a freestanding DLC-textured film. The process provides the rapid production of these films, thus enabling mass production upscaling.

Ion beam bombardment methods are under development for the production of extremely fine precision micro-cutting and molding tools. The process of ion beam etching provides excellent precision in the design of micrometer-sharp structures by the so-called focused ion beam (FIB) techniques. Conversely, the process is slow and somewhat expensive as it requires advanced vacuum facilities and ion acceleration sources, presently available within research laboratories. Ultraprecision diamond micro-shaped endmills for glass micro-cutting were produced by FIB etching for the prototyping of a new micro-array chip for DNA assembly [71]. Micro-structured glass surfaces were produced using

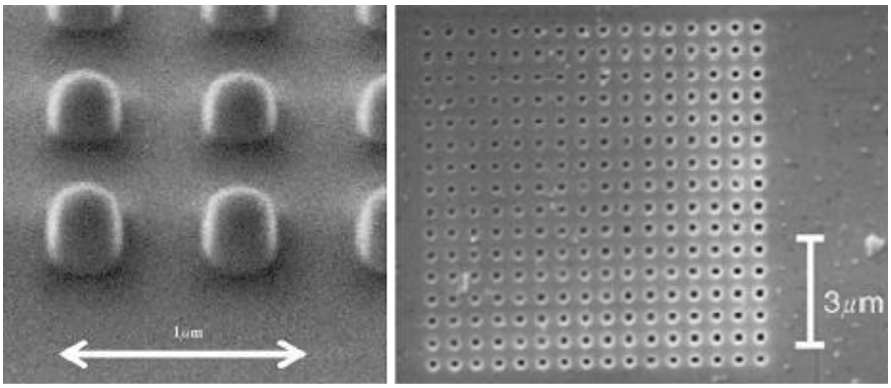

FIGURE 14

SEM images of (left) nano-structured diamond tool produced by focused ion beams techniques and (right) imprinted pattern on glass by the prototyped micro-molding tool.

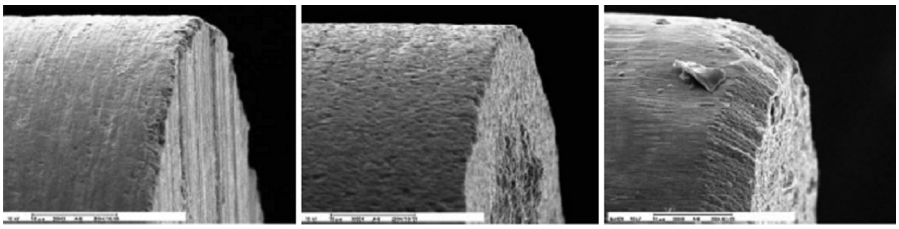

FIGURE 15

Surface finish of micro-dies by ion irradiation—(left) before ion irradiation, (center) ion irradiation with 45° beam incidence, and (right) ion irradiation with 10°beam incidence with respect to the tool parallel axis.

micro-embossing tools previously prototyped by FIB techniques (Figure 14). The textured surfaces provided the micro-array chip with the functional properties required for their performance: low surface energy, low COF, and high transparency.

Micro-featured punches for sheet micro-forming tools have been semifinished by FIBs methods and finally coated with low friction DLC films deposited using ion beam-assisted deposition [72] (see Figure 15 for 0.15 mm diameter punches, after different ion beam regrinding cycles). Micro-forming tool finishing is a complex process which requires nonconventional polishing techniques, such as electrochemical etching, which become difficult to control at the micrometer scale, and is strongly dependent on the properties of the tool material. Contrarily, net-shape finishing by FIB mostly depends on the ion beam properties and less on the intrinsic properties of the tool material.

SUMMARY

In this chapter, a concise review of recent progress in surface engineering for tooling protection has been presented, with particular focus on applications in micro- and nano-production technologies. As a general conclusion, it can be stated that surface engineering has the potential for great impact in the further development of miniature and micro-manufacturing. In this context, research and development in this field should focus on new concepts of flexible surface modification systems, in order to achieve an optimal performance on nonstandard tooling elements. Moreover, the implementation of reliable testing tools and standards needs to be addressed in detail. The development of surface/interface modeling tools is envisaged to help in the integration of both process design and surface engineering for micro-manufacturing. Substantial integrative endeavors need to be undertaken between the scientific community and the relevant industrial stakeholders to obtain the full potential of surface engineering and to convert it in a true enabling technology for micro-manufacturing.

ACKNOWLEDGMENTS

The author gratefully acknowledges the support of the European Commission for Research and Development through the project MicroFAST (contract Nr FP7-NMP-FoF-608720)

REFERENCES

[1] Veprek S. The search for novel superhard materials. J Vac Sci Technol A 1999;17:2401−20.
[2] Holmberg K, Mathews A. In: Briscoe BJ, editor. Coatings tribology. 2nd ed. Tribology and interface engineering series, vol. 56. Elsevier; 2009.
[3] Xie Y, Williams JA. The prediction of friction and wear when a soft surface slides against a harder rough surface. Wear 1996;196:21−34.
[4] Tung SC, McMillan ML. Automotive tribology overview of current advances and challenges for the future. Tribol Int 2004;37:517−36.
[5] Engel U. Tribology in microforming. Wear 2006;260:265−73.
[6] Lee J-M, Jin W-H, Kim D-E. Application of single asperity abrasion process for surface micro-machining. Wear 2001;251:1133−43.
[7] Lee S-Y. Mechanical properties of $TiN_x/Cr_{1-x}N$ thin films on plasma nitriding-assisted AISI H13 steel. Surf Coat Technol 2005;193:55−9.
[8] de Souza SD, Olzon-Dionysio M, Miola EJ, Paiva-Santos CO. Plasma nitriding of sintered AISI316L at several temperatures. Surf Coat Technol 2004;184:176−81.
[9] Wei R, Booker T, Rincon C, Arps J. High intensity plasma ion nitriding of orthopaedic materials Part I: tribological study. Surf Coat Technol 2004;186:305−13.
[10] García JA, Fuentes GG, Martínez R, Rodríguez RJ, Abrasonis G, Rivière JP, et al. Temperature-dependent tribological properties of low-energy N-implanted V5Ti alloys. Surf Coat Technol 2004;188−189:459−65.

[11] Fuentes GG, García JA, Rodríguez RJ. Method for nitriding metal alloys and device for carrying out said method. EP 11156311.0, Patent Number EP2369028.
[12] Corujeira Gallo S, Dong H. Study of active screen plasma processing conditions for carburising and nitriding austenitic stainless steel. Surf Coat Technol 2009;203: 3669−75.
[13] Avelar-Batista JC, Spain E, Housden J, Mathews A, Fuentes GG. Plasma nitriding of Ti6Al4V alloy and AISI M2 steel substrates using D.C. glow discharges under a triode configuration. Surf Coat Technol 2005;200:1954.
[14] Rodríguez R, Sanz A, Medrano A, García-Lorente JA. Tribological properties of ion implanted aluminium alloys. Vacuum 1999;52:187−92.
[15] Rodríguez RJ, Medrano A, García JA, Fuentes GG, Martínez R, Puertolas JA. Improvement of surface mechanical properties of polymers by helium ion implantation. Surf Coat Technol 2007;201:8146−9.
[16] Mitterer C, Holler F, Reitberger D, Badisch E, Stoiber M, Lugmair C, et al. Industrial applications of PACVD hard coatings. Surf Coat Technol 2003;163−164:716−22.
[17] Erdemir A. Genesis of superlow friction and wear in diamondlike carbon films. Tribol Int 2004;37:1005−12.
[18] Böhlmark J. Fundamentals of high power impulse magnetron sputtering, Dissertation No. 1014, Linköping Institute of Technology, Sweden; 2006. ISSN:0345-7524.
[19] Fuentes GG, Díaz de Cerio MJ, Rodriguez R, Avelar-Batista JC, Spain E, Housden J, et al. Study on the sliding of aluminium thin foils on the PVD-coated carbide forming-tools during micro-forming. J Mat Proc Tech 2006;177:644−8.
[20] Hultman L. Thermal stability of nitride thin films. Vacuum 2000;57(200):1−30.
[21] Fuentes GG, Cáceres D, Vergara I, Elizalde E, Sanz JM. Elastic properties of hard TiCxNy coatings grown by dual ion beam sputtering. Surf Coat Technol 2002; 151−152:365.
[22] Bull SJ, Bhat DG, Staia MH. Properties and performance of commercial TiCN coatings. Part 2: tribological performance. Surf Coat Technol 2003;163−164:507−14.
[23] PalDey S, Deevi SC. Single layer and multilayer wear resistant coatings on (Ti,Al)N: a review. Mater Sci Eng A 2003;342:58−79.
[24] Fuentes GG, Rodriguez R, Avelar-Batista JC, Housden J, Montala F, Carreras LJ, et al. Recent advances in the chromium nitride PVD process for forming and machining surface protection. J Mater Process Technol 2005;167:415−21.
[25] Fuentes GG, Díaz de Cerio MJ, García JA, Martínez R, Bueno R, Rodríguez RJ, et al. Gradient Cr(C,N) cathodic arc PVD coatings. Surf Coat Technol 2008;203: 670−4.
[26] Arndt M, Kacsich T. Performance of new AlTiN coatings in dry and high speed cutting. Surf Coat Technol 2003;163−164:674−80.
[27] Rodríguez RJ, García JA, Martínez R, Lerga B, Rico M, Fuentes GG, et al. Tribological metal-carbon coatings deposited by PVD magnetron sputtering. Appl Surf Sci 2004; 235:53−9.
[28] Carrera S, Salas O, Moore JJ. Performance of CrN/MOS2 (Ti) coatings for high wear low friction applications. Surf Coat Technol 2003;167:25−32.
[29] Voevodin AA, Walck SD, Zabinski JS. Architecture of multilayer nanocomposite coatings with super-hard diamond-like carbon layers for wear protection at high contact loads. Wear 1997;203:516−27.
[30] Hoya R, Kammingaa J-D, Janssen GCAM. Scratch resistance of CrN coatings on nitrided steel. Surf Coat Technol 2006;200:3856−60.

[31] Avelar-Batista JC, Spain E, Fuentes GG, Sola A, Rodriguez R, Housden J. Triode plasma nitriding and PVD coating: a successful pre-treatment combination to improve the wear resistance of DLC coatings on Ti6Al4V alloy. Surf Coat Technol 2006;201: 4335−40.
[32] Klimek KS, Ahn H, Seebach I, Wang M, Rie K-T. Duplex process applied for die-casting and forging tools. Surf Coat Technol 2003;174−175:677−80.
[33] Holmberg K, Matthews A, Ronkainen H. Coatings tribology—contact, mechanisms and surface design. Tribol Int 1998;31:107−20.
[34] Diserens M, Patsheider J, Lévy F. Improving the properties of titanium nitride by incorporation of silicon. Surf Coat Technol 1998;108−109:241−6.
[35] Vaz F, Rebouta L, Ramos S, da Silva MF, Soares JC. Physical, structural and mechanical characterization of $Ti_{1-x}Si_xN_y$ films. Surf Coat Technol 1998;108−109:236−40.
[36] Kim SK, Vinh PV, Kim JH. Deposition of superhard TiAlSiN thin films by cathodic arc plasma deposition. Surf Coat Technol 2005;200:1391−4.
[37] Ribeiro E, Rebouta L, Carvalho S, Vaz F, Fuentes GG, Rodriguez R, et al. Characterization of hard DC-sputtered Si-based TiN coatings: the effect of composition and ion bombardment. Surf Coat Technol 2004;188−189:351−7.
[38] Fuentes GG, Almandoz E, Pierrugues R, Martínez R, Rodríguez RJ, Caro J, et al. High temperature tribological characterisation of TiAlSiN coatings produced by cathodic arc evaporation. Surf Coat Technol 2010;205:1368−73.
[39] Feng J, Qin Y, Zeng Q, Almandoz E, Fuentes GG, Dong H, et al. Parameterized finite element modeling of the surface systems with coatings which considers the cracking of the coatings and influences of the case-hardening of the substrate. J Multiscale Model 2011;3:1−22.
[40] Vollertsen F, Schulze Niehoff H, Hu Z. State of the art in micro forming. Int J Mach Tools Manuf 2006;46:1172−9.
[41] Robinson GM, Jackson MJ. A review of micro and nanomachining from a materials perspective. J Mater Process Technol 2007;167:316−37.
[42] Chae J, Park SS, Freiheit T. Investigation of micro-cutting operations. Int J Mach Tools Manuf 2006;46:313−32.
[43] Qin Y. Forming-tool design innovation and intelligent tool-structure/system concepts. Int J Mach Tools Manuf 2006;46:1253−60.
[44] Hanyu H, Kamiya S, Murakami Y, Kondoh Y. The improvement of cutting performance in semi-dry condition by the combination of DLC coating and CVD smooth surface diamond coating. Surf Coat Technol 2005;200:1137−41.
[45] Perucca M, Durante S, Semmler U, Rüger C, Fuentes GG, Almandoz E. Cast iron cutting with nano TiN and multilayer TiN-CrN coated inserts. IOP Conf Ser Mater Sci Eng 2012;40:012004.
[46] Aramcharoen A, Mativenga PT, Yang S, Cooke KE, Teer DG. Evaluation and selection of hard coatings for micro milling of hardened tool steel. Int J Mach Tools Manuf 2008; 48:1578−84.
[47] Biermann D, Steiner M, Krebs E. Investigation of different hard coatings for micromilling of austenitic stainless steel. Procedia CIRP 2013;7:246−51.
[48] Yao SH, Su YL, Kao WH, Liu TH. On the micro-drilling and turning performance of TiN/AlN nano-multilayer films. Mater Sci Eng A 2005;392:340−7.
[49] Kopac J, Sokovic M, Dolinsek S. Tribology on coated tools in conventional and HSC machining. J Mat Proc Tech 2001;118:377−84.

[50] Yang S, Wiemann E, Teer DG. The properties and performance of Cr-based multilayer nitride hard coatings using unbalanced magnetron sputtering and elemental metal targets. Surf Coat Technol 2004;188−189:662−8.
[51] Bouzakis K-D, Hadjiyiannis S, Skordaris G, Mirisidis I, Michailidis N, Erkens G. Wear development on cemented carbide inserts, coated with variable film thickness in the cutting wedge region. Surf Coat Technol 2004;188−189:636−43.
[52] Giorleo L, Ceretti E, Giardini C. CIRP Ann−Manuf Technol 2011;60:595−8.
[53] Guo Y, Liu G, Xiong Yi, Tian Y. Study of the demolding process—implications for thermal stress, adhesion and friction control. J Micromech Microeng 2007;17:9−19.
[54] Heckele M, Schomburg WK. Review on micro molding of thermoplastic polymers. J Micromech Microeng 2004;14:R1−R14.
[55] Erdemir A. Review of engineered tribological interfaces for improved boundary lubrication. Tribol Int 2005;38:249−56.
[56] Bech J, Bay N, Eriksen M. Entrapment and escape of liquid lubricant in metal forming. Wear 1999;232:134−9.
[57] Tallal J, Gordon M, Berton K, Charley AL, Peyrade D. AFM characterization of anti-sticking layers used in nanoimprint. Microelectron Eng 2006;83:851−4.
[58] Byeon K-J, Yang K-Y, Lee H. Thermal imprint lithography using sub-micron sized nickel template coated with thin SiO_2 layer. Microelectron Eng 2007;84:1003−6.
[59] Park S, Schift H, Padeste C, Schnyder B, Kötz R, Gobrecht J. Anti-adhesive layers on nickel stamps for nanoimprint lithography. Microelectron Eng 2004;73−74: 196−201.
[60] Meškinis Š, Kopustinskas V, Šlapikas K, Tamulevičius S, Guobienë A, Gudaitis R, et al. Ion beam synthesis of the diamond like carbon films for nanoimprint lithography applications. Thin Solid Films 2006;515:636−9.
[61] Chiu SM, Hwang SJ, Chu CW, Gan D. The influence of Cr-based coatings on the adhesion force between epoxy molding compounds and IC encapsulation mold. Thin Solid Films 2006;515:285−92.
[62] Hock M, Schäffer E, Döll W, Kleer G. Composite coating materials for the moulding of diffractive and refractive optical components of inorganic glasses. Surf Coat Technol 2003;163−164:689−94.
[63] Wänstrand O, Larsson M, Kassman-Rudolphi A. Mechanical and tribological properties of vapour deposited low friction coatings on Ni plated substrates. Tribol Int 2000;33: 737−42.
[64] Díaz de Cerio MJ, Fuentes GG, Martínez R, Rodriguez R, Spain E, Housden J, et al. Temperature dependent contact phenomena of PVD and CVD deposited DLC films sliding on aluminium thin foils. Int J Adv Manuf Technol 2010;47:931−6.
[65] Cao DM, Jiang J, Meng WJ. Metal micromolding with surface engineered inserts. Microsyst Technol 2004;10:662−70.
[66] Conde A, Muñoz-García C, García I, Fuentes GG, Almandoz E, García JA, et al. Friction, nanowear and corrosion properties of electroplated Nickel surfaces after dual implantation of Cr^+ and N_2^+ ions. Influence of the implantation energy of the N_2^+ ions. Surf Coat Technol 2012;210:46−53.
[67] Saha B, Dirckx M, Hardt DE, Tor SB, Liu E, Chun JH. Effect of sputtering power on friction coefficient and surface energy of co-sputtered titanium and molybdenum disulfide coatings and its performance in micro hot-embossing. Microsyst Technol 2014;20:1069−1078. http://dx.doi.org/10.1007/s00542-013-1783-2.

[68] Saha B, Tor SB, Liu E, Hardt DE, Chun JH. Titanium−aluminum−polytetrafluoroethylene coated stainless steel micromold via co-sputtering deposition: replication performance and limitation in hot-embossing. Sens Actuators B 2012;163:290−8.
[69] Pettersson U, Jacobson S. Tribological texturing of steel surfaces with a novel diamond embossing tool technique. Tribol Int 2006;39:695−700.
[70] Yamamoto R, Miyashita K, Hayashi H, Inoue K. Preparation of microstructure bodies in freestanding diamond-like carbon foil prepared using plasma-based ion implantation. Diam Relat Mater 2007;16:292−5.
[71] Yoshino M, Matsumura T, Umehara N, Akagami Y, Aravindan S, Ohno T. Engineering surface and development of a new DNA micro array chip. Wear 2006;260:274−86.
[72] Fujimoto K, Yang M, Hotta M, Koyama H, Nakano S, Morikawa K, et al. Fabrication of dies in micro-scale for micro-sheet metal forming. J Mater Process Technol 2006;177: 639−43.

CHAPTER

DLC-Coated Tools for Micro-forming

21

Chunju Wang, Debin Shan, Bin Guo

School of Materials Science and Engineering, Harbin Institute of Technology, Harbin, China

CHAPTER OUTLINE

INTRODUCTION

The growing awareness of environmental issues and the requirement to establish solutions reducing impact on the working environment as well as the external environment has initiated ever-increasing efforts to develop new, environmentally benign tribological systems for metal forming [1–3]. In micro-forming, the application of lubricants complicates the cleaning of workpieces, which process is more complex than that in the macro-range due to the smaller dimensions involved. Moreover, the thin workpiece material usually has a more sensitive dependence of the forming limit on the friction between the workpiece and the forming tool. For the high ratio of free-surface-to-volume of micro-parts, the size effect on the coefficient of friction (COF) becomes more evident than that in traditional macro-metal forming when

Micromanufacturing Engineering and Technology. http://dx.doi.org/10.1016/B978-0-323-31149-6.00021-9

liquid lubricants are applied. Tiesler and Engel studied the size effect on the COF in the double-cup-extrusion (DCE) process, their results revealing that the friction factor increased from $m = 0.02$ in the case of the 4 mm specimen up to 0.4 for the smallest specimen [4,5]. Guo et al. studied the size effect on friction in scaled-down strip drawing using thin T2 copper sheet. When a kind of liquid lubricant, e.g., soybean oil, was applied, the average COF increased from 0.138 for $\lambda = 1$ to 0.224 for $\lambda = 0.125$ [6]. From a study of the dependence on the contact pressure at the radius of the die, it was deduced that tribological size effects would be greater with the miniaturization of process dimensions [7].

Engineers have long attempted to reduce friction between tools and materials. Surface modification and micro-texture optimization are two possible solutions to the challenge. By using ion-beam irradiation equipment, a micro-textured surface with many nano-crystal particles was obtained, which was confirmed by micro-deep drawing tests to be very useful in decreasing friction. However, it is difficult to control the micro-textured surface produced using such methods [8]. In surface modification, low wear friction coatings such as diamond-like carbon (DLC) are candidates for substitution as lubricants [9]. The important aspect is the property of DLC film to graphitize the surface at high pressures, so that the coating becomes virtually self-lubricating. Numerous researchers are interested in DLC film for its low COF, high wear resistance, and environmentally benign characteristics. DLC films have been applied widely in the macro-forming process, and the advantages of using DLC film or silicon-doped DLC film (Si-DLC) in cold forming and warm forming, respectively [10–14], have been demonstrated.

The excellent tribological properties of DLC film have been gaining increasingly more attention. The most important feature is that it can eliminate the size effect of friction in micro-forming, and it can also protect the micro-die in respect of its wear resistance and antiadhesion characteristics. The application of DLC-coated tools is also becoming much wider in micro-forming.

CHARACTERISTICS AND PREPARATION OF DLC FILM

CHARACTERISTICS OF DLC FILM

DLC is a metastable form of amorphous carbon containing a significant fraction of sp^3 bonds. It can have a high mechanical hardness, chemical inertness, optical transparency, and low friction. In DLC, carbon is able to exist in three hybridizations, sp^3, sp^2, and sp^1, as shown in Figure 1. The extreme physical properties of DLC derive from its mixture of carbon bonds. In DLC film, the sp^3, as in diamond, has a strong σ bond, which confers on it many beneficial properties, such as high mechanical hardness and chemical inertness. The sp^2, as in graphite, has a strong intralayer σ bond and a weak van der Waals bond between its layers. The great versatility of carbon materials arises from the strong dependence of their physical properties on the ratio of sp^2 (graphite-like) to sp^3 (diamond-like) bonds [9,15].

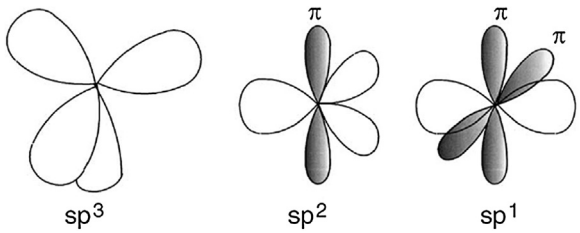

FIGURE 1

The sp^3, sp^2, and sp^1 hybridized bonding [9].

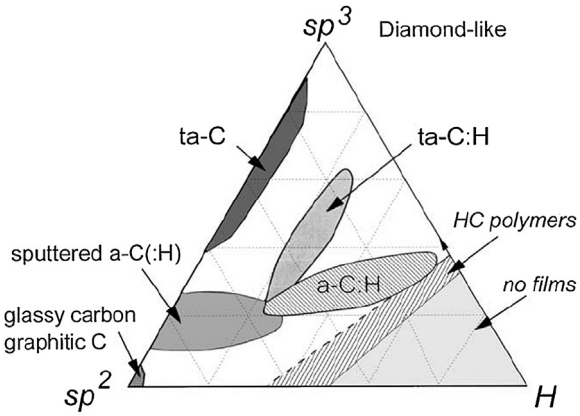

FIGURE 2

Ternary phase diagram of bonding in amorphous carbon–hydrogen alloys [9].

DLC consists not only of the amorphous carbons (a-C) but also of the hydrogenated alloys, a-C:H. It is convenient to display the compositions of the various forms of amorphous C–H alloys on a ternary phase diagram, as shown in Figure 2. The hydrogenated amorphous carbons (a-C:H) have a rather small C–C sp^3 content. DLCs with higher sp^3 content are termed tetrahedral amorphous carbon (ta-C) and its hydrogenated analog ta-C:H. Another crucial parameter is the degree of clustering of the sp^2 phase. Amorphous carbons with the same sp^3 and H content show different mechanical properties according to the clustering of the sp^2 phase [9,16].

DLC films are characterized by high hardness and a high elastic modulus, but also by high internal stress. The hardness of DLC films is in the range 10–30 GPa, with a corresponding Young's modulus 6–10 times larger. The widest use of DLC films is mainly of the hydrogenated DLC in applications exploiting the low friction coefficients and high wear resistance of these materials. The tribological behavior of DLC is controlled by an interfacial transfer layer which is formed by a friction-induced transformation of the top layer of the DLC film into a material of low shear strength. The low friction and ultra-low wear of DLC and its counterparts can be explained by the low shear strength of the transfer layer. In ambient air at

relative humidities of $20\% < RH < 60\%$, the friction coefficients of DLC span a range of $\mu = 0.05-1.0$. The large spread in the values of the friction coefficient is caused by variations in the structure and composition of the films [17,18].

Both the hydrogenated and nonhydrogenated DLC are metastable materials and their structures will change toward graphite-like carbon by either thermal activation or irradiation with energetic photons or particles. Heating of hydrogenated DLC films results in the loss of hydrogen and CHx species, starting at about 400 °C, or even lower, depending on the deposition conditions and the dopant contained in the films. This causes changes in the dimensions and properties of the material and limits the use of DLC in applications involving temperatures above 400 °C, where thermal activation can cause the conversion of some sp^3 carbon bonds into sp^2 bonds [17].

DEPOSITION METHODS OF DLC FILM

In order to obtain the metastable structure of DLC, such films are deposited by plasma-enhanced chemical vapor deposition (PECVD) or physical vapor deposition (PVD) techniques (sputtering or ion beams) using a variety of precursors, as described in detail elsewhere. In the PECVD methods, the substrates have to be at a negative bias relative to the plasma to achieve ion bombardment of the growing film. The growth and properties of DLC films are controlled by the substrate temperature and bias, the latter having the dominant control. Films deposited with this method had polymeric characteristics. A more recent technique for the deposition of DLC films is plasma source ion implantation (PSII). In this technique, substrates are placed directly in a plasma source and then pulse-biased. This is a non-line-of-sight technique and enables the coating of complex structures. Various materials derived from the DLC films have been developed to change and improve their properties. Such materials are similar in structure to DLC, including silicon (Si-DLC), fluorine (F-DLC), etc. Most modifications have been made to DLC to reduce its typically high internal compressive stresses, with the purpose of reducing its surface energy to enable further reduction of its already-low friction coefficients [17].

EVALUATION METHODS FOR DLC FILMS

DLC films are amorphous materials with carbon atoms bonded in mainly sp^3 and sp^2 hybridizations. DLC films can have an sp^3 fraction of up to about 40%. The properties of the films are determined by the relative ratio of the two hybridizations. Raman spectroscopy is widely used, being a routine, nondestructive way to characterize the structural quality of DLC films. Diamond has a single Raman active mode at 1332 cm^{-1}, and single-crystal graphite has a single Raman active mode at 1580 cm^{-1} labeled by "G" for "graphite," while disordered graphite has a second mode at around 1350 cm^{-1} labeled "D" for "disorder," this enabling Raman to be used to derive the structural information of DLCs and their sp^3 fraction [9,19].

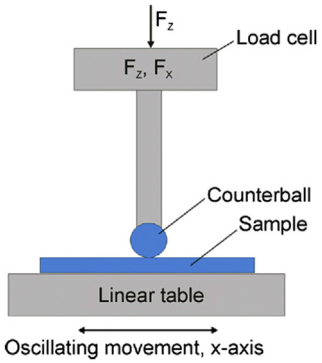

FIGURE 3

Principle of the experimental setup for a wear test on a tribometer [21].

The ball-on-disk test is generally used in the evaluation of the tribological behavior of DLC film [20]. Vollertsen investigate the dry tribological properties of DLC film using the tests as shown in Figure 3. For example, balls made of steel X5CrNi18-10 were used as opposing bodies, under two different loads of 5 and 25 N which is representative of the local contact pressure in deep drawing, to determine an average friction coefficient for the DLC-coated sample of $\mu = 0.166$ under the load of 5N and $\mu = 0.18$ under the load of 25N: as shown in Figure 4, these values are much lower than that for the uncoated sample. This behavior of the friction coefficients is reflected in the wear on the surface of the samples as shown in Figure 5. For the case of the uncoated sample, the groove has a maximum depth of more than 10 μm. In comparison, the groove on the DLC-coated sample has a maximum depth of about 1 μm [21].

Adhesion strength is a concerned parameter for the micro-forming process because of the high contact pressure involved. In the case of metal forming at sub-millimeter scale, the die bears a larger stress on the shoulders or the edges. As a result, the DLC film becomes more easily damaged and the die becomes more easily worn or broken in comparison with larger dies. The adhesive strength can be evaluated by the scratch test and an indentation test. A DLC film with a gradient in mechanical properties was deposited using chemical vapor deposition (CVD) DLC film equipment by changing the bias voltage. The damage of the DLC film due to the concentration of stress/strain was evaluated using the nano-indentation test with larger loads of up to 800 mN. Cracking and/or chipping occurred in the DLC film except for the conditions of a bias voltage of 1 and 3 kV, as shown in Figure 6. There were some minor wrinkles, but no cracking or delamination occurred in these coatings, which means that the coatings have the ability to bear larger strain/stress [22]. Kitamura et al. have also basically evaluated the adhesive characteristics of Si-DLC film by the indentation test [23,24].

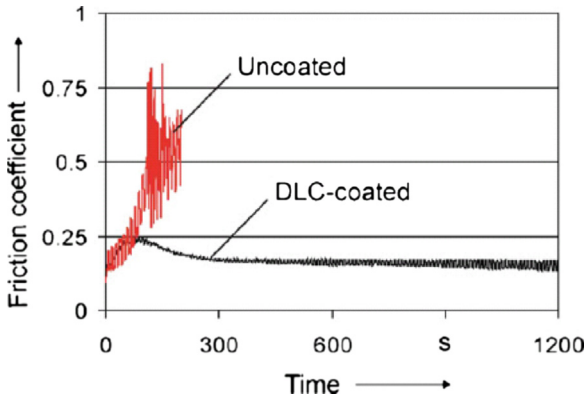

FIGURE 4

Development of the friction coefficient of uncoated and DLC-coated steel X153CrMoV12 by tribotest against the steel X5CrNi18-10 (load 5N, velocity $v = 1$ mm/s, dry friction) [21].

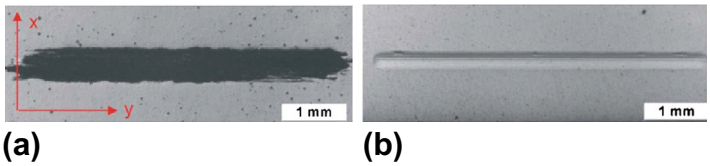

FIGURE 5

Wear of the uncoated (a) and diamond-like carbon-coated (b) samples (load 25N, velocity $v = 1$ mm/s, dry friction) [21].

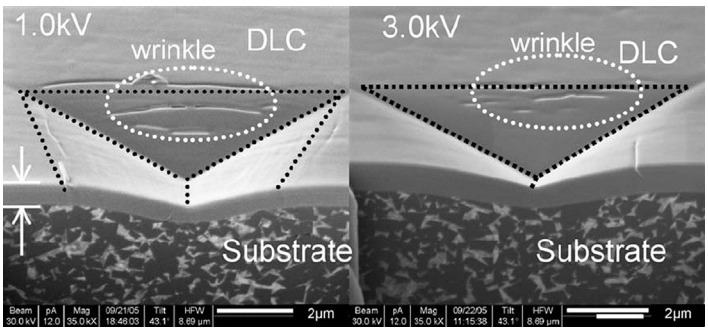

FIGURE 6

Enlarged image of the cross section of diamond-like carbon (DLC) film after indentation [22].

DLC-COATED TOOLS IN MICRO-SHEET FORMING

DEPOSITION OF DLC FILM ON THE INNER SURFACE OF A MICRO-CAVITY OF THE DIE

The small dimensions of micro-die cavity lead to difficulty in the deposition of DLC film on the inner surface. To easily measure the properties of DLC film on the inner surface of a micro-channel, a series of two-body dies with micro-channels of different widths from 0.6 to 1.4 mm were manufactured from SKD11 steel. DLC film was deposited at room temperature with PSII. From analysis of the results of the experiments, ripple topography of the DLC films appears on the inner surface of the micro-cavity, which is different from the situation at the top surface. The direction of the ripple is parallel to the length direction of the micro-channel. With increase of the depth, the ripple topography was transferred into a group of islands. Also, the width of the channel and the depth into the micro-cavity have an obvious effects on the forming of the ripple. The ripple-and-island structure on the inner surface is not helpful in micro-forming applications. With increase of the depth into the micro-cavity from the top surface, the thickness of the DLC film decreases quickly. For example, the thickness the DLC film is reduced from 554 nm for the top surface to 48 nm for a depth of 0.43 mm, i.e., less than one-tenth of that for the top surface. This means that it is difficult for DLC film to be deposited on the inner surface of a micro-cavity. Fortunately, the thickness of DLC film is large at the corner of the opening side, and sufficient for the application in micro-deep drawing process to reduce the friction.

The mechanical properties of DLC film inside the micro-cavity, such as nano-hardness and adhesion strength, were evaluated. With the decrease of channel width, the hardness becomes lower. Also, it decreases with the increase of depth from the top surface. The adhesive strength between the DLC film and the substrate at the upper surface is about 125 mN, as obtained by scratch tests. However, the value of the adhesive strength at the inner surface is not attainable, as the scratch marks show a different failure mode. On the top surface, only a small part of DLC film is peeled off, which indicates that the failure mode is mainly brittle fracture, and that the adhesive strength is greater. With the decrease of channel width, the peeled-off part of the DLC film becomes very small. Even though the DLC film is broken for large plastic deformation of the substrate, the DLC film is not peeled off. The reason may be the different micro-structure of the DLC film because that the distribution of energy is not uniform in the micro-cavity of die during the deposition of the film.

To determine the mechanism for the mechanical properties shown above, the micro-structure of the DLC film was analyzed using Raman spectrum. The ratio of ID/IG decreases with the increase of channel width, which means that the number of sp^3 bonds becomes larger: thus the mechanical properties of a DLC film on a micro-cavity of large width are better than those for one of small width. When the width of the channel is 1.4 mm, the ratio 2.31 of ID/IG is close to the value of 2.23 for the top surface. When the depth is small, the ratio of ID/IG is almost the

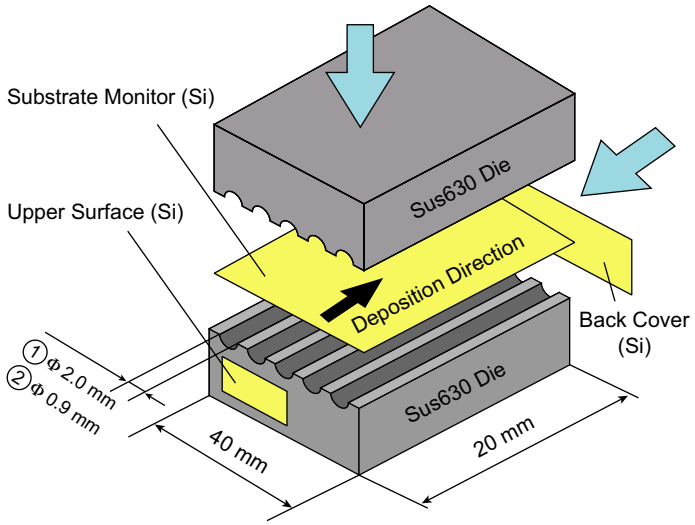

FIGURE 7

Schematic illustration of the die and Si wafers [27].

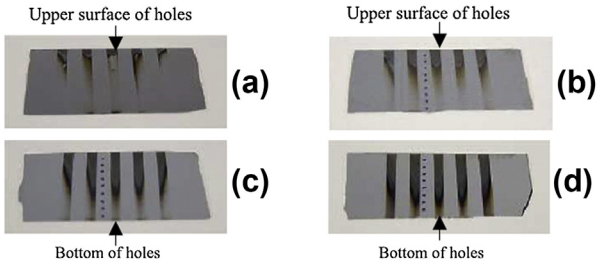

FIGURE 8

Photograph of the side Si monitor substrate inserted between the dies after deposition [27]. (a) 3 Pa (b) 6 Pa (c) 8 Pa (d) 10 Pa.

same. However, when the depth increases to 1.5 mm, the ratio of ID/IG becomes greater [25,26].

In another investigation [27], the effects of deposition pressure on the properties of DLC films were investigated with die holes of diameter of 2 and 0.9 mm, and a depth of 20 mm, using the pulse plasma CVD method (Figure 7), with argon gas being introduced to improve the situation. Photographs of the silicon monitor substrate are shown in Figure 8, the substrate being inserted between the divided dies after deposition. The length of the films deposited on the surface of the silicon wafer increased with increasing deposition pressure from 3 to 10 Pa. The Raman spectroscopic analysis results indicate that all deposited films are typical DLC films. The

measured hardness of films deposited under a pressure of 10 Pa is much lower than that deposited under a pressure of 6 Pa. For thinner holes of 0.9 mm diameter, the deposition time should be extended to ensure the obtaining of good deposition results on the inner wall surface of the dies. At the same time, the long deposition time may lead to the decrease of hardness. In order to improve the situation, it is of value to increase the length of the deposited films when increasing the deposition pressure, and argon gas was introduced to the chamber together with acetylene during the deposition of the DLC films for removing the redundant neutral radicals generated at high deposition pressure. The thickness distribution of films on the back cover of the dies becomes thinner from the center to the side of the dies. To obtain a uniform thickness distribution of the films on the bottom of dies, it is necessary to consider the size relation of the cathode and die in future research.

DLC-COATED TOOLS IN STRIP DRAWING

To evaluate the tribological properties of DLC film in micro-sheet forming, strip drawing tests were carried out as shown in Figure 9. The punch, made with tool steel JIS-SKD11, was deposited with TiN and DLC film in a plasma-based ion implantation and deposition (PBII&D) facility, and a MoS_2 coating with magnetron sputtering technique. With T2 copper sheet, the COF were reduced from 0.3 for no surface modification, to 0.21, 0.15, and 0.13 for DLC, MoS_2, and TiN film, respectively, with specimen of 1 mm width. This means that the surface film is very helpful in the decreasing of friction. When the width of specimen is changed from 1 to 2 mm, the size effects of friction do not occur. After about 100 tests, it is interesting to note that there is no cracking or chipping of the DLC film, which means that the DLC film has the ability to bear larger strain/stress [28]. In the strip-ironing test, the

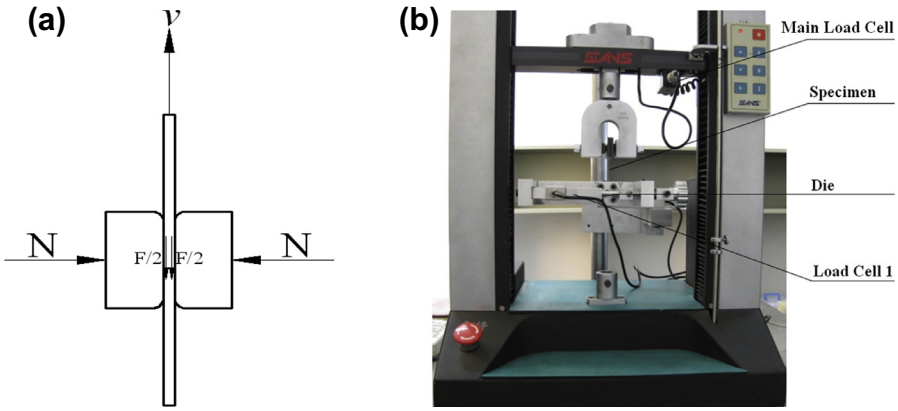

FIGURE 9

Schematic diagram of strip drawing and machine [28]. (a) Strip drawing, (b) machine for strip drawing tests.

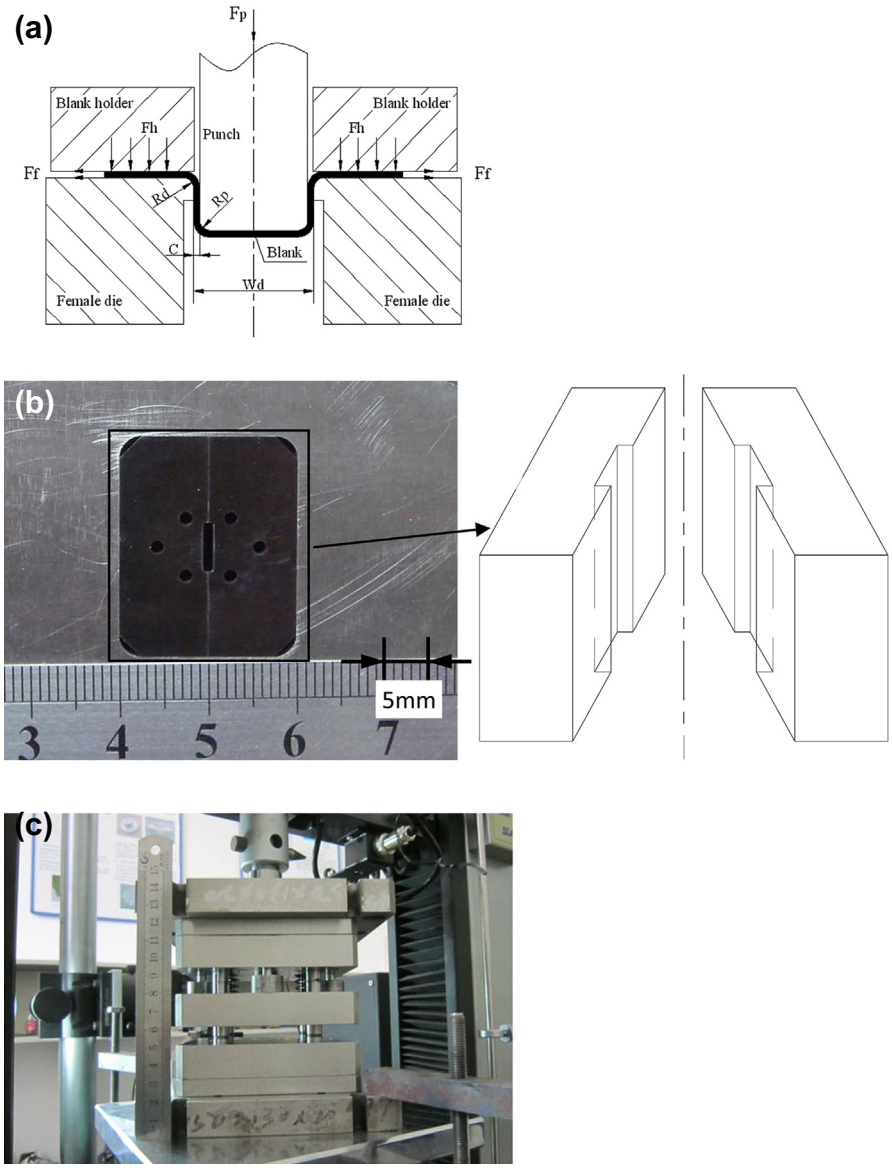

FIGURE 10

U-deep drawing device [29]. (a) Schematic of U-deep drawing. (b) Two-bodies DLC-coated female die. (c) Photograph of the die device.

Si-DLC film shows high potential in tribo-characters such as friction and antipickup, under the heavy conditions of high ironing reduction and no active lubrication. The Si-DLC has the possibility of application in dry forming with a high pressure, a surface expansion, and a long sliding distance [23].

A schematic diagram of the U-deep drawing process (Figure 10(a)) was developed with a set of two-bodies DLC-coated female die (Figure 10(b)) fabricated with JIS-SKD11, and a photograph of the die device is shown in Figure 10(c). The two-bodies female die can be surface modified separately, and then assembled and embedded in a container. With the design of this structure, it is easy to obtain micro-cavities with small dimensions, and helpful for deposition of DLC film in the inner surface of micro-cavities. A contact load such as 15 N is applied to the blank holder. Two kinds of lubricant, such as castor oil and DLC film, are used to investigate the tribological behavior in U-deep drawing during the miniaturization of the specimen under different lubrication conditions. As shown in Figure 11, with a DLC-coated female die, the punch load is smaller than that for no lubrication, but larger than that for castor oil when a specimen of 4.5 mm width is selected. When the width of specimen is reduced to 1 mm, the results indicate that the decreasing of specimen dimension does not lead to the reduction of the COF with the DLC-coated female die. When the surface of the specimen is polished using the electrochemical polishing process, the tribological behavior becomes worse with castor oil than that with DLC film [29].

DLC-COATED TOOLS IN MICRO-BENDING

A micro-bending test was utilized to evaluate the wear properties of DLC films, as shown in Figure 12. The shoulder radii of the die were varied from 30 to 600 μm for changing the concentration of stress on the die-surface during bending. The DLC films were deposited on the micro-bending dies under conditions of bias voltages of 1.0 and 3.0 kV, and a thin sheet (SUS304-H) of 0.1 mm in thickness was employed in the bending test. As shown in Figure 13, the evaluation of damage due to wear indicates a strong wear-proof property but delamination is easier with the condition of 1.0 kV. Contrarily, the DLC film with the condition of 3.0 kV shows strong adhesion to the substrate but is easier to wear [22]. By combining these two coating conditions, a two-layered DLC film deposited with 3.0 and 1.0 kV could supply a gradient in properties with both wear resistance and lower friction, which could be appropriate for metal forming at submillimeter size. Significant damage was not observed after more than 50,000 cycles for the die with a radius of 600 μm, which means that DLC film with a gradient in properties is practical for real production [30].

To improve the coated tool life, the nano-laminated DLC film was invented and deposited using unbalanced magnetron sputtering, and applied in the testing. The bias voltage U_b was alternatively controlled: at zero for the formation of the lower-density graphitic layers, and at -200 V for the formation of the higher-density disordered layers. The applied power was constant at 1.0 kW. The nano-layer ratio

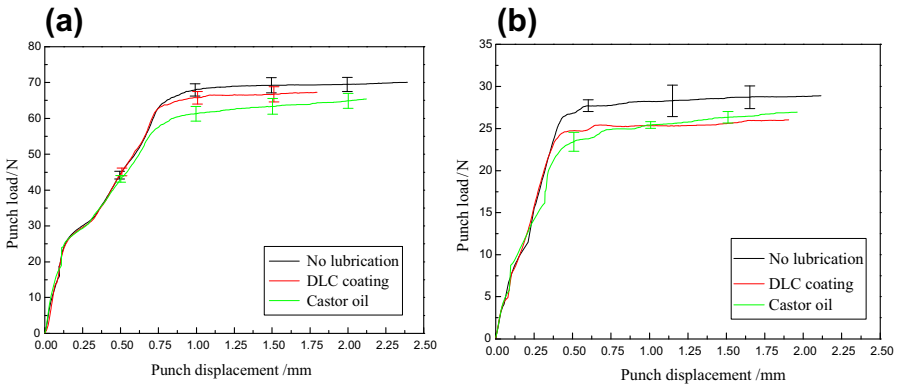

FIGURE 11

Curves of punch load versus punch displacement for different lubricants [29]. (a) 4.5 mm in width (b) 1 mm in width. DLC, diamond-like carbon.

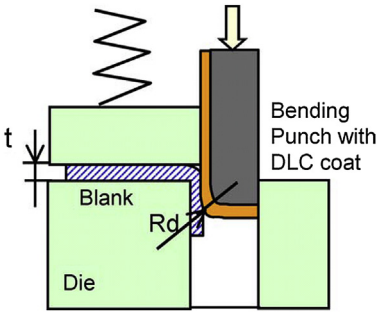

FIGURE 12

Schematic configuration of the micro-bending test [22]. DLC, diamond-like carbon.

affects the mechanical properties of nano-laminated DLC film, which can be controlled by varying the duration time for the formation of the low-density sublayer and the high-density sublayer [3]. The results indicate that both Young's modulus and hardness increase monotonically with decrease of the sublayer thickness. Using a coating with sublayer thickness of 10 nm, no delamination or cracking was detected on the inside of the scratched trace until the applied load was continuously increased up to 100 N. This suggests that the nano-laminated coating has sufficiently high wear resistance and toughness and that its scratching strength is quite rather insensitive to the number of layers. The nano-laminated coating was deposited on the tungsten carbide (WC) upper punch with sublayer thickness of 10 nm. After dry bending and ironing a hundred times, the ironed surface of the coated punch between the monolayer coated and nano-laminated tools are shown in Figure 14. The monolayered

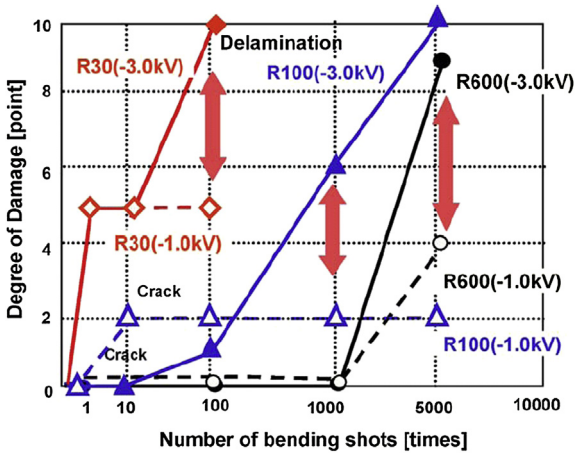

FIGURE 13

Progress of damage in the diamond-like carbon (DLC) film during bending test: (---) DLC film with −1.0 kV; (—) DLC film with −3.0 kV; (△) R30 μm; (◇) R100 μm; (○) R600 μm [22].

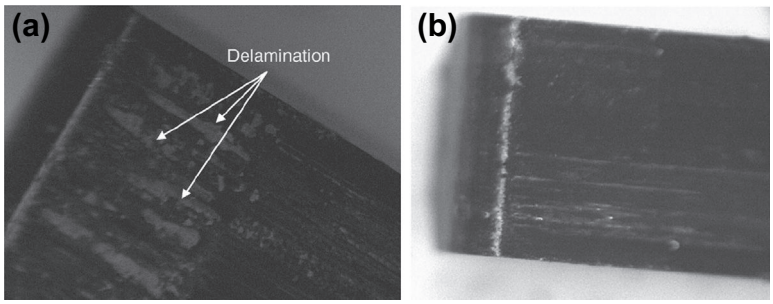

FIGURE 14

Comparison of the contact surface between the monolayered a-C:H coating (a) and the nano-laminated a-C:H coating after bending and ironing for 100 cycles (b) [31].

coating broke away and separated partially from the cemented carbide tool. On the other hand, no delamination or break-away tool place occurred when using the nano-laminated coating. After 2000 cycles under dry conditions there is significant change of the surface of the nano-laminated coating. No adhering work material was seen on the surface. This improvement of wear toughness might be due to the retardation and suppression of cracking with the nano-laminated structure [31,32].

DLC-COATED TOOLS IN MICRO-DEEP DRAWING

The micro-deep drawing of specimens of approximately 1 mm diameter was performed using DLC-coated blank holders and female dies. For the small dimensions

involved, it is very difficult to locate the specimens accurately in the micro-deep drawing process. A blanking/deep drawing multiple-operation mold was developed, as shown in Figure 15. Based on the analysis of friction in micro-deep drawing (Figure 16), the blank holder and female die, both manufactured with tool steel JIS-SKD11, were deposited with DLC film using the PBII&D method. To evaluate the performance of the coating, samples with a diameter of 30 mm and a thickness of 5 mm were also coated at the same time. The micro-structure of the DLC film was

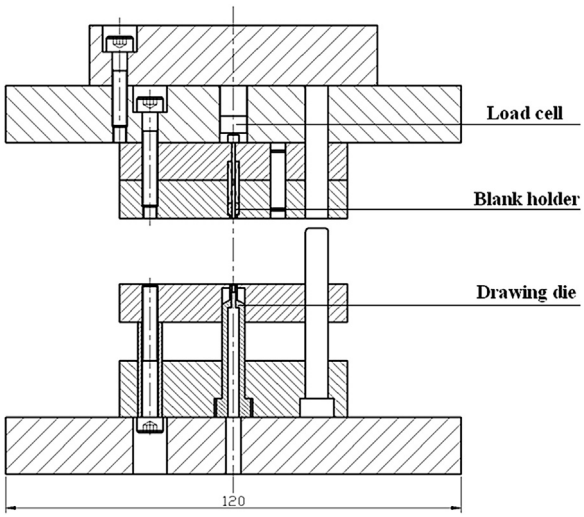

FIGURE 15

Schematic of the micro-blanking-deep drawing die [20].

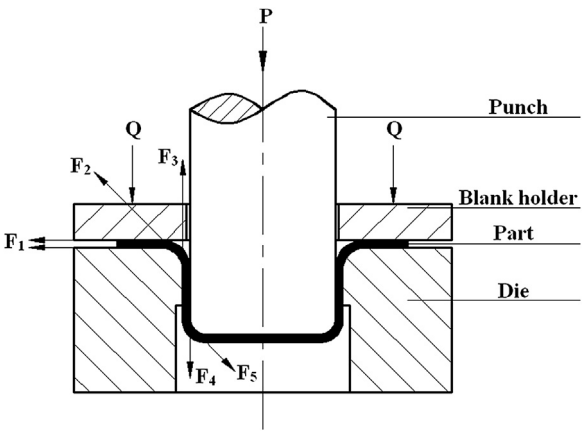

FIGURE 16

Friction in micro-deep drawing [20].

analyzed using Raman spectra (JY, HR800) with an excitation wavelength of 532 nm at a power of 0.1 mW. After Gauss-curve fitting, there are two obvious peaks at 1381.3 cm^{-1} and 1554.1 cm^{-1} as shown, which validates the typical microstructure of DLC film. The adhesive strength of DLC film with a substrate is from 97 to 125.6 mN. With strip-drawing experiments, a COF of 0.15 is obtained under a normal load of 9.6 N and a velocity of 0.01 mm/s. This indicates that the DLC film possesses excellent tribological properties, which can be used in the micro-deep drawing process [20,33].

The micro-deep drawing processes were carried out with T2 copper sheet and pure Au sheet with a thickness of 40 μm. Using pure Au thin sheet, the micro-cup was successfully deep drawn except for small wrinkles in the rim of the cups, using DLC-coated tools. When the plasma-enhanced (PE) film is applied, the situation is quite clearly changed. Numerous wrinkles appear at the upper part of the micro-cup. The limiting drawing ratio (LDR) is urgently pursued in industry in order to reduce the cost of manufacture. A series of drawing punches and dies were manufactured with an LDR ranging from 1.8 to 2.2, whereby micro-cups with different inner diameter were successfully deep drawn, as shown in Figure 17. The LDR was 2.1 under

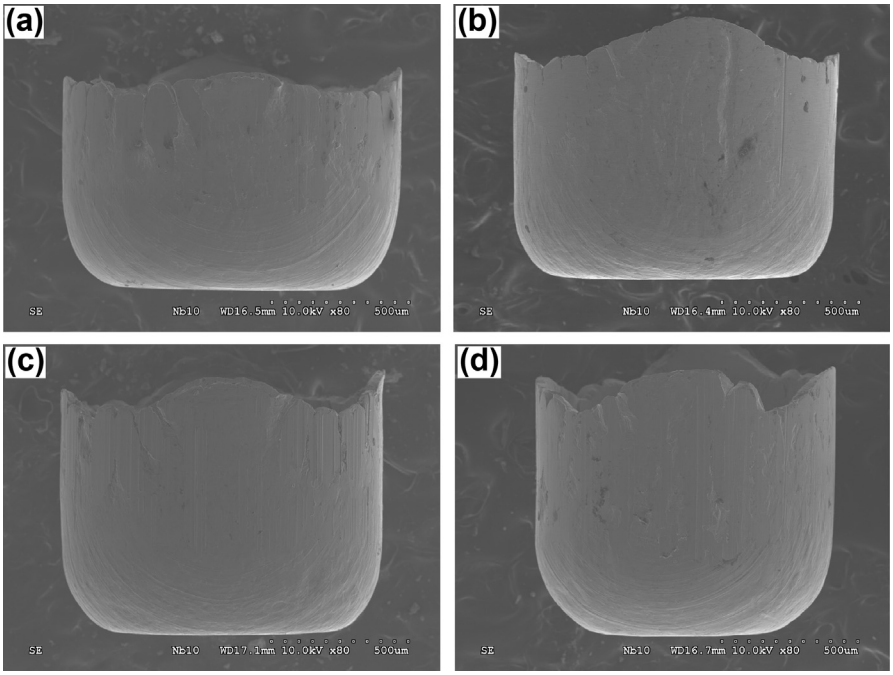

FIGURE 17

SEM images of micro-cups formed under the lubrication of diamond-like carbon film (a) d = 1.1 mm, (b) d = 1.05 mm, (c) d = 1.0 mm, (d) d = 0.95 mm [20].

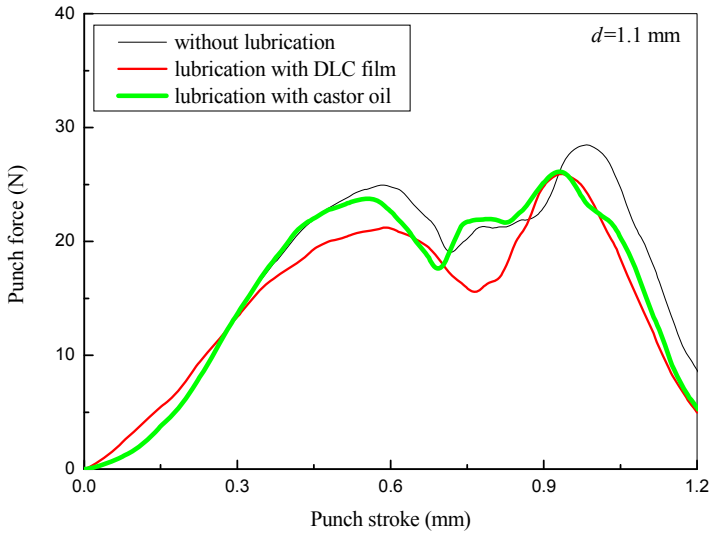

FIGURE 18

Punch stroke–punch force curves [20]. DLC, diamond-like carbon.

the lubrication of DLC film, which was much better than 1.8 without lubrication and 1.9 under the lubrication of castor oil [20,33]. Vollertsen also investigated the micro-deep drawing with DLC-coated dies using stainless steel sheet with a thickness of 25 μm. However, the obtained LDR is smaller [21].

To compare the lubrication properties of different lubrication conditions, tests without lubrication and lubricated with PE film and castor oil were carried out in addition to lubrication with DLC film. The density and viscosity of castor oil was 0.93×103 kg/m^3 and 0.61 Pa s, respectively. The drawing punch stroke–force curves for a drawing punch diameter of 1.1 mm are shown in Figure 18, using heat-treated T2 copper thin sheet. The punch load for lubrication with DLC film was reduced by approximately 15%. The reason is that the friction coefficient between the DLC film and sheet was much lower than that without lubrication, and the friction coefficient was not affected by the size effect throughout the drawing process [20]. When a PE film with excellent tribological properties was applied, the punch load for the PE film increases to 128.7% of that for a DLC film at the latter stages of the accumulation [33]. As more experiments were repeated using stainless steel sheet, the corresponding measured punch force versus stroke curves varied within a certain range. For example, the maximum punch force using the DLC-coated forming tool ranged from 41 to 46 N with a deviation of about ±6.1%, which is better than that for the TiN-coated forming tool. The measured punch force versus stroke for the deep drawing with uncoated forming tools is higher than that with DLC-coated forming tools, although a lubricant (mineral oil HBO) was used for deep drawing with uncoated forming tools [1,21]. This indicates that

the DLC film can reduce friction between the blank and the forming tool in micro-deep drawing more than for the lubricant and TiN coating.

The inner diameter of micro-cups using pure Au sheet was measured using a confocal laser scanning microscope. The diameters of the micro-cups are 1114.598 and 1096.838 μm for lubrication conditions of DLC film and PE film, respectively. The diameter of the micro-cup for DLC film is a little greater than that of the punch due to the springback of the thin sheet. In the case of PE film, the accumulation of PE film decreases the diameter of the female die, and the diameter of the micro-cup is almost the same as the diameter of the punch. The distribution of thickness is one of the important evaluation parameters in the deep drawing process because nonuniform thickness can lead to breakage of the micro-cup due to stress concentration in application. By measuring the thickness of micro-cups obtained under different lubrication conditions, it is shown that the greatest reduction of thickness occurs at the bottom corner of the micro-cup under both lubrication conditions: DLC film and PE film. An interesting feature is that a DLC-coated tool is helpful for the fabrication of micro-cups with uniform wall thickness [33].

After a small number of tests, no obvious cracks or similar damage caused by friction due to the so-called eggshell effect were observed in micro-deep drawing. This means that DLC film possesses excellent wear resistance in the bearing of high strain/stress. Therefore, DLC-coated tools have a great application potential in micro-forming under dry conditions [1,21]. The ratio of ID/IG obtained by Raman spectra increases to 2.1, which indicates that the number of sp^2 bonds becomes greater. Graphitization of DLC film occurs with increase of temperature induced by friction. With the increasing of the time of duration of the experiments, the graphitization of DLC film will become more serious, which may lead to the wear of DLC film [33].

The durability and wear of DLC film in mass production was investigated using a blanking and deep drawing tool combination with a maximum stroke rate of 200 ppm. Experiments with copper foil of 0.05 mm thickness were performed to produce cylindrical micro-cups with a diameter of 1.0 mm. The punch and die of 0.9 and 1.06 mm diameter, respectively, are both made of stainless steel. The results show that an uncoated tool has a longer life than a coated tool, which was not expected. After 5000 strokes, it can be observed that the DLC film starts to delaminate. When the number of strokes reached 15,000, the production of micro-cups in an automatic procedure was not possible due to cup base fractures produced [34]. To discover the mechanism of delamination of DLC film, the micro-structure of the cross section of the blanking and deep drawing tool combination was analyzed. High density of scattered carbides and pores with different size of up to 35 μm was observed. Because of their hardness, the carbides stick out from the rest of the tool material after the manufacturing of the tools, and small mesas can be formed on the carbides' surface during the coating process. The coated carbides can break out during a mechanical stress state as existing in micro-deep drawing, which may damage the DLC film and cause the delamination. Therefore, it is important to analyze the micro-structure before using a DLC-coated tool in micro-deep drawing [34].

When the dies and punches were made using WC, and coated by the nano-laminated DLC film, even after 50,000 strokes with Cu-alloy sheet, no delamination and damage took place on any surface of the punches and dies, together with no scratches on the surface of the drawn cups [3].

DLC-COATED TOOLS IN MICRO-BULK FORMING

DLC-COATED TOOLS IN MICRO-EXTRUSION

The validity of using high strength/low friction die coating was investigated in micro-extrusion by observing the tribological characteristics. Micro-extrusion tests with pure aluminum were carried out at room temperature using a segmented die to facilitate the deposition of the surface coating and the removal of the pins after extrusion. The segmented die was fabricated with a base diameter of 1.71 mm and the corresponding extrude diameter was 1.09 mm, while the diameter of the punch was 1.47 mm. The forming assembly was placed inside a novel experimental press. The coatings used in the test are DLC disposed by two different coating methods (DLC-Spatter and DLC-Arc): chromium nitride (CrN) and titanium nitride (TiN). The typical extrusion indicates that the maximum extrusion force for the DLC-Spatter-coated die is the lowest (25 kN) and that of the uncoated die is the highest (32 kN). The corresponding values for the DLC-Arc-coated die, CrN-coated die, and TiN-coated die were about 28, 30, and 29 kN, respectively. These results show that the DLC-Spatter coating produces the least friction and therefore has the lowest extrusion force [35]. In another similar micro-extrusion experiment, Si-DLC film deposited using PECVD shows the lowest extrusion force and the greatest pin-length extruded [36,37].

DLC-COATED TOOLS IN EMBOSSING/COINING

For mint application, the performance of proof coinage dies can be improved by DLC film with the filtered cathodic vacuum arc method. High-quality DLC films are prepared and emphasis is placed on the lifetime of the proof mint dies coated with the DLC films, which can be extended to approximately eight and four times corresponding to that of uncoated and hard chromium plating dies. The adhesive critical load value was observed to be more than 30 N. The sp^3 bond fraction in DLC films as examined by Raman spectroscopy and X-ray photoelectron spectroscopy was approximately 72%. DIN 2550 was selected as the die material due to its uniform and homogeneous structure that had no trace of bending, was free from undissolved primary carbides, and had a small level of porosity. Annealed silver (99.99%) and aluminum bronze (92Cu2Ni6Al) blanks were used in the investigation. Prior to the actual deposition of the DLC films, a thin titanium interlayer of thickness less than 0.1 μm was deposited onto the substrate to increase the adhesive strength of the coating. Figure 19 shows the schematic illustrations of the coining process. Significant plastic deformation during coining can be noticed. Three

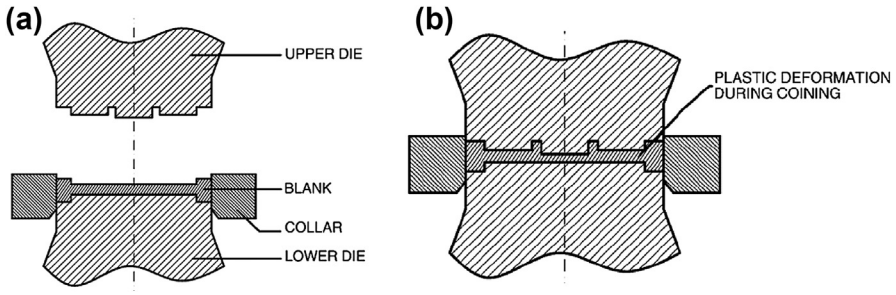

FIGURE 19

Schematic illustration of the coining process (a) coining setup, (b) press and induce plastic deformation [38].

loading−unloading cycles were performed to make one single coin. Even at 30,000 strokes, failure of the die surface at the conjunction point did not occur. This implies that the adhesion and quality of the DLC film are excellent. When the number of strikes exceeded 200,000 in silver and aluminum−bronze coin production, the failure mechanisms of DLC film for the coining process were summarized as (1) die sinking and/or die settling due to the plastic deformation of substrates, (2) microcracks and local DLC film breakdown due to surface pinholes of the DIN 2550 substrate, and (3) high-stress abrasion and/or impact wear due to inclusions within the blank [38].

DLC film can also be etched to mold-die tools for micro-forming. Differently from conventional plasma etching with use of chemically active agents, only oxygen gas or oxygen−argon mixtures are employed as a carrier gas to make etching carbon-based bulk and coating materials. The unmasked regions of DLC film are selectively removed by this plasma etching. A two-dimensional mask pattern for micro-hole patterning with a hole-diameter of 50 μm is made. The geometric deviation of hole-diameter and periodicity in the imprinting lies in the range of 1 μm [39]. Its geometric accuracy is essentially determined by the micro-etching behavior and the resolution in micro-texturing. The slender walls of micro-grooved DLC would have a risk of collapsing if the aspect ratio of its width to depth is greater than 3.0. Using the micro-embossing system, these micro-textures on larger-area products were duplicated onto aluminum sheets without wrinkling and damage [40].

DIAMOND TOOLS IN EMBOSSING

For the purpose of improving the die life and lubrication, diamond micro-dies were fabricated with a hot-filament CVD method using silicon negatives seeded with diamond nano-crystals, as shown in Figure 20. PMMA using the diamond dies were fabricated by hot embossing at 423 K under 980 N without a lubricant (shown in Figure 21). The PMMA specimen was a plate of 20 mm in length and width, and 1.0 mm in thickness, and molded according to the configurations of the diamond

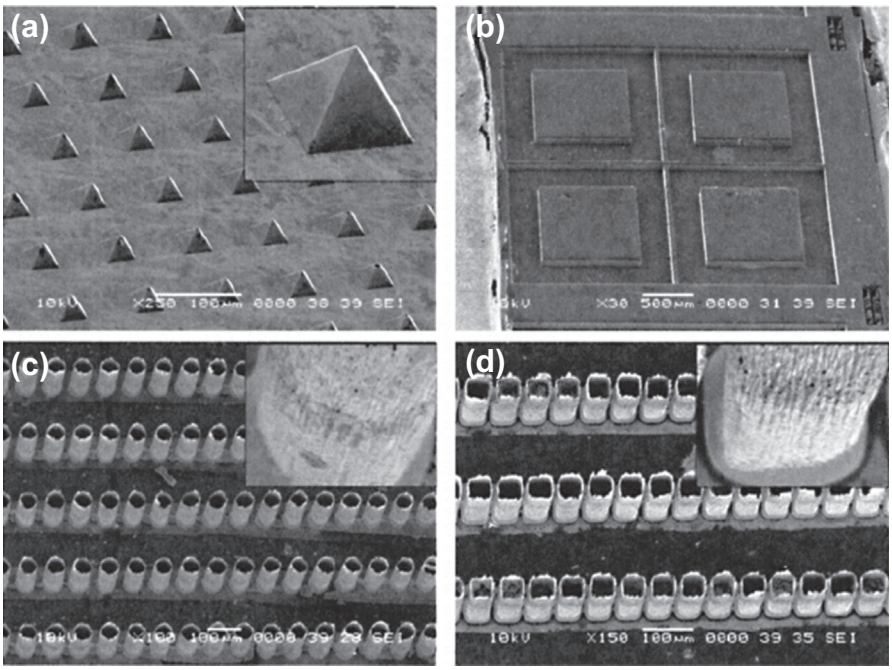

FIGURE 20

SEM micrographs of the fabricated diamond dies: (a) pyramids, (b) square poles and crossed wall, (c) round, and (d) square hollow [41].

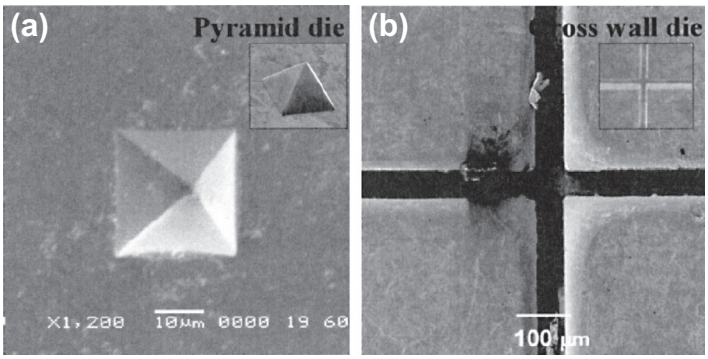

FIGURE 21

SEM micrograph of the micro-structures fabricated by micro-forming with the diamond dies: (a) pyramid and (b) crossed channels [41].

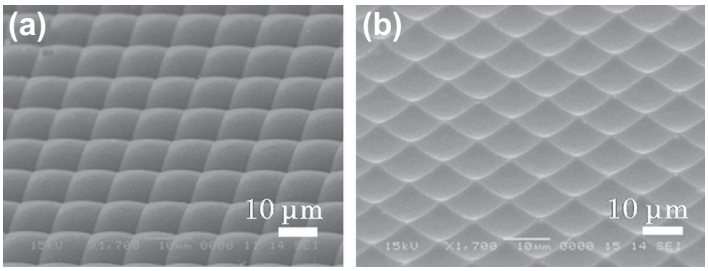

FIGURE 22

SEM surface image of (a) the diamond mold for the micro-lens array, and (b) the imprinted glass [42].

dies. Scratch marks and droops introduced by releasing the die from the workpiece were not observed. This indicates that the diamond dies have good lubricating ability under dry conditions. The diamond die is therefore more appropriate for micro-forming than conventional silicon and nickel dies [41].

For the nano-imprinting tests of glasses at high temperature, the surface smoothing of the diamond film was performed by conventional high-frequency inductively coupled plasma reactive ion etching. Figure 22(a) shows the diamond mold used for imprinting glass micro-lens arrays. Figure 22(b) shows the typical appearance of the silicate glass micro-lens array fabricated by imprinting at 600 °C. The figures reveal that there were no defects either on the diamond mold or on the imprinted glass. Quartz glass micro-lenses were also fabricated by imprinting at a higher temperature (1330 °C). Cracks were absent in the obtained micro-lens array. The quartz glass micro-lens array had a three-dimensional (3D) ultrafine surface structure with a maximum depth of 5 μm, which was close to the structure with the maximum depth of 6 μm in the mold. The results indicate that the diamond dies have good releasability and shape transcription properties at temperatures above 1330 °C [42].

DLC-COATED TOOLS IN NANO-FABRICATION/IMPRINTING

Three-dimensional structures are required in various devices such as optical devices (micro-lens, photonic crystals, etc.). Focused-ion-beam chemical vapor deposition is very useful for the fabrication of 3D structures [43]. Nano-imprinting of Pd-based metallic glass (MG) was performed with fabricated dot arrays of 13−18 nm diameter and 7−34 nm gap widths in a vacuum atmosphere of 10^{-3} Pa. The concave hole array was clearly replicated on the MG surface. The flow distance into the hole was proportionately correlated with the gap width, which depended upon the ratio of specific surface to volume [44].

The DLC is well known to have the advantages of lower surface energy, lower friction, and high hardness. These excellent properties are of importance in

application as an antiadhesion layer in ultraviolet nano-imprint lithography. To ensure UV transparency for use as a UV stamp, it is important to control the DLC film thickness because a thick DLC layer has the shortcoming of low UV transparency. A DLC film of less than 10 nm is found to have a UV transparency of approximately 80% with good antiadhesion characteristics. From the results, excellent correlations between 3D multilayered stamps and imprinted features can be observed without any problems. This indicates that micro-scaled structures can be created in a single step using the DLC-coated stamps. However, intensive investigation into working life, the yield of antiadhesion measures, and the variation of the coating thickness of a DLC layer still remain to be resolved by further study [45].

Although the surface energy of the DLC film is relatively low, it is still not low enough for achieving smooth and easy postimprint separation. Thus, an additional surface treatment is required. It has already been demonstrated that the in situ fluorination of DLC during growth significant lowers its surface energy. The advancing contact angle of water was found to increase from 70° for bare DLC to 90°−100° upon plasma fluorination under different conditions for both C_4F_8 and CHF_3 [46−48]. The DLC film could also be fluorinated using a Plasmalab 80+ reactive ion etcher with CF_4 as the fluorine source to improve the durability in the nano-imprint lithography. Comparisons between SiO_2 imprinters and <3-nm thick F-DLC SiO_2 imprinters have shown a significant improvement in the quality of the pattern transfer along with the durability of the imprinter after multiple samples were imprinted utilizing the same imprinter [49,50].

Not only as an antistick layer, the DLC film was deposited and patterned for imprint templates that offer high wear resistance and robust antistick surfaces. The abrasive wear of DLC films on Si and quartz indicates that the wear resistance of a DLC template is 3 times better than that of quartz and almost 2 times better than that of Si [51].

WEAR MECHANISM OF DLC FILM

The deposited DLC films can be characterized by small clusters of sp^2-bonded carbon that are interconnected with a network of sp^3 carbon-bonded hydrogen. The sp^3-oriented carbon structure in DLC can be thought of as formed by compressing several hydrogen atoms into one carbon vacancy. Sliding-induced heat accumulating on local contact areas can probably cause a gradual destabilization of carbon−hydrogen bond in the sp^3 tetrahedral structure. The removal of hydrogen atoms, as has been reported by calorimetry experiments, can thus trigger the transformation of the sp^3 structure into a graphite-like sp^2 structure [52].

The wear of DLC film is different from that of simple rigid contact sliding because of the plastic deformation of the surface micro-asperities. As shown in Ref. [29], the wear mechanism of DLC film was analyzed in micro-U-deep drawing using DLC-coated tools. As shown in Figure 23, the peak frequency of the G peak increases slightly, which indicates that some important changes occur in the

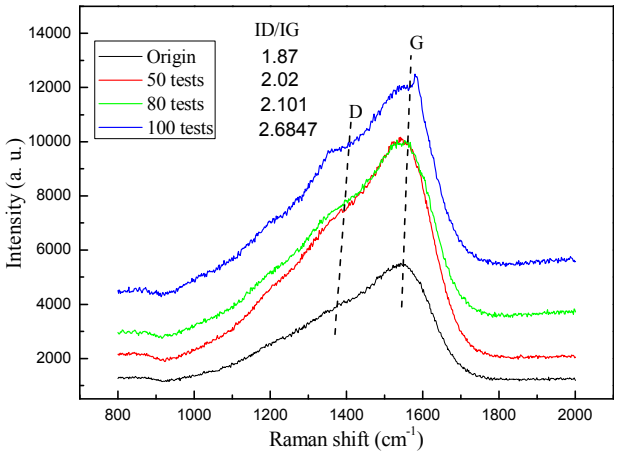

FIGURE 23

Raman spectra of a DLC film after tests (normal load 15 N) [29].

micro-structure of the DLC film. The integrated intensity ratio of the D and G bands (ID/IG) derived from curve-fitting increases with the increasing of the test duration. This means that a part of the sp^3 bonds transform to sp^2 bonds, and graphitization of the DLC film appears clearly after 100 times of testing.

The internal energy change per unit volume accompanying the conversion process of the sp^3 carbon structure to pure sp^2 structure is shown in Eqn (1):

$$Q = C_{\mathrm{DLC}}\rho\Delta T \tag{1}$$

where C_{DLC} is the specific heat of the DLC, ρ is the density, and ΔT is the temperature increment at which the sp^3 structure is converted into sp^2 structure.

The graphitization of DLC film can be analyzed considering the frictional work. Considering the micro-topography of the specimen surfaces, a micro-asperity can be treated as a micro-pin, and the real contact area can be obtained using Eqn (2):

$$a = 0.0182(PDC_E)^{1/3} \tag{2}$$

Here, P is the normal load applied to the micro-asperity, D is the diameter of the micro-asperity, and C_E can be obtained by the elastic moduli and Poisson's ratio of the specimen and the DLC film. As shown in Figure 24, the real contact area is the summation of every contact area of the micro-pins. The friction work per test can be calculated using Eqn (3):

$$W = \sum Pf(2a) = 0.0364\sum fP^{4/3}(DC_E)^{1/3} \tag{3}$$

where f is the COF. When the frictional work overcomes the energy barrier of transformation from sp^3 bond to sp^2 bond, the graphitization of DLC film occurs. This means that the wear of the DLC film begins.

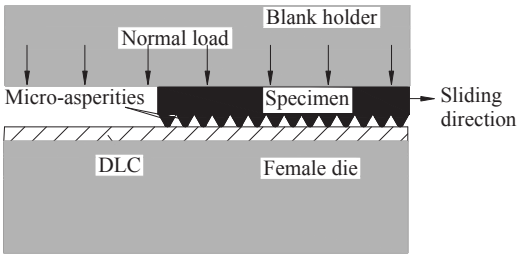

FIGURE 24

Schematic diagram of the contact state in U-deep drawing [29]. DLC, diamond-like carbon.

REFERENCES

[1] Hu Z, Wielage H, Vollertsen F. Economic micro forming using DLC- and TiN-coated tools. J Technol Plast 2011;36(2):51−8.
[2] Bay N, Azushima A, Groche P, Ishibashi I, Merklein M, Morishita M, et al. Environmentally benign tribo-systems for metal forming. CIRP Ann Manuf Technol 2010; 59(2):760−80.
[3] Morita H, Aizawa T, Yoshida N, Kurozumi S. Dry transfer stamping by nano-laminated DLC-coated tool. In: Proceeding of 10th Int Conf Techn Plast IBF (RWTH Aachen)& IUL (TU Dortmund); 2011. p. 1103−8.
[4] Tiesler N, Engel U. Microforming-effects of miniaturization. In: The 8th international conference on metal forming; 2000. p. 355−60.
[5] Engel U. Tribology in microforming. Wear 2006;260:265−73.
[6] Guo B, Gong F, Wang CJ, Shan DB. Size effect on friction in scaled down strip drawing. J Mater Sci 2010;45:4067−72.
[7] Vollertsen F, Hu Z. Tribological size effects in sheet metal forming measured by a strip drawing test. CIRP Ann Manuf Technol 2006;55(1):291−4.
[8] Wang C, Shan DB, Guo B, Xu J, Zhang H. Effect of nano-crystals at surfaces induced by ion beam irradiation on the tribological behaviour in microforming. Vacuum 2013; 89:267−70.
[9] Robertson J. Diamond-like amorphous carbon. Mat Sci Eng R 2002;37:129−281.
[10] Reisel G, Dorner-Reisel A, Wielage B. Silicon doped diamond like carbon as substitute for lubrication in spin-extrusion. Diamond Relat Mater 2005;14:1810−4.
[11] Murakawa M, Jin M, Hayashi M. Study on semidry/dry wire drawing using DLC film dies. Surf Coat Technol 2004;177−178:631−7.
[12] Wank A, Reisel G, Wielage B. Behavior of DLC film in lubricant free cold massive forming of aluminum. Surf Coat Technol 2006;201:822−7.
[13] Reisel G, Wielage B, Steinhäuser S, Hartwig H. DLC for tools protection in warm massive forming. Diamond Relat Mater 2003;12:1024−9.
[14] Reisel G, Steinhäuser S, Wielage B. The behavior of DLC under high mechanical and thermal load. Diamond Relat Mater 2004;13:1516−20.
[15] Jacob W, Moller W. On the structure of thin hydrocarbon films. Appl Phys Lett 1993;63: 1771−3.
[16] Ferrari AC, Robertson J. Interpretation of Raman spectra of disordered and amorphous carbon. Phys Rev B 2000;61:14095−107.

[17] Grill A. Diamond-like carbon: state of art. Diam Relat Mater 1999;8:428−34.
[18] Erdemir A, Donnet C. Tribology of diamond-like carbon films: recent progress and future prospects. J Phys D Appl Phys 2006;39:R311−27.
[19] Lifshitz Y. Diamond-like carbon-present status. Diamond Relat Mater 1999;8:1659−76.
[20] Gong F, Guo B, Wang CJ, Shan DB. Micro deep drawing of micro cups by using DLC film coated blank holders and dies. Diamond Relat Mater 2011;20:196−200.
[21] Hu ZY, Schubnov A, Vollertsen F. Tribological behaviour of DLC-films and their application in micro deep drawing. J Mater Process Tech 2012;212:647−52.
[22] Fujimoto K, Yang M, Hotta M, Koyama H, Nakano S, Morikawa K, et al. Fabrication of dies in micro-scale for micro-sheet metal forming. J Mater Process Tech 2006;177: 639−43.
[23] Kitamura K, Ymamoto T, Tsuchiya Y, Dohda K. Application of DLC-coating to metal forming die. In: ICTMP. Yokohama; 2007. p. 169−74.
[24] Wang Z, Kuboda H, Taniguchi V, Tsuchiya Y. Fracture behavior of DLC films coated on tool materials in indentation test. In: ICTMP. Yokohama; 2007. p. 189−93.
[25] Wang CJ, Guo B, Shan DB, Tian XB. Properties of DLC film inside of micro-channel cavities prepared with PSII. Rev Adv Mater Sci 2013;33:119−25.
[26] Wang CJ, Guo B, Shan DB, Zhang H. Properties of DLC film deposited on mould with micro-cavity used in microforming. Integr Ferroelectr 2012;136:35−42.
[27] Yang XD, Saito T, Nakamura Y, Kondo Y, Ohtake N. Mechanical properties of DLC films prepared inside of micro-holes by pulse plasma CVD. Diamond Relat Mater 2004;13:1984−8.
[28] Wang CJ, Wang CJ, Guo B, Shan DB. Effects of tribological behaviors of DLC film on micro-deep drawing processes. Trans Nonferrous Met Soc China 2014;24:2877−82.
[29] Wang CJ, Guo B, Shan DB, Bai XM. Tribological behaviors of DLC film deposited on female die used in strip drawing. J Mater Process Tech 2013;213:323−9.
[30] Yang M, Manabe K, Ito K. Micro press forming and assembling of micro parts in a progressive die. J Mech Sci Technol 2007;21:1338−43.
[31] Aizawa T, Iwamura E, Itoh K. Nano-lamination in amorphous carbon for tailored coating in micro-dry stamping of AISI-304 stainless steel sheets. Surf Coat Technol 2008;203:794−8.
[32] Aizawa T, Itoh K, Iwamura E. Nano-laminated DLC film for dry micro-stamping. Steel Res Int 2010;81(9):1169−72.
[33] Wang CJ, Guo B, Shan DB, Bai XM. Experimental research on micro-deep drawing processes of pure gold thin sheet using DLC-coated female die. Int J Adv Manuf Technol 2013;67:2477−87.
[34] Flosky H, Vollertsen F. Wear behavior of a DLC-coated blanking and deep drawing tool combination. Key Eng Mater 2013;549:511−7.
[35] Takatsuji N, Dohda K, Makino T, Yoshimura T. Friction behavior in aluminum microextrusion. In: International conference on tribology in manufacturing processes. Yokohama; September 2007. p. 157−62.
[36] Krishnan N, Cao J, Dohda K. Microforming : study of friction conditions and the impact of low friction/high strength die coatings on the extrusion of microparts. In: Proceeding of ASME international mechanical engineering conference and exposition; November 2005. p. 1−10. Orlando.
[37] Krishnan N, Cao J, Dohda K. Study of the size effects on friction conditions in microextrusion-Part I: microextrusion experiments and analysis. J Manuf Sci Eng 2007;129:669−76.

[38] Lin W, Leu MS, Lin CK, Su CY. The failure mechanism of diamond like coating prepared by the filtered cathodic arc technique for minting application. Surf Coat Technol 2006;201:4430−5.
[39] Aizawa T, Itoh K, Fukuda T. Fine micro-stamping system for micro-pattern printing onto polymers and glasses. In: Proceeding of 10th international conference technology of plasticity; 2011. p. 1097−102.
[40] Aizawa T. Micro-texturing onto amorphous carbon materials as a mold-die for microforming. Appl Mech Mater 2013;289:23−37.
[41] Hanada K, Zhang L, Mayuzumi M, Sano T. Fabrication of diamond dies for microforming. Diamond Relat Mater 2003;12:757−61.
[42] Takezawa N, Yamanoi T, Iizuka K, Hiraide T, Yoshikawa H, Ando Y, et al. Fabrication of a diamond-based imprint mold by applying diamond CVD on silicon master molds for a glass microlens array. Diamond Relat Mater 2011;20:866−70.
[43] Watanabe K, Morita T, Kometani R, Hoshino T, Kondo K, Kanda K, et al. Nanoimprint using three-dimensional microlens mold made by focused-ion-beam chemical vapor deposition. J Vac Sci Technol B 2004;22(1):22−6.
[44] Fukuda Y, Saotome Y, Nishiyama N, Inoue A. Influence of wetting behavior on nanoprint of metallic glass in sub-10 nm scale. In: Proceeding of the 6th Asian workshop on Micro/Nano forming technology. Jeju Island; October 2013. p. 8−11.
[45] Park SH, Lim TW, Yang DY, Jeong JH, Kim KD, Lee KS, et al. Effective fabrication of three dimensional nano/microstructures in a single step using multilayered stamp. Appl Phys Lett 2006;88:203105.
[46] Houle FA, Rettner CT, Miller DC, Sooriyakumaran R. Antiadhesion considerations for UV nanoimprint lithography. Appl Phys Lett 2007;90:213103.
[47] Schvartzman M, Mathur A, Kang Y, Jahnes C, Hone J, Wind SJ. Fluorinated diamondlike carbon templates for high resolution nanoimprint lithography. J Vac Sci Technol B 2008;26(6):2394−8.
[48] Schvartzman M, Mathur A, Hone J, Jahnes C, Wind SJ. Plasma fluorination of carbon-based materials for imprint and molding lithographic application. Appl Phys Lett 2008; 93:153105.
[49] Fillman RW, Carroll J, Krchnavek RR. Toward a universal anti-stick layer for nanoimprint lithography imprinters: ultra-thin F-DLC. In: 2009 IEEE nanotechnology materials and device conference. Traverse City; June 2009. p. 186−9.
[50] Fillman RW, Krchnavek RR. Ultrathin fluorinated diamondlike carbon coating for nanoimprint lithography imprinters. J Vac Sci Technol B 2009;27(6):2869−72.
[51] Ramachandran S, Tao L, Lee TH, Sant S, Overzet LJ, Goechner MJ, et al. Deposition and patterning of diamondlike carbon as antiwear nanoimprint templates. J Vac Sci Technol B 2006;24(6):2993−7.
[52] Liu Y, Erdemir A, Meletis EI. A study of the wear mechanism of diamond-like carbon films. Surf Coat Technol 1996;82:48−56.

CHAPTER

22 Micro- and Nano-fibers by Electrospinning Technology: Processing, Properties, and Applications

Ioannis S. Chronakis

Technical University of Denmark, DTU-Food, Søltofts Plads, Lyngby, Denmark

CHAPTER OUTLINE

Micromanufacturing Engineering and Technology. http://dx.doi.org/10.1016/B978-0-323-31149-6.00022-0

INTRODUCTION

Human beings have used fibers for centuries. In 5000 BC, our ancestors used natural fibers such as wool, cotton silk, and animal fur for clothing. Mass production of fibers dates back to the early stages of the industrial revolution. The first man-made fiber—viscose—was presented in 1889, at the World Exhibition in Paris. Developments in the polymer and chemical industries—as well as in electronics and mechanics—have led to the introduction of new types of man-made fibers, especially the first synthetic fibers, such as nylon, polypropylene, and polyester. The needs and further progress allowed the production of high-functionality fibers (antistatic, flame-resistant, etc.) and high-performance fibers (carbon fibers in 1960 from viscose and aramid fibers in 1965) that showed high strength, a high modulus, and great heat-resistance. These fibers are used not only in clothing but also in hygienic products, medical and automotive applications, geotextiles, and other applications.

Traditional methods for polymer fiber production include melt spinning, dry spinning, wet spinning, and gel-state spinning. These methods rely on mechanical forces to produce fibers by extruding a polymer melt or solution through a spinneret and subsequently drawing the resulting filaments as they solidify or coagulate. These methods allow the production of fiber diameters typically in the range of 5−500 μm. At variance, *electrospinning technology* allows the production of fibers of much smaller dimensions. The fibers are produced by using an electrostatic field [1].

Electrospinning is a fiber-spinning technology used to produce long, three-dimensional (3D), ultrafine fibers with diameters in the range of a few nanometers to a few microns (more typically 100 nm−1 μm) and lengths of up to kilometers (Figure 1). When used in products, the unique properties of nano-fibers are utilized, such as extraordinarily high surface area per unit mass (∅ of 100 nm−1000 m^2/g), very high porosity, tuneable pore size, tuneable surface properties, layer thinness, high permeability, low basic weight, ability to retain electrostatic charges, and cost-effectiveness, among others [2].

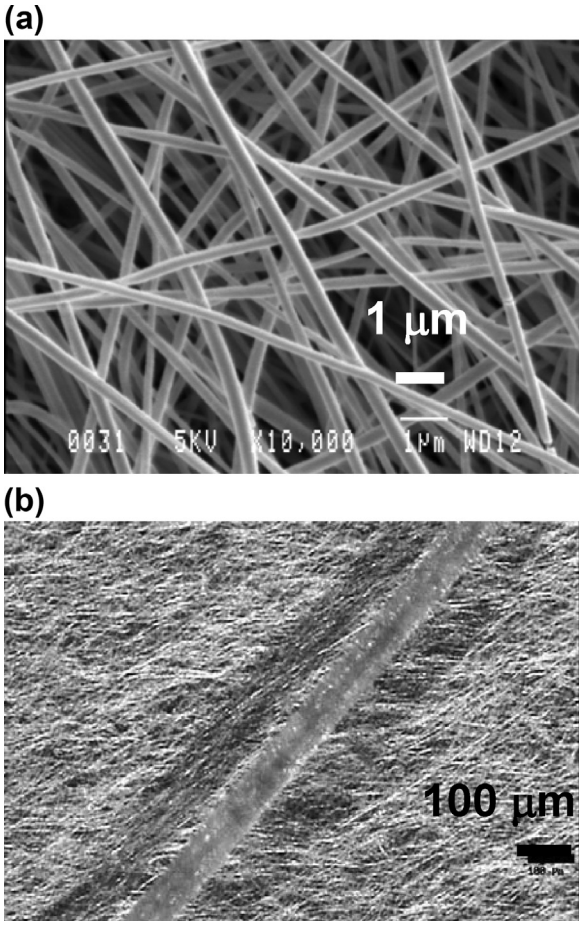

FIGURE 1

(a) SEM image of poly(ethylene terephthalate) (PET) nanofiber web. The nanofibers were electrospun from a PET solution in THF:DMF. The diameter of the fibers is about 200 nm. (b) PET nanofiber web - comparison with human hair [1].

While electrospinning technology was developed and patented by Formhals [3] in the 1930s, it was only about 20 years ago that actual developments were triggered by Reneker and coworkers [4]. Interest today is greater than ever and this cost-effective technique has made its way into several scientific areas, such as biomedicine, filtration, electronics, sensors, catalysis, and composites [5,6]. Electrospinning is a continuous technique and is hence suitable for high-volume production of nanofibers. The ability to customize micro- and nano-fibers to meet the requirements of specific applications gives electrospinning an advantage over other, larger scale, micro- and nano-production methods. Carbon and ceramic nano-fibers made of polymeric precursors further expand the list of possible uses of electrospun nanofibers [7].

WORKING PRINCIPLE AND CONFIGURATION OF ELECTROSPINNING PROCESSING

Electrospinning is increasingly being used to produce ultrathin fibers from a wide range of polymer materials. This nonmechanical, electrostatic technique involves the use of a high-voltage electrostatic field to charge the surface of a polymer-solution droplet, thereby inducing the ejection of a liquid jet through a spinneret (Figure 2). In a typical process, an electrical potential is applied between a droplet of a polymer solution held at the end of a capillary tube and a grounded target. When the electric field that is applied overcomes the surface tension of the droplet, a charged jet of polymer solution is ejected. On the way to the collector, the jet will be subjected to forces that allow it to stretch immensely. Simultaneously, the jet will partially or fully solidify through solvent evaporation or cooling, and an electrically charged fiber will remain, which can be directed or accelerated by electrical forces and then collected in sheets or other useful shapes.

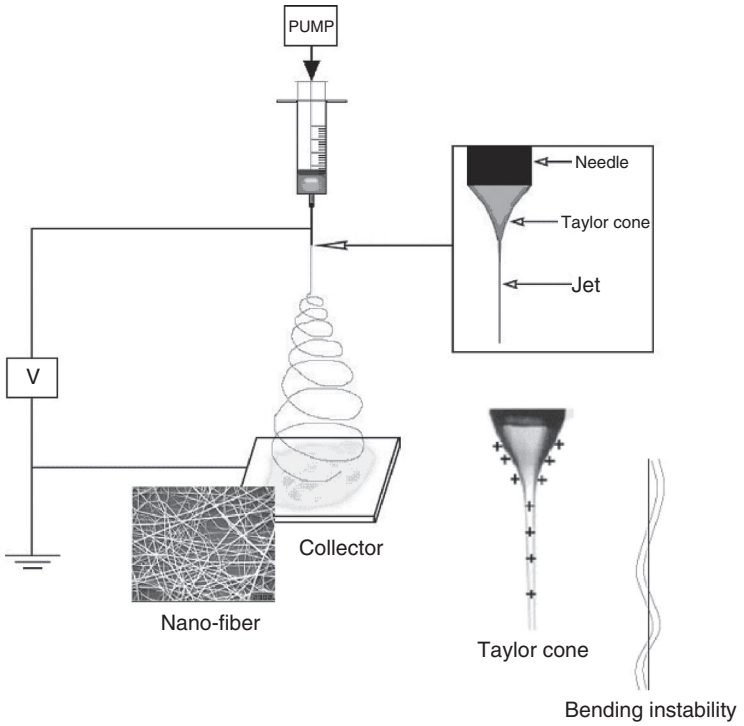

FIGURE 2

Schematic illustration of the conventional setup for electrospinning. The insets show a drawing of the electrified Taylor cone, bending instability and a typical SEM image of the non-woven mat of PET nanofibers deposited on the collector. The bending instability is a transversal vibration of the electrospinning jet. It is enhanced by electrostatic repulsion and suppressed by surface tension.

A characteristic feature of the electrospinning process is the extremely rapid formation of the nano-fiber structure, which occurs on a millisecond scale. Other notable features of electrospinning are a huge material elongation rate of the order of 1000 s^{-1} and a reduction of the cross-sectional area of the order of 10^5 to 10^6, which have been shown to affect the orientation of the structural elements in the fiber.

THE ELECTROSPINNING MECHANISM

In spite of the simple setup for electrospinning, the actual spinning mechanism is quite complex. Although extensive studies have been conducted to explore the mechanism, some aspects and phenomena are not yet fully understood.

FORMATION OF THE TAYLOR CONE AND SUBSEQUENT FLUID JET

When the high-voltage field is applied, the droplet of polymer solution at the tip of the needle will become highly electrified and the charges induced will be evenly distributed over the polymer solution surface. The droplet will experience two types of electrostatic forces: electrostatic repulsion between the charges on the surface and Coulombic forces in the external field. Under the influence of these two forces, the droplet will be elongated and finally distorted into a so-called Taylor cone. As the voltage increases, the electrostatic forces will become stronger and eventually overcome the surface tension, and a charged jet of fluid will be ejected.

Both electrostatic and fluid dynamic instabilities can contribute to the basic operation of the process.

Reznik et al. [8] experimentally and numerically studied the shape evolution of small droplets attached to a conducting surface that was subjected to relatively strong electric fields. Three different scenarios of droplet shape evolution are distinguished, based on numerical solution of the Stokes equations for perfectly conducting droplets:

1. In sufficiently weak (subcritical) electric fields, the droplets are stretched by the electric Maxwell stresses and acquire steady-state shapes where equilibrium is achieved by means of surface tension.
2. In stronger (supercritical) electric fields, the Maxwell stresses overcome the surface tension, and jetting is initiated from the droplet tip if the static (initial) contact angle of the droplet with the conducting electrode is $\alpha_s < 0.8\ \pi$; in this case, the jet base acquires a quasi-steady, nearly conical, shape with a vertical semiangle of $\beta \leq 30^\circ$, which is significantly smaller than that of the Taylor cone ($\beta_T = 49.3^\circ$).
3. In supercritical electric fields acting on droplets with a contact angle in the range $0.8\ \pi < \alpha_s/<\pi$, there is no jetting and almost the whole droplet jumps off: this is similar to gravity or drop-on-demand dripping.

The droplet-jet transitional region and the jet region proper are studied in detail for the second case using quasi-one-dimensional equations, taking into account the inertial effects and additional features such as the dielectric properties of the liquid (leaky dielectrics). The flow in the transitional and jet region is matched to that in the

droplet. This is used to predict the current−voltage characteristic, $I = I(U)$, and the volumetric flow rate, Q, in electrospun viscous jets, given the potential difference applied. The predicted dependence, $I = I(U)$, is nonlinear due to the convective mechanism of the charge redistribution superimposed on the conductive (Ohmic) mechanism. Realistic current values $I = O(10^2\ \text{nA})$ have been predicted for $U = O(10\ \text{kV})$ and fluid conductivity $\sigma = 10^{-4}$ S/m.

THINNING OF THE FLUID JET

Beyond the conical base, immediately at the end of the capillary tip, the jet continues to become thinner. This jetting mode is known as the electrohydrodynamic cone jet. The jet will initially travel in a straight line toward the collector but will eventually become unstable. To the naked eye, it looks like the jet splits into multiple jets and it was thought before 1999 that this was the main reason for the small diameter of the electrospun fibers. However, when the jet is examined with a high-speed camera, it can clearly be seen that the splaying is actually one single fiber rapidly bending or whipping, causing the fiber to make lateral excursions that grow into spiraling loops.

Jet splitting does occur, but it is not as common as previously thought and it is not the dominant process that occurs during spinning. Bending or whipping is caused by a phenomenon called *bending instability* and can occur in electrified fluid jets. Every loop then grows larger in diameter and the jet becomes thinner. New bending instabilities arise when the jet is thin enough and enough stress relaxation of the viscoelastic stress has taken place. This is called the second instability region and is very similar to the first instability region but acts on a much smaller scale. A tertiary-bending instability has also been documented. Each cycle of bending instability can be described in three steps:

1. A smooth, straight, or slightly curved segment starts to bend.
2. The segment of the jet in each bend elongates and a spiral of growing loops develops.
3. As the perimeter of the loops increases, the diameter of the jet decreases. When the perimeter of the loop is large enough and the diameter of the jet is small enough, the conditions of the first step of the cycle are fulfilled. The next cycle of bending instability then begins.

Several research groups have attempted to explain the bending instability by mathematical models.

ELECTROSPINNING PROCESSING PARAMETERS—CONTROL OF THE MICRO- AND NANO-FIBER MORPHOLOGY

The fiber morphology has been shown to be dependent on process parameters, namely solution properties (system parameters), process conditions (operational parameters), and ambient conditions [1,2].

SOLUTION PROPERTIES

Solution properties are those such as molecular weight, molecular weight distribution and architecture of the polymer, and properties such as viscosity, conductivity, dielectric constant, and surface tension. The polymer solution must have a concentration high enough to cause polymer entanglements, yet not so high that the viscosity prevents polymer motion induced by the electric field. The resulting fibers' diameters usually increase with the concentration of the solution according to a power law relationship. Decreasing the polymer concentration in the solution produces thinner fibers. Decreasing the concentration below a threshold value causes the uniform fiber morphology to change into beads [9]. The main factors affecting the formation of beads (Figure 3) during electrospinning have been shown to be solution viscosity, surface tension, and the net charge density carried by the electrospinning jet. Higher surface tension results in a greater number of bead structures, in contrast to the parameters of viscosity and net charge density, for which higher values favor fibers with fewer beads. This reduction in thickness is due to the solution conductivity, which reflects the charge density of the jet and thus the elongation level. The surface tension also controls the distribution and the width of the fibers, which can be decreased by adding a surfactant to the solution. Adding a surfactant or a salt to the solution is a way to increase the net charge density and thus reduces the formation of beads. Finally, the choice of solvent(s) directly affects all of the properties mentioned and is of major importance to the fiber morphology.

PROCESS CONDITIONS

The parameters in the process are spinning voltage, distance between the tip of the capillary and the collector, solution flow rate (feed rate), needle diameter and, finally, the motion of the target screen. Voltage and feed rate show different tendencies and are less effective in controlling fiber morphology as compared to the solution properties. Too high a voltage might result in splaying and irregularities in the fibers. A bead structure is evident when the voltage is either too low or too high. However, a higher voltage also leads to a higher evaporation rate of the solvent, which in turn might lead to solidification at the tip and instability in the jet. Morphological changes in the nano-fibers can also occur upon changing the distance between the syringe needle and the substrate. Increasing the distance or decreasing the electrical field decreases the bead density, regardless of the concentration of the polymer in the solution.

AMBIENT CONDITIONS

Ambient conditions include factors such as humidity and temperature, air velocity in the spinning chamber, and atmospheric pressure. Humidity primarily controls the formation of pores on the surface of the fibers. Above a certain threshold level of humidity, pores begin to appear and, as the level increases, so does the number and size of the pores.

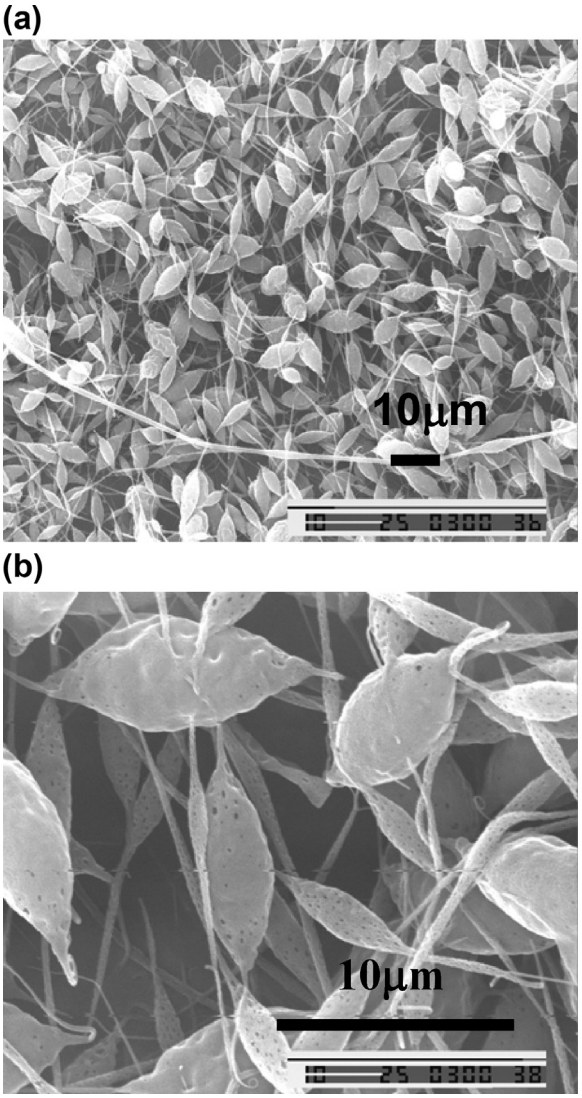

FIGURE 3

Example of bead formation during electrospinning: SEM micrographs of poly(propyl carbonate) (PPC) beads prepared by electrospinning a PPC solution in dichloromethane [9].

The precise mechanism behind the formation of pores and texturing on the surface is complex and is thought to be dependent on a combination of breath figure formation and phase separation. Breath figures are imprints formed due to the evaporative cooling during evaporation of the solvent, which results in condense solvent drops on the surface and, later, pores. Surface porosity (Figure 4) can also be achieved by selective removal of one of the components in the polymer blend after

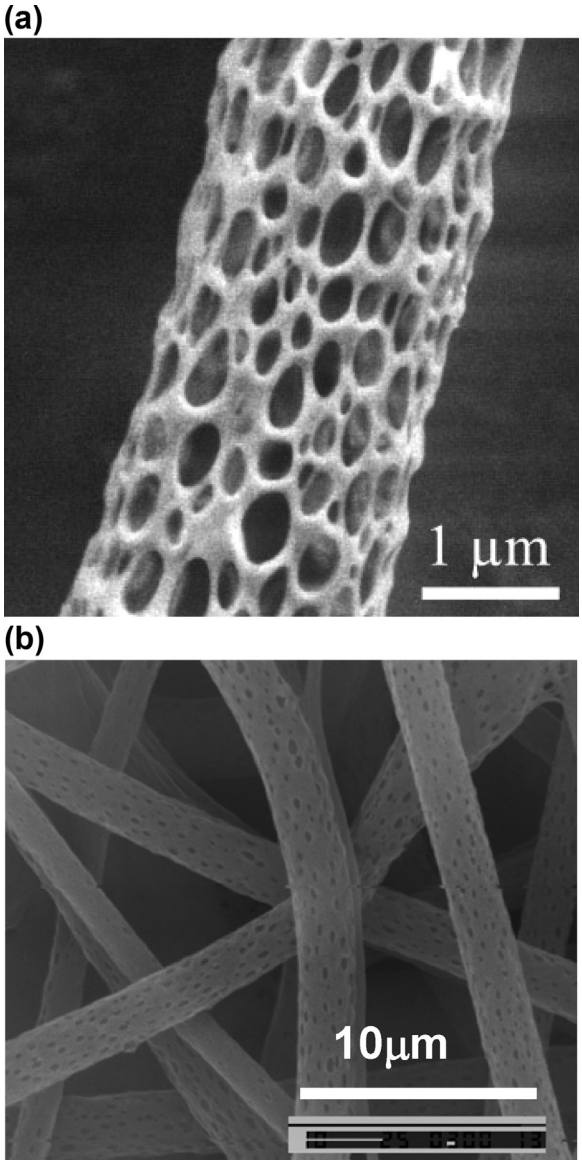

FIGURE 4

SEM images of (a) porous poly(L-lactide) (PLA) nanofibers prepared by electrospinning a solution of PLA in dichloromethane [5]. (b) Poly(propyl carbonate) (PPC) nanofibers with a porous surface electrospun from a PPC solution in dichloromethane [9].

spinning. The pores formed on the fiber surface can be used, for example, to capture nano-particles, act as a cradle for enzymes or increase the surface area for filtration applications.

Baumgarten studied the spinning velocities in addition to the effect of the flow rate, voltage, gap, and the surrounding atmosphere [10]. He was able to determine the spinning velocity using the power balance:

$$IV = \frac{\dot{m}_s \dot{v}_s^2}{2} \tag{1}$$

where V is the potential, I is the current, and $\dot{m}_s$ and $\dot{v}_s$ are the mass flow rate and the spinning velocities, respectively. The calculation showed velocities close to the velocity of sound in air. Other researchers calculated velocities of the fibers reaching the collector to be 140–160 m/s. Obviously, these speeds must depend on the process parameters and solution used.

Increasing the solution temperature is also a method for speeding up the process, but it might cause morphological imperfections, such as the formation of beads. Furthermore, the regulation of scale and bifurcation-like instability in electrospinning are intriguing problems that remain to be solved. Regulatory mechanisms for controlling the radius of electrospun fibers at the different states are clearly illustrated in the work by He et al. [11].

ELECTROSPINNING SETUPS AND TOOLS

NOVEL SETUPS

The traditional setup for electrospinning has been modified in a number of ways during the last few years in order to be able to control the electrospinning process and tailor the structure of micro- and nano-fibers.

Yarin and Zussman achieved upward electrospinning of fibers from multiple jets without the use of nozzles; instead using the spiking effect of a magnetic liquid [12]. The concept (Figure 5) consists of a bath filled with a layer of magnetic liquid (a). This liquid is covered by the solution to be spun (b). An electrode is submerged into the magnetic fluid (d). A counter electrode (c) as a collector is placed a certain

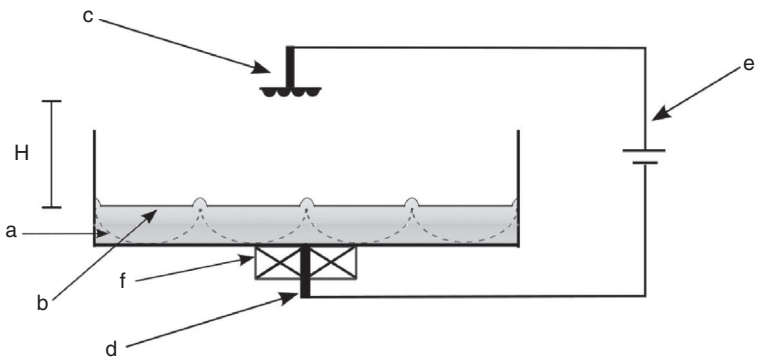

FIGURE 5

Schematic representation of the upward electrospinning set-up [12].

distance above this bath. A strong permanent magnet or electromagnet (f) is placed under the bath around the electrode. When a magnetic field is applied, the spiking effect causes some of the polymer solution to protrude into the electrical field applied between the electrodes (c and d). The protrusion is sufficient to initiate multiple jets of polymeric fibers traveling toward the collector. The production rate was reported to be about 12 times that of a conventional setup. This approach also avoids clogging problems.

Using supercritical CO_2-assisted electrospinning, polymer fibers of high molecular weight polydimethylsiloxane and poly (D,L-lactic acid) (PLA) were produced by means of only electrostatic forces and without the use of a liquid solvent. The fibers were formed between two electrodes in a high-pressure view cell. This supported the idea that the supercritical CO_2 reduces the polymer viscosity sufficiently to allow fibers to be pulled electrostatically from an undissolved bulk polymer sample.

Electrospinning in a vacuum is also a novel setup. Compared to electrospinning in air, a vacuum allows higher electric field strength over large distances and higher temperatures compared to what can be achieved in air, which influences both the spinning process and the morphology of the fibers that are produced. Other attempts have been made to incorporate vibration technology in polymer electrospinning. The idea is to produce finer nano-fibers under lower applied voltage by vibration technology. Other electrospinning setups are discussed in a recent review by Teo and Ramakrishna [6].

SETUPS INVOLVING DUAL SYRINGES

A setup was developed for electrospinning involving a dual syringe spinneret (Figure 6). The development enables spinning highly functional nano-fibers such as hollow nano-fibers, nano-tubes, and fibers with a core–shell structure [13]. A recent study describes the formation of hollow nano-tubular fibers in a single step using electrospinning and sol–gel chemistry. The method exploits electrohydrodynamic forces that form coaxial jets of liquids with microscopic dimensions. A high voltage is applied to a pair of concentric needles used to inject two immiscible liquids that lead to the formation of a two-component liquid cone that elongates into coaxial liquid jets and forms hollow nano-fibers.

SETUPS CONTROLLING THE ORIENTATION AND ALIGNMENT OF MICRO- AND NANO-FIBERS

A number of setups that allow control over the orientation of fibers have been developed. The orientation is crucial for different applications of nano-fibers and opens new opportunities for manufacturing yarn, micro- and nano-wire devices, etc. Most of the setups are based on rotating collection devices.

A technique called *dry rotary electrospinning* involves the organization and alignment of electrospun nano-fibers into planar assemblies [14]. The technique (Figure 7) involves a rotating disk as a grounded collector that stretches the coils into aligned rings. The dry fibers in a ring shape can be collected into linear strands to form a nano-fibrous yarn.

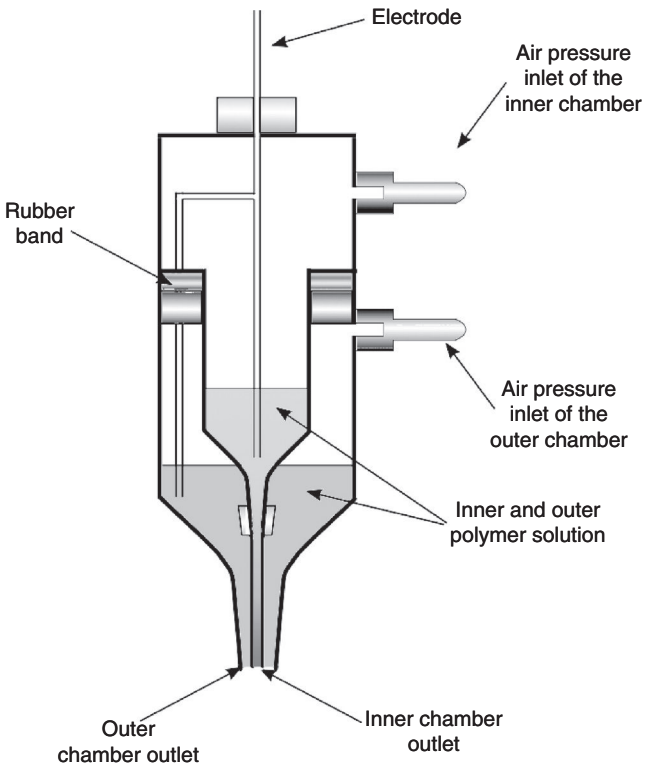

FIGURE 6

Schematic illustration of the setup used to co-electrospin compound core-shell nanofibers. It involves the use of a spinneret consisting of two coaxial capillaries through which two polymer solutions can simultaneously be ejected to form a compound jet [13].

Another method for controlled deposition of oriented nano-fibers uses a micro-fabricated scanned tip as an electrospinning source [15]. The tip is dipped in a polymer solution to gather a droplet as a source material. A voltage applied to the tip causes the formation of a Taylor cone and, at sufficiently high voltages, a polymer jet is extracted from the droplet. By moving the source relative to a surface, thus acting as a counter-electrode, oriented nano-fibers can be deposited and integrated with micro-fabricated surface structures. This electrospinning technique is called a *scanned electrospinning nano-fiber deposition system*. In addition to achieving uniform fiber deposition, the scanning tip electrospinning source can produce self-assembled composite fibers of micro- and nano-particles aligned in a polymeric fiber.

Using a frame as a countered electrode also allows an oriented deposition of fibers [16]. The same effect can be accomplished by placing two electrodes parallel to each other that are separated by a void [17]. A modified method for electrospinning that generates uniaxially aligned arrays of nano-fibers over large areas

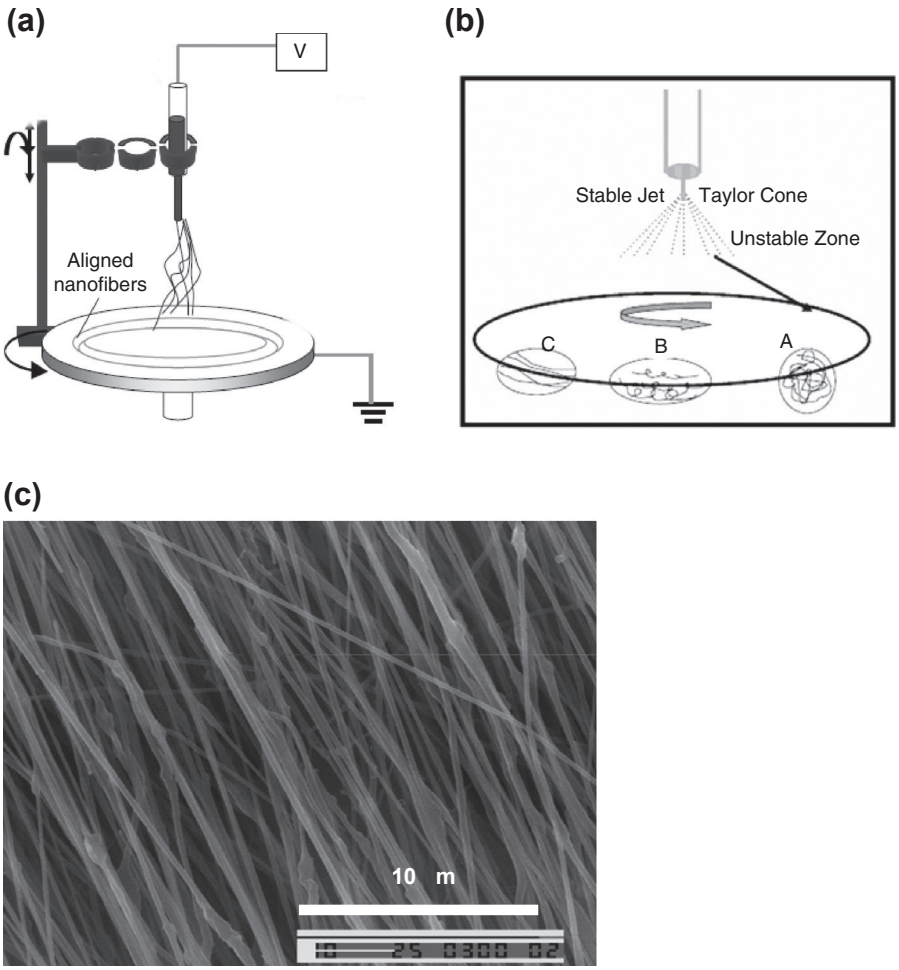

FIGURE 7

The rotary electrospinning apparatus: (a) schematic illustration of the setup used for electrospinning nanofibers as uniaxially aligned arrays. (b) Schematic illustration of the effect of the rotating speed on the formation of fibers [14]. (c) Aligned Poly(vinylidene-fluoride) (PVDF) nanofibers (Chronakis et al., unpublished results).

has also been reported. A collector composed of two conductive strips separated by an insulating gap of variable width was used. Directed by electrostatic interactions, the charged nano-fibers are stretched to span across the gap and become uniaxially aligned arrays. Two types of gaps were demonstrated: void gaps and gaps made of a highly insulating material. When a void gap was used, the nano-fibers could readily be transferred onto the surfaces of other substrates for various applications. When an insulating substrate was involved, the electrodes could be patterned into various designs on the solid insulator. In both cases, the nano-fibers could be conveniently stacked into multilayered architectures with controllable hierarchical structures.

Zussman et al. reported an approach to a hierarchical assembly of nano-fibers into crossbar nano-structures [18]. The polymer nano-fibers are created through an electrospinning process with diameters in the range of 10–80 nm and lengths up to centimeters. When the electrostatic field and the polymer rheology of the nano-fibers are controlled, they can be assembled into parallel periodic arrays. These authors also observed failure of nano-fibers owing to a multiple necking mechanism, sometimes followed by the development of a fibrillar structure, during electrospinning using a rotating tapered accumulating wheel (electrostatic lens). This phenomenon was attributed to a strong stretching of solidified nano-fibers by the wheel, if its rotation speed became too high. Necking has not been observed in the nano-fibers collected on a grounded plate.

Various other setups have been reported in the production of oriented, continuous nano-fibers such as using copper wires spaced evenly in the form of a circular drum as a collector and the use of a rotating wheel. In particular, the work by Theron and coworkers described an electrostatic field-assisted assembly technique that was combined with an electrospinning process used to position and align individual nano-fibers on a tapered and grounded wheel-like bobbin [19]. The bobbin is able to wind a continuous as-spun nano-fiber at its tip-like edge. The alignment approach resulted in nano-fibers with diameters ranging from 100 to 300 nm and lengths of up to hundreds of microns.

As described previously, one of the most important factors influencing the deposition of the fibers produced through conventional electrospinning is the whipping effect. The chaotic motions of the fiber jet originated by the whipping effect, causes difficulties in controlling the structure of the deposited fiber meshes. A *near-field electrospinning* (NFES) process has been developed to deposit solid nano-fibers in a direct, continuous, and controllable manner [20,21]. A tungsten electrode with tip diameter of 25 μm was used to construct nano-fibers of 50–500 nm line width on silicon-based collectors while the liquid polymer solution is supplied in a manner analogous to that of a dip pen. The minimum applied bias voltage is 600 V, and minimum electrode-to-collector distance is 500 mm to achieve position controllable deposition. Charged nano-fibers can be orderly collected, and can be assembled into controlled complex patterns such as circular shapes and grid arrays on large and flat areas, thus, making NFES a potential tool in direct write nano-fabrication for a variety of materials.

CHARACTERISTICS AND DESIGN CONSIDERATIONS OF ELECTROSPUN MICRO- AND NANO-FIBERS

MOLECULAR ORIENTATION

In traditional fiber spinning, the molecular orientation obtained by stretching the fibers after their formation is critical for their strength. The molecular orientation of electrospun fibers has also been a subject of various studies.

Dersch and coworkers studied the intrinsic structure of polyamide (nylon 6) and PLA electrospun fibers [16]. They found that the fibers do not differ a great deal from as-spun thicker fibers obtained by melt spinning and showed rather disordered crystals and different degrees of crystal orientations. The orientation seems to be almost absent in the PLA fibers and to be locally strong, yet inhomogeneous, in the polyamide fibers. However, stretching the PLA fibers did lead to an increased orientation of the crystals along the fibers' axis. On the other hand, the electrospinning of polyethylene oxide (PEO), for example, causes some molecular orientation but a poorly developed crystalline micro-structure.

Collecting electrospun fibers onto a high-speed rotating drum can enhance the molecular orientation up to an optimal speed, after which the orientation can decrease slightly [22]. In the report of a study using a high-speed winder, it was suggested that a critical winding speed exists that just matches the "natural" velocity of the fiber (due to electrohydrodynamic forces) and that additional drawing of the fiber should occur for higher winding speeds. This work concluded that the degree of molecular orientation, which develops only due to electrohydrodynamic forces and, hence, would be expected in nonwoven electrospun fabrics, is quite low.

SHAPES AND SIZES

In addition to circular fibers, a variety of cross-sectional shapes and sizes can be obtained from different polymers during electrospinning. Koombhongse and coworkers actually obtained branched fibers, flat ribbons, ribbons of other shapes, and fibers that were split longitudinally from larger fibers in electrospinning a polymer solution [23]. Studies of the properties of fibers with these cross-sectional shapes from a number of different kinds of polymers and solvents indicate that effects of the fluid mechanics, the electrical charge carried with the jet, and evaporation of the solvent all contributed to the formation of the fibers.

Sung and Gibson used polycarbonate in another study [24]. Electrospun fibers created in this process showed a wrinkled structure that was found to depend on the rate of evaporation of the solvent from the surface related to the rate of evaporation from the core. Indeed, as the solvent on the surface evaporated and a "skin" formed, the solvent entrapped in the core diffused into the ambient atmosphere and caused what they called a "raisin-like structure." A rapid evaporation of solvent from the jet that creates a skin, as mentioned above, can in fact give rise to hollow fibers that can collapse into a ribbon.

ALTERATIONS OF SECONDARY STRUCTURE AND FUNCTIONALITY

The electrospinning process is highly versatile and allows not only the processing of many different polymers into polymeric nano-fibers but also the coprocessing of polymer mixtures and mixtures of polymers and low-molecular-weight nonvolatile materials. This is done simply by using ternary solutions of the components for electrospinning to form a combination of nano-fiber functionalities. Polymer blends,

core–shell structures, and side-by-side bicomponent electrospinning are growing research areas that are connected with the electrospinning of multicomponent systems. The targets are either to create nano-fibers of an "unspinnable" material or to adjust the fiber morphology and characteristics.

The option of spinning a polymer blend renders possible the creation of core–shell nano-fibers through phase separation as the solvent evaporates. Another method for creating a structure of this kind is to coelectrospin two different polymer solutions through a spinneret consisting of two coaxial capillaries (see Figure 6). Nano-fibers with hollow interiors are used in several applications, such as nanofluidics and hydrogen storage. Electrospun tubular fibers can also be used as sacrificial templates.

The electrospinning technique also provides the capacity to lace together a variety of types of nano-particles or nano-fillers to be encapsulated into an electrospun nano-fiber matrix (Figure 8) [25]. Several functional components (e.g., nanometer-sized particles, nano-fillers, carbon nano-tubes, drugs, enzymes, and DNA) can be

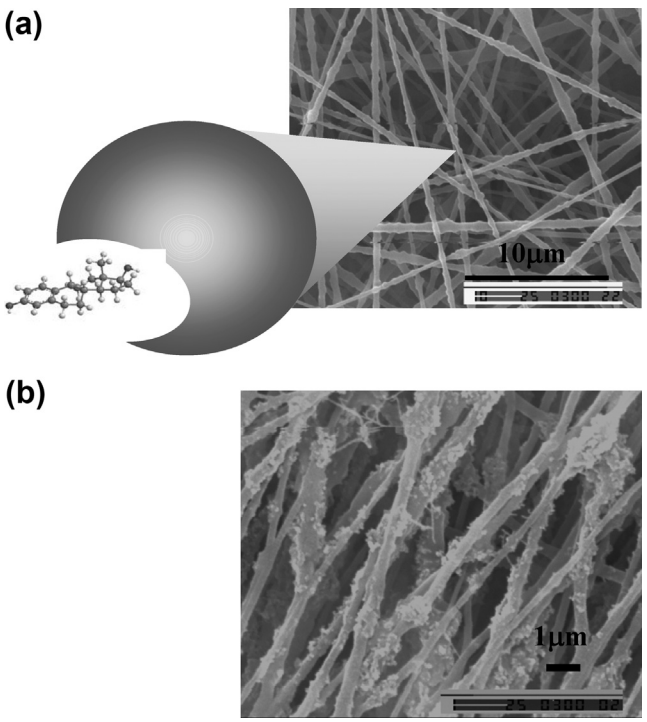

FIGURE 8

SEM images of (a) electrospun poly(ethylene terephthalate) (PET) nanofibers containing encapsulated molecular imprinted 17beta-estradiol nanoparticles (50% of the nanofibers content) [25]. (b) electrospun polyurethane (PU) nanofibers coated with SiC ceramic nanoparticles (Chronakis et al., unpublished results).

dispersed in the initial polymer solutions, which are then electrospun to form composites in the form of continuous nano-fibers and nano-fibrous assemblies.

Another interesting aspect of nano-fiber processing is that it is feasible to modify not only their morphology and their (internal bulk) content, but also their surface structure in order to carry various chemically reactive functionalities. Thus, nano-fibers can be easily postsynthetically functionalized, for example, by using plasma modification, physical or chemical vapor deposition, and chemical modifications such as cross-linking or grafting. By varying the processing parameters, it is also possible to produce fibers with unique surface features and secondary structures such as micro-textured/nano-porous fibers and micro- and nano-webs.

Besides traditional two-dimensional (2D) nano-fibrous structures, electrospinning is powerful in fabrication of *three-dimensional* (*3D*) *fibrous macro-structures*, especially for tissue engineering applications. A recent article summarizes recent advances in electrospinning techniques, including multilayering electrospinning, postprocessing after electrospinning, liquid-assisted collection, template-assisted collection, porogen-added electrospinning, and the self-assembly of some typical electrospun 3D fibrous macro-structures such as fibrous honeycomb structure, nano-fiber yarns, and fibrous stacks [26]. These 3D nano-fibrous macro-structures have been demonstrated to have potential applications in tissue engineering, energy harvesting and storage, and filtration.

APPLICATIONS OF ELECTROSPUN FUNCTIONAL MICRO- AND NANO-FIBERS

Electrospun micro- and nano-structures are a class of novel materials that is exciting because of several of the unique characteristics discussed above. Significant progress has been made in this field in the last few years, and the resulting micro- and nano-structures may serve as a highly versatile platform for a broad range of important technological applications in areas such as biomedicine, pharmacy, sensors, catalysis, filter, composites, ceramics, electronics, and photonics. Some of the most recent developments in their processing and the relevant applications that are considered are presented below.

BIOMEDICAL APPLICATIONS

Tissue engineering

Electrospun 3D nano-fibrous structures meet the essential design criteria of an ideal tissue engineered scaffold based upon their unique action in supporting and guiding cell growth [27,28]. Most studies confirm that the electrospun nano-fibrous structure is capable of supporting cell attachment and proliferation. The structure features a morphological similarity to the extracellular matrix (ECM) of natural tissue, which is characterized by a wide range of pore diameter distribution, high porosity, and effective mechanical properties (Figure 9).

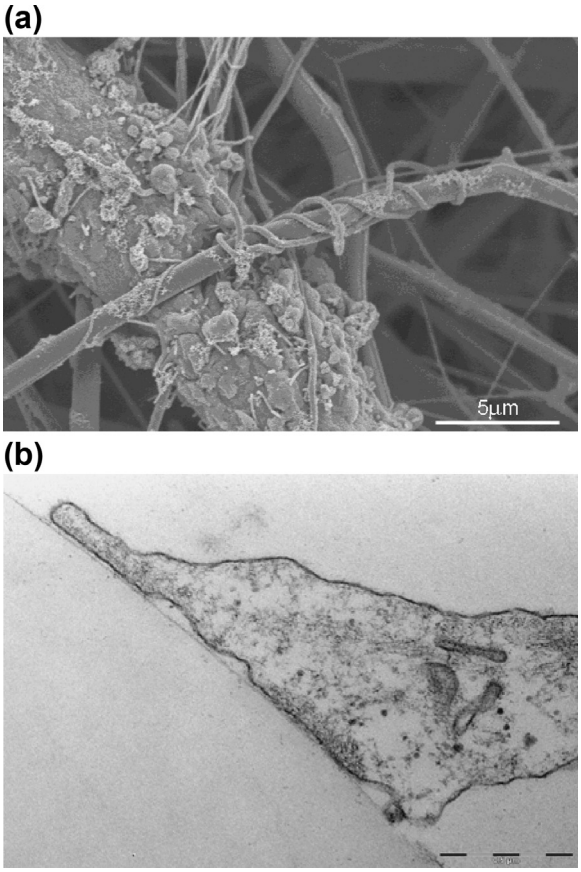

FIGURE 9

(a) SEM image showing fibroblast (human MRC-5) extension wrapping around the electrospun nanofiber. (b) TEM image showing a fibroblast extension in close contact with electrospun Artelon® nanofiber [28].

Nano-fibers have been studied for engineering *cardiovascular tissues* such as heart tissue constructs and blood vessels. Ramakrishna's group published several articles on the use of nano-fibers as a scaffold for blood vessels and looked at the influence of fiber diameter, orientation and other parameters on cell proliferation [29]. Nano-fibers made of poly(L-lactide-co-ε-caprolactone) or poly(ethylene terephthalate) (PET) were primarily used.

Biomimetism toward human ligament has been considered, and the effects of fiber alignment and direction of mechanical stimuli on the ECM generation of human ligament fibroblast was studied [30]. An elastic biodegradable material in a tubular form was produced by combining polylactide with cross-linked elastin [31]. The tubular material obtained showed excellent mechanical properties equal to those of blood vessel and peripheral nerve tissue.

Nano-fibers are potential structures for *bone tissue engineering*. Yoshimoto et al. used poly(ε-caprolactone) scaffolds to grow mesenchymal stem cells derived from bone marrow [32]. Polylactide combined with cross-linked elastin shows a potential for *neural applications* [31]. The regeneration of peripheral nerve axons was observed in transplantation using a rat model with sciatic trauma. Silk-like polymers with fibronectin functionality (ECM proteins) have been electrospun to make biocompatible films for use in prosthetic devices intended for implantation in the central nervous system [33].

It has been shown by Jayasinghe's group that it is possible to directly electrospin living organisms under stable threading conditions at a level of resolution that is constrained only by the size of the cells being electrospun [34]. The treated cells were safe in terms of growth and survival and this has not been achieved by any other competing jet-based technology. This has far reaching implications and will enable significant advances to be made in technologies ranging from tissue engineering to regenerative medicine. For instance, for the development of 3D biological models, for the development of preorientated and organized architectures for repairing, replacing, and rejuvenating damaged and/or aging tissues, while also adding a novel approach to the delivery of biological therapeutics.

Wound dressings and healing

Electrospun nano-fibrous membranes can be used in the production of novel wound dressings. These membranes are particularly important because of their favorable properties, such as high-specific surface area, combined with antibacterial and drug release functionality. Recent studies support that nano-fibrous dressings promote hemostasis, have better absorptivity, semipermeability and conformability and allow scar-free healing [35]. The nano-fibrous membrane also shows controlled evaporative water loss, excellent oxygen permeability, and promoted fluid drainage ability, but it can still inhibit exogenous microorganism invasion because its pores are ultrafine. Histological examinations also indicate that the rate of epithelialization is increased and that the dermis becomes well organized when wounds are covered with electrospun nano-fibrous membrane.

A nano-fiber mat made of fibrinogen, a soluble protein that is present in blood, has been produced by electrospinning [36]. The mat could be placed and left on a wound, thereby minimizing blood loss and encouraging the natural healing process. Fibrinogen increases the "stickiness" of clotting cells, thickens the blood, and promotes the formation of fibrin (the stringy protein that forms the basis of blood clots). Electrospinning can also be used to create biocompatible, thin films with a useful coating design and a surface structure that can be deposited on implantable devices in order to facilitate the integration of these devices in the body.

Drug carrier and delivery systems

Electrospun fiber mats have also been explored as drug delivery vehicles, with promising results. The application of electrostatic spinning in pharmaceutical applications resulted in dosage forms with useful and controllable dissolution properties.

The compatibility of the drug with the polymers, the drug distribution in polymeric matrices, the release behavior of various incorporated drug forms and the stability of drugs during the electrospinning process have been well investigated. Polymeric matrices such as fibrinogen, chitosan, collagen, and poly(ethylene glycol), poly(vinyl alcohol) (PVA), are a few of the polymers that have being studied as electrospun drug delivery matrices due to their biocompatibility.

For instance, hydroxy propoxy methylcellulose, a cellulose derivative commonly used in pharmaceutical preparations, together with a drug has also been tested [37]. Poly (L-lactic acid) and poly (D,L-lactide-coglycolide) nano-fibers are other polymers that have been electrospun with an encapsulated drug and have shown promising drug release properties. In another study, PVA nano-fibers were studied as carriers of drugs for transdermal delivery systems, using four types of nonsteroidal anti-inflammatory drugs with varying water solubility property. The molecular weight of the model drugs played a major role on both the rate and total amount of drugs released, despite the different drug solubility [38]. Incorporation of an antibiotic in fibers developed for scaffold applications has also been reported. The combination of mechanical barriers based on nonwoven nano-fibrous biodegradable scaffolds and their capability for local delivery of antibiotics makes them desirable for applications in the prevention of postsurgical adhesions and infections.

Nutraceutical delivery

Electrospun nano-fibers can be instrumental in food sector as vectors for nutrients, protective entities for encapsulated active compounds (e.g., vitamins, probiotics, functional lipids, and amino acids) during food processing and bioseparation materials to enhance food safety [39]. Recently electrospun edible nano-fibrous mats have been prepared from blend solutions of cellulose acetate (CA) in acetic acid and egg albumin in formic acid, via the fine tuning of electrical conductivity and surface tension by addition of Tween40® (surfactant) [40]. It is pertinent to mention that use of egg albumin, an excellent source of proteins, to develop fibrous nutraceutical carriers facilitate to withstand stomach's severe acidic conditions and release the bioactive material at the alkaline pH of the intestine. In another report, release mechanism of gelatin from coaxially electrospun core–shell CA fibers was found to be anomalous diffusion and exhibited a near zero-order release pattern with release half-life of ~7.4 days [41]. The membranes have been envisaged as suitable matrix for sustained release of proteinaceous pharmaceutical/food compounds in the gastrointestinal tract.

Moreover, fast-dissolving drug delivery systems became of importance for developing new strategies for drug delivery applications, due to their advantages such as enhancing drug solubility, onset of action and bioavailability. These delivery systems are usually in the form of solid tablets or films and designed to instantly wet by saliva and dissolve/disintegrate in the patient's mouth without the need to drink or chew. Fast-dissolving drug delivery systems were prepared by electrospinning using PVA as the filament-forming polymer and drug carrier [42]. Caffeine and riboflavin were used as the model drugs. The SEM images showed that nano-fibers prepared

from electrospinning PVA/drugs aqueous solutions possessed an ultrafine morphology with average diameter in the range of 260−370 nm. Pharmacotechnical tests showed that both PVA/caffeine and PVA/riboflavin nano-fibrous mats had almost the same dissolution time (about 1.5 s) and wetting time (about 4.5 s). The release measurements indicated that drugs can be released in a burst manner (caffeine of 100% and riboflavin of 40% within 60 s) from the PVA nano-fibrous matrices.

Micro- and nano-fibers as support for enzymes and catalysts

Electrospun micro- and nano-fibers are an attractive class of supports for enzymes and catalysts due to their ultrathin sizes and large surface areas. Reneker and coworkers demonstrated the possibility of using nano-fibers for the immobilization of enzymes, showing catalytic efficiency for biotransformations [43]. Enzyme-modified nano-fibers of PVA and PEO achieved by loading the enzymes, i.e., casein and lipase, into the polymer solutions have also been reported. The membranes with encapsulated enzymes were six times more reactive than cast films from the same solutions.

Electrospun CA nano-fibers on hydrolysis and subsequent oxidation by $NaIO_4$ (to generate surface aldehyde groups) acted as suitable immobilization platform for *Candida rugosa* lipase [44]. The authors have reported significant increment in thermostability and durability postimmobilization in comparison to the free counterpart. In yet another system, using glutaraldehyde as the coupling agent, *C. rugosa* lipase was covalently attached to cellulose membrane (containing pentaethylenehexamine as spacer) regenerated from electrospun CA [45]. The authors have reported a high activity (9.83×104 U/m^2) of this biphasic enzyme-immobilized membrane bioreactor for the reaction model involving the hydrolysis of olive oil.

Investigations have been made of the catalytic activity of nano-fibers obtained by incorporating catalysts. For instance, the incorporation of palladium (Pd) nano-particles has been studied in detail using carbonized and metal oxide nano-fibers [46].

GENERATION OF MICRO- AND NANO-MECHANICAL AND MICRO- AND NANO-FLUIDIC DEVICES THROUGH ELECTROSPINNING

As mentioned earlier, electrospun micro- and nano-fibers can serve as sacrificial templates for the generation of micro- and nano-structures with hollow interiors. Czaplewski and coworkers prepared nano-fluidic channels [47]. The channels obtained were elliptical and presented no sharp corners, as in conventional lithographic techniques, which promotes a smoother fluid flow through them. Furthermore, the spin-on glass is optically transparent and compatible with chemical analysis, thereby opening applications in biomolecular separation and single molecule analysis. They also demonstrated the use of these templates for the fabrication of micro-electromechanical devices, such as nano-scale mechanical oscillators.

Deposits of oriented poly(methyl methacrylate) nano-fibers, combined with contact photolithography, created silicon nitride nano-mechanical oscillators with dimensions in the order of 100 nm. The fibers were used as etch masks to pattern

nano-structures in the surface of a silicon wafer. The oriented polymeric nano-fiber deposition method that was used in this experiment offers an approach for rapidly forming arrays of nano-mechanical devices, connected to micro-mechanical structures, that would be difficult to form using a completely self-assembled or completely lithographic approach. This approach may provide a useful method for realizing nano-scale device architectures in a variety of active materials.

Furthermore, magnetite nano-particles were incorporated as a colloidally stable suspension into PEO or PVA solutions [48]. After electrospinning, the nano-particles were aligned along the fibers' axis. These nano-fibers exhibited superparamagnetic behavior and deflected when subjected to a magnetic field at room temperature. A micro-aerodynamic decelerator based on permeable surfaces of nano-fiber mats was reported by Zussman and Yarin [49]. The mats were positioned on light, pyramid-shaped frames. These platforms fell freely through the air, apex down, at a constant velocity. The drag of this kind of passive airborne platform is of significant interest in a number of modern aerodynamics applications including, for example, dispersion of "smart dust" carrying various chemical and thermal sensors, dispersion of seeds, and movement of small organisms with bristle appendages.

MICRO- AND NANO-FIBERS IN SENSORS

Recent advances in micro- and nano-technology and the electrospinning technique offer great potential for the construction of cost-effective, next-generation chemical, and biosensor devices. The high surface area per volume unit makes electrospun micro- and nano-structures great candidates for a variety of sensing applications as they can offer high sensitivity and response time. These sensors can find applications in medical diagnosis and environmental and bioindustrial analysis, among others [1,25].

Conducting electroactive polymers have remarkable sensing applications because of their ability to be reversibly oxidized or reduced by applying electrical potentials. For biosensing applications, conducting electroactive polymers combine the role of a matrix immobilization template and the generation of analytical signals. The most common conducting electroactive polymers include polypyrrole, polyaniline, and polythiophene and are characterized by an electronic conductivity of up to $10^4\ \Omega^{-1}$. Resistive-type sensors made from undoped or doped polyaniline nano-fibers outperform conventional polyaniline on exposure to acid or base vapors, respectively [50].

Electrospinning of lead zirconate titanate, $Pb(Zr_xTi_{1-x})O_3$ (PZT) fibers should be mentioned because of its technological importance in the field of sensors, electronics, and nonvolatile ferroelectric memory devices. PZT is one example of one-dimensional nano-structures, the smallest dimension structures for efficient transport of electrons and optical excitation that can be used as building blocks in a bottom-up assembly in diverse applications in nano-electronics and photonics [51]. Wang et al. showed that ultrafine PZT fibers could be synthesized from metallo-organic compounds simply by using metallo-organic decomposition and vacuum heat treatment electrospinning techniques [51].

Other developments are electrospun nano-fibers of polyvinylpyrrolidone (PVP) containing the urease enzyme that show a potential as a urea biosensor and nano-fibers coated with metal oxides (TiO_2, MoO_3) for the detection of toxic gases [52].

To use molecular imprinting polymers (MIPs) in applications such as sensing or affinity separation, it is often required that MIPs be immobilized on solid surfaces. This procedure usually results in a low surface area and leads to relatively low binding capacity. A substantial increase in the surface area to volume ratio is obtained if MIPs are synthesized in the form of nano-particles. Studies by Chronakis et al. [25] demonstrate that by entrapping premade MIP nano-particles in electrospun polymer nano-fibers, it is possible to exploit the favorable molecular selectivity of MIPs, for example, to develop new fiber-based materials for chemical sensing and bio-separation. MIP nano-particles can be prepared with a high level of cross-linking density, making the imprinted binding sites intact even after treatment with harsh processing conditions. Chronakis et al. have used electrospinning to encapsulate two types of well-established MIP nano-particles (imprinted against theophylline and β-estradiol), and tested molecular binding property of the composite nano-fibers. The nano-fibers containing the encapsulated MIP nano-particles showed selective binding for the original templates used in the imprinting reaction, suggesting that the encapsulation by electrospinning can be a general approach to introduce MIP nano-particles into functional membrane devices. Molecular imprinted nano-fibers with selective molecular recognition ability and signal transduction ability have been also developed [53].

MICRO- AND NANO-FIBERS IN ELECTRIC AND ELECTRONIC APPLICATIONS

Electrospun nano-fibers with electrical and electro-optical activities have received a great deal of interest in recent years because of their potential application in nano-scale electronic and optoelectronic devices, such as nano-wires, LEDs, photocells, etc. PZT and carbon nano-fibers are two typical and challenging examples of one-dimensional nano-structures that can be used as building blocks in bottom-up assembly in diverse applications in nano-electronics and photonics [51].

Studies support that electrospinning can be a simple method for fabricating a one-dimensional polymer field-effect transistor, which forms the basic building block of logic circuits and switches for displays [54,55]. In addition, the excellent adherence of the nano-fibers to SiO_2 and to gold electrodes may be useful in the design of future devices. By means of electrospinning processing, extremely low-dimensional conducting nano-wires have been made from, e.g., polyaniline or polypyrrole for use in nano-electronics [56] (Figure 10).

Other studies report the development of carbon nano-fiber webs from the oxidation and steam activation of a polyacrylonitrile (PAN) nano-fiber web for use as an electrode in a supercapacitor, poly(vinylidene fluoride) nano-fibers for applications as a separator or as an electrolyte in batteries [57] and fabrication of a lithium secondary battery comprising a fibrous film made by electrospinning [58].

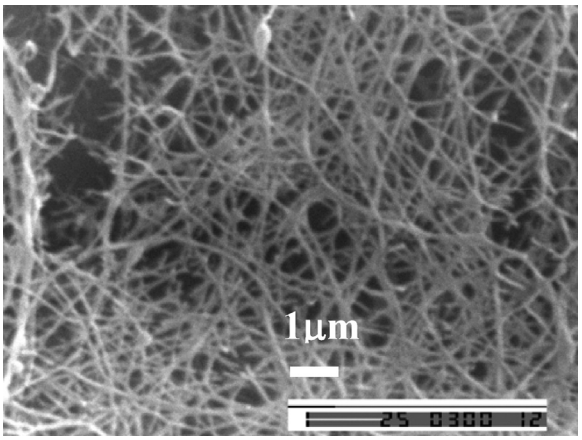

FIGURE 10

SEM micrograph of conductive polypyrrole nanofibers. The nanofibers were electrospun from a solution of [(PPy3)+ (DEHS)-]x in DMF [56].

Electrospinning mixtures of ceramic particles with polymers and subsequent pyrolysis of the polymer to form pure ceramic nano-fibers is an area of intense research [7]. Because of their large surface-to-volume ratios and narrow-band optical emission, these nano-fibers can be used as selective emitters for thermophotovoltaic applications and as emitting devices in nano-scale optoelectronic applications.

MICRO- AND NANO-FIBERS IN FILTERS

The efficiency of nano-fibers in filtration has been studied by several groups. Generally, the electrospun webs have been found to be much more effective than other commercial high-efficiency air filter media. In most cases, the nano-fiber webs are applied on a substrate chosen to provide mechanical properties, while the nano-fiber dominates the filtration performance. Electrospinning can also be used to produce charged fibers for use in filtration media. Obviously, the charge-induction and charge-retention characteristics are related to the polymer material used for electrospinning.

Controlling the parameters of electrospinning allows the generation of micro- and nano-fiber webs with different filtration characteristics. A study done by Schreuder-Gibson and Gibson showed that it is possible to tailor pore size, air permeability, and aerosol filtration of elastic nonwoven media by applying very light-weight layers of electrospun elastic fibers to the coarser webs [59]. It has been found that a significant deformation of the elastic webs increases air flow, and it might be possible to design controlled flow filters or air bags that are modulated by a pressure drop across elastic webs with correspondingly variable porosities. Many filtering applications of electrospun micro- and nano-fibers are related to air filtration, but liquid filtration can also occur [60].

Moreover, ion exchange materials (such as resins, membranes, etc.) have been widely used in various industries for water deionization or softening, metal recovery, biological process, food and beverages, pharmaceuticals, and fuel cell applications. Polymer nano-fiber ion exchangers are new, promising materials as they have a much higher surface area than common ion exchangers.

MICRO- AND NANO-FIBERS IN TEXTILES

Electrospun micro- and nano-membranes composed of elastomeric fibers are of particular interest in the development of several protective clothing applications. The excellent ability to capture aerosols and the possibilities to incorporate any kind of active substances make electrospun nano-fiber materials potential candidates for use in protective clothing and smart cloths responding to changes in the surrounding environment. Much work is being done with the aim to develop garments that reduce soldiers' risks for chemical exposure [61]. The idea is to lace several types of polymers and fibers to make protective ultrathin layers that would enhance, for example, chemical reactivity and environmental resistance. Such mats have been found to have a higher convective resistance to air flow while the transport of water vapor is much higher than in normal clothing materials. These products exhibit remarkable "breathing" properties, which are now required in clothing applications.

In some other uses of protective clothing, thermal and flammability properties are essential [62]. Electrospun poly(methyl methacrylate-co-methacrylic acid) and its layered silicate nano-composites have shown good thermal stability, reduced flammability, and increased self-extinguishing properties. The possibility of using submicron and nano-scale fibers and fibrous assemblies based on conductive Poly(3,4-ethylenedioxythiophene) (PEDOT) for wearable electronics has also been explored [14]. Finally, the development of electrospinning apparatuses for fiber orientation that allow the fabrication of yarns is of considerable interest [63].

MICRO- AND NANO-FIBERS AS COMPOSITE REINFORCEMENT

The strength of a composite material is effectively enhanced by fiber-based reinforcement. Thus, the high surface-to-volume ratio of nano-fibers significantly improves the stiffness and mechanical strength of the composites compared to conventional fibers due to the increased interaction between the fibers and the matrix [64]. Another positive aspect is that the composites are able to maintain their optical transparency related to the small cross-section of the nano-fibers.

MICRO- AND NANO-FIBERS FOR PACKAGING APPLICATIONS

In order to improve the barrier properties of fully renewable microbial biopolyesters, a novel methodology based on electrospun interlayers was presented by Lagaron's group, with significant interest in food packaging applications. They have prepared multilayer films of PLA containing a zein electrospun fiber interlayer that showing good adhesion between the layers and having considerably improved oxygen

barrier properties up to 71% [65]. Moreover, multilayer structures based on polyhydroxybutyrate-co-valerate with a valerate content of 12% PHBV12 as the outer layers (prepared by casting or by compression molding) and electrospun zein fibers as the inner layer have been successfully developed [66]. The effect that zein interlayer had on water vapor and limonene permeability values depended on the zein deposition time and on the film-processing method, although the structures prepared by casting were more permeable to water vapor and limonene than their counterparts prepared by compression molding. A significant decrease in oxygen permeability values was observed in the zein-containing multilayer films in comparison with the pure PHBV12-based films. These results have demonstrated the potential of this processing method for the development of biodegradable multilayer PHBV-based films in which the intermediate electrospun zein nano-fibers were able to improve barrier properties (more efficiently for the longest deposition time) with minimum changes in mechanical and optical properties.

Encapsulation of bacteriophages in the form of electrospun nano-fibers have been also investigated by few groups [67,68]. Bacteriophage incorporated electrospun nano-fibers have been prepared using aqueous suspensions of M13 bacteriophage and PVP. The bacteriophage-encapsulated fibers instantly released the M13 bacteriophage, which exhibited some activity, and were able to infect the bacterial host. Similarly, the same suspension electrospinning process was used to investigate the encapsulation of T4, T7, and k bacteriophages in PVA fibers [69]. Although exposure of bacteriophages to a PVA aqueous solution showed no effect on their viability, a very low activity (T4: 1%, T7: 2%, k: 6%) was reported after release from the PVA fibers. The loss of activity was mainly attributed to the rapid dehydration of the bacteriophages and solvent evaporation during fiber formation. To overcome the sensitivity of bacteriophages to the electrospinning process and increase bacteriophage viability, Korehei and Kadla [68] have investigated two different electrospinning processes: emulsion and coaxial electrospinning. The aim was to "protect" the bacteriophage from the harsh conditions of the electrospinning process by either pre-encapsulating and/or allocating the bacteriophage to the core of a core/shell fiber. Coaxial electrospinning was shown to be capable of encapsulating T4 bacteriophages with high loading capacity, high viability, and long storage time. These results are significant in the context of controlling and preventing bacterial infections in perishable foods during storage.

The lactoperoxidase (LP) system is a naturally occurring antimicrobial system in milk that is effective against many microorganisms. In some developing countries, where milk is susceptible to temperature abuse and poor sanitary conditions during transportation and storage, H_2O_2 has been added to raw milk to activate the LP system to preserve the milk during transportation. Activation of the LP system in milk prior to pasteurization can also increase the margin of safety with respect to milk-borne pathogens. Potentially, the use of LP may offer an opportunity to decrease the thermal requirement for pasteurization or reduce the refrigeration requirement during storage. In a study by Zhou and Lim, glucose oxidase (GOX) was immobilized in polylactide (PLA) fibers that were used to activate the LP system in milk

[70]. The GOX-containing micro-fibers were electrospun from emulsions prepared by dispersing aqueous GOX in PLA dissolved in a chloroform and *N*,*N*-dimethylformamide blend, using sorbitan monopalmitate as an emulsifier. The enzymatic activity of GOX-in-PLA fibers (1100 ± 400 nm diameter) was more than 19 times higher than that of the GOX-in-PLA membrane formed by direct casting, due to the larger surface area of the electrospun fibers. The activation of LP in model solutions using GOX-in-PLA fibers provided a more sustained generation of antimicrobial OSCN—than direct activation using H_2O_2. Preliminary evaluation on milk samples showed that the electrospun GOX-in-PLA micro-fibers are capable of activating the naturally present LP system, indicating that they may be promising for active food packaging applications to extend the shelf life of milk.

ATTEMPTS TO INCREASE THE PRODUCTION RATE OF ELECTROSPUN MICRO- AND NANO-FIBERS

ELECTROSPINNING USING MULTIPLE NOZZLES

The most obvious way to increase the rate of production of micro- and nano-fibers is to increase the number of nozzles used in the spinning process. In a patent, Chu et al. described an electrospinning apparatus with multiple nozzles, as shown in Figure 11 [71]. The essential invention in this patent was not the use of multiple nozzles but the possibility to better control the jet formation, jet acceleration, and fiber collection for individual jets. This was achieved using several additional electrodes to homogenize the electric field that accelerates the jets from the nozzles to the collector. The possibility of controlling both the flow of the conducting fluid (polymer solution or

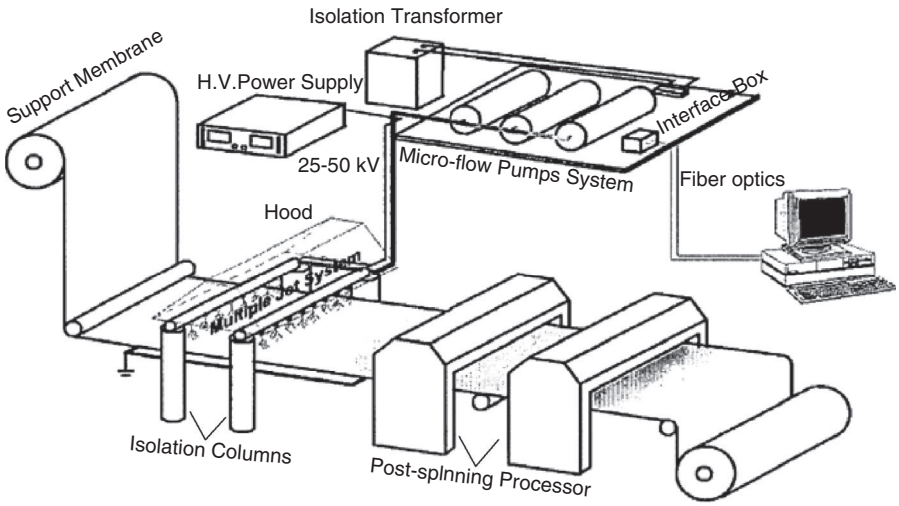

FIGURE 11

Schematic drawing of an apparatus for large-scale electrospinning of nanofibers [71].

melt) and the properties of the electric field for each jet was described as essential for producing nano-fibers using multiple nozzles. A later patent by the same group focused on controlling multiple fiber jets as opposed to individual jets or adding the possibility of blowing a temperate gas in the fiber spinning direction. The gas flow gives a higher production rate than traditional electrospinning, as well as lower energy consumption.

ELECTROSPINNING WITHOUT NOZZLES

Perhaps the most successful way to increase the electrospinning production rate that can be recognized thus far is the Nanospider™ technology, patented by O. Jirsak et al. [72]. This technology is now owned by ElMarco (Czech Republic). Instead of using capillaries as a spinneret for introducing the polymer solution into the electric field, a rotating charged electrode is used that is partly immersed into the polymer solution. This setup allows the creation of many Taylor cones and hence many jets that travel upward to a conveyor belt that can be covered with a material to be coated.

A great advantage of this method is the possibility to create multiple jets of nanofibers without the risk of the nozzles clogging. Another advantage of the technique is that the spinning direction is upward, which minimizes the risk of solution droplets forming in the product. The process is schematically shown in Figure 12.

The polymer solution (2) is applied to the charged cylindrical electrode (3) as it rotates partly immersed in the solution. Multiple fiber jets are formed from the surface of the electrode toward the oppositely charged electrode (40). The fibers are drawn to the electrode (40), not only by the electric force but also due to the action of a vacuum chamber (5). The patent also covers rotating cylindrical electrodes with different patterned surfaces. Using this technology, ElMarco claims that they will have a production capacity of 3000 m^2/day (1 m in width) (2006).

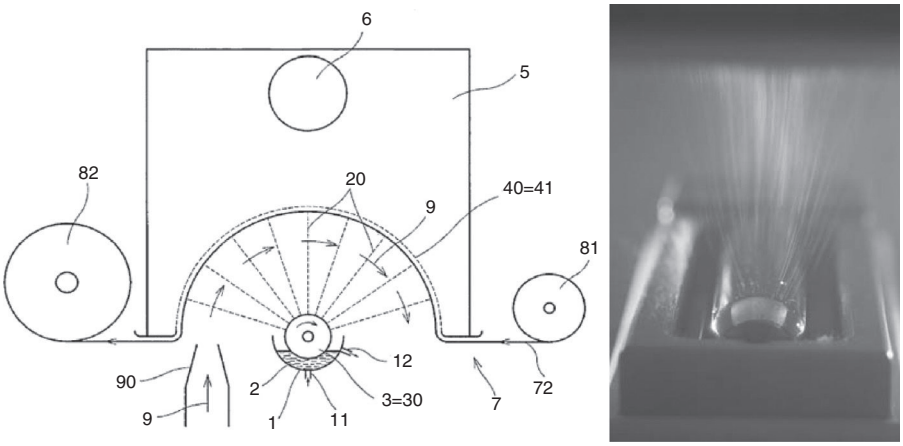

FIGURE 12

(a) Schematic drawing of the Nanospider™ technology [72], (b) Picture of the Nanospider™ technology in action (from www.nanospider.cz).

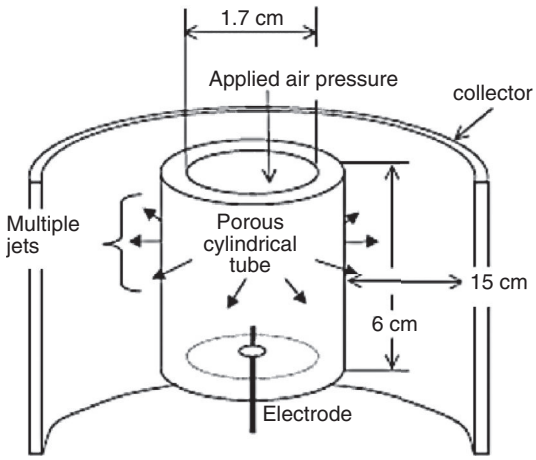

FIGURE 13

Schematic illustration of the electrospinning setup using a porous polyethylene tube [73].

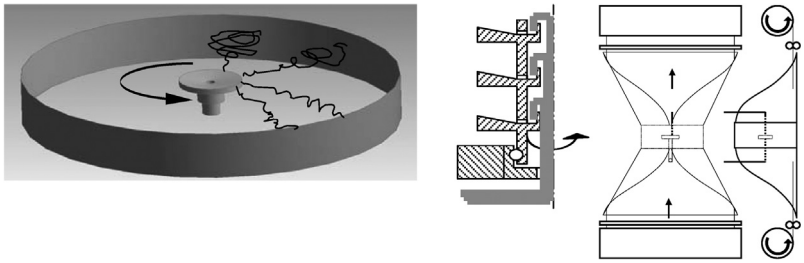

FIGURE 14

Schematic illustration of the micro- and nano-fiber formation from rotating disc [74].

Another approach to spinning nano-fibers without nozzles is to use a porous tube of polyethylene, as reported by Reneker et al. [73]. By applying air pressure to a polymer solution inside a cylindrical porous tube, these authors were able to form multiple jets of polymer solution in the electric field. With this porous tube, the production rate could be increased to about 250 times that of the corresponding production rate for a single needle (Figure 13).

Recently, a new technology with the use of centrifugal forces has been developed and patented from Swerea IVF [74]. The process is schematically shown in Figure 14.

COMMERCIAL PRODUCTS

It should be noted that some companies already have commercial products based on electrospun nano-fibers. One of the first companies to start an industrial production

line of nano-fiber web is NanoTechnics Co., Ltd., in Korea. The company offers nano-fiber webs of PA6 and PA66 for application in filters and PAN for electrodes in batteries. Other companies that claim to be able to electrospin webs for use in filters are Hollingsworth & Vose, Germany, and eSpin Technologies, USA. Donaldson Company Inc., USA is also an important actor in the field of nano-fiber-based filters. Donaldson has several US and international patents that cover nano-fiber innovations, configurations, and uses.

TECHNOLOGICAL COMPETITIVENESS AND OPERATION ECONOMICS

Electrospinning is a very simple and versatile method for creating polymer-based, high-functional, and high-performance micro- and nano-fibers that can revolutionize the world of structural materials. The process is versatile in that there is a wide range of materials that can be spun (Table 1). At the same time, electrospun micro- and nano-fibers possess unique and interesting features. The ability to customize micro- and nano-fibers to meet the requirements of specific applications gives electrospinning an advantage over other larger scale micro- and nano-production methods. Combining well-established technologies of today with the emerging field of electrospun micro- and nano-fibers can potentially lead to the development of new technologies and new micro- and nano-structured smart assembles and stimulate opportunities for an enormous number of applications. Thus, electrospinning technology can provide a connection between the worlds of the nano-scale and the macro-scale.

Another advantage of this top-down micro- and nano-manufacturing process is its relatively low cost compared to that of most bottom-up methods. The electrospinning method itself is environment-friendly because it consumes only a small amount of electrical energy. In spite of the high potential difference (10,000−40,000 V) that is applied, only a small electrical current flows through the nano-fibers (in the order of nano-amperes). In addition, the electrospinning method provides nano-fiber structures that imply a large reduction in material consumption. For instance, the formation of a true nano-coating (monolayer-like) will result in a thickness of only a few nanometers, while current coatings have a thickness of a few micrometers. This means that the consumption of materials is also about 1000 times less for nano-coatings while it results in the same surface properties as are obtained with micro-coatings. Moreover, the resulting micro- and nano-fiber samples are often uniform and continuous and do not require expensive purification (unlike submicrometer-diameter whiskers, inorganic nano-rods and carbon nano-tubes). Overall, despite the existence of some commercial products, it is evident that an upscaling of the electrospinning process and productivity improvements are essential features and merit more effort to ensure full success in socioeconomic terms.

Table 1 Examples of Some Polymer-Biopolymer Materials that have been Electrospun and Solvents Used (In Alphabetical Order).

Materials	Solvents
ABS	N,N-Dimethyl formamide (DMF) or Tetrahydrofuran (THF)
Cellulose	Ethylene diamine
Cellulose acetate	Dimethylacetamide (DMAc) and Acetone or Acetic acid
Ethyl-cyanoethyl cellulose [(E-CE)C]	THF
Chitosan and chitin	1,1,1,3,3,3-hexafluoro-2-propanol (HFIP)
Dextran	Water, DMSO/Water, DMSO/DMF
Gelatine	2,2,2-Trifluoroethanol
Nylon	Formic acid
Poly(2-acrylamido-2-methyl-1-propane sulfonic acid) (PMAPS)	Ethanol/Water
Polyacrylonitrile (PAN)	DMF
Polyalkyl methacrylate (PMMA)	Toluene/DMF
Polycarbonate	THF/DMF
Poly(ethylene oxide) (PEO)	Water, Ethanol, DMF
Polyethylene terephthalate (PET)	Trifluoroacetic acid (TFA) and Dichloromethane (DCM)
Polylactic based polymers	Chloroform, HFIP, DCM
Pol(ε-caprolacone) based polymers	Acetone, Acetone/THF, Chloroform/DMF, DCM/Methanol, Chloroform/Methanol, THF/Acetone
Poly(3-hydroxybutyrate-co-3-hydroxyvalerate) (PHBV)	2,2,2-Trifluoroethanol
Polyphosphazenes	Chloroform
Polystyrene	1,2 Dichloroethane, DMF, Ethylacetate, Methylethylketone (MEK), THF
Bisphenol-A Polysulfone	DMAc/Acetone
Polyurethane (PU)	THF/DMF
Polyvinyl alcohol (PVA)	Water
Polyvinyl chloride (PVC)	DMF, DMF/THF
Poly(vinylidene fluoride) (PVDF)	DMF/THF
Poly(vinyl pyrrolidone)	Ethanol, DCM, DMF
Silk	Hexafluoroacetone (HFA), Hexafluoro-2-propanol, Formic acid

ACKNOWLEDGMENT

The author would like to thank the Danish Strategic Research Council for financial support (DSF -10-93456, FENAMI Project).

REFERENCES

[1] Frenot A, Chronakis IS. Polymer nanofibers assembled by electrospinning. Curr Opin Colloid Interface Sci 2003;8:64−75.

[2] Li D, Xia Y. Electrospinning of nanofibers: reinventing the wheel? Adv Mater 2004;16: 1151−70.

[3] Formhals. Process and apparatus for preparing artificial threads. US Patent, 1-975-504; 1934.

[4] Reneker DH, Chun I. Nanometre diameter fibres of polymer produced by electrospinning. Nanotechnology 1996;7:216−23.

[5] Dersch R, Steinhart M, Boudriot U, Greiner A, Wendorff JH. Nanoprocessing of *polymers*: applications in medicine, sensors, catalysis, photonics. Polym Adv Technol 2005; 16:276−82.

[6] Teo WE, Ramakrishna S. A review on electrospinning design and nanofibre assemblies. Nanotechnology 2006;17:R89−106.

[7] Chronakis IS. Novel nanocomposites and nanoceramics based on polymer nanofibers using electrospinning process − a review. J Mater Process Technol 2005;167:283−93.

[8] Reznik SN, Yarin AL, Theron A, Zussman E. Transient and steady shapes of droplets attached to a surface in a strong electric field. J Fluid Mech 2004;516:349−77.

[9] Welle A, Kröger M, Döring M, Niederer K, Pindel E, Chronakis IS. Electrospun aliphatic poly(carbonate)s nanofibers as tailored tissue scaffold materials. Biomaterials 2007;28:2211−9.

[10] Baumgarten PK. Electrostatic spinning of acrylic microfibers. J Colloid Interface Sci 1971;36:71−9.

[11] He JH, Wan YQ, Yu MY. Allometric scaling and instability in electrospinning. Int J Nonlinear Sci Numer Simul 2004;5:243−52.

[12] Yarin AL, Zussman E. Upward electrospinning of multiple nanofibers without needles/ nozzles. Polymer 2004;45:2977−80.

[13] Sun Z, Zussman E, Yarin AL, Wendorff JH, Greiner A. Compound core-shell polymer nanofibers by co-electrospinning. Adv Mater 2003;15:1929−32.

[14] El-Aufy AK. Nanofibers and nanocomposites poly(3,4-ethylene dioxythiophene)/poly (styrene sulfonate) by electrospinning [Ph.D. Thesis]. Drexel University; 2004.

[15] Czaplewski D, Kameoka J, Craighead HG. Nonlithographic approach to nanostructure fabrication using a scanned electrospinning source. J Vac Sci Technol B (Microelectron Nanom Struct) 2003;21:2994−7.

[16] Dersch R, Liu T, Schaper AK, Greiner A, Wendorff JH. Electrospun nanofibers: internal structure and intrinsic orientation. J Polym Sci Part A: Polym Chem 2003;41: 545−53.

[17] Li D, Xia Y. Direct fabrication of composite and ceramic hollow nanofibers by electrospinning. Nano Lett 2004;4:933−8. and Li D, Wang Y, Xia Y. Electrospinning nanofibers as uniaxially aligned arrays and layer-by-layer stacked films. Adv Mater 2004;16:361−366.

[18] Zussman E, Theron A, Yarin AL. Electrostatic field-assisted building 3-D nanostructures from electrospun nanofibers. Appl Phys Lett 2003;82:973−5.

[19] Theron A, Zussman E, Yarin AL. Electrostatic fields-assisted alignment of electrospun nanofibres. Nanotechnology 2001;12:384−90.

[20] Sun D, Chang C, Li S, Lin L. Near-field electrospinning. Nano Lett 2006;6:839−42.

[21] Chang C, Limkrailassiri K, Lin L. Continuous near-field electrospinning for large area deposition of orderly nanofiber patterns. Appl Phys Lett 2008;93:123111.
[22] Fennessey SF, Farris RJ. Fabrication of aligned and molecularly oriented electrospun polyacrylonitrile nanofibers and the mechanical behavior of their twisted yams. Polymer 2004;45:4217−25.
[23] Koombhongse S, Liu W, Reneker DH. Flat ribbons and other shapes by electrospinning. J Polym Sci Polym Phys Ed 2001;39:2598−606.
[24] Sung C, Gibson H, Ravi Varma NK. Electrospinning of polycarbonates and their surface characteristics. J Text Appar Technol Manag 2001;1(special issue). The Fibre Society Spring Conference, Raleigh NC.
[25] Chronakis IS, Jakob A, Hagström B, Ye L. Encapsulation and selective recognition of molecularly imprinted theophylline and 17beta-Estradiol nanoparticles within electrospun polymer nanofibers. Langmuir 2006;22:8960−5. and Romeo V, Gorrasi G, Vittoria V, Chronakis IS. Encapsulation and exfoliation of inorganic lamellar fillers into polycaprolactone by electrospinning. Biomacromolecules 2007;8: 3147−3152.
[26] Sun B, Long YZ, Zhang HD, Li MM, Duvail JL, Jiang XY, Yin HL. Advances in three-dimensional nanofibrous macrostructures via electrospinning. Prog Polym Sci 2014;39: 862−90.
[27] Pham QP, Sharma U, Mikos AG. Electrospinning of polymeric nanofibers for tissue engineering applications: a review. Tissue Eng 2006;12:1197−211.
[28] Borg E, Frenot A, Walkenström P, Gisselfält K, Gatenholm P. Electrospinning of degradable elastomeric nanofibers with various morphology and their interaction with human fibroblasts. J Appl Polym Sci 2008;108:491−7.
[29] Ma Z, Kotaki M, Yong T, He W, Ramakrishna S. Surface engineering of electrospun polyethylene terephthalate (PET) nanofibers towards development of a new material for blood vessel engineering. Biomaterials 2005;26:2527−36.
[30] Lee CH, Shin HJ, Cho IH, Kang Y-M, Kim IA, Park K-D, et al. Nanofiber alignment and direction of mechanical strain affect the ECM production of human ACL fibroblast. Biomaterials 2005;26:1261−70.
[31] Kitazono E, Kaneko H, Miyoshi T, Miyamoto K. Tissue engineering using nanofiber. Yuki Gosei Kagaku Kyokaishi/J Synth Org Chem Jpn 2004;62:514−9.
[32] Yoshimoto H, Shin YM, Terai H, Vacanti JP. A biodegradable nanofiber scaffold by electrospinning and its potential for bone tissue engineering. Biomaterials 2003;24: 2077−82.
[33] Buchko CJ, Chen LC, Shen Y, Martin DC. Processing and microstructural characterization of porous biocompatible protein polymer thin films. Polymer 1999;40: 7397−407.
[34] Jayasinghe SN. Cell electrospinning: a novel tool for functionalising fibres, scaffolds and membranes with living cells and other advanced materials for regenerative biology and medicine. Analyst 2013;138:2215−23.
[35] Zhang Y, Lim CT, Ramakrishna S, Huang Z-M. Recent development of polymer nanofibers for biomedical and biotechnological applications. J Mater Sci Mater Med 2005; 16:933−46. and Katti DS, Robinson KW, Ko FK, Laurencin CT. Bioresorbable nanofiber-based systems for wound healing and drug delivery: optimization of fabrication parameters. J Biomed Mater Res 2004;70B:286−296.
[36] Bowlin G. Natural bandages from fibrinogen. Med Text 2003;13:4.

[37] Verreck G, Chun I, Peeters J, Rosenblatt J, Brewster ME. Preparation and characterization of nanofibers containing amorphous drug dispersions generated by electrostatic spinning. Pharm Res 2003;20:810−7.
[38] Taepaiboon P, Rungsardthong U, Supaphol P. Effect of cross-linking on properties and release characteristics of sodium salicylate-loaded electrospun Poly(vinyl alcohol) fiber mats. Nanotechnology 2007;18:175102 (11p).
[39] Konwarh R, Karak N, Misra M. Electrospun cellulose acetate nanofibers: the present status and gamut of biotechnological applications. Biotechnol Adv 2013;31:421−37.
[40] Wongsasulak S, Patapeejumruswong M, Weiss J, Supaphol P, Yoovidhya T. Electrospinning of food-grade nanofibers from cellulose acetate and egg albumen blends. J Food Eng 2010;98:370−6.
[41] Sakuldao S, Yoovidhya T, Wongsasulak S. Coaxial electrospinning and sustained release properties of gelatin-cellulose acetate core-shell ultrafine fibres. Sci Asia 2011;37:335−43.
[42] Li X, Kanjwal MA, Lin L, Fu J, Chronakis IS. Electrospun polyvinyl-alcohol nanofibers as oral fast-dissolving delivery system of caffeine and riboflavin. Colloids Surf B: Biointerfaces 2013;103:182−8.
[43] Jia H, Zhu G, Vugrinovich B, Kataphinan W, Reneker DH, Wang P. Enzyme-carrying polymeric nanofibers prepared via electrospinning for use as unique biocatalysts. Biotechnol Prog 2002;18:1027−32.
[44] Huang X-J, Chen P-C, Huang F, Ou Y, Chen M-R, Xu Z-K. Immobilization of *Candida rugosa* lipase on electrospun cellulose nanofiber membrane. J Mol Catal B: Enzym 2011;3−4:95−100.
[45] Chen P-C, Huang X-J, Huang F, Ou Y, Chen M-R, Xu Z-K. Immobilization of lipase onto cellulose ultrafine fiber membrane for oil hydrolysis in high performance bioreactor. Cellulose 2011;18:1563−71.
[46] Demir MM, Gulgun MA, Menceloglu YZ, Erman B, Abramchuk SS, Makhaeva EE, et al. Palladium nanoparticles by electrospinning from poly(acrylonitrile-co-acrylic acid)-PdCl2 solutions. Relations between preparation conditions, particle size, and catalytic activity. Macromolecules 2004;37:1787−92.
[47] Czaplewski DA, Kameoka J, Mathers R, Coates GW, Craighead HG. Nanofluidic channels with elliptical cross sections formed using a nonlithographic process. Appl Phys Lett 2003;83:4836−8.
[48] Wang A, Singh H, Hatton TA, Rutledge GC. Field-responsive superparamagnetic composite nanofibers by electrospinning. Polymer 2004;45:5505−14.
[49] Zussman E, Yarin AL, Weihs D. A micro-aerodynamic decelerator based on permeable surfaces of nanofiber mats. Exp Fluids 2002;33:315−20.
[50] Huang J, Virji S, Weiller BH, Kaner RB. Nanostructured polyaniline sensors. Chem − A Eur J 2004;10:1314−9.
[51] Wang Y, Furlan R, Ramos I, Santiago-Aviles JJ. Synthesis and characterization of micro/nanoscopic $Pb(Zr_{0.52}\ Ti_{0.48})O_3$ fibers by electrospinning. Appl Phys A 2004; 78:1043−7.
[52] Gouma PI. Nanostructured polymorphic oxides for advanced chemosensors. Rev Adv Mater Sci 2003;5:147−54.
[53] Yoshimatsu K, Ye L, Stenlund P, Chronakis IS. A simple method for preparation of molecularly imprinted nanofiber materials with signal transduction ability. Chem Commun 2008;7:2022−4.

[54] Pinto NJ, Johnson AT, MacDiarmid AG, Mueller CH, Theofylaktos N, Robinson DC, et al. Electrospun polyaniline/polyethylene oxide nanofiber field-effect transistor. Appl Phys Lett 2003;83:4244−6.
[55] Kim C, Yang KS. Electrochemical properties of carbon nanofiber web as an electrode for supercapacitor prepared by electrospinning. Appl Phys Lett 2003;83: 1216−8.
[56] Chronakis IS, Grapenson S, Jakob A. Conductive polypyrrole nanofibers via electrospinning: electrical and morphological properties. Polymer 2006;47:1597−603.
[57] Choi S-S, Lee YS, Joo CW, Lee SG, Park JK, Han K-S. Electrospun PVDF nanofiber web as polymer electrolyte or separator. Electrochimica Acta 2004;50:339−43.
[58] Cho WB, Choi SW, Mu JS, Kim HS, Kim US, Cho WI. A lithium secondary battery comprising a super fine fibrous polymer separator film and its fabrication method, Patent WO0189022 and WO0189023; 2001.
[59] Gibson P, Schreuder-Gibson H, Rivin D. Transport properties of porous membranes based on electrospun nanofibers. Colloid Surf A − Physicochem Eng Aspects 2001; 187:469−81.
[60] Yoshimatsu K, Ye L, Lindberg J, Chronakis IS. Selective molecular adsorption using electrospun nanofiber membranes. Biosens Bioelectron 2008;23:1208−15.
[61] Schreuder-Gibson H, Gibson P, Senecal K, Sennett M, Walker J, Yeomans W, et al. Protective textile materials based on electrospun nanofibers. J Adv Mater 2002;34: 44−55.
[62] Wang M, Hsieh AJ, Rutledge GC. Electrospinning of (MMA-co-MMA) copolymers and their layered silicate nanocomposites for improved thermal properties. Polymer 2005;46:3407−18.
[63] Ko F, Gogotsi Y, Ali A, Naguib N, Ye H, Yang G, et al. Electrospinning of continuous carbon nanotube-filled nanofiber yarns. Adv Mater 2003;15:1161−5.
[64] Bergshoef MM, Vancso GJ. Transparent nanocomposites with ultrathin electrospun nylon-4,6 fiber reinforcement. Adv Mater 1999;11:1362−5.
[65] Fabra MJ, Lopez-Rubio A, Lagaron JM. High barrier polyhydroxyalcanoate food packaging film by means of nanostructured electrospun interlayers of zein. Food Hydrocoll 2013;32:106−14.
[66] Fabra MJ, Busolo MA, Lopez-Rubio A, Lagaron JM. Nanostructured biolayers in food packaging. Trends Food Sci Technol 2013;31:79−87.
[67] Lee SW, Belcher AM. Virus-based fabrication of micro- and nano-fibers using electrospinning. J Nano Lett 2004;4:387−90.
[68] Korehei R, Kadla J. Incorporation of T4 bacteriophage in electrospun fibres. J Appl Microbiol 2013;114:1425−34.
[69] Salalha W, Kuhn J, Dror Y, Zussman E. Encapsulation of bacteria and viruses in electrospun nanofibers. Nanotechnology 2006;17:4675−81.
[70] Zhou Y, Lim L-T. Activation of lactoperoxidase system in milk by glucose oxidase immobilized in electrospun polylactide microfibers. J Food Sci C: Food Chem 2009; 74:C170−6.
[71] Chu B, Hsiao BS, Fang D. Apparatus and methods for electrospinning polymeric fibers and membranes. US2002175449.
[72] Jirsak O, Sanetrnik F, Lukas D, Kotek V. A method of nanofibres production from a polymer solution using electrostatic spinning and a device for carrying out the method. WO2005/024101A1.

[73] Dosunmu OO, Chase GG, Kataphinan W, Reneker DH. Electrospinning of polymer nanofibers from multiple jets on a porous tubular surface. Nanotechnology 2006;17: 1123−7.
[74] Hagström B. Method and device for manufacturing nanofibers. Swedish Patent, SE530751C2; 2007.

CHAPTER

Micro-factories 23

Eeva Järvenpää, Riku Heikkilä, Niko Siltala, Timo Prusi, Reijo Tuokko
Department of Mechanical Engineering and Industrial Systems, Tampere University of Technology, Tampere, Finland.

CHAPTER OUTLINE

INTRODUCTION

Miniaturization of products has been a strong trend already for several years. As technology continues to develop, products are getting smaller and more complex. Production processes have to be faster, more precise, and more accurate. This implies that at least partial automation of the processes will become compulsory. Although the need for such production of small-sized products has been rapidly

Micromanufacturing Engineering and Technology. http://dx.doi.org/10.1016/B978-0-323-31149-6.00023-2

increasing, the size scale of the manufacturing systems has not changed much. Small products are still commonly being produced with relatively large machines. This leads to inefficient space utilization and unnecessarily high operating costs. Furthermore, these large-size production systems and machines do not provide flexibility in their location, but need to be placed in traditional large factories even though, in many cases, it would be desirable to produce products closer to the customer.

Besides the miniaturization, two other paradigms—adaptive manufacturing and sustainable manufacturing—set new requirements to the modern production systems. The market calls for customer specific products, which means that the production systems need to cope with high variation and demand fluctuation, small volumes, and short product life cycles. This turbulent production environment requires adaptive and rapidly responding production systems that can adjust to required changes both in production capacity and processing functions. The production ramp-up has to be fast and the effort of changing the production system for the production of new products or different volumes should be minimized. Customers are not willing to pay more for the customization, speed, and flexibility. This means that the production systems need to be able to produce customized products with the price of mass products. Furthermore, the regulatory requirements toward sustainable manufacturing are forcing the companies to minimize the ecological footprint of their production operations in terms of energy and material consumption and waste generation.

Miniaturization of production systems is believed to answer to the industrial demand and challenges discussed above. First of all, miniaturized production systems, micro-factories, provide solution for eco-friendly production. Second, the trend toward modular "construction kit"-type micro-factory solutions enable rapid configuration and reconfiguration of the system based on the need, and in a location where it is needed. Therefore they enable strong customer orientation and flexibility for manufacturing of small-size products.

This chapter will give a thorough introduction to micro-factories. It first discusses about the characteristics of micro-factories in Section Characteristics of Micro-factories. Second, in Section Evolution of micro- and desktop factories, the existing micro-factory solutions, both academic and commercial, are reviewed, followed by detailed introduction to a specific TUT-micro-factory concept, developed in Tampere University of Technology (TUT), in Section Introduction to TUT-micro-factory concept. In Section Potential applications for micro-factory solutions, the potential application areas of micro-factory solutions in general, are discussed. Finally, Section Summary and conclusions concludes the chapter.

CHARACTERISTICS OF MICRO-FACTORIES

This section first gives the definition for micro-factories. After that the challenges related to micro- and desktop manufacturing are highlighted, followed by the discussion of the benefits of micro-factories compared to traditional larger size production systems.

DEFINITION OF MICRO-FACTORIES

Micro- and desktop factories are small-size production systems suitable for the manufacture of small products with micro- and/or macro-sized features. The development of micro-factories originates from the early 1990s Japan [1], where small machines were developed in order to save resources when producing small products, and to reduce the size of the machinery and systems to match the product dimensions. Energy saving and economizing were some of the primary goals. It is worth noting that, in this context and chapter, the term "micro" does not necessarily refer to the size of the manufactured or assembled parts or their features. Neither does it refer to the size of the micro-factory itself. Instead, micro-factories can be seen as a general philosophy to downscaling the production systems and processes closer to the size of the produced goods [1]. The term "desktop factory" is often used interchangeably with the term "micro-factory." Generally speaking, and within this chapter, those terms are used to refer to the same concept: Minimizing production equipment down to level where they can be placed on desktop and manually moved without any lifting aids [2].

The micro- and desktop factories are often characterized by modularity, reconfigurability, plug-and-play interfaces, extreme portability and mobility [2]. In general, micro-factories are composed of similar components and devices than larger scale production systems, but just in a miniaturized size. Due to their small size, several challenges and limitations in their operation exist, which will be discussed in the next section.

CHALLENGES AND LIMITATIONS RELATING TO MICRO- AND DESKTOP MANUFACTURING

The first limiting factor is obviously the size of the production system, which limits the size of the products that can be manufactured and handled with the system. In general, the micro- and desktop factories are designed for handheld size or smaller products. Second, the small size and lightweight of the miniaturized equipment incurs challenges relating to, for example, high accuracy demands, high movement speeds, vibration, and temperature changes. In large-scale equipment, these types of challenges are usually resolved using heavy frames. This is not possible in desktop scale. Instead, alternative solutions have to be used. For example, accuracy can be increased by using active closed-loop control. Vibration can be reduced by using new stiff, but lightweight, materials and structures, such as composites. Also, optimizing the movement control can reduce vibration. Since the equipment is small, the effect of thermal expansion is not as big as in large equipment and also in this case the new materials can help the situation. Similarly, due to the small size, the transfer distances are relatively short and therefore the maximum movement speed is not as important as in large-scale equipment.

Two main concerns of micro-manipulation are the fragile components and sticky effect. As the objects get smaller, the gravity becomes insignificant. Instead, adhesion and other surface forces become dominant, which hampers

the manipulation of the components. In addition, small parts tend to be fragile. As a result, traditional type grippers might destroy the small parts and releasing them becomes difficult. Therefore, more sophisticated grippers need to be developed.

In addition to the challenges relating to the mechanical design of the miniaturized production systems, the small size of desktop equipment creates other difficulties, such as weak accessibility or visibility of the work space to the operator and difficulties in service operations. Operator needs to be aware of what is happening inside the factory. Therefore, when direct visibility is limited, other methods and techniques for visualizing the work space are needed. Often this requires advanced sensors and measurement methods. Service and maintenance operations can be made easier with modular structure so that, for example, a broken piece of equipment can be removed and serviced off-line.

One more challenge resulting from the small size of equipment is feeding of components to the process, e.g., in case of assembly process. Large component trays used to transport the parts from suppliers and small equipment are difficult to match, and therefore additional equipment for unloading components from large trays to smaller ones, or alternative feeding methods, is needed.

Currently micro- and desktop manufacturing is still relatively new and, at least partially, unproven technology and therefore some prejudices against it probably exist. Furthermore, the availability of small-size equipment and components is currently limited and therefore they might not be a practical or economically feasible solution in all cases. Standard components like actuators, controllers, amplifiers, sensors, pneumatic valves, and cylinders are large and if small components are available they are often very expensive. This forces the system providers to develop smaller components by themselves [3].

BENEFITS OF MICRO-FACTORIES COMPARED TO TRADITIONAL LARGER SIZE FACTORIES

The benefits of micro-factories compared to traditional larger size factories can be viewed from three sustainability perspectives, namely ecological, economical, and social. These will be discussed in the following sections.

Ecological perspective

The micro-factory platforms comprise of small-sized production devices. According to Refs [1] and [4], compared to traditional larger factories, they require less factory floor space, consume less energy and raw material, and create less waste and emissions. Due to the smaller size of the overall factory, also less energy is needed for lighting, air-conditioning, and heating. Moreover, less waste heat, which needs to be cooled down, is generated.

Energy saving is one of the most often cited advantage of micro- and desktop factories. For example, Kawahara et al. [5] estimated that downscaling equipment to size 1/X reduces the consumed energy by factors presented in Table 1. They

Table 1 Average Energy Consumption in Actual Factories and Energy Saving Effect when the Factories are Miniaturized to 1/X [5]

	Average Consumption in Actual Factories (%)	Energy-Saving Effect (1/X Miniaturization)
Operating energy	13	$1/X^3$
Environmental energy		
Illuminating	23	$1/(1.5*X^3)$
Air-conditioning	56	$1/(3*X^3)$
Processing energy and others	8	1

separated the energy consumption to three categories: (1) operating energy, which is proportional to moving the parts of the equipment; (2) environmental energy, which is affected by the space needed for the equipment and the number of operators; and (3) process energy, which is needed to remove material from the workpiece (e.g., cutting and grinding). As can be seen from Table 1, majority of the energy is used for illumination and air-conditioning, and therefore these also have the largest potential for energy savings. On the other hand, according to Ref. [5], the needed processing energy does not decrease at all when miniaturizing the equipment.

The case studies conducted in 2003 in Japan proved high potentials in energy and space savings by micro-factories. A desktop factory by Sankyo for assembling motor bearings was reported to reach 98% savings in energy consumption and 95% reduction in space consumption compared to their traditional production systems [6].

Further empirical evidence of the reduced energy consumption of miniaturized resources was obtained in a study conducted at TUT in 2010 by Ref. [7]. The results, reported in [8], indicate that there is a great potential for operating energy savings and possibly even greater savings in, for example, air-conditioning. Therefore, it can be assumed that the environmental impact is smaller for products manufactured in small-size micro-factories, compared to those manufactured in traditional factories.

Economical perspective

The micro- and desktop factories offer an affordable solution to manufacturers, because of lower investment and operating costs compared to traditional larger factories. Same manufacturing capacity can be fitted into smaller space and there is a possibility to use micro-factory automation to aid human worker without the need to reserve huge, expensive factory spaces. Due to their small-size, micro-factories do not need big factory halls requiring heating, lighting, air-conditioning, and so on. Furthermore, as discussed in the previous section, the energy consumption and waste generation of the system itself is much lower compared to traditional large-scale systems, leading to substantial savings in the operating costs. The cost reduction

factors have been discussed in the literature (e.g., Refs [9,10]). Micro-factories allow also special controlled environment, such as a clean room, to be built into a small module space, eliminating the need for big expensive clean rooms. Experiences from one full-scale desktop factory, realized in Takashima Sangyo in Japan, have shown remarkable competitiveness improvements compared to the company's earlier traditional factory: investment 1/5 and running costs 1/5 with the same production capacity [11].

In the era of customization, the desire of the manufacturers is to be able to cost-efficiently serve the customers in their individual demands and to bring the manufacturing closer to the customer. Due to the plug-and-play interfaces of the modular micro-factory system components, the full-scale system can be rapidly build and reconfigured to different functional and volume demands. The system setup and ramp-up time and engineering effort for new process requirements can be radically reduced. Due to shorter setup times, the inventories may also be reduced.

Small-size equipment provides improved portability of the production capacity to the place where it is needed, thus enabling new business models as well as production and logistic strategies. With the novel micro-factory solutions the production does not need to be located anymore to traditional factories, but can be brought to the most convenient location. Few examples could be fabricating customized shoe soles or assembling customized watches in a retail shop, fabricating spare parts in a battlefield, manufacturing products in a ship while being transported, building prototypes in an office room, teaching students about production systems in a classroom, or fabricating customized medical implants in doctor's operating room in hospital [2]. This allows faster response to the individual customer requirements and more personalized service. In case of consumer products, the fact that customer can see his/her product to be manufactured or assembled, can bring competitive advantage against competitors and especially manufacturers abroad.

Especially for small companies and start-ups circumstances like clean room, quality, skilled workers, and investments in high-level equipment are predominant strategic and economic factors that hinder them to upscale from the lab to the full production. In addition, the unknown response from the market after launching the product, the life cycle of the product and the evolution of the product are other issues that are taken in account when setting up the commercial production. Thus, such a modular and mobile micro-factory increases the ability to rapidly follow the market dynamics by means of fast production and delivery of customized final products. Such a mobile micro-factory could also be leased (hired) for a time by a company preparing the launch of a new product, a start-up, a research institute, etc. Micro-factories offer flexibility to try out new ideas without huge investments [8].

Social perspective

The micro-factory solutions could also have a wider societal impact for different economic regions. First of all, they can create more attractive and safe workplaces.

Second, they offer possibility to maintain the manufacturing or even bring it back from low labor cost countries by enabling cost-efficient production of customized, green products on the spot.

From the social point of view it is important to minimize hazardous work environments, improve the ergonomics of the work environments and to pursue the efficiency, creativity, and health of the workers. The risks of the manufacturing environment to the human worker are not only physical, but also psychological. For example, extremely simple, monotonous work can cause psychological issues and lack of motivation. Due to their small size, micro-factories can be placed, e.g., on the desktop of human worker to help him/her with boring repetitive tasks, tasks which require special accuracy, or tasks that are ergonomically difficult. The human can then concentrate on more interesting activities which require special skills. Compared with large production equipment, e.g., industrial robots, micro-factory solutions do not expose the human workers to danger. Due to small forces, for example, the collisions are not fatal. Therefore, they enable safer human−machine cooperation compared to traditional large-size equipment.

The micro-factories cannot only improve the manufacturing work environments, but also provide better service for the end customers. As the small size of the micro-factory solutions allows them to be brought closer to the end customer, even to the point-of-sales or point-of-use, it ensures faster and more customized service and satisfied customers. The offered products can fit better to the individual customer's needs. For example, in the field of medical devices the customization is extremely important. Today, the customization of medical devices, such as medical implants, is not yet common, causing imperfect fit and possible complications to the patients. Therefore, the manufacturing of customized medical implants on the spot (in the surgeon's room or dentist's office) is expected to have a drastic impact on the quality of the implant customization and thus lead to a better fit of the implant in each patient's body. Therefore fewer complications are expected and consequently less expensive and possibly painful reoperations will be needed. This will lead to notable savings in health care costs and also in the time that is needed to treat individual patient. Moreover the quality of the treatment will be better resulting in increased well-being of the patients. Therefore, the societal impacts can be wide.

EVOLUTION OF MICRO- AND DESKTOP FACTORIES

According to Okazaki et al. [1], the idea of a micro-factory originates from the research conducted in Japan in the 1990s. The research was based on an idea that smaller machines are needed to produce micro-parts and machines. Energy saving and economizing were the primary goals. Ideas of "desktop," "palmtop," and "mobile" factories were awoken. In the late 1990s, the research spread around the world, and since then multiple miniaturized production systems, i.e., micro- and desktop factories, modular micro-factory platforms as well as miniaturized production equipment in general, including, e.g., desktop-size machining units,

robotic cells, and rapid prototyping units, have been developed. Despite of large amount of research, the level of commercialization and adoption of micro-factory solutions remains still relative low. The discipline lacks of empirical cases and industrial practice on micro-factory-related business. However, few commercial desktop factories, small-size machining units and desktop-size stand-alone automation units have been developed for different purposes. The following sections will first list the research conducted in the academic world, followed then by the commercial solutions related to micro- and desktop factories. Finally a more detailed introduction to a selected set of micro-factory solutions will be given.

ACADEMIC MICRO-FACTORY DEVELOPMENT

Table 2 presents the summary of academic micro-factory developments. In the table, the developments are divided into the following categories:

- **Miniaturized machining units**—multiple highly miniaturized machining units have been developed since the mid-1990s. Some of them have been developed as part of complete micro-factory concepts and some are developed for stand-alone use. They are usually high-speed and high-precision machines designed to produce metallic precision mechanics components.
- **Miniaturized robotic and assembly cells**—the miniaturized robotic and assembly cells are stand-alone systems. They usually have one or few manipulators and one or few cameras for teleoperation (they work in semiautomatic mode) or for process control.
- **Micro-factory as a set of small-size production equipment**—the original Japanese approach to micro-factories was to develop a fixed set of integrated small-size production machines. The micro-factory systems usually include miniaturized machining units and/or micro-press to produce components, a small-size manipulator, transfer arm or conveyor system to transport the components, and a small-size assembly unit or a micro-manipulator to assemble the components.
- **Modular micro- and desktop factory concepts**—the research on modular micro- and desktop factory concepts is mainly concentrated on modular micro-factory platforms and/or architectures. The main focus of the research is on developing the platform. Development of the machines is usually only a secondary goal.

For more information about the individual concepts, please refer to the sources indicated in the table.

COMMERCIAL MICRO-FACTORY DEVELOPMENT

Even though micro- and desktop factories have been under research for several years, large industrial breakthrough still remains unseen. At the moment, it appears that miniaturized machining units have the largest coverage and also

Table 2 Academic Micro-factory Developments

Year	Country Code	Concept	Institution	Source
Miniaturized Machining Units				
1996	JP	Micro-lathe	MEL	[12]
1999	JP	Multifunction desktop machine	AIST	[13]
2000	JP	NC micro-lathe	AIST	[14]
2001	JP	Desktop NC milling machine, 200 krpm "El Chuchito"	AMRI	[15]
2004	JP	Desktop milling machine, 300 krpm	AIST	[6]
2004	MX	Mexican first generation MMT	UNAM	[16]
Miniaturized Robotic Cells and Assembly Units (Stand-alone Cells)				
2002	CH	Flexible micro-assembly cell	EPFL/LSRO	[10]
2003	GER	μFemos	KIT (IEF Werner)	[17]
2004	FIN	TOMI—mini assembly cell	TUT	[18]
2008	TR	Versatile and reconfigurable micro-assembly workstation	Sabanchi University	[19]
2008	FR	Flexible micro-assembly system with automated tool changer	FEMTO-ST	[20]
Micro-factory Concepts (Including e.g., Miniaturized Machining Units, Manipulators, Transfer Arms, and Conveyor Systems)				
1994	JP	Micro-factory by MMC	MMC	[21]
1998	JP	Portable micro-factory	MEL	[12,22]
2000	FIN	TOMI micro-factory	TUT	[23,24]
2006	USA	Automated Illinois micro-factory	UIUC	[25,26]
2006	KR	Mosaic	KIMM	[27]

Continued

Table 2 Academic Micro-factory Developments—cont'd

Year	Country Code	Concept	Institution	Source
Modular Micro-factory Concepts (Modular Micro-factory Architectures and Platforms)				
2001	USA	Agile assembly architecture	CMU	[28]
2001	GER	AMMS, advanced modular micro-assembly system	Frauenhofer IPA	[29]
2004	FIN	ABAS desktop platform	TUT	[30]
2005	CH	Microbox Pocket-Factory	EPFL/LSRO	[31]
2005	FIN	TUT micro-factory	TUT	[3,32]
2008	JP	On demand manufacturing system	AMRI	[33,34]
2010	CH	Desktop rotary assembly line	EPFL/LSRO	[35]
2010	FIN	Desktop assembly	VTT	[36]
2011	GER	MicroFLEX	KIT (IEF Werner)	[37]

desktop-size stand-alone automation units have been developed for multiple purposes. Furthermore, desktop-size 3D printers and rapid prototyping units are appearing rapidly on the market. Instead, only a few modular desktop factories have been developed.

Table 3 presents the summary of the commercial micro-factory solutions. In the table, the solutions are divided into the following categories:

- **Small-size stand-alone machining units**—since the millennium, multiple commercial small-size and stand-alone machining units have been developed. The miniature machining systems are designed for versatile materials and applications, e.g., metal (micro-mechanics, jewelry, and watches), glass (micro-optics), plastic (hearing aids), ceramics (dental), and biodegradables (implants).
- **Small-size stand-alone process cells**—the small-size stand-alone process cells have been developed for different processes, such as laboratory automation, hot embossing, nickel plating, and molding.
- **Small-size stand-alone robotic cells**—the small-size stand-alone robotic cells are stand-alone cells consisting of robotic unit and needed auxiliary devices. They have been developed for a certain task, such as pipetting, palletizing, or screwing.
- **Multifunctional micro- and desktop factories**—the multifunctional micro- and desktop factories are complete factory concepts able to perform multiple operations and processes, such as machining, cleaning, assembly, or coating.

FURTHER INTRODUCTION TO A SELECTED SET OF ACADEMIC AND COMMERCIAL MICRO-FACTORY DEVELOPMENTS

Figure 1 and Table 4 summarize a selection of development milestones in micro- and desktop factories. These will be discussed in more detail below.

The first, and one of the most commonly cited, miniaturized production unit is the micro-lathe developed in MEL in Japan in 1996. The lathe revealed the possibility to downsize machining units. The lathe has dimensions of 32 × 25 × 30 mm and it weighs only 100 g. The main spindle motor uses power only 1.5 W, and it can spin up to 10,000 rpm. It has an accuracy of 1.5 μm in the feed direction and a roundness of 2.5 μm. The minimum diameter of workpiece is 60 μm [1,12]. Four years later, in 2000, the micro-lathe was further developed and equipped with a precision digital control system. A desktop milling machining unit, with a footprint or 550 × 450 mm, was build based on the numerical-controlled micro-lathe [1,14].

Another famous Japanese micro-factory concept is the portable micro-factory developed by MEL in 1998. Dimensions of the system are 625 × 490 × 380 mm, and it is teleoperated. The system has a micro-lathe, a micro-milling machine, a micro-press machine, a transfer arm, and a two-fingered micro-manipulator. The user interface consists of two joysticks and a 5.8-in LCD monitor, showing live video of three miniature CCD cameras. Miniature ball bearing was used as the first case product [22].

Table 3 Commercial Micro-factory Developments

Year	Country Code	Product	Company	Source
Small-size Stand-alone Machining Units				
2002	JP	Nanowave MTS2 • Precision lathe	Nano Corporation	[38,39]
2003	JP	Multi-Pro • Versatile 3-axis desktop machine platform	Takashima Sangyo Co.	[40]
2003	JP	Multi-function Turning Center	DTF	[41]
2004	JP	TRIDER-X • 4 Axis grinder	Rinken Co.	[42]
2004	JP	Desktop milling machine	PMT Co.	[1]
2004	JP	Cylindrical cells • Turning and grinding	SII Co.	[1]
2005	JP	Nanowave MTS3, MTS4, MTS5/MTS6 • Precision mill	Nanowave Co.	[39]
2008	USA	G4-ULTRA CNC • 3/4/5-Axis micro-machining	Atometric Inc.	[43]
2008	USA	Microlution 363-S • 3-Axis micro-mill/grill	Microlution Inc.	[44]
2008 2009	USA	EM203, GM703, MM903 • Micro-milling/turning/EMD/drilling/polishing nano-grinding	SmallTec Inc.	[45]
2009	JP	Micromill CVN-2000 • 4-Axis CNC mill	Enomoto Kogyo Co.	[46]
2010	GER	Impression line: cam4-02, cam5-02, cam4-K1, cam4-K2 • 4/5-Axis CNC machine	Vhf camfacture AG	[47]
2011	FIN	Kolibri • 3/4/5-Axis CNC machine	Wegera	[48]

Small-size Stand-alone Process Cells				
2003	JP	Ultra Compact Hot Embossing Machine	DTF	[41]
2003	JP	Desktop Nickel Plating Machine	DTF	[41]
2007	UK	DS2TM and DSXTM • Laboratory/diagnostics automation	DYNEX Technologies	[49]
2009	IT	Global240 and Keylab • Laboratory/chemistry automation	BPC BioSed SRL	[50]
2010	IT	Sesame • Nano-molding	Medical Murray	[51]
Small-size Stand-alone Robotic Cells				
2009–2011	CH	Asyfeed Pocket • Flexible multi-function robot cell, e.g., assembly pelletizing and sorting	Asyril	[52]
2019	FIN	J505-62 • Desktop screw inserting cell	JOT Automation	[53]
2011	FIN	Roboline • Desktop cell for automated pipetting	Biohit	[54]
Multifunction Micro- and Desktop Factories				
2003	JP	Desktop Factory DTF® • Multiple processes, e.g., cleaning, coating, screwing measuring, and assembly	Sankyo Seiki Co.	[55]
2003	JP	Multi-Pro • Versatile 3-axis desktop machine platform	Takashima Sangyo Co.	[40]
2004	USA	Nexar® and Araya® • Laboratory automation	Douglas Scientific	[56]
2007	GER	Lean Desktop Factory • Modular floor-standing “desktop” assembly system	Bosch Rexroth AG	[57]

Continued

Table 3 Commercial Micro-factory Developments—cont'd

Year	Country Code	Product	Company	Source
2009	GER	LabFab • Laboratory automation	Festo AG & Co.	[58]
2010	FIN	MAG Lean • 3/4-Axis multi-function automation cell, e.g., pick and place, and screwing	MAG	[59]
2011	FIN	JOT Lean Desktop • Lean assembly cells	JOT Automation	[53]
2011	GER	MicroFLEX	IEF Werner	[37]
2012	FIN	GIN Kolibri • 5-Axis high precision CNC milling machine	Global Innovation Network (GIN)	[60]

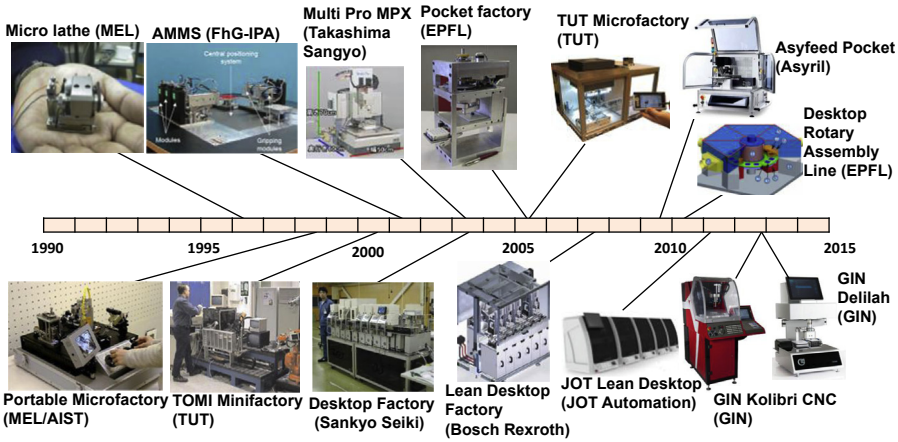

FIGURE 1

Selected milestones in micro- and desktop factory developments (both academic and industrial).

One of the first micro-factory concepts, developed outside Japan, was the TOMI micro-factory developed by TUT in Finland in 2000. TOMI (Towards Mini and Micro Assembly Factories) was a pilot project for TUT micro-factory research. The goal was to develop an integrated high performance assembly system for a miniature product. The case product was a planetary gearhead with a diameter of 8 mm and variable gear ratios. As a result, a small-size floor-standing system was developed. Dimensions of the production system are 1800 × 500 mm and the system consists of modules of 500 × 500 mm. All the assembly phases were packed into one module [24].

One of the first modular desktop-size micro-factory concepts was the advanced modular micro-assembly system, developed by Fraunhofer IPA in Germany in 2001. The "plug-and-produce" system is based on a 600 × 400 mm planar motor table. Products and/or components are placed on moving carriers, which move with a friction-free air bearing on the planar table. The fixed process modules have dimensions of 100 × 200 mm, standardized interfaces, and they are placed next to the planar table. The complete system has dimensions of 800 × 800 mm. The XY planar stage has a positioning accuracy of 20 μm. The accuracy of the Z-axis depends on the used process module. A miniaturized laser diode was used as a case product. It is argued that a wide range of micro-products, e.g., mini-encoders, micro-valves, or fiber optics, could be assembled with a similar system [61].

One of the first commercial micro-factory units was the Desktop Factory® developed by NIKED Sankyo (former Sankyo Seiki) in 2003. The modules are 170 mm wide and they are designed for multiple purposes, e.g., cleaning, coating, screwing, measuring, and assembly [55].

Takashima Sangyo introduced in 2003 a multifunctional desktop process machine Multi-Pro MPX. It is applicable to various machining, such as milling, grinding, and laser processing. The current version has footprint of

Table 4 References to Micro- and Desktop Factories Shown in Figure 1

Year	Country Code	Concept	Institution	Source
1996	JP	Micro-lathe	MEL	[12]
1998	JP	Portable Micro-factory	MEL	[12,22]
2000	FIN	TOMI Micro-factory	TUT	[23,24]
2001	GER	AMMS, advanced modular micro-assembly system	Frauenhofer IPA	[29]
2003	JP	Desktop Factory DTF®	Sankyo Seiki Co.	[55]
2003	JP	Multi-Pro MPX	Takashima Sangyo Co.	[40]
2005	CH	Microbox Pocket-Factory	EPFL/LSRO	[31]
2005	FIN	TUT micro-factory	TUT	[3,32]
2007	GER	Lean Desktop Factory	Bosch Rexroth AG	[57]
2009–2011	CH	Asyfeed Pocket	Asyril	[52]
2010	CH	Desktop Rotary Assembly Line	EPFL/LSRO	[35]
2011	FIN	JOT Lean Desktop	JOT Automation	[53]
2012	FIN	GIN Kolibri	GIN	[60]
2012	FIN	GIN Delilah	GIN	[60]

480 × 725 mm and repeatability of 2 μm. The granite base is used to reduce the thermal changes and deformation during machining [40].

The first micro-factory concept with an integrated clean room was the Microbox Pocket-Factory developed by LSRO (a laboratory of EPFL) in Switzerland in 2005. Microboxes have clean rooms capable of clean class 100 or ISO 5 (maximum 100,000 articles of size ≥0.1 μm in a cubic meter). In addition, the units include an entry port enabling clean transfer into unit, a 4 degrees of freedom (DOF) scara robot for easy assembly tasks, sensors for process control, a laminar airflow generator, and a filtration system. The units have about 1 dm^3 clean working area. A "pocket factory" can be constructed out of multiple Microbox units and different feeders. Each unit can conduct one or multiple assembly operations (e.g., gluing, insertion) [31].

The modular TUT-micro-factory concept was introduced by TUT, Finland, in 2005. The concept is based on small independent micro-factory modules of size 300 × 200 × 220 mm, which are designed to work as a stand-alone unit or as a part of "plug-and-produce" production line. The concept includes an integrated clean room as well [3]. More detailed introduction to the TUT-micro-factory concept will be given in the next section.

In Europe, one of the first commercial "desktop factories" was developed by German Bosch Rexroth AG in 2007. Despite the name, it is a modular floor-standing system. However, the width of the modules is only 220 mm. An example of squeezing a 30-m long automated assembly line down to 4.5 m, has been reported [57].

In addition, small-size and stand-alone robotic cells have been developed for specific applications. In 2009, Swiss company Asyril published their first version of a tabletop cell, Asyfeed Pocket. The overall size of the cell is 850 × 900 × 900 mm. It is a miniaturized version of the floor-standing cell, Asyfeed Desktop (800 × 800 × 2250 mm). They both include a PocketDelta Robot (highly miniaturized and high precision delta robot), an Asycube (flexible feeding system), and an Asyview (vision system). They are primary designed for sorting and palletizing of bulky micro-components. In addition, the cells can be modified to assembly and measurement tasks. Work-cycles up to three components per second can be achieved [52].

The micro-factory research at EPFL continued in 2010 with another concept, Rotary Assembly Line. It is developed to achieve higher class cleanliness than with linear concept. The circular concept has a central unit including clean air inlet, rotary table for transportation of standard 2 in trays and interfaces (mechanic, data, and power) for the production modules. The production modules around include working area with laminar and horizontal airflow, space for a manipulator, air outlet, as well as inlets and outlets for the components. The modules have dimensions of about 250 × 250 mm and height of 75 mm. The overall system has a footprint smaller than a square meter [35].

In 2010, a Finnish automation provider, Master Automation Group, introduced MAG Lean cells. In contrary to Bosch modules, MAG Lean is truly a desktop-size system. The dimensions of the three to four axis cells are 250 × 500 × 500 mm and they weigh only between 25 kg and 40 kg, depending

on the configuration. Applications include, e.g., pick and place, screw inserting, testing and laser marking of aluminum, steel and plastic components. In 2011, Master Automation Group merged together with another Finnish automation provider, JOT automation. The recently published JOT Lean cell includes two sizes, 533 × 600 × 710 mm and 333 × 600 × 710 mm. It is an improved version of the previous MAG Lean generation in all ways. Plasma treatment has been stated as a new potential application [53].

In 2012, a Finnish company Global Innovation Network launched two micro-factory solutions, GIN Kolibri and GIN Delilah. GIN Kolibri is a floor-standing 5-axis high precision compact size computer numerical control (CNC) milling machine. It can mill practically all materials from titanium to plastics. GIN Kolibri is a full-scale milling machine for versatile CNC needs and efficient high-volume manufacturing. The guaranteed precision level within the working envelope is 5 μm. The typical applications are medical devices, their components, and medical and dental implant manufacturing. GIN Delilah is a modular robot platform for Laboratory Automation. Typical applications are sample, liquid, tube handling, and drug development [60].

INTRODUCTION TO TUT-MICRO-FACTORY CONCEPT

TUT has a strong background on micro-factory research since 1999. In this section the TUT-micro-factory concept and some of its applications are introduced.

TUT-MICRO-FACTORY CONCEPT

The TUT-micro-factory is a modular construction kit type concept with easy and rapid reconfigurability for different manufacturing processes of handheld size, or smaller, products. The system structure is designed with an idea that a base module (Figure 2) can work as an independent unit including all the needed auxiliary systems. The base module includes a clean room class work space, a control cabinet and the equipment needed by the clean room. Since the production module does not need a separate control cabinet, the factory can be aggregated fast and easily on a desktop table or other flat surface. This and small size of the modules enable extreme mobility of the production capacity. The outer dimensions of one base module are 300 × 200 × 220 mm and the inside work space is 180 × 180 × 180 mm [3,62].

The production module can be tailored to certain processes by placing process modules on top of the base module (Figure 3). Process module can be, e.g., a robot, laser, or machining unit. In addition to the top side of the base module, both sides and the front side can be left open when adjacent cells compose one integrated work space. Feeders and other devices can be placed in the opening on the sides. Examples of different configurations of TUT-micro-factory modules for different applications can be seen in Figure 4 [3,62].

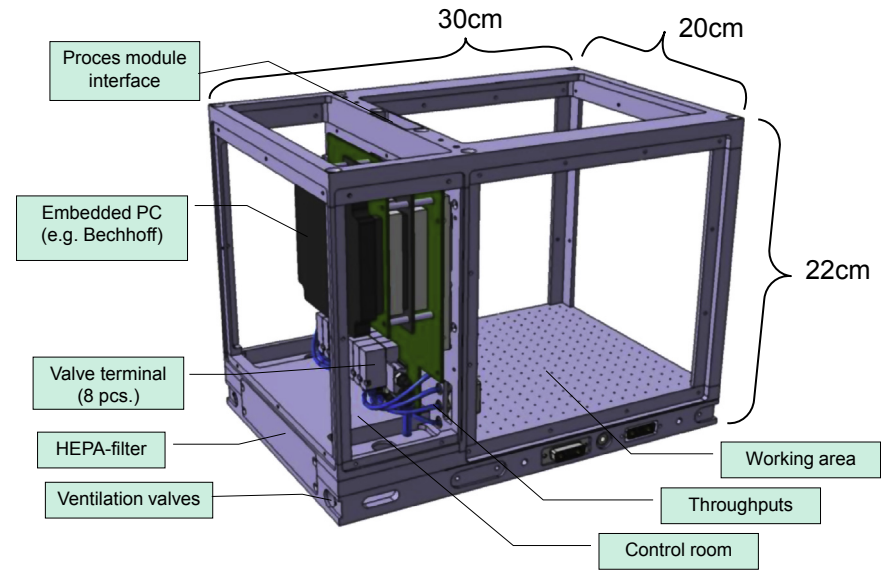

FIGURE 2

TUT-micro-factory base module.

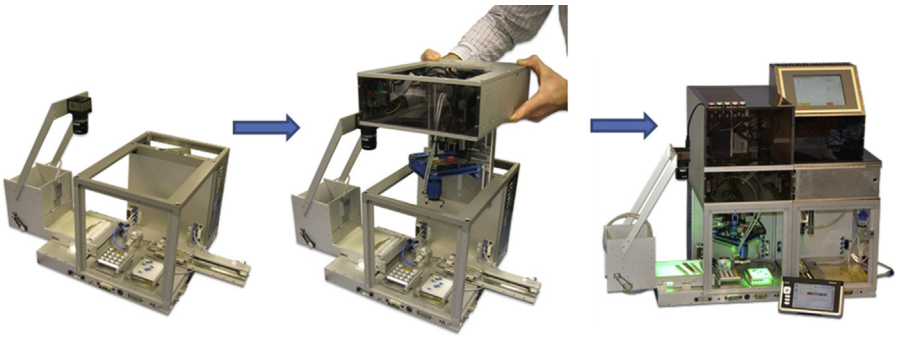

FIGURE 3

Plug-and-play interfaces for easy configuration of a complete TUT-micro-factory system.

All interfaces in the TUT-micro-factory concept have been designed to be as simple as possible. The base modules can be locked next to each other side by side, front by side, or front by front allowing nearly unlimited number of factory layouts, ranging from a simple line type to a freely branching one. The physical interface between two base modules includes two hybrid connectors for electrics/electronics, an interlocking system, and connectors for pressurized air and vacuum. Each module has an individual control unit and standardized interfaces. They can communicate with each other through the physical connections or through WLAN. User interface

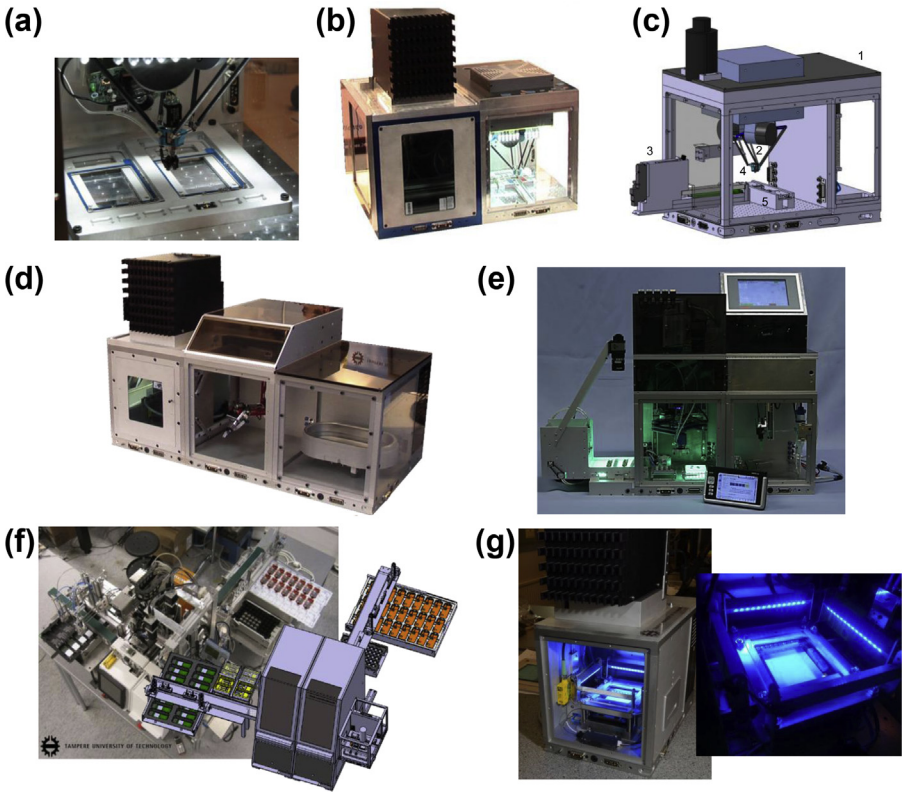

FIGURE 4

TUT-micro-factory applications: (a) a loudspeaker assembly, (b) laser marking, (c) spring assembly, (d) manufacturing of medical implant, (e) gas sensor assembly, (f) cell phone assembly, (g) laser welding.

for a tablet PC has been developed and, with that, one or multiple cells can be controlled using only a single interface device [3,62].

Due to the modular structure of the TUT-micro-factory concept and plug-and-play interfaces of the modules, it is easy to reconfigure the system to different product requirements. This reconfigurability is also supported by the fact that the small-size and lightweight equipment can be lifted manually without any lifting aids.

APPLICATIONS OF TUT-MICRO-FACTORY CONCEPT

Several demonstrations, some of those shown in Figure 4, have been realized with the TUT-micro-factory concept during the past and ongoing research projects. One of the first case processes was assembly of a cell phone loudspeaker in 2005 (Figure 4(a)). The assembly operation was a pick and place operation of the loudspeaker from a jig to the cell phone cover. The component size was

10.9 × 7.4 × 2 mm and weight less than 1 g. As a manipulator a PocketDelta robot from Asyril [52] was used [32].

The laser marking micro-factory (Figure 4(b)) was built as a demo for the Laser 2007 fair in Germany. The case products were personalized aluminum business cards with sizes of 4 × 9 mm and 9 × 20 mm. The case was a good introduction to the point-of-need manufacturing. The visitors could personalize their own business cards and get them manufactured right away [3].

As a part of the Desk project, in 2008, the first industrial demonstration was conducted. The case process was a small spring placement in a micro-electro-mechanical systems (MEMS) sensor component (Figure 4(c)). The small size (D 0.7 mm, L 2.54 mm) and complex shape made the spring extremely difficult to handle. The factory was built using only one TUT-micro-factory module. Besides the base module (1), a PocketDelta robot (2) was used as a manipulator, and the springs were fed by a machine vision-based flexible feeding system, the Wisematic Minifeeder™ (3). The vacuum gripper (4) had a fiber-optic sensor to detect the spring in the gripper. In addition, a small lead frame stepper (5) was designed to move the base components. The stepper used pneumatic actuators and an optical sensor to detect the position of the lead frame [3].

The first process chain level three-cell demonstration was a manufacturing process of a medical implant, a laser-machined silicon rubber ear tube (D 3 mm, L 5 mm) (Figure 4(d)). The manufacturing process consisted of machining and cleaning. Three base modules and two process modules were used in the demonstration. The first module included a 20 W laser lathe with a scanner and an online inspection system. The online inspection system was used for measuring the dimensions of the tube. The second module included a 5 DOF articulated joint robot, which reached the adjacent cells as well. It was used to load the lathe and move the implants to washing. The final module included an ultrasonic washing system [62].

The gas sensor assembly was a good introduction to different joining processes (Figure 4(e)). The case product was a gas sensor (L 78 mm, D 12 mm), including two identical plastic frame parts, a detector in a metal package and an exciter. There were three phases in the assembly process. First, the detector was placed in the plastic frame in right orientation. Second, the exciter was placed in a correct position and angle. Third, another plastic frame was glued on top of the other. The micro-factory assembly system consisted of two TUT-micro-factory modules and a machine vision-based flexible feeder for the frame parts. The first micro-factory module was responsible for the part handling and assembly operations. A new TUT H-Scara robot was used for the manipulation. Besides the robot, the cell included a vacuum gripper, two standard 2-in trays for component feeding, a turning unit, and cameras. The second micro-factory module provided the gluing process. It consisted of a low cost Cartesian TUT linear motor robot, a dispensing valve, an assembly jig for the base frame, a controller, and a human-machine interface (HMI) unit [63].

In the Mz-DTF project (2009−10) the factory level integration of micro-factory modules was considered and implemented. As a demonstration, a complete mobile phone assembly line was built out of commercial components and the

TUT-micro-factory modules (Figure 4(f)). The assembly process consisted of pick-and-place, manipulation, and screwing operations. The TUT-micro-factory module was used as a flexible screwing cell and larger desktop prototypes from industrial partners were used for the pick-and-place operations. The implementation was successful, but also some challenges came up. Even though handheld-size products fit perfectly into the TUT-micro-factory, the subcontractors in the electronic industry still tend to use rather large trays. Compact feeding systems, e.g., tape-and-reel, bowl, and machine vision-based flexible feeding, need to be further developed and accepted as an industry standard [64].

In the ReDia-project (2011−13) the laser-welding process of medical diagnostic device was miniaturized and implemented to TUT-micro-factory module. In the process, a transparent plastic plate, containing micro-fluidic channels, was welded together with dark plastic cover plate. A conveyor transported the micro-fluidic cartridge to the clamping device and the finished product out of the module. The clamping device ensured good contact between materials during the welding process. A machine vision-based measurement system was used to position the micro-fluidic channel locations. The measurement ensured precise welding around the micro-fluidic channels which is needed to achieve proper sealing and to prevent leakages. Special attention was paid to the laser safety. The micro-factory module was designed to be one phase in a complete manufacturing system of the micro-fluidic-based immunoassay cartridge. The complete manufacturing line would consist of several dispensing, washing, and handling modules as well as incubation chambers. These were all modeled, but not implemented during the project.

POTENTIAL APPLICATIONS FOR MICRO-FACTORY SOLUTIONS

This section will draw a vision about potential application areas for micro-factory solutions. As the small size of the micro-factories ensure extreme portability of the manufacturing capacity, the production systems do not need anymore to be located into traditional factory spaces. Therefore three principal motivation scenarios for the use of micro-factories can be identified:

1. Replacing the traditional size equipment and systems with miniaturized equipment and systems;
2. Relocating the production further into the downstream;
3. Manufacturing “on the spot.”

Application area examples for micro-factory technologies from these three perspectives will be discussed in the next three sections.

REPLACING TRADITIONAL SIZE EQUIPMENT WITH MINIATURIZED EQUIPMENT

The first scenario takes place in a traditional production chain. In this scenario the traditional large-scale production machines are replaced and/or supplemented with

the micro- and desktop production systems. Here, the production process itself and the supply chain remain unchanged. Basically, smaller equipment needs smaller factory buildings and consumes less energy and resources or, what seems to be quite important in many cases, enables more production capacity in the existing factory buildings. Other benefits, and obviously the motivating factors, of replacing the large-size equipment with miniaturized equipment have already been discussed in Section Benefits of micro-factories compared to traditional larger size factories.

Figure 5 represents the potential application areas speculated in the literature. In general, micro- and desktop factories could be applied to all products and processes, which fit into the reduced working space. However, it does not mean that the miniaturization would necessarily be feasible. Usually there already exists large-scale machinery for any given process. A desktop machine or a factory is bought instead if it is better for the application or if it can cut costs.

Replacing traditional size equipment with miniaturized equipment				
Application area	**Material production** 	**Component manufacturing** 	**Assembly** 	**Finishing and inspection** 
Products	• Medical • Chemistry • Low-volume process industry products	• Metal (e.g., jewelry and watches) • Glass (e.g., micro-optics) • Plastic (e.g., hearing aids) • Ceramics (e.g., dental) • Biodegradables (e.g., implants) • Silicon (e.g., semiconductors)	• Portable devices • Precision mechanics, e.g., watches, micro-motors, gears • Micro-optics • Jewelry • Life science • Medical/dental • Semiconductors • Sensors • MEMS products	• Small products or components, e.g., CE marking, optical control of assembly, sterilization of medical implants
Processes	• Chemical reactions of dangerous materials • Micro-cultivation • Drug fabrication and encapsulation	• Injection moulding • Machining • Additive manufacturing (3D printing) • Lithography	• Pick and place • Screwing • Dispensing • Laser processes • Ultrasonic welding • Heat treatment • Palletizing	• Marking (scratching/laser) • Coating (Paint/UV-printing) • Washing • Cleaning • Sterilization • Optical control • Packing • Processes under special condition

FIGURE 5

Motivation scenario 1: replacing traditional size equipment with miniaturized equipment.

Kawahara et al. [5] argue that micro- and desktop factories could be used as micro-chemical plants. Applications include, e.g., drug fabrication, micro-cultivating, and chemical reaction of dangerous materials. Multiple benefits relate to the small reaction space. The reaction starts and ends quickly. Thus, risky exothermic reaction can be safely achieved. In addition, truly homogeneous chemical reaction becomes possible as the concentration differences decrease [5]. However, micro-factories are not suitable for large volumes. For example, instead of pharmaceutics industry, micro-cultivation, and micro-reactors might suit better for laboratory environments.

Component and micro-part manufacturing was one of the original applications for micro-factories. The benefits relate mostly to floor space reduction and relating costs. In addition, the small-size machining units enable few additional business models for the equipment providers and subcontractors. Furthermore, the small machines can support Lean and Just-In-Time production as components can be produced on the spot based on requirements. The small components are made of multiple materials: metal (e.g., jewelry, gears, and watches), glass (e.g., microscopes, laboratory instruments, and contact lenses), plastic (e.g., hearing aids and implants), ceramics (e.g., dental products and molds), biodegradables (e.g., implants), and silicon (semiconductors, e.g., sensors). Potential miniaturized processes include injection molding (e.g., Ref. [51]), machining and additive manufacturing, including 3D printing, and lithography. In addition, components can be fabricated in a clean room or under a special condition (e.g., Refs [5,31,35]).

Assembly operations are other promising application for micro-factories. Suitable small-size products include, e.g., portable electronic devices [53], precision mechanics (e.g., watches, micro-motors, and planetary gearheads) [18,65], micro-optics, life science products (e.g., test kits) and other small medical products, dental products, semiconductors, sensors, and measuring devices, as well as other MEMS products [33]. Suitable miniaturized assembly processes include, e.g., pick and place, screwing, dispensing, ultrasonic welding [53] as well as palletizing [52].

Finally, micro- and desktop factories could be used for finishing, inspection, or packing, as well as for CE marking, visual control of assembly or sterilization of small medical implants. Other miniaturized processes include, e.g., marking, laser carving [3], painting, UV-printing, ultrasonic washing [62], cleaning, and sterilization [2]. In addition, a micro-factory with a clean room enables processes under special conditions. Again, the only restriction is that the small products and components have to fit into the working space.

RELOCATING THE PRODUCTION FURTHER INTO DOWNSTREAM

The second motivation scenario is relocating production further into the downstream. Small size and easy portability of desktop size equipment enables, at least in theory, locating manufacturing capacity and organizing logistics freely. This means that some of the production steps could be relocated to three different phases between a factory and a customer. First, the products could be produced during the

transportation, e.g., on a ship or in an aeroplane. Second, the products could be personalized at, or before, the wholesaling level. Third, the personalization could be placed at the retailing level. Figure 6 shows some example applications speculated in the literature.

First option is a mobile factory that was first introduced by Kawahara et al. [5]. Because of the small machine size, the production system could be integrated, e.g., into a car, train, boat, or aeroplane. The materials could be loaded into the car and the manufacturing would happen during transportation. In the end, the car could deliver completed products [5]. The process could shorten delivery and enable production of perishable products on the way. The shorter delivery could gain add-on sales. In

Relocating production further into the downstream			
Application areas	**Transportation, on the way/fly** 	**Storage and wholesaling** 	**Retailing** 
Products	• Small products having long time of delivery and stabile demand • Perishable products (e.g., grocery)	• Small products having modular design and intermediate level of personalization	• Small highly personalized products, e.g., contact lenses, watches, jewelry, cosmetics, small sports equipment, craft shops, medical
Reasons /how	• To shorten delivery • To protect the perishable products	• Dynamic supply chain and delivery • Wholesale level mass customization	• Coating (Paint/UV-printing, e.g., laptops) • Marking (Scratching/laser, e.g., iPods) • Final assembly (e.g., eye glasses) • Final design (e.g., custom-fit sports equipment) • Drug dosage and encapsulation

FIGURE 6

Motivation scenario 2: relocating production further into the downstream.

addition, capital costs are expected to decrease, as delivery is faster and stocks of finished products decrease. Suitable products would be small and perishable products having a long time of delivery and a stabile demand.

The second option to relocate production further into the downstream is to place some production phases at the wholesaling and/or retailing level. At wholesaling level, the model would suite well for personalization of small products having modular design and an intermediate level of personalization. At retail level, micro-factories could be used to personalize small and highly personalized products, e.g., contact lenses, watches, jewelry, cosmetics, small sport equipment, pharmaceutics, and other medical products. Potential processes include coating and UV-printing (e.g., electronics), marking (e.g., jewelry), final assembly (e.g., optics), machining (e.g., custom-fit sport equipment), and sorting (e.g., drug dosage and encapsulation). The advantages relate mostly to add-on sales. Customers might choose the product because it is more personalized. In addition, decentralized production hubs are expected to increase dynamics of the supply chain, adapting more easily to a fluctuating demand and decreasing costs of logistics. Goldsmiths, opticians, and orthotics are examples of current businesses, relating to retail level personalization.

However, a lot of uncertainty relates to the advantages of bringing the production further into the downstream. Production during transportation is speculated to shorten delivery times. However, since the duration of actual transportation (especially air cargo) is usually short compared to the actual delivery time, this might not be the case. It is also speculated that the costs of logistics and capital tied to stocks would decrease with mobile factories. On the other hand, production equipment requires space in the transportation vehicle and therefore transportation capacity decreases. In addition, the impact of personalization on the costs of logistics depends highly on the processes. If the personalization happens during the assembly process, the components have to be transported to many locations instead of one factory. As a result, the costs of logistics might even increase. Therefore, subtractive manufacturing, coating, and marking are more potential processes compared to assembly.

ON THE SPOT MANUFACTURING

The last scenario, on the spot manufacturing, relates to the speculated "ubiquitous manufacturing" [4], "point-of-need manufacturing," and "decentralized manufacturing." As micro-factories are small, they could be used to produce products on the spot (in the place where the products are actually used) in various locations. There are three principal reasons for manufacturing on the spot: (1) no space for a traditional factory (e.g., urban fabrication in a city center); (2) no time to order and deliver (e.g., battlefield); or (3) impossible logistics (e.g., isolated places such as oceans or space) (Figure 7).

"On the spot manufacturing" would be ideal for small products having critical time of delivery, e.g., exchange parts [5], spare parts [4], and medical products [62].

On the spot manufacturing		
Application areas	**Production in the place of ordering** 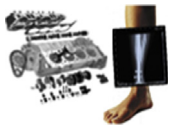	**New applications** 
Products	• Exchange parts • Spare parts • Small products having critical time of delivery • Medical products (e.g., custom implants, dental implants, drugs fabrication, dosage, encapsulation, sterilization)	• New applications for automation and industrial machinery
Reasons	• No space for factory • No time to deliver • Impossible logistics	• The process is the product (education) • Impossible sub-contracting (laboratory)
Where	• Urban factory • Space • Oceans and air • Researchers' special conditions • Battlefield • The third world	• Prototyping, e.g., in an office (designing, engineering, or architecture) • Education (At school or Fablabs) • Laboratory automation • Processes inside of industrial and laboratory equipment • Craft shops • At home (consumers, communities)

FIGURE 7

Motivation scenario: on the spot manufacturing.

Micro-factories could be used for fabrication of customized medical implants [62]; dental applications [4,47]; drug fabrication, dosage, and encapsulation; as well as sterilization. Battlefield, trouble spots, and the third world are examples of situations or locations where logistics can be problematic [2]. "On the spot manufacturing" concept allows, on one hand, producing the product in the place of use instead of ordering. On the other hand, it provides a solution for situations in which ordering is not an option, such as in education or prototyping.

SUMMARY AND CONCLUSIONS

This chapter gave a thorough introduction to micro-factories, which were defined as miniaturized production systems suitable for fabricating small products with

micro- and/or macro-sized features. Several different academic and commercial micro-factory equipment and systems were reviewed and one specific micro-factory concept, TUT-micro-factory, was introduced in detail. The advantages of miniaturized production systems compared to traditional larger scale factories were highlighted based on their sustainability from three perspectives, namely ecological, economic, and social. As a conclusion, it can be said, that micro-factory solutions can bring remarkable improvements to the manufacturing sustainability from all these three perspectives. The primary benefits are smaller investment and operating costs, as well as smaller energy and raw material consumption compared to conventional factories. The small-size micro-factories can be flexibly located to the most convenient locations, and modular concepts allow easy adaptivity and reconfigurability to different demands.

This chapter discussed also the potential application areas of micro-factories. The literature speculates with a broad range of different applications and associated advantages. As micro- and desktop factories are not suitable for high volume production, especially the "on the spot" manufacturing of customized products, such as medical implants, and nonmanufacturing applications, like educational and laboratory use, as well as prototyping, are considered promising.

REFERENCES

[1] Okazaki Y, Mishima N, Ashida K. Microfactory - concept, history, and developments. J. Manuf. Syst. Eng. 2004;126(4):837−44.

[2] Tuokko R, Heikkilä R, Järvenpää E, Nurmi A, Prusi T, Siltala N, et al. Micro and desktop factory roadmap. Tampere, Finland: Tampere University of Technology. Department of Production Engineering; 2012, ISBN 978-952-15-2984-9. Available at: http://URN.fi/URN.

[3] Heikkilä R, Järvenpää E, Tuokko R. Advances in the TUT microfactory concept development. Int. J. Autom. Technol. 2010;4(2):117−26.

[4] Okazaki Y. Microfactories - a new methodology for sustainable manufacturing. Int. J. Autom. Technol. 2010;4(2):82−7.

[5] Kawahara N, Suto T, Hirano T, Ishikawa Y, Kitahara T, Ooyama N, et al. Microfactories; new applications of micromachine technology to the manufacture of small products. Microsyst. Technol. 1997;3(2):37−41.

[6] Okazaki Y. Development of a desk-top milling machine with a 300 krpm spindle and a linear motor stage. In: IWMF 2004, 4th international workshop on microfactories, Shanghai, China, October 15−17; 2004. p. 29−33.

[7] Escribano Gimeno L. An Overview of microfactory concept and Analysis of fit principal advantages [MSc thesis]. Tampere University of Technology; 2010. 107 p.

[8] Järvenpää E, Heikkilä R, Tuokko R. TUT-microfactory − a small-size, modular and sustainable production system. In: Seliger G, editor. Proceedings of the 11th global conference on sustainable manufacturing (GCSM), 23rd − 25th September 2013, Berlin, Germany, ISBN 978-3-7983-2608-8. p. 81−6.

[9] Koelemeijer Chollet S, Benmayor L, Uehlinger J-M, Jacot J. Cost effective microsystem assembly automation. In: 7th international conference on emerging technologies and factory automation; 1999. p. 359−66.

[10] Koelemeijer Chollet S, Bourgeois F, Benmayor L, Moll B, Wulliens C, Jacot J. A flexible microassembly cell for small and medium sized batches. In: International symposium on robotics; October 7−11, 2002 [Stockholm, Sweden].
[11] Tuokko R. Desktop factories − actual knowledge status and experiences from far East. In: Manufuture 2011 conference, October 24, 2011; 2011.
[12] Kitahara T, Ashida K, Tanaka M, Ishikawa Y, Oyama N, Nakazawa Y. Microfactory and microlathe. In: International workshop on microfactories; 1998. p. 1−8.
[13] Kurita T, Watanabe S, Hattori M. Development of hybrid micro machine tool. In: 2nd international symposium on environmentally conscious design and inverse manufacturing; 2001. p. 797−802.
[14] Okazaki Y, Kitahara T. NC microlathe to machine micro-parts. In: Proc. 2000 ASPE annual meeting; 2000. p. 575−8.
[15] Okazaki Y, Mori T, Morita N. Desk-top NC milling machine with 200 krpm spindle. In: ASPE 16th annual meeting, 10−15.11.2001, Crystal city, Virginia, USA; 2001. p. 192−5.
[16] Ruiz-Huerta L, Caballero-Ruiz A, Ascanio G, Baidyk T, Kussul E. In the way to the second generation of microequipment. In: IWMF 2004, 4th international workshop on microfactories, October 15−17; 2004. p. 86−91.
[17] Bär M. Modulare Montagemaschine − Tischfabrik. In: Bär M, editor. μFEMOS - Mikro-Fertigungstechniken für hybride mikrooptische Sensoren; 2006. Available at: http://www.ubka.uni-karlsruhe.de/shop/download/1000003769 [assessed 10.12.11].
[18] Uusitalo JJ, Viinikainen H, Heikkilä R. Mini assembly cell for the assembly of mini-sized planetary gearheads. Assem. Autom. 2004;24(1):94−101.
[19] Kunt ED, Naskali AT, Cakir K, Sabanovic A. A versatile and reconfigurable microassembly workstation. In: 6th IWMF; 2008. p. 37−41.
[20] Clévy C, Hubert A, Chaillet N. Flexible micro-assembly system equipped with an automated tool changer. J Micro - Nano Mechatronics 2008;4(1):59−72.
[21] Ataka T. The experimental microfactory system in japanese national R&D project. 1999 [Shizuoka, Japan].
[22] Tanaka M. Development of desktop machining microfactory. RIKEN Rev. 2001;34: 46−9. Available at: http://www.riken.go.jp/lab-www/library/publication/review/pdf/No_34/34_046.pdf [accessed 10.12.11].
[23] Tuokko R, Lastra J, Kallio P. TOMI - a finnish joint project towards mini and micro assembly factories. In: 2nd international workshop on microfactories, Fribourg, Switzerland, October 9−10, 2000; 2000. p. 183−6.
[24] Tuokko R. Towards mini and micro assembly factories. In: Proceeding of international symposium on robotics, October 7−11, 2002, Stockholm, Sweden; 2002. p. 623−8.
[25] Honegger AE, Langstaff GQ, Phillip AG, VanRavensway TD, Kapoor SG, DeVor RE. Development of an automated microfactory: Part 1: microfactory architecture and subsystems development. Trans. NAMRI/SME 01.05.2006;34:333−40.
[26] Honegger AE, Langstaff GQ, Phillip AG, VanRavensway TD, Kapoor SG, DeVor RE. Development of an automated microfactory: Part 2: experimentation and analysis. Trans. NAMRI/SME 01.05.2006;34:341−9.
[27] Park J-K, Lee N-K, Lee DW, Song J-Y. Development of microfactory systems for the next generation - 3rd year report. In: 3th international workshop on microfactory technology; 2007. p. 5−12.
[28] Rizzi AA, Gowdy J, Hollis RL. Distributed coordination in modular precision assembly systems. Int. J. Robotics Res. 2001;20(10):819−38.

[29] Gaugel T, Dobler H. Advanced modular microproduction system (AMMS). In: SPIE, 29−30 October 2001. Newton, USA; 2001. p. 278−85.
[30] Lastra, JLM. Reference mechatronic architecture for actor-based assembly systems [Doctoral thesis]. Tampere University of Technology, Institute of Production Engineering; 2004. p. 140.
[31] Verettas I, Clavel R, Codourey A. "Pocket factory": concept of miniaturized modular cleanrooms. In: 1st topical meeting of desktop MEMS and nanofactories (TMMF2005), Tsukuba, JP, October 17−19, 2005; 2005.
[32] Heikkilä R, Karjalainen I, Uusitalo J, Vuola A, Tuokko R. Possibilities of a microfactory in the assembly of small parts and products - first results of the M4-project. ISAM; 2007. pp. 166−171.
[33] Ashida K, Nakano S, Park J, Akedo J. On-demand MEMS device production system by module-based microfactory. Int. J. Autom. Technol. 2010;4(2):110−6.
[34] Nakano S, Ashida K, Akedo J. On demand manufacturing system - a solution of ecological MEMS factory. In: 6th international workshop on micro- factories IWMF 2008, October 5−7 2008. Evanston, Illinois, USA. Northwestern University, USA; 2008. p. 73−6.
[35] Kobel P, Clavel R. Circular concept of a miniaturized assembly line with an integrated clean room. In: 7th international workshop of micro-factories. IWMF; 2010. p. 25−9.
[36] VTT. Research project desktop assembly. Technical Research Centre of Finland; 2010. Available at: http://www.vtt.fi/files/research/ism/manufacturingsystems/desktop_assembly_poster2.pdf [accessed 12.12.11].
[37] Hofmann A, Hummel B, Firat O, Bretthauer G, Bär M, Meyer M. Microflex - a new concept to address the needs for adaptable meso and micro assembly lines. ISAM; 2011. 5 p.
[38] Iijima D, Ito S, Hayashi A, Aoyama H, Yamanaka M. Micro turning system: a super small CNC precision lathe for microfactories. In: 3rd IWMF; 2002. p. 37−40.
[39] Nano Co. Nanowave products. Available in: http://www.nanowave.co.jp/proeng/products/index_e.html [accessed 10.10.13].
[40] Sangyo T. Takashima Sangyo Co., Ltd. Available at: http://www.takashima.co.jp/en/index_e.html; 2011 [accessed 10.12.11].
[41] DTF. "DTF" technological foundation of nagano prefecture. Suwa Techno Lakeside Regional Center; 2011. Available at: http://www.dtf.ne.jp/en/ [accessed 10.11.11].
[42] Lin W, Ohmori H, Uehara Y, Asami M, Ohmori M. Development and characteristic on the desk-top 4-axes machine "TRIDER-X" for micro-fabrication. In: 4th IWMF; 2004. p. 74−9.
[43] Atometric Inc. G4-ULTRA CNC MicroMachining centers. 2008. Available at: http://www.atometric.com/index-1.html [accessed 10.12.11].
[44] Microlution Inc. The microlution solution − the 363-S 3axis, CNC horizontal micro milling machine. 2007. Available at: http://microlution-inc.com/products/363.php [accessed 10.12.11].
[45] SmalTech. Manufacturing advanced micro machining equipment. Available in: http://www.smaltec.com/index.cfm, [accessed 10.10.13].
[46] Enomoto K. Desktop micro CNC milling machine CVN-2000. 2009. Available at: http://tubasa-kikai.co.jp/wordpress/wp-content/uploads/2011/07/8ea3339b5231ad4fe0263c2c30a1f754.pdf [accessed 12.10.11].
[47] Vhf camfacture. Impression line. 2010. Available at: http://www.vhf.eu/en/machines/BasicSystems/ImpressionLine [accessed 10.12.11].

[48] Wegera. Compact CNC module variations: KOLIBRI CNC system basic data. 2011. Available at: http://www.wegera.com/images/kolibri_englanti.pdf [accessed 10.12.11].
[49] Dynex Technologies. Products. Available in http://www.dynextechnologies.com/#, [accessed 10.10.13].
[50] BPC BioSed. Home. Available in: http://www.bpcbiosed.it/, [accessed 10.10.13].
[51] Murray Medical. Nanomolding. 2011. Available at: http://www.medicalmurray.com/Development/Nanomolding.aspx [accessed 10.12.11].
[52] Asyril. Products. Available in: http://www.asyril.ch/en/products.html, [accessed 21.10.13].
[53] JOT Automation. Products and solutions. Available in: http://www.jotautomation.com/en/products-solutions.html, [accessed 22.10.13].
[54] Biohit. Biohit RobolineTM - your automate. 2011. Available at: http://www.biohit.com/resource/files/media/brochures/liquid-handling/all/roboline-brochure-490100en-screen.pdf [accessed 10.12.11].
[55] Tuneda H. Sankyo's steps toward realization of desktop factory. In: International forum on desktop factory, international forum on DesktopFactory in SUWA (DTF2005); 2005. p. 119−26.
[56] Douglas S. Products of Douglas scientific. 2011. http://www.douglasscientific.com/Products/ [accessed 10.1.12].
[57] Klemd O. Desktop factory − new approaches for lean micro assembly. In: International symposium on assembly and manufacturing, ISAM 2007, Ann Arbor, Michigan, USA; 2007. p. 161−5.
[58] Festo. Partner for laboratory automation with pneumatics and electrics. Flyer; 2011. Available in: http://www.festo.com/net/SupportPortal/Files/142210/MedLab_KompFlyer_en_V08.pdf [accessed 10.1.12].
[59] MAG. MAG Lean: solutions for industry. 2010. Available at: http://www.mag.fi/products_and_services/electronics/mag_lean [accessed 10.12.11].
[60] GIN, Global Innovation Network. Home. Available in http://www.go-gin.com/, [accessed 21.10.13].
[61] Gaugel T, Bengel M, Malthan D. Building a mini-assembly system from a technology construction kit. Assem. Autom. 2004;24(1):43−8.
[62] Heikkilä R, Uusitalo J, Heikkilä R, Tuokko R. A microfactory concept for laser-assisted manufacturing of personalized implants. IWMF; 2008. pp. 77−80.
[63] Siltala N, Prusi T, Vuola A, Heikkilä R, Tuokko R. Modular microfactory system for gas sensor assembly. ISAM; 2011.
[64] Tuokko R, Järvenpää E, Heikkilä R, Nurmi A. Micro and desktop factories for micro/meso-scale manufacturing applications and future visions. Appl. Mech. Mater. 2013; 289:1−12. ISSN:978-3-03785-628-4.
[65] Järvenpää E, Heikkilä R, Tuokko R. Factory level logistics and control aspects for flexible and reactive microfactory concept. In: Lee S, Suarez R, Choi B-W, editors. Frontiers of assembly and manufacturing: selected papers from Isam'09'. Springer-Verlag; 2010, ISBN 978-3-642-14115-7. p. 127−40.

This page intentionally left blank

CHAPTER

Micro-mechanical Assembly

24

Hans Nørgaard Hansen[1], **Mogens Arentoft**[2], **Guido Tosello**[1]

Department of Mechanical Engineering, Technical University of Denmark, Kgs. Lyngby, Denmark[1]*; IPU Technology Development, Kgs. Lyngby, Denmark*[2]

CHAPTER OUTLINE

INTRODUCTION

This chapter gives an introduction to micro-mechanical assembly and proposes a classification and characterization of micro-mechanical assembly methods. Micro-mechanical assembly is defined as assembly methods on micro-scale, where the relative position of components is retained by exchange of contact forces provided by mechanical constraints. Based on this definition, the current chapter will not deal with solid bonding, welding, gluing, etc.

In view of the high quality and accuracy requirements on the mechanical assembly of miniaturized products in the precision mechanical engineering industry, manual methods still prevail. Manual micro-assembly procedures are extremely demanding on the human operators performing them, time consuming, costly, and frequently they give rise to quality problems in terms of uniformity. Automatic procedures with a low level of flexibility have been adopted only where high product volumes occur [1–3]. Hence, highly automated systems for micro-assembly are not suitable for medium/small production batches for not respecting the minimum cost of manufacturing principle. These problems are rendered more severe by the

Micromanufacturing Engineering and Technology. http://dx.doi.org/10.1016/B978-0-323-31149-6.00024-4

trend toward further miniaturization of mechanical components and by the increasing variety of products and models.

Forms of flexibility have been developed in classical macro-scale assembly technology, which can also be adopted in principle when assembling micro-components. Assembly systems can be adjusted to various models by means of a modular product design which uses easily interchangeable product-specific system components. Furthermore, hybrid micro-systems to be assembled should be constructed on a modular principle, dependent on the particular application, by using standard components [1,3].

The actual mechanical assembly function can be divided into the following constituent functions:

- Handling and positioning.
- It has the function for putting two or more objects into a particular mutual position and orientation. Handling comprises processes of selection and preparation of components for composing or checking and transportation to the following production, assembly, or packaging systems.
- Mechanical assembly.
- It has the function of ensuring the mutual relationship between components against outside effects. By mechanical assembly, connections between the components can be created by means of mechanical constraints. The assembly process can be achieved by means of shape, material, force, etc.
- Quality control.
- It has the function of ascertaining whether the mechanical assembly process has been carried out as specified. Checking represents those processes by which the component's presence and position are checked in addition to the quality of the finished product.

Assembly becomes particularly challenging when dealing with micro-products. A first approach may be to miniaturize macro-scale solutions by simple downscaling of dimensions. This approach reaches a limit with respect to obtainable tolerances in manufacturing processes and handling solutions. Another natural approach is then to try to reduce as much as possible the mechanical manipulation of micro-components, through a higher level of integration as compared to that of conventional size products. This involves a high degree of integration with the design phase when the product development is still in the early stage as well as the materials choice, which determines obviously the process choice itself [1].

Finally it should be considered that the assembly of two or more components may result in a subassembly which will then be subject to further processing or assembly (Figure 1).

Mechanical assembly of micro-components presents quite a few challenges because of the reduced dimensions, which include [3]:

- In the micro-world, submicron precision is often required, comparable to wafer stepper precision. This degree of precision is beyond the calibration range of conventional open-loop precision assembly devices used in mechanical

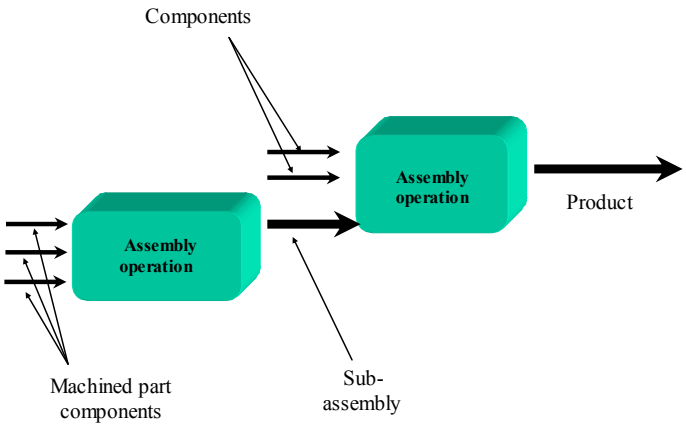

FIGURE 1

Levels of micro-assembly.

industry. Closed-loop strategies are required to compensate for poor kinematic models and thermal effects: real-time vision feedback is perfectly suited for this application.

- In the micro-world, forces other than gravity dominate due to scaling effects. Surface-related forces, such as electrostatic, van der Waals, and surface tension forces, become dominant over gravitational forces.
- Manual handling of micro-parts shows the problem of the loss of direct hand−eye coordination. It implies a series of interconnected problems: because of the dimensions in the micro-range, microscopes for vision and micro-grippers for manipulation are suitable to be used. In order to achieve a good resolution, high magnification is used, but then problems related to restriction of field of view (smaller than the object), very short depth of focus (an unclear image), and short working distance arise. Magnification could be reduced, but then issues of trade-off between field of view and resolution emerge. Furthermore, micro-grippers have less degree of freedom than the human hand and lack of force feedback.
- Manual handling is time consuming because slow and operating with one or few objects at a time, which implies high production costs.

CLASSIFICATION OF MICRO-MECHANICAL ASSEMBLY METHODS

Micro-mechanical assembly methods can be classified according to the mechanical constraint and the way the material is processed in order to achieve this constraint (Table 1). The mechanical constraint is divided into two categories: possibility for disassembly or no possibility for disassembly. The material conditioning characteristics: no deformation, elastic deformation, plastic deformation, flow, and

Table 1 Overview of Mechanical Assembly Methods at the Micro-scale

	Characteristic		Material Constraint			
	No Disassembly	**Disassembly Possible**	**No Deformation**	**Elastic Deformation**	**Plastic Deformation**	**Flow and Solidification**
Snap fit	X			X		
Screw		X		(X)	X	
Velcro	X			X		
Joinery		X	X			
Injection molding	X					X
Riveting, folding, clinching	X	X			X	

solidification. The micro-mechanical assembly methods listed in the table are those typically found in the literature when searching for micro-assembly. This implies that methods and technologies may exist which are not mentioned in this chapter. However, it is believed that the most relevant technologies are mentioned in Table 1. A more specific description of the single technologies will be given in the following sections.

MICRO-SNAP FITS

Micro-snap fit is a mechanical joining method, based on the elastic deflection of joint features on one micro-part that are inserted into a mating feature on another micro-part, to obtain an elastic interference.

Complicated micro-structures consisting of multiple components can be assembled together using snap fasteners. They also have great potential when being lifted out of plane and used as vertical plug-in connectors.

A snap fastener consists of a mating pair of an anchor and flexible latches. As an example, it may have two outer latches and a central anchor. The latches are supported on flexible beams. In its disengaged state, the anchor and the latches can move freely with respect to each other.

In this type of assembly, only a linear movement is required to engage the components. The relative positioning accuracy required depends on the absolute dimensions, but is relatively large due to the self-aligning nature of the joint. The design can be modified in such a way that the required force for engagement is small. See Refs [4–8] for examples of micro-snap fits.

MICRO-SCREWING

Screws are components with a thread (a uniform cross section following a spiral or helical path) either on the inside or outside surface. Threads may be right-handed or left-handed. The screw may be cylindrical or tapered. Cylindrical screws need a counterpart geometry, whereas tapered screws usually create the geometry in the counterpart. Assembly operations involving screws require a combined translational and rotational movement. Furthermore, a certain alignment accuracy of the screw with respect to the counterpart is required. The level of this accuracy depends on screw dimensions and tolerances.

Very few literature exists on micro-screwing although it is extensively used, for example, in the watch industry. ISO standard geometries are not necessarily scaled down to micro-scale (metric screws according to ISO 68-1) in these applications (Figure 2). Micro-screws are used in medical devices (e.g., hearing aids) as one of the simplest fastening components. In some of the products, the screw has another functionality, namely creating an electrical connection.

MICRO-VELCRO

Micro-velcro is a micro-mechanical fastening system, based on silicon micro-machining technology, which results in a strong, permanent bond without chemical

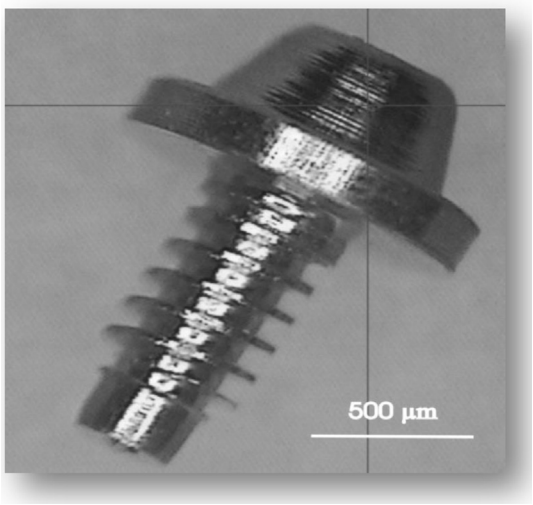

FIGURE 2

Example of micro-screw with non-ISO dimensions and geometry [9].

adhesives. The working principle is based on arrays of micro-mechanical mating structures, which act as mechanical adhesives.

The joining principle of micro-velcro is based on the matching of silicon wafers with high-density micro-structured surface, with an areal density of approximately 200.000 units/cm^2. The micro-structures on two identical surfaces will self-align and interlock with each other under application of adequate external pressure. A tensile strength per unit interlocked area of the order of 0.2 MPa has been achieved [10].

The principle of bonding is a button snap, or a zipper, but in a two-dimensional configuration. The bonding principle is depicted by the schematic cross section in Figure 3. Under application of adequate external pressure, the tabs of the structures deform and spring back, resulting in an interlocking of the two surfaces. In this way, a permanent bond is achieved. Other examples are reported in Refs [11,12].

MICRO-JOINERY

Micro-joinery is the fabrication and assembly of micro-joints to realize three-dimensional (3D) micro-structures. Each micro-joint contains two or more mating surfaces which join the various parts together as a single unit. This technique involves primarily silicon but virtually any single crystalline material of virtually any crystalline orientation (GaAs, Ge, quartz, metals, etc.) is suitable to be used [13]. In macro-scale mechanical assembly, this technique is well known. It is therefore also applicable for metallic, ceramic, or polymer micro-components providing that adequate processing technologies exist and can be applied. A critical point is, of course, the tolerances of the parts. On one hand, they should ensure mating, and on

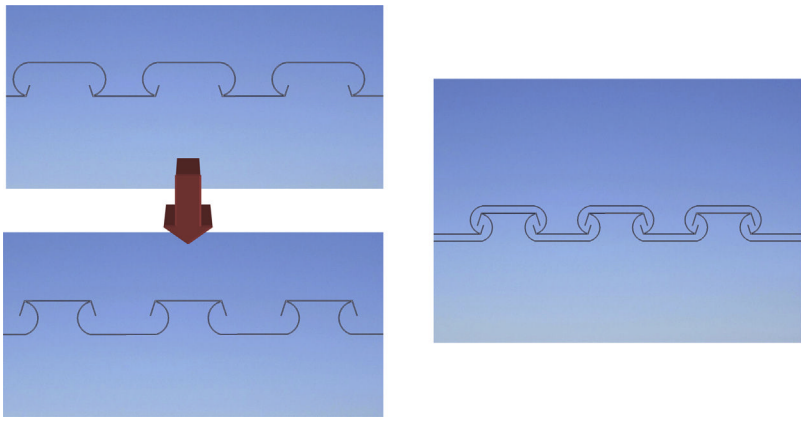

FIGURE 3

Principle of a micro-velcro assembly. Left: two initial parts. Right: assembled unit.

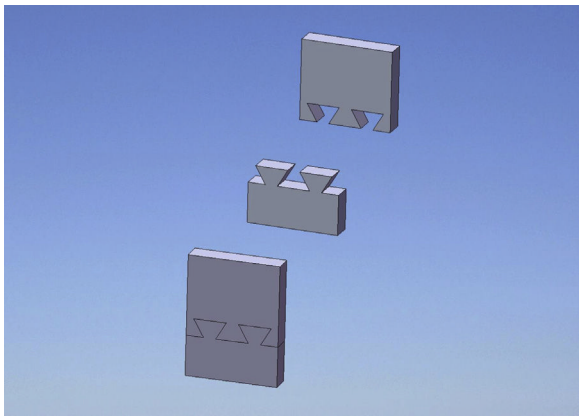

FIGURE 4

Dovetail assembly.

the other hand they should be as small as possible in order to secure the assembly. The surface area to volume ratio favors the strength of the joint on micro-scale but it also is a potential challenge in terms of actual assembly.

The dovetail micro-joint is a particular adaptation of the micro-joinery concept and it is commonly used in 3D (x, y, z) positioning devices requiring linear translation—see Figure 4 for an example.

The slot joint is similar in function to the dovetail micro-joint in that it also constrained translation, but method and geometry are slightly different. The slot joint has a rectangular-shaped cross section (Figure 5). A number of techniques are

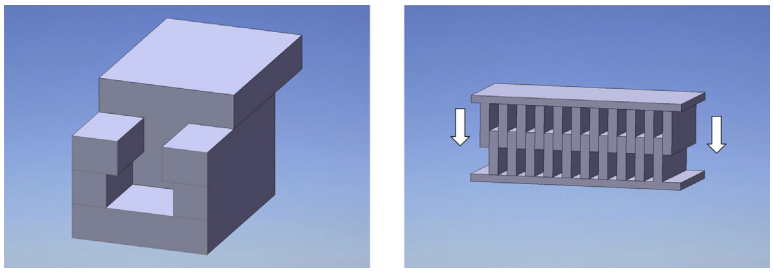

FIGURE 5

Slot joint (left) and finger joint (right).

suitable to be used for the fabrication of a slot joint: micro-milling, sawing, LIGA (German acronym for lithography-electroplating-molding), or anisotropic etching of silicon wafers. Finger joints are interlocking structures that feature a periodic assembly of mating fins as shown in Figure 5. Finger joints are used to attach two substrates rigidly together, paying attention to the fact that large mating surfaces of the finger impart considerable strength and stability to the joint.

MICRO-INJECTION MOLDING

Micro-injection molding is a manufacturing technique that can be used not only for the production of monolithic micro-structures but also for the assembly of hybrid structures. As components and functional structures become smaller, they cannot be regarded in terms of steps in a single process, but as an integrated production concept. A process called micro-assembly injection molding has been developed and combines the joining of hybrid elements with the generation of functional structures [14,15].

Micro-injection molding allows the production of movable micro-structures by using incompatible polymers, soft/hard combinations of materials, the generation of fluidic hollow structures by lost core technology, and the over molding of wires and optical system like optical fibers.

The differences of materials used, the temperature layout of the process, and the mechanical strain of inlay parts play a fundamental role. Most of all, the precision in positioning of inlay parts and the demolding of hybrid structures have a relevant importance. For these reasons, a mold technology with flexibility, precision, and special processing equipment is required. The mold is characterized by using a special system for positioning of inlay parts and complex sensor equipment for measuring pressure and temperature, which are relevant process parameters. Thus, a new mold concept has to consider the possibility of various thermal processes, such as heating the cavity before injection, cooling down again before demolding. It has to be characterized by acceptable cycle times and the possibility to evacuate the cavity. Figure 6 illustrates hybrid micro-structures produced by injection molding. Over

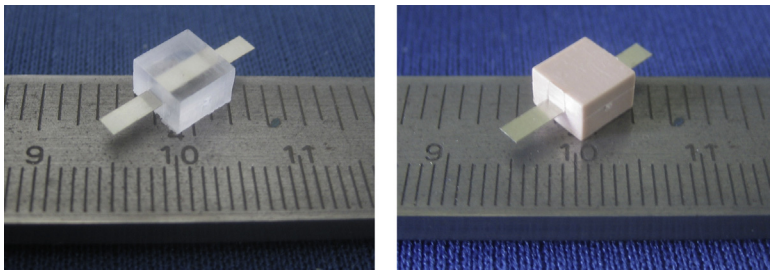

FIGURE 6

Hybrid (metal—polymer) structures manufactured by injection molding. Material: polystyrene (left) and PA66 + GF50% (right). Metal foil thickness up to 100 μm [16].

molding of other polymer parts is used in two-component micro-injection molding, for example, for the creation of molded interconnect devices [17].

MICRO-RIVETING, FOLDING, AND CLINCHING

Riveting, folding, and clinching are mechanical assembly processes based on plastic deformation of the materials involved. This excludes brittle materials from these particular processes although micro-electronics mechanical systems-based riveting has been reported [18]. In macroscopic assembly processes, these technologies are used in metal joining/assembly. They require the use of molds/dies and tools and are based upon sheet metal operations: Reference can be made to a relevant chapter for the basis of these technologies. Figure 7 illustrates a micro-rivet which was produced by a micro-cold forging operation.

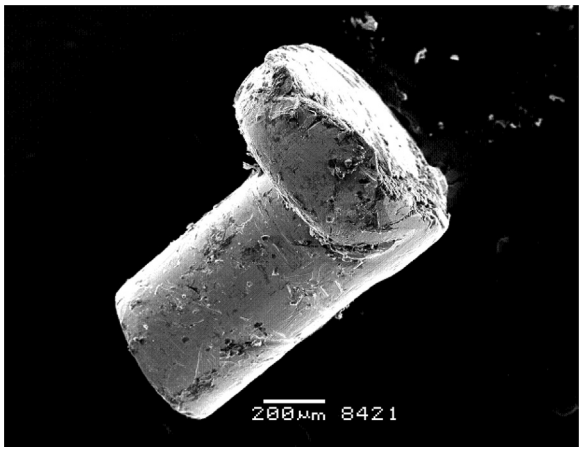

FIGURE 7

Micro-rivet in Ag.

SYSTEMATIC APPROACH TO MICRO-MECHANICAL HANDLING AND ASSEMBLY

The handling of the small parts has been studied for almost half a century and different micro-handling principles are summarized in Ref. [1]. A classification scheme for the quantified analysis of micro-gripping principles has been proposed in Ref. [3] and describes basic features of the gripping operation on micro-scale. Different handling classification schemes have been introduced in recent years. Different realizations of micro-grippers have been reported (their diversity is large) addressing different handling situations, materials, and dimensions.

However, when developing solutions for micro-mechanical handling and assembly, a systematic approach is beneficial. Figure 8 illustrates the contents of a proposed methodology. Object characteristics (material, weight, dimension, geometry) are considered as the basic information of the problem. Depending on what should be done with the objects (referred to as functionality) a choice of gripping principle and assembly method can be made. The description of the desired functionality is important due to the fact that the resulting feedback may also involve a redesign of the component to make it more suitable for the assembly operation.

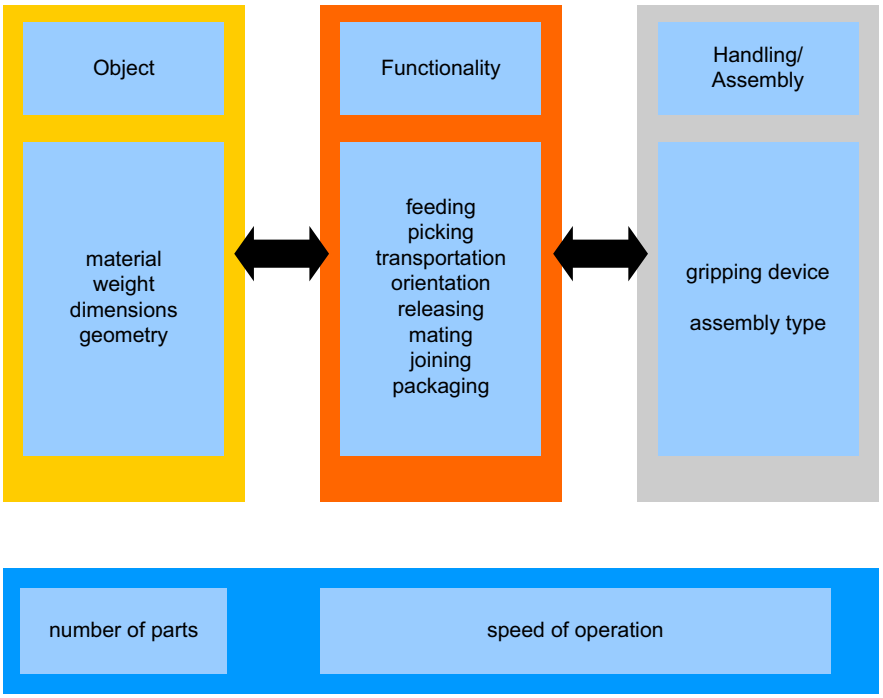

FIGURE 8

Systematic approach to micro-mechanical handling and assembly [9,19].

It is not the methodology to automatically result in an optimized overall handling and assembly process. However, by considering all the points in the methodology, a characterization of the entire situation is possible and an identification of the most important steps in the process is possible. The systematic consideration of what exactly is needed in terms of operations will hopefully result in gripper designs that are tailor-made. The next section will illustrate how the methodology has been applied.

APPLICATION EXAMPLE: MECHANICAL ASSEMBLY OF PUSH BUTTON PARTS

As an example of mechanical assembly, a hearing aids push button will be taken. The push button consists of seven different parts both geometrically and in respect of the material (see Figure 9). All parts have an axis-symmetrical geometry but different diameters and shapes. The screw is shown in detail in Figure 2. Different geometrical dimensions of the parts are up to 2 mm, but dimensions of the functional structures are less than 1 mm, what allows calling these parts micro-objects. Assembly of these parts is usually done by putting parts number 1−3 onto each other, then screwing a screw through part 3 to part 1. A lid with two wires is placed on the top of it and fastened by thermal heating and gluing, for sealing purposes: the lid and wires are not used in this example. Presently, these assembly operations are performed manually or on semiautomatic stations involving manual labor.

The requirements to the handling and assembly process can be summarized as follows:

- The assembly operations should be performed using a small standard industrial robot.
- The parts (all axisymmetrical) need to be aligned with respect to each other.
- The screwing process must be achieved by a combined rotational and translational movement using a certain torque. In this process, either the screw or its counterpart should be moving while the other is kept in a fixed position.

It was chosen to work with small pallets as carriers for the components because the industrial company already had good experience with this type of system. The parts were therefore placed in separate fixtures and then picked and placed during the assembly process. Two types of tools were needed for handling and assembly:

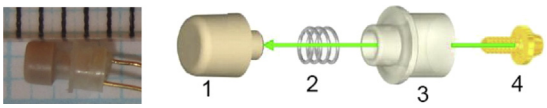

FIGURE 9

A picture of a push button. Schematic view of a push button parts: 1, knob; 2, spring; 3, holder; and 4, screw. Scale on left picture in millimeters.

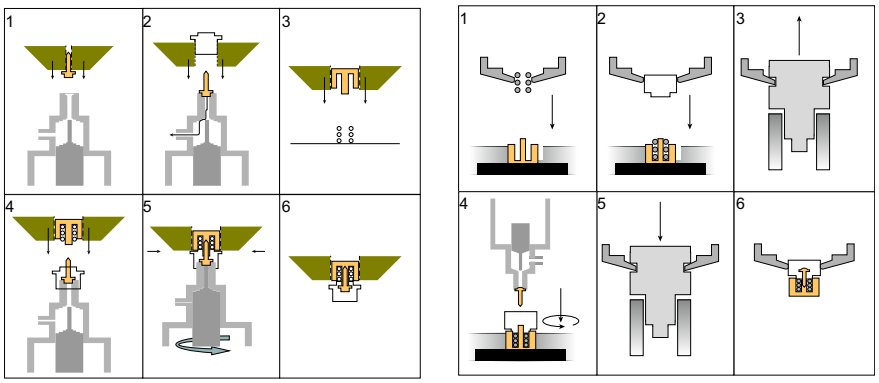

FIGURE 10

Assembly scenarios of push button [20–22].

one capable of executing a combined rotational/translational movement and one capable of picking and releasing axisymmetrical parts.

Two assembly scenarios were considered (Figure 10): In Figure 10(a) a screwdriver is fixed and the parts are manipulated one by one using a mechanical gripper. In the first step, the screw is fixed in the screwdriver by means of vacuum. Subsequently, the remaining parts are fitted over the screw one by one, and finally the screwing process is performed. In the second scenario (Figure 10(b)), three of the parts are picked and placed on top of each other by a mechanical gripper. Then a screwdriver is used to pick and screw the small screw into place and to perform the screwing operation [9].

The design of the mechanical gripper is a subject of high importance. On one hand, the gripper should match the shapes of the objects—preferably of all the objects—and on the other hand, a custom-made design for each part would ensure a better picking and releasing operation. As a compromise, a two-finger gripper design was investigated (see Figure 11). Various angles of the slots as well as surface textures were investigated in order to optimize the design. It was concluded that a flexible design with a V-groove would accommodate all the various diameters of the parts. Furthermore, the use of micro-structured surfaces facilitates the release of objects, especially in case of the plastic parts, which have weights 10 times smaller than that of the screw [23].

The detail-designed screwdriver (Figure 12) is composed of two different mechanisms. The first is an air suction-based mechanism (11 shows where it has to be connected) for picking up the screw (1) and holding it in the required position while transporting it. The vacuum system consists of a pump, tubes, and a manipulator (not shown in the figure). The second mechanism is a screwing mechanism that is composed of a screwdriver (2), a screwdriver shaft holder, bearings, a hexagonal key, a coupling, and a motor with a gearbox (9). The remaining parts are designed

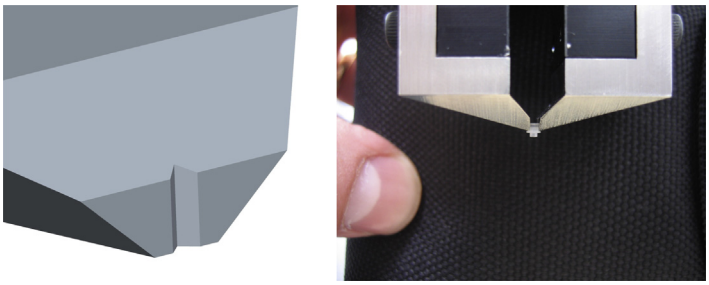

FIGURE 11

Mechanical gripper. V-groove design (left) and mounted on robot (right).

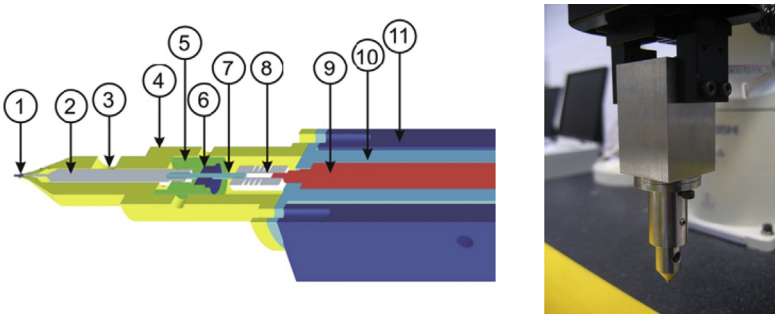

FIGURE 12

Detailed screwdriver design. 1, micro-screw; 2, shaft; 3, vacuum connection place; 4, corpus; 5, holder; 6, bearings; 7, shaft; 8, shaft coupling; 9, motor and gearings; 10, motor holder; and 11, corpus.

for supporting the screwdriver. The corpus consists of two parts: (4) and (11). The corpus has a chamber for air and air connection place (3). The motor is kept in the corpus, while fastened to a motor holder (10). The screwdriver shaft holder and the motor are kept in place by two screws. Four screws connect both parts of the corpus and the motor holder. The corpus is fastened by (11) holes on the sides, by which it is held by a robot hand [24].

With the use of the described gripping and screwing device, the relative limited accuracy of the robot was compensated for. The described assembly process was successfully tested in a laboratory environment and is currently considered for industrial implementation.

CONCLUSION

Mechanical micro-assembly methods are among the most highly relevant methods in micro-manufacturing. They allow the assembly of different materials, primarily

nonsilicon, and potentially they can incorporate possibilities for disassembly. The challenges related to micro-mechanical assembly include the almost total lack of guidelines (i.e., standards, best practice, etc.) and the need for tailor-made tools for the processes. This often is used as an argument against the automation of such processes.

REFERENCES

[1] Alting L, Kimura F, Hansen HN, Bissacco G. Micro engineering. Ann CIRP 2003; 52(2):1−23.
[2] Van Brussel H, Peirs J, Reynaerts D, Delchambre A, Reinhart G, Roth N, et al. Assembly of Microsystems. Ann CIRP 2000;49(2):451−72.
[3] Fantoni G, Santochi M, Dini G, Tracht K, Scholz-Reiter B, Fleischer J, et al. Grasping devices and methods in automated production processes. CIRP Ann 2014;63(2): 679−701.
[4] Prasad R, Bohringer K-F, MacDonald NC. Design, fabrication, and characterization of single crystal silicon latching snap fasteners for micro assembly. Proc 1995 ASME Int Mech Eng Congr Expo 1995;57(2):917−23.
[5] Dechev N, Cleghorn WL, Mills JK. Tether and joint design for microcomponents used in microassembly of 3D microstructures. Proc SPIE - Int Soc Opt Eng MEMS/MOEMS Compon Their Appl 2004;5344(1):134−46.
[6] Yeh R, Kruglick EJJ, Pister KSJ. Surface-micromachined components for articulated microrobots. J Microelectromech Syst 1996;5(1):10−7.
[7] Oh YS, Lee WH, Stephanou HE, Skidmore GD. Design, optimization, and experiments of compliant microgripper. In: Proceedings of 2003 ASME international mechanical engineering Congress, vol. 5; 2003. p. 345−50.
[8] Koester D, Cowen A, Mahadevan R, Stonefeld M, Hardy B. PolyMUMPs design handbook − a MUMPs® process. MEMSCAP; 2003. Revision 10.0.
[9] Gegeckaite A. Handling and assembly of microproducts [Ph.D. thesis]. Department of Mechanical Engineering, Technical University of Denmark; 2007, ISBN:978-87-89502-73-1.
[10] Han H, Weiss LE, Reed ML. Micromechanical velcro. J Microelectromech Syst 1992; 1(1):34−43.
[11] University of Limerick web site, Ireland, http://www.plato.ul.ie/academic/Vincent.Casey, January 2005.
[12] Han H, Weiss LE, Reed ML. Mating and piercing micromechanical structures for surface bonding applications. In: Proceedings of IEEE micro electro mechanical systems: an investigation of micro structures, sensors, actuators, machines and robots; 1991. p. 253−8.
[13] Collins SD, Gonzalez C, Smith RL, Howitt DG. MicroJoinery: concept, definition, and application to microsystems development. Sens Actuators - A: Phys 1998;66(1−3): 315−32.
[14] Michaeli W, Rogalla A, Ziegmann C. Micro assembly injection moulding of hybrid microsystems. J Polym Eng 2001;21(2):99−109.
[15] Michaeli W, Ziegmann C. Micro assembly injection moulding for the generation of hybrid microstructures. Microsyst Technol 2003;9(6):427−30.

[16] Tosello G. Precision moulding of polymer micro components [Ph.D. thesis]. Department of Mechanical Engineering, Technical University of Denmark; 2008. ISBN: 978-87-89502-77-9.
[17] Islam A. Two component micro injection moulding for moulded interconnect devices [Ph.D. thesis]. Department of Mechanical Engineering, Technical University of Denmark; 2008. ISBN:978-87-89502-75-5.
[18] Shivkumar B, Kim CJ. Microrivets for MEMS packaging: concept, fabrication, and strength testing. J Microelectromech Syst 1997;6(3):217−25.
[19] Gegeckaite A, Hansen HN. A methodology for characterization and categorization of solutions for micro handling. In: Proc. of the 5th international conference of euspen, Montpellier 2005; 2005. p. 397−400.
[20] Erikson T, Hansen HN, Gegeckaite A, Arentoft M. Automated assembly of micro mechanical parts in a microfactory setup. In: Proc. of the 5th international workshop on microfactories, Besancon, France, October 2006; 2006.
[21] Gegeckaite A, Hansen HN. Automation of 3D micro object handling process. In: 7th international conference of the European society for precision engineering and nanotechnology (Euspen), Bremen (Germany), 20−24 May 2007, vol. 2; 2007. p. 233−6.
[22] Hansen A, Langhans C, Ingham D, Dahl-Hansen HK, Olsen MH. Automated assembly of micro components, student report (in Danish). Department of Mechanical Engineering, Technical University of Denmark; 2008.
[23] Gegeckaite A, Hansen HN, De Chiffre L, Pocius P. Handling of micro objects: investigation of mechanical gripper functional surfaces. In: 7th international conference of the European society for precision engineering and nanotechnology (Euspen), Bremen (Germany), 20−24 May 2007, vol. 2; 2007. p. 185−8.
[24] Gegeckaite A, Hansen HN, Eriksson T. A screwing device for handling and assembly of micro screws. In: 7th international conference of the European society for precision engineering and nanotechnology (Euspen), Bremen (Germany), 20−24 May 2007, vol. 2; 2007. p. 481−4.

This page intentionally left blank

CHAPTER

Self-assembly of Micro-parts

25

Matthias Burgard

Fraunhofer Institute for Manufacturing Engineering and Automation IPA, Stuttgart, Germany

CHAPTER OUTLINE

INTRODUCTION

Micro-devices can be divided into monolithic and hybrid systems. The monolithic micro-devices are created on one single substrate and are built by one process after the other on this substrate. The processes are highly optimized for one substrate material. A typical example is the manufacturing of semiconductor devices. The processes are adapted, e.g., for silicon substrates. There are very strict design rules to fulfill the process requirements. High functional density can be achieved but only with a very limited functional variety. For complex devices, a combination of different components is mostly unavoidable—they are built up as hybrid devices. Hybrid devices are manufactured by combining various single components. This implicates the advantage to use optimized materials and processes for each function. The assembly of the subcomponents becomes an essential process step for the manufacturing of hybrid products.

Elementary processes for assembly are

- Singularization
- Arranging
- Storing
- Feeding
- Picking/grasping
- Transporting and positioning
- Placing
- Affixing

Micromanufacturing Engineering and Technology. http://dx.doi.org/10.1016/B978-0-323-31149-6.00025-6

They are relevant in micro-manufacturing to achieve a high quality of the product. The production with high throughput is achieved by automated assembly systems. Components for mass production are often manufactured in batch processes. Afterward they have to be separated from each other. Injection molded parts have to be separated by cutting and usually provided as bulk good. For a further processing, the single parts are arranged in a defined order in a tray. Specially designed trays can also be used for storage. The providing of the components for the core assembly process is called feeding. The components are provided on defined positions, where they can be picked up. The automated core assembly process is usually a pick-and-place system. Components are provided in a tray and picked with a gripper transported to the final position where they are placed. The affixing is dependent on the functionality of the component. Often an electrical connection is additionally needed.

Micro-components are commonly assembled and packaged using robotic pick-and-place. Modern pick-and-place machines have an adequate throughput for typical consumer electronics [1]. "However, pick-and-place is confronted with a trade-off between throughput and component placement accuracy. Moreover, this method is serial, it requires closed-loop control and it becomes more expensive as device dimensions shrink to smaller scales and registration constraints become more stringent. Also, stiction problems become inevitable for device sizes smaller than 300 μm" [2], pp. 1–2.

The assembly of micro-parts implies specific challenges due to the small dimensions:

- Position accuracy
- Interfering forces (e.g., adhesion, electrostatic)
- Sensitivity of parts

In Ref. [3], a classification of the micro-assembly approaches is presented with two major categories: deterministic and stochastic (Figure 1). The conventional processes are all classified as deterministic processes and in contrast the self-assembly process as statistic. He stated that self-assembly is using usually a stochastic approach. But in recent publications [4–6], self-assembly is described as a supporting process for pick-and-place systems and can be seen as a deterministic and parallel process.

"Self-assembly is the autonomous organization of components into patterns or structures without human intervention" [7], p. 2418. But Kosar et al. [8] raised the legitimate question "if we strictly follow this definition, is anything not self-assembly, including the origins of life? From replication of DNA in the molecular scale to the formation of galaxies in the astronomical scale, all the structures and motifs in nature form without human intervention." Whitesides [9], p. 146 stated that "it is easiest to define by what it is not. A self-assembling process is one in which humans are not actively involved, in which atoms, molecules, aggregates of molecules and components arrange themselves into ordered, functioning entities without human intervention." And he continues: "People may design the process,

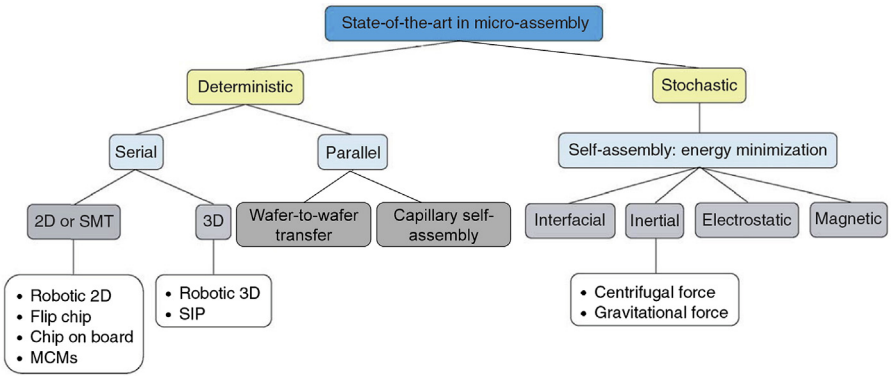

FIGURE 1

Categories of state-of-the-art micro-assembly techniques. MCM, multichip module; SIP, system in package [3], p. 405. Added capillary self-assembly.

and they may launch it, but once under way it proceeds according to its own internal plan, either toward an energetically stable form or toward some system whose form and function are encoded in its parts." It was inspired by nature. But focusing in this chapter on the assembly of micro-parts we will restrict "self-assembly as a manufacturing strategy for creating useful entities such as patterns, structures, components, and devices" [8], p. 1.

Self-assembly techniques are mainly based on energy minimization, what implies a lot of advantages especially for the assembly of micro-parts [3]. They are using the forces, which are in general detrimental, in a controlled way to sort, arrange, or position small components. This ensures an easy handling of mirco-parts, a parallel and fast assembly, and a positioning with high accuracy.

Self-assembly can be applied to a wide size range, from millimeter to nanometer scales. It may avoid direct contact manipulation of components, thus overcoming the stiction issue. It can achieve yield and throughput comparable to those of pick-and-place techniques [2], p. 2.

There are recent publications summarizing the achievements in the field of self-assembly for the manipulation of micro-parts [2,3,10]. But assembly methods that rely on fluidic forces and fluidic mediums show particular promise at the micro-scale [10]. This chapter gives an overview of the current state of art of the self-assembly of micro-parts using surface tensions.

THEORY/PRINCIPLE

In general, a substrate is patterned with an array of energy traps. On an assembly substrate, agitated components are attracted to these energy traps and then permanently attached [3]. Using capillary forces is most interesting for the self-assembly of micro-parts as the surface tension force scales linearly with the length,

but the gravity quadratic. This means that the gravity force loses influence but the surface tension gains influence when the parts are getting smaller. Magnitudes of capillary forces are adequate enough for manipulating micro-components [10].

Fluidic self-assembly methods can be classified in two major groups. In the first group, fluids are used as environment in which the assembly is carried out [1,11,12]. In the second group, capillary forces and surface tensions are used for positioning or transporting of parts [1,4,23]. But also a combination, using fluid as environment and surface tension for capturing and positioning of the parts has been presented [13].

In Ref. [14], the principle and the dynamic behavior of the self-alignment of components using functionalized surfaces and the surface tension of fluids are described and characterized. Macroscopic foils of 18×18 m^2 are used but the principle and the conclusions can be transferred to micro-components. The foils are handled with a vacuum gripper and onto the binding site, the 125-µm-thick water layer is dispensed. The foils are prealigned with defined offsets and released onto the water layer, where the self-alignment positioned the foils according to the functionalized pattern on the substrate (Figure 2).

In contrast, for smaller droplets and micro-parts with 500×500 µm^2 size Boufercha et al. [15] simulated the duration from the deposition of the part onto the droplet to the final position. Within less than 1 ms the part is at its final position Figure 3(a). Figure 3(b) shows the relation between the time needed for the horizontal adjustment and the starting deviation from the final position.

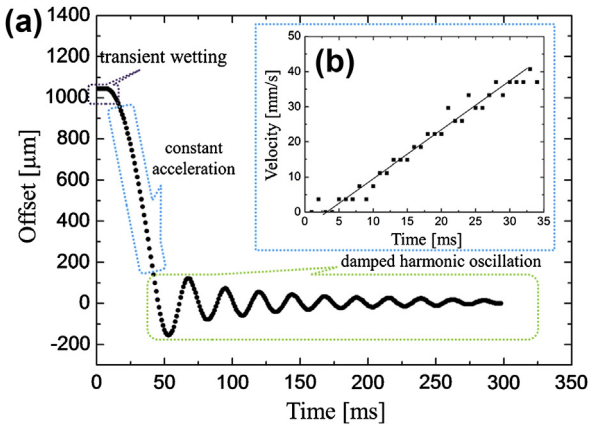

FIGURE 2

(a) Typical self-alignment trajectory of a foil die (0.80 mg/mm^2). Data extracted from high-speed video recording starting upon die contact with water. The three regimes (transient wetting, constant acceleration, and damped oscillation) are evidenced. (b) Numerical derivative of the parabolic regime depicted in (a) showing the linear progression of velocity in time [14].

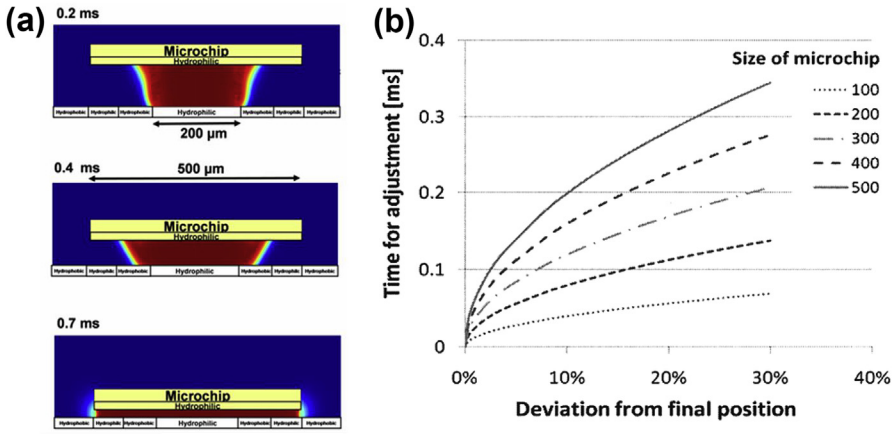

FIGURE 3

(a) Simulation of the self-alignment capability of a micro-chip; (b) Alignment of the micro-chip [15].

PROCESSES

Surface tension driven self-assembly can be used for a wide range of processes within the assembly procedure: (1) singularization and arranging of parts, (2) gripping of parts, and (3) positioning of parts. Examples for (1) and (3) will be highlighted and their functionality explained.

SINGULARIZATION AND ARRANGEMENT OF MICRO-PARTS

Common vibratory conveyor technology reaches its limits for micro-parts due to its impact to the components and the occurring surface effects. Therefore, specialized equipment with grippers is used for palletizing of the micro-parts. The separation and the arranging into a tray of the micro-parts for further assembly are getting more time-consuming and less cost efficient. As already described above, there are a lot of investigations and publications regarding the positioning of micro-parts using surface tension. In contrast, the feeding of the micro-components is still a conventional process with all its disadvantages for the handling of the small parts.

In Ref. [16], the singularization of micro-parts using surface tension is described. It can be used for components with feeding size of 1 mm and smaller. The parts can be provided as bulk good. A selection of possible components (coated O-rings, gears, lenses, spheres, LEDs, screws, springs, stamped parts) is presented in Figure 4.

The fluidic sorting is based on the phenomenon to be found in nature that water striders can stay and glide on the water surface due to the surface tension. If small components are applied on a surface of a fluid, it shows the same behavior.

FIGURE 4

Selection of miniaturized components tested with fluidic sorting.

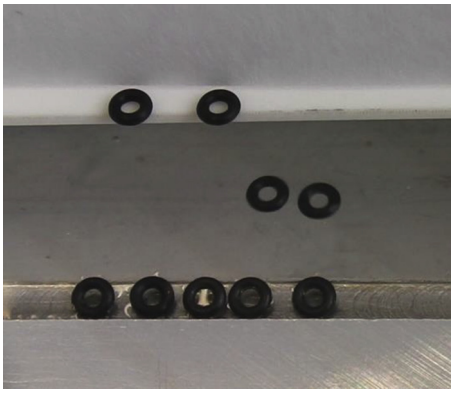

FIGURE 5

Sliding o-rings on a convex fluidic surface [16].

In addition, the friction is minimized and therefore the components can be moved easily on the surface for instance due to the gravity. Fluids can be easily shaped to concave or convex surfaces on which the components can slide to a lower level, e.g., to the fluid rim or a present barrier (Figure 5).

For the fluidic sorting process, a curved liquid surface is required (Figure 6). Therefore a reservoir is filled with fluid. After the reservoir is filled, it is possible to continue with supplying and the surface is bent. In doing so, a convex surface

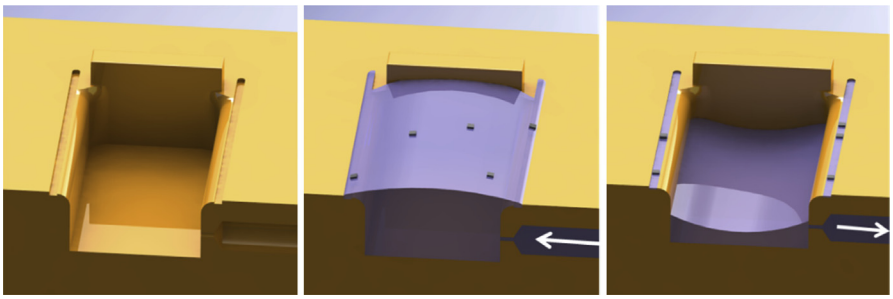

FIGURE 6

Principle of the fluidic sorting process [16].

is realized and the surface curvature can be controlled with the volume. The applied components can move due to surface tension and gravity to the rim of the fluid, where they concentrate. Possible agglomerations are resolved by applying vibration. The components are arranging themselves along the border. When extracting the fluid, a barrier at the rim prevents the components of returning into the reservoir. The components are staying arranged and can be delivered to the next assembly process (Figure 7).

A setup has been presented in Ref. [16]. Further developments have been carried out and the first prototype is now available. It consists of following components:

1. feeding device,
2. reservoir,
3. removable tray,

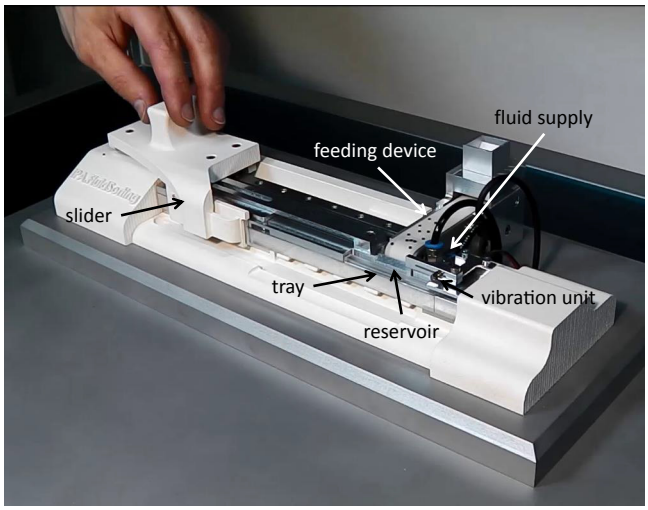

FIGURE 7

Prototype of fluidic sorting system with visible slider, feeding device, and reservoir.

4. slider for stable surface generation,
5. vibration unit, and
6. fluid supply.

The procedure is described below (Figure 8):

1. The slider is moved toward the reservoir and closes the reservoir,
2. Filling the reservoir with fluid,
3. By moving the slider back, the excessive fluid is pouring out,
4. The components are placed on the fluid by conveyor belt and are self-arranging on the border,
5. If necessary a vibration can be applied,
6. Extracting of the fluid,
7. Removing of the tray with arranged components.

Components that can be arranged into a tray can be of a wide range of shape and dimensions. Also different materials have been positively tested positive, e.g., brass, glass, sapphire, silicone, and various polymers (e.g., silicone) can be processed.

A new process and system for separating, arranging, and feeding micro-components have been described using the surface tension for a gentle handling.

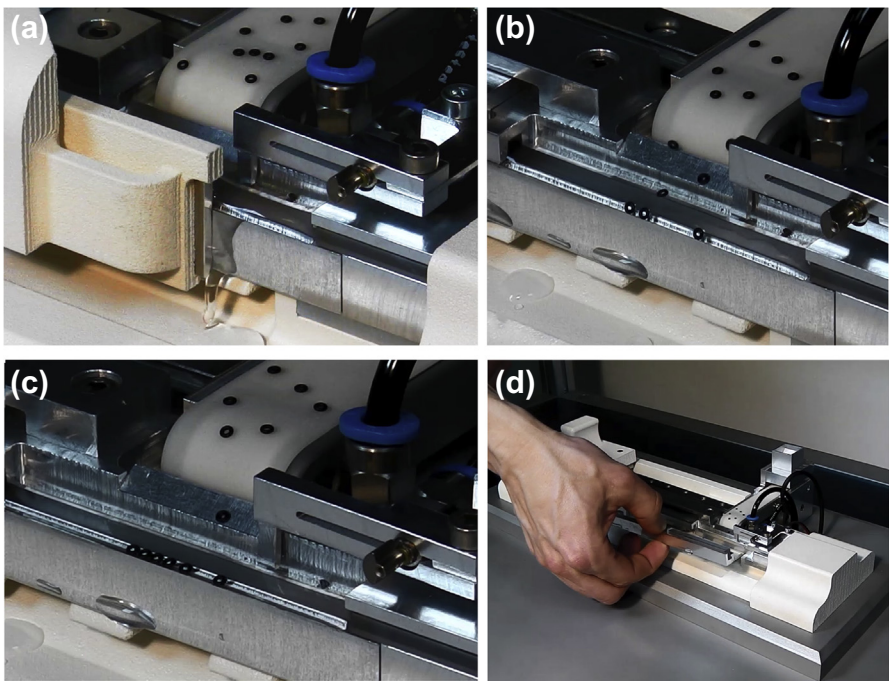

FIGURE 8

(a) Moving the slider to generate a stable surface curvature. (b) The components are put on the fluid surface. (c) Self-arranging of the components on the border. (d) Removing the tray for processing in next assembly step.

A parallel processing of multiple parts is feasible with this method. Micro-components made of various materials and many shapes can be processed with this method and system. A prototype has been realized which can be used for application-specific developments and characterization which are component-dependent, e.g., reliability, failure ratio, or throughput.

POSITIONING OF MICRO-PARTS

A high-throughput manufacturing technology used for flexible substrates is the roll-to-roll manufacturing. It is commonly used in the printing industry, but its importance for the electronic industry is steadily increasing, especially for the manufacturing of organic and printed electronics and the manufacturing of microsystems [17]. A main characteristic of the roll-to-roll manufacturing is the continuous processing, whereby a high yield is achieved. It is based on a layer by layer approach to avoid serial processes, which would slow down the production speed. On the other hand, the integration of components is a sequential process. Therefore, an integration of devices during the roll-to-roll manufacturing is not feasible nowadays. But the combination of conventional devices (e.g., semiconductor circuits, LEDs, sensors) with a roll-to-roll organic and printed electronics could take specific advantages of both technology platforms and could lead to new products with high functionalities [18].

The self-assembly process is a known method for a highly parallel assembly of small parts [19,24]. It could provide a precise handling and positioning of micro-parts as well as high-throughput and cost-efficient assembly for an in-line integration of components in a roll-to-roll manufacturing. The described processes chain in Ref. [24] using the self-assembly effect have a sequential arrangement (Figure 9). The fluidic self-assembly for the integration of GaAs devices that utilizes fluid transport and shape differentiation for placement and orientation requires well-defined structures as well on the device as on the substrate [19]. For a roll-to-roll manufacturing, a seamless processing has to be provided and to keep the manufacturing costs of devices as low as possible, their design restrictions should be minimized. In Ref. [20], a solution for the self-assembly of components in a roll-to-roll manufacturing is described.

For the generation of controlled surface tensions, the surface has to be functionalized in hydrophobic and hydrophilic areas. The hydrophilic areas have to be surrounded with hydrophobic characteristics. The dimension of the hydrophilic area and the micro-part has to be identical. Placing ultrapure water on the surface, it will be aligned within the hydrophilic area. A part, placed on the water layer, will be positioned by the surface tension according to the hydrophilic shape.

Hydrophilic and hydrophobic functionalized surfaces and structures are needed (Figure 10). The requirements of the functionalized areas are

- sharp transition from hydrophobic to hydrophilic characteristic and
- same shape and size of functionalized area and device, e.g., 500 × 500 μm.

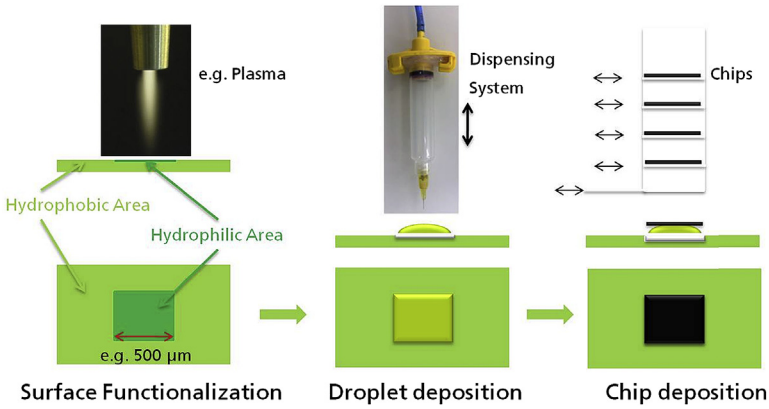

FIGURE 9

Schematic diagram of the process steps for the self-assembly of micro-parts [20].

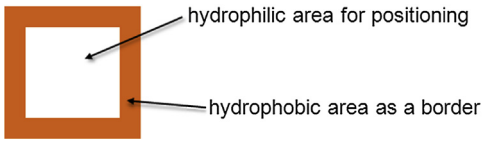

FIGURE 10

Schematic of the functionalized area [20].

The surface functionalization can be realized with different methods. Investigations have shown that two technologies are feasible: (1) atmospheric plasma and (2) the technology for the manufacturing of offset-printing plates.

For the *atmospheric plasma* functionalization, a polymer is used as substrate. A surface mounted device mask with apertures of 500 µm is placed on the polymer. The plasma nozzle with exhausting atmospheric plasma is moved across the mask apertures. The plasma increases the surface energy where it has access to the surface. It is hydrophilizing the substrate through the mask apertures.

The results can be seen in Figure 11 (right), where droplets are positioned on the hydrophilic areas to show the effect. The sharp transition is demonstrated by the quadratic shaped droplets with 500 µm lateral length. A 100-µm gap between two squares is also an indication for the sharp transfer of mask shape to the surface.

Offset-printing plates are established devices in the printing industry for hydrophilic and hydrophobic surfaces. A laser is structuring the Teflon-covered aluminum to realize hydrophilic and hydrophobic surfaces. In Figure 12, the water droplet on the functionalized area shows even better characteristics as the atmospheric plasma functionalization. Structures with 200-µm size can be realized easily with this method. This method is optimized for one substrate material. Therefore the self-assembly cannot be carried out directly onto the product substrate. But it can be used as a transfer substrate.

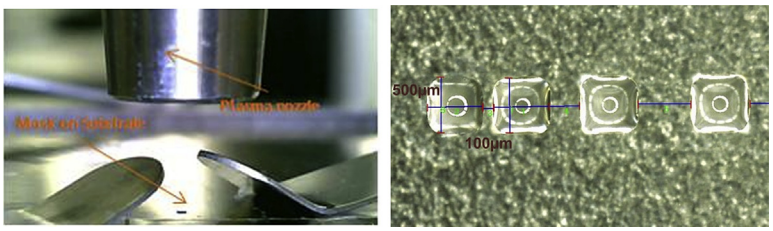

FIGURE 11

Left: Surface mounted device mask on polymer substrate and plasma nozzle above. Right: Droplets on functionalized surface with 500 µm edge length and minimal spacing of 100 µm [20].

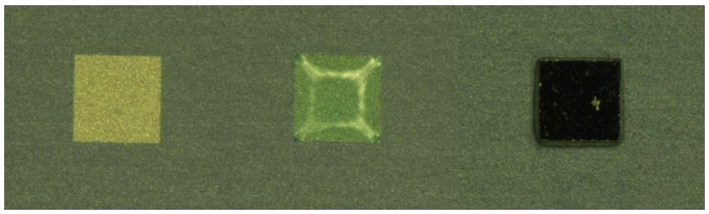

FIGURE 12

Left: 500-µm hydrophile square on an offset-printing plate. Center: Inked water (for better visualization) on hydrophile area. Right: Self-assembled chip [20].

In the next step, the ultrapure water is deposited onto the hydrophilic areas. The water evaporates within seconds residue-free [21], so that a contamination of the devices can be excluded. To generate a well-formed droplet on a 500-µm square, a droplet diameter of 400 µm is required. A standard air-powered dispenser with a passive magnetic valve was used, which was developed at Fraunhofer IPA [22]. The valve supports a reproducible volume for a reliable processing. Figure 13 shows the miniaturized valve integrated into a capillary. For a high-throughput production, a parallel applying of droplets can be achieved by an application-specific arrangement of capillaries with integrated valves.

The parts are applied onto the droplet without using a gripper. The parts are placed adjacent directly one after the other inside an opened channel. The row of parts is moved as far until the first part protrudes from the channel edge. The substrate with the droplet on the hydrophilic area is moving just below. As the droplet is on the top of the surface, it hits the protruding part and pulls it out of the channel. The part stays on the droplet and the self-assembly takes place. The part is positioned according to the hydrophilic structure on the substrate (Figure 14).

As already mentioned, the roll-to-roll process is a continuous process, and so the applying of the parts has to be realized on a moving substrate. A structured offset-printing plate is mounted on a rotating cylinder in Figure 15. It has hydrophilic

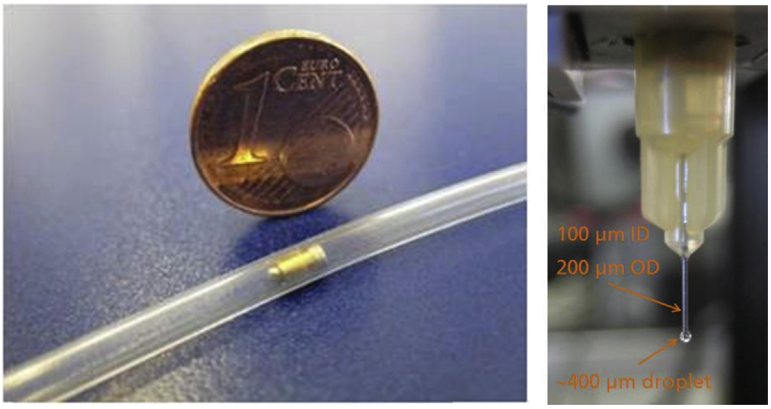

FIGURE 13

Left: Miniaturized IPA. VALVE in a 1-mm tube. Right: 400-µm droplet [20]. OD, outer diameter; ID, inner diameter.

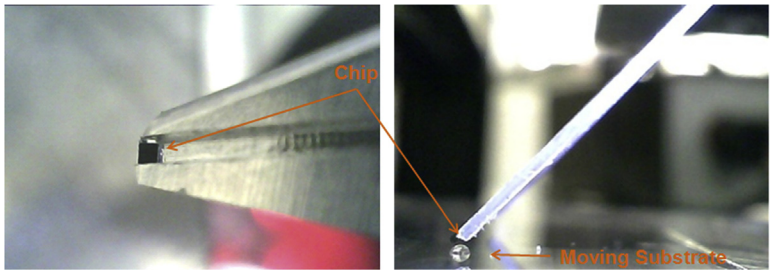

FIGURE 14

Left: Top view onto the channel with a single chip protruding from the edge. Right: Side view with moving substrate and droplet underneath the chip [20].

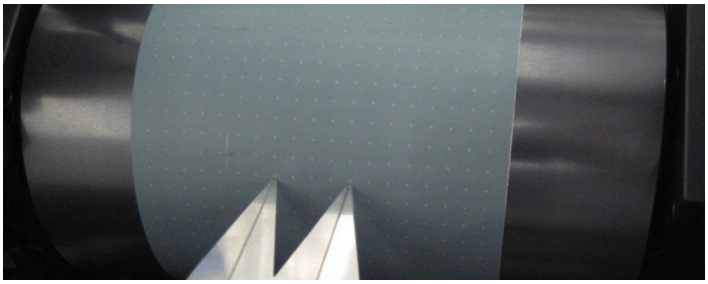

FIGURE 15

Cylinder with functionalized surface and parallel deposition of devices [20].

squares with 500-µm lateral length. On this rotating surface the droplets and parts have been applied in parallel. The self-assembled micro-parts are then transferred on the product substrate.

A self-assembly process using surface tension for the assembly for micro-parts has been adapted for the continuous roll-to-roll manufacturing. The assembly of parts with 500-µm lateral dimension has been presented. The requirements for a parallel positioning of devices within a roll-to-roll manufacturing are fulfilled with the above described method. Future work will be focused on the automation of the processes to meet the requirements of production equipment.

CONCLUSION

Self-assembly has an extremely wide field of applications. For the assembly of micro-parts, surface tensions can be used for a precise and fast positioning. The self-assembly approach is also applicable for the feeding, sorting, and gripping of micro-parts. There are versatile approaches, but only very few have managed the step toward implementation. But there are self-assembly processes available for application-specific developments. Further effort is fundamental to adapt these processes to industrial requirements.

REFERENCES

[1] Morris CJ, Stauth SA, Parviz BA. Self-assembly for microscale and nanoscale packaging: steps toward self-packaging (4). 2005. Available online at: http://www.cpmt.org/scv/meetings/parviz2.pdf [checked on 26.10.14].

[2] Mastrangeli M, Abbasi S, Varel C, van Hoof C, Celis J-P, Böhringer KF. Self-assembly from milli- to nanoscales: methods and applications (8). 2009. Available online at: http://iopscience.iop.org/0960-1317/19/8/083001/pdf/0960-1317_19_8_083001.pdf [checked on 16.06.14].

[3] Fang J, Böhringer KF. Self-assembly. In: Gianchandani YB, Tabata O, Zappe HP, editors. Comprehensive microsystems, vol. 1. Amsterdam: Elsevier; 2008. p. 403−29. Available online at: http://www.ee.washington.edu/research/mems/publications/2008/chapters/Fang-ComprehensiveMicrosystems-2008.pdf [checked on 11.07.14].

[4] Chang B. Hybrid microassembly with surface tension driven self-alignment: handling strategies and microfabricated patterns. Doctoral Dissertations. Espoo: Unigrafia Oy (117); 2013. Available online at: http://lib.tkk.fi/Diss/2013/isbn9789526052625/isbn9789526052625.pdf [checked on 16.06.14].

[5] Sariola V, Zhou Q, Laass R, Koivo HN. Experimental study on droplet based hybrid microhandling using high speed camera. In: 2008 IEEE conference on automation science and engineering. Arlington, VA, 23−26 August 2008. Automation science and engineering. Arlington, VA, 23−26.8.2008. Piscataway, N.J: Institute of Electrical and Electronics Engineers (IEEE); 2008. p. 919−24.

[6] Zhou Q, Sariola V. Unified view of robotic microhandling and self-assembly. In: Gauthier M, Régnier S, editors. Robotic microassembly//robotic micro-assembly. Hoboken, N.J: John Wiley & Sons; 2010. p. 107−43 [checked on 30.10.14].

[7] Whitesides GM, Grzybowski B. Self-assembly at all scales. Science 2002;295: 2418−21. Available online at: http://gmwgroup.harvard.edu/pubs/pdf/793.pdf [checked on 27.10.14].
[8] Kosar TF, Rioux RM, Dickey M. What is self-assembly?. In: NNIN Nanotechnology open textbook; 2008. Available online at: http://www.nano.umn.edu/assets/pdf/textbook/ch_6-2.pdf [checked on 27.10.14].
[9] Whitesides GM. Self-assembling materials. Sci Am 1995;273:146−9. Available online at: http://gmwgroup.harvard.edu/pubs/pdf/431.pdf [checked on 27.10.14].
[10] Crane NB, Onen O, Carballo J, Ni Q, Guldiken R. Fluidic assembly at the microscale: progress and prospects. Microfluid Nanofluid 2013;14(3−4):383−419. Available online at: http://download.springer.com/static/pdf/585/art%253A10.1007%252Fs10404-012-1060-1.pdf?auth66=1414764115_69ed2eac0ad5dbd7af13d1e233194110&ext=.pdf [checked on 29.10.14].
[11] Shrinivasam U, Liepmann D, Howe RT. Microstructure to substrate self-assembly using capillary forces. J Microelectromechanical Syst 2001;10. Available online at: http://pdf.aminer.org/000/333/813/integration_of_silicon_circuit_components_onto_plastic_substrates_using_fluidic.pdf [checked on 11.04.13].
[12] Alien Technology Corporation. In: Fluidic self assembly. White Paper; 1999. Available online at: http://venturebeat.files.wordpress.com/2008/10/alienfsa_white_paper.pdf [checked on 28.11.12].
[13] Zheng W, Jacobs HO. Fabrication of multicomponent microsystems by directed three-dimensional self-assembly. Adv Funct Mater 2005;15(5):732−8.
[14] Arutinov Gari, Mastrangeli Massimo, Smits Edsger CP, Schoo Herman FM, Brugger Jürgen, Dietzel Andreas. Dynamics of capillary self-alignment for mesoscopic foil devices (14). 2013. Available online at: http://infoscience.epfl.ch/record/185896/files/Arutinov%20-%20Dynamics%20of%20capillary%20self-alignment%20for%20mesoscopic%20foil%20devices.pdf [checked on 26.10.14].
[15] Boufercha Nourdin, Sägebarth Joachim, Burgard Matthias, Othman Nabih, Schlenker Dirk, Schäfer Wolfgang, et al. Fluidassem − a new method of fluidic-based assembly with surface tension. In: Ratchev Svetan, Koelemeijer Sandra, editors. Micro-assembly technologies and applications. IFIP international federation for information processing, vol. 260. Boston: Springer; 2008. p. 149−59. Available online at: http://dx.doi.org/10.1007/978-0-387-77405-3_14.
[16] Burgard Matthias, Othman Nabih, Mai Uwe, Schlenker Dirk, Verl Alexander. Feeding of small components using surface tension of fluids. In: Proceedings of the international precision assembly seminar, IPAS 2014, Chamonix, France, February 16−20, 2014. Berlin: Springer; 2014 (will be published In: Svetan Ratchev, editors).
[17] Hecker K. Organic and printed electronics. 3rd ed. Frankfurt am Main: VDMA Verlag GmbH; 2009.
[18] Gourlay J, Götzen R, Reinhardt A, Bohlmann H, Gonzalez D, Queipo P, et al. 79.4: Light-rolls: high throughput manufacture for LED lighting and displays. In: SID symposium digest of technical papers, vol. 41; May 2010. John Wiley & Sons Ltd; p. 1184−1187.
[19] Yeh H-JJ, Smith JS. Fluidic self-assembly for the integration of GaAs light-emitting diodes on Si substrates. IEEE Phot Technol Lett 1994;6(6):706−8.
[20] Burgard Matthias, Schläfli Norbert, Mai Uwe. Processes for the self-assembly of micro parts. In: Ratchev Svetan, editor. Precision assembly technologies and systems. 6th IFIP WG 5.5 international precision assembly seminar, IPAS 2012, Chamonix, France,

February 12−15, 2012. Proceedings. IFIP advances in information and communication technology, vol. 371. Springer Berlin Heidelberg; 2012. p. 36−41 [checked on 27.10.14].

[21] Boufercha Nourdin, Sägebarth Joachim, Burgard Matthias, Othman Nabih, Schäfer Wolfgang, Sandmaier Hermann. Selfassembly of micro components with microfluidics. In: Proceedings of the international workshop on micro- and nano- production technologies and systems. Moskau; 2007. p. 44−52.

[22] Schlenker D. Schließventillösung für unterschiedlichste Anwendungen. In: adhäsion Kleben & Dichten, vol. 11; 2010. p. 16−8.

[23] Fang J, Böhringer KF. Parallel micro component-to-substrate assembly with controlled poses and high surface coverage (4). 2006. Available online at: http://iopscience.iop.org/0960-1317/16/4/008/pdf/0960-1317_16_4_008.pdf [checked on 26.10.14].

[24] Fang J, Bohringer KF. Wafer-level packaging based on uniquely orienting self-assembly (the DUO-SPASS processes). J Microelectromech Syst 2006;15(3):531−40. Available online at: http://ieeexplore.ieee.org/ielx5/84/34353/01638479.pdf?tp=&arnumber=1638479&isnumber=34353 [checked on 30.10.14].

This page intentionally left blank

CHAPTER

Laser Beam Micro-joining 26

Felix Schmitt, Alexander Olowinsky
Fraunhofer Institute for Laser Technology ILT, Aachen, Germany

CHAPTER OUTLINE

INTRODUCTION

The joining processes in electronic device manufacturing are today still dominated by conventional joining techniques such as press fitting, crimping, and resistance welding. Laser beam joining techniques have been under intensive investigation and subsequently new processes for mass manufacturing and high-accuracy assembling have been established. With the newly developed SHADOW® (Stepless High Speed Accurate and Discrete One Pulse Welding) welding technology, technical aspects such as tensile strength, geometry, and precision of the weld can be improved. This technology provides the greatest flexibility in weld geometry with a minimum welding time as well as new possibilities in using application-adapted materials. Different parts and even different metals can be joined by a noncontact process. The application of a relative movement between the laser beam and the part to be joined at feed rates of up to 60 m/min produces weld seams with a length of from 0.6 to 15.7 mm using a pulsed Nd:YAG laser with a pulse duration of up to 50 ms. Due to the low-energy input, typically 1−6 J, a weld width as small as 50 μm and a weld depth as small as 20 μm have been attained. This results in low distortion of joined watch components.

Micromanufacturing Engineering and Technology. http://dx.doi.org/10.1016/B978-0-323-31149-6.00026-8

In the field of micro-production, a variety of materials with individual product-specific dimensions are commonly used. Especially, the manufacturing of hybrid micro-systems, built up of different functional groups, affords variable joining technologies tailored to the specific demands of each components or material combination. Soldering with metal solder alloys is an established and well-known process in electronic industries [1].

LASER BEAM SOLDERING

During the soldering process, a liquid phase is caused by melting of a solder alloy or by diffusion processes within the intermediate layer. In principle, the joining process is based on interaction reactions between the joining partners and the melted solder. Therefore, a direct, oxide-free, and contamination-free contact between the metal surfaces of the joining partners and the solder alloy is one of the most important process requirements. If the melting temperature of the additional material is below 450 °C (840 °F) the process is called soldering, while when above 450 °C the process is called brazing. Characteristic features of soldering include the following [2]:

- The melting temperature of the joining partners is higher than the melting temperature of the solder alloy.
- In most cases, the service temperature of the assembly must be lower than the melting temperature of the solder alloy. In a diffusion soldering process, called transient liquid phase bonding, the service temperature can be higher than the soldering process temperature.
- Prior to the joining operation, the surfaces have to be cleaned to remove oxides and organic films. The use of a flux can avoid these prior processing. However, there are some constrictions associated with the use of flux, e.g., the residues that they leave behind, which are often corrosive and can be difficult to remove.
- Complex assemblies can be produced with low distortion, high fatigue resistance, and good resistance to thermal shock.
- Joints tend to be strong if well filled, unless embrittling phases are produced by reaction between the solder alloy and the components.
- By using a broad variety of solder alloys, it is possible to match the solder with the required process temperature and reduce the melting temperature by using elements with a low melting point (e.g., indium, bismuth).
- Compensation and gap bridging by using an additional filler material as solder alloy.
- For a molten solder alloy to wet and bond to a metal surface, the surface has to be free from nonmetallic surface films. Despite a precleaning process and ensuring this condition at the beginning of the process, significantly oxidation will occur if the components are heated in air. An active flux fulfills the following functions [2]:
  - Removal of oxides and other films on surfaces by either chemical or physical means,

- Protection of the cleaned joint from oxidation during the soldering process,
- Wetting the joint surfaces, but being displaced by the molten solder as the latter spreads, and
- Reducing the surface tension between the solder alloy and the joint surface, thereby enhancing spreading.

- The heating cycle involves four important parameters: the heating period with heating rate and dwell time for heating, the peak soldering temperature, the dwell time above the melting point of the solder alloy, and the cooling rate (Figure 1). In general, it is desirable to use a high heating rate but the maximum heating rate is normally constrained by the form of the energy input. By means of laser energy and its high energy density, it is possible to realize a maximum heat rate. The dwell time for heating is necessary for the evaporation of vapor and constituents of the flux and for the uniform heating of the joining partners up to the wetting temperature. This temperature is below the melting temperature of the solder alloy. The soldering temperature should be such that the solder alloy is certain to melt, but at the same time the solder alloy should not be overheated so that it degrades through the loss of constituents. The peak temperature is normally set at about 20−30 °C above the melting point.

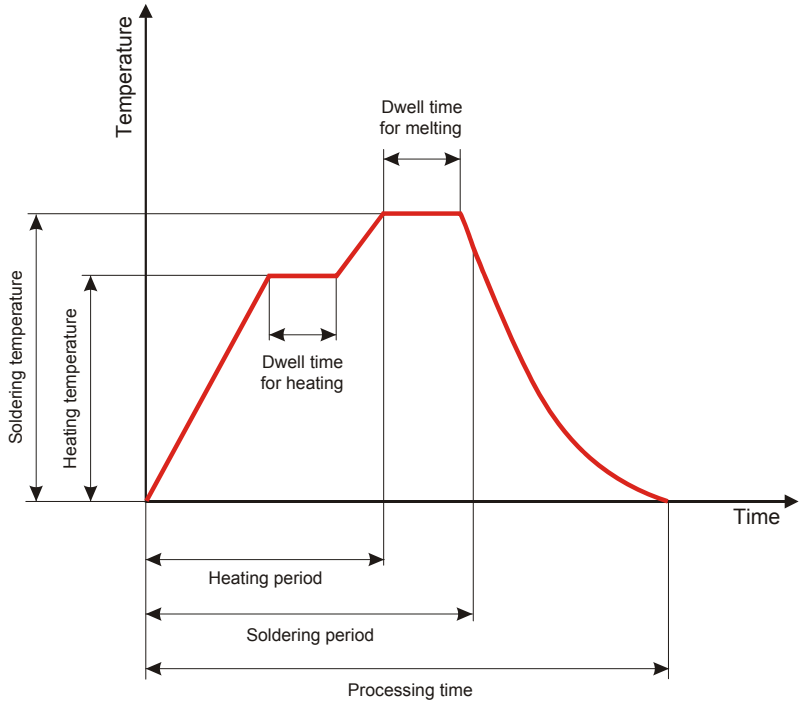

FIGURE 1

Heating cycle for soldering.

The minimum time that the joint geometry is held at this temperature must be sufficient to ensure that the solder alloy has melted over the entire area of the joint. Extended holding times tend to result in excessive spreading of the molten solder alloy, possible oxidation gradually taking place, and deterioration of the properties of the parent materials. The cooling stage of the cycle is not controlled by the operator but normally governed by the thermal mass of the joint geometry. For laser processing, it is very fast because of the instantaneous switch-off of the laser power, resulting in a fine-grained micro-structure of the joint.

Apart from light beam soldering and electron beam soldering, laser beam soldering is a soldering technique using radiation as an energy source (DIN 8505 1979). In contrast to other conventional selective soldering techniques, laser beam soldering features a contactless, temporally and spatially well-controllable energy input. Because of these characteristics, laser beam soldering is predestined for joining tasks where miniaturization and reduced thermal and mechanical stresses are required. Special features of laser beam soldered joints are fine-grained microstructure and a low amount of intermetallic phases due to the high heating and cooling rates of this process. In principle, laser beam soldering is characterized by temporally and spatially selective energy input by surface absorption in the joining area, successive heat conduction, and interface processes. The joining process is determined by characteristics of the laser beam source, the chosen process parameters, and the thermophysical properties of the joining partners.

The first tests on soldering with laser radiation were conducted in 1974 by C. F. Bohmann [3]. Here, a continuously emitting CO_2 laser was used for selective contacting of electronic components, the influence of laser power, irradiation time, and geometry of laser beam interaction zone on the quality of the joints being explored. Although different research teams were working on the industrial implementation of this process, the CO_2 laser did not become a widely accepted tool for soldering tasks despite the good automation possibilities [4,5]. There are some technological and economical reasons, which are inhibiting the use of CO_2 lasers as a laser source for soldering applications. Widely used basic materials in electronic production (e.g., FR4) have an absorption of more than 90% at the emission wavelength of CO_2 lasers ($\lambda = 10{,}600$ nm), but soldering alloys (e.g., tin−lead) have a reflection of about 74% at the same wavelength [6]. In consequence, the risk of burning or partial carbonization of the circuit board is high by primary or diffused scattered laser radiation. Apart from these process-specific drawbacks, the investment and operation costs, maintenance effort, and dimensions of this laser source are not an advantage compared to the use of technological alternatives.

Nd:YAG lasers were used for the first time for soldering applications in the 1980s [7,8]. Compared to CO_2 lasers, these laser sources have different positive features and emit light at near-infrared ($\lambda = 1064$ nm). Apart from smaller dimensions, the shorter emission wavelength enables flexible and cheaper beam shaping and guidance. Here, fiber optics are used for beam guidance and optical components need

not be made from materials such as germanium, zinc−selenium, or cadmium−telluride but can be made of cheaper optical glasses. Metallic materials have a higher absorption in the near-infrared, resulting in a more efficient and reproducible process. The main applications for laser soldering systems based on Nd:YAG lasers are electrical and mechanical joints from sectors, which require a greater level of reliability. Here, precision applications are known from civil fields, e.g., computer technology, automotive, aviation, aerospace, but there are also applications from military fields [6,9]. Because of high investment and operational costs, even laser beam soldering with solid-state lasers is only established in small market segments compared to competing selective soldering technologies.

Since the development of high-power diode lasers, laser beam soldering has become increasingly more important in industrial applications. Diode lasers feature a simple layout, a high electrical efficiency factor, and small dimensions and are appropriate for manifold industrial applications on this account. In combination with not requiring maintenance, being of simple operation, and having long lifetimes, these laser sources fulfill the requirements of industry due to providing an economic operation by lasers [10,17].

The latest developments in laser technology have resulted in fiber lasers becoming a versatile tool for laser-based production processes. Even if they are currently not used for soldering, very often it can be seen that they will penetrate laser beam soldering applications within the next few years. Due to their excellent beam quality, only these laser sources provide minimal focus geometries meeting the requirements for further miniaturization. Furthermore, these laser sources feature continuous emission, small emission wavelengths ($\lambda = 1030$ nm), and high-anticipated lifetimes, combined with small dimensions.

Table 1 shows the important characteristics of these four laser sources for soldering applications.

Table 1 Comparison of Different Laser Sources for Laser Beam Soldering

	Diode Laser	Fiber Laser	Nd:YAG Laser	CO_2 Laser
Dimension (ratio)	1	1	100	1000
Electro-optical efficiency	40–50%	30%	3–17%	10–15%
Emission wavelength	800–1000 nm	1030–1090 nm	1064 nm	10,600 nm
Lifetime	>100,000 h	>100,000 h	>1000 h	~10,000 h
Maintenance	Low maintenance	Low maintenance	200–1000 h	Every 500 h
Investment/ power	10–50 €/W	15–30 €/W	50–100 €/W	10–50 €/W
Beam guiding (fiber optics)	Yes	Yes	Yes	no

Although the beam quality of high-power diode lasers cannot be compared to that of conventional laser sources, these laser sources excel at flexibility. The decisive factor in this is the dimension ratio between the single different laser beam sources. The beam-generating dimensions of a high-power diode laser are smaller by a factor of 100 compared to a Nd:YAG laser at the same power. For the CO_2 laser, this difference is even greater (a factor of 1000). Compactness of semiconductors and the higher efficiency resulting in smaller and low-power consumptive peripheral devices are responsible for the small system design. This saves space in the production environment and increases the mobility of these laser sources. Therefore, it is possible to integrate diode lasers directly into production cells. With respect to economical aspects, modern high-power diode lasers are an attractive alternative to Nd:YAG and CO_2 lasers. Investment costs related to the optical output are at the lower range of competitive laser sources. Due to the epitaxic layout, diode lasers offer the possibility for cost-efficient mass production. Hence, forecasts see a decreasing price for diode bars so that high-power diode lasers will gain an advantage compared to other laser beam sources [10]. With an electro-optical efficiency of about 50%, diode lasers work much more efficiently compared to Nd:YAG ($<17\%$) and CO_2 lasers ($<15\%$), resulting in lower power consumption as well as in required cooling power: this influences directly the operational costs. Diode lasers work almost maintenance free because there are no components wearing out (e.g., flashlights in Nd:YAG).

Due to the demands for high-quality soldered joints, many process control mechanisms have been examined over the last few years. An essential requirement for laser beam soldering is the stability of the material and geometry conditions due to the energy input into the materials being independent of environmental conditions. Compared to other selective soldering methods, laser beam soldering enables temporally and spatially adapted energy input by pyrometric process monitoring. The development of a closed-loop feedback of process information by thermal radiation gives the possibility of process control.

There are numerous different application-specific solutions available commercially for laser beam soldering machines. In principle, they are based on flexible beam shaping and guidance using galvanometric scanners or axis systems. For fiber-guided systems, the processing optics are moved but there are also systems where the entire laser beam source is being moved. In Figure 2 a production cell and laser processing optics are shown based on a galvanometric scanner.

The machine is designed for the laser beam soldering of an automotive microelectronic module (an alternator regulator realized in thick film technology) with solder pads printed on an alumina substrate (Figure 3). The housing has seven terminal leads to be soldered to the substrate. The entire alumina substrate is glued by a heat conducting adhesive to an aluminum base plate [11,12].

Major components of the production cell are a fiber-coupled, continuous wave (cw) diode laser system and a processing head with integrated pyrometric and power sensors.

The diode laser system has a maximum optical output power of 500 W, which can be modulated by controlling the pump current. The collimated laser beam passes

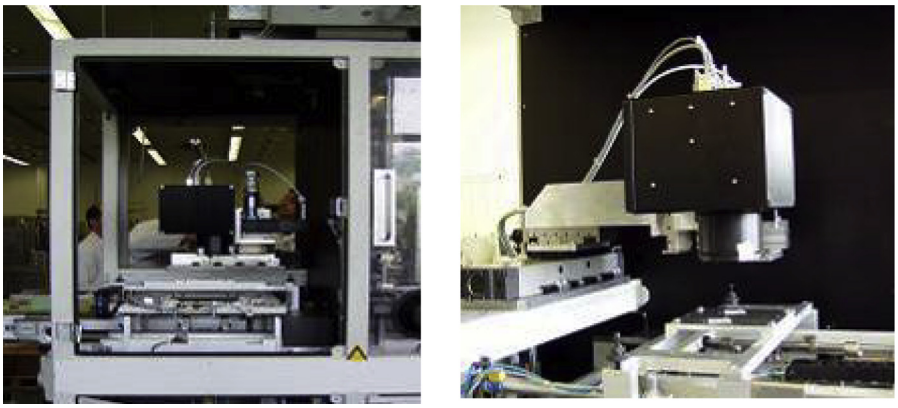

FIGURE 2

System design for laser beam soldering based on a galvanometric scanner: production cell (left) and laser processing optics (right).

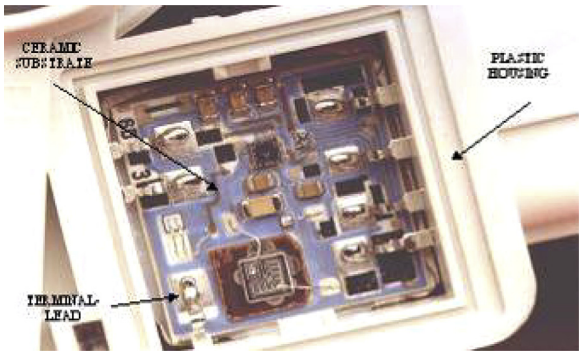

FIGURE 3

Automotive micro-electronic module in a plastic housing—alternator regulator.

through a galvanometer scanner and is focused by an f-Theta lens onto the lead/solder pad area to generate the joint. The circular focus geometry of the laser beam is aligned to the center of the semicircle at the end of the terminal lead (Figure 4). The working distance between the optics and the laser beam interaction area is about 80 mm. With an image projection ratio of 1:2 the minimum focal diameter is 1.2 mm, which is double the fiber core diameter of 0.6 mm.

Thermal radiation emitted from the surface follows the beam delivery system of the galvanometer scanner and passes through a dichroic mirror, which is transparent for this wavelength range. After passing the dichroic mirror, the thermal radiation is focused by a lens on a photodetector (Ex. InGaAs, peak wavelength 2.3 μm). The output signal of the detector is conditioned by a logarithmic amplifier circuit.

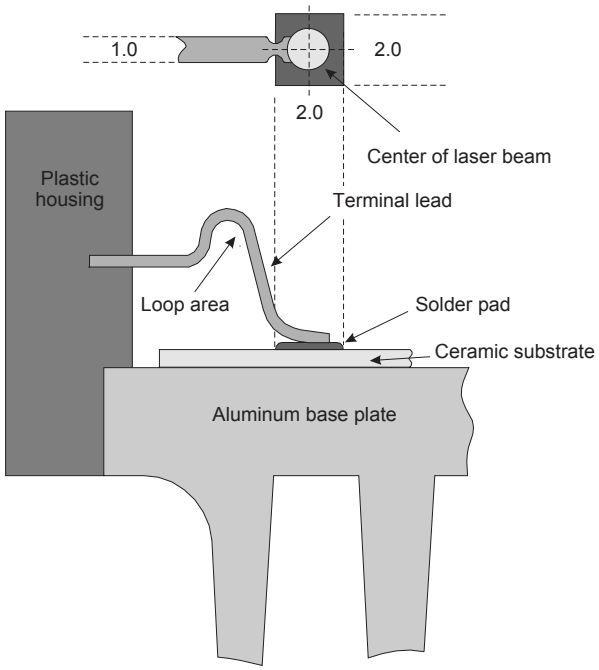

FIGURE 4

Solder joint configuration (dimensions in mm).

The integrated pyrometric sensor is conditioned for laser beam applications with process temperatures in the range of 150 °C, e.g., welding of plastics or soldering. The pyrometric sensor is calibrated by means of a standardized blackbody and the response time of the sensor is about 1 ms at 150 °C.

The surface of the lead/solder pad area is imaged onto a charge-coupled device camera via a deflecting mirror.

Apart from interconnection requirements, a high production rate has to be ensured for the process to remain attractive for mass production. For this reason the total process period, especially the irradiation time, has to be as short as possible. However, to achieve an adequate solder joint with reduced irradiation time the laser power has to be increased. To avoid the hazard of superheating, the laser power has to be limited and controlled. Therefore the thermal radiation from the interaction zone is detected and analyzed in more detail. In a series of experiments the following features could reproducibly be observed in the recorded pyrometric signal. A typical profile is presented in Figure 5, where the laser is switched on at time $t = 0.2$ s. At point (A) the reduction of the ascending slope indicates the initial activation of the applied adipic acid. The second change in the pyrometric signal at point (B) is related to the onset of localized melting of the solder pad and outgassing of volatile components. Due to the continued energy input by the laser beam, the terminal lead

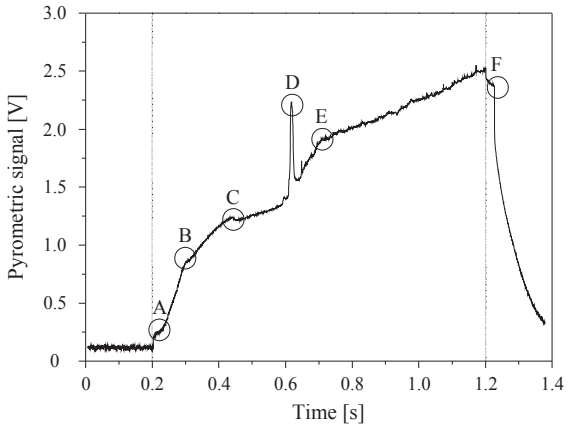

FIGURE 5

Pyrometric signal detected during soldering; irradiation time: 1000 ms.

reaches the wetting temperature (point (C)). In the next phase there is a sudden improvement in heat dissipation due to the wetting of the terminal lead, which often results in a temperature decrease (point (C)−(E)). At point (D) a gas bubble consisting of volatile components leaves the molten solder. The variation of the signal curve following point (E) is induced by self-optimization of the surface tension and by superheating of the molten solder pool. After the laser beam is switched off at $t = 1.2$ s, very high cooling rates are observed. This high rate is caused by the optimized heat transfer into the aluminum base plate. At point (F) the solder solidifies. The change of the descending slope in the signal curve at the crystallization point (F) is known from the thermal analysis of solidification reactions in the literature [13,14].

Based on a set of characteristic curves, benchmarks can be determined and by changing specific process parameters a thermal and temporal optimized profile can be generated. Using these analytic profiles as set point settings for a closed-loop control system, the energy input can be controlled individually for each joining application or product (Figure 6).

Figure 7 shows a detailed view of two solder joints and a cross section of a laser-soldered joint.

An innovative application for laser beam soldering is the electrical contacting of solar cells for photovoltaic module production (Figure 8). Due to the decreasing thickness of the solar cells (at the present time 220 μm but in future likely to be below 150 μm) the demand for a soldering method without any mechanical contact has led to the development of the laser beam soldering process [15]. The process is controlled by pyrometric sensors to avoid thermal damage of the thin silicon wafer.

Laser soldering is playing an increasingly important role as an alternative to the gluing or clamping of micro-optical components into metallic mountings. In contrast

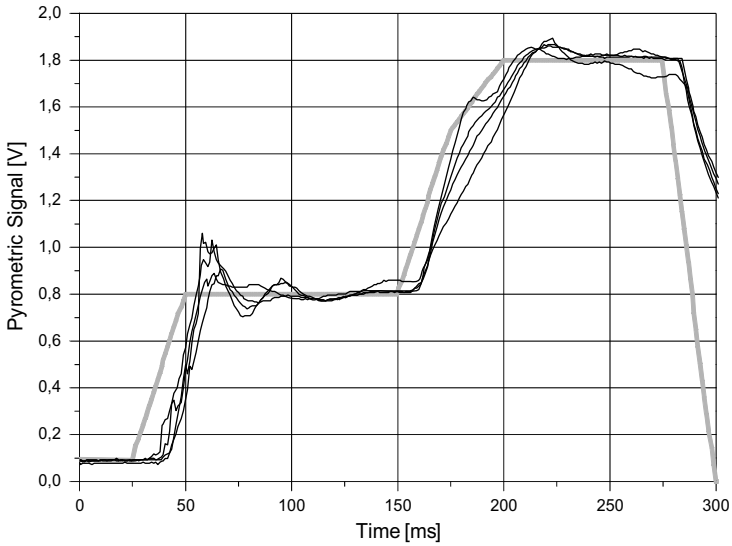

FIGURE 6

Array of pyrometer signals recorded during different closed-loop controlled laser beam soldering processes. The gray curve represents the defined set point settings.

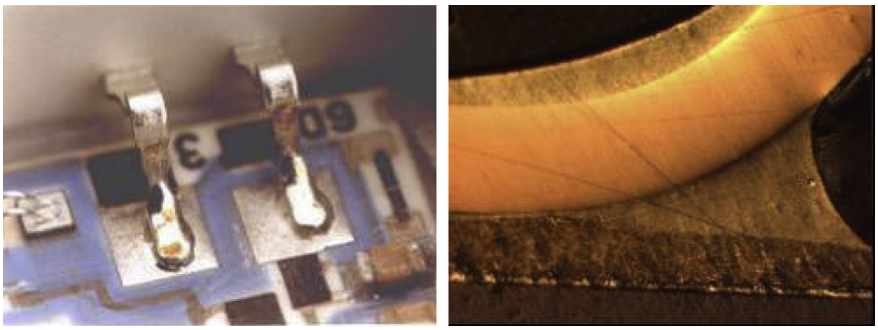

FIGURE 7

Detailed view of two solder joints (left) and a cross section of a laser-soldered joint (right).

to laser soldering, the energy input by induction is difficult for miniaturized optics with a diameter smaller than 1 mm and mounting widths below 50 μm because of the smaller amount of material for heating. Similarly, manual soldering using a soldering iron raises problems because of the small dimensions and therefore the resulting insufficient reproducibility. An alternative to these processes is soldering by using a high-power diode laser or a fiber laser. For these experiments the joining components consist of a gold metalized stainless steel mounting and sapphire optics,

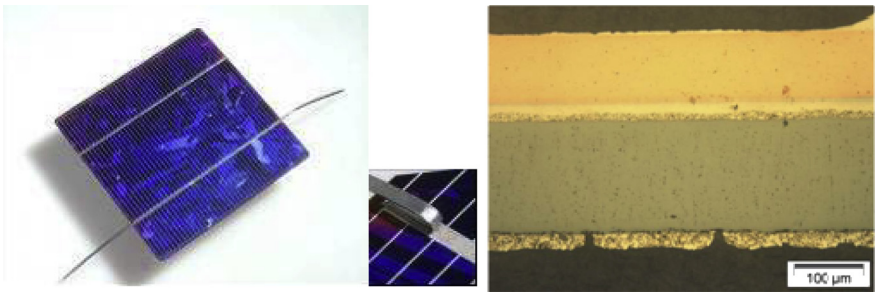

FIGURE 8

Electrical contacting for solar cell interconnection.

also metalized with gold. An AuSn solder alloy with a melting temperature of 280 °C is used. By using a fluxing agent, the surfaces are cleaned of oxides before soldering and the joining area is prevented from oxidation during the soldering process. This flux causes pores in the soldering joint and therefore pores can be detected. By means of a pyrometer, it is possible to set a controlled process and a two-step temperature profile, as recommended in the literature for soldering. At the beginning of the laser soldering process the flux is activated at a lower temperature (∼150 °C), while in the second step the necessary energy for the melting of the solder alloy is applied. This process management reduces the number of pores within the soldered joint significantly (Figure 9 (right)).

The gap is filled homogeneously with the solder by capillary forces: Excessive solder does not wet the surfaces of the sapphire but wets the mounting on the laser facing side. Both diode lasers focused to 1 mm and fiber lasers collimated to 1 mm diameter or lower can be used as laser sources. The advantage of the fiber laser is that the focal position does not have to be aligned because of the Rayleigh length of greater than 1600 mm.

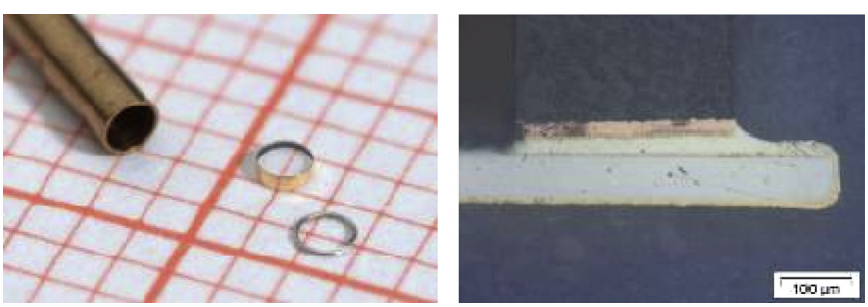

FIGURE 9

Joining components: bushing, sapphire optics, solder preform (left). Cross section of a soldering joint (right).

Application areas of selective laser beam soldering using high-power diode lasers are manifold and are not confined to a special branch of industry. Currently industrial applications are focused on electronics assembly, especially for the automotive sector. Discrete mounting of critical components, soldering of cable strands, soldering and brazing of micro-electronic and micro-mechanical components, and cable assemblies are industrial applications of laser beam soldering.

LASER BEAM MICRO-WELDING

Laser beam micro-welding is a versatile and flexible manufacturing technology, which has found its way into various industrial applications. Electron guns for cathode ray tube displays have been produced using Nd:YAG lasers since the 1970s. Such an electron gun contains more than 150 spot welds to assemble the different parts. This sums up to 15 million laser pulses per day. In many other industrial fields, laser beam welding tends to become a standard manufacturing technology for small products.

In the watch industry, gear wheels and arbors will no longer be joined in a press fit process, but by means of laser beam welding. In the automotive industry, increasingly more sensors and components such as relays and control units are being mounted directly under the hood and have to undergo heavy vibrations and high temperatures. The joints in these components have to survive these stresses with a long estimated lifetime and a very low failure probability, as they are part of the safety equipment.

As a variety of different geometries and different accessibilities have to be joined securely, only a joining technology with high flexibility at reasonable cost and the ability to provide short cycle times can be used. Alternative joining methods often reach their limits in terms of product quality and reliability (Table 2).

Laser beam micro-welding is a noncontact process without any tool wear out. The process duration is shorter than that of comparable techniques. The joining process may be finished within a few milliseconds, whereas the whole cycle time is

Table 2 Alternative Joining Methods

Joining Method	Disadvantage in Comparison to Laser Beam Welding
Adhesive bonding	Elaborate surface preconditioning Lower bond strength Long process time
Swedging or border crimping	Tool wear out Additional forces
Resistance welding	Two-sided accessibility Limited material choice
Soldering	Reduced high-temperature strength

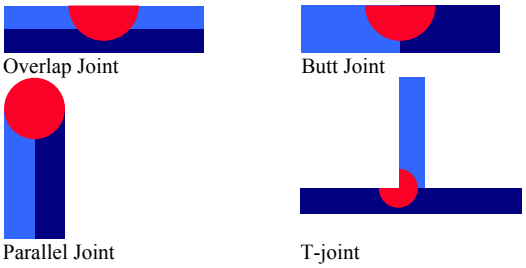

FIGURE 10

Joint geometries for micro-welding.

determined by loading and unloading of the components to be joined as well as by the specifications of the laser source.

One main advantage of laser beam welding is its flexibility: Part geometry, material and material combinations can be changed very easily because the energy input can be controlled and the intensity and the power can be adapted to the task over a wide range. Spot welds as well as continuous weld seams can be applied. Process monitoring as a main requirement in industrial production lines can easily be integrated as in-line weld monitoring or off-line inspection of the weld.

Laser beam welding requires good contact between the joining partners. To obtain good results the following joint geometries have been established (Figure 10).

PROCESSES AND RESULTS

The most commonly used laser source is a pulsed flashlamp-pumped Nd:YAG laser at a wavelength of $\lambda = 1064$ nm with a low absorption in nearly all material. Typical data of commercially available laser sources are listed in Table 3.

Pulsed flashlamp-pumped Nd:YAG lasers offer some advantages compared to continuously emitting cw Nd:YAG lasers, which include:

- high maximum pulse power at moderate average power,
- better beam quality,
- affordable investment costs and low cost-of-ownership,

Table 3 Typical Specifications of Pulsed Nd:YAG Laser Sources and Fiber Lasers

		Pulsed Nd:YAG	Fiber Laser
Average power	(W)	10–400	100–200
Pulse power	(kW)	1–7	–
Pulse energy	(J)	1–50	–
Pulse duration	(ms)	0.1–20	Cw
Beam quality	(mm mrad)	8–16	0.4
Beam diameter	(μm)	50–400	35
Fiber diameter	(μm)	100–500	10–50

- lower requirements for cooling,
- steeper slopes for pulse rise time, and
- pulse forming capability.

The applicability of optical fibers to guide the laser light offers new possibilities for industrial use within manufacturing equipment. The separation of the laser source itself and the working head inside the machine or even the possibility of using one laser source for different machines by energy-sharing or time-sharing mechanisms. By means of this, the use of lasers becomes more economic.

The new sources, e.g., fiber lasers, now combine better beam quality with reduced costs.

BEAM DELIVERY

For Nd:YAG lasers, there are two possible ways for beam delivery: direct beam and fiber delivery [10]. The beam quality of a direct beam (BPP[1] 8−20 mm mrad) is better than the beam quality of a fiber-guided system (BPP 15−30 mm mrad)[1]. The intensity distribution of a direct beam is normally a Gaussian distribution, whereas the fiber-guided system has a top-hat distribution. Thus the Gaussian distribution can be focused better to smaller beam diameter.

A disadvantage of Nd:YAG rod lasers is the influence of the thermal lens. Beam quality and intensity distribution are depending on duty cycle, pulse duration, and laser power. They also can change from pulse to pulse as well as within one pulse. Therefore a laser beam guided through an optical fiber by multiple reflections is homogenized. Beam quality and intensity distribution are predetermined by the diameter of the fiber and its numerical aperture (NA) and vary only slightly. Furthermore, the maximum temperature of the weld bead using a Gaussian distribution is normally higher, so the top-hat distribution is normally more appropriate for laser beam welding.

The positioning of the beam can be made by using a Cartesian positioning system to move the workpiece or by moving the beam by means of a galvanometer scanner (Figure 11).

Typical applications of laser beam micro-welding are dealing with wires and thin sheets ranging from several tens of microns to one millimeter in thickness. The diameter of the laser beam should be of the dimension of the thickness of the parts to be welded, although in certain applications it can be larger. As a particularity the parts are sometimes already placed in a polymer housing (e.g., a premolded package). Here it has to be taken into account that the housing material must not be influenced by diverging laser radiation or by the heat created by the joining process. The main materials are steel and coated and uncoated copper alloys.

[1]The beam parameter product (BPP) of a laser beam is defined as the product of beam radius and the beam divergence half-angle (measured at the beam waist and the far field respectively). The usual unit for the BPP are mm mrad and can be used to specify the beam quality of a laser beam: the higher the beam parameter product, the lower is the beam quality.

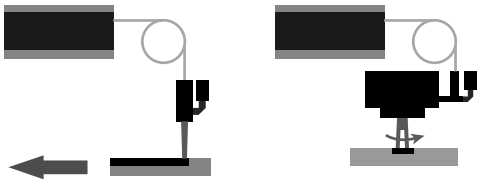

FIGURE 11

Positioning of the laser beam for micro-welding.

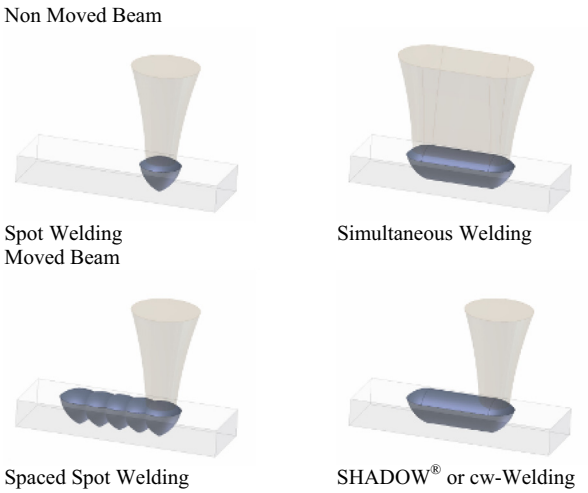

FIGURE 12

Classification of laser beam micro-welding. SHADOW®, Stepless High Speed Accurate and Discrete One Pulse Welding; cw, continuous wave.

Often combinations of materials have to be joined, e.g., steel/copper or steel/brass. In this situation, the joint geometry determines the weldability. As the joining tasks differ very much in terms of geometry, dimensions, and material, attention has to be paid to the heat conduction in the parts. Sheets with a thickness of below 500 µm cannot be treated as semi-infinite bodies. Therefore, heat accumulation at the back face of the sheet influences heavily the welding as well as the heat losses into the surrounding material of the parts and the clamping devices.

In micro-technology three different types of joining methods are applied: spot welding, spaced spot welding to create lines, and continuous seam welding (Figure 12).

SPOT WELDING

Spot welding will be applied if only small connection cross sections are needed or if the available space is not sufficient for elongated weld seams. The diameter ranges from 100 to 800 µm depending on the beam diameter, the material, and the laser power. The spot welding process can be divided into four phases: heating, melting,

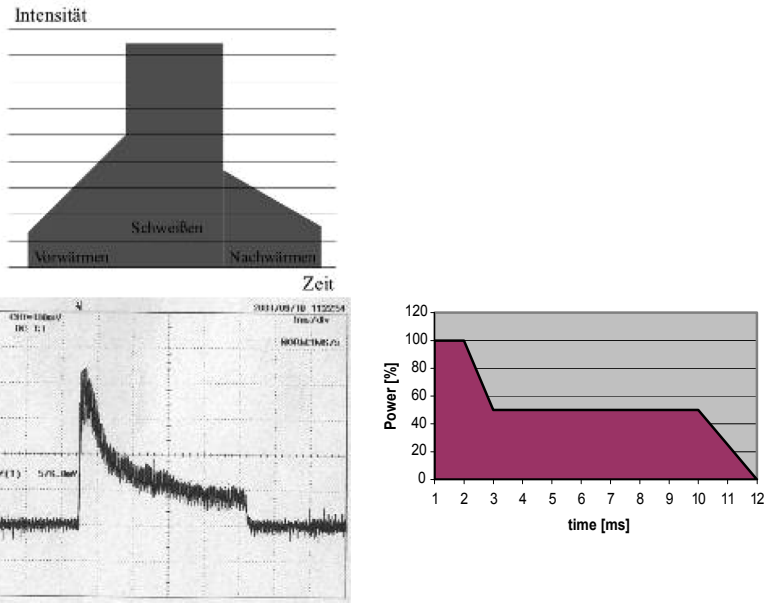

FIGURE 13

Typical pulse form.

melt flow dynamics, and cooling. Depending on the intensity, evaporation of material may occur.

By means of pulse forming, the intensity can be adapted to the sequence of the process phases. A typical pulse form is given in Figure 13.

For some materials a preheating, as shown on the left above, is favorable. Other materials such as copper alloys require high intensities at the beginning of the pulse in order to crack existing oxide layers and to assure stable uncoupling of the laser energy.

Post heating with well-controlled cooling conditions may reduce the risk of cracks. Therefore a pulse form as shown on the right above can be used. Typical pulse durations range from 1 to 15 ms.

For pure heat conduction welding, the weld depth amounts to the radius of the weld spot diameter. Increasing the intensity leads to evaporation of material and to the establishing of a capillary. The presently developing keyhole welding process creates deeper weld depths. The discrimination between pure heat conduction welding and keyhole welding cannot be given for micro-parts due to the given facts of heat accumulation and the dimensions of the parts.

Spaced spot welding

Spaced spot welding is realized by placing several spot welding at a certain overlap in order to achieve a seam weld. The length of the seam is scalable, but the heat input is very high because for each spot all process phases of spot welding have to be

FIGURE 14

Typical application for spaced spot welding.

Lasag.

passed through. This may lead to distortion or thermal damage of the parts. Figure 14 shows a cover of battery housing for a pacemaker.

Important process parameters beside pulse power and pulse duration are pulse repetition rate and feed rate. The latter two determine together with the spot diameter the overlap of two consecutive spots, which is usually in the range of 60%.

CONTINUOUS WELDING

Continuously emitting lasers are seldom used in micro-technology to realize weld seams because of the large beam diameter.

Up to the present time, cw laser welding has been used only for longer joints and for larger parts. A high average laser power, $P_{av} > 500$ W, and a high-processing velocity, $v > 5$ m/min, are required for cw laser welding. Above all, cw laser sources are more expensive than pulsed laser sources. Nevertheless, the joints obtained by cw laser welding show a smooth surface and an optimized micro-structure almost entirely without pores. The energy per length is less for cw laser welding than for pulsed laser welding.

The idea is to apply cw welding to micro-parts with a part geometry of less than 500 μm and a weld width of less than 100 μm. The use of pulse forming (temporal shape of the laser pulse) enables the joining of dissimilar materials such as steel to copper. As the length of the weld seam will be very short, cw lasers tend to be off rather than being used for welding. Therefore a new technique called SHADOW® was developed to realize extended weld seams with a pulsed laser using one single pulse and sweeping the laser beam over the surface during the duration of the pulse.

SHADOW® stands for Stepless High Speed Accurate and Discrete One Pulse Welding. It was invented to weld small axisymmetric parts, which can be rotated quickly during one single laser pulse. This technique combines the advantages of cw welding, such as a smooth surface and a high process speed, with the possibilities of the pulsed laser systems, such as lower costs and the capability of forming the temporal lapse of a pulse. Since the parts are small the latter advantage of the process enables the application in micro-technology, where the thermal load of the assembled parts has to be well controlled (Figure 14).

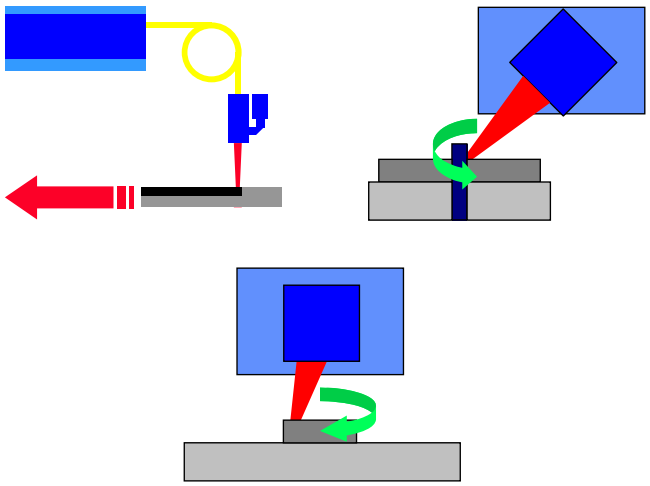

FIGURE 15

Schematic drawing of the setup.

Pulsed laser sources at present are able to generate a maximum pulse duration of $\tau_{H,max} = 20$ ms. To weld parts over a length of $l = 2$ mm a processing velocity of $v = 6$ m/min is therefore required.

Comparing the energy input ($E_{H,SHADOW} = 6$ J) with the energy input for a similar joint using the multipulse technique where 10 pulses without overlap are needed ($E_{H,p} = 10 \times 2.4$ J $= 24$ J), it is seen to be less by a factor of 4. Moreover, the joined parts show less debris or pollution on the surface and neglecting the time needed to accelerate the process, and the processing time is dramatically reduced.

The effect of reduced energy input can be seen in Figure 15. As the transition from solid to liquid is limited to the initial instant of the process, no particles or melt ejections occur. The result is a smooth and even surface of the weld seam.

SHADOW® can be used for welding difficult materials and to improve the weld quality (Figure 16). The applications are shown in the following section.

Applications of SHADOW® in fine mechanics and electronics

The accuracy of a mechanical watch depends on the quality of the rotating spring assembly (balancer). For high-end watches this balancer consists of a ring with four pins. Here SHADOW® is used to weld the pin to the ring. As the outer surface is diamond turned after the welding process, the weld seam can no longer be seen. The diameter of the annular weld seam can be adjusted to achieve either a ring around the pin or, by reducing the diameter, the pin can be molten in total (Figure 17).

Instead of moving the laser beam by means of a scanning head the complete part can be turned, especially for the joining of a wheel to an axis or, as shown in the

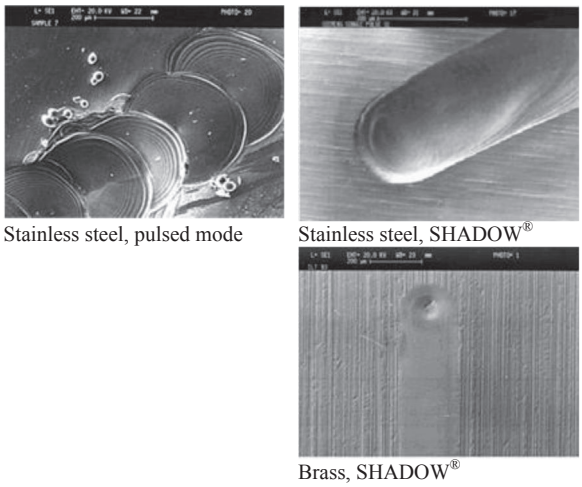

FIGURE 16

Examples of the weld seam with Stepless High Speed Accurate and Discrete One Pulse Welding (SHADOW®).

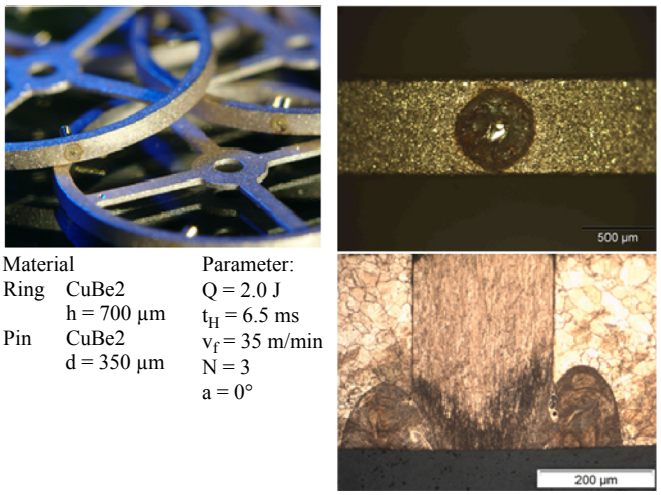

FIGURE 17

Balancer for mechanical watches.

following example, the inner cage of a ball bearing (Figure 18). The axis in the middle of the part prohibits the use of a scanning head where the beam comes from the center of the field of view. This application is done with a high-speed rotating workpiece with a tilted beam targeting from the outside to the center of the part at an inclination angle of 45° (Figure 15).

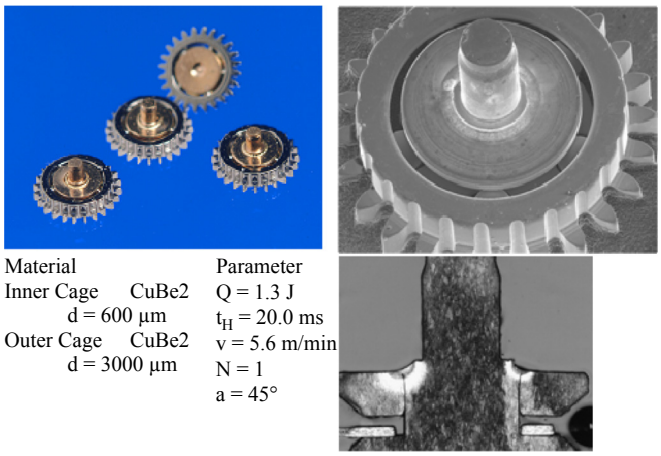

FIGURE 18

Ball bearing.

Comparison of conventional pulsed mode welding to SHADOW®

The already mentioned advantages of the SHADOW® technique can be discussed in an example from the watch industry. The application is the second hand of a gear wheel. The typical combination of steel and brass with its problem of evaporation of zinc is shown in Figure 19. Two different methods are applied and the results are discussed in the following.

In pulsed mode, 130 pulses with a pulse energy Q = 0.1 J are applied. The total energy amounts to 14 J. In comparison, the SHADOW® technique only uses one pulse with an energy Q = 1.3 J. The reduction of the energy results in a smooth surface without any ejection or particles on the part.

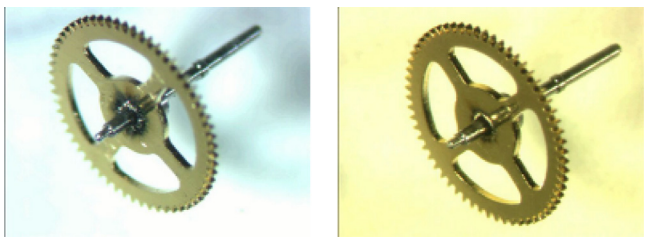

FIGURE 19

Comparison of conventional pulsed mode (left) welding to Stepless High Speed Accurate and Discrete One Pulse Welding (SHADOW®) (right). Material: Axis S20AP; Wheel CuZn37 Ø 0.3 mm.

PRECONDITIONS AND LIMITS OF LASER BEAM MICRO-WELDING

To determine the applicability of laser beam micro-welding for a specific joining problem, there are some crucial points that have to be investigated.

Offsets in the butt joint configuration and gaps at all instances commonly create kerfs at the edges of the weld seam, which decrease the stability and strength of the joint. Furthermore, the surface conditions such as oxidation or contamination with lubricants due to preceding manufacturing steps, e.g., stamping, change the absorption and therefore the welding result. As a consequence more pores may occur.

Reproducible clamping conditions are one major precondition to assure reproducible weld results. The thermal mass and the dimensions of the parts are so small that differences in the positioning within the clamping, varying gaps or clamping forces, may not be compensated for.

Furthermore, the position of the focal plane with respect to the surface of the workpiece is crucial for the weld result. Defocusing due to misalignment will lead to broadening of the weld seam, taking into account that the intensity distribution may seriously change the process behavior. Finally, the mode of operation of the laser source itself influences the weld results. At the limits of the working range the focusing conditions vary from pulse to pulse in terms of pulse power, pulse form, and intensity distribution.

CONCLUSIONS AND REMARKS

Laser beam joining offers the advantage of well-controlled energy input into the parts with low effects on the surrounding material.

For welding micro-parts, two different kinds of laser sources can be chosen: diode-pumped systems such as fiber or thin disk lasers for longer weld seams and flashlamp-pumped rod lasers used for the SHADOW® technique. Fiber laser systems of up to 200 W are able to weld stainless steel as well as copper up to thicknesses of at least 250 mm. It is also possible to weld dissimilar metals in an overlap configuration. The beam diameter has to be small to obtain a keyhole. However, the Rayleigh length of a laser beam with 15 μm beam diameter is smaller than 200 μm, so the requirements for beam positioning are quite high.

The flashlamp-pumped rod laser used for the SHADOW® technique is more economic for weld seams length of up to several half centimeters. The welding technique SHADOW® combines the advantages of continuous welding such as low contamination and smooth weld beads with the lower investment costs of a pulsed solid-state laser, with its capability of pulse forming and the good focus ability due to its comparable beam quality. As most micro-parts need only short weld seams, the SHADOW® technique often is the most economic welding technique. To further increase productivity an increase in throughput by parallelization can be achieved. By using special diffractive optics to split the laser beams, the soldering process can be performed on multiple spots simultaneously [16].

Fiber lasers with their unique beam quality at reasonable cost and extremely small footprints are at their point of entry into industrial use. The possibility to realize very small weld seams due to their achievable focus diameter opens up new fields of use in micro-mechanics and micro-electronics, such as the replacement of thermosonic ribbon bonding for high-power electronics.

The current development of laser sources with high beam qualities enables to increase the quality of the welding process. With further and fine-grained control over the process parameters even difficult material combination could be addressed. To package temperature-sensitive glass/glass and glass/ceramics component groups, especially those with large substrate surfaces to be sealed, the laser-based joining process using glass solder is becoming more and more significant. Unlike other processes, the laser beam is able to apply energy to a limited space in order to melt the glass solder precisely, thus generating a bond with long-term, stable hermeticity.

High-temperature processes such as anodic bonding and glass frit bonding are widely used methods for hermetically sealing components made of silicon and glass. The heat needed for joining is introduced into the component by a kiln process at temperatures of 300−600 °C. Because the most temperature-sensitive component determines the maximum allowable temperature of the entire system, these two processes cannot be used for temperature-sensitive functional elements. They are, for example, unsuitable for encapsulating organic light-emitting diodes, because the functional organic layers would be destroyed at a temperature of even 100 °C [18].

REFERENCES

[1] Bosse L, Göbbels N, Olowinsky A, Gillner A, Poprawe R. Production cell for laser joining of microsystems with modular pick-&-join-tools. In: Proc. third int. wlt-conf. On lasers in manufacturing LIM; 2005. p. 785−9.
[2] Humpston G, Jacobson DM. Principles of soldering. Materials Park: ASM Int; 2004.
[3] Bohmann CF. The laser and microsoldering. 1974. SME Technical +Paper No 10: AD74−810.
[4] Burns F, Zyetz C. “Laser Microsoldering”. In: Electronic Packaging and Production; May 1981. p. 109−20.
[5] Chang D. Experimental investigation of laser beam soldering. Weld J 1986;65(10): 33−41.
[6] Meyer FG. Laserlöten unter besonderer Berücksichtigung der SM-Technologie und des Lötens an schwer zugänglichen Stellen, vol. 122. DVS-Verlag Düsseldorf; 1989. p. 70−71.
[7] Vanzetti R, Dustoomian AS. Intelligence comes to laser soldering. Electronics July 1986:75−7.
[8] Meyer FG, Klimt BH. Laser soldering of surface mounted devices. In: Proc, SPIE; 1987. vol. 744, p. 8−90.
[9] Keeler R. Lasers for high-reliability soldering − for soldering military, computer, and other high-rel products lasers surpass mass-soldering methods. Electron Packag Prod 1987;27(10).
[10] Haag M, Brandner M. Diodenlaser-innovatives Werkzeug für die Produktion. In: Proc, laser opto; 2000. vol. 3.

[11] Bosse L, Koglin A, Olowinsky A, Kolauch V, Nover M. Laser beam soldering − an attractive alternative to conventional soldering technologies. In: Proc. SPIE; 2003. vol. 4977, p. 473−480.
[12] Bosse L, Gillner A, Poprawe R. Temperature controlled selective soldering with laser radiation. In: Proc. of the 6th international symp. on laser precision microfabrication; 2005.
[13] Bosse L, Schildecker A, Gillner A, Poprawe R. High quality laser beam soldering. Microsyst Technol 2002;7:215−9.
[14] Bosse L, Gillner A, Poprawe R. Adapted time-power profile for laser beam soldering with solder paste. In: Proc. SPIE; 2001. vol. 4406, p. 76−81.
[15] Britten S, Olowinsky A, Gillner A. Stress-minimized laser soldering of h-pattern multi-crystalline silicon solar cells. In: International conference on lasers in manufacturing (LiM); 2013.
[16] Ferstl M, Kratz C, Röder H, Hummelt C. Simultaneous laser soldering by the use of multi-beam optics. In: Conference "Advanced solid state lasers" (ASSL); 2013.
[17] Petring D, Polzin R, Becker M. Series in Optical Sciences. "Applications" in high power diode lasers, vol. 128. Springer; 2007. p. 285−533.
[18] Banse H, Beckert E, Eberhardt R, Stöckl W, Vogel J. Laser beam soldering − a new assembly technology for microoptical systems. Microsyst Technol February 2005; 11(2−3):186−93.

This page intentionally left blank

CHAPTER

Handling for Micro-manufacturing

27

Antonio J. Sánchez
Universitat Politècnica de València, Valencia, Spain

CHAPTER OUTLINE

Micromanufacturing Engineering and Technology. http://dx.doi.org/10.1016/B978-0-323-31149-6.00027-X

INTRODUCTION

Presently, a large number of industrial developments are being made for compact products. The trend toward miniaturizing products such as electronic, optical, and mechanical devices is motivating fundamental innovation in production processes. These compact products are composed of micro-components, which are fabricated using different kinds of micro-manufacturing machines. Therefore, a micro-manufacturing plant must be composed of different kinds of manufacturing machines, and several inspection, assembling, and packaging stations.

At a micro-manufacturing facility, the handling process includes transporting components from one location to another, orientation control, and sorting. It is essential that the components are presented in a specific position, are facing the right direction, and are at a suitable rate at all workstations. These points are the main objectives of a handling system. The aim of this chapter is to emphasize the importance of the handling process in micro-manufacturing, compared to conventional manufacturing at a meso-scale.

Several definitions can be found in the literature to characterize meso-handling and micro-handling domains. In this chapter, the following definitions have been adopted. Micro-handling is basically the manipulation of small parts with high accuracy. Typical part dimensions are in the range of micrometers up to a few millimeters. The typical location accuracy is in the range of $0.1-10\ \mu m$. Meso-handling is concerned with the transport and location of parts greater than a few millimeters (as a reference, the meso-domain is defined as products fitting in a box of $200 \times 200 \times 200\ mm^3$).

Automated positioning at the meso-scale is easily solved using conventional closed-loop control and a variety of sensors. In meso-handling, the main challenge concerns the picking of objects and the subsequent development of tools that are stiff enough to resist the effects of gravity and inertial forces. However, automated positioning at a micro-scale becomes a difficult problem. When the size of the components decreases, handling becomes the bottleneck in the fabrication process and the most expensive task, owing to automation difficulties. This is especially true for very small components that require very restricted positioning tolerances. The main handling challenges at an automated micro-manufacturing plant are (1) how to transport the micro-components between the different stations (intermachine transport problem) and (2) how to handle the micro-components at an intramachine station (intramachine micro-handling problem).

One key feature that characterizes micro-manufacturing facilities is the need to manipulate a large number of different micro-components. This chapter is focused on the serial pick-and-place approach. However, given that micro-fabrication processes can yield thousands of micro-parts, it is interesting to consider whether a large number of micro-parts can be handled simultaneously. This class of micro-handling is called the parallel approach [1].

SERIAL PICK-AND-PLACE TASK

The handling task of picking a part from #P location and placing it at #R location is called a "pick-and-place" task (see Figure 1). Serial micro-handling is a concept used in conjunction with a manipulator and a gripper, which must perform pick-and-place cycles for each object. A serial pick-and-place task is composed of the following subtasks:

1. Picking subtask
2. Hold and transport subtask
3. Placing subtask

Each subtask is composed of a sequence of actions. Consider the following list of possible actions for the pick-and-place task:

1. Grasp actions (close the gripper, set vacuum, etc.)
2. Move actions (approach, depart, transport, etc.)
3. Release actions (open the gripper, reset vacuum, vibrate, etc.)

The "move" actions will be performed by a manipulator and the "grasp" and "release" actions will be performed by a gripper, which will be based on different types of grasping principles (stick, friction, suction, magnetic, etc.).

The complete sequence of actions in a pick-and-place task is described in Table 1. The picking subtask includes the actions for grasping the part from #P location. The hold and transport subtask includes the actions to transport the part from #A to #B location. Finally, the placing subtask includes the actions to place the part at #R location.

This chapter provides an overview of the fundamentals of the micro-handling process, with particular reference to the serial pick-and-place task. After a brief description of intermachine transport systems, the principal requirements, methods, and components of intramachine micro-handling systems are presented. The chapter ends with a short discussion of different handling applications.

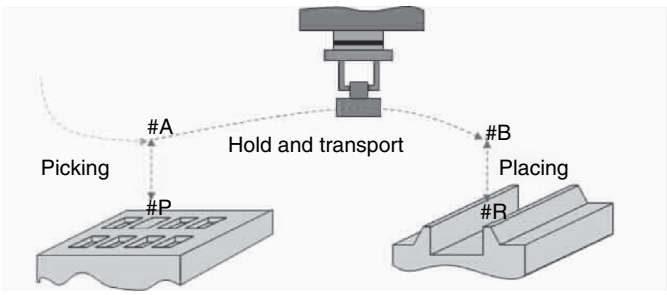

FIGURE 1

Pick-and-place task.

Table 1 Sequence of Actions in a Pick-and-Place Task

Subtask	Action	Velocity	Trajectory
Picking	**0.** Move to #A	100%	Joint space
	1. Approach to #P	30%	Cartesian space
	2. Grasp	0%	Cartesian space
	3. Depart to #A	70%	Cartesian space
Hold and transport	**4.** Transport to #B	100%	Joint space
Placing	**5.** Approach to #R	30%	Cartesian space
	6. Release	0%	Cartesian space
	7. Depart to #B	70%	Cartesian space

INTERMACHINE TRANSPORT SYSTEMS

The evolution of new types of micro-components has contributed to an inefficient proliferation of separate, and sometimes even unique special purpose machines. For example, the use of specialized stand-alone equipment for assembling, inspection, packaging, etc., inherently requires multiple queuing steps for each machine as well as returning the components to an interim packaging mode between stations.

A flexible and automated transport system must be integrated in a fully automated micro-manufacturing facility. In any multitask automation system, the need to simultaneously perform operations with different time cycles presents a difficult challenge. It is also important to build flexibility into multifunction stations to accommodate variations in overall production requirements. Some automation approaches include rotary turret architectures and linear pick-and-place architectures based on carriers.

Rotary dial indexers are well established in the industry for their efficiency, flexibility, and ability to deliver high-speed performance. These systems generally use central, high-accuracy, direct drive indexing to synchronize a number of operations nested around the circumference of the dial. Rotary turret system designs offer a simple, rugged-core mechanism that can be used for integrating a variety of assembling, inspection, and other processing operations on individual stations around the periphery of the rotary indexer platform. Some of the primary advantages of rotary-indexed architectures are simplicity, precision, reliability, durability, and high throughput within a relatively small footprint.

Although rotary turret architectures generally provide the most efficient approach for the high-speed integration of most applications, linear pick-and-place architectures can also be the best choice for certain applications. For example, systems that process parts from carrier-to-carrier or carrier-to-tape often can benefit from using a linear pick-and-place strategy instead of rotary turret architecture. The use of carriers throughout the stations makes it most efficient and appropriate to feed the machines directly from carriers (see Figure 2). By combining advanced

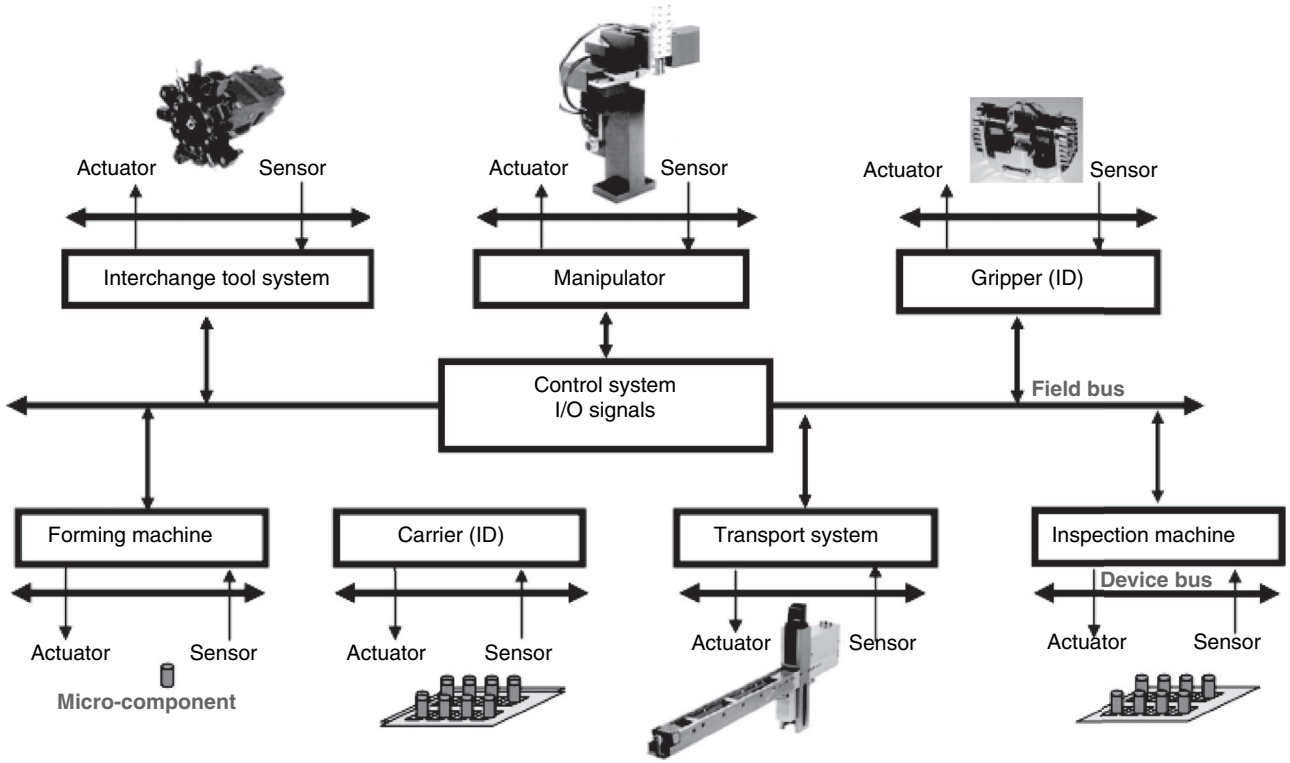

FIGURE 2

Linear pick-and-place concept based on carriers.

carrier-scan techniques with multihead pick-and-place systems, linear architecture can deliver a balanced combination of flexibility and speed that fits smoothly into carrier-oriented production-floor operations.

STANDARD CARRIERS

A key problem area limiting the emergence of automated micro-handling technology is the lack of standardization, which causes equipment makers to spend an excessive amount of time and resources on custom automation solutions [2,3].

A carrier or tray is a flat magazine that can take up pieces for storage, transport, and handling in an orderly manner and is adaptable to automatic piece feeding to the production equipment.

A cassette or cartridge is a container for carriers, which can be plugged into production equipment for the purpose of automatic feeding.

There are some standards defined for micro-handling issues. However, many standardized systems are available in the semiconductor industry, where some examples are given below:

1. **Trays:** standardized plastic carriers (2 or 4 inches) (50.8 or 101.6 mm) with depressions for the individual placement of components. The parts move freely within the limits of these depressions. Manufacturers offer standard-sized depressions in a range of variations. To protect the components, the trays are closed with a lid with accompanying retaining clips.
2. **Gel packs:** components are held by adhesion to glass or plastic carrying materials with gel coatings. Gels with different levels of adhesive strength are available depending on the sizes of the components.
3. **Belt magazines:** a belt magazine has a band made with depressions into which the component is locked by a covering layer of foil. For small pieces, plated and embossed belts are available to enclose the components.
4. **Tube magazines:** in the case of tube magazines, the components are either stacked or lined up. The lengths of the tubes, which are made of plastic, are shaped like the components themselves, thus preventing the components from becoming distorted.

In general, a dimensionally specific carrier is well suited for large volume production, where changes of micro-component types are not frequent.

CONVENTIONAL TRANSPORT EQUIPMENT

Conventional transport equipment such as stockers, vehicles, conveyors, manipulators, indexers, and lifters are used for transporting materials, components, and tools between the different stations in a linear pick-and-place plant based on carriers.

Conveyors usually consist of a looped belt or chain moving along a predetermined path. Instead of conveyors, vehicles could be more flexible and easier to adapt

to changes in the environment. Both conveyors and vehicles are used to transport the carriers and cassettes between the different stations. Some examples of transport equipment are a person-guided vehicle (PGV), an overhead hoist transport (OHT), a rail-guided vehicle (RGV), and an autonomous-guided vehicle (AGV).

1. An OHT is a conveyor suspended from the ceiling that loads/unloads carriers or cassettes.
2. An AGV is a trackless mobile robot typically with a single gripper, a single manipulator, and two buffers. A buffer refers to a place on the vehicle where one or two carriers can be placed. Loading/unloading of carriers and transfer between two carriers can be performed.
3. An RGV is a rail-guided mobile robot of which there are several types with various numbers of grippers, manipulators, and buffers.
4. Finally, a PGV is a person-guided vehicle. There are several types of vehicle, as with the RGV.

Other components such as optical character recognition, ionization units, carrier ID, or light curtains are occasionally added, based on system requirements.

INTRAMACHINE MICRO-HANDLING SYSTEMS

A key problem area limiting the emergence of automated micro-handling technology is the nonavailability of flexible and highly precise micro-handling machinery [2].

The most significant difference between meso- and micro-handling is the required positional accuracy of automatic handling systems. Micro-handling often requires submicron precision. This degree of precision is beyond the calibration range of the normal open-loop precision handling devices used in industry. Closed-loop strategies, such as real-time vision feedback, are required to compensate for poor kinematic models and thermal effects. Additionally, in micro-handling, the structural vibration due to link flexibility must be controlled at a submicron level.

Another major difference between handling in the meso- and micro-domains is the mechanics of object interactions. People usually think in meso-scale terms, but when talking about handling methods at the micro-scale, gravity and inertial forces cannot be considered the main forces being applied to the part. In the micro-world, surface forces dominate due to scaling effects, and the mechanics of manipulation can be unpredictable. For example, when a gripper opens, the part may not drop downward.

Finally, it is necessary to emphasize that micro-handling requires greater care in manipulation and in cleanliness because the micro-parts are very fragile. Usually it is mandatory to control the grasping forces and to work under clean room conditions.

Since micro-scale positioning becomes a difficult problem, manual micro-handling is the most commonly used method. In this case, micro-handling tasks are carried out by operators, who position and align objects manually in a specific

station. The application of teleoperating micro-handling, which transforms the human operator's hand motion by means of a joystick into the finer 3D motion of the system's manipulator systems, is normally tailored to specific complex tasks. Finally, an automated serial pick-and-place task is only applied to micro-parts, which can be handled and released using a well-suited gripper.

A micro-handling system is composed of the following subsystems:

1. Micro-part feeder subsystems;
2. Fixture and gripper subsystems;
3. Sensor and control subsystems.

SIGNIFICANT FORCES AT THE MICRO-SCALE

In micro-handling, surface forces such as friction or adhesion are immensely more significant than in meso-handling. Therefore at the micro-scale (masses $<10^{-6}$ kg), gravity forces are not significant compared to surface forces, and releasing an object becomes a real challenge due to adhesion between the micro-part and the tool (see Figure 3).

Formally, a force is defined to be short range if it decreases with distance quicker than d^{-n}, where n is the dimensionality of the system (usually 3). Short-range interactions are commonly dealt with by imposing a cutoff to the potential $V(d)$, d_c, beyond which $V(d)$ is set to 0. On the other hand, long-range forces have a range of infinity.

Intermolecular and surface force interactions are classified into several categories. The first category includes long-range attractive interactions that bring particles to surfaces and establish adhesive contact. These forces include van der Waals, electrostatic, and magnetic forces. The second category of forces is focused on

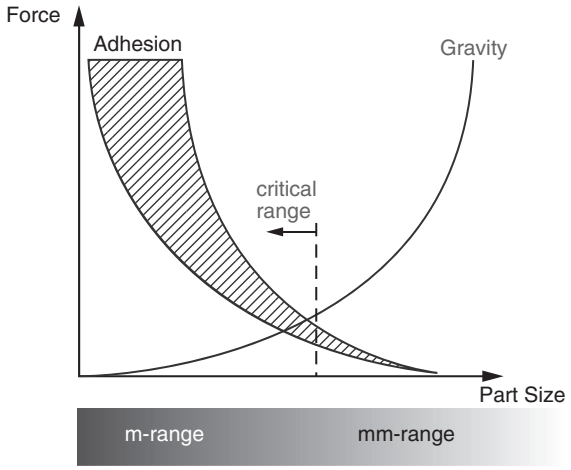

FIGURE 3

Significant forces depending on part size.

adhesion, including diffusion, condensation, diffusive mixing, mutual dissolution, liquid and solid bridges between particles and surfaces, and capillary forces. The third category includes very short-range interactions that can contribute to adhesion only after an adhesive contact area has been established. These forces include chemical bonds, intermediate bonds, and hydrogen bonds.

Balancing these forces depends on environment conditions, such as humidity and temperature, the surface condition, material properties, geometry, and relative motion. Micro-handling is quite different from meso-object manipulation. To manipulate micro-objects, one must consider micro-physics and pay attention to environmental conditions.

There are three main adhesive forces that are important for handling micro-parts: van der Waals, capillary, and electrostatic forces [4]. van der Waals forces come from intermolecular potentials and are always present. Capillary or surface tension forces depend on the humidity of the environment, and electrostatic forces are due to the triboelectrical phenomenon. Much work has been done by several authors, who have presented the principles of van der Waals forces, surface tension forces, and electrostatic forces [5,6]. Some authors have described numerical methods to compute the van der Waals force between a smooth sphere and a smooth rectangular block [7] or to compare capillary effects with surface tension forces [8]. However, micro-parts have different shapes with considerable surface roughness and often show large deformation in the contact region. As a consequence, theoretical predictions are rarely applicable in practice.

In order to improve micro-part manipulation, different strategies have been set up to deal with these surface forces [7,9]. First, the effects of surface forces, F_{adhesion}, can be reduced by choosing an adapted set of manipulation parameters. This can, for example, be done by changing the coating. Surface tension effects can be reduced with hydrophobic coatings, electrostatic forces by using conductive materials, and van der Waals forces by increasing the roughness profile.

MICRO-PART FEEDERS

A micro-part feeder always uses a certain number of functions to ensure the perfect treatment of a micro-part at the workstation. These functions are to index; extract (isolate, disentangle, separate); sort; turn over; locate; guide; move; load/unload; release/seize; and recognize a micro-component. Micro-part feeders, which singularize and orientate parts prior to the station processes, are a significant bottleneck in successful automation.

The basic kinds of part feeding, which are designed to feed and to orient the micro-parts, may be classified as follows:

1. Mechanical feeders;
2. Manipulator-based part feeders.

Mechanical feeders

Commonly used mechanical feeders for micro-handling are vibratory bowl feeders and tape-and-reel systems.

The most common approach to automated feeding is the vibratory bowl feeder, which consists of a bowl filled with parts guided by a mechanical track. The bowl and track are made to vibrate, causing parts to move on the track, where they encounter a sequence of mechanical devices such as grooves, gaps, balconies, etc. Most of these devices are filters that reject parts in all orientations except for the desired one. Thus a stream of oriented parts emerges at the end after successfully running the full track.

Another particular form of mechanical feeder is known as tape-and-reel for feeding parts of relatively small sizes, which can be placed on tapes of standard width. Tape-and-reel is a method of housing parts in separate cavities in a long continuous strip. The cavities are covered with a plastic sheet to facilitate winding the strip around a reel for component presentation or feeding to automated placement equipment. These particular mechanical feeders are based on standard belt or tube magazines.

For large volume manufacturing, the employment of a dedicated mechanical part feeding apparatus may be justified. However, mechanical feeders often fail due to jamming and, most significantly, generally require retooling when a micro-component is changed.

Manipulator-based part feeders

Another common feeding concept is the use of a specially designed carrier for each micro-part family to maintain sufficient accuracy for a completely preprogrammed manipulator. In this case, the manipulator will perform a serial pick-and-place task using a specific gripper mounted on the manipulator.

Conventional manipulators do not meet the repeatability and accuracy requirements needed in the micro-world because joint backlash, temperature drift, and structural vibration must be controlled at the submicron level.

The state-of-the-art of precision industrial manipulators is summarized in Table 2. This table shows the most important parameters of the workspace, the accuracy, the velocity, and the load capacity of different manipulators. The most common configurations are SCARA (RRP) and Cartesian (PPP) manipulators, but other configurations are also available. There are important differences in degrees of freedom (DOF), accuracy, workspace, and load. The most accurate manipulators have reduced speeds. Cartesian manipulators are usually slower than SCARA-type robots, but have greater precision.

Micro-handling flexibility would denote that different products with similar scales and complexity levels are handled at the same station without any hardware modifications, but with software changes. Although there are technological and economic limitations to reach in such a goal, shorter product life and constant product changes demand greater flexibility in the handling process. The most common principle for achieving flexibility is vision-based flexible part feeding, which is a concept used in conjunction with a manipulator, whereby the manipulator uses a vision system to locate micro-parts that can be randomly scattered on a conveyor belt. Randomly oriented parts have to be positively identified and accurately located everywhere within the camera's field of view.

Table 2 Some State-of-the-Art Industrial Micro-manipulators

Model	By	Type	DOFS	Rep. Acc. (um)	WS (mm)	Load (kg)	Speed (mm/s)
E2C	Epson	SCARA	4	8	R250 Z100	5	P&P[{(br)}]0.39 s
RP-1AH	Mitsubishi	SCARA	4	±5	150 × 105 × 25	1	400[{(br)}]P&P 0.28 s
YK-120X[{(br)}]YK-150X	Yamaha	SCARA	4	5–10	R110 Z30	0.5	700–2000[{(br)}] P&P < 300
Tusboscara[{(br)}] SR4-Plus	Bosch	SCARA	4	±50	R400 Z200	2	1600
Autoplace 400	Sysmelec	Cart	4	±2.5	150 × 150 × 150 [{(br)}]85 × 85 × 75	4	
MP63-25DC	Feinmess	Cart	3	5	25 × 25 × 25	2	5
MP84	Feinmess	Cart	3	3	25 × 25 × 25[{(br)}] 100 × 100 × 100	1.5	250
1940	Kopf	Cart	3	1	128 × 128 × 128		
MM3A	Kleindiek	RRR [{(br)}](antr)	3	1	100 cm^3[{(br)}]z:12 x,y:180°		10
Klocke	Nanomanip	RRP [{(br)}](spher)	3	0.001	5 × 5 × 19		5
MRSI							
Exfo	PCS-4100	RPPPR	5	0.4	25 × 25 × 25		2
Semprex	Univ. pipette manipulator	PPPRPP	6		75 × 33 × 25[{(br)}] 95° 75,200		
Somapatch	MW3R/L	CART	3	0.25	5 × 5 × 5		
MRSI	Newport	PPPR	4	±10	415 × 415		9000

The cost and performance of a micro-handling system can be significantly improved by carefully considering issues at multiple scales: precision, compliance, modeling, gripping, fixturing, tolerance, and control. One of the basic challenges in precision handling is the need for very high accuracy over a large range of motion. This fact involves the design of handling tools and processes at multiple scales, and their integration into coherent system architectures. One possible approach to micro-handling systems is to improve the performance of standard manipulator systems. A conventional robot for coarse motion with low accuracy but long traveling distance is used and there is a fine positioning device between the end effector and the robot with high accuracy and a very small traveling distance.

Existing solutions have the common feature of being expensive and bulky. Due to their dimensions, they are sensitive to environmental perturbations such as vibrations or temperature drifts. A general trend is to reduce manipulator size. The aim is to improve the system's immunity to environmental perturbations such as vibrations and thermal drifts. The development of such robots is now being made possible by new technologies, in particular, by zero-backlash micro-gears and highly dynamic micro-motors with integrated incremental encoders, which allow manipulator structures to be miniaturized.

FIXTURES AND GRIPPERS

Fixtures are used to hold micro-components during machining, inspection, and assembly processes. The use of precision fixtures can mitigate the need for high positional accuracy. V-groove structures, datum points, or other minimum energy surfaces should be used as much as possible to guide the micro-parts into their desired positions and orientations.

Micro-grippers are used to grasp, hold, and release micro-components during the handling process. Compliance analysis of micro-handling, including both the gripper and the micro-part, is critical for reducing the necessary positional accuracy of the system, and therefore the cost. The handling system need not require the same precision as the tolerance of the locations if proper use is made of compliance, gripping, and fixturing.

Grasping principles

A grasping principle is the physical principle that produces the necessary force to get and maintain a part in a position with respect to the gripper. Some grasping principles are well known in the meso-domain: friction-based gripping [10], form-closed gripping [11], suction-based gripping [12,13], and magnetic gripping.

Other principles, based on adhesive forces, are particularly applicable in the micro-domain [14]. One example is the use of electrostatics, or the charge difference between the gripper and the part [15–17]. For small, low-weight parts, the capillary force and the surface tension of a liquid between the gripper and the part can be sufficient to hold the part [18,19]. van der Waals force is another grasping principle [20]. Cryogenic gripping means that a small amount of liquid is frozen between the

gripper and the part, so that the adhesive property of ice produces the required force. To release the part, the frozen material is broken, and/or molten, and evaporated [21]. Ultrasonic pressure waves can also be used to lift a part. Since these forces are small, only extremely light parts can be handled in this way [22]. A focused light source, for example, a laser source, can produce a pressure that is sufficient to lift small parts. To compensate for the mass of the part, the operation may take place in a liquid [23,24]. The Bernoulli effect has also been demonstrated to be applicable for raising small parts; an airflow between gripper and part causing a force, which brings the gripper and the part close together.

Grasping requirements

Some grasping principles can only be applied when the environment in which the operation takes place meets certain demands, or, the other way around, the environment puts constraints on the selection of the grasping principle. In some cases, conditioned environments are applied. Micro-handling may, for instance, take place in clean environments, in dry environments, or in a vacuum. The substrate is important because adhesive forces occur between both the part and the gripper and also between the part and the substrate. One possible attractive alternative is to manipulate parts while they are immersed in a fluid, which eliminates electrostatic and surface tension effects. Fluidic transport provides a powerful means for handling components in many micro-systems and is increasingly being employed in a number of such applications.

Some grasping principles put constraints on the type of material that can be gripped. Where appropriate, the material type of the top layer, a coating, for example, must be considered. Adding coatings to parts is a possibility that enables the application of a grasping principle, which could not have been applied otherwise. Some examples of the relation between the grasping principle and the material type are (1) the hydrophilic properties of the material are important for the application of adhesive gripping; (2) gripping using magnetism demands ferromagnetic materials.

The interaction between the gripper and the part takes place via the part's force interaction surface. This surface must be available for force operation throughout the entire pick-and-place cycle, for example, from picking up a part at a feeding position through to releasing the part in the final position. Technical executions of grasping principles demand a certain configuration and shape of the force interaction surface. Friction-based gripping will demand at least two locations on the side of the part for finger placement. Several other principles only demand one accessible part surface. In developing a grasping solution, it should be noted that geometric constraints may impose limitations on the availability of part surfaces.

In the case of a contact-grasping principle, one possible situation that may occur during the release procedure is that the part may stick to the gripper and not remain static during the release action. In this case, F_{adhesion} is greater than F_{gravity} (see Figure 4). This situation would require a device that would hold the part in place during the gripper-release procedure. Such devices do not have to be complicated to design; one common method to overcome this problem is to use sticky paper with an adhesive force slightly greater than that of the adhesive force acting on the part and gripper.

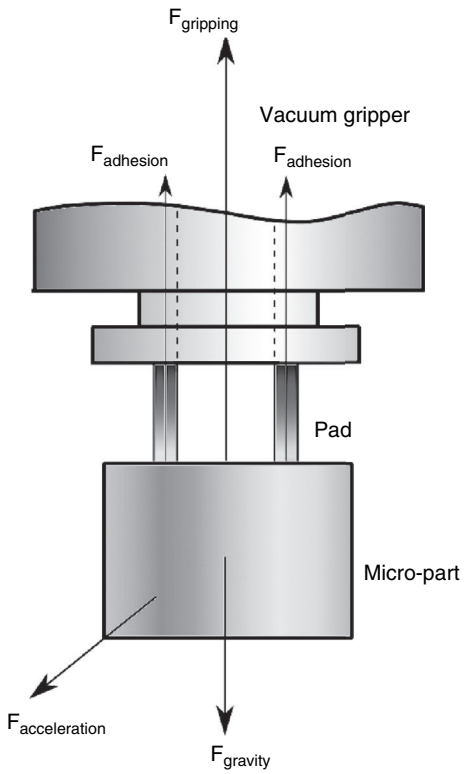

FIGURE 4

Force vectors in a contact-handling principle.

Grippers

Suction grippers, such as vacuum grippers, consist mainly of a thin tube or pipette connected to a vacuum pump. This makes this kind of gripper cheap and easy to replace. This is important since micro-tools are fragile and have to be replaced frequently. The disadvantage is that the vacuum gripper can obviously not be employed in a vacuum.

Tong grippers grasp a part employing friction between the part and the gripper, usually implemented using a pair of fingers. Gripping parts based on friction certainly provide sufficient force in many cases. Another advantage of this kind of gripper is the ability to center the part between the gripping jaws and to align it parallel to the jaws. This allows more precise handling of micro-parts by putting them in a defined location after being gripped. This is an important attribute in a handling system with a high degree of accuracy and speed. The more reference points that can be applied to the location of the micro-part, the fewer sensors that will be needed to determine the same information. However, with decreasing part

size, the parameters of the gripper-finger dimensions need to be small also. Here, a technical problem may occur with this method having to be eliminated due to technical or cost perspectives.

Adhesive grippers utilize the surface forces discussed earlier. The easiest force to control is the electrostatic force, but it is not suitable for the manipulation of charge-sensitive devices. Surface tension forces due to air humidity can be controlled by incorporating a micro-heater in the gripper. In cold conditions, an object can be picked up simply by touching it. To release the object, the heater evaporates the water in the contact. Common manipulation methods with surface forces include vibration of the gripper, sliding and inclining tools, or using dual manipulators.

The disadvantage of contact strategies is that friction between the tool and the part may generate micro-dust from the object. Contactless grippers have several advantages compared to conventional contact grippers. A homogeneously distributed force enables the sensitive gripping of fragile parts. Disadvantages include low flexibility for different part shapes and the need for additional equipment, such as ultrasonic sources and pressure supplies. Contactless grippers include air-cushion grippers and ultrasound levitation.

The principle of an air-cushion gripper is based on a vacuum prestressed air bearing. The gripper includes several arrays of pressure and vacuum nozzles. These create an air cushion, separating the gripper and the micro-part, which is levitated about 10 μm underneath the gripper. The weight of the part has to be in equilibrium with the pushing and pulling forces exerted by the air cushion.

Another contactless gripping method is ultrasound levitation, which is based on a squeeze film or acoustic standing waves. Parts can be picked from above by the combination of ultrasonic waves and vacuum. The vacuum forces the parts to the gripper surface. The air cushion generated by the high-frequency oscillation of the ultrasound sonotrode produces a repulsive force on the part. Finally, there is balancing of these two forces and the weight of the handled part. A further phenomenon that can be used for handling parts without contact is levitation based on acoustic standing waves. The arrangement consists of a reflector and a vibrating sonotrode, the assembly being called a resonator. The distance between the two elements is an integer multiple of half the wavelength. In the resonator, small parts are levitated in the pressure nodes of the standing wave.

SENSORS AND CONTROL SYSTEMS

Obtaining accurate sensor information is difficult at a micro-scale as sensors can be too large to be placed in a tiny environment. The main sensors used at a micro-scale are displacement, vision, and force sensors because motion control, visual servoing, and force control strategies are often required at micro-domains. These sensors have to be extremely sensitive as the forces and displacements involved are very small. Thus, to enable micro-manipulation, miniature sensitive sensors are needed.

Vision sensors

Vision systems are often used for the recognition and positioning processes to locate the individual micro-components. The camera resolution must be compatible with the size of the manipulated objects. Optical microscopes and scanning electron microscopes are therefore used. Applications in confined spaces require compact camera systems such as fiberscopes or micro-cameras.

In a meso-domain, visually servoing has been shown to effectively compensate for uncertainty in the calibration of camera lens systems, manipulators, and workspaces. However, manufacturing engineers usually prefer strongly calibrated parts-handling systems due to cost and reliability issues. In micro-domains, precise calibration is highly dependent on precisely modeled kinematics, which is subject to thermal growth errors. Two common techniques for compensating thermal errors include the use of expensive cooling systems, or waiting several hours for the thermal equilibrium of the device to stabilize. These types of factors greatly affect the cost and reliability of handling systems, therefore real-time visual feedback can be used effectively and economically in a micro-domain. However, there are problems with visual control or image processing in controlling these systems. Some of the main problems are low processing speeds, high costs, programing difficulties, and being error prone due to glare, reflection, and other unwanted contaminants. Moreover, the manipulation tools may obstruct the view. Additionally, it is important to emphasize the problems in setting up image-processing equipment and the long downtimes that are involved if an error occurs. Even processes that may seem straightforward such as focusing and aligning the camera properly become complicated and extremely difficult to carry out at these micro-scales.

In micro-handling, structural vibrations due to link flexibility must be controlled at the submicron level. Control of machine vibration becomes very important as designers attempt to advance the state-of-the-art with faster and lighter machines. Many researchers have examined different controller configurations in order to control machines without exciting resonances. Even with a sophisticated controller it is difficult to rapidly move flexible machines without deflections and vibrations. A more achievable goal is to eliminate residual vibration once the machine has achieved a desired set point. Input shaping is a command-generation technique that reduces residual vibration when a machine is moved from one set point to another. Input shaping works like a notch filter that is designed to eliminate decaying sinusoidal responses.

Micro-force sensors

A typical micro-force sensor structure is fabricated by micro-machining technology on a silicon wafer. A diode sensor has a cold-field emission cathode, which is a sharp silicon tip, and a movable diaphragm anode. When a positive potential difference is applied between the tip and the anode, an electric field is generated, which allows electrons to tunnel from inside the cathode to the vacuum. The field strength at the tip and the quantity of electrons emitted (emission current) are controlled by

the anode potential. When an external force is applied, the anode deflects and changes the field and the emission current.

Impedance control is a strategy adequate for both free motion and constrained motion control. It consists of an imposition of behavior on the system rather than tracking a reference value. Mechanical impedance is the dynamic relation between a force acting on a body and its motion:

$$Z(s) = F(s)/v(s) = M(s) + B(K/s)$$

where Z is the impedance, F is the force, v is the velocity, M is the mass, B is the damping, and K is the stiffness of the system.

Opposition of the body to the force consists of its stiffness, viscous damping, and mass. The function of the impedance control is to impose the desired values for these three parameters instead of the real values.

APPLICATIONS

The serial pick-and-place task has been used extensively in the micro-manufacturing industry. There are specific pick-and-place machines used for placing micro-components. The aim of this section is to show a few examples of handling applications, which may refer to different kinds of processes, for example, in micro-fabrication, inspection, and assembly.

MICRO-FABRICATION

The main intramachine micro-handling task in a micro-fabrication station is the packaging of the fabricated micro-parts into a standard carrier.

INTRAMACHINE HANDLING SYSTEM IN A MICRO-FORMING APPLICATION

This example consists of the design of a micro-handling system, which arranges the micro-parts produced by a bulk-forming machine into a standard carrier [25,26].

The forming machine is set in a specific location and will leave the micro-pieces in an output buffer. This buffer guides the micro-parts along a mechanical track, like a vibratory bowl feeder system. A vision control strategy for actuating on the vibration will allow the individual micro-parts to flow in order to synchronize the buffer release process with the load process into the carrier cells.

The carrier has been defined following the DIN-32561 standard. This carrier is a small tray able to store hundreds of small pieces on it (see Figure 5). The shape of the cells for locating the pieces depends on the piece shape. An empty carrier will be attached to a 2-DOF manipulator, which will move the carrier under the vibration subsystem, so that the empty cells in it are exactly below the buffer output, permitting the pieces to fall into them. The vision system indicates to the manipulator when a micro-part is into the cell to proceed to locate the next empty cell.

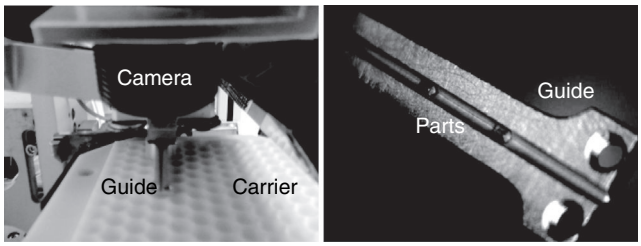

FIGURE 5

Vibration subsystem details.

When the carrier is full, the 2-DOF manipulator will move it to a specific location where the unload subsystem will take the carrier and put it into a cassette. The load subsystem will take another empty carrier and load it on the manipulator.

INSPECTION

Usually component inspection requires different points of view. A micro-handling system can be used to obtain all the views required for a complete inspection. For example, a rotational movement can be used for inspecting cylindrical surfaces.

Stent inspection system

A cardiovascular stent is a small, expandable, slotted, metal tube that acts like a mechanical scaffold in an artery. Cardiovascular stents have hundreds of critical features with tight tolerances. These stents require 100% inspection over all surfaces.

Stent inspection has been traditionally accomplished by manually operated stereomicroscopy. The typical drawbacks of inspecting cylindrical surfaces with this method are nonreferenced fields of view and the focal depths of stereomicroscopes, which increase operator fatigue and error. Often parts are rotated under the microscope while the operator is looking from checkpoint to checkpoint.

Nowadays the quality control of stents is made by an automatic visual inspection system but the handling process is usually manual. In the sampling plant, the stent is inside a plastic tube, which protects it throughout the process. This tube is also useful for identifying one stent from the others. An operator manually extracts the stent from the plastic tube and inserts it into a needle. The operator fixes the needle on a rotary gripping system in front of a vision system, and then the system rotates the needle while the vision system scans the stent surface. Once the automated inspection has been done, the operator removes the needle and extracts the stent from it, puts the stent into the tube again and screws its top on.

The aim of this example is to describe a stent quality control application without human intervention. In this application, all the manipulation is done by a 6-DOF manipulator. The whole handling system is composed of different subsystems (carriers, unscrewing/screwing gripper, manipulator, funnel system, rotating disk, insertion pin).

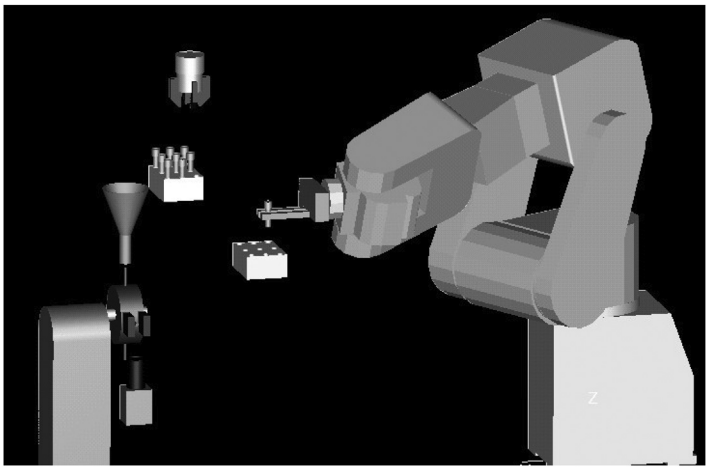

FIGURE 6

Stent inspection concept.

The intermachine transport system consists of a linear pick-and-place architecture based on carriers. The tube arrives in a carrier that is able to transport nine tubes (Figure 6). This carrier approaches the inspection station on a powered belt conveyor. The manipulation process is divided into the following parts:

1. **Picking:** the manipulator picks the plastic tube from the carrier.
2. **Unscrewing:** the manipulator carries the tube to the unscrewing/screwing gripper and removes the screwed cap.
3. **Extraction:** the manipulator transports the uncapped tube to the funnel zone and empties its content (the stent).
4. **Gripping:** the funnel guides the stent to a vertical pin on the rotating disk, where it is inserted by gravity and vibration principles. A piezoelectric system mounted on the pin holds the stent.
5. **Inspection:** the pin is rotated to the horizontal inspection zone. There is a horizontal position to perform the machine vision quality control.
6. **Collection:** the pin carrying the analyzed stent is transported to the collection position, where the stent is released and put into the tube.
7. **Screwing:** the tube with the stent is taken to the unscrewing/screwing gripper where its cap is located and then screwed on.
8. **Placing:** the tube is placed in a new carrier.

The first task must be the opening of the tube. This must be done by a rotating four-fingered gripper. The fingers of the gripper are developed in order to accurately grip the top of the transporting tube.

A 6-DOF manipulator is needed, in order to be able to move the tube around the working area. A FANUC manipulator (LR Mate 200iB model), which is a six-axis,

modular construction, AC electric servo-driven robot, is used. It is optimized for operations in sensitive, contamination-controlled environments and occupies minimal floor space. It provides high throughput, industry-leading reliability, and sophisticated motion control for part handling. It can move along three-dimensional curved paths and approach any position from virtually any direction.

The stent is very fragile, but is heavy enough to be subject to the effects of gravity. If the stent is allowed to fall into the pin vertically, it is possible to feed the pin without problems. In any case, this process must be done with extreme accuracy because subjecting the stent to a little stress renders it useless. Therefore a rotating disc can be used to locate a pin in the vertical position to load the stent, after which the disc rotates the pin to a horizontal location to perform the inspection of the stent surface and finally, the disc rotates the pin to the unload vertical position to release the stent.

ASSEMBLY

Micro-handling and micro-assembly are closely linked topics because several positioning movements are always involved in micro-assembly processes.

Optical fiber communication systems are increasing because of the demand for large-capacity and high-speed data transmission on local area networks. With the growth in optical fiber communications, fiber alignment has become a key production process because its efficiency greatly influences the overall production rates for the optoelectric products used in optical fiber communications. Fiber alignment is necessary when two optical fibers are connected, when an optical fiber is connected to a photodiode or a light emission diode, and when an optical fiber array is connected to an optical waveguide (Figure 7). Connecting optical fibers is difficult because the connecting edges should be aligned with submicrometer resolution. Therefore, it is time consuming even for human experts.

Active optical fiber alignment

The technique for aligning the optical fiber to maximize optical coupling efficiency while monitoring the signals, in respect of the amount of light coupled to the input fiber, is known as active alignment. This widely adopted method consists of rough and fine searches. In the rough search, a coordinate where the coupled light is maximized is found approximately. In the fine search, a peak coordinate is strictly identified to the order of submicrons. More specifically, in the rough search, a scan is made in a zigzag or spiral manner. In the fine search, a cross-scan is repeated around the (coarse search) coordinate showing a maximum amount of coupled light, to seek a new coordinate showing a maximum amount of coupled light. The fiber alignment ends when the distance between the newly found coordinate showing a maximum amount of coupled light and the previous coordinate showing a maximum amount of light converge to less than a given value.

In this application, a precision manipulator is needed in order to move the optical fibers while monitoring the signals during the automated alignment process.

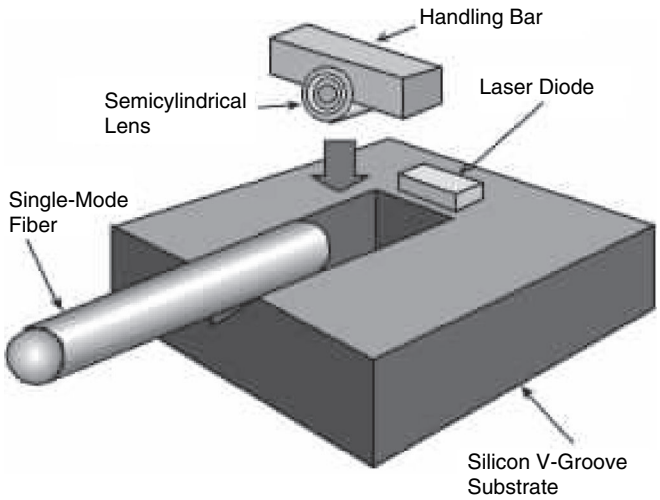

FIGURE 7

Optical fiber alignment.

CONCLUSIONS

A review of existing systems for handling of micro-parts was carried out in this chapter. A key problem area limiting the emergence of micro-handling technology is the nonavailability of flexible, highly precise, micro-handling machinery.

Due to the increasing number of topics related to MEMS, some standards for automated gripping and handling of micro-parts have arisen. Irrespectively, the standardization of these micro-systems is quite new, so there are few standards defined at this moment. For example, to deal with different part sizes, an automated interchange tool system can be used (DIN 32565). This norm is the result of the work committee "NAFuO." It specifies requirements of a mechanical interface between an end effector and a handling device for micro-systems.

The combination of different grip principles in the same gripper is recommended to increase flexibility. Additionally, sensors mounted on smart grippers can help to compensate for inaccuracies in part gripper relations. Machine vision is a widespread technology for high precision handling of parts in industrial environments. In micro-scale, machine vision can be used to "see" exactly what it is going in the working place and to "actuate" in consequence. With dedicated algorithms, the features of an object in the image can be extracted for robot localization and control. For the latter, a real-time processing of images is a crucial issue.

Compliance analysis of micro-handling, including both gripper and part is critical for reducing the necessary positional accuracy of the system, and therefore the cost. The handling system need not require the same precision as the tolerance of the locations if a proper use of positioning, sensing, modeling, and control tools is

made. The use of precision fixtures can mitigate the need for high positional accuracy. V-groove structures, datum points, or other minimum energy surfaces should be used as much as possible to guide the micro-parts into desired positions and orientations.

The following are key areas of the research in micro-handling systems:

- "Contactless" and smart micro-grippers;
- Modeling of micro-assembly processes using molecular dynamics simulation;
- High-resolution micro-feeding techniques;
- Plug and produce micro-assembly modules (control and hardware integration);
- Integration of automated assembly processes applicable to "super clean room."

ACKNOWLEDGMENTS

This work was financially supported by the European Community FEDER funds and European Community research funds (MASMICRO, Project number 500095-2). The authors also would like to thank the R&D&I Linguistic Assistance Office at the "Universidad Politècnica de València."

REFERENCES

[1] Bohringer KF, Fearing RS, Goldberg KY. Microassembly, the handbook of industrial robotics. In: Shimon YN, editor. 2nd ed. John Wiley & Sons; February 1999. p. 1045–66.
[2] Sanchez AJ, Lopez R, Gunman R, Ricolfe C. Recent development in micro-handling systems for micro-manufacturing. J Mater Process Technol 2005;167(22):499–507.
[3] Sanchez AJ, Lopez R, Gunman R, Ricolfe C. An inter-machine material handling system for micro-manufacturing based on using a standard carrier. Int J Adv Manuf Technol 2010;47(9–12):937–43.
[4] Israelachvili J. Intermolecular & surface forces. 2nd ed. Academic Press Ltd; 1992.
[5] Bowling RA. A theoretical review of particle adhesion. In: Mittal KL, editor. Particles on surfaces I: detection, adhesion, and removal. New York: Plenum; 1988. p. 129–55.
[6] Fearing RS. Survey of sticking effects for micro parts handling. In: Proc. IEEE-RSJ intelligent robots and systems; August 3–5, 1995. Pittsburgh, PA.
[7] Feddema JT, Xavier P, Brown R. Micro-assembly planning with Van Der Waals force. In: Proceedings of the 1999 IEEE international symposium on assembly and task planning; July 1999. p. 32–8. Porto, Portugal.
[8] de Lazzer A, Dreyer M, Rath HJ. Particle-surface capillary forces. Langmuir 1999;15: 4551–9.
[9] Arai F, Ando D, Fukuda T, Nonoda Y, Oota T. Micro manipulation based on micro physics – strategy based on attractive force reduction and stress measurement in Proc. IEEE/RSJ 1995;2:236–41.
[10] Kohl M, Krevet B, Just E. SMA microgripper system. Sens Actuators A 2002;97–98: 646–52.
[11] Ok J, Chu M, Kim C-J. Pneumatically driven microcage for micro-objects in biological liquid. IEEE MEMS 1999;459–63.

[12] Zesch W, Brunner M, Weber A. Vacuum tool for handling micro-objects with a Nano-Robot. In: IEEE int. conf. on robotics and automation, vol. 2. April 20−25, 1997. p. 1761−6.
[13] Petrovic D, Popovic G, Chatzitheodoridis E, Del Medico O, Almansa A, Sümecz F, et al. Gripping tools for handling and assembly of microcomponents. In: Proc. 23rd international conference on microelectronics, vol. 1. May 2002. p. 247−50.
[14] Rollot Y, Régnier S. Micromanipulation par adhésion. Nano et Micro Technologies 2000;1(2):213−41.
[15] Tsuchiya K, Murakami A, Fortmann G, Nakao M, Hatamura Y. Micro assembly and micro bonding in nano manufacturing world. SPIE 1999;3834:132−40.
[16] Enikov ET, Lazarov KV. Optically transparent gripper for microassembly. SPIE 2001; 4568:40−9.
[17] Hesselbach J, Büttgenbach S, Wrege J, Bütefisch S, Graf C. Centering electrostatic microgripper and magazines for microassembly tasks. In: Proc. of SPIE microrobotics and micromanipulation 4568; 2001. p. 270−7.
[18] Bark C, Binnenböse T, Vögele G, Weisener T, Widmann M. Gripping with low viscosity fluids. In: IEEE micro electro mechanical systems workshop Heidelberg, Germany; February 1998. p. 301−5.
[19] Grutzeck H, Kiesewetter L. Downscaling of grippers for micro assembly. Microsyst Technol 2002;8:27−31.
[20] Arai F, Fukuda T. A new pick up and release method by heating for micromanipulation. In: IEEE micro electro mechanical systems workshop Nagoya, Japan; January 1997. p. 383−8.
[21] Kochan A. European project develops ice gripper for micro-sized components. Assem Autom 1997;17(2):114−5.
[22] Reinhart G, Hoeppner J. Non-contact handling using high-intensity ultrasonic. Ann CIRP 2000;49(1):5−8.
[23] Bancel PA, Cajipe VB, Rodier F, Witz J. Laser seeding for biomolecular crystallization. J Cryst Growth 1998;191:537−44.
[24] Rambin CL, Warrington RO. Micro-assembly with a focused laser beam. IEEE MEMS 1994;285−90.
[25] Sanchez AJ, Ricolfe C. A flexible packaging station for micro-bulk-forming applications based on a standard carrier. Int J Adv Manuf Technol 2012;61(5−8): 529−36.
[26] Sanchez AJ, Ricolfe C. A bi-linear-vibratory feeder system for micro-bulk-forming applications. Steel Res Int 2010;89(9):1205−8.

This page intentionally left blank

CHAPTER

Robotics in Micro-manufacturing and Micro-robotics

28

Rafa López Tarazón
Robotnik Automation SLL

CHAPTER OUTLINE

INTRODUCTION: ROBOT DEFINITIONS

A robot can be seen as an electromechanical system programmable in three or more axes and with some degree of intelligence and ability to make choices based on its environment. Based on its size (and scale), robots may be classified as follows:

1. Macro-robots (macro-scale)
2. Micro-robots (micro-scale)
3. Nano-robots (nano-scale)

Micromanufacturing Engineering and Technology. http://dx.doi.org/10.1016/B978-0-323-31149-6.00028-1

In 1954, the first modern macro-robot was invented, called the Unimate. This robot was installed to automatically remove hot metal from a die casting machine. From that time up to the present, millions of robots have been developed and manufactured. Numerous companies are currently selling robots, two examples are shown in Figure 1.

Nowadays macro-robots are used for many applications: car production, packaging, palletizing, printed circuit board (PCB) manufacturing, goods transportation, vacuum cleaning, lawn mowing, care assistance for the elderly, and even for military applications or laparoscopic surgeries. Although new applications are arising, this kind of robot is used mainly in industrial environments.

On the other hand, a micro-robot is basically a small robot usually capable of operating at the microscopic scale. Micro-robotics is used widely for biologic applications, mainly biotechnology (cells localization, particles separation, chromosome cutting, or even genetic manipulation), but also for a large number of micro-manufacturing applications.

An example of an industrial micro-robot suitable for micro-manufacturing is the RP-1AH robot from Mitsubishi Electric [1], which is a miniature-format robot designed specifically for high-precision micro-handling applications. Its footprint is no larger than that of a DIN A5 sheet of paper. The RP-1AH is designed for small, cramped work areas and applications such as the placement of components on surface mount device circuit boards and micro-mechanics.

Finally, a nano-robot can be defined as a robot at or close to the scale of nanometers. Another definition sometimes used is a robot that allows precise interactions with nano-scale objects, or can manipulate with nano-scale accuracy. In general, nano-robots are still under development, but some initial results and tests have been made. An example is the first single-molecule car with buckyballs for wheels (by Rice University) (Figure 2).

Possible applications for nano-robots are nano-surgery, nano-manufacturing, weaponry, and cleaning.

Table 1 summarizes the main features of the different robot technologies.

Very closely related to micro-robotics are micro-electromechanical systems (MEMS), which can be defined as the technology of small things. MEMS are usually used to make sensors by incorporating silicon-based mechanical and electrical

FIGURE 1

Two different commercially available robots from Robotnik Automation Company.

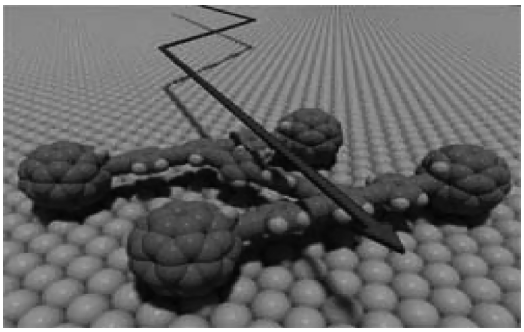

FIGURE 2

The Nanocar.

Courtesy of Rice University.

components. Sensing devices are generally two dimensional in shape and use the electrical and mechanical properties of bulk silicon and deposited thin film.

Nowadays, there are numerous applications in which MEMS take part, such as in pressure measurement, material straining, fluid flowing, and chemical compounding.

MICRO-ROBOTICS APPLICATIONS

Something about the actual applications of micro-robotics in micro-manufacturing is now explained. Many of these have arisen with the growth of the MEMS market. One of the first applications is in micro-assembly, which can be defined as the assembly of micro-products, where the main goal is the construction of a micro-structure by means of several micro-components under microscopic tolerances. Micro-assembly may combine many different techniques from many different disciplines, such as robotics, chemistry and pneumatics or computer vision. The second main application is in micro-handling, where not only is the accuracy of the movement important, but also that of the physical gripper that holds the micro-part.

Table 1 Robot Technologies

Type	Size	Interaction with Environment	Main Application
Macro-robot	Centimeters to meters	Mechanical	Industrial
Micro-robot	Micrometers to centimeters	Mechanical, chemical, and electromagnetic	Micro-assembly
Nano-robot	Nanometers to micrometers	Chemical	Surgery (future)

MICRO-ASSEMBLY

In general, assembly applications are very well known in the robotic macro-world, as they are spread over numerous industrial applications, but these applications are completely different and relatively unknown when referring to the micro-scale.

As explained in Ref. [1], there are two main differences between micro- and macro-assembly:

1. **The final accuracy needed:** as an example, a typical assembly SCARA robot has an accuracy of 0.01 mm, while the precision needed by a micro-assembly application is below the submicron level. This problem is further increased by the accuracy needed by the sensors placed on the micro-robot, as the displacements and movements involved are very small and slow.
2. **Manipulation strategies:** the interaction between objects is completely different for the micro-world and the macro-world. In the former, gravity is not the main force, and other forces that appear, as surface-related forces (electrostatic, van der Waals) and surface tension forces, are dominant over gravitational force. This means that in the macro-world, mechanical interaction between objects will not perform as one might think it should. As an example, if a gripper is opened in the macro-world, the object being gripped will be released and will fall to the floor. If the same experiment is made in the micro-world, the object will not fall, as it will probably remain in place, adhering to the micro-gripper due to surface-related forces.

A review of many different types of micro-assembly systems is made next:

1. Teleoperated micro-assembly systems [2]
2. Master slave micro-assembly systems [3]
3. Automatic micro-assembly machines [4]
4. Serial or parallel micro-assembly [5,6]
5. Environment-controlled micro-assembly systems [7]
6. Hybrid micro-assembly systems [8]
7. Micro-assembly by micro-robots [9,10]

A good example of a micro-assembly system can be found in Ref. [11], where 3D MEMS micro-structures are created by assembling multiple surface, micro-machined micro-components together. In this case, the micro-assembly process consists of the following subprocesses: grasping a micro-component with a micro-gripper, removing the micro-component from a chip substrate, reorienting the micro-component to a new location, and joining the micro-component to another micro-component.

Another good example of micro-assembly of MEMS is found in Ref. [12]. In this case, the assembly process is done using adhesive films, and the example case is a micro-part being assembled on a PCB.

The last example presented of micro-assembly systems is the Pocket Delta robot, developed at CSEM (the Swiss Center for Electronics and Microtechnology). Based

on parallel kinematics, this micro-assembly robot has a repeatability of 2.5 μm and a pressing force of up to 2 N (Figure 3).

MICRO-HANDLING

The second main application for micro-robotics is in micro-manipulation or micro-handling. Micro-manipulation consists basically in moving a micro-component from one location to another. To achieve this task, the end effector plays an important role as it has the task of physically picking up and releasing the micro-part.

There are many different end effectors used for micro-handling operations. The most commonly used are the micro-grippers, which have been designed in many types. They usually use flexure or rotatory joints and also piezoelectric actuators.

An example of a micro-gripper is found in Ref. [13], where a flexible micro-gripper is designed for the high-precision handling of very small components. This micro-gripper uses flexure hinges, an inchworm piezoelectric actuator, and exchangeable gripping jaws.

Finally, another example is shown in Ref. [14], where a new micro-gripper that can realize a parallel movement of the gripping arms is developed. The piezoelectric actuation principle is used to move the micro-gripper mechanism. The micro-gripper was fabricated by means of a UV-lithographic process and chemical wet-etching technology from micro-structurable photosensitive glass.

SENSORS AND ACTUATORS IN MICRO-ROBOTICS

SENSORS

In robotics, sensors play important roles as they are responsible for collecting information about the environment. In robotics, sensors are used for a large number of tasks, such as finding locations, measuring parameters (internal or external), avoiding collisions, etc.

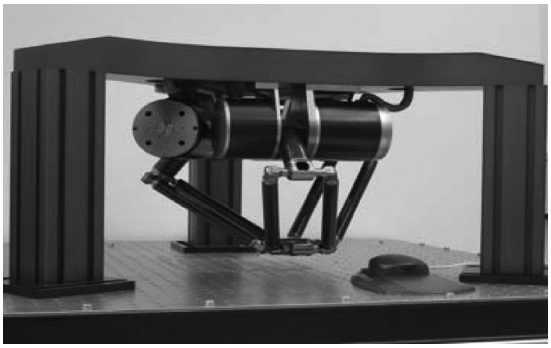

FIGURE 3

The Pocket Delta robot.

Courtesy of CSEM, SA Switzerland.

On the other hand, example applications, where sensors are used, are as follows:

- Displacement measurement
- Temperature measurement
- Velocity measurement
- Obstacle avoidance
- Distance measurement
- Beacon detection
- Collision detection

When considering micro-world applications, sensors are even more important, as they must be more precise and accurate than those for normal macro-world applications.

Basically, a sensor makes a conversion of energy from one form to another. To achieve this conversion, the sensor makes use of a transducer and an electronic circuit. A transducer is a device that converts a quantity of energy to a signal able to be measured electrically. Some examples are as follows:

- **Thermistor:** temperature-to-resistance
- **Electrochemical:** chemistry-to-voltage
- **Photocurrent:** light intensity-to-current.

After the transducer, the electronic circuit conditions the obtained signal into an electrical signal that can be processed further.

Combining signals from several sensors to form a world model is known as sensor fusion.

In robotics, sensors are basically classified into two groups: internal and external. Internal sensors (also called proprioceptive) are used to measure robot parameters relative to the reference frame of the robot, such as a joint angle, a linkage deflection, and a gripping force. External sensors (also called extereoceptive) are used to measure the environment and the position of the robot relative to that environment.

Sensors can be also classified as active, if they transmit energy into the environment, or passive, if they receive energy from the environment.

Finally, the sensors that are most commonly used in robotics can be summarized as follows:

- Resistive sensors (i.e., potentiometer)
- Tactile sensors (i.e., bumpers)
- Infrared sensors (i.e., proximity sensors)
- Ultrasonic distance sensors
- Inertial sensors (i.e., accelerometers)
- Orientation sensors (i.e., compasses)
- Laser range sensors
- Vision sensors

Almost every sensor has its micro-sensor, so it is possible to find micro-sensors for a large number of micro-robotics applications. A review of micro-sensors (strain,

pressure, acceleration, force, and angular rate sensing) is presented in Ref. [15]. As an example, Sippola et al [16] show a ceramic capacitive sealed-gage pressure micro-sensor, which is able to work under high-temperature applications.

ACTUATORS

An actuator is a device (usually mechanical) responsible for generating a movement in a mechanism or system. While sensors make conversions between different forms of energy, actuators make a conversion from one form of energy to a mechanical movement. From another point of view, an actuator is the provider of the motion to the robot. Current actuators for macro-robots are electrical, pneumatic, or hydraulic.

Obviously, micro-robots need micro-actuators to generate their movement. There are many different micro-actuators that can be used in micro-robotics, such as piezoelectric actuators, micro-motors, micro-pneumatic actuators, shape memory alloy composite micro-actuators (based on materials that deform at low temperature and regain their original shape when they are heated), electrostatic actuators, or even ferrofluid actuators. Next, the most important are explained: piezoactuators and micro-motors.

PIEZOELECTRIC ACTUATORS

This type of actuator generates motion in the subnanometer range. These actuators make use of piezoelectric materials, and the movement is based on the frequencies derived from solid-state crystalline effects. There are no moving parts in contact, so there are no friction forces generated.

Piezoactuators usually have a very short response time (below 1 ms) and a very long life time (i.e., require no maintenance). Figure 4 shows an example of a piezoelectric actuator from the CEDRAT Group.

MICRO-MOTORS

There are two main types of micro-motors: electromagnetic and piezoelectric. A good review of electromagnetic micro-motors is reported in Ref. [17], where their main types are illustrated (variable reluctance, induction, and permanent magnet micro-motors), the permanent magnet micro-motor being confirmed to be the best in terms of developed power. These electromagnetic micro-motors operate the same as the bigger ones in the macro-world, but with their parts reduced to the minimum possible size. Numerous companies are selling electromagnetic micro-motors, among which the Faulhaber Group and Maxon Motor stand out.

On the other hand, piezoelectric micro-motors are based on the change in shape of a piezoelectric material. The motion is produced from the ultrasonic vibrations of the material when applying an electrical field. There are both linear- and rotary-motion micro-motors (Figure 5).

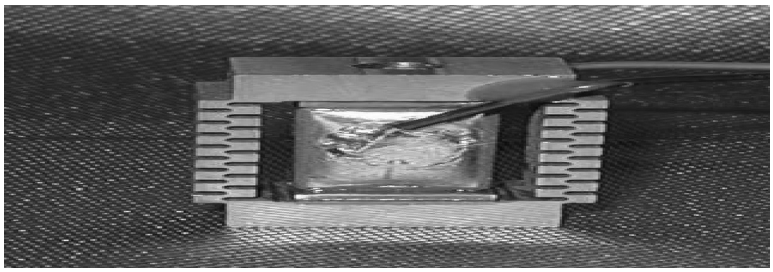

FIGURE 4

A piezoactuator.

Courtesy of CEDRAT Group.

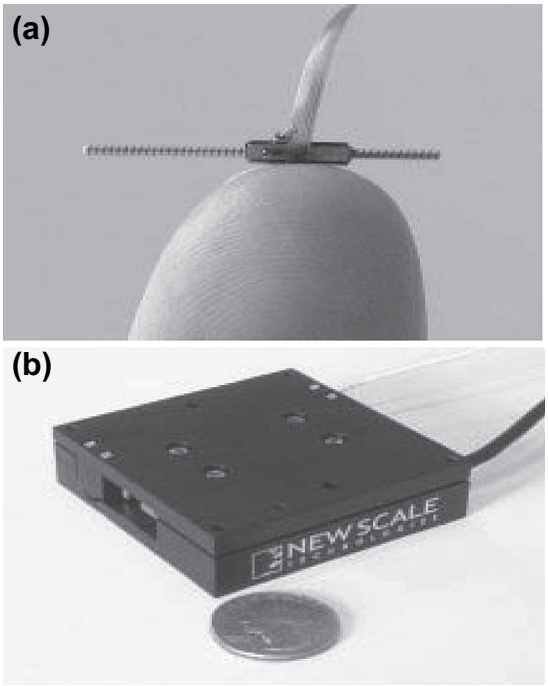

FIGURE 5

(a) Piezoelectric rotary micro-motor and (b) linear nano-positioning stage.

Courtesy of CEDRAT Group.

MICRO-ROBOT EXAMPLES

Next, some state-of-the-art micro-robots are presented. Their applications are countless, although the Hexapod M-850 Micro-robot is especially designed for micro-manufacturing tasks. Some of them are still in the development stage, but they show real examples of their importance in this field.

MICRO-AIR VEHICLE

The first example of a micro-robot can be found in Ref. [18], where a micro-air vehicle (MAV) is designed and prototyped. This 10 cm, 2 g MAV is capable of autonomous flight, target sensing, and obstacle avoidance and makes use of articulated and rigid composite micro-structures, high-performance micro-actuators, and low-power biomimetic sensors. Figure 6 shows this MAV.

The electronics and control are located on a PCB at the center of the fuselage. The power is placed on the front part and consists of a 20-mAh lithium polymer battery. There are also two bimorph piezoelectric actuators and an optical flow sensor for obstacle avoidance.

HEXAPOD M-850 MICRO-ROBOT

Produced by Physik Instrumente (PI) GmbH & Co. KG, the M-850 Hexapod is a micro-positioning system for all complex positioning tasks that require high load capacity and accuracy in six independent axes (Figure 7). Its main features are as follows:

- Six degrees of freedom
- Repeatability to ± 1 μm
- Actuator resolution to 0.005 μm

Current applications for this micro-robot are given below:

- Surgical robots
- Micro-machining

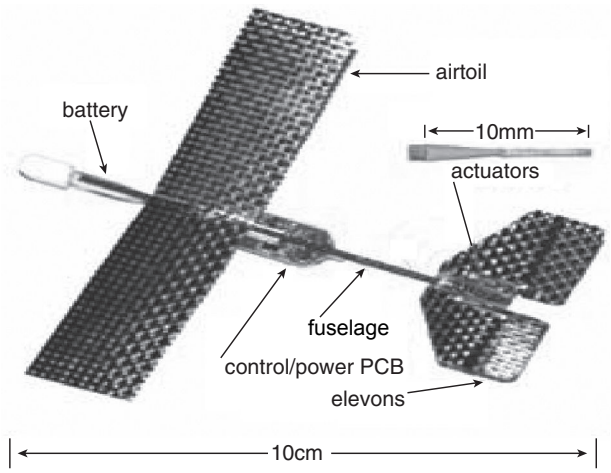

FIGURE 6

A micro-air vehicle. PCB, printed circuit board.

Courtesy of UC Berkeley.

FIGURE 7

The Hexapod M-850.

Courtesy of Physik Instrumente (PI) GmbH & Co. KG.

- Micro-manipulation (life sciences)
- Semiconductor handling systems

OPEN-SOURCE MICRO-ROBOTIC PROJECT

This Open-source micro-robotic project aims to develop a cheap, reliable, and swarm-capable micro-robot. Currently, there are two developed robot versions: "Jasmine II" and "Jasmine III" (Figure 8). The robots (hardware, software, and simulations) are available under the GNU General Public License.

WAALBOT [19]

This robot (developed at Nano-Robotics Laboratory, Carnegie Mellon University) is a new approach to wall-climbing robots (Figure 9). Using two actuated legs with rotary motion and two passive revolute joints at each foot, this robot can climb and steer in any orientation. The main applications for this robot are inspection and surveillance, and space missions.

STRIDER MICRO-ROBOT [20]

This micro-robot (also developed at Nano-Robotics Laboratory, Carnegie Mellon University) was inspired by water strider insects (Figure 10). The robot (as with the insects) uses surface tension force to balance its weight on water by using hydrophobic Teflon-coated wire legs. The maximum forward speed has been measured to be 3 cm/s and its rotational speed is 0.5 rads/s.

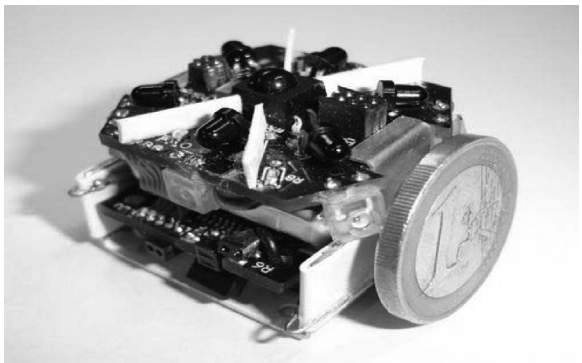

FIGURE 8

The Jasmine III robot.

Courtesy of open-source micro-robotics project.

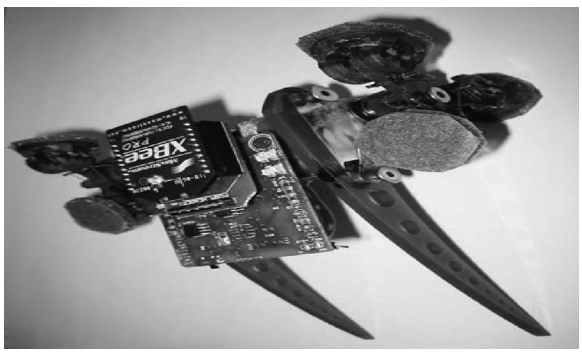

FIGURE 9

The waalbot robot.

Courtesy of Metin Sitti, Nano-Robotics Laboratory, Carnegie Mellon University.

FIGURE 10

The strider micro-robot.

Courtesy of Metin Sitti, Nano-Robotics Laboratory, Carnegie Mellon University.

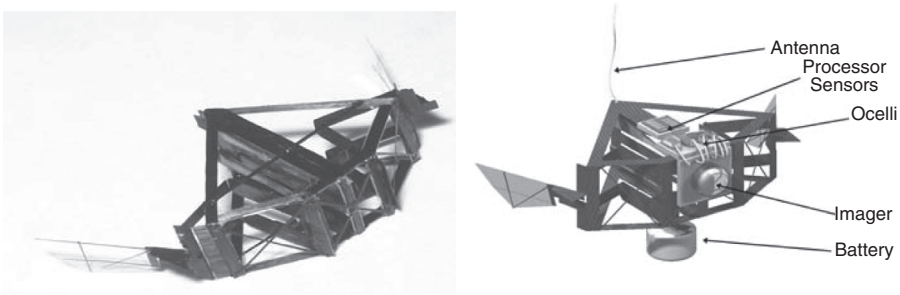

FIGURE 11

The micro-mechanical flying object project at UC Berkeley.

MICRO-MECHANICAL FLYING OBJECT PROJECT

Closely related to the strider micro-robot (inspired by insects) and the MAV (autonomous flying micro-robot) is the micro-mechanical flying object (MFI) developed at the Biomimetic Millisystems Lab, at UC Berkeley (Figure 11).

The goal of the project is to develop a very small device capable of sustained autonomous flight, based on the flight performance of flies and by means of piezoelectric actuators and flexible thorax structures.

CONCLUSIONS

As has been seen throughout this chapter, micro-robotics is a relatively new field with a large amount of research still to be done. Numerous laboratories and investigation centers are concentrating their efforts toward obtaining increasingly more sophisticated and smaller robotic devices.

Future applications of micro-robots are numerous and extend from searching for survivors during rescue missions to extremely precise surgical operations (even autonomously by a micro-robot inside the patient's body) all the way up to top-secret espionage missions.

REFERENCES

[1] Cohn MB, Böhringer K-F, Novorolski JM, Singh A, Keller CG, Goldberg K, et al. Microassembly technologies for MEMS. In: Proc. SPIE micromachining and microfabrication, conference on micromachining and microfabrication process technology IV Santa Clara, CA; September 21−22, 1998. p. 2−16.

[2] Reinhart G, Anton O, Ehrenstrasser M, Patron C, Petzold B. Framework for teleoperated microassembly systems. Proc SPIE 2002;4570:86−96. M.R. Stein editor. Telemanipulator and Telepresence Technologies VIII.

[3] Kaneko K, Tokashiki H, Tanie K, Komoriya K. Impedance shaping based on force feedback bilateral control in macro-micro teleoperation system. Proc ICRA 1997: 710−7.
[4] Shimamura K, Sasaki Y, Fujii M. Low cost microassembly machine. FUJITSU Sci Tech J Jan. 2007;43(1):59−66.
[5] Danuser G, Pappas I, Vögeli B, Zesch W, Dual J. Manipulation of microscopic objects with nanometer precision: potentials and limitations in nano-robot design. Int J Robot Res 1997:1−47.
[6] Cohn MB, Liang Y-C, Howe RT, Pisano AP. Wafer-to-wafer transfer of microstructures for vacuum packaging. In: Solid-state sensor and actuator workshop, Hilton Head Island, SC, USA (June 2−6, 1996); 1996.
[7] Zhou Q, Aurelian A, Chang B, del Corral C, Koivo HN. Microassembly system with controlled environment. J Micromechatronics 2004;2(3):227−48.
[8] Kim B, Kang H, Kim D-H, Park J-O. A flexible microassembly system based on hybrid manipulation scheme for manufacturing photonics components. Int J Adv Manuf Technol (Springer Lond) 2005;28(3−4):379−86.
[9] Zhu T, Tan D. Research on microrobot-based microassembly system. Intell Control Autom 2002;2:1236−40.
[10] Fatikow S, Seyfried J, Fahlbusch S, Buerkle A, Schmoeckel F. A flexible microrobot based microassembly station. J Intell Robotic Syst Jan. 2000;27(1−2):135−69.
[11] Dechev N, Cleghorn WL, Mills JK. Construction of 3D MEMS microstructures using robotic microassembly. In: International conference on robots and intelligent systems (IEEE/RSJ IROS 2003) Las Vegas, Nevada, USA; October 27−31, 2003.
[12] Karjalainen I, Sandelin T, Uusitalo J, Tuokko R. Robotic assembly and joining of miniature and MEMS components using adhesive films − test environments and experiences. J Assem Autom 2004;24(1):58−62.
[13] Henein S, Thurner M, Steinecker A. Flexible micro-gripper for micro-factory robots. Created by SHe/Rev. July 2003.
[14] Keoschkerjan R, Wurmus H. A novel microgripper with parallel movement of gripping arm. In: Proceedings of the eighth international conference on new actuators Bremen, Germany; June 10−12, 2002. p. 321−4.
[15] Goldfarb M, Strauss A, Barth EJ. Overview of mechatronics. Chapter 5: an introduction to micro and nanotechnology. CRC Press LLC; 2002.
[16] Sippola CB, Ahn CH. A thick film screen-printed ceramic capacitive pressure microsensor for high temperature applications. J. Micromechanics Microengineering 2006;16(5):1086−91.
[17] Dereine E, Dehez B, Grenier D, Raucent B. A survey of electromagnetic micromotors. In: Proceedings of the 1st international precision assembly meeting (IPAS 2003) Bad Hofgastein, Austria; March 17−19, 2003. p. 85−94.
[18] Wood RJ, Avadhanula S, Steltz E, Seeman M, Entwistle J, Bachrach A, et al. An autonomous palm-sized gliding micro air vehicle. IEEE Robotic Autom Mag 2007: 82−91.
[19] Murphy MP. Waalbot: an agile small-scale wall-climbing robot utilizing dry elastomer adhesives. IEEE/ASME Trans Mechatronics 2007;12(3):330−8.
[20] Song YS, Sitti M. Surface tension driven biologically inspired water strider robots: theory and experiments. IEEE Trans Robotic June 2007;23(3):578−89.

FURTHER READING

[1] McKerrow PJ. Introduction to robotics. Ed. Addison Wesley; 1990.
[2] Sanchez AJ, Lopez R, Guzman R, Ricolfe C. Recent development in micro-handling systems for micro-manufacturing. J Mater Process Technol 2005;167(22):499−507.
[3] Lin G, Lawton RA. 3D MEMS in standard processes: fabrication, quality assurance and novel measurement microstructures. NASA Tech Rep 2000. JPL Internal Report.
[4] Bell J. Automated packaging of MEMS devices. J SMT 2003;16(2):22−6.

CHAPTER

Measurement, Testing, and Diagnosis for Micro-manufacturing Systems

29

Pietro Larizza
MASMEC SpA, Bari-ITALY

CHAPTER OUTLINE

INTRODUCTION

Testing and diagnosis are terms often associated with the same topic, nevertheless their true sense is commonly related to a different meaning. A main difference is that testing does not deal with fault repairing but focuses only on fault detection, while diagnosis consists of determining the nature of a detected fault, of locating it and hopefully repairing it. There is another difference between the two topics: this is related to the work conditions and functional states which permit the execution of testing or diagnostic procedures. Testing is often considered as an *off-line* procedure conducted by proper, prefixed excitation signals using suitable testing models; however, it is ever more frequent to implement testing procedures as *online* conditions thanks to automated test bench and computer-based measurement equipment.

Micromanufacturing Engineering and Technology. http://dx.doi.org/10.1016/B978-0-323-31149-6.00029-3

Diagnosis procedures can also be executed under normal working conditions, permitting real-time response and fast fault identification and compensation. A common application area for testing and diagnosis procedures is measurement, which can be performed following both classical and modern approaches. The classical approach generally provides a number of sensors that are equal to the number of signals to be acquired, while the modern, or model-based, approach provides a number of sensors (observations) that are less than the number of signals (variables) to be acquired. In such a type of approach, more information is provided by the knowledge model of the system.

Testing or diagnostic procedures applied to micro-manufacturing systems, or miniaturized systems for processing and machining, could be assisted by the use of measurement techniques based on the modern approach, principally due to the minimum space available and difficulties associated with the location of the sensors. In order to achieve a further reduction of the problem related to the allocation of the sensors, especially with reference to micro-systems, testing and diagnostic procedures often require noncontact sensors or special transducers in order to avoid external influences, under normal working conditions, of the reduced size of parts and devices to be tested. Other important aspects are the precision and accuracy of the measurement system, which for the specific micro-manufacturing area have to be related to the local and global concepts.

Precision is defined as the degree to which further measurements, or calculations, show the same or comparable results, so the concept of precision is linked to that of repeatability. The accuracy is the degree of conformity of a measured or calculated quantity to its actual or true value (Figure 1). Often the two concepts have to be related to the local and global meaning because local measurement space and global measurement space could be several orders of magnitude apart. This imposes strong requirements in terms of accuracy and stability of the measurement system which can be overcome by proper local reference points and (auto) calibration procedures.

Typically, a measurement system consists of sensors, conditioning, acquisition, and processing systems. Depending on the nature of the measurement, the sensor

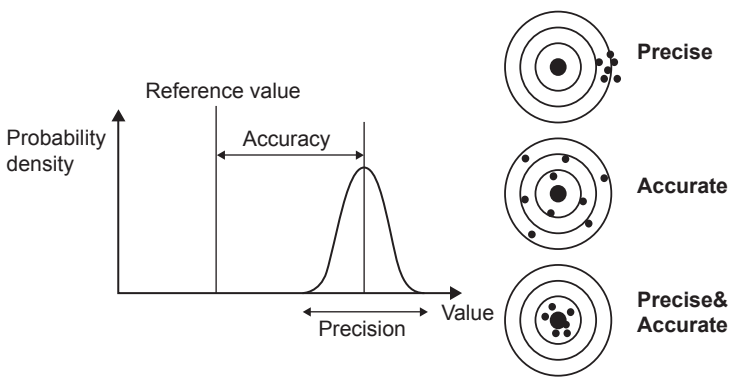

FIGURE 1

Definition of precision and accuracy.

system could be considered as a complex transducer system or could even be reduced to a simple sensing element. For example, dimensional measurements could require, as sensing element, a simple linear encoder or a complex charge-coupled device (CCD) camera joined with a laser beam. If the dimensional measurement of micro-parts is considered, performed with the aid of a microscope, a precise positioning of the sensing element (optics, lenses, camera) is required. Often this task is accomplished by a servo actuator connected in a closed-loop configuration. Precise positioning is also required for the focusing of the camera's optical system, in order to accomplish inspection of micro-parts both in static and dynamic mode (dependent on shape and dimensions of the part).

Precise positioning devices are largely used in modern measurement systems either as single-stage devices (1D) or multistage devices (2D−3D or even more). Characterized by a precision of a few nanometers, up to micrometers, the linear movements are implemented either with piezodevices or electromagnetic devices (moving coil, brushless linear motor). These devices are either coupled directly with the end-moving part, without a mechanical joint, or, depending on the final application, using several very precise kinematic configurations (serial-Cartesian, or parallel-Tripod or Hexapod). Many measurement systems suitable for micro- or nano-technology areas are based on the laser interferometer principle. A laser interferometer together with a CCD or position sensing detector (PSD) and galvanometer motor, are used to realize precise 1D to 6D measurements (orders of nanometer or below) by exploiting laser tracking techniques. Very fast sampling times are also possible (up to 100 kHz), rendering this kind of measurement suitable for the ultraprecise real-time measurement of vibrating parts.

Within micro-manufacturing processes, both testing and diagnostic procedures are of great importance for quality assurance (QA). The main *scenario* of QA involves statistical process control (SPC) as a set of tools capable of controlling the quality of the products by statistical analysis methodologies [1]. The SPC techniques use data and measurements coming from testing and diagnostic equipment in order to take decisions on quality levels of the production, and ensure eventual corrections of the production process. There are several tools which permit the control of the incoming data from a process. When the measurement data are collected, they are analyzed by extracting *means* and *ranges* that are plotted on *charts*. More complex analyses can be accomplished by calculating the *indices of capability,* which become tools suitable for the evaluation of how much the process or subprocesses meet the initial requirements. While the precision of a process is related to the spread of the collected data around a mean value, the capability relates the precision to the range of the permitted values fixed by the specifications (or specification tolerance). Generally, if the precision is characterized by the *standard deviation* σ, the capability index relates the specification tolerance to the value of 6σ.

From a more general point of view, the testing and diagnostic decision-making processes can be viewed as a series of transformations, or mappings, on process measurements. Figure 7 shows the various transformations that process data go

through during diagnosis [2]. The measurement space defines a set of measurements incoming from sensors and transducers. These are the input to the diagnostic system. The feature space is a space of points that are obtained as a function of the measurements by utilizing a priori knowledge. Here, the measurements are analyzed and combined with the aid of a priori process knowledge, in order to extract useful features about the process behavior to aid diagnosis. The mapping from the feature space to decision space is usually designated to meet some objective function (such as minimizing of misclassification). Typically, this transformation is achieved by using either threshold functions or template matching. In the class space, the features are separated by suitable classifiers. The class space is thus the final interpretation of the diagnostic system delivered to the user.

In the following sections, a deeper analysis of some aspects of the diagnosis and testing for micro-manufacturing systems will be detailed. In the first section, the main noncontact measurement techniques used in the micro-applications area are recalled. The second section focuses on testing and diagnostic methods, in particular, related to quantitative techniques such as Kalman filters (KFs). The third section reports an application where model-based testing is used to detect the failures and performance of a piezoelectric micro-positioning device.

PRECISION MEASUREMENT SYSTEMS

Starting from the measurement space, it results that primary importance is usually given to how signals and data are collected in order to proceed through a testing or diagnostic process. The main elements involved in the capturing of signal are the sensors.

The production of *meso*-, *micro*-, and *nano*-devices requires a high level of precision due the millimeter or submillimeter dimensions of the devices to be assembled, handled, or tested. Within the submillimeter range of dimensions, many phenomena are no longer negligible with respect to the macro-world (adhesion, deformation, thermal variation), so the external influences of probes or tools for handling purposes are to be avoided in order to achieve the required precise measurements. For example, even some well-defined procedures, in the vibration detection and analysis area, can no longer be applied by adopting standard sensing elements (contact accelerometers).

Nowadays, noncontact sensors are largely used in order to avoid external influences on the measurement system, thus enabling ultrahigh precision measurements (i.e., up to the 10^{-9} range of the whole dimensions of the part to be measured). Due to the property of coherence in the emitted radiation, the laser is the main technique applied within high-precision applications, not only within the realm of dimensional control, but also within a wide range of applications where the physical characteristics of materials have to be measured in a direct or indirect manner.

Laser applications on measurement systems go from dimensional analysis to vibration measurement. Some applications in material characterization even use

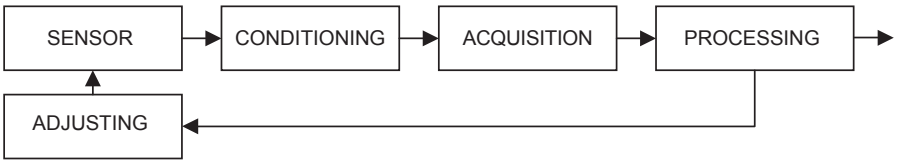

FIGURE 2

A typical measurement system suitable for micro/nano-applications.

the laser as a power source in order to produce mechanical waves. This is achieved by impacting the laser beam onto targets and then measuring the ultrasound reflections (Laser Ultrasound Inspection).

The laser is also used within optical applications in order to inspect transparent or semiopaque materials using a coherence light source (OCT—optical coherence tomography). However, even high-resolution image analysis is increasing its influence within the high-precision measurement domain, especially when in-line inspection and testing of micro-parts are required. Laser interferometers, LUS, OCT, and image processing can easily ensure resolutions of below 1 μm with very simple equipment and, in some cases, at a very competitive cost.

Recalling these applications, one may also recognize the wide use of precise positioning systems suitable to move the probe or the sensor, as shown in Figures 2 and 3. Precision movements are often achieved with mechatronic systems based on piezoactuators, submicrometric brushless motors, galvo motors, moving coil motors, etc. Note also that high-precision mechanical devices have to ensure optimal isolation from vibration and other external disturbances.

FIGURE 3

Hexapod system with six degrees of freedom.

Of particular importance, dimensional measurement sensors are especially valuable because by dimensional measurement, it is possible to retrieve a large amount of information about the observed system, and not only from a purely dimensional point of view. For example, laser displacement sensors can report information about dimensional, dynamical, thermal, and vibrational behavior. Therefore, it may be useful to briefly detail a number of such sensors, especially of the noncontact type, which are particularly suited for micro-testing applications.

MONO- AND MULTIDIMENSIONAL MEASUREMENT

Precise noncontact dimensional measurement systems are largely based on the laser interferometer technique (i.e., the Michelson interferometer). Comprising just the interferometer, i.e., being a system capable of detecting only differences on beam paths, it is suitable for incremental, or displacement, measurements. Typically, the time response is very fast (typ. <100 μs) and the measuring accuracy, by the use of interpolator devices, easily reaches values below 10^{-8} m. The laser interferometer system is very suitable for coordinate measuring machine applications. Very accurate measurements on micro-parts are possible by placing the part on a positioning system (one stage: X or multistage: X-Y or X-Y-Z table) provided with reflectors.

Other dimensional measurement techniques are based on different principles, such as laser beam triangulation, which use a laser source and a detector (CCD or PSD as represented by Figures 4–9). In this case, the system performances depend

FIGURE 4

1D laser-based displacement measurement system.

FIGURE 5

A motorized, vision-based measurement system (X, Y, Z resolution: 50 nm).

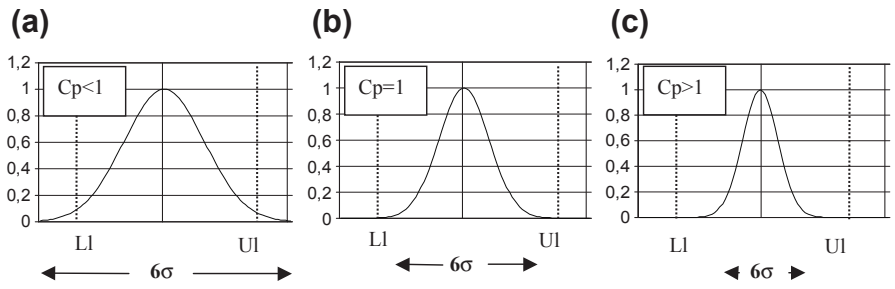

FIGURE 6

Capability index for a low capability (a), medium capability (b), high capability (c) system (process). (Cp: capability index, Ll: tolerance lower limit, Ul: tolerance upper limit, σ: standard deviation).

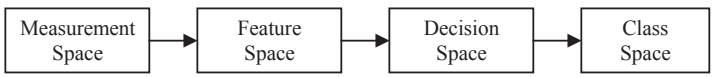

FIGURE 7

Transformations in a testing/diagnostic system.

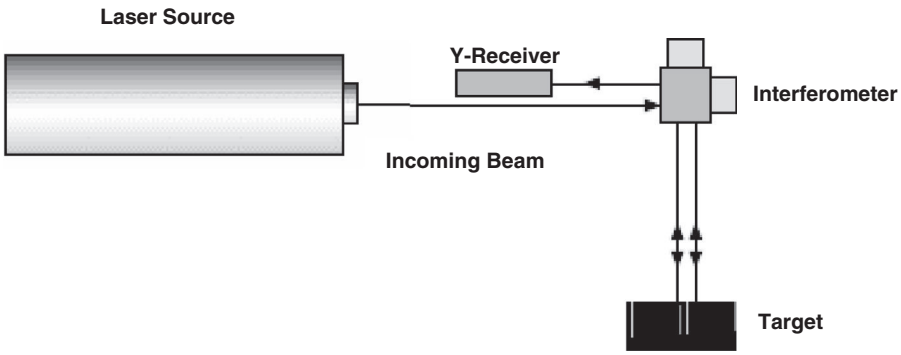

FIGURE 8

One-dimensional displacement measurement by laser interferometer.

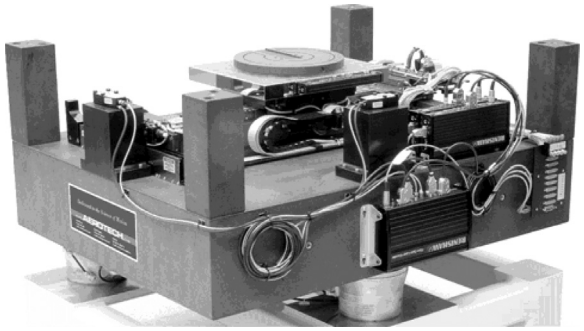

FIGURE 9

High-precision X-Y feedback system (Aerotech Inc.) using two laser interferometers (Renishaw) with total precision up to 10 nm. The system is suitable also for testing 2D tables and precise linear motors.

on the surface characteristics of the target material. Both the precision and the distance range are affected by material typology and surface texture.

THICKNESS MEASUREMENT

There are several techniques which are suitable for the precise and ultraprecise measurement of thickness. Inductive measurement, based on differential measurement techniques, is a methodology often adopted for low-cost applications. This method is affected by the type of material being measured. Higher levels of stability and precision are achieved by laser techniques which consist of a laser beam shaped by the target. A sensor, in these systems, consists of emitter and receiver elements, with the field of measurement situated between them. The width of the "shading" (e.g., behind an object) or the light (e.g., through a gap) can thus be measured (Figure 10). Alternative techniques are possible, mainly by using two displacement sensors as

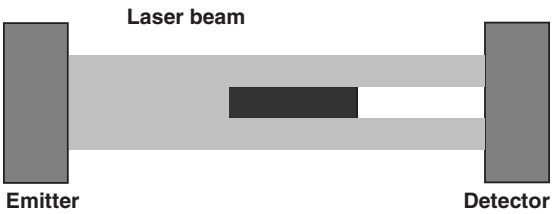

FIGURE 10

Thickness measurement using a laser beam.

represented in Figures 11–17. This kind of technique requires, however, highly accurate calibrations (usually accomplished with the use of a calibrated target).

In this domain, great importance is given to the laser ultrasound system (LUS), which is capable of reaching high levels of precision by using a hybrid technique. The technique is based on a very narrow pulsed laser beam, which is launched toward the target with the reflected ultrasound wave being received by an acoustic sensor. The variations of the acoustic impedance of the material are analyzed subsequently by a processing unit in order to deliver a map of the discontinuity of the material. The accuracy of this measurement, depending on the type of material, sound velocity, and time resolution of the signal processing unit, can reach a few micrometers.

2D PROFILE AND SHAPE MEASUREMENT

Profile and shape measurements are often accomplished by a combined use of laser and image analysis techniques.

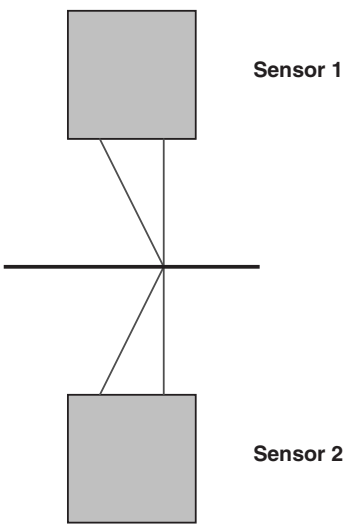

FIGURE 11

Thickness measurement using two displacement sensors.

Model	**Micro-Epsilon ILD 2200-2**
Measuring range	2 mm
Start of measuring range SMR	24 mm
Midrange MMR	25 mm
End of measuring range EMR	26 mm
Linearity	1 µm ±0.05 % FSO
Resolution(at 10 kHz without averaging)	0.03 µm
Measuring rate	10kHz
Permitted ambient light	30,000 lx
Spot diameter	SMR 80 µm MMR 35 µm EMR 80 µm
Light source	semiconductor laser <1 mW, 670 nm
Temperature stability	0.01 % FSO/°C

FIGURE 12

Thickness measurement systems.

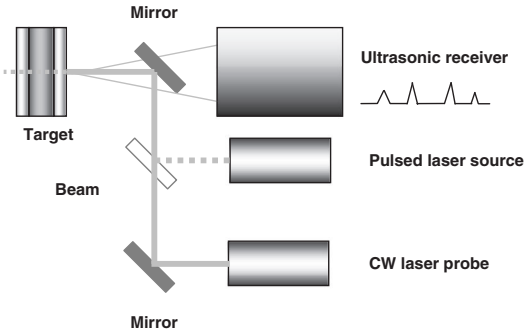

FIGURE 13

LUS principle and a system by TECNAR working on the B scan and C scan mode.

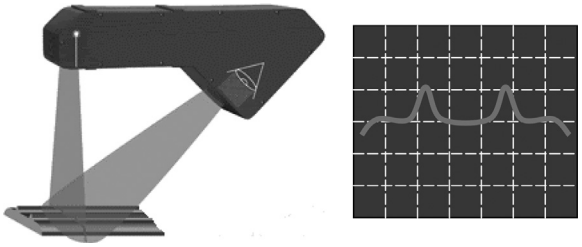

FIGURE 14

A profile measurement system using laser and charge-coupled devices.

A very thin laser beam is projected onto the part to be measured. The projection is analyzed by a CCD linear array camera. A precise 1D linear movement may be imposed onto the measurement system or onto the part to be measured. Depending on the laser beam thickness, linear array CCD, optics and positioning system resolution, submicrometric accuracy can easily be achieved.

Suitable calibration procedures, using master profiles, are used to calibrate the analyzed image, thus permitting compensation for optical field deformations.

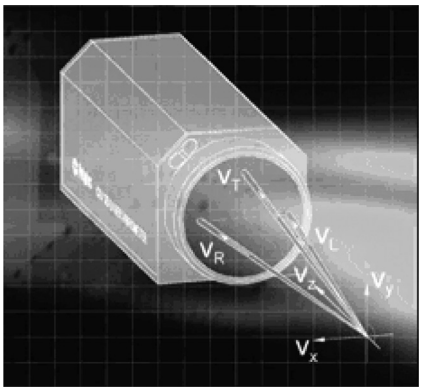

FIGURE 15

3D laser vibrometer by Polytec. The system is capable of detecting speed components with a resolution of 0.2 μm/s using a laser spot of 65 μm.

FIGURE 16

The Polytec MSA-400 Micro System Analyzer: by scanning laser-doppler vibrometry it is capable of performing the precise 3D dynamic characterization of MEMS and MOEMS micro-structures.

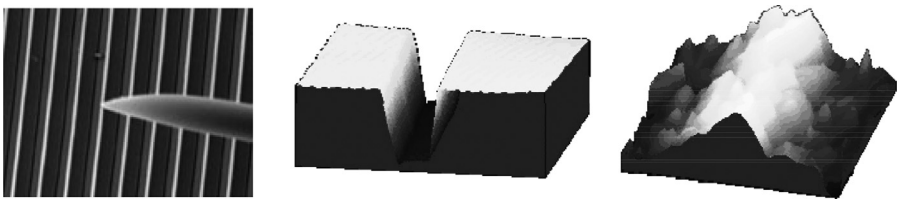

FIGURE 17

SEM image of a Nanonics® AFM Probe in contact with sample. 10 × 10 μm AFM image of a 10 μm deep/2 μm wide trench and a 1 × 1 μm AFM image of the bottom of the deep trench.

This kind of equipment is particularly suitable in continuous-control processes when the parts to be measured are brought by a linear transportation system or by tape. In such cases, high efficiency image analysis algorithms and high-speed computational systems are required.

Shape and profile analyses are also accomplished by suitable image analysis techniques (subpixeling) that adopt high-resolution CCD linear or matrix sensor arrays. High resolution (below 1 μm) bidimensional and stereoscopic image analysis can be carried out by 2D arrays of sizes greater than 20 megapixels or by linear arrays of sizes greater than 300 pixels × mm. As with laser beam profilers, a continuous and very accurate movement of the analyzed part, or the linear array, has to be considered.

VIBRATION MEASUREMENT AND ANALYSIS

Vibration analysis is a very wide and complex domain which exploits several aspects of the testing and diagnosis disciplines, from condition monitoring to defect detection. Improvements in sensor technology now permit the use of vibration analysis methodology within the micro-/meso-world also. Noncontact high-speed (wide bandwidth) laser sensors (typically displacement sensors) can overcome the traditional limits exhibited by accelerometers, so highly accurate and localized analyses can be performed.

Vibration analysis methodology could be subdivided into four principal domains:

- Time domain
- Frequency domain
- Joint domain (time/frequency domain)
- Modal analysis

Each domain provides specific information on the working conditions and features of the vibrating part.

Typically, time-domain analysis is devoted to detecting the integral performance of the tested part: peak, average, root-mean-square, envelope values of vibration

amplitude. These values are compared with threshold values in order to detect abnormal performance or latent defects.

Frequency domain is able to provide more information as the measured signal is decomposed into a sequence of frequency components (spectrum) by a Fourier transform calculation (or fast Fourier transform—FFT). Local analysis of the different frequency components permits the association of a signature with the processed signal, such that the tested part can be identified precisely by its own signature (signature analysis). Due to the time-varying property of the signal, calculating many spectrums on the time observation window can be found to be useful. To do so, a joint time/frequency technique (Gabor–Wigner–Wavelet) can be used very efficiently. In a particular case of time/frequency analysis, the spectrums are related to the rotational speed of the tested devices (order analysis), such that the analysis of the single order which is represented by a frequency component varying with the speed is rendered possible.

Modal analysis permits the study of the dynamic properties of structures under vibration excitation. This technique uses FFT in order to carry out a transfer function which shows one or more resonances, by means of which it is possible to estimate the characteristic mass, damping, stiffness, and other properties of the tested part. Using a laser interferometer, and suitable software tools, it is possible to apply noncontact vibration analysis for the test and measurement of MEMS (microelectromechanical system) and MOEMS (micro-optical electromechanical system) dynamics and topography.

MIXED QUALITATIVE–QUANTITATIVE ANALYSIS SYSTEMS

Surface-texture analysis

This is a typical application of image analysis techniques whereby properties, or features, of analyzed surfaces are compared with known properties belonging to a sample image. Due to its mainly qualitative aspect, surface-texture analysis could be considered more properly as an inspection methodology; however, its output may provide information on both processes and good working conditions of machines (typically in machining or assembly areas) and may provide quantitative evaluations through proper morphological analyses on shapes and forms.

Principally, the features extraction is performed by a joint domain (spatial-frequency) transformation (Gabor, Wavelet) [3] and the features comparison is performed by a suitable statistical classifier: for example, the Mahalanobis distance, which is scale invariant with respect to the Euclidean distance (minimum distance classifiers), or maximum likelihood classifiers of which the Mahalanobis distance is a particular case. A more complex classifier tool is represented by the neural network.

A neural network (typically of the back-propagation type) is able to activate particular output ports when a set of input signals determines the satisfaction of conditions for which the network was previously trained. Independently of the classifier

used and the analysis methodology, image acquisition is the more critical aspect that involves both the optical system and the illumination technique. In the testing of micro-parts, the additional use of a microscope and coherent light paths is a primary requirement. Quantitative aspects and morphological analyses are performed mainly in the spatial domain.

SCANNING ELECTRON MICROSCOPY, ATOMIC FORCE MICROSCOPY, AND SCANNING TUNNELING MICROSCOPY

Scanning electron microscopy (SEM), atomic force microscopy (AFM), and scanning tunneling microscopy (STM) are all widely used surface analysis techniques capable of very high accuracies (in the range from 10^{-9} to 10^{-7} m [4]).

In SEM, the primary electrons hit a surface with an energy of 0.5−30 keV, and generate many low-energy secondary electrons. The intensity of these secondary electrons is affected by the surface topography of the target. An image of the target surface can then be constructed by measuring the secondary electron intensity as a function of the position of the scanning primary electron beam.

AFM systems detect the z-displacement of a cantilever by the reflection of a laser beam focused onto the top surface of the cantilever. The feedback from this sensor maintains the probe at a constant force. STM systems measure the quantum tunneling current between a wire or a metal-coated silicon tip and the object surface. An electronic feedback system maintains a constant current by positioning the tip to just make contact with the surface.

SEM is often used to survey surface analysis problems before proceeding to techniques that are more surface sensitive and more specialized, such as AFM or STM. High-resolution images of surface topography, with excellent depth of field, are produced using a highly focused SEM. These kinds of SEM are also able to provide high spatial resolution, except when the target consists of very narrow and deep wells. This is the case, for example, of a trench in a semiconductor wafer in which an SEM cannot view the bottom or the sidewall of the trench structure. In these cases, the combination of SEM and AFM (or STM) analysis has to be considered.

TESTING AND DIAGNOSIS METHODS

As mentioned earlier in the introduction, testing and diagnosis for micro-manufacturing products/machines may now take advantage of new approaches in measurement and control system methodologies. Contactless sensor systems and model-based measurement systems are two examples of such approaches. Both methodologies aim to minimize interaction between the measurement system and the tested workpiece, in order to:

- save space for sensor allocation;
- retrieve more information from the observed system.

Another advantage is that, in the model-based measurement systems, the number of sensors is minimized. This characteristic is an important requirement because the sensors are fault sensitive, and critically increase the production costs of the systems.

Basic foundations of testing and diagnosis rest upon fault detection and isolation techniques and can be based on qualitative, quantitative, or history-based information/data with the use of modeling techniques. These methods permit process adjustment and tuning in order to achieve optimal performance and to ensure product QA approaches [5]. The term "fault" is generally defined as "a departure from an acceptable range of an observed variable or a calculated parameter associated with a process." This defines a fault as a process abnormality or symptom, such as a high vibration level in a machine or a high positional error in a controlled device. The underlying cause of this abnormality, such as a failed ball bearing, or a defective controller, is called the *basic event* or the *root cause*.

Note that there are several main characteristics that a testing/diagnostic system has to satisfy and that these will not usually be met by any single diagnostic method. Therefore, it may be useful to benchmark various methods in terms of the a priori information that needs to be provided, the reliability of the solution, and the generality and efficiency in computation. Tables 1 and 2 summarize the main requirements of a generalized diagnostic system.

Diagnostic systems can be classified according to the a priori knowledge used (Figure 18). The basic a priori knowledge that is needed for fault diagnosis is the set of failures and the relationship between the observations (symptoms) and the failures. The relationship between observations and failures could be explicit (as in a look-up table), or it may be inferred from some source of knowledge. In particular, such knowledge is referred to as causal or model-based knowledge. On the other hand, it may be gleaned from past experience with the process. This knowledge is referred to as process history-based knowledge. The model-based knowledge can be broadly classified as qualitative or quantitative. The model is usually developed based upon some fundamental understanding of the physics of the process. In quantitative models, this understanding is expressed in terms of mathematical functional relationships between the inputs and outputs of the system. In contrast, in qualitative model equations, these relationships are expressed in terms of qualitative functions centered around different units in a process.

Process history-based methods differ from the model-based approaches, where a priori knowledge about the model of the process is assumed (either quantitative or qualitative), in that only the availability of large amounts of historical process data is assumed.

The remainder of this chapter will focus on diagnostic methods based on a quantitative approach.

QUANTITATIVE MODEL-BASED TESTING

In model-based methodology, the feature space is characterized by the use of suitable analytical techniques which permit the achievement of features starting from

Table 1 Performance of Measurement Systems

Measurement	Measurement Technique	Size of Parts (mm)	Accuracy (μm)	Measurement Time (μs)	Online Analysis
[1,0]Dimensional measurement	1D, 2D, 3D Laser interferometer	>0.01	0.01	>1	Yes
	1D Laser triangulation	>0.1	0.1	>10	Yes
Thickness measurement	Laser barrier	>0.001	0.1	>10	Yes
Profile and shape measurement	Laser optics	>0.01	0.1	>10	Yes
Vibration measurement	Laser interferometer	>0.1	0.1	>10	Yes
[1,0]Surface texture and profile measurement	Optics/Laser	>0.1	1	>100	Yes
	SEM, AFM, STM	>0.01	0.001	>100	No

Table 2 Main Characteristics of a Testing/Diagnostic System

Quick detection and diagnosis	The diagnostic system should respond quickly in detecting and diagnosing process malfunctions. These characteristics are related to the bandwidth of the diagnostic system.
Isolability	It is the ability of the diagnostic system to distinguish between different failures.
Robustness	Rejection to various noise and uncertainties.
Novelty identifiability	The diagnostic system is able to decide, given current process conditions, whether the process is functioning normally or abnormally, and, if abnormal, whether the cause is a known malfunction or an unknown, novel, malfunction.
Classification error estimate	An important practical requirement for a diagnostic system is in building the user's confidence on its reliability. This could be greatly facilitated if the diagnostic system could provide a priori estimates of classification errors that can occur.
Adaptability	Processes in general change and evolve due to changes in external inputs or structural changes due to retrofitting and so on. Process operating conditions can change not only due to disturbances but also due to changing environmental conditions. Thus the diagnostic system should be adaptable to changes.
Explanation facility	Besides the ability to identify the source of malfunction, a diagnostic system should also provide explanations of how the fault originated and propagated to the current situation.
Modeling requirements	Modeling is any a priori knowledge about the system to be observed. For fast and easy deployment of a real-time diagnostic system, the modeling effort should be minimal.
Storage and computational requirements	Usually, quick real-time solutions would require algorithms and implementations which are computationally less complex, but might entail high storage requirements. One would prefer a diagnostic system that is able to achieve a reasonable balance of these two competing requirements.
Multiple fault identifiability	The ability to identify multiple faults. In a general nonlinear system, the interactions would usually be synergistic and, hence, a diagnostic system may not be able to use the individual fault patterns to model the combined effect of the faults.

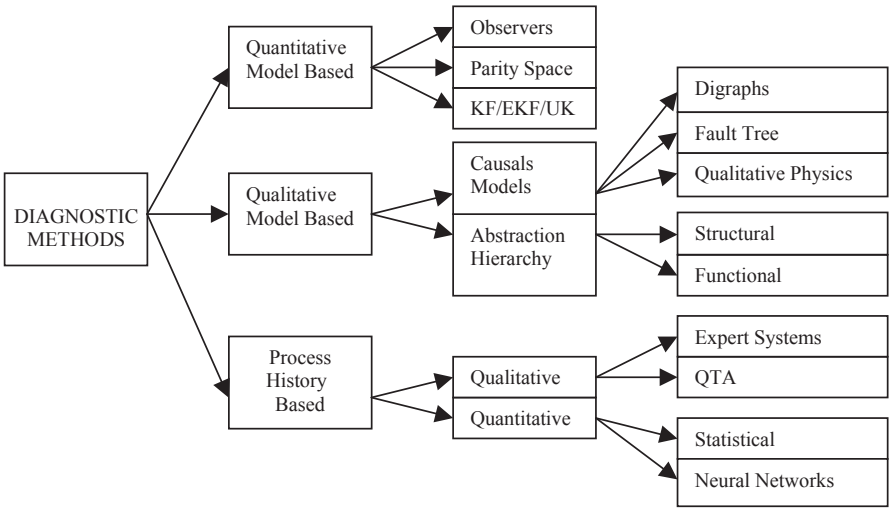

FIGURE 18

Classification of diagnostic techniques.

measurements (observed signals), mathematical or experimental models of the observed system, some statistical information about model uncertainties and signal noise. Some of the most suitable techniques are as follows:

- Adaptive observers;
- Parity relations;
- KFs; and
- Parameters estimation algorithms.

The performances of various methods are summarized in Table 3, with reference to feature extraction capability, nonlinear systems handling, noise rejection, and the possibility to estimate not only state, but also parameter deviations. In particular, extended (EKF) and unscented (UKF) formulations are very efficient and can be implemented with a low/medium level of computation complexity. These will be described in the following paragraph as *state estimators*.

A state estimator permits the extraction of a greater number of features than the observed signals, for example, by measuring the position of a slide, driven by a linear motor, and the currents in the motor coils, it is possible to estimate velocity, force, friction, stiffness, and other system parameters. Of course, it is necessary to exploit a model of the system to be observed and this task can be carried out by the use of suitable simulation software. The advantages of using state estimators for testing application in the micro-manufacturing area are clear; in fact, in order to enhance both the fault detection and classification sensibility, it is possible to minimize the number of sensors by increasing the estimated features.

Figures 19–21 illustrate a typical Kalman state estimator representation.

Table 3 Performance Comparison of the Main Quantitative Model-Based Estimators

	Features Greater than Measurements	Nonlinear System	Disturbance Rejection	Parameters Estimation
Parity space	No	Yes	Poor	No
Observers	Yes	Yes	Good	Yes
Kalman filters				
LKF (linear)	Yes	No	High	No
EKF (extended)	Yes	Yes (critical)	High	Yes
UKF (unscented)	Yes	Yes	High	Yes

Abbreviation: LKF, linear Kalman filter; EKF, extended Kalman filter; UKF, unscented Kalman filter.

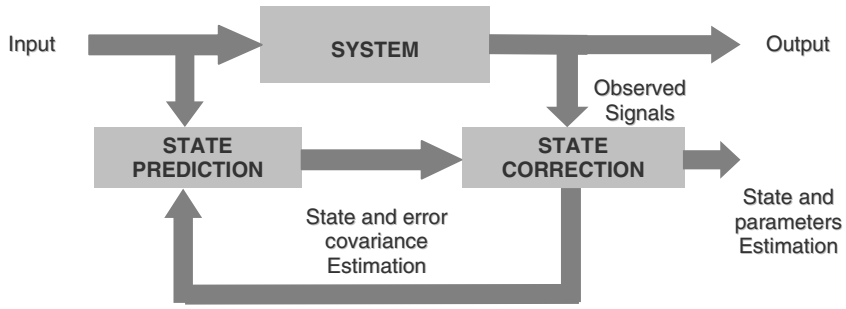

FIGURE 19

Standard Kalman state estimator representation.

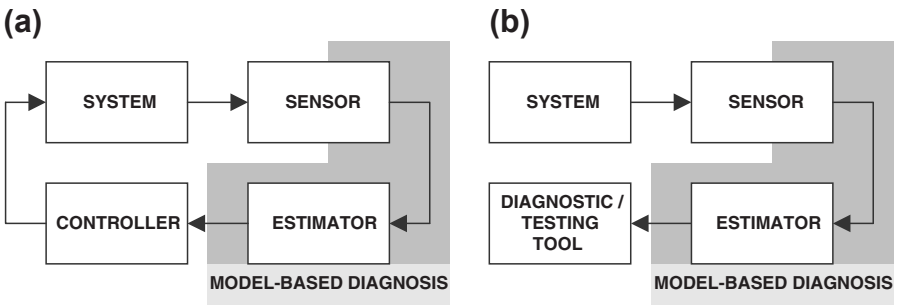

FIGURE 20

Architectures of model-based diagnosis: (a) controlled systems; (b) diagnostic systems.

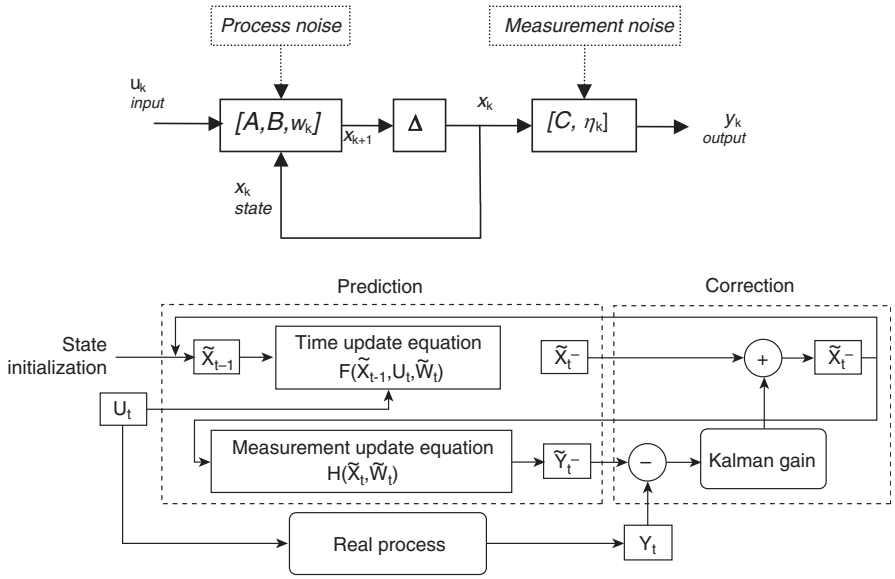

FIGURE 21

General "prediction—correction" structure of the Kalman filter. Model parameters are assumed to be known.

This approach, thanks to knowledge of the model, allows both the observed signals (as part of the output system) and input to be used to produce a prediction of the current state of the observed system. The prediction is then used to correct the current state in order to produce an estimation of the next system state by a recursive cycle. If the system model, which represents the knowledge, includes both variables and parameters of interest (features), then these will be used as failure detectors when the deviation (residual) referred to the nominal value is greater than a prefixed threshold.

The generation of residuals is a recursive and online procedure capable of controlling the behaviors of the system and can even provide a forecast of possible faults (detection) and their classification.

Differently from diagnostic procedures, those of testing can involve test pattern generation for the inputs to the system to be tested. Therefore, achieving optimal performance of the testing system will require both a suitable choice for the system model (the estimation of the most suitable variables and parameters) and the best selection of test pattern input for target faults.

The major advantage of using the quantitative model-based approach is that full control over the behavior of the system will be attained. The mathematical relationships give an analytical redundancy that is useful for relating the internal state variation to the measurements. As the states can be associated to the particular physical characteristics of components inside the system, a fault can be detected rapidly by the abnormal change of states and incorrect component identified.

The main problems associated with the model-based diagnosis methods refer to the complexity of the system, high dimensionality, and process nonlinearity. Such problems often result in difficulties in developing accurate mathematical models of the system. Another problem in these approaches is the simplistic approximation of the disturbances that include modeling errors. In most cases, the disturbance includes only additive uncertainty. However, in practice, it may be advisable to proceed as follows, where appropriate:

1. Begin with a simple model, stating the assumptions in order to focus on particular aspects of the phenomenon.
2. Identify important variables and constants and determine how they relate to each other.
3. Develop the equations that express the relationships between the variables and constants.

Mathematical models typically contain three distinct types of quantities: *input variables*, *dynamic state output variables*, and *parameters*. Output variables give the model solution. When parameters depend on environment interaction, then the choice of what to specify as input variables and what to specify as parameters is somewhat arbitrary and, often, model dependent. Input variables may raise severe modeling uncertainties in the form of multiplicative uncertainties. Another disadvantage with these methods is that, if a fault is not specifically modeled (novelty identifiability), there is no certainty that the residuals will be able to detect it.

When a large-scale process is considered, the size of the bank of filters may seriously increase the computational complexity, although, with the recent increase in computational power and the essential linear nature of these problems, this may no longer be a serious bottleneck.

The core of a quantitative model-based testing procedure is the state estimator. The important issue in the estimators is the knowledge of the system model. Building a mathematical model for a system can be a difficult, yet interesting, task: it is essential to know all the features of the process and, therefore, a thorough understanding of the underlying scientific concepts is necessary. Although problems may require very different methods of solution, the following steps outline a general approach to the mathematical modeling process [6]:

1. Identify the problem, define the terms, and draw diagrams which characterize a single physical problem while the parameters determine the context or setting of the physical problem. Dynamic systems are also characterized by a set of variables called states that represent the memory of the system. A typical representation in state variables is

$$\frac{d\mathbf{x}(t)}{dt} = \mathrm{f}(t, \mathbf{x}(t), \mathbf{u}(t), \boldsymbol{\theta}(t)) \tag{1}$$

$$\mathbf{y}(t) = \mathbf{h}(t, \mathbf{x}(t), \boldsymbol{\theta}(t)) \tag{2}$$

where **x** are the states, **u** the inputs, **y** the outputs, and **θ** the parameters.

2. The simplest case is when the system is time invariant and is modeled with linear differential equations:

$$\begin{aligned} \frac{d\mathbf{x}(t)}{dt} &= \mathbf{F}\mathbf{x}(t) + \mathbf{G}\mathbf{u}(t) \\ \mathbf{y}(t) &= \mathbf{H}\mathbf{x}(t) + \mathbf{L}\mathbf{u}(t) \end{aligned} \tag{3}$$

3. The equations are typically continuous, but for computer processing purposes they are expressed in discrete time:

$$\begin{aligned} \mathbf{x}_{k+1} &= \mathbf{A}\mathbf{x}_k + \mathbf{B}\mathbf{u}_k \\ \mathbf{y}_k &= \mathbf{C}\mathbf{x}_k + \mathbf{D}\mathbf{u}_k \end{aligned} \tag{4}$$

The problem of a state estimator is to measure the output **y** and, by knowledge of input **u** and the matrices of the model **A**, **B**, **C**, **D**, to extract the state **x.**

During the design and analysis of technical systems that encompass several physical domains, the use of adequate models is of great importance. Using suitable techniques of modeling and simulation, these models are easy to create and can be updated rapidly when this is required. Generally, an important aspect of systems is their dynamic behavior. This is especially true for systems that exhibit fast changes or systems that should behave accurately: in such cases, it is useful to choose the most appropriate model that meets the achievement of performance and then simulate to update the best parameter values.

In micro-engineering, the characterization of materials, micro-structures and properties is frequently carried out through simulations. This is often done to better understand and reproduce mechanical behavior. During the development of a new micro-device, mathematical equations governing the physics of the process are known. Due to this feature, model-based techniques for fault diagnosis or testing can be applied in this field. In fact, a reduced number of sensors are often required for systems having reduced dimensions. The state estimator method can easily reduce the number of sensors because there is an analytical redundancy introduced by the mathematical relationship. In this manner, some sensors can be omitted because the measurements are estimated. Some techniques, such as the KFs, are also useful because they produce reliable estimates from noisy measurements. This permits the reduction of the scale of the application without serious problems.

Together, the state and parameter estimations are useful to follow the performance alterations of internal components of a complex system. If the characteristics of a component vary slowly, and the maximum allowed displacement is known, then the time at which a substitution will be necessary may be calculated. This is the core of predictive diagnosis. With parameter estimation, the

changes in some machine parameter (for example, the friction) may be estimated, such that the coefficients of a software controller may be rapidly reconfigured. This is an autocompensation technique which leads to autorepairing strategies.

All these features of the model-based diagnosis methods meet the most important requirements of a micro-application system, as evidenced in Tables 4 and 5.

THE KALMAN ESTIMATOR

The Kalman estimator, or KF, is a mathematical algorithm that provides efficient computational and recursive methods to estimate the state of a process by minimizing the variance of the estimate error. The filter is very powerful in several aspects: it supports estimations of past, present, and even future states, and it can do so even when the precise nature of the modeled system is unknown [7,8].

The basic framework for the discrete KF involves the estimation of the state of the dynamic system: this can be a discrete-time linear or a nonlinear system represented in state variables. The dynamic system behavior is assumed as a well-known model with Eqn (4) modified in order to take into account model inaccuracy $\mathbf{w}_k$ and measurement noise $\boldsymbol{\eta}_k$:

$$\begin{aligned} \mathbf{x}_{k+1} &= \mathbf{A}\mathbf{x}_k + \mathbf{B}\mathbf{u}_k + \mathbf{w}_k \\ \mathbf{y}_{k+1} &= \mathbf{C}\mathbf{x}_{k+1} + \boldsymbol{\eta}_k \end{aligned} \tag{5}$$

Table 4 How Model-Based Diagnosis Meets the Requirements of a Micro-application

	Sensors Reduction	Predictive Diagnosis	Disturbance Rejection	Autorepairing
Space saving	X			
High efficiency	X	X	X	X
High reliability	X	X	X	X
Low cost	X	X		

Table 5 Number of Measurements (=2) versus Number of Estimated Features (=5)

[0,1–2]Estimated State Variables		[0,3–4]Estimated Parameters		[0,5–6]Measurement (sensors)	
Position Velocity Drag force	*X* (m) d*x*/d*t* (m/s) *Fl* (N)	Stiffness Piezovoltage coefficient	K_R (N/m) *Kv* (N/V)	Voltage Transducer Linear encoder	*V* *Xl*

The KF estimates a process by using a feedback concept: the filter estimates the *state* at a given time and then obtains feedback in the form of innovations or residuals.

The equations for the KF fall into two groups: time update equations and measurement update equations. In order to obtain the a priori estimates for the next time step, the time update equations are responsible for projecting forward (in time) the current state and error covariance estimates. The measurement update equations are responsible for the feedback; i.e., for incorporating a new measurement into the a priori estimate to obtain an improved a posteriori estimate.

The time update equations can also be thought of as predictor equations, while the measurement update equations can be thought of as corrector equations: the time update projects the current state estimate forward in time. The measurement update adjusts the projected estimate by an actual measurement at that time. The final estimation algorithm resembles that of a predictor−corrector algorithm for solving numerical problems [9].

The KF, also called the LKF (linear KF), is only used for linear systems; unfortunately, many real-world systems, especially mechanical systems, are nonlinear in nature. Since even the measurement relationships to the process are often nonlinear, the KF cannot be used to estimate the states. The extended Kalman filter (EKF) was developed to account for these nonlinearities: in order to estimate the state, even if the system is nonlinear, this evolution of the KF obtains a linearization around the current mean and covariance. This filter is based upon the principle of linearizing the measurements and evolution models using Taylor series expansions (truncated at the first-order term, with the assumption that the error incurred by neglecting the higher-order terms is small in comparison to the first-order terms). The series approximations in the EKF algorithm can, however, lead to poor representations of the nonlinear functions and probability distributions of interest.

It is important to note that a fundamental flaw of the EKF is that the distributions (or densities in the continuous case) of the various random variables are no longer normal after undergoing their respective nonlinear transformations. When the system has strong nonlinear transformations, the EFK may be an inadequate state estimator, because the system loses its features, especially for estimation of convergence time.

For heavily nonlinear systems, the UKF (unscented Kalman filter) solves the approximation issues of the EKF. The state distribution is represented by a Gaussian random variable (GRV), using a minimal set of carefully chosen sample points (called sigma points). These sample points completely capture the true mean and covariance of the GRV, and, when propagated through the true nonlinear system, capture the posterior mean and covariance accurately to the third order (Taylor series expansion) for any nonlinearity. The unscented Kalman filter is based on the unscented transform and does not require linearization to handle nonlinear equations [10].

The UKF leads to more accurate results than the EKF and, in particular, it generates much better estimates of the covariance of the states (the EKF seems to underestimate this quantity). The UKF has, however, the limitation that it does not apply to general non-Gaussian distributions.

The SRUKF (square-root unscented Kalman filter) is a filter based on UFK and it reduces the algorithm complexity by the adequate use of the Cholesky and QR decompositions (computation of eingenvalues).

APPLICATION ON MICRO-DEVICES AND MACHINES

As an example of how model-based testing can be applied to the testing of devices particularly suited for micro-positioning application, the case of piezoelectric inchworm motors may be considered. These devices take advantage of piezoceramic characteristics to produce displacements with nanometer resolution, while large travel is assured by an inchworm technique. The inchworm technique is based on the simple concept of the incremental sum of the relatively small displacements produced by piezoceramic elements in order to generate a large displacement.

As shown in Figure 22, a typical inchworm-type linear motor has three major components: two clamping mechanisms (referred to as brakes B1 and B2) and an extending mechanism (referred as mover M). During the greater part of a typical inchworm cycle, only one clamping device is to be activated at any given time, thus allowing the extender to extend and retract freely. The clamping mechanisms are normally designed to create a frictional force that can withstand the static forces produced by a constant load and dynamic forces produced by the extending mechanism. The purpose of the extending mechanism is to generate the small displacements which the inchworm technique sums to produce a large displacement.

The typical cycle of an inchworm technique linear motor reveals that the velocity of the motor is directly dependent on the step size of the motor and on the rate at which the cycle is repeated. To determine a model for a designed motor, the important parameters to be considered all relate to the behavior of the model [11]. The chosen parameters are the stiffness and damping of the extending mechanism, the mass of the clamping mechanisms, the forces applied to the motor, and the forces generated by the motor. Using these parameters, a second-order (mass−spring−damper) system is used to model the behavior of the model.

Figure 22 also shows a diagram of the chosen model, supposing that the central point of the extender is fixed in space. The symbols are as follows:

$x1$: displacement of brake 1
Fr: stiffness force of the extending actuator
Fm: force generated by the extending actuator
Fd: damping force of the extending actuator
Fl: force of the applied load
V: voltage supply

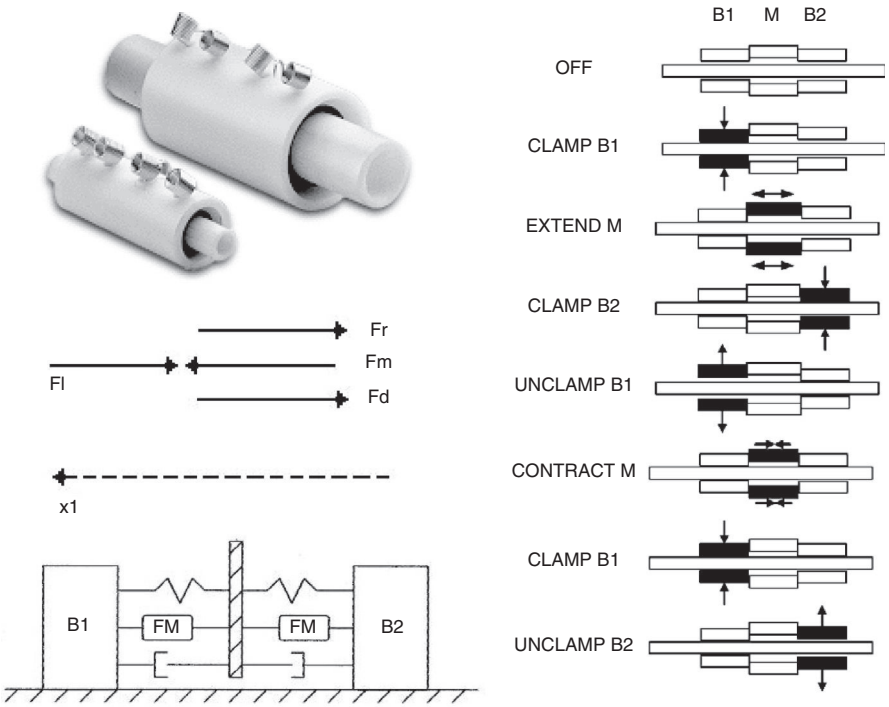

FIGURE 22

Modeling of an inchworm piezomotor and cycle.

By summing the forces shown in the diagram, the equations of motion are derived according to Newton's second law:

$$M\frac{d^2x1}{dt^2} = Fm - Fr - Fd - Fl = Kv * V - Kr * x1 - Kd * \frac{dx1}{dt} - Fl \qquad (6)$$

The parameters in this equation are as follows:

M: mass of brake
Kv: voltage constant of the piezoelectric effect
Kr: stiffness coefficient
Kd: damping coefficient

Assuming $\frac{dx1}{dt} = v1$ and writing Eqn (6) in a state-space form, provides

$$\begin{bmatrix} \frac{dx1}{dt} \\ \frac{dv1}{dt} \end{bmatrix} = \begin{bmatrix} 0 & 1 \\ -\frac{Kr}{M} & -\frac{Kd}{M} \end{bmatrix} \begin{bmatrix} x1 \\ v1 \end{bmatrix} + \begin{bmatrix} 0 & 0 \\ \frac{Kv}{M} & -\frac{1}{M} \end{bmatrix} \begin{bmatrix} V \\ Fl \end{bmatrix} \qquad (7)$$

which represents the first of Eqn (5).

The second equation depends on the outputs chosen to observe the system. In order to estimate, for example, position, velocity, load force, the stiffness, and the voltage constant parameter, all that is needed is the voltage supply V, an input to the system, and the measurement of mover position $x1$, an observation represented by the following equation:

$$[yx] = [1 \quad 0] \begin{bmatrix} x1 \\ v1 \end{bmatrix} \tag{8}$$

Figure 23 shows the applied load force (dashed line) and its estimate (solid line). The signal is modulated by the control signal on the piezoelement. Figure 24 shows the estimation of the piezoelectric coefficient (solid line) and its true value (dashed line). The variation corresponds to a fault which changes the coefficient from 7 N/V to 5.25 N/V. As shown in the figure, the convergence time to the second value is 0.3 s because the mover is controlled by an ON/OFF signal and the estimated curve tends to reach the right value only when the control is ON. This means that the system needs to be in an excited state in order to enable possible fault detection.

Figure 25 shows the estimation of the stiffness coefficient. The very low convergence time (below 0.1 s) shows the high dynamic capability of the Kalman estimator.

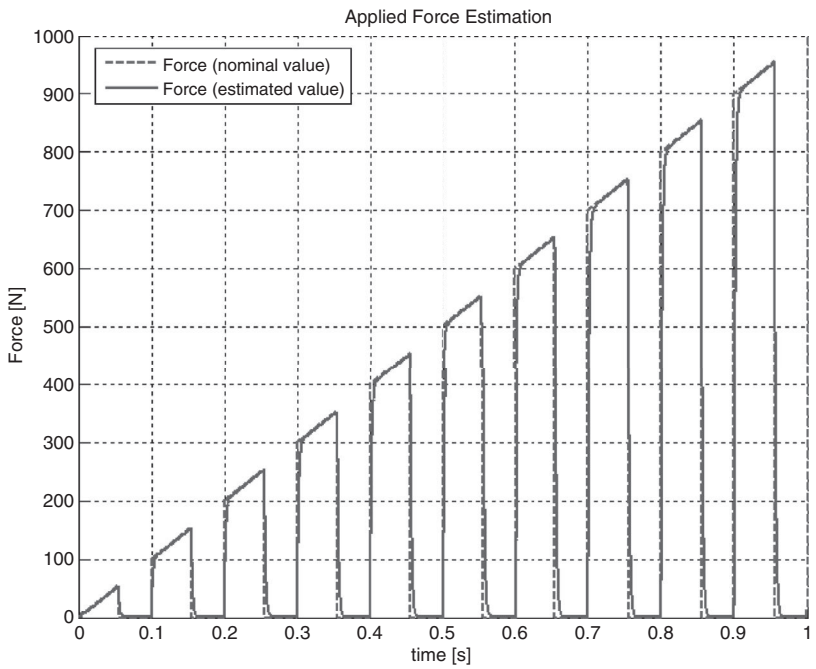

FIGURE 23

Force of a load applied to the inchworm.

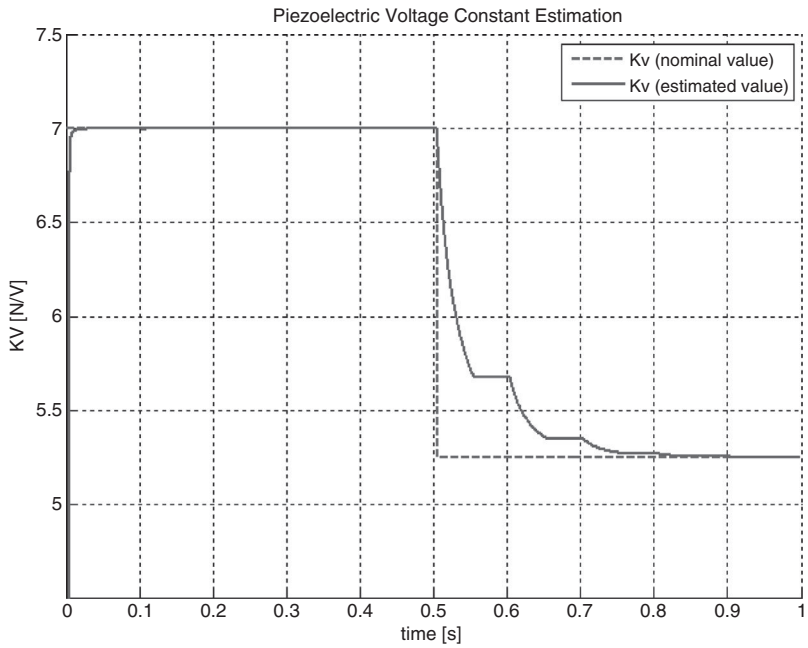

FIGURE 24

Piezoelectric parameter variation.

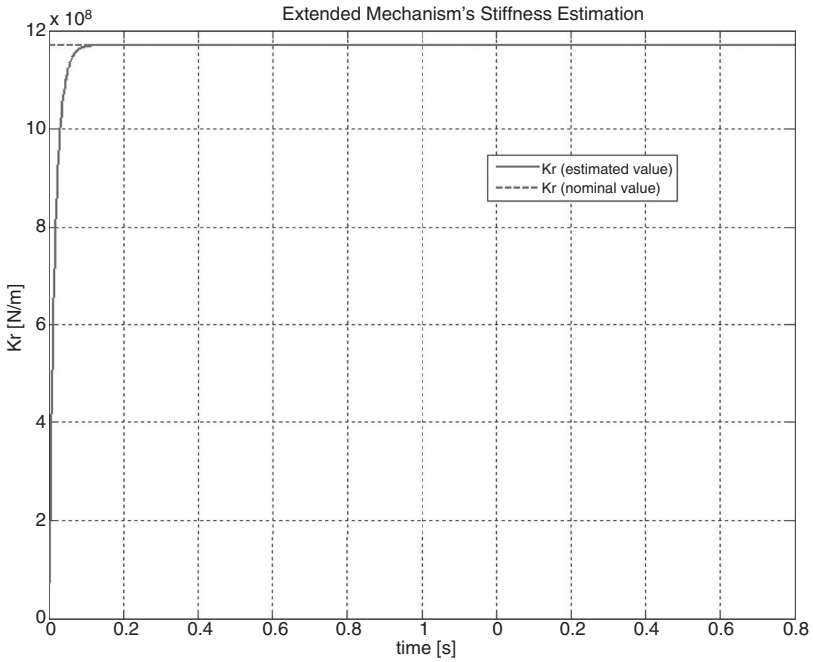

FIGURE 25

Stiffness estimation.

CONCLUSIONS

Testing for micro-manufacturing processes is characterized by requirements on:

- precision;
- noninvasiveness;
- being contactless;
- minimization of the number of sensors;
- low complexity.

Noncontact measurement techniques based on laser sensors and precise movement systems represent the best choice in order to achieve a complete testing system based on direct measurement. When a great number of signals have to be acquired in order to improve the monitoring of the normal working conditions of devices or complex machines, model-based testing can be used to reduce the number of direct measurements (without a reduction of the number of interested signals).

Model-based testing and diagnosis for micro-manufacturing may exploit advantages from the application of estimation techniques in order to extract features from modeled systems. The reduction of the number of sensors is possible by increasing the information flow from the tested system. This information could be well represented by a proper system model. Estimation techniques, such as the KFs, can aid the extraction of variables and parameters which cannot be measured in a direct way, allowing a number of available features greater than the number of signals measured.

The application of model-based testing and diagnostic procedures to the micro-/meso-devices world represents a very efficient and powerful way to increase quality and reliability, while at the same time reducing system complexity.

ACKNOWLEDGMENTS

Special thanks to Professor Biagio Turchiano, Full Professor of Automatic Control and Head of Department, Dipartimento di Elettrotecnica ed Elettronica, Politecnico di Bari, Italy, and to Professor Mauro Onori, Associate Professor, Evolvable Production Systems Group, KTH, Stockholm, Sweden. Thanks also to colleague Eng. Orlando Petrone, Mechatronic Group leader of MASMEC Research and Development Department. Many issues included in this work are related to results achieved by MASMEC Srl, Bari, Italy, for the European Research Project MASMICRO.

REFERENCES

[1] Oakland JS. Statistical process control. Butterworth-Heinemann; 1996.
[2] Isermann R. Model-based fault detection and diagnosis – status and applications. IFAC; 2004.

[3] Chen CH, Pau LF, Wang PSP, editors. The handbook of pattern recognition and computer vision. 2nd ed. World Scientific Publishing Co; 1998. p. 207–48.
[4] Sarid D. Scanning force microscopy, Oxford series in optical and imaging sciences. New York: Oxford University Press; 1991.
[5] Venkatasubramanian V, Rengaswamy R, Yin K, Kavuri SN. A review of process fault detection and diagnosis, Part I: quantitative model-based methods. Comput Chem Eng 2003;27:293–311.
[6] Ljung L, Kailath T, editors. System identification, theory for the user. 2nd ed. Prentice Hall PTR; 1999.
[7] Bishop G, Welch G. An introduction to the Kalman Filter, technical report. Chapel Hill, NC 27599-3175: Department of Computer Science, University of North Carolina at Chapel Hill; May 2003.
[8] Haykin S, editor. Kalman filtering and neural networks. John Wiley & Sons, Inc; 2001.
[9] Dewallef P, Léonard O. On-line measurement validation and performance monitoring using robust Kalman filtering techniques, ASME Paper GT-2003-38379, 2003.
[10] LaViola Jr. A comparison of unscented and extended Kalman filtering for estimating quaternion motion, Joseph J. Brown American Control Conference, 2003. Proceedings of the 2003, vol. 3.
[11] Hagood N, Chung W, von Flotow A. Modelling of piezoelectric actuator dynamics for active structural control. J Intell Mat Syst Struct July 1990;1:327–54.

CHAPTER

30

Optical Coherence Tomography for the Characterization of Micro-parts and Structures

David Stifter

Center for Surface and Nanoanalytics (ZONA), Johannes Kepler University Linz, Linz, Austria

CHAPTER OUTLINE

INTRODUCTION

Optical coherence tomography (OCT) was presented in 1991 for the first time as a powerful technique for applications in the field of medical diagnostics [1]. It was demonstrated that with OCT high-resolution cross-sectional images of biological tissue can be obtained in a contactless and noninvasive way. The investigation of retinal diseases, such as glaucoma, belonged to the first applications, with a main consequence being that commercial retinal OCT scanners are already available and used in eye clinics and hospitals. The OCT method has been further refined in the meantime, and a multitude of new developments and extensions for this technique have been introduced, as also summarized in several books and reviews (e.g., [2,3]). The main applications and driving forces for these developments in the field of OCT research can still be found in the area of biomedical diagnostics, ranging from the investigation of the eye (e.g., also cornea), skin (e.g., melanoma), teeth (caries), or of interior organs and vessels (e.g., by OCT endoscopy) to life science applications providing image details down to the subcellular level.

Although the main route of OCT developments is for biomedical purposes, the potential of OCT for contactless and nondestructive evaluation of nonbiological materials and components has been recognized due to the fact that depth-resolved

Micromanufacturing Engineering and Technology. http://dx.doi.org/10.1016/B978-0-323-31149-6.00030-X

structural information can be obtained with high accuracy in a fast and easy way from the interior of materials, even for those of highly scattering nature. Consequently, a variety of technical applications for OCT have now emerged, as compiled in a recent comprehensive review [4], anticipating a future increase in their number with respect to their biomedical counterparts.

In this chapter, initially, an introduction is provided to the underlying measurement principle of OCT and a short overview on different alternative and advanced OCT measurement concepts is given. A selection of proven applications of classical and advanced OCT techniques for the evaluation of micro-structures is then presented. It is worth noting that due to the novelty of the herein-introduced OCT techniques and results, testing and evaluation of micro-structures by OCT is not yet a routine task but is expected to fully emerge in the next few years, as OCT measurement technology further develops and matures.

MEASUREMENT PRINCIPLES OF STANDARD AND SELECTED ADVANCED OCT TECHNIQUES

The basic physical principle of OCT is low-coherence interferometry (LCI): an interferometer, mostly built in Michelson geometry, is illuminated with spectrally broad light, as depicted in Figure 1(a). The sample is placed in one arm of the interferometer, the reference arm itself is equipped with a movable mirror. Since low-coherence light is used, interference is only observed if the length of the optical path between the beamsplitter and a backscattering feature within the sample,

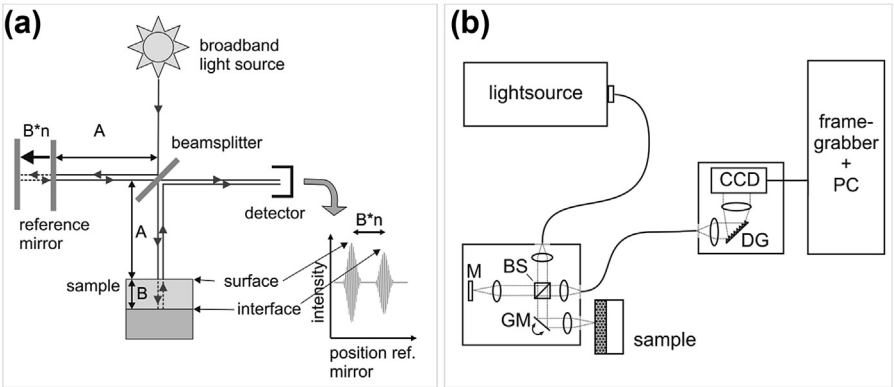

FIGURE 1

(a) Schematic sketch of a standard (time-domain) optical coherence tomography (OCT) setup with a broadband light source illuminating a Michelson interferometer. A, B: path lengths, n: refractive index of sample layer; (b) layout of a spectral-domain OCT setup. Abbreviations: beamsplitter (BS), reference mirror (M), galvano scanner mirror for lateral scanning (GM), diffraction grating (DG), line camera (CCD).

such as a buried interface, equals the optical path length of the reference arm. In this way, the absolute positions of backscattering and backreflecting features can be determined. In the example of Figure 1(a), two interference peaks are observed when moving the reference mirror (from surface and interface). Usually, the envelope of the interference signal is taken and it represents a reflectivity depth profile of the sample at a fixed lateral position (so-called A-scan). By measuring several depth profiles at adjacent positions, e.g., by scanning the focused light beam over the sample, cross-sectional images (B-scans) and 3D volume data can be acquired.

The width of the peaks in a depth profile, determining the axial resolution of the system, is given by the coherence length of the used light source: the broader the spectrum, the higher the axial resolution [5]. Standard OCT systems exhibit axial resolutions in the 5−15 μm range, ultrahigh resolution OCTs [6] have been reported showing even submicron resolution with very broadband light sources, like thermal or super continuum sources. The light sources are spectrally situated mostly in the near-infrared region (800−1500 nm) with an average power in the milliwatt range, ensuring damage-free (noninvasive) investigation of living tissue. Consequently, no special safety precautions have to be taken when handling an OCT apparatus, as it is mandatory for, e.g., X-ray computed tomography.

For OCT, the axial resolution is decoupled from the lateral one, which is determined by the spot size of the focused light beam on the sample. Due to the decoupling, a high axial resolution can be maintained even for long working distances, in contrast to confocal microscopy where high numerical aperture (NA) optics has to be used for good depth discrimination [7]. The axial resolution in OCT should not be mistaken for the accuracy with which the position of the envelope peaks can be determined: on smooth surfaces and interfaces, precision in the nanometer range is feasible. In this context, scanning white light interferometry (SWLI) and coherence probe microscopy (CPM) shall be mentioned, since these methods share the same principle (LCI) and a similar setup as OCT [8]: in contrast to conventional OCT, mostly whole surface areas are illuminated at once, and area cameras are used to register the interference signal when moving a reference mirror. Such systems were optimized for the measurement of surface topographies with subnanometer accuracy and are now widely employed in the semiconductor industry for the inspection of integrated circuits [9] or for the characterization of micro-electromechanical structures [10]. Although transparent layers can also be measured with these systems (e.g., thickness), only OCT is also capable of determining the internal structure of scattering and turbid media with reasonable penetration depth (in the millimeter range). However, the border between the different techniques start to blur, as a combination of the CPM technique and OCT leads, e.g., to full-field OCT (FF-OCT) and FF optical coherence microscopy (FF-OCM) by using high NA optics, area illumination, and area cameras [11].

The concept of obtaining depth information by moving the reference mirror (Figure 1(a)) is referred to as time-domain (TD) OCT configuration. A new trend is to build OCT devices preferably in the Fourier-domain (FD) configuration. In FD-OCT, the reference mirror is fixed and the wavelength of a narrowband

light source is rapidly tuned (swept-source OCT (SS-OCT)) or the spectrum of a broadband light source is acquired by a spectrum analyzer as depicted in Figure 1(b) (spectral-domain OCT (SD-OCT)). The obtained spectral data are Fourier transformed to obtain at once the desired depth information in form of a whole A-scan. The main advantages of FD-OCT over TD-OCT can be found in the fact that no movable parts are needed for depth scanning, in the increased system sensitivity and in the high measurement speed with A-scan rates of several hundreds of kHz for SD-OCT [12] reaching up to the megahertz range for SS-OCT [13].

Besides measuring the intensity of the back reflected light to gain structural information, further sample properties and enhanced contrast can be obtained by taking additional physical phenomena into account with advanced OCT extensions: a determination of the frequency shift of the reflected light from moving particles leads to optical Doppler tomography (ODT) for the depth-resolved measurement of flow velocities [14]. Finally, polarization-sensitive OCT (PS-OCT) shall be mentioned: the evaluation of the polarization state of the light gives insight into the birefringence properties of the sample [15].

APPLICATION OF OCT FOR THE EVALUATION OF STRUCTURES ON THE MICRON SCALE

In the following, a short selection of instructive examples for OCT applied by the author to measurement tasks in micro- and miniature manufacturing are given, especially with the intention to familiarize the reader with the potential of the novel OCT techniques for these kinds of applications and to promote OCT for future routine tasks in the characterization and testing of micro- and miniature structures.

At first, an OCT study on photoresist molds for the production of miniature gear wheels with the LIGA molding technology (LIGA, German acronym for lithography-electroplating-molding) is presented, with the results depicted in Figure 2. High aspect ratio trenches exhibiting widths down to 30 μm were etched in thick photoresist layers deposited on gold-coated silicon wafers. Residual particles in the trenches as well as the defects of the resist/wafer interface are of primary concern since they affect the quality of the molds, crucial for the subsequent electroplating step. As can be seen from the OCT cross-sectional image in Figure 2(a), the thickness of the photoresist layer can easily be determined. However, since the optical path length within the material is different to the path length in the (air-filled) trenches, a virtual step is observed at the wafer surface. From the height of this virtual step, the refractive index of the material can be determined and therefore also the geometrical (and not only the optical) thickness of the resist layer can be obtained. Furthermore, it should be noted that the rather low NA optics of OCT is of significant advantage in order to access the bottom of the high aspect ratio trenches.

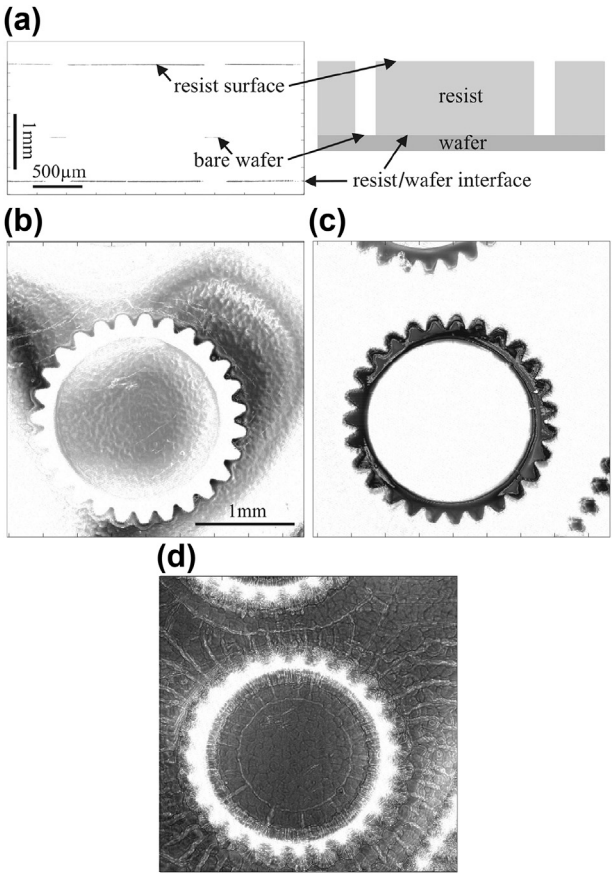

FIGURE 2

(a) Cross-sectional scan and schematic drawing of a mold for a miniature wheel in a 1.3-mm thick photoresist layer on a gold-coated wafer; (b)–(d) 3×3 mm^2 *en face* scans of the structure. In (a), only the surfaces of the bare resist and the wafer, and the resist/wafer interface can be distinguished. In (b)–(d), the full geometric information of the structure at these levels is obtained. In (b), the resist surface is imaged, (c) and (d) were recorded at depth positions of the optical path length corresponding to the bare wafer surface and the resist/wafer interface (as shown in (a)), respectively.

From Ref. [16], © Optical Society of America, 2005.

By using so-called *en face* scanning OCT [16], single planes parallel to the sample surface can be at once imaged at defined depth locations, as shown in Figure 2(b)–(d). In addition to the geometrical form of the wheel, surface corrugations with a maximum height of less than 100 nm (Figure 2(b)), residual particles in the trenches (white spots in the black wheel structure, Figure 2(c)) and a network of ridges (most probably caused by underetching, Figure 2(d)), could be observed and evaluated.

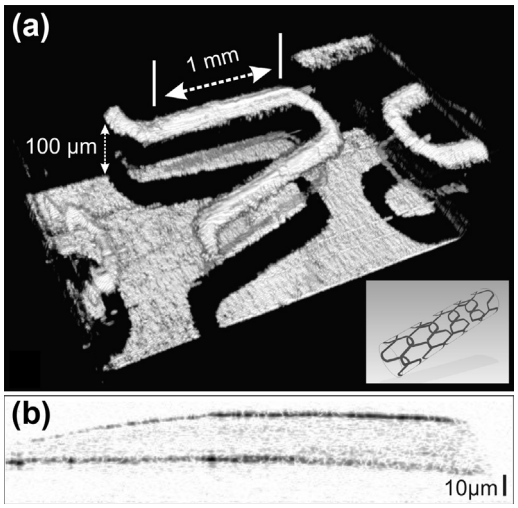

FIGURE 3

Optical coherence tomography inspection of a coated (drug-eluting) medical stent: (a) topography of one stent segment with schematic structure of the whole stent in the inset; (b) cross section of the polymer coating on the metal surface of the stent (scan taken along the straight part of the segment as indicated in (a)); measurements performed in cooperation with K. Wiesauer, UAR GmbH, Linz/Austria.

A second example is presented in Figure 3, where a drug-eluting medical stent has been investigated. The stent structure is essentially a thin metallic network in the shape of a tube (see also schematic sketch in the inset of Figure 3(a)) which is inserted, e.g., in blood vessels and expanded to counteract a disease-induced decrease of vessel and duct diameter and helps in this way to maintain the blood flow. Of interest is the topography and roughness of the individual metallic meanders (Figure 3(a)). The stent structure is also coated with a thin ($\sim$5–20 µm) drug-containing polymer layer. Its homogeneity and thickness is crucial for a determined delivery of a drug—enclosed in the polymer layer—to the surrounding tissue in order to hinder the formation of thick tissue at the interior of the expanded vessel, which could again obstruct the blood flow. As can be seen in the cross section of Figure 3(b), taken along one of the linear segments of the meander structure, the polymer layer can easily be resolved with OCT on the rough metal surface and exhibits in this case inhomogeneous regions with thickness variations of more than 100%.

The extension of OCT toward PS-OCT leads to additional contrast and information, exemplified in Figure 4. *En face* PS-OCT has been performed on resist molds, similar to those depicted in Figure 2: PS-OCT is capable to detect the birefringence caused by residual stress in the photoresist layer allowing in this way high-resolution strain/stress mapping within the wheel mold structures.

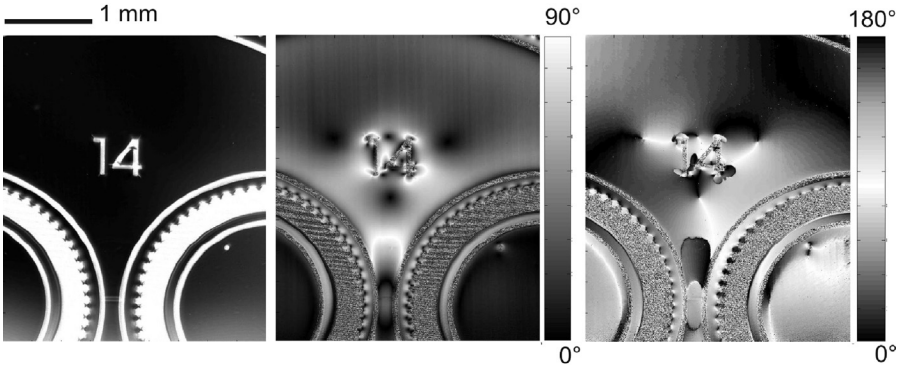

FIGURE 4

En face images of photoresist molds for miniature gear wheels. Left: optical coherence tomography intensity image; middle: optical retardation image (phase lag grayscale coded from 0° to 90°); right: orientation of optical axis indicating the direction of the internal stress within the image plane (orientation grayscale coded from 0° to 180°).

From Ref. [19], © Oldenbourg Verlag 2007.

In addition to the standard intensity image, a retardation image (middle image in Figure 4) is obtained. This image is grayscale coded and gives the phase lag of the reflected light of one polarization direction with respect to the other, orthogonal one. Highly strained areas show strong birefringence leading to higher optical retardation and are depicted in light gray and white in the image. By calibration procedures, i.e., determining the stress-optical coefficient of the material under investigation, even a quantitative evaluation of the strain distribution is possible [17,18]. Furthermore, the orientation of the optical axis, which is related to the orientation of the internal stress within the sample, can also be measured, as shown in the right image of Figure 4. With the help of PS-OCT, valuable insight for the optimization of the production process with its individual photolithographic steps can consequently be gained, especially focusing on the minimization of internal stress, which can cause distortions of the wheel geometries and may lead to detrimental cracks at the wafer/resist interface and between trenches.

This section on selected measurement applications for micro-structures is concluded by recalling the evaluation of micro-fluidic devices with OCT. As an example, in Figure 5 the 3D reconstruction of internal channel structures of such a device measured with a customized high-speed FF-OCM system [20] as dimensional metrology tool is depicted. In addition, also the knowledge of the flow characteristics in micro-fluidic networks and devices, such as micro-mixers and lab-on-a-chip systems, helps to assess the predicted performance and verify the functionality of novel fluidic chip designs. In this view, the flow behavior of micro-mixers was studied by conventional OCT imaging: two liquids with a different concentration of scatterers were used to visualize flow patterns in the

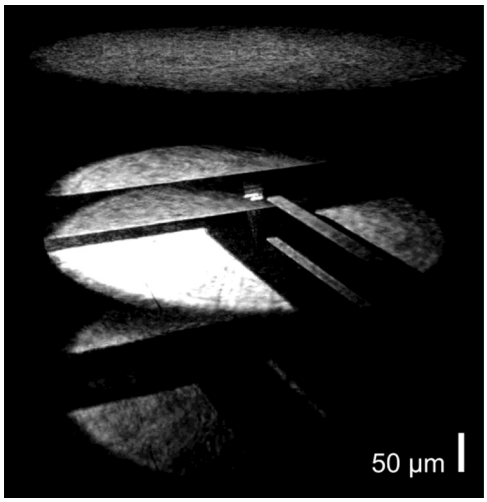

FIGURE 5

3D reconstruction of micro-fluidic channel structures acquired by full-field optical coherence microscopy for dimensional metrology.

Image by S. Schausberger and B. Heise (CDL-MS-MACH/ZONA, Johannes Kepler University Linz/Austria), micro-fluidic sample provided by Fraunhofer IPHT Jena/Germany.

OCT images, giving in this way information on the status of intermixing and the spatial distribution of vortices in the fluidic structure [21]. Besides the retrieval of geometrical information of the flow structure, ODT can now be applied to measure even the flow velocity profiles in the micro-channels in a spatially resolved way, as reported in, e.g., Ref. [22].

CONCLUSIONS AND OUTLOOK

Classical OCT and advanced OCT techniques, providing high resolution and taking advantage of different contrast mechanisms such as birefringence or flow velocity, have been introduced for the evaluation of micro-structures and micro-parts. The fact that depth-resolved information can be obtained—even from the interior of scattering materials—in a contactless way by OCT using harmless infrared light renders this method especially promising for future routine applications in metrology of micro-structures. From the technological point of view, the advantage of FD-OCT with respect to robustness, speed, and achievable sensitivity will further promote its breakthrough. The same is true for the ultrahigh lateral and axial resolution provided by, e.g., high-speed FF-OCM. Currently, the overall potential of OCT is recognized by companies which offered up to now only commercial biomedical OCT systems but are

preparing their products also for the industrial metrology market, such as, e.g., automated inspection solutions for thin multilayer materials. Routine applications for advanced OCT techniques such as PS-OCT or for phase-resolved OCT microscopy providing subnanometer accuracy [23] are yet to come. Finally, it shall be considered that hybrid techniques based on SWLI, CPM, and OCT will allow tailoring the characteristics of measurement systems to the exact requirements imposed by the specific micro-structure evaluation tasks.

ACKNOWLEDGMENTS

Financial support by the Austrian Science Fund as well as by the Federal Ministry of Economy, Family and Youth and by the National Foundation for Research, Technology and Development is acknowledged.

REFERENCES

[1] Huang D, Swanson EA, Lin CP, Schuman JS, Stinson WG, Chang W, et al. Optical coherence tomography. Science 1991;254:1178–81.
[2] Fercher AF, Hitzenberger CK. Optical coherence tomography. Prog Opt 2002;44: 215–301.
[3] Drexler W, Fujimoto JG, editors. Optical coherence tomography, technology and applications. Berlin Heidelberg: Springer; 2008.
[4] Stifter D. Beyond biomedicine: a review of alternative applications and developments for optical coherence tomography. Appl Phys B 2007;88:337–57.
[5] Swanson EA, Huang D, Hee MR, Fujimoto JG, Lin CP, Puliafito CA. High-speed optical coherence domain reflectometry. Opt Lett 1992;17:151–3.
[6] Drexler W, Morgner U, Kartner FX, Pitris C, Boppart SA, Li XD, et al. In vivo ultrahigh-resolution optical coherence tomography. Opt Lett 1999;24:1221–3.
[7] Sheppard CJR. Confocal Laser scanning microscopy. New York: Springer; 1997.
[8] Sheppard CJR, Roy M, Sharma MD. Image formation in low-coherence and confocal interference microscopes. Appl Opt 2004;43:1493–502.
[9] Davidson M, Kaufman K, Mazor I, Cohen F. An application of interference microscopy to integrated circuit inspection and metrology. Proc SPIE 1987;775:233–47.
[10] O'Mahoni C, Hill M, Brunet M, Duane R, Mathewson A. Characterization of micromechanical structures using white-light interferometry. Meas Sci Technol 2003;14: 1807–14.
[11] Dubois A, Boccara AC, Lebec M. Real-time reflectivity and topography of depth-resolved microscopic surfaces. Opt Lett 1999;24:309–11.
[12] Potsaid B, Gorczynska I, Srinivasan VJ, Chen Y, Jiang J, Cable A, et al. Ultrahigh speed spectral/Fourier domain OCT ophthalmic imaging at 70,000 to 312,500 axial scans per second. Opt Express 2008;16:15149–69.
[13] Wieser W, Biedermann BR, Klein T, Eigenwillig CM, Huber R. Multi-Megahertz OCT: high quality 3D imaging at 20 million A-scans and 4.5 GVoxels per second. Opt Express 2010;18:14685–704.

[14] Chen Z, Miller TE, Srinivas S, Wang XJ, Malekafzali A, van Gemert MJC, et al. Noninvasive imaging of in vivo blood flow velocity using optical Doppler tomography. Opt Lett 1997;22:1119−21.
[15] Hitzenberger CK, Götzinger E, Sticker M, Pircher M, Fercher AF. Measurement and imaging of birefringence and optic axis orientation by phase resolved polarization sensitive optical coherence tomography. Opt Express 2001;9:780−90.
[16] Wiesauer K, Pircher M, Götzinger E, Bauer S, Engelke R, Ahrens G, et al. En-face scanning optical coherence tomography with ultra-high resolution for material investigation. Opt Express 2005;13:1015−24.
[17] Wiesauer K, Sanchis Dufau AD, Götzinger E, Pircher M, Hitzenberger CK, Stifter D. Non-destructive quantification of internal stress in polymer materials by polarisation sensitive optical coherence tomography. Acta Mater 2005;53:2785−91.
[18] Stifter D, Leiss-Holzinger E, Major Z, Baumann B, Pircher M, Götzinger E, et al. Dynamic optical studies in materials testing with spectral-domain polarization-sensitive optical coherence tomography. Opt Express 2010;18:25712−25.
[19] Stifter D, Wiesauer K, Pircher M, Götzinger E, Engelke R, Ahrens G, et al. Optische Kohärenztomografie als neues Werkzeug für die zerstörungsfreie Werkstoffprüfung. TM 2007;74:51−6.
[20] Schausberger SE, Heise B, Bernstein S, Stifter D. Full-field optical coherence microscopy with Riesz transform-based demodulation for dynamic imaging. Opt Lett 2012;37:4937−9.
[21] Xi C, Marks DL, Parikh DS, Raskin L, Boppart SA. Structural and functional imaging of 3D microfluidic mixers using optical coherence tomography. Proc Natl Acad Sci 2004;101:7516−21.
[22] Ahn YC, Jung W, Zhan J, Chen Z. Investigation of laminar dispersion with optical coherence tomography and optical Doppler tomography. Opt Express 2005;13: 8164−71.
[23] Joo C, Akkin T, Cense B, Park BH, de Boer JF. Spectral-domain optical coherence phase microscopy for quantitative phase-contrast imaging. Opt Lett 2005;30:2131−3.

CHAPTER

In situ Testing of Mechanical Properties of Materials[1]

31

Fredrik Östlund, Karolina Rzepiejewska-Malyska, Laetitia Philippe, Patrick Schwaller, Johann Michler

Laboratory for Mechanics of Materials and Nanostructures, EMPA, Swiss Federal Laboratories for Materials Testing and Research, Thun, Switzerland

CHAPTER OUTLINE

INTRODUCTION

The mechanical properties of small structures, typically with dimensions within the range of a few hundred microns down to several microns or below, cannot simply be extrapolated from the properties of bulk samples. This is due to two effects. First, samples used for bulk mechanical testing usually have dimensions which are much larger than the micro-structural features, such as grains or particles. Second, mechanical behavior is controlled by certain fundamental length scales. For example, plasticity in metals is controlled by dislocation motion and when obstacles are more closely spaced than about 100 nm can hinder dislocation propagation, leading to decreased plasticity and increased strength. Additionally, fracture in brittle

[1]Figures 1–3 and Table 1, plus similarities in this Chapter are reproduced with permission of MRS *Journal of Materials Research.*

Micromanufacturing Engineering and Technology. http://dx.doi.org/10.1016/B978-0-323-31149-6.00031-1

materials is initiated at flaws with a critical size of several tens of micrometers [1]. The mechanical properties of a material will necessarily change as the sample dimensions become smaller than these fundamental length scales. It is therefore necessary to measure the mechanical properties at a length scale comparable to the feature sizes used in miniature or micro-electromechanical devices. The flow stress dependence on pillar size in micro-compression experiments was shown by Uchic et al. [2], who performed compression tests on Ni pillars having different diameters ranging from 40 μm down to 5 μm and found that for the smallest samples the flow stress is almost three times greater than for bulk Ni.

Accurate prediction of a material's response also requires an understanding of the fundamental mechanisms of material deformation and fracture in the micro- and nano-scale. It is therefore essential that small specimens, for instance, for tensile or compression testing, can be manufactured for which appropriate handling and manipulation techniques and equipment with appropriate load and displacement resolution are available. Also, it has to be possible to observe the material under load in situ to study plastic deformation and crack propagation mechanisms. The scanning electron microscope (SEM) is an ideal platform for in situ mechanical testing, as it covers a magnification range from 10 to 10^6 times, exhibits a relatively large specimen chamber that can accommodate mechanical testing equipment, and has analytical capabilities for determining local chemical composition and crystal structure.

In this chapter, the reader will be introduced to the peculiarities of integrating materials testing within an SEM. The most popular techniques will be explored, i.e., miniaturized tensile tests, compression tests, and nano-indentation tests. Then the subject of image analysis will be touched upon and finally a case study combining the use of compressive and tensile testing methods will be presented.

INTEGRATING A MECHANICAL TESTING SETUP IN AN SEM

Integrating a mechanical testing setup within an SEM raises some difficulties. In the following, some important details about this process will be described.

It is of course necessary to use actuators and load sensors that can deliver the required displacements and measure the low loads encountered at these scales. Due to the limited space available in an SEM chamber. The actuators and sensors must have small dimensions. In particular, to achieve an optimal performance of the SEM, the distance between the objective lens of the SEM and the sample has to be kept to a minimum. Typically, the optimal working distance is between 2 and 5 mm.

The vacuum in the chamber also has to be taken into account when designing a mechanical testing device. All elements of the device have to be vacuum compatible, meaning that they do not emit gas in vacuum. Special care should be taken to avoid, for example, plastics and oil.

Note that some materials which normally do not emit gas in vacuum can do so when exposed to an electron beam. Teflon, for example, releases fluorine when

exposed to high-energy electrons. To facilitate the evacuation of the chamber, parts that contain threads should have extra channels to allow air to exit the components.

Magnetic materials should be avoided, since their magnetic fields can affect the electron beam of the SEM, resulting in a distorted image with bad resolution. Similarly, electrical components must have sufficient electrical shielding. All parts close to the electron beam should also be conductive and grounded in order to avoid electrical charging. In particular, this applies to the tip used in compression and indentation tests. Usually, these tips are made of diamond because of the high hardness requirements. Pure diamond, however, is a very poor electrical conductor. Therefore, boron-doped diamond is a preferred choice. Even if these rules are followed, the maximum resolution of the SEM will generally not be achieved.

Note that not all experiments have to be performed in situ: cost and time have to be weighted against gain of information. In addition, not all materials can be tested in situ. The electron beam might affect the sample by, for example, breaking chemical bonds or the sample might become too highly charged to be imaged. Charging problems can often be solved by depositing a thin metal layer on the samples before the testing. However, this can potentially change the mechanical properties of the material.

TENSILE TESTS

Tensile testing is probably the most commonly used standardized [3] method to determine the mechanical properties of materials [4]. In a typical tensile test, a specimen having a small, uniform cross section is strained until failure. The deformation (increase in length) and applied load are continuously measured during the whole experiment. The applied engineering stress σ is defined by the load F divided by the initial cross-sectional area A_0 of the sample. The engineering strain ε is defined by the measured length change Δl divided by the initial length l_0:

$$\sigma = \frac{F}{A_0} \tag{1}$$

$$\varepsilon = \frac{\Delta l}{l_0} \tag{2}$$

A schematic representation of an engineering stress/strain curve obtained this way is shown in Figure 1.

From such a curve, the following properties can be inferred. The linear increase at low strain is an elastic deformation that is described by Young's modulus E (the slope of the stress/strain curve). The transition between elastic and plastic deformation is defined by the 0.2% offset yield stress $R_{p0.2}$ commonly used in materials technology. In Figure 1, a straight line shifted by a strain of 0.002 is drawn parallel to the linear elastic portion. The intersection of this line with the stress/strain curve is taken as the yield stress.

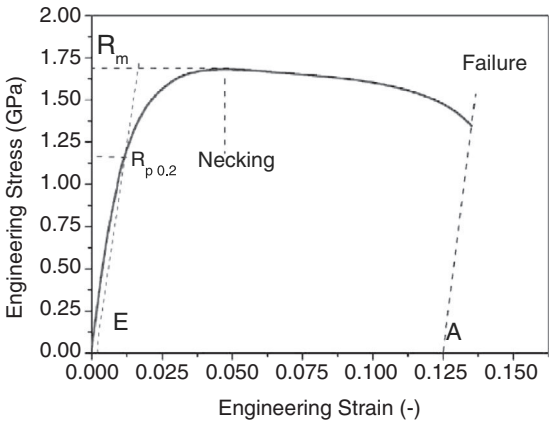

FIGURE 1

Engineering stress/strain curve for an NiCo sample indicating the relevant quantities that can be extracted from the curve (see text for the details).

The tensile strength R_m indicates the deformation where necking of the sample starts. Finally, the elongation at rupture, A, indicates the strain at failure of the sample. The uniaxial deformation is usually applied using a constant strain rate, i.e., using a displacement control, in contrast to a load control. This is because as a sample yields there can be a decrease in the load. If that occurs with load control, the feedback system will try to reestablish the load by increasing the strain. This causes the sample to be rapidly deformed until failure in an uncontrolled manner.

It is also worthwhile mentioning the difference between engineering and true stress and strain values. Engineering stress and strain are defined by Eqns (1) and (2) as shown above. Both quantities refer to the initial cross section and initial length. True stress σ_{true} and true strain $\varepsilon_{\text{true}}$ values take small changes of the deformation into account starting from an instantaneous elastic or plastic deformation. σ_{true} and $\varepsilon_{\text{true}}$ can be calculated as follows:

$$\sigma_{\text{true}} = \sigma(1 + \varepsilon) \tag{3}$$

$$\varepsilon_{\text{true}} = \ln(1 + \varepsilon) \tag{4}$$

For samples in the millimeter range, tensile tests can be performed under an optical microscope. If the samples are smaller, the higher resolution of an SEM is required imaging. This is especially important if the images are used to extract the strain.

From the image sequence, it is sometimes interesting to observe the propagation of cracks induced by the tensile strain and to correlate the crack path or the crack type with other material properties that can be inferred from SEM images. Instead of imaging the sample using secondary electrons, chemical mapping can be done using energy-dispersive X-ray spectroscopy and the orientation of grains of the sample can be recorded using electron backscatter diffraction.

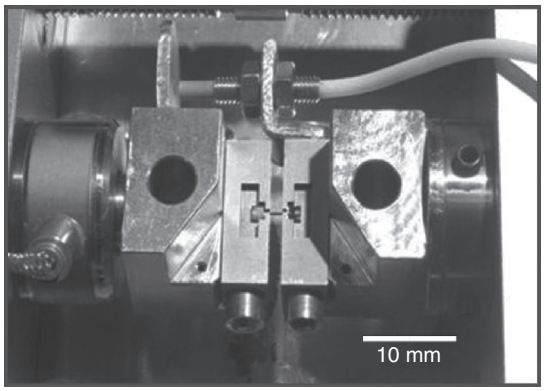

FIGURE 2

A specimen for tensile testing positioned in the sample holder of a tensile testing setup.

Due to the limited overall size of the test stage, the sample dimensions also have to be small (typically only several millimeters in length and a few 100 μm thick). This means that surface properties gain importance and rough surface regions or a slightly different composition in the surface region may influence the measured stress/strain curves. The most critical issue, however, is the correct fixing of the tensile test specimen. Mechanical clamping may be unsuitable because a deformation could already have been induced prior to the actual test. A suitable solution is to use sample holders having the "negative" shape of the specimen and to fit the specimen inside these holding forms: an example of this is shown in Figure 2.

Due to the small dimensions of the tensile test specimens, extensometers or conventional strain gauges cannot be clamped onto the samples. However, the SEM images can be used to calculate strain values. The quantitative evaluation of the strain values from SEM images recorded during the tensile tests, however, is difficult. The total elongation until fracture in the images is often only a few pixels and specialized image analysis routines allowing subpixel resolution have to be used to obtain reliable strain data: this will be further discussed below. In contrast to the displacement measurements, the load measurements can be performed using conventional load cells.

COMPRESSION TESTS

As an alternative and complement to tensile testing, materials can be tested by compression tests. This method has been extensively used for decades and has the advantage that the specimen does not have to be attached at the ends of the testing setup. Compression tests are analogous to tensile tests: a cylindrical sample with uniform diameter is compressed by applying an increasing force on the ends until it fractures; typically starting with a purely elastic region followed by plastic

deformation with strain hardening and finally fracture. Throughout the compression the load on the sample and the deformation are recorded. Typically, these numbers are then converted to engineering stress and strain and these are plotted against each other, providing characterization of the material as described above for tensile tests.

As for tensile tests, it is beneficial if the actuators can be run with displacement control. Although there is no necking phenomenon as for tensile tests, crystalline samples can exhibit a load drop at the onset of plasticity which can cause an uncontrolled compression if load control is used. In addition, the mechanical behavior of a material is often dependent on the rate of compression, making constant displacement more logical than load control.

New load cells and piezoactuators have made it possible to perform compression tests in the submicrometer scale [5]. Also vital for this type of testing is the possibility to manufacture rods or pillars using, for example, lithography or focused ion beams (for an excellent example of compression tests on FIB (focused ion beam)-machined metal pillars, cf. [2]).

Figure 3 shows an image series from a compression test on a gallium arsenide pillar of 4.2 μm diameter. This pillar was manufactured by photolithography and reactive-ion etching. The crystallographic direction of the surface is (001). (a) and (d) show the pillar before and after compression, respectively. (c) shows plastic deformation along three different (111) slip planes and (d) reveals cracking along 110 planes.

The stress/strain curve recorded during this experiment is shown in Figure 4. The letters a–d correspond to the images in Figure 3. It is impossible to determine strictly from this curve whether the first load drop is due to cracking or slip. However, since the experiment was performed in an SEM it is easily shown that the slip planes

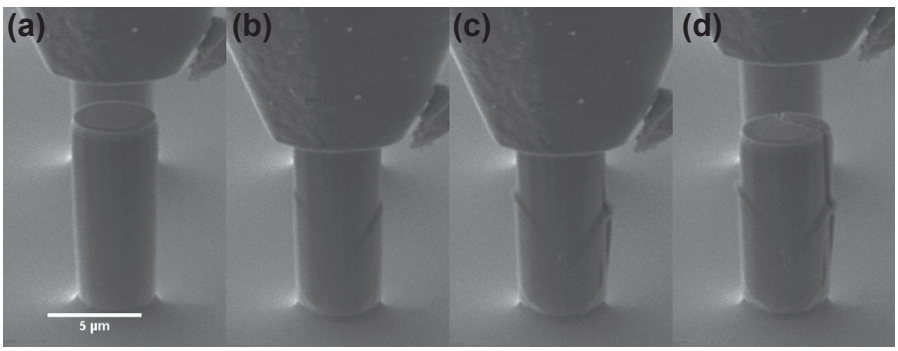

FIGURE 3

Image sequence from the video captured during the compression of a gallium arsenide pillar. The total time of the compression experiment was about 90 s and the frame rate of the video 0.58 frames/s. In (b), plastic deformation along three different slip planes can be seen. (c) reveals some cracking of the pillar. (d) shows the pillar after compression. The stress/strain curve for this particular experiment is shown in Figure 4.

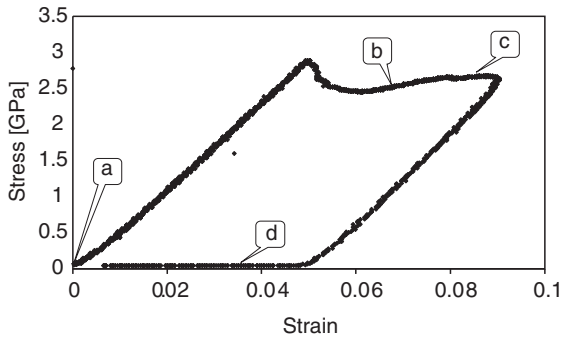

FIGURE 4

Stress–strain curve for a compression experiment of a gallium arsenide pillar. The letters refer to the images in Figure 3. Note that after the initial elastic part of the curve there is a drop in the measured force. This is common for crystalline samples and is caused by the introduction and subsequent multiplication of dislocations within the material [6].

develop first followed by cracking of the pillar (Figure 3 (b) and (c)), demonstrating the power of in situ testing. In this particular study, the transition from brittle to ductile behavior of gallium arsenide as a function of the dimensions was investigated [7].

Micrometer-sized compression experiments do not necessarily have to be performed within an SEM, but doing so offers some advantages. First, being able to see the sample and tip (compression punch) facilitates the positioning of the sample under the tip. Additionally there will not be any doubt as to whether the tip only partially contacts the sample, which could be possible in an experiment that does not use direct observation. Also, contaminants on the sample, which potentially can affect the experiment, can be detected immediately.

If the pillar and tip are poorly aligned, the pillar might buckle or bend, thus producing an entirely different load/displacement curve. Such effects are easily detected in an in situ experiment so that experiments showing these effects can be discarded. By analyzing the video with image analysis software (see below), it is possible to extract more information than just load and displacement. For example, the lateral expansion can be measured from which the value of Poisson's ratio can be calculated. Also, during a typical compression experiment the pillar sinks into the substrate. This effect, called sink-in, can easily be measured. In fact, because it is possible to measure the top and bottom of the pillar, the strain extracted from a video will be entirely free of instrumental compliance.

In principle, the image from an SEM only gives two-dimensional information. This complicates the approach of the tip to the sample. In order to make the alignment of the tip over the pillar possible, it is necessary that the setup be tilted to the electron beam so that the sample substrate can be seen (as seen in Figure 3). The focus of the SEM can be used to give an estimation of the height difference between the sample and the tip. When the tip is very close to the substrate a "shadow" of the

tip can be seen. This shadow arises from the constrained geometry, preventing a fraction of the secondary electrons from reaching the detector of the SEM. Most configurations allow for physically touching the substrate with the tip at a position close to the pillar before the experiment. After this, the distance between the sample and the tip is known and positioning becomes easier.

INSTRUMENTED INDENTATION/NANO-INDENTATION

Instrumented indentation or nano-indentation is an excellent tool for the determination of the hardness and Young's modulus of thin coatings or small objects. In a typical experiment, a diamond indentation body is pressed into the specimen. The term nano-indentation is commonly used for indentation depths ranging from a few nanometers to 100 nm. The load P and the displacement into the surface h are continuously measured during loading and unloading: for an overview, cf. [8]. An example of such a load–displacement curve is shown in Figure 5. Young's modulus, E_{Indent}, can be calculated from the initial portion of the unloading curve, since unloading is a purely elastic recovery process. However, the analysis is not as straightforward as for tensile and compression tests; therefore, a method to determine E_{Indent} in more detail is described. The full procedure is presented by Oliver and Pharr in [9].

The first step of the Oliver–Pharr data analysis procedure consists of fitting the unloading part of the load–displacement data to a power law relation derived from contact mechanics theory:

$$P = B(h - h_{\text{f}})^m \tag{5}$$

where P denotes the applied load, h, the penetration into the surface, h_{f}, the final displacement after complete unloading (cf. Figure 5), and B and m are empirically

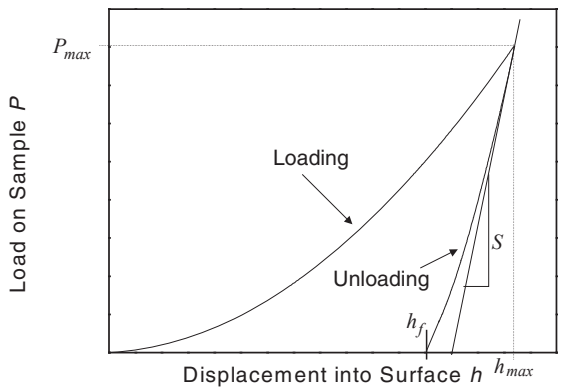

FIGURE 5

A typical load–displacement curve from an indentation experiment.

determined fitting parameters. From this equation, the unloading stiffness $S = dP/dh$ can be calculated by differentiating the equation and evaluating it for $h = h_{\max}$:

$$S = Bm(h_{\max} - h_f)^{m-1} \tag{6}$$

Using S, the so-called contact depth, h_c, can be calculated according to:

$$h_c = h - \varepsilon P/S \tag{7}$$

where ε is a constant depending on the indenter geometry. For three-sided pyramidal indenters (Berkovich tips), $\varepsilon = 0.75$. Note that the correction for h_c has to be used with some caution because it is not valid in the case of material pile-up around an indentation. Using h_c, the projected contact area as a function of the penetration, $A(h_c)$ can be calculated. With S and A, the so-called reduced Young's modulus, E_r, can be determined:

$$E_r = \frac{\left(\sqrt{\pi \cdot S}\right)}{2\beta \cdot A} \tag{8}$$

β depends on the indenter geometry and is equal to 1.034 for Berkovich pyramids. However, the reduced Young's modulus does not take the finite stiffness of the tip into account. The Young's modulus of the sample, E_{Indent}, can be extracted from the relation:

$$\frac{1}{E_r} = \frac{\left(1 - \nu^2\right)}{E_{\text{Indent}}} + \frac{\left(1 - \nu_i^2\right)}{E_i} \tag{9}$$

Here, ν is the Poisson's ratio of the sample and E_i (1141 GPa) and ν_i (0.07) are the Young's modulus and Poisson's ratio, respectively, of the diamond indenter. It may seem counterintuitive that the Poisson's ratio of the investigated material has to be known. However, ν is about 0.3 for most metals and even an uncertainty of ± 0.1 produces an error for E_{Indent} of only about $\pm 5\%$. The scattering of E_{Indent} values from measurements on the same material with fixed measurement parameters is within $\pm 10\%$.

The hardness of the material is defined by:

$$H = \frac{P}{A(h_c)} \tag{10}$$

The largest error source for the calculation of hardness and Young's modulus is the expression used to calculate the area as a function of the displacement. Only for an ideal (i.e., infinitely sharp) Berkovich indenter is the relation $A = 24.5 \cdot h_c^2$ valid. In reality, each tip will be blunted and may have other defects. This can be corrected to some extent by using an area function of the form:

$$A(h_c) = a_0 \cdot h_c^2 + \sum_{i=1}^{n} a_i \cdot h_c^{1/2^i}. \tag{11}$$

The parameters a_i can be obtained by performing nano-indentation experiments on materials with a known value of Young's modulus.

INDENTATION INSIDE THE SEM

As was mentioned previously, nano-indentation enables the measurement of hardness and Young's modulus of small samples or thin coatings. However, it is not possible to have an insight of the deformed zone of the sample during the indentation process. As a consequence, no information about possible crack formation or pile-up (cf. Figure 6) can be obtained. In Figure 6, an SiO_2 surface was indented by a cube corner tip. The information about cracking can be used to evaluate the fracture toughness of the material. Likewise, information about pile-up and sink-in can be used to evaluate plasticity models, providing more accurate data about the material. Another advantage of in situ indentations is the possibility to precisely position the tip with respect to the sample surface. This makes indentation experiments on small structures or at specific locations possible. Finally, there is no need to locate the indent after a test for measuring the area of the residual imprint. For ex situ indentations, this can be a very time-consuming task since the size of the imprints is on the order of nanometers and is thereby very difficult to locate and measure post-indentation. In the next paragraph, issues that have to be addressed for in situ SEM devices will be briefly described.

As for all in situ mechanical tests, the SEM environment induces several "design boundaries" that do not have to be considered in a standard indentation

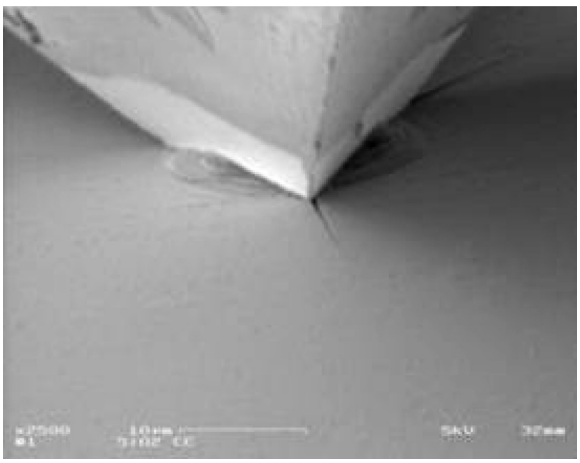

FIGURE 6

In situ indentation showing cracking and pile-up.

device working in air. Firstly, the setup must allow for an unobstructed view of the indentation region. Therefore, indentation tip axis normal to the sample surface has to be inclined with respect to the beam axis of the SEM. In addition, the indenter tip geometries which are normally used in indentation experiments (the four-sided Vickers pyramid or the three-sided Berkovich pyramid [10]) cannot be used because they have too large an opening angle (140.6°), which would obstruct the view of the indent. For measurements inside the SEM, sharper indenters such as the cube corner (opening angle 84.6°) have to be used.

Figure 7 shows a custom-made instrumented indentation device working inside the SEM [11]. The indentation head (4) is composed of a parallel mechanism (flexure hinges) that holds the diamond tip. The head is driven by a stack piezo (5) with 20 μm range and a built-in displacement sensor (strain gauge). The indentation head and its actuator are assembled on a coarse positioning stage (6) (also a flexure mechanism) and driven by a fine-pitch precision screw, remotely controlled with a cable connected to a knob installed on the SEM chamber's door. The stage is fixed on the main body by a dovetail sliding bearing. An XY slip-stick piezo stage (2) holds the load cell (1) and the sample (3).

As a demonstration of the benefits of in situ nano-indentation, Figure 8 shows the result of an indentation experiment of a thin nano-composite coating. Where the load−displacement curve does not show any irregularities, while the SEM images recorded simultaneously show the formation of pile-up and the formation of a crack upon unloading. Interestingly, the crack almost closes completely after full unloading and would therefore be very difficult to detect by inspection of the residual impression only. This demonstrates the added value that can be gained by in situ SEM indentation experiments.

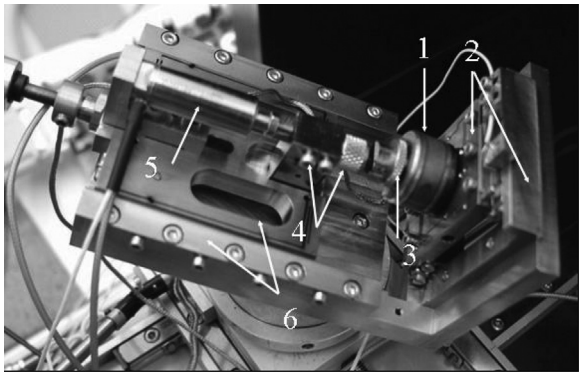

FIGURE 7

The SEM-micro-indenter: 1, load cell; 2, XY-positioning table; 3, sample holder; 4, tip holder and adapter; 5, piezoactuator, displacement sensor; 6, sample coarse positioning.

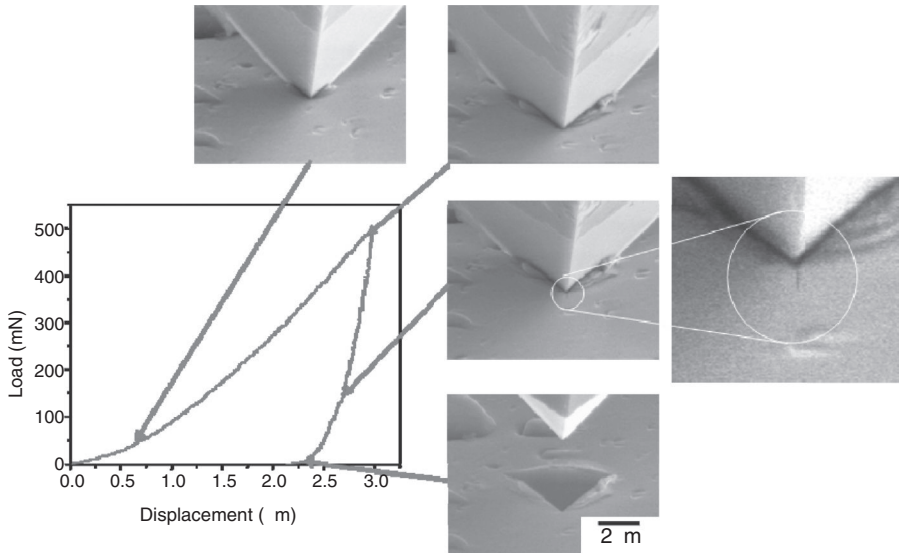

FIGURE 8

In situ SEM indentation of a thin nano-composite coating.

IMAGE ANALYSIS

Most modern SEMs allow the recording of a video, which can be later used to extract the displacement of different features of the sample. Rough measurements can be done simply by directly measuring distances with some imaging software. However, image analysis tools can do this with a far greater resolution. Also, through image analysis algorithms, it is possible to track features throughout a whole video automatically in order to construct, for example, a time versus strain relationship.

There are several algorithms available for tracking motion in an image sequence. Here, it will be assumed that an algorithm called cross-correlation is employed. For a description of this algorithm, cf. [12]. This algorithm takes a small image and a large image as inputs. The output will be a map showing how similar the small image is to each position in the larger one. By taking the peak value, the position of the smaller image in the larger image is found. This algorithm works even if there is no exact copy of the small image within the larger. By selecting a small feature in the first frame of the video and trying to find this part in the following frames gives the displacement of this particular feature. For the case of compressive or tensile tests, if two features that are close to the ends of the sample are tracked, the strain can be calculated. This strain will be entirely independent of instrument compliance. As mentioned above, strain is not the only property that can be measured from the images. For example, by tracking several parts on the samples, buckling and lateral expansion of the samples can be measured.

The cross-correlation algorithm can be improved, making it possible to track changes with a subpixel resolution, provided that the image is well focused and that the level of noise is low. This is important because the total size of an image is often about 500 pixels in width. In this case, one single pixel corresponds to 0.2% strain assuming that the sample covers the whole image. This low resolution would normally be considered insufficient.

When working close to the resolution limit of an SEM, the signal is usually very weak, requiring a very long integration time for each image. In this case, the acquisition time for a single frame can be several seconds. It must therefore be taken into account also that different parts of the image are scanned at different times, usually starting from the top and ending at the bottom.

CASE STUDY: A COMPARISON OF IN SITU MICRO-TENSION AND MICRO-COMPRESSION FOR STUDYING THE PLASTIC PROPERTIES OF NANO-CRYSTALLINE ELECTRODEPOSITED NICKEL AT DIFFERENT LENGTH SCALES

In order to evaluate the effects of grain size or geometrical constraints on measured mechanical properties, there is a need to understand the influence of the measurement technique, load distribution, strain rate, etc., on the measurement values and to correlate the measurements with deformation mechanisms. Uniaxial in situ methods are interesting tools for this purpose. In the following case study, a comparison of in situ and ex situ micro-compression with in situ micro-tensile tests is shown for electrodeposited nano-crystalline (nc) nickel. Since the material is nano-crystalline, it would be expected that the size of the probed volume does not influence the mechanical properties as long as it is at least of the order of a cubic micrometer. Micro-tensile tests that probe a volume of more than 2×10^6 μm^3 show reasonable agreement with results from micro-compression tests that probe much smaller volumes of a few μm^3. In situ uniaxial solicitation in compression mode reveals several advantages for studying stress−strain properties.

In the same way as for tensile measurements, a quantitative evaluation of the deformation during compression using individual video frames [13] is possible. The material investigated was electrodeposited nc nickel. Figure 9 shows a high-resolution SEM picture of the nc Ni surface. The sizes of the grains vary between 30 and 200 nm with an average of 50 nm. The inset in Figure 9 displays a transmission electron microscope (TEM) cross section of the film indicating the grains have a predominantly columnar structure parallel to the deposition direction.

These samples for tensile testing were manufactured by a LIGA (German acronym for lithography-electroplating-molding) process, as well as the 10 μm pillars for in situ compression, whereas the 2 μm pillars for ex situ compression were produced by FIB machining.

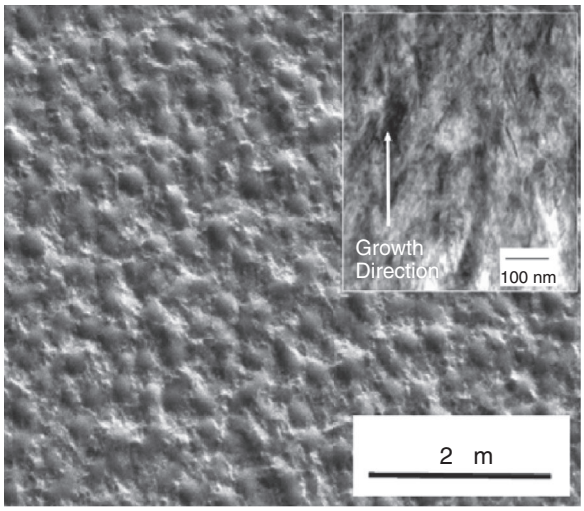

FIGURE 9

High-resolution scanning electron microscope image of the nc Ni surface; roughness and grain size are easily identified on this picture. The inset of the right of the picture shows a transmission electron microscope bright-field image of the specimen indicating the growth direction of the electrodeposition.

The in situ tensile tests were carried out at a constant strain rate of $0.2 \times 10^{-3}\ s^{-1}$. Figure 10 shows the average true stress–strain (σ-ε) curve (i.e., measurements made prior to necking) obtained from micro-tensile measurements. The curve indicates weak strain hardening leading to an increase of the required stress for further deformation of the tested specimen. Figure 10(a) shows an SEM image of the dog-bone central section extracted from the video frames recorded at the beginning of a measurement and Figure 10(b) represents SEM video frame of the micro-tensile bars just before fracture, revealing necking in the central part. An inset on the left part of the graph shows an optical picture of the typical dog bone specimen used.

The in situ compressive tests were carried out using a flat diamond punch of 15 μm diameter. The strain rate was $0.2 \times 10^{-3}\ s^{-1}$. Figure 11 displays true σ-ε curves obtained on 10-μm-diameter pillars (aspect ratio 3:1) with in situ compressive tests. Figure 11(a) and (b) for the 10-μm-diameter pillar tested represent the video frames extracted at the beginning and end of a typical in situ compressive test, respectively. Buckling or crack formation was found only rarely in the video recording and were not included in the analysis. Finally, for comparison, ex situ compressive tests were performed in a commercial MTS NanoXP nano-indentation system with a truncated diamond tip of 8 mm diameter.

Table 1 lists the respective material properties inferred from σ-ε curves obtained with the different testing methods. The yield stress values listed are equal to the

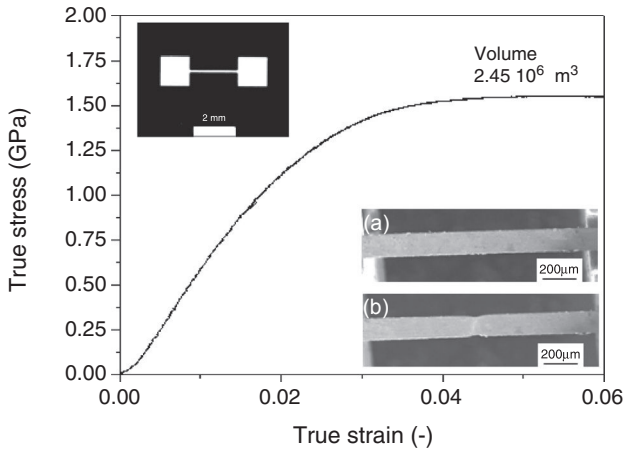

FIGURE 10

Average tensile stress–strain curves obtained from four samples. The inset of the left part of the graph shows an optical picture of the typical dog-bone specimen tested.

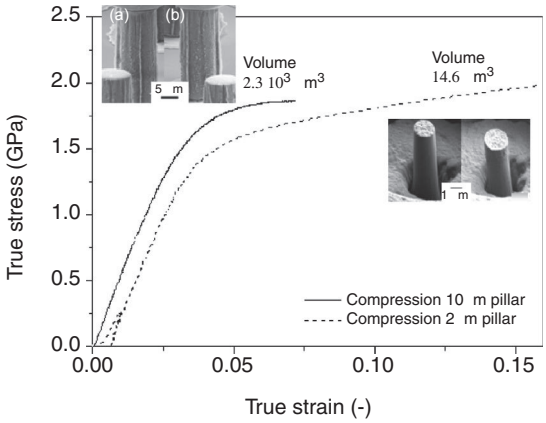

FIGURE 11

Average micro-compressive stress–strain obtained from five measurements for in situ compressive tests (10 μm pillars) and for ex situ compressive tests (2 μm pillars). On the ex situ curves, a reloading procedure at the beginning of the compressive test in order to rectify the misalignment of the pillar with the tip is visible.

0.2% offset yield stress as described by Figure 1. The complete stress–strain curves determined in four different ways reveal that there is reasonable agreement between the two compressive tests and the single tensile test despite the fact that the probed volume differs by 5 orders of magnitude.

Table 1 Young's Modulus, E, and Yield Stress, σ_y for Nano-Crystalline Ni as Determined from Micro-Tensile and Micro-Compression Testing. Also Shown is a Comparison of the Strain Rate Values Used for Each Method

Method	E (GPa)	σ_y (GPa)	Strain Rates (s^{-1})
Tensile	63 ± 16	1.2 ± 0.1	0.2×10^{-3}
Compression (2 μm pillar)	51 ± 13	1.3 ± 0.2	0.9×10^{-3}
Compression (10 μm pillar)	54 ± 14	1.4 ± 0.2	1.5×10^{-3}

Measurement errors that are intrinsic to each technique are prone to give differences in σ-ε curves. For tensile tests, the major source of uncertainty in the stress calculation is the measurement of the specimen cross section. As all tensile bars tested were fabricated from the same plating batch, it is assumed that an average value of their cross sections gives sufficient accuracy. For compression measurements, the cross section was measured at 10 different positions over the entire length of the pillar. For 2-μm pillars, 10 measurements of the cross section were made directly on the pillar SEM image over its entire length, for obtaining an average value of the pillar volume, i.e., the pillar shape is a source of error as the diameter is not constant over its length. In both cases, for micro-compressive and micro-tensile tests, the pillar sizes (length, L, and surface area, A) and the tensile bar sizes (length, L, and cross section, A) can be measured to within an error of 5% for L and L_0 (displacement), and to within an error of 15% for A. These induce statistical errors, with a scatter of 25% in the Young's modulus estimation and 15% for σ_y. Such experimental errors in the measurements might explain the discrepancies found between tensile and compressive tests.

A comparison between ex situ and in situ micro-compressive tests reveals the advantage of the in situ method. First, for the ex situ compressive tests, the measured displacement values had to be corrected by accounting for the sink-in of the pillar into the substrate, whereas this correction is not necessary when strain values are determined from SEM images recorded during compression. Also, this correction has to take into account the complex geometry of the postbase connection to ensure the avoidance of an overestimation of Young's modulus with a simple elastic contact model [14]. Finally, without continuous video control, a misalignment of the tip to the pillar can lead to a decrease of the measured elastic modulus or, in excessive cases, to the buckling of the pillars.

In nc Ni, the difference of probed volume in the different tests, i.e., external size effects, should not have a significant influence on the σ-ε curves. The Young's moduli and the yield stresses are somewhat lower than already reported for fully densified nc electrodeposited nickel [15], suggesting that the influence of textures,

pre-existing voids, columnar grain structure, and hydrogen on the mechanical response cannot be neglected [16,17]. In this case, it is expected that pores and flaws within the matrix tested are prone to play a bigger role on the mechanical response in the tensile mode.

Cheng et al. proposed a deformation mechanism map for face-centered cubic (FCC) metals [18]. The model predicts not only the strength as a function of grain size, but also the observed tensile/micro-compressive asymmetry of the yield strength. It is predicted that a greater yield stress will be found in compression than in tension for FCC metals with grain sizes ranging from 2 nm up to 100 nm. The tension/compression asymmetry which is explained by a pressure dependence of the dislocation self-energy during bow-out may be responsible for the difference in the yield/stress values plotted in Table 1 for the tested FCC nc nickel.

To summarize, the potential of in situ micro-compression and micro-tensile methods to characterize nc nickel has been assessed and potential measurement errors have been discussed. Due to the small size of the micro-structure, size effects could be neglected, which allowed the revelation on the one hand of the importance of the load cases particular to each method, and on the other hand the influence of the probed volume and of the micro-structure. Whether surface effects, stress state or strain rate is the most important could not be distinguished. It was found that in situ uniaxial tensile and compression testing is able to provide accurate data and similar mechanical insights of the tested materials ranging over 5 orders of magnitude of probed volume. Comparing the aforementioned advantages and drawbacks of the different approaches, it may be concluded that uniaxial in situ methods are appropriate to study the mechanical properties of isotropic nc metals.

CONCLUSION AND OUTLOOK

Discussed above are instrumented micro-indentation, micro-compression, and micro-tensile testing methods for use inside an SEM and the application potential of the techniques is presented in a case study on UV-LIGA materials. Coupled with advanced image analysis techniques, these in situ SEM micro-mechanical testing methods are used to study scale-dependent material properties and to observe deformation and fracture mechanisms in situ. Also, the SEM enables for accurate sample positioning and visual control of the experiment. Current leading edge research in instrumentation is focused on micro-electromechanical systems for the tensile testing of nano-wires and carbon nano-tubes, and on nano-bending experiments on nano-wires using (1) atomic force microscopy techniques and (2) vibrational analysis of different types of nano-structures inside the SEM. Both of these techniques require, however, high-resolution SEMs or alternatively TEMs.

REFERENCES

[1] Arzt E. Size effects in materials due to microstructural and dimensional constraints: a comparative review. Acta Mater 1998;46(16):5611−26.

[2] Uchic MD, Dimiduk DM, Florando JN, Nix WD. Sample dimensions influence strength and crystal plasticity. Science 2004;305:986.

[3] Current standards for metals: EN 10002-1 and -5, ISO 6892, ASTM E 8, ASTM E 21, DIN 488, DIN 501.

[4] Mencik J. Mechanics of components with treated or coated surfaces. Doordrecht (Netherlands): Kluwer Academic Publishers; 1996.

[5] Philippe L, Schwaller P, Bürki G, Michler J. A comparison of microtensile and micro-compression methods for studying plastic properties of nanocrystalline electrodeposited nickel at different length scales. J Mater Res 2008;23(5):1383−8.

[6] Hull D, Bacon DJ. In: Introduction to dislocations. 4th ed. Oxford: Butterworth-Heinemann; 2001.

[7] Michler J, Wasmer K, Meier S, Östlund F, Leifer K. Plastic deformation of gallium arsenide micropillars under uniaxial compression at room temperature. Appl Phys Lett 2007;90:043123.

[8] Bhushan B. Handbook of micro/nano tribology. New York: CRC Press; 1999. C 433.

[9] Oliver WC, Pharr GM. Measurement of hardness and elastic modulus by instrumented indentation: advances in understanding and refinements to methodology. JMR 2004;19: 3−20.

[10] Fischer-Cripps AC. Nanoindentation. New York: Springer; 2002.

[11] Rabe R, Breguet JM, Schwaller P, Stauss S, Haug FJ, Patscheider J, et al. Observation of fracture and plastic deformation during indentation and scratching inside the scanning electron microscope. Thin Solid Films 2004;469−470:206−13.

[12] Kropatsch WG, Bischof H. Digital image analysis: selected techniques and applications. New York: Springer; 2001.

[13] Moser B, Wasmer K, Barbieri L, Michler J. Strength and fracture of Si micropillars: a new scanning electron microscopy-based micro-compression test. J Mater Res 2007; 22(4):1004−11.

[14] Zhang H, Schuster BE, Wie Q, Ramesh KT. The design of accurate micro-compression experiments. Scr Mater 2006;54:181−6.

[15] Nix WD, Greer JR, Feng F, Lilleodden ET. Deformation at the nanometer and micrometer length scales: effects of strain gradients and dislocation starvation. Thin Film Solids 2007;515(6):3152−7.

[16] Kumar KS, Van Swygenhoven H, Suresh S. Mechanical behavior of nanocrystalline metals and alloys. Acta Mater 2003;51:5743−74.

[17] Asaro RJ, Suresh S. Mechanistic models for the activation volume and rate sensitivity in metals with nanocrystalline grains and nano-scale twins. Acta Mater 2005;53:3369−82.

[18] Cheng S, Spencer JA, Milligan WW. Strength and tension/compression asymmetry in nanostructured and ultrafine-grain metals. Acta Mater 2003;51:4505−18.

CHAPTER

Micro-mechanics Modeling for Micro-forming Processes

32

Shiwen Wang[1], Weimin Zhuang[2], Jian Cao[1], Jianguo Lin[1]
Department of Mechanical Engineering, Imperial College London, London, UK[1]; College of Automotive Engineering, Jilin University, Changchun, Jilin, PR China[2]

CHAPTER OUTLINE

INTRODUCTION

In recent decades, the development toward miniaturization of products and devices in industries such as electronics, optics, communications, etc., has increased the demand for metallic parts manufactured at micro-scale. Such parts encompass a wide variety of geometries, materials, functionalities, and production processes. Examples of micro-parts include screws, fasteners, connector pins, springs, micro-gears, and micro-shafts. These are manufactured by employing a variety of manufacturing processes such as machining, folding, bending, stamping, drawing, molding, lithography, and forward/backward extrusion [1]. Some examples of extruded micro-parts are shown in Figure 1 [2]. Forming is a particularly appropriate manufacturing technique for these parts, as often they have a complicated shape and machining would be time-consuming and produce low yield. Process modeling plays an ever-increasing role in these areas, for product design and for reducing lead time and manufacturing costs.

Micromanufacturing Engineering and Technology. http://dx.doi.org/10.1016/B978-0-323-31149-6.00032-3

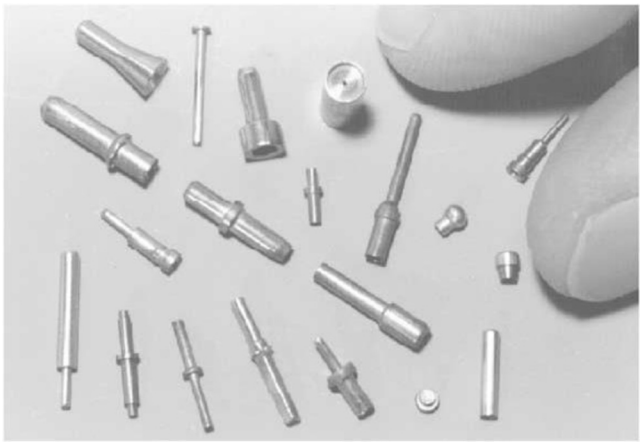

FIGURE 1

Examples of micro-pins (Shinko, NME) [2].

To enable process design to be undertaken on a scientific basis, knowledge of the underlying theory of micro-mechanics is essential. Plastic deformation can be observed at various length scales, which can be from the atomic scale where the atomic arrangement and individual defect properties of a material are of crucial importance, up to the macroscopic scale where the actual material micro-structure is not resolved and plasticity is described on phenomenological grounds. A schematic diagram of the length scales at which plasticity may be addressed: the nanometer scale (atomistic), the mesoscopic scale (tens of microns), and the macroscopic scale; is given in Figure 2.

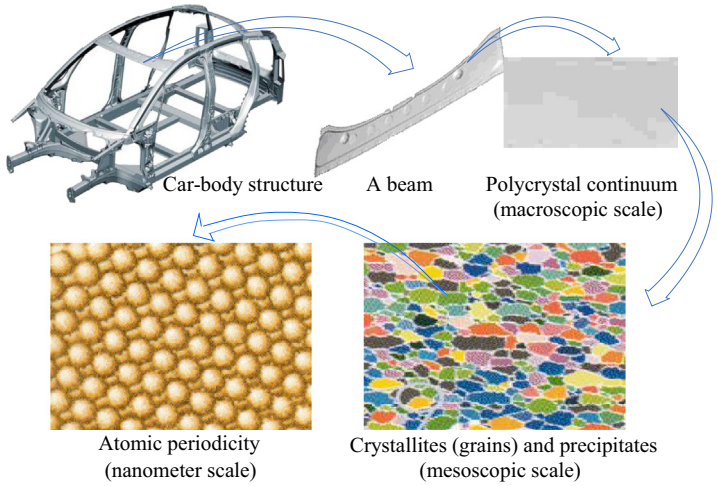

FIGURE 2

Plasticity in metals at various length scales.

In conventional metal forming processes, the size of the workpiece is usually large compared with the grain size of the metal from which it is constituted. Standard continuum plasticity models are local in the sense that the stress at a material point is assumed to be a function of a strain at that point only. Local theories do not make reference to the characteristic length scale for dislocations and, therefore, are not able to resolve dislocation structures. As a consequence, such models also exhibit no size dependence. The crystals and their inherent directions of preferred slip (slip plane) are usually oriented randomly. Thus, although a workpiece may be deformed by an external force (or stress) in a clearly defined direction, internally the crystal deformations are multidirectional. It is the resolution of the multidirections along a common axis that gives rise to the macro-deformation, resulting in the change in shape of the workpiece. Because of the large number of crystals and the randomness of crystal orientation, at the macro-scale a material appears homogeneous and different samples of the same material in the same thermomechanically treated condition exhibit the same properties.

At the micro-level, the grain size can be similar to that of the part being formed. Thus a cross section of a workpiece may contain a single digit number of grains, compared with the tens or hundreds at the macro-level. Thus the metal is not homogeneous and the deformation characteristics are likely to be different, as the resolved crystal deformation exhibited as the workpiece shape will be the result of slip on relatively few slip planes and a common outcome between different workpieces is unlikely. Due to this influence of the micro-structure on the forming process, the workpiece for a micro-part can no longer be regarded as a homogeneous continuum for process simulation purposes. Thus in the process simulation of forming micro-parts, it is important to choose appropriate finite element (FE) simulation theories, so that the length scale of material deformation can be considered. In most of the cases in the forming of micro-parts, continuum mechanics theories break down and crystal plasticity finite element (CPFE) methods have to be used. Thus, in this chapter, numerical procedures for CPFE are introduced.

CPFE THEORY

PHYSICAL BASIS FOR SINGLE-CRYSTAL DEFORMATION

Crystal plasticity is a physically based plasticity theory that represents the deformation of a metal at the micro-scale. The flow of dislocations in a metallic crystal along slip systems is represented in a continuum framework. Plastic strain is assumed to be due solely to crystallographic dislocation slip. Slip is the dominant mechanism for deformation, which occurs due to dislocation motion. A crystalline material is constructed of a periodic packing of atoms. A crystal structure refers to a group of atoms that is situated in repeating or periodic arrays or a unit cell. For metals, there are three simple crystal structures, namely FCC (face-centered cubic), BCC

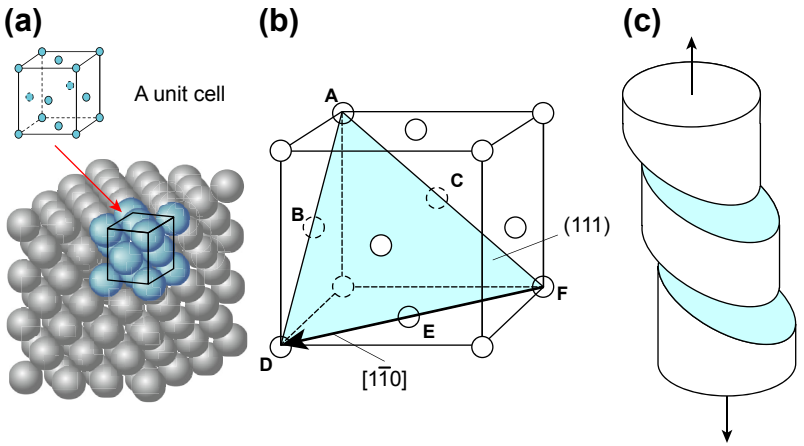

FIGURE 3

(a) Face-centered cubic (FCC) structures in a crystalline material; (b) a particular slip system $(111)[1\bar{1}0]$ in an FCC lattice; and (c) a schematic diagram representing single slip.

(body-centered cubic), and HCP (hexagonal close packed) structures. Figure 3(a) shows the pure crystal structures for FCC metals.

Observation of single crystals shows that slip tends to take place most readily in specific directions (i.e., slip directions) on certain crystallographic planes (i.e., slip planes). A slip plane refers to the plane of greatest atomic density and the slip direction is the closest packed direction within the slip plane. A combination of preferred slip planes and slip directions is called a slip system. For FCC crystals, the most densely packed planes are the diagonal planes of the unit cell, see Figure 3(b). The full family of slip systems in an FCC crystal may be written as $\langle 1\bar{1}0\rangle\{111\}$. There are 12 such systems in an FCC crystal (four planes each with three directions).

Considered a single crystal of zinc, this is a few millimeters in width and has been loaded beyond its yield in tension. The planes that can be seen are those on which slip has occurred resulting from many hundreds of dislocations running through the crystal and emerging at the edge. Each dislocation contributes just one Burger's vector of relative displacement, but with many such dislocations, the displacements become large (Figure 3(c)).

CRYSTAL KINEMATICS

The general kinematics of the elastic−plastic deformation of a crystal at finite strains were given by Taylor [3], Hill [4], Rice [5], Hill and Rice [6], Asaro and Rice [7], and Asaro [8]. The total deformation gradient of finite strain from the reference frame to the current frame, F_{ij}, is defined by:

$$F_{ij} = \frac{\partial x_i}{\partial X_j} \tag{1}$$

where X_j and x_i denote the reference and current particle positions, respectively. Here, tensor conventions for subscripts are adopted. All indices i, j, k, and l are running from 1 to 3 throughout this chapter.

In crystal plasticity theory, a crystalline material is embedded on its lattice, which undergoes elastic deformation and rotation. The inelastic deformation of a single crystal is assumed here to arise solely from crystalline slip. The material flows through the crystal lattice via dislocation motion. The total deformation gradient F_{ij} is given by:

$$F_{ij} = F^*_{ik} F^P_{kj} \tag{2}$$

where F^P_{kj} denotes plastic shear of the material to an intermediate reference configuration in which the lattice orientation and spacing are the same as in the original reference configuration, and where F^*_{ik} denotes stretching and rotation of the lattice. These are shown in Figure 4. The rate of change of F^P_{ij} is related to the slipping rate $\dot{\gamma}^\alpha$ of the α-th slip system by:

$$\dot{F}^P_{ik} F^{P-1}_{kj} = \sum_\alpha \dot{\gamma}^\alpha s^\alpha_i m^\alpha_j \tag{3}$$

where the sum ranges over all activated slip systems and unit vectors s^α_i and m^α_j are the slip direction and the normal to the slip plane in the reference configuration, respectively. The number of slip systems and their orientations depend on the crystal lattice, e.g., an FCC crystal contains four slip planes and each slip plane has three slip directions, which results in $\alpha = 1,2,\ldots,12$.

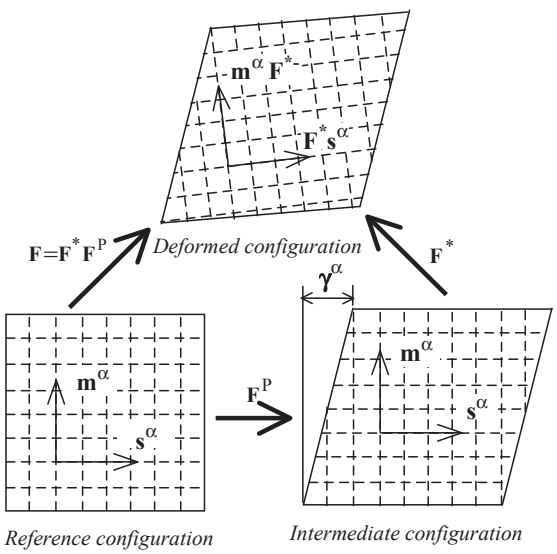

FIGURE 4

Schematic diagram of single-crystal kinematics.

It is convenient to define the vector $s_i^{*\alpha}$, lying along the slip direction of the system α in the deformed configuration, by:

$$s_i^{*\alpha} = F_{ik}^* s_k^\alpha \tag{4}$$

A normal to the slip plane which is the reciprocal base vector to all such vector in the slip plane is:

$$m_i^{*\alpha} = m_k^\alpha F_{ki}^{*-1} \tag{5}$$

The velocity gradient in the current state is:

$$L_{ij} = \dot{F}_{ik} F_{kj}^{-1} = D_{ij} + \Omega_{ij} \tag{6}$$

where the symmetric rate of stretching D_{ij} and the antisymmetric spin tensor Ω_{ij} may be decomposed into lattice parts (superscript *) and plastic parts (superscript $^{\mathrm{P}}$) as follows:

$$D_{ij} = D_{ij}^* + D_{ij}^P, \quad \Omega_{ij} = \Omega_{ij}^* + \Omega_{ij}^P \tag{7}$$

Satisfying:

$$D_{ij}^* + \Omega_{ij}^* = \dot{F}_{ik}^* F_{kj}^{*-1}, \quad D_{ij}^P + \Omega_{ij}^P = \sum_\alpha \dot{\gamma}^\alpha s_i^\alpha m_j^\alpha \tag{8}$$

Finally, it is noted that the plastic parts of the rate of stretching and the rate of spin are given by the symmetric and skew part of Eqn (8). If it is defined that:

$$P_{ij}^\alpha = \frac{1}{2}\left(s_i^{*\alpha} m_j^{*\alpha} + s_j^{*\alpha} m_i^{*\alpha}\right), \quad W_{ij}^\alpha = \frac{1}{2}\left(s_i^{*\alpha} m_j^{*\alpha} - s_j^{*\alpha} m_i^{*\alpha}\right) \tag{9}$$

then:

$$D_{ij}^P = \sum_\alpha P_{ij}^\alpha \dot{\gamma}^\alpha, \quad \Omega_{ij}^P = \sum_\alpha W_{ij}^\alpha \dot{\gamma}^\alpha, \tag{10}$$

It is worth noting that the plastic part of the rate of stretching, D_{ij}^P, is that part of the rate of stretching arising from slip in the current lattice direction $s_i^{*\alpha}$, in a plane where the current normal is $m_i^{*\alpha}$, while the plastic part of the rate of spin, Ω_{ij}^P, is that part of the rate of plastic spin resulting from the summation of rotation on each slip system.

CRYSTAL PLASTICITY CONSTITUTIVE EQUATIONS

The main feature of the crystal plasticity constitutive theory will be briefly introduced here. For each grain, linear elasticity constitutive relations are given by the generalized Hooke's law:

$$\tau_{ij}^{\nabla *} = L_{ijkl} D_{kl}^* \tag{11}$$

where L_{ijkl} the fourth order stiffness tensor and D^*_{ij} the second order symmetric rate of stretching of the lattice. $\tau^{\nabla *}_{ij}$ represents the Jaumann rates of Kirchhoff stress formed on axes that spin with the *lattice*:

$$\tau^{\nabla *}_{ij} = \dot{\tau}_{ij} - \Omega^*_{ik}\tau_{kj} + \tau_{ik}\Omega^*_{kj} \tag{12}$$

where $\dot{\tau}_{ij}$ is the material rate of Kirchhoff stress. The Kirchhoff stress τ_{ij} is defined as $(\rho_0/\rho)\sigma_{ij}$, where σ_{ij} is the Cauchy stress and ρ_0 and ρ are the material density in the reference and current states. On the other hand, τ^{∇}_{ij} is the Jaumann rate of Kirchhoff stress formed on axes that rotate with the *material*:

$$\tau^{\nabla}_{ij} = \dot{\tau}_{ij} - \Omega_{ik}\tau_{kj} + \tau_{ik}\Omega_{kj} \tag{13}$$

The difference between these two rates is:

$$\tau^{\nabla *}_{ij} - \tau^{\nabla}_{ij} = \sum_{\alpha}\left(W^{\alpha}_{ik}\tau_{kj} - \tau_{ik}W^{\alpha}_{kj}\right)\dot{\gamma}^{\alpha} \tag{14}$$

When Eqns (9)–(11) and Eqn (14) are combined, the resulting constitutive law becomes:

$$\tau^{\nabla}_{ij} = L_{ijkl}D_{kl} - \sum_{\alpha}\left(L_{ijkl}P^{\alpha}_{kl} + W^{\alpha}_{ik}\tau_{kj} - \tau_{ik}W^{\alpha}_{kj}\right)\dot{\gamma}^{\alpha} \tag{15}$$

In crystal plasticity, plastic deformation is assumed to be caused solely by crystalline slip and crystalline slip to be driven by Schmid stress (or resolved shear stress), τ^{α} [3], which is defined by:

$$\tau^{\alpha} = m^{*\alpha}_i \tau_{ij} s^{*\alpha}_j \tag{16}$$

where $m^{*\alpha}_i$ and $s^{*\alpha}_j$ are slip plane normals and directions for the α-th slip system, respectively. The rate changes of this Schmid stress is given by [9]:

$$\dot{\tau}^{\alpha} = m^{*\alpha}_i\left(\tau^{\nabla *}_{ij} - D^*_{ik}\tau_{kj} + \tau_{ik}D^*_{kj}\right)s^{*\alpha}_j \tag{17}$$

The slipping strain rate $\dot{\gamma}^{\alpha}$ is assumed to be governed by the resolved shear stress τ^{α} given by a constitutive equation shown below:

$$\dot{\gamma}^{\alpha} = \dot{a}\left(\frac{\tau^{\alpha}}{g^{\alpha}}\right)\left(\left|\frac{\tau^{\alpha}}{g^{\alpha}}\right|\right)^{n-1} \tag{18}$$

where $\dot{a}$ is the reference strain rate, n is the stress sensitivity parameter, and g^{α} is the current strain hardened state of the crystal. In the limit as n approaches infinity, this power law approaches that of a rate-independent material. The current hardened state g^{α} is defined by:

$$\dot{g^{\alpha}} = \sum_{\beta} h_{\alpha\beta}\dot{\gamma}^{\beta}, \quad \beta = 1, 2, \ldots, 12 \text{ for FCC crystals} \tag{19}$$

Table 1 Material Parameters for the Crystal Plasticity Model

n	$\dot{a}$ (s^{-1})	h_0 (MPa)	τ_s (MPa)	τ_0 (MPa)
10.0	0.001	541.5	109.5	60.8

where $h_{\alpha\beta}$ is the slip hardening moduli. Self- ($h_{\alpha\alpha}$) and latent- ($h_{\alpha\beta}$) hardening moduli are defined as:

$$h_{\alpha\beta} = \begin{cases} h_0 \operatorname{sech}^2 \left| \dfrac{h_0 \gamma}{\tau_s - \tau_0} \right| & \alpha = \beta \\ q h(\gamma) & \alpha \neq \beta \end{cases} \tag{20}$$

$$\gamma = \sum_{\alpha=1}^{12} |\gamma^{\alpha}| \tag{21}$$

where h_0 is the initial hardening modulus, τ_0 is the initial shear strength of the material; at $t = 0$, all g^{α} are equal to τ_0; τ_s is the breakthrough stress when plastic flow initiates; γ is the cumulative slip strain and q is a hardening factor. The material constants within the crystal plasticity constitutive equations are determined from experimental data. As an example, a set of the constants is listed in Table 1 for a single-crystal copper [9]. The high value of n is used here to reduce the viscoplastic behavior of the material, as it is used in room temperature forming processes.

INTEGRATED CPFE ANALYSIS FOR THE FORMING OF MICRO-PARTS

CPFE IMPLEMENTATION

CPFE calculations can be carried out using commercial FE software. While detailed implementations can be found either in the form of implicit [10] or explicit [11] format, a brief introduction of the explicit implementation will be given in this section and a sample simulation on the forming of micro-pins with an integrated micro-mechanics analysis system will be given in the following section.

In crystal plasticity, the constitutive equations are expressed in an intermediate configuration, shown in Figure 4, obtained by unloading the deformed crystal from the current configuration. Because the total deformation applied to the crystal is provided by the FE solution, only single-crystal response is needed. A set of crystal constitutive equations can be implemented into ABAQUS/Explicit via a user-defined subroutine VUMAT. In explicit FE calculation procedures, the task can be split up easily and solved by a number of processors. Hence, VUMAT can be constructed with a vectorized interface. This means that when a simulation is carried out using multiple processors, the analysis data can be split up into blocks and solved

independently. Thus, vectorization can be preserved in the writing of the subroutine in order that optimal processor parallelization can be achieved.

The time integration of the set of constitutive equations can be carried out by discretizing the deformation history in time and integrating the equations numerically over each time increment. For this purpose, the configuration of the body is considered at t_n and t_{n+1}, with $t_{n+1} = t_n + \Delta t$. The integration scheme developed assumes that: (1) a given crystal deformation represented by F_{ij} (or L_{ij}) is given at each time increment, Δt; (2) the variables (τ^α, g^α, γ^α) in each crystal are known at time t_n; and; (3) the slip systems ($m^{*\alpha}$, $s^{*\alpha}$) are known. The purpose of the integration scheme is to determine the updated values (τ^α, g^α, γ^α), which are then used to calculate the stress–strain response of the crystal at time t_{n+1}.

An explicit integration method is employed in ABAQUS/Explicit. In this approach, the accelerations and velocities at a particular point in time are assumed to be constant during a time increment and are used to solve for the next point in time. To reduce the dynamic effects, a value of the ratio of the duration of the load and the fundamental natural period of the model of greater than five is recommended [12]. It has been found that by keeping the ratio of kinetic energy to the total internal strain energy at $<5\%$, dynamic effects in the model are negligible [13,14].

The overall numerical calculation procedure for the CPFE implementation into the commercial FE code ABAQUS via the user-defined subroutine VUMAT is summarized in Figure 5.

DEVELOPMENT OF THE CPFE MODEL

In crystal plasticity modeling, a workpiece contains a number of grains which are in random shapes that also possess random grain orientation [15–18]. The FE mesh, which takes account of different orientations of grains, requires that different mechanical properties be assigned to individual grains.

The grain structures and grain boundaries are described in terms of vector graphics by means of differentiation between points of different colors in the micrograph. The scale of the specimen is defined and the axes of a coordinate are assigned. The grain objects must be assigned with mechanical properties according to the data from an EBSD (electron backscatter diffraction) micrograph. An EBSD micrograph of a low-carbon steel has been used for preparation of a sample mesh according to the above principle. The original micrograph is shown in Figure 6(a). The extracted grains with orientations have been created (see Figure 6(b)) from the EBSD micrograph. The selected grains can be further discretized and the final mesh for CPFE analysis is shown in Figure 6(c).

The above process for creating an FE mesh is complicated and time-consuming. Thus Voronoi tessellation, like the stochastic method, was introduced recently to generate grain structures based on probability theories [19–23]. The concept of the Voronoi polygon has been used extensively in material science, especially for modeling random micro-structures such as aggregates of grains in polycrystals. If the micro-structure information of a material is known, such as average,

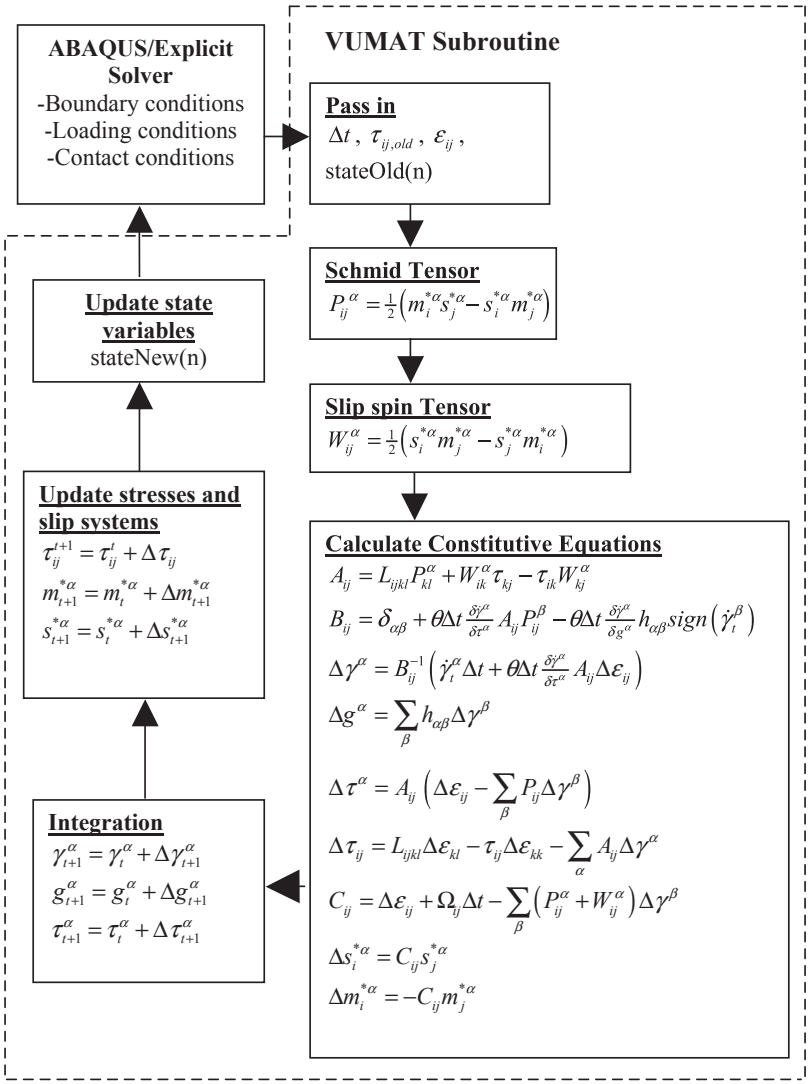

FIGURE 5

The implementation procedure for CPFE analysis using ABAQUS.

After Ref. [11].

minimum, and maximum grain sizes, then the one parameter gamma distribution, which proved valid can be used for representing the distribution probability of grain structures [24–26].

Significant progress had been made to control the virtually generated CPFE model to be more representative to real material micro-structures and their failure

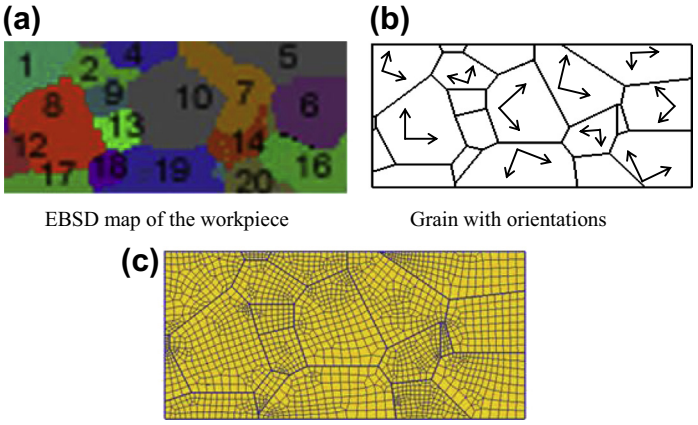

FIGURE 6

An approach to create a finite element mesh from the physical micro-structure of a material. EBSD, electron backscatter diffraction; CPFE, crystal plasticity finite element.

modes [27–31]. In this progress, controlled Poisson Voronoi tessellation (CPVT) model had been proposed [27–29], which can produce two-dimensional (2D) virtual grain structures that are statistically equivalent to metallographic observations of polycrystalline materials in terms of the tessellation's regularity and grain size distribution.

To address the intergranular crack initiation and propagation of material failure at micrometer level, a finite thickness cohesive zone interfaces, which representing the grain boundaries and multiple junctions, had been incorporated into the virtual grain structures of CPFE model with an efficient grain boundary offsetting algorithm [30].

The concept of CPVT has also been further implemented to generate 3D polycrystalline grain structures for micro-mechanics simulations [31]. In particular, relations between the regularity and distribution parameter, for a range of regularity values, had been determined by a comprehensive set of statistical experiments, in which data fitting for the grain size distribution model had been obtained by an evolutionary optimization algorithm.

In summary, virtual grain generations technology had made dramatic progress to truly characterize real material micro-structures. With the advancement of new parallel computing technologies and powerful computers, large-scale CPFE analysis could be used widely in the design and manufacturing of micro-products.

THE INTEGRATED NUMERICAL PROCESS

In this process, a virtual grain structure is generated according to the physical parameters of a material, such as the dimensions of the workpiece and the grain size

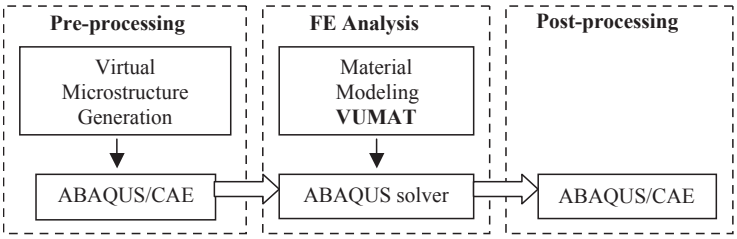

FIGURE 7

An integrated numerical procedure for micro-mechanics modeling. FE, finite element.

information [32]. The orientation of grains is assigned according to a probability distribution, either in the random form or with a designed distribution. The generated grain structure, together with its orientation, can be transferred to commercially available FE codes, where further preprocessing, such as meshing, boundary conditions, and loading assignment, can be carried out. In this research, the generated virtual grains with their orientation information are transferred into ABAQUS/CAE for further preprocessing.

Figure 7 shows the overall scheme of the integrated numerical procedure for CPFE modeling using ABAQUS. In the preprocessing, virtual grain structures with their orientation information are generated and input into ABAQUS/CAE, which is employed for further preprocessing. A complete CPFE model with meshing, contact interaction, boundary and loading conditions are created using ABAQUS/CAE. The crystal plasticity material model is implemented into ABAQUS via the user-defined subroutine VUMAT. This enables explicit micro-mechanics analyses to be carried out.

PROCESS SIMULATION FOR THE FORMING OF MICRO-PINS

Extruded micro-pins are now used widely in electronics devices. It is estimated that 24 billion micro-pins are used annually for IC carriers [33]; they have diameters of the order of 100 μm−2 mm. The quality of the formed micro-pins is affected by the grains size, grain orientation, and grain distributions of the material and the geometrical defects cannot be captured using conventional continuum-based FE forming simulation techniques.

Figure 8(a) shows micro-pins of 0.57 mm diameter extruded using the same material, but which was heat treated to produce different grain sizes [34]. It was reported that for material with a grain size of 32 μm, or about 16−18 grains across the extruded diameter, and the deformation ratio is about 1.3, fairly straight micro-pins can be extruded and continuum FE analysis can be used for this prediction. However, for material with a grain size of 211 μm, i.e., about 2−3 grains across the diameter of the extruded micro-pins, uncontrollable bending and

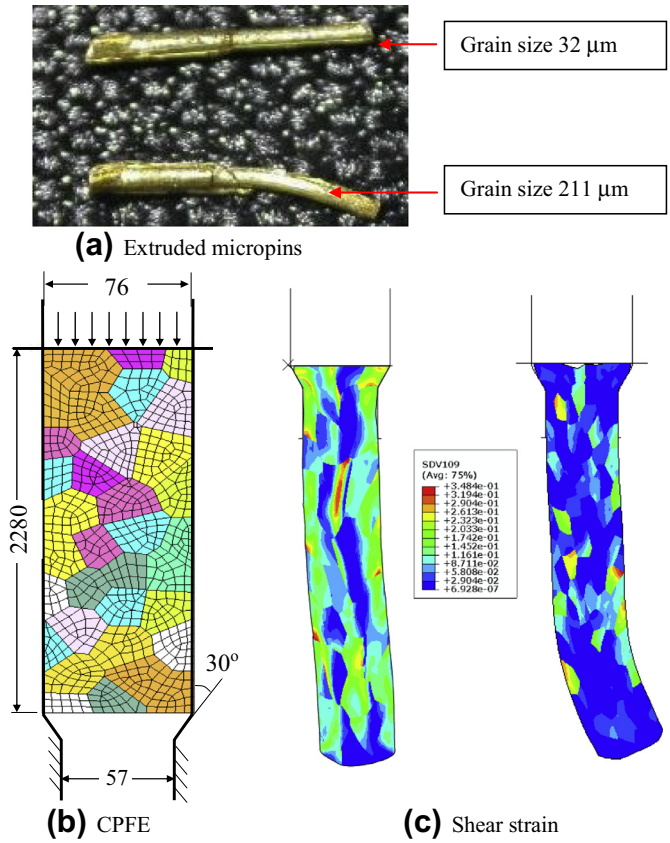

FIGURE 8

Extrusion of micro-pins. CPFE, crystal plasticity finite element.

curvature of the extruded micro-pins usually can be observed experimentally for the same extrusion ratio [34].

Numerical investigations have been carried out using the developed integrated CPFE simulation system. Randomly distributed grains with an average grain size of 211 µm were generated using the Voronoi tessellation method (Figure 8(b)). The dimensions of the workpiece and the die are also shown in Figure 8(b) and the FE mesh was created using ABAQUS/CAE with quad-dominated elements (CPE4R). The subroutine VUMAT was used for the crystal plastic model simulation. A displacement of 2280 µm is applied on the extrusion punch. The friction coefficients are 0 at the interfaces between the punch and the workpiece and 0.1 between the die and the workpiece: the latter value is commonly used for cold extrusion processes. In Figure 8(b), the grain orientation is assigned randomly. It should be noted that the CPFE model described above is based on a plane strain description,

which is a simplified model and different from that for the extrusion of circular micro-pins. However, similar features of the geometric variations between the extruded and simulated micro-pins can be observed.

Figure 8(c) shows the virtually "formed" micro-pins and the contours of cumulative shear strain distribution for the results of two CPFE analyses. Both use the same FE model and grain structure and the only difference is that the grain orientations are assigned to the grains using the same probability theories twice: thus the grain orientations are different from the two CPFE models. It can be seen clearly that the geometric errors for the extruded micro-pins are different. This could confirm the results obtained experimentally, that if the ratio of the diameter of the micro-pins and the grain size of the material is small, uncontrollable bending and curvature of the extruded micro-pins are the major geometrical defects. This CPFE analysis result demonstrates the validity of the developed CPFE tools in capturing the grain size effects in the process of the forming of micro-pins. It can be observed also from the figure that the maximum cumulative shear strains occur locally along grain boundaries, the effect of which is induced by strong mismatches of the orientations among the grains. The uncontrollable curvature feature (Figure 8(a) and (c)) cannot be modeled, if continuum FE analysis is used. This shows clearly the grain size effect during the micro-forming process and that CPFE needs to be employed to predict such features.

CONCLUSIONS

In traditional metal forming processes, continuum mechanics-based FE techniques can be used for process simulation. However, in micro-forming processes, if the ratio of the minimum dimension of a micro-part and the grain size of the material is small, CPFE analysis has to be used, otherwise, the important features of the forming of micro-parts cannot be captured. CPFE analysis can be carried out using existing commercial FE codes, such as ABAQUS: there is no need to generate special FE codes for this purpose. The main progress in the simulation of micro-forming processes using CPFE are: (1) the creation of the CPFE with controlled Voronoi tessellation, which includes the generation of the micro-structures of materials, material orientations, grain boundaries, and the creation of an FE mesh within grains and; (2) crystal plasticity material models, which include the development and determination of micro-mechanics material models and the implementation of the models into commercial FE codes.

To demonstrate the validity of the proposed integrated micro-mechanics forming simulation system, CPFE analysis had been carried out to simulate the typical forming process of a micro-pin. The failure pattern of large-scale crack initiation and mixed mode propagation had been demonstrated through the example of micro-film under tension and three-point bending [27,30]. The effects of regularity and grain size upon local deformation had been demonstrated by a three-dimensional micro-pillar compression simulation [31].

REFERENCES

[1] Geiger M, Kleiner M, Eckstein R, Tiesler N, Engel U. Microforming. CIRP Ann 2001; 50(2):445−62.

[2] Engel U, Eckstein R. Micro-forming − from basic research to its realization. J Mater Process Technol 2002;125−126:35−44.

[3] Taylor GI. Plastic strain in metals. J Inst Met 1938;62:307−25.

[4] Hill R. Generalized constitutive relations for incremental deformation of metal crystals by multislip. J Mech Phys Solids 1966;14(2):95−102.

[5] Rice JR. Inelastic constitutive relations for solids: an internal-variable theory and its application to metal plasticity. J Mech Phys Solids 1971;19(6):433−55.

[6] Hill R, Rice JR. Constitutive analysis of elastic-plastic crystals at arbitrary strain. J Mech Phys Solids 1972;20(6):401−13.

[7] Asaro RJ, Rice JR. Strain localization in ductile single crystals. J Mech Phys Solids 1977;25:309−38.

[8] Asaro RJ. Micromechanics of crystals and polycrystals. Adv Appl Mech 1983;23: 1−115.

[9] Peirce D, Asaro RJ, Needleman A. An analysis of nonuniform and localized deformation in ductile single crystals. Acta Metall 1982;30:1087−119.

[10] Huang Y. A user-material subroutine incorporating single crystal plasticity in the ABAQUS finite element program. Harvard University Report, MECH 178. 1991.

[11] Harewood FJ, McHugh PE. Comparison of the implicit and explicit finite element methods using crystal plasticity. Comput Mater Sci 2007;39:481−94.

[12] Kutt LM, Pifko AB, Nardiello JA, Papazian JM. Slow-dynamic finite element simulation of manufacturing processes. Comput Struct 1998;66(1):1−17.

[13] Chung WJ, Cho JW, Belytschko T. On the dynamic effects of explicit FEM in sheet metal forming analysis. Eng Comput 1998;15(6):750−76.

[14] Choi H-H, Hwang S-M, Kang YH, Kim J, Kang BS. Comparison of implicit and explicit finite element methods for the hydroforming process of an automobile lower arm. Int J Adv Manuf Technol 2002;20(6):407−13.

[15] Riesch-Oppermann H. VorTess, generation of 2-D random Poisson-Voronoi Mosaics as framework for the micro-mechanical modelling of polycrystalline materials. Report FZKA 6325. Karlsruhe, Germany: Forschungszentrum Karlsruhe; 1999.

[16] Kobayashi K, Sugihara K. Crystal Voronoi diagram and its applications. Future Gener Comp Sy 2002;18(5):681−92.

[17] Kocks UF, Tomé CN, Wenk H-R. Texture and anisotropy. Cambridge, UK: Cambridge University Press; 1998.

[18] Zhang KS, Wu MS, Feng R. Simulation of micro-plasticity induced deformation in uniaxially strained ceramics by 3-D Voronoi polycrystal modelling. Int J Plast 2005; 21(4):801−34.

[19] Cao J, Zhuang W, Wang S, Ho K, Zhang N, Lin J, et al. An integrated crystal plasticity FE system for micro-forming simulation. J Multiscale Model 2009;1:107−24.

[20] Cao J, Zhuang W, Wang S, Lin J. Development of a VGRAIN system for CPFE analysis in micro-forming applications. Int J Adv Manuf Technol 2010;47:981−91.

[21] Zhu HX, Thorpe SM, Windle AH. The geometrical properties of irregular two-dimensional Voronoi tessellations. Philos Mag A 2001;81(12):2765−83.

[22] Okabe A, Boots B, Sugihara K. Spatial tessellations: concepts and applications of Voronoi diagrams. New York: Wiley; 1992.

[23] Stoyan D, Kendall WS, Mecke J. Stochastic geometry and its application. New York: Wiley; 1987.
[24] Vaz Fātima M, Fortes MA. Grain size distribution: the lognormal and the gamma distribution functions. Scr Metall 1988;22:35−40.
[25] Zhu B, Asaro RJ, Krysl P, Zhang K, Weertman JR. Effects of grain size distribution on the mechanical response of nanocrystalline metals: part II. Acta Mater 2006;54: 3307−20.
[26] Wang C, Liu G, Wang G, Xue W. On the quasi-stationary grain size distribution from two gamma size distributions in three-dimensional grain growth. Mater Lett 2007;61: 4262−6.
[27] Zhang P, Karimpour M, Balint D, Lin J, Farrugia D. A controlled Poisson Voronoi tessellation for grain and cohesive boundary generation applied to crystal plasticity analysis. Comput Mater Sci 2012;64:84−9.
[28] Zhang P, Balint D, Lin J. Controlled Poisson Voronoi tessellation for virtual grain structure generation: a statistical evaluation. Philos Mag 2011;91(36):4555−73.
[29] Zhang P, Balint D, Lin J. An integrated scheme for crystal plasticity analysis: virtual grain structure generation. Comput Mater Sci 2011;50:2854−64.
[30] Zhang P, Karimpour M, Balint D, Lin J. Cohesive zone representation and junction partitioning for crystal plasticity analyses. Int J Numer Methods Eng 2012;92:715−33.
[31] Zhang P, Karimpour P, Balint DB, Lin J. Three-dimensional virtual grain structure generation with grain size control. Mech Mater 2012;55:89−101.
[32] Ho KC, Zhang N, Lin J, Dean, TA. An integrated approach for virtual microstructure generation and micromechanics modelling for micro-forming simulation. In: Proceedings of ASME, MNC2007, MicroNanoChina07, 10−13 January 2007, Sanya, Hainan, China. 1−9.
[33] Cao J, Krishnan N, Wang Z, Lu H, Wing K, Swanson A. Micro-forming: experimental investigation of the extrusion process for micropins and its numerical simulation using RKEM. Trans ASEM 2004;126:642−52.
[34] Krishnan K, Cao J, Dohda K. Study of the size effect on friction conditions in micro-extrusion: part 1: micro-extrusion experiments and analysis. J Manuf Sci E-ASME 2007;129:669−76.

CHAPTER

Manufacturing Execution Systems for Micro-manufacturing

33

Matthias Meier[1], **Ursula Rauschecker**[2]

Robert Bosch GmbH, Stuttgart, Germany[1]*; Fraunhofer Institute for Manufacturing Engineering and Automation IPA, Stuttgart, Germany*[2]

CHAPTER OUTLINE

INTRODUCTION

Looking at manufacturing from a bird's-eye perspective reveals two important generic processes that characterize these enterprises—the *product life cycle process* on the one hand and the *customer order process* on the other. Figure 1 shows a sketch of these processes and their interrelation. The product life cycle process that is shown on the x-axis describes the activities that are executed to develop new products, i.e., to generate innovations and to bring them to the market. The customer order process on the y-axis shows the activities performed to produce these products based on market needs and to deliver them to customers. Over the last few years, the

Micromanufacturing Engineering and Technology. http://dx.doi.org/10.1016/B978-0-323-31149-6.00033-5

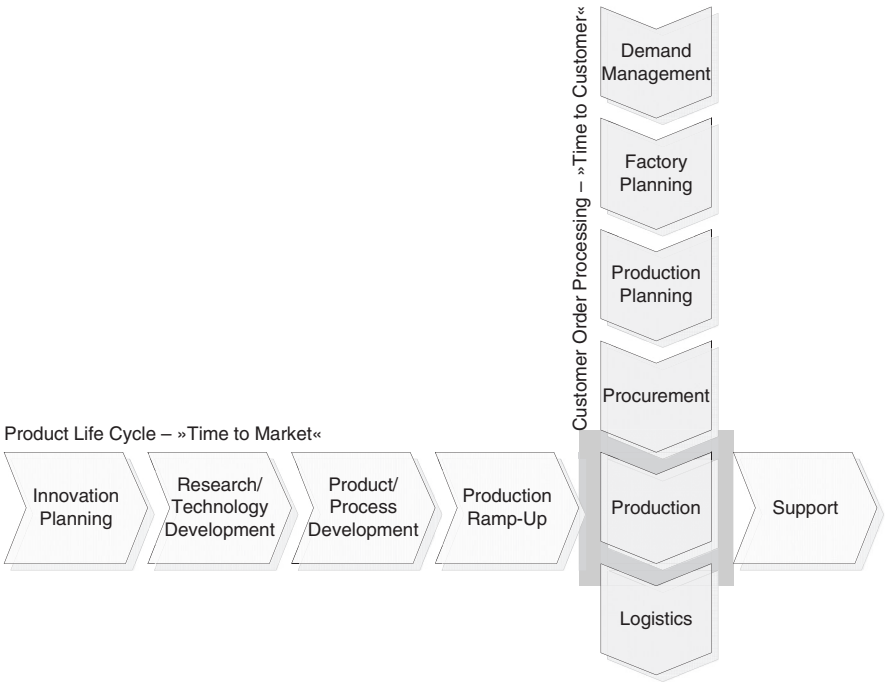

FIGURE 1

Product life cycle and customer order process.

integration of activities within both of these processes has been recognized as a major capability for optimization. Furthermore, the time required for the execution of these processes on the one hand and the efficiency and effectiveness of the execution of activities within these processes on the other are considered as generic optimization goals. Adjusting these potentials requires a significant amount of *information technology* (IT) support, as complex control loops have to be built up—some of them even bridging multiple process activities, with large amounts of data needing to be collected and to be processed in order to change the process variables in the right way. The production activity is the linchpin where both processes overlap and is therefore definitely an activity to be considered when designing the overall IT architecture of an enterprise.

While the foregoing remark is already true for today's state-of-the-art factories, there are a number of reasons that even argue for an increasing need of IT support for the manufacturing of micro-products in future, such as:

1. Operating new manufacturing processes at the edge of technical feasibility in series production often requires sophisticated IT support for monitoring and controlling these processes.
2. There is increasing pressure in terms of quality control, which arises from the automotive industry, for example. While extremely high quality requirements

have been known for a long time in aerospace, in defense, and in the medical industry, the quality requirements *original equipment manufacturer*s (OEMs) request from their suppliers in the automotive industry have significantly risen over the last few years. The goal of the OEMs is to reduce the number of quality issues as experienced with several car series in recent years—which were often caused by defective electronic components. The IT environment is one building block for implementing zero-defect strategies as requested by the OEMs.

3. Increasing low-cost production capacities in several parts of the world put additional cost pressure on numerous industries. Adjusting optimization potentials throughout the process chains is another goal to be supported by IT systems.

Further discussions within this chapter are focused on the "production" activity and the IT environment supporting it. This chapter aims to deliver insights into concepts, standards, and technologies used to implement the production-related IT environment for micro-/nano-manufacturing. The first section provides a general overview of the production IT landscape. It explains important terms, architecture layers, and corresponding systems and their scope. In the second section, the scope is narrowed to the manufacturing execution systems, which are investigated in more detail. The third section briefly reviews approaches to implement the concepts discussed earlier. The last section closes the chapter with some considerations on relevant standardization work.

PRODUCTION IT OVERVIEW

For the following considerations, the scope is narrowed to discrete manufacturing. Investigating a micro-manufacturing enterprise from a production IT point of view requires some initial discussion of the organizational structure of the physical assets of such an enterprise. The hierarchical structure shown in Figure 2, which is

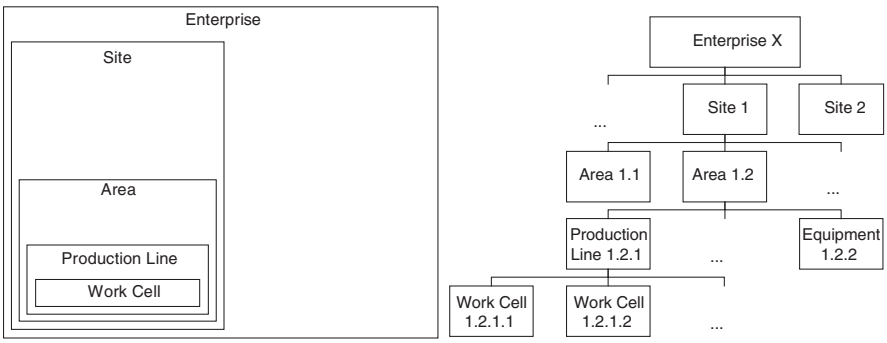

FIGURE 2

Hierarchical model of physical assets—conceptual model (left) and example (right).

based on reference [1], is commonly used for this purpose. As the root of the hierarchy, the *enterprise* defines the products to be manufactured and how and where these products are to be manufactured. Each enterprise comprises one or multiple *sites*. A site is mainly characterized by its physical or geographical location and its major *manufacturing capabilities* and serves as a grouping element for the enterprise. Each site contains one or multiple *area*s. Similar to a site, an area is usually characterized by its physical or geographical location within the site and its major manufacturing capabilities. The actual production capabilities are provided by lower-level entities that are grouped within the area, such as *production lines* and *work cells*. Both production lines and work cells are again characterized by their physical location within the area. Additionally, they have well-defined manufacturing capabilities and capacities. A modular precision assembly line for hard disks would be an example for a production line that is made up of several modules (work cells), each providing specific capabilities required to execute the overall assembly process. For some of the concepts described later, the detailed distinction between production lines and work cells is no longer required. In this case, the generic term *equipment* is used to represent both levels in the hierarchy.

Besides physical enterprises, the concept of *virtual enterprises* (VEs) is becoming increasingly more popular—both in research and industry. VEs are temporary organizations bridging the classical system boundaries described above. Therefore, their structure will look different compared to that discussed earlier. Although the specific requirements of VEs in terms of production IT are not considered here, many of the generic concepts discussed in the following can be adjusted to support VEs. However, additional concepts need to be established from an IT point of view to implement VE organizations.

Figure 3 shows a simplified operational scenario within such an enterprise. Based on demand information a site receives from the enterprise level, the site generates and schedules *work orders* for a given quantity of products or components to be manufactured at the site using the capabilities available within one or multiple areas of the site. The goal of the schedule is to deliver the requested product or component at the right point in time while optimizing the utilization of any *resources* required. Resources in this context comprise employees, equipment, *durables*, *consumables*, and *material*. Durables are auxiliary materials required in addition to equipment in order to process material, such as tools, tensioning media, carriers, cassettes, etc. In contrast to durables that can be reused many times, consumables are a class of auxiliary materials that are consumed while being used, such as coolant, for example. The work orders are executed according to corresponding *route*s, which define the sequence of *steps* required to manufacture a product or component of the requested type starting from raw material. Each step in the route contains information on the resources required to perform the step. The route is complemented by a corresponding *bill of material* that describes in a structured way the parts and components required to manufacture the product or component. In order to monitor the progress of work orders over time, sufficient feedback needs to be provided from the equipment level to higher levels while the route is being executed. Besides the information

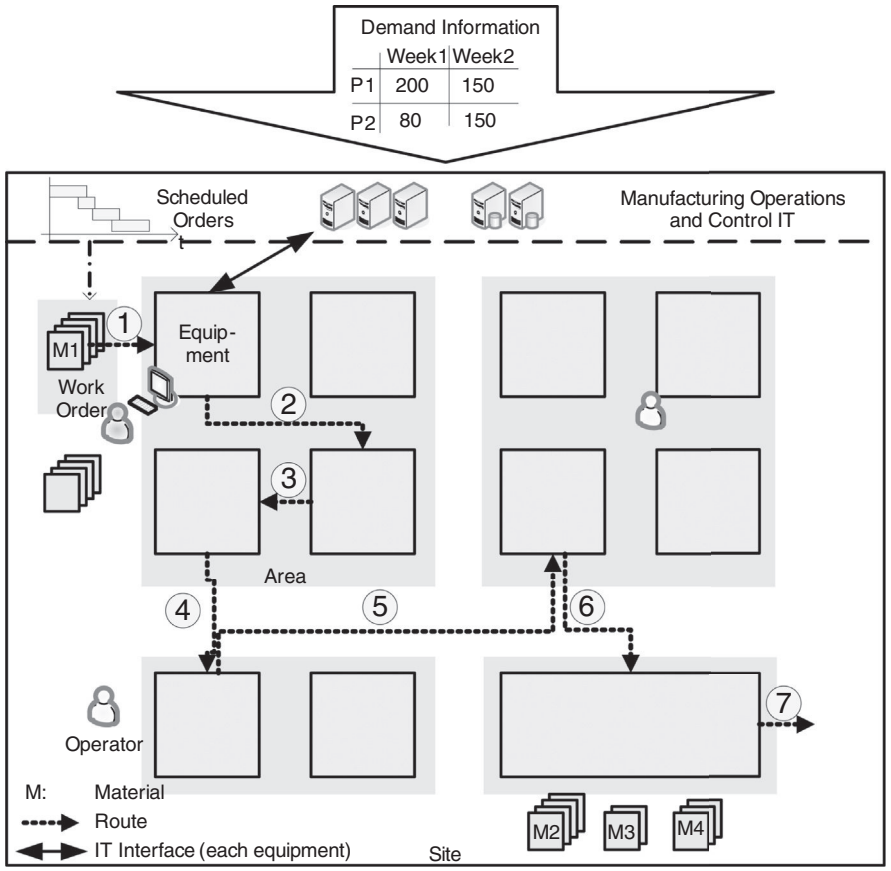

FIGURE 3

Operational scenario (example).

on progress and process results in terms of quantities, feedback on quality needs to be collected to detect possible issues early and to ensure the required level of quality upon completion of the job.

The term "production IT" refers to the IT landscape that is dedicated to support the specific subprocess and activities within the "production" activity shown in Figure 1, i.e., it provides tools to efficiently and effectively operate production. Furthermore, the production IT landscape serves as a building block for process integration within both of the generic processes described earlier—the product life cycle process and the customer order process. The production IT landscape:

1. supplies both processes with accurate information from production in a timely manner, such as information on the processing status of customer orders, available capacities—both are essential for the customer order process—and

process and quality data from production, which complement product life cycle-related data that have been generated in other phases. Access to data from production is required as a first prerequisite to control and optimize the overall processes.

2. provides other activities of the generic processes with suitable interfaces to influence production, which is the second prerequisite to establish overall control loops, including production.

Although the specific requirements to be fulfilled by the production IT environment differ from industry to industry on the one hand and from company to company on the other, there exists a set of generic concepts that many industries have in common: these concepts will be discussed in the following. The common approach to define both the scope and responsibility of the production IT landscape is derived from the *scheduling and control hierarchy*, which is based on the organizational structure of the enterprise, as described earlier. Each level within the hierarchy has corresponding spheres of responsibility and planning horizons and is mapped to corresponding levels or layers of the IT architecture shown in Figure 4 (tasks based on

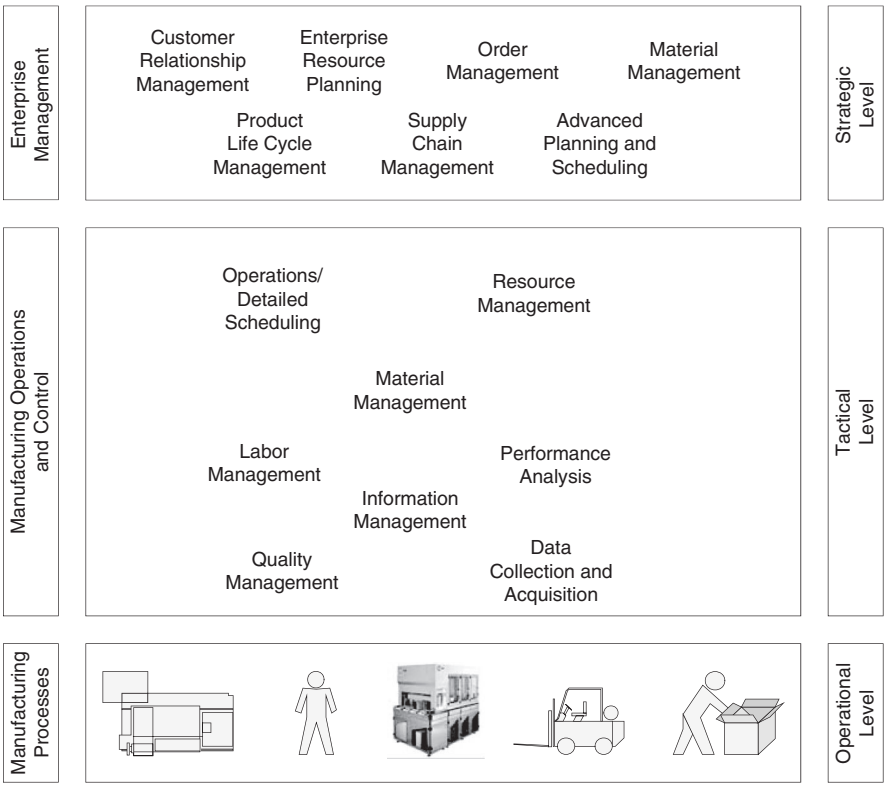

FIGURE 4

Production IT landscape—an overview.

Ref. [2]). On the top-most level, the enterprise management level, the whole enterprise needs to be considered. Thus, planning and control activities on this level cover all sites, have a response time of the order of magnitude of days, span multiple weeks, or months, and incorporate the complete list of available orders (strategic level). The sphere of responsibility of the manufacturing operations and control level is limited to single sites. Therefore, the scope of planning and control activities is limited to this site, spanning only one or several shifts while providing a response time in the order of magnitude of a few seconds to a single shift. At the same time, the number of orders to be considered is rather limited (tactical level). The bottom-most level, which reflects the actual manufacturing processes, is finally concerned with the execution of single process steps. Thus, the planning horizon is further limited to the order of magnitude of seconds or minutes. At the same time, a response time of the order of magnitude of milliseconds to seconds has to be provided. In addition to its specific tasks, each level has to present a sufficient amount of transparency, i.e., to supply the upper layer with accurate and meaningful information with a defined maximum delay and with suitable interfaces to propagate information.

Although the specific shape and the boundaries of these levels differ slightly from industry to industry and from solution to solution, the basic concept—including the levels discussed above—is widely spread throughout many industries.

EXPLORING THE MANUFACTURING OPERATIONS AND CONTROL LEVEL

Based on the overall picture of the production IT landscape described above, the following sections will discuss the role of the manufacturing operations and control layer in more detail—especially the class of *manufacturing execution system*s (MES), which plays a major role in this context. MES bridge the gap between manufacturing processes—including their control systems—and the enterprise management systems as shown above. They control and monitor operations in production, are targeted to adjust optimization potentials within production, and facilitate the level of transparency between enterprise management and production that is required to implement complex process integration scenarios, as described above. The task-oriented view defined in Ref. [2] has been selected as the basic structure for this discussion, as it gives good insight into the MES world from a user's perspective. The description of the MES tasks is complemented by a discussion of major concepts and terms to be considered in the MES environment.

OPERATIONS/DETAILED SCHEDULING

Operations/detailed scheduling optimizes the execution of available work orders—which have usually been generated by higher level systems—based on a set of

predefined optimization goals, while considering the constraints of the production under consideration. Generic optimization goals are:

1. The generation of a schedule that is actually executable while considering the availability of resources and material.
2. The reduction of setup times, cycle time, and *work in progress* (WiP).
3. An increase of throughput, resource utilization, and on-time delivery.

A major characteristic of this task at the MES level is its real-time behavior, i.e., the schedule is continuously adjusted based on events and disturbances that occur on the shop floor. These changes are immediately enforced in production. Thus, the MES is able to handle unforeseen events, such as resource breakdowns, missing material, issues with production processes, and quality issues. Generally, there are two approaches to be distinguished, based on the planning horizon: the *scheduling* approach and the *dispatching* approach. The scheduling approach attempts to generate a plan for assigning a set of *jobs* (task in the context of the architecture level considered) to a set of resources based on given constraints and optimization criteria within the range of a *scheduling horizon*. The dispatching approach is aimed at the optimization of resources in real time by evaluating context information based on a given set of rules. Two typical questions answered by the dispatching subsystem in the case of job shop production are:

1. **What is next for a given resource?**—i.e., which of the jobs within the job queue of this resource should be executed first based on the current context information and the set of dispatching rules? Examples for context information are: resource states, job priorities, time constraints, delivery dates, etc.
2. **Where is next for a given material?**—i.e., what is the best-suited next location for some material after completing a process job on a given resource? In this case, the context to be considered could be the next step based on the route assigned to this work order, the state of resources of the type that is required next, etc.

Due to the ad hoc nature of decisions in the case of dispatching, this approach is mainly followed in highly dynamic environments as known from semiconductor manufacturing, for example, as the large number of disturbances within the production environment would require very frequent rescheduling. As the schedule generation is rather resource consuming (in terms of computational resources) and time-consuming, it is difficult to implement the scheduling approach in this environment.

To deal with scheduling conflicts that arise due to disturbances as described above or due to competing optimization goals caused by committed delivery dates and varying job priorities, for example, is an important aspect of the operations/detailed scheduling task. The system needs to provide the capability to handle these conflicts automatically, if possible, or to supply responsible people with sufficient information to be able to take the right decision manually.

RESOURCE MANAGEMENT

Resource management is mainly concerned with the task of ensuring the availability of the resources required for executing work orders. In this context, the term "resource" comprises machines, equipment, durables, and nonmaterial durables. The former terms were explained earlier—the latter notion of nonmaterial durables refers to auxiliary resources such as *numerical control* (NC) programs or *process programs* (PP) in general. In several industries, PP are also referred to as *recipes*. Recipes are programs that are executed by the equipment control system in order to control a specific process. The behavior of the control system can be adjusted by selecting different recipes or by adjusting parameters within given recipes.

The first aspect of the resource management task comprises the management of resource-related master data. For each resource, a record of generic information needs to be maintained, including properties such as the *identifier* (ID), the location, and capacities and maintenance-related data. Furthermore, resources have to be modeled in sufficient detail in order to support the selected operations/detailed scheduling approach and other MES functionalities. Usually, resources are modeled in the form of a hierarchical structure that describes relevant components and their relationship. A simple example would be some cluster equipment, i.e., a class of items of equipment which have several process chambers that can be operated in parallel. Each process chamber offers specific process capabilities. An internal logistics system is responsible for the material transport within the equipment. The mainframe could be modeled as the root of a tree that contains a set of load ports and a set of process chambers. If single chambers are being considered within the process of detailed scheduling, equipment has to be modeled down to the chamber level. Each object within the tree has a specific state model assigned, including states such as "idle," "processing," or "locked" that reflect the current state of the component at run-time. This state model is used to specify rules for operating the resource at run-time. A rule of that type could define that a resource in state "locked" may not be used for processing, for example. Furthermore, resources have a set of *capabilities* assigned that define the type of jobs that can be executed. At the same time, resources are often integrated into an overall resource hierarchy, such as equipment groups, areas, and facilities, and are linked with related resources. Machine/tool relations would be an example of this type of link. In addition to the equipment model-related master data, resource management has to cover the subtasks of recipe and parameter management.

The second aspect of resource management is related to the run-time behavior of resources. The resource tracking task performs bookkeeping on any relevant dynamic data related to resources, including information on jobs and recipes executed on the resource, state changes based on the resource model and maintenance-related information. The tracking task makes use of events that are gathered online from resources or manually logged at user terminals. If the physical resource starts processing, for example, a corresponding event is either automatically or manually logged for the resource, together with a time stamp. Upon receipt of this event, resource

management will update the corresponding resource state model, i.e., transition it from "idle" to "processing," and store the event in the *history* to allow for further analysis. The updated state information is visible for other MES tasks. Up-to-date resource information is an important requirement for realizing complex automation scenarios with the MES, as other MES tasks, especially the detailed scheduling functionality, rely on this data. Furthermore, resource management plays an important role in the process of resource allocation, especially for the appropriate *setup* of resources before some production job is executed on the resource. The setup comprises anything that is required in addition to the pure resource in order to process the job, such as the appropriate tools, tensioning media, recipes, and parameters. In the case of fully automated scenarios, the setup is performed automatically, e.g., the durables are requested from connected logistics systems, and recipes and parameters are downloaded to the resource. As soon as the setup is complete and material is loaded, remote-controlled resources can even be automatically started via resource management.

The third aspect of resource management is also related to the run-time behavior of resources and is mainly concerned with the availability of resources. Resource properties reflecting the *qualification* state are continuously monitored, such as the operating hours, the number of production jobs executed, or even specific resource- or process-related properties. If limits defined within the master data model are exceeded, requalification of the resource is triggered to ensure the resource does actually provide the expected process capability. Similarly, the maintenance state of resources is monitored. Based on data collected from the resource and corresponding rules maintained in the form of resource master data, *preventive* or *predictive maintenance* strategies can be implemented in order to control the availability of resources to the maximum extent.

With a preventive maintenance strategy, maintenance activities would be triggered as soon as predefined threshold values of given resource properties are exceeded. Exchanging the coolant after a given number of operational hours would be an example for a preventive maintenance strategy. If required, the resource is locked for productive use until the maintenance job has been executed. In the case of a predictive maintenance strategy, resource parameters are monitored, correlated, and evaluated against a set of rules. Maintenance tasks are triggered based on the evaluation results at the best-suited point in time before the resource breaks. The idea of this approach is to reduce the amount of waste that is potentially generated by implementing a purely periodic maintenance strategy, while securing a well-known level of availability for the set of resources. For the coolant example, this would mean changing the coolant only after required material properties have changed, which are continuously monitored. In the event of a resource breakdown, which causes an unscheduled downtime in contrast to the scheduled downtime triggered by preventive or predictive maintenance activities, a maintenance request needs to be generated based on the corresponding resource state change. Additional data acquired from the resource can be linked to the maintenance request in order to speed up the error detection and repair process.

MATERIAL MANAGEMENT

Material management involves all tasks related to material logistics in production. Special focus is put on the WiP management. WiP comprises material that is not residing in managed inventories, i.e., raw material, partially completed material, and final products. Similar to resources, material has a set of properties that are monitored while it is transferred from the raw state toward the final product. The major properties of a material are its ID, its location, its quality, and its quantity. The material ID allows the unique identification of an entity of material, based on a serial number, for example. Due to the amount of data that needs to be handled if single entities of material are individually tracked and due to the fact that many processes treat multiple entities of material at the same time, the concept of *lots* (*batches*) is frequently used to group materials for tracking. Multiple entities of material are grouped to a lot, which has an ID assigned. In addition, lots can have similar properties as single entities of material, such as quality, quantity, and state. Managing lots is part of the material management domain, which includes the tasks to *create*, to *split*, to *merge*, or to *terminate* them. *Create* supports the process of building lots from single entities. *Split* divides a given parent lot into multiple children. *Merge* combines multiple lots into a single lot. *Terminate* removes the lot from the system.

Maintaining the history of lots or single material entities is a major task within the material management domain, which is also referred to as *material tracking* or *WiP tracking*. These terms describe the process of documenting the complete history (*genealogy*) of lots or single entities of material within production. The history contains information such as links to raw material data, information on the equipment the material has been processed on, process data that have been collected while processing the material on the equipment, information on quality and quantity after each process step, and material-related measurement and inspection data. These data are recorded with time stamps and thus lay the foundation for a comprehensive material-related audit trail, which is an important building block for implementing a traceability strategy.

Like the resource states, the material state, which is continuously updated while generating history information, is an important input parameter for the detailed scheduling functionality, as it contains relevant data from an operations perspective. Some examples for material state-related information that needs to be considered for operations are:

1. Material might be locked for further processing (on *hold*). The hold status is set if quality problems are detected that need further investigation, for example.
2. Time constraints caused by specific process properties might require the next process step to occur within a given time window or after a minimum waiting time. If such constraints are violated, this might result in scrap.

Furthermore, information on available material quantities and material locations needs to be evaluated for planning and operations. However, material management does not only monitor material movements, it also triggers material movements by internal or external logistic systems.

LABOR MANAGEMENT

The task of labor management is closely related to resource management. It takes the specific properties of "human resources" into account and supports the task of allocating sufficient personnel with the right level of qualification on schedule for the production. Similar to the resource management domain, the run-time functionality is based on a set of master data for single employees, groups of employees, and the organizational structure. Typical attributes of a single employee are the personnel ID, name, qualification, or certification, etc. Furthermore, the availability of personnel is maintained in the context of the deployment scheduling.

Based on the master data described above, personnel-related status information needs to be maintained. Time recording allows for gathering information on the actual availability of staff and the jobs or tasks executed within this time frame. This information is required as a basis to implement complex work schedule and wage models, including flexible working hours, piecework models, etc. Tracking the association of staff information with production jobs constitutes another building block for implementing traceability strategies, as it documents who did what and whether the person who performed a given job or task had the right level of qualification or not. Functionality supporting the resource deployment gives an overview on the available staff capacities, provides support to manage these capacities, and helps to assign jobs and tasks to personnel in an efficient and effective way.

DATA COLLECTION AND ACQUISITION

The availability of data of sufficient quality with little delay from production is an important prerequisite for all of the MES tasks discussed earlier (and those to be described later). Data collection and acquisition realizes the connectivity to the manufacturing processes with a suitable maximum delay. Thereby, it lays the foundation for an up-to-date, correct, and consistent process image of the situation in production within the MES. This image is used to *monitor and control* processes in production in real time—as described in other MES tasks. The meaning of "suitable delay" and "real time" depends on the actual monitoring and control problem to be solved. Usually, the minimum response time on the MES level is of the order of magnitude of a few seconds.

Generally, three approaches to data collection and acquisition can be distinguished: manual, semiautomated, and automated data collection. In the case of manual data collection, an operator manually enters data records using some kind of input device. Manual data collection is frequently performed using electronic forms that the operator has to complete at a user terminal. Semiautomated data collection needs manual interaction by a user—however, part of the data is acquired automatically. Data collection using barcode guns or radio frequency identification readers are examples of semiautomated applications. Automated data collection requires the implementation of suitable IT interfaces for data acquisition. The collection is either triggered by events that occur within the data source or by cyclically polling the data source. Sophisticated mechanisms have been designed to

specify both the amount of data to be collected and the frequency, based on the current need. The concept of *data collection plan*s allows users to dynamically determine the data to be collected for a given process. The user specifies the collection plan by selecting process variables to be monitored from a set of available variables and the desired collection frequency. As soon as the plan is activated on the corresponding resource, the selected data are available through the IT interface.

Whenever raw data are collected, it needs to be checked for plausibility and consistency before being further processed. These checks are required independently of the approach used for data collection. As correct and consistent data are an important prerequisite for successfully operating an MES, these checks are considered to be part of the data collection and acquisition task in order to prevent the further processing of incorrect data. After performing the plausibility and consistency checks, most of the data records collected have to be preprocessed and consolidated to simplify the downstream tasks. Converting dimensions or evaluating counters to physical values are two examples of consolidation and preprocessing steps.

PERFORMANCE ANALYSIS

Performance analysis targets the evaluation of the performance on the shop floor, both short term and long term. Thus, it provides support for establishing control loops to influence operations on the one hand and to optimize processes in the long run on the other. Data that have been collected by the MES are consolidated to suitable *key performance indicators* (KPIs) that lay the foundation for further analysis. These KPIs can be compared against organizational and technical targets: suitable corrective actions are derived from the results, if necessary. The following list provides a set of examples of KPIs that are used throughout many industries:

1. **Cycle time**. This is the analysis for all components of the cycle time for jobs, including nonproductive time, and the sum of these components.
2. **Equipment utilization**. This is the fraction of time the equipment is performing its intended function during a specified time period [3]. Measurement of the remaining capacity of equipment or workplaces provides the ability to detect bottlenecks.
3. **Overall equipment efficiency (OEE)**. This is the fraction of the total time that equipment is producing effective units at theoretically efficient rates [4]. This is used widely to measure process efficiency.

The following explanation for OEE calculation is given in order to visualize performance analysis and its relevance and application of results. To do so, some theoretical foundations have to be given: The OEE is the product of *availability efficiency*, *performance efficiency*, and *quality efficiency* (refer to Table 1). Thereby, availability is defined based on the time, during which the equipment is in operational mode, i.e., not in unscheduled or scheduled down mode which applies, e.g., for maintenance and repair activities. Further availability losses are caused by nonscheduled times such as unworked shifts, shutdown, or start-up times. The

Table 1 Overview on Equipment Times and Efficiency Losses

Nonscheduled Time *unworked shifts*, *shutdown/start-up*, *etc*.	*Availability Efficiency Losses*
Unscheduled downtime *Repair time*, *maintenance delay*, *etc*.	
Scheduled downtime *Production tests*, *preventive maintenance*, *etc*.	
Engineering time *Process experiments*, *Software qualification*, *etc*.	*Performance Efficiency Losses*
Standby time *No operator/product/support tool*, *etc*.	
Productive time *Regular production*, *work for third party*, *Engineering runs*	*Quality Efficiency Losses* *Theoretical production time for effective units*

performance of an equipment is affected by standby engineering times, when process experiments or software qualification is executed, standby times when, e.g., resources are not available as they are needed, and productive times, when regular production is executed. The rework and scrap occurring during such productive times is the basis for calculation of the quality efficiency.

Based on the monitoring and analysis of the theoretical production time for effective units and related performance figures, there are numerous ways to make use of these results and to trigger corresponding actions. In the simplest case, the results are incorporated into management reports and lay the foundation for further decisions. This is especially true for the long-term case. For the short-term case, the results of the performance analysis could automatically trigger actions within the system such as updates to dispatching and scheduling decisions or could be fed into the dashboards of control centers or information systems on the shop floor to trigger immediate action by operational personnel.

QUALITY MANAGEMENT

The quality management task supports organizations in reaching the required level of product and process quality as far as the shop floor is concerned. It comprises the aspects of *quality planning*, *management of test equipment*, and *quality inspection*. Quality planning requires a variety of input data from previous process stages in the product life cycle on the one hand and overall quality targets on the other that define the requirements for quality inspection. Test plans need to be transformed into suitable system configurations to ensure that routes and data collection plans are appropriately set up and that the data acquired from the shop floor are evaluated as needed. The *sampling* functionality is responsible for selecting lots or single products for

quality inspection based on *sampling plans* that need to be configured according to the test plan. A simple sampling plan could define every 50th lot to be inspected, for example. *Dynamic sampling* is an extension that allows for dynamic adjustments of sampling plans at run-time. The sampling rate could be automatically increased, if issues are detected in production that might affect quality, for example. Quality assurance processes and measures need to be modeled within the MES system in order to enforce and to document their execution. Access control based on the current certification level of operators, the ability to issue directives to operators that need to be confirmed after reading, and quality gates are examples of measures to be supported by the MES environment. Managing test equipment is closely related to resource management. However, some specific characteristics of test equipment have to be taken into consideration. Especially, the support for calibration traceability needs to be taken into account.

Another aspect of the quality management task is related to documentation, reporting, and control. Depending on the quality management system, corresponding documentation has to be generated which confirms that the defined quality assurance measures have been properly executed. The quality information collected lays the foundation for reporting the level of quality reached and thus allows for implementing countermeasures early, if issues are detected. Sample data collected can be evaluated using the methodology of *statistical process control* (SPC). SPC provides the means to monitor processes and thus to detect possible quality issues and to correct them in the early stages of the overall production process for a product. The methodology of *fault detection and classification* (FDC) is used to analyze quality-related data, to detect and recognize possible issues, and to derive suitable actions from these issues. Example actions that could be triggered automatically are:

1. Put lots on hold;
2. Stop process equipment.

INFORMATION MANAGEMENT

Information management is a cross-sectional task that is built on top of the tasks that have been described earlier. It makes use of data and context information available in the system, provides suitable views of the data—both for users as well as for other MES tasks—and complements this information by suitable reports and evaluation results. Furthermore, the task of information management has an active component—it responds to events reported from production in real time. Both aspects lay the foundation for establishing complex control loops for production that take a variety of parameters into account.

Suitable views providing information in the appropriate context are not only relevant for management reporting, production management, and control or quality assurance, they also provide the tools required to implement *paperless* production

concepts or at least strategies that require a minimum amount of paper in production. Replacing paper-based *lot traveler*s by electronic lot travelers is one element of paperless strategies. A lot traveler contains basic properties of the lot, such as: its ID and priority information; information on the route to be used, i.e., the process steps to be performed; and additional information to be considered by the operator. Furthermore, it is often used to collect feedback from production, such as the signatures of operators confirming that certain instructions have been executed, quality inspection results, process data, etc. An electronic lot traveler provides users with the type of information required in a given context using IT systems. In this case, "context" could mean a given job at a given equipment instance. Other views could provide operators with specific information on quality trends achieved at a particular work station which would help to achieve a constant level of quality. The capability to access relevant documents in a given context, such as drawings, manuals, and work instructions, helps operators to work efficiently and effectively.

The ability to design, execute, and monitor workflows for the shop floor environment that allow the guidance of operational sequences on the shop floor is a major task to be supported by the MES. These workflows describe sequences of actions, roles, and responsibilities and drive all operational sequences in a defined way. Implementing this task might require the MES to support additional classes of master data, if this data cannot be supplied by other tasks or external systems. *Exception management* is an additional subtask of information management. It targets the automatic resolution of exceptions that occur in production, if possible, or at least the support of users for resolving exceptions. Semiautomated exception resolution would provide responsible users with information on possible corrective actions and generate exception notifications for these users by E-mail or short message service, for example. More sophisticated approaches to influence production based on collected information are covered by the methodologies of *advanced process control* (APC). This term covers a variety of process control methods and tools, such as SPC and FDC as described above, *run to run* (R2R) control, and others.

MES IMPLEMENTATION AND INTEGRATION INTO THE PRODUCTION IT

There exists a variety of approaches to implement MES solutions supporting the tasks described above. In most cases, these tasks will not be supported by a single system, but rather by a collection of cooperating systems. Furthermore, the set of implemented tasks heavily depends on the requirements of the industry or group of industries that a given solution targets and—most importantly—the specific requirements of the organization to be supported. The same holds true for the complexity of the IT landscape and the enterprise architecture of the production IT environment. In the following, two approaches for MES implementation and integration into the production IT are given.

COMMON HIERARCHICAL IT INFRASTRUCTURE

Figure 5 shows a simplified example of a production IT environment that contains some typical concepts used. It is based upon the hierarchical structure shown in Figure 4.

1. The bottom-most layer is the equipment layer. Equipment provides one or multiple manufacturing process capabilities that are monitored and controlled by internal process control systems, such as *programmable logic controllers* (PLC), *computer numeric controller*s, *embedded PCs*, or *industry PCs* (IPC). Typically, these control systems are connected to *sensors* and *actuators* using standardized *field bus* systems, such as PROFIBUS and CANopen. Depending on the complexity of the equipment, it might again use a hierarchical IT

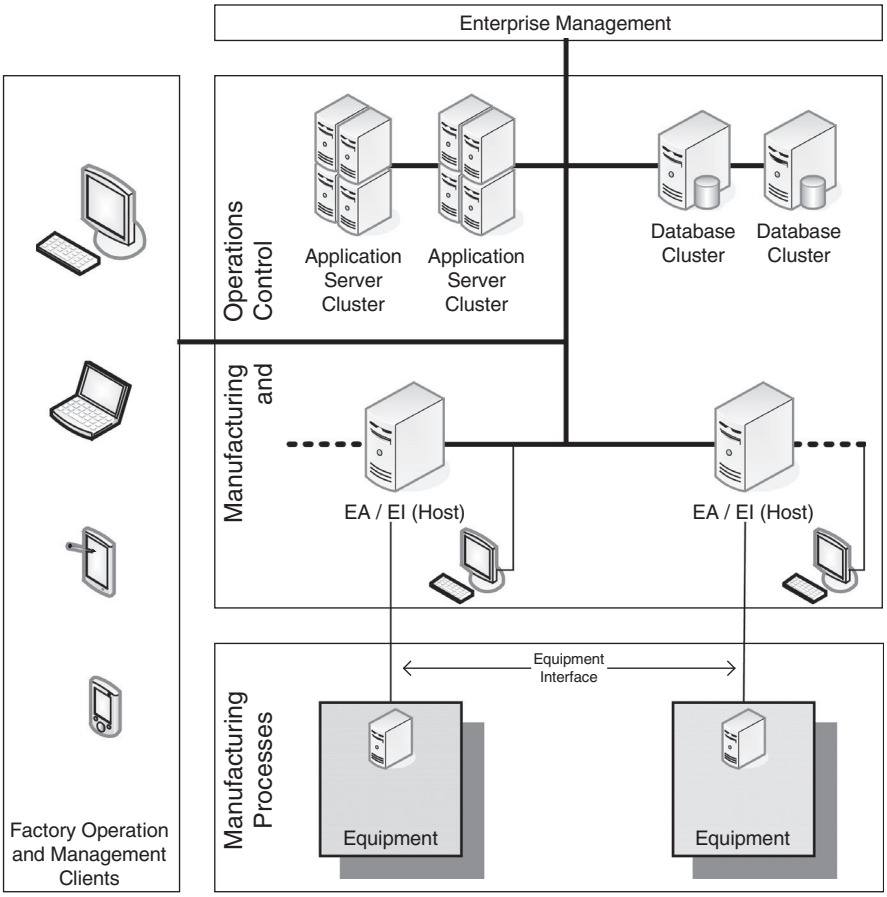

FIGURE 5

IT Infrastructure (example).

infrastructure internally. Examples of complex equipment would be cluster equipment, automated lines, or transport systems. Equipment is able to autonomously control at least their basic process capabilities using these internal control systems. IT interfaces (in Figure 5 marked as "Equipment Interface") expose selected properties of the internal control system of the equipment to the outside world. In the simplest cases, the interfaces provide access to data available within the internal control system, such as process variables that contain sensor results. Furthermore, such interfaces can provide notification of events or alarms that occur within the equipment, configurable data collection based on collection plans, remote control, and other capabilities. Sufficient equipment interface capabilities are an important prerequisite for supporting the tasks described above on the MES layer. For this reason, they provide a broad field for standardization, which will be described in more detail in the following section.

2. The *equipment automation* (EA)/*equipment integration* (EI) layer connects equipment to IT systems on higher layers by using the equipment interfaces discussed earlier. The main goal of the EI is to provide a common view of all types of production equipment to be monitored and controlled within the factory and to connect equipment to the factory communication system (usually Ethernet based). Thus, it implements part of the resource management tasks. At the same time, several of the data collection and acquisition-related tasks described earlier are implemented on the EI layer, such as unit conversion and data verification. EA refers to the implementation of equipment (type)-specific operational scenarios, i.e., it provides the IT support required to execute process steps of equipment in a defined way at a given instance. These scenarios comprise equipment-related material logistics, material verification, setup instructions, remote control commands, and data collection, for example. User interface clients are attached to single items of equipment or to groups of equipment, if operational scenarios require user interaction or supervision. These user interface clients support the information management tasks in the context of a given item of equipment or equipment group. In many installations, the EA/EI components and the user clients are either deployed on dedicated PCs or IPCs for single items of equipment or equipment groups or deployed on larger server systems within the factory's computational center.
3. The majority of tasks described above are implemented on top of the EA/EI layer. Older implementations of MES solutions followed a rather database-centered approach and were usually based on mainframe technologies. This turned out to be a limitation during recent years, especially in terms of agility. One of the nonfunctional requirements to be taken into account for implementing MES solutions is the ability to change, i.e., to support new requirements. Reasons for change and new requirements are the introduction of new technologies, new equipment, new products, and process improvements, for example. Furthermore, there is a need for horizontal integration within the manufacturing and control level. Due to the variety of tasks to be supported,

there is usually the need to integrate multiple applications—in many cases even from different suppliers—in order to realize the required level of IT support for production. However, all applications require a correct and consistent view of the current situation in production. Both issues were not sufficiently supported by the old mainframe solutions. Fortunately, current state-of-the-art architectures promise to do better. To use the paradigms of a *service-oriented architecture* (SOA) looks particularly promising: the MES tasks described above are implemented by a collection of independent *services*. Each service covers a well-defined functional scope (such as recipe management) and exposes its capabilities through public service interfaces. In order to implement a given business process in production, a corresponding set of services needs to be *orchestrated*, i.e., to be combined, in the right way. This approach does not only improve agility, as services can be rewired or complemented by additional services to support changing requirements, it also greatly simplifies both horizontal as well as vertical integration within the production IT landscape.

OUTLOOK TOWARD INTELLIGENT, NETWORKED PRODUCTION

Beyond the hierarchical IT infrastructure described above, the trend toward networked production based on CPS (cyber-physical systems) and cloud computing currently increases. The underlying concepts are based on the exploitation of the potential provided by the integration of additional intelligence and network capabilities to manufacturing infrastructures. To realize this, mainly the following approaches are considered:

- Uncoupling the hardware infrastructure from the logical, in most cases still hierarchically ordered, software functionalities: Running software in cloud infrastructures while the related hardware or processes are operating on shop floor level is currently mainly implemented for applications which are not depending on real-time capabilities, i.e., it applies, e.g., for data collection, MES, and enterprise level features. As soon as there apply real-time requirements for communication between control software and connected sensors and actuators, this has to be considered during the overall IT infrastructure setup which currently excludes remote cloud infrastructures to be used for this purpose [5].
- Integration of additional intelligent components to the manufacturing environment: The term of CPS emerged during the past years also in the production domain. It stands for the integration of sensors, actuators, and software functionalities into one system while considering security and networking aspects [6]. For manufacturing, those systems are, e.g., implemented in the form of smart carriers, or by enhancing existing manufacturing equipment, transport systems, etc., with additional intelligence, i.e., sensors and IT features, in order to provide additional information and services to the MES and enterprise level.
- Closer integration of existing IT systems such as MES, APC, ERP, CRM, CAx systems, etc., in order to generate additional knowledge and context

awareness: In addition to accessing additional data sources such as CPS, the integration of existing systems provides potential for the exploitation of existing data by interlinking the systems in order to identify, e.g., additional interdependencies among processes and conditions which are currently not considered to be related to each other by the corresponding stand-alone IT systems.

All of these efforts have in common that they intend to enable or support additional intelligence and flexibility in manufacturing.

When focusing on intelligence, those systems are the basis for additional IT systems for data analysis and decision-making which contribute to the optimization of manufacturing environments. However, the potential of these emerging technologies strongly depends on the applications for which they are implemented. Their benefit, for example, can be related to an added value which could be provided to customers such as full traceability of products, or to cost reductions, i.e., increased manufacturing efficiency.

Flexibility with regard to products or processes is mainly supported by intelligent components which are providing self-descriptions to enable fast integration and (re-)configuration, and by additional software components supporting this. The benefit provided by them is mainly shorter ramp-up times. However, their potential strongly depends on the degree of standardization throughout automation levels and industry branches.

PRODUCTION IT STANDARDIZATION

As shown in the preceding sections, establishing a pervasive shop floor IT environment requires a variety of software systems to cooperate—starting from the enterprise layer down to the equipment layer. For each type of software system, there exists a variety of products and suppliers in the market. Therefore, accepted and implemented industry standards turn out to be an important enabler for realizing production IT environments. Among others, standards are created to serve the following goals:

1. They provide common definitions of important terms and concepts and thus facilitate a common understanding, which is especially important for the specification phase of MES solutions.
2. They define system classes and their scope and thus create transparency regarding the capabilities of a given system class.
3. They provide unified interface definitions and enable or simplify the task of integrating different systems, even if they are provided by different suppliers.

Standardization activities are performed throughout all layers of the shop floor IT—usually based on specific needs. There exists a variety of organizations that provide platforms for standardization that have to be considered in the shop floor IT environment—some of them targeting on specific industries

(e.g., Semiconductor Equipment and Materials International—SEMI [7]), some of them approaching cross-industry topics (e.g., Manufacturing Enterprise Solutions Association—MESA international [8]), others focusing on specific technologies (e.g., Internet Society—ISOC [9]). The following sections give a rough overview of selected organizations and standard collections in the shop floor IT area—both on the factory automation layer and on the equipment automation layer.

GENERAL PRODUCTION IT STANDARDS

Several organizations have made a number of attempts over the last few years to create extensive standard frameworks or reference models describing approaches to realize a pervasive production IT landscape that integrates well with the overall IT landscape within the enterprise and thus supports the goal of process optimization described at the beginning of this chapter. One approach that shaped the discussion for several years, especially in the early 1990s, was the "Reference Model for Computer Integrated Manufacturing (CIM)" [10]. This describes a hierarchical IT architecture that is built up from six levels based on the scheduling and control hierarchy and has been designed as a guideline for establishing a vertically integrated production IT landscape. Although the concept has not yet been implemented to its full extent, it served as a basis for many successors. In 1997, MESA [8] presented a definition for MES, which is still considered to be valid, and its potential scope by describing a set of 11 functional groups. The scope of a concrete MES solution was defined to be a subset of the potential scope based on the user's priorities and requirements. A few years later, in 2000, ISA-95 Part I was published. This is based on the concepts of CIM (especially the scheduling and control hierarchy) and focuses on the specification of interface between business systems and manufacturing operations and control systems. Furthermore, ISA-95 integrates the functional groups defined by MESA to describe the functionalities of the manufacturing operations and control, i.e., the MES, level. ISA-95 Part II [11] and Part III [12] followed later and complement Part I with the detailed specification of the data model on the one hand and the activity model and dataflow specification for the manufacturing operations and control level on the other. VDI 5600 [2] is currently the latest standard in this series. It comes from a task-oriented view of the MES that rather reflects the user's perspective than the system perspective and updates and extends the MESA MES model.

EQUIPMENT INTERFACE STANDARDS

An important prerequisite for implementing several requirements described in the preceding sections is the ability to communicate with process equipment in order both to remotely control the equipment and to acquire a variety of data from the

equipment, such as operational data, machine data, and process data. As a factory usually houses equipment from a variety of suppliers, the effort to connect them to the production IT environment of a given factory is comparably high, as a specific connector has to be implemented for each equipment type. This is where the idea of the definition of a standard IT interface for equipment, as shown in Figure 5, comes into play.

One of the standard frameworks that is frequently used to integrate equipment with higher levels of the production IT landscape is the OPC [13] framework. In the past, the OPC standards enabled basic data access between MES level and PLC level. However, during the past years, the OPC UA (OPC Unified Architecture) standard has been emerging. It provides the ability to access shop floor data on MES and enterprise level via Web services while it also fulfills real-time requirements which apply for communication with the devices and related sensors and actuators [14].

To do so, the standard specifies abstract services such as session, query, method, or subscription, an address space model, an information model, and the mapping of the abstract services to concrete technologies such as UA native, Web services, etc. A further advantage of OPC UA in comparison to other PLC-level communication standards is that it deals with security issues.

However, for further discussion, an industry-specific framework from the semiconductor industry has been selected, as it refers to industry-specific communication standards. It provides a comprehensive approach, which can serve as a generic example. Figure 6 (based on Ref. [15]) gives a compressed overview of the standards framework that is widely used in the semiconductor industry. The communication protocol defined by E5 lays the foundation of the standard framework. Today, it is usually bound to a TCP/IP-based message transport layer according to E37 (HSMS-SS), which enables communication with equipment using a unified message format. While this protocol basically allows for the communication of a host system with an equipment instance, it leaves the supplier with a high degree of freedom regarding the actual implementation of the interface. For this reason, the effort for integrating equipment into the shop floor IT still turned out to be rather high. Furthermore, different interface implementations provided largely varying capabilities that needed to be taken into account. To overcome these limitations, additional standards have been added on top of E5. The "Generic Model for Communications and Control of Manufacturing Equipment" (GEM) defines the semantics of the interface, i.e., the behavior of the equipment from the IT interface perspective. This step led to a significant reduction of the effort required for the integration of equipment and allowed for the introduction of standard compliance tests. E30 is complemented by a standard for *recipe* management and standards for specific equipment models. While E30 contains specifications that have to be considered for all types of semiconductor equipment, specific equipment models comprise equipment characteristics and behavior definitions that have to be implemented in addition to GEM for specific equipment types only, for example, transport systems: these take the specific needs based on the equipment type into account.

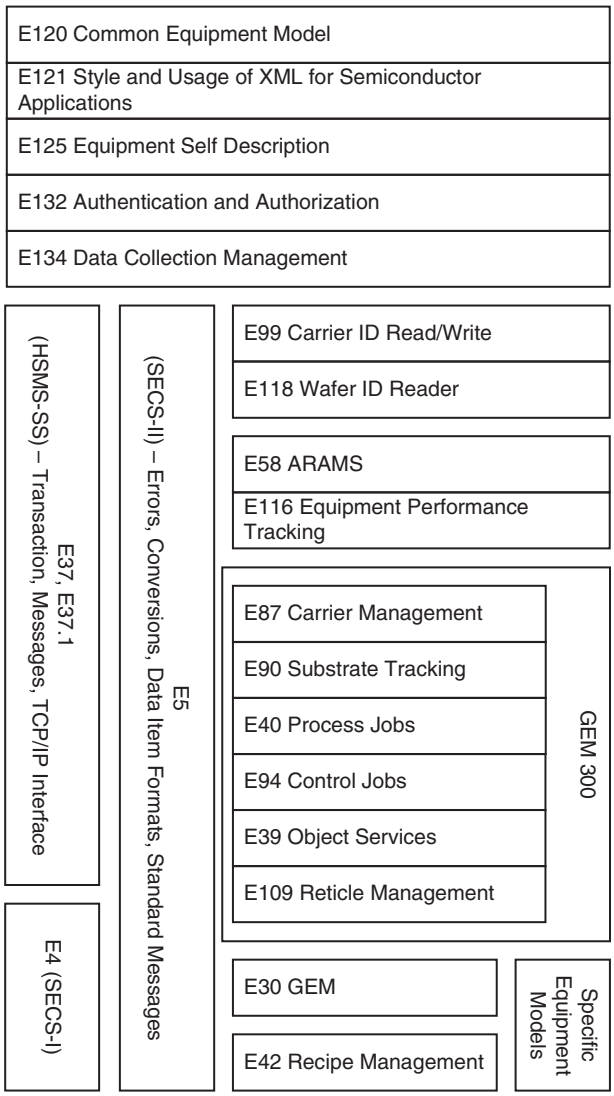

FIGURE 6

Equipment interface standard framework—as defined by Semiconductor Equipment and Materials International. SECS, SEMI Equipment Communication Standard.

The standard framework is completed by the family of GEM300 and a couple of auxiliary standards. As the transition from 200 to 300 mm wafer processing was accompanied by the demand for a higher level of automation, the requirements for additional automation capabilities on top of E5 arose and led to the definition

of these standards, such as the capabilities to manage carriers or to track substrates. Additionally, there was an increasing need to acquire data from process equipment. The family of Equipment Data Acquisition (EDA) standards has been created to meet these requirements. The EDA stack is implemented in parallel with the GEM/SECS (SEMI Equipment Communication Standard) interface, is limited to data acquisition and allows an arbitrary number of clients to acquire data from equipment based on Web technologies.

CONCLUSIONS

Today, it is virtually unthinkable to operate state-of-the-art manufacturing facilities without a variety of IT systems supporting production. Several classes of IT systems can be found over the different layers of these facilities—from enterprise resource planning systems as an example on the enterprise management layer down to programmable logic controller-based applications on the manufacturing processes layer. The term MES usually refers to a collection of integrated software applications that is located between those two layers—on the manufacturing operations and control layer. On the one hand, the MES ensures the right level of information transfer between upper and lower layers and thereby supports the integration of processes on the shop floor into the overall business process framework. On the other hand, the MES provides a rich set of functionalities to optimize operations on the shop floor in different dimensions, such as product quality, resource utilization, and the adherence to delivery dates. A variety of standards have been created in different industries to enable and simplify the setup of the MES environment. Looking at the potential provided by an MES, the relevance of this topic in the area of micro-manufacturing will continue to grow in the future.

REFERENCES

[1] Enterprise-control system integration, part I: models and terminology. ANSI/ISA-S95.00.01−2000. Research Triangle Park (NC, USA): Instrument Society of America; 2000.

[2] Manufacturing execution systems − production management systems. VDI 5600 Blatt 12006−08. Verein Deutscher Ingenieure. 10772 Berlin (Germany): Beuth Verlag GmbH; 2006.

[3] Specification for definition and measurement of equipment reliability, availability and maintainability (RAM). SEMI E10. 3081 Zanker Road, San Jose (CA, USA): Semiconductor Equipment and Materials International; 2004.

[4] Specification for definition and measurement of equipment productivity. SEMI E79. 3081 Zanker Road, San Jose (CA, USA): Semiconductor Equipment and Materials International; 2006.

[5] Stock D, Rauschecker U, Stoehr M, Bauernhansl T. Cloud-based platform to facilitate access to manufacturing IT. In: The 8th international conference on digital enterprise technology, Stuttgart, Germany; 2014.

[6] Geisberger E, Broy M. AgendaCPS – integrierte forschungsagenda cyber-physical systems. acatech STUDIE; March 2012.
[7] Semiconductor Equipment and Materials International – SEMI. http://www.semi.org [Last accessed: 07.03.2014].
[8] Manufacturing Enterprise Solutions Association – MESA International. http://www.mesa.org [Last accessed: http://www.mesa.org].
[9] Internet Society – ISOC. http://www.isoc.org/ [Last accessed: http://www.mesa.org].
[10] Williams TJ. A reference model for computer integrated manufacturing (CIM), a description from the viewpoint of industrial automation. Research Triangle Park (NC, USA): Instrument Society of America; 1989.
[11] Anonymous, enterprise-control system integration, part II: object model attributes. ANSI/ISA–S95.00.02–2001. Research Triangle Park (NC, USA): Instrument Society of America; 2001.
[12] Anonymous, enterprise-control system integration, part III: activity models of manufacturing operations management. ANSI/ISA-S95.00.03–2005. Research Triangle Park (NC, USA): Instrument Society of America; 2005.
[13] The OPC foundation. http://www.opcfoundation.org/ [Last accessed: 07.03.2014].
[14] Meier M, Dreiss P, Seidelmann J. Potentials and limitations of standardization of shop floor IT based on examples from semiconductor industry. PPS Manag 2007;12:4. Gito Verlag mbH, Klixstr. 1 A, 13403 Berlin, Germany.
[15] Leitner SH, Mahnke W. OPC UA – service-oriented architecture for industrial applications. ABB Res Cent 2006;11.

This page intentionally left blank

CHAPTER

34 Life Cycle Assessment in Nanotechnology, Materials and Manufacturing

Sergio Durante[1], **Mauro Comoglio**[2], **Nicola Ridgway**[3]
Diad Group ES, Spain[1]*; Diad Group, Italy*[2]*; Teks, France*[3]

CHAPTER OUTLINE

Micromanufacturing Engineering and Technology. http://dx.doi.org/10.1016/B978-0-323-31149-6.00034-7

INTRODUCTION

Nanotechnology and micro-manufacturing and the production of nano-materials is a rapidly developing field with great scope for innovation and development. For example, the US government increased their expenditure for nanotechnology from $464 to $1554 million between the years 2000 and 2008 [1]. However, the economic potential of nanotechnology has not only been recognized by the United States with the EU investing $1.7 billion in nanotechnology research and development in 2008 [2]. To guide the research and development of nanotechnology-related activities, the National Nanotechnology Initiative (NNI) was established in 2000 by the US Government. The NNI define nanotechnology as "the understanding and control of matter at dimensions between approximately 1 and 100 nm" A nanometer is one-billionth of a meter. To give some perspective to this size, a sheet of paper is 100,000-nm thick and the average finger-nail grows 1 nm a second. The use of nano-technologies is evident in a wide range of disciplines such as science, engineering, and technology and can be used in a wide range of applications including measuring, modeling, and imaging. An example of how nanotechnology has impacted on modern-day life is the use of nanotechnology in nano-engineered batteries. Such technologies have contributed to the explosion of portable electronics and revolutionized how we communicate [3]. Nanotechnologies are also impacting health care and revolutionizing the way we treat chronic disease, among other things. For example, the use of nanotechnology has allowed the development of oral chemotherapy, which will enable "at home" treatment for cancer [4]. Not only will this include the ease at which patients seek health treatments but it may also enable a reduction of side effects which are currently often experienced by those living with cancer. Current chemotherapy regimes are delivered using IV infusions/injections with high doses, often causing peaks above the maximum tolerable concentration of the drug in the plasma [4]. Such peaks can cause serious side effects [4]. Oral chemotherapy could maintain a sustained moderate concentration, which would avoid high peaks above the maximum tolerable concentration. The development of an oral chemotherapy regimen has only been possible through the use of nanotechnology. More pertinently, our bodies are designed to protect us from external toxins, so many drugs (especially anticancer drugs) are not absorbable in the gastrointestinal tract. Nanotechnology has been researched and applied to drug formulation and drug delivery in order to overcome these difficulties. Just from the few examples outlined here, it is easy to understand the potential impact that nanotechnology can have across varied aspects of everyday life. However, despite the benefits of nanotechnology, we still do not know enough about the long-term impacts of such techniques. In particular, knowledge of exposure rates as well as the potential environmental impacts of nano-materials is limited.

Therefore, there is a clear need for in-depth research to establish a fuller understanding of the benefits and drawbacks of nanotechnologies compared with conventional technologies.

NANO-MATERIALS AND THE ENVIRONMENT

Little is currently known about the impact of nano-materials on the environment and society. The environmental impact of nanotechnologies is particularly interesting as Dhingra et al. [5] outline that the apparent benefits of nano-enabled products are often discussed and focused on while the environmental impacts upstream and downstream of the life cycle often get ignored. Kim and Fthenakis [6] summarize the importance of considering the environmental impact across the full life cycle of nanotechnologies in their review of the current evidence base. They summarize that most reviewed studies suggest that the cradle-grave energy demand and global warming impact from nanotechnologies are lower than from conventional technologies. This evidence is a belief held by many people as nano-materials are used in small amounts to improve functionality and offer increased energy efficiency. However, in-depth analyses of the findings suggest that nano-materials have high cradle to gate energy demands per functional unit and therefore have higher global warming potential when compared with conventional materials and processes. These higher energy demands, early in the life cycle, are attributed to the energy intensive synthesis processes or additional mechanical processes that are needed to reduce particle size. Kim and Fthenakis (2013) conclude that depending on the synthesis method, it could take anywhere from 1 to 900 GJ per kilogram (GJ/kg) of energy to produce carbon-based nano-particles. In contrast, it would only require around 200 MJ/kg for aluminum, a material often used prior to the development of nano-materials. Such an energy-intensive phase of development will have a large impact on the environment and potential to harm human health. Overall, nanotechnologies can be considered energy and resource intensive due to the stricter purity requirements, lower process yields, repeated processing/postprocessing, use of toxic or acidic chemicals and organic solvents, the need for moderate to high vacuums, and the use of or generation of greenhouse gases [7]. For this reason, it is imperative to investigate the potential impact of nanotechnologies and consider the impact across the full life cycle of the materials/products. Life cycle engineering (LCE) is the primary methodology to investigate the impact of materials and processes.

THE PRINCIPLES OF LCE

LCE is a methodology for the assessment of the environmental and economical impact of products, usually considering their whole life cycle: production, use phase, and end of life. The analysis is conducted taking into account technical boundaries (technical feasibility).

LCE is structured by life cycle assessment (LCA) and life cycle costs (LCC), devoted to the analysis of the environmental and economic impact assessments.

THE LIFE CYCLE ASSESSMENT

"LCA studies the environmental aspects and potential impacts throughout the product's life (i.e. cradle to grave) from raw materials acquisition through production, use and disposal. The general categories of environmental impacts needing consideration include resource use, human health, and ecological consequences." **ISO 14040**.

LCA is a technique used by industry, environmentalists, governments, researchers, and commercial organizations to identify and measure the cumulative environmental burdens associated with industrial processes during a complete life cycle. An LCA does not include economic (or social) parameters but only takes into account those physical phenomena that may produce significant changes in terms of energy consumption, raw materials use, and waste production as outlined in Figure 1.

The manufacturing industry requires inputs of raw materials and fuels for the generation of useful products. At the same time, outputs in the form of air emissions, water emissions, and solid waste are also produced. Additional inputs of raw materials and fuels and outputs of waste materials may be associated with a product during its lifetime (including transportation, selling, use, maintenance, etc.), even when disposed of at the end of its useful life. Several initiatives to set up a concrete LCA methodology started in the early 1990s, when some handbooks and calculation tools were published and widely used by researchers. The most famous manuals are the

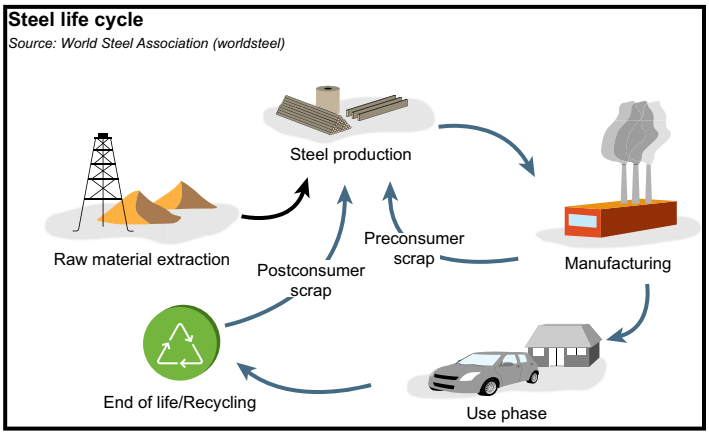

FIGURE 1

Example of life cycle taken from the World Steel Association.

ones from Environmental Protection Agency (EPA, USA), Centre of Environmental Science in Leiden (the Netherlands), and Society of Environmental Toxicology and Chemistry (SETAC, USA).

The ISO Technical Committee 207 SC 5 has published the ISO14040 series, in order to internationally standardize LCA's methodology and its main steps. The series have been recently reorganized as follows:

- ISO14040: 2006—Environmental Management—Life Cycle Assessment—Principles and Framework.
- ISO14044: 2006—Environmental Management—Life Cycle Assessment—Requirements and Guidelines.
- ISO14040: 2006 and ISO14044: 2006 have replaced:
  - ISO14040:1997—Environmental Management—Life Cycle Assessment—Principles and Framework.
  - ISO14041:1998—Environmental Management—Life Cycle Assessment—Goal and Scope Definition and Inventory Analysis.
  - ISO14042:2000—Environmental Management—Life Cycle Assessment—Life Cycle Impact Assessment.
  - ISO14043:2000—Environmental Management—Life Cycle Assessment—Life Cycle Interpretation.

The ISO14040/44 series provide a set of principles and framework, which provides a clear overview of the practice, applications, and limitations of LCA to a broad range of potential users and stakeholders, including those with a limited knowledge of LCA.

According to the International Organization for Standardization (ISO) 14040/44 standards, an LCA study consists of four phases: (1) goal and scope (framework and objective of the study); (2) life cycle inventory (input/output analysis of mass and energy flows from operations along the product's value chain); (3) life cycle impact assessment (evaluation of environmental relevance, e.g., global warming potential); and (4) interpretation (e.g., optimization potential) (ISO 14040: 2006, ISO 14044: 2006).

More recently, the European Commission's Joint Research Centre (JRC) through its Institute for Environmental and Sustainability has developed the ILCD Handbook that is a series of technical documents that provide guidance for good practice for LCA. The ILCD Handbook further specifies the provisions of ISO 14040 and 14044 standards on environmental LCA. The ILCD system is a collection of publications, documents, and tools supporting LCA and LCI high quality data sets development, publication, and sharing.

On the basis of the normative ISO 14040 (subspecifications ISO 14041, 14042, 14043) and the ILCD, the LCA is therefore split into four distinct phases (see below) as illustrated in Figure 2:

Goal and scope definition

The aim of this initial phase is the identification of the decision context, application, and target of the analysis.

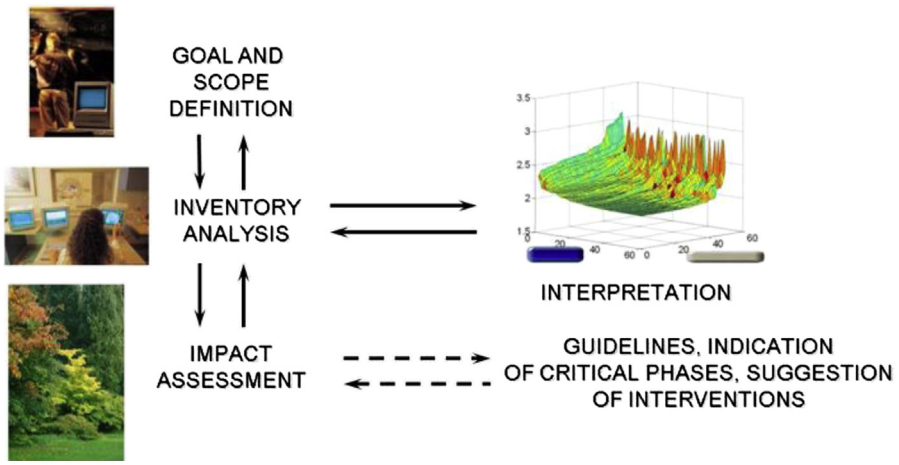

FIGURE 2

Life cycle assessment framework according to ISO14040 and ILCD.

- The goal and scope phase outlines the rationale of the study, the anticipated use of the results of the study, the boundary conditions, the data requirements, and the assumptions made to analyze the product system under consideration, and other similar technical specifications for the study.
- The goal of the study is to answer the specific questions that have been raised by the target audience and the stakeholders involved, while considering potential uses of the study's results.
- The scope of the study defines the system's boundary in terms of technological, geographical, and temporal coverage of the study, attributes of the product system, and the level of detail and the complexity addressed by the study.
- Furthermore, an additional objective of this phase is to define the function and functional unit of the study.

Life cycle inventory

In this phase are defined in detail the different cases to be studied, its functions, the functional unit (e.g., mass, amount, etc.), the life cycle stages, the environmental impacts to be considered, the interpretation approaches, the assumptions, and the limitations.

- The life cycle inventory (LCI) phase qualitatively and quantitatively analyzes the materials and energy used (inputs) and the products and by-products generated and the environmental releases in terms of nonretained emissions to specified environmental compartments and the wastes to be treated (outputs) for the process system being studied.
- The LCI data can be used on its own to: understand total emissions, wastes, and resource use associated with the material or the process being studied; improve production performance; be further analyzed and interpreted to provide insights

into the potential environmental impacts from the system (life cycle impact assessment and interpretation or LCIA).

Life cycle impact assessment

In this phase, the estimated inventory process data for inputs (e.g., energy consumption, raw material use) and outputs (e.g., emissions to air and water, waste produced) are elaborated. The LCI results are assigned to the selected impact categories and it calculated the potential environmental impact in each category.

- The impact assessment is aimed at understanding and evaluating the magnitude and significance of the potential environmental impacts of the products or processes considered.
- It is a technical and/or quantitative process to characterize and assess the effects of the environmental loading identified in the inventory.

Interpretation and improvement

In this phase, it is carried out as an interpretation of the LCIA results, providing indications for the improvement of the environmental impact of the cases studied.

- The findings of either the inventory stage or the impact assessment are analyzed and interpreted (consistent with the defined goal and scope) to reach conclusions and recommendations.
- The significant issues (the processes, resources/emissions that quantitatively contribute most to the results) are identified.
- The completeness, sensitivity, and consistency of the analysis are checked.
- The conclusions of the interpretation take to indications and recommendations for the improvement, highlighting limitations, and assumptions done.

Considering the micro- and nano-manufacturing, it is important that the selection of the impact assessment method will be used to associate the quantities of substances indicated in the LCI with the environmental burdens.

One of most widely used methods is the **CML 2001 (baseline) method**, which conforms to ISO 14040 and ILCD, including the following impact categories:

Depletion of abiotic resources

This impact category indicator is related to extraction of minerals and fossil fuels due to inputs in the system. The abiotic depletion factor is determined for each extraction of minerals and fossil fuels (kg antimony equivalents/kg extraction) based on concentration reserves and rate of deaccumulation.

Acidification

Acidifying substances cause a wide range of impacts on soil, groundwater, surface water, organisms, ecosystems, and materials (buildings). Acidification potentials (AP) for emissions to air are calculated with the adapted RAINS 10 model, describing the fate and deposition of acidifying substances. AP is expressed as kg SO_2 equivalents/kg emission.

Climate change

Climate change can result in adverse affects upon ecosystem health, human health, and material welfare. Climate change is related to emissions of greenhouse gases to air. The characterization model as developed by the Intergovernmental Panel on Climate Change is selected for the development of characterization factors. Factors are expressed as global warming potential for time horizon 100 years, in kg carbon dioxide/kg emission. The geographic scope of this indicator is at global scale.

Stratospheric ozone depletion

Due to stratospheric ozone depletion, a larger fraction of UV-B radiation reaches the earth surface. This can have harmful effects on human health, animal health, terrestrial and aquatic ecosystems, biochemical cycles, and on materials. This category is output related and at global scale. The characterization model is developed by the World Meteorological Organisation and defines ozone depletion potential of different gasses (kg CFC-11 equivalent/kg emission). The geographic scope of this indicator is at a global scale. The time span is infinity.

Human toxicity

This category concerns the effects of toxic substances on the human environment. Health risks of exposure in the working environment are not included. Characterization factors, human toxicity potentials (HTP), are calculated with the Uniform System for the Evaluation of Substances adapted for LCA purposes (USES-LCA), describing fate, exposure, and effects of toxic substances for an infinite time horizon. For each toxic substance, HTPs are expressed as 1,4-dichlorobenzene equivalents/kg emission. The geographic scope of this indicator determines on the fate of a substance and can vary between local and global scale.

The substances that contribute to an impact category are multiplied with a characterization factor that expresses the relative contribution of the substance, as such it can be seen as an equivalence factor. In Table 1, the CLM 2001 impact categories are indicated and their units expressed in equivalence factor.

Another method used is the Eco-indicator 99 that defines damage categories. The different damage categories have been clustered as:

Human health

This category includes the number and duration of diseases, and life years lost due to premature death from environmental causes. The effects included are: climate change, ozone layer depletion, carcinogenic effects, respiratory effects (organics and inorganics), and ionizing (nuclear) radiation (unit: DALY = disability adjusted life years; this means different disability caused by diseases are weighted).

Ecosystem quality

This category includes the effect on species diversity, especially for vascular plants and lower organisms. The effects included are: ecotoxicity, acidification, eutrophication, and land use (unit: PDF*m2yr; PDF = potentially disappeared fraction of plant species).

Table 1 CML 2001 (baseline) method impact categories and their units expressed in equivalence factor.

Impact Category	Unit
Abiotic depletion	kg Sb eq
Acidification	kg SO2 eq
Eutrophication	kg PO4— eq
Global warming (GWP100)	kg CO2 eq
Ozone layer depletion (ODP)	kg CFC-11 eq
Human toxicity	kg 1,4-DB eq
Fresh water aquatic ecotoxicity	kg 1,4-DB eq
Marine aquatic ecotoxicity	kg 1,4-DB eq
Terrestrial ecotoxicity	kg 1,4-DB eq
Photochemical oxidation	kg C2H4

Resources

This category includes the surplus energy needed in future to extract lower quality mineral and fossil resources (unit: MJ surplus energy additional energy requirement to compensate lower future ore grade).

The data obtained from the LCIA can be reported in impact assessment characterization tables and represented diagrams. On the other hand, as above mentioned, the different impact categories have different measurement units and are not comparable. In practice, it is possible to compare the environmental burdens of different micro- and nano-manufacturing (or products), but not to verify for the single process or product what are the most significant environmental burdens.

In order to make the interpretation of the impact assessment easier, an impact assessment normalization can be used to create a uniform unit for all impact categories and to show the relative contribution of all impact categories to the environmental problems in a region. This is achieved by dividing the characterization results by a reference value per impact categories (as example the reference can be calculated from the yearly emissions per inhabitant in an area like Europe).

In the LCIA, the software tools may also allow discrimination between environmental impact including the overall emissions and impact excluding the long-term emissions.

COMMERCIAL AND CUSTOMIZED SOFTWARE TOOLS

Commercial LCA and environmental auditing softwares are usually based on well-known and reliable databases, which are used to build the LCI. The costs and the success of these commercial tools depend on their valuable databases that make

the analysis of many industrial products and processes possible. Open source software is available, but they may require the separate purchase of external databases. The external databases are sometimes cost free, but the most reliable, complete, and updated databases containing life cycle inventory of innovative materials and processes are commercialized by annual licensing.

As example, the commercial software SimaPro8 Analyst (PRé Consultants) is based on Ecoinvent database (www.ecoinvent.org/database), US-LCI, US Input Output, EU and Danish Input Output, Swiss Input Output, LCA Food, Industry data v.2. The Ecoinvent database is one of the most widely used LCA database in the world, developed by Swiss Ecoinvent Center and itself represents the result of a large effort to update and integrate the well-known ETH-ESU 96, BUWAL250 (Swiss Bundesamt für Umwelt, Wald und Landschaft), and several other databases.

To give an idea of how widely used Ecoinvent is, some examples of other LCA softwares adopting it are outlined: GaBi, AMEEdiscover, Aveny GmbH, eBalance (new Chinese software, www.itke.com.cn), EMIS, iPoint Compliance Agent LCA Module, Open LCA, Quantis Suite 2.0, REGIS, Umberto, Life Cycle Tracker, Bilan Produit, CPMLCA, Green-E, KLC-ECO, LEGEP, OGIP V, Regis, TEAM, VITRUVIUS, and WRATE.

The application of Ecoinvent database is not only limited to LCA, but also used for Environmental Product Declaration (EPD), carbon footprinting (CF), Integrated Product Policy (IPP), Life Cycle Management (LCM), Design for Environment (DfE), ecolabeling, and other applications related to sustainability aspects.

Another well-known LCA commercial tool, suitable for the environmental analysis innovative materials, processes, and products, is GaBi (Thinkstep, formerly PE International): it integrates a GaBi database (developed, maintained, and regularly updated since 1990 by PE International jointly with LBP and the University of Stuttgart), together with other databases like the ELCD (European Life Cycle Database, the official LCA database of European Commission provided by EC JRC, the Joint Research Center), Ecoinvent (mentioned above), APME, and EDIP (Denmark).

Other LCA databases that include life cycle inventory data of innovative materials are: UBA Database (Germany), DIM (Italy), ECODESIGN X-Pro (Spain), IVAM (Netherlands), CLCD (Chinese Life Cycle Database developed by Sichuan University and IKE Environmental Technology), IDEMAT (Netherlands), Franklin (US), EIME (France), Esu-services database, Eurofer data sets (cost free), GEMIS (cost free), IO-database for Denmark, 1999 (cost free), Option data pack (Japan), ProBas (cost free), Boustead Model (UK), and Umberto library (Germany).

Obviously this list is not exhaustive, but it gives an idea on how disperse the data are and the degree of difficulty to carry out an LCA adopting a single database and software tool. The recovery of inventory data became even more difficult considering micro- and nano-materials as well as micro- and nano-manufacturing.

It is important to consider how to conduct a comprehensive LCA. One of the key phases to conducting a comprehensive LCA is the "interpretation of the results," where the industrial experience and technical background of the engineers are still playing the main role. It is not possible to carry out an effective and comprehensive LCA, without the correct guidance from trained personnel from well-established industries. So even if you have the best software in the world, but you do not have a detailed understanding of the underlying processes, it can be very difficult to interpret the results. It is exactly the same situation as having a state-of-the-art FEM software and trying to design a race car or an airplane without having ever done it before. The result will most probably be disastrous.

For example, it can be observed that the inventories offer a vast amount of data about the extraction, the refining, the casting, the shaping of most common metals (e.g., aluminum, brass, bronze, cast iron, chromium, cobalt, copper, lead, magnesium, manganese, mercury, molybdenum, nickel, unalloyed steels, low alloyed steels and stainless steels, zinc, palladium, platinum, rhodium, etc.). On the other hand, the modern European Industries are gaining in world competitiveness by focusing on high tech and high quality products that require development and application of innovative materials and processes: looking from this perspective to the available inventory databases, it is evident that there is an urgent need to integrate more data. For example, it is difficult to find information on emerging materials (and their production processes) for the automotive applications like ADI cast irons (Austempered ductile irons), CGI cast irons (compacted graphite irons), hypereutectic aluminum alloys (e.g., AS13, A390), or the aeronautic and motorsport applications like the reinforced aluminum alloys (e.g., MMCs). Also information on traditional and widely used aeronautic superalloys like Inconel 718 and Rene 80 are not available in most of the databases, the industries must be refer to generic Iron Nickel data. In the area of manufacturing and micro-manufacturing, data on both traditional and innovative cutting tools materials and coatings are frequently not available: for example, High Speed Steel by Powder Metallurgy and hard metal are often not considered as well as micro- and nano-structured tool materials. Titanium alloys obtained from casting or sintering processes, e.g., Ti6Al4V, that are applied by the automotive, aeronautic, sport, biomedical, and food industries are not included in main databases. There is a dramatic need for the data regarding micro- and nano-materials and their manufacturing.

In order to carry out an LCA of micro- and nano-materials and manufacturing, two main approaches can be followed: the first is to buy from the databases producers new models customized ad hoc, the second is to personally build them. In fact, in certain cases, the LCA softwares allow the users to build their owns models, therefore micro- and nano-materials and manufacturing not included on the databases can be "created" implementing the necessary data inputs (manually) or combining data from other materials and processes listed. At this purpose, it is

important to mention that main LCA softwares allow to import and export models using common file formats (e.g., .xls,.txt,.csv,.xml), therefore, the transfer of data from different LCA tools and databases can be attempted.

It is hard for the users of LCA software to collect reliable information about the input resources, emissions, and by-products for micro- and nano-materials and their processing: only the active collaboration (and information purchase) of the overall process chain actors can lead to a successful LCI creation and comprehensive LCIA results for micro- and nano-manufacturing.

It is clear that the European Industries and Institutions perceive a stringent need of life cycle inventory data on micro- and nano-materials, their production filler, and their end of life: the extensive industrial application these materials will go hand in hand with the capability to prove their sustainability.

Two more general aspects must be considered in the evaluation of sustainability software tools:

- the high purchase prices of state-of-the-art commercial environmental analysis software tools and the expensive periodic updates of the databases.
- the steep learning curve to use them, as often they require basic training course and then various advanced optional course modules.

These conditions make the access to LCA, environmental auditing of micro- and nano-materials and manufacturing for the SMEs very difficult. Therefore, it would be recommended that the development of cheap and easy-to-use environmental assessment software tools and databases, having different steps of analysis (requiring limited inputs and elaborating data quickly at the earlier design stage and allowing more granularity at the final assessment phase). This issue is relevant in Europe, where the SMEs are the average of the 99% of European companies, representing more than 67% of total employment.

LCA AS A METHODOLOGY FOR PRODUCT DESIGN GUIDELINES AND DESIGN FOR LIFE CYCLE

As mentioned above, the interpretation of the LCIA can be used to provide indications for the improvement of the environmental impact of micro- and nano-products and processes. This powerful tool, conceived for the evaluation of existing products and processes, can also be used for addressing the "green" design of new products and new processes, addressing, from an environmental point of view, alternative solutions for the most critical design steps.

In fact, LCA simulations can be conducted during the products design, adopting estimated LCI data, and can be used for calculating and comparing the environmental impact of different alternatives of product materials, geometry, quality, etc., considering the overall product life cycle.

This approach takes to many advantages:

- estimating the potential environmental impact of micro- and nano-products and manufacturing since design phase.
- identification of significant issues that quantitatively contribute most to the environmental impact of the overall life cycle.
- production and update of design guidelines for reducing the environmental impact of the final product.
- achievement of a "green design" for life cycle.

ENERGY CONSUMPTION

Energy is needed to create, use, and dispose micro- and nano-materials as well as for the micro- and nano-manufacturing. Each life cycle stage of a product, process, or activity needs energy.

The energy consumption of the manufacturing processes has a relevant environmental and cost impact, therefore, every intervention for reducing the energy need of micro- and nano-manufacturing leads to double the advancement in decrease of both environmental and economical burdens. Therefore, the consideration of the energy consumption (or production) must be included in the LCA and LCC and it is fundamental to the selection of the correct energy mix.

ENERGY MIX

The energy mix is the share of various energy sources typical of a country or a region: fossil fuels (e.g., hard coal, crude oil, natural gas liquid, gasses), nuclear, renewables, waste, etc. Many options of energy mix are available on the LCI commercial databases and the selection of one mix will impact significantly on the final results of the environmental assessment (e.g., CO_2 emissions). The location of the product life cycle must be defined here: production, use, and end of life may happen at same place or in different countries: for each life cycle phase must be selected the correct country energy mix. Sometimes it is not possible or correct to define specific locations: in those cases a more general energy mix value must be used. This is the case of LCA of micro-/nano-materials or manufacturing made considering the European Union territory (US, etc.), where an average EU27 energy mix is adopted (average value of the energy shares of 27 EU Countries): this assumption is fundamental to obtain the LCA environmental impact data that are significant at European scale and not just at the National level. Other aspects to be considered are the electricity voltage (high, medium, low) and the transmission network. The voltage must be selected on the basis of the electric power supply at the micro-/nano-manufacturing production site (usually medium voltage), at the usage site, and at the end-of-life site. The transmission network

(grid) is the average technology used to transmit and distribute electricity and will depend on the location of the life cycle phases and the electric voltage supplied. It is important to outline that usually energy consumption of micro-/nano-manufacturing is one of the main sources of environmental (and cost) impact, therefore, the selection of correct data is dramatically important: luckily the existing commercial databases allow a great granularity in the selection of energy mix/voltage/grit.

EMBODIED ENERGY, EMBODIED CO_2

As above mentioned, the commercial LCA softwares require consistent purchase and maintenance costs as well as personnel training effort. From this point of view, the embodied energy analysis and embodied carbon analysis represent easy and useful methodologies for a quick preliminary environmental evaluation, before producing a more complete and detailed LCA.

The life cycle energy analysis (LCEA), used since late 1970s, consider the energy as the only measure of environmental impact of products. The purpose of this methodology is not to substitute the LCA, but deeply analyze the energy attributable to products, processes, or activities. In particular (and compared), the initial energy (capital), recurrent energy (operational), and the end-of-life energy (required to recycle, remanufacture or dispose) of materials and products can be evaluated. This kind of environmental analysis can be used as an example to estimate the energy use/savings over a product life, comparing energy payback periods for different design or production solutions.

The embodied energy values can be converted in kg eq. of CO_2 allowing to consider the life cycle carbon assessment methodology and materials/products carbon footprint evaluation.

RELEVANT INDUSTRIAL CASE STUDIES

In this section, an example analysis carried out in an EU R&D project named RAPOLAC (Rapid Production of Large Aerospace Components) is presented. The project was focused on an innovative additive manufacturing technology, called Shaped metal deposition (SMD), which is basically a near-net shape prototyping system licensed to the University of Sheffield that allows complex parts to be built directly from the CAD model with minimum finishing. The system creates components in a layer-wise fashion, depositing weld material without the need for tooling. Complex parts can be made with improved material properties, and it is possible for hybrid components to be created. The time and material savings are expected to make SMD an attractive option for the manufacture of large aerospace parts.

No quantitative results will be presented because of confidentiality rules among the partners, but the overall methodology will be presented.

Concerning the LCA activity, in this research project, it was decided to consider that the manufacturing process of one element starts from the raw material and finishes with the waste treatment of the element. So it was decided to perform the assessment of environmental impact starting from the titanium raw materials. To produce a component, it is necessary to use the raw material and a combination of energy to carry out the transformation. After this phase, there is the use of the product and the recycling, if it is possible, or the waste treatment. With this last option, it is possible to produce the energy for the same or another process. If it is possible to reuse the material in the same process, the loop is closed, and if the material will be used in other process or in the same but adding some other raw materials, the loop is considered open.

In the outside of the system, there is the environment and also the other process that can be considered in the external of this process. So it is possible to divide the life cycle in different processes and evaluation of different effects. Practically, all the data collected from end users have been grouped in reference categories and were inserted in the questionnaire available online in the partners server. In particular, the tests have been analyzed in details and the data have been implemented in the model.

In the analysis carried out, different categories of input/output have been analyzed. In particular, the component is produced in the inner of a factory and there is a person (or an automatic system) that must control all its operations, as occurs in conventional plants. There is also the heat of the place where the SMD component is mounted. In fact, the person cannot start the SMD component manufacturing if, for example, at the inner of the factory the temperature is under a certain value. So in this case, the heat created must come into the balance of the environmental releases, in particular the air releases, if the heat is made with gas or petroleum derived. The partners decided also to consider the impact of transport because of their impact on the environmental releases. Just as an example, it is possible to compare the situation in the factory where the transports are based on diesel trolley with the electrical trolley: the situation is much different. In fact, on the basis of literature reports and on the basis of historical data collected in industries, there is a different incidence on the health of the people that work, for the pollution presence, and on the air emission at the inner of the factory. For this last point in particular, there is the possibility to estimate also the total reduction of the air emission of some particular gas (CO_2, SO_2). With the electrical power in the inner of the factory, there are not the gas releases but for the production of the energy power, there are the electric power station that create some gas emission and there is also all the consequence of the recycle of the battery of the trolley. In the case of the project on SMD, it has been decided not to go into too much in details of this analysis, not because of limits of the models, but for the difficulty to recover all the necessary information and also because of the fact that the RAPOLAC process

was in continuous evolution and some parameters were changing day by day. Anyway a comprehensive analysis has been conducted to compare SMD with conventional manufacturing process. The picture below shows the ARC voltage measurements carried out during advanced tests.

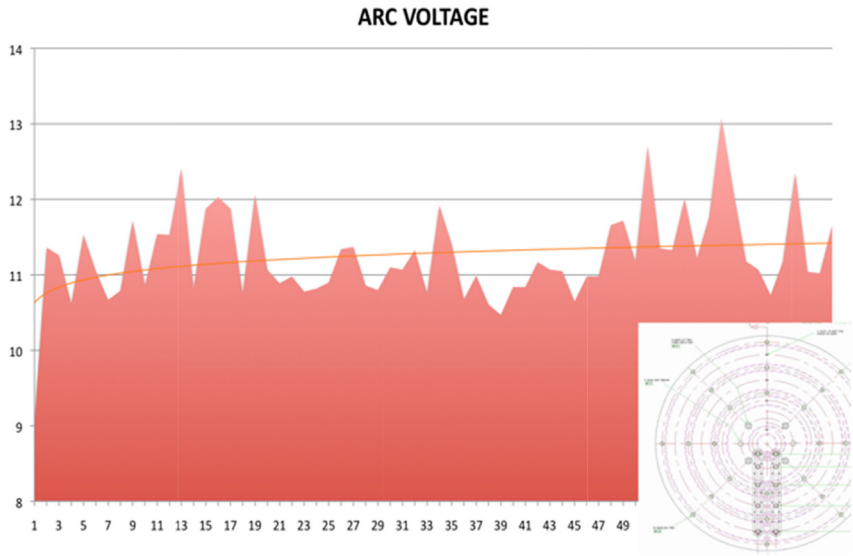

The final component was a very complex shape from the point of view of the deposition system, and so it was possible to divide its manufacturing process in some steps. So in the single step, it was important to evaluate the raw material that enters and the energy applied in these phases. In the same way, it was necessary to evaluate all the outputs in the environment.

Moreover, it has been decided to analyze in deep details the convenience of application of some new materials also in hybrid parts.

With the goal and the scope that the process leaders have established, it has been decided that all the common phase for the manufacturing process and the waste treatment and the life use of the two different manufacturing processes (SMD and traditional one) components should be removed from the study. In fact, this kind of phase produces the same kind of environmental impact, and the differences between the two parts are not present.

HYBRID PARTS APPROACH

The Consortium decided to carry out the study considering all the steps of the manufacturing process for the construction of the SMD conventional and hybrid component and all the environmental impacts that are created. That means that in order to permit a better comparison among results, the same approach has been followed also on hybrid parts.

In the inventory analysis, the collections of all elements that can have a possible environmental impact during the life of the SMD components and components manufactured have been carried out.

In the case under study not all these kind of data were available and so a screening of the parameters that in the SMD components (hybrid) can have an effect on the environmental impact have been carried out.

In particular, there is a first phase for dividing the manufacturing process in some unit process to obtain the single step for a specific study.

For the configuration of the RAPOLAC SMD component, the impact of the electric and the hydraulic systems was less relevant (only the actuator of the machine equipped with the welding device) and it will not be considered, because the focus of the research activity is the welding process itself. Moreover, there are no differences between the processes for creating the electrical and hydraulic components because at the inner of the project in the part change only one element in term of material there are no variations on the circuit that supply to all the other components.

The assessment starts from titanium production, evaluating the two most important sources in order to permit the choice of the best one for the efficiency and the environmental compatibility of SMD. A similar analysis has been conducted to compare SMD with respect to the reference state of the art manufacturing processes.

This study cannot be performed without considering the different energy mix.

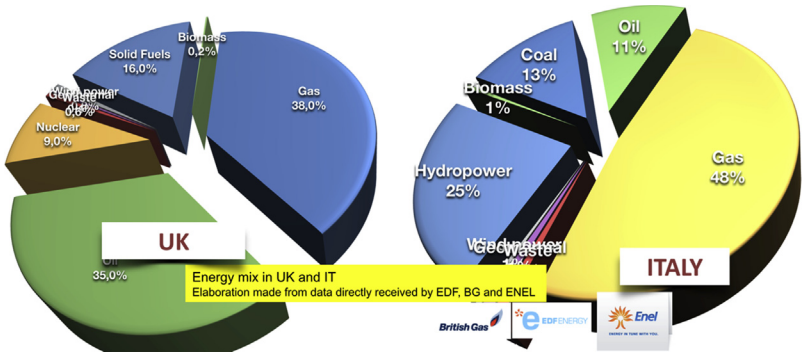

The energy mix varies from country to country. All the calculations on nonrenewable energy, oil consumption, emissions, have been carried out using the European average energy mix. Of course in the case of setting up future productions, the values should be corrected recalculating the chosen country and eventually going into detail in the specific production area.

It means that an SMD factory has a different impact at the environmental level if located in UK or Italy.

The energy mix shown above are based on the data available at the time of the activities. So the analysis carried out into RAPOLAC have also taken into account the difference in the energy mix country from country.

The analysis started with the comparison of two production processes for the titanium material used in SMD process.

Process (a): The raw materials disposable in the environment to obtain titanium are different: rutile, brookite, and some different "titaniti" and in particular from this last group the titanite. These materials are not simple to find in the environment and with some chemical process it is possible

Electrolytic process under vacuum and creation of a sponge that, with some heat and under pressure, produce the final traditional foundry shape of the titanium to obtain the pure titanium

From this, the titanium is able to support all the typical deformation process valid for the steel material (cold and hot process) enough problems (big use of chemical products for eliminate the impurity)

Process (b): Another process able to reduce the environmental impact but it is not yet always applied. Some balls of titanium dioxide are put on a solution of calcium chloride and here crossed from some electricity. So there is the creation of pure titanium with a less environmental impact.

A reduction of the chemical agent able to pollute the environment and also the reduction of the major part of the gas produced during the reaction. The energy absorption is also less than the first process. At the end of this

process, there is a creation of some traditional foundry shape. From now, there is a collection of all the traditional processes that are able to transform the initial foundry shape in the final element. In particular, there is two different ways for do this now: foundry process and laminate process.

Both of these two different systems, there is the creation of an intermediate shape and there is also some common point to reach the final shape.

Process (A): For the foundry process, there is the creation of some different part with the press casting process and after there is the mechanical joint of these different parts. So for this the environmental impact is the same of the initial process because here the supplier buys the raw material from a foundry and after in some furnace it melts this material and after with a cooling process it obtains the final shape in a mould. So for the environmental impact, there is the creation of some gas during this phase and there is also the use of electrical energy. The creation of some component is necessary to obtain the final shape because it is very difficult or impossible to create with a single mould.

Process (B): The second chance is the creation through the laminate process of some different titanium sheet and after, with the same process of the electro-welding, the creation of the final shape. In this case, there is no production of the gas because the titanium is not melting but there is an environmental impact for the electrical energy absorption. In this case, the laminate process can be applied at environmental temperature or at hot temperature for obtain an increase of the working thickness.

In particular for the first, there is major energy absorption for the heating of the raw material but there is also a reduction of the energy necessary to laminate the material. The two processes have so for a great quantity of working material about the same energy absorption.

The SMD welding-based deposition process is for both of the processes. The welding process has a very high electrical absorption for the environmental impact but there are not some other particular problems. The only particular in this kind of process is that it must be do in inert atmosphere. This atmosphere is created with different gas like argon. In both of these cases (as also in SMD), there is no particular problem for the human health because there are no toxic gases and they are not dangerous. The electrical energy absorption for the treatment of this gas and the sufficient compression of them at the inner working area (which is similar to SMD).

After the joints of the different parts of the element are disposed, the final shape and the working (machining) phases for creating the necessary precision of the surface and the holes for interfacing with the other components of the system are done. Also in this case, there are no particular environmental impacts during this working phase and also during the electrical energy absorption.

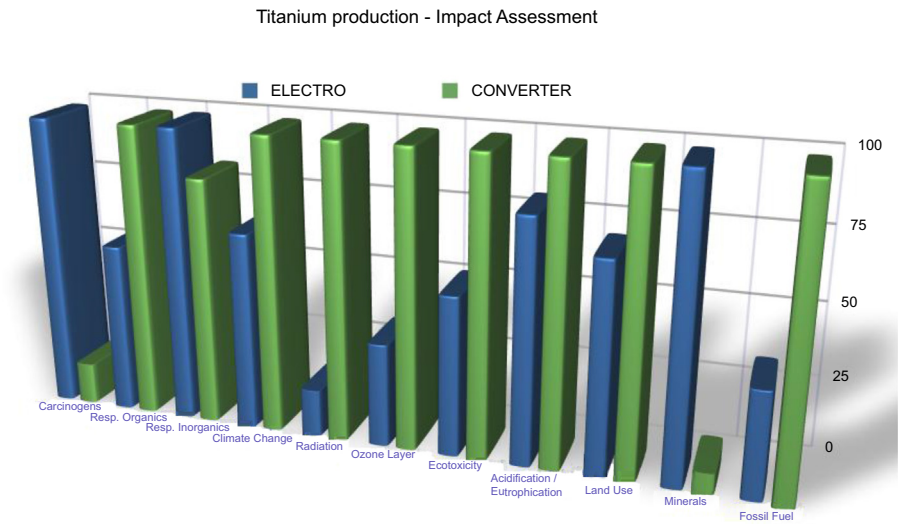

Titanium production—impact assessment: Qualitative comparison of human and environmental impacts between two ways of producing titanium ("converter" vs "electro")

Monte Carlo results of a comparison. In this graph, the number of outcomes where converter titanium has a higher score than the electrotitanium are shown per impact category. This allows us to see whether the differences shown in the previous figures are indeed significant. In general, we can assume that if 90–95% of the Monte Carlo runs are favorable for a product, the difference may be considered significant. Applying this rule means that only the difference between the two processes is not significant for Land use, Acidification, and Respiratory inorganic.

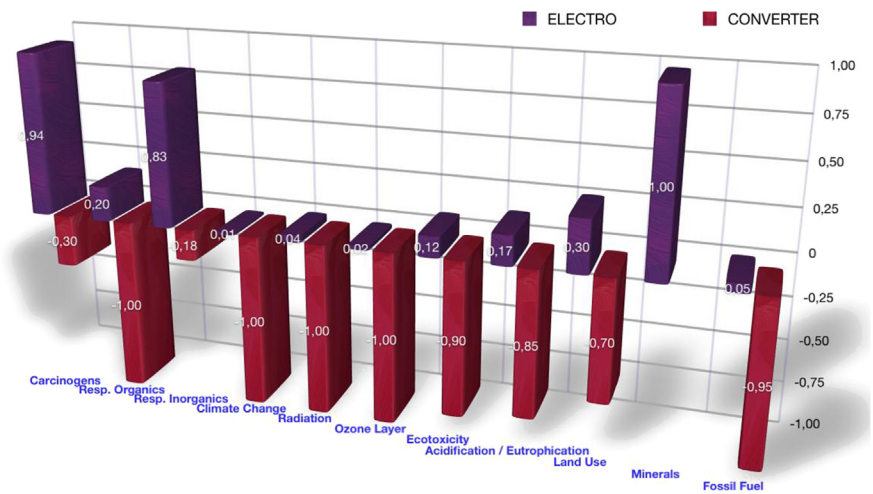

Monte Carlo Impact assessment

Essentially, the program will move around a marker in multidimensional space, tending to move in directions which lead to a lower function, but sometimes moving against the gradient.

Probabilistic formulation of inverse problems leads to the definition of a probability distribution in the model space. This probability distribution combines a priori information with new information obtained by measuring some observable parameters (data from titanium purifying process). As, in the general case, the theory linking data with model parameters is nonlinear, the a posteriori probability in the model space may not be easy to describe (it may be multimodal, some moments may not be defined, etc.).

When analyzing an inverse problem, obtaining a maximum likelihood model is usually not sufficient, as we normally also wish to have information on the resolution power of the data. In the general case, we may have a large number of model parameters, and an inspection of the marginal probability densities of interest may be impractical, or even useless. However, it is possible to pseudorandomly generate a large collection of models according to the posterior probability distribution and to analyze and display the models in such a way that information on the relative likelihoods of model properties is conveyed to the spectator. This can be accomplished by means of an efficient Monte Carlo herein optimized for RAPOLAC method, even in cases where no explicit formula for the a priori distribution is available.

During a meeting, it became apparent that there was a need to compare the impacts and costs of production of titanium ingots or wires for SMD, so a more detailed analysis was conducted. On the basis of the data available at the time of the activity, it emerged that the production of wire requires an important percentage more of energy.

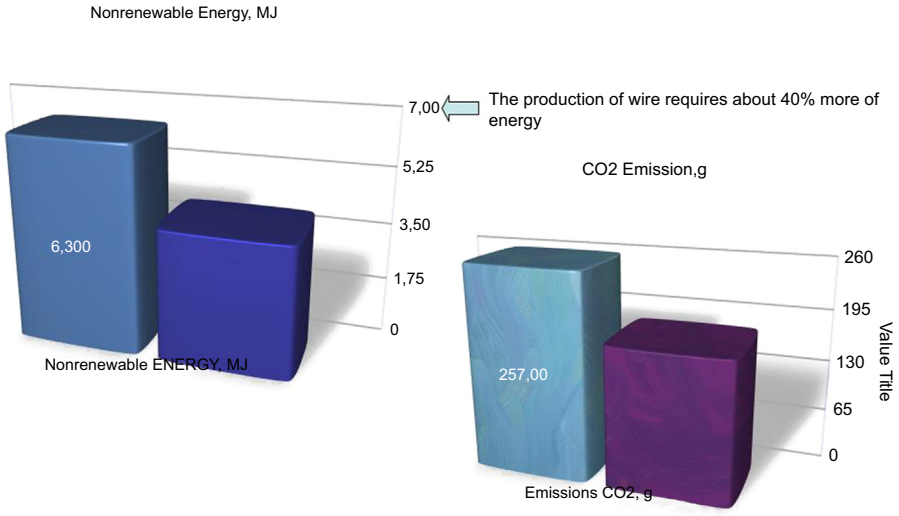

Another activity conducted was related to the optimization of the assessment procedures and adaptation to the case study identified.

From the few details reported here, it is easy to imagine that the SMD process could become a must for aerospace components, but also in some niche automotive and consumer goods fields. The idea was to evaluate also from the LC point of view the SMD as manufacturing process of the RAPOLAC demonstration. The use of SMD has been compared with the use of the traditional processes typical of the sectors. The RAPOLAC activity was so focused on the comparison of a conventional well-tuned manufacturing process with the new SMD one. In particular, the calculation was carried out making the hypothesis to produce the engine case in titanium alloys as shown in the following picture. The choice of titanium for this kind of components is:

Picture of a prototype engine case produced by SMD

The following pictures show a qualitative comparison in the consumption of nonrenewable energy, in emissions of CO_2 and SO_2 between the conventional process and new RAPOLAC SMD taking into account all the parameters as described before.

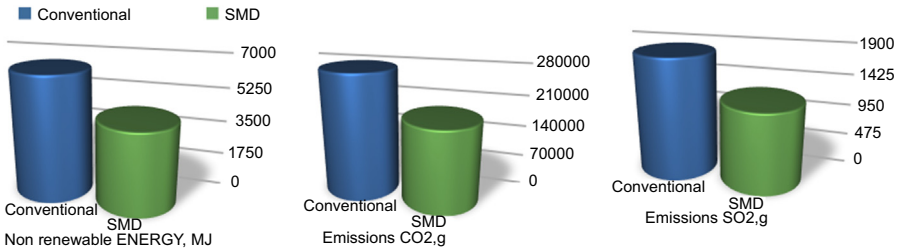

These results are an interesting anticipation on what the analysis will bring, as described in a more detailed way in the following chapters.

The impact at energy level of the SMD process applied to manufacturing an aeronautic titanium engine case part has been carried out. So it is possible to evaluate and compare the conventional process with the new one, in the production of a complex shape part, considering all the aspects illustrated in this and previous reports. A comparison between the energy used in the original-SMD and the optimized-SMD processes has been carefully calculated using the most advanced algorithms. In particular, the conventional process has been split into the main phases and for each of them a calculation has been made.

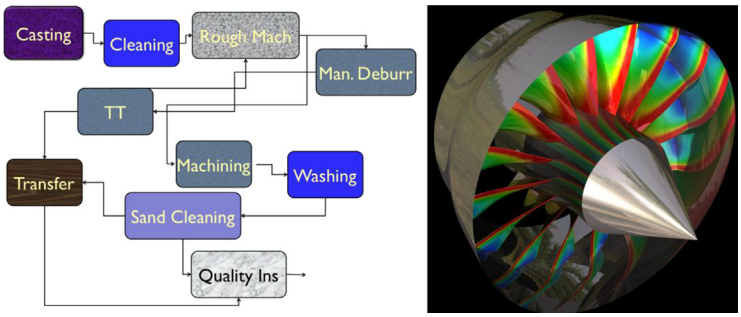

Business case conventional process flow chart

The same splitting procedure has been applied on the new SMD process using the data that emerged during the technical meetings of the project. It is important to highlight that the evolution of the process during the RAPOLAC project has been quite sensible and these Pert diagrams are not able to show the important improvements introduced during the 3 years on the process parameters. Some extensive analysis carried out on the approach itself shows that it is good enough to permit interesting evaluation with a much more than acceptable approximation.

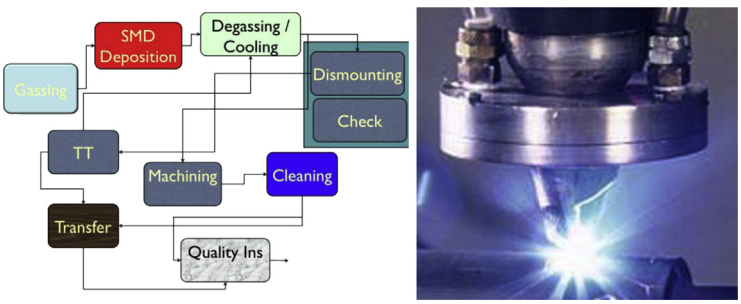

Business case SMD Hybrid process flow chart

To better understand the quality and variance of the data in the analysis, the time domain of the arc voltage for a complex component like the aeroengine case is illustrated.

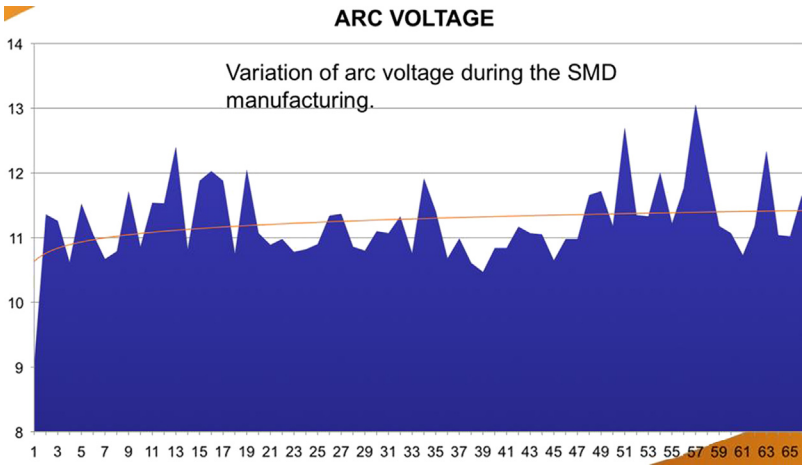

The environmental cost/benefit evaluation of RAPOLAC hybrid part with respect to conventional methods has been carried out using both commercial and in-house customized software for the business case analyzed.

The methodology developed in the project made it possible to carefully analyze the cost/benefits between conventional manufacturing process and hybrid SMD process, to produce a reference engine case. The analysis showed impact at different levels:

- Nonrenewable energy
- Oil consumption
- CO_2 emissions
- No_x emissions

Then the analysis has been normalized on the different energy mix considering to better understand the different impact to the Earth and human economy when establishing a production facility in UK or IT. Of course the internal difference between conventional versus hybrid SMD process is proportional but the global impact per categories is different.

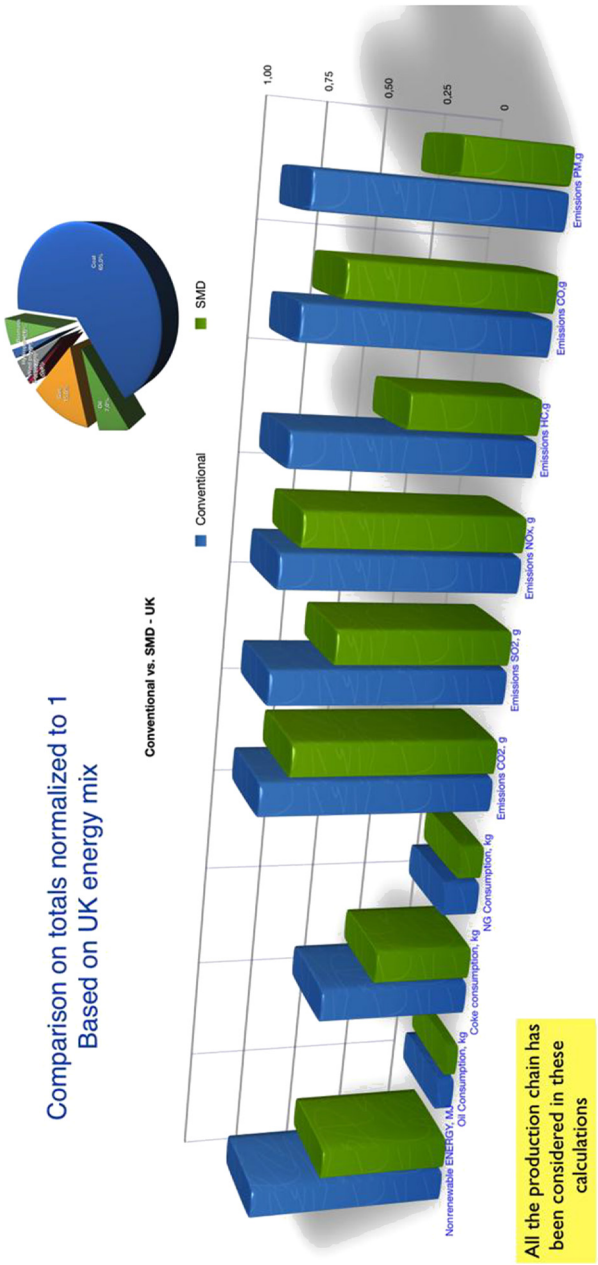
Comparison on totals normalized to 1
Based on UK energy mix
Conventional vs. SMD - UK
Conventional
SMD
1.00
0.75
0.50
0.25
0
Nonrenewable ENERGY, MJ
Oil Consumption, kg
Coke consumption, kg
NG Consumption, kg
Emissions CO2, g
Emissions SO2, g
Emissions NOx, g
Emissions HC,g
Emissions CO,g
Emissions PM,g
All the production chain has been considered in these calculations

LCA FOR NANOTECHNOLOGY AND MICRO-MANUFACTURING

Past experience has taught us that an LCA across the full life cycle of emerging technologies such as nanotechnologies is difficult due to limited data availability. In particular, for nanotechnologies there is a distinct lack of inventory data since their manufacturing processes are new and often protected by confidentiality constraints [8]. Such obstacles mean that an LCA is often not considered until the technology has matured. Good practice should encourage us to conduct LCAs at a much earlier stage of product/technology development as it offers an opportunity for proactive action to influence design and minimize potential adverse effects to both the environment and human health. As outlined previously, the LCA for a nanotechnology should consider the full life cycle in order to gain a realistic understanding of the impacts on both the environment and human health. Theoretically, this process can follow the framework outlined by the ISO 14040 and 14044 standards but it is important to consider that there are few areas that need careful considerations. The following sections will consider the recommended stages of an LCA and highlight particular areas that may be problematic or require special attention.

GOAL AND SCOPE DEFINITION

When defining the scope of interest for the LCA, it is important to consider the functional unit for assessment [9]. The functional unit acts as a reference unit for the flow information to be considered and enables the comparison of different products but this may prove a problematic issue when assessing nanotechnologies [10]. As nanotechnologies are still relatively new and it may therefore be difficult to quantify and define a functional unit that could act as a fair comparison for the analysis. Without a functional alternative, it is impossible to conduct a comparative analysis and gain a clear understanding of how nanotechnologies compare to conventional technologies. Furthermore, the manufacturing processes adopted for the development of nano-materials are not yet standardized and are therefore continually changing. This proves problematic when trying to define the goal and scope for the LCA and compare it to a state-of-the art alternative. Continually changing methods make it impossible to restrict the analysis to a boundary and will affect the generalizability of the results, as the analysis will not reflect a standardized process/material. To overcome these issues, it may be beneficial to plan to conduct scenario analyses to consider the inherent uncertainties associated with nanotechnologies and nano-materials.

LIFE CYCLE INVENTORY

One of the biggest challenges when conducting LCA investigating the impacts of nanotechnologies and nano-materials is the paucity in available and reliable data [11]. Even though this problem was highlighted a number of years ago, a large number of data gaps remain [8]. This problem is particularly pertinent for the

manufacture, release, transport, and ultimate fate of nano-materials. The lack of standardized data comes from the fact that many of the processes/materials are relatively new and often protected by confidentiality agreements. Confidentiality constraints are particularly problematic when attempting to model process data meaning and the collection of data from companies is almost impossible. In addition, when modeling potential impacts in such a rapidly evolving area, as quick as we manage to obtain/estimate data, it quickly becomes outdated and new data are required. Data are also lacking outlining maintenance and end-of-life processes. As nanotechnologies and nano-materials are still developing, the maintenance and recycling options for the products are currently unclear. As highlighted earlier in the chapter, it is imperative to consider the entire life cycle (cradle to grave) but this is difficult when it is currently unknown how materials will react with other materials in an incinerator or dump, for example [11]. This suggests that an input−output based life cycle assessment approach (IO-LCA) may aid some of the problems discussed. An IO-LCA adopts an aggregate view of sectors and therefore covers an entire economy [12]. In this way, it does not draw boundaries like we do in a conventional LCA. All elements of a product's supply chain are therefore analyzed by default. It is thought that this aggregated view may prove useful as the existing data sources may aid in the assessment of new nanotechnologies and nano-materials [11]. More pertinently, similar processes can be adapted to more adequately reflect the nano-process under review. For example [11], we suggest that an IO-LCA semiconductor manufacturing may be a good starting point when assessing nano-materials.

A final area of consideration within the life cycle inventory is the potential change in surface chemistry of nano-particles [5]. Changes in surface chemistry will increase agglomeration and therefore create larger particles [13]. As these larger, secondary particles are created, the material properties will differ from those associated with the original, primary particles. The potential impacts of these secondary particles are uncharacterized and difficult to quantify within a model. Often the elementary flows within the LCA model only characterize the primary particles so additional characteristics will need to be considered and described to ensure that an accurate representation is modeled [11]. Manufacturers are attempting to minimize the potential to agglomerate with the use of coatings but once again this is an evolving area restricted by confidentiality constraints. Lowry et al. [14] conducted a review to further investigate the transformations of nano-particles and suggested that the nano-particle tranformations which will alter the fate, transport, and toxicity of nano-materials. Although not enough is currently known about the process and impacts of nano-particle transformations [14], review highlights that research is working toward investigating the issue further.

LIFE CYCLE IMPACT ASSESSMENT

Many of the impact assessments that are frequently used in LCIA can be adopted for the assessment of nanotechnologies and nano-materials. However, due to the current

level of understanding concerning particle transformations and dose–response relationships, the toxicological impacts may need further consideration [13]. Currently, not enough is known about the toxic reactions of nano-materials but the material characteristics exhibited may well lead to greater toxic reactions. For example, research conducted by [15] assessed the impact of inhalation of fibers from carbon nano-tubes. The distinctive shape of the nano-tube fibers have been compared with asbestos suggesting that they may produce similar health effects [15]. By exposing the mesothelial lining of the body cavity of mice to carbon nano-tubes, it resulted in asbestos-like pathogenic behavior. Such behavior included inflammation and the formation of lesions. These findings are of great importance and may highlight the need for occupational management plans and greater caution before introducing products to market.

When modeling the LCIA, particular consideration should also be given to the dose–response relationship as traditional measures such as dose or mass may be linked to other aspects of the nano-materials. If adequate consideration is not given to these additional aspects such as particle size, shape, and surface area, then results will be limited and not accurate.

Due to the aspects discussed, it is currently difficult to address and model the potential toxic impacts of nano-materials. Further research is needed to improve the clarity of this but for the time being, any available information on nano-material reactivity, degradability, ecotoxicity should be incorporated where possible in an attempt to model the toxic impacts within the LCIA. Alternatively, it may be useful to consider a "worst-case" scenario and explore the possibility that nano-materials have an impact potential as high as that of the most toxic chemicals [11].

Dhingra et al. [5] suggest that a risk assessment may aid our understanding of the health impacts outlined above and help us to better understand the adverse health impacts of toxic substances. Such an approach accounts for quantities of pollutants and their effects as well as the consideration of various exposure pathways. Specifically, Dhingra et al. (2010) suggest that the combination of LCA and risk assessment may work well as the two methodologies would complement each other. One example of this combined approach is the 10-step Nano LCRA (Life Cycle Risk Assessment) framework for nano-materials as outlined by Shatkin [16]. Nano-LCRA is based on adaptive management as it involves the reconsideration of prior decisions and analysis with the development of new information [16].

LIFE CYCLE INTERPRETATION

The interpretation stage of the LCA for nanotechnologies and nano-materials should follow the ISO 14040 and 14044 standards and be conducted in the conventional manner. As outlined repeatedly throughout this chapter, uncertainty and sensitivity analyses are particular important and should be assessed during this interpretation stage.

CONSIDERATION OF LCC

To gain an in-depth perspective of the impact of nanotechnology, it will often be appropriate to also consider the corresponding cost implications. This can be done by adopting an assessment of the LCC. When conducting LCC analysis of nanotechnology, it is important to consider many of the environmental issues discussed previously in this chapter. In particular, it may be difficult to collect the data needed for the LCC due to the confidentiality constraints outlined. Without in-depth knowledge of materials, processes, disposal/recycling methods, and implications, it will be difficult to model an accurate model of the associated costs. As with an environmental assessment (LCA), it will be necessary to include uncertainty and sensitivity analyses to compensate for the data quality. As the field of nanotechnology develops, the data needed to conduct an in-depth LCC will hopefully become more readily available and make the process easier to conduct and result in a more accurate cost estimate.

CONCLUSIONS

Conducting LCAs for nanotechnologies/nano-materials are important to enhance our understanding of the impact of such approaches. Importantly, the analysis should cover the whole life cycle from cradle to grave to ensure that it captures important up- and downstream environmental and health impacts. The current evidence base often restricts the boundary for analysis to the use phase due to the constraints in collecting data across the full life cycle. In particular, since the techniques and materials are still relatively new, the end-of-life and recycling processes and impacts are not yet fully understood. The ISO standards should be adhered to when conducting the nanotechnology/nano-material LCA but it is imperative that some further consideration is given to the toxicity impacts. To gain a clearer understanding of the potential impact of nanotechnologies, uncertainty and sensitivity analyses need to be conducted. In particular, it may be useful to conduct "worst-case" scenario analysis.

Future work needs to be collaborative in nature in order to push the evidence forward. Practitioners, engineers, as well as nanotechnological companies, need to all work together to pool their knowledge and generate greater clarity into the impacts of nanotechnology. For the assessment of the impacts on human health, practitioners of LCA and risk assessment need to work together to produce LCRAs so that we can understand the longer term health impacts for the production of nano-materials and their impacts in wider society.

REFERENCES

[1] National Nanotechnology Initiative (NNI). www.nano.gov.
[2] Roco MC, Mirkin CA, Hersam MC. Nanotechnology research directions for societal needs in 2020. Retrospective and Outlook; 2010.

[3] Bruce D, Liu P, Meng S. Nanoscience and nanotechnology in next generation lithium batteries. Nanotechnology 2013;24.
[4] Mei L, Zhang Z, Zhao L, Huang L, Yang XL, Tang J, et al. Pharmaceutical nanotechnology for oral delivery of anticancer drugs. Adv Drug Deliv Rev 2013;65:880−90.
[5] Dhingra R, Naidu S, Upreti G, Sawhney R. Sustainable nanotechnology: through green methods and life-cycle thinking. Sustainability 2010;2:3323−38.
[6] Kim HC, Fthenakis V. Life cycle energy and climate change implications of nanotechnologies. J Industrial Ecol 2013;17(4):528−41.
[7] Sengul H, Theis TL, Ghosh S. Toward sustainable nanoproducts: an overview of nanomanufacturing methods. J Industrial Ecol 2008;12(3):329−59.
[8] Meyer D, Curran MA, Gonzalez M. An examination of existing data for the industrial manufacture and use of nanocomponents and their role in the life cycle impact of nanoproducts. Environ Sci Technol 2009;43(5):1256−63.
[9] Rebitzer G, Ekvall T, Frischknecht R, Hunkeler D, Norris G, Rydberg T, et al. Environ Int 2004;30:701−20.
[10] Bauer C, Buchgeister J, Hischier R, Poganietz WR, Schebek L, Warsen J. Towards a framework for life cycle thinking in the assessment of nanotechnology. J Clean Prod 2008;16:910−26.
[11] Kloepffer W, Curran MA, Frankl P, Heijungs R, Kohler A, Olsen SI. Nanotechnology and life cycle assessment: a systems approach to nanotechnology and environment. Washington: Woodrow Wilson International Center for Scholars; 2007.
[12] Hendrickson CT, Lave LB, Matthews HS. Environmental life cycle assessment of goods and services: an input-output approach. Washington, DC, USA: Resources for the Future; 2006.
[13] Rivera JL, Seely B, Sutherland JW. Societal implications of nanotechnology: occupational perspectives. Environ Dev Sustain 2012;14:807−25.
[14] Lowry GC, Gregory KB, Apte SC, Lead JR. Transformations of nanomaterials in the environment. Environ Sci Technol 2012;46:6893−9.
[15] Poland C, Duffin R, Kinloch I, Maynard A, Wallance W, Seaton A, et al. Carbon nanotubes introduced into the abdominal cavity of mice show asbestos-like pathogenicity in a pilot study. Nat Nanotechnol 2008;3(7):423−8.
[16] Shatkin JA. Health and environmental risks. 2nd ed. Boca Raton, FL, USA: CRC Press/Taylor & Francis Group; 2013.

Index

Note: Page numbers followed by "f" and "t" indicate, figures and tables respectively.

D

E

F

G

H

I

J

K

L

M

N

O

P

Q

R

S

T

U

V

W

X

Z